

2.01 Fundamentals in Reverse Osmosis

G Jonsson, Technical University of Denmark, Lyngby, Denmark

F Macedonio, University of Calabria, Arcavacata di Rende (CS), Italy

© 2010 Elsevier B.V. All rights reserved.

2.01.1	Introduction	2
2.01.2	Phenomenological Transport Models	3
2.01.2.1	Irreversible Thermodynamics-Phenomenological Transport Model	3
2.01.2.2	IT-Kedem–Spiegler Model	4
2.01.3	Nonporous Transport Models	4
2.01.3.1	Solution–Diffusion Model	4
2.01.3.2	Extended Solution–Diffusion Model	5
2.01.3.3	Solution–Diffusion-Imperfection Model	5
2.01.4	Porous Transport Models	5
2.01.4.1	Friction Model	5
2.01.4.2	Finely Porous Model	6
2.01.5	Comparison and Summary of Membrane Transport Models	7
2.01.6	Influence from Operating Conditions on Transport	7
2.01.6.1	Effect of Pressure	7
2.01.6.2	Effect of Concentration	8
2.01.6.3	Effect of Feed Flow	8
2.01.6.4	Effect of Temperature	8
2.01.6.5	Effect of pH	9
2.01.7	Experimental Verification of Solute Transport	10
2.01.7.1	Single-Salt Solutions	12
2.01.7.2	Mixed-Salt Solutions	13
2.01.7.3	Organic Solutes and Nonaqueous Solutions	16
2.01.7.4	Mixed Organic Solutes	18
2.01.7.5	Membrane Charge	18
2.01.7.6	Membrane Fouling and Concentration Polarization Phenomena: Limits of Membrane Processes	19
References		20

Nomenclature

A	hydraulic permeability	$(\bar{c}_s)_{ln}$	logarithmic mean solute concentration in the membrane
b	friction parameter defined by Equation (36)	\bar{c}_v	concentration of water in the membrane
B	salt permeability	D_2	solute diffusion coefficient
c'_s	bulk solute concentration at high-pressure side ($g\ l^{-1}$)	\bar{D}_s	diffusivity of the solute in the membrane ($m^2\ s^{-1}$)
c''_s	solute concentration at low-pressure side ($g\ l^{-1}$)	\bar{D}_v	diffusivity of the solvent in the membrane ($m^2\ s^{-1}$)
c'''_s	solute concentration at high-pressure side of the membrane (at membrane surface) ($g\ l^{-1}$)	E_0	apparent activation energy for solvent transport ($kJ\ kmol^{-1}$)
\bar{c}_s	mean solute concentration in the membrane	F_i	driving force on component i
		F_{ij}	frictional force between i and j
		J_i	flux of component i

J_s	molar flux of solute ($\text{kmol m}^{-2} \text{s}$)	x	coordinate direction perpendicular to the membrane (m)
J_v	solvent volume flux ($\text{m}^3 \text{m}^{-2} \text{s}$)	X_{ij}	friction coefficient between mol i and surrounding j
k	distribution coefficient of solute	ε	frictional pore area of the membrane
k_1, k_2, k_3	transport parameters in the solution–diffusion imperfection model as defined by Equations (23) and (24)	λ	thickness of the membrane skin layer
K	distribution coefficient of solute between bulk solution and pore fluid	$\Delta\mu_s$	solute chemical potential difference across the membrane (kJ kmol^{-1})
l_p	hydraulic permeability coefficient ($\text{m s}^{-1} \text{kPa}$)	$\Delta\pi$	osmotic pressure difference across the membrane (kPa)
l_{sp}	pressure-induced solute transport parameter ($\text{kmol m}^{-2} \text{s kPa}$)	Δx	membrane thickness (m)
$l_{\pi p}$	coupling coefficient	ΔP	pressure difference across the membrane (kPa)
L_p	hydraulic permeability	ρ_v	density of water
p_s	solute permeability coefficient ($\text{m}^2 \text{s}^{-1}$)	σ	reflection coefficient
p_v	water permeability coefficient ($\text{m}^2 \text{s}^{-1} \text{kPa}$)	τ	tortuosity factor
R and R	solute retention	ω	transport parameter defined by Equation (6) ($\text{kmol m}^{-2} \text{s}^{-1} \text{kPa}^{-1}$)
R_{max}	maximum solute rejection		
\mathcal{R}	universal gas constant ($\text{kJ kmol}^{-1} \text{K}$)		
T	temperature (K)		
u	linear velocity of the pore fluid		
u_i	linear velocity of component i		
V_s	solute partial molar volume ($\text{m}^3 \text{kmol}^{-1}$)		
V_v	partial molar volume of water ($\text{m}^3 \text{kmol}^{-1}$)		
		Subscripts	
		p	in the pore
		il	intermediate layer
		sl	skin layer
		pl	porous layer
		1 and/or v	solvent (water)
		2 and/or s	solute
		3 and/or m	membrane

2.01.1 Introduction

Several models on reverse osmosis (RO) transport mechanisms and models have been developed to describe solute and solvent fluxes through RO membranes. The general purpose of a membrane mass transfer model is to relate the fluxes to the operating conditions. The power of a transfer model is its ability to predict the performance of the membrane over a wide range of operating conditions. To realize this objective, the model has to be integrated with some transport coefficients often determined based on some experimental results.

When theories are proposed to describe membrane transport, either the membrane can be treated as a black box in which a purely thermodynamic description is used, or a physical model of the membrane can be introduced. The general description obtained in the first case gives no information on the flow and separation mechanisms. On the other hand, the correctness of data on the flow and

separation mechanisms obtained in the second case depends on the chosen model.

The transport models can be divided into three categories:

1. phenomenological transport models which are independent of the mechanism of transport and are based on the theory of irreversible thermodynamics (irreversible thermodynamics – phenomenological transport and irreversible thermodynamics – Kedem–Spiegler models);
2. nonporous transport models, in which the membrane is supposed to be nonporous or homogeneous (solution–diffusion, extended solution–diffusion, and solution–diffusion-imperfection models (SDIMs)); and
3. porous transport models, in which the membrane is supposed to be porous (preferential sorption-capillary flow, Kimura–Sourirajan analysis, finely porous and surface force-pore flow, and friction models).

Most models for RO membranes assume diffusion or pore flow through the membrane while charged-membrane theories include electrostatic effects. For example, Donnan exclusion models can be used to determine solute fluxes in the often negatively charged nanofiltration membranes.

Moreover, RO membranes have, in general, an asymmetric or a thin-film composite structure where a porous and thin top layer acts as selective layer and determines the resistance to transport. Macroscopically, these membranes are homogeneous. However, on the microscopic level, they are systems with two phases in which the transport of water and solutes takes place. **Figure 1** provides a schematic presentation of a thin-film composite membrane structure with (1) the highly selective skin layer which acts as a barrier, (2) the intermediate porous layer where the selectivity decreases to zero, and (3) the nonselective porous sublayer.

The porous sublayer influences the total hydraulic permeability (L_p) from Reference 1:

$$\frac{1}{L_p} = \frac{1}{(L_p)_{sl}} + \frac{1}{(L_p)_{il}} + \frac{1}{(L_p)_{pl}} \quad (1)$$

But it has almost no influence on the solute rejection properties of the membranes. Therefore, most transport and rejection models of RO membranes have been derived for single-layer membranes focusing almost only on the surface thin layer.

Transport models can help in identifying the most important membrane structural parameters and showing how membrane performance can be improved by varying some specific parameters. One of the main membrane intrinsic parameters is the reflection coefficient, σ , introduced by Staverman [2] and defined as

$$\sigma \equiv \frac{-l_{\pi p}}{l_p} = \left(\frac{\Delta P}{\Delta \pi} \right)_{\mathcal{F}_v = 0} \quad (2)$$

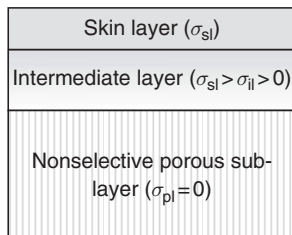


Figure 1 Schematic presentation of thin-film composite membrane structure.

where σ describes the effect of the pressure driving force on the flux of solute and represents the relative permeability of the membrane to the solute:

1. $\sigma = 1$ for a high-separation membrane and
2. $\sigma = 0$ for a low-separation membrane in which the solute is significantly carried through the membrane by solvent flux.

In RO, the intrinsic retention R_{\max} is related to σ and normally $\sigma \leq R_{\max}$ (as reported in Reference 3). Pusch [4] derived the following relationship between R_{\max}

$$\text{and } \sigma: R_{\max} = 1 - (1 - \sigma) \cdot \frac{\bar{c}_{s\max}}{c'_s}$$

where $\bar{c}_{s\max}$ is the mean salt concentration at infinite \mathcal{F}_v .

2.01.2 Phenomenological Transport Models

2.01.2.1 Irreversible Thermodynamics-Phenomenological Transport Model

The membrane is treated as a black box when nothing on the transport mechanism and membrane structure is known. In this case, the thermodynamics of irreversible thermodynamics (IT) processes can be applied to membrane systems. According to the IT theory, the flow of each component in a solution is related to the flows of other components. Then, different relationships between the flux through the membrane and the forces acting on the system can be formulated.

Onsager [5] suggests that fluxes \mathcal{F}_i are related to the forces F_j through the phenomenological coefficient L_{ij} :

$$\mathcal{F}_i = L_{ii}F_i + \sum_{i \neq j} L_{ij}F_j \quad \text{for } i = 1, \dots, n \quad (3)$$

For systems close to equilibrium, the cross-coefficients are equal:

$$L_{ij} = L_{ji} \quad \text{for } i \neq j \quad (4)$$

Kedem and Katchalsky [6] used the linear phenomenological relationships (Equations (3) and (4)) to derive the phenomenological transport:

$$\mathcal{F}_v = l_p(\Delta P - \sigma \Delta \pi) \quad (5)$$

$$\mathcal{F}_s = \omega \Delta \pi + (1 - \sigma) \mathcal{F}_v (\bar{c}_s)_{in} \quad (6)$$

where parameters l_p , ω , and σ are simple functions of the original phenomenological coefficient L_{ij} .

Usually RO systems are far from equilibrium; therefore, Equation (4) may not be correct. Moreover,

phenomenological transport equations (5) and (6) have been rarely applied for describing RO membrane transport both because the often large concentration difference across the membranes invalidates the linear laws and because this analysis does not give much information regarding the transport mechanism.

2.01.2.2 IT-Kedem–Spiegler Model

Spiegler and Kedem [13] bypassed the problem of linearity by rewriting the original IT equations for solvent and solute flux in differential form:

$$\mathcal{J}_v = p_v \left(\frac{dP}{dx} - \sigma \frac{d\pi}{dx} \right) \quad (7)$$

$$\mathcal{J}_s = p \frac{d\bar{c}_s}{dx} + (1-\sigma)\bar{c}_s \mathcal{J}_v \quad (8)$$

where p_v is the water permeability, x the coordinate direction perpendicular to the membrane, and p_s the solute permeability. Integrating Equations (7) and (8) over the thickness of the membrane by assuming p_v , p_s , and σ constant, the following equations for the solvent flux \mathcal{J}_v and retention R are achieved:

$$\mathcal{J}_v = \frac{p_v}{\Delta x} (\Delta P - \sigma \Delta \pi) \quad (9)$$

$$R = \frac{\sigma \{1 - \exp[-\mathcal{J}_v(1-\sigma)\Delta x/p_s]\}}{1 - \sigma \exp[-\mathcal{J}_v(1-\sigma)\Delta x/p_s]} \quad (10)$$

where Δx is the membrane thickness. Equation (10) can be rearranged as follows:

$$\frac{c'_s}{c''_s} = \frac{1}{1-\sigma} - \frac{\sigma}{1-\sigma} \exp \left[-\mathcal{J}_v(1-\sigma) \frac{\Delta x}{p_s} \right] \quad (11)$$

However, similar to phenomenological transport equations, Spiegler and Kedem relationships also do not give information on the membrane transport mechanism.

2.01.3 Nonporous Transport Models

2.01.3.1 Solution–Diffusion Model

The solution–diffusion model assumes that (1) membrane surface layer is homogenous and nonporous and (2) both solute and solvent dissolve in the surface layer and then they diffuse across it independently. Water and solute fluxes are proportional to their chemical potential gradient. The latter is expressed as the pressure and concentration difference across the membrane for the solvent, whereas it is assumed

to be equal to the solute concentration difference across the membrane for the solute:

$$\mathcal{J}_v = A(\Delta P - \Delta \pi) \quad (12)$$

$$A = \frac{\bar{D}_v \bar{c}_v V_v}{\mathcal{R} T \Delta x} \quad (13)$$

$$\mathcal{J}_s = B(c_s''' - c_s'') \quad (14)$$

$$B = \frac{\bar{D}_s k}{\Delta x} \quad (15)$$

where A is the hydraulic permeability constant l_p , B is the salt permeability constant, c_s''' and c_s'' are, respectively, the salt concentrations on the feed and permeate sides of the membrane. \bar{D}_v and \bar{D}_s are the diffusivities of the solvent and the solute in the membrane, respectively; \bar{c}_v is the concentration of water in the membrane; V_v is the partial molar volume of water; \mathcal{R} is the universal gas constant; T is the temperature; k is the partition or distribution coefficient of solute defined as follows:

$$K = \frac{\text{kg solute m}^{-3} \text{ membrane}}{\text{kg solute m}^{-3} \text{ solution}} \quad (16)$$

k measures the solute affinity to ($k > 1$) or repulsion from ($k < 1$) the membrane material.

Following Equations (12)–(15), differences in solubilities and diffusivities of the solute and solvent in the membrane phase are important in this model since these differences strongly influence the fluxes through the membrane. Moreover, these equations prove that the solute flux through the membrane is independent of water flux.

Because the concentration of salt in the permeate solution c'_s is usually much smaller than c_s''' , Equation (14) can be simplified as follows:

$$\mathcal{J}_s = B c_s''' \quad (17)$$

Equations (12) and (17) show that the water flux is proportional to the applied pressure, whereas the solute flux is independent of pressure. This means that the membrane selectivity increases with increasing pressure. The membrane selectivity can be measured as solute rejection R given by

$$R = \left[1 - \frac{c''_s}{c_s''} \right] \times 100\% \quad (18)$$

By combining Equations (12)–(18) with the relationship (19) between c''_s , \mathcal{J}_v , and \mathcal{J}_s , the membrane rejection can be expressed as follows:

$$c''_s = \frac{\mathcal{J}_s}{\mathcal{J}_v} \rho_v \quad (19)$$

$$R = \left[1 - \frac{\rho_v B}{A(\Delta P - \Delta \pi)} \right] \times 100\% \quad (20)$$

where ρ_v is the density of water.

The main advantage of the solution–diffusion model is its simplicity. One of its restriction is that it foresees rejection equal to 1 at infinite flux ($\Delta P \rightarrow \infty$), a limit not reachable for many solutes. Therefore, this model is appropriate for solvent–solute–membrane systems where the separation is close to 1. Moreover, it can be noted that Equation (5) is reduced to the solution–diffusion model when $\sigma = 1$.

2.01.3.2 Extended Solution–Diffusion Model

In the solution–diffusion model, the effect of pressure on solute transport is neglected [8, 19]. In order to include the pressure term, the salt chemical potential gradient has to be written as

$$\Delta \mu_s = RT \ln \left(\frac{c_s'''}{c_s''} \right) + V_s \Delta P \quad (21)$$

where $\Delta \mu_s$ is the solute chemical potential difference across the membrane and V_s is the solute partial molar volume.

For sodium chloride–water separation, Burghoff *et al.* [8] suggest ignoring the pressure term $\left(\frac{V_s \Delta P}{RT} \right)$

when $\ln \left(\frac{c_s'''}{c_s''} \right) \gg 8.0 \times 10^{-6} \Delta P$.

Including pressure, particularly for organic-water systems, the solute flux is given by

$$\mathcal{J}_s = \frac{\bar{D}_s k}{\Delta x} (c_s''' - c_s'') + l_{sp} \Delta P \quad (22)$$

where l_{sp} is the pressure-induced transport parameter.

Equation (22) has been proved to be accurate for different organic solutes with cellulose acetate membranes [8].

2.01.3.3 Solution–Diffusion-Imperfection Model

The solution–diffusion model is one of the most referred membrane models. It presupposes that the membrane surface is homogenous/nonporous and it has the limitation that the intrinsic value of retention is always unity.

The SDIM developed by Sherwood *et al.* [9] considers that small imperfections exist on the membrane surface due to the membrane-making process,

and solvent and solute can flow through them without any change in concentration. Therefore, SDIM includes pore flow as well as diffusion of solute and solvent through the membrane and it can be considered a compromise between solution–diffusion and porous models. Moreover, Jonsson and Boesen [10] proved that SDIM can be used to determine a parameter identified with the reflection coefficient. According to the model, water and solute fluxes can be written as

$$\begin{aligned} \mathcal{J}_v &= \underbrace{k_1(\Delta P - \Delta \pi)}_{\text{diffusion}} + \underbrace{K_3 \Delta P}_{\text{pore flow contribution to water flux}} \\ &= (k_1 + k_3) \left(\Delta P - \frac{k_3}{k_1 + k_3} \Delta \pi \right) \end{aligned} \quad (23)$$

$$\mathcal{J}_s = k_2 \Delta \pi + \underbrace{K_3 \Delta P c_s'}_{\text{pore flow of solute through the membrane}} \quad (24)$$

where $K_3 \Delta P$ is the term proportional to the pressure-driving force; k_1 and k_2 are the transport parameters for diffusive water and solute flux, respectively; and k_3 is the transport parameter for the pore flow.

Equations (23) and (24) can be rearranged to give the reduction factor [3]:

$$\frac{c_s'}{c_s''} = \frac{c_s' \mathcal{J}_v}{\mathcal{J}_s} = \frac{(\Delta P - \Delta \pi) + \frac{k_3}{k_1} \Delta P}{\frac{k_2}{k_1} \frac{\Delta \pi}{c_s''} + \frac{k_3}{k_1} \Delta P} \quad (25)$$

and comparing Equation (23) with Equation (5), σ can be obtained:

$$\sigma = \frac{1}{1 + \frac{k_3}{k_1}} \quad (26)$$

where the ratio k_3/k_1 is a measure of the relative contribution of pore flow compared to diffusive flow.

This model has been successfully applied for the performance description of several solutes and membranes [10], particularly it is proper for those membranes exhibiting lower separation than that calculated from solubility and diffusivity measurements.

2.01.4 Porous Transport Models

Among the transport models in which the membrane is supposed to be porous, friction and finely porous models are described in this section.

2.01.4.1 Friction Model

Friction model considers that the transport through porous membrane occurs both by viscous and diffusion flow. Therefore, the pore sizes are considered so

small that the solutes cannot pass freely through the pores but friction between solute-pore wall and solvent-pore wall and solvent-solute occurs. The frictional force F is linearly proportional to the velocity difference through a proportional factor X called friction coefficient indicating the interaction between solute and pore wall:

$$F_{23} = -X_{23}(u_2 - u_3) = -X_{23}u_2 \quad (27)$$

$$F_{13} = -X_{13}(u_1 - u_3) = -X_{13}u_1 \quad (28)$$

$$F_{21} = -X_{21}(u_2 - u_1) \quad (29)$$

$$F_{12} = -X_{12}(u_1 - u_2) \quad (30)$$

Equations (27)–(30) are derived considering the membrane as reference ($u_3 = 0$). Considering that the frictional force per mole of solute F_{23} is given by

$$F_{23} = -X_{23}u_2 = -X_{23} \frac{\mathcal{F}_{2p}}{c_{2p}} \quad (31)$$

Equation (27) can be written as

$$F_{23} = -X_{23} \frac{\mathcal{F}_{2p}}{c_{2p}} \quad (32)$$

Jonsson and Boesen [10] have presented a detailed description of this model and they have shown that, as F_{21} is the effective force for diffusion of solute in the center of mass system, the solute flux per unit pore area \mathcal{F}_{2p} is given by

$$\mathcal{F}_{2p} = \frac{1}{X_{21}} c_{2p} (-F_{21}) + c_{2p} \cdot u \quad (33)$$

A balance of applied and frictional forces is equal to

$$F_2 = -(F_{21} + F_{23}) \quad (34)$$

Neglecting the pressure term and in the case of dilute solution behavior, F_2 is equal to

$$F_2 = -\frac{RT}{c_{2p}} \frac{dc_{2p}}{dx} \quad (35)$$

Defining b as the term that relates the frictional coefficients X_{23} (between solute and membrane) and X_{21} (between solute and water)

$$b = \frac{X_{21} + X_{23}}{X_{21}} \quad (36)$$

and inserting in Equations (29), (32), and (34)–(36), \mathcal{F}_{2p} can be written as

$$\mathcal{F}_{2p} = -\frac{RT}{X_{21} \cdot b} \frac{dc_{2p}}{dx} + \frac{c_{2p} \cdot u}{b} \quad (37)$$

The coefficient for distribution K of solute between bulk solution and pore fluid is given by

$$K = c_{2p}/c_2 \quad (38)$$

with $\mathcal{F}_v = \varepsilon \cdot u$, $\mathcal{F}_i = \mathcal{F}_2 \cdot \varepsilon$, and $\xi = \tau \cdot x$, using the product condition

$$c_2' = \frac{\mathcal{F}_{2p}}{u} \quad (39)$$

and integrating Equation (37) with the boundary conditions $x = 0 : c_{2p} = Kc_2'$; $x = \tau \cdot \lambda : c_{2p} = Kc_2''$ the following equation for the ratio c_2'/c_2'' is obtained:

$$\frac{c_2'}{c_2''} = \frac{1 + \frac{b}{k} [\exp(u\varepsilon \frac{\tau \cdot \lambda}{\varepsilon} \frac{X_{21}}{RT}) - 1]}{\exp(u\varepsilon \frac{\tau \cdot \lambda}{\varepsilon} \frac{X_{21}}{RT})} \quad (40)$$

In this derivation K , b , and X_{21} are assumed to be independent from the solute concentration.

2.01.4.2 Finely Porous Model

The finely porous model was developed by Merten [11] using a balance of applied and frictional forces proposed by Spiegler [12]. It is a combination between viscous flow and frictional model presented in detail by Jonsson and Boesen [10]. The premise of the model is to describe, reasonably, the transport of water and solutes in the intermediate region between solution-diffusion model and Poiseuille flow:

1. the first is reasonable when applied to very dense membranes and solutes which are almost totally rejected, whereas
2. Poiseuille flow can be used to describe the transport through porous membranes consisting of parallel pores.

Jonsson and Boesen [10] showed that the following equation can be used to determine R_{\max} from RO experiments:

$$\frac{c_2'}{c_2''} = \frac{b}{K} + \left(1 - \frac{b}{K}\right) \exp\left(-\frac{\tau \cdot \lambda}{\varepsilon} \cdot \frac{\mathcal{F}_v}{D_2}\right) \quad (41)$$

where D_2 is the solute diffusion coefficient.

From Equation (41), the maximum rejection R_{\max} (at $\mathcal{F}_v \rightarrow \infty$) is given by

$$R_{\max} = \sigma = 1 - \frac{K}{b} = 1 - K \frac{1}{1 + \frac{X_{23}}{X_{21}}} \quad (42)$$

Equation (42) shows how rejection is related to a kinetic term (the friction factor b) and to a thermodynamic equilibrium term (K). Spiegler and Kedem [13] derived the following corresponding expression:

$$\sigma = 1 - K \frac{1}{1 + \frac{X_{23}}{X_{21}}} \left(1 + \frac{X_{23} \bar{u}_2}{X_{21} \bar{u}_1}\right) \quad (43)$$

Equations (42) and (43) are identical apart the correction term $X_{13} \bar{u}_2 / X_{21} \bar{u}_1$ which is much smaller than 1 for

highly selective membranes because the solubility of the solute in the membrane must be as low as possible. This can be achieved by a proper choice of the polymer.

2.01.5 Comparison and Summary of Membrane Transport Models

In this section, an overview of several transport models commonly used to describe solute and solvent transport mechanisms through the membranes is presented. As discussed, each of the models is based on substantially different assumptions. However, some of them have nearly similar mathematical forms. Certainly, a model is suitable for describing experimental data if agreement between the adopted model and experimental results exists. However, the simple agreement does not guarantee that the model is correct. The real power of a model is when it is suitable also for predicting the behavior of real membranes under various experimental conditions. Moreover, in each model, some coefficients emerge that must be determined based on experimental data. Therefore, the success of a model is also measured in terms of its ability and simplicity to describe mathematically the data with coefficients reasonably constant over the range of operative conditions.

Without doubt there is not a certain model if the membrane structure is not known. In this situation, information on the diffusion and solubility is obtained through the application of the solution–diffusion model, whereas a porous model will give information about the porous nature of the membrane.

2.01.6 Influence from Operating Conditions on Transport

In the previous sections, an overview of several transport models commonly used to describe membrane transport was presented. As earlier stated, the power of a transport model is to describe and to predict the behavior of membranes under various experimental conditions. The real performance of a membrane is, in fact, a strong function of operating conditions and this has to be seriously taken into account when a membrane system is designed. Predicting the effect of operating conditions on the membrane performance requires the use of one of the described transport models. For example, applying the solution–diffusion model to limited data, the transport parameters A and B can be determined.

These parameters can then be used to predict the effect of operating conditions on membrane performance.

In this section, the influence of various operating conditions on the membrane performance and, therefore, the application of transport model for predicting membrane performance is presented. In particular, the effects of pressure, concentration, feed–flow rate, temperature, and pH are described in succession.

2.01.6.1 Effect of Pressure

The effect of feed pressure on water flux and salt rejection is clearly shown in Figure 2(a).

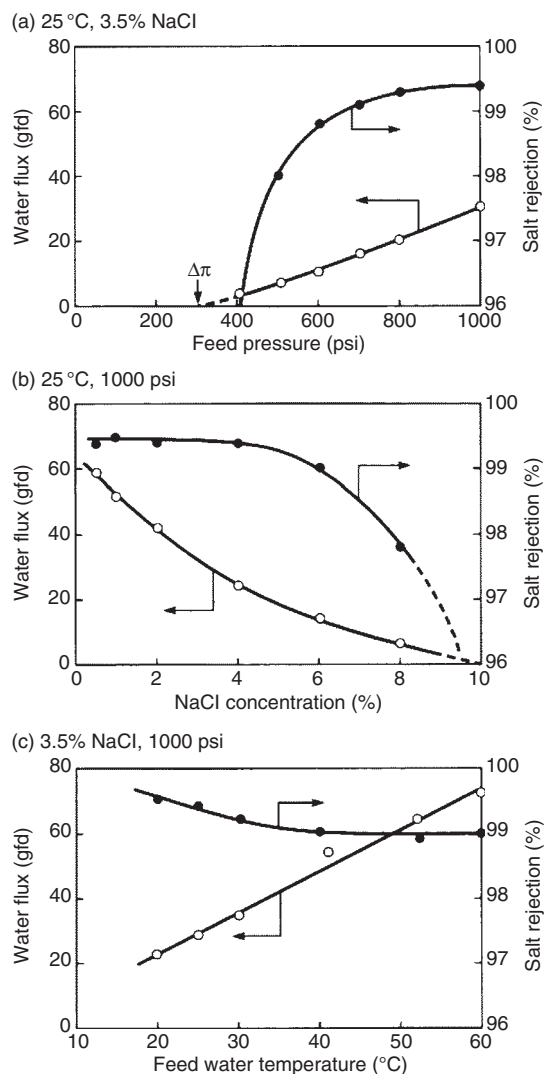


Figure 2 Effect of pressure (a), feed salt concentration (b), and temperature (c) on the properties of good-quality seawater desalination membranes (SW-30) [14, 17].

The primary effect of increasing the operating pressure is to enhance the driving force which, in turn, increases water flux (as predicted by Equation (5) or (12)) and salt rejection (through Equation (20)). In fact, at a pressure equal to the feed osmotic pressure, the water flux approaches zero and is similar for the salt rejection. As the pressure increases, water flux grows linearly whereas salt rejection rises fast and approaches the limiting rejection higher than 99%.

2.01.6.2 Effect of Concentration

Feed concentration has marked effects on membrane performance due to the increase in osmotic pressure with increasing concentration (Figure 2(b)). At a constant feed pressure, as concentration increases, water flux and salt rejection fall and approach zero when the osmotic pressure equals the applied hydrostatic pressure. Dickson [15] highlights the interesting trend of separation with increasing concentration (Figure 3): it first increases (due to the flux drop off which reduces the concentration polarization phenomena) and then decreases (because the further rise in concentration lowers the driving force and the separation).

2.01.6.3 Effect of Feed Flow

The changing of feed-flow rate influences the pressure drop and the mixing in the system and, therefore, the mass transfer coefficient k . The dependence of k on feed-flow rate, cell geometry, and solute system is described by the following equation:

$$Sh = a \cdot Re^b \cdot Sc^{1/3} \quad (44)$$

where a and b are parameters that can be determined experimentally. Equation (44) is a generalized correlation of mass transfer which illustrates the relationship among Sherwood (Sh), Reynolds (Re), and Schmidt (Sc) number.

The effect of changing feed-flow rate on the RO performance for different cellulose acetate membranes is shown in Figure 4.

2.01.6.4 Effect of Temperature

The increasing of temperature causes a growth in water flux and a reduction in salt rejection (Figure 2(c)). This happens because transport of both salt and water, as represented by Equations

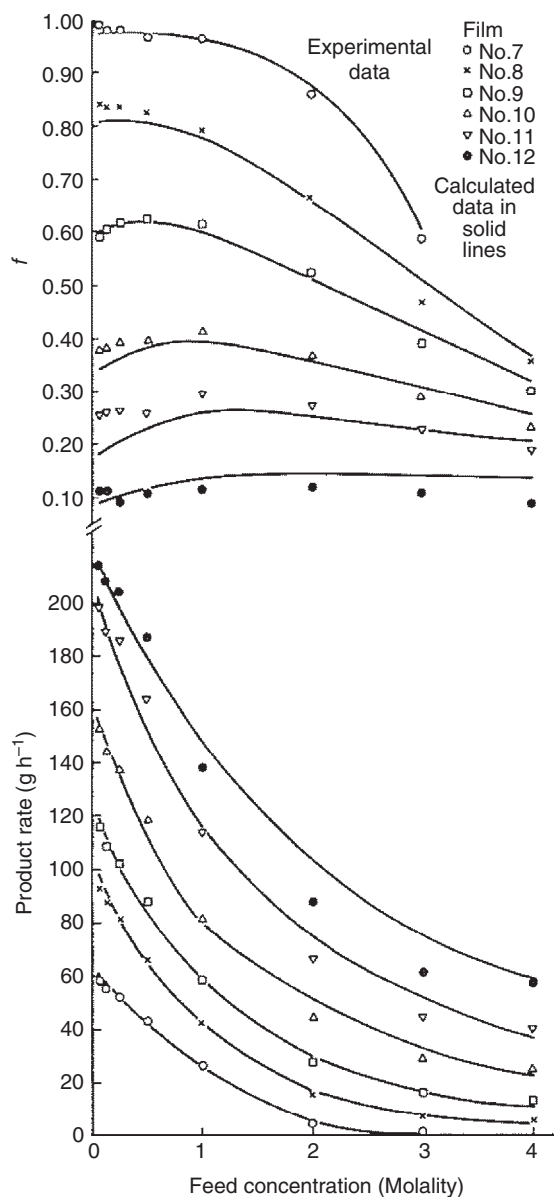


Figure 3 Comparison of the experimental and calculated reverse osmosis performance for NaCl-water system for a variety of cellulose acetate membranes with different porosities [15].

(12) and (17), increases exponentially with increasing temperature as described by the following Arrhenius dependence for the pure water permeability coefficient A :

$$A = A_0 \exp\left(\frac{-E_0}{RT}\right) \quad (45)$$

where E_0 is the apparent activation energy associated with the solvent transport process. For most membranes,

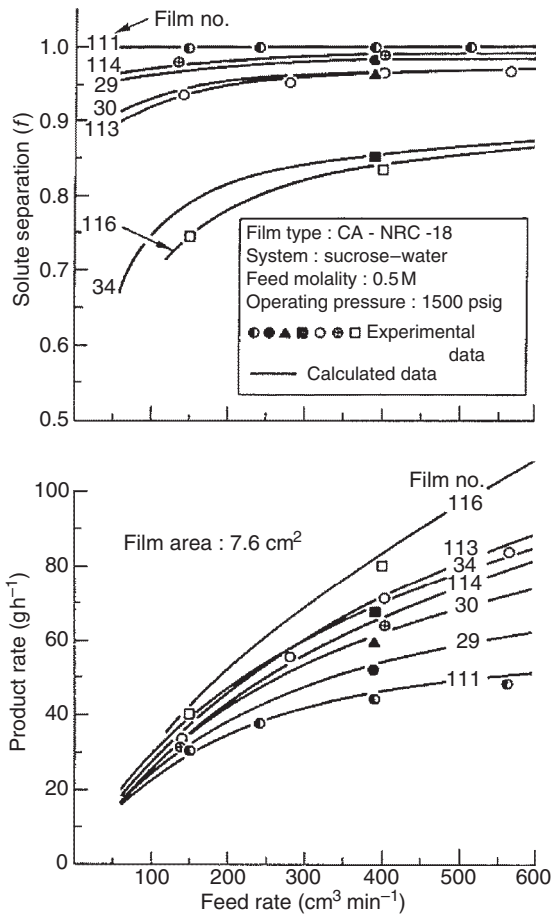


Figure 4 Effect of feed-flow rate on RO performance for different membranes [15].

the activation energy is around $-0.0017 \text{ kJ kmol}^{-1}$ [15]. As shown in Figure 2(c), the water flux more than doubles when temperature is increased by 30°C , whereas the salt rejection coefficient (depending on the ratio B/A in Equation (20)) decreases as the temperature increases.

2.01.6.5 Effect of pH

Unlike concentration, pressure, feed flow, and temperature, the effect of pH cannot be predicted by any of the described transport models. pH effect becomes significant and needs to be taken into account either when it is so high or low to irreversibly damage the membrane, or in the presence of solutes which ionize with pH changing. In order to avoid membrane replacement due to mistaken operating conditions, manufacturers usually supply limits on the pH for their membranes. In the case of ionizable solutes, the separation can be strongly effected by pH change, for example, in the case of phenol and boron.

Figure 5 shows how the phenol separation changes with the pH of feed solution: at low pH, the separation is about zero because the phenol is completely undissociated; with increasing pH, separation increases due to the phenol dissociation; at pH higher than 12, the separation becomes independent of pH because phenol is now completely dissociated.

A situation similar to that described in the case of phenol can be also found in the case of boron. At the natural pH of most of seawater used in desalination

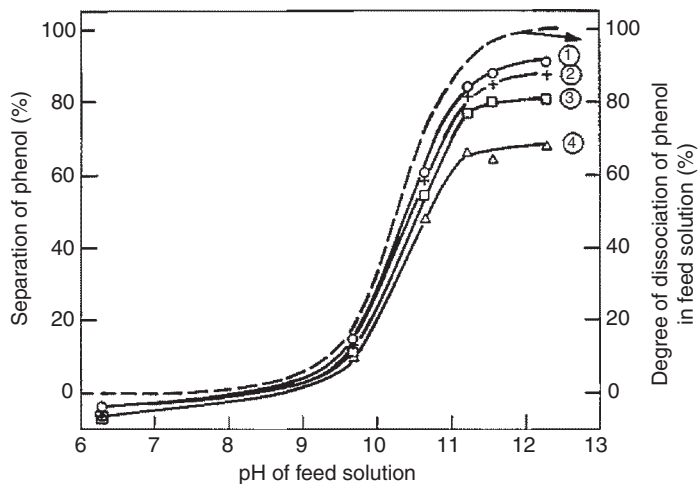


Figure 5 Effect of feed solution pH and phenol degree of dissociation on the separation of phenol for several cellulose acetate membranes (rearranged from [15]).

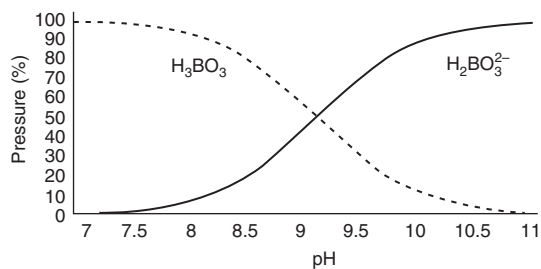


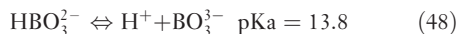
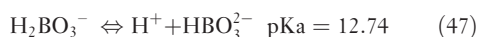
Figure 6 Distribution of $H_3BO_3/H_2BO_3^{2-}$ in function of pH [16].

(pH \approx 7–8), boron is mainly present as boric acid in molecular form. As can be seen from **Figure 6**, at these pH values, the percentage of the nondissociated species H_3BO_3 is between 99.3% (pH 7) and 93.2% (pH 8) of the total boron.

At pH \approx 7–8, the rejection of H_3BO_3 is in the range of 82–92% for most seawater RO membrane products in the market, and between 30% and 80% for brackish water RO products (**Figure 7**).

The boron rejection performance is increased in the alkaline region due to the two following effects:

1. *Effect of atomic or molecular size.* At high pH values (alkaline conditions), boric acid dissociation proceeds according to Equations (46)–(48), ionization takes place, and a hydration radius is achieved which is greater than that of the boron molecule. The rejection performance of the RO membrane therefore improves.



2. *Effect of electrical charge of the molecule.* In the alkaline region, ionization of boron causes a negative charge, and since the RO membrane also has a negative charge, the two repel each other and the rejection performance of the RO membrane is enhanced.

As normal seawater is in the range of neutral pH, boron does not dissociate and the boron molecular form exists without electrical charge. Therefore, the two effects described above do not occur and the boron rejection by the RO membrane is low. A treatment in which normal seawater would be directly rendered alkaline to achieve the boron to dissociation but cannot be adopted because the many hardness components contained in the seawater would give scaling problems at high pH levels. Given the above conditions, nowadays, most parts of seawater desalination plants use RO systems with several pass-stages. At the first pass-stage, the salt in the seawater is removed along with most of the boron. By treating the resulting product water with other boron removal RO membrane elements at ultralow pressure working at high pH and, eventually, with boron-selective resins, the boron concentration is brought to below the regulation value.

2.01.7 Experimental Verification of Solute Transport

As earlier stated, the power of a transport model is to predict the behavior of a specific membrane toward solutes never tested. This capability is of extreme

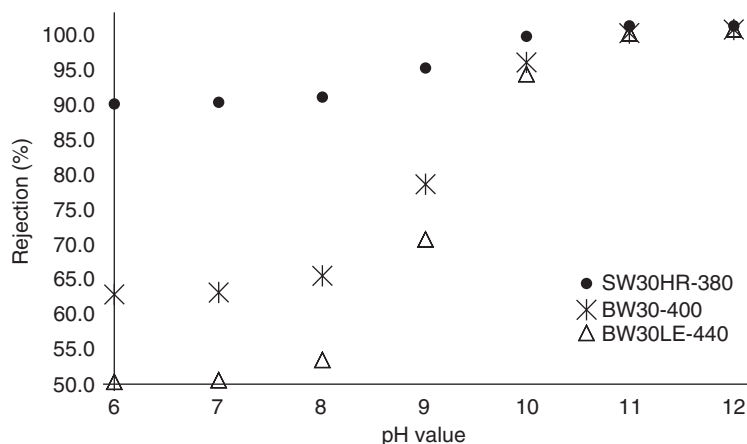


Figure 7 Rejection of total boron with FILMTEC membrane elements (SW for seawater elements, BW for brackish water elements) [16].

importance esteemed the large number of existing solutes that can be removed through the commercially available membranes. Taking into account that RO is not a filtration process but rather a solution–diffusion process, the retention by RO membranes also depends on the used membrane material. Therefore, the prediction can be realized only if the relationship between the transport model parameters and the physicochemical nature of the solute for a specific solvent–membrane system is known. In fact, whereas low molecular weight organic solutes often have a poor rejection on many types of RO membranes, the rejection of electrolytes, such as sodium chloride and magnesium sulfate, is high. An example of the different rejection performance of high-pressure RO membranes, medium-pressure brackish water desalting membranes, and low-pressure nanofiltration membranes for various solutes is provided in **Table 1**.

Examples on the influence of membrane intrinsic characteristics on permeate flux and solute rejection are shown in **Figures 8 and 9**.

The effect of various degrees of acetylation on solute rejection is shown in **Figure 8**. It is shown that, for example, as sodium chloride rejection decreases from 99.5% to 99% the degree of acetylation of cellulose acetate membranes diminishes from 39.8% to 37.6%.

Figure 9 shows the effect of annealing temperatures on flux and rejections of cellulose acetate membranes. As it can be seen, the salt rejection of the membrane can be raised if it is heated for few minutes in a bath of hot water (i.e., the annealing procedure). Through this conventional procedure, the micropores are eliminated and a denser and higher salt-rejecting skin is created. Therefore, whereas NaCl rejection is improved, permeate flux decreases.

Table 1 Rejection of current good-quality commercial membranes [17]

Parameter	Seawater membrane (SW-30)	Brackish water membrane (CA)	Nanofiltration membrane (NTR-7250)
Pressure (psi)	800–1000	300–500	100–150
Solution concentration (%)	1–5	0.2–0.5	0.05
Rejection (%)			
NaCl	99.5	97	60
MgCl ₂	99.9	99	89
MgSO ₄	99.9	99.9	99
Na ₂ SO ₄	99.8	99.1	99
NaNO ₃	90	90	45
Ethylene glycol	70	NA	NA
Glycerol	96	NA	NA
Ethanol	NA	20	20
Sucrose	100	99.9	99.0

NA, not available.

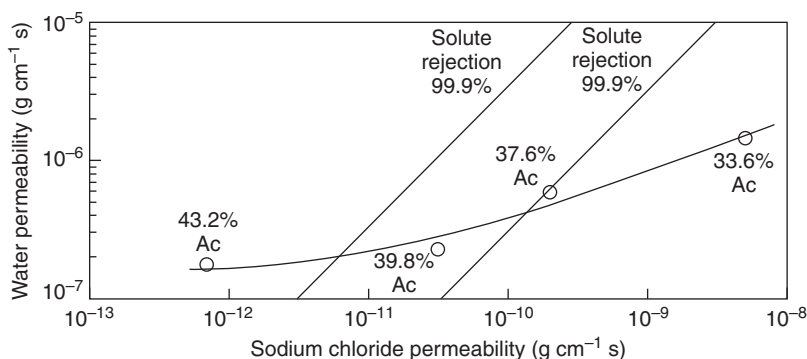


Figure 8 Water vs. sodium chloride permeability for cellulose acetate membranes with various degrees of acetylation. The reported rejection coefficients were calculated using the Equation (20) for dilute salt solutions [17].

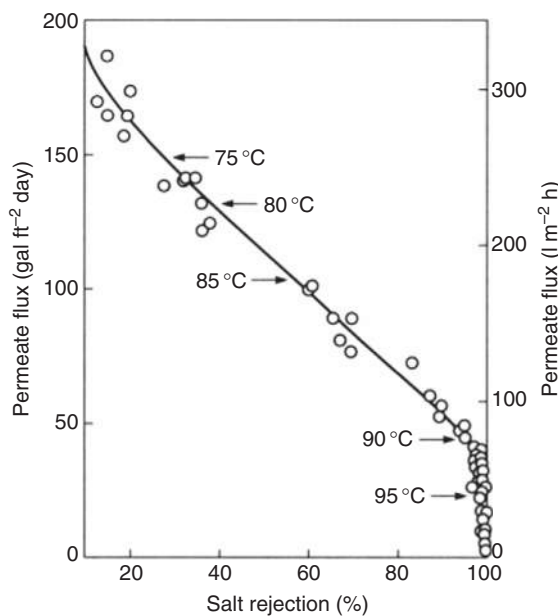


Figure 9 Permeate flux vs. salt rejection for different annealing temperatures [17,18].

The reported examples describe the strong dependence of flux and separation from the physical and chemical nature of the solute–solvent–membrane system.

In this section, the experimental verification of solute transport in various solutions (single salt, mixed salt, organic solute, and mixed organic solutes) is described. The behavior in the presence of membrane charge is also briefly discussed. Further, the topic of transport in nonaqueous solutions is also presented. Finally, the effect of fouling and concentration polarization in membranes is also discussed.

2.01.7.1 Single-Salt Solutions

The separation of single electrolytes is determined by electrostatic forces which force ions to avoid regions of low dielectric constant. In fact, the retention of electrolytes changes with concentration (Figure 10) and in the presence of other solutes.

Figure 10 shows that the NaCl retention level decreases when its concentration increases in the range 0.0002–0.01 eq. l⁻¹ due to Donnan exclusion: RO cellulose acetate membrane contains small amount of carboxylic groups which gives it the properties of a weak cation-exchange membrane. Figure 11 is the confirmation of this theory: the dissociation of carboxylic acid groups and the consequent Donnan exclusion raise with increasing pH.

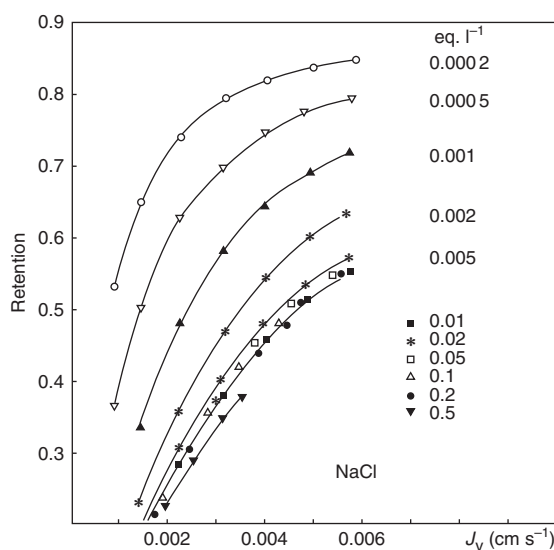


Figure 10 Retention vs. permeate flux for different NaCl concentration on a DDS 930 cellulose acetate RO membrane [7].

At low pH, the dissociation of carboxylic acid groups does not occur and the Donnan exclusion disappears.

Whereas for NaCl the selectivity is almost constant in the concentration range of 0.01–0.2 eq. l⁻¹ (Figure 10), the MgSO₄ selectivity is approximately constant in the concentration range 0.005–0.02 eq. l⁻¹ and increases with increasing concentration from 0.02 to 0.5 eq. l⁻¹ (Figure 12).

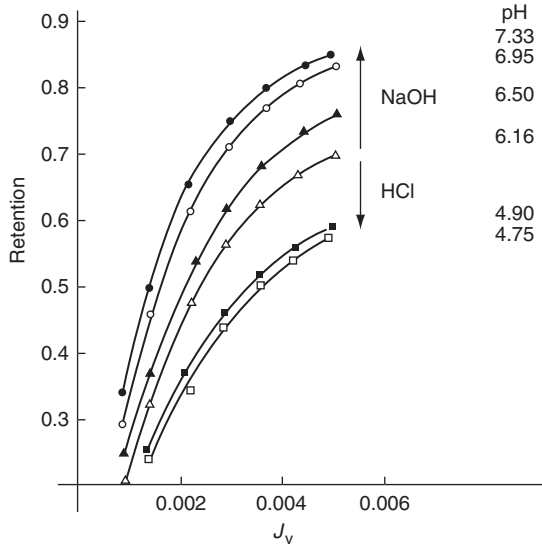


Figure 11 Retention vs. permeate flux for 0.001 eq. l⁻¹ NaCl at different pH values on a DDS 930 membrane [7].

If the retention is calculated from activity values using Equation (49)

$$R_a = 1 - \frac{a''_j}{a'_i} = 1 - \frac{c''_i \gamma''_i}{c'_i \gamma'_i} \quad (49)$$

it is more constant than the retention based on concentration (Figure 13, which shows that selectivity is now constant in the concentration range 0.05–0.35 eq. l⁻¹, whereas it increases with decreasing concentration from 0.05 to 0.005 eq. l⁻¹).

The different behavior reported in Figures 12 and 13 is due to the fact that the activity coefficient for 2:2 electrolytes drops drastically with increasing concentration. Moreover, the activity coefficient between bulk and permeate is completely different due to the high retention. Therefore, the equilibrium at the membrane–solution interface is better expressed by activities rather than concentration. For this reason, retention in activity is more constant than retention based on concentration. Further, for MgSO₄, similar to NaCl, the selectivity increases at low concentrations due to the Donnan exclusion. However, the Donnan effect is more evident at much higher concentrations for MgSO₄ than for NaCl because, at neutral pH, divalent ions dissociate the carboxylic acid groups to a much higher extent than monovalent ions.

2.01.7.2 Mixed-Salt Solutions

The prediction of performance for mixed-solute systems can be considerably more complex than the

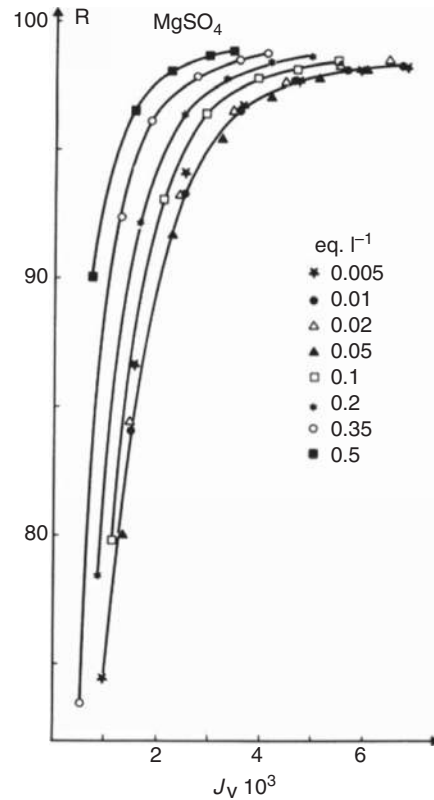


Figure 12 Retention vs. permeate flux for different MgSO₄ concentration on a DDS 930 cellulose acetate RO membrane [7].

prediction for single-solute systems. In general, there may be a strong interaction between the various solutes which results in a complex relationship between operating conditions and performance. In particular, due to primary charge effects and differences in the mobilities of cations and anions, electrolytic interactions can be rather strong. Many results on single-salt solutions have been published [19], whereas very little can be found in the literature on mixed-salts solutions. The general trend found is that in a mixture of more and less permeable ions, the retention of the more permeable ions decreases and that of the less permeable ions increases [20, 21].

Heyde and Anderson [22] studied the influence of added electrolyses upon ion sorption by membranes. They found that membrane sorption of permeable ions is substantially increased by the addition of membrane impermeable salts to the bulk solution and vice versa. This change in sorption was explained in terms of constrained phase equilibria using the ideas developed by Donnan [23].

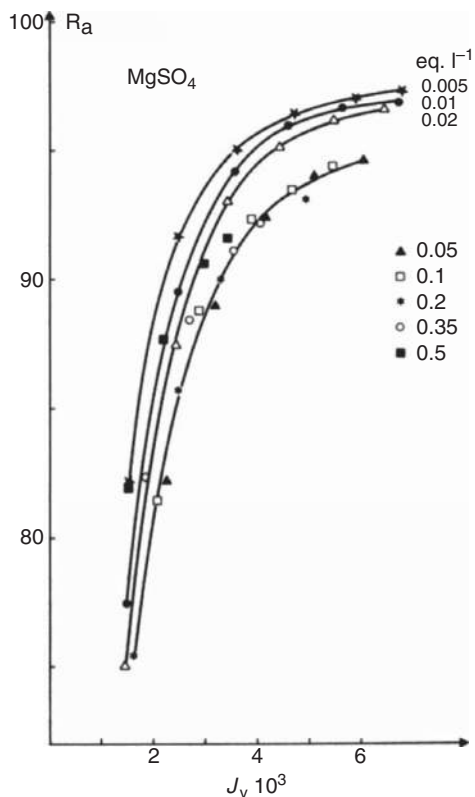


Figure 13 Retention in activity R_a vs. permeate flux for different MgSO_4 concentration on a DDS 930 cellulose acetate RO membrane [7].

Lonsdale *et al.* [24] were able to pass from positive to negative rejection of Cl^- upon addition of membrane-impermeable sodium citrate. The experimental results were explained by a solution–diffusion model coupled to the Donnan equilibrium theory.

Jonsson [25] demonstrated both experimentally and theoretically how the rejection of the separate ions in the binary system $\text{HCl}-\text{CaCl}_2$ was influenced by the induced boundary, diffusion, and streaming potentials under RO conditions. The experimental results were explained from a theory developed by using a combined frictional and exclusion model together with the extended Nernst–Planck equations. Jonsson found a strong coupling between the retentions of HCl and CaCl_2 on medium-tight cellulose acetate (CA) membranes. In fact, the determined retention curves (Figure 14) indicate a complex interaction between the fluxes of the individual H^+ , Ca^{2+} , and Cl^- ions.

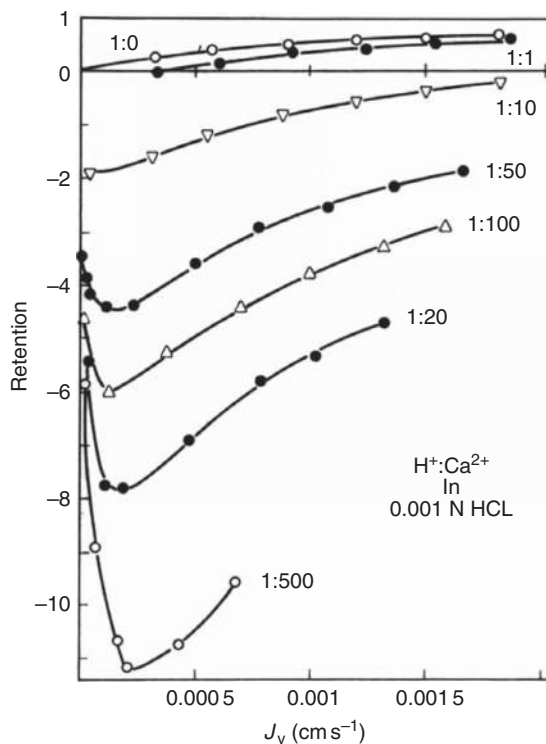


Figure 14 Retention vs. permeate flux for H^+ ion in a 0.001 N HCl solution at different CaCl_2 concentrations. The indicated numbers are the normality ratio $\text{H}^+:\text{Ca}^{2+}$.

In Figure 14, the retention of H^+ ion decreases with increasing CaCl_2 concentrations from 0 to 0.5 N and it has a minimum at low permeate flux. When CaCl_2 concentration increases, the minimum goes to higher pressures and, therefore, to higher fluxes. Jonsson [25] explained the experimental results by the combined frictional and exclusion model together with the extended Nernst–Planck equation. In particular, his theoretical treatment of two-salt solutions was based on a combined viscous flow and frictional model with the extension of a flux-dependent electrical potential term together with a boundary potential causing the distribution coefficients of the individual ions (K_i) to be concentration dependent.

The presence of the minimum can be explained from the three induced potential terms: the boundary potential on the permeate side has a maximum value corresponding to a pure HCl solution, which is attained at a quite low permeate flux. At low permeate flux, the potential gradient in the membrane is determined mainly by the diffusion potential arising

from the diffusion of CaCl_2 , which increases H^+ concentration. With increasing permeate flux, the streaming potential arising from the convective motion of HCl partly cancels the diffusion potential, thereby decreasing H^+ concentration. From a practical point of view, the results show that the retention of the separate ions in multisalt solutions is strongly dependent on the induced potentials which are caused by all ions present in the bulk solution. Therefore, the retention of a single ion can be quite different from the measured retention of the same ion in a single-salt solution. Thus, the results explain why pH is normally found to be one pH unit lower in the permeate than in the bulk solution, when using RO on natural waters.

Vonk and Smit [26] applied the extended Nernst–Planck equation to the separate ions and derived analytically expressions describing the rejection curves in ternary systems valid under the limiting cases of either high-volume fluxes or low-volume fluxes.

Nielsen and Jonsson [27] used the extended Nernst–Planck equations as starting equations for calculating the change in the rejection of a given ion under nanofiltration conditions when adding other salts to the bulk solution. The theoretical treatment of multicomponent salt solutions used by Nielsen and Jonsson [27] is based on a combined viscous flow and frictional model with the extension that the individual ion fluxes are coupled with each other by an induced membrane potential. The procedure has been restricted only to loose RO membranes (nanofiltration) in order to be able to obtain an analytical solution and a titration function has been derived. From the latter, the change in rejection of a given ion by adding other salts to the solution can be calculated from the change in the bulk solution composition and knowledge of the self-diffusion coefficient of the individual ions in that solution. Using the multisalt system NaNO_3 – Na_2SO_4 – HCl as an example, the nitrate rejection plane was calculated from the derived titration function, which represents the magnitude of the induced electrical potentials. Thus, **Figure 15** shows the line for the concentration ratios of Na_2SO_4 : HCl , where the sign of the nitrate rejection changes from positive to negative values. The experimental nitrate rejection data fit very nicely into this plane, showing increased negative rejections with increasing Na_2SO_4 concentration (**Figure 16**), which can be reversed by the addition of HCl to the bulk solution (**Figure 17**).

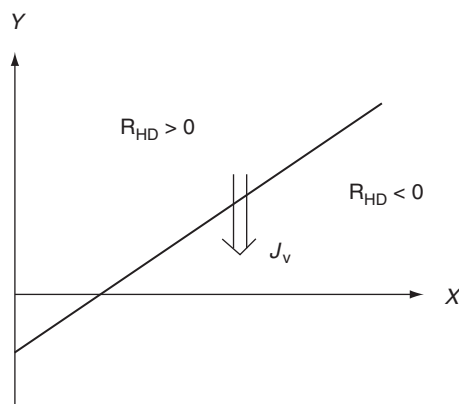


Figure 15 Outline showing that negative nitrate rejection can be inverted to positive rejection with increasing volume flux [27].

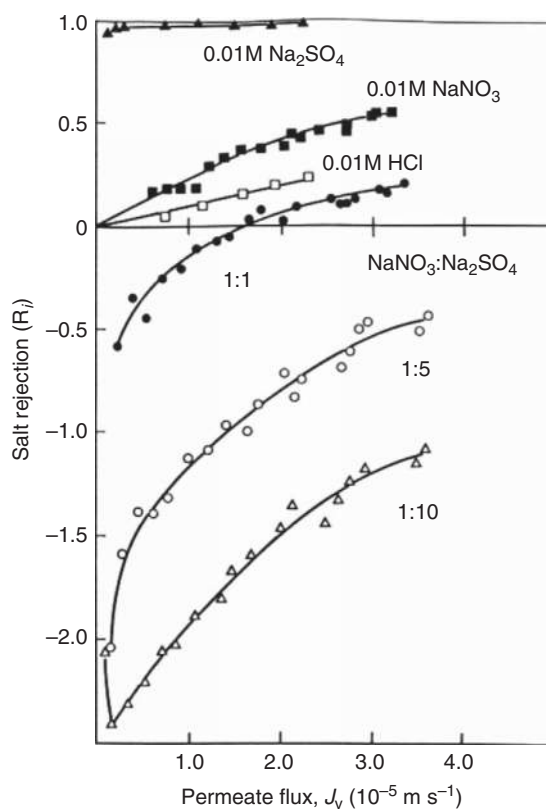


Figure 16 Salt rejection vs. permeate flux for the three single-salt solutions and for the nitrate rejection with increasing Na_2SO_4 in the two-salt solutions [27].

Figure 16 shows the measured rejections versus the permeate flux for the single-salt solutions NaNO_3 , Na_2SO_4 , and HCl . As expected, there are positive rejections for the single-salt solutions with HCl showing the lowest rejection, NaNO_3 an

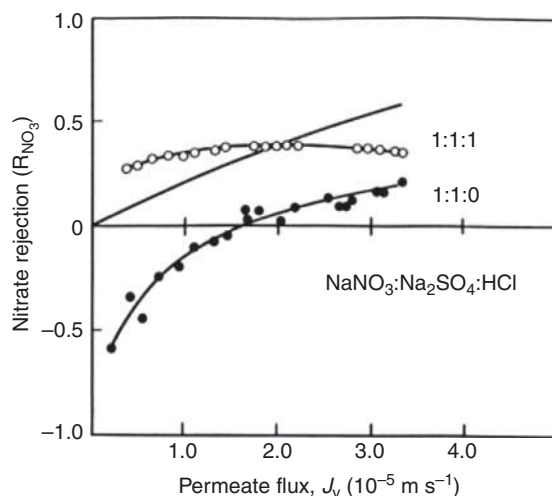


Figure 17 Comparison of the nitrate rejection vs. permeate flux for the single-, two-, and three-salt solutions in the concentration ratio as indicated [27].

intermediate rejection, whereas Na_2SO_4 shows the highest rejection by far because of the divalent sulfate ion. For all the three salts, there is an increased rejection with increasing permeate flux. **Figure 16** also shows data for the two-salt solutions, $\text{NaNO}_3 + \text{Na}_2\text{SO}_4$, showing a similar trend for the system sulfate/nitrate ions as was found for the system calcium/hydrogen ions in **Figure 14**.

Figure 17 shows the measured nitrate rejections versus the permeate flux for the system $\text{NaNO}_3:\text{Na}_2\text{SO}_4:\text{HCl}$ equal to 1:1:1 compared to the system 1:1:0. As can be seen, the titration of the system by the addition of HCl increases the rejection of the nitrate ion back to a positive value which is close to the average value for the single-salt solution.

Figures 16 and 17 highlight, moreover, how important but also complicated, in RO desalination, the prediction of rejection of ionic solutes in mixed systems from experimental data obtained in simplified single-salt solutions can be.

2.01.7.3 Organic Solutes and Nonaqueous Solutions

Low molecular weight organic solutes often have a poor rejection on many types of RO membranes. Sourirajan and Matsuura [28] have correlated the RO solute separation with some polar, steric, and nonpolar parameters. However, the real separation mechanism cannot always be determined by retention data alone. **Figure 18** and **Table 2** show the

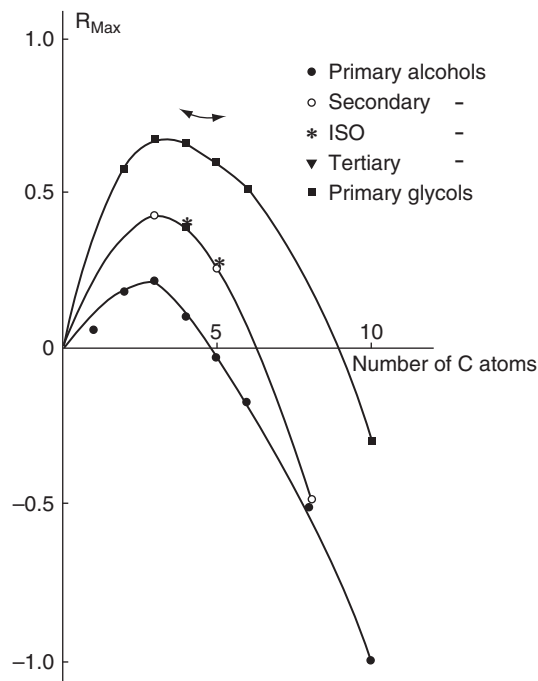


Figure 18 Maximal retention vs. chain length determined from reverse osmosis on an asymmetric cellulose acetate membrane.

maximal retention R_{\max} on CA membranes versus the number of carbon atoms of the solutes for different kinds of alcohols: there is a maximum in R_{\max} at about three C atoms and then a strong decrease in selectivity with increasing number of C atoms. The negative value of retentions indicates that the permeate is enriched in the solute.

In **Table 3**, some values of the distribution (K_i) and diffusion (D_i) coefficient of different alcohols determined from desorption experiments on homogeneous CA membranes are listed. Whereas the diffusion coefficient is mainly a function of the hydrodynamic volume of the molecule (determined by the chain length and the branching of the chain), the distribution coefficient is mainly a function of the aliphatic chain length or the hydrophobic nature of the alcohol molecule. Thus, with increasing branching of the butanols the diffusivity decreases much more than the distribution coefficient, which gives rise to the strong increase in rejection by RO. Further, passing from methanol, to butanol, and hexanol the distribution coefficient increases much more than the diffusion coefficient decreases. This explains why, in RO, methanol and butanol have almost the same positive rejection (though the mechanism is quite different) and why hexanol has a negative

Table 2 Maximal retention for different organic solutes determined from reverse osmosis on an asymmetric cellulose acetate membrane

<i>Solute</i>	R_{max}	<i>Solute</i>	R_{max}
Methanol	0.06	1,2-ethanediol	0.58
Ethanol	0.18	1,3-propanediol	0.68
Propanol	0.22	1,2-propanediol	0.73
Butanol	0.10	1,4-butanediol	0.66
Pentanol	-0.03	1,3-butanediol	0.73
Hexanol	-0.17	1,5-pentanediol	0.60
Cyclo-hexanol	0.61	2,2-dimethyl-propanediol	0.89
Octanol	-0.51	1,6-hexanediol	0.51
Decanol	-1.00	1,10-decanediol	-0.30
2-propanol	0.43		
2-butanol	0.39		
2-pentanol	0.26	Glycerol	0.90
2-octanol	-0.48	Pentaerythritol	0.99
Iso-butanol	0.39	Benzylalcohol	-0.15
Iso-pentanol	0.28	Diphenylcarbinol	-0.41
2-methyl-butanol	0.28		
		Phenol	-0.34
<i>Tert</i> -butanol	0.76	Hydroquinone	-0.12
<i>Tert</i> -pentanol	0.75	<i>p</i> -cresol	-0.46

Table 3 Estimated values of the distribution coefficient and the diffusion coefficient of different alcohols [7]

<i>Solute</i>	R_{max}^a	K_i^b	$D_i \times 10^9$ (cm^2/s^{-1}) ^b	K_i^c	$D_i \times 10^9$ (cm^2/s^{-1}) ^c
Methanol	0.06	0.10	45	0.22	NA
Ethanol	0.18	0.21	12		
Propanol	0.22	0.50	7.7		
2-propanol	0.43	0.44	6.0		
Butanol	0.10	1.2	4.3		
2-butanol	0.39	1.0	3.4		
<i>Tert</i> -butanol	0.76	0.8	0.9		
Hexanol	-0.17	14	0.7	0.23	9
Cyclo-hexanol	0.61	5.7	0.14		
Phenol	0.34	30	0.9	0.8	10

^a Determined from RO experiments on asymmetric CA membranes.

^b Determined from desorption experiments on homogeneous CA membranes.

^c As in note b, but with methanol as solvent instead of water.

NA, not available.

rejection (because the exclusion term increases much more than the kinetic term has decreased).

In **Table 3**, further shown are some estimated values of the distribution and diffusion coefficients determined on the same homogeneous CA membranes, but with methanol as solvent instead of water. A promising new application of RO is, in fact, in the chemical industry for the separation of organic/organic mixture. These separations are difficult due to the high osmotic pressures that must be

overcome and because they require membranes sufficiently solvent resistant to be mechanically stable but also sufficiently permeable for good fluxes to be reached.

In **Table 3**, it is shown that for hexanol the distribution coefficient decreases with a factor 60 to almost the same value as the methanol content in the membrane, while the diffusivity increases with a factor 15. This proves that the main reason for the very strong sorption of higher aliphatic alcohols and

similar flavors components on CA membranes is not a solute–membrane interaction but rather a lack of solute–water interaction.

As discussed by Kozak *et al.* [29], nonpolar groups tend to adhere to one another in an aqueous environment, known as hydrophobic bonding. This tendency reflects the aversion of these solutes to an aqueous environment. When brought into contact with a membrane, where the polymer phase is hydrophobic and the interstitial water is hydrophilic, the solutes will be squeezed into the membrane phase, which acts as a much better solvent medium for the solute than the water phase alone.

The first dense, solution–diffusion, RO membranes for processing organic solvent solutions appeared in the 1990s. Kiryat Weitzmann Ltd produced cross-linked silicone composite membranes that have some uses in the hyperfiltration of nonpolar solvent. The flux of different simple solvents through these membranes is shown in Figure 19.

2.01.7.4 Mixed Organic Solutes

Very few results have been published for mixed nonelectrolyte systems. Jonsson and Boesen [10] studied and presented some data on two-solute systems using two different cellulose acetate membranes. They found, for the glucose–raffinose system, that the two-solute data are in good agreement with the single-solute data. Therefore, a postulated interaction can be explained from the convection term of the finely porous model (see Section 2.01.3.2). An increasing concentration of glucose involves a lower

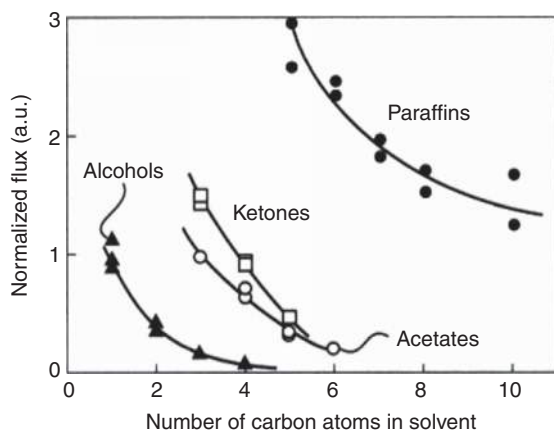


Figure 19 Normalized flux of homologous solvent series vs. the number of carbon atoms in the solvent molecules (MFP-60 Kiryat Weitzmann membranes) [17,30].

retention of raffinose, which corresponds to the variation in the permeate flux. Principally, the same could be observed by decreasing the pressure to get the same permeate flux as in the two-solute experiment. For glucose, it is further seen that the lower retention for the higher concentration is retained in the two-solute experiments, so that the effect is due to the glucose concentration only. This means that the change in retention of component i by introducing another solute j is caused by the water–solute coefficient X_{vi} and X_{vj} whereas the coupling coefficients X_{ij} disappear.

Matsuura and co-workers [31, 32] analyzed the behavior of systems with mixed alcohols. They observed an opposite trend of the retention with concentration. In particular, they noted that the retention does not change at low concentrations where the permeate flux is constant, whereas a change can be observed at high concentration. In this second case, the retention could be calculated from the retentions of the single-solute systems of the same total molality. However, from the data, neither the coupling between the solutes can be really identified nor can it be concluded whether the convection is effectively the term responsible for the change in retention.

Boesen and Jonsson [33] found a significant change in the retention of the organic solute when an alcohol is introduced in the solution. In particular, they noticed a change in the retention of *tert*-butanol when ethanol or phenol is added to the feed solution. According to the measurements of the distribution coefficients of *tert*-butanol on homogeneous membranes, they concluded that the virtual coupling between the flows of the two solutes and not the changes in permeability caused the retention change.

2.01.7.5 Membrane Charge

The models illustrated in Section 2.01.4 can be applied for a wide range of solutes in neutral membranes. However, a different behavior can be observed with charged solutes in membranes containing fixed charged groups. In fact, membrane composition combined with solvent and solute characteristics can influence rejection via electrostatic double-layer interactions or other hindrances: if a solution containing ions is brought in contact with membranes possessing a fixed surface charge, the passage of ions possessing the same charge as the membrane (coion) can be inhibited. This condition is termed Donnan exclusion. Moreover, the

membrane can exchange ions between the feed solution and the ion exchange groups on the membrane. This can lead to swelling of the membrane structure and, as a consequence, to variations in the transport properties of the membrane. As a first approximation, the discussed models can be used also in the case of charged membranes, but the transport parameters are a strong function of the operating conditions.

For the salt $M_{zy}Y_{zm}$, which ionizes to M^{zm+} and Y^{zy-} , a dynamic equilibrium occurs when a charged membrane is placed in the salt solution. At equilibrium and in the case of the negatively charged membranes usually utilized in nanofiltration, the following equations for the salt distribution coefficient K^* and the rejection R' can be used [34]:

$$K^* = \left[\frac{c_{y(m)}}{c_y} \right] = \left[z_y^{z_y} \left(\frac{c_y}{c_m^*} \right)^{z_y} \left(\frac{\gamma}{\gamma_m} \right)^{z_y z_m} \right]^{1/z_m} \quad (50)$$

$$R' = 1 - K^* \quad (51)$$

where z_i is the charge of species i , c_y and $c_{y(m)}$ are the concentrations of coion y in the bulk solution and in the membrane phase, respectively, γ and γ_m are activity coefficients, and c_m^* is the charge capacity of the membrane.

Equations (50) and (51) furnish a qualitative description of the solute rejection, which is a function of both the membrane charge capacity, and the solute concentration in the feed and the charge of the ions. However, they do not take into account diffusive and convective fluxes that are also important in the charged membrane processes.

2.01.7.6 Membrane Fouling and Concentration Polarization Phenomena: Limits of Membrane Processes

Real RO processes are limited by concentration polarization phenomena and membrane fouling. These phenomena strongly reduce the performance of membrane operations because they decrease mass flux and/or separation performance, that is, salt rejection. As a consequence, concentration polarization phenomena and membrane fouling negatively affect the economy of the membrane-separation processes and their control is one of the major problems in the design of membrane systems.

But, what are concentration polarization and fouling? Rejection of dissolved matter by the membrane leads to accumulation of these substances in front of the membrane, with highest concentrations directly at the membrane surface. This phenomenon is called

concentration polarization. Thus, a concentration gradient between the solution at the membrane surface and the bulk is established which leads to a back transport of the material accumulated at the membrane surface by diffusion. Although concentration polarization can also be found on the permeate side, it is usually neglected in RO since it is much less pronounced than feed-side polarization. A typical concentration profile is shown in Figure 20.

While the causes of concentration polarization are identical in membrane filtration (MF), ultrafiltration (UF), and RO, the consequences are rather different. In RO, mainly low molecular weight materials are separated from a solvent such as water. The feed solutions often have a considerable osmotic pressure. For example, seawater has an osmotic pressure of about 24 bar. In RO, concentration polarization leads to an increase in the osmotic pressure which is directly proportional to the solute concentration at the membrane surface, and thus a decrease in the transmembrane flux at constant applied hydrostatic pressure. Furthermore, the quality of the filtrate is impaired since the solute leakage through the membrane is also directly proportional to the solute concentration at the membrane feed-side surface.

In MF and UF, only macromolecules and particles are retained by the membrane. The osmotic pressure of the feed solution is generally not as high as in solutions treated by RO. However, the applied hydrostatic pressure is also quite low and, under certain conditions, the increased osmotic pressure due to concentration polarization phenomenon could effect the transmembrane flux. Due to the rather high molecular weight of the components

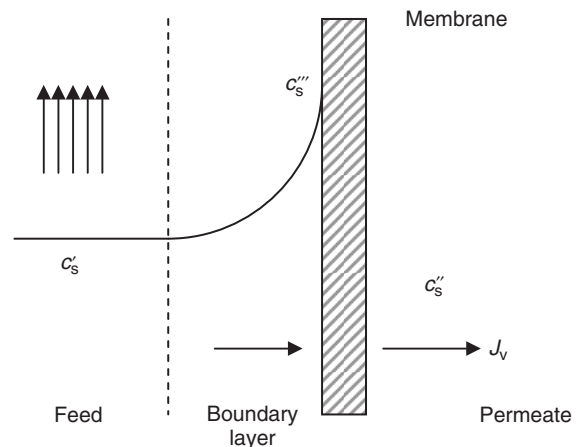


Figure 20 Concentration profile.

separated in UF and MF, their diffusion from the membrane surface back into the bulk solution is relatively slow. Therefore, the retained components often are precipitated and form a solid layer at the membrane surface. This layer, which often exhibits membrane properties itself, can affect the membrane-separation characteristics significantly by reducing the membrane flux and by changing the rejection of the lower molecular weight components. This is especially problematic in the fractionation of different molecular weight materials.

Concentration polarization complicates the modeling of membrane systems because experimental calculation of the wall concentration is difficult. For high feed-flow rates, it has often been assumed that the wall concentration is equal to the bulk concentration due to the high mixing which is, however, seldom the case. At low flow rates, this assumption is certainly no more applicable and can cause substantial errors. In order to estimate the extent of concentration polarization, the film theory is the most well-used technique [35, 36]:

$$\frac{c_s''' - c_s''}{c_s' - c_s''} = \exp\left(\frac{J_v}{k}\right) \quad (52)$$

In Equation (52), k denotes the mass transfer coefficient which can be estimated using a Sherwood correlation such as the following derived by Gekas and Hallstrom [37]:

$$Sh = 0.023 Re^{0.8} Sc^{0.33} \quad \text{for turbulent flow} \quad (53)$$

$$Sh = 1.86(Re \cdot Sc \cdot d_h/L)^{0.33} \quad \text{for laminar flow} \quad (54)$$

Concentration polarization phenomena can be reduced by promoting a good mixing of the bulk feed solution with the solution near the membrane surface. This goal can be achieved by modifying the membrane module in order to encourage mixing, for example, including turbulence promoters in the feed channel, or increasing feed-flow rate (thus increasing the axial velocity and promoting turbulent flow).

The adverse effects of the concentration polarization are intensified when a deposition and/or an adsorption of certain feed constituents occurs at the membrane surface, causing a decline in flux over time when all operating parameters, such as pressure, flow rate, temperature, and feed concentration are kept constant. This phenomenon is referred to as membrane fouling. Membrane fouling may be the result of concentration polarization but it may also be only the consequence of adsorption of feed solution constituents at the membrane surface and,

especially in microfiltration, also within the membrane structure.

Possible negative effects of fouling include:

- membrane flux decline resulting from the formation of a permeability-reducing film on the membrane surface;
- membrane biodegradation due to the production of acidic by-products by microorganisms, which are concentrated at the membrane surface where they can cause the most damage;
- increased salt passage thereby reducing the quality of the product water;
- increase in energy consumption. To maintain the same production rate differential pressure and feed pressure must be increased to counteract the reduction in permeability brought on by the increase in resistance due to fouling. But, damage to the membrane elements may be possible if the operating pressure exceeds the manufacturer's recommendations.

While concentration polarization can be minimized by hydrodynamic means, the control of membrane fouling is more difficult. Fouling can be prevented through the following means: pretreatment of the feed solution; modification of membrane surface; hydrodynamic optimization of the membrane module; recourse to proper chemical agents for the cleaning; and back flushing.

Fouling can never fully be prevented even with optimized pretreatment. Therefore, periodical membrane cleaning has to be performed. Good operating practice calls for chemical cleaning of the membranes if either normalized permeate flow decreases by 10%, feed channel pressure loss increases by 15%, or normalized salt rejection decreases by 10% from initial conditions during the first 48 h of plant operation [38]. However, complete fouling removal is not possible and it has to be tolerated up to a decrease of mass flux down to 75% of original flux [39].

References

- [1] Jonsson, G. Selectivity in Membrane Filtration. In *Synthetic Membranes: Science, Engineering and Applications*; Bungay, P. M., Lonsdale, H. K., de Pinho, M. N., Eds.; D. Reidel: Dordrecht, 1986; pp 343–366.
- [2] Staverman, A. J. *Rec. Trav. Chim. Pays-Bas.* **1951**, *70*, 344.
- [3] Jonsson, G. *Desalination* **1978**, *24*, 19–37.
- [4] Pusch, W. *Ber. Bunsenges. Phys. Chem.* **1977**, *81*, 269.
- [5] Onsager, L. *Phys. Rev.* **1931**, *37*, 405–425.

- [6] Kedem, O., Katchalsky, A. *Biochem. Biophys. Acta* **1958**, *27*, 229–246.
- [7] Jonsson, G. *Desalination* **1980**, *35*, 21–38.
- [8] Burghoff, H.-G., Lee, K. L., Push, W. *J. Appl. Polym. Sci.* **1980**, *25*, 323–347.
- [9] Sherwood, T. K., Brian, P. L. T., Fisher, R. E. *Ind. Eng. Chem. Fundam.* **1967**, *6*, 2–12.
- [10] Jonsson, G., Boesen, C. E. *Desalination* **1975**, *17*, 145–165.
- [11] Merten, U. Transport Properties of Osmotic Membranes. In *Desalination by Reverse Osmosis*; Merten, U., Ed.; MIT Press: Cambridge, MA, 1966; Chapter 2, pp 15–54.
- [12] Spiegler, K. S. *Trans. Faraday Soc.* **1958**, *54*, 1408–1428.
- [13] Spiegler, K. S., Kedem, O. *Desalination* **1966**, *1*, 311.
- [14] Cadotte, J. E., Petersen, R. J., Larson, R. E., Erickson, E. E. *A New Thin Film Seawater Reverse Osmosis Membrane*; Presented at the 5th Seminar on Membrane Separation Technology, Clemsom University, 1980.
- [15] Dickson, J. M. Fundamental Aspects of Reverse Osmosis. In *Reverse Osmosis Technology*; Parekh, B. S., Ed.; Marcel Dekker: New York, 1988; pp 1–51.
- [16] Redondo, J., Busch, M., De Witte, J.-P. *Desalination* **2003**, *156*, 229–238.
- [17] Baker, R. W. *Membrane Technology and Applications*; Wiley: Chichester, 2004.
- [18] Sourirajan, S. *Reverse Osmosis*; Academic Press: New York, 1970.
- [19] Sourirajan S., Ed. *Reverse Osmosis and Synthetic Membranes*; National Research Council: Ottawa, ON, 1977.
- [20] Erickson, D. L. Glater, J. McCutchan, J. W. *Ind. Eng. Chem. Prod. Res. Develop.* **1966**, *5*, 205–211.
- [21] Hodgson, T. D. *Desalination* **1970**, *8*, 99–138.
- [22] Heyde, M. E., Anderson, J. E. *J. Phys. Chem.* **1975**, *79*, 1659–1664.
- [23] Donnan, F. G. *Chem. Rev.* **1924**, *1*, 73.
- [24] Lonsdale, H. K., Pusch, W., Walch, A. *J. Chem. Soc. Faraday Trans.* **1975**, *71*, 501.
- [25] Jonsson, G. Coupling of Ion Fluxes by Boundary-, Diffusion- and Streaming-Potentials Under Reverse Osmosis Conditions. In *Proceeding of the 7th International Symposium on Fresh Water from the Sea 2*, 1980; pp 153–163.
- [26] Vonk, M. W., Smit, J. A. *J. Colloid Interface Sci.* **1983**, *96*, 121.
- [27] Nielsen, D. W., Jonsson, G. *Sep. Sci. Technol.* **1994**, *29* (9), 1165–1182.
- [28] Sourirajan, S., Matsuura, T. In *Reverse Osmosis and Synthetic Membranes*; Sourirajan, S., Ed. National Research Council: Ottawa, ON, 1977; pp 5–43. Chapters 2,3.
- [29] Kozak, J. J., Knight, W. S., Kaufmann, W. *J. Chem. Phys.* **1968**, *48*, 675–690.
- [30] Machado, D. R., Hasson, D., Semiat, R. *J. Membr. Sci.* **1999**, *163*, 93–102.
- [31] Matsuura, T., Bednas, M. E., Sourirajan, S. *J. Appl. Polym. Sci.* **1974**, *18*, 567–588.
- [32] Matsuura, T., Sourirajan, S. *Ind. Eng. Chem. Process. Des. Develop.* **1971**, *10*, 102–108.
- [33] Boesen, C. E., Jonsson, G. Solute–Solute Interactions by Reverse Osmosis of Three Component Solutions. In *Proceeding of the 6th International Symposium on Fresh Water from the Sea 3*, 1978; pp 157–164.
- [34] Bhattacharyya, D., Cheng, C. Separation of Metals Chelates by Charged Composite Membranes. In *Recent Developments in Separation Science*; Li, N. N., Ed.; Boca Raton, FL: CRC Press, 1986; Vol. 9, p 707.
- [35] Bhattacharyya, D., Williams, M. E. Reverse Osmosis. In *Membrane Handbook*; Winston Ho, W. S., Sirkar, K. K., Eds.; Springer: New York, 1992; Chapter VI, pp 312–354.
- [36] Fritzmann, C., Löwenberg, J., Wintgens, T., Melin, T. *Desalination* **2007**, *216*, 1–76.
- [37] Gekas, V., Hallstrom, B. *J. Membr. Sci.* **1987**, *30*, 153.
- [38] Cleaning Chemicals, DOW FILMTEC Membranes, Tech Manual Exerpt, Form No. 609-02091-704.
- [39] Rautenbach, R., Melin, T. *Membranverfahren (Grundlagen der Modul- und Anlagenauslegung)*, 2nd edn.; Springer: Heidelberg, 2003.

Biographical Sketches



Gunnar Jonsson is currently a professor at the Department of Chemical and Biochemical Engineering at the Technical University of Denmark (DTU) in Lyngby. Here, he has been responsible for teaching and research in membrane technology for almost 40 years. His current research focuses on dynamic and integrated membrane processes, such as high-frequency back flushing, vibrating membrane systems, electro-ultrafiltration, and reverse electro-enhanced dialysis (REED) used in membrane bioreactor systems. He also works on membrane contactors, membrane formation, and surface modification of membranes. He is an editorial board member of the journals *Desalination*, *Purification and Separation Technology*, *Recent Patents on Chemical Engineering*, and *Desalination and Water Treatment – Science and Engineering*. Currently, he is the chairman of the Danish Society for Chemical Engineers and the Nordic Filtration Society. He is the author of about 150 scientific papers and six patents in membrane science and technology and is the co-founder of the spin-off company Jurag Separation A/S.



Francesca Macedonio graduated in chemical engineering from the University of Calabria (Italy) in July 2005 and obtained her doctorate degree in 2009. Her primary research interests are in the fields of membrane processes for sea-, brackish-, and wastewater treatment, integrated membrane desalination processes, membrane distillation and membrane crystallization, energetic and exergetic analyses, as well as economical evaluations of membrane systems.

She was the winner of the Premio Sapio per la Ricerca Italiana 2008 – Premio Sapio Speciale Decima Edizione, and the recipient of the international award for poster presentation of the conference Euromembrane 2006, 24–28, September 2006, Taormina, Italy, for the paper titled ‘Integrated membrane systems for seawater desalination’.

She is currently member of the Section on Membrane Engineering of the European Federation of Chemical Engineering and has authored and co-authored eleven scientific papers in international journals, three chapters of books, and participated in 25 conferences in the field of Membrane Science and Technology.

2.02 Preparation of Industrial RO, NF Membranes, and Their Membrane Modules and Applications

M Kurihara and H Tomioka, Toray Industries, Inc., Shiga, Japan

© 2010 Elsevier B.V. All rights reserved.

2.02.1	Introduction	23
2.02.2	Preparation of RO Industrial Membranes	24
2.02.2.1	Asymmetric Membrane	24
2.02.2.1.1	Cellulose acetate membrane	24
2.02.2.1.2	Aromatic polyamide hollow fiber membrane	24
2.02.2.2	Composite Membrane	25
2.02.2.2.1	Cellulose acetate membrane	25
2.02.2.2.2	Cross-linked aromatic polyamide membrane	25
2.02.2.2.3	Cross-linked poly ether membrane	25
2.02.3	Applications of RO Membrane	26
2.02.3.1	Low-Pressure Brackish Water Desalination Membrane	26
2.02.3.2	Seawater Desalination Membrane	27
2.02.3.2.1	Brine conversion system	27
2.02.3.2.2	Boron removal membrane	29
2.02.3.3	Low Fouling Membrane for Wastewater Reclamation	30
2.02.4	Integrated Membrane System	31
References		32

Abbreviations

BWRO RO (membrane) for brackish water applications

CA Cellulose acetate

CTA Cellulose tri-acetate

PA Polyamide

SWRO RO (membrane) for seawater applications

TDS Total dissolved solids

TOC Total organic carbon

2.02.1 Introduction

Population explosion and industrial activities have been responsible for both large consumption of water resources and water pollution; consequently, sustaining adequate water balance, both in terms of quantity and quality, is one of the most serious issues in the world today. Therefore, the twenty-first century is the so-called 'water century,' instead of the 'oil century' of the twentieth century.

In the twentieth century, some new technologies for water treatment were developed as countermeasures to the water shortage, and the membrane technology is recently regarded as indispensable since it ensures plenty of high-grade water with low

cost and the maintenance of sustainable water resources. The membrane technologies have made great progress and their key features are as follows:

1. Materials: Molecular design of high-performance materials suitable for each separation mode.
2. Morphology: Morphological design of high-performance membrane.
3. Element/module: Element and module design to maintain high performance of membrane.
4. Membrane process: Plant design and operation technology.

Especially in desalination fields, reverse osmosis (RO) and nanofiltration (NF) membranes have been widely applied not only to seawater desalination but

also to brackish water desalination including industrial and wastewater treatment. Today, their commercial use is spreading rapidly and worldwide.

2.02.2 Preparation of RO Industrial Membranes

2.02.2.1 Asymmetric Membrane

2.02.2.1.1 Cellulose acetate membrane

The history of materials for RO membranes is shown in **Figure 1**. RO systems were originally presented by Professor Reid in 1953 [1a,b]. The first membrane which was industrially available in actual water production plants was cellulose acetate membrane invented by Loeb and Sourirajan in 1960 [2]. This membrane had a cross-sectional structure called asymmetric or anisotropic with a very thin separating functional layer on a coarse supporting layer as shown in **Figure 2**. The material of this membrane was exclusively a polymer such as cellulose acetate, and the nonsolvent-induced phase separation method was used for the formation of the membrane. Following the invention by Loeb and Sourirajan, spiral-wound membrane elements using the asymmetric cellulose acetate flat sheet membranes were

developed and manufactured by several companies in the United States and Japan. RO technologies had become commercially available since *c.* 1964 [3]. Asymmetric cellulose acetate membranes were widely used from the 1960s through the 1980s mainly for pure water for industrial processes and ultrapure water for semi-conductor industries, and some of them are still used even today.

2.02.2.1.2 Aromatic polyamide hollow fiber membrane

Many intensive and continuous research and development efforts were made mainly in the United States and Japan to meet the demands from markets, and many inventions and breakthroughs in membrane materials and configurations had also been suggested to improve the membrane performances.

To overcome the difficulties involved in using cellulose acetate membranes, which had comparatively low water permeability and filtration performance, many synthetic polymeric materials for RO were proposed. However, except for the linear aromatic polyamides with pendant sulfonic acid groups shown in **Figure 3**, none were successful. This material, invented by DuPont, was fabricated into a very fine hollow fiber membrane, and the

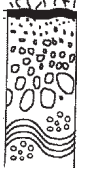
Year	Stage	Remarkable topics	
1950	Early	First concept of RO membrane (Reid)	 <p>Asymmetric membrane</p>
1960	Research for asymmetric membranes	First CA asymmetric membrane (Loeb and Sourirajan)	
		First spiral-wound element of CA (General Atomic Co.)	
		First hollow fiber membrane of CTA (Dow)	
1970	Rapid progress by composite membranes	First hollow fiber membrane of linear aromatic PA (Du Pont)	 <p>Composite membrane</p>
		Start of research for composite membrane (Riley)	
		Linear polyamide composite membrane by interfacial condensation (Scala)	
1980		Cross-linked aromatic PA composite membrane by interfacial condensation (Cadotte)	
		High performance cross-linked aromatic PA composite membrane (Toray)	

Figure 1 History of materials for reverse osmosis (RO) membrane.



Figure 2 Cross section of asymmetric cellulose acetate.

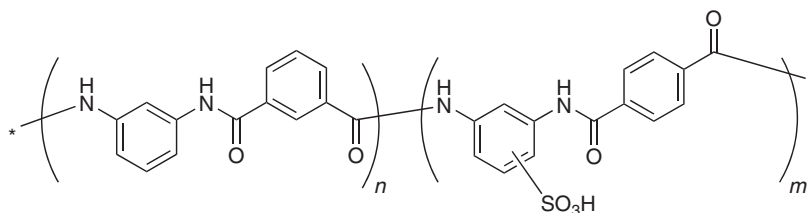


Figure 3 Representative chemical structure of linear polyamide membranes (B-9 and B-10).

modules of this membrane were designated B-9 and B-10 [4]. They showed high rejection performance, which could be used for single-stage seawater desalination with low water recovery, and hence were widely used mainly for seawater or brackish water desalination and recovery of valuable materials such as electric deposition paints, until DuPont withdrew it from the market in 2001.

2.02.2.2 Composite Membrane

2.02.2.2.1 Cellulose acetate membrane

Other approaches to obtain a high-performance RO membrane had been followed by some institutes and companies since the 1970s. Many methods to prepare composite membranes had been proposed. In the early stage, a very thin film of cellulose acetate polymer coating on a substrate such as a porous substrate of cellulose nitrate was tried, but in spite of the best efforts, only the Riley group of Gulf General Atomics (Koch Membrane Systems at present) succeeded in manufacturing it on an the industrial scale.

2.02.2.2.2 Cross-linked aromatic polyamide membrane

The next approach was to use the interfacial condensation reaction to form a very thin polymeric layer onto a substrate. Morgan [5] first proposed this method, and then Scala and Van Hauben actually

applied the same to obtain a RO membrane [6a,b]. Cadotte [7] invented a high-performance membrane using an *in situ* interfacial condensation method. In this method, the interfacial condensation reaction between polymeric polyamine and monomeric polyfunctional acid halides or isocyanates was carried out on a substrate material to deposit a thin-film barrier layer.

Later, many companies succeeded in the development of composite membranes using this method, and the membrane performance has drastically improved ever since. The composite membrane of cross-linked fully aromatic polyamide is already regarded as the most popular and reliable material for use in RO membranes [3, 8].

2.02.2.2.3 Cross-linked poly ether membrane

Some of the composite membranes were succeeded in industrial fabrication by those manufactured by another company. Riley and coworkers developed cross-linked poly ether membranes designated as PA-300 and RC-100 (Figure 4), which showed high salt rejections and productivity [4]. The RC-100 membrane is known as the first composite RO membrane, which was installed in many areas. However, many other methods to prepare RO membranes had also been proposed. Figure 5 summarizes RO membrane materials including the related information of membrane morphology, module configuration, and their suppliers.

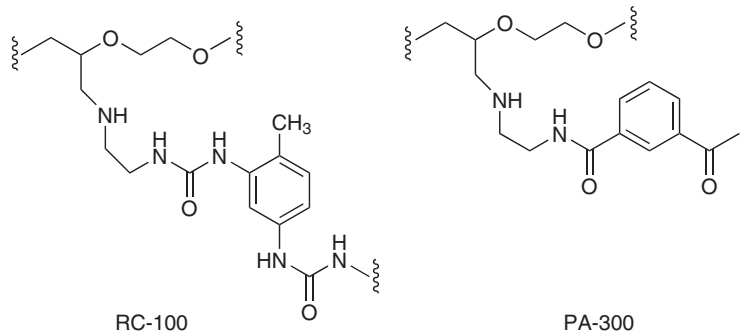


Figure 4 Representative chemical structure of cross-linked poly ether membranes (RC-100 and PA-300).

Membrane material	Membrane morphology	Module configuration	Example of membrane and module, Membrane Suppliers	
Cellulose acetate		Spiral	1. Toray, UOP, Environgenics, Osmonics, Desalination, Ajax, Hydranautics, Daiseru 4. Toray-polyamidic acid, Du Pont-DP-1, Monsanto 6. Celanese-polybenzimidazole 9. UOP-CTA 10. North Star-NS-100, UOP-PA-300, -100, LP-300, RC-100 12. North Star-NS-200, Osmonics-NS-200, Environgenics-SPFA(NS-200), Desalination-NS-200 14. North Triangle Inst.-Plasma Polym. Toray-PEC-1000, FilmTec-FT-30, Asahi Glass-MVP, Nihon Syokubai	
Polyamide			Hollow fiber	2. Dow, Monsanto, Toyobo 5. DuPont 7. Celanese-Polybenzimidazole 13. FRL-NS-200, Gulf South Research Inst.-NS-100
Heterocyclic polymer				Tubular
Cross-linked water-soluble polymer	Composite membrane			
Polymerizable monomer (crosslinking)				

Figure 5 Summary of materials for RO membrane.

2.02.3 Applications of RO Membrane

RO membranes have been widely used for water treatment such as the production of ultrapure water and boiler pure water for industrial use; seawater and brackish water desalination for drinking water and agricultural water use; wastewater reclamation for industrial, agricultural, and indirect drinking water use, and so on. The expansion of RO membrane applications promoted the redesign of suitable membrane material taking into consideration the chemical

structure, membrane configuration, chemical stability, and ease of fabrication. Along with improvements of the membranes, their applications are further developed. Recent technology trends in RO membranes are shown in Figure 6.

2.02.3.1 Low-Pressure Brackish Water Desalination Membrane

Figure 7 shows the progress of low-pressure membrane performance in brackish water desalination in

Operating pressure (MPa)	Super low	Ultralow	Low	High	Ultrahigh	Notes
	0.3	0.5	1.0	2.0	5.5 10.0	
SWRO	Second stage					High TDS removal High boron removal
	First stage					High TDS removal High boron removal
BW RO						Cost reduction Low fouling
Ultra-pure water						High TOC removal High quality Cost reduction
Waste water reuse						Low fouling Cost reduction

Figure 6 Technology trends in RO membranes.

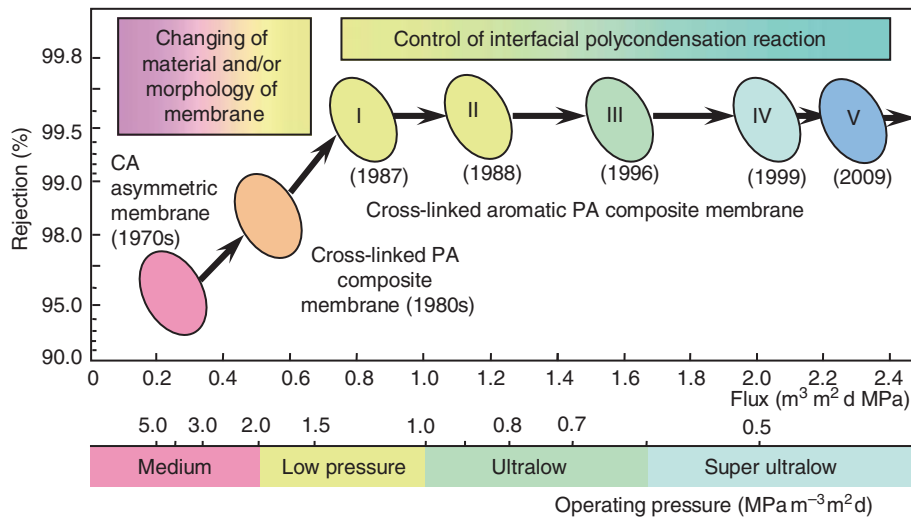


Figure 7 Performance changes in brackish water RO membrane.

these four decades, including industrial water treatment such as ultrapure water production. In the first decade from 1970, many efforts were made for developing high-performance membrane materials and improving the membrane performance, and as a result, membrane performance improved well with a newly developed material of cross-linked aromatic polyamide by appropriate modification of membrane morphology and fabrication technology. The membrane developed in 1987, which is depicted as I in **Figure 7**, had 4 or 5 times higher water productivity and 5 times lower salt passage (100-rejection (%)) than those of cellulose acetate membranes [3]. After 1987, based on the adoption of cross-linked fully aromatic polyamide composite membrane, the performance of brackish water RO membrane has

rapidly improved. Typical performances of the RO elements in these two decades for brackish water desalination are shown in **Table 1**.

2.02.3.2 Seawater Desalination Membrane

2.02.3.2.1 Brine conversion system

The progress of RO membranes for seawater desalination is shown in **Figure 8** [9]. In the operation of seawater desalination system, the increase of recovery rate of permeate water is crucial for cost reduction. Most seawater RO desalination systems were confined to approximately 40% conversion of the feed-water in the case of 3.5% of salt concentration, since usual commercially available RO

Table 1 Typical performance of Toray's brackish water RO elements

Types of membrane	Low pressure		Ultralow pressure	Super ultralow pressure	
	I	II	III	IV	V
Name of the membrane element	TM720-400	TM720L-400	TMG20-400	TMH20-400A	TMH20-400C
(Year in which the product is launched)	(1987)	(1988)	(1996)	(1999)	(2009)
Performance					
Salt rejection (%)	99.4	99.0	99.4	99.4	99.3
Water permeability ($\text{m}^3 \text{d}^{-1}$)	26.0	22.0	26.0	26.0	32.0
Test condition					
Operating pressure (MPa)	1.5	1.0	0.75	0.5	0.5
Temperature ($^{\circ}\text{C}$)	25	25	25	25	25
Feed concentration (mg l^{-1})	1500	1500	1500	1500	1500
Brine flow rate (l min^{-1})	80	80	80	80	80

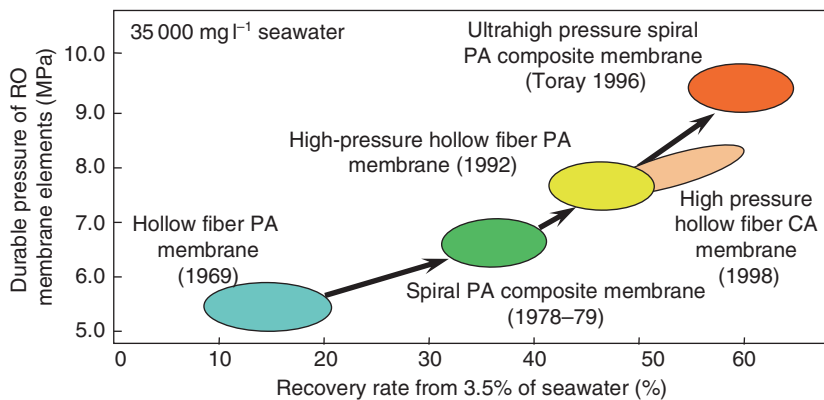


Figure 8 Performance trends in RO membranes for seawater desalination.

membrane did not allow high-pressure operation at more than 7 MPa.

Toray developed a low-cost seawater desalination system called the brine conversion system (BCS), which provides 60% of the recovery rate [10–12]. Process flow of the BCS system is shown in **Figure 9**. The concentrated seawater (5.8% of salt concentration) from the first-stage RO modules is pressurized to 8–10 MPa by pressure booster; then, the concentrate is supplied to the second-stage RO modules. Additional fresh water is obtained from the second stage, and the feed water is finally concentrated to approximately 8.7% of salt concentration. The 60% of the total recovery rate can be obtained in which 40% comes from the first stage and a further 20% from the second stage. The total recovery rate is determined considering the salt concentration that does not generate the precipitation of salt, and the

operating pressure is determined to desalt second-stage brine water.

Further, for achieving the 60% of recovery RO seawater desalination system, the RO membrane element must be durable under very severe operating conditions with 10 MPa of high pressure and 5.8% of high feed water concentration. Toray developed an ultrahigh-pressure-resistant membrane called the TM820BCM, which enabled 60% of the high recovery rate operation.

The advantages of the BCS system compared with the conventional system are as follows:

1. Plant installation space can be reduced by two-thirds.
2. Plant capacity is easily expanded by 1.5 times by just adding BCS second stage into the conventional plant.

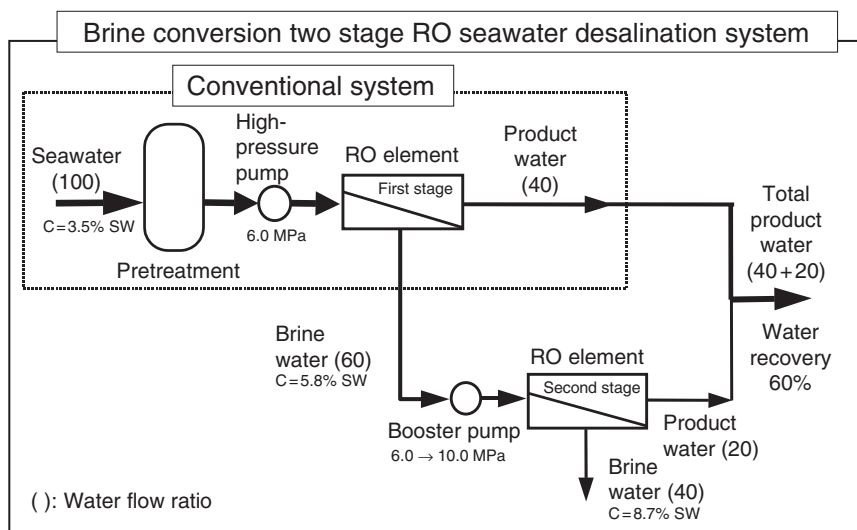


Figure 9 Typical flow diagram of brine conversion system.

3. Disposed concentrated brine water is reduced by two-thirds.

Therefore, the BCS is a useful method to save footprint, power, and cost of the SWRO desalination plant.

Some cost-related parameters for a recent RO operation are shown in **Table 2**. According to the table, first, possible recovery rate has greatly increased. For example, the membrane technology progress enabled high-recovery operations as mentioned earlier. Second, power consumption is remarkably reduced because of the progress of pump and power recovery device. Thus, the total water cost has been dramatically reduced in past few decades [13, 14].

2.02.3.2.2 Boron removal membrane

Water-quality improvement and energy saving are the two main concerns in seawater RO desalination. As for the water quality, boron removal is one of the most important issues [15–19], because it is known that reproductive toxicity was shown in per oral administration to laboratory animals. Boron exists as boric acid in seawater, and its concentration is 4–7 mg l⁻¹, which is 20 times higher than that of surface water. Further, it is difficult for RO

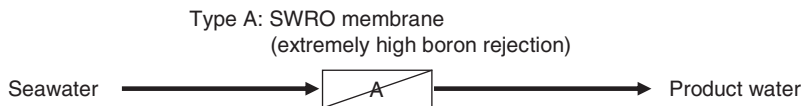
membrane to remove boric acid from water due to the following reasons: first, the molecular size of boric acid is too small to be effectively removed by size exclusion. Second, since boric acid has a pK_a of 9.14–9.25, it is was shown in not ionized in the natural seawater at pH 7.0–8.0 and dissociates at pH 9 or more [20], and the boron rejection by the electric repulsive force between boric acid and the membrane cannot be expected under neutral conditions. From the viewpoint of energy savings, RO membrane with high water permeability is preferable since lower pressure operation becomes possible. However, there is a tradeoff between the increase of water permeability and the decrease of boron removal.

Accordingly, the required boron concentration value in product water of each plant is varied by its circumstance, such as the system design, the usage of water, the policy of country, and so on. In the recent design of RO system corresponding to the respective boron regulations, the optimal operating conditions, which include the membrane to be used, must be chosen according to the required total water cost and quality, and the character of feed water. The RO processes are roughly classified into two groups as shown in **Figure 10**, namely, single-stage RO

Table 2 Technology progress in seawater RO operation

	Period		
	1980–90	1990–2000	2000–
Recovery rate %	25	40–50	55–65
Operating pressure psig (MPa)	1000 (6.9)	12 000 (8.25)	14 000 (9.7)
Product TDS conc. mg l ⁻¹	500	300	<200
Power consumption kwh/kgal (kwh m ⁻³)	45 (12)	21 (5.5)	10.2 (2.7)
Total water cost \$m ⁻³	>1.5	0.7–1.5	0.4–1.0

1. Single-stage SWRO for boron regulation



2. Multistage SWRO for severe boron regulation

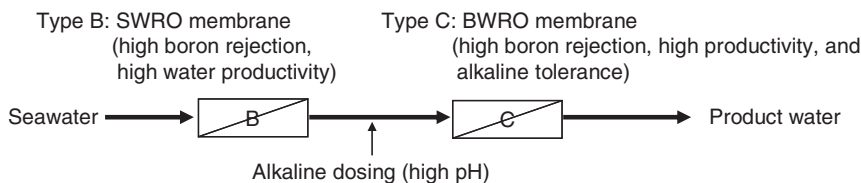


Figure 10 Flow diagrams of typical SWRO processes for corresponding to boron regulations.

process and multistage RO process. The single-stage process is characterized by simple composition without supportive processes for boron removal. In addition, in this process, extremely high boron rejection membrane (type A) in which the performance for boron removal is enhanced as well as maintaining water permeability is needed. The multistage process is generally used for water quality corresponding to severe boron regulation. In this method, after the preceding SWRO, BWRO treatment with alkaline dosing is adopted. Alkaline dosing ionizes boric acid and enhances the efficacy of its rejection. Therefore, the SWRO membrane element (type B) must have both high performance for boron removal and high water productivity to maintain energy saving and water quality, and the BWRO element (type C) must have alkaline tolerance with high performance for boron removal and high water productivity (as same as type B, depicted as **Figure 10**).

Furthermore, RO membrane with extremely high water permeability will be required for the effective

energy-saving operation. RO membrane must perform adequately for the removal of salt and other harmful compounds. Consequently, there are three courses for the development of seawater RO membranes:

1. pursuit of highest boron removal performance;
2. high water permeability with high boron removal performance; and
3. extremely high water permeability.

Recently, Toray has been investigating SWRO membranes with focus on the removal of boron by the improvement of membrane performance. Toray's SWRO product line-up is shown in **Tables 3 and 4**.

2.02.3.3 Low Fouling Membrane for Wastewater Reclamation

With the increase of demands for the preservation of sustainable water resources, the number of wastewater reclamation plant construction has been increasing every year. In a wastewater reclamation

Table 3 Toray's SWRO product line-up

<i>Element type^a</i>	<i>Product name</i>	<i>Salt rejection (%)</i>	<i>Product flow rate GDP (m³ d⁻¹)</i>	<i>Boron rejection (%)</i>
Type A	TM820A-400	99.75	6000 (23)	93
Type B	TM820C-400	99.75	6500 (25)	93
	TM820E-400	99.75	7500 (28)	91
Type C	TM720C-400	99.2	8800 (33)	95

^a Test condition: Type A and B: Feed water; NaCl 32 000 mg l⁻¹, Boron 5 mg l⁻¹, Temperature 25 °C pH 6.5, Operating pressure 5.52 MPa, Flow rate; 80 l min⁻¹, Recovery rate 8%; Type C: NaCl 1500 mg l⁻¹, Boron 5 mg l⁻¹, Temperature 25 °C, pH 10, Operating pressure 1.03 MPa, Flow rate; 80 l min⁻¹, Recovery rate 15%.

Table 4 List of world's largest SWRO plants (investigated in November 2008)

	<i>Country</i>	<i>Location</i>	<i>Capacity (m³ d⁻¹)</i>	<i>Operation (year)</i>	<i>Membrane manufacturer</i>
1	Israel	Ashkelon	330 000	2005	Dow
2	Saudi Arabia	Shuqaiq	216 000	2008	Toyobo
3	Saudi Arabia	Rabigh	205 000	2008	Toyobo
4	Algeria	Hamma	200 000	2008	Toray
4	Algeria	Mostaganem	200 000	2010	Dow
4	Algeria	Souk Tleta	200 000	2010	Nitto/Hydranauties
4	Algeria	Beni Saf	200 000	2008	Nitto/Hydranauties
8	UAE	Fujairah	170 000	2003	Nitto/Hydranauties
9	Saudi Arabia	Shuaiba	150 000	2009	Toray
10	Spain	Valdelentisco	140 000	2007	Dow
11	Trinidad & Tobago	Point Lisas	136 000	2002	Toray
11	Singapore	Tuas	136 000	2005	Toray
11	UAE	Fujairah II	136 000	2010	Toray
11	Kuwait	Shuwaikh	136 000	2010	Toray
11	Australia	Perth	136 000	2006	Dow

plant, the wastewater is first treated with biological technology, such as activated sludge method and membrane bioreactor (MBR), and the biologically treated water is again treated with RO membranes. In the RO membrane process, stable operation is one of the most important concerns. Many operational issues have been reported, with problems of membrane fouling occupying 80%. In order to avoid membrane fouling, it is imperative to take the following precautions: (1) RO membrane with low fouling property; (2) adequate pretreatment before RO membrane treatment; and (3) suitable cleaning operation of RO membrane [21].

Membrane fouling phenomena are categorized into chemical fouling and biological fouling. Chemical fouling is caused by the adsorption of organic matters such as humic substances and surfactants in the feed water onto membrane surface. Humic substances and surfactants have various chemical structures depending on the water origin; however, without exception they have both hydrophobic groups and ionic groups. Since RO membrane material is generally polyamide, which also possesses both the hydrophobic and ionic properties, it strongly interacts with humic substances and surfactants. In the case of biological fouling, the following estimations are reported: (1) microbe adsorption by hydrophobic or electrostatic interaction; (2) propagation of microbes with nutrition in the feed water; and (3) deposition of exhaust material of biological metabolism. Process (1) is reversible; however, (2) and (3) are irreversible, and are impossible to be removed by chemical cleaning.

Toray developed a low fouling RO membrane called TML for wastewater reclamation, which has water permeability similar to the conventional RO membranes [22]. The low fouling performance was evaluated with a nonionic surfactant aqueous solution as shown in Figure 11. The low fouling RO membrane shows a small permeability decline rate

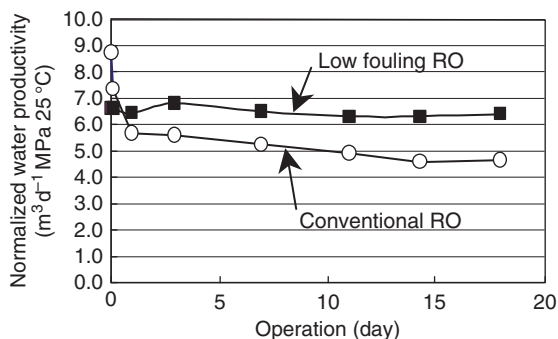


Figure 11 Evaluation of antichemical fouling performance.

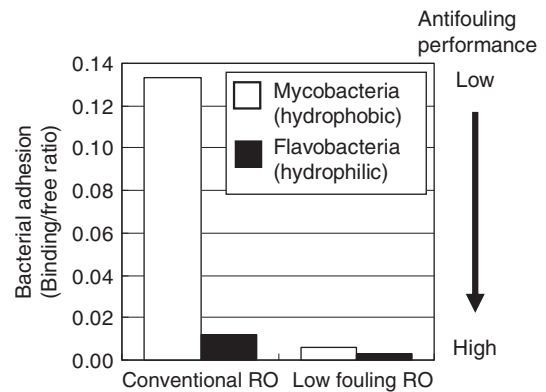


Figure 12 Evaluation of antibiological fouling performance.

of 27%, and stable operation, whereas the conventional RO membrane shows 36–47% decline rate. In addition, the low fouling RO membrane shows better recovery of permeability after chemical cleaning.

In order to evaluate antibiological fouling, an adhesion assay of a certain hydrophobic microbe and other hydrophilic microbes was performed as shown in Figure 12. The hydrophobic microbe is tightly adhered to conventional RO membrane and it causes biological fouling of an RO membrane. However, in the low fouling RO membrane, the adhesion property of the hydrophobic microbe is quite low, which is less than one-tenth of the conventional RO membrane.

In the near future, even the further polluted water, which is difficult to be treated due to fouling, is also necessary to be utilized as a resource. Therefore, stable operation requires that low fouling RO membrane is easily available.

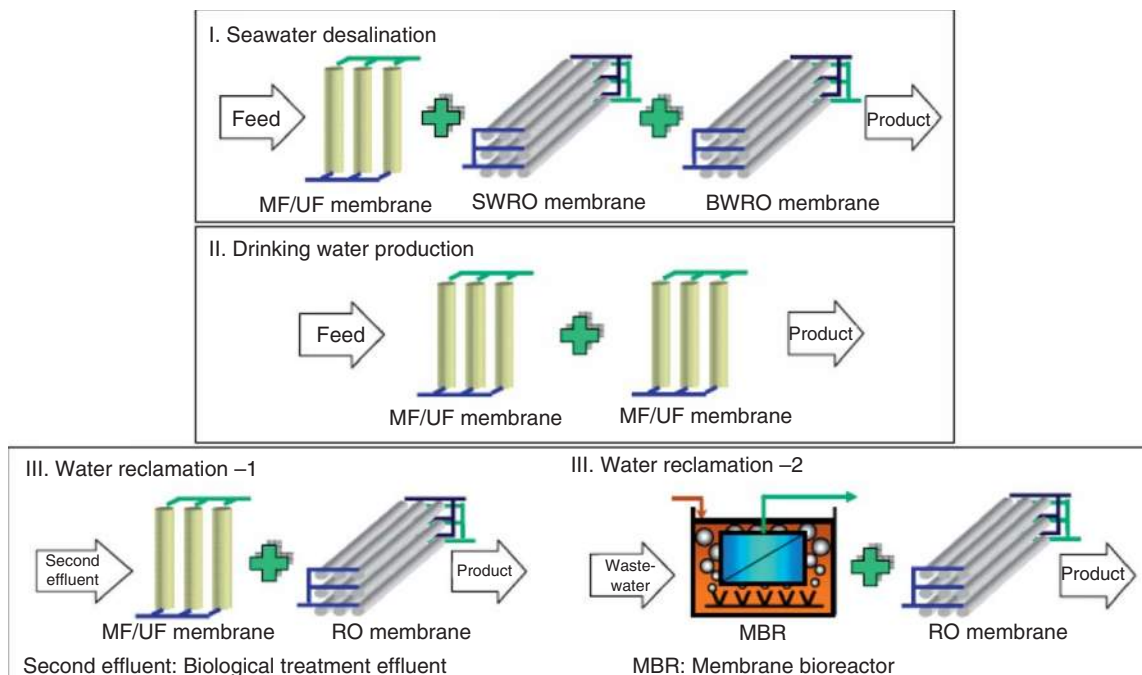
2.02.4 Integrated Membrane System

As mentioned above, large water reclamation plants have been launched as shown in Table 5. In these plants, the selection of pretreatment process is significant as well as that of RO membrane because the property of feed water severely influences operational durability even in using a low fouling membrane.

The water treatment process by combining multiple classes of membranes is called an integrated membrane system (IMS) [23]. The concept of IMS is that the optimal process which exerts strong points of each membrane for the cost and operation is designed according to various water resources and their purposes. The flow diagrams of typical IMS

Table 5 List of world's largest wastewater reclamation plants using RO membrane (investigated in August 2008)

	Country	Location	Capacity ($m^3 d^{-1}$)	Operation (year)	UF/MF membrane manufacturer	RO membrane manufacturer
1	Kuwait	Sulaibiya	32 000	2005	Norit	Toray
2	Singapore	Changi	228 000	2009	Siemens (Memcor)	Toray
3	USA	Fountain Valley	220 000	2007	Siemens (Memcor)	Hydranauties
4	Singapore	Ulu Pandan	140 000	2006	Asahi Kasei	Hydranauties
5	USA	Mest Basin	75 000	1997–2001	Siemens (Memcor)	Hydranauties
6	Australia	Luggage Point	66 000	2008	Pall	Toray
7	Singapore	Kranji	40 000	2003	Siemens (Memcor)	Hydranauties
8	Singapore	Bedok	32 000	2003	GE (Zenon)	Hydranauties
9	China	Tianjin	30 000	2006	Siemens (Memcor)	Toray
10	Singapore	Seletar	24 000	2004	Hyflux	Toray

**Figure 13** Integrated membrane systems corresponding to various purposes of water use.

corresponding to each purpose of water use are shown in **Figure 13**. The practical IMSs are exemplified as follows: (1) the BCS in **Figure 9** consists of MF + RO; (2) the world's largest wastewater reclamation plant in Sulaibiya consists of UF + low fouling RO; and (3) an industrial wastewater reuse plant in India consists of MBR + low fouling RO, and so on. Thus, the membrane systems of diverse combinations have already been suggested and are already functioning in the world. Therefore, membrane manufacturers need to know about each class of membrane types for the concept of IMS.

References

- [1a] Breton, E. J., Jr. Water and Ion Flow through Imperfect Osmotic Membranes. *Research and Development Progress Report* 1957, No. 16.
- [1b] Reid, C. E., Breton, E. J., Jr. *J. Appl. Polym. Sci.* **1959**, *1*, 133.
- [2] Loeb, S., Sourirajan, S. *Adv. Chem. Ser.* **1963**, *38*, 117.
- [3] Kurihara, M., Himeshima, Y., Uemura, T. In *Preprints of the 1987 International conference on membrane and Membrane Process*; The Aseanian Membrane Society: Tokyo, 1987; p 428.
- [4] Petersen, R. J. *J. Membr. Sci.* **1993**, *83*, 81–150.
- [5] Morgan, P. W. *Condensation Polymers: By Interfacial and Solution Methods*; Polymer Reviews; Wiley: New York, 1965; Vol. 10, xviii, 561pp.

- [6a] Scala, R. C., Ciliberti, D. F., Berg, D. Interface Condensation Desalination Membranes. US Pat. 3,744,642, 10 July 1973.
- [6b] Van Heuven, J. W. Dynamic Membrane. US Pat. 3,996,318, 7 December 1976.
- [7] Cadotte, J. E. Interfacially Synthesized Reverse Osmosis Membrane. US Pat. 4,277,344, 7 July 1981.
- [8] Kurihara, M., Uemura, T., Himeshima, Y., Ueno, K., Bairinji, Y. *Nippon Kagaku Kaishi* **1994**, 2, 97–107.
- [9] Kurihara, M., Fusaoka, Y., Sasaki, T., Bairinji, R., Uemura, T. *Desalination* **1994**, 96, 133.
- [10] Yamamura, H., Kurihara, M., Maeda, K. Reverse Osmosis Separation Method. Jpn. Pat. 3963304, 1 July 2007.
- [11] Ohya, H., Suzuki, T., Nakao, S. *Bull. Soc. Seawater Sci. Jpn.* **1996**, 50, 389.
- [12] Nakao, S. *Bull. Soc. Seawater Sci. Jpn.* **1996**, 50, 406.
- [13] Wilf, M., Bartels, C. *Desalination* **2005**, 173, 1.
- [14] Moch, I. *ADA 2000*, Lake Tahoe, USA, 2000.
- [15a] Taniguchi, M., Kurihara, M., Kimura, S. *J. Membr. Sci.* **2001**, 183, 249–257.
- [15b] Taniguchi, M., Kurihara, M., Kimura, S. *J. Membr. Sci.* **2001**, 183, 259–267.
- [16] Taniguchi, M., Fusaoka, Y., Nishikawa, T., Kurihara, M. *Desalination* **2004**, 167, 419–426.
- [17] Fukunaga, K., Matsukata, M., Ueyama, K., Kimura, S. *Membrane* **1997**, 22, 211–216.
- [18] Redondo, J., Busch, M., Witte, J. D. *Desalination* **2003**, 156, 229.
- [19] Tomioka, H., Taniguchi, M., Okazaki, M., Goto, S., Uemura, T., Kurihara, M. *Proceedings of IDA World Congress on Desalination and Water Reuse*, Singapore, 11–14 September 2005.
- [20] Rodriguez, M., Ruiz, A. F., Chilon, M. F., Rico, D. P. *Desalination* **2001**, 140, 145.
- [21] Kurihara, M., Matsuka, N., Fusaoka, Y., Henmi, M. *Proceedings Water Reuse & Desalination Conference*, Suntec Singapore, Singapore, 25–27 February 2003.
- [22] Yamamura, H. *Proceedings the 2nd International Conference on Application of Membrane Technology*, Beijing, China, 27–29 September 2002.
- [23] Kurihara, M., Henmi, M., Tomioka, H., Kawakami, T. *ICOM 2008*, Honolulu, Hawaii, 13–18 July 2008.

Biographical Sketches



Dr. Masaru Kurihara, currently an advisor to Toray Industries, Inc., holds posts ranging from director to managing director in many organizations: Director of International Desalination Association (IDA), President of Asia Pacific Desalination Association (APDA), President of Japan Desalination Association (JDA), and Managing Director of Japan Membrane Separation Association (AMST). Dr. Kurihara completed his doctoral dissertation in 1970 at the University of Tokyo; he graduated from Gunma University, Technical Department of Applied Chemistry in 1963. He pursued membrane research during 1970–72 at the University of Iowa, USA, as a research associate.

His professional experience began in 1963 when he joined Toray Industries, Inc. During 1963–70, he carried out polymer research at the Basic Research and Pioneering Research Laboratories. In 1992, he was a research fellow of Toray Ind. Inc. He was both director and general manager at Chemicals Research Lab. and Polymers Labs during 1997–2001. From 2002 to 2005, he was a visiting professor of Kyoto University. Almost during the same time (2003), he also held the position of senior director at the Water Treatment Division Water Treatment, Technology Center and R&D Division. Between 2005 and 2006, he also held another professorship (visiting professor of Tianjin Polytechnic University and Shanghai, Jiao tong University). In 2006, he resigned from Toray but stayed on as its advisor. In 2007–08, he was appointed the Council Member of Industry Competiveness by Keidanren.

The awards received by Dr. Kurihara during his career include Technical Award of Chemical Society of Japan (1992); Technical Award of Japan Chemical Engineering Society (1994); Technical Award of Japan Seawater Society and President Award of International Desalination Association (both in 2002); and Production Award of Okouchi Memorial (2003).

Dr. Kurihara's major fields of interest are membrane separation and membrane water treatment process.



Mr. Hiroki Tomioka is presently a research associate at the Global Environment Research Laboratories, Toray Industries, Inc. In 1992, he graduated from Waseda University, Faculty of Science and Engineering, Department of Chemistry and obtained his MSc in science in 1994 from Waseda University. He joined Toray Industries, Inc. in 1994. From 1994 to 2002, he was a researcher at Basic Research Laboratories. Since 2002, he has been working at Global Environment Research Laboratories. His major fields of interest are membrane separation and organic chemistry.

2.03 Current and Emerging Developments in Desalination with Reverse Osmosis Membrane Systems

J-C Schrotter, S Rapenne, J Leparc, P-J Remize, and S Casas, Water Research Center of Veolia Environnement, Maisons Laffitte, France

© 2010 Elsevier B.V. All rights reserved.

2.03.1	Introduction	36
2.03.2	Context	36
2.03.3	RO Unit	38
2.03.3.1	RO Membranes Characteristics	38
2.03.3.2	Membrane Fouling and Autopsy	42
2.03.3.3	Membrane Cleaning	44
2.03.4	Pretreatments	46
2.03.4.1	Introduction	46
2.03.4.2	Water Quality Parameters and Analytical Methods	46
2.03.4.2.1	Inorganic characterization	46
2.03.4.2.2	Characterization of NOM with LC-OCD chromatography or size-exclusion chromatography	46
2.03.4.2.3	Flow cytometry for enumeration of picophytoplankton and bacteria	47
2.03.4.2.4	Global measurement of fouling potential	49
2.03.4.3	Raw Water Quality	50
2.03.4.3.1	Ion content	50
2.03.4.3.2	Natural organic matter	51
2.03.4.3.3	Phytoplankton and algal content of raw SW	52
2.03.4.3.4	Correlations between conventional SW quality parameters and advanced analytical tools	52
2.03.4.4	Performances of Various Pretreatment Processes	53
2.03.4.4.1	General presentation of pretreatment processes	53
2.03.4.4.2	Performances of pretreatment processes	55
2.03.5	Reducing Cost, Energy Consumption, and Environmental Impact	58
2.03.5.1	Energy Consumption	58
2.03.5.1.1	Energy-saving devices	58
2.03.5.1.2	PX Pressure Exchanger® Technology	59
2.03.5.1.3	DWEER™ work exchanger	60
2.03.5.2	Environmental Impact	60
2.03.5.3	Current Trends in Operations for Cost Saving	61
2.03.5.4	Other Trends	61
2.03.6	Conclusion	61
References		62

Abbreviations

AFM	Atomic Force Microscopy	EDS	Energy Dispersive Spectroscopy
BW	Brackish Seawater	EPS	Exo-Polymeric Substances
CIP	Cleaning In Place	EMF	Electro-Magnetic Field
DOC	Dissolved Organic Carbon	FTIR	Fourier Transform Infrared Spectroscopy
DMF	Dual-Media Filtration	HNA	High Nucleic Activity
DO	Direct Osmosis	HP	High Pressure or Hydrogen Palladium
DP	Pressure Drop	ICP-OES	Inductively Coupled Plasma – Optical Emission Spectrometry

LC-OCD	Liquid Chromatography – Organic Carbon Detection	RO	Reverse Osmosis
LNA	Low Nucleic Activity	SEM	Scanning Electron Microscopy
LP	Low Pressure	SDI	Silt Density Index
MF	Microfiltration	SW	Seawater
MFI	Modified Fouling Index	TDS	Total Dissolved Solids
NF	Nanofiltration	TOC	Total Organic Carbon
NOM	Natural Organic Matter	UF	Ultrafiltration
		VBNC	Viable But Non-Cultivable

2.03.1 Introduction

Desalination by reverse osmosis (RO) is by far the most widespread application for membrane in water treatment. It is capable of removing nearly all colloidal and dissolved matter from an aqueous solution, producing a brine concentrate and an almost pure water permeate.

RO is based on the ability of certain polymer-based materials to separate water from dissolved substances. The objective over the past three decades has been to enhance the transport of water molecules, while minimizing the one of any dissolved substances. By applying a pressure difference across the membrane, the water contained in the feed is forced to permeate through the membrane. In order to overcome the feed-side osmotic pressure, high feed pressure is required, which commonly ranges from 55 to 75 bar for seawater (SW) desalination application. RO-based desalination plants include the following stages, as described in [Figure 1](#):

- water intake;
- pretreatment;
- membrane separation unit, including bore treatment if required;
- energy recovery system;
- posttreatment; and
- concentrate (treatment and) disposal.

An advanced control system is also used to operate the plant.

The growing interest of RO membrane for SW desalination applications is spurring all market players – RO membrane and system manufacturers as well as plant design engineers and operators – to concentrate their research and development (R&D) efforts on three main topics:

1. membrane products and processes;
2. pretreatment processes to ensure suitable characteristics of membrane feed streams; and
3. reducing cost, energy consumption, and environmental impact.

2.03.2 Context

Due to the world water crisis, SW desalination has been a growing industry for the past few decades. The growth of this market is exponential, as can be seen in [Figure 2](#), cumulating thermal and reverse osmosis SW desalination processes.

Although thermal desalination has dominated the market for more than 30 years, the tendency now seems to reverse since RO has become the dominant technology in use for SW and BW desalination. As shown in [Figures 3\(a\) and 3\(b\)](#), the overall capacity of SW and BW RO plant reaches $56.5 \times 10^6 \text{ m}^3 \text{ d}^{-1}$, representing 51% of the market, while the number of membrane desalination installations accounts for 78% of all desalination facilities. In fact, this ratio is likely to change, since most of the new contracted desalination plants are based on membrane technology ([Table 1](#)). Large SWRO plants, already in service, have proved to be cost effective. Despite new plants in Europe, the Gulf area has still the greatest installed capacity. Due to prolonged drought conditions, new plants using membrane technology are now under construction in Australia (Gold Coast, Kurnell). One of the biggest tenders has been launched in Melbourne in 2008 for a $600\,000 \text{ m}^3 \text{ d}^{-1}$ RO desalination plant. The global growth for RO desalination from 2005 to 2015 is expected to be around 100%.

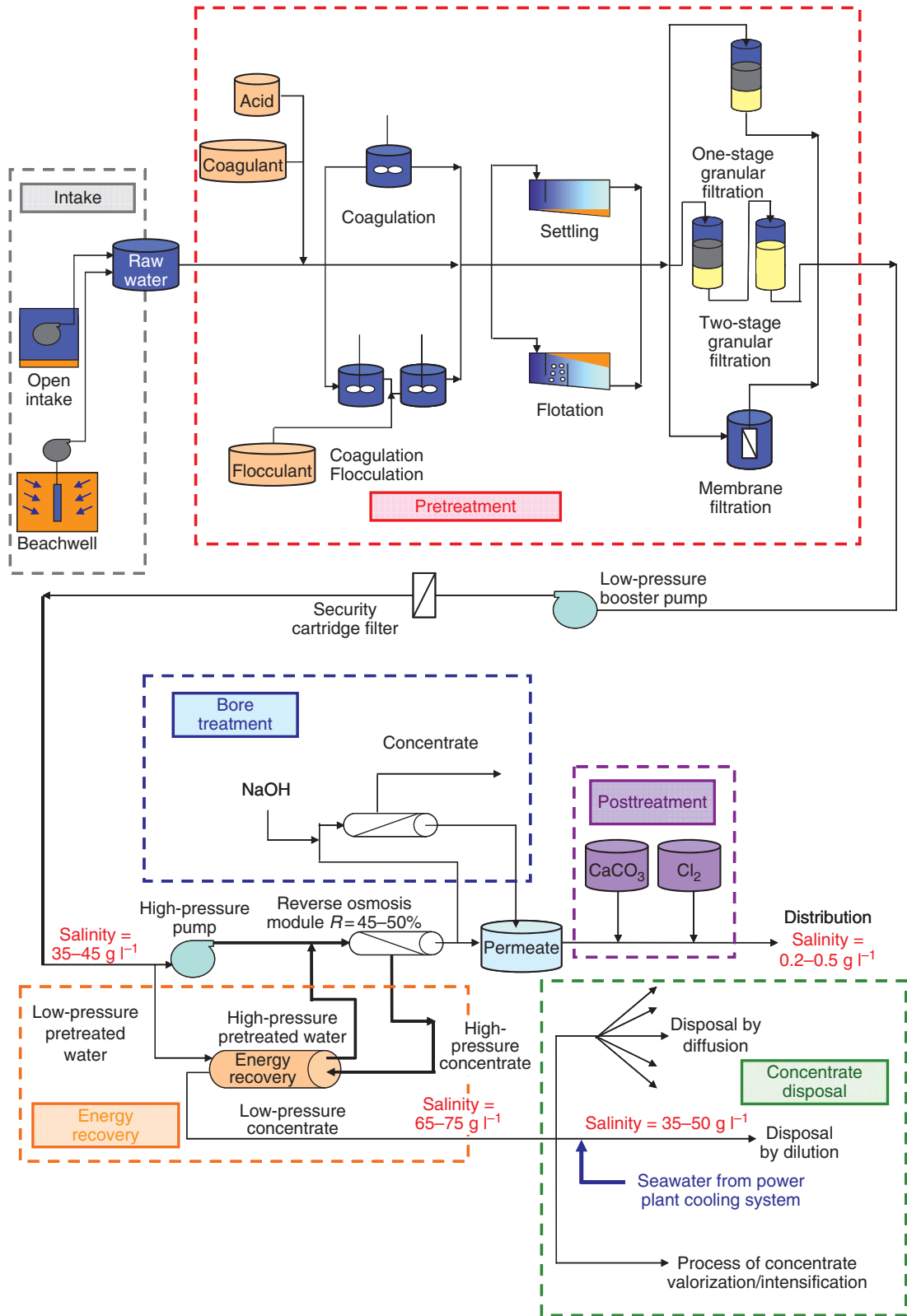


Figure 1 Schematic flow diagram of a seawater reverse osmosis desalination plant.

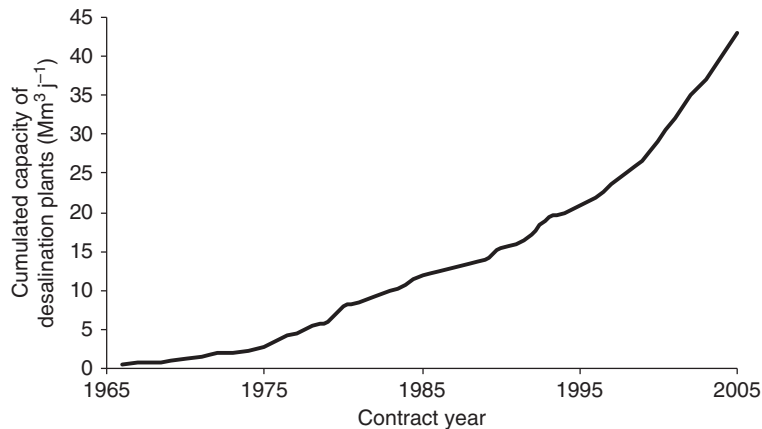


Figure 2 Global installed desalination capacity since 1966.

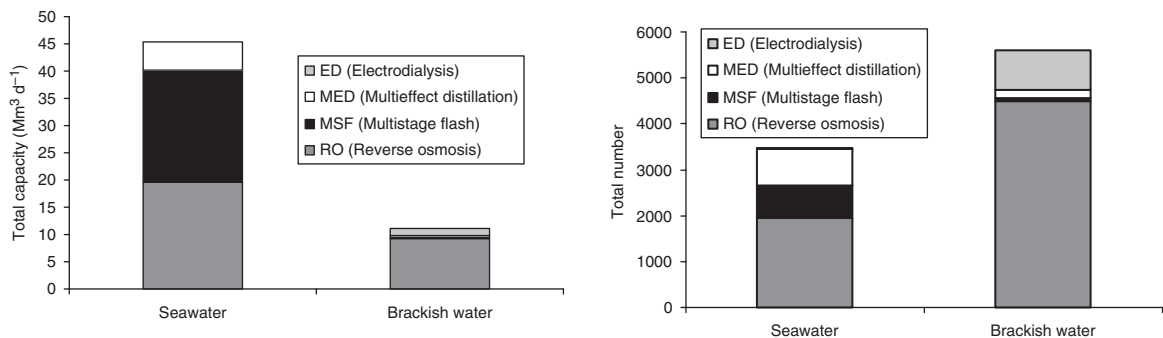


Figure 3 Desalination processes repartition in 2007 expressed (a) in plant capacity or (b) in plants number. From Global Water Intelligence, <http://www.desaldata.com> (accessed November 2009).

2.03.3 RO Unit

2.03.3.1 RO Membranes Characteristics

Historically, in the 1960s, the first membrane desalination plants were operated with hollow-fiber cellulose-acetate-based materials produced according to the formulation of Loeb and Sourirajan. Due to the low mechanical resistance of this type of membranes, Dupont de Nemours developed hollow-fiber polyamide-based material in the 1970s. Nowadays, although hollow-fiber membrane has managed to maintain its presence in this market with Toyobo Company Ltd. (Japan), the future belongs to spiral-wound membranes, because the intense competition in this segment is spurring further developments.

Major developments are based on thin-film composite, spiral-wound membranes with the 8-inch-diameter module that represent a standardized product today. Dow and Hydranautics are the two market leaders (Figure 4), followed by Toray. Koch

Membrane Systems (USA), GE Osmonics (USA), and Saehan (Korea) are also key market shareholders.

The most recent technological improvements are aimed at developing spiral-wound membranes with the following characteristics:

- *Membranes with minimized clogging and fouling by colloidal solids and microorganisms, respectively.* This can be achieved by ensuring the smoothest possible membrane surface to prevent the occurrence of tiny dead zones, and by reducing the electrostatic charge of the membrane surface to limit the attraction of elements of the opposite charge.
- Membranes with high salt rejection factors, but with the lowest possible energy requirement for operation.
- Membranes tolerant to oxidants, especially chlorine.
- Membranes able to withstand high operating pressure levels.

Table 1 Main RO seawater desalination plants

Site	Capacity $m^3 d^{-1}$	Start-up year
Ashkelon (Israel)	320 000	2005
San Francisco (US)	300 000	2008
Hadera (Israel)	275 000	2010
Kurnell (Australia)	250 000	2010
El Hamma (Algeria)	200 000	2008
Beni Saf (Algeria)	200 000	2008
Tlemcen Hounaine (Algeria)	200 000	2010
Valdelentisco (Spain)	200 000	2007
San Diego (US)	190 000	2006
Aguilas (Spain)	180 000	2007
Fujairah (UAE)	170 000	2003
El Prat del Llobregat (Spain)	165 000	2009
Fujairah 2 (UAE)	136 500	2010
Tuas (Singapore)	136 000	2005
Al Taweelah (Saudi Arabia)	136 500	2008
Point Lisas (Trinidad)	130 000	2002
Medina/Yambu (Saudi Arabia)	128 000	1995
Kwinana, Perth (Australia)	150 000	2006
Gold Coast (Australia)	125 000	2009
Carboneras, Almeria (Spain)	121 000	2003
Tampa Bay, Florida (US)	110 000	2003

From Global Water Intelligence, <http://www.desaldata.com> (accessed November 2009).

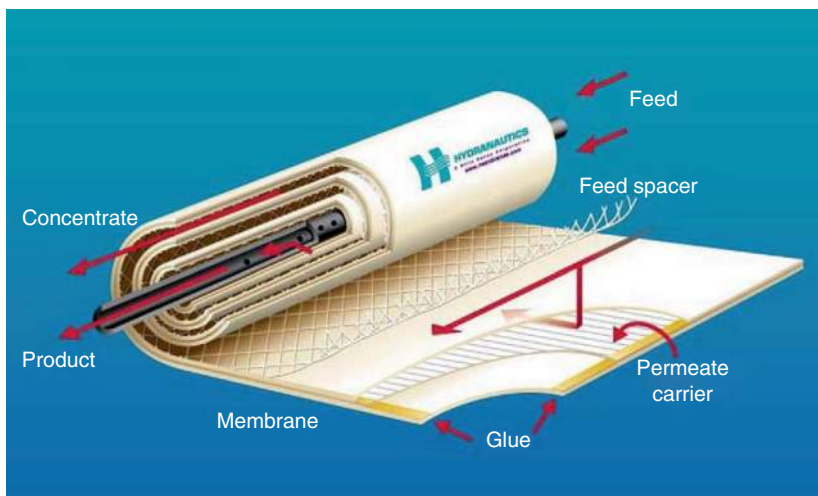


Figure 4 Spiral-wound modules.

- Membranes configured in elements designed to offer the greatest possible surface area, thanks to increased size.

Furthermore, three major advances have been achieved with the market launch of:

- Membranes able to withstand feedwater pressures of 84 bar, compared to the typical service pressure of 70 bar for

conventional membranes. This new specification paves the way for the design of two-stage systems in which the brine concentrate from the first stage – equipped with conventional membranes – becomes the feed stream for a second stage equipped with hydrogen palladium (HP) membranes. A booster pump raises the pressure in order to overcome the higher mean osmotic pressure of the second-stage brine concentrate. This design, developed by Toray, gives

recovery ratios of 60%, versus the 40–50% attainable using conventional single-stage systems.

- *Larger spiral-wound elements.* For example, the Koch Membrane Systems company has introduced large elements (diameter: 18" (457 mm) × length: 61" (1.549 m)), versus standard elements of 8" (203 mm, diameter) × 40" (1016 mm, length). The surface area of the Koch membranes is 7.5 times larger than that of typical elements. This specification allows for a smaller system footprint and reduces the number of pressure vessels and seals between elements. Dow-Filmtec (USA), Hydranautics (USA and Japan), Toray (Japan), and Saehan (Korea) followed suit with the launch of 16" (406 mm, diameter) elements. Also noteworthy is the market launch of medium-pressure (40 bar) and high-pressure (HP; 80 bar) tubes to house the 16" (406 mm) and 18" (457 mm) elements. In addition, a new proprietary RO system by GrahamTek Singapore Pte Ltd has been launched. GrahamTek claims that these innovations prevent fouling and scaling during operation, eliminating the need for chemicals and achieving higher performances than conventional water-treatment systems. This system is based on patented electromagnetic field (EMF) coil and flow distributor that are incorporated into a commercial 16" (406 mm) spiral-wound RO elements (Figure 5). The integrated flow distributor is incorporated at the front end of the spiral-wound membrane elements and generates a higher flux with improved recoveries through the continuous disruption of the concentration polarization on the membrane surface releasing micro-bubbles, thereby improving the cross-flow



Figure 5 Eight-inch spiral-wound membranes vs. 16-inch spiral-wound modules.

shear force, easing mass transfer across the membrane surface. The micro-bubbles thus generated actively scour the membrane surface, preventing foulants from settling. The EMF device is encapsulated within the pressure vessels and is applied throughout the length of each vessel and prevents fouling on the membrane surface by inhibiting active crystal formation. Crystals that form under these conditions are amorphous and therefore do not grow or scale. The water in the feed channel is encapsulated by the EMF, generating a net movement in the direction of the concentrated stream. All the ions within the concentrated stream become electrically charged, inducing the feed channel to act as a semiconductor, which moves forward in the direction of the magnetic field.

Nevertheless, the benefits of these innovations still need to be confirmed and validated as only few side-by-side pilot-plant trials have been performed today.

- *Membranes with improved total dissolved solid (TDS) rejection or with higher productivity.* In standardized test conditions, some membranes achieved salt rejection factors of 99.75–99.80%: the usual factor is 99.4% (Figures 6(a) and 6(b)). In the case of very warm and highly saline water, this gain means that a second pass is not needed to produce permeates with TDSs, chlorides, and sulfate values compatible with drinking water quality requirements.

Historically, the rejection of 99.40–99.70% (which is required to achieve acceptable permeate quality of 350 ppm TDS) was only available with elements having a flow rate of 23 000 m³ d⁻¹ (6000 gpd) or less. In 2004, Bush and Mickols [2] described new commercially available elements with higher flow rates (28 000–34 000 m³ d⁻¹, 7500–9000 gpd) and with a NaCl rejection of 99.70%. In 2008, ultra-low-energy RO modules have been introduced into the market with 41 500 m³ d⁻¹ (11 000 gpd) and 99.70% NaCl rejection.

Other recent developments are:

- *Membranes with high boron rejection factors.* This characteristic is required by certain irrigation applications, particularly when the water is used to irrigate fruit trees, because boron causes spots on the fruit, thus reducing its commercial value. In some projects, the required boron level is so low (typically 0.5 mg l⁻¹) that an additional treatment, such as selective boron ion-exchange resin or typically a second pass RO fed with a high pH feedwater quality, is needed. The increase in pH is important

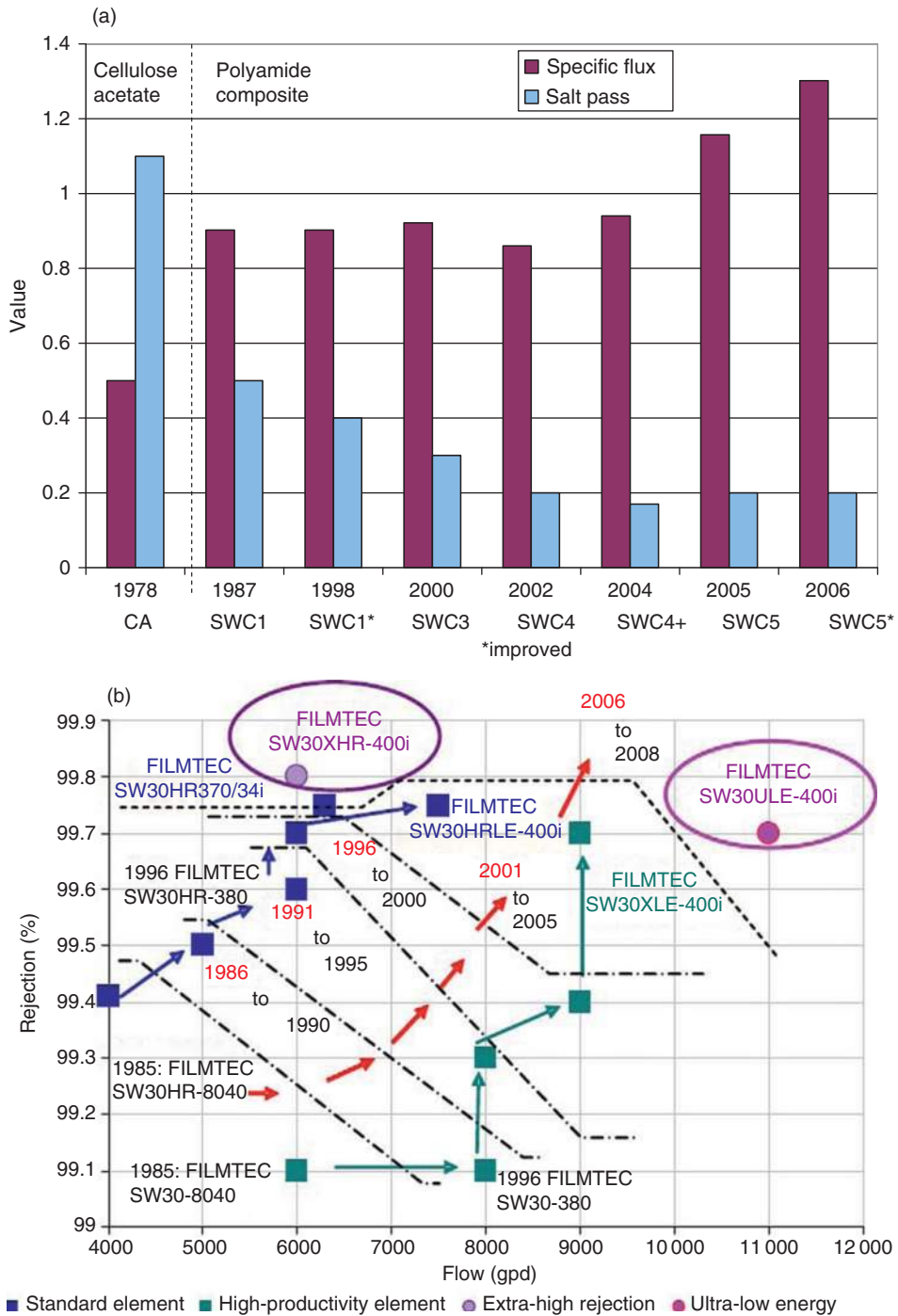


Figure 6 (a) Evolution of performances of Hydranautics seawater reverse osmosis (SWRO) membranes. (b) Evolution of salt rejection and productivity of Filmtec™ SWRO elements in standard conditions.

as RO membranes are very efficient at removing charged species such as the borate ion, rather than neutral molecules such as boric acid and as the pK_a of $H_3BO_3/H_3BO_2^-$ is 9.2; therefore, the equilibrium

$H_3BO_3 \rightleftharpoons H_3BO_2^- + H^+$ is typically toward the left at standard SW pH 8. Increasing the pH shifts the equilibrium $H_3BO_3 \rightleftharpoons H_3BO_2^- + H^+$ to the right in order to have the dominant form of boron as borate

H_3BO_2^- and, therefore, improves boron removal at the second pass as shown in **Figure 7**.

- *Internally staged element design* [3, 4]. Due to the high fouling tendency in the front position of the vessel, the flow has to be reduced. At the same time, the overall production of the vessel has to be kept constant. The internally staged design uses elements of relatively low permeability in the first positions and high flow elements in the rear of the vessel. The effect is similar to a two-stage design which has a booster in the second stage or a permeate backpressure in the first stage. With these lower flow elements in the lead position, the design will not violate engineering recommendations and the high-productivity elements will achieve the same amount of permeates at a lower pressure (**Figure 8**).

- *Locking systems to interconnect elements and prevent slippage typical of interconnectors fitted with O-ring joints.*

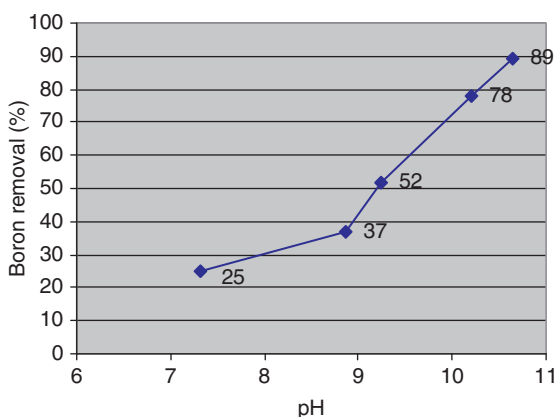


Figure 7 Pilot plant experiment for boron removal vs. pH.

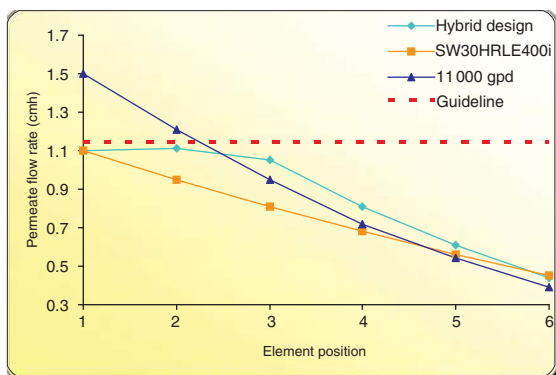


Figure 8 Permeate flow rate of an internally staged element design. Courtesy of The Dow Chemical Company.

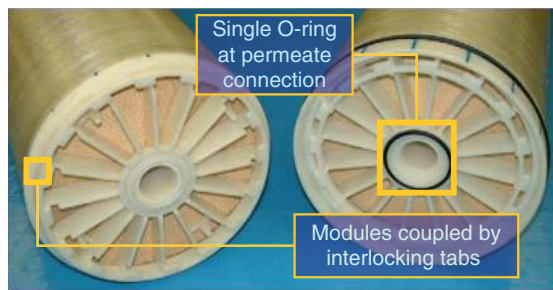


Figure 9 Interlocking system. Courtesy of The Dow Chemical Company.

The new locking devices improve leak control, thereby ensuring consistent permeate quality (**Figure 9**).

2.03.3.2 Membrane Fouling and Autopsy

SW contains microorganisms, organics, and minerals mixed in a saline water matrix. Scaling, organic fouling, particulate fouling, and biofouling are the four major types of fouling that can occur on RO membrane surfaces [5]. The fouling mechanism at the membrane surface is initiated by a concentration gradient that occurs at the separating surface due to the concentration polarization phenomenon. Within this boundary layer, salts may precipitate and suspended solids can start to deposit on the membrane surface, leading to fouling.

Several inorganic scales may be present in fouled RO membranes: calcium carbonate (CaCO_3), calcium sulfate (CaSO_4), and barium sulfate (BaSO_4). Calcium carbonate is the most likely inorganic scale to be deposited.

Deposit of colloidal/particulate species can also be observed, depending on the feedwater quality and the pretreatment before the RO unit: ferric or aluminum oxide/hydroxide, silica, organic debris, colloidal particles, and humic acids [6].

Unlike the other types of fouling, it is difficult to both understand and prevent biofouling. Examination of numerous membranes has led to conclude that biofouling is the most common type of fouling encountered, as shown in **Figure 10**.

This is primarily due to the accumulation of extracellular polysaccharide substances (EPSs) secreted by microorganisms entering the membranes in the feedwater. This adhesive polysaccharide material first accumulates at the membrane surface and

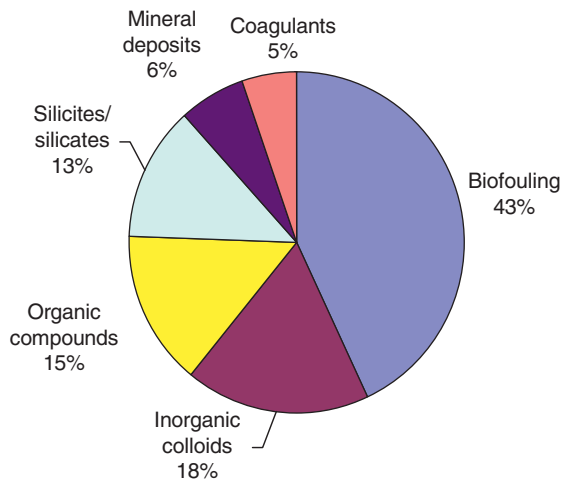


Figure 10 Repartition of fouling types on seawater reverse osmosis (RO) membranes.

can act as a trap for other organic debris and as a source for microbiological growth. Then, these biopolymers are excreted by the bacteria entrapped in the biofilm at the membrane surface. This results in a consolidated structure that is difficult to remove.

Different types of fouling may be found at different locations along the length of an element, along the modules of a pressure vessel, and at different stages of the plant (**Figure 10**). For example, due to concentration factors, scale will deposit first at the outlet end, whereas suspended matter will remain in the early stages of a pressure vessel.

Control of membrane fouling is essential for successful long-term performances of desalination plants. Therefore, an identification of the foulants is necessary in order to use the most adequate pretreatment and/or cleaning sequences. A membrane autopsy provides information on the history of the operating membrane facility, which can help resolve operational problems.

In the autopsy process, membranes are cut open and their surfaces are scientifically examined. The autopsy analyses can include chemical, microbiological, and microscopic examinations, as well as the use of cross-flow test cells to characterize membrane performances. The autopsy is a destructive procedure. The most significant reason for sending membrane for autopsy is usually a fall-off in system performances. This fall-off can be either an increase in differential pressure or a decrease in permeate flux or permeate water quality.

This examination requires a sacrificial membrane element to be removed from the plant for destructive analyses.

After removal from the plant, the element must be kept wet and wrapped immediately in a plastic bag and sent to the autopsy laboratory. No preservative is added at this stage, as microbiological investigations cannot be performed otherwise. The module must be dissected as soon as possible after removal from the plant. If the element cannot be dissected immediately, it is kept wet and stored in a cool place.

At the autopsy laboratory, the fiberglass casing is first inspected in order to put into evidence any mechanical damages. Such damages can be an indication of excessive pressure drops across the membrane due to a high degree of fouling.

After this inspection, the membrane ends and casing are removed and the leaves are unwound (**Figure 11**). Deposit samples are collected for analysis from a known surface area. A wide range of methods is available for the analysis of membranes and deposit. Standard analyses are usually conducted to identify the type of fouling. Advanced analyses can be performed if more complete information is needed.

Membrane samples can be tested in a flat-sheet test rig to compare their performances in terms of flux and salt rejection against a clean unused membrane of the same model.

Loss on ignition, total organic carbon (TOC), and dissolved organic carbon (DOC) measurements give general information on the organic content in the deposit. More specific analyses, such as Fourier transform infrared spectroscopy (FTIR) or liquid chromatography-organic carbon detection (LC-OCD), presented in a more detailed manner in Section 2.03.4.2, can help identify the specific structures implied



Figure 11 Membrane dissection.

in the fouling phenomenon. As mentioned before, EPSs (exopolymeric substances) are usually found to be an abundant component of the fouling layer.

Inductively coupled plasma optical emission spectrometry (ICP-OES) analyses allow quantifying most of the inorganic components. X-ray diffraction and energy dispersive spectroscopy (EDS) can help in the final diagnosis. High iron concentrations are often observed in the membrane deposit. They likely originate from the pretreatment since ferric chloride is usually used as a coagulant. Aluminosilicates have also been detected in many autopsies of SWRO membranes.

Microscopic methods, such as atomic force microscopy (AFM), scanning electron microscopy (SEM), and confocal laser microscopy, can be powerful tools; however, depending on the magnification, their use must be conducted with care since information remains very local.

For example, the SEM is a microscopic method capable of producing very high magnification images of a membrane surface, as shown in **Figure 12**. Due to the manner in which the image is created, SEM images have a characteristic three-dimensional appearance and are useful for judging the surface structure of the sample. Microbial structures have been observed using this tool.

Bacteria counts give an indication of the degree of biofouling on the membrane surface. Bacteria in SW are usually in the viable-but-noncultivable (VBNC) state. Therefore, cultivating methods cannot be used in this case and total counts are usually performed using 4'-6-diamidino-2-phenylindole (DAPI) staining. Active cells are also enumerated based on their respirometric activity (chlorotetracycline (CTC)

staining). Cultures on specific media can also be performed to help identify the implied bacteria, such as iron- or manganese-oxidizing bacteria (**Figure 13**).

2.03.3.3 Membrane Cleaning

As a consequence of membrane fouling, the effectiveness of the membrane filtration process decreases. The diagnosis can be established through a monitoring of membrane performances. A decrease in membrane flux or retention is an indicator of membrane fouling, which will cause an increase in the energy demand. To prevent these negative effects on the membrane process, appropriate membrane cleaning actions need to be applied periodically.

The moment and frequency of membrane cleaning is essential. The frequency of cleaning will be determined by the rate of fouling. Cleaning cannot be performed too often from an economical point of view and due to a risk of membrane deterioration. However, if some limits are reached, cleaning becomes unavoidable.

In general, cleaning is recommended when any of the following changes by 10–15% (Hickman [7]):

- an increase in salt rejection,
- an increase in pressure drop (DP),
- an increase in feed pressure, or
- a decrease of product flux.

The pressure drop, corresponding to the longitudinal pressure drop along the pressure vessel, is usually the most-used criterion as it is the most sensitive parameter for fouling detection. Usually, a decrease in permeate flux or retention follows an

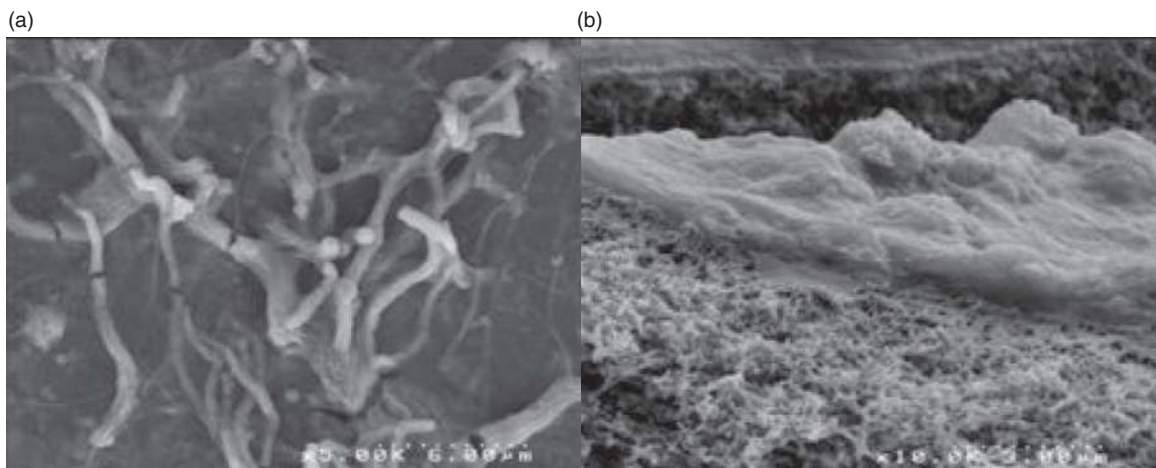


Figure 12 Scanning electron microscopy (SEM) pictures: (a) membrane surface ($\times 5000$); and (b) cross section ($\times 10\,000$).

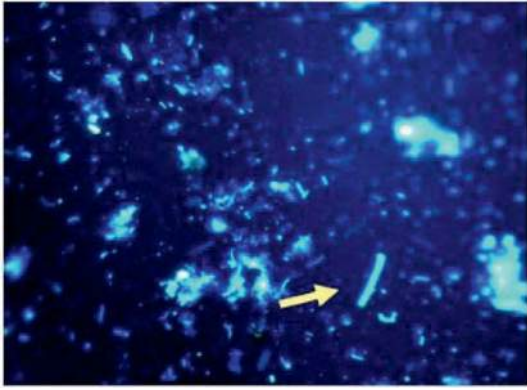


Figure 13 Analysis by epifluorescence microscopy of the deposit after 4'-6-diamidino-2-phenylindole (DAPI) staining.

increase in pressure drop. An example is given in **Figures 14 and 15**.

For spiral-wound elements, few cleaning methods are available. Unlike hollow fibers, mechanical or hydrodynamic cleanings cannot be performed. Therefore, chemical cleaning methods are mainly used for the removal of foulants at the membrane surface.

Chemical cleaning agents are used to complexate, oxidize, inactivate, solubilize, hydrolyze, and denaturalize the membrane fouling layer. During cleaning, the membrane installation is temporarily

taken out of operation and cleaned by a cleaning-in place (CIP) procedure with different cleaning agents. CIP can be performed on any part of the membrane installation according to the requirement. It is usually performed on one membrane stage or on the process line at the time.

There is a variety of different cleaning chemicals available for membrane cleaning. However, the properties of some chemicals are not suitable or compatible with some membrane materials. Cleaning agents are selected depending on function of the type of foulants to be removed typically identified by membrane autopsy. The usual cleaning agents are acids, alkalines, complexing agents or anti-precipitants, biocides, detergents, and enzymes. For example, weak acids are known to help remove iron and metal oxides, whereas the biofilm is usually cleaned with an alkaline-based cleaner.

After selecting the adapted cleaning agents, several cleaning conditions must be adjusted: the temperature and concentration of cleaning solutions, cross-flow velocity, and transmembrane pressure during membrane cleaning. Moreover, the cleaning sequence must be optimized with care to have a better action on the removal of foulants. The order of cleaning-agent application, the duration of each step, and the rinsing time will be chosen as function of the desired effect. Procedures may consist of a

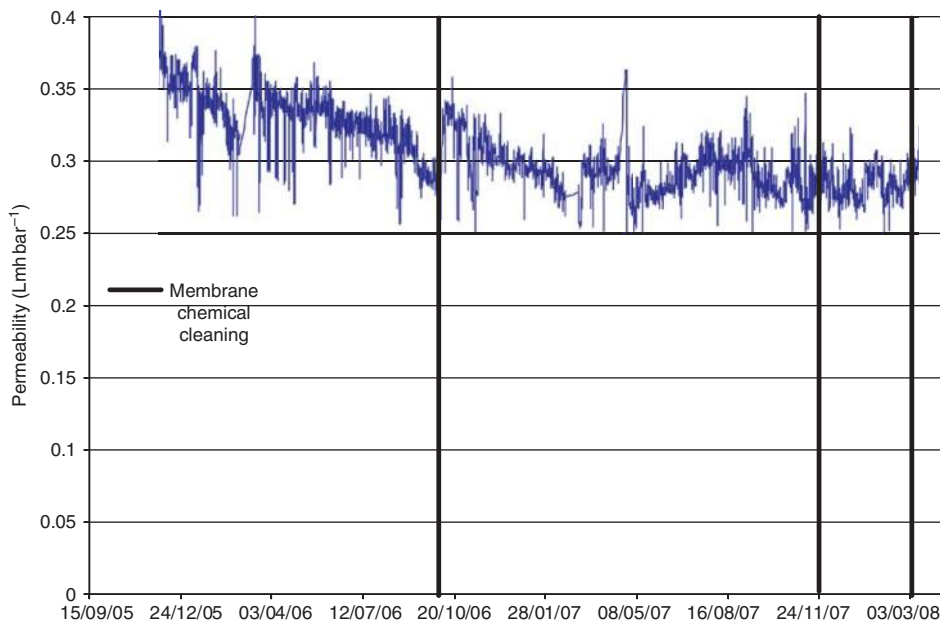


Figure 14 Permeability evolution on a reverse osmosis (RO) unit.

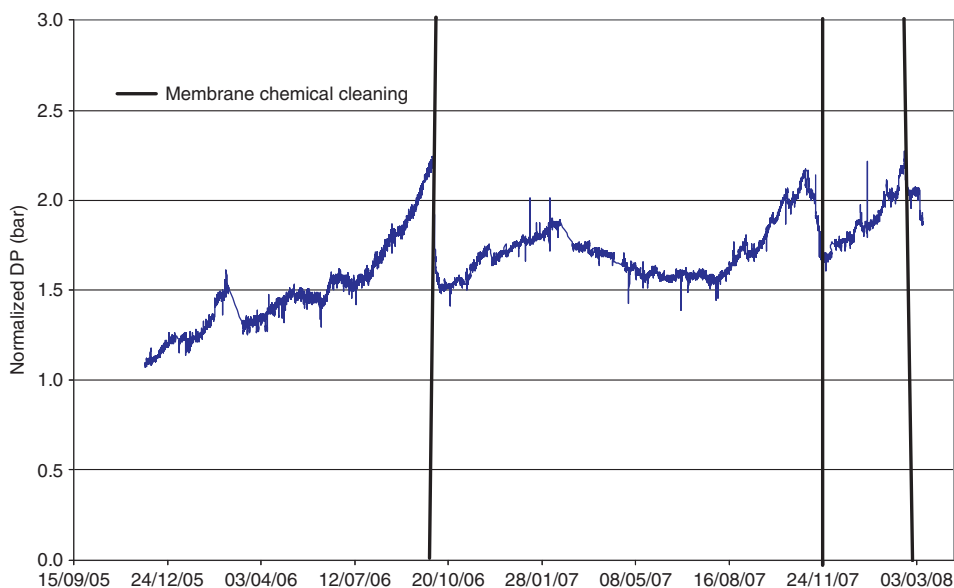


Figure 15 Normalized DP evolution on a reverse osmosis (RO) unit.

two-stage cleaning with a soaking time in between recirculation of the cleaning solution.

2.03.4 Pretreatments

2.03.4.1 Introduction

Design and operation of SWRO plants strongly depend on the raw SW quality to be treated. To exceed the 3-year guarantee given by manufacturers of RO elements and extend membrane life to 5 or 10 years, the feed stream must be pretreated to prevent, or at least limit, membrane clogging, scaling, and fouling. The selection of the best pretreatment technology depends on the raw SW quality and its variations.

To date, membrane manufacturers have greatly emphasized on the silt density index (SDI) as a surrogate parameter for water quality to prevent fouling on RO membranes. However, this SDI measurement is based on the reduction of permeability with time of a water sample through a microfiltration (MF) membrane. As the transfer mechanisms through an RO membrane are very different from those occurring through an MF membrane, it is highly likely that the fouling mechanisms and occurrences will greatly differ from an SDI membrane and an RO membrane. Therefore, while the SDI measurement can be a useful indicator with respect to the particulate content and MF fouling compounds, this index does not

provide any information regarding the nature of the foulants passing through a 0.45- μm membrane and the risks of biofouling. Advanced analytical methods are therefore needed to characterize raw SW samples as well as the performance of SW pretreatment processes. Advanced analytical tools have recently been developed focusing mainly on: (1) inorganic characterization, (2) characterization of the natural organic matter (NOM), (3) enumeration of picophytoplankton and bacteria through flow cytometry, and (4) global measurement of fouling potential.

2.03.4.2 Water Quality Parameters and Analytical Methods

2.03.4.2.1 Inorganic characterization

The ion makeup of the raw SW sources is characterized according to the analytical methods listed in [Table 2](#).

2.03.4.2.2 Characterization of NOM with LC-OCD chromatography or size-exclusion chromatography

The LC-OCD system consists of a size-exclusion chromatography column, which separates hydrophilic organic molecules according to their molecular size [8, 9]. The underlying principle is the diffusion of molecules into the resin pores, which means that larger molecules elute first as they cannot penetrate the pores very deeply, while smaller molecules take

Table 2 Analytical methods for inorganic characterization

Parameter	Analytical method
Cations (sodium, potassium, calcium, magnesium, strontium, and baryum)	ICP – optical emission spectroscopy
Boron	Spectrophotometry
Chloride	Potentiometry
Bromide	Ionic chromatography
Hydrogenocarbonate	Alkalimetric titration
Sulfate	Ionic chromatography
Silica	Colorimetry
Fluoride	Ionometry

more time to diffuse into the pores and out again. The separated compounds are then detected by two different detectors: an ultraviolet (UV) detector (absorption at 254 nm) and a DOC detector (after inorganic carbon purging). Depending on the size of the molecules, the composition of the organic matter can be obtained. With a bespoke algorithm program, the different peaks can be integrated to evaluate the proportion of each organic fraction. The DOC measurement can be carried out using a bypass mode. In this case, the samples go straight through the TOC reactor and analyzer. **Figure 16** depicts a typical chromatograph with the different peaks and their associated organic fractions.

2.03.4.2.3 Flow cytometry for enumeration of picophytoplankton and bacteria

Picophytoplankton species corresponds to the smaller-size species of phytoplankton (size ranging from 0.2 to 10 μm). The concentrations of picophytoplankton species are interesting to monitor in both raw and pretreated SWs as

1. picophytoplankton species are by very far the most abundant phytoplankton species in SW

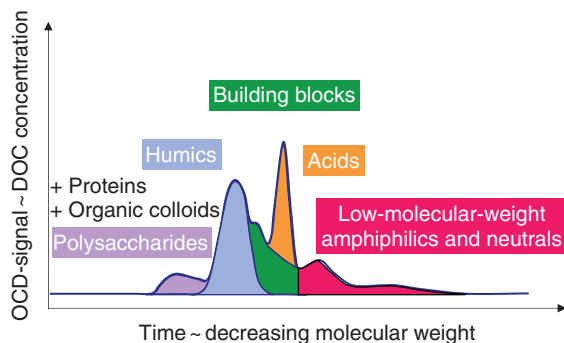


Figure 16 Chromatograph obtained with liquid chromatography-organic carbon detection (LC-OCD).

- (concentration between 10^3 and 10^5 ml^{-1}) as compared to phytoplankton species with a size $>100 \mu\text{m}$; and
2. phytoplankton species with a size $>100 \mu\text{m}$ are very likely to be removed through conventional pretreatment processes (e.g., coagulation + dual-media filtration), and through the cartridge filters located upstream of the RO membrane units, and, therefore, smaller-size algal organisms, such as picophytoplankton, are the most likely to pose a threat to the RO membranes.

The main picophytoplankton species are:

- nanoeukaryotes: algal species $>2 \mu\text{m}$ and
- smaller species $<2 \mu\text{m}$: *Synechococcus*, Picoeukaryotes, and *Prochlorococcus*

Flow cytometry is an individual, qualitative, and quantitative characterization technique for particles (cells, bacteria, etc.) in a liquid field. The sample is injected in a measurement chamber by a sheath fluid. The whole flows to a circular neck and, thanks to hydrodynamic convergence, cells are separated in a sharpened capillary tube and cells cross a laser beam light. Optical and physical signals are then collected by four photomultipliers. Two tubes detect the light diffused under two different angles: forward-angle light scatter (FSC), for the light diffused under the axis of the incident ray and side-angle light scatter (SSC), for the light diffused with a 90° angle. The two other tubes detect fluorescence emissions. Populations are hence differentiated according to their signals of diffusion and fluorescence [10].

For picophytoplankton and algae enumeration, samples are divided into two aliquots and fixed with formaldehyde (2% final concentration) and then frozen in liquid nitrogen. Prior to analysis, the samples are rapidly thawed. Samples are then analyzed using a FACSort flow cytometer (Becton Dickinson).

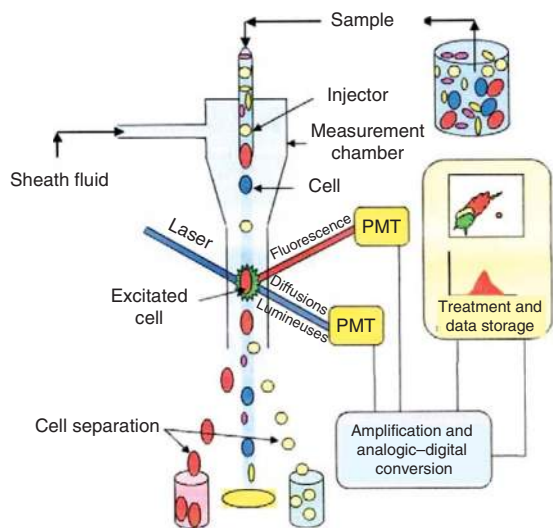


Figure 17 Principle of the flow cytometry technique for enumeration of picophytoplankton and bacteria in seawater.

Figure 17 shows the principle of flow cytometry used for phytoplankton and algal counts. For all experiments, FACSFlo is used as sheath fluid. The first aliquot is analyzed directly and used for

autotrophic population counts. The second aliquot is incubated for 15 min in the presence of SYBR Green I (SYBR-I; 1:10 000 final concentration; Molecular Probes), which is a dye that stains DNA, in order to obtain bacterial counts.

Parameters acquired on nonincubated samples are cell concentration, FSC, orange phycoerythrin fluorescence, and red chlorophyll fluorescence. On SYBR-I-stained samples, green fluorescence from the DNA-dye complex is also measured. For unstained samples, pico- and nanoeukaryotes are discriminated from *Synechococcus* cyanobacteria on the basis of the orange phycoerythrin fluorescence. *Prochlorococcus* has very low red chlorophyll fluorescence, typical of oligotrophic surface waters and cannot be easily differentiated from background noise. On SYBR-I-stained samples, both picoeukaryotes and *Synechococcus* cyanobacteria could be discriminated from heterotrophic bacteria because of their red chlorophyll fluorescence. Data acquisition is performed at a high rate for unstained samples ($90\text{--}100\ \mu\text{l min}^{-1}$) and at a low rate for SYBR-I stained samples ($15\text{--}20\ \mu\text{l min}^{-1}$). **Figure 18** depicts a set of cytograms obtained on an SW sample, and

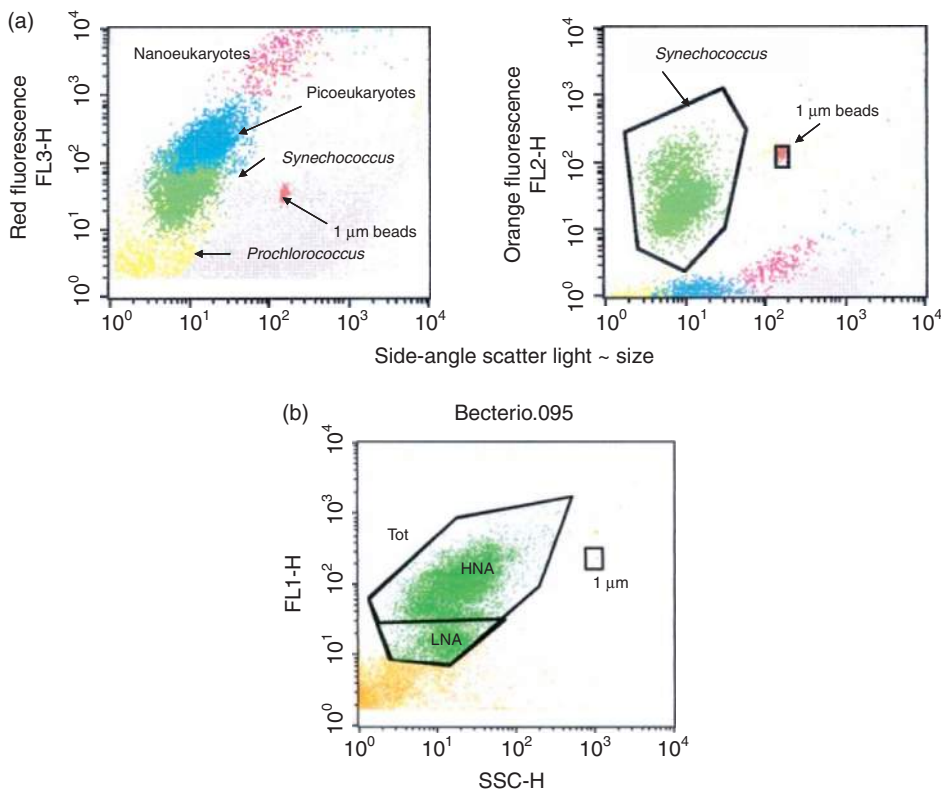


Figure 18 Cytograms for differentiating/enumerating (a) phytoplankton species and (b) bacteria [11].

shows how the picophytoplankton species and bacteria (high nucleic acid (HNA) bacteria equivalent to active bacteria; low nucleic acid (LNA) bacteria equivalent to dormant bacteria) can be differentiated and enumerated.

2.03.4.2.4 Global measurement of fouling potential

As mentioned previously, SDI remains the most commonly used global parameter for evaluating SW quality before RO membranes. Nevertheless, despite an intensive use of this fouling index and its recommendation from membrane manufacturers, some studies showed that SDI is inappropriate for measuring the fouling potential of SW. For instance, Moody *et al.* [12] and Kaakinen and Moody [13] reported a severe fouling of RO membranes fed by SW with $SDI < 1$. The RO membrane autopsy revealed that the fouling material was mostly clay and organic matter. On the contrary, Potts *et al.* [14] showed the economic viability for RO plants fed by SW with $SDI > 5$.

To overcome this issue of nonadapted water fouling index, modified fouling index (MFI) and mini plugging fouling index (MPFI) tests have been developed.

- *MFI and MPFI.* Schippers and Verdouw [15] proposed a fouling index called MFI, which takes into account fouling mechanisms. They considered that the fouling of a flat-sheet membrane in dead-end filtration at constant transmembrane pressure takes place in three steps:
 1. pore blocking;
 2. formation of an incompressible cake; and
 3. formation of a compressible cake.

This mechanism is based on the laws of dead-end filtration at constant transmembrane pressure or constant flux stated by Hermans and Bredee [16], taken up by Hermia [17], and quoted by Minier and Jolivald [18]. These laws give explicit relationships between filtration time and permeate flow rate. This is illustrated by Figure 19, which represents the evolution of the ratio t/V as a function of V , where t is the filtration time and V the cumulated permeate volume.

According to these filtration laws, there should be a linear relationship between t/V and V during the formation of a compressible cake [15]. The parameter $MFI_{0.45}$ specifically corresponds to the fouling by cake formation at the membrane surface. Practically, the measurement of MFI is similar to that of SDI, with the same equipment. The volume of permeate is measured every 30 s, during a maximum time of 20 min. Test results consist in a series of time measurements and cumulated permeate volumes. The MFI value is the slope of the linear part of the graph, that is, the tangent of the angle α .

The MPFI is defined as the slope of the linear part of the curve representing the instantaneous permeate flow rate as a function of time. This curve also presents three parts corresponding to the fouling steps mentioned previously.

Requirements have been set up for water feeding RO and nanofiltration (NF) systems [19] as reported in Table 3.

Even if $MFI_{0.45}$ and MPFI represent a significant improvement of the evaluation of fouling potential compared to SDI, these indexes still present some limits for predicting NF and RO fouling:

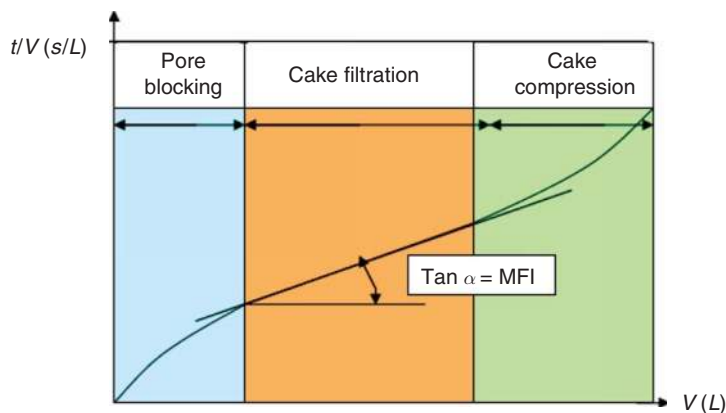


Figure 19 Evolution of t/V as a function of V .

Table 3 Approximations of fouling indexes for NF and RO

Fouling index	Range	Application
MFI	$(0-2) \text{ s} \times \text{l}^{-2}$ $(0-10) \text{ s} \times \text{l}^{-2}$	OI NF
MPFI	$(0-3 \times 10^{-5}) \text{ l} \times \text{s}^{-2}$ $(0-1.5 \times 10^{-4}) \text{ l} \times \text{s}^{-2}$	OI NF
SDI	(0-2) (0-3)	OI NF

- Measurements of $\text{MFI}_{0.45}$ and MPFI are carried out in dead-end filtration, while NF and RO operate in cross-flow filtration that slows down or limits the particle deposit on the membrane.
- Permeate flux in NF or RO is much lower than in MF, modifying the force equilibrium on a particle.
- A high part of colloidal matter retained at the surface of an NF or RO membrane passes through the filter used for $\text{MFI}_{0.45}$ measurement. Hence, the fouling ability of these colloids is not taken into account and the particles constituting the cake at the NF or RO membrane surface will have a different structure.
- Operating pressures in NF or RO are much higher than 30 psi (2.07 bar), which is the pressure applied for SDI and $\text{MFI}_{0.45}$ measurement. Hence, the cake should be much more compressed in NF or RO than in MF.
- Salt retention through NF or RO membranes and the accumulation of these salts in the polarization boundary layer modify the ionic neighborhood next to the membrane, which can affect the structure of the fouling deposit.

Some of the limits have been removed through the development of a new index based on the use of an ultrafiltration (UF) membrane: MFI-UF.

• *MFI with UF and NF membranes.* Boerlage *et al.* [20–23] have developed a new fouling index called MFI-UF. Unlike the previous indexes (SDI and

$\text{MFI}_{0.45}$), this index is measured with a UF membrane, hence with pores smaller than 0.45 μm . This choice aims at a better characterization of the fouling ability of water containing colloids, which can pass through an MF membrane with a porosity of 0.45 μm . Boerlage *et al.* [21] have selected a membrane with a molecular weight cutoff of 13 000 Da for the measurement of MFI-UF. This cutoff would be the best according to filtration tests. Filtration mechanisms considered for MFI-UF are exactly the same as for $\text{MFI}_{0.45}$ (see **Figure 19**).

Currently, studies are moving toward the development of not only a fouling index using NF membranes [24] but also a cross-flow sampler providing a fouling index operating under flow conditions closer to RO processes than SDI or MFI [25].

2.03.4.3 Raw Water Quality

These new tools, combined with conventional SW quality parameters (turbidity, SDI, and TOC), were used at various full-scale and pilot-scale desalination facilities for raw SW characterization. SW samples were collected at these various sites capturing a wide variety of source waters. **Table 4** lists the various sites with their location and intake type.

2.03.4.3.1 Ion content

The ion makeup of the raw SW sources is characterized according to the analytical methods listed in **Table 2**. As shown in **Table 5**, the ion content of a same body of SW is fairly similar, and no significant changes of ion content are observed over a year at the participating sites (no significant seasonal variations of ion content). Based on the samples collected at the various sites, the main observations are as follows:

- the overall ion content of the Arabian Gulf is higher as compared to the oceans and the Mediterranean Sea; and

Table 4 Desalination sites involved in the seawater characterization study

Site ID	Location	Intake type
Sites A, B	Pacific Ocean	Open intake
Sites C, D, E	Mediterranean Sea	Open intake
Site F	Atlantic Ocean	Open intake and beachwell
Site G	Arabian Gulf	Open intake
Site H	Brackish water	Estuarine surface water
Site I	Atlantic Ocean	Open intake and beachwell

Table 5 Ion content of various seawaters

	<i>Pacific Ocean (sites A, B)</i>	<i>Mediterranean Sea (sites C, D, E)</i>	<i>Atlantic Ocean (Site I)</i>	<i>Arabian Gulf (Sites G)</i>
Sodium (mg l ⁻¹)	10 200–10 500	11 800–12 500	10 100	12 300–13 800
Potassium (mg l ⁻¹)	370–380	435–455	360	505–610
Calcium (mg l ⁻¹)	400	450–470	430	430–570
Magnesium (mg l ⁻¹)	1200–1235	1410–1500	1340	1510–1790
Chloride (mg l ⁻¹)	18 300–18 700	21 000–22 600	21 200	23 100–24 900
Sulfate (mg l ⁻¹)	2710–2830	2960–3210	2490	3040–3110
Bicarbonate (mg l ⁻¹)	152	170	162	162–170
Boron (mg l ⁻¹)	4.6	5.4	4.3	5.1–6.7
Fluoride (mg l ⁻¹)	1.1	1.5–1.7	1.2	2.4–2.7
Strontium (mg l ⁻¹)	7.7	8.4	7.5	9.5–10.5
Barium (µg l ⁻¹)	<10	<10–20	14	<10
Salinity (g l ⁻¹)	33.4–34.4	38.8–41.0	33.2	43.7–44.3

- the sites located on the Pacific Ocean and the Atlantic Ocean show a slightly lower salt content than the Mediterranean Sea, and this could impact, in some cases, the design of the RO systems, notably with respect to the boron removal.

Overall, these differences of salt content will not impact the selection of the pretreatment strategy, but will impact the sizing of the RO systems. For the more saline SW, adequate desalination through RO will require slightly higher pumping requirements, and/or slightly lower conversion rates, and/or slightly higher dosing rates of antiscalant, and more advanced treatment (additional RO passes) for boron removal.

2.03.4.3.2 Natural organic matter

The NOM contained in different raw SWs is characterized with the LC-OCD analytical method. TOC analyses are also performed using a Shimadzu TOC-V analyzer (high-temperature catalytic oxidation).

Overall, SWs collected from open intakes at various sites have a fairly low and stable TOC level ranging from 0.8 to 1.5 mg l⁻¹. Figure 20 demonstrates the advantage of using beachwell as SW feed as compared to surface SW (open intake). First, the TOC levels of beachwell SW are slightly lower, but most importantly, the polysaccharides are almost completely removed through the slow filtration occurring when beachwells are used. Beachwells are, therefore, an excellent line of

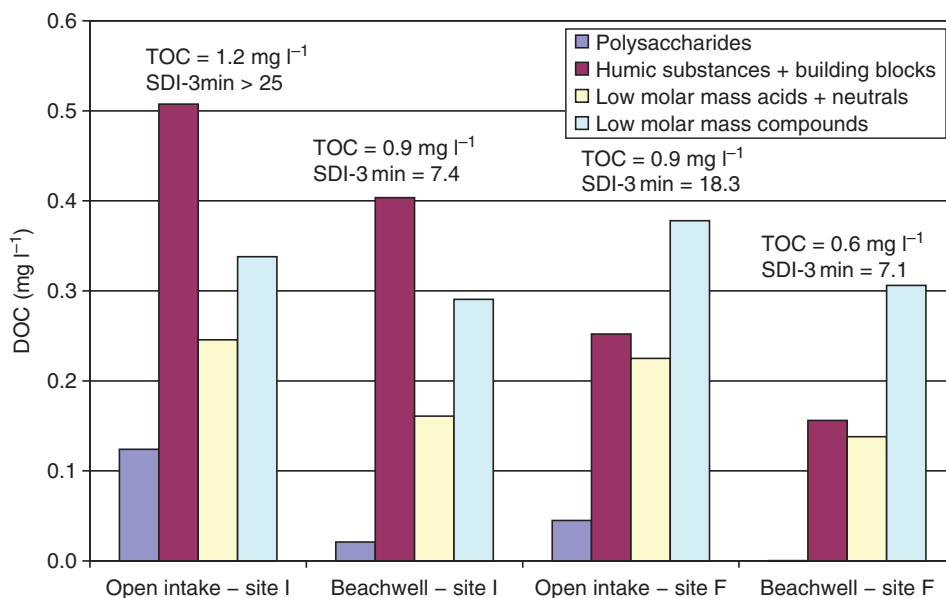


Figure 20 Impact of the seawater intake type on the natural organic matter (NOM) content.

defense against organic and biological fouling on the RO membranes as polysaccharides are easily absorbed onto spiral-wound membranes. Then, polysaccharides foster the microbial attachment onto the RO membranes, and these high-molecular-weight compounds can also be used as nutrients by the bacteria, thus facilitating the development of a biofilm onto the membranes (biofouling). It is also interesting to note the major impact that the use of beachwells can have on the SDI values, as the slow filtration through the seabed can lead to a threefold decrease of the $SDI_{3, \min}$ values.

With the exception of major storm events or extreme influence of inland activities, the TOC levels do not show any major variations. On the other hand, the NOM characterization through LC-OCD chromatography allows one to demonstrate that the NOM content may vary depending on the seasons. **Figure 21** notably shows that samples collected during fall have lower polysaccharide levels than samples during summer. These lower polysaccharide levels during colder seasons also correspond with lower $SDI_{3, \min}$ values and lower bacterial counts. It already appears that the bacterial and algal activities, enhanced with warmer water temperatures and higher sun exposure, are major water quality factors impacting the fouling potential of open intake SWs, and, therefore, will impact the selection of the pretreatment strategy.

2.03.4.3.3 Phytoplankton and algal content of raw SW

Figure 22 shows the concentrations of phytoplankton species at the various SW desalination sites. The following observations can be made:

- the Arabian Gulf SW has a significantly higher algal activity as compared to the Mediterranean Sea (and other oceans – data not shown) and
- the positive impact of the beachwell is again demonstrated, as concentration of phytoplankton species in beachwell SW is more than one level of magnitude lower than that of surface SWs.

Figure 23 compares the time profile of the bacterial counts. It appears that the bacteria content of the raw SW in summer (June and August samples) is higher than that of the sample collected in fall (October sample). However, beyond the simple comparison of total bacteria counts, the variation of distribution between active and dormant bacteria is very interesting. Indeed, the proportion ratio between active and dormant bacteria seems to invert between the summer samples and the fall sample, with bacteria having a higher activity in summer. This observation could have a great impact on the fouling kinetics occurring on the RO membranes. Of course, this observation can be related to higher sun exposure and higher water temperature in summer (around 30 °C in summer against 15 °C in fall).

2.03.4.3.4 Correlations between conventional SW quality parameters and advanced analytical tools

This comprehensive monitoring approach notably shows that

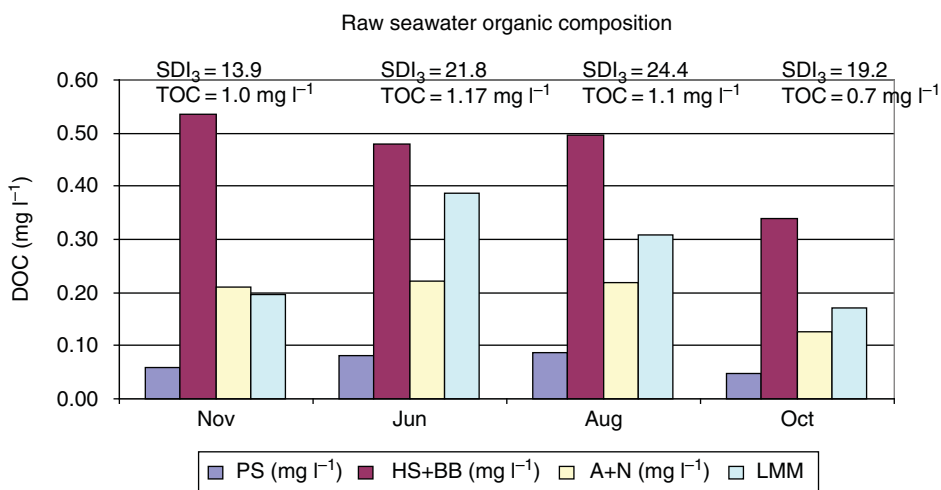


Figure 21 Seasonal variations of the natural organic matter (NOM) content of the raw seawater: Mediterranean Sea – open intake.

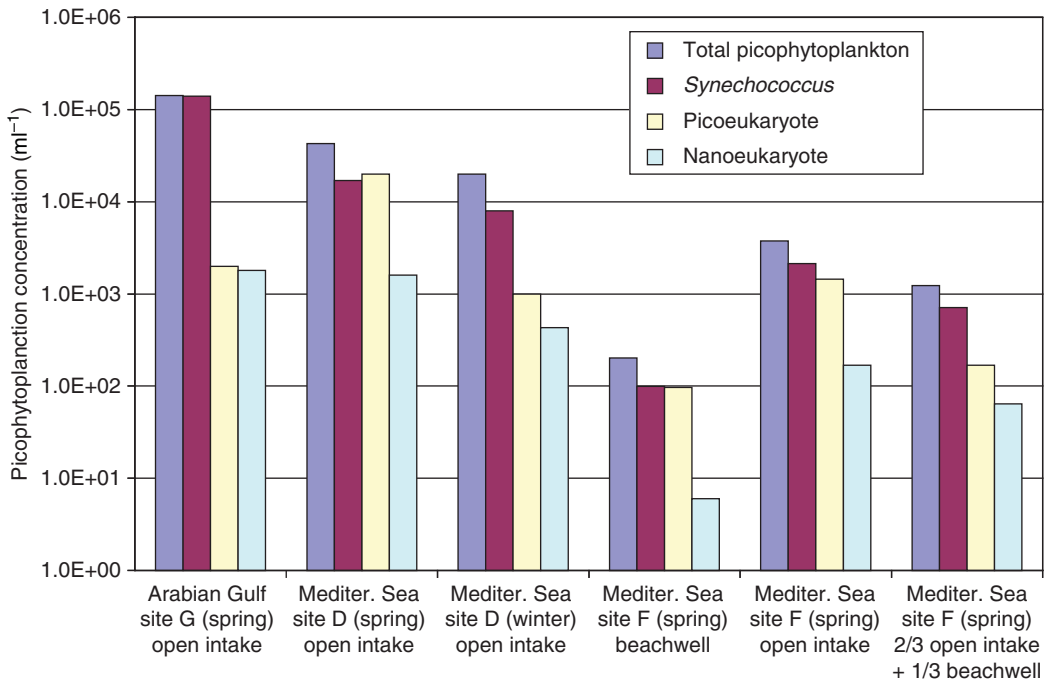


Figure 22 Phytoplankton concentrations in various raw seawaters (Log scale).

1. the $SDI_{15\ min}$ values at the outlet of the pretreatment process seem to be closely correlated with the total bacteria count (see **Figure 24**); and
2. the polysaccharide content is also correlated with the total bacterial count, and this for both the raw SW and the pretreated SW (see **Figure 25**).

2.03.4.4 Performances of Various Pretreatment Processes

2.03.4.4.1 General presentation of pretreatment processes

Figure 26 shows the various pretreatment process options that can be implemented on an RO desalination plant, depending on the raw SW quality and its variations. In general, pretreatment processes consist of

- removing algae, plankton, hydrocarbons, via, for example, a flotation process;
- capturing colloidal solids via a clarification-filtration line;
- preventing the precipitation of dissolved solids and metal salts in the brine concentrate zone by injecting an acid and/or chelating agent; and
- controlling microorganism growth and the introduction of biodegradable organics that constitute

a food supply for microbes and foster their proliferation at the membrane surface.

As seen in Section 2.03.4.3, feedwaters from coastal wells are generally of very high quality. The same cannot be said, however, of water taken directly from the sea, especially warm seas, which call for the use of multibarrier treatment processes to ensure low levels of turbidity and a low SDI, specifically

- turbidity below 0.1 NTU and
- average SDI of 2.5 with peaks not exceeding 3 or 4.

Meeting these requirements allows plant design to be based on the highest possible transmembrane flux (with a proportionate reduction in the necessary membrane surface area), and presents the following operational advantages:

- reduced frequency of chemical cleaning;
- consistently high permeate quality;
- limited head loss across the elements, allowing the use of the energy recovery device (to recover energy from brine concentrate), leading to energy savings; and
- longer membrane service life, thanks to a lower rate of irreversible fouling.

Biofouling remains the major problem; therefore, development efforts have focused on achieving the

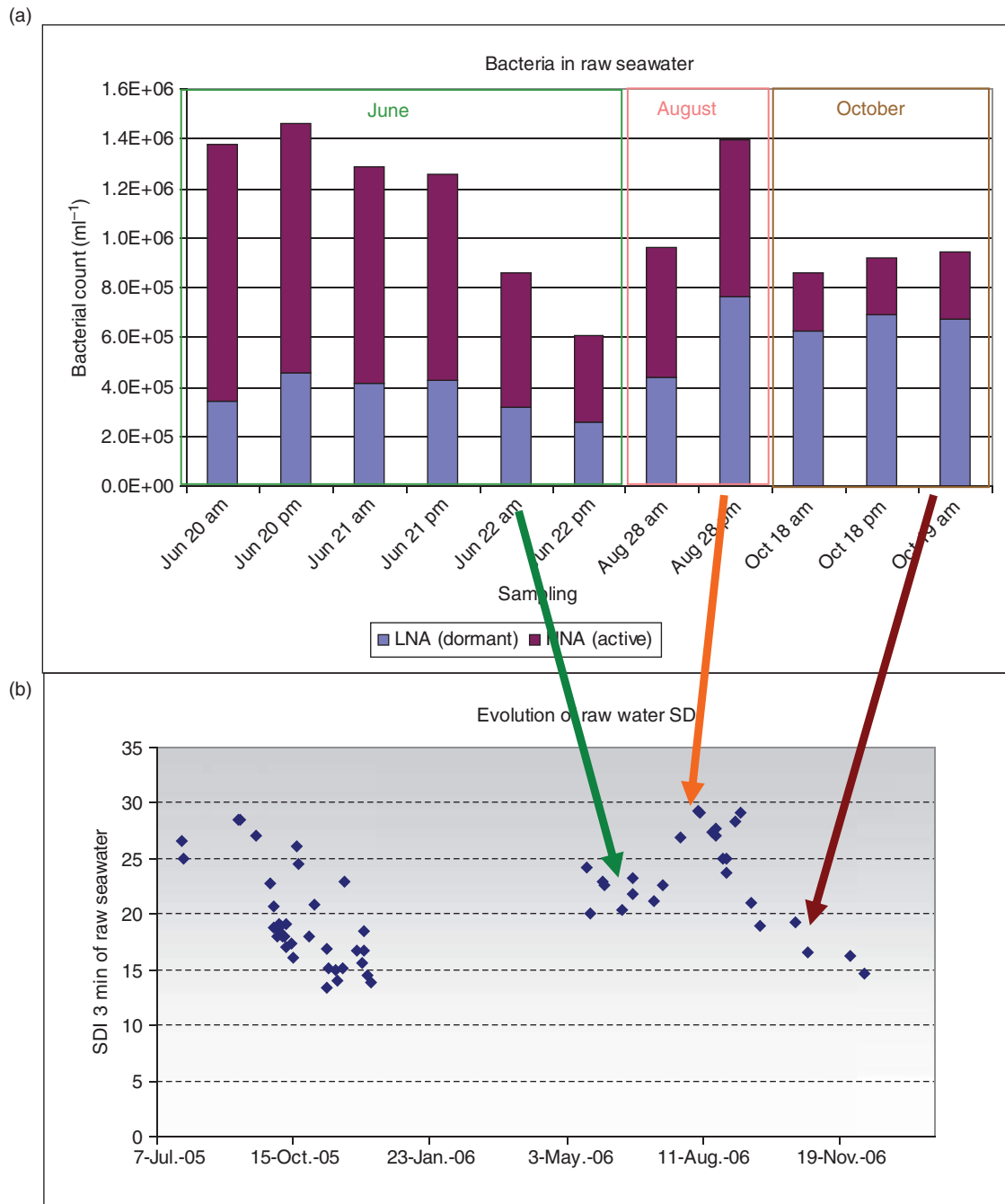


Figure 23 Seasonal variations of bacteria counts (a) and silt density index (SDI) 3-min values (b): Mediterranean Sea – open intake.

highest possible rejection factors for microorganisms and organic matter.

Trends in current practice consist of:

- Elimination of continuous prechlorination, which has the significant drawback of transforming

certain nonbiodegradable organics (such as humic acids) into biodegradable compounds, which, in turn, constitute a nutrient supply for microorganisms. Continuous prechlorination is being successfully replaced by shock chlorination followed by dechlorination. Other alternatives for

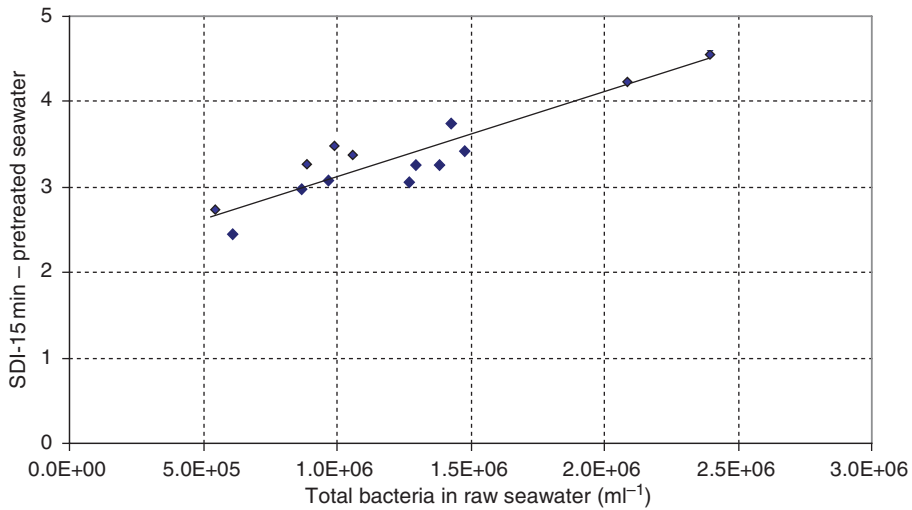


Figure 24 Impact of raw seawater bacteria concentration on silt density index (SDI) 15-min values of pretreated water (coagulation + dual-media filtration): Mediterranean Sea – open intake.

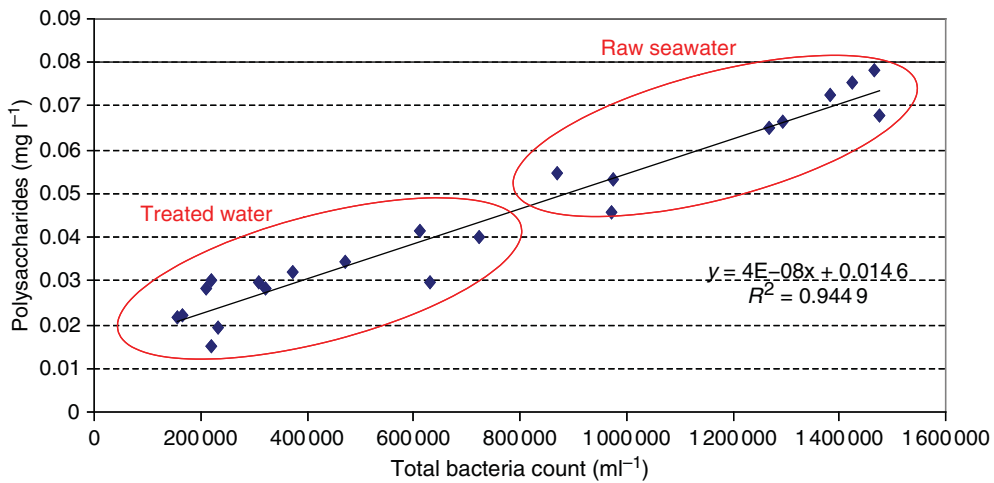


Figure 25 Impact of bacteria concentration in raw seawater on silt density index (SDI) 15-min values of pretreated water (coagulation + dual-media filtration): Mediterranean Sea – open intake.

controlling microorganism populations are periodic injections of specific biocides or UV oxidation.

- Use of membrane clarification techniques, especially UF, to replace conventional granular media filtration. Although UF yields a high-quality pretreatment effluent (turbidity lower than 0.1 NTU; SDI averaging 1.5–3), it is not an effective solution for organic removal, because only organic macromolecules are retained on the membrane, and only partially. For this reason, UF must be supplemented with a coagulation step.

2.03.4.4.2 Performances of pretreatment processes

Performances of the various pretreatment processes presented in Figure 26 strongly depend on the raw SW quality they are fed with. This section presents the performances, based on conventional and advanced analytical tools, of the pretreatment trains corresponding to the various desalination sites discussed in Section 2.03.3.

Table 6 lists the various sites with their location, intake type, and pretreatment process.

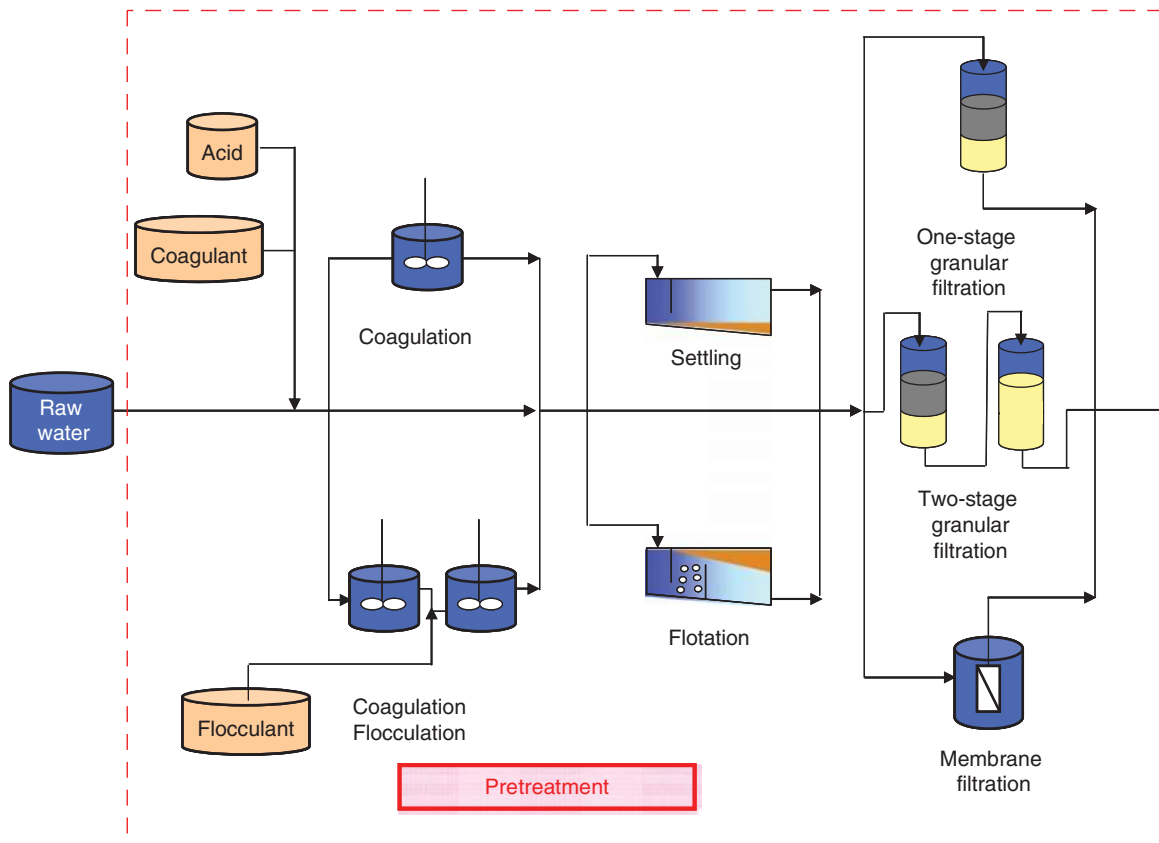


Figure 26 Pretreatment process options.

Table 6 Desalination sites involved in the seawater characterization study

Site ID	Location (intake type)	Pretreatment technology
Site A	Pacific Ocean (OI)	Coagulant + granular filtration
Site B	Pacific Ocean (OI)	1. Coagulant + granular filtration 2. MF/UF
Site C	Mediterranean Sea (OI)	Actiflo + granular dual-media filtration
Site D	Mediterranean Sea (OI)	Coagulant + granular dual-media filtration
Site E	Mediterranean Sea (OI)	Coagulant + granular dual-media filtration
Site F	Atlantic Ocean (OI and BW)	Coagulant + granular dual-media filtration
Site G	Arabian Gulf (OI)	Actiflo + granular dual-media filtration
Site H	Brackish Water (ES)	Coagulant + granular dual-media filtration + UF
Site I	Atlantic Ocean (OI and BW)	None – raw seawater samples only

Intake type: OI, open intake; BW, beachwell; ES, estuarine surface.

Table 7 shows the main results and allows a thorough performance comparison between various processes, even though most of them were not operated at the same site. From a scientific perspective, sound process comparison can be performed only when operating two or more processes using a side-

by-side approach (i.e., strictly similar raw water quality feeding the processes being evaluated). Nevertheless, this requirement cannot be easily met, notably at full scale. Only extensive pilot-scale studies can allow such an approach, which was the case for site D (Mediterranean Sea – open intake).

Table 7 Performance comparison of various pretreatment processes

	<i>Raw water</i>		<i>Pretreated water</i>					
	<i>SDI_{3min}</i>	<i>TOC (mg l⁻¹)</i>	<i>SDI_{15min}</i>	<i>TOC removal</i>	<i>Polysac. removal</i>	<i>Bacteria removal</i>	<i>Picoplankton removal</i>	<i>Chlorophyll removal</i>
Dual-media filtration								
Site A – Pacific Ocean coagulation + DMF	Avg: 19 16–25	1.4	Avg: 2.9	0%	0%	0.5 Log	0.5 Log	-
Site C – Mediterranean Sea actiflo + DMF	16–19	0.7	Avg: 2.7	5%	10–20%	-	-	90–95%
Site D – Mediterranean Sea coagulation + DMF	Avg: 20 12–29	1.3	3–3.5: 21% 3.5–4: 40% >4: 37%	15%	-	0.3 Log	0.6 Log	90–99%
Site E – Mediterranean Sea coagulation + DMF	13–30	0.8–1.2	2.6–4.0	15–20%	20–50%	0.3–0.6 Log	0.2–0.7 Log	92–97%
Microfiltration/Ultrafiltration								
Site B – Pacific Ocean MF/UF	>25	1.4	2.0	5%	35%	3.5 Log	>3.7 Log	90%
Site D – Mediterranean Sea MF/UF	Avg: 20 12–29	1.3	<3: 90% 3–3.5: 10%	5%	-	3.0 Log	>4.1 Log	>99%
Site H – Estuarine brackish water – MF/UF	>25	11	3.1	40%	62%	2.8 Log	3.5 Log	99%

The two water quality parameters showing the higher level of variation and sensibility between conventional pretreatment processes (process strategy based on dual-media filtration) and MF/UF processes are the bacteria calculation and the phytoplankton enumeration. Analyses of polysaccharide concentration also provide interesting information, but further data are required at this stage. The main observations from the data contained in **Table 7** are the following:

- Pretreatment processes with dual-media filtration provide limited removal of picophytoplankton and bacteria (<1 Log removal), while membrane-based pretreatment (MF/UF) achieves high removal of both types of microorganisms (removal >2.8 Log).
- While the chlorophyll removals through various granular filtration systems and low-pressure (LP) membrane units (MF and UF) were greater than 90%, the picophytoplankton and bacteria counts were found to be more sensitive to capture differences of pretreatment performance. This demonstrates that picophytoplankton and bacteria enumeration can be a very useful tool for the selection and optimization of the pretreatment based on the site-specific raw SW quality challenges.
- TOC removal appears fairly limited for all tested pretreatment technologies, and further polysaccharide analyses are needed at this stage to draw more robust conclusions. Nevertheless, TOC removal on site D (where side-by-side process comparison is performed at pilot scale) seems higher at the outlet of the coagulation + dual-media filtration (DMF) pretreatment (15%) than at the outlet of the UF/MF membrane pretreatment, which could have a significant impact on the subsequent RO membrane biofouling extent.
- $SDI_{15\ min}$ values are lower after MF or UF pretreatment as compared to dual-media filtration (see results from site D). Nevertheless, dual-media filtration can also consistently achieve $SDI_{3\ min}$ values lower than 3 when the raw SW quality is of fairly good quality (low raw SW $SDI_{3\ min}$ values, no major algal blooms, etc.), and when optimal operating conditions are found (type and dosing of coagulant, type and dosing of polymer, and optimal filtration velocity).

2.03.5 Reducing Cost, Energy Consumption, and Environmental Impact

2.03.5.1 Energy Consumption

2.03.5.1.1 Energy-saving devices

Energy is the single largest cost factor when producing freshwater from SW, and can be estimated to represent 30–40% of the overall cost. Energy costs depend on plant capacity, the cost of power generation per kilowatt-hour, and the system defined for recovering the hydraulic energy of the brine concentrate.

The first generation of desalination plants, based on a thermal process, required the equivalent of 20 kWh of electricity to produce 1 m³ of freshwater. Over a quarter of a century ago, the power consumption of desalination plants based on the RO principle was about 8 kWh m⁻³. With the introduction of systems based on Pelton turbines to recover energy from the brine concentrate, the power requirement dropped to about 5.0 kWh m⁻³. Today, in large-scale desalination plants, power consumption is 3.2 kWh m⁻³. This gain can be attributed to the commercialization of high-capacity pumps and turbines, coupled with improvements in their hydraulic design and better machining techniques. As efficiency varies as a function of flow rate, it is always preferable to present power consumption data in reference to plant capacity, although this is not always done. For example, for a plant capacity of 800 m³ d⁻¹ and a recovery ratio of 40%, the overall efficiency is 60% for the pumps and turbines alone. If plant capacity increases to 10 000 m³ d⁻¹, the overall energy efficiency rises to 75%.

About 5 years ago, another system for recovering the hydraulic energy from brine concentrate appeared on the market. The new system is based on energy exchangers, which allow direct energy recovery without a transformation to mechanical energy (contrary to Pelton turbines).

Providing an efficiency of 95%, energy exchangers can considerably boost the amount of energy recovered from the brine concentrate, as illustrated by the calculation for a plant with a capacity of 10 000 m³ d⁻¹ capacity (recovery ratio: 45%; feed-water pressure: 65 bar; and back pressure on permeate: 1 bar). Applying a similar calculation for a plant of similar characteristics, but using a Pelton

turbine for energy recovery, leads to an increase in energy consumption of 0.4 kWh m^{-3} .

The direct energy recovery device thus translates to a significant 13% in energy savings. However, this figure should be considered optimistic because the calculation was carried out using maximum efficiencies for the pumps and turbines, which, unfortunately, may not always be the case in terms of both design and operation, since the actual operating parameters may be quite different from the optimum values.

On the other hand, the energy savings are greater for small- and medium-capacity desalination plants, because the efficiency of direct energy recovery devices remains constant regardless of flow rate, in contrast to turbine efficiency, which declines with flow rate.

It is worth mentioning that all improvements in membrane performance (increase in the transmembrane flux density, the recovery ratio, and the rejection factor of dissolved solids) are achieved at the cost of higher energy consumption. Nevertheless, some recent membrane developments have focused on lower energy consumption. This required the development of high-productivity membrane elements and compatible design concepts that enable operation at lower pressure [2, 3].

Accordingly, the optimum, in terms of investment and operating costs, must be sought on a case-by-case basis, based on the technical parameters of the site, the plant economics, and the expectations of the operator.

Today, the market of energy exchangers is led by two companies: Calder with the commercialization of the DWEER system and Energy Recovery Inc. with

their Pressure Exchanger[®] Technology (PX[®]) system. Both devices are two different design concepts of pressure exchangers – rotating or nonrotating devices [26]. The rotating concept is represented by the PX system using a spinning, self-floating rotor in a sealed housing, which transfers the pressure energy from the brine to the feed flow. Nonrotating devices, as they are used by DWEER/Calder, employ stationary vessels being pressurized and depressurized by means of actuated valves. Both concepts are installed in many SWRO plants and have been proven for reference.

2.03.5.1.2 PX Pressure Exchanger[®] Technology

The PX device captures the hydraulic energy from the HP reject stream of RO processes. It transfers this energy to LP feedwater with an efficiency of nearly 98%. Pressurized feedwater from the PX device is sent to the membrane feed, merging with an approximately equal stream of pressurized water from a HP pump. This significantly reduces the amount of water pressurized by the HP pump. As the PX device itself consumes no electrical power, the overall energy consumption of an SWRO process is cut in half or less.

The PX device (Figure 27) contains a single cylindrical rotor that spins inside a sleeve between two end covers. The rotor is driven by the flow so that no power is required to make the device operate.

Rotor speed is self-adjusting, maintaining the interface between the feed streams, and thus eliminating mixing. This design results in no pressure spikes or pulsations, nor does it require pistons,

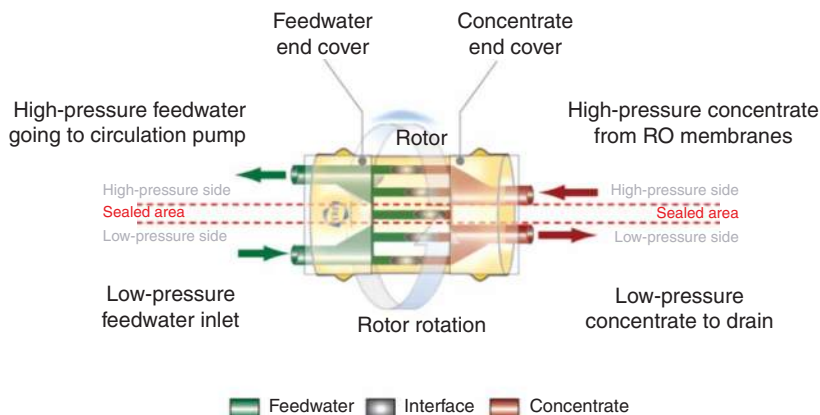


Figure 27 Schematic diagram of a Pressure Exchanger[®] (PX[®]) device.

valves, or timers. PX technology maintains consistent high-energy transfer efficiency, regardless of salinity, temperature, and recovery rate variations.

2.03.5.1.3 DWEER™ work exchanger

In order not to interrupt the brine flow, the DWEER™ work exchanger has a minimum of two pressure vessels in parallel [27]. One vessel is in the working stroke, while the other is filled with fresh SW. As soon as the piston of the working pressure vessel finishes its working stroke and the filling vessel is fully filled with fresh feed water, the brine and feed line are switched (Figure 28). The DWEER™ work exchanger consists of three main subassemblies: the LinX™ valve, the pressure vessels, and the check valve nest. The main difference, compared to a typical arrangement with a Pelton turbine, is that the feed flow is split into the LP feed to the HP pump and to the energy recovery device. Only a flow slightly greater than the product flow will be handled by the HP pump; therefore, the size of the HP pump is reduced. A booster pump needs to be installed in the system to compensate for the differential pressure over the membranes and pressure losses in the piping and over the energy recovery device. Typically, such a pump is designed for a differential head of about 30–40 m. Thus, compared to the HP pump this is a low power consumer. The booster pump needs to be designed for HP (Figure 29).

2.03.5.2 Environmental Impact

Several studies have been undertaken on the socioeconomic and environmental impacts of desalination plants [28–33]. Nevertheless, there have been very few studies dealing with the impact of hypersaline brine inputs on marine environment.

The magnitude of the high salinity impact will depend on the size of the plant, the sensitivity of the ecosystem that receives the spill, and on the general hydrodynamic field [34, 35]. This hypersaline wastewater emanates dense discharge plumes that can potentially affect marine organisms and communities.

In addition, a number of other substances (such as antiscaling additives, biocides, surface-active agents, or



Figure 29 DWEER™ systems.

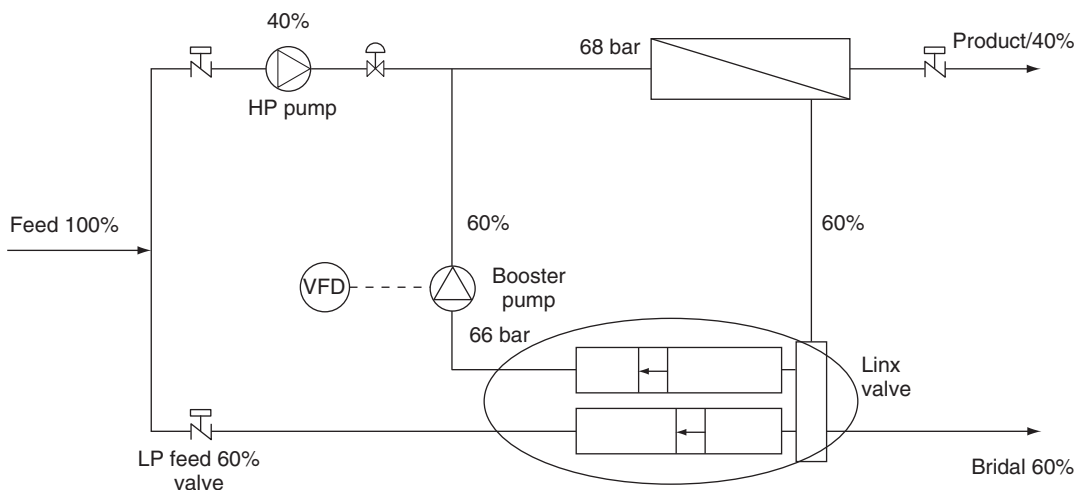


Figure 28 Integration of a DWEER™ system in a reverse osmosis (RO) desalination system.

solid residues from back flushing of filters) may continuously or sporadically accompany the release and are also likely to have an environmental impact.

In fact, while technical improvements of the desalination process has led to increasing efficiency and cost reductions, very little attention has been given to the associated environmental issues.

Future studies in this field should focus not only on energy issues but also on the fate and potential effects on receptor environment.

2.03.5.3 Current Trends in Operations for Cost Saving

Studies have highlighted the biocidal benefits of osmotic shock treatment for preventing a microbial invasion of filter media and membranes. The explanation for this effect is that the cytoplasm, which is the inner part of the cell composed mainly of water, is surrounded by a semipermeable membrane. Increasing the salinity of the medium surrounding the microorganisms causes the water to pass from inside the cells to the surrounding environment (through natural (direct) osmosis). This leads to the dehydration and death of the cells. It is therefore recommended that filters be washed periodically using the concentrate from the RO modules.

Osmotic shock with a biocidal effect can also be triggered by washing the membranes with permeate. In this case, freshwater flows into the cells, altering the salinity of the cytoplasm (direct osmosis) and degrading the cell membrane.

A membrane cleaning system (direct osmosis-high salinity (DO-HS) system), based on the principle of direct osmosis, is currently being developed by Membrane Recovery Ltd. Membranes are cleaned daily during the production process. According to the developer of the process, it is an effective substitute for periodic chemical cleaning. The DO-HS process entails applying a concentrated solution of sodium chloride to the SW feed stream for a brief period of time. This sends a wave of water characterized by high osmotic pressure through the feed-concentrate channels of the element. As the wave passes through, the RO phenomenon is replaced by direct osmosis, that is, the permeate passes into the feed-concentrate compartment. The direct osmosis triggers a flow counter-current to the production flow that dislodges any accumulated debris from the membranes and carries it off in the concentrate flow. At the same time, an

osmotic shock occurs, dehydrating the microorganism cells and leading to their death (as discussed above), with an accompanying dissolution of microcrystals formed on the membranes and spacers.

According to the developers, this process allows for a constant output and quality of permeate, limits head loss (which saves on energy costs), and extends the service life of membranes. Nevertheless, the benefit of this operating procedure still needs to be confirmed today as certain limitations, due to concentration polarization on the feedwater side when the salt concentration increases, have been observed.

2.03.5.4 Other Trends

Thanks to thorough mastery of RO techniques in SW desalination coupled with technological progress achieved in recent years, large-scale desalination plants have now been built. The Ashkelon SWRO plant in Israel, for example, has a production capacity of $326\,000\text{ m}^3\text{ d}^{-1}$ with relatively low production costs of US\$0.53 m^{-3} . However, in countries where low-cost energy resources are available, the cost of producing freshwater by RO is comparable to that of thermal-process desalination. Accordingly, rather than pitching these two desalination processes in competition with each other, the strategy in the Middle East has been to combine them in hybrid plants (RO/multistage flash evaporation) coupled to power generation facilities. The Fujairah complex (United Arab Emirates) is one example.

Unlike distillation-only plants, hybrid facilities offer the advantage of greater operating flexibility in terms of water output: it can maximize the use of RO capacity during periods of low power demand.

2.03.6 Conclusion

Assuming that the efficiencies of pumping equipment ($\sim 90\%$) and direct energy recovery systems ($\sim 95\%$) have reached their upper limit, the most significant developments now to be expected lie in the areas of membranes and process, with the aims of boosting productivity, improving permeate quality, and reducing feedwater pressure requirements, while at the same time extending membrane service life and resistance to all types of fouling.

It is also necessary to draw the lessons learned from the 25-year operating experience in order to optimize the principles for designing and operating

SWRO desalination plants, especially those of small and medium capacities.

Further efforts are also needed to master the quality of membrane feedwater, an essential parameter for smooth and cost-effective operation of desalination facilities.

In addition, efforts have to be made to focus on the development of efficient adapted tools and probes for computer-aided operations. Real-time monitoring of water productivity and quality at many different locations of the plant are essential to anticipate membrane degradation and fouling issues. The deployment of such tools must be supported by appropriate operator-training programs. Scheduling membrane autopsy on a regular basis and eventually planning cleaning operation and partial replacement of membrane elements according to needs are important to control the system and maintain water productivity and quality.

We have thus entered a phase of optimization of systems, equipment, and operations. The cost of the necessary investments can only be reduced by an expansion of the market for RO desalination plants; such growth will itself be spurred by the growing demand for water, water shortages, as well as by the competitiveness of RO processes compared to the cost of the treatment required for conventional water resources and the cost of water conveyance.

References

- [1] By Global Water Intelligence, <http://www.desaldata.com> (accessed November 2009).
- [2] Busch, M., Mickols, W. E. *Desalination* **2004**, *165*, 299–312.
- [3] Garcia-Molina, V., Busch, M., Sehn, P. *Proceedings of the EDS Euromed Conference*, Dead Sea, Jordan, 9–13 November 2008.
- [4] Mickols, W. E., Busch, M., Maeda, Y., Tonner J. *Proceedings of the IDA World Congress on Desalination and Water Reuse*, Dubai, UAE, 7–12 November 2009.
- [5] Goosen, M. F. A., Sablani, S. S., Al-Hinai, H., Al-Obeidani, S., Al-Belushi, R., Jackson, D. *Sep. Sci. Technol.* **2004**, *39*, 2261–2297.
- [6] Dudley, L. Y., Annuziata, U. A., Rabinson, J. S., Latham, L. J. *Proceedings of the IDA World Congress on Desalination and Water Reuse*, Abu Dhabi, UAE, 18–24 November 1995.
- [7] Hickman, C. E. *Proceedings of the AWWA Seminar on Membrane Cleaning Techniques*, Orlando, FL, USA 10–13 March 1991.
- [8] Huber, S. A., Frimmel, S. H. *Environ. Sci. Technol.* **1994**, *28*, 1194–1197.
- [9] Huber, S. A. *Ultrapure Water* **1998**, 16–20.
- [10] Lefebvre, A., Guelorget, O., Perthuisot, J.-P., Courties, C., Millet, B. *Oceanol. Acta* **1996**, *20*, 757–767.
- [11] Rapenne, S. *Seawater Desalination by Reverse Osmosis: Impact of Conventional Processes on Physicochemical and Microbiological Characteristics of the Feed Water and Fouling Study*. PhD Thesis, University of Poitiers, France, 2007.
- [12] Moody, C. D., Kaakinen, J. W., Lozier, J. C., Laverty, P. E. *Desalination* **1983**, *47*, 239–256.
- [13] Kaakinen, J. W., Moody, C. D. Characteristics of Reverse-Osmosis Membrane Fouling at the Yuma Desalting Test Facility. In *Reverse Osmosis and Ultrafiltration*; Sourirajan, S., Matsuura, T., Eds.; ACS Symposium Series; American Chemical Society: Washington, DC, 1985; Vol. 281, pp 359–382.
- [14] Potts, D. E., Ahlert, R. C., Wang, S. S. *Desalination* **1981**, *36*, 235–264.
- [15] Schippers, J. C., Verdouw, J. *Desalination* **1980**, *32*, 137–148.
- [16] Hermans, P. H., Bredee, H. L. *J. Soc. Chem. Ind.* **1936**, *55*, 1–4.
- [17] Hermia, J. *Inst. Chem. Eng.* **1982**, *60*, 183–187.
- [18] Minier, M., Jolival, C. *Les Techniques Séparatives à Membranes: Théories, Applications et Perspectives*; Pontié et Coll., U. I. E.: Paris, France, 2001; Chapter 3.
- [19] Sung, L. K., Morris, K. E., Taylor, J. S. *Intl. Desalination Water Reuse J.* 1994, *4/3*.
- [20] Boerlage, S. F. E., Kennedy, M. D., Aniye, M. P., et al. *Desalination* **2000**, *131*, 201–214.
- [21] Boerlage, S. F. E., Kennedy, M. D., Dickson, M. R., El-Hodali, D. E. Y., Schippers, J. C. *J. Membr. Sci.* **2002**, *197*, 1–21.
- [22] Boerlage, S. F. E., Kennedy, M. D., Aniye, M. P., Abogrean, E. M., Tarawneh, Z. S., Schippers, J. C. *J. Membr. Sci.* **2003**, *211*, 271–289.
- [23] Boerlage, S. F. E., Kennedy, M. D., Aniye, M. P., Schippers, J. C. *J. Membr. Sci.* **2003**, *220*, 97–116.
- [24] Khirani, S., Ben Aim, R., Manero, M.-H. *Desalination* **2006**, *191*, 1–7.
- [25] Adham, S. S., Fane, A. G. Cross Flow Sampler Fouling Index. *NWRI Final Project Report*; National Water Research Institute: Fountain Valley, CA, 2008.
- [26] Kochanowski, W., Schwarz, G., Klemm, T., Bross, S. *Proceedings of the IDA World Congress on Desalination and Water Reuse*, Canarias, Spain, 21–26 October 2007.
- [27] Schneider, B. *Desalination* **2005**, *184*, 1177–1190.
- [28] Hoepner, T. *Desalination* **1999**, *124*, 1–12.
- [29] Einav, R., Harussi, K., Perry, D. *Desalination* **2002**, *152*, 141–154.
- [30] Al Malek, S. A., Mohamed, A. M. O. *Desalination* **2005**, *185*, 9–30.
- [31] Weiss, J. M., Reice, S. R. *Ecolog. Appl.* **2005**, *15* (2), 599–617.
- [32] Gacia, E., Invers, O., Manzanera, M., Ballesteros, E., Romero, J. *Estuar. Coast. Shelf Sci.* **2007**, *72*, 579–590.
- [33] Lattemann, S., Hopner, T. *Desalination* **2008**, *220*, 1–15.
- [34] Hoepner, T., Widdelberg, J. *Desalination* **1996**, *108*, 11–18.
- [35] Del Pilar Ruso, Y., De la Ossa Carretero, J. A., Giménez Casalduero, F., Sanchez Lizaso, J. L. *Mar. Environ. Res.* **2007**, *64*, 492–503.

Biographical Sketches



Dr. Jean Christophe Schrotter is currently a recognized membrane expert with 17 years of experience in membrane processes. Previously he was a lecturer at the University of Bath (UK) in the chemical Engineering Department; then he joined Anjou Recherche, the Water Research Centre of Veolia Company in September 2000, as a membrane R&D director. He is currently supervising a team of 23 people to develop innovative membrane processes for drinking, waste, and industrial water as well as for desalination applications with a recent emphasis on hybrid processes and membrane contactors. He has worked as a technical advisor for companies, as well as for public institutions. He has authored 6 patents and more than 90 publications and presentations related to membrane technology and applications.



Sophie Rapenne is a project leader of desalination and membrane R&D projects for Anjou Recherche – Veolia Water. She has an engineer degree in chemistry and chemical engineering with an MSc. in analytical chemistry and PhD in water chemistry and microbiology (University of Poitiers, France). Her thesis was on seawater desalination by reverse osmosis. She has experience in international and national research projects involving academic partners. She is involved in several pilot-scale studies for process evaluation and optimization. She is author and co-author of about 15 papers on desalination technologies.



Jerome Leparc has a Master of Science degree in chemical engineering from the National Polytechnique Institute of Nancy, France. Currently he is project manager in charge of the desalination R&D projects for Anjou Recherche – Veolia Water. He specialized in drinking water processes and membrane technologies, notably through international research projects involving academic partners, water treatment design and operating companies. He has also been a member of funding agencies (European Community, AWWARF). He is involved in numerous feasibility and pilot-scale studies for process evaluation and optimization on drinking water plants. He has authored/co-authored over 30 publications/proceedings on drinking water and desalination technologies.



Pierre-Jean Remize is a project leader on desalination R&D projects for Anjou Recherche – Veolia Water. He has a degree in chemical engineering (National Institute of Applied Sciences – INSA Toulouse, Fr) with an MSc in process engineering (University of Toulouse) and a PhD in environmental process engineering (INSA Toulouse). His thesis was on water treatment by ultrafiltration. He has been at Anjou Recherche since 2006. He is involved in several projects about desalination (water characterization, pretreatment, SWRO optimization).



Stello Casas is an experienced scientist in marine biology and chemistry. He is currently involved in Veolia R&D projects on the environmental impact assessment of discharges in marine environment using biological indicators. He has a PhD (2005) from Ifremer (French Institute of Marine Research). His thesis was on modelling trace metal bioaccumulation in the Mediterranean mussel *Mytilus galloprovincialis*. He held a postdoctoral position (2006) at the CSIC (Spanish national Research Council), where he worked on bioaccumulation of organic chemicals. He aims to develop integrative biomonitoring strategies to assess environmental impacts of coastal industrial activities, e.g. wastewater treatment plants and desalination plants.

2.04 Transport Phenomena in Nanofiltration Membranes

S Bandini and L Bruni, Università di Bologna, Bologna, Italy

© 2010 Elsevier B.V. All rights reserved.

2.04.1	Introduction	68
2.04.2	Theoretical Background: The DSP&DE Model	70
2.04.2.1	The General Physical Problem	70
2.04.2.2	Mass Transfer through the Membrane	71
2.04.2.2.1	Total flux	71
2.04.2.2.2	Solute flux	72
2.04.2.3	Solute Partitioning	72
2.04.2.3.1	Dielectric exclusion	74
2.04.2.4	Statement of the Problem	76
2.04.2.4.1	Rejection of neutral solutes	78
2.04.2.4.2	Rejection of single salts in neutral membranes	78
2.04.3	Model Applications	79
2.04.3.1	Approximated Versions of the DSP&DE Model	83
2.04.3.2	Parameter-Calculation Procedures	84
2.04.3.2.1	Some remarks on the volume membrane charge	86
2.04.4	Conclusions	87
References		87

Nomenclature

0^-	feed/membrane interface, feed side	K_{id}	diffusive hindrance factor
0^+	feed/membrane interface, membrane side	K_{eff}	effective convective coefficient, defined in Equation (28)
A	parameter defined in Equation (30)	K_{ieff}	effective convective coefficient, defined in Equation (26)
B	parameter defined in Equation (30)	L_p	hydraulic membrane permeability ($m s^{-1} Pa^{-1}$)
c	mole concentration ($mol m^{-3}$)	$L_p' = L_p * \delta$	permeability parameter defined in Equation (15) ($m^2 s^{-1} Pa^{-1}$)
C_{eq}	equivalent concentration ($mol m^{-3}$)	n	number of ionic species
D_{eff}	effective diffusive coefficient, defined in Equation (25) ($m^2 s^{-1}$)	N_A	Avogadro number ($= 6.023 \times 10^{23}$) (mol^{-1})
D_{ip}	hindered diffusivity inside the pore ($m^2 s^{-1}$)	P	pressure (Pa)
$D_{i\infty}$	bulk diffusivity at infinite dilution ($m^2 s^{-1}$)	Pe	hindered Peclet number defined in Equation (30)
e	elementary charge ($=1.602 \times 10^{-19}$) (C)	Pe_i	parameter defined in Equation (15)
F	Faraday constant ($=96485$) ($C mol^{-1}$)	r_B	parameter defined in Tables 2 and 3 (m)
I	$= \frac{1}{2} \sum_{i=1}^n z_i^2 c_i$ ionic strength ($mol m^{-3}$)	r_i	Stokes radius (m)
I_{el}	electric current density ($A m^{-2}$)	$r_{i,cav}$	cavity radius defined in Equation (10) (Table 2) (m)
j	mole solute flux ($mol m^{-2} s^{-1}$)	r_p	average pore radius (average slit semi-thickness) (m)
J_v	total volume flux ($m s^{-1}$)	R_i	real rejection defined in Equation (34) (Table 4)
k_B	Boltzmann constant ($=1.381 \times 10^{-23}$) ($J K^{-1}$)	\bar{V}	partial molar volume ($m^3 mol^{-1}$)
k_j	parameter defined in Equation (31)		
K_{ic}	convective hindrance factor		

x	axial coordinate in the membrane (m)	ε_r	dielectric constant
X	volume charge density (mol m^{-3})	ε_{rm}	membrane dielectric constant
z	ionic valence	ε_{rp}	dielectric constant of the pore solution
γ_{DE}	parameter defined in Table 2	ε_{rs}	dielectric constant of the bulk solution
γ_i	activity coefficient	η	water dynamic viscosity inside the pore ($\text{Pa}\cdot\text{s}^{-1}$)
δ	effective membrane thickness, accounting for tortuosity and porosity (m)	η_0	water dynamic viscosity in the external bulk ($\text{Pa}\cdot\text{s}^{-1}$)
δ^-	membrane/permeate interface, membrane side	κ^{-1}	Debye length (m)
δ^+	membrane/permeate interface, permeate side	λ_i	$= r_i/r_p$
Δ	difference	$\tilde{\mu}$	electrochemical potential (J mol^{-1})
ΔP	pressure difference across the membrane (Pa)	π	osmotic pressure (Pa)
ΔP_{eff}	effective pressure difference (Pa)	ϕ_i	steric partitioning coefficient, defined in Table 1
ΔW_{DE}	excess energy due to dielectric exclusion	ψ	dimensionless electrostatic potential
ΔW_{Born}	excess energy due to Born partitioning defined in Equation (9) (Table 2)	Ψ	electrostatic potential (V)
ΔW_{im}	excess energy due to image forces, defined in Equations (10) and (11) (Table 3)		
$\Delta\psi_D$	Donnan potential		
ε_0	vacuum permittivity ($=8.854 \times 10^{-12}$) ($\text{C}^2 \text{J}^{-1} \text{m}^{-1}$)		

Subscripts

0	at the feed/membrane interface
1	cation
2	anion
asym	asymptotic conditions
<i>i</i>	ion or uncharged solute
δ	at the membrane/permeate interface

2.04.1 Introduction

The recent extensive developments of nanofiltration (NF) technology have shown evidence for the real application potentialities of this innovative pressure-driven membrane process used for the separation and the purification of liquid mixtures. The development of mathematical models describing transport mechanisms through the membrane is essential to predict and to optimize membrane performances, in the case of both simple systems and multicomponent systems containing electrolyte mixtures and neutral solutes.

Polymeric or ceramic NF membranes typically show separation characteristics, which are intermediate between ultrafiltration and reverse osmosis (RO). The most interesting feature of the process is the possibility to separate electrolyte solutions based on ion valence and to obtain a relatively complete retention of neutral substances such as complex sugars.

In the case of neutral solutes, partitioning between feed and membrane is mainly related to

size-exclusion effects, and molecular weight cutoff is generally sufficient to describe the separation efficiency of the membrane. In the case of electrolyte solutions, rejection properties of the membrane are remarkably affected by type and valence of the ionic species as well as by the type of membrane material and strongly depend on operative conditions such as pH and ionic strength values existing in the feed side [1–29].

With single symmetric salts, such as NaCl or KCl, salt rejection generally decreases as the concentration increases at constant pH values, whereas rejection goes through a minimum value as feed pH increases [1–29].

In the case of nonsymmetric electrolytes, on the contrary, physical–chemical interactions of the salt with the membrane can be relevant; trends are often reversed with respect to the NaCl-type behavior [5, 9–12, 14–16, 18, 24, 25, 28]. As an example, with polyamide membranes in aqueous solutions, at low salt concentrations, MgCl_2 rejection as well as CaCl_2 rejection increase as the concentration increases and

a maximum rejection value is obtained when both the salt concentration and the feed pH increase. Such general behavior is basically obtained also in the case of inorganic membranes [15, 16, 24].

Conversely, electrochemical characterizations of the membrane material (e.g., electrokinetic measurements of streaming potential [5, 6, 17, 30–37], membrane potential measurements [26, 27, 38, 39], and titration experiments [40, 41]) have shown evidence that the membrane surface is endowed with charges which are strictly dependent on feed pH, as well as on type and concentration of electrolytes; amphoteric behavior is also frequently observed for a wide class of polymeric as well as of ceramic membranes. In addition, physical–chemical interactions of multivalent ions with the membrane are stronger than the ones typically existing with univalent electrolytes; in particular, at fixed pH values, calcium binding on ionized sites of the membrane can be so remarkable that zeta potentials switch from negative to positive values and the points of zero charge are greatly affected by salt concentration [35]. In general, the amphoteric behavior of NF membranes is related to the presence of a surface membrane charge whose value and sign are due to the contribution of both a proper charge (strictly connected with the membrane material and caused by the acid/base dissociation of hydrophilic sites), which is counterbalanced by the dissolved ions (giving rise to site-binding phenomena on the dissociated hydrophilic sites), as well as an adsorption charge located on the hydrophobic sites of the membrane [31, 38, 39, 42–46].

The question about the mathematical modeling of electrolytes and neutral solute transport through charged membranes is well known for about 40 years [47–50]. The key points of the problem can be basically identified both in the characterization of the membrane, which can be seen as a homogeneous or as a porous medium, and in the understanding of the electrostatic phenomena giving rise to ion partitioning and affecting the transport of ionic species through the membrane. Such aspects must account for the presence of a surface membrane charge.

Atomic force microscope measurements indicate that, for most of NF membranes, pores do exist [51–54]: average pore radii are in the range from 0.3 to 1 nm, only one order of magnitude greater than atomic dimensions. The combination of nanoscale pore dimensions with electrically charged materials makes the partitioning and transport problem extremely complex, involving several phenomena.

Original descriptions of ion transport in NF were based on phenomenological approaches derived from

irreversible processes of thermodynamics [47–49], in which the membrane is assumed basically as a black box; in these models, it is difficult to characterize the structural and electrical properties of the membrane and the extension to multicomponent systems is very complex. However, some authors applied these types of models successfully [55–60].

Transport of uncharged solutes has been first described by continuum hydrodynamic models [61]; later, porous membranes were modeled as bundles of straight cylindrical pores and solute transport was corrected on account of hindered diffusion and convection caused by solute–membrane interactions, owing to the moving of a species in a confined spaces [62].

Nowadays, it is recognized that the separation mechanism of the process is remarkably related to the steric and electrostatic partitioning effects between the membrane and the external solutions. Most of the recently developed models accept a porous vision of the membrane and propose to describe mass transfer through the extended Nernst–Planck (ENP) equation. Some of them are the application of the space charge model (SCM), originally proposed by Gross and Osterle [63] and by Jacazio *et al.* [64], in which the volumetric flux is described through the Navier–Stokes equation, ions are treated as point charges moving across the membrane according to the NP equation, and the radial distribution of electric potential and ion concentration is accounted for by using the Poisson–Boltzmann equation [62, 63, 65–68].

Because of its numerical complexity, SCM is used in simplified forms, which are versions of the fixed-charge model proposed by Teorell [69, 70] and Meyer and Sievers [71].

At present, the most widely used models derive from the SCM with the approximation that ion concentration and electric potential are radially homogeneous across the pore and that the fixed charge is uniformly distributed in the membrane volume [6–8, 20, 42, 51, 65, 73–76]. This approximation is valid for sufficiently weak membrane charges and tight pores as indicated by several authors [42, 72, 73].

In addition, NP equation is appropriately modified by some authors for taking into account of the hindered transport through narrow pores comparable with the molecular dimensions of the permeating species.

All those models, however, assume Donnan equilibrium as the only electrostatic phenomenon involved in the ion partitioning at the interfaces between the membrane and the liquid phases. It was only after the 2000s that some authors began to extensively introduce the dielectric exclusion (DE) phenomenon as an additional

electrostatic partitioning effect, which could explain the high rejection values measured for multivalent counterions, for which the only Donnan equilibrium would have erroneously predicted a more favorable partitioning inside the membranes. The mechanism of DE of ions from membranes was originally considered by Glueckauf [77] and recently by other authors as well [4, 5, 9, 14, 78–81].

Finally, all the models make use of several parameters to characterize the membrane: there are structural parameters, such as average pore radius, membrane thickness, tortuosity, and porosity; electrical parameters, such as the surface or volume membrane charge; and electrochemical parameters, such as the dielectric constants of the membrane and of the solutions inside/outside the pores. In addition, depending on the authors, all the parameters are considered as adjustable parameters or, alternatively, some of them can be obtained by independent measurements, such as tangential streaming potential, filtration potential, membrane potential, atomic force microscopy, and titration experiments.

From a general viewpoint, the description of transport phenomena occurring in NF membranes is a problem characterized by manifold aspects, which are discussed in detail in the following sections. Although many papers are published on this topic every year, the problem to be solved is the development of a model which can be a reasonable compromise between very complex models (able to describe the variation of membrane properties as well as the mass transfer through the membrane, as a function of the position inside the membrane itself) and extremely simplified models (the phenomenological models), requiring few parameters to be calculated as a function of operative variables and of the solute type whenever any condition changes.

In the following, the statement of the general physical problem is first defined and the more advanced models are considered that describe

1. solute partitioning at the interfaces between the membrane and the external phases;
2. solute transport across the membrane; and
3. water or total flux across the membrane.

The choice is made of describing in detail the general version of the most used model at present, the DSP&DE, which is a revised and extended version by some authors of the original DSP model (DSPM) introduced by Bowen and Mukhtar [8].

A detailed discussion of the model potentialities in simulating NF membrane performances is provided, and a critical analysis of the numerical complexity of

the mathematical problems encountered in the treatment of multicomponent systems as well as membrane parameters is presented.

In this chapter, the phenomena involved in membrane characterization are presented, assuming the solute concentrations, existing at the feed/membrane interface, as known values. For the evaluation of mass transfer resistance in the external phases of the membrane, the typical techniques can be used such as the film theory model or any other specific application of it to NF modules with multicomponent solutions [82, 83]. The DSP&DE model is indeed introduced as a local model, with reference to a generic membrane section, whose equations can be implemented in any simulation program to describe the performances of the module under investigation.

2.04.2 Theoretical Background: The DSP&DE Model

2.04.2.1 The General Physical Problem

An NF membrane separates two aqueous liquid phases (the feed and the permeate) kept at different pressure values (ΔP); the main operative variables are related to the feed conditions (kind of solutes, concentration, pH, temperature, pressure, and flow rate) and to the permeate conditions (the pressure downstream the membrane). Depending on the membrane material as well as on the feed conditions, the membrane generally assumes a surface charge located at each interface existing between a liquid phase and the polymeric material [5, 6, 17, 26, 27, 30–45].

In order to characterize the membrane performances (solute rejection and total transmembrane flux), the solute flux as well as the water flux through the membrane must be calculated. With reference to a generic section of the membrane (**Figure 1**), the problem can be considered in a plane geometry. In the case in which electrolyte solutions are processed, it generally requires the description of the basic mechanisms determining

1. total transmembrane flux;
2. solute transport across the membrane; and
3. solute partitioning at the interfaces between the membrane and the external phases.

Outputs of the problem are the concentration profile of the species and the electric potential profile through the pore, as well as the solute and total fluxes across the membrane. From a general viewpoint, operating in steady-state conditions, the concentration

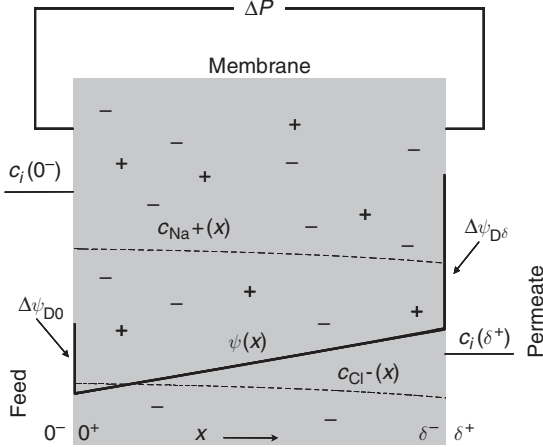


Figure 1 Scheme of a generic membrane section. Coordinate system for the Donnan steric pore and dielectric exclusion (DSP&DE) model: electric potential and concentration profiles are reported with reference to NaCl-water solutions. Net membrane charge is negative and it is uniformly distributed.

of each specie varies with the radial as well as with the axial coordinate along the membrane pore; the surface membrane charge depends on the axial coordinate, whereas the fluxes of each species are constant along the pore.

The problem solution requires the knowledge of some parameters:

- structural parameters of the membrane (pore geometry, pore radii distribution, porosity, thickness, and tortuosity);
- electric parameters of the membrane (surface/volume membrane charge distribution); and
- electrochemical parameters (dielectric constants of the membrane material and of the solutions outside and inside the membrane pore).

Thus, the problem appears very complex, even in the case of aqueous solutions containing a single strong binary electrolyte. The most general model developed at present is the SCM [63–68], in which the volumetric flux is described through the Navier–Stokes equation, ions are treated as point charges moving across the membrane according to the NP equation, and the radial distribution of electric potential and ion concentration is accounted for by using the Poisson–Boltzmann equation. Owing to its numerical complexity, SCM is used in simplified forms, which are versions of the fixed-charge model proposed by Teorell, and Meyer and Sievers, with the approximations that ion concentration and electric potential are radially homogeneous

across the pore and that the fixed charge is uniformly distributed in the membrane volume (the approximation is valid for weak membrane charges and narrow pores). Based on this idea, some successful unidimensional models were developed by some authors [8, 9, 14, 51, 52, 74, 75, 80, 81, 84–90]. Each author named the model with a different abbreviation and introduced improvements in the description of the partitioning phenomena; however, the models are basically an extension of the original DSPM developed by Bowen and Mukhtar [8].

In the following sections, a synthesis of the work mentioned above is reported and the general features are discussed. The general model is termed as DSP&DE model, for historical reasons. Basically, it can be applied to polymeric as well as to ceramic membranes, although most of the results concern polymeric materials. Reference is made to the coordinate system shown in **Figure 1**, according to which the membrane is considered as a bundle of identical pores whose length is much larger than their diameter and the motion of the species is assumed as unidirectional through the membrane.

2.04.2.2 Mass Transfer through the Membrane

2.04.2.2.1 Total flux

Experimental data obtained in NF of pure water, as well as of aqueous solutions containing electrolytes and/or neutral solutes [8, 9, 21, 23, 28, 51, 85], have clearly shown evidence that there is a linear proportionality between the total transmembrane flux and the driving force maintained across the membrane. As a consequence, the standard relationships, typically used for RO membranes, can be considered in which the volume flux linearly depends on the effective pressure difference existing across the membrane ΔP_{eff} , through the water permeability L_p [91], according to the following relationship:

$$\mathcal{J}_v = L_p \Delta P_{\text{eff}} = L_p (\Delta P - \Delta \pi) \quad (1)$$

in which $\Delta \pi$ is the osmotic pressure difference across the membrane, which must be calculated at the composition values existing at the membrane/external phases interfaces in the case in which concentration polarization occurs. In general, since NF can be seen as an RO operation with more permeable membranes, the effective driving force should contain the Staverman reflection coefficient also; in the

most cases investigated, however, its contribution was clearly negligible. In addition, in view of the porous nature of the membrane, the Hagen–Poiseuille flow can be considered under the hypothesis of constant pressure gradient along the membrane pore, according to the corresponding relationships for the various pore geometries:

$$\mathcal{F}_v = \frac{r_p^2}{8\eta\delta} \Delta P_{\text{eff}} \quad (\text{cylindrical pores}) \quad (2)$$

$$\mathcal{F}_v = \frac{r_p^2}{3\eta\delta} \Delta P_{\text{eff}} \quad (\text{slit pores}) \quad (3)$$

in which η represents the viscosity of the solution inside the pore. L_p can be obtained through NF experiments with pure water, by data reduction according to Equation (1). As far as Equation (1) holds true, L_p represents the water permeability; as a consequence, we can assume that the viscosity of the solution inside the pore corresponds to the water viscosity inside the pore. Unfortunately, there is a certain level of uncertainty in determining that quantity, since the assumption of bulk solvent properties may not be valid within narrow pores: the use of bulk water viscosity η_0 may lead to an overestimation of L_p , since the actual viscosity η may be increased with respect to η_0 by interactions of water dipole with the charge pore walls. The problem has been studied in detail by Bowen and Welfoot [9], and it was recognized that η/η_0 can be close to 10. This aspect is also considered in Section 2.04.3.2 related to the calculation of parameters. Recently, Geens *et al.* [92] performed an extensive investigation on which parameters determine membrane permeability and concluded that Hagen–Poiseuille-type equations were sufficiently accurate to describe the behavior of hydrophilic NF membranes.

2.04.2.2.2 Solute flux

The basic equation for the description of mass transfer of a generic specie across the membrane is the ENP equation. Under the approximation of no direct coupling between species fluxes (since dilute aqueous solutions are generally processed), the flux of each species, j_b can be written as a function of the electrochemical potential:

$$j_i = K_{ic} c_i \mathcal{F}_v - \frac{c_i D_{ip}}{RT} \frac{d\tilde{\mu}_i}{dx} \quad (4)$$

in which D_{ip} is the hindered diffusivity of the specie inside the pore ($D_{ip} \eta = K_{id} D_{i\infty} \eta_0$, $D_{i\infty}$ is the diffusivity of the specie in water at infinite dilution), and K_{ic} and K_{id} are the hindrance factors for convection

and diffusion, respectively. It must be observed that the axial coordinate x accounts for also the tortuosity and the porosity of the membrane; the membrane thickness resulting from the integration of Equation (4) is then an effective membrane thickness.

Equation (4) can be rewritten in an explicit form, accounting for the dependence of the electrochemical potential on activity, pressure, as well as on the electrostatic potential, according to Equation (5):

$$j_i = K_{ic} c_i \mathcal{F}_v - c_i D_{ip} \frac{d \ln \gamma_i}{dx} - D_{ip} \frac{dc_i}{dx} - \frac{c_i D_{ip} \bar{V}_i}{RT} \frac{dP}{dx} - z_i c_i D_{ip} \frac{F}{RT} \frac{d\Psi}{dx} \quad (5)$$

which can be easily simplified into Equation (6), neglecting the contributions of the gradient of $\ln \gamma_i$ as well as of the pressure gradient on the solute flux:

$$j_i = K_{ic} c_i \mathcal{F}_v - D_{ip} \frac{dc_i}{dx} - z_i c_i D_{ip} \frac{F}{RT} \frac{d\Psi}{dx} \quad (6)$$

Equation (6) is a simplified form of the ENP equation, accounting for convection, diffusion, and electromigration (in the case of charged solutes) through the membrane pores; it is appropriately modified to account for the hindered transport of the permeating species through narrow pores comparable with the molecular dimensions. The meaning and relevance of hindrance factors K_{ic} and K_{id} have been widely documented by Deen [62], as well as by many other authors [93–100]. K_{ic} is a drag factor accounting for the effects of the pores walls on the specie motion; K_{id} represents the effect of the pore to reduce the solute–solvent diffusion coefficient below its value in the free bulk solution ($D_{i\infty}$). Hindrance factors are related to the hydrodynamic coefficients calculated from the solution of the motion problem of a spherical specie inside cylindrical as well as slit-like pores of infinite length; they depend on the solute to pore-size ratio, λ_i . A collection of the various relationships proposed to calculate hindrance factors is reported in Table 1, for cylindrical as well as for slit geometry; various solutions are considered in which the solute particle is located at different radial coordinates of the pore (centerline approximation, cross-sectional average, solvent velocity parabolic profile, etc.).

2.04.2.3 Solute Partitioning

Partitioning of the i specie at the interfaces between the membrane and the external solutions is described through the following equations:

Table 1 Hindrance factors

<i>Cylindrical pores</i>	<i>Ref.</i>
$\phi_i = (1 - \lambda_i)^2$ $K_{ic} = (2 - \phi_i)^{\#} \left(1 - \frac{2}{3}\lambda_i^2 - 0.163\lambda_i^3\right)$ $K_{id} = (1 - 2.1044\lambda_i + 2.089\lambda_i^3 - 0.948\lambda_i^5)$ Centerline approximation $0 \leq \lambda_i < 0.4$	[93]
$K_{ic} = (2 - \phi_i)^{\#} K_{i,s} / (2K_{i,t}); K_{id} = \frac{6\pi}{K_{i,t}}$ $K_{i,t} = \frac{9}{4} \pi^2 \sqrt{2} (1 - \lambda_i)^{-5/2} \left[1 + \sum_{n=1}^2 a_n (1 - \lambda_i)^n\right] + \sum_{n=0}^4 a_{n+3} \lambda_i^n$ $K_{i,s} = \frac{9}{4} \pi^2 \sqrt{2} (1 - \lambda_i)^{-5/2} \left[1 + \sum_{n=1}^2 b_n (1 - \lambda_i)^n\right] + \sum_{n=0}^4 b_{n+3} \lambda_i^n$ $a_1 = -73/60, a_2 = 77.293/50.400, a_3 = -22.5083, a_4 = -5.6117, a_5 = -0.3363, a_6 = -1.216,$ $a_7 = 1.647$ $b_1 = 7/60, b_2 = -2.227/50.400, b_3 = 4.0180, b_4 = -3.9788,$ $b_5 = -1.9215, b_6 = 4.392, b_7 = 5.006$ Centerline approximation $0 \leq \lambda < 1$	[98]
$K_{ic} = (2 - \phi_i)^{\#} (1.0 + 0.054\lambda_i - 0.988\lambda_i^2 + 0.441\lambda_i^3)$ $K_{id} = 1.0 - 2.30\lambda_i + 1.154\lambda_i^2 + 0.224\lambda_i^3$ Centerline approximation $0 \leq \lambda_i < 0.8$	[94]
$K_c = \frac{\phi_i (1 + 2\lambda_i - \lambda_i^2) (1 - 2/3\lambda_i^2 - 0.20217\lambda_i^5)}{(1 - 0.75857\lambda_i^5)}$ $K_d = \frac{\phi_i (1 - 2.105\lambda_i + 2.0865\lambda_i^3 - 1.7068\lambda_i^5 + 0.72603\lambda_i^6)}{(1 - 0.75857\lambda_i^5)}$ Centerline approximation $0 \leq \lambda_i < 0.9$	[97]
$K_{ic} = \left(\frac{1 + 3.867\lambda_i - 1.907\lambda_i^2 - 0.834\lambda_i^3}{1 + 1.867\lambda_i - 0.741\lambda_i^2} \right)$ $K_{id} = (1 + a_1\lambda_i \ln\lambda_i - a_2\lambda_i + a_3\lambda_i^2 + a_4\lambda_i^3 - a_5\lambda_i^4 + a_6\lambda_i^5 + a_7\lambda_i^6 - a_8\lambda_i^7) / \phi_i$ $a_1 = 9/8; a_2 = 1.56034; a_3 = 0.528155; a_4 = 1.91521;$ $a_5 = 2.81903; a_6 = 0.270788; a_7 = 1.10115; a_8 = 0.435933$ Cross-sectional average $0 \leq \lambda_i < 1$	[100]
<i>Slit-like pores</i>	<i>Ref.</i>
$\phi_i = (1 - \lambda_i)$ $K_{ic} = \frac{1}{2} (3 - \phi_i^2) \left(1 - \frac{\lambda_i^2}{3} + O(\lambda_i^3)\right)$ $K_{id} = 1 - 1.004\lambda_i + 0.418\lambda_i^3 + 0.21\lambda_i^4 - 0.169\lambda_i^5 + O(\lambda_i^6)$ Centerline approximation $0 \leq \lambda_i < 1$	[62,99]

(Continued)

Table 1 (Continued)

<i>Slit-like pores</i>	<i>Ref.</i>
$K_{ic} = (1 - b_1\lambda_i^2 + b_2\lambda_i^3 - b_3\lambda_i^4 + b_4\lambda_i^5 - b_5\lambda_i^6 + b_6\lambda_i^7) / \phi_i$ $K_{id} = (1 + a_1\lambda_i \ln \lambda_i - a_2\lambda_i + a_3\lambda_i^3 - a_4\lambda_i^4 + a_5\lambda_i^5) / \phi_i$ <p> $a_1 = 9/16; a_2 = 1.19358; a_3 = 0.4285; a_4 = 0.3192; a_5 = 0.08428$ $b_1 = 3.02; b_2 = 5.776; b_3 = 12.3675; b_4 = 18.9775; b_5 = 15.2185; b_6 = 4.8525$ </p>	[100]
Cross-sectional average $0 \leq \lambda_i < 0.95$	
# $(2 - \phi_i)$ accounts a parabolic profile for solvent velocity.	

$$\frac{c_i(0^+)}{c_i(0^-)} = \phi_i \frac{\gamma_i(0^-)}{\gamma_i(0^+)} \exp(-z_i \Delta \psi_{D0}) \exp(-z_i^2 \Delta W_{DE0}) \quad (7)$$

$$\frac{c_i(\delta^-)}{c_i(\delta^+)} = \phi_i \frac{\gamma_i(\delta^+)}{\gamma_i(\delta^-)} \exp(-z_i \Delta \psi_{D\delta}) \exp(-z_i^2 \Delta W_{DE\delta}) \quad (8)$$

With reference to charged solutes, the ion partitioning coefficient at each interface takes into account of four contributions: steric exclusion, through ϕ_b , nonideality of the solutions, through activity coefficients γ_i , Donnan equilibrium, through $\Delta \psi_D$, and DE, through ΔW_{DE} , defined through Equations (9)–(13) in **Table 2**, which are discussed in detail in the next section.

Steric exclusion and activity coefficients are the only partitioning effects existing in the case of neutral solutes.

Steric exclusion accounts for the sieve effect, due to the intrinsic porosity of the membrane; it depends on the pore geometry and it is in the range between 0 (for solutes larger than the pore radius) and 1 (for point solutes) [62] (**Table 1**).

Activity coefficients of the ionic species can be expressed according to the Debye–Hückel theory or its developments, depending on the concentration range of the solutions processed. A collection of some relationships proposed by various authors to calculate ion activity coefficients is reported in **Table 3**. It must be observed that, in general, the ideal solution hypothesis is not valid for electrolytes solutions, even at the typical low concentrations existing in NF operations. Experience shows that for NaCl solutions the limiting Debye–Hückel theory is a good approximation, whereas in the case of multivalent nonsymmetric salts more advanced models should be used [101]. Finally, the relationships reported in **Table 3** should be used carefully in that they refer to the description of electrolyte solution behaviors, which are not influenced by the confinement in narrow pores; their use inside the pore gives

only an estimation of the properties, since in that case modifications of the water dipole can occur and the hypotheses of the corresponding theories cannot be fully fulfilled (e.g., the hypothesis of local electroneutrality condition in the Debye–Hückel theory could not be fully valid). In the case of neutral solutes, activity coefficients can be expressed making use of the typical models used in thermodynamics.

Donnan equilibrium plays a relevant role in the case of charged membranes and it is effective in the partitioning of ions owing to the Donnan potential arising both at the feed/membrane and at the membrane/permeate interfaces; it always offers favorable partitioning for counterions and unfavorable partitioning for coions.

DE arises as a consequence of the difference existing between the dielectric properties of the aqueous solution inside and outside the membrane pores and the dielectric properties of the membrane material. The main macroscopic effect is the presence of polarization charges induced by the ions of the aqueous solution on the boundary surface between the two dielectric media (the pore surface). In the DSP&DE model, as a simplification, all the partitioning effects related to the DE are collected in the partitioning coefficients at the feed/membrane as well as at the membrane/permeate interfaces. As shown in Equations (7) and (8), the DE partitioning effect is always unfavorable for any ion, independent of the ion sign. It is important to observe that the DE phenomenon is remarkably relevant also in the case of uncharged membranes, whereas electric exclusion related to Donnan equilibrium approaches zero.

2.04.2.3.1 Dielectric exclusion

The mechanism of DE of ions from membranes was originally considered by Glueckauf [77] and recently by other authors as well [4, 5, 9, 14, 78–81]. In the

Table 2 Dielectric exclusion: Excess solvation energies

Dielectric exclusion

$$\Delta W_{\text{DE}} = \Delta W_{\text{im}} + \Delta W_{\text{Born}}$$

Born exclusion

$$\Delta W_{\text{Born},i} = \frac{e^2}{8\pi\epsilon_0 k_B T r_{i,\text{cav}}} \cdot \left(\frac{1}{\epsilon_{\text{rp}}} - \frac{1}{\epsilon_{\text{rs}}} \right) \quad (9)$$

Image force – cylindrical pores

$$\Delta W_{\text{im}}(0) = \frac{2r_{\text{B}}(0^+)}{\pi r_{\text{p}}} \int_0^\infty \frac{K_0(k)K_1(v(0)) - \tilde{\beta}_0(k)K_0(v(0))K_1(k)}{I_1(v(0))K_0(k) + \tilde{\beta}_0(k)I_0(v(0))K_1(k)} dk \quad (10)$$

$$\Delta W_{\text{im}}(\delta) = \frac{2r_{\text{B}}(\delta^-)}{\pi r_{\text{p}}} \int_0^\infty \frac{K_0(k)K_1(v(\delta)) - \tilde{\beta}_\delta(k)K_0(v(\delta))K_1(k)}{I_1(v(\delta))K_0(k) + \tilde{\beta}_\delta(k)I_0(v(\delta))K_1(k)} dk \quad (11)$$

in which

$$\tilde{\beta}_0(k) = \frac{k}{v(0)} \frac{\epsilon_{\text{rm}}}{\epsilon_{\text{rp}}}; \quad \tilde{\beta}_\delta(k) = \frac{k}{v(\delta)} \frac{\epsilon_{\text{rm}}}{\epsilon_{\text{rp}}}$$

$$v^2(0) = k^2 + (r_{\text{p}}\kappa(0^+))^2; \quad v^2(\delta) = k^2 + (r_{\text{p}}\kappa(\delta^-))^2;$$

I_0, I_1, K_0, K_1 : modified Bessel functions

Image force – slit-like pores

$$\Delta W_{\text{im}}(0) \cong -r_{\text{B}}(0^+) \frac{1}{r_{\text{p}}} \ln \left[1 - \gamma_{\text{DE}} \exp(-2r_{\text{p}}\kappa(0^+)) \right] \quad (12)$$

$$\Delta W_{\text{im}}(\delta) \cong -r_{\text{B}}(\delta^-) \frac{1}{r_{\text{p}}} \ln \left[1 - \gamma_{\text{DE}} \exp(-2r_{\text{p}}\kappa(\delta^-)) \right] \quad (13)$$

in which

$$r_{\text{B}}(0^+) = r_{\text{B}}(\delta^-) = \frac{F^2}{8\pi\epsilon_0\epsilon_{\text{rp}}RTN_{\text{A}}}; \quad \kappa^{-1}(0^+) = \frac{1}{F} \sqrt{\frac{\epsilon_0\epsilon_{\text{rp}}RT}{2I(0^+)}}; \quad \kappa^{-1}(\delta^-) = \frac{1}{F} \sqrt{\frac{\epsilon_0\epsilon_{\text{rp}}RT}{2I(\delta^-)}};$$

$$\gamma_{\text{DE}} = \frac{1 - \epsilon_{\text{rm}}/\epsilon_{\text{rp}}}{1 + \epsilon_{\text{rm}}/\epsilon_{\text{rp}}}$$

case under investigation, in which a dilute aqueous solution is in contact with a polymeric membrane and, more precisely, flows through the charged narrow pores of a membrane, the phenomenon is due to a series of concomitant effects.

The primary effect is caused by the difference existing between the dielectric constant of an aqueous solution and the corresponding value of the polymeric matrix. Electrostatic interactions arise between the ions of the solutions and the polarization charges, induced by the ions themselves on the discontinuity surface located in the boundary between the two dielectric media. Since the dielectric constant of an aqueous solution is remarkably higher than the corresponding value of the polymeric matrix (ϵ_{rm}), the polarization charges have the same sign as the ionic charges of the aqueous solutions. As a consequence,

when the ion enters the pore membrane it faces an image force, created by the ion itself, which is opposite to the ion entrance; these interactions always cause an additional rejection mechanism for each ion, independently of its sign, which can be described making use of an excess solvation energy term (ΔW_{im}).

The phenomenon has been widely studied and described with suitable approximations for NF membranes by Yaroshchuk [78] who developed simple relationships for cylindrical pores as well as for slit-like geometry, as reported in **Table 2**. Applications of these relationships [14, 81] have clearly shown evidence that the slit geometry approximation is more probable for NF membranes, since too much higher rejections are predicted in the case of cylindrical pores. With regard to the relationships for the slit geometry (Equations (12) and (13) in **Table 2**), it

Table 3 Activity coefficients for ions in electrolyte aqueous solutions

	Activity coefficients	Ref.
Debye–Hückel limiting law	$\gamma_i = \exp(-z_i^2(r_B \kappa))$	[14,81]
Debye–Hückel law	$\gamma_i = \exp\left(-z_i^2\left(r_B \frac{\kappa}{1 + \kappa r_i}\right)\right)$	[81,82]
Davies equation	$\gamma_i = \exp\left(-z_i^2\left(\frac{r_B \kappa}{1 + \sqrt{I}} - 0.3I\right)\right)$	[108]

$$r_B = \frac{F^2}{8\pi\epsilon_0\epsilon_rRTN_A}; \quad \kappa^{-1} = \frac{1}{F} \sqrt{\frac{\epsilon_0\epsilon_rRT}{2I}}$$

can be observed that the partitioning contribution related to the image forces depends on the solvent property inside the pore (ϵ_{rp}), the dielectric properties of the membrane material (ϵ_{rm}), as well as the ionic concentration inside the membrane ($\kappa(0^+)$, $\kappa(0^-)$).

For both geometries, the effect of the image forces is assumed to be located at the pore mouth: all the partitioning effects related to the DE are collected in the distribution coefficients at the feed/membrane as well as at the membrane/permeate interface, assuming the separation effect of the polarization charges along the membrane pores as negligible.

The secondary effect is due to the variations of the solvent dielectric properties inside the membrane pores with respect to the external bulk values, which are caused by an alteration of the solvent structure when it is confined in small narrow pores [4, 9, 78, 80, 81, 102–106]. As a consequence, since the solvent dielectric constant inside the pore (ϵ_{rp}) is lower than the corresponding value in the external solutions (ϵ_{rs}), an additional partitioning mechanism occurs, well known as Born partitioning, corresponding to an additional energy barrier for the ion ($\Delta W_{\text{Born},i}$). The original relationship developed by Born accounted for the influence of the solvent on the solute radius; as a simplification, authors generally assume a constant value for the ionic radius ($r_{i,\text{cav}}$) as reported in Table 2. Various approximations can be used to estimate $r_{i,\text{cav}}$: Pauling radius (as Born did), Stokes radius [9], and the radius of the cavity formed by the ion in the solvent [81, 107]. However, independently of the value used to estimate $r_{i,\text{cav}}$, it must be stressed that the partitioning contribution related to the Born energy depends only on the solvent properties (ϵ_{rp} , ϵ_{rs}) and on the ion characteristics; however, it depends neither on the pore geometry nor on the ionic concentration inside the membrane.

2.04.2.4 Statement of the Problem

Basic equations of the DSP&DE model are summarized in Table 4.

The ENP equation (Equation (6)) can be rewritten to obtain a relationship for the concentration gradient of each ionic specie; in addition, it can be rearranged also into Equation (14) (Table 4) in which the parameter Pe_i is defined in a straightforward manner.

In view of the porous nature of the membrane, the Hagen–Poiseuille flow type (Equations (2) and (3)) can be used; in the case of cylindrical pores, the following relationships are obtained to calculate Pe_i . The corresponding equations for slit geometry can be derived straightforwardly basing on Equation (3):

$$\begin{aligned} Pe_i &= \frac{\mathcal{F}_v K_{ic} \delta}{D_{ip}} = \frac{K_{ic} L_p' \Delta P_{\text{eff}}}{D_{ip}} = \frac{K_{ic} r_p^2 \Delta P_{\text{eff}}}{8\eta D_{ip}} = \frac{K_{ic} r_p^2 \Delta P_{\text{eff}}}{8\eta_0 K_{id} D_{i\infty}} \\ &= \frac{\mathcal{F}_v K_{ic} r_p^2}{8\eta_0 K_{id} D_{i\infty} L_p} \propto \mathcal{F}_v r_p^2 \end{aligned} \quad (15)$$

in which L_p' represents a kind of water permeability coefficient including all the membrane characteristics with the exception of the effective thickness. Apparently, independently of the pore geometry, Pe_i can be assumed related to r_p^2 , approximately.

Under the hypothesis of constant volumetric charge density across the membrane, the derivative of Equation (16) can be performed with respect to the axial coordinate of the membrane and the relationships reported in Equation (17) can be obtained to calculate the potential gradient.

It can be observed that Pe_i (quite similar to a sort of Peclet number for the ionic species i) is independent of the membrane thickness δ , since membrane permeability can be considered inversely proportional to δ . (This aspect is very useful when we are

Table 4 Basic equations of the DSP&DE model

Concentration gradient through the membrane:

$$\frac{dc_i}{dx} = \frac{J_V}{D_{ip}} \left[K_{ic} c_i - c_i(\delta^+) \right] - \frac{z_i c_i F}{RT} \frac{d\Psi}{dx} = \frac{Pe_i}{\delta} \left[c_i - \frac{c_i(\delta^+)}{K_{ic}} \right] - \frac{z_i c_i F}{RT} \frac{d\Psi}{dx} \quad (14)$$

Potential gradient through the membrane:

$$\frac{d\Psi}{dx} = \frac{\sum_{i=1}^n z_i \frac{J_V}{D_{ip}} [K_{ic} c_i - c_i(\delta^+)]}{\frac{F}{RT} \sum_{i=1}^n z_i^2 c_i} = \frac{\sum_{i=1}^n z_i \frac{Pe_i}{\delta} \left[c_i - \frac{c_i(\delta^+)}{K_{ic}} \right]}{\frac{F}{RT} \sum_{i=1}^n z_i^2 c_i} \quad (17)$$

Electroneutrality conditions:

$$\sum_{i=1}^n z_i c_i + X = 0 \quad (16)$$

$$\sum_{i=1}^n z_i c_i(\delta^+) = 0 \quad (22)$$

Partitioning at the membrane/external solutions interfaces:

$$\frac{c_i(0^+)}{c_i(0^-)} = \phi_i \frac{\gamma_i(0^-)}{\gamma_i(0^+)} \exp(-z_i \Delta\psi_{D0}) \exp(-z_i^2 \Delta W_{DE0}) \quad (7)$$

$$\frac{c_i(\delta^-)}{c_i(\delta^+)} = \phi_i \frac{\gamma_i(\delta^+)}{\gamma_i(\delta^-)} \exp(-z_i \Delta\psi_{D\delta}) \exp(-z_i^2 \Delta W_{DE\delta}) \quad (8)$$

Total flux

$$J_V = L_p (\Delta P - \Delta \pi) \quad (32)$$

Solute flux

$$j_i = J_V c_i(\delta^+) \quad (33)$$

Real rejection

$$R_i = 1 - \frac{c_i(\delta^+)}{c_i(0^-)} \quad (34)$$

in which

$$D_{ip} = K_{id} D_{i\infty} \frac{\eta_0}{\eta} \quad (35)$$

$$Pe_i = \frac{J_V K_{ic} \delta}{D_{ip}} \quad (15)$$

 $\phi_i, \gamma_i, K_{ic}, K_{id}$ defined in **Tables 2 and 3**

faced with the problem of calculating the membrane parameters, in that r_p calculation can be performed separately from the determination of the effective membrane thickness.) As a consequence, both the potential and the concentration gradients are inversely proportional to the membrane thickness. Therefore, the concentration difference across the membrane obtained from the integration of those functions will be independent of the membrane thickness and the rejection of each ion will be independent of δ as well. However, this conclusion does not mean that one can calculate rejection by

assuming an arbitrary membrane thickness, rather that, after the right calculation of Pe_i , any membrane thickness value can give the right rejection. The problem is then transferred into the determination of the parameter Pe_i which can be expressed according to one of the relationships reported in Equation (15), depending on which parameters are known with a better precision. The knowledge of δ is, however, required for the calculation of concentration and potential profiles.

The general DSP&DE model is a set of first-order differential equations which can be solved to

calculate total volume flux as well as the flux and the concentration profile of each species across the membrane, once the membrane parameters and the pore geometry are known. The electric potential profile through the membrane is also calculated straightforwardly, besides the Donnan potentials at the membrane/external solutions interfaces. The great interest in this model is related to its easy extension to dilute multicomponent solutions.

By supposing as known data, the operative variables related to the feed conditions (concentration $c_i(0^-)$, pH, temperature, and dielectric constant ε_{rs}), as well as the pressure difference ΔP , the model parameters are: the membrane parameters (L_p , pore geometry, δ , r_p , ε_{rm} , and X) and the dielectric constant of the solution inside the pore ε_{rp} . In the case in which the model parameters are known, equations in **Table 4** can be solved to characterize membrane performances and can be introduced in any other model aimed to the simulation of a membrane module in an NF process. Alternatively, the same set of equations can be used to calculate all the model parameters, or any one of them, as adjustable parameters.

All the model parameters can be assumed as constant values (some of them are strictly connected with water properties), with the exception of the volume membrane charge X . Several studies of different nature (electrokinetic measurements of streaming potential [5, 17, 30–37], membrane potential measurements [26, 27, 38, 39], titration experiments [40, 41], and modeling [8, 9, 31, 45]) have shown evidence that the membrane charge depends on the feed pH, as well as on the type and concentration of electrolytes and that amphoteric behavior is also frequently observed for a wide class of polymeric as well as of ceramic membranes.

In general, although some parameters might be estimated as reasonable values, such as ε_{rm} and ε_{rp} , some others require the prior determination on experimental basis, such as L_p , pore geometry, δ , r_p , and X .

2.04.2.4.1 Rejection of neutral solutes

In the case of uncharged solutes, Equation (6) becomes a very simple form, since the electromigration contribution is negligible; in addition, only steric exclusion and nonideality of the solution are to be considered in the partitioning coefficients between the membrane and the external solutions (Equations (7) and (8)). As a consequence,

integration of Equation (14) (**Table 4**) over the membrane thickness leads to a simple analytical relationship for the solute rejection reported in Equation (18):

$$R_i = 1 - \frac{K_{ic} \phi_i \frac{\gamma_i(0^-)}{\gamma_i(0^+)}}{1 - \left(1 - K_{ic} \phi_i \frac{\gamma_i(\delta^+)}{\gamma_i(\delta^-)}\right) e^{-Pe_i}};$$

$$R_i^{\text{asym}} = 1 - K_{ic} \phi_i \frac{\gamma_i(0^-)}{\gamma_i(0^+)} \quad (18)$$

In this case, Pe_i assumes the meaning of a hindered Peclet number of the uncharged solute.

Apparently, the solute rejection depends on the pore geometry and on r_p , through ϕ_i , K_{ic} , and K_{id} , contained in Pe_i , as well as on the solute concentration through γ_i . At very high volume fluxes, the asymptotic rejection is obtained in the limiting case of $Pe_i \rightarrow \infty$; apparently, asymptotic rejection depends on the pore geometry, the pore radius, as well as on the partitioning at the feed/membrane interface only.

2.04.2.4.2 Rejection of single salts in neutral membranes

In the case of a single strong electrolyte, Equation (6) can be written as reported in Equations (19) and (20), in which cations and anions are indicated by subscripts 1 and 2, respectively:

$$j_1 = -D_{1p} \left(\frac{dc_1}{dx} + z_1 c_1 \frac{F}{RT} \frac{d\Psi}{dx} \right) + K_{1c} c_1 \mathcal{F}_V \quad (19)$$

$$j_2 = -D_{2p} \left(\frac{dc_2}{dx} + z_2 c_2 \frac{F}{RT} \frac{d\Psi}{dx} \right) + K_{2c} c_2 \mathcal{F}_V \quad (20)$$

The potential gradient inside the membrane can be calculated [14] applying the zero electric current condition (Equation (21)), that is equivalent to the electroneutrality condition in the permeate side (Equation (22), **Table 4**); when the electrostatic potential is eliminated, Equations (19) and (20) can be rewritten as Equations (23) and (24):

$$I_{el} = F \sum_{i=1}^n z_i j_i = 0 \quad \Rightarrow \quad z_1 j_1 + z_2 j_2 = 0 \quad (21)$$

$$j_1 = -D_{\text{eff}} \frac{dc_1}{dx} + K_{1\text{eff}} c_1 \mathcal{F}_V \quad (23)$$

$$j_2 = -D_{\text{eff}} \frac{dc_2}{dx} + K_{2\text{eff}} c_2 \mathcal{F}_V \quad (24)$$

in which

$$D_{\text{eff}} = \frac{D_{1p}D_{2p}(z_1^2c_1 + z_2^2c_2)}{D_{1p}z_1^2c_1 + D_{2p}z_2^2c_2} \quad (25)$$

$$K_{2\text{eff}} = z_1c_1 \frac{z_1D_{1p}K_{2c} - z_2D_{2p}K_{1c}}{D_{1p}z_1^2c_1 + D_{2p}z_2^2c_2}; K_{1\text{eff}} = -z_2c_2 \frac{K_{2\text{eff}}}{z_1c_1} \quad (26)$$

The flux of each ion is obviously the result of the diffusive and convective contribution to motion inside the membrane. The coefficients D_{eff} , $K_{1\text{eff}}$ and $K_{2\text{eff}}$ are a combination of the hindered diffusivities and of the convective hindrance factors of each specie and depend on the ionic concentrations inside the membrane, which in turn depend on the membrane charge. The diffusive term, D_{eff} , is a sort of harmonic average of the hindered diffusion coefficients of the single ions inside the membrane and it can be seen as a hindered diffusion coefficient of the electrolyte, considered as a single specie permeating through the membrane. Analogous considerations hold true for the convective terms $K_{1\text{eff}}$ and $K_{2\text{eff}}$.

The validity of Equations (19)–(21) and (23)–(26) is, however, general, independently of the membrane nature, positively or negatively charged as well as neutral. In the case of neutral membranes, or alternatively for amphoteric membranes at their corresponding isoelectric points (more precisely, at their points of zero charge), the coefficients D_{eff} , $K_{1\text{eff}}$ and $K_{2\text{eff}}$ become independent of the membrane charge. In that case, Equations (25) and (26) can be easily combined with the electroneutrality condition inside the membrane (Equation (16), Table 4); for symmetric electrolytes, the flux equation for cation becomes

$$j_i = -D_{\text{eff}} \frac{dc_1}{dx} + K_{\text{eff}}c_1\mathcal{F}_V \quad (27)$$

in which

$$D_{\text{eff}} = \frac{2D_{1p}D_{2p}}{D_{1p} + D_{2p}} \quad (28)$$

$$K_{\text{eff}} = \frac{D_{1p}K_{2c} + D_{2p}K_{1c}}{D_{1p} + D_{2p}}$$

The relationship (27) holds true not only for the cation, but also for the anion as well as for the salt flux. In this case, D_{eff} and K_{eff} are the effective hindered diffusion coefficient and the effective hindrance factor of the salt inside the membrane, respectively.

Integration of Equation (27) with the proper boundary conditions (details are reported in Reference 14) leads to the following relationship for salt rejection:

$$R = \frac{A-1 + (1-B)e^{Pe}}{e^{Pe} + A-1} \quad (29)$$

in which

$$Pe = \frac{K_{\text{eff}}\mathcal{F}_V\delta}{D_{\text{eff}}}; A = K_{\text{eff}} \frac{c_1(\delta^-)}{c_1(\delta^+)}; B = K_{\text{eff}} \frac{c_1(0^+)}{c_1(0^-)} \quad (30)$$

Equation (29) is formally very similar to the well-known relationships introduced by Spiegler and Kedem [109], as well as by Mason and Lonsdale [91] to describe RO of aqueous solutions containing single salts. In the case in which the same values for A and B can be assumed, the parameter A , or, alternatively, the parameter B , has the meaning of $1 - \sigma$, with σ being the typical reflection coefficient appearing in the phenomenological RO models. The result obtained in Equation (29) is particularly interesting for some aspects. It not only reconfirms that the phenomenological model is a particular case of a more general transport-equilibrium model, but the latter can also predict values and behavior of the phenomenological parameters, such as the σ dependence on the salt concentration.

2.04.3 Model Applications

The DSP&DE model, as presented in Table 4, is the more simple and complete approach developed at present to describe transport phenomena in NF membranes.

The strong point is related to its applicability to dilute multicomponent solutions, making use of the same model parameters used for/calculated from single-salt solutions (L_p , δ , pore geometry, r_p , ε_{rm} , and ε_{rp}) with suitable mixing rules to estimate the membrane charge (X). It can be observed that, in principle, ε_{rp} should also be considered as a function of salt type and composition; however, even an estimated value is sufficient to perform a good process simulation.

The weak points are mainly related to the presence of

1. numerical problems of convergence as the number of ionic species increases;
2. complex and tedious statistical analyses for the calculation of some model parameters, which require extensive experimentation; and
3. a high level of uncertainty in the estimation of those model parameters which are interdependent of each other.

The former point can be solved by developing specific algorithms for the solution of the corresponding differential equations [82, 88–90, 108], or, alternatively, by developing simpler approximated versions of the general differential model [14, 84].

The latter points are remarkably critical. The partitioning contributions appearing in Equations (7) and (8) cannot be estimated separately, since they are strictly connected to each other, with the exception of the steric hindrance. At the feed/membrane interface, for instance, the Donnan potential, $\Delta\psi_{D0}$, can be calculated through the electroneutrality condition reported in Equation (16) (Table 4); in this case, it is easy to observe that the $\Delta\psi_{D0}$ value is the result of the concomitant effects of the nonideality of the solution (γ_i), of the membrane charge (X), and of the DE (ΔW_{DE0}), which in turn depends on ε_{rp} as well as on X through ionic concentrations inside the membrane ($\kappa(8^+)$), with regard to (ΔW_{im}), and depends on ε_{rp} only, with regard to (ΔW_{Born}). In other words, assuming a low value of ε_{rp} with respect to ε_{rs} leads to an overestimation of Born partitioning and, consequently, a low X is sufficient to obtain the experimental rejection. In principle, there are infinite couples (X, ε_{rp}), which give the same rejection of single-salt solutions [82]. A good approach to the problem passes through the determination of the model parameters by independent methods and/or by using different kinds of experimental data.

In the past 10 years, the DSP&DE model has been used with different levels of approximation, which have represented the various steps of development of the general model.

First, Bowen and coworkers [8, 51, 74] developed the DSPM, which is basically the DSP&DE model without DE, which was good for solutions containing single salts, such as NaCl or Na₂SO₄. It was extremely successful in modeling NaCl + Na₂SO₄ solutions, but it failed in the prediction of divalent ions rejection, such as calcium or magnesium salts [14, 75]. The same model is the basis of the computer simulation program Nanoflux developed by Lefebvre and coworkers [88–90].

Second, Hagmeyer and Gimbel [5] as well as Bowen and Welfoot [9, 80] introduced DE as a further partitioning mechanism accounted only for the Born model, and proposed empirical approaches to the problem, in which ε_{rp} could be calculated as an adjustable parameter. At the same time, Bandini and Vezzani [14] adapted the DSPM model by Bowen into the DSPM&DE model, introducing the DE as a further partitioning mechanism accounted for only

by the contribution of image forces, in association with the description of the nonideality of the solutions according to the limiting Debye–Hückel theory. In that model, since the properties of water inside the membrane pore were assumed equal to those existing in the external bulk ($\varepsilon_{rp} = \varepsilon_{rs}$), no further adjustable parameters were introduced with respect to the original DSPM model.

Finally, using the steric, electric, and dielectric exclusion (SEDE) model, Szymczyk and Fievet [81] accounted for both the contributions related to DE, image forces and Born partitioning, and ε_{rp} appeared as an adjustable parameter.

All those models differ in the description of the partitioning mechanisms, whereas the mass transfer through the membrane is described by the extended Nernst–Planck equation in all cases. All the models were good in the prediction of membrane performances, in their field of validity, with the model parameters adjusted through a fitting procedure performed with the same equations of the corresponding models.

Some noteworthy results are reported in Figures 2–4.

Figure 2 shows the ability of the DSPM model [8] to simulate NF performances in the case of NaCl–Na₂SO₄–water mixtures, starting from model

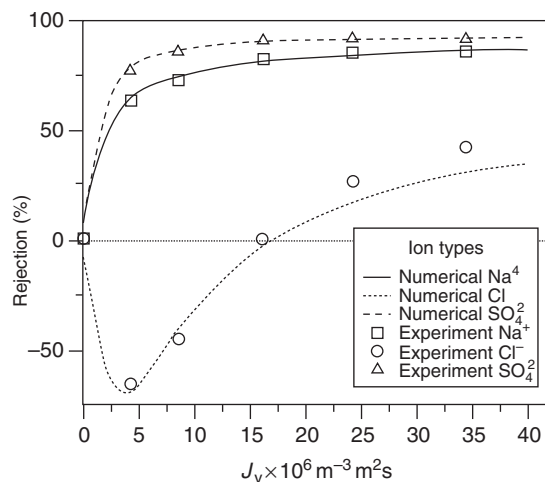


Figure 2 Nanofiltration (NF) of aqueous solutions containing 10^{-3} M NaCl + Na₂SO₄, NaCl/Na₂SO₄ = 0.2 mol mol⁻¹, through a polyethersulfone membrane. Comparison between experimental rejection values (symbols) and model predictions (lines). Lines = Donnan steric pore model (DSPM) [8] (ideal mixtures; cylindrical pores; no dielectric exclusion (DE); $r_p = 0.72$ nm, $\delta = 17$ μ m, $X = -10^{0.874} C_{eq}^{0.508}$ mol m⁻³, calculated from NaCl data). Reproduced with permission from Bowen, W. R., Mukhtar, H. *J. Membr. Sci.* **1996**, *112*, 263–274.

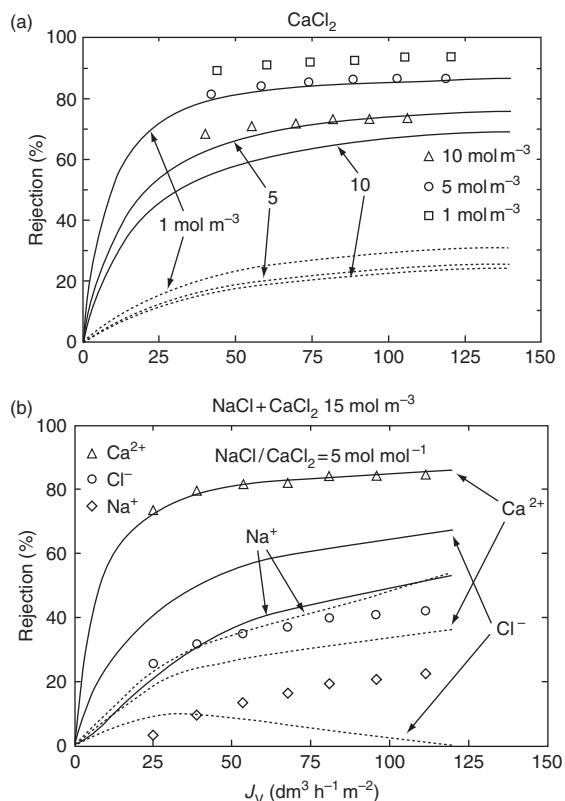


Figure 3 NF of aqueous solutions containing (a) CaCl_2 and (b) $\text{NaCl}-\text{CaCl}_2$, through a polyamide membrane. Comparison between experimental rejection values (symbols) and model predictions (lines). Solid lines = integral version of Donnan steric pore model and dielectric exclusion (DSPM&DE) model [14] (see Equation (31)) (γ_i from Debye–Hückel limiting law (Table 3); slit geometry; DE, $\epsilon_{rp} = \epsilon_{rs} = 80$, $\epsilon_{rm} = 3$; $r_p = 0.67$ nm, calculated from lactose data; $\delta = 27.1$ μm , $X = -0.479 C_{\text{eq}}^{1.05}$ mol m^{-3} , calculated from NaCl data). Dashed lines = integral version of DSPM [14] (see Equation (31)) (ideal mixtures; cylindrical pores; no DE; $r_p = 0.67$ nm, calculated from lactose data; $\delta = 31.9$ μm , $X = -4.37 C_{\text{eq}}^{0.76}$ mol m^{-3} , calculated from NaCl data). Reproduced with permission from Bandini, S., Vezzani, D. *Chem. Eng. Sci.* **2003**, 58, 3303–3326.

parameters fitted by data with NaCl–water solutions. In particular, the membrane charge is assumed to vary with the equivalent concentration in the mixture according to a Freundlich isotherm, calculated by NaCl–water solutions data only.

The same idea, about the extension of single-salt data to multicomponent mixtures, is at the basis of the results reported in Figure 3 [14], which demonstrates with no doubt that the description of NF of multivalent nonsymmetric salts requires the introduction of DE. Apparently, accounting only for Donnan partitioning (DSPM) is not sufficient to

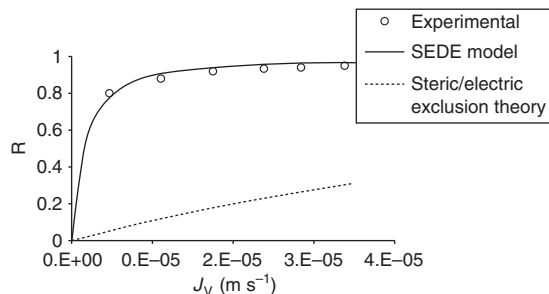


Figure 4 Nanofiltration (NF) of aqueous solutions containing 50 mol m^{-3} KCl, through a polyamide membrane. Comparison between experimental rejection values (symbols) and model predictions (lines). Solid lines = steric, electric, and dielectric exclusion (SEDE) model [81] (γ_i from Debye–Hückel limiting law (Table 3); slit geometry; dielectric exclusion (DE), $\epsilon_{rp} = 42$, $\epsilon_{rs} = 78$, $\epsilon_{rm} = 3$; $r_p = 0.50$ nm, $\delta = 6.7$ μm , $X_{\text{TSP}} = -113$ mol m^{-3}). Dashed lines = SEDE model [81] (γ_i from Debye–Hückel limiting law (Table 3); slit geometry; no DE; $r_p = 0.50$ nm, $\delta = 6.7$ μm , $X_{\text{fit}} = -1210$ mol m^{-3}). Reproduced with permission from Szymczyk, A., Fievet, P. *J. Membr. Sci.* **2005**, 252, 77–88.

explain the high values measured for CaCl_2 rejection (Figure 3(a)). Furthermore, the presence of DE phenomena can explain the experimental rejection sequence observed for the ions in ternary mixtures ($\text{NaCl}-\text{CaCl}_2$ –water solutions, Figure 3(b)).

The relevance of DE partitioning has also been shown as evidence by Szymczyk and Fievet [81] in Figure 4, in which the authors proposed to use the value obtained by tangential streaming potential measurements as volume membrane charge (X) and, consequently, to calculate the dielectric constant inside the pore (ϵ_{rp}) as a fitting parameter. In that case, also for a single symmetric salt, such as KCl, DE is to be accounted for in addition to Donnan partitioning in order to achieve the high rejection values experimentally observed.

It is therefore evident that it is difficult to indicate which model correctly describes ion partitioning in the membrane: in our opinion, a reasonable test can be represented by the ability of the model (1) to predict separation performances in operative conditions different from those for which the adjustable parameters were calculated and (2) to predict a behavior of adjustable parameters with operative conditions which is very close to that obtained for the same parameters by experimental techniques different from NF experiments.

Basically, all the versions of the DSP&DE model fulfill the requirement of the above-mentioned point (1), as suggested by the results reported in

Figures 2–4. However, although it is possible to perform a simulation by keeping (L_p , δ , pore geometry, r_p , ε_{rm} , and ε_{rp}) as constant values and equal to the ones obtained from pure water and single-salt experiments (NaCl, typically), the membrane charge remains a fitting parameter to calculate as a function of pH, concentration, and of the mixture type.

From a general viewpoint, the question is not related to the quality of the DSP&DE model, rather to the knowledge level about the correct mechanism of membrane charge formation. DSP&DE model is essentially a partitioning and transport model in which the membrane charge is a parameter. As a partitioning-transport model it is quite satisfactory; however, it requires a good relationship which expresses how the membrane charge depends on the operative variables. Some authors [5, 81, 110] tried to solve the problem by using the values calculated from streaming potential measurements, although they are not representative of the real conditions at which the membrane operates in NF processes. Since the values are not the real ones, the model requires to adjust the dielectric constant inside the pore (ε_{rp}) in order to fit the experimental data, as an example. Other authors [9, 14, 82], on the contrary, decided to assume a value for the dielectric constant inside the pore and calculated the membrane charge accordingly.

Apparently, the problem is still open: there is no univocal answer. The studies reported in References 9, 81, 82, 107, and 110 have shown evidence that the confinement clearly leads to a decrease of the water dielectric constant inside the pore; on the other hand, it is difficult to obtain the exact value of ε_{rp} . However, it can be estimated in the range between 40 and 70, depending on the salt type. In our opinion, the correct estimation of ε_{rp} is not a real problem; it mainly determines the contribution of image forces with respect to Born partitioning, and it influences the membrane charge value. Nevertheless, the key problem is not to obtain the real value of the membrane charge, rather to determine the qualitative behavior of the membrane charge as a function of operative conditions. The correct model, for instance, is one that is able to give the correct membrane charge behavior, which may fit streaming potential charges. However, this condition is not sufficient, since streaming potential measurements are significant for low concentration solutions only.

Finally, the DSP&DE model has been used as a predictive tool [8, 9, 14, 15, 86–89], to investigate membrane performances in multicomponent mixtures, as well as the behavior of concentration and potential

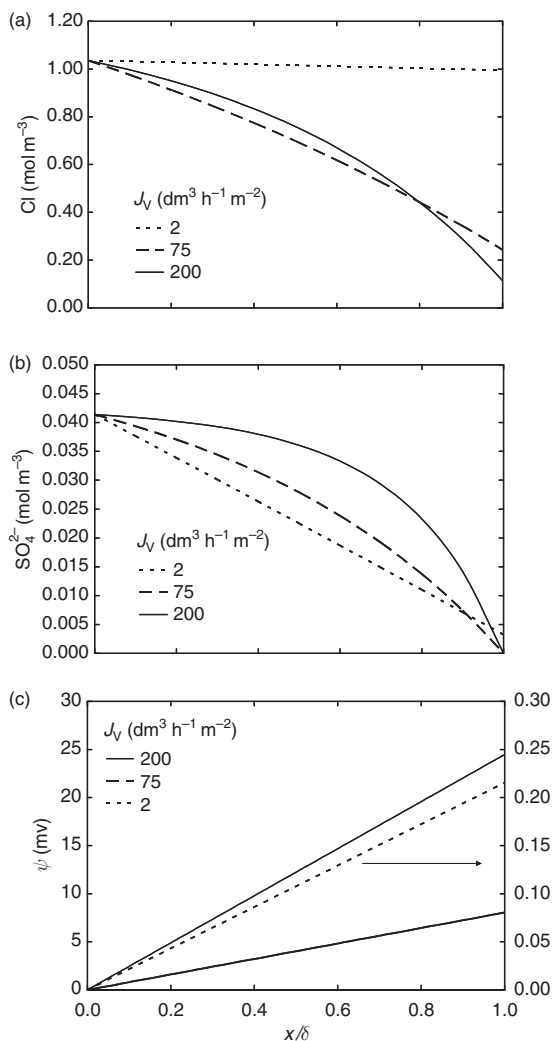


Figure 5 Nanofiltration (NF) of aqueous solutions containing NaCl (5 mM) + Na_2SO_4 (10 mM), through a polyamide Desal-type membrane: concentration (a, b) and electric potential (c) profiles inside the membrane at different volume fluxes. Calculations are performed by Donnan steric pore and dielectric exclusion (DSP&DE) model (γ_i from Debye–Hückel limiting law (Table 3); slit geometry; dielectric exclusion (DE), $\varepsilon_{rp} = \varepsilon_{rs} = 80$, $\varepsilon_{rm} = 3$; $r_p = 0.50 \text{ nm}$, $\delta = 20 \mu\text{m}$, $X = -5 \text{ mol m}^{-3}$).

profiles across the membrane. The case of a ternary mixture is reported in Figure 5, in which a polyamide membrane (Desal-type) is simulated. The behavior observed is quite general for the NF membranes tested and for the process operative conditions typically maintained for single salts as well as for multicomponent mixtures of electrolytes. Apparently, the electric potential behavior is very close to a linear trend, whereas the concentration profiles are not strictly linear, above all, at the higher volume fluxes. At high

fluxes, indeed, the convective contribution to ion flux is dominant with respect to the diffusive contribution.

That behavior strongly depends on the membrane charge value. An interesting investigation about the analysis of the role of each transport mechanism across the membrane was performed by Bowen and Mohammad [74]; the results, confirmed also by other authors [86, 87], are reported in Figure 6. For the case of NaCl–water mixtures in negatively charged membranes, at high membrane charges, the transport is controlled largely by diffusion, although convection and electromigration contributions are not negligible. At low membrane charges, on the contrary, all the contributions are remarkable.

2.04.3.1 Approximated Versions of the DSP&DE Model

In order to simplify the solution procedures of the general DSP&DE model (the set of first-order

differential equations – Table 4) as well as the statistical procedures for the model parameters calculation, some simplified versions have been developed. These models can be used for predictive purposes, for process optimization, and they can be particularly advantageous in those cases in which a feasibility study of the process is pursued.

Three types of simplifications were introduced, aimed to obtain analytical relationships for rejection of single salts, or, alternatively, to switch the mathematical problem to the solution of a set of algebraic equations.

A first simplified version was introduced in Reference 14. Under the hypothesis of complete co-ion exclusion, in the case of a single symmetric salt, Equations (23) and (24) can be easily integrated with the proper boundary conditions (Equations (7) and (8), Table 4) (since the coefficients D_{eff} , $K_{1\text{eff}}$ and $K_{2\text{eff}}$, defined in Equations (25) and (26) become independent of the membrane charge), and an analytical

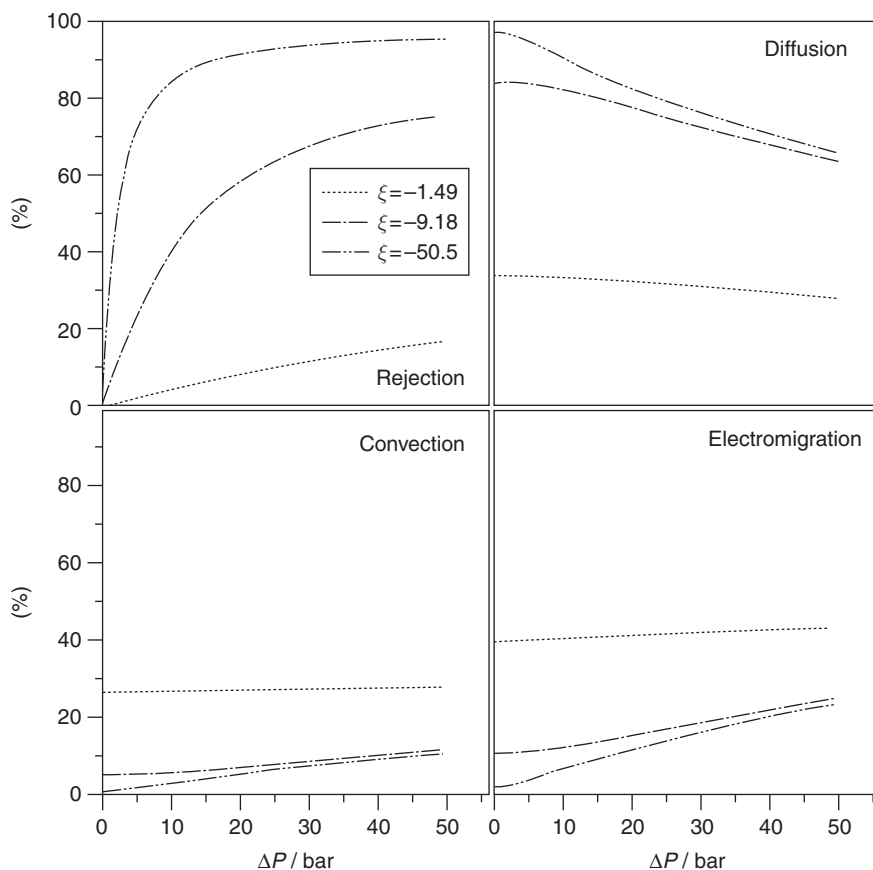


Figure 6 Nanofiltration (NF) of aqueous solutions containing NaCl. Analysis of transport mechanisms at various $\xi = X/C_{\text{eq}}$, performed by Donnan steric pore model (DSPM) [74] (ideal mixtures; cylindrical pores; no dielectric exclusion (DE); $r_p = 0.66$ nm, $\delta = 4.76$ μm). Reproduced with permission from Bowen, W. R., Mohammad, A. W. *Chem. Eng. Res. Des., Inst. Chem. Eng.*, 1998, 76A, 885–893.

relationship can be obtained to relate salt rejection to membrane charge, pore radius, and membrane thickness. The approximation is particularly advantageous as an alternative procedure for the adjustable-parameters calculation. The application should be avoided in the cases of low charged membranes [53].

Advantages in the ion rejection calculation could be achieved also in the case in which linear behaviors for the concentration profiles as well as/or for the electric potential profile might be assumed, as it can be observed in Equation (6).

Bandini and Vezzani [14] made the assumption of a constant potential gradient through the membrane; the hypothesis is proved by the results reported in Figure 5 as well. As a consequence, Equation (14) (Table 4) can be easily integrated over the membrane thickness, thus obtaining the following relationships for the concentration profile through the membrane of each ionic specie:

$$\frac{c_i(x) - \frac{j_i \delta}{k_i D_{ip}}}{c_i(0^+) - \frac{j_i \delta}{k_i D_{ip}}} = e^{\left(k_i \frac{x}{\delta}\right)}; \quad k_i = Pe_i - z_i \frac{F \delta}{RT} \frac{\Delta \Psi}{\delta} \quad (31)$$

The quantity $\Delta \Psi / \delta$ is the potential gradient, which can be evaluated according to the general relationship reported in Equation (17) (Table 4); detailed information is reported in Reference 14.

The integral version represented by Equation (31) greatly simplifies calculations: it switches the mathematical problem from a set of first-order differential equations to a set of algebraic equations. It can be applied to binary as well as to multicomponent systems, and it requires the prior calculation of the membrane parameters, which can be performed through the various fitting procedures discussed in the following sections; the version itself can be used to adjust the parameters. The ability of the integral version to simulate membrane performances was demonstrated by the comparison with the results obtained by the general differential version in Reference 14; however, no estimation about the confidence range of the integral model was performed in detail: as a rule of thumb, authors recommended that the integral model had to be used in all multicomponent cases in which no solute is a trace component.

Bowen *et al.* [84, 85], on the contrary, operated a finite difference linearization of the concentration gradient. Although the authors do not report any recommendation about the validity range of the

linearization, the approximation seems to be counterbalanced by the adjustable-parameters values calculated accordingly. However, the analytical solution derived for multicomponent mixtures is rather complex and must be performed case by case.

2.04.3.2 Parameter-Calculation Procedures

Contemporary to the development of the various DSP&DE model versions, many procedures have been proposed for the calculation of the membrane parameters. The best procedure would be the independent determination of each parameter, basing on different sets of experimental data. Unfortunately, as discussed in the previous sections, this is not feasible ($\gamma_{1\text{eff}}$ and $K_{2\text{eff}}$, defined in Equations (25) and (26) become independent of the membrane charge), and an analytical relationship can be obtained to relate salt rejection to membrane charge, pore radius, and membrane thickness. The approximation is particularly advantageous as an alternative procedure for the adjustable-parameters calculation. The application should be avoided in the cases of low charged membranes [53].

Key points of the parameter-calculation procedure are the following:

1. Calculate hydraulic membrane permeability (L_p) from NF experiments with pure water, according to Equation (1).
2. Choose the pore geometry (cylindrical or slit-like). Experience shows that in the case of neutral solutes, both the geometries are equivalent to simulate solute partitioning; on the contrary, with electrolytes, the slit geometry seems to be more suitable.
3. Calculate the average pore radius (r_p). The use of neutral solutes with spherical molecular shape is preferential (e.g., sugars); in addition, the use is recommended of solutes which are not completely rejected. Rejection data can be fitted according to Equation (18). In the case in which measurements in a wide range of ΔP are used, Pe_i can be expressed according to one of the relationships reported as Equation (15); alternatively, only those data which approach asymptotic conditions can be fitted. In both cases, quite close r_p values are obtained, thus indicating that the Hagen–Poiseuille flow hypothesis inside the pores (Equations (2) and (3)) is acceptable.
4. Calculate the effective membrane thickness (δ). It can be calculated based on neutral-solutes data or on rejection of single salts. When possible, the use of

neutral-solutes data is recommended, since, in this case, rejection is independent of the membrane charge value. In the latter case, NaCl data are generally suitable, and the calculation is performed together with the membrane charge evaluation, at pH conditions far from the membrane isoelectric point.

Calculation must be performed by using rejection data as a function of total volume flux. The use of relationships derived from the application of the Hagen–Poiseuille flow hypothesis must be careful, since it could lead to an underestimation of the membrane thickness by 5–10 times [9, 81, 84, 85, 107]. This is a crucial and very delicate question. It is a matter of fact that ionic rejection is independent of membrane thickness, as discussed in Section 2.04.2.4, which does not mean that any membrane thickness can be assumed to perform rejection calculations, rather that there is a unique curve which relates rejection as a function of Pe_i , if the correct value of membrane charge is used (i.e., if the asymptotic rejection is well predicted). However, in order to calculate the correct Pe_i number by using experimental data, the correct value of δ is required (Equation (15)). The problem is put in evidence by the results reported in Figure 7(a) in which the same NaCl rejection data versus total experimental fluxes are fitted by using $\delta = 28.5 \mu\text{m}$ and $\delta = 5.7 \mu\text{m}$ (calculated from the elaboration of the hydraulic membrane permeability according to the relationship reported in Equation (3), with $\eta = \eta_0$) in correspondence with different membrane charge values, both performing best fits

(no Born partitioning was accounted for). Apparently, both the sets of parameters can give a good fit of the data, but only $X = -7 \text{ mol m}^{-3}$ can simulate the experimental asymptotic rejection correctly. In addition, by using $\delta = 5.7 \mu\text{m}$ and $X = -7 \text{ mol m}^{-3}$, we can observe that correct asymptotic rejections are achieved at volume fluxes which are much higher than the experimental ones and the curve rejection versus volume flux is predicted wrongly. In Figure 7(b), the corresponding curves are reported as a function of the corresponding Pe values, calculated with the experimental total fluxes and the thickness values indicated. The conclusion is self-evident: in the case in which NaCl data are used, the correct thickness value is the δ , which can give, at the same time, both the correct Pe value and the best fit of rejection versus flux data, in correspondence with a membrane charge value that predicts the asymptotic rejection correctly.

Furthermore, in the case in which a wrong δ value is used to simulate the membrane rejection in association with a wrong membrane charge, a wrong prediction might be performed also of asymptotic conditions, as it clearly occurred in References 9, 84, and 85, although a good fit of data was performed in the pressure range investigated. The same kind of problem also exists in Reference 107, partially hidden and counterbalanced by a high Born partitioning prediction. In this case, since the membrane charge was assumed equal to the value obtained from streaming potential measurements, in correspondence with a low thickness value, a high Born

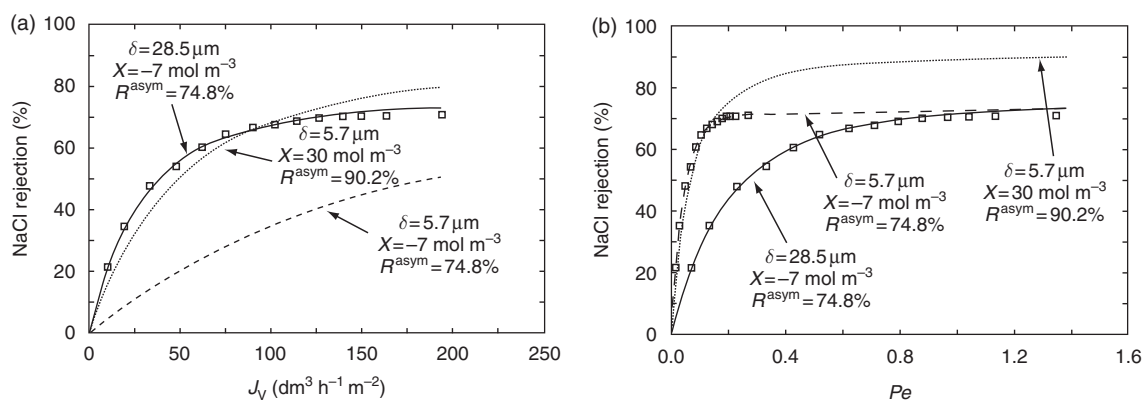


Figure 7 Nanofiltration (NF) of aqueous solutions containing 10 mM NaCl, through a Desal DK membrane. Comparison between experimental rejection values (symbols) and model predictions (lines) vs. (a) total transmembrane flux and (b) salt Peclet number. Calculations are performed by Donnan steric pore and dielectric exclusion (DSP&DE) model (γ_i from Debye–Hückel limiting law (Table 3); slit geometry; dielectric exclusion (DE), $\epsilon_{rp} = \epsilon_{rs} = 80$, $\epsilon_{rm} = 3$; $r_p = 0.59 \text{ nm}$; $L_p = 7.07 \cdot 10^{-8} \text{ m h}^{-1} \text{ Pa}^{-1}$). $Pe = J_V \delta / D_{\text{eff}}$, $D_{\text{eff}} = 2 / (1/D_{1p} + 1/D_{2p})$. Data taken with permission from Bandini, S., Drei, J., Vezzani, D. *J. Membr. Sci.* **2005**, 264, 65–74.

partitioning was also required in addition to the image force DE to perform a good fit of rejection data versus the total flux.

In conclusion, we can observe that we are facing the same indetermination problem previously discussed: since the same value of asymptotic rejection can be simulated by accounting for different contributions of image forces and Born partitioning, that is by different values of the couples (X and ε_{rp}), there are various sets of the parameters (X , ε_{rp} , and δ) which can give a good fit of rejection data. As a consequence, we strongly recommend using rejection data of neutral solutes to calculate the effective membrane thickness.

Finally, the results reported in Figure 7(a) show that the calculation of δ can be postponed to the membrane charge determination, which could be performed by fitting only asymptotic rejection data.

5. Calculate the volume membrane charge (X) and the dielectric constant in the pore (ε_{rp}). This calculation is affected by a high level of uncertainty, since the two parameters are interdependent on each other, as previously discussed in Section 2.04.3. Typically, the problem has been solved by assuming a value for one parameter and by calculating the other one as an adjustable quantity. The interesting feature of these procedures is related to the quality of the results obtained, which had allowed to draw some general conclusions.

In References 14, 23, 28, and 29, authors made the assumption of $\varepsilon_{rp} = \varepsilon_{rs}$ and calculated X values as fitting parameters, by keeping all the other parameters as constant values and equal to those calculated from NaCl data at pH = 5.8. The calculation of X has been also performed by using only asymptotic rejection data [14, 23]. The results obtained show evidence that there are different membrane-charge behaviors as a function of operative conditions, depending on the salt type, which can be explained accounting for the same mechanisms involved in the membrane-charge formation [45, 46].

Bowen and Welfoot [9] suggested first to calculate ε_{rp} from NaCl data at the point of zero charge and, second, to use it as a constant value in the calculation of X by fitting rejection data at different pH conditions. Other authors [82] applied the same idea by using rejection data at high concentrations, under the hypothesis that the membrane charge approaches an asymptotic value (X completely screened by adsorbed ions).

Finally, Szymczyk and coworkers [81, 107, 110] proposed to use the value obtained by tangential streaming potential measurements as volume membrane charge and, consequently, to calculate (ε_{rp}) as a fitting parameter. These studies, together with the results obtained in References 5, 6, 9, and 82, show evidence that the confinement clearly leads to a decrease of the solvent dielectric constant inside the pore, which can be estimated in the range between 40 and 70, depending on the salt type.

2.04.3.2.1 Some remarks on the volume membrane charge

In NF membranes, in view of the narrow pores, the surface charge is the most important membrane characteristic in the determination of salt rejection. Several experiments of different nature, as well as many models, demonstrate the presence of a charge located at the membrane/liquid interface, which is strictly dependent on salt type, salt concentration, and on pH. Conversely, all the authors basically agree with the interpretation of the phenomena determining the membrane charge: mechanisms, such as acid/base dissociation and ionic adsorption, can be recognized as the main mechanisms determining the membrane-charge formation. Empirical models, such as Freundlich or Langmuir isotherms, have been proposed to relate the membrane charge with the equivalent concentration [8, 31, 38, 39, 42, 43]. Some recent studies [45, 46, 111] made a distinction between specific and nonspecific adsorption and recognized counterion site-binding phenomena as remarkable in the membrane-charge formation, above all, in the case of nonsymmetric electrolytes.

However, the question is not yet well defined about how the data obtained for single salts might be used for the extension of the models to multi-component mixtures. By now, the mixing rules which have shown better results are those proposed by Bowen and Mukhtar [8] and by Nakao and coworkers [42]. In Reference 8, the membrane charge was assumed to vary with the equivalent concentration in the mixture according to a Freundlich isotherm, calculated by NaCl–water solutions data only; in Reference 42, mixing rules of the charge values calculated for the corresponding single salts were proposed according to the salt molar fraction.

2.04.4 Conclusions

The study of transport phenomena in NF or loose RO membranes covers the period of the past 40 years. Although many models have been developed so far, in the past decade, scientific production has been devoted to the improvement of the partitioning-transport model, originally introduced by Bowen *et al.* in 1996. Remarkable improvements have been performed in the description of the phenomena involved; the most important is certainly the introduction of dielectric exclusion as partitioning mechanism.

The general model, termed DSP&DE model, has been assessed in this chapter and a detailed discussion has been carried out about advantages and disadvantages of this tool.

The most interesting strong points are related to the wide generality of the model and to the easy extension to multicomponent mixtures.

Some questions are still open, such as the independent calculation of electric and dielectric parameters (membrane charge and dielectric constant inside the pore), as well as the correct determination of the mechanisms involved in the membrane-charge formation in the case of multicomponent ion mixtures.

References

- [1] Tsuru, T., Urairi, M., Nakao, S., Kimura, S. *J. Chem. Eng. Jpn* **1991**, *24*, 518–520.
- [2] Lipp, P., Gimbel, R., Frimmel, F. H. *J. Membr. Sci.* **1994**, *95*, 185–197.
- [3] Nyström, M., Kaipia, L., Luque, S. *J. Membr. Sci.* **1995**, *98*, 249–262.
- [4] Hall, M. S., Starov, V. M., Lloyd, D. R. *J. Membr. Sci.* **1997**, *128*, 39–53.
- [5] Hagemeyer, G., Gimbel, R. *Desalination* **1998**, *117*, 247–256.
- [6] Hagemeyer, G., Gimbel, R. *Sep. Purif. Technol.* **1999**, *15*, 19–30.
- [7] Afonso, M. D., de Pinho, M. N. *J. Membr. Sci.* **2000**, *179*, 137–154.
- [8] Bowen, W. R., Mukhtar, H. *J. Membr. Sci.* **1996**, *112*, 263–274.
- [9] Bowen, W. R., Welfoot, J. S. *Chem. Eng. Sci.* **2002**, *57*, 1121–1137.
- [10] Xu, Y., Lebrun, R. E. *J. Membr. Sci.* **1999**, *158*, 93–104.
- [11] Wang, X., Wang, W., Wang, D. *Desalination* **2002**, *145*, 115–122.
- [12] Szoke, S., Patzay, G., Weiser, L. *Desalination* **2002**, *151*, 123–129.
- [13] Tanninen, J., Nyström, M. *Desalination* **2002**, *147*, 295–299.
- [14] Bandini, S., Vezzani, D. *Chem. Eng. Sci.* **2003**, *58*, 3303–3326.
- [15] Labbez, C., Fievet, P., Szymczyk, A., Vidonne, A., Foissy, A., Pagetti, J. *J. Membr. Sci.* **2002**, *208*, 315–329.
- [16] Tsuru, T., Hironaka, D., Yoshioka, T., Asaeada, M. *Desalination* **2002**, *147*, 213–216.
- [17] Ernst, M., Bismark, A., Springler, J., Jekel, M. *J. Membr. Sci.* **2000**, *165*, 251–259.
- [18] Paugam, L., Taha, S., Dorange, G., Jaouen, P., Quéméneur, F. *J. Membr. Sci.* **2004**, *231*, 37–46.
- [19] Quin, J., Oo, M. H., Lee, H., Coniglio, B. *J. Membr. Sci.* **2004**, *232*, 153–159.
- [20] Timmer, J. M. K., van der Horst, H. C., Robbertsen, T. *J. Membr. Sci.* **1993**, *85*, 205–216.
- [21] Freger, V., Arnot, T. C., Howell, J. A. *J. Membr. Sci.* **2000**, *178*, 185–193.
- [22] Nilsson, M., Trägårdh, G., Östergren, K. *J. Membr. Sci.* **2008**, *312*, 97–106.
- [23] Bandini, S., Drei, J., Vezzani, D. *J. Membr. Sci.* **2005**, *264*, 65–74.
- [24] Van Gestel, T., Vandecasteele, C., Buekenhoudt, A., *et al.* *J. Membr. Sci.* **2002**, *209*, 379–389.
- [25] Condom, S., Larbot, A., Youssi, S. A., Persin, M. *Desalination* **2004**, *168*, 207–213.
- [26] Fievet, P., Szymczyk, A., Aoubiza, B., Pagetti, J. *J. Membr. Sci.* **2000**, *168*, 87–100.
- [27] Fievet, P., Aoubiza, A., Szymczyk, B., Pagetti, J. *J. Membr. Sci.* **1999**, *160*, 267–275.
- [28] Mazzoni, C., Bandini, S. *Sep. Purif. Technol.* **2006**, *52*, 232–240.
- [29] Mazzoni, C., Bruni, L., Bandini, S. *Ind. Eng. Chem. Res.* **2007**, *46*, 2254–2262.
- [30] Afonso, M. D., Hagemeyer, G., Gimbel, R. *Sep. Purif. Technol.* **2001**, *22–23*, 529–541.
- [31] Ariza, M. J., Benavente, J. *J. Membr. Sci.* **2001**, *190*, 119–132.
- [32] Childress, E., Elimelech, M. *J. Membr. Sci.* **1996**, *119*, 253–268.
- [33] Peeters, J. M. M., Mulder, M. H. V., Strathmann, H. *Colloids Surf. A: Physicochem. Eng. Aspects* **1999**, *150*, 247–259.
- [34] Tay, J. H., Liu, J., Sun, D. D. *Water Res.* **2002**, *36*, 585–598.
- [35] Teixeira, M. R., Rosa, M. J., Nyström, M. *J. Membr. Sci.* **2005**, *265*, 160–166.
- [36] Zhao, Y., Xing, W., Xu, N., Wong, F. *Sep. Purif. Technol.* **2005**, *42*, 117–121.
- [37] Szymczyk, A., Fievet, P., Mullet, M., Reggiani, J. C., Pagetti, J. *J. Membr. Sci.* **1998**, *143*, 189–195.
- [38] Takagi, R., Nakagaki, M. *J. Membr. Sci.* **1990**, *53*, 19–35.
- [39] Takagi, R., Nakagaki, M. *J. Membr. Sci.* **1992**, *71*, 189–200.
- [40] Schaep, J., Vandecasteele, C. *J. Membr. Sci.* **2001**, *188*, 129–136.
- [41] Afonso, M. D. *Desalination* **2006**, *191*, 262–272.
- [42] Tsuru, T., Nakao, S., Kimura, S. *J. Chem. Eng. Jpn* **1991**, *24*, 511–517.
- [43] Takagi, R., Nakagaki, M. *Sep. Purif. Technol.* **2003**, *32*, 65–71.
- [44] De Lint, W. B. S., Biesheuvel, P. M., Verweij, H. *J. Coll. Interface Sci.* **2002**, *251*, 131–142.
- [45] Bandini, S. *J. Membr. Sci.* **2005**, *264*, 75–86.
- [46] Bruni, L., Bandini, S. *J. Membr. Sci.* **2008**, *308*, 136–151.
- [47] Hoffer, E., Kedem, O. *Desalination* **1967**, *2*, 25–39.
- [48] Dresner, L. *Desalination* **1972**, *10*, 27–46.
- [49] Simons, R., Kedem, O. *Desalination* **1973**, *13*, 1–16.
- [50] Jitsuhara, I., Kimura, S. *J. Chem. Eng. Jpn* **1983**, *16*, 394–399.
- [51] Bowen, W. R., Mohammad, A. W., Hilal, N. *J. Membr. Sci.* **1997**, *126*, 91–105.

- [52] Bowen, W. R., Doneva, T. A. *Desalination* **2000**, *129*, 163–172.
- [53] Otero, J. A., Lena, G., Colina, J. M., Prádanos, P., Tejerina, F., Hernández, A. *J. Membr. Sci.* **2006**, *279*, 410–417.
- [54] Otero, J. A., Mazarrasa, O., Villasante, J., *et al.* *J. Membr. Sci.* **2008**, *309*, 17–27.
- [55] Wang, X. L., Tsuru, T., Togoh, M., Nakao, S., Kimura, S. *J. Chem. Eng. Jpn.* **1995**, *28*, 186–192.
- [56] Perry, M., Linder, C. *Desalination* **1989**, *71*, 233–245.
- [57] Gupta, V. K., Hwang, S. T., Krantz, W. B., Greenberg, A. R. *Desalination* **2007**, *208*, 1–18.
- [58] Ahmad, A. L., Chong, M. F., Bhatia, S. *J. Membr. Sci.* **2005**, *253*, 103–115.
- [59] Garba, Y., Taha, S., Gondrexon, N., Dorange, G. *J. Membr. Sci.* **1999**, *160*, 187–200.
- [60] Garba, Y., Taha, S., Cabon, J., Dorange, G. *J. Membr. Sci.* **2003**, *211*, 51–58.
- [61] Ferry, J. D. *J. Gen. Physiol.* **1936**, *20*, 95–104.
- [62] Deen, W. M. *AIChE J.* **1987**, *33*, 1409–1425.
- [63] Gross, R. J., Osterle, J. F. *J. Chem. Phys.* **1968**, *49*, 228–234.
- [64] Jacazio, G., Probst, R. F., Sonin, A. A., Yung, D. *J. Phys. Chem.* **1972**, *76*, 4015–4023.
- [65] Wang, X. L., Tsuru, T., Nakao, S., Kimura, S. *J. Membr. Sci.* **1995**, *103*, 117–133.
- [66] Szymczyk, A., Fievet, P., Aoubizab, B., Simon, C., Pagetti, J. *J. Membr. Sci.* **1999**, *161*, 275–285.
- [67] Hijnen, H. J., Smit, J. A. M. *J. Membr. Sci.* **1995**, *99*, 285–302.
- [68] Hijnen, H. J., Smit, J. A. M. *J. Membr. Sci.* **2000**, *168*, 259–274.
- [69] Teorell, T. *Progr. Biophys.* **1953**, *3*, 305.
- [70] Teorell, T. *Z. Elektrochem.* **1951**, *55*, 460.
- [71] Meyer, K. H., Sievers, J. F. *Helv. Chim. Acta* **1936**, *19*, 649, 665, 987.
- [72] Wang, X. L., Tsuru, T., Nakao, S., Kimura, S. *J. Membr. Sci.* **1997**, *135*, 19–32.
- [73] Combe, C., Guizard, C., Aimar, E., Sanchez, V. *J. Membr. Sci.* **1997**, *129*, 147–160.
- [74] Bowen, W. R., Mohammad, A. W. *Chem. Eng. Res. Des., Inst. Chem. Eng.* **1998**, *76A*, 885–893.
- [75] Schaep, J., Vandecasteele, C., Mohammad, A. W., Bowen, W. R. *Sep. Purif. Technol.* **2001**, *22–23*, 169–179.
- [76] Lefebvre, X., Palmeri, J., David, P. *J. Phys. Chem. B* **2004**, *108*, 16811–16824.
- [77] Glueckauf, E. *Proceedings of the First International Symposium on Water Desalination*, Washington, DC, 1967; Vol. 1, p 143.
- [78] Yaroshchuk, A. E. *Adv. Colloid Interface Sci.* **2000**, *85*, 193–230.
- [79] Yaroshchuk, A. E. *Sep. Purif. Technol.* **2001**, *22–23*, 143–158.
- [80] Bowen, W. R., Welfoot, J. S. *Chem. Eng. Sci.* **2002**, *57*, 1393–1407.
- [81] Szymczyk, A., Fievet, P. *J. Membr. Sci.* **2005**, *252*, 77–88.
- [82] Déon, S., Dutournié, P., Bourseau, P. *AIChE J.* **2007**, *53* (8), <http://europa.sim.ucm.es/compludoc/AA?a=Bourseau%2c+P&donde=otras&zfr=01952-1969> (accessed November 2009).
- [83] Geraldès, V., Afonso, M. D. *J. Membr. Sci.* **2007**, *300*, 20–27.
- [84] Bowen, W. R., Welfoot, J., Williams, P. M. *AIChE J.* **2002**, *48*, 760–773.
- [85] Bowen, W. R., Cassey, B., Jones, P., Oatley, D. L. *J. Membr. Sci.* **2004**, *242*, 211–220.
- [86] Fievet, P., Labbez, C., Szymczyk, A., Vidonne, A., Foissy, A., Pagetti, J. *Chem. Eng. Sci.* **2002**, *57*, 2921–2931.
- [87] Szymczyk, A., Labbez, C., Fievet, P., Vidonne, A., Foissy, A., Pagetti, J. *Adv. Colloid Interface Sci.* **2003**, *103*, 77–94.
- [88] Palmeri, J., Sandeaux, J., Sandeaux, R., *et al.* *Desalination* **2002**, *147*, 231–236.
- [89] Lefebvre, X., Palmeri, J., Sandeaux, J., *et al.* *Sep. Purif. Technol.* **2003**, *32*, 117–126.
- [90] NanoFlux programme web site: <http://www.iemm.univ-montp2.fr> (accessed November 2009).
- [91] Mason, A., Lonsdale, H. K. *J. Membr. Sci.* **1990**, *51*, 1–81.
- [92] Geens, J., Van der Bruggen, B., Vandecasteele, C. *Sep. Purif. Technol.* **2006**, *48*, 255–263.
- [93] Anderson, J. L., Quinn, J. A. *Biophys. J.* **1974**, *14*, 130–150.
- [94] Bowen, W. R., Sharif, A. O. *J. Colloid Interface Sci.* **1994**, *168* (2), 414–421.
- [95] Deen, W. M., Satvat, B., Jamieson, J. M. *Am. J. Physiol.* **1980**, *238*, F126.
- [96] Paine, P. L., Scherr, P. *Biophys. J.* **1975**, *15* (10), 1087–1091.
- [97] Nakao, S., Kimura, S. *J. Chem. Eng. Jpn.* **1982**, *15*, 200–205.
- [98] Bungay, P. M., Brenner, H. *Int. J. Multiphase Flow* **1973**, *1*, 25–56.
- [99] Faxen, H. *Ann. Phys.* **1922**, *68* (10), 89–119.
- [100] Dechadilok, P., Deen, W. M. *Ind. Eng. Chem. Res.* **2006**, *45*, 6953–6959.
- [101] Zemaitis, J. F., Jr., Clark, D. M., Rafal, M., Scrivner, N. C. *Handbook of Aqueous Electrolyte Thermodynamics*; DIPPR, AIChE: New York, 1986.
- [102] Senapati, S., Chandra, A. *J. Phys. Chem. B* **2001**, *105*, 5106–5109.
- [103] Brovchenko, I., Geiger, A. *J. Mol. Liq.* **2002**, *96–97*, 195–206.
- [104] Zhang, L., Davis, H. T., Kroll, D. M., White, H. S. *J. Phys. Chem.* **1995**, *99*, 2878–2884.
- [105] Hartnig, C., Witschel, W., Spohr, E. *J. Phys. Chem. B* **1998**, *102*, 1241–1249.
- [106] Spohr, E., Hartnig, C., Gallo, P., Rovere, M. *J. Mol. Liq.* **1999**, *80*, 165–170.
- [107] Cavaco Morão, A. I., Szymczyk, A., Fievet, P., Brites Alves, A. M. *J. Membr. Sci.* **2008**, *322*, 320–330.
- [108] Geraldès, V., Brites Alves, A. M. *J. Membr. Sci.* **2008**, *321*, 172–181.
- [109] Spiegler, K. S., Kedem, O. *Desalination* **1966**, *1*, 311–326.
- [110] Szymczyk, A., Fatin-Rouge, N., Fievet, P., Ramseyer, C., Vidonne, A. *J. Membr. Sci.* **2007**, *287*, 102–110.
- [111] Bandini, S., Bruni, L. On the Mechanism of Charge Formation in Nanofiltration Membranes. In *Surface Electrical Phenomena in Membranes and Microchannels*; Szymczyk, A. Ed.; Transworld Research Network: Trivandrum, India, 2008; pp 1–30.

Biographical Sketches

Serena Bandini is currently an associate professor in chemical engineering at the Engineering Faculty of the University of Bologna – Alma Mater Studiorum, at the Chemical and Mining Engineering and Environmental Technologies Departments.

She graduated in chemical engineering at the University of Bologna in 1987 and received her PhD in chemical engineering, from the Italian Ministry of University and Scientific Research, in 1992 with a thesis titled 'Porous hydrophobic membranes-based separation processes.'

She has taught courses in chemical engineering thermodynamics, basic process engineering, electrochemical engineering principles, and chemical processes development, at the Faculty of Engineering and at the Faculty of Industrial Chemistry for first- and second-level degrees in chemical engineering, energy engineering, and industrial chemistry.

Her scientific research has been in the field of membrane separation processes for liquid mixtures (reverse osmosis, nanofiltration, microfiltration, membrane distillation, and electrodialysis). It has been documented by more than 60 papers and several presentations at international scientific congresses. Her fields of main interest include membrane characterization, transport phenomena modeling, and process development on an industrial scale.



Luigi Bruni is currently a PhD student in chemical engineering at the Department of Chemical and Mining Engineering and Environmental Technologies of the University of Bologna.

His research has mainly focused on transport and electrostatic phenomena in nanofiltration membranes under the supervision of Prof. Serena Bandini.

He graduated in chemical engineering at the University of Bologna in 2005. He began studying nanofiltration membranes during the preparation of his graduation thesis in which he performed a preliminary study to investigate which are the main phenomena involved in the mechanism of membrane charge formation.

2.05 Nanofiltration Operations in Nonaqueous Systems

L G Peeva, M Sairam, and A G Livingston, Imperial College London, London, UK

© 2010 Elsevier B.V. All rights reserved.

2.05.1	Introduction	91
2.05.2	Membranes for Separations in OSs	92
2.05.2.1	Polymeric Membranes	92
2.05.2.1.1	Integrally skinned asymmetric polymeric membranes	92
2.05.2.1.2	TFC membranes	93
2.05.2.1.3	Postformation treatment	93
2.05.2.1.4	Commercially available polymeric membranes	93
2.05.2.2	Ceramic OSN Membranes	95
2.05.2.2.1	Commercial ceramic membranes	97
2.05.3	Membrane Characterization	98
2.05.3.1	MWCO and Flux	98
2.05.3.2	Swelling	98
2.05.3.3	SEM and Atomic Force Microscopy	99
2.05.3.4	Pore-Size Measurement	102
2.05.3.5	Positron Annihilation Lifetime Spectroscopy, X-Ray Photoelectron Spectroscopy, Contact Angle, Surface Charge, and Surface Tension	102
2.05.4	Applications of Separation in OSs	103
2.05.4.1	Fine Chemical and Pharmaceutical Synthesis	103
2.05.4.2	Food and Beverage	105
2.05.4.3	Refining	107
2.05.5	Conclusions	109
References		109

2.05.1 Introduction

Membrane-based separation processes, such as gas separation, reverse osmosis (RO), nanofiltration (NF), ultrafiltration (UF), microfiltration (MF), electrodialysis (ED), and pervaporation (PV), have been developed for various applications [1]. NF, which is intermediate between RO and UF, is a pressure-driven process used for removing solutes, such as divalent ions, sugars, dyes, and organic matter, which have molecular weight (MW) in the range of 200–1000 g mol⁻¹, from aqueous feed streams [1]. A recent innovation is the extension of pressure-driven membrane NF processes to organic solvents (OSs). This emerging technology is referred to as organic solvent nanofiltration (OSN), or alternatively as solvent-resistant nanofiltration (SRNF) [2]. Aqueous NF, in many cases, involves separation between charged solutes and other compounds in an aqueous phase, whereas, by contrast, OSN is used for separations between molecules in organic–organic systems. Another membrane-based process widely

used with OSs is PV where separation occurs by differential permeation of liquids through a membrane, with transport of liquids through the membrane effected by maintaining a vapor pressure gradient across the membrane [3]. Membrane-based separations, in general, use significantly less energy than thermal processes, such as distillation, and this is of particular interest given the current high energy prices. This chapter focuses on describing the state of the art in OSN.

Sourirajan [4] reported the first application of membranes to nonaqueous systems in 1964 for the separation of hydrocarbon solvents using a cellulose acetate membrane. Later, Sourirajan and coworkers [5–7] used membranes to separate OS mixtures and organic and inorganic solutes using cellulose acetate membranes. From 1980 onward, major oil companies, such as Exxon [8–11] and Shell [12, 13], and chemical companies, such as Imperial Chemical Industries (ICI) and Union Carbide [14], began to file patents on the use of polymeric membranes to separate molecules present in organic solutions. The applications include

oil recovery [8–10], enrichment of aromatics [15–18], and homogeneous catalyst recycle [14]. Major membrane producers, including Grace Davison [19–22] and Koch [23], began research and acquisition programs, and products started to be commercially available from the mid-1990s onward. The largest success so far industrially has been the MAX-DEWAXTM process installed at ExxonMobil Beaumont refinery for the recovery of dewaxing solvents from lube oil filtrates [20], while the most recent addition to commercial offerings is the launch by Membrane Extraction Technology (MET) in 2008 of the DuraMemTM series of highly solvent-stable OSN membranes for the separation of organic solutes from various OSs [24]. These efforts have prompted a rapid rise in the number of academic publications and process development projects in industry. By way of illustrating the surge in interest in OSN, **Figure 1** shows a rough estimate of the number of patents and papers published on the application of membranes for nonaqueous operations before the 1990s, during the 1990s, and from 2000 onward.

2.05.2 Membranes for Separations in OSs

Both polymeric and inorganic materials have been used for the preparation of OSN membranes. In what follows, we present a brief summary of the currently commonly available OSN membranes.

2.05.2.1 Polymeric Membranes

Compatibility of polymeric membranes with a wide range of OSs is a very challenging issue in the OSN membrane production. Polymeric membranes generally fail to maintain their physical integrity in OSs because of their tendency to swell or dissolve. Nevertheless, several polymeric materials exhibit satisfactory solvent resistance (e.g., polyimides (PIs)) or can be made more stable, for example, by increasing the degree of cross-linking (e.g., silicone and polyacrylonitrile (PAN)). An overview of solvent-resistant polymeric materials used for membrane preparation can be found elsewhere [1, 25]. Most polymeric OSN membranes have an asymmetric structure, and are porous with a dense top layer. This asymmetry can be divided into two major types: the integrally skinned asymmetric type, wherein the whole membrane is composed of the same material; and the thin-film-composite (TFC) type, wherein the membrane-separating layer is made of a different material from the supporting porous matrix.

2.05.2.1.1 Integrally skinned asymmetric polymeric membranes

Integrally skinned asymmetric membranes are most commonly prepared by the phase-inversion immersion precipitation process. A solution of the polymer is cast as a thin film onto a nonwoven fabric, dried for a few seconds to create a dense top layer, and then immersed in a coagulation bath, which contains a

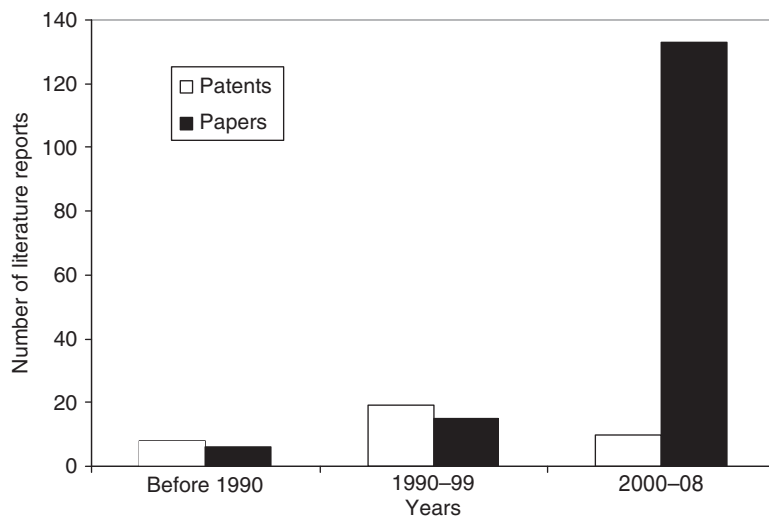


Figure 1 Number of patents and papers published before 1990s, during 1990s, and 2000s on membranes for nonaqueous operations.

nonsolvent for the polymer. The solvent starts to diffuse out of the homogeneous liquid polymer film, while the nonsolvent simultaneously diffuses into the film. Due to the presence of a nonsolvent, phase separation takes place in the polymer film and the polymer precipitates as a solid phase, forming a porous asymmetric membrane structure. The thermodynamic properties of the casting system and the kinetics involved in the exchange of solvent and nonsolvent affect the morphology of the membrane, and, consequently, its permeability and solute rejection [26]. The phase separation can also be induced by other methods, such as lowering the temperature (thermal precipitation), by evaporating the volatile solvent from the polymer film (controlled evaporation), or by placing the cast polymer film in a nonsolvent vapor phase (precipitation from the vapor phase) [2]. More detailed information about membrane preparation techniques can be found elsewhere [1].

2.05.2.1.2 TFC membranes

Composite membranes consist of at least two different materials. Usually, a selective membrane material is deposited as a thin layer upon a porous sublayer, which serves as support. The advantage of this type of membrane over the integrally skinned ones is that each layer can be optimized independently in order to achieve the desired membrane performance. There are several well-established techniques for applying a thin top layer upon a support: dip coating, spray coating, spin coating, interfacial polymerization, *in situ* polymerization, plasma polymerization, and grafting. Details of these techniques can be found elsewhere [1]. Due to the large variety of preparation techniques, almost all polymeric materials can be used to produce these types of membranes. The top layer and the support both contribute to the overall membrane performance.

2.05.2.1.3 Postformation treatment

In order to increase the separation performance of asymmetric membranes and to increase their long-term stability, several postformation treatments or conditioning procedures can be used, such as annealing (wet or dry), cross-linking, drying by solvent exchange, and treatment with conditioning agents [2]. Posttreatment procedures could be applied to both types of polymeric membranes mentioned above.

2.05.2.1.4 Commercially available polymeric membranes

Despite the fast development of research in the area of separation in OSs, there are still a limited number of membranes that have been commercialized. According to our knowledge of the membrane market, there are currently five companies producing SRNF membranes. The commercially available solvent-stable membranes include the Koch and StarmemTM membrane series, the SolSep membranes, the newly launched DuraMemTM membrane series, and the Inopor series of ceramic membranes.

Koch SelRO membranes. Koch Membrane Systems (USA) [27] was the first company to enter the OSN market with three different membranes designed for solvent applications. However, the hydrophobic membranes, such as SelRO MPF-60 (molecular weight cutoff (MWCO) 400 g mol⁻¹, based on rejection of Sudan IV (384 g mol⁻¹) in acetone) and SelRO MPF-50 (MWCO 700 g mol⁻¹, based on rejection of Sudan IV in ethyl acetate), have already been removed from the market. Only the hydrophilic MPF-44 membrane (MWCO 250 g mol⁻¹, based on rejection of glucose (180 g mol⁻¹) in water) is still available, in flat sheet as well as in spiral-wound (MPS-44) module configuration [2].

It is believed that the MPF series membranes are TFC-type membranes, comprising a dense silicone-based top layer of submicron thickness on a porous cross-linked PAN-based support. Membrane production may be associated with a patent from Membrane Products Kyriat Weitzman (Israel) [28], in which a cross-linked PAN support was first treated with silanol-terminated polysiloxane as a pore protector, and then immersed in a solution of polydimethylsiloxane (PDMS), tetraethyl silicate, and a tin-based catalyst for final coating and cross-linking. A scanning electron microscopy (SEM) picture [29] of the MPF-50 membrane is presented in **Figure 2**. Koch also distributes a UF membrane (nominal MWCO 20 000 g mol⁻¹), based on cross-linked PAN, available in both flat sheets (MPF-U20S) and spiral-wound (MPS-U20S) elements [2, 27].

According to the manufacturer's information, both membranes are claimed to be stable in methanol, acetone, 2-propanol, cyclohexane, ethanol, methyl ethyl ketone (MEK), butanol, methyl isobutyl ketone (MIBK), pentane, formaldehyde, hexane, ethylene glycol, dichloroethane, propylene oxide, trichloroethane, nitrobenzene, methylene chloride, tetrahydrofuran (THF), carbon tetrachloride, acetonitrile, diethylether, ethyl acetate, dioxane, xylene,

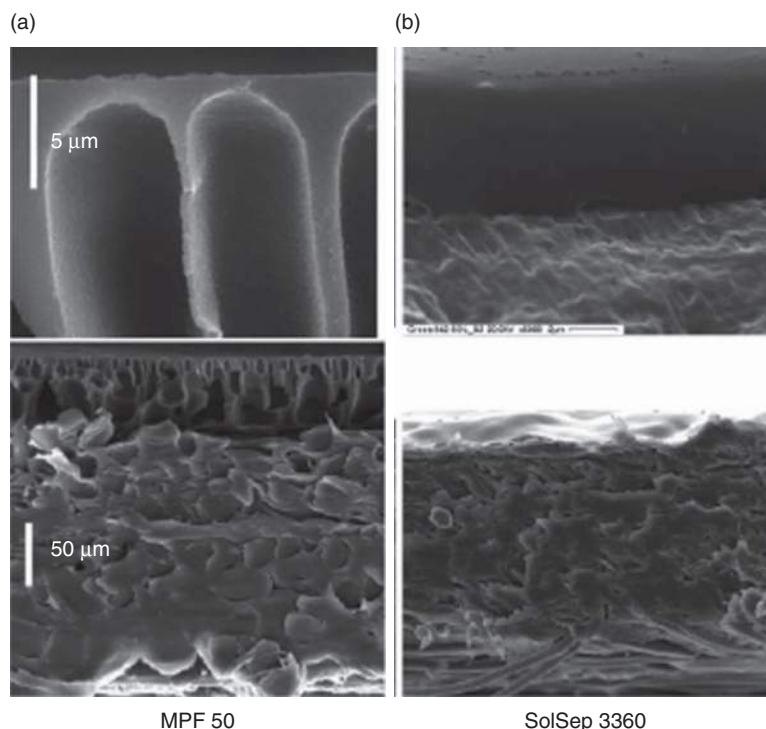


Figure 2 Scanning electron microscopy (SEM) images of the skin layer (top) and the entire cross section of the: (a) Koch membrane MPF-50, (b) SolSep 3360. Reproduced with permission from Van der Bruggen, B., Jansen, J. C., Figoli, A., Geens, J., Boussu, K., Drioli, E. *J. Phys. Chem. B* **2006**, *110*, 13799–13803.

and toluene, and claimed to have limited stability in dimethylformamide (DMF), *N*-methyl pyrrolidone (NMP), and dimethylacetamide [27].

The MPF series of OSN membranes were the first freely available membranes on the market, and, therefore, they have been subjected to extensive studies and have been tested in many applications, for example, the recovery of organometallic complexes from dichloromethane (DCM), THF, and ethyl acetate, and of phase-transfer catalysts (PTCs) from toluene, the separation of triglycerides from hexane, and for solvent exchange in pharmaceutical manufacturing. Extensive fundamental studies on solvent/solute transport mechanisms in OSN membranes have also been performed on MPF membranes [2].

StarmemTM membranes. The StarmemTM membranes series (Starmem is a trademark of W.R. Grace and Company) are distributed by MET (UK) [24]. The series consist of hydrophobic integrally skinned asymmetric OSN membranes with active surfaces manufactured from PIs. An active skin layer less than 0.2 mm in thickness with a pore size of <5 nm covers the PI membrane body [19, 21].

An SEM picture of a typical StarmemTM membrane is presented in Figure 3. StarmemTM 122 has an MWCO of 220 g mol⁻¹, StarmemTM 120 has an MWCO of 200 g mol⁻¹, and StarmemTM 240 has an MWCO of 400 g mol⁻¹. These quoted MWCOs are manufacturer values obtained using toluene as a solvent and are quoted as the MW at 90% solute rejection, estimated by interpolation from a plot of rejection versus MW for a series of *n*-alkanes. The membranes are claimed to be stable in alcohols (e.g., butanol, ethanol, and iso-propanol); alkanes (e.g., hexane and heptane); aromatics (e.g., toluene and xylene); ethers (e.g., methyl-*tert*-butyl-ether); ketones (e.g., methyl-ethyl-ketone and methyl-iso-butyl-ketone); and others (e.g., butyl acetate and ethyl acetate). All membranes are available as flat sheets or spiral-wound elements [24].

StarmemTM membranes have also been widely used to study solute and solvent transport through OSN membranes, and tested in different applications, such as product separation and catalyst recycle; chiral separations; solvent exchange in pharmaceutical manufacturing; ionic liquid-mediated reactions; and microfluidic purification and

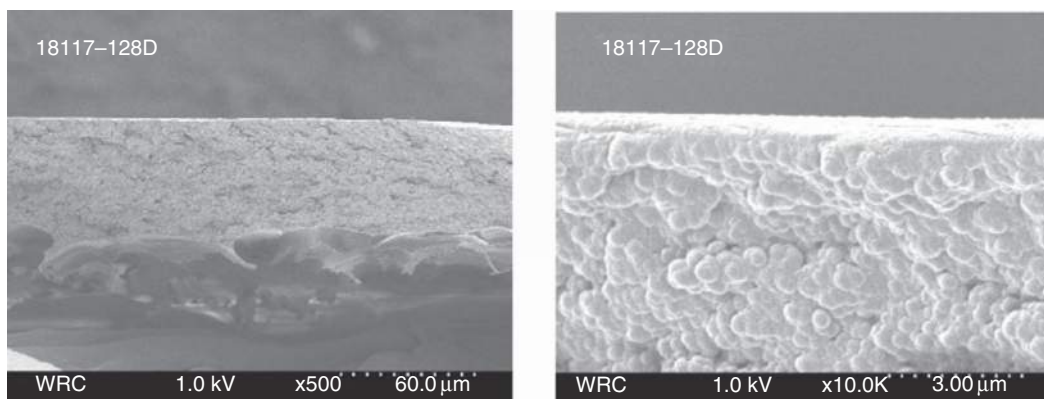


Figure 3 Grace Davison Membranes STARMEM™ polyimide membrane at 500× and 10 000× magnification of active separation layer. Reproduced with permission from White, L. S. *J. Membr. Sci.* **2002**, 205, 191–202.

membrane bioreactors (MBRs) for biotransformations [2]. Starmem™ membranes are the only OSN membranes applied at a large scale, in the refining industry for solvent recovery from lube oil dewaxing (MAX-DEWAX™) [21]. Further details on this large-scale application are provided in the subsequent section.

SolSep membranes. The Dutch company SolSep [30] offers five NF membranes with different stabilities and nominal MWCO values between 300 and 750 g mol⁻¹, and one UF membrane with an MWCO around 10 000 g mol⁻¹. According to the manufacturer, the membranes are stable in alcohols, esters, and ketones, and some of them are also stable in aromatics and chlorinated solvents. Typical characteristics of the SolSep membranes, as presented by the manufacturer, are summarized in **Table 1** and are claimed as being produced as spiral-wound-type modules [31]. While there is not much information available on the type of membrane material used for their preparation, it is believed that the SolSep membranes are of TFC type and some of them were proven to have a silicone top layer [29], as illustrated in **Figure 2**. The top layer of SolSep 3360 is clearly thicker than the barrier layer of MPF-50; consequently, lower solvent permeability is reported for similar MWCO [2, 29]. There is relatively limited information for the performance of these membranes in the literature [2, 29, 31–33]. Filtration data for SolSep NF030306 were recently reported in ethanol, i-propanol, toluene, xylene, hexane, heptane, cyclohexane, and butyl acetate [33].

DuraMem™. DuraMem™ range of highly stable OSN membranes is manufactured by MET [24]. Membranes are of integral asymmetric type and are

based on cross-linked PI [34, 35]. These membranes are available with different MWCO curves (180–1200 g mol⁻¹) and possess excellent stability in a range of solvents, including polar aprotic solvents such as DMF and NMP. The membranes have a sponge-like structure and are stable in most OSs, including toluene, methanol, methylene chloride, THF, DMF, and NMP. The membranes have been operated continuously for 120 h in DMF and THF and showed stable fluxes and good separation performances, with DMF permeability in the range of $(1–8) \times 10^{-5} \text{ L m}^{-2} \text{ h}^{-1} \text{ Pa}^{-1}$ ($1–8 \text{ L m}^{-2} \text{ h}^{-1} \text{ bar}^{-1}$) [35]. Possible re-imidization and loss of cross-linking at elevated temperatures limit their range of application to temperatures <100 °C.

2.05.2.2 Ceramic OSN Membranes

Ceramic materials (silicium carbide, zirconium oxide, and titanium oxide) endure harsh temperature conditions and show stable performance in solvent medium, and, therefore, are excellent materials for membrane preparation. Ceramic membranes generally have an asymmetric structure, in which a thin membrane layer with one or more intermediate layers is applied to a porous ceramic support. The support defines the external shape and mechanical stability of the membrane element. Common configurations are disks, which are produced by film casting or pressing of dry powder, and tubes, which are commonly produced via extrusion of ceramic powders with the addition of binders and plasticizers. These supports are subsequently sintered at 1200–1700 °C and an open-pore ceramic body is obtained with pore size between 1 and 10 μm, depending on the initial

Table 1 Overview of the available SolSep membranes with indicative cutoff and solvent compatibility

<i>Membrane</i>	<i>Maximum operating temperature (°C)</i>	<i>Maximum operating pressure (bar)</i>	<i>Rejection characteristics R (%)</i>	<i>Solvents compatibility</i>
UF10104	90	20	Typical retention of larger molecules ~10 000 g mol ⁻¹	Tested in alcohols, aromatics, esters, ketones
NF010206	120	20	R (95%) ~ 300 g mol ⁻¹	Alcohols, esters
NF010306	150	40	R (95%) ~ 500 g mol ⁻¹ ; ionics/acetone R (99%) ~300 g mol ⁻¹	Alcohols, esters, ketones, aromatics, chlorinated solvents
NF030306	150	40	Acetone: R (95%) ~ 500 g mol ⁻¹ Alcohols R (99%) ~ 300 g mol ⁻¹ Extremely stable	Alcohols, esters, ketones, aromatics, chlorinated solvents
NF030306F	120	40	Acetone: R (95%) ~ 300 g mol ⁻¹ Ethylacetate: R (95%) ~ 300 g mol ⁻¹ Extremely stable	Alcohols, ketones, aromatics, chlorinated solvents
NF030105	90	20	Ethanol, methanol R (95%) ~ 300 g mol ⁻¹ Acetone R (95%) ~ 750 g mol ⁻¹	Alcohols, ketones, aromatics,

Adapted from Cuperus, F. P. *Chem. Ing. Tech.* **2005**, 77, 1000–1001.

particle size and shape. A thin layer is applied to this support, typically by suspension coating using narrowly classified ceramic powders dispersed in an appropriate solvent. The pore size again is controlled by the size of the powder. The finest available powders have a particle size of about 60–100 nm, from which membranes with pore size of about 30 nm can be produced (the upper range of UF) [36]. To reduce the pore size even further, an additional thin defect-free layer is added, usually, by the so-called sol–gel process. The process starts with a precursor, which is often an alkoxide. The alkoxide is hydrolyzed in water or OS, which yields a hydroxide able to polymerize and form polyoxometalate. At this stage, the viscosity of the solution increases, which is an indication that polymerization has started. Viscosity modifiers or binders are frequently added to the sol prior to layered deposition on the porous support via dip or spin coating, where the final gelation occurs. Finally, the gel is dried and, via controlled calcination and/or sintering, the actual ceramic membrane is produced. A typical multilayered structure of a ceramic membrane is presented in **Figure 4**. Further details on the process of membrane preparation can be found elsewhere [1, 2, 36].

The major challenge in opening up the range of molecular separations in solvents that is possible with ceramic membranes was the evolution toward a lower pore size—around 1 nm. For a long time, the MWCO of the membranes was retained $\sim 1000 \text{ g mol}^{-1}$. However, by the end of the last century, NF membranes were developed based on silica membranes doped with zirconia and titania. A TiO_2 -based NF membrane, with a pore size of 0.9 nm and a cutoff of 450 g mol^{-1} , has been commercialized under the name Inopor[®] by

a spin-off company of HITK (Germany) [37], and has been successfully applied since 2002 in a treatment plant for harsh colored textile wastewaters [38, 39].

The intrinsic hydrophilicity of the oxide pore surfaces of the existing ceramic NF membranes lowers the permeability of apolar solvents through these membranes. Approaches to cope with this by preparing mixed oxides were not successful. The modification of the pore surface, by coupling of silane compounds to the hydroxyl groups, has been found to be a better solution. The silylation of ceramic membranes has been patented and is semi-commercially available from HITK (Germany) [36]. The membranes exemplified in the patent show cutoff values of about 600, 800, and 1200 g mol^{-1} in toluene using polystyrene standards [36], and have been used to retain transition-metal catalysts in apolar solvents [2].

2.05.2.2.1 Commercial ceramic membranes

Inopor series membranes. The Inopor[®] company [40] currently offers a range of ceramic UF and NF membranes in the form of monochannel and multi-channel tubes with lengths up to 1200 mm, as summarized in **Table 2**. The membranes are offered as hydrophilic version; however, on customer request, they can be prepared to be hydrophobic. There is no specific information on the company's website regarding the hydrophobic membranes, but it is believed that the literature-cited HITK-T1 (HITK, Germany) is a silylated TiO_2 -based version of the above-mentioned membranes. With a nominal MWCO of 220 g mol^{-1} , this membrane showed methanol and acetone permeabilities ($\sim 0.4 \text{ L m}^{-2} \text{ h}^{-1} \text{ bar}^{-1}$),

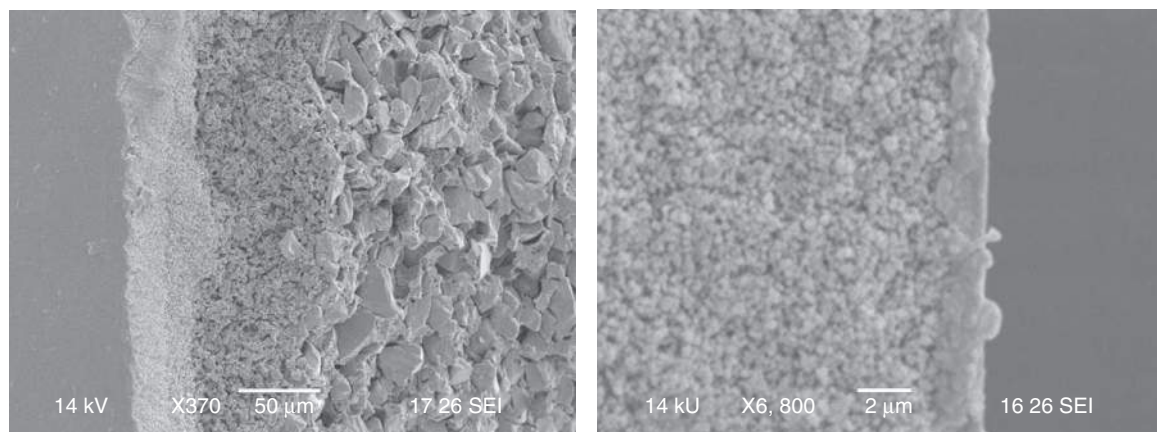


Figure 4 Typical multilayered structure of a ceramic membrane from the Inopor[®] series [40] at magnification 370 \times (edge view) and 6000 \times (top-layer edge view).

Table 2 Ceramic membranes supplied by the Inopor company

Membrane	Top layer material	Mean pore size (nm)	Cutoff (g mol^{-1})	Open porosity (%)
Inopor [®] ultra	TiO ₂	30	-	30–55
	TiO ₂	5	8500	
	ZrO ₂	3	2000	
Inopor [®] nano	SiO ₂	1	600	30–40
	TiO ₂	1	750	
	TiO ₂	0.9	450	

while rejecting Victoria blue (506 g mol^{-1}) for 99% from methanol, and erythrosine B (880 g mol^{-1}) for 97% from acetone, and demonstrated efficient catalyst recovery for Pd–2,2'-bis(diphenylphosphino)-1,1'-binaphthyl (BINAP) (849 g mol^{-1}) with rejections around 94.5% [2].

2.05.3 Membrane Characterization

Membrane characterization methods can be divided into two categories: (1) functional characterization and (2) physical–chemical characterization [41]. Functional parameters, such as flux and rejection, determine the selection of a membrane for a specific application [42]. Physical–chemical parameters include porosity, pore size, pore-size distribution, hydrophobicity, hydrophilicity, skin layer thickness, and charge [41]. One of the current challenges in OSN research is to establish the physical–chemical structure of the membranes, and then to use that to predict the functional performance.

2.05.3.1 MWCO and Flux

Flux or permeation rate is the volume of liquid flowing through the membrane per unit area and per unit time and is generally expressed in terms of $\text{L m}^{-2} \text{ h}^{-1}$ and the permeability by $\text{L m}^{-2} \text{ h}^{-1} \text{ bar}^{-1}$. Rejection of a solute i ($R_i\%$) is calculated by $R_i (\%) = (1 - C_{pi}/C_{ri}) \times 100\%$ where, C_{pi} and C_{ri} are the concentration of solute i in the permeate and retentate, respectively. The separation performance of OSN membranes can also be expressed in terms of MWCO obtained by plotting the percentage rejection of solutes versus their MW (typically $200\text{--}1000 \text{ g mol}^{-1}$) and interpolating the data to find the MW corresponding to 90% rejection. Oligomeric forms of polyisobutylene [43–46], polyethylene glycol (PEG) [47, 48], polystyrene [46, 49], linear and branched alkanes, and dyes have been

used as solutes to estimate MWCO of OSN membranes [49]. The properties of solutes and solvents, such as structure, size, charge, and concentration, are found to affect the performance of OSN membranes [43–51]. Figure 5 shows MWCO curves for StarmemTM 122 in different solvents using polystyrene oligomers. MWCO of some of the commercially available membranes are summarized in Table 3. The selection of membranes for OSN applications depends upon the MWCO specified by the manufacturer. However, different methods used for evaluating MWCO of membranes lead to inconsistencies, making the selection of a suitable membrane for a desired application difficult. A simple and reliable method was developed by See Toh *et al.* [49] to determine MWCO of OSN membranes using a homologous series of polystyrene oligomers spanning the NF range ($200\text{--}1000 \text{ g mol}^{-1}$) and which are soluble in a wide range of solvents.

OSN membranes, with high solvent fluxes and high retention of organic solutes, are required for various applications. Fluxes of OSs through commercial membranes are reported in the literature [29, 52–62]. Initial flux decrease was found to be a common phenomenon, usually attributed to membrane compaction, with the variation between initial and steady-state fluxes depending upon membrane and solvent [56]. Solvent flux through the membrane also increases with rise in temperature driven by reductions in viscosity of solvents, increase in solvent diffusion coefficients [62], or by increases in polymer chain mobility [63, 64]. The nature of the membrane (hydrophilic or hydrophobic), physical properties of solvents, such as dipole moment, dielectric constant, and solubility parameter, affect membrane–solvent interaction, which in turn affects solvent flux [57, 65].

2.05.3.2 Swelling

Polymer swelling plays an important role in flux and rejection of some OSN membranes [65–67]. Ho and

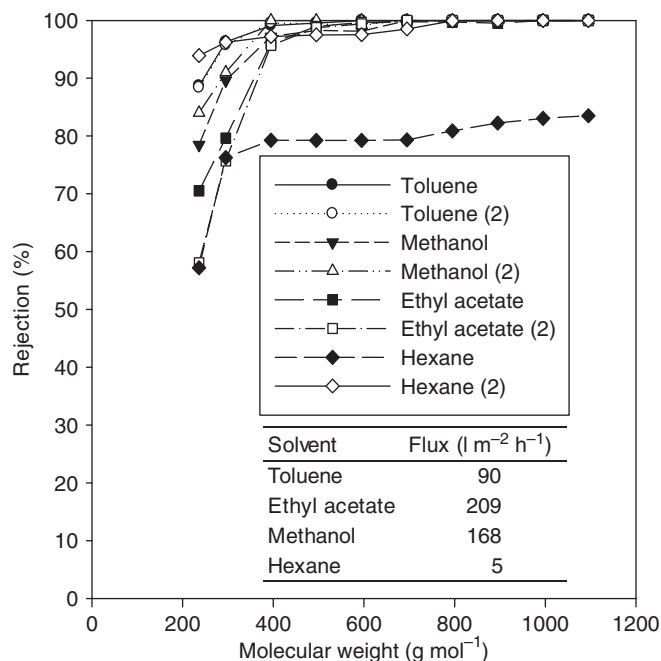


Figure 5 Molecular weight cutoff curves for Starmem™ 122 using different solvent systems at 30 bar. Reproduced with permission from See Toh, Y. H., Loh, X. X., Li, K., Bismarck, A., Livingston, A. G. *J. Membr. Sci.* **2007**, 291, 120–125.

Sirkar [68] developed a method to quantify swelling of polymeric membranes, based on weight difference between dry and solvent-impregnated polymer samples. Swelling experiments were carried out on PDMS, and on hydroxylated PDMS films and blocks, by immersing them in test solutions. Samples were removed at different time intervals, excess solvent was wiped out, and weight was measured [69–71]. Swelling of PDMS approached 205% in hexane–solute systems [69]. Transport in PDMS is strongly influenced by swelling, and viscosity of solvent also plays a role under certain conditions [70]. Geens *et al.* [72] observed significant swelling with a range of solvents. Piccinini *et al.* [73] described an alternative, and relatively complex, technique in which a quartz spring microbalance was used to simultaneously measure solubility, diffusion coefficient, and swelling for a solvent/polymer combination of acetonitrile/polyetherurethane. Tarleton *et al.* [74, 75] described a new apparatus for *in situ* determination of membrane swelling, comprising a linear inductive probe and electronic column gauge with an overall resolution of 0.1 μm . It was used in two configurations to assess the swelling propensity of PAN/PDMS NF membranes in a range of alkane, aromatic, and alcohol solvents. The extent of swelling was closely related to the value of the mixture solubility parameter (δ_{mixture}), where a

higher value of δ_{mixture} led to less swelling [74]. The inductive probe method was also used to measure the swelling of seven PAN/PDMS composite NF membranes in a range of alkane, aromatic, and alcohol solvents [75]. PDMS membranes with thickness between 1 and 10 μm were prepared and were cross-linked by radiation and/or thermal treatments. The tested membranes exhibited a range of swelling dependent on the degree of cross-linking, the initial PDMS layer thickness, and the type of solvent. With no applied pressure, the PDMS layer on some radiation cross-linked membranes swelled by as much as $\sim 170\%$ of the initial thickness, while other membranes were restricted to a maximum swelling of $\sim 80\%$. When a pressure of up to 2000 kPa was applied to a membrane, then swelling could be reduced to $\sim 20\%$ of the value obtained at zero applied pressure. However, results of the swelling experiments could not be correlated with NF performance of membranes in terms of solvent flux and solute rejection [75].

2.05.3.3 SEM and Atomic Force Microscopy

Polymer membranes, with an asymmetric pore distribution in their cross section, represent the most common type of membrane structures used today. Their characteristic feature is the presence of a

Table 3 MWCO data for some of the commercially available membranes

	<i>MWCO</i> (g mol^{-1})	<i>Reported rejection (%)</i> <i>of solute</i>	<i>Solute (molecular</i> <i>weight, g mol^{-1})</i>	<i>Solvent</i>	<i>Nature</i>	<i>Ref.</i>
MPF-60	400		Sudan IV (384)	Acetone	Hydrophobic	
MPF-50	700		Sudan IV (384)	Ethyl acetate	Hydrophobic	[27]
MPF-44	250		Glucose (180)	Water	Hydrophilic	
MPF-U20S	2000		-	-	-	
Starmem TM 120	200		<i>n</i> -Alkanes	Toluene	Hydrophobic	
Starmem TM 122	220		<i>n</i> -Alkanes	Toluene	Hydrophobic	[24]
Starmem TM 228	280		<i>n</i> -Alkanes	Toluene	Hydrophobic	
Starmem TM 240	400		<i>n</i> -Alkanes	Toluene	Hydrophobic	
NF030505	-	-	-	-	-	
SolSep-169	880	91	Erythrosine B (880)	Acetone	-	[52]
		65	Victoria blue (506)	Ethyl acetate	-	
SolSep-3360	880	92	Erythrosine B	Ethanol	-	[29]
HITK-T1	220	99	Victoria blue (506)	Methanol	-	[53]
	220	97	Erythrosine B (880)	Acetone	-	
Desal-5	-	99	Sucrose (342)	-	-	[54]
Desal-5-DK	-	99	Sucrose (342)	-	-	
Membrane YK		43	Sudan IV (384)	Hexane		
		86	Sudan IV (384)	Methanol		[55]
DuraMem TM	250–1200 (tunable)		Polystyrene oligomers	DMF	Hydrophobic	[24]

thin, tighter top layer (skin) and a porous sublayer with large through pores, which minimizes the mass transfer resistance of membranes. Asymmetric membranes can have either a nonporous or a porous skin. The latter membranes can be used as supports for composite diffusion membranes, or as independent porous films in various pressure-driven processes (RO, MF, UF, and NF). Separation characteristics and physical properties vary across membranes and depend upon the membrane morphology. Examination of SEM pictures provides reliable information on membrane morphology and confirms the formation of asymmetric structures during phase-inversion process [76–80].

The skin layer generated after a prolonged evaporation period shows a dramatically different structure compared to that obtained after shorter evaporation times. The cross section of membrane prepared from the shorter evaporation time favors the formation of a sponge-like structure containing macrovoids, while that prepared with longer evaporation time showed sponge-like structure [77–80]. Pinnau and Koros [77] proposed a mechanism for the formation of surface skin layers during asymmetric membrane formation by dry/wet phase inversion. They suggested that the outermost region of the asymmetric membrane undergoes a phase separation by spinodal decomposition during the initial stages of the evaporation process, and that the evaporation step, prior to immersion in the non-solvent, strongly influences the surface skin-layer thickness and is necessary to assure the formation of the defect-free skin. See Toh *et al.* [81] reported no apparent increase of separation-layer thickness with increasing evaporation time or polymer concentration (Figures 6 and 7). The presence of macrovoids was observed at low polymer concentration. The effect of thermal annealing and the differences observed in membrane morphology before and after OSN filtration were reported [81].

SEM images of the MPF-50 membrane showed vague, pore-like features with diameters of 2–3 μm (Figures 8(b) and 8(d)) [70]. SEM images under more surface-sensitive conditions did not show pore-like features at the same magnification; instead, a relatively uniform surface was observed. Local damage to the surface suggested the presence of a thin surface layer (Figures 8(a) and 8(c)). SEM pictures recorded at higher magnification (Figure 8(e)) revealed crack-like features with dimensions of a few tens of nanometers. These cracks were assumed to be artefacts introduced to

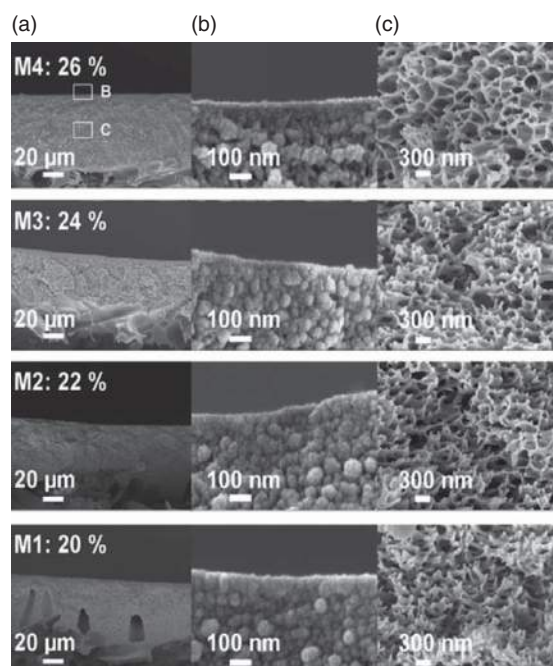


Figure 6 Morphological changes with polymer concentration of polyimide (PI) membranes: (a) cross section 2000 \times ; (b) top layer 400 000 \times ; (c) middle section 100 000 \times . Reproduced with permission from See Toh, Y. H., Ferreira, F. C., Livingston, A. G. *J. Membr. Sci.* **2007**, 299, 236–250.

the surface layer by the electron beam or during the membrane preparation. The pore-like features observed at 20 kV were probably due to subsurface porosity of the membrane. The interpretation was supported by micrographs of cross section, which also showed the presence of a surface layer with a thickness in the 100-nm range (Figure 9) [70]. Figure 10 shows cross-sectional views of the asymmetric PI membrane used for the recovery of solvents from lube oil filtrates [19, 21]. A membrane free of macrovoids was prepared in order to avoid potential weak spots in the membrane during high-pressure operations. The thickness of the skin layer on the membrane surface was reported to be less than 0.2 μm [21].

Atomic force microscopy (AFM) probes the surface of a sample with a sharp tip, located at the free end of a cantilever [82, 83]. AFM provides information about surface roughness, hydrophilicity, and hydrophobicity of membranes [84, 85]. It has also been used to study the roughness of polymeric [86–88] and ceramic membranes [89, 90]. For UF and MF membranes, AFM was also used to study the

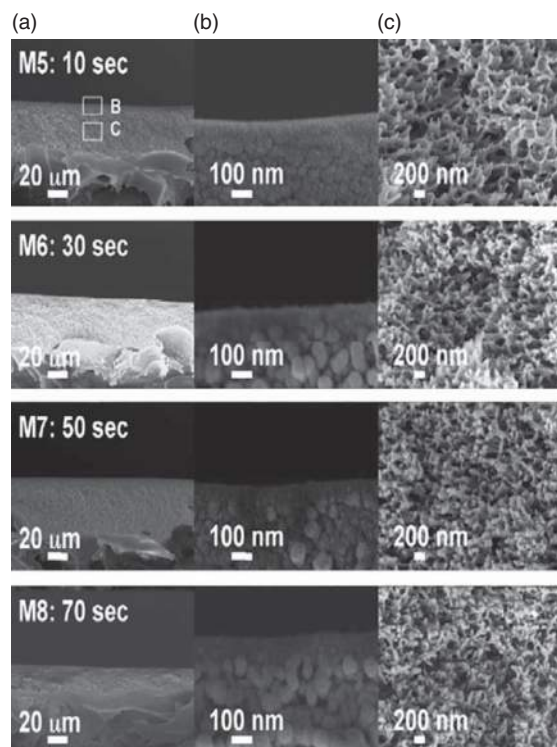


Figure 7 Morphological changes with evaporation time of PI membranes: (a) cross section 2000 \times ; (b) top layer 400 000 \times ; (c) middle section 100 000 \times . Reproduced with permission from See Toh, Y. H., Ferreira, F. C., Livingston, A. G. *J. Membr. Sci.* **2007**, 299, 236–250.

size and the shape of pores on the surface [87, 88]. The pore size in NF and RO membranes will be smaller when compared to UF and MF membranes; therefore, the interpretation of pore diameters needs great care [91, 92]. Another application of AFM in the membrane field is the direct measurement of the force of adhesion between a particle (such as silica or polystyrene) and the membrane surface by immobilizing the particle at the end of the cantilever. This can be of great benefit to membrane technologists, as it makes it possible to predict fouling without process measurements [92]. AFM studies on composite membranes of zeolite-filled PDMS coated on PI and PAN supports showed that good-quality membranes were obtained by coating PDMS on relatively smoother PI supports than PAN [93]. AFM analysis of OSN membranes prepared by alternating deposition of oppositely charged polyelectrolyte showed an increase in thickness with increase in layer growth and an increase in surface roughness with increase in number of bilayers [94].

2.05.3.4 Pore-Size Measurement

Pore diameters of ceramic membranes were estimated based on the dynamic method of humid air permeation [95, 96]. The membranes prepared are asymmetric; therefore, it is important to evaluate the effective pore diameters of membranes. Brunauer, Emmett and Teller (BET) methods, based on nitrogen adsorption and desorption to evaluate the pore diameters of powders, may not be adequate for the evaluation of active pore size of asymmetric membranes. The principle of measuring pore size based on humid air permeation lies in capillary condensation of water vapor in the fine pores at a given humidity and blocking of air permeation through the condensed pores [97, 98]. Pore size of silica–zirconia membranes was estimated from perporometry [99, 100], and pure solvent permeabilities for methanol, ethanol, and 1-propanol were measured at temperatures from 25 to 60 \pm °C through silica–zirconia composite membranes [99]. For membranes with pore sizes as large as 70 nm, the permeation mechanism of alcohols followed the viscous flow mechanism irrespective of types of alcohols. Permeation mechanism through porous silica–zirconia membranes with pore diameters of 1–5 nm was found to be different from the viscous flow mechanism; the flow is dependent on the size of molecules [99]. NF experiments were carried out on porous silica–zirconia membranes with various average pore sizes in a range of 1–4 nm, measured by perporometry [100]. MWCO of these membranes was found to be 300, 600, 1000, and >1000 g mol⁻¹ in ethanol and methanol [100]. Another widely used technique for measurement of pore size in UF is liquid displacement, which may also be useful to estimate pore size in OSN membranes [101–103].

2.05.3.5 Positron Annihilation Lifetime Spectroscopy, X-Ray Photoelectron Spectroscopy, Contact Angle, Surface Charge, and Surface Tension

Some of the other useful techniques to characterize membranes are described briefly. Positron annihilation lifetime spectroscopy (PALS) enables the characterization of the free volume in polymers and was used to determine the pore size in NF membranes. PALS was successfully used to characterize the pore size in the top layer of TFC membranes and used to explain the flux-enhancement mechanism [104]. This technique was also used to measure the size of pores in PV [105] and gas separation [106]

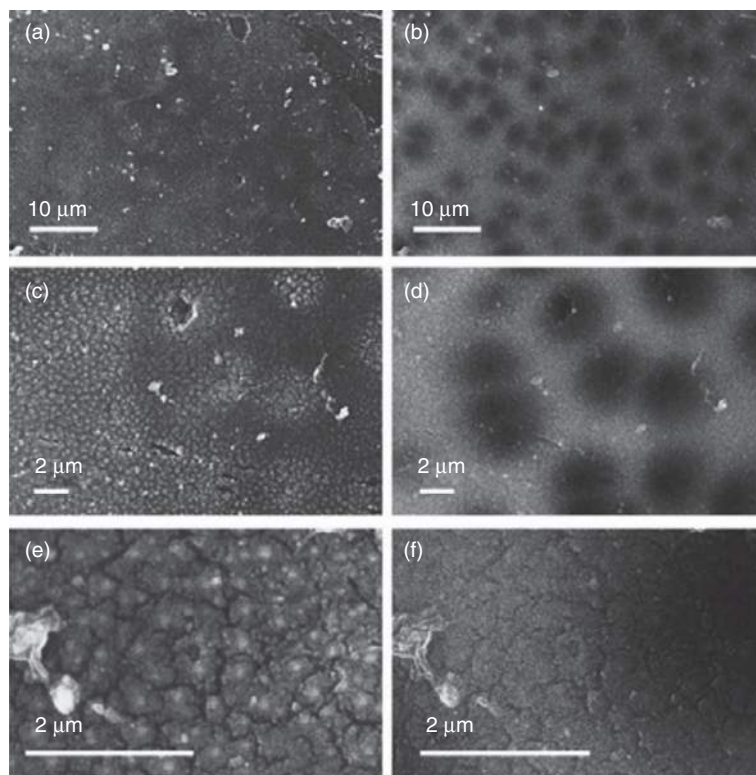


Figure 8 Field emission gun-scanning electron microscopy (FEG-SEM) images of the surface of the MPF-50 membrane. Images at 5 kV (left; images (a), (c), and (e)) and at 20 kV (right; images (b), (d), and (f)) of the same region are compared. Original magnifications were $1000\times$ (a, b); $5000\times$ (c, d); and $25\,000\times$ (e, f). Reproduced with permission from Vankelecom, I. F. J., De Smet, K., Gevers, L. E. M., *et al. J. Membr. Sci.* **2004**, 231, 99–108.

membranes. Pore-size measurement by PALS in some commercially available NF membranes indicated the presence of pores with a radius of 1.25–1.55 and 3.2–3.95 Å [107]. However, no correlation was observed between the MWCO measured with PEG as solutes in water and pore size measured by PALS. X-ray photoelectron spectroscopy (XPS) is a useful technique to determine the elemental composition, variation in chemical composition during cross-linking of membranes [70, 104, 108, 109]. Contact angle [72, 108, 109], surface charge [110, 111, 112], and surface tension [72, 110] are all useful to determine the hydrophobicity and surface charge of membranes.

2.05.4 Applications of Separation in OSs

Membrane separation in OSs is an emerging technology and has not yet been widely exploited. It has a great potential as an alternative – or at least as a complementary process in hybrid processes – for

distillations, evaporations, chromatographical separations, crystallizations, adsorptions, or extractions. Applications have been proposed for a variety of industries, including fine chemical and pharmaceutical synthesis, food and beverage, and refining.

2.05.4.1 Fine Chemical and Pharmaceutical Synthesis

The separation of reaction products from catalysts is a recurrent problem in homogeneous catalysis. The major drawback of the common separation techniques applied in homogeneous catalysis is the extensive (and usually destructive) nature of the postreaction workups required. OSN membranes, being selective between high MW catalysts ($>450\text{ g mol}^{-1}$) and reaction products, are able to perform this separation. Recycling off-the-shelf homogeneous catalysts was described in a 1993 patent assigned to Membrane Products Kiryat Weitzman, and 4 years later in a Union Carbide patent describing Rh catalyst retained by an MPF-50 membrane during a

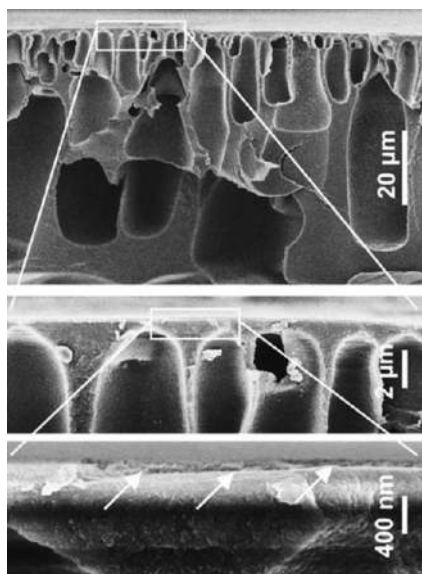


Figure 9 Field emission gun-scanning electron microscopy (FEG-SEM) images at 5 kV of the cross section of the MPF-50 membrane, zooming in (top to bottom) on details of the surface region. An apparent surface layer is indicated with arrows. Original magnifications were 1000 \times (top); 5000 \times (middle); and 25 000 \times (bottom). Reproduced with permission from Vankelecom, I. F. J., De Smet, K., Gevers, L. E. M., *et al. J. Membr. Sci.* **2004**, 231, 99–108.

hydroformylation process in butyraldehyde and acetone with observed rejection of 99% and 93%, respectively [2]. A 2001 study of OSN-coupled reactions with nonenlarged catalysts describes how

Ru-BINAP and Rh-DuPhos catalysts were retained by MPF-50 membranes in methanol for more than 97% [2]. Another extensive study was presented by Scarpello *et al.* [113] who investigated the rejection of Wilkinson catalyst, Jacobsen catalyst, and Pd-BINAP catalyst by a range of StarmemTM membranes, MPF50, and Desal5 membranes in DCM, THF, and ethyl acetate solvents. Nair *et al.* [114] presented a membrane-based (StramemTM 122) process for the separation of a PTC and a Heck reaction transition-metal catalyst from the reaction media. For the PTC catalyst, the process was so efficient that rejections superior to 99% were observed for both pre- and postreaction mixtures, and no reaction rate decline was observed for two consecutive catalyst recycles. Catalyst recovery reported in the literature has mainly been performed using polymeric OSN membranes; however, some successful applications of ceramic membranes can also be found – but typically, low solvent fluxes were observed [115, 116]. Apart from the catalyst metal center, the ligands, which are often even more expensive, can be recycled with OSN membranes as described in a recent patent filed by Lyondell Chemical Technology where the hydrophilic MPF-44 was used to recover triphenyl phosphine from the reaction mixture [117]. Currently, there are a large number of studies reporting recovery and reuse of homogeneous catalysts, a good review of which could be found elsewhere [2].

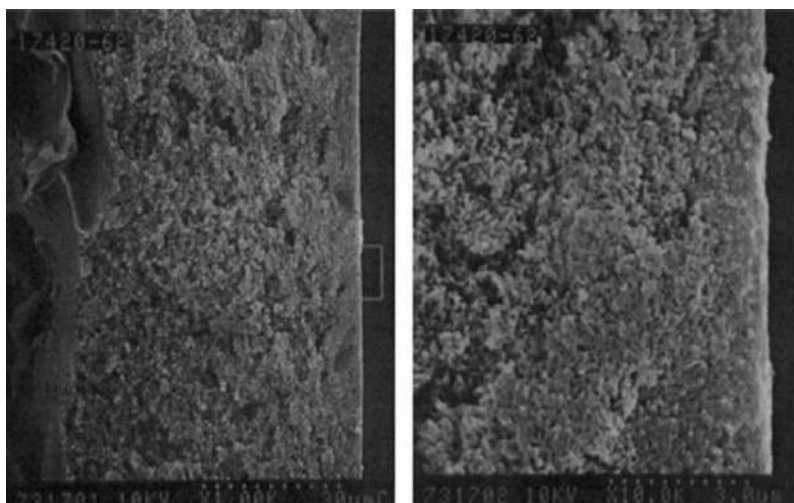


Figure 10 Cross-section scanning electron microscopy views of asymmetric polyimide membrane at 1000 \times and 10 000 \times magnification of the active separation layer. The membrane was first washed with hexane to remove conditioning agents and the backing removed. The active surface layer is on the right. Reproduced with permission from White, L. S., Nitsch, A. R. *J. Membr. Sci.* **2000**, 179, 267–274.

Another important application is the use of OSN membranes in biocatalytic processes. Large numbers of substrates and products of biotransformations are poorly soluble in water, and thus the biotransformation has to be performed in OS or in biphasic aqueous/OS systems. In many cases, the operation of direct-contact biphasic systems is obstructed by irreversible emulsification and/or inhibition of the biocatalyst by the OS. A viable alternative is the use of a membrane contactor utilizing OSN membrane, which separates the two phases and prevents emulsification and inhibition, allowing efficient substrate and product permeation. One such example is the biotransformation of geraniol to R-citronellol by baker's yeast, performed in toluene and *n*-hexadecane, in a membrane contactor equipped with StarmemTM 122 membrane. However, the OSN-based contactor exhibited lower productivities compared to a direct-contact biphasic reactor due to limitations in the transfer rate of the substrate through the membrane [118, 119]. A hybrid biocatalytic/chemocatalytic process was proposed for dynamic kinetic resolution for cases where the catalytic conditions for resolution and racemization are not compatible. StarmemTM122 and Durapore[®], an MF membrane (0.65 μm DVPP, Millipore, USA), were used to separate the two reactive systems, allowing permeation of product and substrate, while retaining the catalysts. The racemization and resolution reactions were catalyzed by a Ru(cymene)/amine base system and a lipase (Novozym 435)/vinyl acetate system, respectively [120].

Synthesis of pharmaceuticals often involves multistep reactions, performed in different solvents, while the isolation of the product also occurs in a specific solvent. The exchange of solvents can be problematic for many synthetic processes, especially if a high boiling solvent is to be exchanged for a low boiling one and/or when solvent azeotrope of thermally labile products is involved. A series of works suggests that membrane technology could be a viable option. Sheth *et al.* [121] demonstrated that OSN could be successfully applied for solvent exchange in multistep organic synthesis of bulk drugs where each reaction may be carried out in a different solvent. Ethyl acetate was reduced to the level of a low-concentration impurity in methanol using OSN membranes MPF-50 and MPF-60 and a solute, erythromycin, representing an active intermediate. Livingston *et al.* [122] have also shown the solvent exchange potential of StarmemTM 122 OSN membrane, for the methanol–toluene system.

MET commercialized this solvent exchange technology as MEMSOLVETM and claims that MEMSOLVETM achieves greater than 99% exchange of solvents at ambient temperature, using up to 80% less energy than distillation [24].

Similarly to membranes designed for aqueous applications, the OSN membranes have been used for isolation, concentration, and purification of active pharmaceutical ingredients (APIs). Specific examples are membrane processes applied for concentration of antibiotics [2]; solvent recovery [123]; and fractionation and purification of APIs in membrane cascade [124]. OSN membranes have found their place even in specific areas such as separation of chiral molecules. One successful example has been demonstrated for enantioselective separation of a D, L phenylethanol racemic mixture using OSN combined with enantioselective inclusion–complexation. A complex is formed with one of the enantiomers, thus leaving the uncomplexed form of the other enantiomer in the solvent. The latter is much smaller and will preferably permeate through an OSN membrane (StarmemTM 122) with MWCO between the MWs of the complexation agent and the racemate. A decomplexation solvent is then added, dissociating the complex and allowing permeation of the de-complexed enantiomer. The complexing agent is retained by the membrane and further reused in consecutive cycles. This approach offers an alternative to distillation–combined enantioselective inclusion complexes and opens up the enantiomer complexation separation to nonvolatile compounds and large-scale applications [125].

2.05.4.2 Food and Beverage

Vegetable oil production is a complex multistage process and membranes, conceptually, can be applied to almost all stages of oil production and purification (Figure 11). In the conventional vegetable oil processing, there are four major drawbacks [126]:

- High energy usage – after the oil extraction with solvent, the oil solvent mixture is then separated by evaporation. This requires a considerable amount of energy and, in addition, safety problems might arise from the released explosive vapors.
- Oil losses – the saponification in the refining step traps a considerable amount of oil.
- Resources – large amounts of water and chemicals are used.

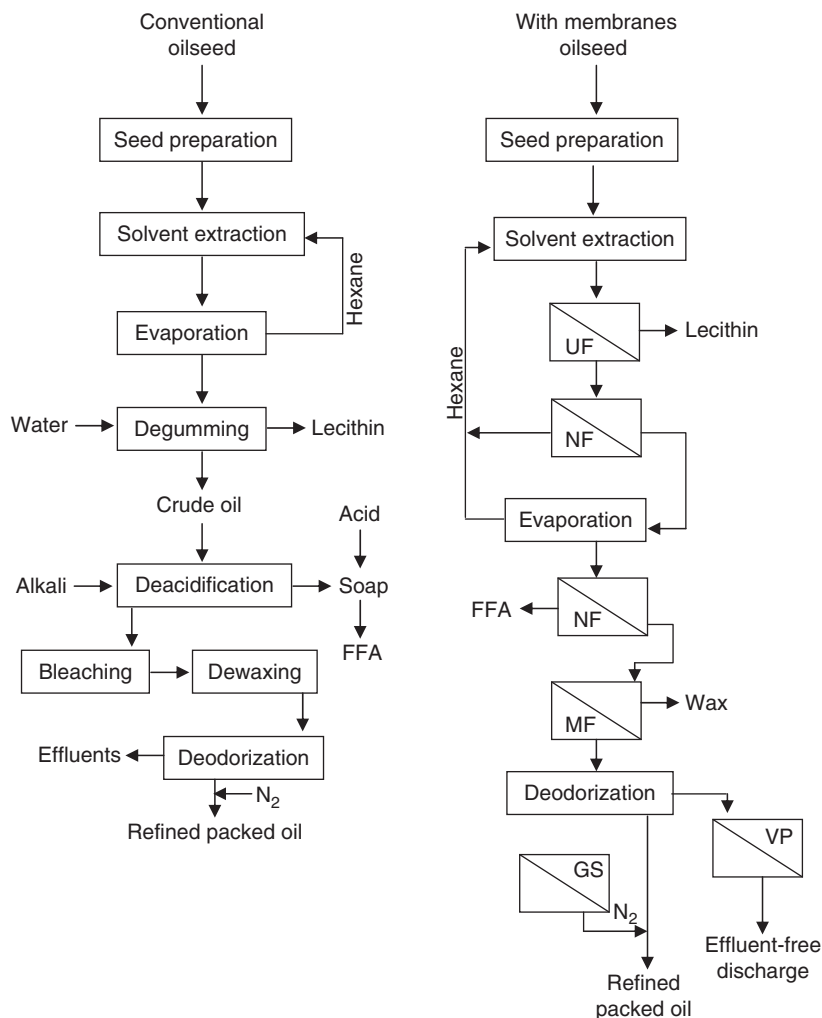


Figure 11 Vegetable oil processing, using a conventional approach and membrane technology. UF, ultrafiltration; NF, nanofiltration; VP, vapor permeation; GS, gas separation; MF, microfiltration; FFA, free fatty acids. Reproduced with permission from Cheryan, M. *Membr. Tech.* **2005**, *2*, 5–7.

- Effluents – heavily contaminated effluents are produced.

The use of solvent-resistant membranes in the vegetable oil industry would allow (Figure 11): minimization of thermal damage, solvent recycle, lower emissions, lower energy consumption, reduced oil losses, and a decrease in bleaching earth requirements. It has been estimated that the introduction of membrane technology in edible oil processing could potentially save 15–22 trillion kilojoules per year of energy in the United States alone, while reducing oil losses by 75%, improving the oil quality, and minimizing thermal damage [2]. Successful examples could be found in the literature for each of the various

membrane-processing steps presented in Figure 11. Pioch *et al.* [127] observed that cross-flow filtration gives promising results for vegetable oil refining, while a Unilever patent suggests that OSN membranes could be quite efficient during the degumming step [128]. The distillation step could be complemented with several membrane steps performed at ambient temperature, thus reducing the energy demands. An added advantage is that the degradation of some thermolabile components of the oils will also be reduced. Separation of corn oil from hexane and isooctane using membranes whose top layer comprises radiation cross-linked PDMS has been claimed in a patent filed by GKSS-Germany [129]. High permeability ($3 \text{ L m}^{-2} \text{ h}^{-1} \text{ bar}^{-1}$) and rejection

values of 90% have been observed. Stafie *et al.* [69] reported similar rejections for sunflower oil/hexane and permeation through a composite PDMS membrane with PAN support. Raman *et al.* [130] and Zwijnenberg *et al.* [131] suggested that OSN could be successfully applied to the final step of the edible oil processing – deacidification. More recent results by Bhosle and Subramanian [132] also confirmed this concept; however, the fluxes are too low for industrial applications.

Other promising applications of the OSN membranes in the food industry are for concentration, fractionation, and purification of high-value natural products. Such examples are the membrane processes proposed for purification and recovery of carotenoids from palm oil [133] and xanthophylls from corn [134], both valuable natural nutraceutical products.

2.05.4.3 Refining

The refining industry is both energy and separations intensive, suggesting that application of large-scale membrane systems can provide significant benefits [2]. Starting in the 1980s and 1990s, oil majors (Exxon [8, 9], Shell [12], and Texaco [135]) began to file patents on the use of polymeric membranes for solvent recovery in lube oil dewaxing. They used existing commercial (aqueous) membranes, or made their own. Finally in 2000, White and Nitsch [21] showed that the commercial polymer, known as Matrimid 5218, can be used to form asymmetric NF

membranes with excellent chemical stability, able to separate light hydrocarbon solvents from lube oil filtrates. More specifically, in a 2-month high-pressure continuous test, this PI membrane was able to achieve a 99% purity chilled solvent (MEK–toluene mixture at 263 K) recovery from lube oil filtrates with a steady permeate rate. The energy requirements for this membrane process are nearly 45% less than those for the usual distillation-based lube processing. This work led to the installation of a commercial OSN plant, located in Mobil's Beaumont, Texas refinery. The process (trademarked as MAX-DEWAX™) (Figure 12) is able to deal with 11 500 m³ of solvent per day. The MAX-DEWAX™ process, combined with selected ancillary equipment upgrades, increased base oil production by over 25 vol.% and improved dewaxed oil yields by 3–5 vol.%. The net annual uplift from the membrane unit is over \$6 million, making it a very attractive technology. The capital expenditure was paid back in less than 1 year by the increase in the net profitability of the lube dewaxing plant. This highly successful application at large scale clearly shows the potential for OSN to impact the energy and chemicals sectors.

In a patent filed by British petroleum (BP), OSN membranes have been used for deacidification of crude oil. Crude oil and the distilled fraction thereof typically contain organic acids, such as naphthenic acids, making it acidic. The acid impurities may cause corrosion and are typically removed by extraction with a polar solvent, such as methanol. The solvent is typically

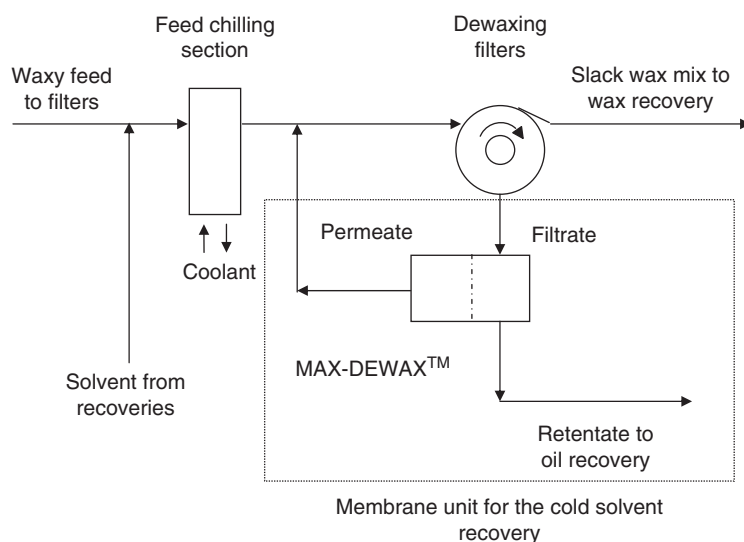


Figure 12 Schematics of the MAX-DEWAX™ process. Reproduced with permission from White, L. S., Nitsch, A. R. J. *Membr. Sci.* **2000**, 179, 267–274.

recovered by distillation; however, in the patented process, the distillation unit is replaced with an OSN unit. The naphthenic acids are retained in the retentate, while the recovered solvent appears in the permeate stream. Commercial membranes from the Desal (Osmonics) series designed for water applications were employed and the highest rejection achieved for the naphthenic acids was $\sim 87\%$ with Desal DK [136].

There are a number of OSN membrane applications suggested for treating aromatics-containing refinery streams. Toluene disproportionation converts toluene to higher value *p*-xylene and benzene. In the toluene disproportionation unit, a fraction of the toluene recycle stream is sent to purge, to avoid accumulation of undesirable nonaromatic hydrocarbons in the recycle loop. It has been shown that an aromatics-selective membrane could provide an

effective recovery ($>50\%$) of toluene from the purge stream and return it to the main reactor loop (Figure 13(a)). Successful trials were demonstrated in over 2000 h of tests with 2-inch-diameter module from the StarmemTM series at 50 °C and 55-bar pressure. After an initial period of membrane compaction, stable flux was achieved. Shorter tests were also run with full-scale 8-inch-diameter modules on a pilot plant. Additional refinery processes that could benefit from this membrane separation include aromatic isomerization, aromatic disproportionation, aromatic hydrogenation, aromatic alkylation, and aromatic dealkylation [137]. Economic calculations have shown that recovering 50% toluene from a purge stream normally run at $160 \text{ m}^3 \text{ d}^{-1}$ (1 000 barrels d^{-1}) at a differential cost of $\$0.053 \text{ l}^{-1}$ of toluene would result in $\$1.5 \text{ million yr}^{-1}$ (US dollars) in proposed savings.

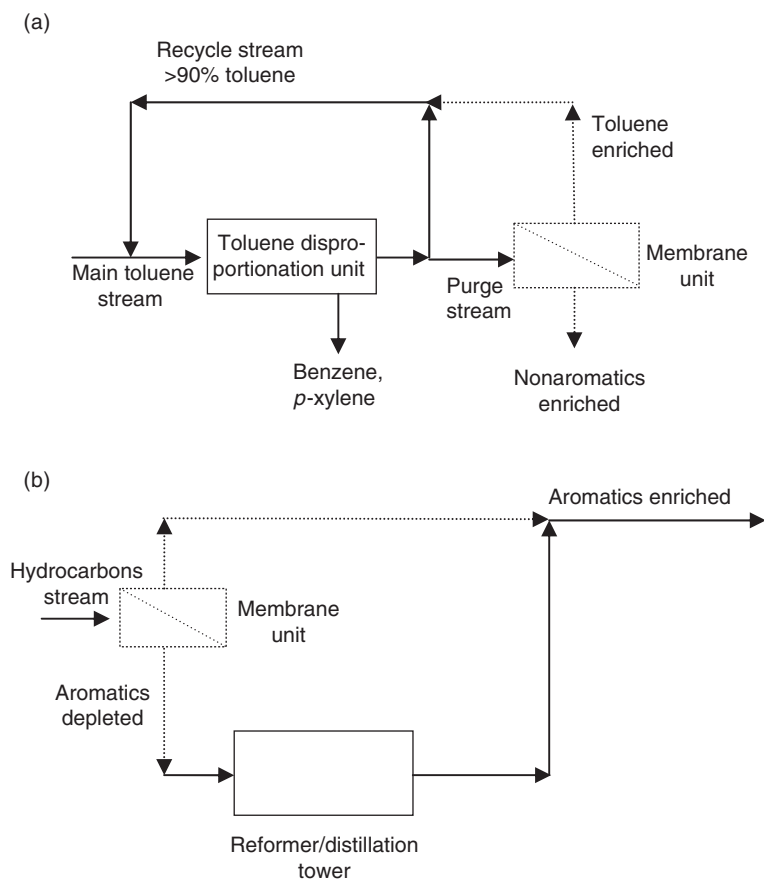


Figure 13 Organic solvent nanofiltration (OSN) membrane applications suggested for treating aromatics-containing refinery streams. (a) Schematics of aromatic-selective membrane unit integrated into the purge stream for toluene disproportionation. (b) Schematics of aromatic-selective membrane unit combined with reforming/distillation in petrochemical operations. Reproduced with permission from White, L. S., Wildemuth, C. R. *Ind. Eng. Chem. Res.* **2006**, *45*, 9136–9143.

Aromatic selective membrane units could be placed prior to reforming or distillation units in refineries [137]. In reforming, a hydrocarbon stream is upgraded in aromatics content, improving octane value, and generating hydrogen as a useful by-product. The aromatics content present in existing naphtha streams also goes through the reformer, so a membrane separation could divert the aromatics stream around the reformer (Figure 13(b)). This would allow for capacity increase with the reformer unit. Similar membrane schemes combined with distillation can also be developed.

Other OSN membrane applications that have also been emphasized are the separation of petroleum fractions, recovery of components from petroleum streams or fuel upgrading. Ohya *et al.* [138] prepared a series of asymmetric PI membranes, and using ones with a MWCO of 170 g mol^{-1} succeeded in separating gasoline–kerosene mixtures, with a separating factor (for gasoline/kerosene) of 19.5 and a $40 \text{ kg m}^{-2} \text{ day}^{-1}$ flux at 423 K and 10 MPa. Separations of light gas-oil from crude oil and kerosene from lower MW mixtures were also possible with membranes presenting 380 and 270 g mol^{-1} MWCO, respectively.

2.05.5 Conclusions

From the above discussion, it can be seen that OSN offers the potential to shift the dominant paradigm for separations from distillation to membrane processing, in the same manner that RO has displaced multiple-effect evaporation for desalination. New membranes, better understanding of transport and fouling processes, and further successful applications will lead this paradigm shift.

References

- [1] Mulder, M. *Basic Principles of Membrane Technology*, 2nd edn.; Kluwer: Dordrecht, 2004.
- [2] Vandezande, P., Gevers, L. E. M., Vankelecom, I. F. J. *Chem. Soc. Rev.* **2008**, *37*, 365–405.
- [3] Smitha, B., Suhanya, D., Sridhar, S., Ramakrishna, M. J. *Membr. Sci.* **2004**, *241*, 1–21.
- [4] Sourirajan, S. *Nature* **1964**, *203*, 1348–1349.
- [5] Kopecek, J., Sourirajan, S. *Ind. Eng. Chem. Proc. Des. Dev.* **1970**, *9*, 5–12.
- [6] Farnand, B. A., Talbot, F. D. F., Matsuura, T., Sourirajan, S. *Ind. Eng. Chem. Proc. Des. Dev.* **1983**, *22*, 179–187.
- [7] Sourirajan, S., Matsuura, T. *Reverse Osmosis/Ultrafiltration Principles*; National Research Council of Canada: Ottawa, ON, 1985; pp 802–805.
- [8] Shuey, H. F., Wan, W. (Exxon Research and Engineering Co.). Asymmetric Polyimide Reverse Osmosis Membrane, Method for Preparation of Same and Use Thereof for Organic Liquid Separations. US Pat. 4,532,041, 30 July 1985.
- [9] Anderson, B. P. (Exxon Research & Engineering Company). Ultrafiltration Polyimide Membrane and Its Use for Recovery of Dewaxing Aid. US Pat. 4,963,303, 16 October 1990.
- [10] Gould, R. M., Nitsch, A. R. (Mobil Oil Corporation). Lubricating Oil Dewaxing with Membrane Separation of Cold Solvent. US Pat. 5,494,566, 27 February 1996.
- [11] Gould, R. M., Kloczewski, H. A., Menon, K. S., Sulpizio, T. E., White, L. S. (Mobil Oil Corporation). Lubricating Oil Dewaxing with Membrane Separation. US Pat. 5,651,877, 29 July 1997.
- [12] Bitter, J. G. A., Haan, J. P., Rijkens, H. C. (Shell Oil Company). Process for the Separation of Solvents from Hydrocarbons Dissolved in the Solvents. US Pat. 4,748,288, 31 May 1988.
- [13] Cossee, R. P., Geus, E. R., Van Den Heuvel, E. J., Weber, C. E. (Shell Oil Company). Process for Purifying a Liquid Hydrocarbon Product. US Pat. 6,488,856, 3 December 2002.
- [14] Miller, J. F., Bryant, D. R., Hoy, K. L., Kinkade, N. E., Zanolalidou, R. H. (Union Carbide Chemicals & Plastics Technology Corporation). Membrane Separation Process. US Pat. 5,681,473, 28 October 1997.
- [15] Black, L. E., Boucher, H. A. (Exxon Research and Engineering Co.). Process for Separating Alkylaromatics from Aromatic Solvents and the Separation of the Alkylaromatic Isomers Using Membranes. US Pat. 4,571,444, 18 February 1986.
- [16] Black, L. E., Miasek, P. G., Adriaens, G. (Exxon Research and Engineering Co.). Aromatic Solvent Upgrading Using Membranes. US Pat. 4,532,029, 30 July 1985.
- [17] Black, L. E. (Exxon Research and Engineering Company). Interfacially Polymerized Membranes for the Reverse Osmosis Separation of Organic Solvent Solutions. US Pat. 5,173,191, 22 December 1992.
- [18] Bitter, J. G. A., Haan, J. P. (Shell Oil Company). Process for Separating a Fluid Feed Mixture Containing Hydrocarbon Oil and an Organic Solvent. US Pat. 4,810,366, 7 March 1989.
- [19] White, L. S., Wang, I. F., Minhas, B. S. (W. R. Grace & Co. Conn. New York, NY). Polyimide Membrane for Separation of Solvents from Lube Oil. US Pat. 5,264,166, 23 November 1993.
- [20] Gould, R. M., White, L. S., Wildemuth, C. R. *Environm. Prog.* **2001**, *20*, 12–16.
- [21] White, L. S., Nitsch, A. R. *J. Membr. Sci.* **2000**, *179*, 267–274.
- [22] Kong, Y., Shi, D., Yu, H., Wang, Y., Yang, J., Zhang, Y. *Desalination* **2006**, *191*, 254–261.
- [23] Linder, C., Nemas, M., Perry, M., Katrar, R. (Membrane Products Kiryat Weitzman Ltd.). Silicon Derived Solvent Stable Membranes. US Pat. 5,265,734, 30 November 1993.
- [24] MET – Membrane Extraction Technology Ltd., <http://www.membrane-extraction-technology.com> (accessed November 2009).
- [25] Livingston, A. G., Peeva, L. G., Silva, P. Organic Solvent Nanofiltration. In *Membrane Technology in the Chemical Industry*; Nunes, S. P., Peinemann, K.-V., Eds.; Wiley-VCH Verlag GmbH&Co. KGaA: Weinheim, Germany, 2006; Chapter 11, pp 203–228.
- [26] Park, J. S., Kim, S. K., Lee, K. H. *J. Ind. Eng. Chem.* **2000**, *6*, 93–99.
- [27] KOCH Membrane Systems, <http://www.kochmembrane.com> (accessed November 2009).

- [28] Linder, C., Nemas, M., Perry, M., Katraró, R. (Weizmann Kiryat Membrane Prod.). Silicone-Derived Solvent Stable Membranes. Eur. Pat. 0532199, 17 March 1993.
- [29] Van der Bruggen, B., Jansen, J. C., Figoli, A., Geens, J., Boussu, K., Drioli, E. *J. Phys. Chem. B* **2006**, *110*, 13799–13803.
- [30] SolSep BV Robust Membrane Technologies <http://www.solsep.com> (accessed November 2009).
- [31] Cuperus, F. P. *Chem. Ing. Tech.* **2005**, *77*, 1000–1001.
- [32] Geens, J., Van der Bruggen, B., Vandecasteele, C. *Sep. Purif. Technol.* **2006**, *48*, 255–263.
- [33] Bargeman, G., Albers, J., Westerlink, J. B., Manahutu, C. F. H., Ten Kate, A. *Proceedings of the International Workshop on Membranes in Solvent Filtration*, Leuven, Belgium, 2006.
- [34] Livingston, A. G., See Toh, Y. H. (Imperial Innovations Ltd.). Method of Separation. Great Britain Pat. 2437519, 31 October 2007.
- [35] See Toh, Y. H., Lim, F. W., Livingston, A. G. *J. Membr. Sci.* **2007**, *301*, 3–10.
- [36] Dudziak, G., Hoyer, T., Nickel, A., Puhlfuerr, P., Voigt, I. (Hermsdoefer Inst Tech Keramik.). Ceramic Nanofiltration Membrane for Use in Organic Solvents and Method for the Production Thereof. Eur. Pat. 1603663, 14 December 2005.
- [37] Hermsdorfer Institut für Technische Keramik, <http://www.hitk.de> (accessed November 2009).
- [38] Ralph, W., Horst, C., Valko, M. *Desalination* **2003**, *157*, 113–125.
- [39] Voigt, I. *Chem. Ing. Tech.* **2005**, *77*, 559–564.
- [40] inopor, <http://www.inopor.com> (accessed November 2009).
- [41] Cuperus, F. P., Smolders, C. A. *Adv. Colloid Interface Sci.* **1991**, *34*, 135–173.
- [42] Mulherkar, P., van Reis, R. *J. Membr. Sci.* **2004**, *236*, 171–182.
- [43] Stamatialis, D. F., Stafie, N., Bua du, K., Hempenius, M., Wessling, M. *Proceedings of the International Workshop on Membranes in Solvent Filtration*, Leuven, Belgium, 2006.
- [44] Stafie, N., Stamatialis, D. F., Wessling, M. *Sep. Purif. Technol.* **2005**, *45*, 220–231.
- [45] Van der Bruggen, B., Schaeep, J., Wilms, D., Vandecasteele, C. *J. Membr. Sci.* **1999**, *156*, 29–41.
- [46] Zwijnenberg, H. J., Boerrigter, M., Koops, G. H., Wessling, M. *Proceedings of the International Conference on Membranes and Membrane Processes (ICOM)*, Providence, RI, 2005.
- [47] Kwiatkowski, J., Cheryan, M. *Sep. Sci. Technol.* **2005**, *40*, 2651–2662.
- [48] Tsuru, T., Sudoh, T., Yoshioka, T., Asaeda, M. *J. Membr. Sci.* **2001**, *185*, 253–261.
- [49] See Toh, Y. H., Loh, X. X., Li, K., Bismarck, A., Livingston, A. G. *J. Membr. Sci.* **2007**, *291*, 120–125.
- [50] Zheng, F., Li, C., Yuana, Q., Vriesekoop, F. *J. Membr. Sci.* **2008**, *318*, 114–122.
- [51] Gevers, L. E. M., Meyen, G., De Smet, K., et al. *J. Membr. Sci.* **2006**, *274*, 173–182.
- [52] Han, S., Wong, H., Livingston, A. G. *Chem. Eng. Res. Des.* **2005**, *83*, 309–316.
- [53] Geens, J., Boussu, K., Vandecasteele, C., Van der Bruggen, B. *J. Membr. Sci.* **2006**, *281*, 139–148.
- [54] Comstock, D. L. *Desalination* **1989**, *76*, 61–72.
- [55] Bhanushali, D., Kloos, S., Bhattacharyya, D. *J. Membr. Sci.* **2002**, *208*, 343–359.
- [56] Yang, X. J., Livingston, A. G., Freitas dos Santos, L. J. *Membr. Sci.* **2001**, *190*, 45–55.
- [57] Machado, D. R., Hasson, D., Semita, R. *J. Membr. Sci.* **1999**, *163*, 93–102.
- [58] Van der Bruggen, B., Geens, J., Vandecasteele, C. *Sep. Sci. Technol.* **2002**, *37*, 783–797.
- [59] Peeva, L. G., Gibbins, E., Luthra, S. S., White, L. S., Stateva, R. P., Livingston, A. G. *J. Membr. Sci.* **2004**, *236*, 121–136.
- [60] Zhao, Y., Yuan, Q. *J. Membr. Sci.* **2006**, *279*, 453–458.
- [61] Silva, P., Han, S., Livingston, A. G. *J. Membr. Sci.* **2005**, *262*, 49–59.
- [62] Rautenbach, R., Albrecht, R. *Membrane Processes*; Wiley: Chichester, 1989.
- [63] Uragami, T., Yono, T., Sugihara, M. *Die Angew. Makromol. Chem.* **1979**, *82*, 89–102.
- [64] Uragami, T., Tamura, M., Sugihara, M. *J. Membr. Sci.* **1979**, *4*, 305–314.
- [65] Bhanushali, D., Kloos, S., Kurth, C., Bhattacharyya, D. *J. Membr. Sci.* **2001**, *189*, 1–21.
- [66] Bhanushali, D., Bhattacharyya, D. *Ann. N.Y. Acad. Sci.* **2003**, *984*, 159–177.
- [67] Paul, D. R., Garcin, M., Garmon, W. E. *J. Appl. Poly. Sci.* **1976**, *20*, 609–625.
- [68] Ho, W. S. W., Sirkar, K. K., Eds. *Membrane Handbook*; Van Nostrand: New York, 1992.
- [69] Stafie, N., Stamatialis, D. F., Wessling, M. *J. Membr. Sci.* **2004**, *228*, 103–116.
- [70] Vankelecom, I. F. J., De Smet, K., Gevers, L. E. M., et al. *J. Membr. Sci.* **2004**, *231*, 99–108.
- [71] Yoo, J. S., Kim, S. J., Choi, J. S. *J. Chem. Eng. Data* **1999**, *44*, 16–22.
- [72] Geens, J., Van der Bruggen, B., Vandecasteele, C. *Chem. Eng. Sci.* **2004**, *59*, 1161–1164.
- [73] Piccinini, E., Giacinti Baschetti, M., Sarti, G. C. *J. Membr. Sci.* **2004**, *234*, 95–100.
- [74] Tarleton, E. S., Robinson, J. P., Smith, S. J., Na, J. J. W. *J. Membr. Sci.* **2005**, *261*, 129–135.
- [75] Tarleton, E. S., Robinson, J. P., Salman, M. *J. Membr. Sci.* **2006**, *280*, 442–451.
- [76] Schossig, T. M., Paul, D. *J. Membr. Sci.* **2001**, *187*, 85–91.
- [77] Pinnau, I., Koros, W. J. *J. Polym. Sci.: Polym. Phys.* **1993**, *31*, 419–427.
- [78] Kawakami, H., Mikawa, M., Nagaoka, S. *J. Membr. Sci.* **1997**, *137*, 241–251.
- [79] Pinnau, I., Koros, W. J. *J. Appl. Polym. Sci.* **1991**, *43*, 1491–1502.
- [80] Pinnau, I., Koros, W. J. *J. Membr. Sci.* **1992**, *7*, 81–96.
- [81] See Toh, Y. H., Ferreira, F. C., Livingston, A. G. *J. Membr. Sci.* **2007**, *299*, 236–250.
- [82] Wickramasinghe, H. K. *AIP Conference Proceedings 241*, American Institute of Physics, Santa Barbara, CA, 1992.
- [83] Wiesendanger, R. *Scanning Probe Microscopy and Spectroscopy: Methods and Applications*; Cambridge University Press: Cambridge, UK, 1994.
- [84] Boussu, K., Van der Bruggen, B., Volodin, A., et al. *Desalination* **2006**, *191*, 245–253.
- [85] Boussu, K., Van der Bruggen, B., Volodin, A., Snauwaert, J., Van Haesendonck, C., Vandecasteele, C. *J. Colloid Interface Sci.* **2005**, *286*, 632–638.
- [86] Khulbe, K. C., Matsuura, T. *Polymer* **2000**, *41*, 1917–1935.
- [87] Bessières, A., Meireles, M., Coratger, R., Beauvillain, J., Sanchez, V. *J. Membr. Sci.* **1996**, *109*, 271–284.
- [88] Kim, J. Y., Lee, H. K., Kim, S. C. *J. Membr. Sci.* **1999**, *163*, 159–166.
- [89] Vilaseca, M., Mateo, E., Palacio, L., et al. *Microporous Mesoporous Mater.* **2004**, *71*, 33–37.
- [90] Marchese, J., Almandoz, C., Amaral, M., et al. *Bol. Soc. Esp. Ceram. Vidr.* **2000**, *39*, 215–219.
- [91] Kwak, S., Yeom, M., Roh, I. J., Kim, D. Y., Kim, J. J. *J. Membr. Sci.* **1997**, *132*, 183–191.
- [92] Bowen, W. R., Doneva, T. A. *Desalination* **2000**, *129*, 163–172.

- [93] Gevers, L. E. M., Aldea, S., Vankelecom, I. F. J., Jacobs, P. A. J. *Membr. Sci.* **2006**, *281*, 741–746.
- [94] Li, X., Feyter, S. D., Chen, D., et al. *Chem. Mater.* **2008**, *20*, 3876–3883.
- [95] Asaeda, M., Kitao, S. *Key Eng. Mater.* **1991**, *61–62*, 295–300.
- [96] Asaeda, M., Okazaki, K., Nakatani, A. *Ceram. Trans.* **1992**, *31*, 411–420.
- [97] Mey-Marom, A., Katz, M. G. *J. Membr. Sci.* **1986**, *27*, 119–130.
- [98] Cuperus, F. P., Bargeman, D., Smolders, C. A. J. *Membr. Sci.* **1992**, *71*, 57–67.
- [99] Tsuru, T., Sudou, T., Kawahara, S., Yoshioka, T., Asaeda, M. *J. Colloid Interface Sci.* **2000**, *228*, 292–296.
- [100] Tsuru, T., Sudou, T., Yoshioka, T., Asaeda, M. *J. Membr. Sci.* **2001**, *185*, 253–261.
- [101] Calvo, J. I., Bottino, A., Capannelli, G., Hernández, A. J. *Membr. Sci.* **2004**, *239*, 189–197.
- [102] Capannelli, G., Becchi, I., Bottino, A., Moretti, P., Munari, S. Computer Driven Porosimeter for Ultrafiltration Membranes. In *Characterization of Porous Solids*; Unger, K. K., Rouquerol, J., Sing, K. S. W., Kral, K., Eds.; Elsevier: Amsterdam, The Netherlands, 1988; pp 283–294.
- [103] Bottino, A., Capannelli, G., Grosso, A., Monticelli, O., Nicchia, M. *Sep. Sci. Technol.* **1994**, *29*, 985–999.
- [104] Kim, S. H., Kwak, S., Suzuki, T. *Environ. Sci. Technol.* **2005**, *39*, 1764–1770.
- [105] Satyanarayana, S. V., Subrahmanyam, V. S., Verma, H. C., Sharma, A., Bhattacharya, P. K. *Polymer* **2006**, *47*, 1300–1307.
- [106] Winberg, P., DeSitter, K., Dotremont, C., Mullens, S., Vankelecom, I. F. J., Maurer, F. H. J. *Macromolecules* **2005**, *38*, 3776–3782.
- [107] De Baerdemaeker, J., Boussu, K., Djourelou, N., et al. *Phys. Stat. Sol. (c)* **2007**, *4*, 3804–3809.
- [108] Aerts, S., Vanhulsel, A., Buekenhoudt, A., et al. *J. Membr. Sci.* **2006**, *275*, 212–219.
- [109] Kim, N., Shin, D. H., Lee, Y. T. *J. Membr. Sci.* **2007**, *300*, 224–231.
- [110] Buonomenna, M. G., Gordano, A., Drioli, E. *Eur. Polym. J.* **2008**, *44*, 2051–2059.
- [111] Xu, P., Drewes, J. E., Kim, T. U., Bellonaa, C., Amy, G. J. *Membr. Sci.* **2006**, *279*, 165–175.
- [112] Shim, Y., Lee, H. J., Lee, S., Moon, S. H., Cho, J. *Environ. Sci. Technol.* **2002**, *36*, 3864–3871.
- [113] Scarpello, J. T., Nair, D., Freitas dos Santos, L. M., White, L. S., Livingston, A. G. *J. Membr. Sci.* **2002**, *203*, 71–85.
- [114] Nair, D., Luthra, S. S., Scarpello, J. T., White, L. S., Freitas, L. M., Livingston, A. G. *Desalination* **2002**, *147*, 301–306.
- [115] Witte, P. T., Chowdhury, S. R., Ten Elshof, J. E., Rozner, D. S., Neumann, R., Alsters, P. L. *Chem. Commun.* **2005**, *9*, 1206–1208.
- [116] Turlan, D., Urriolabeitia, E. P., Navarro, R., Royo, C., Menendez, M., Santamaria, J. *Chem. Commun.* **2001**, *24*, 2608–2609.
- [117] Miller, J. F. (Lyondell Chemical Technology L.P.). Separation Process. US Pat. 7,084,284, 1 August 2006.
- [118] Blanco, R. V., Ferreira, F. C., Jorge, R. F., Livingston, A. G. *J. Membr. Sci.* **2008**, *317*, 50–64.
- [119] Blanco, R. V., Ferreira, F. C., Jorge, R. F., Livingston, A. G. *Desalination* **2006**, *199*, 429–431.
- [120] Roengpithya, C., Patterson, D. A., Taylor, P. C., Livingston, A. G. *Desalination* **2006**, *199*, 195–197.
- [121] Sheth, J., Qin, Y., Sirkar, K., Baltzis, B. J. *Membr. Sci.* **2003**, *211*, 251–261.
- [122] Livingston, A., Peeva, L., Han, S., et al. *Ann. N.Y. Acad. Sci.* **2003**, *984*, 123–141.
- [123] Witte, B. D. Membrane Technology for Solvent Recovery in Pharmaceutical Industry: Outfalls and Opportunities. In *International Workshop – Membranes in Solvent Filtration*, Leuven, Belgium, 2006.
- [124] Lin, J. C. T., Peeva, L. G., Livingston, A. G. Separation of Pharmaceutical Process-Related Impurities via an Organic Solvent Nanofiltration Membrane Cascade. *AIChE Annual Meeting, Conference Proceedings*, San Francisco, CA, 12–17 November 2006; 410g/1–410g/7.
- [125] Ghazali, N. F., Ferreira, F. C., White, A. J. P., Livingston, A. G. *Tetrahedron Asymm.* **2006**, *17*, 1846–1852.
- [126] Cheryan, M. *Membr. Tech.* **2005**, *2*, 5–7.
- [127] Pioch, D., Larguée, C., Graille, J., Ajana, H., Rouviere, J. *Ind. Crops Prod.* **1998**, *7*, 83–89.
- [128] Sen Gupta, A. K. (Lever Brothers Company.). Refining. US Pat. 4,533,501, 6 August 1985.
- [129] Matthias, S., Peinemann, K. V., Scharnagl, N., Friese, K., Schubert, R. Silicone Composite Membrane Modified by Radiation Chemical Means and Intended for Use in Ultrafiltration. WO9627430, 12 September 1996.
- [130] Raman, L. P., Cheryan, M., Rajagopalan, N. *J. Am. Oil Chem. Soc.* **1996**, *73*, 219–224.
- [131] Zwijnenberg, H. J., Krosse, A. M., Ebert, K., Peinemann, K. V., Cuperus, F. P. *J. Am. Oil Chem. Soc.* **1999**, *76*, 83–87.
- [132] Bhosle, B. M., Subramanian, R. *J. Food Eng.* **2005**, *69*, 481–494.
- [133] Darnoko, D., Cheryan, M. *J. Am. Oil Chem. Soc.* **2006**, *4*, 365–370.
- [134] Tsui, E. M., Cheryan, M. *J. Food Eng.* **2007**, *83*, 590–595.
- [135] Pasternak, M. (Texaco Inc). Membrane Process for Treating a Charge Containing Dewaxing Solvent and Dewaxed Oil. US Pat. 5,234,579, 10 August 1993.
- [136] Livingston, A. G., Osborne, G. C. A Process for Deacidifying Crude Oil. WO 0250212, 27 June 2002.
- [137] White, L. S., Wildemuth, C. R. *Ind. Eng. Chem. Res.* **2006**, *45*, 9136–9143.
- [138] Ohya, H., Okazaki, I., Aihara, M., Tanisho, S., Negishi, Y. *J. Membr. Sci.* **1997**, *123*, 143–147.
- [139] White, L. S. *J. Membr. Sci.* **2002**, *205*, 191–202.

Relevant Websites

<http://www.inopor.com> – The Cutting Edge of Ceramic Filtration.

Biographical Sketches

Ludmila Georgieva Peeva was born in Bourgas, Bulgaria, in 1963. She studied chemical engineering at the University of Chemical Technology and Metallurgy – Sofia, Bulgaria, where she graduated in 1986. In 1996, she obtained her PhD in chemical engineering from the Institute of Chemical Engineering (IChemEng), Bulgarian Academy of Sciences, Bulgaria. Until 1999, she worked at IChemEng as an assistant professor in the field of biotechnology. During this period, she spent eight months at the Ben-Gurion University of the Negev (Beersheva, Israel). In 1999, she joined the Separation Engineering and Technology Group at the Department of Chemical Engineering and Chemical Technology, Imperial College London, UK, initially as a postdoctoral researcher and later as a research fellow in membrane technology. Her current interests are in the field of membrane processes, particularly nanofiltration in organic solvents, and separation processes for pharmaceutical/biopharmaceutical manufacture. Her research resulted in more than 30 publications, two patents, and two chapters in books.



Malladi Sairam obtained his MSc in synthetic organic chemistry from Andhra University, Waltair, India. He did his PhD (2004) on the ‘Synthesis, characterization of polyaniline and its nanocomposites for catalytic and electrostatic discharge applications’ at the Indian Institute of Chemical Technology, Hyderabad, India. He worked as a research associate with Prof. T.M. Aminabhavi (2004–06) at the Center of Excellence in Polymer Science, Karnataka University, Dharwad, India on polymeric membranes and drug release systems. Since 2006, he has been working as a postdoctoral researcher at Imperial College London, UK, with Prof. A. G. Livingston, on membranes for organic solvent nanofiltration.



Andrew G Livingston was born and bred in Taranaki, New Zealand (NZ), and studied chemical engineering in NZ. Following graduation, he worked for 3 years at a NZ food processing company doing general chemical engineering. In 1986, he began his PhD at Trinity College, University of Cambridge. Upon completing PhD, he started working as a lecturer in the Department of Chemical Engineering at Imperial College London, UK. His research includes immobilized cell bioreactors, waste treatment, membrane separations, biotransformations, and chemical and separations technology. Livingston has been a full professor from 1999, and has published over 160 papers and granted 15 patents in chemical technology. The awards received by him include Junior Moulton Medal and Cremer and Warner Medal of IChemE. He leads a research group of 15 PhD students and postdoctoral researchers, with current research interests in (bio)chemical technology, including separations for chemical and pharmaceutical applications. In 1993, Livingston graduated with an MSc in economics from the London School of Economics. In 1996, he founded Membrane Extraction Technology, a spinout company, which carries out process development and commercialization of membrane-separation processes. He was elected a fellow of the Royal Academy of Engineering in 2006, and became Head of the Department in 2008.

2.06 Ultrafiltration: Fundamentals and Engineering

H Lutz, Millipore Corporation, Billerica, MA, USA

© 2010 Elsevier B.V. All rights reserved.

2.06.1	General	116
2.06.2	UF Membranes and Modules	116
2.06.2.1	Membranes	116
2.06.2.2	Modules	117
2.06.3	UF Technology Fundamentals	120
2.06.3.1	Surface Polarization	120
2.06.3.2	Retention	120
2.06.3.3	Flux	120
2.06.3.4	Mass Transfer Coefficients	122
2.06.3.5	Fouling	123
2.06.4	UF Processing	123
2.06.4.1	Process Configurations	123
2.06.4.2	Single-Pass Operation	123
2.06.4.3	Batch and Fed-Batch Concentration	124
2.06.4.4	Batch DF	126
2.06.4.5	Continuous Operation	127
2.06.5	UF Process Development	128
2.06.5.1	Standard Test Protocol	128
2.06.5.2	Data Analysis	128
2.06.6	UF Scale-Up	130
2.06.6.1	Batch Configuration Sizing	130
2.06.6.2	Batch Recovery	131
2.06.6.3	Operating Procedure	132
2.06.6.4	Adding Area in Series	132
2.06.6.5	Process Monitoring and Control	132
2.06.6.6	Equipment Selection	133
2.06.6.7	Skid Layout	135
2.06.7	UF Applications	136
2.06.8	UF System Troubleshooting	137
References		137

Glossary

Diafiltration A process of adding a new buffer to an ultrafiltration system to wash out the old buffer and small permeable solutes and replace them with the new buffer.

Flux A measure of membrane productivity calculated as the volumetric flow through a membrane per unit of membrane area.

Fouling Solute adsorption and entrapment within a membrane that can affect the flux and retention properties. A chemical cleaning treatment is needed to remove.

Hydrophobic A characteristic of being water repellent and easily fouled by adsorbing solutes.

Permeability A measure of membrane resistance to flow, calculated as the flux per unit pressure differential across a membrane.

Permeate A fluid stream passing through the membrane in a normal or perpendicular direction to the membrane surface.

Polarization The accumulation of retained solutes at and above the membrane surface that can affect membrane flux and retention properties.

Retentate A fluid stream passing across the membrane in a tangential direction to the membrane surface.

Sieving coefficient or passage The ratio of solute concentrations in the permeate to that in the feed or at the membrane surface.

Ultrafiltration The use of cast membrane filters to retain 10–1000 Å diameter solutes.

2.06.1 General

Ultrafiltration processing (also commonly called ultrafiltration (UF) or ultrafiltration/diafiltration (UF/DF)) employs pressure-driving forces of 0.2–1.0 MPa to drive liquid solvents (primarily water) and small solutes through membranes. UF membranes have retention ratings of 1–5000 K and can retain solutes of 10–1000 Å in diameter (roughly 300–1000 KDa) such as colloids, large molecules, and nanoparticles. UF membranes retain smaller solutes than microfiltration (MF) membranes and larger solutes than reverse osmosis membranes. Most commercial operations are run as tangential flow filtration (TFF) but dilute solutions such as water treatment or small-scale sample preparation are run as normal flow filtration (NFF). Virus-retaining filters, sometimes referred to as nano-filters, are on the most open end of UF and can be run as NFF or TFF.

The first large commercial application of UF was paint recycling, followed by dairy whey recovery in the mid-1970s. Applications can be described as clarification of a permeate product (e.g., water purification), concentration of a retentate product (e.g., paint, dairy, and pharmaceuticals), or solute purification (e.g., virus/protein separation and buffer exchange). UF applications are enabled by low temperature and low-cost operation, particularly with membrane reuse. UF processes can vary significantly between applications due to differing requirements and relative costs.

This chapter is organized into the following sections: membranes and modules, technology fundamentals, processing, process development, scale-up, applications, and troubleshooting.

2.06.2 UF Membranes and Modules

2.06.2.1 Membranes

UF membranes primarily consist of polymeric structures (polyethersulfone, regenerated cellulose, polysulfone, polyamide, polyacrylonitrile, or various

fluoropolymers) formed by immersion casting on a web or as a composite cast on an MF membrane. Hydrophobic polymers are surface modified to render them hydrophilic and thereby reduce fouling, reduce product losses, and increase flux [4]. Some inorganic UF membranes (alumina, glass, and zirconia) are available but only find use in corrosive applications due to their high cost. Physical and chemical properties of commonly used membrane materials are shown in **Table 1**. Chemical compatibility is a critical basis for membrane selection.

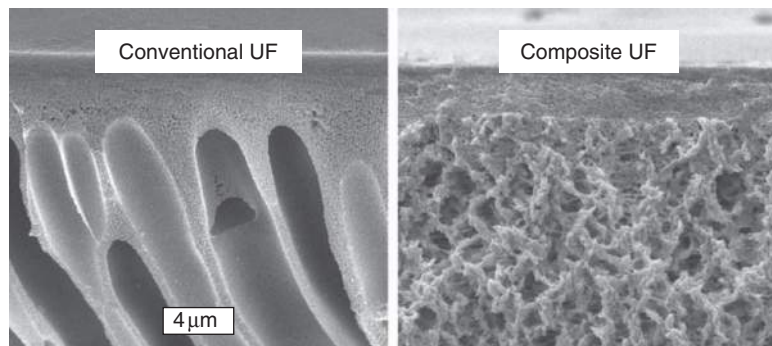
Food and medical applications require additional properties such as extractables, adsorption, shedding, and United States Pharmacopeia (USP) class VI toxicity testing. In addition, these applications require high consistency membranes with vendor quality programs (e.g., international organization for standardization (ISO), current good manufacturing practices (cGMP)).

Early UF membranes had thin surface retentive layers with an open structure underneath as shown in **Figure 1**. These membranes were prone to defects and showed poor retention and consistency. In part, retention by these membranes would rely on large retained components in the feed that polarize or form a cake layer that plugs defects. Composite membranes have a thin retentive layer cast on top of an MF membrane in one piece [12]. These composites demonstrate consistently high retention and can be integrity tested using air diffusion in water.

UF membranes are generally described using a log normal pore size distribution [58]. These distributions can be measured by electron microscopy, porosimetry, or solute retention testing. UF membranes are assigned a nominal molecular weight limit (NMWL) or nominal molecular weight cutoff (NMWCO) rating corresponding to their ability to retain a solute of a particular molecular weight. This is convenient for testing and rough selection but solute retention is based on effective solute dimensions and not on molecular weight. Nonspherical solutes will orient themselves under shear so that their major axis is parallel to the pores. Linear chain

Table 1 Ultrafiltration membrane properties

<i>Material</i>	<i>Advantages</i>	<i>Disadvantages</i>
Polyethersulfone (PES)	Resistance to temperature, Cl ₂ , pH, easy fabrication	Hydrophobic
Regenerated cellulose	Hydrophilic, low fouling	Sensitive to temperature, pH, Cl ₂ , microbial attack, mechanical creep
Polyamide		Sensitive to Cl ₂ , microbial attack
Polyvinylidene fluoride (PVDF)	Resistance to temperature, Cl ₂ , easy fabrication	Hydrophobic, coating sensitive to high pH
Inorganic	Resistance to temperature, Cl ₂ , pH, high pressure, solvents, long life	Cost, brittleness, high cross-flow rates

**Figure 1** Ultrafiltration membrane SEM. Courtesy Millipore Corporation.

dextrans and DNA show a higher passage than globular proteins of the same molecular weight. The effective solute radius can increase more than 4 times as a result of surface charge [37].

Ratings are not standardized among vendors and depend on the marker solute selected (e.g., protein, dextran in a particular buffer) and the level of retention selected for the marker solute (e.g., 90%). Retention is also affected by fouling due to adsorbed components and polarized solutes on the membrane surface (see Section 2.06.3.2 for additional discussion). A rule of thumb for selecting membrane NMWL is to take 0.2–0.3 of the MW of the solute that is to be retained by the membrane. This should be taken as a rough guide to select membranes for testing.

Solvent flow through membranes is described by their normalized permeability, the ratio of their flux to the average transmembrane pressure corrected to 25 °C using a solvent viscosity ratio. Parallel cylindrical pores of the same diameter produce a permeability L of

$$L_M = \frac{J}{\Delta P} = \frac{\varepsilon r^2}{8\mu L} \quad (1)$$

where J is the flux or volumetric flow per unit membrane area, ΔP is the transmembrane pressure difference, r is the pore radius, ε is the membrane porosity, μ is the fluid viscosity, and L is the membrane thickness.

Figure 2 shows the trade-off between water permeability and pore size for several membrane families. Tight membranes with low NMWL provide high retention and have lower solvent permeability.

2.06.2.2 Modules

UF membranes are commonly packaged into cassettes, spirals, hollow fibers, tubes, flat sheets, and inorganic monolith modules for commercial operation. **Figure 3** shows some of the module types, while **Figure 4** shows the flow paths.

Hollow fibers or tubular modules are made by potting the cast membrane fibers or tubes into end caps and enclosing the assembly in a shell. Similar to fibers or tubes, monoliths have their retentive layer coated on the inside of tubular flow channels or lumens with a high permeability porous structure on the shell side.

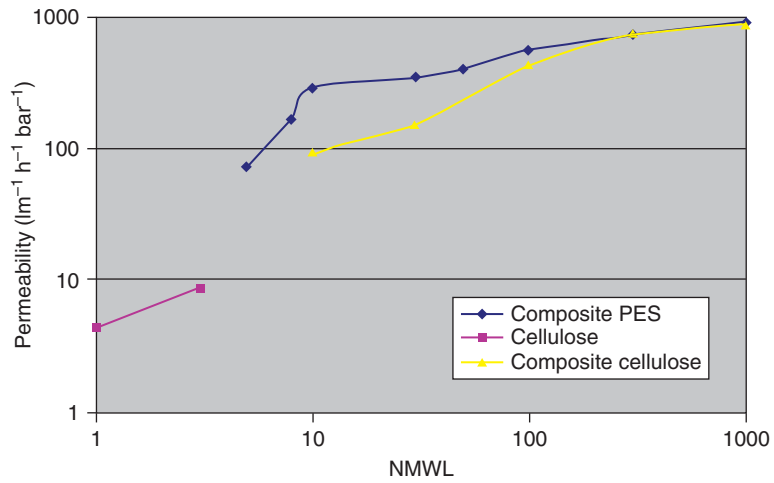


Figure 2 Membrane permeability and rating.



Figure 3 Commercial ultrafiltration modules. Courtesy Millipore Corporation.

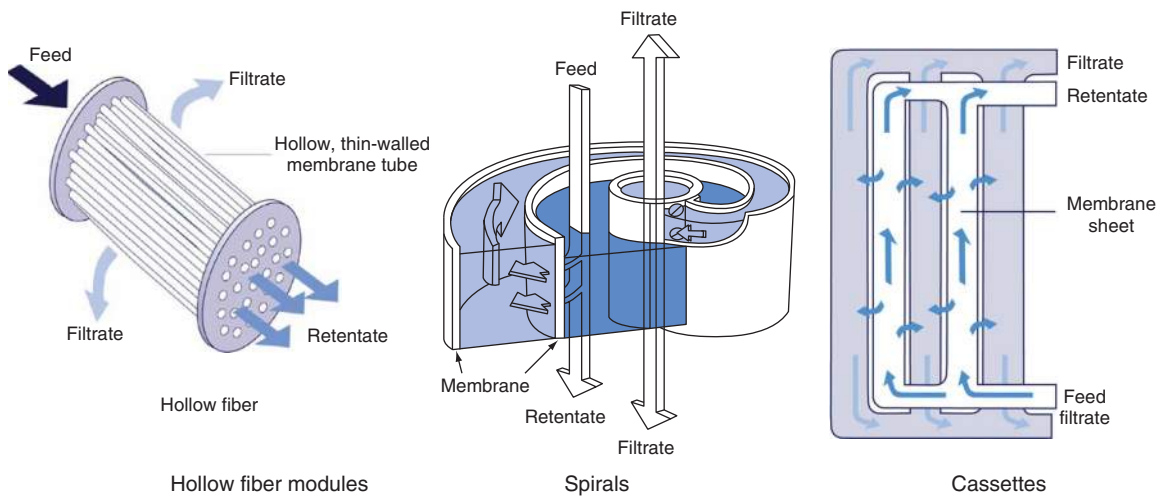


Figure 4 Ultrafiltration (UF) module flow paths. Courtesy Millipore Corporation.

Spiral-wound modules [15] are made by assembling a membrane packet or leaf consisting of a permeate channel spacer sheet with two flat sheets of membranes on either side (facing outward from the permeate sheet). The sides of this packet are glued together, and the top is glued to a central core collection tube containing small holes that allow passage of permeate from the spacer channel into the collection tube. A feed side spacer is placed on the packet and the packet is wound around the core to create the module. The wound packet assembly is sometimes inserted into a shell. Spiral modules frequently use a multileaf construction where several packets are glued to the central core before winding. This design reduces the pressure drop associated with a long permeate path length.

Cassettes use feed and permeate spacers with one set of precut holes for the feed/retentate and another, smaller set of holes, for the permeate. The feed spacer has a raised edge seal around the permeate hole to prevent flow and the permeate spacer has a similar seal around the feed/retentate hole. Similar to spiral assembly, membrane packets are sealed together around their edges, assembled into a stack, and the stack sealed together around the edges.

For fibers or tubular modules, the feed is generally introduced into the inside of the tubes, or lumen, while permeate is withdrawn from the shell side. This flow orientation enhances the shear at the membrane surface for TFF operation. These modules may also be run at high conversion or NFF mode with the feed introduced on the outside of the tubes or shell side. In this case, the shell side offers more surface area.

Additional modules include stirred cell and high shear devices. Stirred cells use a flat disk with a stir bar for small-scale studies where the velocity profiles have been well defined [40]. High-shear devices include surfaces that vibrate or rotate relative to the membrane to induce a high shear field at the membrane surface [6, 16, 51, 55]. These devices are useful for very viscous and high solids applications requiring further dewatering but are limited in their ability to be scaled up.

Module performance properties of interest include mechanical robustness, sealing, flow distribution (low pressure drops, high TFF membrane shear, low dead volumes, and low sensitivity to feed channel plugging), cleanability for reuse, chemical robustness, low extractables, low cost, ease-of-assembly, scalability, high product recovery, high integrity, and high consistency. The importance of these attributes varies considerably among applications.

Table 2 shows some of the performance properties of the different module types. Modular fibers and tubular membranes are inexpensive with low pumping costs and insensitivity to plugging for applications in water purification and juice clarification. Spirals are inexpensive with relatively low pumping costs for dairy applications. Cassettes are relatively more expensive with higher pumping costs. However, they have higher fluxes, lower pump flow rates, and reproducible scaling for pharmaceutical applications with expensive fragile protein products (see Section 2.06.7 for further discussion of module selection).

Table 2 Commercial ultrafiltration module performance

	<i>Spiral</i>	<i>Fiber</i>	<i>Cassette</i>
Screens/spacers	Yes	No	Yes/no
Typical # in series	1–2	1–2	1–2
Packing density (m^2l^{-1})	0.8	1.0–6.0	0.5
Feed flow ($\text{l m}^{-1}\text{h}^{-1}$)	700–5000	500–18 000	400
ΔP Bar/module	0.4–1.0	0.1–0.4	0.7–3.5
Channel height (mm)	0.3–1.0	0.2–3.0	0.3–1.0
Plugging sensitivity	High	Moderate	High
Working volume (l m^{-2})	1	0.5	0.4
Holdup volume (l m^{-2})	0.03	0.03	0.02
Module cost ($\text{\$ m}^{-2}$)	40–200	200–900	500–1000
Ruggedness	Moderate	Low–moderate	High
Module areas (m^2)	0.1–35	0.001–5.0	0.05–2.5
Membrane types	RO–UF	RO–UF–MF	UF–MF
Relative mass transfer efficiency	6	4	10
Ease of use	Moderate	High	Moderate
Scalability	Fair	Moderate	Good

2.06.3 UF Technology Fundamentals

UF is typically operated in TFF mode as shown in **Figure 5**, where the membrane is represented by the cross-hatched region. TFF involves passing a permeate fluid through the membrane (with a flow vector perpendicular or normal to the membrane) and passing fluid across the membrane surface (with a flow vector tangent to the membrane surface).

2.06.3.1 Surface Polarization

Solutes entrained by the permeate normal flow are retained by the membrane and accumulate on the membrane surface to form a region of high concentration called the polarization boundary layer. While this region is also sometimes referred to as the gel layer, one must be careful to distinguish between reversibly held polarized solutes and bound fouling layers deposited on the membrane. A steady state is reached relatively quickly where Brownian diffusion helps the retained solute migrate away from the membrane surface, while tangential convective flow carries solutes along the membrane surface and normal convective flow carries it toward the membrane. The back transport leading to steady-state operation gives TFF a high capacity. The elevated membrane surface concentration is called C_{wall} (as visualized by Vilker *et al.* [53] and McDonough *et al.* [27]). Neglecting tangential convection allows a one-dimensional (1D) mass balance derivation of the single solute, polarization equation [3], where k is defined as the mass transfer coefficient (ratio of Brownian diffusivity D to the boundary layer thickness δ):

$$\text{Polarization } C_{\text{wall}} - C_{\text{perm}} = (C_{\text{bulk}} - C_{\text{perm}}) \cdot \exp(\mathcal{J}/k) \quad (2)$$

The mass transfer coefficient k and the boundary layer thickness are dependent on the tangential flow. At high flux rates, the wall concentration of a fully retained solute can significantly exceed the bulk

concentration by up to 100-fold. This may impact solute aggregation and membrane fouling. Protein mass held up in a polarization layer can be on the order of 1.5 g m^{-2} depending on concentrations, mass transfer, and flux.

2.06.3.2 Retention

The intrinsic membrane passage or sieving coefficient is defined as $S_i = (C_{\text{perm}}/C_{\text{wall}})$, while intrinsic membrane retention or rejection is defined as $R_i = 1 - S_i$. The intrinsic passage is inherent to the membrane and solute, while an observed passage as $S_o = (C_{\text{perm}}/C_{\text{bulk}})$ varies with polarization. Equation (2) is rearranged to show that the observed passage depends on the intrinsic passage and polarization:

$$\text{Observed passage } S_o = \frac{1}{1 + \left(\frac{1}{S_i} - 1\right) \cdot \exp(-\mathcal{J}/k)} \quad (3)$$

Intrinsic and observed passages are equivalent at low flux; at high flux, the wall concentration can increase significantly as a result of polarization. This causes the observed passage to increase and approach 100%, regardless of the intrinsic passage. Rearranging Equation (3) allows one to plot single-solute passage data versus flux to determine the intrinsic passage and mass transfer coefficient from a linear fit.

The intrinsic passage characteristics of a UF membrane can be characterized by using a polydisperse nonadsorbing solute such as the linear chain dextran [44] shown in **Figure 6**. Models of transport in membranes are reviewed by Deen and Dedchadilok (see, e.g., References 8 and 9).

For multicomponent systems, van der Waals interactions occur in the polarization layer and not in the membrane pores. Individual intrinsic solute sieving coefficients can be used [57, 39]. The presence of a large solute that polarizes more on the membrane surface will lower the wall concentration of smaller solutes and lower their passage.

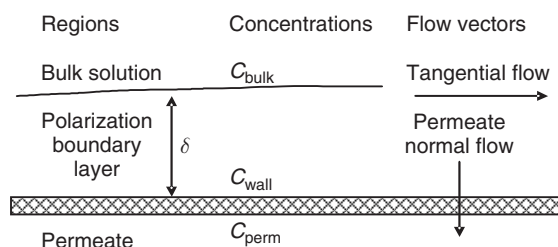


Figure 5 Tangential flow filtration.

2.06.3.3 Flux

An empirical gel flux model for retained solutes is obtained from Equation (2) by taking $C_{\text{perm}} = 0$ and setting C_g (or gel concentration) $= C_{\text{wall}}$ to get Equation (4). Cheryan [5] has compiled C_g values for a variety of fluids:

$$\text{Gel flux model } \mathcal{J} = k \ln(C_g/C_{\text{bulk}}) \quad (4)$$

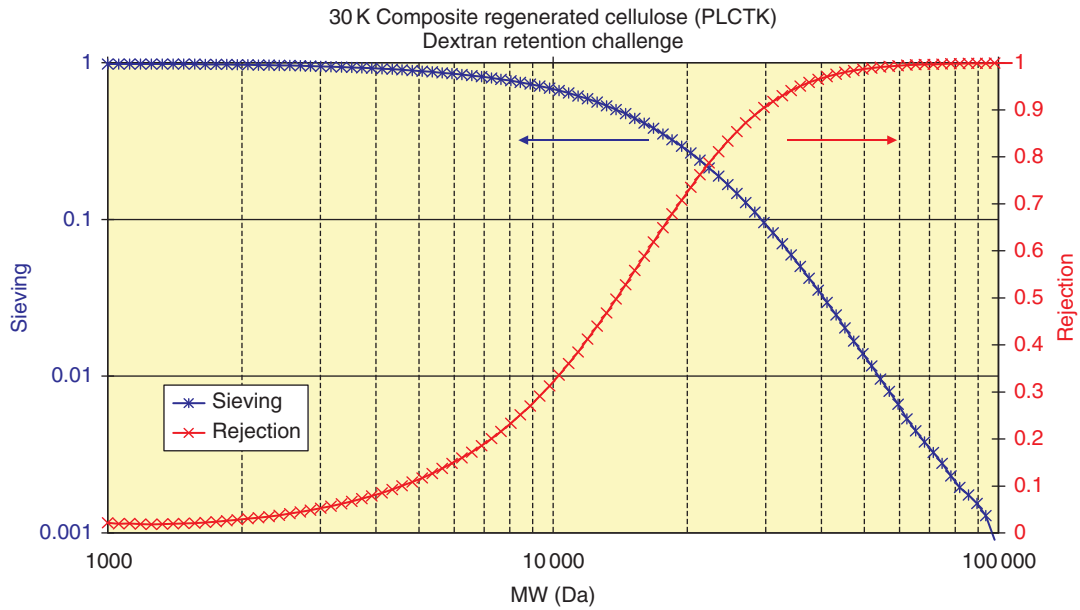


Figure 6 Intrinsic membrane retention. Courtesy Millipore Corporation.

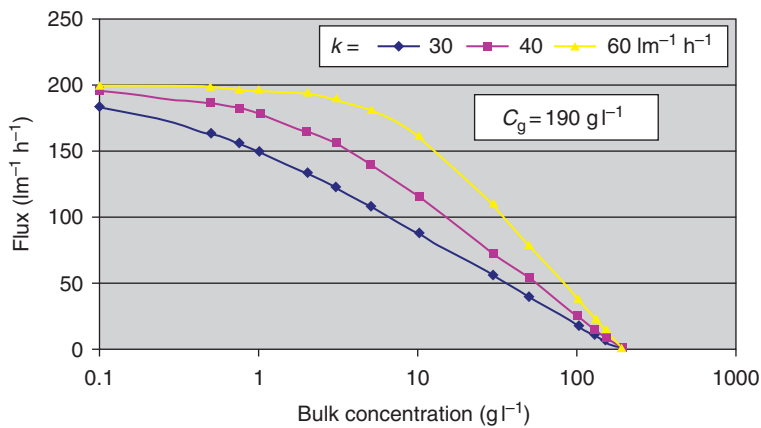


Figure 7 Flux vs. concentration.

The gel model indicates that the flux is independent of the pressures applied across the membrane or the membrane permeability. **Figure 7** shows that Equation (4) can provide a good fit to data over a range of concentrations but break down at lower concentrations where the flux is determined by membrane permeability in buffer. Despite the gel name, solutes at a C_g concentration obtained from such plots do not literally correspond to a separate gel phase. The mass transfer coefficient k is dependent on the tangential flow velocity and the solute type. Both the transfer coefficient and the gel concentration increase with temperature.

Figure 8 shows typical flux versus TMP curves corresponding to just the membrane in buffer ($C_{wall}=0$), fouled membrane in buffer ($C_{wall}=0$), and fouled membrane in a solute solution. For a module where the feed pressure varies along the feed channel, the TMP is calculated as an average: $TMP = (P_{feed} + P_{retentate})/2 - P_{permeate}$. The slope of the buffer curve is the membrane permeability. The fouled membrane in buffer is determined after removing the reversible polarization layer through a buffer flush. The slope of the fouled membrane curve in buffer is the fouled membrane permeability. The presence of adsorbed or entrapped species on the membrane lowers its permeability.

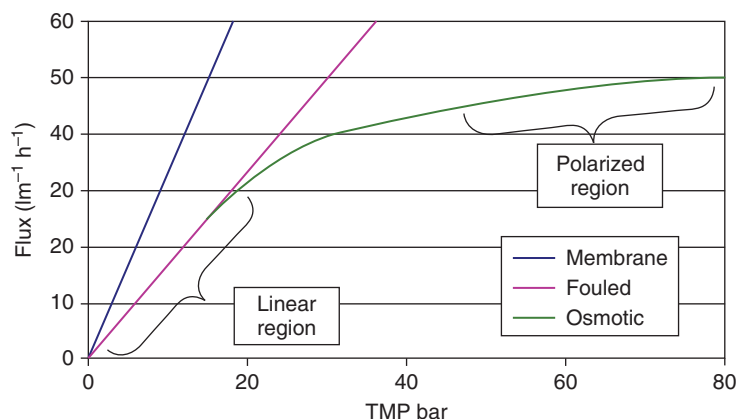


Figure 8 Flux vs. TMP.

The flux behavior of a fouled membrane in a solute solution shows a low flux/low TMP section called the linear region that is dependent on TMP but independent of cross flow and bulk concentration. A high flux/high TMP section is called the polarized region. The polarized region is where the gel model can be applied and where flux is independent of TMP but dependent on cross flow and bulk concentration. It is extremely counterintuitive that flux is independent of pressure differences across the membrane but is dependent on flow (and as a result, pressure differences) parallel to the membrane surface. This peculiar result is the consequence of surface polarization ($C_{\text{wall}} \neq 0$). In between the linear and polarized regions lies the knee of the flux curve.

The effect of high solute wall concentrations in the polarized region on solute flux can be explained by osmotic pressure. Retained antibody protein at a wall concentration of 191 g l^{-1} has an osmotic pressure Π of 2 bar [32]. That is, an elevated pressure of 2 bar must be applied to the protein-rich retentate side of a water-permeable membrane containing 191 g l^{-1} of antibody in order to prevent water back flow from the permeate side of the membrane containing water at 0 bar. An increase in TMP causes an increase in wall concentration and osmotic pressure that results in no change in net driving force for solvent flow through the membrane.

The osmotic flux model shown in Equation (5) is based on this mechanistic picture of the net pressure driving force [52]. In Equation (5), σ_0 is the osmotic reflection coefficient [43], $\Delta\Pi$ is the difference in osmotic pressures between the wall concentration on the upstream side and the permeate concentration on the downstream side, and L_{fouled} is the fouled membrane permeability in the solvent. Equation (5) requires a mass

transfer coefficient k to calculate C_{wall} and a relation between protein concentration and osmotic pressure:

$$\text{Osmotic flux model } \mathcal{J} = L_{\text{fouled}} [\text{TMP} - \sigma_0 \cdot \Delta\Pi(C_{\text{wall}})] \quad (5)$$

One can also write a resistance-based flux model by omitting the osmotic term and adding a compressible polarization resistance term in the denominator [5]. This resistance model does not explain the existence of experimentally seen backward flow when the TMP is shut off.

2.06.3.4 Mass Transfer Coefficients

Mass transfer coefficients for a solute and Newtonian solvent in various modules and flow regimes can be correlated by Equation (6) with values for the constants in Table 3:

$$\text{Sh} = a\text{Re}^b \text{Sc}^c (d_h/L)^e \quad (6)$$

for $\text{Sh} = kD/d_h$; $\text{Re} = \rho v d_h/\mu$ (tube, slit); $\text{Re} = \rho \omega d^2/\mu$ (stirred cell diameter d), or $\text{Re} = 2\rho\omega R d/\mu$ (rotating cylinder inner radius R and gap diameter d) and $\text{Sc} = \mu/\rho D$.

Equation (4) indicates that flux depends on the mass transfer coefficient. Increasing the mass transfer coefficient can be accomplished by (1) increasing the shear rate at the wall through higher tangential flow velocities, smaller channel heights, or mechanically moving the membrane by spinning or vibration; (2) altering the geometry of the feed channel to increase turbulent mixing in the normal direction using feed channel screens or curving channels to introduce Dean or Taylor vortices; (3) introducing pulsatile flow in the feed channel or periodic bursts of gas

Table 3 Mass transfer correlations

Geometry	Flow	a	b	c	e	Comments
Tube	Laminar	1.62	0.33	0.33	0.33	Theoretical [22]
Slit	Laminar	1.86	0.33	0.33	0.33	Theoretical [22]
	Turbulent	0.023	0.80	0.33	NA	Theoretical [14]
Spacer	Turbulent	0.023	0.875	0.25	NA	Theoretical [10]
	NA	0.664	0.50	0.33	0.50	Experimental [7]
Stirred cell	Laminar	0.23	0.567	0.33	NA	Experimental [42]
Rotating	Laminar	0.75	0.50	0.33	0.42	Experimental [18]

NA, not available.

For a spacer geometry with channel height h , porosity ε , and specific surface area s , the hydraulic diameter is given by $d_h = 4\varepsilon/[2/h + (1-\varepsilon)s]$. See also DaCosta [7] for an additional correction k_{do} .

bubbles; (4) introducing body forces (centrifugal, gravitational, or electromagnetic) to augment transport away from the membrane; (5) introducing large particles in the feed (e.g., $>0.5 \mu\text{m}$ polyvinyl chloride (PVC) latex beads) that disrupt boundary layers and cause shear-induced diffusion; and (6) introducing periodic back flushing with reversed permeate flows. These methods alter the simple picture shown in Figure 5 but one can still define an average mass transfer coefficient (e.g., see Schwinge *et al.* [41] for variations in k along a screened channel).

2.06.3.5 Fouling

Fouling refers to the reduction in pure solvent permeability caused by solute adsorption and entrapment on the membrane. It is reversed by cleaning but not by back flushing or changing hydraulic operating conditions such as polarization. As seen in Figure 8, severe fouling can shift the knee to higher pressures. For extreme fouling, one may have to operate in the linear region where the fouled permeability dominates the flux. Fouling may also be progressive and cause a steady decline in flux over time. Fouling can also change membrane retention properties.

Membrane chemistry and surface treatment are designed to minimize the intermolecular forces governing adsorption by making surfaces very hydrophilic for water-solvent applications. Membrane surface roughness can impact the entrapment of solutes on the surface. Long-chain solutes such as DNA align with the flow field and can become entrapped in pores larger than their minor axis. In addition, one can operate above a critical flux where the polarizing layer continues to grow because solutes are convected to the membrane faster than they can back transport away. For sticky solutes, this

polarizing layer can form a fouling cake that is not reversible by a change in operating conditions.

These mechanisms suggest that one can alter solution and membrane chemistries to reduce adsorption, use a smaller pore membrane to prevent solute entrapment, and run at less polarizing conditions (i.e., lower TMP, more dilute solute concentrations, and higher mass transfer coefficients) to reduce caking. The suggestions outlined above under mass transfer coefficients may be applicable for sticky cakes. In addition, the use of a body feed may be helpful.

For UF run in normal flow mode such as virus or water purification filters, the tight skin side of the membrane may not be facing the feed stream and fouling solutes can enter the membrane and become trapped. There are a variety of models for filter plugging in the normal flow mode [56]. Prefiltration or other purification methods can be tried to remove plugging species.

2.06.4 UF Processing

2.06.4.1 Process Configurations

Basic membrane process configurations shown in Figure 9 include single-pass, batch, fed-batch, and continuous. Dilute clarification applications use a single-pass configuration, concentration applications can use any configuration, and purification applications use batch or continuous configurations. Regulatory requirements currently limit pharmaceutical applications to batch processing.

2.06.4.2 Single-Pass Operation

A single-pass configuration is used for an NFF system operation (no retentate) or dilute with assemblies of TFF modules run in an NFF mode

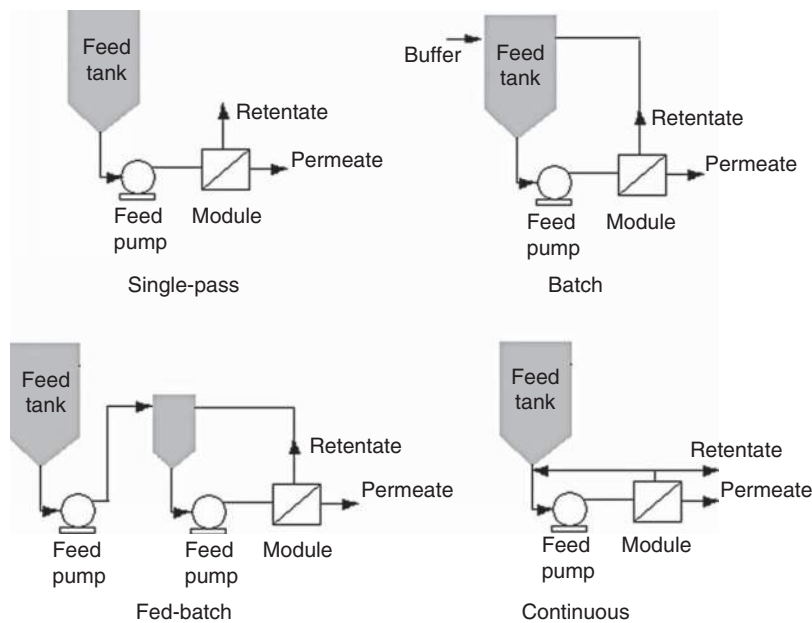


Figure 9 Process configurations.

(retentate closed). Component concentrations change along the length of the retentate channel. For nondilute streams, a single pass through a module may be insufficient to generate either the desired permeate flow or a concentrated retentate.

Steady-state component and solvent mass balances can be written for single-pass operation by considering an incremental area element, dA , in the axial or flow direction for a feed channel, module, or membrane assembly of constant width. For a volumetric cross flow Q in the feed channel, component i with concentration c_i and observed solute passage S_i is

$$\frac{d(c_i Q)}{dA} = c_i \frac{dQ}{dA} + Q \frac{dc_i}{dA} = -\mathcal{F}_i S_i \quad (6a)$$

and

$$\frac{dQ}{dA} = -\mathcal{J} \quad (6b)$$

Combining these equations and integrating yields $c_i = c_{i0} X^{(1-S_i)}$ for a volume reduction factor $X = Q/Q_0$. This allows one to determine either final concentrations from cross-flow rates or the reverse. For a fully retained product ($S_i = 0$), a 10-fold volume reduction ($X = 10$) produces a 10-fold more concentrated product. However, if the product is only partially retained, the volume reduction does not proportionately increase the final concentration due to losses through the membrane.

The area required for processing is $A = (Q_0 - Q)/\bar{\mathcal{J}}$, where $Q_0 - Q$ is the permeate volumetric flow. The Cheryan flux approximation [5] $\bar{\mathcal{J}} \approx 0.33\mathcal{J}_{\text{initial}} + 0.67\mathcal{J}_{\text{final}}$ is useful. In addition, one needs an appropriate flux model relating flux to cross flow, concentration, and pressure, and a hydraulic model showing how retentate pressure profiles vary with flow for spacer-filled channels.

2.06.4.3 Batch and Fed-Batch Concentration

Batch operation involves recycling the retentate to the feed tank to create a multipass flow of the feed through the module. The compositions in batch systems change over time. Recycling is necessary for nondilute streams to generate either the desired permeate flow or a concentrated retentate. Multipass operation increases residence times and pump passes that may degrade retentate components. For systems requiring high pressures to generate permeate flow, it is useful to run the entire system at high pressure to save energy.

An unsteady-state component mass balance (Equation (7a)) can be written for batch operation by assuming a uniform average retentate concentration c_i within the system. Assuming a constant solvent concentration and 100% passage,

$$\frac{d(c_i V)}{dt} = -\mathcal{F}A c_i S_{oi} \quad (7a)$$

$$\frac{dV}{dt} = -\mathcal{F}A \quad (7b)$$

where Equation (7b) represents the solvent balance. Dividing Equation (7a) by Equation (7b) and integrating yields the relationship in **Table 4** between the retentate concentration, the volume reduction factor $X = (\text{initial retentate volume})/(\text{final retentate volume})$, and the observed component passage S_i . For a fully retained product ($S_i = 0$), a 10-fold volume reduction ($X = 10$) produces a 10-fold more concentrated product. However, if the product is only partially retained, the volume reduction does not proportionately increase the final concentration due to losses through the membrane. The component mass in the retentate is obtained as the product of the retentate concentration and retentate volume as shown in **Table 4**.

TFF systems have a maximum volume reduction capability, typically about $40\times$. This arises because tanks must be large enough to hold the batch volume while allowing operation at a minimum working volume. The minimum working volume may be limited by air entrainment into the feed pump, mixing in the feed tank, or level measurement capabilities. Fed-batch operation extends the volume reduction capability to $100\times$ and provides some flexibility in processing a variety of batch volumes in a single skid. For a fed-batch operation, the retentate is returned to a smaller tank, not the large feed tank.

Feed is added to the small retentate tank as permeate is withdrawn so the system volume remains constant. The smaller retentate tank can allow a smaller working volume without entrainment. One could make the retentate tank a section of the pipe or bypass line that returns the retentate directly into the pump feed. Fluid from the feed tank is added slowly into this recirculation loop. This allows a holdup volume consisting of just the recirculation loop. This configuration can be problematic to flush, vent, and drain leading to cleaning and product recovery issues.

Equation (8) is the unsteady-state component mass balance for fed-batch concentration at constant retentate volume V_R . Integration gives the equations for concentration and yield in **Table 4**:

$$V_R \frac{dc_i}{dt} = \mathcal{F}A c_{i0} - \mathcal{F}A c_i S_i \quad (8)$$

Retentate concentration over the course of the process is shown in **Figure 10** for a fully retentive product ($S_i = 0$) as $C/C_0 = 1 + r(1 - 1/X)$ with tank ratio $r = V_o/V_R$, feed concentration C_0 , and feed volume V_o . Fed-batch retentate concentrations exceed the batch concentrations until the curves intersect and any further concentration would proceed in batch mode. The benefits sought from higher concentrations can lead to other problems such as reduced fluxes, larger area and pumps, possible denaturation, and extra lines that may have issues with cleaning and product recovery. This has not only caused significant commissioning and validation delays but also led to the

Table 4 Batch and fed-batch performance equations

	<i>Batch concentration and diafiltration</i>	<i>Fed-batch concentration</i>
Retentate concentration	$c_i = c_{i0} X^{(1-S_i)} e^{-S_i N}$	$c_i = \frac{C_{i0}}{S_i} [1 - (1-S_i) e^{-S_i r(1-1/X)}]$
Retentate mass	$M_i = M_{i0} e^{-S_i [N + \ln(X)]}$	$M_i = \frac{M_{i0}}{S_i} [1 - (1-S_i) e^{-S_i r(1-1/X)}]$
Sizing	$A = \frac{V_o}{t} \left(\frac{1-1/X}{J_{\text{conc}}} + \frac{N/X}{J_{\text{Diaf}}} \right)$	$A = \frac{V_o}{t} \left(\frac{1-1/X}{J_{\text{conc}}} \right)$
Comments	<ul style="list-style-type: none"> • Simplest system and control scheme • Smaller area or process time • Limited to $X < 40$ 	<ul style="list-style-type: none"> • Required for $40 < X$ • Minimize fed-batch ratio (total V_o/recycle tank V) to minimize area • Can require larger area and time • Limited to $X < 100\times$ • Test process performance using proposed fed-batch ratio • $r = \text{batch volume/retentate tank volume} = V_o/V_R$

X , initial volume/final volume; N , buffer volume added/retentate volume.

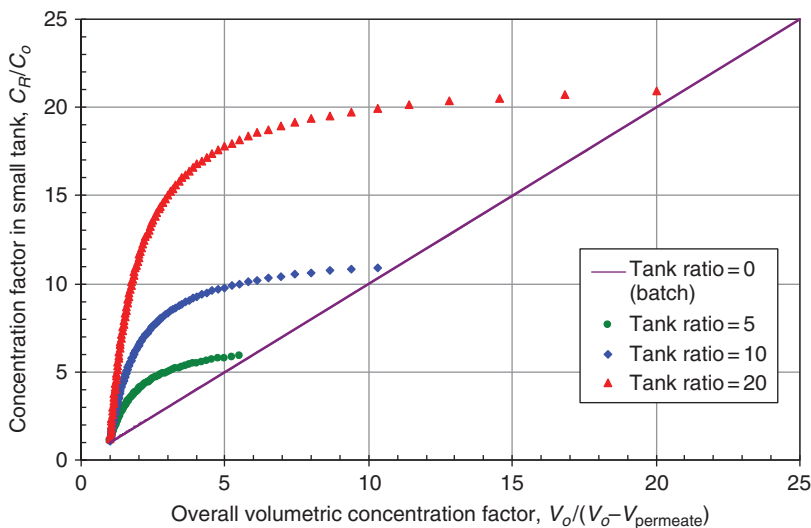


Figure 10 Batch and fed-batch concentration. Courtesy of Millipore Corporation.

scrapping of a process skid as unworkable. The number of pump passes will also be higher, leading to more potential solute degradation. Fed batch and bypass should be used only when necessary.

2.06.4.4 Batch DF

An operating mode known as constant volume DF involves adding a new buffer to the system while withdrawing permeate at the same rate. Equation (9) shows the component mass balance for constant retentate volume V_R :

$$V_R \frac{dc_i}{dt} = -fAc_iS_i \tag{9}$$

Equation (9) is readily integrated and shown in Table 4 in terms of retentate concentration and diavolumes $N = (\text{buffer volumes added}) / (\text{fixed retentate volume})$. Figure 11 shows a washout curve for different membrane-passage characteristics and a starting solute concentration of 100 000 ppm. For a fully passing solute ($S_o = 1$) such as a buffer, the retentate concentration decays 10-fold with each $\ln(10) \sim 2.3$ diavolumes. Partially retained solutes do not decay as quickly and require more diavolumes to reach a final concentration target. A fully retained solute ($S = 0$) maintains its retentate concentration constant at the initial value. For fully passing solutes, >4.5 diavolumes are needed to achieve a specification of $<1\%$ of the original buffer components. Incomplete mixing (due to dead legs and liquid droplets on tank walls)

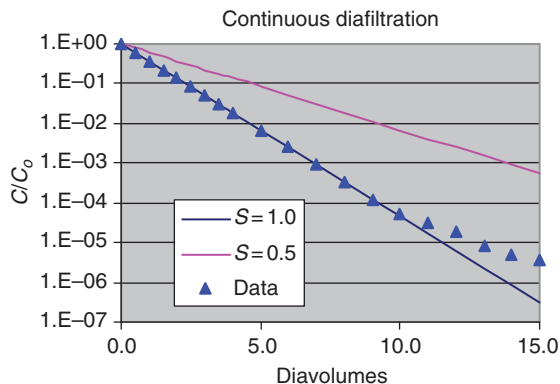


Figure 11 Batch diafiltration.

becomes significant at high diavolumes and causes the curves in Figure 11 to flatten out. It is common to add an extra 1–2 diavolumes as a safety factor to ensure complete buffer exchange.

System sizing involves integration of Equation (7b) using a flux model as shown in Equation (10). This equation also shows the tradeoff between area and process time. The Cheryan flux approximation [5] is useful if a flux model is not readily available. Table 4 shows area requirements where V_o represents the batch volume. In general, flux drops as batch volume is reduced and retained component concentrations increase:

$$\text{Sizing } A = \frac{V}{\bar{f}t}, \text{ where } \frac{1}{\bar{f}} = \int_0^V \frac{dV}{f} \tag{10}$$

Constant retentate weight DF requires variable retentate volumes to compensate for density changes $V = M_R/\rho$ and a diafiltrate buffer flow rate that may differ from the permeate flow rate as $q_D = q_P/\rho_D$. The component mass balance becomes

$$M_R \frac{d(c/\rho)}{dt} = -s c q_D \rho_D / \rho$$

which integrates to $c = c_0(\rho/\rho_0) \exp(-sN')$, where N' is the number of diamasses (buffer mass added/retentate mass). If the concentration of a component is expressed as the mass ratio $y = c_A/c_P$ (gram of A per gram of a fully retained product), the mass ratio becomes $y = y_0 \exp(-sN')$, analogous to a constant volume operation.

The fraction of product mass lost in the permeate can be obtained from the mass in Table 4 as loss = $1 - M_i/M_{i0}$. This loss is shown in Figure 12 and Equation (12). A membrane with 1% passage (99% retention) can have yield losses much higher than 1% because the protein is repeatedly cycled past the membrane during the entire process with losses at every pass. A high-yielding process (<1% loss) requires membrane passage of <0.1% (retention of >99.9%):

$$\text{Permeate loss} = 1 - \exp\{-S[N + \ln(X)]\} \quad (11)$$

Consider a UF process that is designed to fractionate two solutes, product p and impurity i . After a batch concentration and DF, the ratio of the component concentrations is $C_p/C_i = (C_{p0}/C_{i0}) e^{-S_p[N + \ln(X)] + S_i[N + \ln(X)]}$, where C_{i0} and C_{p0} are the initial g l^{-1} concentrations of the two components. Noting that the retentate yield of the product is $Y_p = \exp\{-S_p[N + \ln(X)]\}$, one can rearrange and simplify the concentration ratio to get the purification factor, Equation (12), where ψ is the selectivity (S_p/S_i , the ratio of sieving coefficients). For a product that is

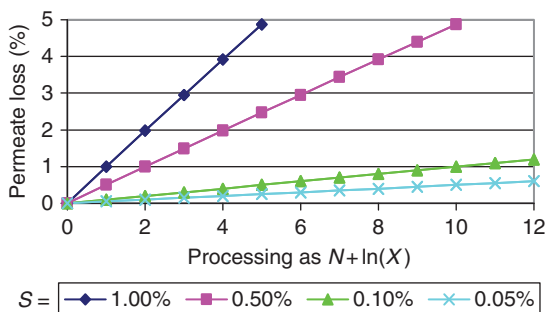


Figure 12 Permeate losses.

retained more than the impurity, $\psi < 1$, $\text{PF} > 1$, and the product becomes enriched in the retentate relative to the impurity.

Equation (13) shows that a high selectivity is needed to achieve high yield and reduce impurity levels. High selectivity requires solutes that differ in the effective size due to molecular weight and charge, the use of charged membranes, and careful control of the polarization layer by running at constant flux and maintaining a uniform TMP along the length of the feed channel [49, 50] (Figure 13):

$$\text{Purification factor PF} = (C_p/C_{p0})/(C_i/C_{i0}) = Y_p^{1-\psi} \quad (12)$$

2.06.4.5 Continuous Operation

Continuous operation (also called feed-and-bleed) involves partial recycle of the retentate. This configuration provides higher productivity of invested capital since setup and cleaning times between batches are significantly reduced. As a result, continuous systems are common for large-scale processing. The residence time and number of pump passes is in between single pass and batch operation, depending on the fraction of retentate recycled. Several continuous units can be plumbed with the retentate flow feeding the next consecutive system. This configuration is commonly used for large-scale membrane systems. For feed flow F , retentate flow R , permeate flow P , and diafiltrate buffer flow D , the steady-state mass balances on the solute and component are: $F + D = R + P$ and $FC_0 = RC_R + PC_{R,S}$. Equation (13) shows the retentate concentration for a volume concentration factor $X = F/R$ and diavolumes $N = D/F$.

$$C_R = C_0 X / [1 - S + SX(1 + N)] \quad (13)$$

The area required is $A = P/\mathcal{J} = F(1 + N - 1/X)/\mathcal{J}$, depending on whether a feed or permeate flow is

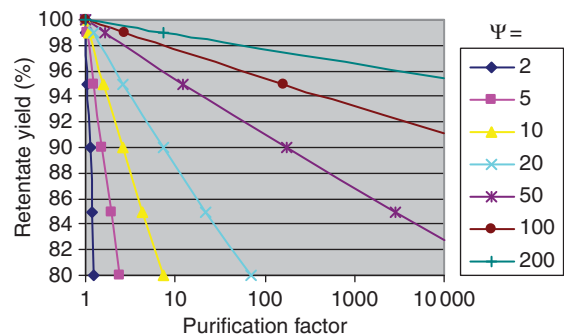


Figure 13 Ultrafiltration (UF) solute purification vs. yield.

specified. The concentration and DF requirements set the retentate concentration for the flux model. There remains to specify the dependence of flux on cross-flow rate in order to solve for the area. Comparison of continuous operation to batch operation shows that more area is needed because the continuous system runs at the final retentate concentration which has the lowest flux, while the batch system operates over a range of concentrations.

Continuous operation can be performed as a multistage operation. The retentate from one system becomes the feed for the next system. Each stage runs at a different concentration so the area requirements are less than for a single stage [38].

2.06.5 UF Process Development

Development of a robust, consistent, and optimized TFF step may be achieved by following a systematic process development protocol. Early phase process development objectives include feasibility for the UF membrane/device to meet the target concentration and buffer exchange specifications. Later phase development objectives include optimization (product yield and quality, system sizing, and costing) and performance validation (reproducibility, sensitivity to variations).

Selection of candidate membranes and modules is made on the basis of applications requirements and vendor recommendations. In addition to the performance factors described under membrane and modules, experience with vendors, vendor support, and product consistency are important factors to consider.

Candidate membranes and modules must be screened using vendor-recommended scale-down test systems for feasibility evaluation. Vendors or the literature may recommend some starting conditions or ranges of operation (TMP, cross flow) to try. Membrane disks can be tested using a low volume, stirred cell device to check critical feasibility characteristics (e.g., product yield and quality, fluxes, membrane fouling and cleaning) even though the flux performance in these devices does not scale. If larger volumes (>50 ml) of feedstock are available, a scale-down representative module is preferred. Other candidate modules with different membrane chemistries, MW ratings, and module design can also be tested if feed volume and time permits.

2.06.5.1 Standard Test Protocol

1. Module verification: Initial flush to wet the membrane; measure normalized water permeability (NWP) as $l\text{m}^{-2}\text{h}^{-1}\text{psi}^{-1}$ or LMH/psi corrected to 298 K; measure air diffusion through wetted membrane as $l\text{m}^{-2}\text{s}^{-1}$ and compare with specification to verify membrane integrity. Flush with buffer to precondition the membrane.
2. Initial dynamics: Add product solution and measure flux and passage versus time in permeate recycle mode to allow for membrane conditioning in product solution.
3. Sensitivity to initial operating conditions: Measure flux, passage, and feed to retentate pressure drop (ΔP) versus TMP and cross flow in permeate recycle mode.
4. Concentration mode: Measure flux, passage, turbidity, retentate concentration, temperature, and permeate volume versus time while withdrawing permeate to achieve target concentration.
5. Sensitivity to final operating conditions: Measure flux, passage, feed to retentate pressure drop (ΔP), and turbidity versus TMP and cross flow in permeate recycle mode.
6. DF mode: Measure flux, passage, impurity concentration in retentate, temperature, and permeate volume versus time while withdrawing permeate and adding diafiltrate to achieve target impurity concentration.
7. Recover retentate product by depolarizing and using a plug-flow flush (see Section 2.06.5.2).
8. Clean membrane under vendor-recommended conditions: For example, flush with buffer, then WFI (water for injection), add 0.1 N NaOH solution, recirculate for 45 min at 293 K in permeate recycle mode, and measure NWP [28, 29, 30].

Additional testing can include repeatability evaluation, cleaning optimization, and further exploration of particular conditions. For high final concentrations and a final formulation buffer leading to significantly different osmotic pressures, it is worth repeating both the operating conditions (step 3) and the concentration mode (step 4) in the new buffer after step 6.

2.06.5.2 Data Analysis

The module used should be integral and show NWP within the normal device range. The initial dynamics should show asymptotic approach to steady-state flux and retention. Continued decline in performance indicates a membrane compatibility issue.

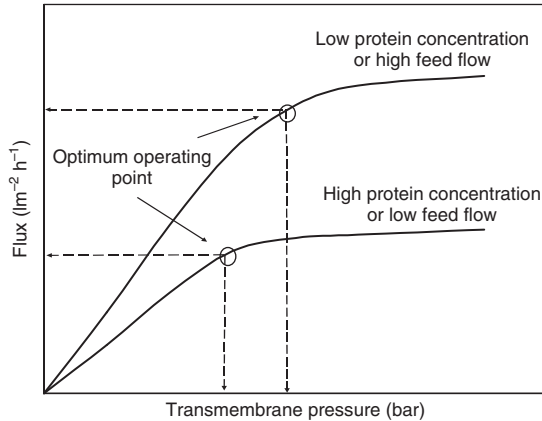


Figure 14 Flux trends. Courtesy of Millipore.

Operating condition data should mirror the trends shown in **Figure 14**. Behavior contrary to these trends may indicate faulty experimental procedures or an unusual new effect that should be confirmed and understood.

The optimum TMP is located at the knee of the flux curve to obtain reasonable flux and avoid formation of aggregates. If there is a difference in the flux curves between the starting solution and the diafiltered solution, a conservative approach for polarization would be to select the lower of the two TMP values.

Vendor recommendations are usually used to select a module cross-flow rate. Increased cross-flow rates are suggested if the flux is very sensitive to cross flow or if the feedstock is prone to polarization or polarization-caused degradation and fouling. In this case, flux-limiting C_{wall} control should also be considered [48]. Decreased cross-flow rates are suggested for feedstocks prone to pumping degradation or if scale-up is limited by available pump sizes. Pump degradation tends to increase with the number of pump passes [54] (volume of fluid pumped/feed volume) as shown in **Figure 15**. Equation (14) shows that pump passes increase with DF and concentration, and decrease with the conversion ratio CR (permeate flow/feed flow). Pump selection and operation is critical to reducing pump degradation. One may also consider a continuous operation configuration with low residence times for sensitive feedstocks.

$$\text{Pump passes PP} = [N + \ln(X)]/\text{CR} \quad (14)$$

Product and target impurity concentrations should be plotted against volume reduction factor X

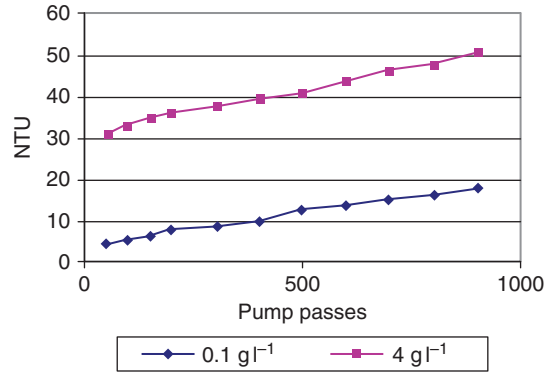


Figure 15 Pump degradation.

and diavolumes N to show agreement with the equations in **Table 4** and ensure high impurity sieving coefficients and low product sieving coefficients. Deviations in performance from expected behavior indicate problems in experimental procedure (e.g., poor tank mixing) or unusual product properties requiring further study (e.g., product precipitation at high concentrations).

A sequence of concentration and DF steps is referred to as the DF strategy. DF is needed for purification applications or for increasing product recovery in a clarification application. Examination of **Table 4** shows that for DF

$$At/V_0 = \left(\frac{N}{X\bar{J}_{\text{Dial}}} \right)$$

That is, the area–time needed per unit volume of feed is reduced by concentration to reduce permeate and buffer volumes during DF. However, flux will also decline during concentration causing an increase in the area–time per unit volume needed. One can plot $X\bar{J}$ values obtained during a concentration step to find an empirical optimum. Application of the gel flux model (Equation (4)) showed that a minimum system area and processing time is obtained by diafiltering at a protein concentration [33] of C_g/e . For human plasma-derived IgG [32] with $C_g = 191.4 \text{ g l}^{-1}$, $C_{\text{DF}} = 68 \text{ g l}^{-1}$. This suggests an optimal DF strategy to concentrate or dilute the initial feed to C_{DF} , diafilter as needed, then concentrate or dilute to the final concentration. The time–area per unit volume is a shallow optimum so operation within $\pm 15\%$ of C_{DF} does not make an appreciable difference. For flux and sieving coefficients that depend significantly on both the retained product and the washed out impurity concentrations, more complex DF strategies should be considered [23].

Table 5 Sources of product loss for batch configurations

Source	Permeate	Adsorption	Holdup	Inactivation
Magnitude	0–1%	0–5%	1–10%	0–20%
Causes	Membrane leakage, operation	Membrane adsorption	Poor system design, poor recovery method	Gas interfaces, high temperatures, polarization, pumping
Correction	Lower MW membrane, sealing issue	Different membrane material	Eliminate dead legs, improve recovery method	Check tank foaming and pump, C_{wall} control

Small-scale test systems may not accurately mirror large-scale systems for product recovery due to differences in holdup and recovery methods. However, one can evaluate product yields for the small-scale process and consider the sources of product loss in **Table 5** to see if further investigation and correction are warranted (see also Section 2.06.6).

Processing times, permeate fluxes, and permeate volumes are recorded during the scale-down experiments to enable a rough system sizing using the equations in **Table 4**. Fluxes scale directly and volumes scale proportionately with the feed volume. A safety factor will be built into the scale-up design so that process times will not be the same.

Feasibility requires demonstration of repeatable performance. The adequacy of the cleaning step is determined by the recovery of at least 80% of the initial normalized water flux [30]. While some variability in water flux is typical, any consistent decline reflects an inadequate cleaning procedure. Additional verification of consistency can involve measuring batch-to-batch yields, buffer passage, process flux, and air integrity. The typical module change-out frequency is 1 year, or 50 runs, or when performance (retention, flux, and integrity) drops below preset specifications.

The data should establish the feasibility of the formulation step in meeting product quality and concentration, buffer composition, robustness (consistency and worst case feed), product recovery, and economical operation goals. Data consistent with the trends shown here should establish confidence in

the results. Further optimization may be appropriate for large-scale operations.

2.06.6 UF Scale-Up

The simplest scaling strategy is linear scale-up [47]. This involves system scaling based on consistent capacity (1m^{-2}) from small scale to large scale. Permeate, buffer, and retentate volumes also scale linearly with feed volume. TFF system performance can be sensitive to hardware design and layout. It is usually not possible to find scale-down hardware that precisely mimics large-scale versions. However, hardware functionality needs to be preserved at both scales. One should also identify potential changes in the feed material in moving from one scale to the next and conduct scale-down testing with worst case feed.

2.06.6.1 Batch Configuration Sizing

Figure 16 shows the concentration and DF steps for an example of a 600-l feed undergoing a $21\times$ volume reduction and $7\times$ DF. The input buffers and permeate waste volumes for this case are calculated from mass balances.

A value of the minimum system area, A_{min} , is calculated from the equations in **Table 4** for each processing step, permeate volumes, and the target processing time (**Table 6**). The average flux over each step is calculated by integrating experimental

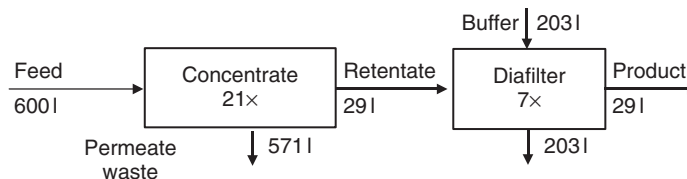
**Figure 16** Ultrafiltration process sequence.

Table 6 Ultrafiltration system sizing

Step	Concentrate	Diafilter	Total
Average flux ($\text{l m}^{-2} \text{h}^{-1}$)	40	30	
Permeate volume (l)	571	203	771
Area-time ($\text{m}^2 \text{h}$)	14	7	21
Time (h)	2.0	1.0	3.0

flux data or by taking the total volume permeated and the total processing time required. The Cheryan flux approximation [5], based on the initial and final fluxes, can also be used with a suitable safety factor.

An area-time term can be calculated for each step as the ratio of the manufacturing scale permeate volume to the average experimental flux. For the concentration step shown in the table, this is $(571 \text{ l}) / (40 \text{ l m}^{-2} \text{h}^{-1}) = 14 \text{ m}^2 \text{h}$. The area-time for each step is then added to give the total area-time for the process, here $21 \text{ m}^2 \text{h}$. When the total area-time is divided by the total processing time, this gives a total area of $A_{\text{min}} = (21 \text{ m}^2 \text{h}) / (4 \text{ h}) = 5.3 \text{ m}^2$.

Safety factors of 1.2–2.0 are used to allow for (1) differences in performance between small and large scale and (2) completing the process within the specified time under batch-to-batch process variations in feedstock, filters, and operating conditions. Differences between scales can include unequal flow distribution, holdup volumes, and poor mixing. For linearly scaled processes, a safety factor of $1.2 \times$ is recommended for an area of $A = 6.4 \text{ m}^2$. For processes with large variability, modules with poor scalability, and limited scale-down data, larger safety factors are recommended. Safety factors on the higher side are also recommended if it is costly for the process to exceed the design time window. The recommended area is now compared with available module sizes. In this case, 13 cassettes of 0.5 m^2 each would give 6.5 m^2 . However, it is convenient to symmetrically array 14 cassettes on a single-level process holder for a configurational area of $A_{\text{config}} = 7 \text{ m}^2$. The system area can be used to size the pump and maintain the same cross flow per unit area.

Process times for each step can be calculated by dividing the area-time for each step by the total area. The expected process time is 3.0 h, well within the

4-h processing target. While this calculation shows the tradeoff between process time and membrane area, the processing time can be a small component of the time it takes to turn around the UF operation (including setup, recovery, and cleaning). The addition of extra area not only ensured consistent processing within the time window allowed but also increased the system holdup and minimum working volume. One must check that the volume reduction factors can still be met with the system.

2.06.6.2 Batch Recovery

Overall product recovery in the final retentate should be $>95\%$ and yields of $>99\%$ are common. **Table 5** lists the largest sources of yield losses as holdup and inactivation. Inactivation can also occur through extensive process times or hold steps, high-temperature spots (nonisolated pump from motor), unflushed cleaning fluid remaining in a dead leg, and contact of the protein solution with buffer solutions that promote instability (i.e., diafiltering through an isoelectric point). Discussions with protein formulation chemists can be useful in diagnosing and correcting inactivation losses.

Holdup losses include unrecovered product liquid left in the system. It is recommended to recirculate the retentate product at the end of processing with a closed permeate to release the product held up in the polarization layer. The bulk of the product in the recycle retentate tank can be pumped out with the feed pump or drained. Appreciable product is still held up in the piping and the modules. Blow down uses compressed air introduced at a high point of the system in the retentate line with the product collection at the lowest point. Care must be taken to gently introduce the air at $\sim 0.13 \text{ bar}$ in order to avoid foaming and product denaturing (**Table 7**).

Additional recovery is obtained by slowly introducing buffer at a high point in the system. This will progress through the wetted components and displace held up product. The buffer will eventually exit the low point drain where a ultraviolet (UV) monitor can readily detect the transition from

Table 7 Product recovery methods

Recovery method	Gravity drain	Blowdown	Plug-flow flush	Recirculation flush
Holdup loss	5–20%	2–10%	0.5–2%	0.1–0.5%
Notes	Design sensitive	Design sensitive		Dilutes product

product to buffer [13]. The transition is generally compact and this procedure is termed a plug-flow flush. One can also use the more extensive recirculation flush where a minimum tank volume of buffer is introduced and recirculated to allow product diffusion out of any dead legs and nooks and crannies in the wetted flow path. The additional recovery using this procedure may not warrant the product dilution effect of using this approach.

2.06.6.3 Operating Procedure

The following procedure is representative of a typical operation. Note that plant standard operating procedures (SOPs) should be written to allow flexibility where possible but must ensure consistently meeting product specifications.

1. WFI flush: Module installation per manufacturing recommendation, flush per recommendation, NWP measurement, and drain.
2. Integrity test: Pressurize to manufacturing specification with sterile air, measure air flow, and compare with manufacturing specification.
3. Buffer rinse preconditioning.
4. Process fluid: Fill tank, concentrate to volumes or retentate concentration, and diafilter to buffer or permeate volume.
5. Recover product: Drain, plug-flow flush.
6. Cleaning: WFI flush, clean per manufacturing recommendation, WFI flush, NWP measurement and comparison with specifications, cleanliness test (limulus amoebocyte lysate (LAL), total organic carbon (TOC)) per application, and drain.
7. Storage: As per manufacturing recommendation.
8. Change out: Based on failing specifications on NWP, ΔP , air integrity, yield, or number of cycles.
9. Allow for reprocessing (if desired).

A well-designed, robust UF process is characterized by the following performance parameters:

1. Yield (overall) $\geq 95\text{--}98\%$.
2. Process flux consistency $\sim \pm 10\%$ run-to-run.
3. Product retention (membrane) $\geq 99.9\%$.
4. NWP recovery (run-to-run) $\sim \pm 20\text{--}35\%$.

2.06.6.4 Adding Area in Series

UF modules are generally scaled by adding area in parallel: feed is distributed among parallel module inlets with a collection of common retentate and

common permeate streams. One can also add area in series where the retentate flow from one module provides the feed flow to the next module. This type of configuration is equivalent to increasing the length of the retentate channel such as increasing the length of hollow fiber modules or using spirals in series. Permeate flows may or may not be plumbed together.

The benefit of this approach is that feed pumping requirements are reduced. However, one cannot add area in series and maintain the same feed flow and pressure profiles used in scale-down testing. In an extreme case, adding extra length to the feed channel can cause the feed channel pressure to fall below the permeate pressure and create backward flow. It is useful to test the series configuration at small scale to verify feasibility.

2.06.6.5 Process Monitoring and Control

A TFF system must be able to implement all the steps in the SOP, deliver the desired product, and meet any process constraints. At a minimum, a batch system contains the membrane modules and holder, tank, feed pump, retentate valve, and pressure sensors for the feed and retentate lines. A representative piping and instrumentation diagram (P&ID) for a typical commercial system is shown in [Figure 17](#). A heat exchanger is sized to maintain uniform temperature of the process to counteract heat added by the pump and ambient heating, but this may be unnecessary during DF. Open systems may be acceptable for early clinical phase production but closed systems with hard plumbed lines are needed for validated consistency, short cycle times, and bioburden control manufacturing. Each step of the process is controlled by switching valves to introduce/discontinue the appropriate solutions to the system (air, buffer, diafiltrate, cleaning fluid, etc.).

Multiproduct facilities process a wide range of batch volumes from clinical trials to marketed products. While fed-batch configurations allow flexibility to handle these wide volume ranges, one can encounter issues with cleaning and product degradation. Separate pilot systems are recommended for small batches to avoid these validation issues and speed time to market.

The monitoring and control strategy should make use of sensors to measure permeate flow (water permeability measurement, processing, and cleaning), retentate flow, air flow during integrity testing, pressures (feed, retentate, and permeate), temperature, tank

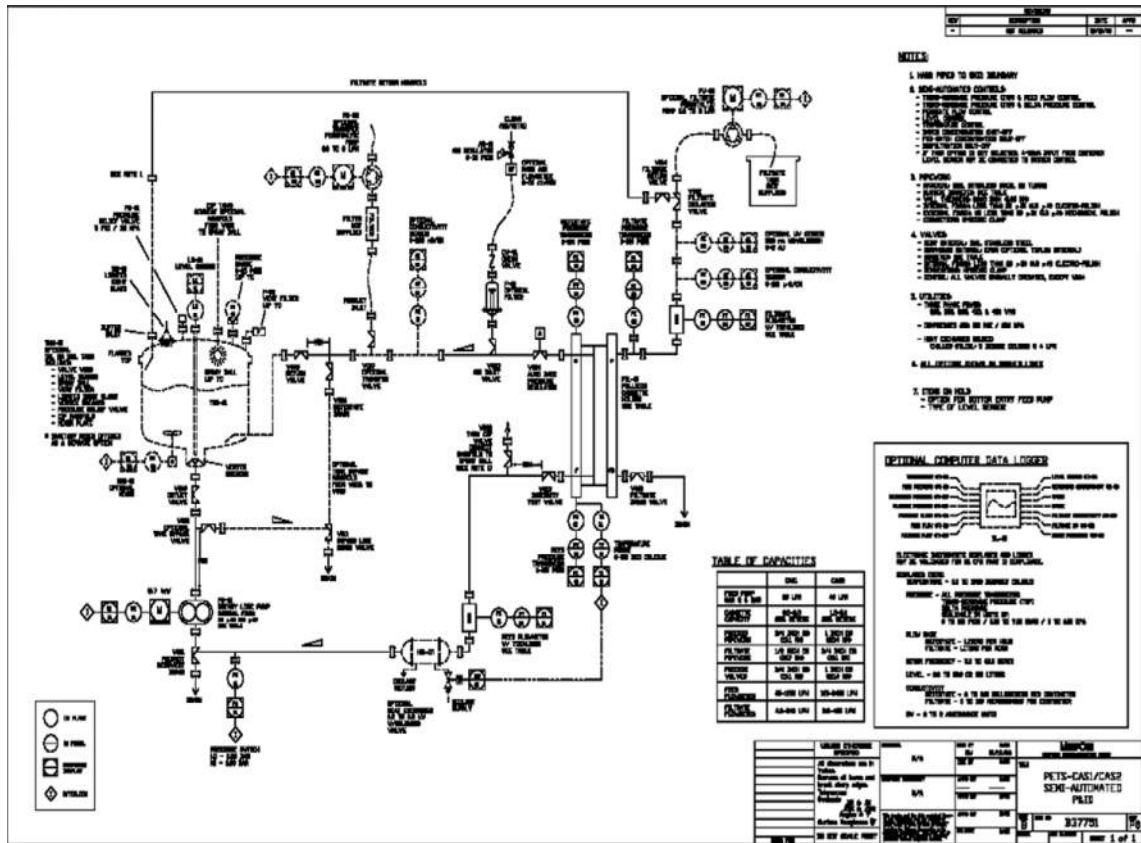


Figure 17 Batch ultrafiltration (UF) process piping and instrumentation diagram (P&ID). Courtesy Millipore Corporation.

level or weight, permeate composition (UV absorbance as an indicator of protein content, pH, and conductivity as desired), process temperature, and coolant temperature. A good design practice is to minimize the number of sensors and identify their optimal placement. These sensor readings may be displayed, logged, and used to trigger alarms and a subsequent step in a process. Alarms may be triggered by abnormal pressure excursions (plugged feed channel and valve froze shut), low tank volumes, high permeate UV absorbance, and high temperatures. The duration of each step is determined by time, permeate volume, or fluid height in the feed tank. Process data are typically logged for cGMP, trending, and diagnosis of any unusual excursions. The flow paths that are active during each step of the SOP should be traced out on the P&ID to show valve configurations along with the relevant sensors used for monitoring and alarms. This includes the ability to vent, drain, clean in place (CIP), and flush the system, and respond to system upsets. It is particularly important to ensure that all flow paths are active during the cleaning step, including sample valves. In some cases, the modules may be

removed from the system during cleaning. Care should also be taken to make sure that the product is not inadvertently flushed to waste through careful automation or the use of transfer panels.

2.06.6.6 Equipment Selection

Table 8 shows equipment requirements. Customer or regulatory requirements ensure that processing objectives are consistently met. Economical requirements include life cycle costs such as capital, operation, validation, maintenance, cost of replacement (and revalidation if needed), staffing required to support ongoing operation (e.g., programming and calibration), and the scope of the supporting documentation and service from the vendor. Standard, easy-to-use, designs and components are less prone to failure with lower labor costs and maintenance. Components must conform to the standards of the country and operating facility (e.g., metric and voltage) to ensure compatibility and reduce the inventory of spare parts. Additional selection criteria

Table 8 Equipment requirements

<i>Component</i>	<i>Customer/regulatory</i>	<i>Economic</i>	<i>Safety</i>
Wetted surface materials	Nontoxic, cleanable/sanitary, consistent, chemically compatible with all process fluids (no swelling or reacting), nonshedding, nonleaching, nonadsorbing, closed system	Availability, can fabricate	
Wetted volume	Low holdup, drainable, ventable, minimize dead legs, cleanable, flushable		Pressure and temperature rating, sealing
Piping, valves, heat exchanger		Compact, can fabricate, drainable, available in a variety of formats	Operator protection from moving parts
Vessels	Handle volume range, mixing, avoid foaming	Availability	
Pumps, filter holders	Low protein degradation, consistent, thermal isolation		Operator protection from moving parts
Sensors/sampling	Reliable, accurate, insensitive to environmental effects (temperature, pressure changes), calibrate in closed system	Design in optimum number – not to excess	Electrical shock, closed system
Skid frame	Compatible with cleaners and sanitizers	Compact	Supports load, ease-of-operation
Display	Capture and store data		Legible
All components	Documentation, easy-to-validate, quality certification	Low cost, reliable, maintainable, conform to plant standards, proven designs, spare parts	Conform to country standards

include experience with components and vendors, and scalability. Long lead components such as specially designed pumps, sensors, and tanks must be designed and ordered early.

Operator safety involves chemical hazards (explosive solvents, biohazards, and toxic or corrosive chemicals), physical hazards (high pressures, moving parts, temperature extremes, use of steam, and obstacles to operation and maintenance), and electrical hazards (high voltages and currents, and inadequate grounding). Safeguards and alarms should be tested to make sure that they work in an emergency. Safety reviews of designs recommended along with formal hazard and operability (HAZOP) analyses and control hazard and operability (CHAZOP) analyses.

Integration of skids with each other and the plant may impose additional constraints. Skids require hardware matching. Retrofit into an existing facility may impose limitations on skid dimensions for the production floor and for access to the facility.

Dead legs shown in **Figure 18** are spaces or pockets in contact with the products that are difficult to vent, flush, and drain [1]. They arise from connecting components to the piping system (e.g., sensors, sampling ports, and rupture disks), within wetted components (e.g., pumps, housings, valves, heat exchangers, and tanks), or as surface roughness. Flow visualization [46], simulations, and testing indicate that the efficiency of cleaning a dead leg is affected by the ratio L/D , the average fluid velocity in the pipe, and the presence of air pockets in the dead leg [11]. While elimination of dead legs is desirable, current ASME American society of mechanical engineers bioprocessing equipment (BPE) guidelines [1] recommend $L/D < 2$ (based on the internal dimensions of the dead leg). Surface roughness can also be considered as dead legs at a microscopic scale. Surface finishes and

cleanability considerations evolved from the dairy industry [45].

The presence of air in piping systems can prevent fluids from wetting the internal surfaces. cGMP is compromised by inadequate contact with cleaning and sanitizing fluids. Fluid velocities of 1.5 m s^{-1} are required to displace air from dead legs or to completely flood a vertical pipe [11]. Avoid vertical pipe bends that create sections where air or solids can accumulate. Liquid retention in undrainable sections represents product loss, growth areas for bioburden, or batch carryover. Venting and draining is aided by a pipe slope of at least 5 mm drop per meter of pipe length. Clean steam lines are self-sanitizing and may be plumbed without a vertical slope. A low point drain is required.

The high CIP flows of 1.5 m s^{-1} required for wetting internal surfaces are typically more demanding than process flows and form the basis for pump sizing. An economic analysis shows that there is a tradeoff between capital and operating costs for piping systems with optimum velocities [36] in the range of $0.9\text{--}3.0 \text{ m s}^{-1}$. Velocities $>0.9 \text{ m s}^{-1}$ are also recommended for cleaning and flushing as part of the 3A standards [45]. These velocities help ensure that air bubbles in dead legs are flushed out of the piping system so that all the internal surfaces are accessible for cleaning [11].

Although pumps do not scale consistently, they are selected to meet the flow, pressure, and pulsation requirements of the scale of operation and avoid damaging protein. Rotary lobe designs recommended for feed pumps should be run below 500 rpm and be mounted in a vertical position to allow product and cleaning solutions to drain out easily. Adding more lobes will reduce pulsation effects but increase protein degradation. Sanitary centrifugal or peristaltic pumps can be used for buffer or CIP solution transfer and for WFI loop recirculation.

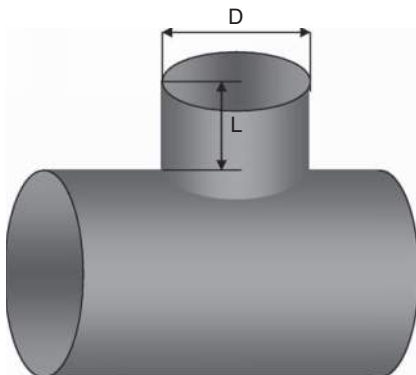


Figure 18 Dead legs.

2.06.6.7 Skid Layout

Skid layout criteria include minimizing the minimum working volume and dead legs, as well as allowing for flushing, cleaning, venting, draining, mixing, sanitizing/steaming, operating and servicing ergonomics, and safety. Holdup volume and the presence of dead legs in the wetted fluid path impact product recovery, separation efficiency (e.g., poor buffer exchange at high diavolumes), fluid volumes required (cleaning, flushing, and processing), system cost and required floor space, and the ease of cleaning and sanitizing. Minimization involves reducing line lengths, employing the full 3D

space using computer-aided design-computer-aided manufacturing (CAD-CAM) to explore design alternatives, and using compact components (e.g., valve assemblies).

Systems must be designed to minimize product degradation by controlling physical and chemical stresses (e.g., hot spots, excessive shear, air interfaces, cavitation, and local concentrations). Mixers are used to eliminate concentration gradients in tanks. Inadequate mixing caused by the addition of diafiltrate in a Tee between the tank and the feed pump will reduce performance. In-line mixing (two fluids are pumped into a Tee connection and blended while flowing in a pipe) for buffer preparation from concentrates reduces waiting time, tankage, and floor space [34].

The 3D layout of process and remote monitoring and control systems should allow operators to set up, operate, and turn around each process without undue strain. In addition, maintenance and service personnel should be able to conduct routine operations (e.g., calibration and gasket replacement) without undue strain. This requires proper orientation of displays and enough space around a processing skid to gain access. Computer 3D models, constructed using CAD-CAM systems, should be examined for ergonomics during design reviews (Figure 19).

The design, construction, commissioning, and validation [35] of a process skid often involve a team of experts from the biopharmaceutical manufacturer, the skid supplier, and an architect and engineering (A&E)

firm. This is facilitated through the use of a process with clear UF step performance requirements, roles of team members, and milestones/reviews [19].

2.06.7 UF Applications

Electrodeposition of cationic paint resin on automobiles (connected to the cathode) provides a uniform, defect-free coating with high corrosion resistance but carries with it about 50% excess paint that must be washed off. UF is used to maintain the paint concentration in the paint bath while generating a permeate that is used for washing (Table 9). The spent wash is fed back into the paint path [56]. Paint recycling with low paint losses and low system costs makes the process economical.

During cheese making, the coagulated milk or curd is used to make cheese while the supernatant whey is a waste product rich in salts, proteins, and lactose. Whey concentration and desalting by UF produces a retentate product that can be used as an animal feed supplement or food additive. The MMV process [26] involves concentrating the milk by UF after centrifugation to remove the cream and before coagulation to improve yields and reduce disposal costs.

UF is used in biopharmaceutical purification (proteins, viral, bacterial vaccines, and nucleic acids) for initial concentration of clarified fluids or lysates (to reduce subsequent column sizes and increase binding),



Figure 19 Ultrafiltration (UF) batch processing skid. Photo courtesy of Millipore.

Table 9 UF modules and systems

<i>Application</i>	<i>Paint recovery</i>	<i>Whey processing</i>	<i>Biologicals</i>	<i>Water treatment</i>	<i>Juice processing</i>
Membrane	PES	PES	Cellulose, PES, PVDF	PES	PES, PVDF
Module	Fibers	Spirals	Cassette	Fibers	Tubes
System	Continuous	Continuous	Batch, NFF	Continuous, single pass	Batch
Characteristics	Cost, plugging	Cost	Recovery	Cost	Plugging, Cost

Table 10 Troubleshooting guide

<i>Symptom</i>	<i>Root cause(s)</i>	<i>Recommended action(s)</i>
Low flux	Fouling, improper cleaning, low cross flow, hardware shedding	Modify cleaning procedure, replace modules, check TMP, replace hardware components
Low yields	Poor recovery, tank foaming, leaky membrane, poor assay, or sampling	Modify recovery, integrity test, check tank, and retentate flow
Failed integrity	Leaky module, improper installation	Reinstall and/or replace modules, tighten hydraulic specification
Failed bioburden	Contaminated feed, buffers, or equipment	Sanitization, check buffers and upstream steps, swab equipment
Inadequate buffer exchange/solute removal	Insufficient diavolumes, poor mixing, poor passage	Increase diavolumes, improve mixing, check for membrane fouling, or solute binding to retained solutes
External leaks	Seals	Integrity test, replace seals

to change buffer conditions (for loading on to columns), and to concentrate and change buffers (for final formulation into a storage buffer) [24]. For these applications, the drug product is recovered in the retentate. For drug products with potential viral contaminants (sourced from mammalian cells or human and animal blood plasma), virus removal filters employed in either a TFF or an NFF mode retain the viruses, while the drug product is recovered in the permeate. UF displaced size exclusion chromatography (SEC) for buffer exchange due to its lower cost and ability to run higher protein concentrations [21]. These applications require high yields, maintaining high purity, consistent operation, and scale-up of the valuable product.

UF is used to clarify various fruit juices (apple, grape, pear, pineapple, cranberry, orange, and lemon) which are recovered as the permeate [2]. UF has also been used to remove pigments and reduce browning in wine production [20]. Low-cost operation is required.

Wastewater treatment and water purification applications employ UF in a TFF or NFF mode to produce permeate product with reduced colloids, pyrogens, and viruses. Oil droplets in wastewater are retained by UF for recycle or disposal at significantly reduced volumes.

2.06.8 UF System Troubleshooting

Table 10 illustrates the typical symptoms, the corresponding causes, and the recommended actions for troubleshooting.

References

- [1] ASME *Bioprocess Equipment Guidelines*; AMSE: New York, 1997.
- [2] Blanck, R. G., Eykamp, W. *AIChE Symp. Ser.* **1986**, *82*, 59–64.
- [3] Brian, P. L. T. Mass Transport in Reverse Osmosis. In *Desalination by Reverse Osmosis*; Merten, U., Ed.; MIT Press: Cambridge, MA, 1966; pp 161–292.
- [4] Cabasso, I. Practical Aspects in the Development of a Polymer Matrix for Ultrafiltration. In *Ultrafiltration Membranes and Applications*; Cooper, A. R., Ed.; Plenum: New York, 1980; pp 57–78.
- [5] Cheryan, M. *Ultrafiltration and Microfiltration Handbook*; Technomic Publishing Company: Lancaster, PA, 1998.
- [6] Culklin, B., Armando, A. D. *Filtr. Sep.* **1992**, *29*, 376.
- [7] DaCosta, A. R., Fane, A. G., Wiley, D. E. *J. Membr. Sci.* **1994**, *87*, 79.
- [8] Dechadilok, P., Deen, W. M. *Ind. Eng. Chem. Res.* **2006**, *45*, 6953–6959.
- [9] Deen, W. M. *AIChE J.* **1987**, *33*, 1409–1425.
- [10] Deissler, R. *Advances in Heat and Mass Transfer*; Harnett, J. P., Ed.; McGraw-Hill: New York, 1961.
- [11] DeLucia, D. *Fundamentals of CIP Design*, ASME Bioprocessing Seminars, San Diego, CA, 1997.

- [12] DiLeo, A. J., Allegrezza, A. E., Jr., Burke, E. T. Membrane Process and System for Isolating Virus from Solution. US Pat. 5,017,292, 21 May 1991.
- [13] Genentech, F. J. Personal Communication, 1998.
- [14] Gekas, V., Hallstrom, B. J. *Membr. Sci.* **1987**, *30*, 153.
- [15] Miller, E. F. General Atomics. US Pat. 3,839,201, 1967.
- [16] Hallstrom, B., Lopez-Leiva, M. *Desalination* **1978**, *64*, 273.
- [17] Ho, W. S. W., Sirkar, K. K., Eds. *Membrane Handbook*; Van Nostrand Reinhold: New York, 1992.
- [18] Holeschovsky, U. B., Cooney, C. L. *AIChE J.* **1991**, *37*, 1219.
- [19] ISPE, Baseline Guide, *Commissioning and Qualification*, Vol. 5, 2001.
- [20] Kosikowski, F. V. Membrane Separations in Food Processing. In *Membrane Separations in Biotechnology*; McGregor, W. C., Ed.; Marcel Dekker: New York, 1986; pp 201–254.
- [21] Kurnik, R. T., Yu, A. W., Blank, G. S., et al. *Biotechnol. Bioeng.* **1995**, *45*, 149–157.
- [22] Leveque, M. D. *Ann. Mines* **1928**, *13*, 201.
- [23] Lutz, H. Membrane Filtration with Optimized Addition of Second Liquid to Maximize flux. US Pat. 5,597,486, 28 January 1997.
- [24] Lutz, H., Raghunath, B. Ultrafiltration Process Design and Implementation. In *Process Scale Bioseparations for the Biopharmaceutical Industry*; Shukla, A. A., Etzel, M. R., Gadam, S., Eds.; CRC Press: New York, 2006; Chapter 10, pp 297–332.
- [25] Lutz, H. Membrane Separation Processes. In *Perry's Chemical Engineering Handbook*, 8th edn.; Green, D. W., Perry, R. H., Eds.; McGraw-Hill: New York; Chapter 10, 2008.
- [26] Maubois, J. L., Mocquot, G., Vassal, L. Procédé de traitement du lait et des sous produits laitiers. Fr. Pat. 2,052,121, 1969.
- [27] McDonough, R. M., Bauser, H., Stroth, N., Grauschoph, U. *J. Membr. Sci.* **1995**, *104*, 51–63.
- [28] Millipore Corporation, *Protein Concentration and Diafiltration by Tangential Flow Filtration*, Lit. No. TB032 Rev. B, 1999.
- [29] Millipore Corporation, *Maintenance Procedures for ProstaK™ Modules*, Lit. No. P17513, 1990.
- [30] Millipore Corporation, *Maintenance Guide*, Lit No TB1502EN00, 2000.
- [31] Mir, L., Michaels, S. L., Goel, V., Kaiser, R. In *Membrane Handbook*; Ho, W. S. W., Sirkar, K. K., Eds.; Van Nostrand Reinhold: New York, 1992.
- [32] Mitra, G., Lundblad, J. L. *Sep. Sci. Technol.* **1978**, *13*, 89–94.
- [33] Ng, P., Lundblad, J., Mitra, G. *Sep. Sci.* **1976**, *2*, 499–502.
- [34] Ogez, J., *Increasing Plant Capacity Using Buffer Concentrates & Linked Unit Operations*, Presentation at IBC 2nd Annual Recovery & Purification of Biopharmaceuticals, San Diego, CA, 13 November 2001.
- [35] PDA, Industrial Perspective on Validation of Tangential Flow Filtration in Biopharmaceutical Applications, PDA Technical Report No. 15, Bethesda, MD, 1992.
- [36] Peters, M., Timmerhaus, K. D. *Plant Design and Economics for Chemical Engineers*, 2nd edn.; McGraw-Hill: New York, 1968.
- [37] Pujar, N. S., Zydney, A. L. *J. Chromatogr. A* **1998**, *796*, 229–238.
- [38] Rautenbach, R., Albrecht, R. *Membrane Processes*; Wiley: New York, 1989.
- [39] Saksena, S. Protein Transport in Selective Membrane Filtration. PhD Thesis, University of Delaware, 1995.
- [40] Schlichting, H. *Boundary Layer Theory*, 6th edn.; McGraw-Hill: New York, 1968; pp 93–99.
- [41] Schwinge, J., Wiley, D. E., Fletcher, D. F. *Ind. Eng. Chem. Res.* **2002**, *41*, 4879–4888.
- [42] Smith, K. A., Colton, C. K., Merrill, E. W., Evans, L. B. *Chem. Eng. Prog. Symp. Ser.* **1968**, *64*, 45.
- [43] Staverman, A. J. *Rec. Trav. Chim.* **1951**, *70*, 344.
- [44] Tkacik, G., Michaels, S. *Biotechnology* **1991**, *9*, 941–946.
- [45] USPHS, *3A Sanitary Standards for Crossflow Membrane Modules*, No. 45-00, 1990.
- [46] Van Dyke, M. *An Album of Fluid Motion*; Parabolic Press: Stanford, CA, 1982.
- [47] van Reis, R., Goodrich, E. M., Yson, C. L., Frautschy, L. N., Dzengeleski, S., Lutz, H. *Biotechnol. Bioeng.* **1997**, *55*, 737–746.
- [48] van Reis, R., Goodrich, E. M., Yson, C. L., Frautschy, L. N., Whiteley, R., Zydney, A. L. *J. Membr. Sci.* **1997**, *130*, 123–140.
- [49] van Reis, R., Gadam, S., Frautschy, L. N., et al. *Biotechnol. Bioeng.* **1997**, *56*, 71–82.
- [50] van Reis, R., Brake, J. M., Charkoudian, J., Burns, D. B., Zydney, A. L. *J. Membr. Sci.* **1999**, *159*, 133–142.
- [51] Vigo, F., Uliana, C., Ravina, E. *Sep. Sci. Tech.* **1990**, *25*, 63.
- [52] Vilker, V. L. C., Colton, C. K., Smith, K. A., Green, D. L. *J. Membr. Sci.* **1984**, *20*, 63–77.
- [53] Vilker, V. L., Colton, C. K., Smith, K. A. *AIChE J.* **1984**, *27*, 632–637.
- [54] Virkar, P. D., Narendranathan, T. J., Hoare, M., Dunnill, P. *Biotechnol. Bioeng.* **1981**, *23*, 425–429.
- [55] Winzeler, H. B., Belfort, G. *J. Membr. Sci.* **1993**, *80*, 35.
- [56] Zeman, L. J., Zydney, A. L. *Microfiltration and Ultrafiltration: Principles and Applications*; Marcel Dekker: New York, 1996.
- [57] Zydney, A. L. *J. Membr. Sci.* **1992**, *68*, 183.
- [58] Zydney, A. L., Aimar, P., Meirles, M., Pimbley, J. M., Belfort, G. *J. Membr. Sci.* **1994**, *91*, 293.

Biographical Sketch



Herbert Lutz is currently principal consulting engineer in the biopharmaceutical division of Millipore Corporation. His research focuses on the development of pharmaceutical manufacturing processes. His areas of interest include virus clearance, filtration, chromatographic purification, and membrane adsorbers. Previously, Mr. Lutz held strategic marketing, product management, and applications positions at Millipore with responsibilities for product development, marketing, validation, and applications development. Mr. Lutz has developed several new product concepts and brought them to market. He has been at Millipore for 10 years.

Mr. Lutz holds degrees in chemistry and chemical engineering from the University of California, Santa Barbara (UCSB). He attended graduate school in business and chemical engineering at Massachusetts Institute of Technology (MIT). He is a frequent presenter and has assisted in organizing several conferences. He holds a filtration patent, is on the scientific advisory board for Biopharm International, and has published in the areas of scaling, ultrafiltration, membrane adsorbers, depth filtration, and virus clearance. He has authored many journal articles, book chapters, and the membrane separation processes section of Perry's *Chemical Engineering Handbook*. Mr. Lutz has taught membrane applications for Millipore, for the ASME Bioprocess course, and for the Society for Bioprocessing Professionals course.

2.07 Fundamentals of Cross-Flow Microfiltration

R Field, University of Oxford, Oxford, UK

© 2010 Elsevier B.V. All rights reserved.

2.07.1	Introduction	141
2.07.2	Separation Mechanism and Associated Transport Phenomena	143
2.07.3	Modeling Membrane Filtration in the Absence of Fouling	146
2.07.4	Fouling: A Brief Overview	147
2.07.5	Modeling Membrane Filtration in the Presence of Fouling	149
2.07.6	Fouling and Choosing between UF and MF	152
2.07.7	Concluding Remarks	152
References		153

Nomenclature

A	area (m^2)
C	concentration (kg m^{-3})
D	diffusion coefficient ($\text{m}^2 \text{s}^{-1}$)
j	solute flux ($\text{kmol m}^{-2} \text{s}^{-1}$)
J	volumetric flux (m s^{-1})
k	mass transfer coefficient (m s^{-1})
l	length, thickness (m)
p	pressure (Pa)
P	permeability ($\text{L m}^{-2} \text{h}^{-1} \text{bar}^{-1}$)
R	resistance (m^{-1})
t	time (s)
z	z-coordinate, normal to membrane (m)

η	dynamic viscosity (Pa s)
π	osmotic pressure (Pa)
ρ	density (kg m^{-3})
Re	Reynolds number
Sc	Schmidt number
Sh	Sherwood number

Subscripts

con	convective
diff	diffusive
F	feed
i, j	component <i>i</i> or <i>j</i>
M	membrane
P	permeate

2.07.1 Introduction

Before focusing upon the fundamentals of cross-flow microfiltration (MF), some introductory remarks are included on the location of MF within the family of membrane processes, on MF applications, and the nature of MF membranes. After this relevant theory, fouling and fouling mitigation are addressed. In the concluding remarks, some reasons for choosing or not choosing MF are addressed.

The pore diameter of MF membranes ranges from about 0.05 to 5 μm . Since not all pores are of equal size, there is a pore-size distribution and the extent of it can be taken as a measure of the quality of the membrane. MF membranes typically have a pore-size distribution with the mean size being between 0.1 and 1 μm . A conventional definition would quote a range of 0.1–10 μm ; however, nominal sizes greater than 1 μm are now rare. Although the pores are smaller than those found in conventional filtration,

they are larger than those found in ultrafiltration (UF) membranes, whose range is from around 4 to 100 nm. While the latter is a separation process that is used for purifying and concentrating both macromolecular ($10\text{--}10^3$ kDa) solutions and certain suspensions, MF is concerned with purifying liquids containing particulate contaminants or concentrating suspensions such as cell broth. Thus, clean MF membranes permit the passage of ions, small molecules, macromolecules, and viruses.

To place the size range of 0.1 and 1 μm in context, the size decade from 1 to 10 μm includes colloids of electropaint, oil emulsions, blue indigo dye, red blood cells, and many bacteria. Of particular relevance to the water industry are pathogens such as giardia cysts and cryptosporidium oocysts. (The importance of avoiding cryptosporidiosis can be gauged by first noting that the 1993 outbreak in Wisconsin, USA made an estimated 403 000 people ill with 4400 people hospitalized and more

than 100 fatalities [1]. More recently in 2008, in the Anglian water region of the UK, around 250 000 consumers were advised to boil their water after *Cryptosporidium* had been found in a local water reservoir. The need for precautionary action lasted for 10 days.) The *cryptosporidium* oocysts are a spherical organism of 4–6 μm in size and are markedly resistant to chlorine disinfection (at least at practical levels). These may well not be removed by conventional water treatment plants, unless their operation is very carefully monitored because the combination of flocculation, sedimentation, and rapid sand filtration does not contain a physical barrier that filters at the appropriate level. Increasingly membranes are used in drinking water treatment due to the fact that microfilters, rated at 0.2 μm or less, are a very effective barrier.

Membrane manufacturing costs have declined so drastically over the last 15 years such that membrane processes, currently, give cost-effective and sustainable solutions. Furthermore, less monitoring of the process is required. MF is used for wastewater treatment (as part of membrane bioreactors (MBRs)) and for water reuse applications, while UF is used for potable water treatment. However, it is also the case that for electropaint recovery, UF is used in preference to MF; the reasons for this are discussed subsequently.

In addition to the rapidly growing number of membrane plants in the water industry, traditional areas of application for MF include the biotechnology industry and certain areas of the food and beverage industries. It is the ability to guarantee a sterile product at the same time allowing the passage of color, sugar, and taste (e.g., cranberry juice manufacture) or color, taste, and alcohol (e.g., wine manufacture) that is crucial. In the biotechnology industry, the process of MF removes suspended solids from the fermentation broth and the filtrate is a clarified liquid containing, for example, proteins. Very high quality water is required in the microelectronics industry and microporous membranes are an integral part of the associated specialist water production facility.

Membranes are thin permselective barriers that are generally polymeric or ceramic. Microporous glasses such as Shirasu porous glass for emulsification applications and sintered metal tubes such as those from the Mott Corporation have found niche applications. The range of polymers includes polytetrafluoroethylene (PTFE), polypropylene, nylon, polysulfones, and others. **Table 1** lists some of the more important materials, their characteristics, and some applications

of these MF membranes. Ceramic membranes are more resistant to chemical attack and can be used at elevated temperatures. Those made of alpha alumina can have pore sizes of around 100 nm; however, for finer pores, an additional coating of gamma alumina or titania or zirconia is required. Indeed, the French company Tami offers inorganic membranes with pores ranging from 2 nm to 1.4 μm .

Ceramic membranes are typically tubular or multiple channels within a circular cross section. An example of the cross section of a CeraMem membrane is shown in **Figure 1**. Polymeric membrane modules can be in tubular, hollow-fiber, spiral, and flat-sheet membrane configurations and the larger companies offer all four options. The tubular membrane is not so compact and has a relatively higher cost per unit of filtration area installed. It is generally used for viscous and fouling feeds for reasons that are explained when discussing fouling. Some hollow-fiber membranes might be considered to consist of genuine fibers (e.g., 0.6 mm outside diameter or less), while the larger ones (up to 2 mm) have also been described as capillary membranes. These come in two formats, either inside-out or outside-in. For the former, the feed is on the inside and the permeate is on the outside (as with the tubular system), but for certain applications, the reverse is to be preferred.

Flat-sheet membranes may be used either in a flat-and-frame module or in a spiral-wound module. The latter has flat sheets that are formed into envelopes (sealed on three sides and which have a plastic permeate space mesh separating the two sides) with the open side of the envelopes being attached to and wound around a central tube that becomes the permeate collector. The individual envelopes are separated by a plastic mesh of feed spacer material. The feed flows through the gaps of the mesh across the surface of the envelopes. Details of the spiral-wound format are available in company brochures such as those issued by Koch Membrane Systems. These modules are compact and of relatively low cost but prone to fouling.

MF is, as the name indicates, a filtration operation, but some of the membranes that are used for MF can also be used for contacting. For example, the Liqui-Cel Membrane Contactors are used around the world for degassing liquids. In general, hollow fibers made from hydrophobic polypropylene provide a barrier between an aqueous phase and a gaseous phase. Such systems can be used for bubble-less oxygenation as well as for O_2 (or CO_2) removal from water. However, such uses of MF membranes are not discussed in this chapter.

Table 1 Materials, characteristics, and applications of main polymeric microfiltration membranes

<i>Material</i>	<i>Characteristics</i>	<i>Typical applications</i>
Polysulfone (PS)	<ul style="list-style-type: none"> - Hydrophilic membrane - High flow rates - Broad chemical compatibility - High mechanical strength and temperature resistance 	<ul style="list-style-type: none"> Food and beverages Pharmaceuticals Microelectronics Water Serum
Nylon	<ul style="list-style-type: none"> - Hydrophilic membrane - Very high flow rates - Excellent chemical compatibility - High tensile strength - Long life cycle 	<ul style="list-style-type: none"> Microelectronics Water Chemicals Beverages
Polytetrafluoroethylene (PTFE)	<ul style="list-style-type: none"> - Hydrophobic membrane than can be laminated to polypropylene support - Superior chemical resistance - Superior temperature resistance - High durability and strength due to support 	<ul style="list-style-type: none"> Air and gases Pharmaceuticals Aggressive chemicals Microelectronics Water
Acrylic copolymers	<ul style="list-style-type: none"> - Hydrophilic co-polymer membrane with nonwoven polyester fabric support - High flow rates - Low differential pressure 	<ul style="list-style-type: none"> Pharmaceuticals Food and beverage Chemicals Microelectronics Pharmaceuticals
Polypropylene (PP)	<ul style="list-style-type: none"> - Hydrophobic membrane - High flow rates - Broad pH stability - High temperature resistance 	<ul style="list-style-type: none"> Water Chemicals Biotechnology
Polyvinylidene fluoride (PVDF)	<ul style="list-style-type: none"> - Hydrophobic membrane - Superior chemical resistance - Superior temperature resistance - More easily processed than other fluoro-polymers - Relatively low cost 	<ul style="list-style-type: none"> Pharmaceuticals Air pollution Laboratory analysis
Polycarbonate (PC)	<ul style="list-style-type: none"> - Hydrophilic membrane - High flow rate - High mechanical stability - Thermal stability 	<ul style="list-style-type: none"> Air pollution Microbiology Foods Pharmaceuticals
Cellulosic	<ul style="list-style-type: none"> - Hydrophilic membrane - Limited thermal stability - Limited mechanical stability 	

From Merry, A.J. Membrane Equipment and Plant Design. In *Industrial Membrane Separation Technology*; Scott, K., Hughes, R., Eds.; Blackie: London, 1996; Chapter 3, pp. 67–113.

As indicated in **Table 1**, the microporous structure of MF material finds applications in gas filtration as it can provide a reliable, long-lasting barrier that excludes liquid, dust, and other contaminants. Such applications will not be considered further in this chapter. The emphasis is on fundamentals that are applicable to liquid-phase applications, such as cell broth concentration, beer filtration, and water purification.

2.07.2 Separation Mechanism and Associated Transport Phenomena

The membrane flux during the filtration of a feed containing solutes and/or particles can be reduced

below that of the corresponding pure water flux (or more generally pure solvent flux) for two reasons: either the driving force across the membrane is less than the transmembrane pressure (TMP) due to osmotic effects or the resistance to fluid flow is greater than the membrane resistance due to extra resistances. In an analogy with electrical current, where the flow of current is given by Ohm's law, $I = V/R$, the current, I , will be reduced if either V is reduced or R is increased.

To understand the reason for a possible reduction in the driving force, it is necessary to understand concentration polarization. This is a natural consequence of the selectivity of a membrane. Particles or solutes that do not pass through a membrane accumulate next to the membrane in a region known as

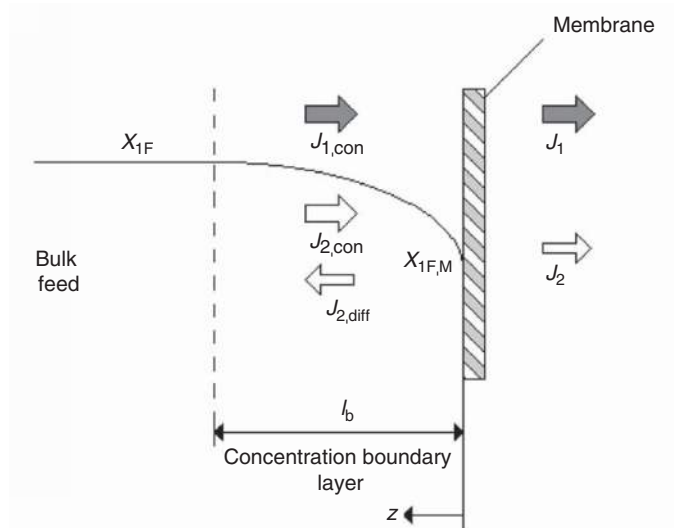


Figure 1 Concentration polarization.

the mass transfer boundary layer. It is relatively thin; the actual thickness depends upon the fluid flow conditions adjacent to the membrane surface. Dissolved molecules accumulating at the surface reduce the solvent activity, which generates an osmotic pressure that reduces the solvent flow through the membrane. This can be represented as a reduction in the effective TMP driving force due to an osmotic pressure difference between the filtrate and the feed solution adjacent to the membrane surface. This phenomenon is inevitable, but is reversible with an elimination of TMP and hence flux. While this effect is generally more important in reverse osmosis and UF, it should be considered in all pressure-driven processes and so a formal derivation of the equations is given.

Consider that the minor component is rejected (e.g., proteins in UF or oil droplets in MF; see [Figure 1](#)). Then the minor component will be of higher concentration in the boundary layer; it is a natural consequence of membrane selectivity and should not be considered as a form of fouling. The resulting higher concentration of the rejected components leads to diffusion of this material back into the bulk. The extent of accumulation in the mass transfer boundary layer and the thinness of it can be estimated using the expressions that will be derived.

Component 1 is not rejected but component 2 is. Now under steady-state conditions the relevant fluxes (in $\text{kmol m}^{-2} \text{s}^{-1}$) are

Component 1:

$$j_{1,\text{con}} = j_1 \quad (1)$$

Component 2:

$$j_{2,\text{con}} = j_{2,\text{diff}} + j_2 \quad (2)$$

Component 2 has a back-diffusion term but component 1, which can be considered to be the solvent, does not. Initially, consideration is given to the dissolved material as this can affect the driving force through osmotic pressure. The following assumptions, which are more precise for dissolved material than they are for particles, allow one to make a mass balance on the feed side of the membrane: consider that

- the behavior is at steady state,
- the diffusion is Fickian (i.e., flux is proportional to concentration gradient),
- there is no chemical reaction,
- the concentration gradient parallel to the membrane is negligible,
- the density is constant; and
- the diffusion coefficient is independent of solute concentration.

Thus, for a general component i ,

$$\mathcal{J} \cdot C_i = \mathcal{J} \cdot C_{i,P} - D_{ji} \frac{dC_i}{dz} \quad (3)$$

where \mathcal{J} is the volumetric flux through the membrane.

Integration of Equation (3) taking the following boundary conditions into account,

$$C_i = C_{i,M}(z = 0)$$

$$C_i = C_{i,b}(z = l_{bl})$$

yields

$$\mathcal{F} = \left(\frac{D_{ji}}{l_{bl}} \right) \cdot \ln \left(\frac{C_{i,M} - C_{i,P}}{C_{i,b} - C_{i,P}} \right) \quad (4)$$

The subscripts M and P refer to the membrane surface and the permeate, respectively, and l_{bl} is the thickness of the mass transfer boundary layer.

From the above equation it can be seen that for every component i , the concentration at the surface is exponentially related to flux:

$$C_{i,M} = (C_{i,b} - C_{i,P}) \cdot \exp \left(\mathcal{F} \cdot \frac{l_{bl}}{D_{ji}} \right) \quad (5)$$

In Equations (4) and (5) the term (D_{ji}/l_{bl}) can be described as a mass transfer coefficient $k_{i,b}$. The mass transfer boundary layer is also referred to as the concentration polarization layer as the average concentration within this layer is significantly higher, due to the exponential relationship (5) than in the bulk. As there is a distinct difference between the two regions, polarization is said to have occurred.

Now for macromolecules (and this may seem surprising), the concentration at the membrane surface, $C_{i,M}$, has been found to be approximately constant and a plot of flux, \mathcal{F} , versus $\ln(C_{i,b})$ is often found to give a straight line of negative slope with an intercept that is taken to be $\ln(C_{i,M})$. However, for particles, the relationship between flux, \mathcal{F} , and the concentration in the feed, $C_{i,b}$, is different because the assumption of Fickian diffusion cannot be made. Indeed, if the diffusion of particles is estimated from the Stokes–Einstein relationship (which shows that for isolated particles the diffusion coefficient is inversely proportional to the particle diameter) then there is a great underestimation of the flux. In a seminal paper [2], this flux paradox was reviewed. The importance of shear gradients and shear forces was highlighted. The former can cause lateral migration; however, as discussed in several papers (e.g., Reference 3), shear-induced diffusion is generally the dominant effect. Both effects increase with increasing particle size and are important for feeds with particulates.

Returning to concentration polarization in general, it is noted that the relationships between mass transfer, fluid flow, and physical properties are given

by equations involving $Sb = kd/D$, $Re = \rho vd/\mu$, and $Sc = \mu/(\rho D)$. Relationships are readily found for a number of geometries and depend upon whether the flow is laminar or turbulent. For turbulent flow through a tube,

$$Sb = 0.023Re^{0.8}Sc^{0.33} \quad (6)$$

The other potentially important dimensionless group is the boundary layer Peclet number ($=\mathcal{F}/k$). It is certainly important for membrane processes, such as MF, where the feed stream is liquid. In the case of gas-phase feeds, the polarization effect is far less important due to the larger (about 10^5 higher) diffusion coefficient in gas phases compared to liquid phases. In addition, the fluxes are smaller, so \mathcal{F}/k is orders of magnitude smaller. In passing, it was mentioned that the mass transfer boundary layer is thin; its thickness is given by $D_{ji}/k_{i,b}$. When D_{ji} is simply small, the boundary layer is thin; but for macromolecules, D_{ji} is very small and the boundary layer is very thin. The resulting highly localized high concentrations are relevant to fouling in UF and MF systems.

Now fouling, that is, a buildup of material (e.g., adsorbed macromolecules, gels, or deposited particles on or in the membrane surface), is not caused by concentration polarization but it is exacerbated by it. Now the nondissolved material that is deposited either on the membrane surface (or on layers that are already adhering to the membrane surface), or in the pore mouths or on pore walls, may take the following forms:

- *Adsorption.* This occurs when specific interaction between the membrane and the solute or particles exists. A monolayer of particles and solutes can form even in the absence of permeation flux, leading to an additional hydraulic resistance. If the degree of adsorption is concentration dependent then concentration polarization exacerbates the amount of adsorption.
- *Pore blockage.* When filtering, pore blockage can occur leading to a reduction in flux due to the closure (or partial closure) of pores.
- *Deposition.* A deposit of particles can grow layer by layer at the membrane surface, leading to an important additional hydraulic resistance. This is often referred to as a cake resistance.
- For certain macromolecules, the level of concentration polarization may lead to gel formation in the immediate vicinity of the membrane surface, for example, a solution of concentrated proteins.

Our attention is restricted to porous membranes and to understand the fundamentals of fouling an appreciation of transport to the membrane surface and the physical laws that govern transport through the membrane will be developed, and an appropriate model given. Fouling leads to an increase in resistance giving less flux for a given TMP difference or a higher TMP if flux is kept invariant by, for example, using a metering pump to maintain a fixed permeate flow rate. Understanding the other resistances is important and it is imperative to distinguish a reduction in driving force across the membrane (which is the effect of concentration polarization) from an increase in resistance due to fouling of the membrane. Therefore, the concept of concentration polarization was introduced with care. This is now used to develop a model for transport in the absence of fouling. This subsequently allows one to place the terms which are due to fouling in context.

2.07.3 Modeling Membrane Filtration in the Absence of Fouling

The basic mechanism of both MF and UF is the sieving mechanism, with rejection of molecules whose size is greater than that of the pores. Furthermore, since both processes use porous membranes, the pore flow model can, in principle, be applied if allowance is made for fouling and concentration polarization.

Darcy's law, which states that flux is proportional to applied pressure difference, can generally be used to describe the flux through an unfouled membrane:

$$\mathcal{J} = P \cdot (p_F - p_P) = P \cdot \Delta p \quad (7)$$

where \mathcal{J} is the volumetric flux and Δp is the TMP. This assumes that osmotic effects are absent. While this might be so, particularly for MF, it is best to allow for the feat that they might be present.

The permeability constant P is a function of membrane structure, including pore-size distribution and porosity of the membrane, as well as viscosity of the permeate. To describe P two approaches are commonly used. When the membrane can be compared to an arrangement of near-spherical particles (as is the case in ceramic membranes), it is possible to apply the Carman–Kozeny equation. However, a different method is required for the majority of membranes.

When the structure of the membrane can be assumed to be uniform capillaries (which is the case

for track-etched membranes), the appropriate approach is to use the Hagen–Poiselle equation. The flux can then be described by

$$\mathcal{J} = \frac{\varepsilon \cdot d_{\text{pore}}^2}{32 \cdot \eta \cdot \tau} \cdot \frac{\Delta p}{l_{\text{pore}}} \quad (8)$$

where τ is the tortuosity of the capillaries and d_{pore} is the diameter of the capillaries. The flux is inversely proportional to the viscosity of the permeate.

In general, the driving force that exists between the bulk feed on one side and that on the permeate side (i.e., $p_F - p_P$) will be reduced by the osmotic pressure difference that occurs due to solute rejection. The term $\Delta p - \Delta \pi$ represents the driving force across the membrane itself. The inclusion of the dynamic viscosity of the permeate, η , as a separate term (as opposed to its inclusion within R_m) is to be preferred. The separate term R_m is then a constant for a given structure.

The flux through most unfouled membranes cannot be described by the above-mentioned idealized equations as these structures do not conform to either of the two idealized forms. In addition, if a solute is present, there will be concentration polarization. Instead, the following equation is used to describe the flux in the absence of any fouling. The inclusion of the dynamic viscosity of the permeate, η , makes due allowance for temperature changes because temperature affects this physical property and little else:

$$\mathcal{J} = \frac{\Delta p - \Delta \pi}{\eta R_m} \quad (9)$$

where R_m is the empirically measured membrane resistance and the term $\Delta \pi$ is zero if the feed is a pure solvent.

If the solute is completely rejected, Equation (4) will link flux and C_{iM} (provided bulk concentration, C_{ib} , and mass transfer coefficient, k_{ib} , are known), while Equation (9) links flux, Δp and $\Delta \pi$ (provided the membrane resistance and permeate viscosity are known). The relationship between solute osmotic pressure and concentration can be expressed by

$$\pi = aC + bC^2 + dC^3 \quad (10)$$

Equation (10) enables one to relate $\Delta \pi$ to C_{iM} ; it is an excellent approximation to make π (at M) = $\Delta \pi$. Sufficient information is now available to plot flux as a function of TMP with the values of $\Delta \pi$ and C_{iM} also being noted.

In MF systems that involve both particles (or cells) and macromolecules (which might well be

extracellular material), it is desirable to estimate any osmotic effects in order to determine whether the effective driving force is being reduced.

2.07.4 Fouling: A Brief Overview

Fouling has sometimes been seen as a reduction in the active area of the membrane, which therefore leads to a reduction in flux below the theoretical capacity of the membrane for the given driving force but it is not necessarily a reduction in available area for permeate flow. If the pores are partially blocked or restricted, this is true; however, a cake layer on the surface of a membrane is a resistance that is in series with the membrane resistance. The various modes of fouling are discussed in the Section 2.07.6. Fouling during filtration clearly has a negative influence on the economics of any membrane process and so it must be understood and counter-measures must be adopted to mitigate the effects. For MF, the fouling can be very severe with the process flux often being less than 5% of the pure water flux, therefore necessitating more membrane area for a given duty. In addition, fouling and subsequent cleaning shorten the life of membranes, leading to membrane replacement expenditure.

Generally, four types of foulants have been distinguished: (1) organic precipitates (macromolecules, biological substances, etc.); (2) colloids; (3) inorganic precipitates (metal hydroxides, calcium salts, etc.); and (4) particulates. A more comprehensive list is given in **Table 2**, the last entry being biofilms. Now for certain applications, the problem is not one of foulants in the feed but biofilms that form from the

constituents in the feed. This is particularly important in water applications. The influence of all of these foulants is made adverse by the effect of concentration polarization; as noted earlier, the surface concentration is expected to increase exponentially with flux (Equation (5)). Thus, lower fluxes will give less fouling, with the effect being nonlinear. Furthermore, this equation indicates that improved mass transfer will also lead to lower surface concentrations, which is why hydrodynamics of the membrane module are important. A higher cross-flow velocity will improve mass transfer and reduce fouling. It can now be understood why tubular membranes are suitable for fouling feeds. The velocities can be relatively high and this, together with the larger dimensions, leads to Reynolds numbers in the turbulent region. In the turbulent region, mass transfer coefficients are about an order of magnitude greater than in the laminar regime.

To the mass balance equation (3), one can add, when appropriate, an electrostatic term and a hydrodynamic term. Such terms are often important. In general, one can view the net flux of material toward the membrane as being a combination of fluxes, some of which tend to move material away from the membrane surface, while others, including the convective flux, move material toward the surface. The overall material flux, N , is given by

$$N = \mathcal{F}C - D \frac{dC}{dz} + p(\zeta) + q(\tau) \quad (11)$$

where D is the Brownian diffusion coefficient, $p(\zeta)$ represents the term for migration of the solutes/particles due to interactions between the membrane surface and the surfaces of the solutes/particles, and

Table 2 Examples of foulants and fouling modes in membrane processes

<i>Foulants</i>	<i>Fouling mode</i>
Large suspended particles	Particles present in the original feed (or developed due to concentration polarization) can block module channels as well as forming a cake layer on the surface.
Small colloidal particles	Colloidal particles can create a fouling layer (e.g., ferric hydroxide from brackish water can become a slimy brown fouling layer). In recovery of cells from fermentation broth, some colloids can be present.
Macromolecules	Gel or cake formation on membrane. Macromolecular fouling within the structure of porous membranes.
Small molecules	Some small organic molecules tend to have strong interactions with some polymeric membranes (e.g., anti-foaming agents, such as polypropylene glycols used during fermentation, adhere strongly to certain polymeric membranes).
Proteins	Interactions with surface or pores of membranes.
Chemical reactions leading to scaling	Concentration increase and pH changes can lead to precipitation of salts and hydroxides.
Biological	Growth of bacteria on the membrane surface and excretion of extracellular polymers.

Modified from Scott, K. *Handbook of Industrial Membranes*, Elsevier: Oxford, 1995.

$q(\zeta)$ represents the effect of the local hydrodynamics on the mass flux. The possible settlement of non-buoyant particles onto the membrane surface has not been included. Now, as discussed elsewhere [4], $p(\zeta)$ can be positive in the case of electrostatic attraction, which corresponds to adsorption of the solute onto the membrane, whereas a negative $p(\zeta)$ corresponds to repulsion. The consequences of this have been developed by several authors [5, 6]. The particle–membrane repulsion is efficient as long as the migration induced exceeds the magnitude of the migration due to the convective flux. This is the case for UF plants treating electro-dip coat paints and may be important in certain applications of MF to oil–water separation.

The term $q(\zeta)$ represents the effect of the local hydrodynamics on the material flux. It depends, but not exclusively, on the shear forces. The term includes migrations (e.g. lateral migration) and diffusive effects, which necessitate concentration gradients. The latter encompass turbulent diffusion and shear-induced diffusion. These effects have been discussed extensively in a review [2] and several papers (e.g., Reference 3).

While theory can be a guide, help to interpret results, the sizing of plants depends crucially upon laboratory and pilot plant data as there are several interacting parameters that influence the fouling rate. These include the membrane type, its pore-size distribution, its surface characteristics, and the nature and concentration of the solutes at the membrane surface. The latter depends upon the hydrodynamic characteristics of the membrane module and the chosen feed velocity.

So far we have mentioned fouling as adversely affecting the hydraulics (decreasing flux (for fixed TMP) or increasing TMP (for a given flux)), but the changing of the effective pore-size distribution will also cause operating problems if transmission of certain solutes is desired. This is the case in beer filtration, where retention of cells but the passing of proteins is essential. Therefore, in the analysis of membrane performance one must remember that it is a separating device.

For MF, it is useful to divide the methods to reduce fouling into direct and indirect methods. Some of the direct methods, such as the use of turbulence, are clearly similar to the measures taken to reduce the intensity of a concentration boundary layer. These methods include turbulence promoters (e.g., modified membrane spacers), rotating or vibrating membranes, and pulsed flow. In the 1990s, the

New Logic Vibratory Shear Enhanced Processing (VSEP) system emerged as an exciting alternative, especially for feeds with high solid levels. While the feed slurry is pumped slowly between parallel membrane leaf elements, a high shear is created by a vigorous vibration of these elements in a direction tangential to the membrane surfaces. The shear waves produced by the membrane's vibration induce solids and foulants to be lifted off the membrane surface and remixed with the bulk feed. The high shear processing allows the membrane to operate closer to the clean water flux. The manufacturer states that the throughput is typically between 3 and 10 times the throughput of conventional cross-flow systems [8].

Included within the indirect methods is the selection of appropriate operating mode. This encompasses the choice of whether one is choosing cross-flow or dead-end (direct) filtration with periodic backflush. For a highly fouling feed, the former is essential, but for drinking water filtration the latter is now the norm because it can be made to work at drastically reduced energy costs compared with traditional cross-flow membrane filtration. Other indirect methods include pretreatment of feed or pretreatment of membrane. In both the cases, the aim is to prevent unwanted adsorption.

One can also mention cleaning in the context of fouling-prevention measures. This may seem strange but regular intermittent cleaning (e.g., chemically enhanced backwash) can reduce the need for major cleaning-in-place procedures. It is suggested that in many industries, the cleaning procedures might be viewed as consisting of two types: those, which are for regular maintenance, and those that are for recovery. Therefore, well-adapted maintenance cleans prevent the need for excessive recovery cleans.

Figure 2 illustrates the approach of flushing to remove cake layers on the feed side and, therefore, reduce the influence of fouling. It is carried out by reversing the flow of the permeate through the membrane. This can dislodge some of the foulants, particularly particulates, and reestablishes the flux at a high level. In order to maintain a high overall flux, backflushing is carried out periodically and requires module types and membranes that can withstand the reverse flow. It is an essential operation in dead-end-operated UF and MF systems. Backflushing with the inclusion of a low concentration of cleaning chemicals, such as parts per million (ppm) levels of chlorine, is labeled a chemically

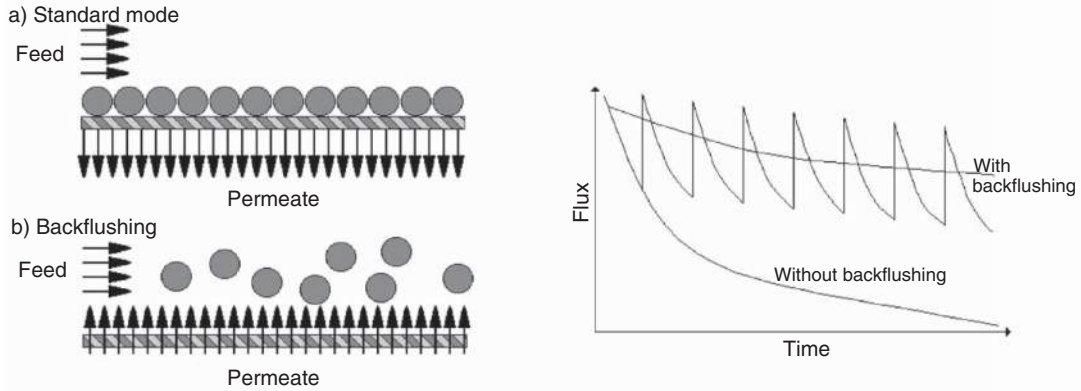


Figure 2 Backflushing: concept and anticipated outcome.

enhanced backwash. These backwashes can clean the membrane pores.

From this brief introduction to prevention and reduction of fouling one can see that a variety of approaches have been developed. While prevention is the aim, and this can sometimes be achieved on the laboratory scale with well-defined feeds, the reality is that the objective is one of reduction. For new applications, pilot plant tests to establish the extent of fouling rates and the efficacy of cleaning methods are essential.

2.07.5 Modeling Membrane Filtration in the Presence of Fouling

Now that a sound basis has been provided, additional terms can be added to account for the hydraulic resistance that is due to material accumulation on the membrane surface and/or in the membrane pores. There is interest in (1) the relationship between flux and TMP and (2) the relationship between flux and time. Whether the fouling is on the membrane surface or in the pores will affect the relationships. At this stage, a three-fold division of the overall fouling resistance is introduced. These resistances can be considered to be in series with the membrane resistance. Hence,

$$\mathcal{J} = \frac{\Delta P - \Delta \pi}{\mu(R_m + R_{ads} + R_{rev} + R_{irrev})} \quad (12)$$

The first of the additional hydraulic resistances, R_{ads} , is for the resistance due to surface or pore adsorption that occurs independently of flux. This

is measured by contacting the membrane with the feed in the absence of flux (for say a few hours) and then measuring a pure solvent flux at a known TMP. This enables the hydraulic resistance of the passively fouled membrane to be calculated and the difference between this resistance and R_m gives R_{ads} . The experiment can be repeated for other contact times.

The other terms reflect the fouling that occurs during operation. The increased resistance that occurs during operation can be divided into a reversible component, R_{rev} (i.e., one that occurs during operation but is not present after switching from the feedback to pure solvent) and an irreversible component, R_{irrev} , that reflects the deposition of material that is only removable (at best) by a cleaning operation.

This classification allows one to distinguish additional resistances (such as adsorption) that are independent of the pressure and permeate flux from fouling phenomena driven by the solvent transfer through the membrane. Fouling of the latter type can be reversible (R_{rev}) or irreversible (R_{irrev}), when the pressure is decreased.

When considering these fouling mechanisms, the strong form of critical flux, \mathcal{J}_{cs} , has been developed to discriminate no fouling conditions (where R_m is the only resistance in Equation (13)) from fouling conditions where other resistances also apply. It has been defined [9] as the flux at which the flux-TMP curve starts to deviate from linearity (Figure 3). So with the assumption that osmotic pressure effects are negligible

$$\text{for } \mathcal{J} < \mathcal{J}_{cs}: \quad \mathcal{J} = \frac{\Delta P}{\mu R_m} \quad (13)$$

$$\text{for } \mathcal{J} > \mathcal{J}_{cs}: \quad \mathcal{J} = \frac{\Delta P}{\mu(R_m + (R_{rev} + R_{irrev}))}$$

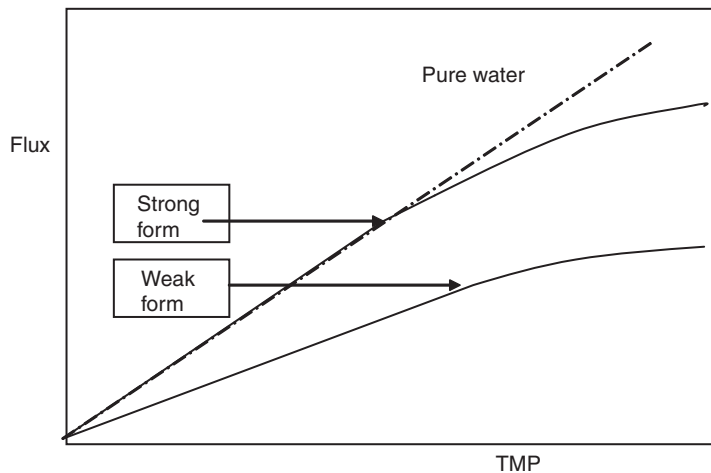


Figure 3 Forms of critical flux as originally defined by Field *et al.* [9].

where at least one of R_{rev} 's or R_{irrev} 's is nonzero and when R_{ads} is considered as negligible.

For UF, the flux through the membrane can ideally be described in analogy to MF, with allowance for osmotic effects due to concentration polarization. This yields a pair of equations:

$$\mathcal{J}_{ideal} = (\Delta p - \Delta \pi) / \mu R_m \quad (14)$$

$$\mathcal{J}_{actual} = \frac{\Delta p - \Delta \pi}{\mu(R_m + R_f)} \quad (15)$$

where the ideal may apply at sufficiently low fluxes. The simplest definition of critical flux is the flux at which fouling is first observed for a given feed concentration and given cross-flow velocity. It should be a design consideration for all pressure-driven processes.

For an advanced discussion of how the concept of critical flux has developed, the reader is referred to Bacchin *et al.* [4].

If there is operation at constant TMP, then Equation (15) shows that increasing of R_f with time will lead to flux decline. Typically, there is an initially rapid decrease followed by a longer more gradual decline, followed in many cases by a steady state being reached. As discussed later, the flux of solutes and particles toward the membrane surface reduces as the volumetric flux decreases. Thus, the accumulation will cease when there is a balance between flux of solids in and removal away. With the accumulation completed, the volumetric flux through the membrane will be steady unless reduced by adverse changes in the accumulated material. In all cases, operation at a high

initial flux is to be avoided as it leads to an excessive flux of foulants toward the membrane surface.

If instead of operation at constant TMP, there is operation at constant flux, then fouling leads to increases in TMP. If the fouling rate is low, this mode of operation has much to commend it. With a constant flux, the rate of TMP increase is generally either linear or concave upwards. In **Figure 4**, the straight line after 15 min is indicative of cake formation on top of the membrane; the slightly higher slope before that time reflects the fact that the initial layers of cells partially blocked the membrane and so had a greater effect per unit mass of yeast cells convected to the membrane surface. The figure also illustrates the distinction between the reversible component of fouling, R_{rev} , that is, one that is readily removed after switching from the feed to buffer (the presence of salts in the buffer is irrelevant) and an irreversible component, R_{irrev} , which reflects the deposition of material that is only removable (at best) by a cleaning operation.

Being able to clearly distinguish between these various types of fouling and understanding how their magnitudes relate to TMP and various operating conditions are important. The subsequent discussion is highly idealized but identification of the fouling mode does aid interpretation of the fouling phenomena.

As shown in **Figure 5**, there are four fouling mechanisms for porous membranes [11]: (1) complete pore blocking; (2) internal pore blocking; (3) partial pore blocking; and (4) cake filtration.

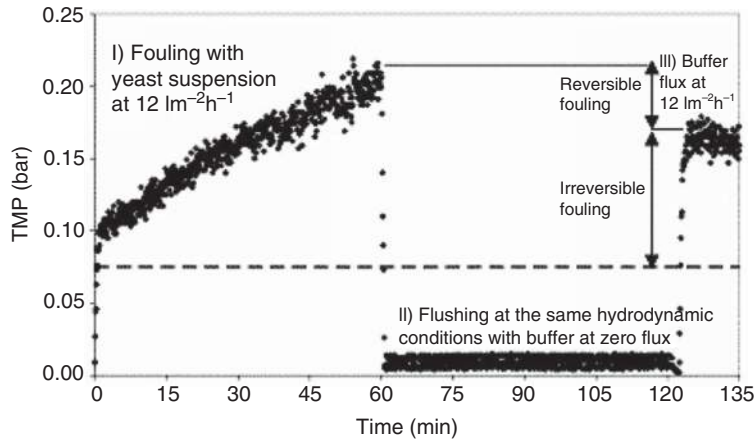


Figure 4 Example of operation at constant flux showing slightly higher fouling rate in the first 15 min compared with post 15 min. The level of irreversible fouling is shown to be greater than that of reversible fouling [10].

Hermia's [11] original unifying equation took the following form:

$$\frac{d^2 t}{dV^2} = k \left(\frac{dt}{dV} \right)^n \quad (16)$$

One may find it strange that the time of filtration is differentiated with respect to the volume of filtrate collected per unit area, but this is the mathematical form that emerges if the focus is upon volume of filtrate collected. For those with a focus upon membrane operations, flux and flux decline are the normal foci and then the above equation takes the simple form:

$$\frac{d\mathcal{F}}{dt} = -k\mathcal{F}^{3-n} \quad (17)$$

In this form, one aspect of the index n becomes immediately clear; the smaller the value of n , the greater the decrease in the magnitude of the rate of flux decline. As \mathcal{F} decreases, the term \mathcal{F}^{3-n} becomes

smaller more rapidly the greater the value of the index.

For $n=2$, particles larger than the pore size, or almost exactly the same size, completely block the pores. In the absence of any removal term, the flux-time equation is

$$\mathcal{F} = \mathcal{F}_0 \cdot K_b \cdot A \cdot t \quad (18)$$

For $n=1.5$, particles smaller than pore size enter the pores and get either adsorbed or deposited onto the pore walls. This restricts the flow of permeate by effectively making the pores smaller. Now $n=0$ represents the formation of a cake on the membrane surface by particles, which neither enter the pores nor seal the pores. The incomplete pore-blocking mechanism ($n=1$) has particles reaching the surface where they may seal a pore or bridge a pore or adhere to inactive regions. Due to the latter possibility, the effect is not as strong. Hermia [11] gives derivations for the mathematical

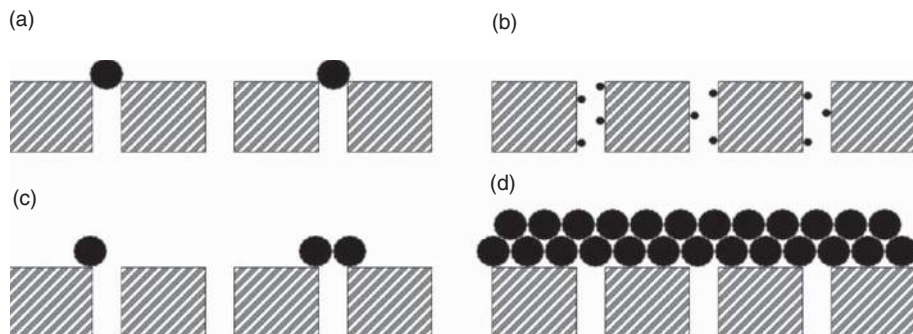


Figure 5 Fouling mechanisms of porous membranes: (a) complete pore blocking; (b) internal pore blocking; (c) partial pore blocking; and (d) cake filtration.

relationships. Those mathematically inclined might like to note that for $n \neq 2$, the following equation can, in the absence of any cross-flow effect, be used to describe the influence of fouling on the flux through the membrane [12]:

$$\mathcal{J} = \mathcal{J}_0 \left(1 + k(2-n)(A \cdot \mathcal{J}_0)^{(2-n)} t \right)^{\frac{1}{n-2}} \quad (19)$$

It must be noted that Equations (18) and (19) include no allowance for cross flow, which can be expected to influence three of the four modes. The exception is internal pore blocking. A more sophisticated approach was developed in the 1990s with allowance for cross flow [9]. Equation (17) is modified to allow for backflux; it then becomes

$$\frac{d\mathcal{J}}{dt} = -k(\mathcal{J} - \mathcal{J}_{ss})\mathcal{J}^{2-n} \quad (20)$$

where \mathcal{J}_{ss} is the steady-state flux reached at long times.

In the presence of cross flow, the flux at long times generally approaches a nonzero value. If a cake has been formed, then the value of \mathcal{J}_{ss} will correspond to the critical flux for cake formation under the specific process conditions (concentration, cross-flow velocity, etc.) for the system under consideration. The integrated forms of Equation (20) can be found in the appendix of Reference 8 for values of n equal to 2, 1, and 0.

2.07.6 Fouling and Choosing between UF and MF

Internal pore blocking is a particularly serious mode of fouling because it is exempt from the mediating effects of cross flow and cleaning may be more difficult. Thus, the correct choice of pore size is very important. One of the reasons for modeling fouling is to determine whether the flux decline is due to internal pore blocking, that is, whether $n = 1.5$ or not. By making this determination, an understanding of why one membrane is performing better than another can be developed. Sometimes a larger pore size gives a higher initial flux (as expected) but an unexpected lower flux than a smaller-pore-sized membrane. This is typical for the MF of cell broth, where $0.2 \mu\text{m}$ is often to be preferred to $0.5 \mu\text{m}$; in many biotechnological applications, the latter size often suffers from excessive internal pore blocking.

An early success for membrane processes, during the 1970s, was the recovery of paint particles from

the washing stage that follows the dip-coat painting/priming of car bodies or the painting of household appliances. Now it might be thought that colloidal paint can be recovered by an MF process but the reported size range is $0.01\text{--}1 \mu\text{m}$ and the former dimension corresponds to UF and, in particular, to a nominal molecular weight cutoff of 50 000 Da.

Two extensively expanding applications for membranes are drinking water filtration and wastewater treatment. While the former principally involves UF, the latter relates particularly to aerobic MBRs. These systems give a combination of biological treatment with excellent filtration that excludes bacteria and viruses from the permeate, which is water of sufficient quality for reuse. With aeration in MBRs providing decent shear at membrane surfaces, the critical flux hypothesis suggests that it is worth exploring whether one can operate below it or close to it. Kubota has exploited this idea with their flat-plate system based on MF membranes. While GE does recommend MF membranes for some water applications, their hollow-fiber ZeeWeed system is based on UF membranes.

The literature suggests that the economic flux is a controlled flux in excess of the critical and thus the system is operated with gentle fouling. The strategy for Kubota may be currently similar but some interesting data for a particular water from Ishida *et al.* [13] with the Kubota system reported that one could obtain $0.5 \text{ m}^3 \text{ m}^{-2} \text{ day}^{-1}$ with a steady pressure of 30 kPa, which was subcritical operation. However, as the storm overload condition necessitated operation at higher fluxes/TMPs, there was some fouling under these conditions. With 70 kPa, they initially obtained $1.05 \text{ m}^3 \text{ m}^{-2} \text{ day}^{-1}$ but this declined to $0.94 \text{ m}^3 \text{ m}^{-2} \text{ day}^{-1}$ due to fouling. On returning from super-critical conditions to the original flux, the TMP was initially a third higher than previously but there was some removal of foulants and the flux settled at 35 kPa. The advantages of simple modes of operation are obvious for unmanned systems. In the UK at least the Kubota system seems to be preferred at the small commercial scale and Zenon at the larger commercial scale.

2.07.7 Concluding Remarks

The successful exploitation of MF membranes is very case specific as fouling, cleaning, and process design are inextricably linked to the process application. Process solutions and the range of applications

will continue to evolve. Water is a huge growth area but biopharmaceuticals remain very important. Knowledge of and an ability to analyze fouling will guide design. Membranes are becoming cheaper and so operating plants around the critical/threshold flux maybe practical. Designs with a larger area for a given task also place less stress on the membrane and reduce the environmental impact of frequent chemical cleaning and membrane replacement.

References

- [1] Corso, P., Kramer, M., Blair, K., Addiss, D., Davis, J., Haddix, A. *Emerg. Infect. Dis.* **2003**, 9 (4); 426–431.
- [2] Belfort, G., Davis, R. H., Zydney, A. L. *J. Membr. Sci.* **1994**, 96, 1–58.
- [3] Li, H., Fane, A. G., Coster, H. G. L., Vigneswaran, S. *J. Membr. Sci.* **2000**, 172, 135–147.
- [4] Bacchin, P., Aimar, P., Field, R. W. *J. Membr. Sci.* **2006**, 281, 42–69.
- [5] McDonogh, R. M., Fane, A. G., Fell, C. J. D. *J. Membr. Sci.* **1989**, 43, 69–85.
- [6] Bowen, W. R., Mongruel, A., Williams, P. M. *Chem. Eng. Sci.* **1996**, 51, 4321–4333.
- [7] Scott, K. *Handbook of Industrial Membranes*; Elsevier: Oxford, 1995.
- [8] New Logic Research, Inc. – Technology, <http://www.vsep.com/technology/index.html> (accessed February 2010).
- [9] Field, R. W., Wu, D., Howell, J. A., Gupta, B. B. J. *Membr. Sci.* **1995**, 100, 259–272.
- [10] Hughes, D., Field, R. W. *J. Membr. Sci.* **2006**, 280, 89–98.
- [11] Hermia, J. *Trans. Ind. Chem. Eng.* **1982**, 60, 183–187.
- [12] Field, R. W. Mass Transport and the Design of Membrane Systems. In *Industrial Membrane Separation Technology*; Scott, K., Hughes, R., Eds.; Blackie: London, 1996; Chapter 4, pp 67–113.
- [13] Ishida, H., Yamada, Y., Matsumura, D., Moro, D. Application of submerged membrane filter to activated sludge process. *Proceedings of the ICOM'93*, Heidelberg, Germany, 1993, Abstract. Quoted in Howell, J.A., *J. Membr. Sci.* **1995**, 107, 165–171.
- [14] Merry, A. J. Membrane Equipment and Plant Design. In *Industrial Membrane Separation Technology*; Scott, K., Hughes, R., Eds.; Blackie: London, 1996; Chapter 3, pp. 67–113.

2.08 Polymeric Membranes for Gas Separation

E Favre, Nancy Université, Nancy, France

© 2010 Elsevier B.V. All rights reserved.

2.08.1	Introduction	158
2.08.1.1	Historical Overview	158
2.08.1.2	Overall Framework and Key Parameters	159
2.08.2	Gas Transport Mechanisms in Polymers	160
2.08.2.1	Permeability Concept	160
2.08.2.2	Equilibrium (Solution) Characteristics	163
2.08.2.2.1	Sorption equilibria in rubbery polymers	163
2.08.2.2.2	Sorption equilibria in glassy polymers	166
2.08.2.3	Diffusion in Polymers: Characteristics	166
2.08.2.3.1	General framework	166
2.08.2.3.2	Diffusion in rubbery polymers (elastomers)	167
2.08.2.3.3	Diffusion in glassy polymers	169
2.08.2.4	Influence of Operating Parameters (T, P, C)	169
2.08.2.4.1	Constant vs. variable permeability behavior	169
2.08.2.4.2	Influence of temperature	170
2.08.2.4.3	Predictive approaches	172
2.08.3	Engineering of Gas Permeation Modules	172
2.08.3.1	General Framework: Separation Factor and Trade-Off Curves	172
2.08.3.2	Membrane Module Design: General Framework and Approximate Analytical Solution	174
2.08.3.3	Membrane Module Design: Methodology	177
2.08.3.3.1	Single module design: Surface and energy requirements	180
2.08.3.3.2	Recycling and multi-stage processes	182
2.08.3.4	Membranes, Modules, and Industrial Installations	184
2.08.3.4.1	Membrane and module structures	184
2.08.3.4.2	Feed pretreatment	187
2.08.3.4.3	Industrial module design: From permeability to permeance and effective selectivity	187
2.08.3.4.4	Pressure drop	188
2.08.3.4.5	Nonisothermal permeation conditions	188
2.08.3.4.6	Hydrodynamic dispersion effects	190
2.08.3.4.7	Fiber variation effects	190
2.08.3.4.8	Additional mass transfer resistances	190
2.08.3.4.9	Multi-component effects 1: Coupling of the frame of references	191
2.08.3.4.10	Multi-component effects 2: Flux coupling and plasticization effects	192
2.08.3.4.11	Membrane deformation	193
2.08.4	Industrial Applications	193
2.08.4.1	General Features	193
2.08.4.2	Hydrogen Purification	196
2.08.4.3	Nitrogen from Air	196
2.08.4.4	Carbon Dioxide Removal in the Treatment of Natural Gas	198
2.08.4.5	Volatile Organic Compounds Recovery	199
2.08.4.6	Drying of Gases	201
2.08.4.7	Miscellaneous Applications	201
2.08.4.7.1	Rare gases	201
2.08.4.7.2	Oxygen	202
2.08.4.7.3	High-value chemicals	202
2.08.4.7.4	Isotopes	202

2.08.5	Future Trends and Prospects	202
2.08.5.1	Membrane Materials	203
2.08.5.1.1	Tackling chemical reactivity	203
2.08.5.1.2	Combining adsorbents and polymers: Mixed matrix membranes	204
2.08.5.1.3	Pushing the limits of ultrathin membrane skin layers	205
2.08.5.1.4	Pushing the operation range of gas separation membranes	205
2.08.5.2	Novel Processes	205
2.08.5.2.1	Operation modes and module design	205
2.08.5.3	Novel Driving Forces	207
2.08.6	Conclusions	207
2.08.6.1		208
2.08.6.1.1	Hydrogen production	208
2.08.6.1.2	Greenhouse emissions mitigation	208
2.08.6.1.3	Isomer separations	208
References		208

Glossary

Asymmetric membrane A membrane constituted of two or more structural planes of nonidentical morphologies.

Co-current flow A flow pattern through a membrane module in which the fluids on the upstream and downstream sides of the membrane move parallel to, and in the same direction as, the membrane surface.

Compaction The compression of a structure due to a pressure difference across its thickness.

Completely mixed (perfectly mixed) flow A flow pattern through a membrane module in which the fluids on both the upstream and downstream sides of the membrane are individually well mixed.

Composite membrane A membrane with chemically or structurally distinct layers.

Continuous membrane column A membrane module(s) arranged in a manner to allow operation analogous to that of a distillation column, with each module acting as a stage.

Counter-current flow A flow pattern through a membrane module in which the fluids on the upstream and downstream sides of the membrane move parallel, and in the opposite direction, to the membrane surface.

Cross-flow A flow pattern through a membrane module in which the fluid on the upstream side of the membrane moves parallel to the membrane surface and the fluid on the downstream side of the membrane moves away from the membrane in the direction normal to the membrane surface.

Dense (nonporous) membrane A membrane without detectable pores.

Diffusion The movement of molecules (or particles) from an area of high concentration to an area of low concentration in a given volume down the concentration gradient. It is a spontaneous process and results in a statistical random motion of molecules.

Downstream The side of a membrane from which the permeate emerges.

Elastomeric (rubbery) The state of matter of a polymer when placed in an environment above its glass transition temperature.

Flux The number of moles, the volume, or mass of a specified component *I* passing per unit time through a unit of the membrane surface area normal to the thickness direction.

Glassy The state of matter of a polymer when placed in an environment below its glass transition temperature.

Glass transition temperature The temperature that corresponds to a pseudo-second-order phase transition at which an amorphous solid, such as a glass or a polymer, becomes brittle upon cooling, or soft upon heating.

Homogeneous membrane A membrane with essentially the same structural and transport properties throughout its thickness.

Ideal separation factor (selectivity) A parameter defined as the ratio of the permeability coefficient of component A to that of component B and equal to the separation factor where a perfect vacuum exists at the downstream membrane face.

Isothermal A process in which the temperature of a system remains constant.

Liquid membrane A liquid phase that exists either in a supported or unsupported form serving as a membrane barrier between two phases.

Membrane A structure with lateral dimensions much greater than its thickness, through which mass transfer may occur under a variety of driving forces.

Module A manifold assembly containing one or several membranes to separate streams of feed, permeate and retentate.

Penetrant (permeant) The entity from a phase in contact with one of the membrane surfaces that passes through the membrane.

Permeability (coefficient) A parameter defined as a transport flux per unit transmembrane driving force per unit membrane thickness.

Permeance (pressure normalized flux) The transport flux per unit transmembrane driving force.

Permeate A stream containing penetrants leaving a membrane module.

Pressure ratio A dimensionless parameter defined as the ratio of the total downstream to upstream (or upstream to downstream) pressure in a gas permeation module.

Recovery (relative or ratio) The amount of substance of a component collected in a useful product divided by the amount of substance of that component entering the process (the useful product may be either the retained material, i.e., the retentate, or the permeated material, i.e., the permeate).

Retentate A stream depleted of penetrants which leaves the membrane module without passing through the membrane to the downstream.

Separation factor A ratio of the compositions of components A and B in the permeate relative to the composition ratio of these components in the retentate.

Sorption (partition) coefficient The parameter equal to the equilibrium concentration of a component in a membrane divided by its partial pressure in the external phase in contact with the membrane surface.

Solution-diffusion (sorption-diffusion) A molecular scale process in which the penetrant is sorbed into the upstream membrane face from the external phase, moves by molecular diffusion in the membrane to the downstream face, and leaves through the external phase in contact with the membrane.

Stage cut A parameter defined as the fractional amount of the total feed entering a membrane module passing through the membrane as permeate.

Steady state The state of a system when all state variables are kept constant and no time dependency is observed.

Sweep A nonpermeating stream directed past the downstream membrane face to reduce the downstream permeant concentration.

Upstream The side of a membrane into which penetrants enter from the feed stream.

Nomenclature

<i>a</i>	activity (–)
<i>A</i>	membrane area (m ²)
<i>c</i>	concentration (mol m ⁻³)
<i>d</i>	diameter (m)
<i>D</i>	mutual diffusion coefficient (m ² s ⁻¹)
<i>D^T</i>	thermodynamic diffusion coefficient (m ² s ⁻¹)
<i>E</i>	energy requirement (J mol ⁻¹)
<i>E_A</i>	activation energy (J mol ⁻¹)
<i>f</i>	fugacity (bar)
<i>F</i>	Faraday constant (96 500 C mol ⁻¹)
<i>H</i>	enthalpy (J mol ⁻¹)
<i>J</i>	diffusion flux (mol m ⁻² s ⁻¹)
<i>k</i>	mass transfer coefficient (m s ⁻¹)
<i>L</i>	phenomenological coefficient (mol ² J ⁻¹ m ⁻¹ s ⁻¹)

<i>L</i>	length (m)
<i>N</i>	total flux (mol m ⁻² s ⁻¹)
<i>n</i>	stage number (–)
<i>p'</i>	membrane module upstream side pressure (bar)
<i>p''</i>	membrane module downstream side pressure (bar)
<i>p</i>	pressure (bar)
<i>P</i>	permeability coefficient (Barrer or mol m ⁻¹ s ⁻¹ Pa ⁻¹ (SI))
<i>Q</i>	flow rate (m ³ s ⁻¹)
<i>r</i>	radius (m)
<i>R</i>	recovery ratio (–)
<i>R</i>	perfect gas constant (8.314 J mol ⁻¹ K ⁻¹)
<i>s</i>	nondimensional membrane surface area (–)
<i>S</i>	entropy (J mol ⁻¹ K ⁻¹)

T	temperature (K)
T_B	boiling temperature (K)
T_C	critical temperature (K)
v_i	partial molar volume ($\text{m}^3 \text{mol}^{-1}$)
v_F	fractional free volume (-)
V	volume (m^3)
x_{in}	mole fraction in the feed mixture (-)
x_{out}	mole fraction in the retentate (-)
y	mole fraction in the permeate side (-)
z	membrane thickness (m)

Greek Letters

α	real separation factor (-)
α^*	ideal separation factor (-)
δ	solubility parameter ($\text{J}^{1/2} \text{m}^{3/2}$)
ε	Lennard–Jones parameter (K)
η	isentropic efficiency (-)
η	viscosity (Pa s)
γ	adiabatic gas expansion coefficient (-)
γ	activity coefficient (-)

γ	plasticization coefficient ($\text{m}^3 \text{mol}^{-1}$)
χ	Flory–Huggins polymer solvent interaction parameter (-)
φ	volume fraction (-)
μ	chemical potential (J mol^{-1})
ϕ	electrical potential difference (V)
ψ	pressure ratio (-)
θ	stage cut (-)

Subscripts

c	continuous
d	dispersed
f	free volume
p	polymer
ref	reference state

Superscripts

sat	saturated
T	thermodynamic

2.08.1 Introduction

2.08.1.1 Historical Overview

The first study on the transport of gases through a polymer is often attributed to Graham [1], who, in 1829, observed that a pig bladder became inflated when placed in an atmosphere of carbon dioxide. Two years later, Mitchell reported on the difference in the collapse rate of small rubber balloons when filled with 10 different gases [2]; he correctly associated the high permeation rate of carbon dioxide with its high solubility [3]. Nevertheless, the foundation of modern membrane science can be dated back to 1866, with the publication of a remarkable paper, again by Graham [4]. For the first time, rubber membranes were described as liquid-like, nonporous materials, and the overall gas permeation process was postulated to follow a solution-diffusion mechanism that can be seen as a cornerstone in today's analysis of dense polymer mass transfer phenomena. Additionally, the gas flux was shown to increase with a decrease in membrane thickness; however, the separation selectivity was not affected. Graham also pointed out an increase in the gas permeability and a decrease in the solubility when the temperature was raised. From a practical point of view, Graham also demonstrated the possibility of achieving an oxygen enrichment of air by natural rubber films.

Figure 1 illustrates the apparatus used by Graham for his experiments.

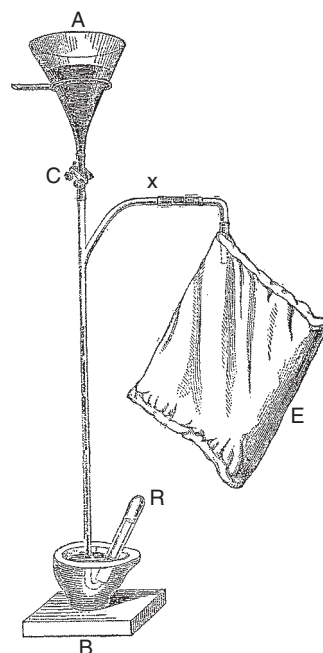


Figure 1 Apparatus used by Graham for his early investigations on gas permeation processes through natural rubber [1]. A-B-C, mercury tube (funnel-mortar-clamp); E, air tight polymer bag; R, gas receiver; X, branch tube.

The first observation of a so-called semipermeable membrane (a name invented by van't Hoff [5]) for gas separations was truly visionary since, as will be shown hereafter, it is nowadays a current industrial application of polymeric membranes.

Nevertheless, it took more than one century for the application envisioned by Graham to become a reality. Indeed, the first large-scale industrial application of polymeric separation membranes started in 1980 with Permea[®] hydrogen separating Prism[®] membranes [6]. Meanwhile, the sole, but nonetheless impressive, use of nonpolymeric membranes for gas separation, namely the isotope separation by microporous metal membranes as part of the Manhattan project, started in 1943 and several very large plants were built worldwide for this unique and very special application.

In fact, in order for polymeric membranes to find applications in industry, several major bottlenecks have had to be overcome. High-flux, defect-free materials, as well as modules with large surface areas were required. In that respect, the development of thin film anisotropic membranes (sometimes called integrally skinned asymmetric membranes), pioneered by Loeb and Sourirajan [7] for reverse-osmosis application in 1961, and the revolutionary concept of resistance composites (or 'caulked' membranes) developed by Henis and Tripodi [8] 20 years later within the Monsanto Company, can be seen as decisive landmarks. More detailed historical perspectives on the development of polymeric membrane materials for gas separation processes have been reported by Lonsdale [9] and Koros [10] and will not be discussed here further.

It can be stated that, due to continuing improvements in materials science, manufacturing, and

process engineering, membrane gas separation processes have been gradually adopted by a large number of industries in a variety of sectors over the past 30 years. The market of polymeric gas separation membranes has recently been estimated [11] to range between \$150 and \$230 million per year, with an annual growth of 15% (i.e., the largest among the various membrane processes [12]). Several thousands of gas separation modules with dense polymeric membranes are currently operated throughout the world and can be roughly divided into four major application fields (Figure 2).

New opportunities for applications, opening additional markets, are expected to emerge in the near future and will be discussed in the last part of this chapter.

Generally speaking, polymeric gas separation membranes have been considered in a wide variety of exhaustive reviews, textbooks [13], and book chapters [14] on topics including materials science aspects [15, 16], scientific challenges, engineering [17], or industrial state of the art [18, 19]. The objective of this chapter is to provide a survey of these various aspects in a condensed and comprehensive form.

The definitions of the terms given in the Glossary section correspond to recommendations [20], also presented in the *Journal of Membrane Science* [21].

2.08.1.2 Overall Framework and Key Parameters

Membranes always occupy a special place in the separations spectrum in that they do not belong to the so-called equilibrium-staged process family, which represents a large majority of industrial

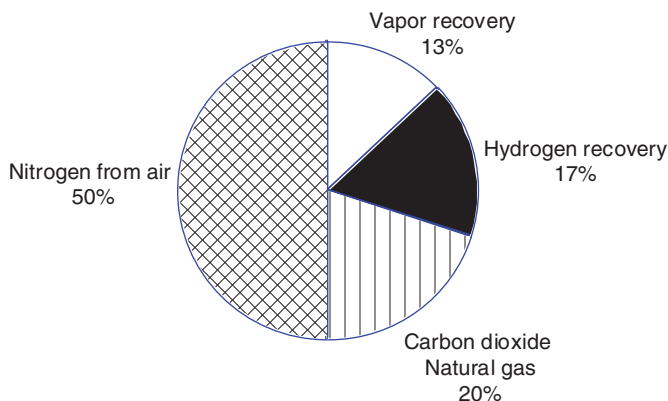


Figure 2 Membrane gas separations: market share in 2000. Modified from Baker R. W. *Ind. Eng. Chem. Res.* **2002**, *41*, 1393–1411.

separation processes (e.g., distillation, absorption, extraction, and adsorption) [22]. Basically, two types of definitions of a membrane operation can be proposed in order to highlight its differences with other separation processes. A membrane separation can first be defined based on a structural view, such as the definition proposed by Hwang and Kammermeyer [23]: “A membrane is a region of discontinuity interposed between two phases.” A different definition has alternatively been proposed by other authors in order to highlight the functional specificities of membrane separation processes: “Any phase that acts as a barrier preventing mass movement but allowing restricted or regulated passage of one or several species through it may be defined as a membrane. This could be a solid or a liquid or even a gas. All membranes are active in an operational sense when used as barriers to separate two solutions or phases unless they are too fragile or too porous” [24].

The key operating principle of a membrane gas separation process indeed demands that a nonequilibrium situation prevails. In what will be developed hereafter, no separation effect occurs at equilibrium, and this represents a fundamental difference when compared to processes based on phase equilibria. From a practical point of view, a difference in partial pressure (or fugacity) of the permeating species between the upstream and downstream sides is a necessity. Such a pressure difference will generate a chemical potential driving force that will induce the permeation of the species through the membrane material. The pressure difference between two compartments separated by a membrane is achieved in a module.

Membrane gas separation is almost systematically operated under a steady-state regime. Moreover, a great number of applications are based on a single stage, a situation that differs considerably from most of the other separation processes for which the stage number is a key issue in the identification of the optimal design. As a result, the general framework of polymeric membrane gas separation units, as shown in **Figure 3**, can, at a first glance, be considered rather simple when compared to other separation processes.

It should however be stressed that, while mass balances can be easily established, an efficient design primarily depends on the precise knowledge of mass transfer expressions as well as on the rigorous description of the conditions (temperature, pressure, composition, velocity, etc.) that prevail in a given

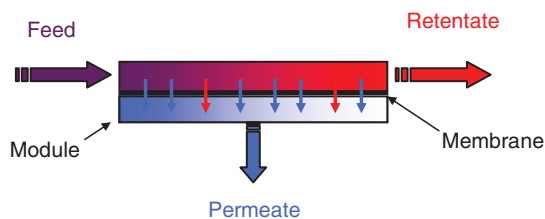


Figure 3 Schematic diagram of a basic membrane gas separation process. The module is usually operated under steady-state conditions and a pressure difference is applied between the upstream and the downstream compartments.

system. In that respect, the detailed analysis of the physical laws governing gas permeability phenomena through dense polymers is of utmost importance. This aspect is developed in the following section.

2.08.2 Gas Transport Mechanisms in Polymers

2.08.2.1 Permeability Concept

The development of rigorous flux computation models is one of the essential targets of mass transfer (field). A crucial prerequisite of mass transfer modeling addresses the driving force issue, which has to be taken into account in order to resolve the problem. The chemical potential μ_i is unanimously considered as the generalized driving force of a given species (i) for mass transfer [25]. This generalized electrochemical potential, introduced by Guggenheim [26], is expressed as

$$\mu_i = \mu_{i,\text{ref}} + RT \ln a_i + \int_{p_{\text{ref}}}^p \bar{v}_i dp - \int_{T_{\text{ref}}}^T S_i dT + z_i F \Phi \quad (1)$$

A chemical potential difference across the membrane is a necessity for penetrant mass transfer to occur. An isothermal process is most often postulated in gas permeation operations, at least for laboratory scale experiments (this point will be discussed later). Moreover, no electrical field is applied in what will be addressed in the following, and based on this, only pressure (p) and concentration (c_i), or, more generally, activity ($a_i = \gamma_i c_i$), can potentially play a role in the variation of the chemical potential. Inside a polymeric gas separation membrane, only three different scenarios can be proposed: (1) a concentration gradient without a pressure gradient, (2) a pressure gradient without a concentration gradient, and

(3) the coexistence of pressure and concentration gradients.

Selecting the correct hypothesis is obviously of prominent importance in order to derive rigorous and efficient mass transfer models. For dense polymers, a great number of studies have, in the 1970s, been reported with this fundamental question as the major issue. It is now commonly admitted that, for dense polymer permeation by gases or liquids, no pressure gradient exists through the membrane, and the pressure inside the membrane is equal to the upstream pressure [27] (Figure 4).

This argument is particularly true for mechanically supported membranes (found in a large majority of situations in laboratory or industry); in this case, on the downstream side of the membrane, the support must indeed exert a pressure that is equal and opposite to that exerted by the gas on the upstream side [28]. Moreover, the existence of a concentration gradient within the membrane has been confirmed by an elegant series of experiments using a stack of rubber membranes [29]. Even though the existence of a pressure gradient inside a dense polymeric membrane is still occasionally proposed for gas [30] or liquid [31] permeation, this option will be excluded in what follows and the celebrated solution-diffusion model can thus be easily derived, based on the situation illustrated in Figure 4. At this stage, single-component permeation is considered for model derivation.

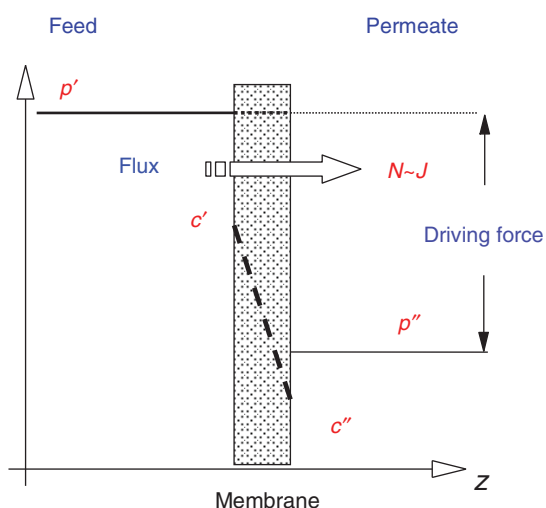


Figure 4 Pictorial view of the steady-state permeation of a pure gaseous species through a dense polymeric membrane.

The derivation of the solution-diffusion model first requires that the hypothesis of local equilibrium conditions on the two sides of the membrane be accepted. From a practical point of view, this assumption corresponds to a much smaller absorption time (upstream side) and desorption time (downstream side) as compared to the intramembrane diffusion time. It is clear that this hypothesis is not necessarily correct for all systems. In fact, it is particularly subject to failure for chemically reacting systems or for extremely thin membrane materials. Chemically reacting systems are employed for liquid membranes where a carrier reacts with one of the penetrant molecules [32], or for hydrogen permeation through metallic membranes. In the latter case, hydrogen dissociates upon adsorption and specific permeation laws have to be employed [33]. For dense polymer permeation however, experimental observations and the comparison of characteristic times for interface equilibrium and diffusional mass transfer demonstrates that the hypothesis of local equilibrium conditions can be considered as valid in a large majority of cases. Since the pressure inside the membrane is constant, and because the system is considered as homogeneous, there exists no direct convection contribution (bulk flow), and the steady-state mass transfer for a fixed reference frame N_i can be written through a strict diffusion mechanism, best expressed by Fick's law:

$$N_i \approx \mathcal{J}_i = -D_i \frac{\partial c_i}{\partial z} \quad (2)$$

It is important to note that the above equation rigorously postulates the occurrence of a counter-diffusion process. For highly swelling membrane, the equation has to be modified in order to take into account the bulk flow contribution resulting from the fact that the polymer is stagnant [34]. This additional term can be disregarded based on the assumption that the amount of sorption of the permeant is negligible (i.e., that the volume fraction of penetrant dissolved in the membrane is $<1\%$). Such a hypothesis is usually considered reasonable in the case of permeation of a pure permeant, but cannot be considered as systematically valid.

The use of an equilibrium relationship between the penetrant pressure (or fugacity) in the gas phase and the corresponding solubility in the polymer can be proposed as

$$c_i = S_i p_i \quad (3)$$

Here, S is the so-called sorption coefficient, which can be experimentally determined or computed from

phase equilibrium considerations. It is more convenient to express the steady-state flux of the penetrant through the membrane with the partial pressure difference, and this can easily be achieved by a combination of the two previous equations. Integration for a membrane of thickness z yields

$$\mathcal{F}_i = \frac{1}{z} \int_{p_i''}^{p_i'} D_i S_i dp_i \quad (4)$$

A mean permeability coefficient can be defined as

$$\bar{P}_i = \frac{1}{p_i' - p_i''} \cdot \int_{p_i''}^{p_i'} D_i S_i dp_i = \frac{\mathcal{F}_i z}{p_i' - p_i''} \quad (5)$$

If the solubility coefficient S and the diffusion coefficient D can be considered as independent of pressure within the limits of the range of pressure, then

$$\bar{P}_i = \frac{P_i(p_i' - p_i'')}{z} \quad \text{with} \quad P_i = S_i D_i \quad (6)$$

Equation (6) can be considered the workhorse of gas permeation in dense polymers, and it applies to the simplest situation that can be proposed. Under the conditions of validity of the various hypotheses that have been used in its derivation, the equation shows that the steady-state flux of a given gas or vapor (i) through a dense membrane \mathcal{F}_i is proportional to the intrinsic permeability coefficient (P_i) and the partial pressure difference ($p_i' - p_i''$), and inversely proportional to the effective thickness of the selective layer (z). Thus, the permeability of gas (i) in a membrane material can be seen as the flux normalized with regard to pressure and thickness. Moreover, it takes on the role of the characteristic mass transfer coefficient. Interestingly, it is a product of two very different terms: a thermodynamic factor (the sorption coefficient S) and a kinetic parameter (the diffusion coefficient D).

For gas separation with polymers, the permeability is most commonly expressed in Barrer, named after the pioneer in gas permeability measurements: R.M. Barrer. For a description of the impressive research carried out by R.M. Barrer, the reader is referred to a review by Michaels [35]. One Barrer represents $10^{-10} \text{ cm}^3 \text{ (STP) cm cm}^{-2} \text{ s}^{-1} \text{ cm}^{-1} \text{ Hg}^{-1}$ and corresponds to $3.347 \times 10^{-16} \text{ mol m}^{-1} \text{ s}^{-1} \text{ Pa}^{-1}$ (SI units). From a quantitative point of view, barrier materials can demonstrate permeability coefficients down to 10^{-6} Barrer, for example, in the case of oxygen permeation through a glassy polymer (dry polyvinylalcohol), whereas values up to 10^4 Barrer have been reported for vapor permeation through elastomeric materials. Ten orders of magnitude can thus be covered for the permeation of gases or vapors through polymers. Such a broad range is remarkable in the field of mass transfer coefficients and it explains the intense efforts carried out during several decades with regard to the understanding of the parameters that affect the polymer permeability (P_i).

The physico-chemical characteristics of the main compounds involved in membrane gas separation at an industrial scale are summarized in **Table 1**, and, for illustrative purposes, a series of permeability data for various gases is reported in **Table 2**.

Several trends, which can be considered as rules of thumb for polymeric gas separations, can be observed when referring to these two tables:

1. While the absolute value of the permeability coefficient varies considerably from one polymer to another, the ranking of the permeability within a limited number of gaseous species remains remarkably similar and can be roughly divided into two categories.

For glassy polymers (i.e., $T_g >$ ambient temperature; cf. **Table 2**), the separation is principally

Table 1 Gas permeabilities in a series of rubbery and glassy polymers under ambient temperature conditions (units: Barrer)

	T_g (°C)	H_2O	H_2	He	CO_2	O_2	N_2	CH_4
PTMSP	~200		13 200	5080	28 000	7730	4970	13 000
PDMS	-123	40 000	890	590	4550	781	351	1430
Polystyrene	95	970	23.8	22.4	12.4	2.9	0.52	0.78
CA	200	6 000	8	16.0	4.75	0.82	0.15	0.15
Polysulfone ^a	190	2 000	12.1	10.8	4.6	1.2	0.19	0.18
Polyimide ^b	>300	640	3.7	8.0	2.7	0.61	0.10	0.59
PMMA	~110	638	2.4	8.4	0.62	0.14	0.02	0.0052

^a Bisphenol-A-polysulfone;

^b PMDA-4,4'-ODA polyimide.

CA, cellulose acetate; PDMS, polydimethylsiloxane; PMMA, polymethylmetacrylate.

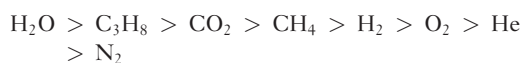
Table 2 Physico-chemical properties of a series of gaseous compounds most often investigated in polymeric gas separation studies or industrial applications

	T_b (K)	T_c (K)	Lennard-Jones diameter (Å)	Kinetic diameter (Å)	Lennard-Jones interaction parameter ϵ (K)
He	4.3	5.3	2.55	2.69	10.2
H ₂	20	33	2.89	2.89	60
O ₂	90	155	3.46	3.46	107
CO	82	133	3.69	3.76	91.7
CH ₄	112	191	3.76	3.87	149
N ₂	77	126	3.80	3.64	71
CO ₂	195	304	3.94	3.30	195
C ₃ H ₈	231	370	5.12	4.30	237.1
H ₂ O	373	647	~3.7		809.1

governed by the size of the permeant and the following sequence is often observed:



For rubbery polymers (i.e., $T_g < \text{ambient temperature}$; cf. **Table 2**), the permeant condensability (expressed through its boiling temperature T_b , for instance) is the major governing factor. As a consequence, water remains the fastest permeating compound, but the order of the other compounds becomes slightly different:



Thus, the glass transition temperature of a polymer is of utmost importance in the analysis of its gas permeation behavior. This point will be further detailed since it corresponds to the basic typology of permeation mechanisms. More generally, gases with high permeabilities, such as water, are logically referred to as fast gases, while others are known as slow permeants. In terms of practical applications, it is obvious that the separation of a given gas pair by a dense polymer is facilitated when the feed mixture contains a fast and a slow gas.

2. For a given permeant, the polymer permeability increases with a decrease in the polymer glass transition temperature (T_g). Elastomeric materials show higher permeability values as compared to their glassy counterparts. It should however be noted that exceptions to this rule are not uncommon. In particular, so-called superpermeable glassy polymers (such as PTMSP in **Table 1**), which show very high free-volume characteristics, are known for their very high permeabilities [36].

Based on this, a direct analysis of the potential of dense polymers for gas separation applications could be directly proposed. Nevertheless, the rational design of a separation unit requires a more detailed understanding of the roles of the operating variables (e.g., pressure and temperature) in the effective permeability. Coming back to the definition of permeability, the best strategy for attaining this target consists in the separate analysis of the solution (thermodynamic step) and diffusion (kinetic step) contributions for single-compound permeation.

2.08.2.2 Equilibrium (Solution) Characteristics

2.08.2.2.1 Sorption equilibria in rubbery polymers

The equilibrium between a gas or vapor and a fluid phase is often considered to be achieved when the criteria of thermal, mechanical, and chemical equilibria are fulfilled. The latter is of great importance since, according to Gibbs, it leads to the hypothesis of chemical potential equality in the various phases of the system. The peculiar situation of equilibria with polymers used for membrane applications, namely the fact that no polymer exists in the gaseous phase, corresponds to a so-called osmotic equilibrium [37]. As a consequence, the only remaining equation is that of the chemical potential equality for gaseous compounds in the two phases of the system. This equation represents the fundamental expression for isotherm analysis or prediction. From a mechanistic point of view, the dissolution of a gaseous species in the polymeric matrix can result from a variety of contributions such as adsorption, absorption, incorporation into microvoids, and cluster formation. The term sorption is usually proposed in order to

indifferently incorporate these various mechanisms, and the S value includes them all.

The simplest situation of equilibrium in gas membrane separation situations is by far the dissolution of a permanent gas in a rubbery material. In this case, the membrane material can be considered as homogeneous and the interactions between the gas molecule and the matrix can be easily described. Permeant/permeant and polymer/permeant interactions are weak as compared to polymer/polymer interactions, and consequently, the sorption coefficient S is most often constant, provided that the gas fugacity coefficient remains close to unity and that material compressibility issues do not play a significant role. Correlations have been proposed in order to predict the solubility of gases in rubbers and an example is, for illustrative purposes, shown in Figure 5.

Here, the gas boiling temperature (T_b) is the only parameter which is taken into account. Other approaches have, for example, related the logarithm of the solubility coefficient to the Lennard–Jones potential well depth or to the critical temperature ratio [38].

From a practical point of view, a linear sorption isotherm, sometimes referred to as of type I, results in

$$c = Sp \quad (7)$$

This type of behavior is expected to occur for permanent gases that are sorbed by rubbery polymers at

low pressure (typically less than a few bar). This situation generally corresponds to a very low solubility (<0.2% of the dissolved gas in volume fraction).

The situation of vapors in elastomers is more complex than that prevailing for gases. In such a case, the thermodynamics theory developed by Flory [39] and Huggins is classically considered to offer the best framework. The equilibrium relationship between the vapor activity (a) and the solubility in the membrane material expressed through the vapor volume fraction in the matrix (φ) is

$$\ln(a) = \ln\varphi + (1-\varphi)\left(1 - \frac{\bar{v}}{\bar{v}_p}\right) + \chi(1-\varphi)^2 \quad (8)$$

with

$$\varphi = c\bar{v} \quad (9)$$

The activity is the ratio of the fugacity over that of the pure compound in the reference state. If the fugacity coefficient is close to 1 – a condition that can be quickly estimated through the corresponding state approach [40] – the expression reduces to the ratio of the vapor pressure over the saturated vapor pressure at the temperature of the system:

$$a = \frac{f}{f^{\text{Sat}}} \approx \frac{p}{p^{\text{Sat}}} \quad (10)$$

Further, c corresponds to the concentration of the penetrant in the membrane (mol m^{-3}) and \bar{v} to its partial molar volume ($\text{m}^3 \text{mol}^{-1}$), which is often

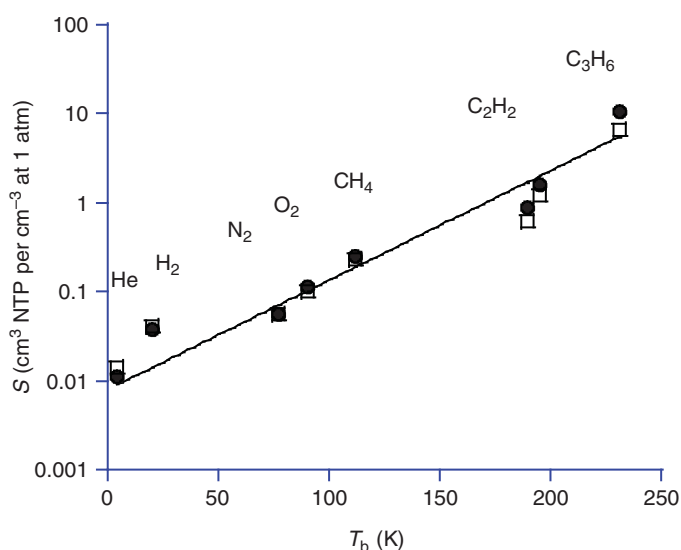


Figure 5 Sorption coefficient (S) of series of gases in natural rubber as a function of boiling temperature (T_b) at 25 °C (circles) and 50 °C (squares). Line correspond to the correlation $\log S = -2.1 + 0.0123T_b$ proposed by van Amerongen.

assumed to be identical to that of the pure liquid at the same temperature.

For the sake of simplicity, the ratio of the partial molar volume of the vapor and the polymer in the membrane is often neglected and the following expression is obtained:

$$\ln(a) = \ln\phi + 1 - \phi + \chi(1 - \phi)^2 \quad (11)$$

Thus, the solubility of the vapor in the membrane can be directly calculated for a given activity provided that the polymer–penetrant interaction parameter χ is known. For weakly interacting species, the regular solution theory can be considered as acceptable and the interaction parameter can be estimated through the solubility parameters:

$$\chi \approx \frac{\bar{v}}{RT} (\delta - \delta_p)^2 \quad (12)$$

Here, \bar{v} is the partial molar volume of the penetrant, and δ and δ_p the solubility parameters of the permeant and polymer, respectively. A series of curves generated by the above expression are presented in **Figure 6**.

When δ and δ_p are identical, the interaction parameter χ is zero and the permeant shows a maximal solubility in the polymer. Otherwise, χ is positive and the extent of sorption decreases as it becomes larger. It should be noted that the Flory–Huggins equation does not take into account the polymer network contribution that offers a mechanical

resistance toward swelling. Consequently, an additional term, as originally proposed by Flory and Rehner [41], is required in this case. This can be of importance for so-called good solvent situations (i.e., for $\chi < 0.5$), where the Flory–Huggins equation predicts a total miscibility of the system (i.e., $\phi \rightarrow 1$ for $a \rightarrow 1$). This condition implies the occurrence of polymer dissolution in a saturated vapor or pure liquid. The fact that this is not the case for a cross-linked elastomer, for instance, demonstrates the importance of the elastic contribution for these systems.

Complications may also arise when discrepancies with regard to the regular solution theory occur for the polymer/permeant interactions. Variable interaction parameter expressions ($\chi = f(\phi)$) are often proposed in this case [42], and such a complication often leads to the impossibility of developing a predictive approach of lattice theories, such as the Flory–Huggins approach [43]. A case of particular importance is that of permeant/permeant interactions that are stronger than polymer/permeant interactions. This leads to an association or clustering of the sorbed molecules as well as to considerable discrepancies when the Flory–Huggins model is used to fit the experimental data. Water is, especially in apolar polymers, a typical example of this, for which hydrogen-bonded clusters, often quite stable, are formed. During this event, alternative equilibrium models

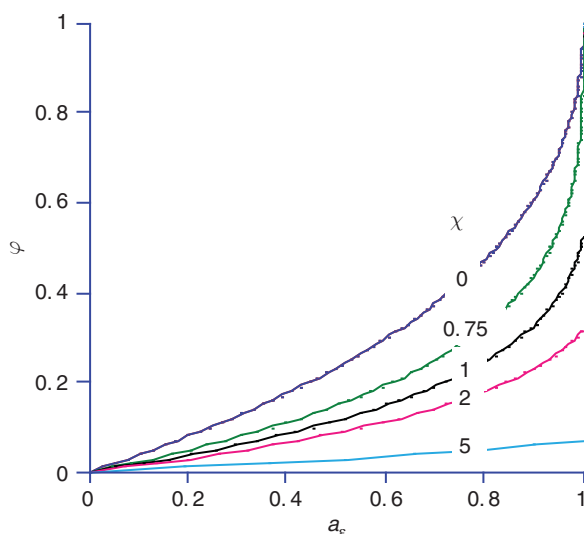


Figure 6 Sorption isotherms according to Flory–Huggins theory. Solute volume fraction in the polymeric membrane (ϕ) at equilibrium as a function of its thermodynamic activity in the gaseous phase in contact with the membrane (a) for different values of the interaction parameter (χ).

that take into account the clustering phenomenon may be proposed [44].

2.08.2.2.2 Sorption equilibria in glassy polymers

The peculiarities of gas sorption equilibria in glassy polymers quickly attracted attention [45], and the existence of microvoids was postulated in order to explain the nonlinear sorption isotherms that were encountered [46]. Figure 7 shows an example of the temperature evolution of a sorption isotherm of a gas in a glassy polymer: the gas solubility decreased when the temperature was raised and a linear relationship could be observed as soon as the temperature exceeded the glass transition temperature (T_g) of the polymer.

This linear relationship at $T > T_g$ was in agreement with what has been detailed above (a linear isotherm was observed when a permanent gas dissolved in an elastomeric matrix).

A simple and efficient model, based on two distinct contributions [47], was proposed in 1976 in order to depict this type of situation: a classical dissolution process in the polymer described by a Henry-type formalism. Moreover, a Langmuir-type mechanism was used for the role played by holes in the glassy matrix. This so-called dual mode model proved to give a consistent and efficient interpretation of the gas/glassy polymer equilibrium problem.

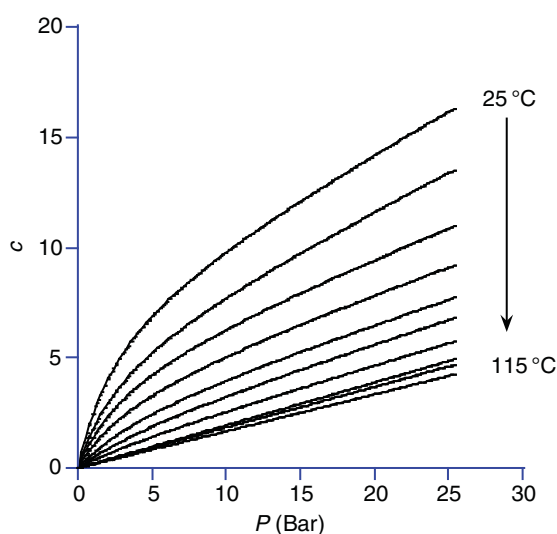


Figure 7 Sorption isotherm of a gas in a glassy polymer ($T_g \sim 105^\circ\text{C}$) for different temperatures according to the dual mode theory.

The solubility isotherm resulting from dual mode sorption is represented by

$$c = c_D + c_H = k_D p + \frac{c_H' b p}{1 + b p} \quad (13)$$

where c_D corresponds to the dissolved Henry contribution and c_H to the Langmuir contribution postulated to occur in microvoids.

This brief overview of the classical models that have been proposed for the dissolution of gases or vapors in rubbery or glassy polymers has been restricted to binary systems (i.e., one penetrant and one polymer), and the discussion has been limited to simple, easy-to-handle expressions. The more complex situation of multi-component equilibria, such as the one that occurs when a binary gas mixture dissolves in a polymer, is, for the sake of simplicity, often treated as the superposition of two binary gas/polymer equilibria. Deviations to this simple approach can, of course, occur and competitive or synergistic phenomena between the different dissolved species can take place; the former is typical of the competitive site adsorption process in glassy polymers, for instance. Conversely, the solubility of a permanent gas can also significantly increase when another more condensable compound is dissolved in the polymeric matrix at a certain level of volume fraction.

The description given above has been restricted to simple, mechanistic models. Given the impressive developments in the field of polymer thermodynamics, more rigorous approaches, such as equations of state, or computational techniques, such as molecular modeling methods [48], play roles of increasing importance in the interpretation or prediction of the sorption coefficient value. For the prediction of equilibria in glassy polymers, nonequilibrium lattice fluid (NELF) models seem to be promising [49]. These various topics are beyond the scope of the present chapter and the interested reader in these modern developments is referred to key articles or textbooks.

2.08.2.3 Diffusion in Polymers: Characteristics

2.08.2.3.1 General framework

In the derivation of the solution-diffusion model, diffusion has been considered as the only mass transfer mechanism in dense membranes. Thus, the knowledge of the sole diffusion coefficient would,

in combination with the sorption coefficient, principally be enough to predict the mass flux in a given membrane. A considerable number of studies have been devoted to the analysis or prediction of the diffusion coefficient D of gases and vapors in polymers for applications such as packaging, devolatilization, chromatography, and membranes separation. The starting point invariably remains the basis of Fick equations, common to any diffusion situation in gases, liquids, or solids [50].

Nevertheless, the peculiarities and the complexity of diffusional processes in polymers often require the development of dedicated models [51]. Similarly to the sorption typology, a distinction is made between the mechanisms that prevail in elastomers and those that are characteristic of glassy polymers. Generally speaking, the former shows similarities with viscous liquids, while the latter is closer to amorphous solids. **Figure 8** displays the evolution of the diffusion coefficient of a series of alcohols in various polymers.

Diffusion coefficients in water as well as in a solid (ZSM zeolite) have been added for the sake of comparison.

It can be seen that:

1. diffusion coefficients in polymers cover a wide range, bridging the gap between liquids and solids;
2. for a given molecule, the diffusion coefficient decreases when the glass transition temperature increases;
3. for a given polymer, the diffusion coefficient decreases when the permeant size, expressed through its molar volume in the figure, increases; and

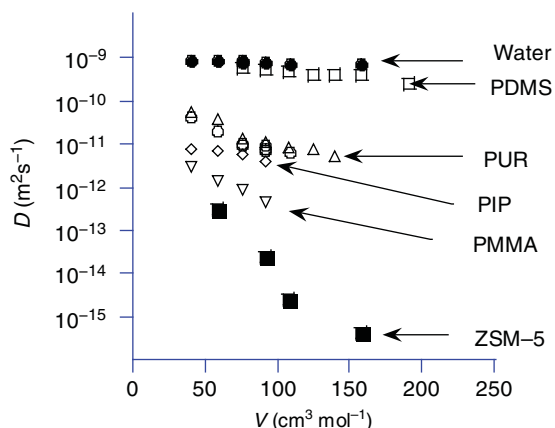


Figure 8 Infinite dilution diffusion coefficient (D in $\text{m}^2 \text{s}^{-1}$) of a series of alcohols in water, polymers, and porous solids (ZSM-5) as a function of their molar volume V (pure liquid). PUR, polyurethane; PIP, polyisopropylene; ZSM-5, Zeolite.

4. the decrease in D with penetrant size is much more pronounced for glassy polymers as opposed to their rubbery counterparts.

The theory of diffusion in isotropic substances is based on the key hypothesis that the rate of transfer through a unit area of a section is proportional to the concentration gradient. The proportionality, namely the mutual diffusion coefficient D , can be a constant, but it can also demonstrate a strong concentration dependence. This latter point is crucial in the development of a rigorous mass transfer expression since the integration of Fick's law is inevitable for flux computation purposes.

Unfortunately, there are very few rigorous solutions to the diffusion equation for a concentration-dependent diffusion. Historically, an empirical exponential dependency was proposed early on for diffusion coefficient variations in polymers [52]:

$$D = D_0 \exp(\gamma c) \quad (14)$$

Here, D_0 is the infinite dilution diffusion coefficient and γ the so-called plasticizing parameter, reflecting the intensity of the increase in D with c . This approach has been indifferently used for elastomers and glassy polymers. In very general terms, the variation appears to be greater for glassy polymers than for rubbers.

2.08.2.3.2 Diffusion in rubbery polymers (elastomers)

For diffusion of simple gases in elastomers, in which case the matrix is isotropic and interactions with the polymer are weak, the diffusion coefficient D is often independent of concentration. When permeant/polymer interactions become significant, D demonstrates a dependency on the permeant concentration, particularly for organic vapors in elastomers. Nevertheless, the variation strongly depends on what polymer system that is studied. For instance, a threefold increase in D as a function of ϕ is observed for a system of benzene/natural rubber, whereas D remains virtually constant for a benzene/polydimethylsiloxane system.

Among the various attempts to interpret and/or predict the diffusion coefficient variation in rubbery polymers, one of the most often employed models is the free-volume model of Fujita [53]. Its key concept is based on the assumption, originally proposed by Cohen and Turnbull [54] in order to explain the viscosity variation in liquids, that a diffusing molecule can move from one place to another only when the

local free volume around it exceeds a critical value V^* . This basic mechanism is illustrated in **Figure 9**.

The fractional free volume (v_F) of the polymer/penetrant system plays a key role, and this parameter is often estimated by a simple mixing law (each compound provides a certain fraction of free volume that is proportional to its volume fraction in the system). For a binary system (permeant i and polymer p , with the corresponding volume fractions $\varphi_i + \varphi_p = 1$), the fractional free volume is expressed as

$$v_F = \varphi_i v_{F,i} + \varphi_p v_{F,p} \quad (15)$$

It is possible to determine the probability of finding a large enough free volume, and the thermodynamic diffusion coefficient related to this probability is written as

$$D^T = D_0 \exp\left(-\frac{B}{v_F}\right) \quad (16)$$

It should be stressed that the thermodynamic coefficient D^T is obtained from a free-volume theory (i.e., Fick's law, that is used in the solution-diffusion model) and makes use of the so-called mutual diffusion coefficient D . Even though the two coefficients can be assumed to be roughly equal when the concentration

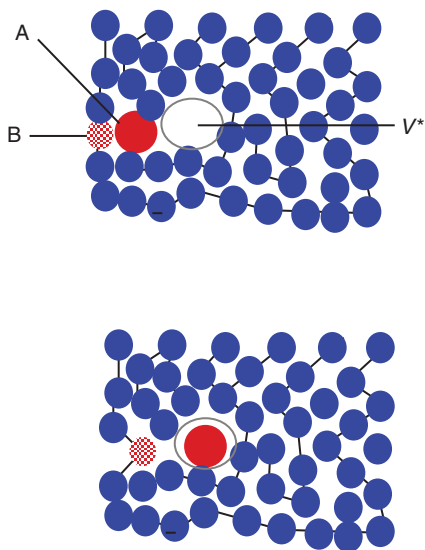


Figure 9 Schematic representation of the diffusion process of a penetrant molecule A in a polymer matrix, according to the free-volume mechanism. An elementary jump of molecule A is possible only if a defined critical volume V^* , which results from the random redistribution of the overall fractional free volume, exists at its contact. The position initially occupied by A has to be taken by another penetrant or polymer segment (B) in order to prevent any retrodiffusion process.

of the penetrant in the polymer is low, care should be taken when directly using Equation (16) in a solution-diffusion framework. In **Figure 10**, Equation (16) was here employed to fit the experimental variation of D as a function of the fractional free volume for a polystyrene–benzene system at 100 °C [55]. As demonstrated in the figure, there was a good agreement between the theoretical and experimental values.

The major interest of the free-volume framework is that it offers a unified interpretation framework and enables the qualitative prediction of the significant trends of diffusion phenomena in polymers:

1. D increases with T , since the fractional free volume increases with temperature, for any system.
2. Since permeants have a larger free volume than polymers, v_F increases with increasing permeant volume fraction φ (or concentration c), and consequently, D increases with the permeant concentration.
3. The fractional free volume of a polymer increases as its T_g decreases, which explains the inverse relationship of D to the temperature of measurement and to T_g .
4. An exponential relationship between D and c , originally proposed on empirical grounds, can be derived and the so-called plasticization coefficient can be expressed [56].

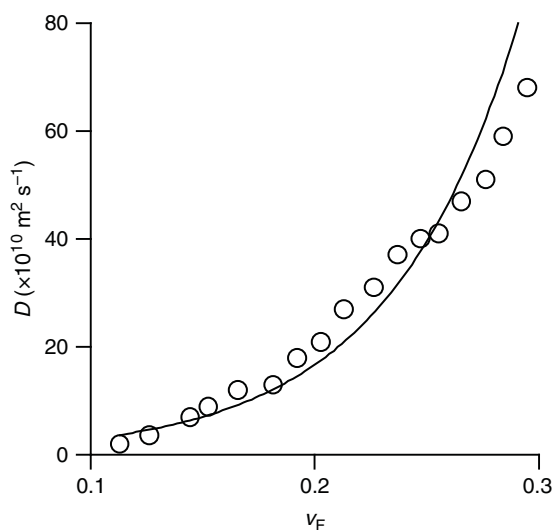


Figure 10 Benzene thermodynamic diffusion coefficient in polystyrene (D^T) at 100 °C as a function of the fractional free volume v_F calculated from the volume fraction of each compound in the system. Circles represent experimental data, line corresponds to an exponential curve fit.

More generally, the free-volume model has been found to present very good correlations with experimental data. For instance, the pressure dependence of the permeability for a number of gases in polyethylene has been successfully interpreted based on a detailed free-volume analysis [57]. However, its major shortcoming is that the constants lack a very precise physical meaning and must be determined experimentally. Other limitations are the complications that arise when the size of the permeant differs significantly from that of a polymer segment, inciting the development of a more comprehensive theory [58]. Unfortunately, this was achieved at the expense of a complex model incorporating supplementary parameters.

2.08.2.3.3 Diffusion in glassy polymers

In the derivation of the solution-diffusion model, a homogeneous polymeric matrix was postulated. Consequently, a single population of diffusing molecules was assumed, leading to a sole diffusion coefficient. This situation can be considered as realistic for a dense homogeneous rubbery membrane. Nevertheless, within the above-mentioned framework of dual mode sorption for glassy polymers, two populations, corresponding to the Henry and Langmuir modes, should logically be taken into account. This hypothesis can further be evidenced by pulsed nuclear magnetic resonance (NMR) experiments, which confirm the existence of two dissolved populations of varying mobility in glassy polymers [59]. Under the hypothesis of a local equilibrium, the two populations can be described by a single chemical potential. As a result, the flux of a gas through a glassy polymer should be expressed as

$$\mathcal{J} = -D_D \frac{\partial c_D}{\partial z} - D_H \frac{\partial c_H}{\partial z} \quad (17)$$

where c_D is the concentration of the penetrant dissolved in the Henry mode and c_H is the concentration of the penetrant dissolved in the Langmuir mode. For the sake of simplicity, the assumption of a complete immobilization of the molecules in the Langmuir mode was first proposed (i.e., $D_H = 0$). Unfortunately, several studies later showed that the pressure dependence of the flux through glassy polymers could be accounted for only if the complete expression was used [60]. This so-called partial immobilization approach was successfully applied to various systems with glassy

polymers such as ethylcellulose [61] and polycarbonate [62], among others.

2.08.2.4 Influence of Operating Parameters (T, P, C)

2.08.2.4.1 Constant vs. variable permeability behavior

Based on the characteristics of the sorption and diffusion coefficients summarized in the previous section, two major types of situations can be proposed to describe the permeability of a given permeant through a known dense polymeric material at a specific temperature. If S and D can be reasonably assumed as constant under the investigated conditions, a constant permeability P will result, as shown in **Figure 11(a)**.

The compositional range that is supposed to exist in the membrane has been expressed through the volume fraction of permeant in the membrane. Nevertheless, as soon as a nonlinear sorption isotherm or a variation in diffusion coefficient occurs, a variable permeability is obtained. This second type of situation induces major complications that are often underestimated or neglected. An effective permeability can indeed always be determined as soon as the flux, membrane thickness, and partial pressure difference for a given case are known. For fundamental purposes, a comparison of the effective permeability data is clearly to be preferred over simply comparing absolute fluxes [63]. Nevertheless, the variable permeability situation should systematically demand the equilibrium (S) and kinetic (D) master curves to be known in order to compute the correct effective permeability value from the membrane boundary conditions that are examined. This is schematically shown in **Figure 11(b)** where the interplay between S and D for a given set of upstream and downstream conditions (corresponding to the boundaries of the shaded area) is demonstrated. In this case, no unique expression of permeability with the pressure difference can be obtained; however, the absolute partial pressure conditions on the two faces of the membrane have to be defined in order to determine the corresponding effective permeability [64].

Typical permeability curves are shown in **Figure 12** and the corresponding basic typology is summarized in **Table 3**.

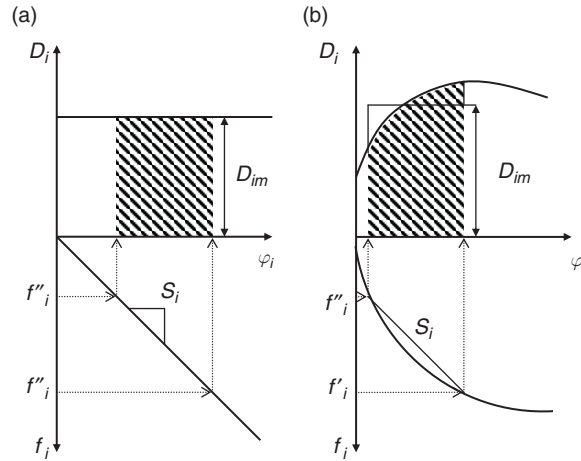


Figure 11 Schematic representation of the sorption and diffusion contributions in the permeability coefficient, according to the solution-diffusion model. The sorption isotherm of the penetrant is obtained through the dissolved volume fraction φ as a function of the fugacity f . The diffusion coefficient can be constant or dependent on volume fraction. For a membrane exposed at a penetrant fugacity f' on the upstream side and f'' on the downstream side, the mean permeability will correspond to the product of the average sorption coefficient and diffusion coefficient (shaded area). (a) For a constant S and D situation, permeability is independent of the pressure difference; (b) The same does not hold for variable diffusion behaviors. Modified from Mauviel, G., Berthiaud, J., Vallières, C., Roizard, D., Favre, E. *J. Membr. Sci.* **2005**, 266, 62–67.

2.08.2.4.2 Influence of temperature

The influence of pressure (or activity) on the permeability has thus far been examined under isothermal conditions. It is useful to also describe the influence of temperature on permeability. The solution-diffusion model offers a utile framework in order to achieve such a purpose.

The temperature dependence of the sorption coefficient S is classically assumed to follow an Arrhenius-type relationship within small temperature ranges:

$$S = S_0 \exp\left(\frac{-\Delta H_S}{RT}\right) \quad (18)$$

Here, ΔH_S is the partial molar heat of sorption that can be expressed as the sum of two contributions: the molar heat of condensation and the partial molar heat of mixing. For regular solutions, the latter can easily be estimated from the solubility parameters:

$$\Delta H_S = \Delta H_{\text{Cond}} + \Delta H_{\text{Mix}} \approx \Delta H_{\text{Cond}} + \bar{v}(\delta - \delta_p)^2(1 - \varphi)^2 \quad (19)$$

For gases that are above their critical temperature, the heat of condensation is necessarily small, thus resulting in a low, positive value of ΔH_S , typically between 0 and 10 kJ mol⁻¹. Consequently, the solubility increases moderately with temperature. In contrast, ΔH_S is negative for more condensable

gases, due to the large contribution of the heat of condensation term. In this case, the solubility decreases with temperature.

The expression of the temperature dependence of the diffusion coefficient has, for a long time, also been proposed through an Arrhenius-type relationship [65]:

$$D = D_0 \exp\left(\frac{-E_D}{RT}\right) \quad (20)$$

The apparent activation energy of diffusion E_D can demonstrate a complex behavior, especially with the dissolved penetrant concentration. In this case, the evolution of E_D can sometimes be interpreted as the result of two terms: the activation energy of diffusion when the polymer chain mobility is unaffected by the permeant (i.e., E_D with $\varphi \rightarrow 0$), and a second term that takes into account the reduction in activation energy due to the sorbed permeant.

It is interesting to note that, for systems of low solubility (such as permanent gases under low to moderate pressure conditions), universal correlations have been proposed in order to quickly estimate the apparent activation energy of diffusion from the only pre-exponential term [66].

For rubbery polymers,

$$\log D_0 = \left(\frac{E_D \times 10^{-3}}{R}\right) - 8.0 \quad (21)$$

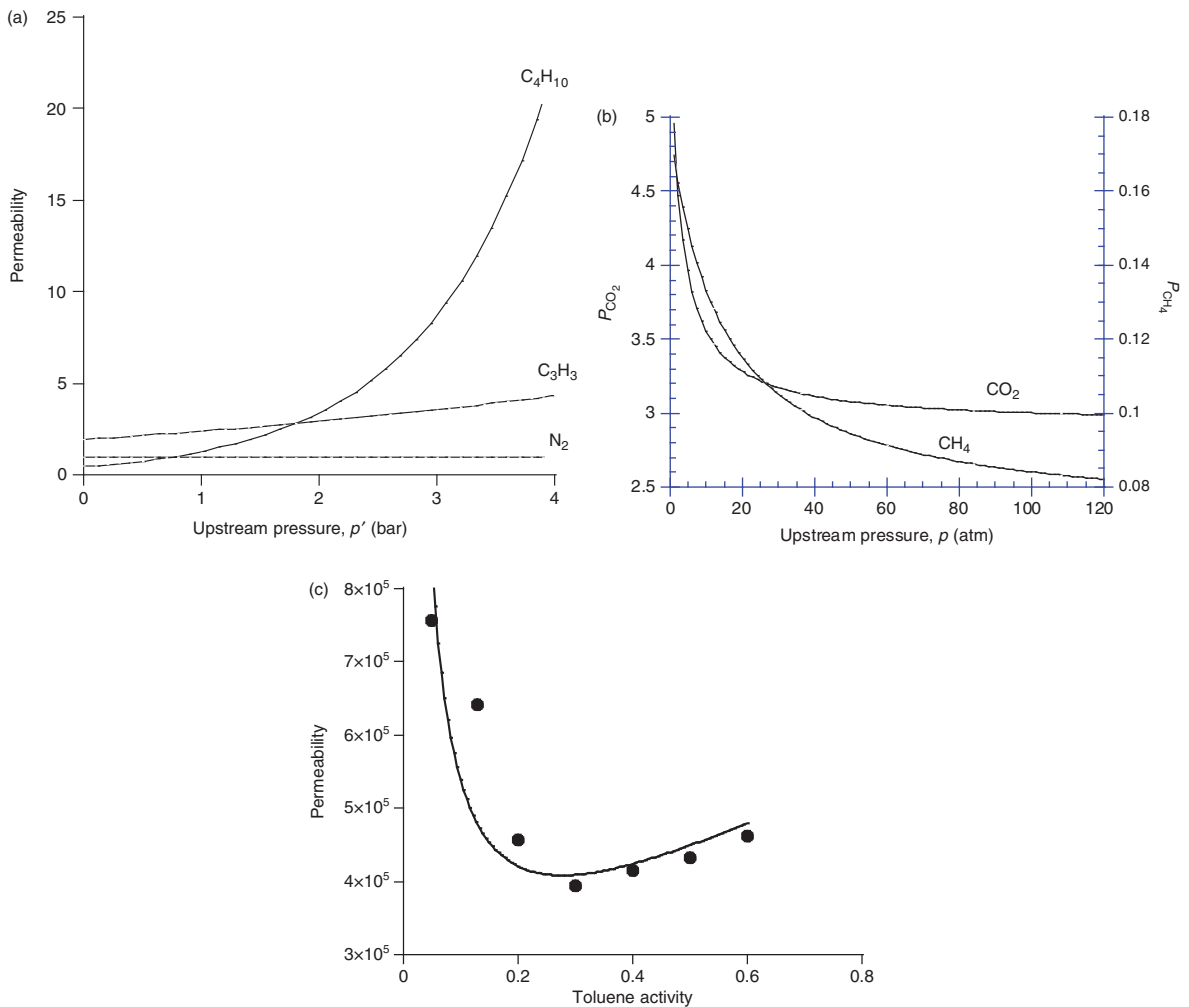


Figure 12 Examples of the evolution of the average permeability of gaseous compounds or vapors through dense polymeric membranes as a function of the upstream pressure (or activity). Vacuum is applied on the downstream side and remains unchanged for the different examples: (a) permeation through a rubbery (silicone rubber) membrane: constant permeability for a permanent gas (N_2) and increase for vapors (propane, butane); (b) carbon dioxide and methane permeability through glassy polysulfone material; permeability decrease (predicted by the dual mode model); (c) A condensable vapor (toluene) through a glassy, high free-volume polymer (polytrimethylsilylpropyne): a complex permeability behavior is observed and can be fitted if a variable diffusion coefficient is added in the dual mode model.

For glassy polymers,

$$\log D_0 = \left(\frac{E_D \times 10^{-3}}{R} \right) - 9.0 \quad (22)$$

In the above expressions, D_0 is given in $m^2 s^{-1}$ and E_D/R in K. Such formalism predicts a change of the slope of D versus T in the vicinity of the glass transition temperature. This has indeed often been observed, with the exception of certain systems with small gas molecules.

Coming back to the temperature dependency of the permeability, the solution-diffusion model

suggests using an Arrhenius-type expression that combines the S and D apparent activation energies:

$$P = P_0 \exp\left(\frac{-E_P}{RT}\right) \quad (23)$$

Here,

$$E_P = \Delta H_S + E_D \quad (24)$$

For permanent gases, the diffusivity is generally a stronger function of temperature (with an E_D ranging between 20 and 80 kJ mol^{-1}) than the solubility. The

Table 3 A summary of the equilibrium (sorption), diffusion, and resulting permeation behavior for the four main situations encountered in gas (or vapor) separation processes with polymeric membranes

	<i>Rubbery polymer</i> ($T > T_g$)	<i>Glassy polymer</i> ($T < T_g$)
$T > 0.7 T_c$ (permanent gas)	Constant S (Henry's law) Constant D Constant E_{AD} P constant (or slight variation for high pressure) Typical permeability expression: $P = DS$	Dual mode sorption Constant or variable D P constant (total immobilization) or decreases with increasing pressure Example of dual mode permeability expression: $P = k_D D \left(1 + \frac{c'_{HB} \cdot \frac{D_H}{k_D \cdot \frac{D_D}{1 + bp}}}{1 + bp} \right)$
$T < 0.7 T_c$ (vapor)	Variable S (Flory–Huggins) $D = f(c)$ (free volume, i.e., exponential dependency) $E_{AD} = f(T, c)$ P usually increases with Δp Permeability expression combines S and D variation and leads to exponential type pressure dependency	Complex sorption with possible significant swelling effects (dual mode with variable D and k_D) History- and time-dependent diffusion Complex permeability behavior (possible occurrence of a minimum) Example of permeability expression with $D = D_0 \exp(\beta c)$: $P = \frac{D_0}{\beta p} \left(\exp \left\{ k_D \beta p \left(1 + \frac{c'_{HB} \cdot \frac{D_H}{k_D \cdot \frac{D_D}{1 + bp}}}{1 + bp} \right) \right\} - 1 \right)$

heat of sorption can be either positive or negative but remains between -10 and $+10 \text{ kJ mol}^{-1}$. As a result, the permeability increases with temperature for E_P values between 30 and 80 kJ mol^{-1} . Due to the predominant role of the heat of condensation term, the situation for vapors is completely different. In this case, a negative apparent energy of permeation is observed and the permeability is found to decrease with temperature [67].

2.08.2.4.3 Predictive approaches

Apart from the experimental determination of the variation of permeability with pressure and temperature, it is also tempting to make use of predictive approaches. Several attempts based on a group contribution approach (such as the so-called Permachor method [68] or free-volume group contribution approaches [69]) or correlations that require physical characteristics [70] have been reported. For rubbery membrane materials, a variety of correlations have been proposed in order to predict the permeability and selectivity of gases and vapors, especially thanks to solubility parameters [71]. Nevertheless, the precise prediction of the polymer permeability remains

a formidable challenge and experimental measurements cannot be discarded if a rigorous evaluation of the separation performances, including a design study, is aimed.

2.08.3 Engineering of Gas Permeation Modules

2.08.3.1 General Framework: Separation Factor and Trade-Off Curves

The ultimate goal of the previous section was to propose realistic and consistent permeation laws in order to achieve a rigorous membrane module design and thus a precise analysis of the separation performances of a given system. Some examples of the different expressions that can be proposed have been shown in Table 3. Tabulations of P , D , and S can be found in the literature for the most common polymers [72].

The interest of a given system for separation purposes can be evaluated when one has knowledge of a consistent permeation law for gases through a polymer. The classical starting point of this type of

analysis consists in first determining the separation performances of a single unit, namely a single gas permeation module, for a given set of operating and feed conditions in a steady-state regime. **Figure 13** depicts the basic corresponding diagram for a binary feed mixture.

Similarly to a flash distillation operation, the feed mixture composition will be modified and split into two distinct flows with a mole fraction x_{out} on the retentate side and a mole fraction y on the permeate side. Logically, the extent of the separation performance of the unit depends on its capability of producing exit streams with the largest possible difference in composition. In separation science on a broad sense, this key variable is called the separation factor α and is expressed as

$$\alpha = \frac{y(1-x_{\text{out}})}{x_{\text{out}}(1-y)} \quad (25)$$

The above expression can be used in order to determine the target separation factor for a given process. The relationship between this process variable and the intrinsic membrane performances is discussed further on.

In order to evaluate the interest of polymeric membranes for a given gas separation problem, the relative permeability of the various compounds present in the feed mixture obviously plays a key role. For a binary mixture, this leads to the so-called ideal separation factor, or membrane selectivity (α^*). Similarly to a convention used in distillation for the relative volatility, it is usually expressed so as to be >1 :

$$\alpha^* = \frac{P_i}{P_j} \geq 1 \quad (26)$$

Taking into account the definition of permeability within the solution-diffusion framework:

$$\alpha^* = \frac{P_j}{P_i} = \frac{S_i D_i}{S_j D_j} = \alpha_S^* \alpha_D^* \quad (27)$$

Thus, a high selectivity can be achieved from a high solubility ratio α_S^* or a high diffusivity ratio α_D^* , or both.

As for any separation problem, in addition to the selectivity, the question of the productivity of a membrane separation system should also be addressed logically. The interplay between these two fundamental characteristics is discussed in a subsequent section through an engineering analysis; nevertheless, it is interesting to first examine the intrinsic performances of various polymers toward these two key properties for a given gas pair. This analysis has been investigated in detail by Robeson for gas separation applications [73]. The systematic antagonism between productivity (i.e., membrane permeability) and selectivity (expressed through the ratio of the gas permeabilities, called ideal selectivity α^* and defined above) is evidenced through this type of chart. An example for the air separation problem (O_2/N_2 gas pair) is presented in **Figure 14**.

More interestingly, the application to different gas pairs shows that an empirical limit seems to be characteristic for each gas mixture. This observation has been further explored by Freeman and a fundamental analysis of the factors playing a role in the position of this limit has been proposed [74]. **Figure 15** shows a comparison of the trade-off curves for three gas pairs of industrial interest, computed by the Freeman approach.

These theoretical limits should not be taken too literally, and modifications have been proposed through a continuous improvement of the membrane materials. Nevertheless, they offer the unique advantage of providing a unified vision of what, in some cases, can be theoretically expected in order for a gas separation problem to be solved by a dense polymer separation process.

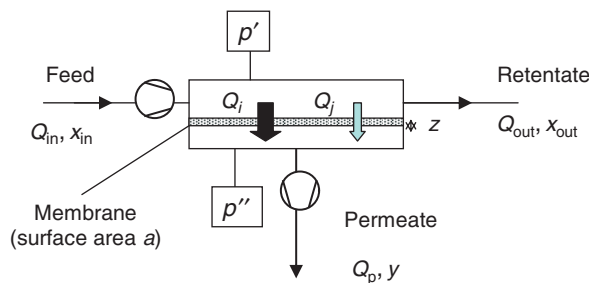


Figure 13 Schematic representation of a gas separation membrane module for a binary mixture separation. A pressure difference between the retentate and permeate side is applied, thanks a compressor and/or a vacuum pump. A fraction of the feed flowrate (Q_{in}) permeates through the membrane and emerges on the permeate side (Q_{p}) as the sum of the fast compound (Q_i) and the slow compound (Q_j) flow rates.

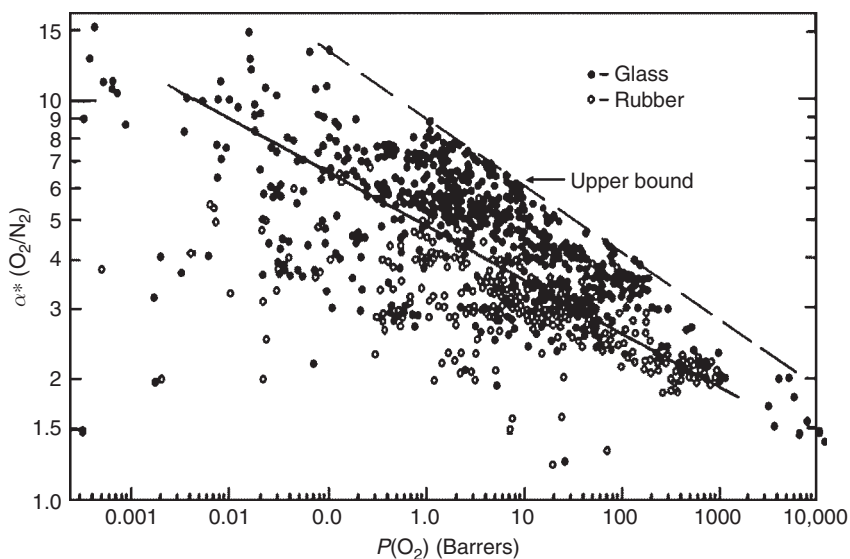


Figure 14 Representation of the selectivity–productivity trade-off curves for the oxygen/nitrogen gas pair. From Robeson, J. L. *J. Membr. Sci.* **1991**, 62, 165.

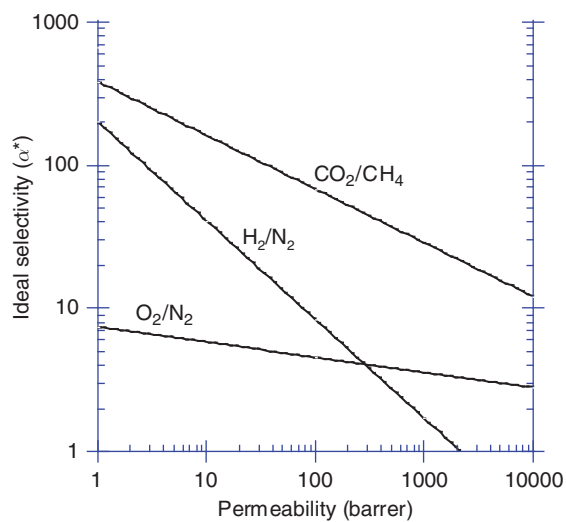


Figure 15 Representation of the theoretical selectivity–productivity trade-off curves for three different gas pairs which find industrial applications.

The quantitative analysis of a single-stage module design for a binary mixture separation will now be developed – at first through a simplified approach.

2.08.3.2 Membrane Module Design: General Framework and Approximate Analytical Solution

The general problem of establishing key equations that describe the separations performances of a gas

separation module can lead to complex formulations if an exhaustive and rigorous approach is taken (i.e., mass, heat and energy transfer, multi-component fluxes including coupling effects, etc.). Fortunately, a simple development can easily be derived for a binary gas mixture, provided that a series of simplifying assumptions is proposed. This strategy offers the major advantage of leading to an analytical solution, where the roles of the different key variables in the separation performances can be explicitly described. A parametric sensitivity analysis can be readily performed according to such an approach; based on this, the possibility of achieving the separation specifications of the problem and the chances of competing with other gas separation technologies can be roughly estimated.

Starting from the general situation depicted in **Figure 13**, the following hypotheses are put forward:

1. a system in steady state;
2. isothermal conditions (a single temperature everywhere in the system);
3. isobaric conditions in each compartment (no pressure drop on the upstream and downstream side);
4. perfect gas law;
5. a constant permeability;
6. the absence of flux couplings (the driving force of each compound is its partial pressure difference); and
7. perfect mixing conditions on both the upstream and downstream sides.

It is important to stress that each of the underlying hypotheses can potentially be questioned, as will be partly discussed later. A classical problem consists in determining the separation efficiency, through the permeate composition y as a function of various parameters such as the feed composition (x_{in}), the upstream (p') and downstream (p'') pressure, the permeability to the fast (P_i) and slow (P_j) permeant, etc. The solution can be obtained by developing mass balance and mass transfer expressions. The mixture composition is expressed in mole fractions (which equal the volume fractions for a perfect gas mixture) with the fast compound as a reference. A binary separation problem is treated below and the employed methodology can be extended to multi-component mixtures.

First, according to the steady-state assumption and since no sweep gas is used on the downstream side, the permeate composition is simply expressed as

$$y = \frac{Q_{p,i}}{Q_p} = \frac{Q_{p,i}}{Q_{p,j} + Q_{p,i}} \quad (28)$$

The mass balance for the fast compound is

$$Q_{in}x_{in} = Q_{out}x_{out} + Q_p y \quad (29)$$

and the global mass balance is written as

$$Q_{in} = Q_{out} + Q_p \quad (30)$$

Mass transfer relationships can be expressed for each compound as

$$Q_{p,i} = \frac{AP_i}{z} \cdot [p'x_{out} - p''y] \quad (31)$$

$$Q_{p,j} = \frac{AP_j}{z} [p'(1-x_{out}) - p''(1-y)] \quad (32)$$

where z represents the membrane thickness and A the membrane surface area.

It is here interesting to note that if one combines the definitions of the permeate composition and mass transfer expressions, the membrane thickness does not affect the composition of the permeate (one of the early observations made by Graham).

Three fundamental adimensional variables can be proposed at this stage:

1. The ideal selectivity α^* , previously defined as the ratio of the fast over the slow permeability, is characteristic of the gas pair/polymer of the system:

$$\alpha^* = \frac{P_i}{P_j} \quad (33)$$

2. The stage cut θ , which corresponds to the ratio of the total permeate to the flow rate of the feed, is linked to the productivity of the module, and can be seen as a key design variable:

$$\theta = \frac{Q_p}{Q_{in}} \quad (34)$$

3. The driving force, expressed exclusively through the pressure ratio and not through the absolute pressure or pressure difference, is a main operating variable governing the energy requirement of the module (i.e., to a large extent, the operating costs):

$$\psi = \frac{p''}{p'} \quad (35)$$

From the permeate composition and mass transfer expressions, it is possible to obtain the following expression:

$$\frac{y}{1-y} = \alpha^* \left(\frac{x_{out} - \psi y}{1 - x_{out} - \psi(1-y)} \right) \quad (36)$$

If the three expressions (permeate composition, mass transfer, and mass balance) are combined, they can be rearranged into a quadratic equation. This result is interesting in that it can be used to determine the permeate composition (y) as a function of the feed composition (x_{in}), the ideal selectivity (α^*), the stage cut (θ), and the pressure ratio (ψ):

$$ay^2 + by + c = 0 \quad (37)$$

With:

$$\begin{aligned} a &= \left(\frac{\theta}{1-\theta} + \psi \right) (\alpha^* - 1) \\ b &= (1-\alpha^*) \left(\frac{\theta}{1-\theta} + \psi + \frac{x_{in}}{1-\theta} \right) - \frac{1}{1-\theta} \\ c &= \alpha^* \left(\frac{x_{in}}{1-\theta} \right) \end{aligned} \quad (38)$$

In the above, the positive root of the second-order polynomial ranging from 0 to 1 was the only physically consistent answer taken as the solution to the problem.

It is, at this stage, interesting to identify the conditions that should maximize the permeate mole fraction of the fast compound (y), that is, the maximal separation performances. Such conditions are obtained for a vanishing pressure ratio (i.e., a perfect vacuum at the downstream side, $p''=0$) and stage cut ($\theta \sim 0$, which corresponds to an infinitely small permeate flow rate and thus a vanishing

productivity). The second condition leads to a simple analysis since the composition in the feed stream remains unchanged ($x_{in} \sim x_{out} = x$). Somehow, this mode of operation corresponds to a distillation column operated under infinite reflux conditions: a maximal selectivity can be obtained at the expense of a vanishingly small productivity. Numerous similar trade-off situations can be found within the topic of separation science [75]. The final expression that applies for $p'' \sim 0$ and $\theta \sim 0$ is written as

$$y = \frac{\alpha^* x}{1 + (\alpha^* - 1)x} \quad (39)$$

Here it is important to note that, for these very specific operating conditions, the separation factor α (defined in the introductory part) equals the ideal selectivity α^* (i.e., the compound permeability ratio). **Figure 16** shows a series of curves generated by the previous expression.

Logically, no separation is obtained when the ideal separation factor $\alpha^* = 1$. For a given feed composition x , an increasing separation effect is found when the fast to slow permeability ratio α^* increases. Interestingly, the same mathematical expression and equivalent master curves are obtained for vapor liquid equilibrium of a perfect binary mixture. In this case, the saturated vapor pressure ratio plays

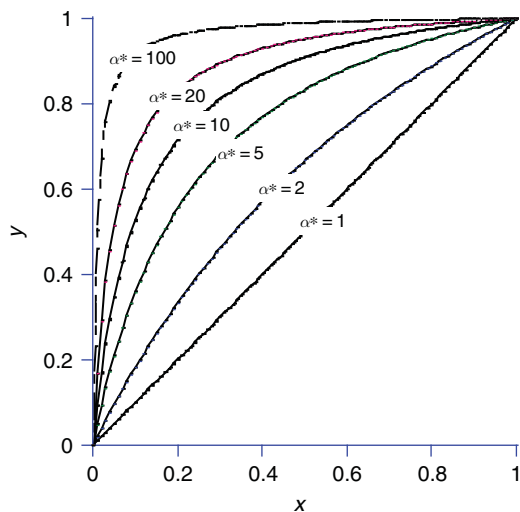


Figure 16 Representation of Equations (25) and (39): maximal permeate purity (y) which can be obtained for a given feed composition (x) for different ideal selectivity values (α^*). The same expression is obtained in order to determine the effective separation factor (α) from the outlet composition of a unit at the retentate (x) and permeate (y) sides.

the same role as the ideal selectivity [76]. This simple expression is of great help for shortcut calculations since, as already mentioned, it provides the highest mole fraction that can be obtained in a single-stage membrane unit on the permeate side. Since the attainment of a target purity is often imposed, this expression can be used in order to verify whether the specification can be obtained with a given polymer material and a known permeability ratio. Furthermore, it can also be used for the determination of the minimal target material selectivity (α^*) if x and y are fixed.

Another asymptotic solution can be derived for perfect mixing conditions if an infinitely small stage cut is assumed ($\theta \sim 0$). In this case, the mole fraction of the outlet retentate is again identical to the feed mole fraction ($x_{out} \sim x_{in} = x$). This expression is of interest as it permits the analysis of the respective influence of the ideal selectivity and the pressure ratio on the separation performances of the module:

$$y = \frac{2}{\psi} \left(x + \psi + \frac{1}{\alpha^* - 1} - \sqrt{\left(x + \psi + \frac{1}{\alpha^* - 1} \right)^2 - \frac{4\alpha^* \psi x}{\alpha^* - 1}} \right) \quad (40)$$

For a binary system, Equation (40) has two limiting cases. When $\alpha^* \gg 1/\psi$, the selectivity is no longer important, and, under the condition that the value of y can never be greater than unity, the permeate composition simply becomes

$$y \approx \frac{x}{\psi} \quad (41)$$

In this case, the separation performances are dictated by the process conditions, and the pressure ratio that is available for the industrial application becomes a key issue. This situation is typical for separations where a very high ideal selectivity is achievable, such as during the removal of hydrogen from mixtures with hydrocarbons in hydrotreaters in refineries or during the dehydration of gas streams. For the latter, the amount of water that can be removed is limited by the ability to maintain a very low partial pressure of water in the permeate.

Conversely, if $\alpha^* \ll 1/\psi$, the influence of the pressure ratio can be neglected and the permeate composition becomes limited by the polymer selectivity. This situation occurs when the membrane is operated with vacuum on the permeate side (i.e., $\psi \rightarrow 0$) or when only a low selectivity is achievable. An example of practical importance is the separation of nitrogen from methane in the

treatment of natural gas. In this case, the N_2/CH_4 selectivity is rarely greater than 2. This induces large losses of methane in the permeate and such losses are often problematic for the application. A significant improvement in the ideal selectivity of the material is clearly required.

Figure 17 summarizes the major conclusions of the above-developed analysis and presents examples of master curves that can be generated when the different relationships between stage cut, pressure ratio, and permeate composition are simultaneously considered. This type of graph depicts the basic framework that needs to be handled for analyzing the module design.

2.08.3.3 Membrane Module Design: Methodology

Historically, the basis of gas permeation module design was first proposed by Weller and Steiner [77] in 1950. Nowadays, modern computation techniques enable numerical solutions to the problems [78], thanks to dedicated routines. Orthogonal collocation methods are reported to be particularly attractive when a minimum resolution time and computational efforts are required [79]. Several of these routines have been implemented in commercial

process simulation softwares, where advantage can be taken of thermodynamics or unit operation design packages in order to simulate hybrid or multi-stage operations with gas separation membranes. Nevertheless, much effort has been devoted to the search of asymptotic analytical solutions to the problem [80] before computing facilities were available. Approximate analytical solutions are still occasionally proposed and they can be of interest, for instance when a broad and systematic sensitivity analysis is desired [81, 82].

In the previous section, a general methodology was proposed in order to predict the performances of a membrane separation module based on a series of simplifying assumptions. The main interest of the approach was to offer the possibility of obtaining a simple, easy-to-handle analytical expression. Nevertheless, the solution obtained through this simplified approach should be taken as a rough estimate, and the hypothesis of perfect mixing conditions must be reconsidered if one expects a more realistic answer with regard to the performance of an industrial module. Similarly to the framework proposed in chemical reactors, heat exchangers, or mass transfer operations, a completely different hypothesis, namely that of a perfect plug flow, is first proposed in order to estimate the incidence of

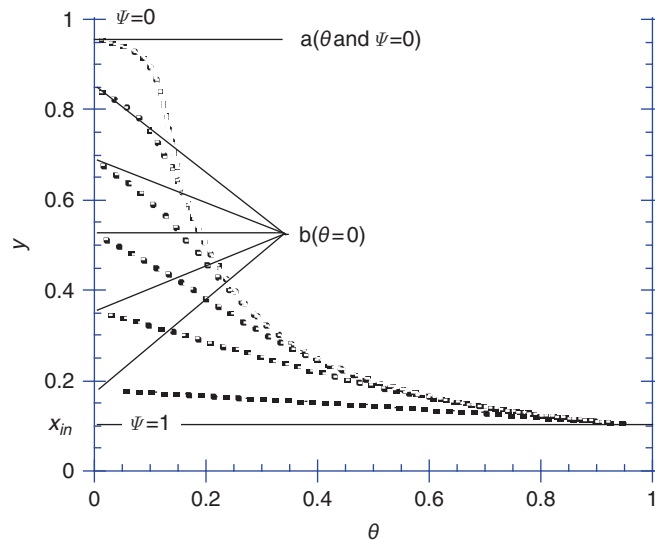


Figure 17 Schematic representation of permeate composition delivered by a membrane separation unit as a function of module stage-cut for different pressure ratio. The membrane ideal selectivity (α^*) is kept constant. When no driving force is exerted ($\psi = 1$), no separation is obtained and $y = x_{in}$. For zero stage cut and zero pressure ratio conditions (noted a on the figure), the maximal permeate purity is obtained and it can be computed by Equation (39). For zero stage-cut conditions (noted b on the figure), Equation (40) can be used. For any other situation, the general solution can be obtained by Equations (37–38) under the assumption of perfectly mixed conditions.

hydrodynamics conditions on the separation performances. This minor modification necessarily leads to a system of ordinary differential equations and, strictly speaking, a rigorous analytical solution can no longer be derived. This difficulty has stimulated much research efforts in the last decades with the aim of identifying approximate analytical solutions to the problem [83]. Basically, different configurations can be proposed and **Figure 18** identifies the four main cases. A fifth one, the so-called one-side mixing (consisting in perfect mixing conditions on the upstream side, and a plug flow on the downstream side), has also been occasionally studied [84]. However, it is rarely taken into account since the performances of industrial modules are most often well covered by the four cases shown in **Figure 18**.

Despite the fact that situations of greater complexity can nowadays be treated, thanks to increasing computing capacities, it is interesting to note that the overall methodology is still employed successfully in numerous cases for module design

purposes [85]. More specifically, hollow-fiber modules may be designed with reasonable precision to approximate an idealized counter-current when the permeate pressure is significant, or to approximate a cross-flow pattern when the permeate pressure is low enough. **Figure 19** displays an example of the excellent agreement that can be obtained between the simulations performed according to the methodology exposed in the present section (i.e., a constant permeability, the absence of coupled fluxes, a plug flow, isothermal conditions, etc.) as well as the experimental results obtained with a hollow-fiber module fed by a multi-component mixture.

The cross-plug-flow model, which remains the cornerstone when it comes to models in this field, is detailed in the following so as to offer a generic framework for module design. As depicted in **Figure 20**, the cross-plug-flow model assumes a plug flow on the upstream, feed side of the membrane, and free flow on the downstream, permeate side.

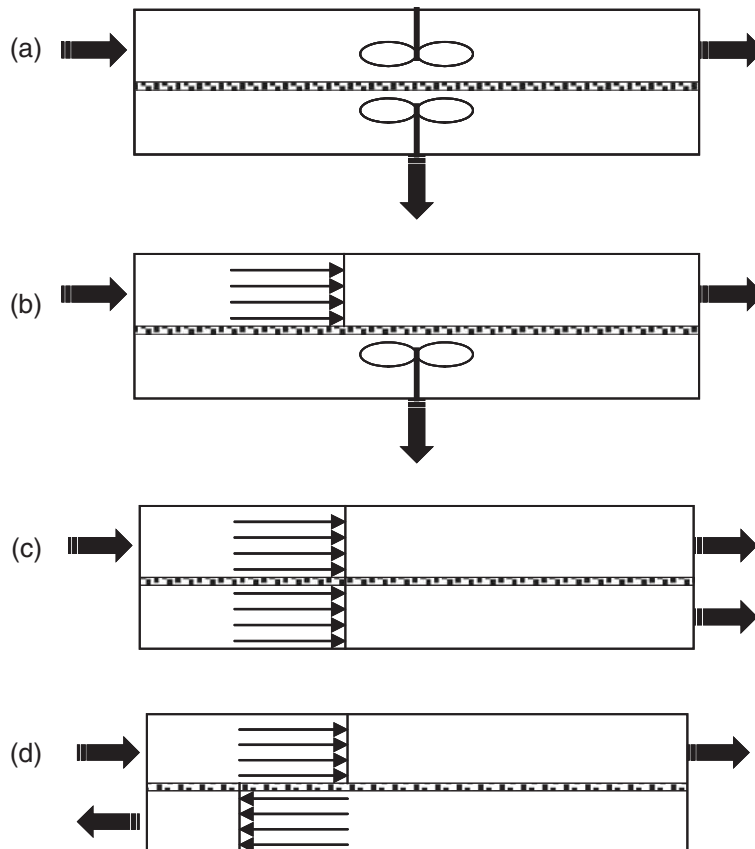


Figure 18 Schematic representation of the four main different flow configurations in polymeric membranes gas permeation processes: (a) perfect mixing, (b) cross plug flow, (c) cocurrent flow, and (d) counter-current flow.

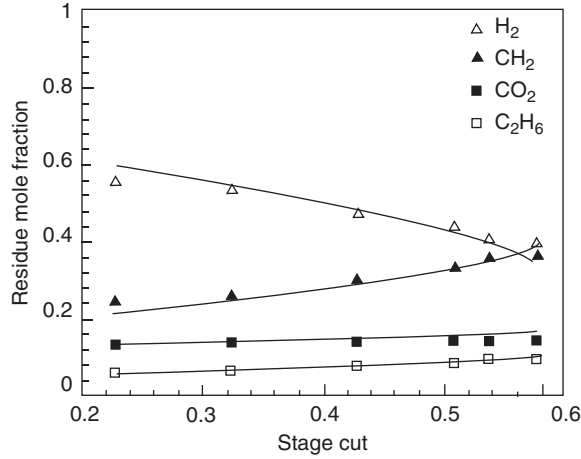


Figure 19 Comparison between experimental data (points) obtained with a multi-component mixture separation and the simulations (lines) obtained according to the classical methodology described in this section [70]. Retentate compositions as a function of the stage cut (θ) at $T = 40^\circ\text{C}$ and $p = 20$ bar.

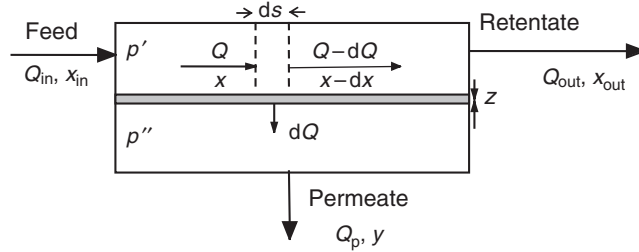


Figure 20 Schematic representation of a gas separation module for cross plug-flow conditions.

Apart from the flow conditions, the hypotheses proposed for the derivation of the solution in the case with perfect mixing conditions are maintained in the under-mentioned analysis.

A mass balance over a differential surface area ds leads to the following differential equation:

$$Q^* \frac{dx}{ds} = - \left(x - \psi y + x \frac{dQ^*}{ds} \right) \quad (42)$$

where x is the upstream fast compound mole fraction and s is the dimensionless membrane area:

$$s = \frac{AP_i p'}{zQ_{in}} \quad (43)$$

Q^* corresponds to the local stage cut $Q^* = Q/Q_{in}$. We can thus write the flux relationships for each component according to

$$-d(Qx) = \frac{P_i p'}{z} (x - y\psi) ds \quad (44)$$

$$-d[Q(1-x)] = \frac{P_j p'}{z} [(1-x) - (1-y)\psi] ds \quad (45)$$

These two equations can be combined, giving rise to the following expression:

$$\frac{dQ^*}{ds} = - \left(x - \psi y + \frac{1}{\alpha^*} (1-x - \psi(1-y)) \right) \quad (46)$$

Finally, from the definition of the equations of the local permeate composition and the mass transfer,

$$\frac{y}{1-y} = \alpha^* \left(\frac{x - \psi y}{1-x - \psi(1-y)} \right) \quad (47)$$

The set of Equations (42), (46), and (47) can be solved numerically and they represent the basis of the cross-plug-flow model. Similar sets of equations have, with the corresponding boundary conditions, been applied by various authors in order to predict separation performances for cross-flow, co-current, or counter-current modes [86]. A correct to excellent agreement has been obtained when predictions are compared to experimental lab-scale data [87]. For multi-component permeation situations, several modeling studies have been reported. Generally, and in

more practical terms, it is interesting to notice that experimental data from on-site pilot modules are often reported as being intermediate between the perfectly mixed and the cross-plug-flow predictions [88].

2.08.3.3.1 Single module design: Surface and energy requirements

A rational analysis of the problem should now be proposed, in order to provide a quantitative answer in terms of size (required surface area) and operating conditions (pressure ratio). The starting point remains the Equations (42) and (46)–(47), offering the possibility of screening the set of solutions which respects the specifications and the feed composition. Basically, two major situations can be found.

The simplest situation corresponds to a single target performance, such as the purity of the permeate (y) or retentate ($1-x_{\text{out}}$). For example, hydrogen, which is a fast compound, can, in certain cases, be imposed to reach a given purity in the permeate, and nitrogen to reach a given purity in the retentate. An example of permeate purity and retentate composition for a single-stage module operated under varying pressure ratios and hydrodynamic conditions is shown in Figure 21. Again, a sensitivity analysis would demonstrate that, in certain cases, the hydrodynamic conditions play a significant role (e.g., a retentate composition for $\psi = 0.5$), while a negligible effect can be obtained in other situations (e.g., a permeate purity y for $\psi = 0.1$).

More generally, the simulations shown in Figure 21 confirm that counter-current conditions systematically provide the best performances, followed by cross-plug-flow, co-current, and perfectly mixed scenarios. As a consequence, either the counter-current model or that of the cross plug flow will most often be proposed for engineering purposes.

The second situation for module design concerns the case of simultaneous purity and recovery constraints. The recovery ratio R , corresponding to the percentage of a target compound that is collected from one of the exit streams of the module, can also be simultaneously imposed. When the target compound is the fast permeating species, such as for hydrogen purification or volatile organic compound (VOC) recovery applications, R is expressed as

$$R = \theta y / x_{\text{in}} \quad (48)$$

In other cases, the target compound is the slow compound of the mixture, obtained at the retentate side. The corresponding recovery ratio is then

$$R = (1-\theta) \frac{(1-x_{\text{out}})}{(1-x_{\text{in}})} \quad (49)$$

This expression can, for instance, be used in order to determine the recovery of natural gas (slow permeant) for sweetening operations.

Before a multi-variate and optimization analysis is performed, it is interesting to examine the set of solutions (θ , ψ , s) enabling a fixed y and R to be obtained when the feed composition and the ideal selectivity of the membrane are fixed. Figure 22 shows an example of a master curve with the interplay between these variables. Numerous curves of this type, demonstrating the large amount of relationships between the different variables, can be found in detailed studies [89].

A general methodology that enables the data set satisfying the constraints to be identified was presented in the previous section. The energy requirement and the membrane surface area needed can now be estimated according to the following:

1. The estimation of the energy requirement for a single-stage process is straightforward and is most often restricted to the contribution of the compressor or vacuum pump. Since the pressure ratio only plays a role in the analysis, it is possible that feed compression or vacuum pumping at the permeate side can be indifferently applied. This is not exactly the case due to the differences in flow rates at the feed and permeate. For instance, for a feed compression with atmospheric pressure at the permeate side ($p'' = 1$), the energy requirement can be estimated as

$$E = Q_{\text{in}} \frac{\gamma RT}{\eta(\gamma-1)} \left[\left(\frac{1}{\psi} \right)^{\frac{\gamma-1}{\gamma}} - 1 \right] \quad (50)$$

where, γ is the adiabatic expansion factor of the gas mixture (e.g., $\gamma = 1.4 \text{ J mol}^{-1} \text{ K}^{-1}$ for nitrogen), η the isentropic efficiency, and T the inlet temperature (K).

For a permeate vacuum pumping strategy with atmospheric pressure at the retentate side ($p' = 1$), the energy requirement becomes

$$E' = Q_{\text{p}} \frac{\gamma RT}{\eta'(\gamma-1)} \left[\left(\frac{1}{\psi} \right)^{\frac{\gamma-1}{\gamma}} - 1 \right] = \theta E \quad (51)$$

Such a simplified analysis would suggest the systematic application of a vacuum pumping strategy, in order to minimize the energy requirement of the process. Industrial feedback shows that this option is very rarely chosen for a variety of reasons. Above all,

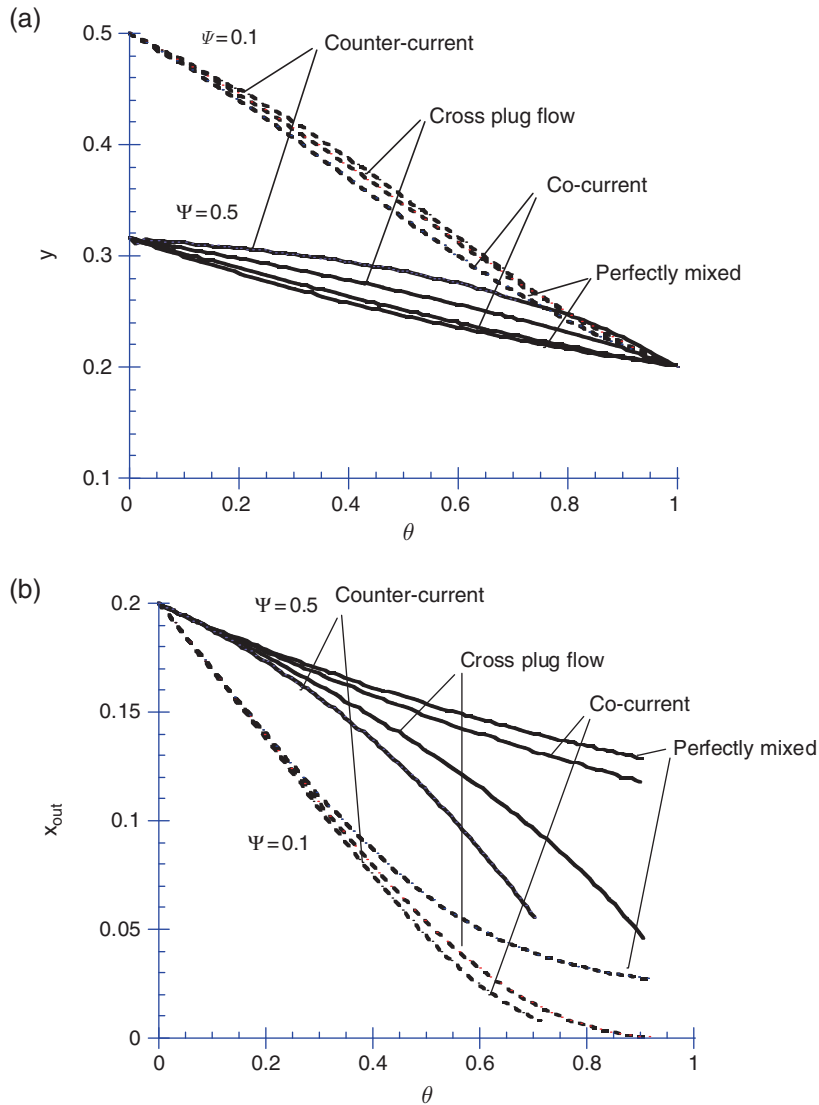


Figure 21 Simulation of a binary gas mixture separation with a single-stage membrane module. Evolution of the separation performances: (a) permeate purity (y) and (b) retentate purity (x_{out}), as a function of the stage cut and the hydrodynamic conditions. Feed mixture composition (x_{in}) 0.2, membrane ideal selectivity (α^*) 5. Two different pressure ratios are compared: 0.5 and 0.1.

vacuum pumping generates a much smaller driving force than the feed compression and a much larger surface area, thus giving rise to a considerably higher capital cost. Other arguments in favor of feed compression include the difficulty of achieving vacuum at an industrial scale, the lower energy efficiency of vacuum pumps as compared to compressors ($\eta' < \eta$ in Equations (50) and (51)), and their large foot prints. Conversely, the risk associated with compression favors the use of vacuum operation for VOC recovery. For permanent gas separations, however, apart

from very specific cases, the practical operation of vacuum pumping is almost never selected. Practically, the operating costs associated with module operation can, be estimated if a unit cost of electricity is available.

2. When the pressure ratio in combination with the feed compression or vacuum option is selected, the corresponding module area can be easily determined from the definition of s . The related capital cost can be estimated as soon as a unit cost of the membrane area is available. It should be noted that, for the latter,

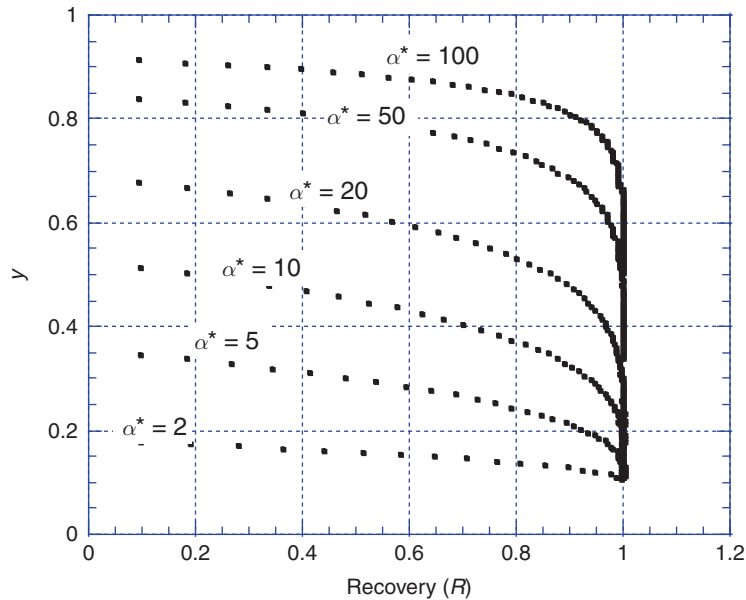


Figure 22 Binary mixture separation by a membrane module. Interplay between permeate composition (y), fast compound recovery ratio (R), and ideal selectivity (α^*). A cross-plug-flow model with a feed composition x_{in} of 0.1 and a constant pressure ratio ($\psi = 0.01$) has been fixed for the simulation.

considerable discrepancies can be found in the literature. Depending on whether or not pretreatment costs are included, and whether a well known and already available membrane material as opposed to a hypothetical one is considered, very different figures are obtained.

Finally, the best set of (s, ψ) data can be determined when the operating costs (estimated from the energy requirement E) and the capital costs (the membrane area estimated from s and compressor unit cost) are considered together. A sketch of the interplay between these two contributions is presented in **Figure 23**.

Again, a trade-off needs to be made between solutions favoring low capital cost (i.e., a low ψ value) at the expense of high operating costs, and the opposite situation. The same operation can be reiterated with another membrane material and a different design would then be obtained through the cost minimization operation. An example of the solution obtained, thanks to this methodology, is illustrated in **Figures 24 and 25**, in which a comparison is performed of the operating conditions, surface area, and energy requirement for producing a defined capacity of a nitrogen stream of 95% purity with two membrane types covering the extremes of the selectivity/permeability trade-off: a highly permeable, poorly selective silicone rubber membrane and a poorly

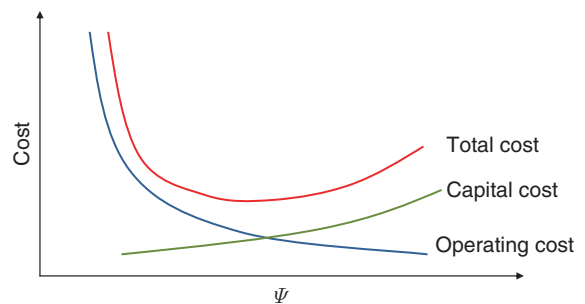


Figure 23 Representation of the evolution of operating costs, which principally result from energy requirement, capital cost, which depend on the membrane surface area required and the total cost as a function of the pressure ratio for a single module design study. At low pressure ratio values, energy requirement is high but a smaller surface area is required. The reverse occurs for high pressure ratio values. The optimal set of pressure ratio and stage-cut data is obtained when the total cost of the installation is minimized.

selective permeable cellulose acetate membrane. A systematic and rigorous cost analysis takes a great number of factors into account.

2.08.3.3.2 Recycling and multi-stage processes

The methodology exposed in the previous section can be said to correspond to a single theoretical stage analysis in conventional separation processes. The

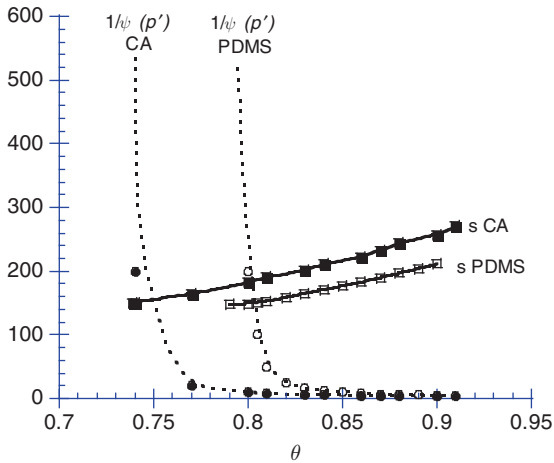


Figure 24 Adimensional membrane area ($s \times 100$) and upstream pressure ($p' = 1/\psi$) required for the production of 95% purity nitrogen ($x_{out}=0.05$) from air ($x_{in}=0.21$) with two membranes having different O_2/N_2 selectivities: CA ($\alpha^*=4$) and PDMS ($\alpha^*=2.2$). Cross-plug-flow conditions have been used for the computations.

impossibility of achieving the target performances with a single stage thus suggests an exploration of the potentialities of multi-staged operations. This classical option in an equilibrium staged process is however completely different for membrane gas separation processes. The main reason is that any supplementary stage requires a recompression step, affecting both the capital and operating costs, whereas staging is easy and relatively inexpensive in absorption or distillation towers. As a consequence, even if improved performances can be obtained as compared to in the single-stage case, industrial practice shows that the number of stages remains limited to 2, or exceptionally 3, in membrane gas separation. Basically, the methodology described for a single stage can be extended to cascades or interconnected networks in order to simulate and evaluate the interest of these more sophisticated processes. A great number of flowsheets can be proposed depending on recycling and connection possibilities. Two such examples, taken from design studies of a VOC recovery [90] and a natural gas treatment [91],

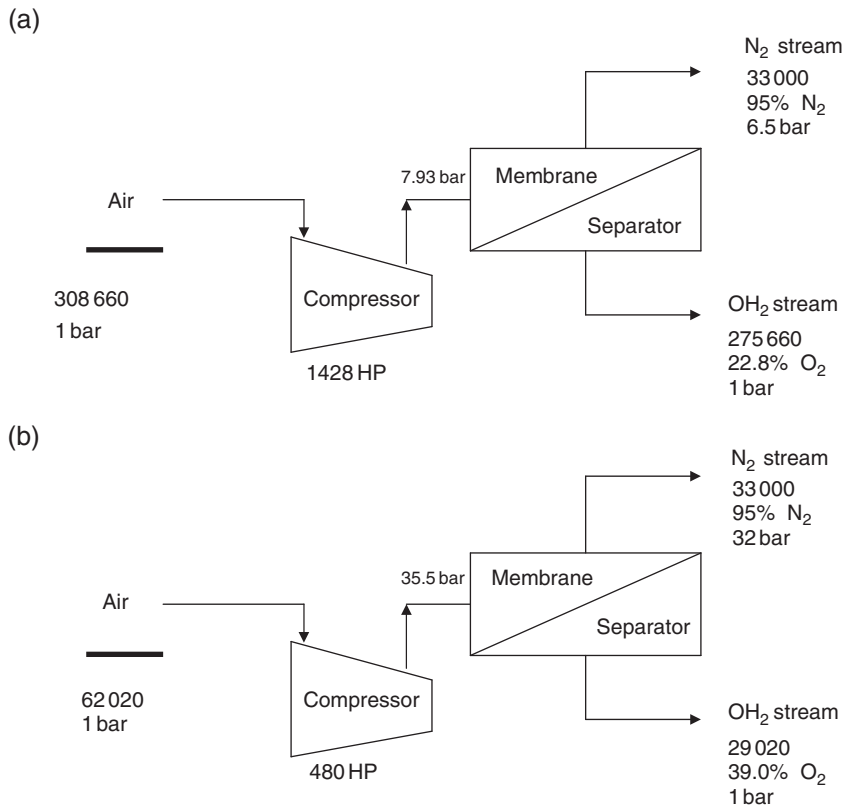


Figure 25 Two different single-stage membrane modules designed for the production of 33 000 SCFD of a 95% purity nitrogen stream, with a highly permeable but poorly selective silicone rubber membrane (a) and a selective, poorly permeable cellulose acetate membrane (b) [124].

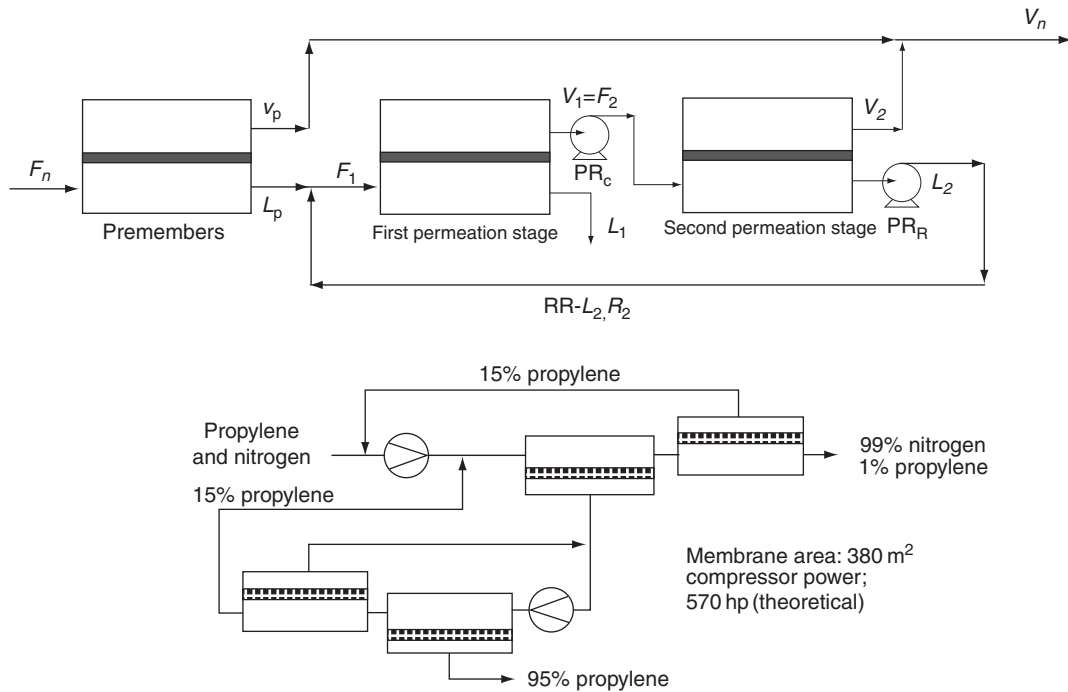


Figure 26 Two examples of multi-stage membrane separation processes for carbon dioxide removal from natural gas [136], and for nitrogen/propylene separation [147].

are shown in **Figure 26**. The search for optimal conditions can logically be very complex and several investigations have addressed the problem of optimizing multi-staged or network gas separation processes, for instance, in the case of carbon dioxide/methane separation [92].

Instead of adding separation stages in a cascade, it can be useful to explore how the single-stage performances can be improved by a modification of the fluid distribution. The recycling of the retentate to the permeate stream can be an effective means of enriching the less permeable component in the retentate stream [93] (**Figure 27**). Comparative studies have confirmed the interest of the technique, including a

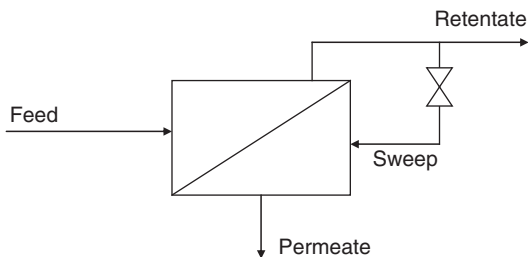


Figure 27 Membrane separation module with retentate recycle for permeate sweeping.

multi-stage cascade, as compared to that of the single-stage operation [94]. This option is often selected for hydrogen purification or drying operations.

2.08.3.4 Membranes, Modules, and Industrial Installations

2.08.3.4.1 Membrane and module structures

There are basically two main types of membranes used for industrial gas separations: skinned asymmetric structures and composites (**Figure 28**).

For industrial application purposes, a polymer is required to be fabricated into a device with a thin active layer of 1 μm or preferably less. For glassy materials, it can be as thin as 50 nm (**Figure 29**).

Membranes can be inserted in three major types of modules for gas separations applications: plate and frame, spiral-wound, and hollow-fiber modules. The main characteristics of these three geometries are summarized in **Table 4**.

Figures 30 and 31 respectively show a hollow-fiber module with typical characteristics and a spiral-wound module.

The tolerable pressure of membrane modules is in the range of 150 bar (for the spiral-wound or hollow-

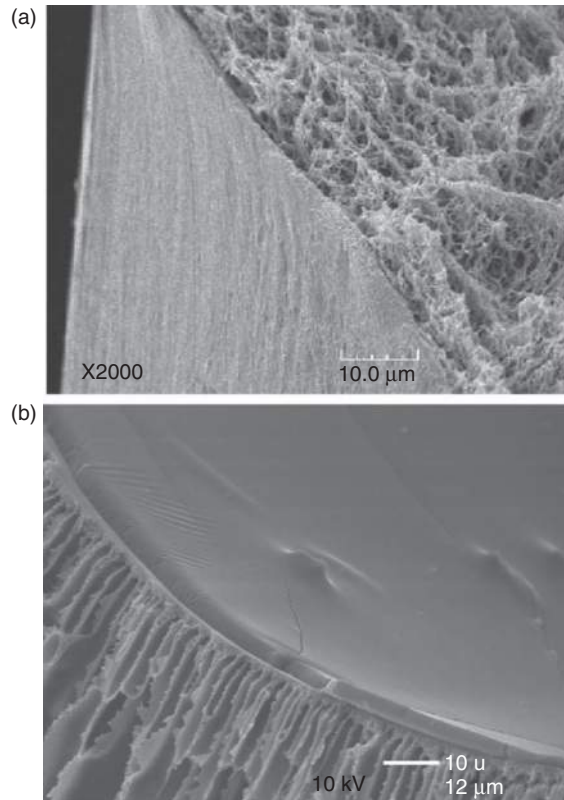


Figure 28 SEM pictures of the two main structures of membranes which can be found for industrial use in gas separation applications: an asymmetric skinned membrane fabricated from a single polymer by a phase inversion process (a) and a composite membrane, with a dense skin layer coated on a porous support made of a different polymer (b).

fiber types), and the maximal operating temperature is 150 °C. From a practical point of view, a module can be used with feed mixture on either the bore side or the shell side. If boundary layer mass resistances are

neglected, there should be no difference between these two operating modes, according to the above-mentioned basic methodology (the pressure ratio is the only influencing variable in the expression).

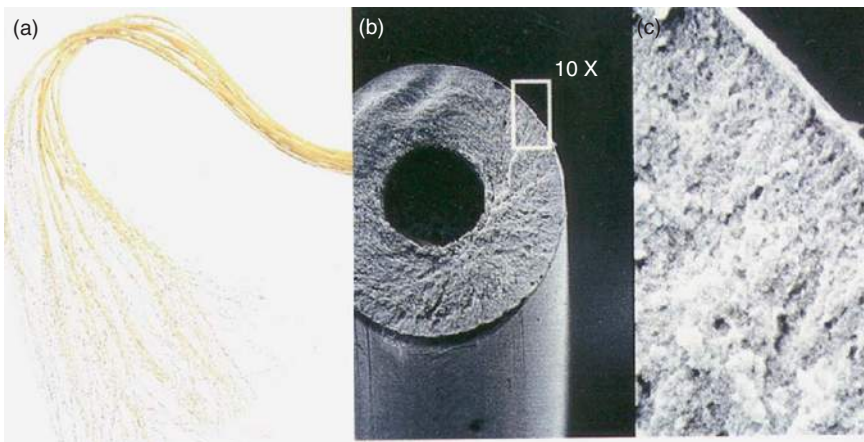


Figure 29 A bundle of hollow fibers such as those used in industrial modules (a) and scanning electron microscopy (SEM) picture of a single fiber (b) showing a detail of the dense outer skin layer (c). Courtesy of Air Liquide/MEDAL™.

Table 4 Key characteristics of the three major types of modules used for industrial applications of gas separation processes with polymeric membranes

	<i>Plate and frame</i>	<i>Spiral wound</i>	<i>Hollow fiber</i>
Packing density ($\text{m}^2 \text{m}^{-3}$)	30–500	200–1000	500–10 000
Approximate area per module (m^2)	5–20	20–40	300–600
Pretreatment requirement	Minimal	Fair	High
Resistance to fouling	Good	Fair	Poor
Pressure drop	Low	Fair	High
Flow distribution	Fair	Moderate	Good
Manufacturing cost	High ($50\text{--}200\text{\$ m}^{-2}$)	Medium ($10\text{--}50\text{\$ m}^{-2}$)	Low ($2\text{--}10\text{\$ m}^{-2}$)

Nevertheless, flow distribution, membrane mechanical resistance, or subtle effects assumed to result from the differential mechanical stress exerted on the skin layer can lead to measurable differences in performances depending on the feed mode. A 15% increase in the permeance has been reported for bore-side feed, as compared to shell-side feed, in an air separation

application [95]. Shell-side feeding is preferred when a high pressure is needed as it displays the advantage of a higher mechanical resistance of the fiber and a larger interfacial area. However, it also has the disadvantage of a more elevated pressure drop on the permeate side, the requirement of a casing that is resistant to the high-pressure conditions, and moreover, channeling

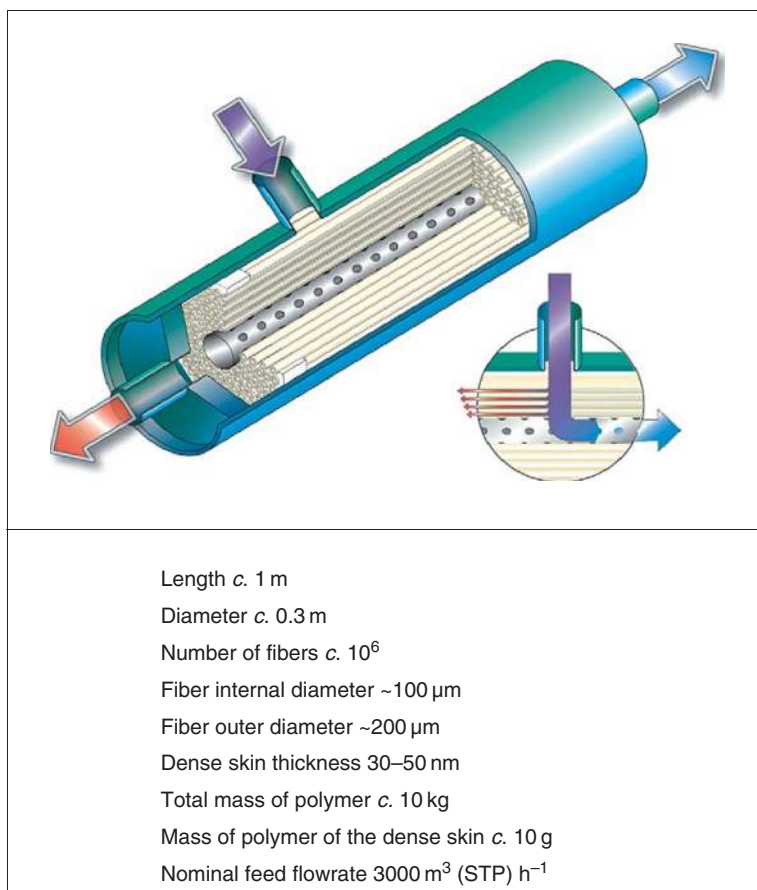


Figure 30 Schematic representation of an industrial hollow-fiber module with shell-side feeding. The retentate emerges through the collecting tube on the left and the permeate from the bore of the fibers on the right. Courtesy of Air Liquide/MEDAL™.

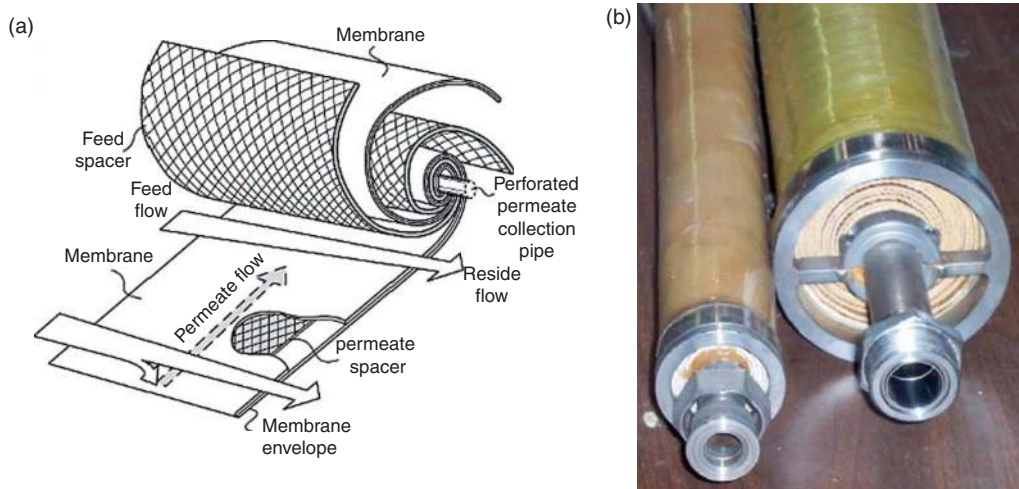


Figure 31 Schematic representation (a) and picture (b) of an industrial spiral wound module. Courtesy of MTR.

problems on the retentate side. Bore-side feeding is applied for low feed pressure conditions. A lower interfacial area is obtained and flow distribution problems can result from internal diameter variations of the fibers.

2.08.3.4.2 Feed pretreatment

When installed in an industrial environment, the selection of the different feed pretreatment operations is a key issue. A traditional pretreatment scheme usually consists of:

1. a coalescing filter for liquid and mist elimination;
2. an adsorbent guard bed for the removal of trace contaminants, such as hydrocarbons (this is often nonregenerable);
3. a particle filter for dust removal after the adsorbent bed; and
4. a heat exchanger to achieve the target feed temperature.

In some cases, a chiller or a turboexpander may be included to reduce the dew point of the gas as well as the hydrocarbon content. The risk associated with the formation of hydrates sometimes requires the addition of inhibitors, or the incorporation of a deep-drying operation, such as glycol absorption.

When the feed composition is subject to changes, a pretreatment retrofit is often needed in order to prevent damage to the membrane.

2.08.3.4.3 Industrial module design: From permeability to permeance and effective selectivity

When studying scanning electron microscopy (SEM) micrographs of industrial membranes, it is difficult to precisely determine the thickness (z) of the dense layer. Furthermore, for different reasons, the membrane properties can vary from those of the bulk at this scale. The discrepancy can be significant, even though a difference of a factor >2 is rarely obtained.

Fortunately, for module design purposes, only the effective proportionality constant is required in combination with the local driving force, as has been previously demonstrated. Thus, it is of greater relevance to express membrane performances through a combined permeability and thickness variable, called permeance [96]. For gas separation with polymer membranes, the permeance is often expressed in gas permeation units (GPUs). One GPU is $10^{-6} \text{ cm}^3 \text{ (STP)/cm}^2 \text{ s cmHg}$, which in SI units corresponds to $3.347 \times 10^{-12} \text{ mol m}^{-2} \text{ s}^{-1} \text{ Pa}^{-1}$. The role of the porous support, which, in general, cannot be neglected from the point of view of mass transfer, is usually included in this effective parameter. In the case of composites, the permeation behavior can be explained according to an analogy between gas permeation and electrical flow [97]. The various portions of the composite are described in terms of their resistance to gas permeation and the support (substrate) and dense layer (coating) contributions

can be matched in order to optimize the flux and separation factor [98].

Table 5 summarizes some major permeance and selectivity characteristics that are currently achieved for industrial gas separations, and a nonexhaustive list of suppliers is given in **Table 6**.

The number of polymeric materials that are commercially available for industrial applications is surprisingly small when considering the hundreds of polymers having undergone investigation and that can be synthesized. This situation can be explained by the fact that the development path to an efficient and reproducible membrane is a long, complex, and expensive process, and includes both technical and commercial activities. Numerous steps and potential bottlenecks can block the development, for instance, the difficulty in achieving the target permeance and effective selectivity, problems of incorporation in a module, the potential incompatibility with sealants (epoxy, polyurethane, silicone, etc.), the sensitivity to contaminants (that, in certain cases, can only be detected on-site), and so forth. On the whole, these issues have limited the development of commercially available membrane modules to a small number of candidates.

From a practical point of view, the tailoring of a polymeric structure is often performed in order to achieve the best performances. The simultaneous increase in fractional free volume and the hindering of chain backbone motions is especially applied. As a result, membrane permeability can be increased by over two orders of magnitude in the best cases, especially through an augmentation of the diffusion coefficient. The sorption and selectivity are definitely more difficult to tune, and improvements by a factor 2–4 as compared to the base material are often considered as upper limits.

Before continuing with a description of the industrial applications of polymeric gas separation membranes and returning to the equations framework that was developed in the previous section, it is important to note that several complications are susceptible of arising. These factors can be roughly divided into two main categories: first, potential changes to the hypotheses proposed for the operating conditions, and second, complications arising from the permeation behavior.

2.08.3.4.4 Pressure drop

The hypothesis, postulated in the analysis above, of a constant total pressure on each side of the membrane

is not necessarily systematically valid. Numerous studies have addressed this problem and, for bore-fed hollow-fiber modules, the results have demonstrated that the pressure drop on the bore side can be adequately estimated by the Poiseuille equation [99]. For a fiber of internal radius r , the pressure gradient in the axial direction principally depends on the total rate of the gas flow Q as well as the mixture viscosity μ :

$$\frac{dp}{dl} = -\frac{8\mu RTQ}{\pi pr^4} \quad (52)$$

The special case where a permeate pressure builds up when hollow fibers are fed to the shell side and vacuum is simultaneously applied to the bore side has been studied in greater detail [100]. Moreover, many studies have addressed the specific problem of a pressure drop in lumen of hollow-fiber modules [101].

2.08.3.4.5 Nonisothermal permeation conditions

Isothermal conditions were postulated in the general framework; however, this hypothesis should be reconsidered, particularly for water permeation, due to the considerable amount of condensation heat released at the upstream side and the possible cooling that may occur due to evaporation on the downstream side. Even though these two effects are expected to be perfectly balanced, temperature gradients are known to occur during steady-state water permeation, causing the temperature polarization to become predominant.

The specific case of temperature changes in a gas permeation module has been investigated by Gorisen [102]. Temperature changes on the retentate side ranging from 1 °C (nitrogen production from air, hydrogen recovery) to more than 7 °C (natural gas treatment) have been estimated. This range in the temperature change depends on the Joule–Thomson coefficient of the gas mixture and a shortcut calculation can be used in order to estimate the effect. A temperature decrease is usually obtained, but an increase can also occur. This is especially true for hydrogen as a result of the negative Joule–Thomson coefficient of this compound. Recent reports have described a general and rigorous modeling framework for gas membrane separation, incorporating nonisothermal conditions [103].

Table 5 A summary of the major industrial applications and material and engineering characteristics of gas separation processes with polymeric membranes

<i>Application</i>	<i>Typical membrane materials</i>	<i>Membrane effective selectivity (a)</i>	<i>Membrane permeance (GPU)</i>	<i>Approximate target design parameters</i>	<i>Remarks</i>
H ₂ purification (H ₂ /CO, H ₂ /N ₂ , H ₂ /CH ₄)	<i>Glassy</i> : polysulfone, polyimides, cellulose acetate	50–200 (H ₂ /CO < H ₂ /N ₂ ~ H ₂ /CH ₄)	50–500	$x_{in} \sim 0.3-0.7$ $v \sim 0.9$ $R \sim 0.9$ $x_{in} = 0.79$	High pressure for ammonia synthesis application (140 bar), medium for refinery (40–70 bar) H ₂ /CO separation is more difficult ($\alpha < 100$)
N ₂ production from air	<i>Glassy</i> : polyimides, polysulfones, ethylcellulose	~7	5–250	$x_{out} \sim 0.9-0.99$	Single stage with feed compression to ~10–15 bar H ₂ O, O ₂ , and CO ₂ are removed Higher N ₂ purity requires multi-stage or hybrid processes
CO ₂ removal from natural gas	<i>Glassy</i> : polyimides, cellulose esters	~30	10–200	$x_{in} \sim 0.05-0.5$ $x_{out} \sim 0.02$ (pipeline) or $v \sim 0.9-0.97$ and $R \sim 0.9-0.95$ (EOR)	Single-stage, hybrid, or multi-stage processes H ₂ O can be removed with CO ₂ Membrane plasticization can be a problem and requires adequate pretreatment
VOC recovery from air or inert gases	<i>Rubbery</i> : silicone rubber (PDMS)	3–100	>1000	$x_{in} \sim 0.01-0.1$ $x_{out} \sim 0.001$ or $R \sim 0.9$	Selectivity depends on VOC type and increases when temperature is decreased. Used in combination with a condenser.
H ₂ O removal (air or permanent gas drying)	<i>Glassy</i> : polysulfone, polyphenyleneoxyde (PPO)...	>200	>200	Relative humidity decrease 50–90%	Temperature and concentration polarization

Table 6 Principal membrane and module suppliers for gas separation processes with dense polymer membranes (nonexhaustive list)

	<i>Membrane</i>	<i>Module</i>	<i>Main applications</i>
Permea (Air Products)	Polysulfone	Hollow fiber	H ₂ recovery Air separation CO ₂ removal Drying
Medal (Air Liquide)	Polyimides, polyaramide	Hollow fiber	H ₂ recovery Air separation CO ₂ removal
Ube	Polyimides	Hollow fiber	H ₂ recovery Air separation CO ₂ removal Drying
Generon (Messer)	Polycarbonate	Hollow fiber	Air separation
Separex (UOP)	Cellulose acetate	Spiral wound	Natural gas treatment (CO ₂)
Nateo Cynara	Cellulose acetate	Hollow fiber	Natural gas treatment (CO ₂)
Parker Hannifin	Polyphenylenoxide	Hollow fiber	Air separation Drying
MTR	Silicone rubber (composite)	Spiral wound	VOC recovery Syngas, natural gas (N ₂ , H ₂ S...)
Sihl GKSS	Silicone rubber (composite)	Plate & Frame	VOC recovery

2.08.3.4.6 Hydrodynamic dispersion effects

In the derivation of the design equations (Section 2.08.3.2), the hydrodynamic conditions were assumed to respect two extreme situations: perfectly mixed or plug-flow scenarios. In reality, an intermediate situation is more likely to occur and this may induce significant deviations. More generally, the incidence of a dispersion effect, best expressed through a dispersion coefficient, has not been investigated in detail. It can be stated that, similarly to any counter-current mass transfer operation, deviations from the plug-flow behavior should be detrimental since they would lead to a decrease in the effective driving force. Basic calculations have shown that, at least for industrial modules and operating conditions, the plug-flow hypothesis is probable for gas flow inside the fibers. The Peclet number, for instance, is very high and the influence of a supplementary term in the radial flow profile is most often negligible [104]. On the shell side, however, the situation is more complex. A detailed analysis has demonstrated that flow patterns, in some cases, affect the overall separation performances [105]. This prediction has been experimentally confirmed by measurements with a thermo-anemograph on hollow-fiber modules [106]. In this study, maldistributions of the shell-side flow were detected, especially for high separation factors and stage-cut conditions. Nevertheless, diffusional contributions were reported to be small on the shell side for industrial hollow-fiber modules in the case of O₂/N₂ separation [107].

2.08.3.4.7 Fiber variation effects

The intrinsic properties of a module, such as the effective permeance, the internal diameter, and the

selectivity, are subject to variations from one fiber to another, and the resulting performances of the module thus become affected. These types of effects have not been investigated in detail, apart from in a study dedicated to air separation [108].

2.08.3.4.8 Additional mass transfer resistances

Upstream and downstream boundary layer resistances can affect the effective flux through a dense polymeric membrane. Concentration polarization effects, which are well known in membrane science [109], are generally less pronounced in gas separation, due to the larger mass transfer coefficients and diffusion coefficients as compared to liquid phases. Nevertheless, the occurrence of non-negligible mass transfer resistances in the upstream boundary layer has been predicted to take place for highly permeable and selective membranes [110]. A case study [111] devoted to air separation and hydrogen purification has suggested that the phenomenon may be significant when the permeation rate of the most permeable compound exceeds $10^{-4} \text{ cm}^3 \text{ (STP) cm}^{-2} \text{ s}^{-1} \text{ cmHg}^{-1}$ (which is equivalent to 100 GPU). The recovery of volatile organic vapors from air or inert gases, which makes use of highly permeable and selective rubbery membrane materials, is one of the applications where concentration polarization phenomena can play a significant role, both at the upstream side (feed-side boundary layer) and at the downstream side (in the porous support) [112].

Drying operations are also subject to this additional phenomenon, due to the very high selectivity and permeability obtained during the extraction of water. For CO₂/CH₄ applications, however, the

concentration polarization is expected to play a minor, if not negligible, role; gas-phase nonidealities and plasticization are the main effects to take into account if a consistent simulation is desired [113].

For overall mass transfer analysis, it is more convenient for the concentration difference to be maintained as the effective driving force in a manner similar to that of the classical mass transfer approach. The overall flux of a compound i thus incorporates the contributions of the various mass transfer resistances in series:

$$N_i = \frac{c_i' - c_i''}{\frac{1}{k_i'} + \frac{1}{k_i^m} + \frac{1}{k_i''}} = \frac{c_i' - c_i''}{\frac{1}{k_i'} + \frac{z}{D_i^{\text{eff}}} + \frac{1}{k_i''}} \quad (53)$$

The membrane mass transfer resistance can be computed from the ratio of the membrane thickness to the effective diffusion coefficient. A simple calculation shows that 1 Barrer corresponds to an effective diffusion coefficient of $8.3 \times 10^{-13} \text{ m}^2 \text{ s}^{-1}$. The upstream (retentate) and downstream mass transfer resistances can be estimated through correlations described in chemical engineering textbooks. For an open, smooth tube with laminar flow conditions, such as those found on the bore side of hollow fiber, k can be determined as

$$k = \frac{1.86 D Re^{0.33} Sc^{0.33}}{d} \left(\frac{d}{L}\right)^{0.33} \quad (54)$$

Here, Re is the Reynolds number, Sc the Schmidt number, D the diffusion coefficient in the gaseous

phase, d the fiber diameter, and L the fiber length. Based on this, the potential variation range of the mass transfer coefficients for the membrane, gas phase, and support (porous matrix) can be estimated, and a synthetic picture is presented in **Figure 32**.

Finally, it should be noted that, for very thin selective layers (i.e., one of the major goals in membrane development), the hypothesis of infinitely rapid equilibrium kinetics, as compared to the diffusion kinetics, can be questioned. In such a case, the permeate flux will not be strictly inversely proportional to the dense layer thickness [114].

2.08.3.4.9 Multi-component effects 1: Coupling of the frame of references

It is well known that mass transfer modeling for systems involving more than two components, that is, multi-component systems, is considerably more complex than the modeling of a simple binary system [115]. Any gas separation problem that involves a membrane becomes a multi-component problem, since at least two permeating species are dissolved and transferred into a third compound, namely the polymer matrix. In this case, the question of the frame of reference is of crucial importance [116]. Surprisingly, this problem has only recently been addressed in detail for gas separation through dense membranes [117], although it has been occasionally mentioned before [118].

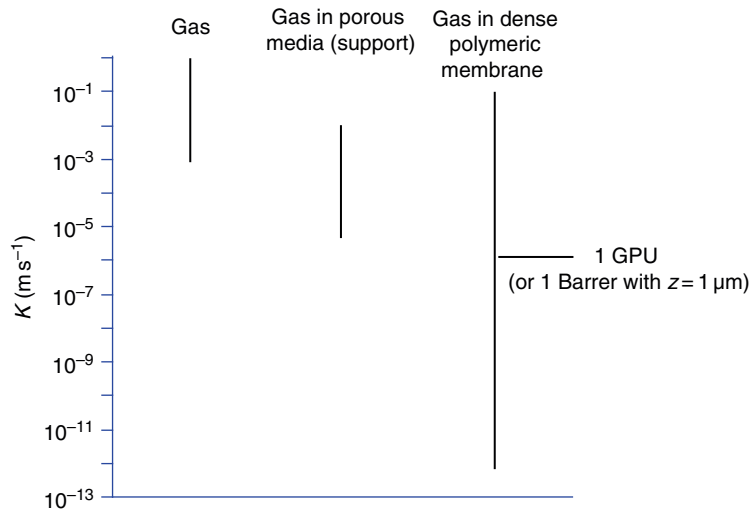


Figure 32 Approximate range of mass transfer coefficients (k in m s^{-1}) of gaseous species in gaseous phase (left bar), in a porous media such as the support layer of a composite membrane (middle) and in a dense polymeric or skinned membrane (right, 1 Barrer = $8 \times 10^{-13} \text{ m}^2 \text{ s}^{-1}$). For a composite membrane, if the right and medium bars overlap, the support mass transfer resistance cannot be neglected. If the right and left bar overlap, polarization concentration (on the retentate side) takes place.

To this respect, it might be useful to recall that “the purely kinematical presumptions leading to Fick’s law are unsupported by any principle or method of mechanics or physics and cannot be expected to explain or predict motions except under particularly simple circumstances [119].”

For a multi-component system, the transmembrane flux in steady state with the volume-average bulk velocity can be expressed as

$$N_i = \mathcal{J}_i + \frac{\varphi_i}{\bar{v}_i} \sum_{k=1}^n \bar{v}_k N_k \quad (55)$$

For pure compound permeation, that is, one penetrant in one polymer, with the stationary frame of reference ($N_p = 0$), the expression (55) reduces to expression (56):

$$N_i = -\frac{1}{\bar{v}_i(1-\varphi_i)} D_i \frac{d\varphi_i}{dz} \quad (56)$$

Interestingly, if anisotropic swelling is assumed, the membrane thickness z can be expressed as a function of the dry orthogonal coordinate Z through: $dZ = \Phi_p dz = (1-\Phi_i)dz$, and one obtains the classical diffusion proposed in the introductory part of this chapter:

$$N_i = -\frac{D_i}{\bar{v}_i} \frac{d\varphi_i}{dZ} = -D_i \frac{dc_i}{dZ} \quad (57)$$

The situation is very different for a multi-component system, where, for a fixed frame of reference, the flux of the permeating component i is a combination of diffusion and convection (the so-called bulk flow) contributions. The latter, which is often neglected, plays a significant role on the flux of the less permeable compound when the relative flux of the other (more permeable) component is high. This supplementary term has been investigated, for instance, in the case of carbon dioxide/methane separations by glassy polypyrrolone membranes [117]. The separation has been shown to become significantly less efficient, due to the enhanced bulk flux of the slow (methane) compound. Consequently, the specificity of multi-component systems should not be underestimated in the rigorous prediction of separation of binary mixtures by membranes.

2.08.3.4.10 Multi-component effects 2: Flux coupling and plasticization effects

In the general methodology described in the module design section, no effects of one gas upon another have been assumed for the description of the steady-state permeation. This hypothesis can be considered

as valid especially for mixtures of permanent gases. An often invoked reason for this is the extremely small solubilities (<0.2%) for these systems at normal temperatures, which imply that a dissolved gas has little effect on polymer properties and thus diffuses independently (i.e., gas–gas contacts are rare). Nevertheless, as the solvent power and the concentration of the dissolved species increase, flux interdependencies are likely to arise and demand the development of a more complex framework.

The most rigorous approach makes use of an irreversible thermodynamics framework, which for a two-compound permeation process (binary mixture separation) can be expressed as

$$\begin{aligned} \mathcal{J}_i &= L_{ii} \frac{d\mu_i}{dz} + L_{ij} \frac{d\mu_j}{dz} \\ \mathcal{J}_j &= L_{jj} \frac{d\mu_j}{dz} + L_{ji} \frac{d\mu_i}{dz} \end{aligned} \quad (58)$$

A classical question concerns the consistency of the solution-diffusion model and the above equations. It is important to note at this point that the permeability concept is compatible with the phenomenological approach that is most often proposed for the rigorous analysis of transport processes. When taking the chemical potential gradient as the general driving force for mass transfer, one obtains

$$\mathcal{J}_i = -L_{ii} \left(\frac{\partial \mu_i}{\partial z} \right) = -L_{ii} \left(\frac{\partial \mu_i}{\partial c_i} \right) \cdot \left(\frac{\partial c_i}{\partial z} \right) \quad (59)$$

where μ is the chemical potential of species i (penetrant gas) in the membrane phase:

$$\mu_i(T, P, c_i) = \mu_i^0 + RT \ln(\gamma_i c_i) + v_i(P - P^{\text{Ref}}) \quad (60)$$

With the hypothesis of an inexistent pressure change through the membrane, postulated by the solution-diffusion model (Figure 4), the flux can be expressed as

$$\mathcal{J}_i = -\left(\frac{L_{ii} RT}{c_i} \right) \left(1 + \frac{\partial \ln \gamma_i}{\partial \ln c_i} \right) \cdot \frac{\partial c_i}{\partial z} = -D_i^T \left(\frac{\partial c_i}{\partial z} \right) \quad (61)$$

From a practical point of view, the evaluation of mixed gas transport through polymeric membranes is a tedious task since it requires the precise determination of both the pure compound and mixture permeation, ideally on the same experimental setup. As a result, experiments on mixtures are scarce in comparison to those on pure compounds. An example of a laboratory setup dedicated to mixture permeation studies for flat membrane samples is shown in Figure 33.

The temperature, pressure, flow rates, and compositions have to be either controlled or determined

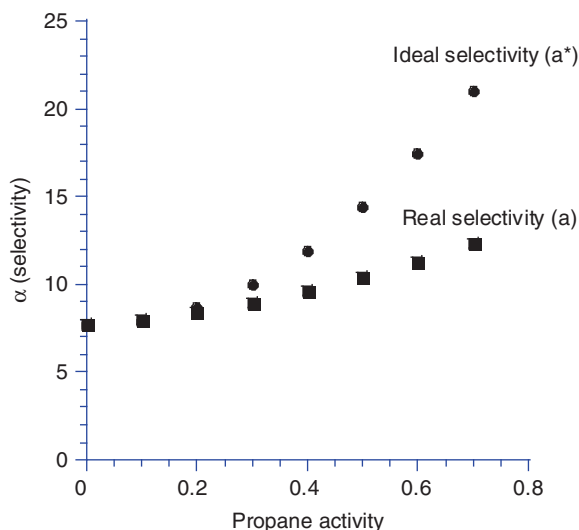


Figure 33 Example of significant discrepancy observed between the ideal selectivity (determined from pure compounds permeability ratio) and the real selectivity which is obtained when a mixture is permeated for a so-called reverse selective operation: separation of hydrogen/propane mixture through a silicone rubber membrane. The significant swelling of the rubbery membrane by propane strongly increases hydrogen permeability compared to the pure compound situation. A noticeable coupling effect results above a critical propane activity in the feed mixture (which corresponds to a critical propane volume fraction on the upstream membrane side). This undesired phenomenon is principally the consequence of the increased diffusion of hydrogen and, to a lesser extent, its higher solubility.

in order for the mass balance on the module to be verified. In general, a very large feed flow rate, as opposed to the permeate flow rate, is applied. This condition, which corresponds to a small stage cut θ (typically in the range of 0.05–0.1), prevents the incidence of hydrodynamic conditions on the separation performances (i.e., for a low stage-cut value, the various hydrodynamic regimes show the same results). The direct comparison of the obtained experimental results, for instance, expressed through the real separation factor, with the ideal separation factor α^* , demonstrates the importance of coupling effects.

An example is shown in **Figure 34** for the propane/hydrogen separation with a rubbery polymer. Depending on the membrane material, the mixture composition and the operating conditions, a variety of behaviors can be obtained. These include increases, decreases, or the lack of differences with regard to the permeability of a given compound in a mixture as compared to its pure component permeability.

2.08.3.4.11 Membrane deformation

In the general methodology described in the previous section, a constant membrane thickness (z) and a constant specific surface area were postulated.

These assumptions should be reconsidered if fiber deformation effects occur. An extreme situation corresponds to self-standing rubbery hollow fibers, capable of demonstrating significant dimensional changes under pressure. This effect, which can be beneficial in terms of permeability, has been modeled and experimentally evidenced for external pressurization conditions [120]. Nevertheless, all the membranes that are presently used at an industrial scale have a supporting porous matrix that is supposed to prevent such changes.

Table 7 provides a tentative synoptic summary of the various concepts and experimental situations that have been covered, from the permeability definition to the module design methodology. The table also presents the approximate frequency of occurrence of the concepts in literature.

2.08.4 Industrial Applications

2.08.4.1 General Features

The selection of a separation process for a given application depends on a great number of variables. For instance, a defined purity or composition can be the only (or main) target for certain applications (the production of nitrogen of a given purity from

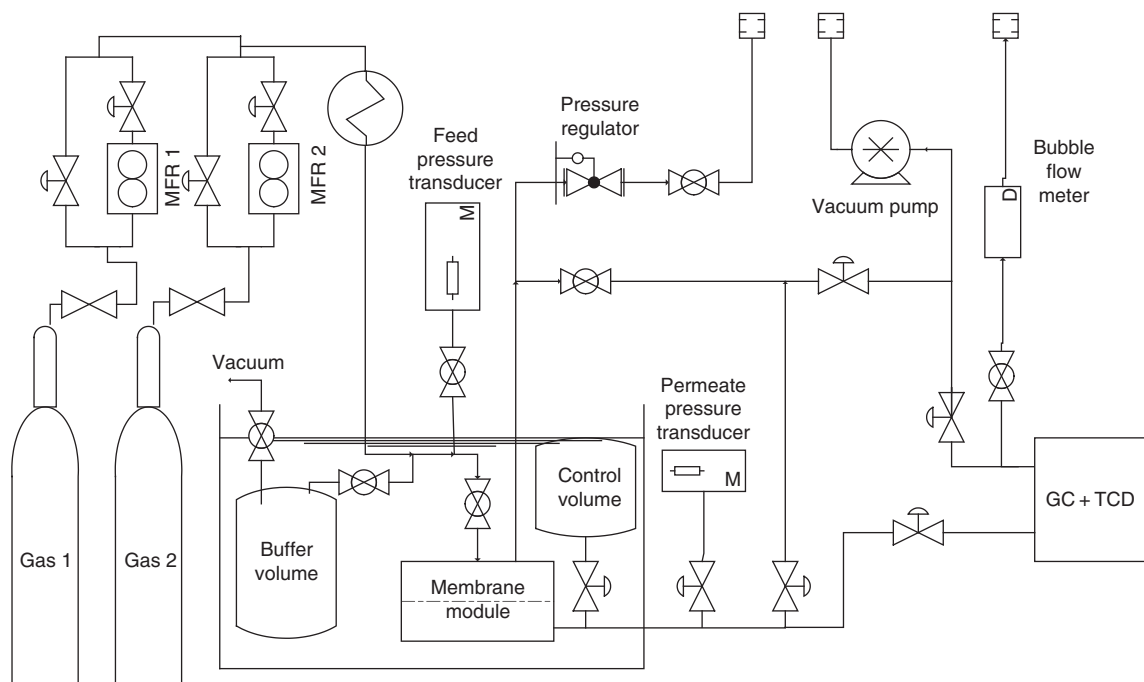


Figure 34 Example of setup dedicated to the permeation of mixture of gases through flat membrane sample [64]. If the separation performances are close to the predictions obtained with the ideal selectivity (α^* , determined from pure compound permeability data), flux coupling or plasticization effects can be neglected and design is straightforward. If discrepancies between simulation and results are obtained, a more rigorous and complex methodology is required. GC, gas chromatograph; M, manometer; MFR, mass flow regulator; TCD, thermal conductivity detector.

air, the capture of VOCs from a vent stream with requirements of respecting emission standards, the drying of air, etc.). A recovery or capture ratio R is often taken into account in order to minimize compound losses during, for example, hydrogen production or the treatment of natural gas. These types of constraints must obviously be precisely defined before the rational design of a separation process becomes possible.

Naturally, membranes do not represent the only means of achieving gas separation in industry, nor is their use the most dominating. Basically, three major competing processes can be identified for industrial applications [121]:

1. Cryogenic distillation or condensation, thanks to a cold box, can be utilized for air separation or the recovery of volatile organic compounds, for instance.
2. Adsorbent-based processes, such as pressure swing adsorption (PSA), temperature swing adsorption (TSA), or vacuum swing adsorption (VSA), are often selected for hydrogen purification, oxygen production, gas drying, or the recovery of organic compounds.

3. Solvent-based processes are also considered for natural gas treatment (i.e., carbon dioxide removal by amine wash), gas drying with heavy and hydrophilic solvents such as glycols, or the removal of sour gases by physical solvents.

It is obvious that the ultimate choice of a separation process is dictated by a technico-economical comparison. This task is generally achieved through a balance between capital and operating costs. Several studies, including sophisticated optimization methods, have been reported for specific applications. Given the number of variables that have to be taken into account as well as case-to-case specificities, it is obvious that a generic and systematic positioning of the different techniques can hardly be achieved. Furthermore, it is important to note that the conclusions that are drawn from these analyses are subject to changes; a breakthrough development in material selectivity, a change in membrane production costs, or energy costs can drastically affect the optimal domain of a given process.

A more subtle effect concerns the fact that the evaluation of membrane separation processes is usually performed according to the specifications for

Table 7 A tentative synopsis of the experimental situations and the associated concepts and methodologies that can be used in polymeric gas separation operations

Experimental situation	Key results	Notes
1. Pure compound permeation through a dense polymer sample	P_i, P_j, α^*	Usually performed at lab scale on thick polymer samples. Numerous data reported in the literature
2. Pure compound permeation through a skinned or composite (i.e., industrial) membrane	GPU for i and j and effective pure compound-based selectivity: $\alpha^{*'} = (GPU_i/GPU_j)$	Few results in the literature (membrane supplier data). The role of the support can be estimated when the effective pure compound selectivity $\alpha^{*'}$ and the ideal selectivity α^* are compared
3. Mixed gas permeation performed on homogeneous or industrial membrane samples	Permeance and effective gas mixture selectivity α_{eff}	Some results on homogeneous membrane samples, few results on industrial membranes. Flux coupling effects can be estimated when comparing the effective selectivity of the pure compound (step 2) and the effective mixture selectivity (step 3).
4. Pilot tests with a membrane module	Effective module separation performances	The possibility to rigorously predict separation performances from permeability data can be estimated. In case of failure, complicating factors must possibly be taken into account: variable permeability, pressure drop, temperature variation, concentration polarization, flow distribution, etc.
5. Rigorous and exhaustive design study (process simulation softwares)	Selection and design of the optimal installation based on a comparative analysis including capital and operating costs (NB: Feed pretreatment costs have to be included)	Schematically, single-stage module, recycling module, multi-stage units (usually limited to three stages) or hybrid processes can be compared

The various steps have been identified in order to fit the parts described in the text. They do not necessarily reflect the sequence of operation that is performed for industrial module design.

an established separation technique (e.g., cryogeny or adsorption). This constrained framework can sometimes lead to the conclusion that membranes are noncompetitive, while the opposite conclusion is obtained when the process is optimized for membrane separation [122]. A notable exception to the previous statement concerns the production of nitrogen from air. For this specific application, a well-known and constant feed composition is naturally available and decades of design studies performed on the three major separation processes can be summarized in a single map, shown in **Figure 35**.

It is remarkable that the three dominating separation techniques have found a domain in which they offer the minimal overall cost. More interestingly, it has to be noticed that membranes represent a superior technology when the lowest purity and the smallest capacity are needed. This observation is

often extended, possibly too rapidly, to membrane gas separation processes in general.

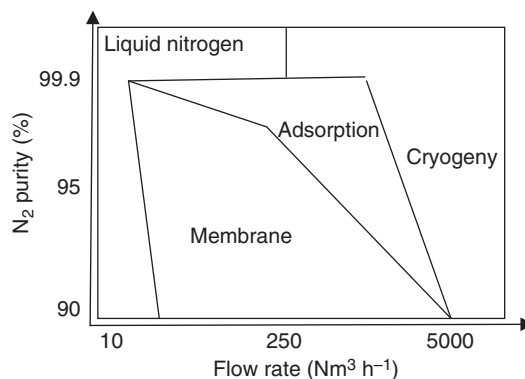


Figure 35 Example of the influence of purity and capacity on different technologies: economic operating regimes for different nitrogen supply options.

Given the difficulty of obtaining a complete and rigorous picture, a more qualitative analysis of the advantages and limitations of membrane separation versus other separation processes is of interest. The advantages can be summarized as follows:

1. operating flexibility causing membranes to tolerate fluctuating feed conditions without losing in quality;
2. low energy requirement and/or high energy efficiency [123] leading to low operating costs;
3. the absence of chemicals, make-up and solvent emissions;
4. easy start-up and shut-down;
5. no moving parts, a minimal maintenance, and operator attention (remote control is sometimes possible);
6. modular design, easy to scale up when an increased capacity is required (a numbering-up approach: additional modules);
7. small footprint and compact system (can be a decisive argument for off-shore applications); and
8. minimal utilities required, easy to control, simple sensors required (pressure, flow rate).

The major drawbacks of membrane processes for gas separation are outlined in the following:

1. No economy of scale due to the modular design (unit capital costs do not decrease with capacity, contrarily to for absorption, adsorption, and cryogenic processes), thus representing a decisive penalty for large capacity applications.
2. Pretreatment can be heavy, and, in some cases, as expensive as the cost of the modules (particulates, aerosols, organic compounds, moisture, etc.).
3. Sensitivity to chemical compounds can be problematic in certain cases (the plasticization effect exerted by trace amounts of hydrocarbons on glassy polymers is a typical example).
4. Requires a high-quality energy source (namely electrical power for compression with most applications), whereas TSA or absorption processes can make use of low-quality energy such as heat.

Membrane-based gas separation processes became a reality in industry in the 1980s [124]. Since then, applications have evolved and have been subject to numerous reviews [125, 126]. Similarly to membrane and module fabrication, a tentative review of the existing industrial applications is a complex and risky task; a large part of the information is considered by membrane equipment suppliers to

be proprietary and trade, or closely guarded information.

2.08.4.2 Hydrogen Purification

The first large-scale application of gas separation with polymeric membranes was for the recovery of hydrogen. Indeed, hydrogen applications provide a combination of factors that favor membrane applications. First, the high permeability of hydrogen in glassy polymers such as polysulfones or polyimides leads to a high selectivity over nitrogen, carbon monoxide, or hydrocarbons. Second, the fast permeating compound is available at a high concentration in the feed mixture. Furthermore, a pressurized feed is most often present and, thus, no further compression is required. In addition, the target hydrogen purity needed is not extreme. Last but not least, applications principally concern feed streams that correspond to purge and that would normally be vented. Membranes are in this case the best means of achieving hydrogen recovery. The main disadvantage of membrane operations resides in the fact that hydrogen is recovered on the low pressure side (permeate), which can lead to redhibitory recompression costs in certain cases.

A large variety of industrially interesting applications exist:

1. hydrogen recovery from an ammonia purge gas;
2. hydrogen recovery from a methanol purge gas;
3. CO/H₂ synthesis gas ratio adjustment;
4. units for steam methane reforming;
5. carbon monoxide purification; and
6. hydrogen recovery from refinery purge gases.

For these various applications, a recovery of 95% or more is often achievable, combined with a purity of above 98%.

An example of an industrial hydrogen recovery unit is shown in [Figure 36](#) and a flowsheet of a hydrotreater unit using a membrane is presented in [Figure 37](#).

2.08.4.3 Nitrogen from Air

Due to a higher solubility in many polymers, oxygen can be fivefold faster than nitrogen. As a result, moderate purity N₂ (i.e., 95–99.5%) can be obtained from single-stage membrane units. For low-to-moderate capacities, membrane separation has proved to be economical and a great number of applications are currently operated. A description of the respective



Figure 36 An industrial hydrogen purification plant with several hollow-fiber modules for refinery applications. Courtesy of Air Liquide/MEDAL™.

domains of cryogeny, adsorption, and membranes for nitrogen production is reproduced in **Figure 35**. The target purity and the plant capacity can be seen to be the two main differentiating variables. This decision map is illustrative of the positioning of membranes, which find applications when the aims include a not too stringent purity and a small-to-medium capacity.

A classical process can be described as follows: atmospheric air is compressed in a compressor and passed through a series of filters in order for moisture and any other condensable compounds (e.g., oil) to be removed. The compressed feed is further heated in a heat exchanger before entering the membrane module. Air travels through a bundle of hollow fibers where oxygen, carbon dioxide, water, and hydrocarbons permeate in preference to nitrogen. Argon, being less permeable, accumulates on the retentate side with nitrogen. The oxygen-enriched stream (i.e., the permeate) can be vented to the atmosphere or used, for instance, to improve the efficiency of combustion units.

In the search for more efficient membrane materials for the oxygen/nitrogen separation, hundreds of polymers have been screened during recent years. Reports continue to appear on studies with novel

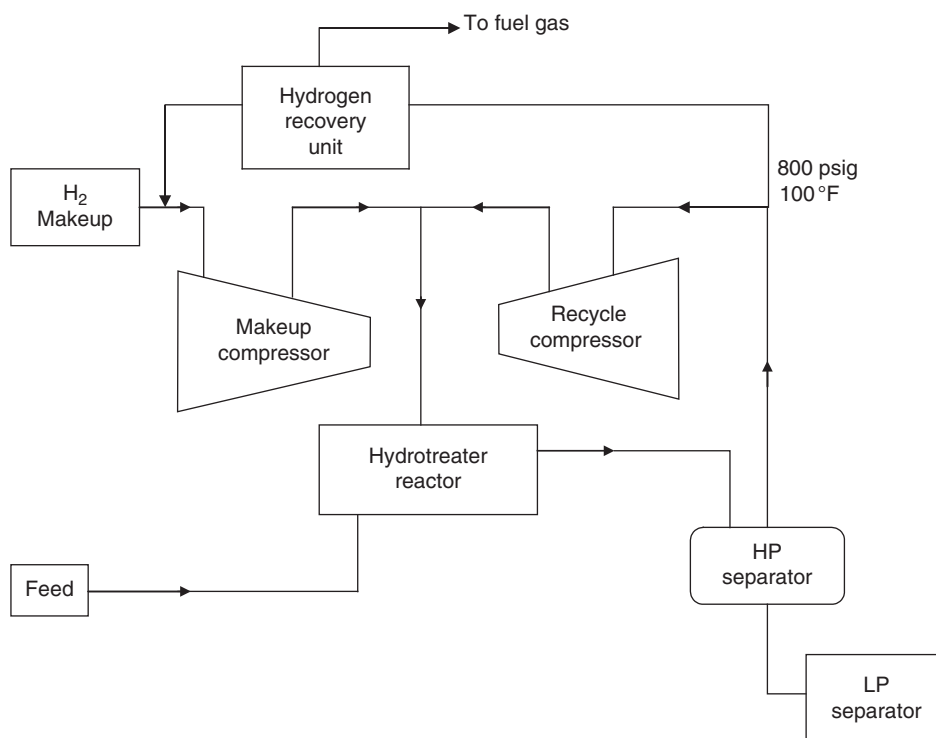


Figure 37 Example of flowsheet for hydrotreater unit with a membrane hydrogen recovery unit [124].

compounds but the performances should be systematically compared to existing materials. For instance, an oxygen/nitrogen selectivity above 11 has been reported for the O₂/N₂ gas pair with sulfonated polystyrene, where the best combination was Mg²⁺ form polymers with the largest extent of sulfonation [127].

More generally, the O₂/N₂ diffusion selectivity (α_D^*) is probably the variable that should be tuned in order to maximize the separation performances. Maximal values around 8.7 have been reported for the O₂/N₂ pair in hyperrigid polypyrrolone polymers exhibiting a performance lying on or above the tradeoff line [128]. However, this value is much smaller than the one reported in rigid zeolite or carbon molecular sieves, where a diffusion selectivity as high as 104 can be obtained. A detailed analysis suggests that this large difference results from entropic selectivity effects.

It should be noted that a very different situation, namely the CO₂/N₂ separation from combustion exhaust gases, has also been occasionally investigated at a pilot scale for nitrogen generation. No significant change was detected after 4 months of operation, even with interrupted feed admissions and shut downs. Moreover, a purity of 98.5% N₂ could be achieved. Nevertheless, the exact potential of this specific application remains to be evaluated.

2.08.4.4 Carbon Dioxide Removal in the Treatment of Natural Gas

Most of the natural gas produced in the world is co-produced with acid gases such as carbon dioxide and/or hydrogen sulphide. These compounds, which, in glassy polymers, are faster permeants than methane, have to be removed in order to achieve pipeline specifications. While the diffusion selectivity is clearly the key factor for hydrogen purification, carbon dioxide removal through glassy polymers often shows a combined diffusion and solubility effect, with an α_D ranging from 4 to 15 and an α_S from 2 to 7 [129]. The significant solubility of carbon dioxide can, in turn, affect the permeation performances and the prediction of a mixed gas permeability has been the subject of numerous efforts for this system.

Membrane operation has proven to be economically competitive, especially for small to intermediate-sized systems. For the treatment of natural gas, reviews on applications, including technico-economic analyses, have been published [130, 131]. A rough

conclusion is that membranes can either compete with or be combined with absorption processes, as soon as the carbon dioxide content in the natural gas exceeds 10% [132]. The potential of hybrid processes appears to be particularly attractive: in this case, the membrane removes the bulk quantities of the CO₂ with a relatively small area and the amine absorption process is used for the final clean-up [133]. Such a configuration takes advantage of the respective characteristics of the two processes: indeed, amine units require more energy when the CO₂ concentration increases, whereas membranes, on the other hand, are more effective at high concentrations of CO₂. A process design study concludes that, under most of the tested conditions, gas absorption processes are not competitive with either hybrid processes or independent membrane processes [134].

Further complications arise when carbon dioxide and hydrogen sulfide are simultaneously present in natural gas. In this case, the use of two different membranes, one with a high CO₂/CH₄ selectivity and the other with a high H₂S/CH₄ selectivity, can be proposed and a detailed technico-economic analysis has been performed for such a situation [135]. More generally, the applications in the field of natural gas treatment are continuously increasing and very large installations have recently been started [136].

In order for membranes to find applications, it is useful to indicate the compositional specifications for a delivery of natural gas by pipeline. For instance, in the US, the maximal tolerable composition is the following: 2% (or less) of carbon dioxide, 120 ppm of water, 4 ppm of hydrogen sulfide, and 4% of inert gases (N₂, He, etc.). More specifically, if membranes are to compete with other separation processes, the partial pressure of the carbon dioxide should be sufficiently high as this would lead to the necessary driving force for the membrane transport. In this case, there is no unique configuration and, depending on the values of the carbon dioxide concentration and the price of the natural gas, single-stage or multi-stage (usually limited to three stages) units can be proposed based on optimization studies [137].

It is generally recommended that membranes be restricted to a bulk removal, typically down to a carbon dioxide content of 8–10%. Any remaining CO₂ is further removed by polishing techniques, such as amine absorption. A detailed study of hybrid schemes that combine membrane and amine processes, including a technico-economic analysis, has been reported. A recycling stream can also be

achieved, in order to increase the hydrocarbon recovery. Each system is designed to minimize the overall compression requirements. Pretreatments generally include air cooling, liquid knock-out, and reheating, with a possibility of achieving the latter in combination with compression.

Polymeric membranes are hardly competitive with conventional absorption processes when the partial pressure of carbon dioxide in the feed stream is low. More specifically, for partial pressures of carbon dioxide in the feed mixture lower than 0.5 bar, advanced processes require the use of thin (i.e., 4 μm) membranes for a facilitated transport to be competitive [138].

Carbon dioxide is often vented but can, in some cases, also be recovered in order to be reinjected for enhanced oil recovery. With the increasing demand on oil and the issues associated to greenhouse gas mitigation, it is likely that this type of application will undergo a significant increase. A 90–95% recovery ratio, combined with purities ranging from 90% to 97%, is often typical in such cases, and field tests were started as early as 1983 for this application [139].

A difficulty associated to the treatment of natural gas resides in the fact that the mixture to be treated is complex and contains numerous compounds such as oil, hydrocarbons, water, glycol, drilling fluids, and particulates (especially iron sulfide particles resulting from the reaction of hydrogen sulfide with iron contained in the pipes). Consequently, pretreatment is a key issue and problems of membrane fouling can occur if this operation is not carefully designed. A major bottleneck of polymeric membranes in the treatment of natural gas comes from the so-called plasticization effect that can be exerted by hydrocarbons or carbon dioxide on glassy polymers. In most applications, hydrocarbons have to be removed in the pretreatment step. Alternatively, the operating temperature of the membrane can be maintained sufficiently high (65–100 °C) to prevent their condensation. From a practical point of view, plasticization, which can occur over large timescales when trace compounds are involved, simultaneously induces a decrease in the selectivity and an increase in the permeability. This effect is by no means negligible and can be quite impressive. For polyimide materials, for instance, considered to be subject to plasticization by hydrocarbon impurities (hexane, toluene) to a higher degree than cellulose acetate membranes, a twofold decrease in selectivity has been reported [140]. This phenomenon is

irreversible, complex, and history dependent, and has been subject to substantial research efforts given its negative implications. It is basically different from competitive sorption or flux coupling effects, even though a subtle balance between these two types of phenomena can be observed [141]. Strategies to minimize plasticization include the selection of adequate materials, chemical crosslinking [142], and membrane posttreatments, such as thermal annealing.

Current carbon dioxide/methane selectivities of membrane gas separation units range from 15 to 25. A major change in the competitiveness toward the amine absorption technology would be achieved if membranes with a selectivity of 40 or more could be produced at an industrial scale, and it is interesting to note that the probability of accomplishing this target is high. For instance, laboratory-scale studies performed with multilayer composite poly(4-vinylpyridine)/polyetherimide hollow-fiber membranes have recently shown ideal separation factors for CO_2/CH_4 up to 62 [143].

Another specific application concerns the treatment of low-quality natural gas or biogas. The upgrading of low-quality natural gas from a well was investigated for more than 20 months [144], and the retentate was found to always meet pipeline specifications. There is an increased interest in biogas, containing 30–45% carbon dioxide, especially as a renewable energy source for electricity production or as a transport vehicle fuel [145]. There are emerging needs for efficient and cheap scrubbing techniques and membranes should logically play a role in this field.

2.08.4.5 Volatile Organic Compounds Recovery

The recovery of VOCs from contaminated gas streams started in the US in the 1980s, and has since then become an established process. The use of highly permeable elastomeric membranes, such as silicone rubber, enables selectivities of organic compounds over permanent gases on the order 20–100 to be achieved. This is often sufficient in order to compete with other technologies, for example, adsorption, condensation, or incineration, especially when the vapor concentration is roughly in the range of 0.1–10%. Adsorption is often more competitive for diluted streams, while condensation and incineration techniques require concentrated mixtures.

Schematically, the applications are driven by two factors; in some cases, the recovery of a high-value

solvent from the vent streams is rendered possible. Similarly to in hydrogen recovery applications, the driving force is clearly economic and a payback time on the order of 1 year or less can be obtained. The recovery of halogenated compounds (CFCs), monomers or solvent vapors (chlorinated solvents, ethers, ketones, etc.) are typical examples. Another method showing a great potential in the petrochemical and refinery areas is the separation of propylene from nitrogen in polyolefin resin degassing vents [146]. An example of such a propylene recovery unit is shown in **Figure 38**.

In other cases, environmental regulations push for membrane installations in order for the limiting emission range to be respected. This is particularly the

situation for hydrocarbon vapor recovery in various operations, especially when a transfer is operated.

VOC membrane recovery units are often designed as hybrid processes with a condenser. The membrane can be installed either before or after the condenser, depending on the feed concentration design constraints (**Figure 39**).

Composite membranes with active layers of rubbery silicone are employed, and industrial modules are of either spiral-wound or plate-and-frame type. Vacuum operation is often applied. A liquid ring pump is frequently selected rendering it possible to achieve vacuum down to 10–100 mbar.

As already stated, the high solubility of organic vapors in elastomers (Flory–Huggins-type isotherm)

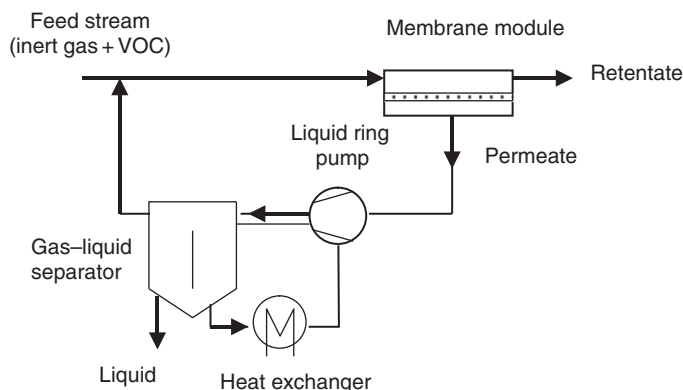


Figure 38 Recovery of volatile organic compounds (VOCs) from a gaseous stream by a single-stage membrane unit (vacuum operation).



Figure 39 Example of an industrial membrane vapor recovery unit (propylene purge treatment). Courtesy of MTR.

can lead to high ideal VOC/N₂ selectivities. This, in combination with the very high permeability of silicone rubber, has two major implications. First, the support mass transfer resistance plays a significant role and the active layer thickness has to be tailored in order for the effective selectivity to remain compatible with the application. **Table 8** displays a series of effective selectivities of composite silicone rubber membranes for various VOCs.

Second, the high selectivity, combined with a high effective permeability, favors the occurrence of concentration [147, 148] and temperature polarization [149] phenomena. Gas-phase nonidealities should also be taken into account for a rational mass transfer analysis [150].

2.08.4.6 Drying of Gases

Water is the fastest permeant in polymers and, for permanent gases, selectivities of several thousands can be achieved with numerous materials. As a consequence, air-drying operations by hydrophilic polymeric membranes can be competitive with other techniques such as condensation or molecular sieve beds. Membrane materials for air drying often include polyphenyleneoxide and Nafion [151], where the latter is an ion-exchange polymer widely used in electrodialysis and in fuel cells. A simple formula for water permeability is frequently proposed for Nafion for design purposes, even though unexpected effects of the membrane thickness on the water permeability have been observed for this polymer [152].

When it comes to membrane air drying, two major problems have to be faced, both of which have to do with boundary layer effects (which were neglected in the design analysis presented before). The very high permeability of water, combined with an extremely high selectivity, induces a strong concentration polarization, especially on the downstream side, causing the effective driving force to be dramatically decreased. The mass transfer can often be enhanced by recycling some of the retentate as a sweep stream on the permeate side. Mass transfer resistance and sweep stream may interact in a subtle way such that the smallest membrane area for a given task may require a less selective membrane [153].

2.08.4.7 Miscellaneous Applications

2.08.4.7.1 Rare gases

Helium, a fast permeating gas, can be recovered from natural gas wells by polymeric membrane processes. The low concentration that is encountered (typically <1%) translates into a low driving force. Multi-stage units would thus be needed in order to achieve the target purity level. Methane losses are also one of the major bottlenecks for this application. Another field of application where membranes are best suited concerns the recovery of helium after it has been used and become diluted. Classical examples include deep-diving gases or blimps, in which cases the contaminants are rejected by small units, sometimes on-board, consisting of a compressor and a membrane module. The purified helium stream is recycled. Polyphosphazene has been proposed as a potential

Table 8 An approximate range of effective selectivity data of composite silicone rubber membranes for various compounds for VOC recovery applications

<i>Volatile organic compound</i>	<i>Membrane selectivity</i> (α VOC/N ₂)
Octane	90–100
1,1,2-Trichloroethane	60
Isopentane	30–60
Methylene chloride	50
CFC-11 (CCl ₃ F)	23–45
1,1,2-Trichloroethane	30–40
Isobutane	20–40
Tetrahydrofuran	20–30
Acetone	15–25
Propane	10
Halon-1301	3

Courtesy of MTR.

material candidate for this application [154], but glassy materials already available in industrial membrane modules can generally be more adequate.

Argon recovery from oxygen feed streams represents another potential application that would take place after a cryogenic air separation unit. Unfortunately, this separation is difficult to achieve since the diameters of the two permeants are very close (3.40 Å and 3.46 Å for argon and oxygen, respectively). Moreover, experimental studies have shown that the solubility selectivity is in favor of argon, while the diffusion selectivity is in favor of oxygen [155].

The separation of rare gases such as of the krypton (Kr)/xenon (Xe) pair through silicone rubber membranes has also been occasionally reported for the treatment of nuclear reactor atmospheres [156]. However, this prospective application has apparently not been further investigated.

2.08.4.7.2 Oxygen

Oxygen is the third largest commodity chemical. As a consequence, oxygen production from air has attracted considerable efforts given the large market and the large number of applications requiring oxygen of a given purity. Cryogenic distillation and adsorption (PSA or VSA) are established technologies for high- and medium-purity applications, respectively. Up until now, membrane separation can hardly compete with these technologies, unless a low purity, typically of a maximum of 30–45% mole, and a small plant capacity, typically no more than 20 ton equivalent pure oxygen per day, are needed. These conclusions were put forward in two detailed technico-economical analyses [157, 158]. The design analysis showed that, for this application, a process with a feed compression was not competitive because of the electricity requirement. Instead, a vacuum pump was more interesting since, as discussed above, a smaller power consumption was required due to the low stage cut of the unit. The major utilizations of oxygen-enriched air streams are for medical use (breathing): improved combustion, claus and fluid catalytic cracking (FCC) catalyst regeneration applications, and aerobic fermentation or wastewater treatments. For such applications, highly permeable and moderately selective materials, such as silicone rubber, represent the best choice. Nevertheless, alternative materials, such as polyvinyltrimethylsilane, have also been proposed for these purposes. For higher oxygen purities (60% or more), multi-stage operation, or, improved, hybrid

processes, such as membrane/adsorption (vacuum swing adsorption), can be proposed.

2.08.4.7.3 High-value chemicals

In terms of specific applications, the recovery of trace amounts of SF₆ is illustrative to the extreme range of concentrations that can be found for gas permeation processes [159]. Glassy polyimide membranes have been proposed for the separation of chlorofluorocarbons (e.g., CFC-12) from air [160]. In this case, flux coupling effects are not negligible. As compared to the performances of pure compounds, a substantial decrease in the permeability of the more permeable gas (air) was observed together with a decrease in selectivity.

The recovery of silane (SiH₄) mixed with hydrogen has been investigated in the production of ultrahigh purity silicon for the electronics industry. The objective was to reuse silane, which was not completely converted in one pass, in the process. For reasons of simplicity and energy efficiency, a comparative engineering analysis was proposed for using membranes for absorption or condensation [161].

Ammonia can be selectively permeated through polymers with very large separation factors, especially in ion-exchange materials, such as perfluorsulfonic acid polymers in H⁺ form under wetted conditions [162]. A selectivity over hydrogen as high as 500 has been reported with composite membranes [163], which could be of interest for applications in ammonia synthesis. The mechanical resistance to the high-pressure conditions that prevail in ammonia production units is however a critical issue for this application.

2.08.4.7.4 Isotopes

The separation of isotopes by polymeric membranes is almost systematically discarded since the separation factors are very small [164], thus preventing the technique from competing with other technologies such as Knudsen diffusion or centrifugation. One of very few existing studies was devoted to isotope-exploded membrane cascades for boron isotopes in a BF₃ application [165]. Experimental selectivity data in the range of 1.02–1.09 were reported and used for the design analysis of a multi-stage unit.

2.08.5 Future Trends and Prospects

The increasing role of separation operations [166], and more specifically of membrane processes [167]

have been discussed recently, with particular emphasis on energy and sustainability challenges. The role of membranes is expected to significantly increase in a large variety of industrial sectors due to their unique features: separation performances, energy efficiency, ease of operation, absence of chemicals, intensification, and associated productivity.

2.08.5.1 Membrane Materials

In 1990, Stern published a visionary paper on the developments that could be expected in the field of polymeric materials for gas separations [168]. More recently, Koros and Mahajan [169] have also explored how to push the limits for large-scale applications. It is clear that the continuing development of new polymeric materials is a major source of improvement and can open new fields of applications. The search for plasticization-resistant polymers for high-pressure CO₂ separations, for instance, is a typical example [170].

Another recent trend consists in systematically exploring the potentialities of solubility selectivity, in contrast to the diffusion selectivity obtained by glassy polymers, which for some reason has been favored up until now. The major industrial application of solubility-selective membrane separations concerns the recovery of VOCs, thanks to silicone rubber. It is possible that other rubbery materials, showing large permeabilities and being less subject to plasticization effects, display promising potentialities for new separations [171]. In a recent study, this concept was demonstrated to offer promising separation properties for hydrogen purification [172]: if a carefully selected temperature and operating pressure was applied, rubbery, molecularly engineered cross-linked poly(ethylene oxide) membranes demonstrated a remarkable reverse selectivity toward the CO₂/H₂ pair, one of the most difficult mixtures where membrane gas separation is concerned. For industrial applications, this result is very promising since hydrogen is recovered at the high pressure side. Thereby, the main drawback of membranes for hydrogen purification can thus be circumvented. From a fundamental point of view, the plasticization effect of CO₂ is in this case harnessed, contrary to the unwanted plasticization that is observed for applications of glassy membrane materials. Interestingly, the presence of moisture in the feed is not detrimental as it improves the selectivity and permeability performances.

More generally, breakthrough material developments could occur from innovative nanotechnological methods, including techniques such as self-assembly in solution, molecular templating or bottom-up designs. Tailored free-volume topologies that make use of the inclusion of judicious templating molecules in glassy polymers have recently been reported to present outstanding separation properties surpassing the limits dictated by trade-off relationships [173].

2.08.5.1.1 Tackling chemical reactivity

Nowadays, gas separation operations by membranes at an industrial scale are still operated with strictly physical interactions (i.e., without the involvement of chemical reactions). To a certain extent, this situation could be compared to gas absorption processes with only physical solvents as separating agents. The use of chemical reactions is known to provide exceptional potentialities in terms of separation selectivities. This strategy is already widely applied for gas-liquid absorption (chemical solvents), liquid-liquid extraction, and chromatographic processes, among others. Thus, it is not surprising that chemically reacting membrane systems have been investigated for decades, in order to enhance separation performances. Nevertheless, attempts in this field remain essentially restricted to laboratory scale or pilot studies. It is expected that new applications will emerge in the near future, due to the considerable improvement offered by chemically reacting systems.

More specifically, two major possibilities of chemical reaction utilization can be potentially proposed:

1. Species that are specifically involved in a chemical reaction with a gaseous permeant are bound to the matrix (e.g., by covalent bonds). These so-called fixed site carrier membranes have been examined from a theoretical point of view by Noble [174] and the interest in the concept has been validated through numerous laboratory studies. The particular case of selective oxygen permeation has been intensively investigated by the incorporation of a metal salt [175], such as CuCl₂, or chelates, which reversibly bind oxygen in rubbery copolymers [176], EDTA-acrylates copolymers [177], polyurethanes [178], or cellulosic materials [179]. Cobalt(III) complexes have been tested and reports reveal impressive improvements of the O₂/N₂ selectivity (with values up to 50!) together with oxygen permeabilities of 6000 Barrer. It is however imperative to confirm

these results by long-term experiments, due to the fact that complex desactivation is a major concern.

2. Another approach consists in using a mobile carrier that reacts with and transports the target species. This concept leads to applications for liquid membranes, a topic that has received considerable attention for decades and that will not be detailed further in that chapter [180].

2.08.5.1.2 Combining adsorbents and polymers: Mixed matrix membranes

The upper-bound limit of polymeric gas separations can be seen as a major bottleneck for certain industrial applications. Therefore, considerable efforts have been dedicated to identifying a means of going beyond this limit. For gas separation in glassy polymers, the diffusion selectivity plays a key role, and this boundary is supposed to result from so-called entropic selectivity effects [181]. The same does not hold true in the rigid cage of nonpolymeric structures such as molecular sieves, zeolites, or mineral adsorbents, which show much higher intrinsic selectivities (usually, however, at the expense of lower permeabilities). Thus, the incorporation of porous selective powdered adsorbents intimately dispersed in a polymeric matrix can be a promising method for improving the performances of gas separation membranes. This concept is generally referred to as mixed matrix membranes and was initiated for separation purposes rather recently, whereas the fundamental problem of gas transport in a polymer/adsorbent heterogeneous matrix was addressed long ago [182].

Porous adsorbent fillers were first shown to diversely affect the separation performances of poorly selective rubbery polymers [183, 184]. Depending on the adsorbent structure (dead-end or interconnected pores), intrinsic permeability, and the possibility of achieving an intimate contact between the polymer and the adsorbent particle, the permeability and selectivity can either increase or decrease. If a correct contact is achieved between the dispersed phase (i.e., the particles) and the continuous phase (i.e., the polymer), the effective permeability can be estimated according to one of the numerous models that have been proposed for heterogeneous media transport properties. Results are often compared to the outcome of an expression derived by Maxwell [185] for the prediction of the electrical properties of two-phase systems. For a matrix with a filler volume fraction φ , the effective permeability of a permeant can be computed from the pure compound permeability of the polymer (P_c) together with that of the adsorbent (P_d) through

$$P = P_c \frac{P_d + 2P_c - 2\varphi(P_c - P_d)}{P_d + 2P_c + \varphi(P_c - P_d)} \quad (62)$$

An example of a mixed matrix membrane and some observed improvements on oxygen/nitrogen selectivity [186] is shown in Figure 40.

A more specific analysis has to be carried out for the incorporation of impermeable nanoparticles in a dense polymeric membrane. This type of operation has, in material science, been performed for decades for reinforcement or cost purposes, and examples include the use of silica in silicone rubber [187].

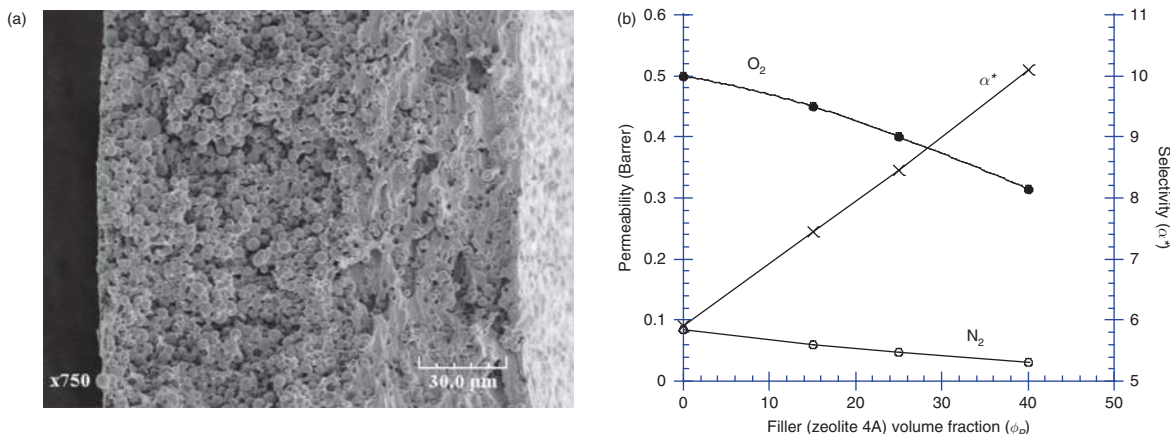


Figure 40 (a) SEM picture of a mixed matrix membrane for gas separations: a powdered adsorbent is dispersed in a dense polymeric membrane. (b) Example of the potentialities of mixed matrix membranes for air separation applications [146]: Evolution of oxygen and nitrogen permeability and membrane selectivity with filler content. Polymer: PVAc, filler: zeolite 4A.

For permeation applications, nanoparticles can significantly increase the glass transition temperature due to the restriction of segmental chain mobility. This can induce beneficial effects in terms of permeability and selectivity and possibly push the performances beyond the trade-off limit. Several observations confirm these effects for silicon dioxide particles for O₂/N₂ separation [188], or butane/methane separation by PTMSP nanocomposites, where a sixfold increase in the butane permeability has been reported [189]. However, the most impressive results have been obtained with fumed silica nanoparticles incorporated in glassy amorphous poly(4-methyl-2-pentyne); surprisingly, a considerable enhancement in both the permeability and selectivity of large organic vapors over small permanent gases was obtained, in contrast to the results found for conventional filled polymer systems [190]. Nanoscale hybridization could be an innovative means of tuning the molecular packing, and consequently, the separation properties in glassy polymers.

2.08.5.1.3 Pushing the limits of ultrathin membrane skin layers

In terms of membrane preparation processes, the search for ultrathin defect-free active layers can possibly lead to breakthrough techniques. Up until now, the productivity of membrane modules for gas separation can roughly be considered to have a lower limit of 50 nm for the best film-forming materials, based on extrusion/coating techniques. This performance is remarkable and will probably be hard to overcome, unless a revolutionary fabrication technique proves to be more efficient. It is interesting to note that alternative and essentially unexplored approaches have been occasionally proposed for such purposes and these include polymerizable ultrathin Langmuir–Blodgett structures [191], or the use photochemical reactive assemblies [192]. The surface structure of the support material and the stability of the thin layer are obviously key issues in this case.

Specific surface treatments that make use of chemical vapor deposition (CVD) or plasma techniques also harbor great potential. The influence of surface fluorination [193], bromination [194], ozonation [195], or ultraviolet (UV) posttreatment [196] has been investigated in greater detail. A completely different strategy would consist in promoting corrugated structures in order to increase the flux [197]; this approach, already applied in certain cases for reverse-osmosis membrane manufacturing,

apparently has yet to attract attention for gas separation purposes.

2.08.5.1.4 Pushing the operation range of gas separation membranes

Aggressive environments are of particular concern for polymeric materials in general, and are often a key issue for membrane applications. The sensitivity of the active layer, of the support, or of the module (such as the casing material, glue, sealants, etc.) to reacting gases, acids, volatile organic compounds, or heavy substances is decisive in terms of process selection, and this certainly constitutes one of the main causes for rejecting gas separation membranes for use in numerous applications. Unfortunately, these aspects are poorly documented in the open literature and the feedback of end-users is very limited.

The difficulties associated with plasticization effects and the necessity of achieving an efficient pretreatment of heavy compounds and hydrocarbons have been discussed above. Moreover, various studies have addressed the durability of membrane materials when exposed to aggressive gases such as chlorine [198] or ozone [199].

Another challenge consists in extending the applicability of gas separation with polymeric membranes in extreme environments of temperature and pressure. Pressure operations up to 380 bar have been occasionally reported for the separation of CO₂/H₂ with a polyamid membrane [200]. The effective transport properties under these conditions are difficult to predict since they result from a competition between swelling and membrane compaction, but a substantial increase in selectivity can, in some cases, be gained.

Gas permeation studies with polymer membranes under high-temperature conditions are scarce. Nevertheless, polypyrrolone has been studied to that extent due to its exceptional thermal stability. Experimental results up to 200 °C have been reported for this polymer [201].

2.08.5.2 Novel Processes

2.08.5.2.1 Operation modes and module design

Innovative processes or operating modes are relatively unexplored issues for membrane gas separation. One could say that the development of polymeric membranes for gas separation has up until now been driven mostly by achievements in materials science: thin active layer membranes, hollow-fiber

modules, and, above all, new polymeric materials. The process development part remains modest, apart from the classical cascade or recycling approach.

Historically, one of the main attempts of promoting novel membrane gas separation processes has been the continuous membrane column, originally proposed by Hwang and Thorman [202]. Here, the key idea is to take advantage of the countercurrent flow principle in a reflux cascade, in order to maximize local driving forces. Similarly to a continuous distillation column, two product flow rates can be continually extracted: a bottom depleted of and a top enriched with a fast permeating compound. Unfortunately, this mode of operation has, in several case studies, been shown to consume more energy and require more membrane area than a simple single-stage process [203].

It is interesting to note, however, that a series of recently published studies has proposed alternative modes of operation, making use of gas separation modules. A common point of several of these new approaches is to take advantage of transient operation. Methods such as the preferential accumulation of the fast compound of a mixture [204], cyclic pressurization and evacuation [205], pressure swing permeation [206], or pulsed feed operation [207] have been explored toward different mixtures. At first glance, this could be regarded as a deadlock; the fact that membrane modules can be operated under steady conditions is often considered a decisive advantage in terms of productivity and ease of operation for process control. Nevertheless, working under unsteady conditions offers the possibility of extending the range of performances in terms of selectivity and productivity.

The key concept of unsteady membrane gas separations was originally proposed for microporous carbon or glass membranes [208]. The idea is based on the fact that, in a closed two-compartment system in transient state, the characteristic curves of two permeating compounds displaying differing diffusion coefficients but identical permeabilities should show different breakthrough times. In this case, the sorption selectivity ($\alpha_S = S_1/S_2$) is strictly inverse to the diffusion selectivity ($\alpha_D = D_1/D_2 = 1/\alpha_S$). Such a situation is not at all systematic, although it may occur occasionally with gas pairs, for example, rare gases.

It is not possible to obtain selectivity under steady operation ($\alpha = 1$); however, a very pure fraction of the fast permeating compound can be extracted for a

short time. Thus, a selectivity–productivity trade-off again needs to be solved. Paul [209] has reported on a pioneering theoretical analysis of the problem, thanks to a dual volume recovering setup with a cyclic feed and a permeate mode of operation. The separation of He/CH₄ was explored and, through an analytical solution of the problem, it could be concluded that the loss of productivity could not be compensated for by the impressive increase in selectivity. A similar conclusion was later obtained for the separation of O₂/N₂ [210]. The concept has recently been re-explored, thanks to modern simulation and optimization methods for separation of the CO₂/H₂ gas pair and a more positive conclusion has been drawn [211]. Further studies are clearly necessary before the real potential of these operating modes can be precisely identified.

Another possibility for achieving multi-component separation consists in utilizing different membranes; this concept has been experimentally and theoretically explored, in particular for the ternary mixture of He–CO₂–N₂ [212]. This mixture was chosen since it is possible to find two different membranes that are inversely selective to the two fast components of the feed (cellulose acetate and silicone rubber). From a practical point of view, the separation can be carried out using a single module equipped with two different membranes [213], or alternatively with two single membrane permeators in series. More recently, various process alternatives for gas separation with membranes have been explored, such as a so-called sorp-vection concept [214].

Significant progress has been made in the design of membrane modules and it is reasonable to state that no major change can be expected within this field in the near future. Generally speaking, hollow-fiber modules take advantage of the better mass-to-momentum transfer efficiency of open tubular contactors as compared to packed beds [215]. The general question of the thermodynamic energy efficiency of modules, which depends, among other things, on the membrane selectivity and pressure ratio, has been investigated for binary mixture separation by one-compressor [216] and two-compressor [217] cascades. These studies confirm that membranes are less adequate for the production of products of extremely high purity. The use of a sweep stream has also been shown to have a strong impact on the energy efficiency, but this mode of operation has remained essentially unexplored in gas permeation applications. The key to thermodynamic efficiency improvement is to

reduce the irreversible entropy production term associated with the separation. This topic was recently explored for membrane separations [218], but the implications in module design with respect to entropy minimization approaches [219], which could possibly open new strategies for module design or driving force distributions, have yet to be addressed.

2.08.5.3 Novel Driving Forces

In addition to the pressure driving force employed for membrane gas separations, alternative approaches could be considered. An electrical potential may also be used, principally in order to achieve a selective transport when examining the general electrochemical potential expression. This option has remained almost unexplored for membrane gas separation purposes, even though the electric potential can be a very strong driving force as compared to pressure. A simple calculation indeed shows that for a species with a net electric charge of ± 2 , a potential difference of 60 mV can be equivalent, in terms of the concentration difference, to 100 bar for an uncharged species [220]. Nevertheless, the application of an electric driving force for gas separation remains largely hypothetical, despite that it could be potentially investigated with electronically conductive polymers, such as polyaniline, having been reported to demonstrate interesting permeation performances in pressure difference operations [221]. Apart from early investigations on electroconvective liquid membranes for gas separation based on liquid crystals [222], this strategy has not attracted attention.

The sensitivity of polymers to specific compounds, usually referred to as solvents, is well known and affects the permeation performances of a gas separation membrane to a large extent. The previous discussion on the negative effect of carbon dioxide or hydrocarbons on glassy polymers due to plasticization belongs to this category. Nevertheless, the swelling effect exerted by one of the compounds present in the feed mixture but not showing an interest can be beneficial. The best example is probably the significant performance changes observed with certain hydrophilic materials when a humid gaseous mixture is treated. This effect has been investigated in detail for cellulosic membrane materials, for which the dry and water-swollen membrane performances have been compared

[223]. Nevertheless, a similar study performed on cellulose acetate, polyethersulfone, and polysulfone for the separation of CO_2/CH_4 reported a decreasing separation factor with an increasing content of feed water [224].

Finally, an unconventional approach consists in exploring the potentiality of visible light or specific wavelengths as an effective driving force for membrane gas separation. Such photoactivated processes would be very appealing when one considers a free energy source. The concept has been experimentally validated for the selective transport of CO through liquid membranes based on a reversible photochromic carrier [225].

2.08.6 Conclusions

In 1955, Weller and Steiner listed a series of what could be considered as impressive, if not utopic, challenges to be overcome for polymeric membranes to find applications in industry:

1. a three- or fourfold increase in flux (permeance) as compared to the performances achieved in the mid-1960s;
2. a sufficient selectivity, generally higher than 20 (NB: air separation is clearly an exception to this rule);
3. the capability of functioning under high pressure differences (up to 150 bar);
4. a good stability in the presence of contaminants within a large temperature range (0–100 °C); and
5. the possibility of developing large-scale, efficient, and stable modules.

Today, these challenges have been achieved to a large extent. As a result, membrane gas separation processes have gained confidence in industry and are nowadays almost systematically considered as one of the possibilities in terms of processes for gas or vapor separation [226].

Given the current and future challenges of the manufacturing and chemical process industries, it can be expected that their use and role will show a considerable development. The number of different markets that can potentially emerge is large. Three main opportunities and their associated challenges are listed below. Overcoming one of these challenges would lead to a major breakthrough and a very large market can be expected.

2.08.6.1

2.08.6.1.1 Hydrogen production

Hydrogen is considered as one of the most promising energy sources when taking into account global climate change and local air pollution issues. The demand for hydrogen is continuously increasing and the separation of hydrogen from other gases by membrane separation processes is often considered to be an extremely promising technology [227]. Nevertheless, breakthrough performances are required in order for polymeric membranes to compete with other technologies in this field. Enhanced selectivities are needed, especially for CO₂/H₂ separation, and higher tolerable operating temperatures would be of interest.

2.08.6.1.2 Greenhouse emissions mitigation

The capture of carbon dioxide from flue gases, generally called postcombustion capture, in order to mitigate greenhouse gas emissions is surely a formidable challenge for membrane gas permeation processes. While polymeric membranes were discarded in the earliest studies, principally because of too low selectivities [228], recent studies have reported a more promising situation [229, 230]. Nevertheless, the exact place and potential of polymeric membranes for this application remains controversial [231] and further investigations are necessary before a clear picture of their practical use can be identified.

2.08.6.1.3 Isomer separations

Isomer separations, mostly among hydrocarbon pairs, represent a very large ratio of the energy requirement for separations in the chemical process industries (e.g., ethylene/ethane and propylene/propane). Glassy polymers, such as poly(phenylene oxide), polysulfone, cellulose acetate, and ethylcellulose, have been considered as potential candidates for separation of the propylene/propane pair, for instance, [232]. Rubbery silicone membranes have also been considered. A major difficulty in this field resides in the strong permeant coupling effect, which drastically decreases the real (effective) selectivity down to a range of 5–10. This is in some cases two- to tenfold lower than the ideal selectivity (α^* , computed from pure gases performances).

Finally, various major arguments support a promising future for gas separation with polymeric membranes:

1. Energy is already a key challenge for industrial manufacturing and membranes are known to offer smart, energy-efficient answers for gas separation. Thus, numerous solutions making use of membranes, which have been discarded due to relatively low energy costs, are expected to be reconsidered.

2. With an increasing amount of sustainable development concerns, constraints such as green engineering or sustainable chemistry issues are becoming more significant. To this respect, membranes combine a unique set of arguments: the absence of chemicals, energy-efficient solutions for recovery or recycling applications, the possibility of working under moderate conditions, etc.

3. It has up until now been said that membrane separation processes often have to fit and be adapted to industrial flowsheets designed for other separation technologies. As a consequence, membrane units have, in a great number of cases, been installed at the process boundaries (e.g., purges, effluents, retrofit of an existing installation, etc.). When new units are designed within an original framework, membrane gas separation processes will have the possibility of playing an increasing role in the heart of the process.

4. Industrial evolution could promote new concepts such as a distributed or consumer-oriented production. In that event, membrane gas separation modular units as well as easy-to-control units would represent an ideal solution.

References

- [1] Graham, T. Q. *J. Sci.* **1829**, *II*, 88–89 (Re-edited in *J. Membr. Sci.* **1995**, *100*, 9.).
- [2] Mitchell, J. K. *Philadelphia J. Med. Sci.* **1831**, *13*, 36.
- [3] Stannett, V. J. *J. Membr. Sci.* **1978**, *3*, 97–115.
- [4] Graham, T. *Philos. Magaz.* **1866**, *32*, 401.
- [5] Mason, E. A. *J. Membr. Sci.* **1991**, *60*, 125–145.
- [6] Henis, J. M. S., Tripodi, M. K. *Sep. Sci. Technol.* **1980**, *15*, 1059.
- [7] Loeb, S., Sourirajan, S. *Adv. Chem. Ser.* **1962**, *38*, 117.
- [8] Henis, J. M. S., Tripodi, M. K. *Science* **1983**, *220*, 4592, 11–17.
- [9] Lonsdale, H. K. *J. Membr. Sci.* **1987**, *33*, 121–136.
- [10] Koros, W. J. Gas Separation. In *Membrane Separation Systems: Recent Developments and Future Directions*; Bakel, R. W., Ed.; Noyes Publishing: Park Ridge, NJ, 1991; pp. 189–241.
- [11] Baker, R. W. *Ind. Eng. Chem. Res.* **2002**, *41*, 1393–1411.
- [12] Strathmann, H. *AIChE J.* **2001**, *47*(5), 1077–1087.
- [13] Paul, D. R., Yampolskii, Y. P. *Polymeric Gas Separation Membranes*; CRC Press: Boca Raton, FL, 1994.
- [14] Baker, R. *Membrane Technology and Applications*, 2nd edn.; Wiley: New York, 2004.
- [15] Ghosal Freeman, B. D. *Polym. Adv. Technol.* **1993**, *5*, 673–697.

- [16] Yamploskii, Y., Freeman, B. D. *Materials Science of Membranes for Gas and Vapor Separation*; Wiley: New York, 2006.
- [17] Rautenbach, R., Albrecht, R. *Membrane Processes*; Wiley: New York, 1989.
- [18] Ho, W. S., Sirkar, K. K. *Membrane Handbook*; Van Nostrand Reinhold: New York, 1992.
- [19] Peinemann, K. V., Nunes, S. *Membrane Technology in the Chemical Industry*; Wiley-VCH: New York, 2001.
- [20] Koros, W. J., Ma, Y. H., Shimidzu, T. *Pure Appl. Chem.* **1996**, 68(7), 1479–1489.
- [21] Koros, W. J., Ma, Y. H., Shimidzu, T. *J. Membr. Sci.* **1996**, 120, 149–159.
- [22] Hwang, S. T., Kammermeyer, K. L. *Membranes in Separations*, Wiley Interscience: New York, 1975.
- [23] Lakshminarayanaiah, N. Transport Processes in Membranes. In *Subcellular Biochemistry, Volume 6*; Roodyn, D., Ed.; Plenum: New York, 1979; pp 401–494.
- [24] Lee, C. H. *J. Appl. Pol. Sci.* **1975**, 19, 83–95.
- [25] Guggenheim, E. A. *Thermodynamics*; North Holland: Amsterdam, 1965.
- [26] Wijmans, J. G., Baker, R. W. *J. Membr. Sci.* **1995**, 107, 1.
- [27] Paul, D. R. *J. Appl. Polym. Sci.* **1972**, 16, 771–782.
- [28] Paul, D. R., Ebra-Lima, O. M. *J. Appl. Polym. Sci.* **1970**, 14, 2201–2224.
- [29] Islam, M. A., Buschatz, H. *Chem. Eng. Sci.* **2002**, 57, 2089–2099.
- [30] Vesely, D. *Polymer* **2001**, 42, 4417–4422.
- [31] Way, J. D., Noble, R. D., Flynn, T. M., Sloan, E. D. *J. Membr. Sci.* **1982**, 12, 239–259.
- [32] Barrer, R. M. *Diffusion in and through Solids*; Cambridge University Press: London, 1951.
- [33] Paul, D. R. *J. Polym. Sci.* **1973**, 11, 289.
- [34] Michaels, A. S. *J. Membr. Sci.* **1996**, 109, 1–19.
- [35] Srinivasan, R., Auvil, S. R., Burban, P. M. *J. Membr. Sci.* **1994**, 86, 67–74.
- [36] Hillaire, A., Favre, E. *AIChE J.* **1998**, 44, 1200–1206.
- [37] Stanett, V. *J. Membr. Sci.* **1978**, 3, 97.
- [38] Flory, P. J., *Principles of Polymer Chemistry*, Cornell University Press: Ithaca, NY, 1953.
- [39] Walas, S. M. *Phase Equilibria in Chemical Engineering*; Butterworths: London, 1985.
- [40] Flory, P. J., Rehner, J., Jr. *J. Chem. Phys.* **1943**, 11, 512–526.
- [41] Favre, E., Nguyen, Q. T., Schaetzel, P., Clement, R., Néel, J. *J. Chem. Soc. Faraday Trans.* **1993**, 89, 4339–4346.
- [42] Prausnitz, J. M., Lichtenthaler, R. N., de Azevedo, E. G. *Molecular Thermodynamics of Fluid Phase Equilibria*; Prentice-Hall: Englewood Cliffs, NJ, 1999.
- [43] Favre, E., Nguyen, Q. T., Clément, R., Néel, J. *J. Membr. Sci.* **1996**, 117, 227–236.
- [44] Barrer, R. M., Barrie, J. A., Slater, J. J. *Polym. Sci.* **1958**, 27, 177.
- [45] Meares, P. *J. Am. Chem. Soc.* **1954**, 66, 3415.
- [46] Vieth, W. R., Howell, J. M., Hsieh, J. H. *J. Membr. Sci.* **1976**, 1, 177–220.
- [47] Theodorou, D. N. *Chem. Eng. Sci.* **2007**, 62, 5697–5714.
- [48] Doghieri, F., Sarti, G. C. *J. Membr. Sci.* **1998**, 147, 73–86.
- [49] Crank, J. *The Mathematics of Diffusion*; Oxford Science Publications: Oxford, 1975.
- [50] Crank, J., Park, G. S. *Diffusion in Polymers*; Academic Press: London, 1968.
- [51] Kokes, R. J., Long, F. A. *J. Am. Chem. Soc.* **1953**, 75, 6142–6146.
- [52] Fujita, H. *Fortschrit Hochpolym. Forsch.* **1961**, 3, 1.
- [53] Cohen, M. H., Turnbull, D. *J. Chem. Phys.* **1954**, 31, 1164–1168.
- [54] Kosfeld, R., Zunkley, L. *Ber. Bunsenges. Phys. Chem.* **1979**, 83, 392–396.
- [55] Peterlin, A. *J. Macromol. Sci. Phys.* **1975**, B11(1), 57–87.
- [56] Stern, S. A., Fang, S. M., Frisch, H. L. *J. Polym. Sci.* **1972**, A-2(10), 201.
- [57] Duda, J. L., Vrentas, J. S., Ju, S. T., Liu, H. T. *AIChE J.* **1982**, 28, 279.
- [58] Assink, R. A. *J. Polym. Sci., Polym. Phys. Ed.* **1975**, 13, 1665–1673.
- [59] Petropoulos, J. H. *J. Polym. Sci. Part A-2* **1970**, 8, 1797–1801.
- [60] Chan, A. H., Koros, W. B., Paul, D. R. *J. Membr. Sci.* **1978**, 3, 117–130.
- [61] Koros, W. J., Chan, A. H., Paul, D. R. *J. Membr. Sci.* **1977**, 2, 165–190.
- [62] Wijmans, J. G. *J. Membr. Sci.* **2003**, 220, 1–3.
- [63] Mauviel, G., Berthiaud, J., Vallières, C., Roizard, D., Favre, E. *J. Membr. Sci.* **2005**, 266, 62–67.
- [64] Barrer, R. M. *Nature* **1937**, July 17th Issue, 106–107.
- [65] Van Krevelen, D. W. *Properties of Polymers*, 2nd edn.; Elsevier: New York, 1976, Chap 18.
- [66] Hillaire, A., Favre, E. *Ind. Eng. Chem. Res.* **1999**, 38, 211–217.
- [67] Salame, M. *J. Polym. Sci.* **1973**, 41, 1–15.
- [68] Park, J. Y., Paul, D. R. *J. Membr. Sci.* **1997**, 125, 23–39.
- [69] Teplyakov, V., Meares, P. *Gas Sep. Pur.* **1990**, 4, 66–74.
- [70] LaPack, M. A., Tou, J. C., McGuffin, V. L., Enke, C. G. *J. Membr. Sci.* **1994**, 86, 263–290.
- [71] Pauly, S. Permeability and Diffusion Data. In *Polymer Handbook*, 4th edn. Bandrup, J., Immergut, E. H., Grulke, E. A., Eds.; Wiley: New York, 1999; pp 435–449.
- [72] Robeson, J. L. *J. Membr. Sci.* **1991**, 62, 165.
- [73] Freeman, B. D. *Macromolecules* **1999**, 32, 375.
- [74] Humphrey, J. L., Keller, G. E. *Separation Process Technology*; MacGraw-Hill: New York, 1997.
- [75] Seader, J. D., Henley, E. J. *Separation Process Principles*; Wiley: New York, 2006.
- [76] Weller, S., Steiner, W. A. *Chem. Eng. Prog.* **1950**, 46 (11), 585–590.
- [77] Coker, D. T., Freeman, B. D., Fleming, G. K. *AIChE J.* **1998**, 44(6), 1289.
- [78] Kaldis, S. P., Kapantaidakis, G. C., Sakellaropoulos, G. P. *J. Membr. Sci.* **2000**, 173, 61–71.
- [79] Boucif, N., Majumdar, S., Sirkar, K. K. *Ind. Eng. Chem. Fund.* **1984**, 23, 470.
- [80] Krovvidi, K. R., Kovvali, A. S., Vemury, S., Khan, A. A. *J. Membr. Sci.* **1992**, 66, 103–118.
- [81] Rautenbach, R., Dahm, W. *J. Membr. Sci.* **1986**, 28, 319–325.
- [82] Naylor, R. W., Backer, P. O. *AIChE J.* **1955**, 1, 95–99.
- [83] Shindo, Y., Hakuta, T., Yoshitome, H., Inoue, H. *Sep. Sci. Technol.* **1985**, 20, 445–459.
- [84] Zolandz, R., Fleming, G. K. Gas Permeation Applications. In *Membrane Handbook*; Ho, W. S., Sirkar, K. K., Eds.; Van Nostrand Reinhold: New York, 1992; pp 17–85.
- [85] Thundiyil, M. J., Koros, W. J. *J. Membr. Sci.* **1997**, 125, 275.
- [86] Stern, S. A., Vaidyanathan, R., Pratt, J. R. *J. Membr. Sci.* **1990**, 49, 1–14.
- [87] Li, K., Acharya, D. R., Hughes, R. *J. Membr. Sci.* **1990**, 52, 205–219.
- [88] Pan, C. Y., Hagbood, H. W. *Ind. Eng. Chem. Fundam.* **1974**, 13, 323–331.
- [89] Baker, R. W., Wijmans, J. G., Kaschemekat, J. H. *J. Membr. Sci.* **1998**, 151, 55–62.
- [90] Bhide, B. D., Stern, S. A. *J. Membr. Sci.* **1998**, 140, 27–49.
- [91] Qi, R., Henson, M. A. *J. Membr. Sci.* **1998**, 148, 71–89.
- [92] Tsuru, T., Hwang, S. T. *J. Membr. Sci.* **1994**, 94, 213–224.

- [94] McCandless, F. P. *J. Membr. Sci.* **1985**, *24*, 15–28.
- [95] Rautenbach, R., Struck, A., Melin, T., Roks, M. F. M. *J. Membr. Sci.* **1998**, *146*, 217–223.
- [96] Zhu, Z. *J. Membr. Sci.* **2006**, *281*, 754–756.
- [97] Henis, J. M., Tripodi, M. K. *J. Membr. Sci.* **1981**, *8*, 233–246.
- [98] Pinnau, I., Wijmans, J. G., Blume, I., Kuroda, T., Peinemann, K. V. *J. Membr. Sci.* **1988**, *37*, 81–88.
- [99] Thorman, J. M., Rhim, H., Hwang, S. T. *Chem. Eng. Sci.* **1975**, *30*, 751–754.
- [100] Feng, X., Huand, R. Y. M. *Can. J. Chem. Eng.* **1995**, *73*, 833–843.
- [101] Lim, S. P., Tan, X., Li, K. *Chem. Eng. Sci.* **2000**, *55*, 2641.
- [102] Gorisen, H. *Chem. Eng. Process* **1987**, *22*, 63–67.
- [103] Coker, D. T., Allen, T., Freeman, B. D., Fleming, G. K. *AIChE J.* **1999**, *45*(7), 1451.
- [104] Kao, Y. K., Chen, S., Hwang, S. T. *J. Membr. Sci.* **1987**, *32*, 139–157.
- [105] Lemanski, J., Lipscomb, G. G. *AIChE J.* **1995**, *41*(10), 2322.
- [106] Chen, H., Cao, C., Xu, L., Xiao, T., Jiang, G. *J. Membr. Sci.* **1998**, *139*, 259–268.
- [107] Lemanski, J., Lipscomb, G. G. *J. Membr. Sci.* **2002**, *195*, 215–228.
- [108] Lemanski, J., Lipscomb, G. G. *J. Membr. Sci.* **2000**, *167*, 241–252.
- [109] Bhattacharya, S., Hwang, S. T. *J. Membr. Sci.* **1997**, *132*, 73–90.
- [110] Haraya, K., Hakuta, T., Yoshitome, H., Kimura, S. *Sep. Sci. Technol.* **1987**, *22*, 1425–1438.
- [111] He, G., Mi, Y., Yue, P. L., Chen, G. *J. Membr. Sci.* **1999**, *153*, 243–258.
- [112] Ludtke, O., Behling, R. D., Ohlrogge, K. *J. Membr. Sci.* **1998**, *146*, 145–157.
- [113] Wang, R., Liu, S. L., Lin, T. T., Chung, T. S. *Chem. Eng. Sci.* **2002**, *57*, 967–976.
- [114] Islam, M. A., Buschhatz, H., Paul, D. *J. Membr. Sci.* **2002**, *204*, 379–384.
- [115] Taylor, R., Krishna, R. *Multicomponent Mass Transfer*; Wiley: New York, 1993.
- [116] Bird, R. B., Stewart, W. E., Lightfoot, E. N. *Transport Phenomena*; Wiley: New York, 1960.
- [117] Kamaruddin, D. H., Koros, W. J. *J. Membr. Sci.* **1997**, *135*, 147.
- [118] Frisch, H. L. *Polymer J.* **1991**, *23*(5), 445–456.
- [119] Truesdell, C. *J. Chem. Phys.* **1962**, *37*, 2336.
- [120] Stern, S. A., Onorato, F. J., Libove, C. *AIChE J.* **1977**, *23*, 567–578.
- [121] Isalski, W. H. *Separation of Gases*; Clarendon: Oxford, 1989.
- [122] Hinchliffe, A. B., Porter, K. E. *Ind. Eng. Chem. Res.* **1997**, *36*, 821–829.
- [123] Koros, W. J. *AIChE J.* **2004**, *50*(10), 2326.
- [124] Schell, W. J. *J. Membr. Sci.* **1985**, *22*, 217–224.
- [125] Spillman, R. W. *Chem. Eng. Prog.* **1989**, *1*, 41–62.
- [126] Koros, W. J., Fleming, G. K. *J. Membr. Sci.* **1993**, *83*, 1–80.
- [127] Chen, W. J., Martin, C. R. *J. Membr. Sci.* **1994**, *95*, 51–61.
- [128] Zimmerman, C. M., Koros, W. J. *Macromolecules* **1999**, *32*, 3341–3346.
- [129] Koros, W. J. *J. Polym. Sci., Pol. Phys. Ed.* **1985**, *23*, 1611–1628.
- [130] Tabe-Mohammadi, A. *Sep. Sci. Technol.* **1999**, *34*, 2095–2111.
- [131] Baker, R. W., Lokhandwala, K. *Ind. Eng. Chem. Res.* **2008**, *47*, 2109–2121.
- [132] Cook, P. J., Losin, M. S. *Hydrocarbon Process* **1995**, *4*, 79–84.
- [133] McKee, R. L., Changela, M. K., Reading, G. J. *Hydrocarbon Process* **1991**, *4*, 63–65.
- [134] Bhide, B. D., Voskericyan, A., Stern, S. A. *J. Membr. Sci.* **1998**, *140*, 27–49.
- [135] Hao, J., Rice, P. A., Stern, S. A. *J. Membr. Sci.* **2002**, *209*, 177–206.
- [136] Dortmund, D., Doshi, K. *Chem. Eng. World*, **2003**, September Issue, 55–66.
- [137] Datta, A. K., Sen, P. K. *J. Membr. Sci.* **2006**, *283*, 291–300.
- [138] Gottschlich, D. E., Roberts, D. L., Way, J. D. *Gas Sep. Purif.* **1988**, *2*, 65–71.
- [139] Parro, D. *Energy Prog.* **1985**, *5*(1), 51–54.
- [140] White, L. S., Blinka, T. A., Kloczewski, H. A., Wang, I. F. *J. Membr. Sci.* **1995**, *103*, 73–82.
- [141] Visser, T., Koops, G. H., Wessling, M. *J. Membr. Sci.* **2005**, *252*, 265–277.
- [142] Wind, J. D., Paul, D. R., Koros, W. J. *J. Membr. Sci.* **2004**, *228*, 227–236.
- [143] Shieh, J. J., Chung, T. S., Wang, R., Srinivasan, M. P., Paul, D. R. *J. Membr. Sci.* **2001**, *182*, 111–123.
- [144] Lee, A. L., Feldkirchner, H. L., Stern, S. A., Houde, A. Y., Gamez, J. P., Meyer, H. S. *Gas Sep. Purif.* **1995**, *9*(1), 35–43.
- [145] Kapdi, S. S., Vijay, V. K., Rajesh, S. K., Prasad, R. *Renew Energy* **2005**, *30*, 1195–1202.
- [146] Baker, R. W., Wijmans, J. G., Kashemekat, J. H. *J. Membr. Sci.* **1998**, *151*, 55–62.
- [147] Lüdtkke, O., Behling, R. D., Ohlrogge, K. *J. Membr. Sci.* **1998**, *146*, 145–157.
- [148] Yeom, C. K., Lee, S. H., Lee, J. M., Song, H. Y. *J. Membr. Sci.* **2002**, *204*, 303–322.
- [149] Hillaire, A., Favre, E. *Ind. Eng. Chem. Res.* **1999**, *38*, 211–217.
- [150] Alpers, A., Keil, B., Lüdtkke, O., Ohlrogge, K. *Ind. Eng. Chem. Res.* **1999**, *38*, 3754–3760.
- [151] Ye, X., LeVan, D. *J. Membr. Sci.* **2003**, *221*, 147–161.
- [152] Ye, X., LeVan, D. *J. Membr. Sci.* **2003**, *221*, 163–173.
- [153] Wang, K. L., McCray, S. H., Newbold, D. D., Cussler, E. L. *J. Membr. Sci.* **1992**, *72*, 231–244.
- [154] Peterson, E. S., Stone, M. L. *J. Membr. Sci.* **1994**, *86*, 57–65.
- [155] Haraya, K., Hwang, S. T. *J. Membr. Sci.* **1992**, *71*, 13–27.
- [156] Stern, S. A., Leone, S. M. *AIChE J.* **1980**, *26*, 881–890.
- [157] Bhide, B. D., Stern, S. A. *J. Membr. Sci.* **1991**, *62*, 13–35.
- [158] Bhide, B. D., Stern, S. A. *J. Membr. Sci.* **1991**, *62*, 37–58.
- [159] Li, Y., Duchateau, E. Process and System for Selective Abatement of Reactive Gases and Recovery of Perfluorocompound Gases. US Pat. 5,759,237.
- [160] Chung, I. J., Lee, K. R., Hwang, S. T. *J. Membr. Sci.* **1995**, *105*, 177–185.
- [161] Hsieh, S. T., Keller, G. E. *J. Membr. Sci.* **1992**, *70*, 143–152.
- [162] Timashev, S. F., Vorobiev, A. V., Kirichenko, V. I., Popkov, M., Volkov, V. I. *J. Membr. Sci.* **1991**, *59*, 117–131.
- [163] Tricoli, V., Cussler, E. L. *J. Membr. Sci.* **1995**, *104*, 19–26.
- [164] Agrinier, P., Roizard, D., Ruiz Lopez, M., Favre, E. *J. Membr. Sci.* **2008**, *318*, 373–378.
- [165] McCandless, F. P., Herbst, S. *J. Membr. Sci.* **1990**, *54*, 307–319.
- [166] Noble, R. D., Agrawal, R. *Ind. Eng. Chem. Res.* **2005**, *44*, 2887.
- [167] Drioli, E., Romano, M. *Ind. Eng. Chem. Res.* **2001**, *40*, 1277–1300.
- [168] Stern, S. A. *J. Membr. Sci.* **1994**, *94*, 1–65.
- [169] Koros, W. J., Mahajan, R. *J. Membr. Sci.* **2000**, *175*, 181–196.
- [170] Kosuri, M. R., Koros, W. J. *J. Membr. Sci.* **2008**, *320*, 65–72.
- [171] Freeman, B. D., Pinnau, I. *Trends Polym. Sci.* **1997**, *5*, 167.

- [172] Lin, H., Van Wagner, E., Freeman, B. D., Toy, L. G., Gupta, R. P. *Science* **2006**, *311*, 639–642.
- [173] Park, H. B., Jung, C. H., Lee, Y. M., et al. *Science* **2007**, *318*, 254–258.
- [174] Noble, R. J. *J. Membr. Sci.* **1990**, *50*, 207.
- [175] Lai, J. Y., Huang, S. J., Chen, S. H. *J. Membr. Sci.* **1992**, *74*, 71–82.
- [176] Wang, C. C., Cheng, M. H., Chen, C. Y., Chen, C. Y. *J. Membr. Sci.* **2002**, *208*, 133–145.
- [177] Wang, C. C., Chen, C. C., Huang, C. C., Chen, C. Y., Kuo, J. F. *J. Membr. Sci.* **2000**, *177*, 189–199.
- [178] Chen, S. H., Yu, K. C., Hwang, S. L., Lai, J. Y. *J. Membr. Sci.* **2000**, *173*, 99–106.
- [179] Bellobono, I. R., Muffato, F., Selli, E., Righetto, L., Tacchi, R. *Gas Sep. Purif.* **1987**, *1*, 103–106.
- [180] Way, J. D., Noble, R. D., Flynn, T. M., Sloan, E. D. *J. Membr. Sci.* **1982**, *12*, 239–259.
- [181] Singh, A., Koros, W. J. *Ind. Eng. Chem. Res.* **1996**, *35*, 1231–1236.
- [182] Paul, D. R., Kemp, D. R. *J. Polym. Sci.* **1973**, *41*, 79–93.
- [183] Duval, J. M., Folkers, B., Mulder, M. H. V., Desgrandchamps, G., Smolders, C. A. *J. Membr. Sci.* **1993**, *80*, 189–198.
- [184] Jia, M., Peinemann, K. V., Behling, R. D. *J. Membr. Sci.* **1991**, *57*, 289–292.
- [185] Maxwell, J. C. *Treatise on Electricity and Magnetism*; Oxford University Press: London, 1873.
- [186] Gonzo, E. E. *J. Membr. Sci.* **2006**, *277*, 46–54.
- [187] Robb, W. L. *Ann. N.Y. Acad. Sci.* **1968**, *146*, 119–137.
- [188] Moaddeb, M., Koros, W. J. *J. Membr. Sci.* **1997**, *125*, 143–163.
- [189] Gomes, D., Nunes, S. P., Peinemann, K. V. *J. Membr. Sci.* **2005**, *246*, 13–25.
- [190] Merkel, T. C., Freeman, B. D., Spontak, R. J., et al. *Science* **2002**, *296*, 519–522.
- [191] Albrecht, O., Laschewsky, A., Ringsdorf, H. *J. Membr. Sci.* **1985**, *22*, 187–197.
- [192] Liu, C., Martin, C. R. *Nature* **1991**, *352*, 50–52.
- [193] Mohr, J. M., Paul, D. R., Pinnau, I., Koros, W. J. *J. Membr. Sci.* **1991**, *56*, 77–98.
- [194] Barbari, T. A., Datwani, S. S. *J. Membr. Sci.* **1995**, *107*, 263–266.
- [195] Henis, J. M. S., Kramer, P. W., Murphy, M. K., Stedronsky, E. R., Stookey, D. J. Membranes Having Enhanced Selectivity and Method of Producing Such Membranes. US Pat. 5,215,554, 1993.
- [196] Wright, C. T., Paul, D. R. *J. Membr. Sci.* **1997**, *124*, 161–174.
- [197] Gronda, A. M., Buechel, S., Cussler, E. L. *J. Membr. Sci.* **2000**, *165*, 177.
- [198] Hagg, M. B. *J. Membr. Sci.* **2000**, *170*, 173–190.
- [199] Polyakov, A., Yamploskii, Y. *Desalination* **2006**, *200* (1–3), 20.
- [200] Hartel, G., Puschel, T. *J. Membr. Sci.* **1999**, *162*, 1–8.
- [201] Costello, L. M., Walker, D. R. B., Koros, W. J. *J. Membr. Sci.* **1994**, *90*, 117–130.
- [202] Hwang, S. T., Thorman, J. M. *AIChE J.* **1980**, *25*(4), 558.
- [203] Rautenbach, R., Dahm, W. *Chem. Eng. Process* **1987**, *21*, 141–150.
- [204] LaPack, M. A., Dupuis, F. Dynamic Membrane Separation Process for Improved Selectivity. US Pat. 5,354,474, 1994.
- [205] Ueda, K., Haruna, K., Inoue, M. Process for Separating Gas. US Pat. 4,955,998, 1990.
- [206] Feng, X., Pan, C. Y., Ivory, J. *AIChE J.* **2000**, *46*, 724–733.
- [207] Beckman, I. N., Shelekhin, A. B., Teplyakov, V. V. *J. Membr. Sci.* **1991**, *55*, 283–297.
- [208] Ash, R., Barrer, R. M., Foley, T. *J. Membr. Sci.* **1976**, *1*, 355–370.
- [209] Paul, D. R. *Ind. Eng. Chem. Process Des. Dev.* **1971**, *10*, 375–379.
- [210] Higuchi, A., Nakagawa, T. *J. Appl. Polym. Sci.* **1989**, *37*, 2181–2190.
- [211] Corriu, J. P., Fonteix, C., Favre, E. *AIChE J.* **2008**, *54*, 1224–1234.
- [212] Sengupta, A., Sirkar, K. K. *J. Membr. Sci.* **1988**, *39*, 61–77.
- [213] Stern, S. A., Perrin, J. E., Naimon, E. J. *J. Membr. Sci.* **1984**, *20*, 25–43.
- [214] Damle, S., Koros, W. J. *AIChE J.* **2005**, *51*, 1396.
- [215] Engasser, J. M., Horvath, C. *Ind. Eng. Chem. Fundam.* **1975**, *14*, 107–110.
- [216] Xu, J., Agrawal, R. *J. Membr. Sci.* **1996**, *112*, 115–128.
- [217] Agrawal, R., Xu, J. *J. Membr. Sci.* **1996**, *112*, 129–146.
- [218] Hwang, S. T. *AIChE J.* **2004**, *50*, 862–870.
- [219] Tondeur, D., Kvaalen, E. *Ind. Eng. Chem. Res.* **1987**, *26*, 50–56.
- [220] Winnick, J. *Chem. Eng. Prog.* **1990**, *1*, 41–46.
- [221] Kuwabata, S., Martin, C. R. *J. Membr. Sci.* **1994**, *91*, 1–12.
- [222] Collins, J. P., Noble, R. D., Parkand, C. H., Clark, N. A. *J. Membr. Sci.* **1995**, *99*, 249–257.
- [223] Wu, J., Yuan, Q. *J. Membr. Sci.* **2002**, *204*, 185–194.
- [224] Paulson, G. T., Clinch, A. B., McCandless, F. P. *J. Membr. Sci.* **1983**, *14*, 129–137.
- [225] Schulz, J. S. *Nature* **1997**, *197*, 1177–1179.
- [226] Häring, H. W. *Industrial Gases Processing*; Wiley-VCH: Weinheim, 2008.
- [227] Adhikari, S., Fernando, S. *Ind. Eng. Chem. Res.* **2006**, *45*, 875–881.
- [228] Van der Sluis, J. P., Hendriks, C. A., Blok, K. *Energy Conv. Manag.* **1992**, *33*(5–8), 429.
- [229] Hägg, M. B., Lindbrathen, A. *Ind. Eng. Chem. Res.* **2005**, *44*, 7668–7675.
- [230] Ho, M. T., Allinson, G. W., Wiley, D. E. *Ind. Eng. Chem. Res.* **2008**, *47*, 1562–1568.
- [231] Favre, E. *J. Membr. Sci.* **2007**, *294*, 50–59.
- [232] Sridar, S., Khan, A. A. *J. Membr. Sci.* **1999**, *159*, 209–219.

Biographical Sketch

Eric Favre is a professor of chemical engineering at the Ecole Nationale Supérieure des Industries Chimiques (ENSIC) at Nancy Université, France. He holds a PhD degree in chemical engineering from INPL as well as graduate degrees from Dijon University (France) and EPFL (Switzerland). His research activities on membranes started in 1987 with studies on ultrafiltration operations and membrane bioreactors performed at EPFL and at the Department of Chemical Engineering and Materials Science at the University of Minnesota (USA), where he was a visiting scientist. In 1991, he moved to ENSIC Nancy to join Professor Néel's team in a CNRS laboratory of macromolecular physical chemistry. There, he investigated thermodynamics and mass transfer phenomena in dense polymers for pervaporation applications. Since 1998, he is based at the Laboratoire des Sciences du Génie Chimique, CNRS, Nancy. His current research activities are mainly concerned with chemical engineering studies of polymeric gas separation membranes. Eric Favre is the author of more than 60 publications in scientific journals, and he has been a member of the editorial board of the *Journal of Membrane Science* since 2005.

2.09 Membranes for Recovery of Volatile Organic Compounds

K Ohlrogge, J Wind, and T Brinkmann, GKSS Research Centre Geesthacht GmbH, Geesthacht, Germany

© 2010 Elsevier B.V. All rights reserved.

2.09.1	Introduction	214
2.09.2	History of VOC-Selective Membranes	214
2.09.3	Membranes for Organic Vapor Separation	216
2.09.4	Design Criteria	217
2.09.5	Membrane Modules	218
2.09.6	Development of Simulation Tools	219
2.09.6.1	Description of Multicomponent Permeation	220
2.09.6.2	Nonideal Thermodynamic Behavior	221
2.09.6.3	Concentration Polarization	222
2.09.6.4	Pressure Drops on the Retentate and Permeate Sides of the Membrane Module	223
2.09.6.5	Transport Resistances of Porous Support Layers	223
2.09.6.6	Modeling of Membrane Modules	223
2.09.7	General Layout Criteria	227
2.09.8	Technical Applications	229
2.09.8.1	Gasoline Vapor Recovery	229
2.09.8.2	Vapor Recovery at Gasoline Stations	231
2.09.8.3	PE Powder Treatment	235
2.09.8.4	Polyolefin Production	236
2.09.8.5	Ethylene Oxide and Vinyl Acetate Production	237
2.09.9	Conclusions and Outlook	238
	References	239

Glossary

EOS Equation of state for describing the pressure–volume–temperature relationship of gas mixtures.

Flow sheeting program Computer tool for process design.

Fugacity Corrected partial pressure taking into account the real gas behavior.

GKSS German government-founded research center, member of the Helmholtz Association of German Research Centres.

GKSS GS Module Flat sheet gas separation membrane module developed by GKSS.

JFE Holdings, Inc. Merger of Nippon Kokan Kabushiki (NKK) and Kawasaki Steel Corporation,

J for Japan, F for steel as in Fe, the atomic symbol for iron, E for engineering.

Joule–Thomson effect Temperature change due to expansion of a real gas.

PDMS Polydimethylsiloxane hydrocarbon selective membrane material.

POMS Polyoctylmethylsiloxane hydrocarbon selective membrane material.

Property package Assembly computer programs for calculating physical properties of substances and their mixtures.

RVP Reid vapor pressure, vapor pressure at 38 °C.

VRU Vapor recovery unit mostly used in tank farm applications.

Nomenclature

A	area (m ²)
b	breadth (m)
c	Concentration (kmol m ⁻³)
d_h	hydraulic diameter (m)
dz	differential length element (m)
D	diffusion coefficient (m ² s ⁻¹)
E_{act}	activation energy (kJ kmol ⁻¹)
F	function
H	molar enthalpy (kJ kmol ⁻¹)
k	heat transfer coefficient (kW m ⁻² K ⁻¹)
L	permeance (m ³ _(STP) bar ⁻¹ m ⁻² h ⁻¹)
L_∞⁰	permeance for $T \rightarrow \infty$ and $p \rightarrow 0$ (m ³ _(STP) bar ⁻¹ m ⁻² h ⁻¹)
m₀	parameter in free-volume model (bar ⁻¹)
m_T	parameter in free-volume model (K ⁻¹)
nc	number of components
\dot{n}	molar flow rate (kmol h ⁻¹)
\dot{n}''	molar flux (kmol m ⁻² h ⁻¹)
p	pressure bar
P	permeability (m ³ _(STP) m bar ⁻¹ m ⁻² h ⁻¹)
\dot{q}''	heat flux (kW m ⁻²)
R	resistance
R	ideal gas constant (0.083 143 3 m ³ bar kmol ⁻¹ K ⁻¹)
S	solubility coefficient (kmol m ⁻³ bar ⁻¹)
T	temperature (K)
v	velocity (m s ⁻¹ , m h ⁻¹)
\dot{V}	volumetric flow rate (m ³ h ⁻¹)
y	mole fraction
α	selectivity

β	mass transfer coefficient (m h ⁻¹)
ζ	friction coefficient
θ	temperature (°C)
ρ	density (kg m ⁻³)
σ	Lennard-Jones molecule diameter (Å)
φ	fugacity coefficient
Φ	pressure ratio

Subscripts

av	average
A	component
B	component
EOS	equation of state
H	high pressure
i	component
j	component
k	permeation cell number
L	low pressure
M	membrane
P	permeate
PM	permeate–membrane surface interface
R	retentate
RM	retentate–membrane surface interface
std	at standard conditions
STP	standard temperature (273.15 K) and pressure (1.01325 bar)
T	total

Superscripts

G	gas phase
----------	-----------

2.09.1 Introduction

Membrane technology to separate volatile organic compounds (VOCs) from gas streams is a well-established technology in several industrial processes since the early 1990s. Membrane processes are used to treat vent streams according to stipulated clean air regulations or to separate organic components from process streams. Often, membrane technology competes with processes such as absorption, adsorption, or cryogenic technology. In the case of the recovery of VOCs, the combination of membrane separation with absorption, adsorption, or condensation could be the favorable design in terms of efficiency and competitiveness.

Membrane technology for VOC separation has captured several niche applications. Typical examples are gasoline vapor recovery, monomer

separation in polymer production, and solvent separation from high organic vapor concentrated off-gas streams.

Research Centre Geesthacht (GKSS) and its licensees as well as Membrane Technology and Research (MTR), USA, in cooperation with Nitto Denko, Japan, can be considered front-runners in the technology transfer of membrane-based organic vapor recovery into industrial use.

2.09.2 History of VOC-Selective Membranes

Silicone materials have been used to understand and to explore gas permeation through dense films. J. K. Mitchell [1,2], as early as in 1831, and Sir

Thomas Graham [3], in 1866, published papers on gas absorption in rubbery materials and on the first quantitative measurements of gas permeation rates. Besides this fundamental research, a patent on process for concentrating hydrocarbons was filed by Fredrik E. Frey from Phillips Petroleum Company. The US patent 2159434 was granted in 1939. Years later, Jean P. Jones, also from Phillips Petroleum Company, filed a patent application titled 'Separation of hydrocarbons from non-hydrocarbons by diffusion.' This patent application was granted as US patent 2167493 in 1952. No technical applications based on these patents have been realized because of the lack of efficient membranes.

G. J. Amerongen (1950) and R. M. Barrer (1951) published very important and useful contributions for a better knowledge and understanding of permeation through polymers. In 1981, Roger W. Fenstermaker filed the US patent 4370150 'Engine performance operating on field gas engine fuel.' Hydrogen sulfide and heavier hydrocarbons as compounds of natural gas have to be separated in order to upgrade the quality of gas engine fuel. Fenstermaker claimed a process to separate interfering substances from natural gas used as engine fuel gas by means of silicone-based membranes.

The introduction of technically feasible processes failed because of the lack of membranes with appropriate selectivities and permeances. In the 1980s, research activities commenced in the United States, Japan, and Germany to develop suitable membranes and membrane separation processes to separate organic vapors from air, off-gas, or process streams. MTR, in cooperation with Nitto Denko (Japan), developed membranes for organic vapor recovery. GKSS Research Center Geesthacht was also active in the development of VOC-selective membranes. GKSS Research Center was focused on the development of membranes, modules, and processes. Several GKSS licensees introduced the developments into industrial use. MTR utilized its own developments as an engineering company. Nitto Denko was the membrane supplier for the Japanese engineering company Nippon Kokan Kabushiki Kaisha (NKK).

The following three process patents show the focus of initial activities to implement organic vapor recovery by means of membrane technology. R.W. Baker from MTR filed the US patent 4553983 'Process for organic vapor recovery from air' in 1985. The patent describes a process to separate organic vapors from effluent streams with a maximum

concentration of 2 vol.% organic vapors. In 1986, Kato *et al.* from NKK (now JFE) invented a process to separate and recover organic vapors from off-gases as a combination of absorption and membrane separation (EP 0247858). The GKSS patent 'Method for extracting organic compounds from air/permanent gas mixtures' (EP 0329962) filed in 1988 is based on compression of organic-vapor-laden gas streams in order to enhance the recovery of organic vapors by condensation, adsorption, or absorption in combination with a membrane separation stage. The first realized unit based on this patent was a gasoline vapor recovery unit (VRU) in a gasoline tank farm in Munich. The unit was commissioned in 1989. G. Hauk, in 1989, filed the German patent DE 3940855 'Process-integrated waste air purification system for vacuum pumps.' Organic vapors contained in outlet streams of vacuum pumps are separated by means of membranes. The required pressure difference needed to support the permeation of organic vapors through the membranes is provided by the same vacuum pump. The pump is used to suck gas mixtures from processes, to feed the gas to the membrane separation stage, and to apply a vacuum at the downstream side of the membrane.

By the late 1980s, several industrial plants were commissioned in the United States, Japan, and Germany. In 1989, MTR commissioned plants to vent streams from refrigerant units. NKK, in 1988, installed the first gasoline vapor recovery in Japan. The GKSS licensee Aluminium Rheinfelden (these activities are now owned by Borsig Membrane Technology) built the first VRU in 1989 to treat the off-gases from a gasoline loading terminal.

Organic vapor recovery by means of membranes is now an accepted technology for different applications in off-gas treatment and gas processing. It is a small market in comparison with the widely accepted adsorption technology; however, membrane technology is established in niches where membrane separation shows the best performance regarding efficiency, safety, and process reliability. Typical examples are gasoline vapor recovery, olefin separation, and separation of solvents from high concentrated off-gas streams. Because of its continuous operation mode, membrane technology is very suitable as a process-integrated separation unit.

A membrane stage can also be used for the pretreatment of gas streams with fluctuating organic vapor concentrations to optimize a posttreatment stage in

order to achieve very stringent clean air requirements. The references are spread throughout the industrial world and the customers include the chemical, petrochemical, and pharmaceutical industries.

2.09.3 Membranes for Organic Vapor Separation

The basic polymer for separation of organic vapors is polydimethylsiloxane (PDMS). PDMS shows a sufficient selectivity for various organic vapors over nitrogen and oxygen. PDMS is known for a preferable permeation of organic compounds. The solution–diffusion model describes gas permeation through nonporous polymer films. It is assumed that the gas at the upstream side of the membrane dissolves into the polymer, diffuses along a concentration gradient through the film, and desorbs at the downstream side. The permeability of a gas through a membrane depends on its solubility and diffusion.

The ideal selectivity is defined as the permeability coefficient of compound A over compound B:

$$\alpha = \frac{P_A}{P_B} = \frac{D_A}{D_B} \times \frac{S_A}{S_B} \quad (1)$$

The ratio D_A/D_B can be explained as mobility selectivity, whereas the ratio S_A/S_B as solubility selectivity. The preferred mobility or solubility is highly dependent on the chemical and physical properties of the polymeric material. The diffusion coefficient commonly decreases with an increase of the molecule size. The transport of smaller molecules is preferential. The solubility of gases increases with the increase of molecule size. Generally, glassy polymers show a dominant mobility selectivity in comparison to a higher solubility selectivity of rubbery polymers. Reviews published by A. Stern [4], M. R. Pixton and D. R. Paul [5], and B. D. Freeman [6] provide an excellent overview on polymer structure and transport behavior of gases through polymers.

The diffusion and solubility coefficients of different gases in silicone rubber are shown in **Figure 1**.

Comparing pentane over oxygen, it can be seen that the diffusion coefficient of pentane is 3.6 times smaller than that of oxygen. On the other hand, the solubility of pentane is approximately 200 times higher than that of oxygen. The relative low diffusion

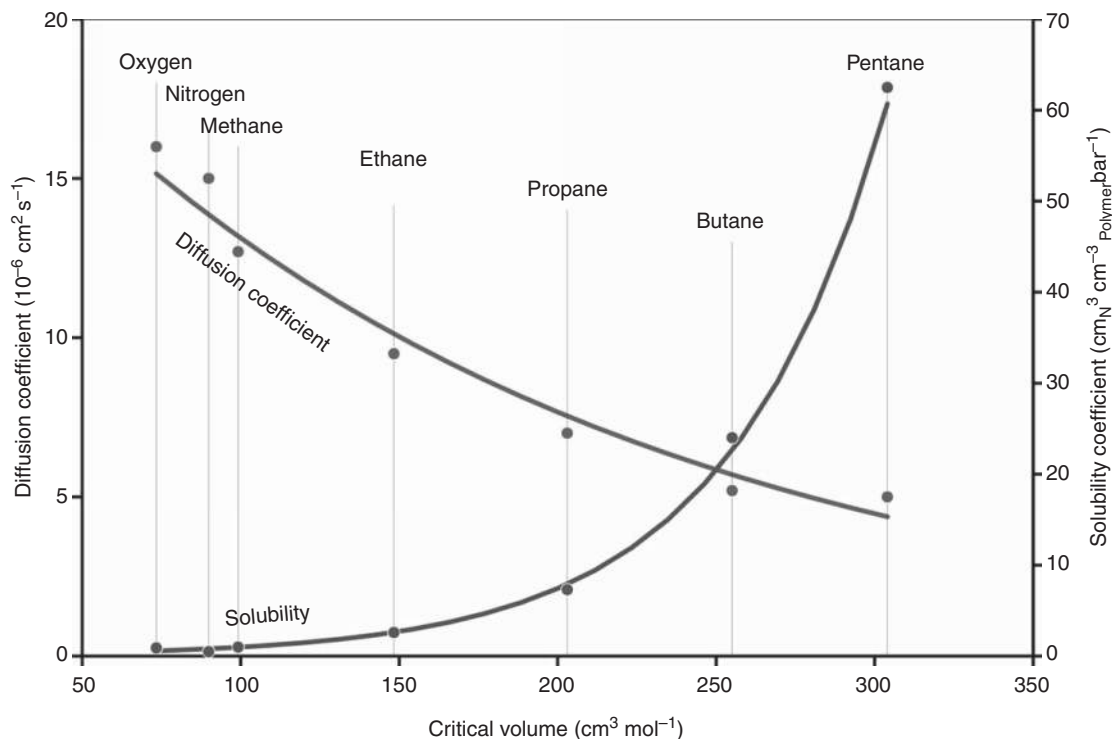


Figure 1 Diffusion and solubility coefficients of various gases in silicone rubber at 30 °C. Reproduced with permission from Ohlrogge, K., Stürken, K. Membranes: Separation of Organic Vapors from Gasstreams. In *Ullmann's Encyclopedia of Industrial Chemistry*; Wiley-VCH Verlag GmbH & Co. KGaA, 2005 [46].

coefficient of pentane is remarkably overcompensated for by its high solubility. This results in a higher permeance of pentane through silicone rubber films in comparison with oxygen.

Thin-film composite membranes have been designed in order to achieve reasonable flux rates through the technical membrane. The membrane consists of a three-layer sandwich. A nonwoven material is used as a substructure to provide the necessary mechanical strength. A microporous membrane is used as substrate to apply the thin pore-free organic-vapor-selective film. Set parameters to cast the substrate membrane are pore size and pore distribution to provide an unhindered permeation through the membrane arrangement. The thickness of the selective film is a compromise between mechanical stability and achievable flux rates.

PDMS has some limitations regarding organic vapor/nitrogen selectivity. It depends on the application whether a high-flux membrane with moderate selectivities or lower flux densities and higher selectivities are the preferred choice. A higher organic-vapor-selective polymer is polyoctylmethylsiloxane (POMS) [7]. **Figure 2** shows the comparison of PDMS and POMS membranes for different organic vapors over nitrogen – the overall selectivities of a

multicomponent mixture are represented taking into account further interaction effects.

Lower permeation rates require more membrane area to achieve a given outlet purity. The advantage of the higher selectivity is a reduced and higher concentrated permeate stream, which leads to smaller vacuum pump and compressor capacity and a lower energy consumption of the separation process. PDMS and POMS membranes have particular advantages and are selected depending on site-specific requirements.

2.09.4 Design Criteria

The challenge of the design of a membrane separation stage is to convert the selectivities obtained from single gas measurements as efficient as possible into a technical process. Operating temperature, feed pressure, feed composition, and module design have a strong influence on the separation efficiency.

The gas permeation through a membrane is dependent on the operation temperature. The permeation of permanent gases, such as oxygen or nitrogen, increases with the increase in temperature. As explained previously, the permeation of organic

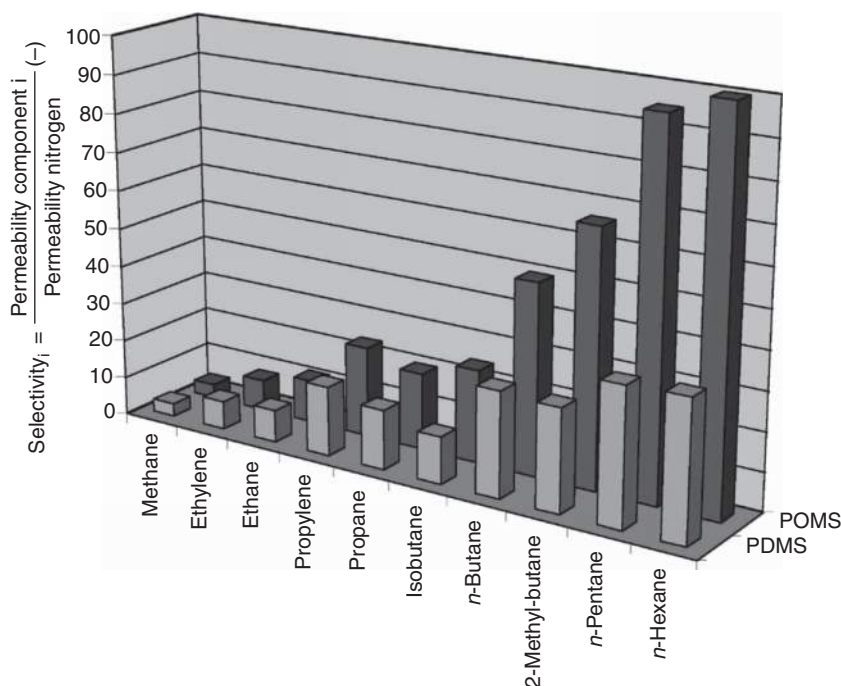


Figure 2 Comparison of selectivities of polydimethylsiloxane (PDMS) and polyoctylmethylsiloxane (POMS) membrane of various organic vapors over nitrogen. Reproduced with permission from Ohlrogge, K., Ebert, K. *MEMBRANEN, Grundlagen Verfahren und industrielle Anwendungen*; WileyVCH Verlag GmbH & Co. KGaA, 2006; pp 299, 306, 379, 425 [48].

vapors is governed by its solubility and the solubility increases with a decrease in temperature. A temperature decrease leads to a higher selectivity of organic vapors over nitrogen. To benefit from this behavior, it is advantageous to operate the separation stage at the lowest possible temperature.

Most vapor recovery processes operate at moderate pressures from atmospheric pressure up to 10 bar. In the case of operations at pressures higher than 10 bar, the nonideal gas behavior has to be taken into account [8]. According to Dalton's law, the ideal driving force for permeation increases directly proportional to higher pressures. In the case of high-pressure application, the partial pressure difference as driving force has to be replaced by the fugacity difference. This is because the real gas behavior has a stronger impact on nonideal vapors than on permanent gases. The effect of higher pressure must be taken into account regarding membrane and module design.

High permeation rates of organic vapors could influence the selectivity of a membrane. The feed channel of a membrane module consists of a turbulent and a laminar part. On top of the selective layer, a boundary layer is formed that depends on the flow velocity of the feed flow and the permeance of the feed components through the membrane. The boundary layer is enriched by the lower permeating feed compound and creates an additional resistance

for the fast compound. The diffusion through the boundary layer is dependent on the feed pressure and decreases with increasing pressure. The achievable selectivity is determined by the resistance in (1) the boundary layer, (2) the selective layer, and (3) the substructure of the composite membrane.

The partial pressure profile of a binary mixture within the boundary layer is depicted in Figure 3 and shows the flow resistance of membrane separation comparable with electrical series connection.

2.09.5 Membrane Modules

Flat-sheet membranes are commonly used for organic vapor separation applications. Typical module configurations are spiral wound modules or envelope-type modules, based on a design developed by GKSS. Capillary or hollow fiber modules are only known for some small-scale laboratory applications. The spiral wound module design is well known and widely accepted, which has the advantages of a simple manufacturing process and relatively low costs of the pressure vessel. The so-called packing density – the ratio of installed membrane area over pressure vessel housing volume varies from 300 to approximately $1000 \text{ m}^2 \text{ m}^{-3}$. A possible disadvantage for highly efficient separation applications is the long

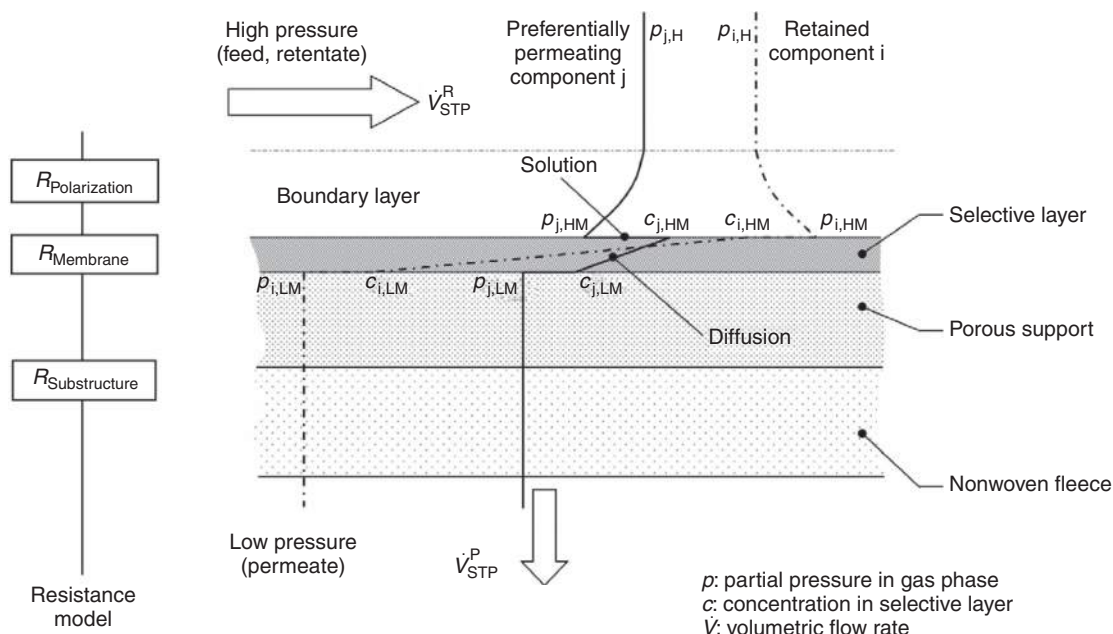


Figure 3 Partial pressure profile of a binary mixture within a boundary layer. Reproduced with permission from Ohlogge, K., Stürken, K. Membranes: Separation of Organic Vapors from Gasstreams. In *Ullmann's Encyclopedia of Industrial Chemistry*; Wiley-VCH Verlag GmbH & Co. KGaA, 2005 [46].

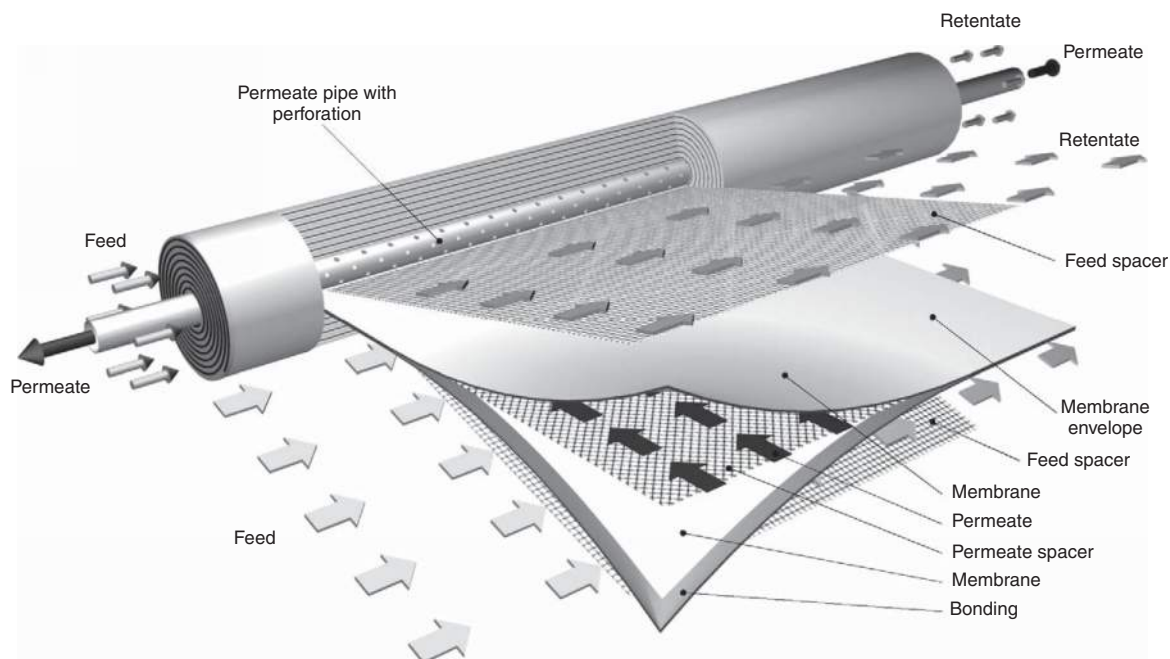


Figure 4 Spiral wound module for gas separation applications.

feed and permeate path. The spiral wound module is the first choice for high volume or bulk removal applications (**Figure 4**).

Some membrane separations require a flow pattern and pressure drop optimized module design to achieve an optimized mass transfer. Elastomeric membranes swell in the presence of organic vapors. The degree of swelling depends on the nature of the organic compound and the vapor concentration. The swelling causes an increase in gas permeation. Permeate has to be discharged as efficiently as possible in order to avoid a pressure buildup on the permeate side. A short permeate path and sufficient free volume between the membrane sheets have to provide the conditions for an unrestrained permeate drainage. The GKSS GS envelope-type module refers to the requirements of high-flux membranes. The design is based on disk filter arrangements. Two round-shaped membrane sheets with layers of nonwoven fabrics and spacers in between are welded at the cutting edge to form an envelope. The envelope inlays are selected in accordance to the expected permeate drainage in order to provide an unrestrained permeate discharge. The permeate flow is directed to the drainage ring at the central hole. The permeate of the envelope is directed to permeate pipe. The permeate pipe is also used to align the membrane stack.

A number of envelopes are arranged to build a membrane stack. The stack can be divided into compartments by means of baffle plates. The number of envelopes in a

compartment varies in accordance to the reduction of feed volume flow caused by permeation. The required flow velocity over the membrane surface to achieve the most efficient separation determines the reduction of membrane area assembled in a compartment. The feed is introduced at the front flange inlet and is directed to the first compartment by means of a baffle plate, which, in turn, is directed in meander form to the module outlet. Permeate is collected in the central permeate pipe. The permeate discharge is optionally single or double sided, depending on the expected permeate volume flow and the pressure drop. The schematic design of the GKSS GS module is depicted in **Figure 5**.

2.09.6 Development of Simulation Tools

Numerous models have been presented for the simulation of gas permeation modules. The majority deals with the module as a stand-alone unit (see, e.g., References 9–14). The shift from end of pipe to more process-integrated applications for gas permeation units equipped with membranes selective for hydrocarbons and other VOCs necessitated a more stringent design of these units. For this task, process simulation tools are required. Ideally, these tools should be compatible commercial process simulators. Far fewer examples for these models can be

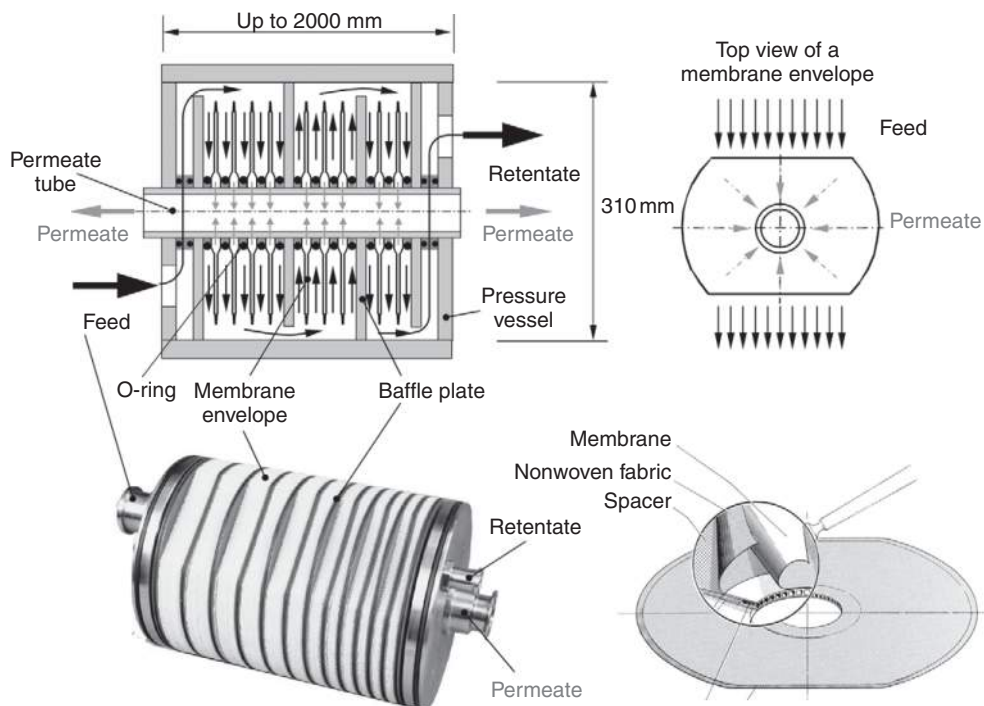


Figure 5 GKSS envelope-type module.

found in literature. Examples are given in References 15–17. Research work at GKSS in this field focused on the modeling of the envelope-type module to address the following points:

- prediction of module sizes and numbers for a given separation task;
- prediction of the separation achievable for a given module configuration;
- sizing of up- and downstream equipment;
- influence of recycle streams in complex process topologies;
- comparison with conventional unit operations;
- determination of the process economics; and
- application of process simulators in early design stages, that is, technologically new unit operations are often only considered, if a reliable model is available.

In order to accurately predict the operation performance of a membrane module used to separate VOCs and other components from permanent gases, mass and energy transport phenomena as well as thermodynamics have to be taken into account as discussed in the previous sections. These effects are:

- selective mass transfer resistance of the active membrane layer, that is, the permeance of a

component in a membrane material as a function of temperature, pressure, and composition;

- thermodynamically correct description of the driving force, that is, the application of fugacities;
- consideration of the Joule–Thomson effect;
- the buildup of boundary layers between the bulk phase and the membrane surface, that is, concentration polarization;
- pressure drops on the retentate and permeate sides; and
- mass transfer resistances and pressure drops of the porous support layers.

The listed phenomena are described by functions of local temperatures, pressures, and compositions on the retentate and permeate sides of the module. As these variables are typically changing along the membrane surface, the listed local phenomena have to be coupled to the material, energy, and momentum balances describing the flow patterns inside the module.

2.09.6.1 Description of Multicomponent Permeation

The temperature and pressure dependence of the permeance of *n*-butane and nitrogen in a silicone-based membrane material is illustrated in [Figure 6](#).

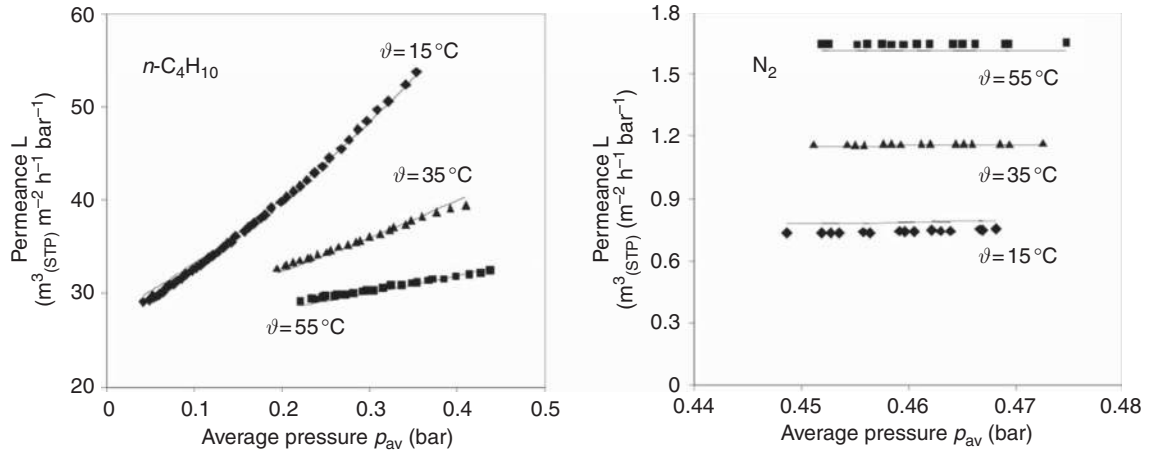


Figure 6 Permeance of *n*-butane (left) and nitrogen (right) in a silicone-based material as function of average pressure and temperature.

It is apparent that *n*-butane has a solution-controlled permeation behavior, while that of nitrogen is diffusion controlled. The permeance of the former decreases with increasing temperature, while the temperature dependence of the latter is vice versa. Furthermore, the exponential increase of the butane permeance with increasing average pressure indicates that the silicone-based material is plasticized by higher hydrocarbons. As expected, the butane permeance is considerably higher than that of nitrogen. The measurements were collected using an automated single gas permeation measurement apparatus [18]. The lines fitted to the experimental data are predictions by the free-volume model Equation (2) [19] where the parameters $L_{i,\infty}^0$, $E_{i,\text{act}}$, $m_{i,0}$, and $m_{i,T}$ were determined by means of a nonlinear least square method [18].

$$L_i = L_{i,\infty}^0 \cdot \exp \left[-\frac{E_{i,\text{act}}}{R \cdot T} + m_{i,0} \cdot (p \cdot y_i \cdot \varphi_i)_{\text{av}} \cdot \exp(m_{i,T} \cdot T) \right] \quad (2)$$

However, Equation (2) describes only the single gas permeation behavior, that is, the interaction of individual, permeating species with the polymer matrix is described. No information on how the impact on the mass transfer of other species is can be deduced. This information is crucial for the correct design of membrane modules, since the permeation of plasticizing components loosens the structure of the polymer matrix and hence creates additional pathways for components that by themselves do not swell the membrane, that is, the selectivity of the process is reduced. In order to predict these phenomena, an extension of Equation (2) was suggested [19, 20]:

$$L_i = \underbrace{L_{i,\infty}^0}_{\text{Permeance for } T \rightarrow \infty} \cdot \exp \left[-\underbrace{\frac{E_{i,\text{act}}}{R \cdot T}}_{\text{Activation Energy}} + \sum_{j=1}^{nc} \underbrace{\left(\frac{\sigma_j}{\sigma_i} \right)^2}_{\text{Ratio of Lennard-Jones diameters}} \cdot \underbrace{m_{j,0} \cdot (p \cdot y_j \cdot \varphi_j)_{\text{av}} \cdot \exp(m_{j,T} \cdot T)}_{\text{Swelling}} \right] \quad (3)$$

This model employs the same parameter as the single-component relationship (Equation (2)). Hence, only single gas permeation experiments are required to predict the multicomponent permeation behavior. Herein lies the great practical importance of Equation (3). That this equation can indeed be used to give an excellent prediction of the separation performance of a membrane module is shown later in this section.

2.09.6.2 Nonideal Thermodynamic Behavior

The importance of using fugacities instead of partial pressures for the description of the transmembrane driving force at absolute pressures exceeding 10 bar has already been discussed. The fugacity of a component is calculated as the product of the partial pressure $p_i = y_i \cdot p$ and fugacity coefficient φ_i . The latter is a function of temperature, pressure, and

composition and can be calculated by means of an equation of state (EOS). Examples are the Soave–Redlich–Kwong EOS [21] or the Peng–Robinson EOS [22]. The molar transmembrane flux can then be expressed as

$$\dot{n}_{i,M}'' = L_i \cdot (p_{Std} / (R \cdot T_{Std})) \cdot (\varphi_{i,RM} \cdot p_{i,RM} - \varphi_{i,PM} \cdot p_{i,PM}) \quad (4)$$

Another thermodynamic phenomenon to be taken into account is the Joule–Thomson effect accounting for the change of temperature when throttling a real gas. The temperature change can be determined by means of an energy balance around an element of membrane area of infinitesimal length dz as shown in Figure 7.

The expansion of the permeate when desorbing out of the membrane material is considered to be isenthalpic. The molar enthalpies on the retentate and permeate sides can also be determined by an EOS. Hence, it is possible to predict the permeate temperature according to Equation (5), when the retentate temperature, the composition of the permeate flux, and the retentate and permeate pressures are known.

$$\tilde{H}_M^G(T_R, p_R, y_{i=1, \dots, nc, M}) = \tilde{H}_M^G(T_P, p_P, y_{i=1, \dots, nc, M}) \quad (5)$$

Equation (5) considers the membrane as a thermal insulator. This is, in practice, not the case and the heat conduction has to be taken into account as well.

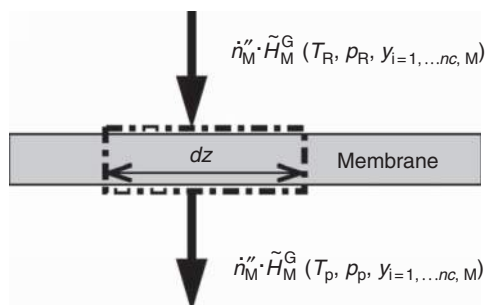


Figure 7 Energy balance for determination of the Joule–Thomson effect. Reproduced with permission from Ohlrogge, K., Ebert, K. *MEMBRANEN, Grundlagen Verfahren und industrielle Anwendungen*; WileyVCH Verlag GmbH & Co. KGaA, 2006; pp 299, 306, 379, 425 [48].

2.09.6.3 Concentration Polarization

The influence of concentration polarization was already introduced previously. In order to quantitatively describe the mass transfer in a boundary layer for a binary system, the following equation can be employed:

$$\dot{n}_{i,M}^s = y_{i,RM} \cdot \dot{n}_{T,M}^s + c_{T,R} \cdot \beta_{i,j} \cdot (y_{i,R} - y_{i,RM}) \quad (6)$$

It is derived from the differential description given, for example, by [23]. The mass transfer coefficient $\beta_{i,j}$ can be determined by means of a Sherwood correlation appropriate for the module geometry under consideration. Equation (6) is solved for only one component, since the composition for the second component is always given by

$$\sum_{i=1}^{nc} y_{i,RM} = 1 \quad (7)$$

For a multicomponent mixture Equations (6) and (7) can still be employed if the binary mass transfer coefficient $\beta_{i,j}$ is replaced by an approximation for a multicomponent mass transfer coefficient, that is, the diffusion coefficient required for the Sherwood correlation was determined using some mixing rule as, for example, listed by Froment and Bischoff [24]. However, this approach will cause some errors, since the characteristics of multicomponent mass transfer are not described accurately. For this, the frictional drag between the species present has to be taken into account, which is described by the Stefan–Maxwell equations. A rigorous treatment of this subject is given by Taylor and Krishna [25]. One of their results is a linearized expression similar to Equation (6):

$$\dot{n}_{i,M}'' = \sum_{j=1}^{nc-1} \beta_{i,j} \cdot c_{T,R} \cdot (y_{j,R} - y_{j,RM}) + y_{i,RM} \cdot \sum_{j=1}^{nc} \dot{n}_{j,M}'' \quad (8)$$

However, here, the mass transfer coefficient $\beta_{i,j}$ is an element of a $(nc - 1) \times (nc - 1)$ matrix, implying that the mass transfer of one component i is dependent not only on its composition gradient but also on those of the other components. Analogous to the binary case, here, only $(nc - 1)$ equations are independent. Equation No. nc again is provided by the summation of mole fractions (Equation (7)). Since the mass transfer coefficients are elements of a matrix, the Sherwood correlation also has to be evaluated in this manner. Some mathematical expenditure is required here, since this involves the power of a

matrix, which is a mathematically difficult task. Alopaeus and Nordén [26] suggested a highly efficient method to simplify this operation with not much loss of accuracy.

2.09.6.4 Pressure Drops on the Retentate and Permeate Sides of the Membrane Module

The consideration of the pressure drops in the flow channels of the module leads to a simplified form of the momentum balance itself. It can be expressed as

$$\frac{dp}{dz} = -\zeta \cdot \frac{1}{d_h} \cdot \frac{\rho}{2} \cdot v^2 \quad (9)$$

The hydraulic diameter d_h results from the geometry of the channel, while the friction coefficient ζ is determined by means of experiments for a given module type and typically expressed as a function of the Reynolds number.

2.09.6.5 Transport Resistances of Porous Support Layers

These resistances will not be discussed further as they were found to be of little influence on the operation performance of the processes discussed here.

2.09.6.6 Modeling of Membrane Modules

In order to model a membrane module and not just the phenomena occurring at and in an infinitesimally small element of membrane area, it is necessary to consider the flow patterns inside the module. Typical flow patterns are cocurrent and counter-current flow, which are realized in hollow fiber modules; cross-flow occurs in spiral wound modules, while the GKSS GS module can be represented by the assumption of unhindered permeate withdrawal for the applications under consideration in this section.

The flow patterns are described by the differential material, momentum, mass, and energy balances. The boundary conditions of these equations, orthogonal to the main flow direction, are posed by the mass and heat transfer through the membrane as well as a possible heat transfer to the environment. In flow direction, they are given by the conditions enforced at the feed, retentate, and permeate ports. This results in a system of partial differential and algebraic

equations representing a membrane module, which involves, in its most general case, three spatial and one temporal domain. The mathematical expenditure to solve this system is too high for typical design problems. Hence, they are simplified, for example, by the assumption of steady-state operation and the assumption of one spatial coordinate for co- and counter-current flow as well as free permeate withdrawal. Cross-flow can be well represented by two spatial coordinates [18, 27]. The boundary conditions orthogonal to the flow directions, that is, the transfer terms, are implemented directly into the resulting ordinary differential equations. For their solution, a numerical approximation of the differentials is required. This can be done by applying an appropriate discretization scheme or by subdividing the considered membrane area into permeation cells and casting the balance equations for each of those cells. The individual cells are then interconnected in such a way as to represent the membrane module. For unhindered permeate withdrawal applicable to the GKSS GS module, this approach is shown in **Figure 8**.

Assuming that transport resistances on the permeate side and dispersion effects can be neglected, the following equations have to be solved for each permeation cell k , where the feed conditions are always provided by the previous cell $k - 1$. For cell 1, the feed conditions are identical to those of the module itself. In order not to completely overload the list, the transfer coefficients are assumed to be constant. These are the friction factor $\zeta_{k,R}$, the elements of the mass transfer coefficient matrix $\beta_{ij,k,R}$, and the heat transfer coefficient $k_{k,R}$ (**Table 1**).

The unknowns of the given system of equations are the molar flow rates for each component i on the retentate and permeate sides, as well as the transmembrane flow $\dot{n}_{i,k,R}$, $\dot{n}_{i,k,P}$, and $\dot{n}_{i,k,M}$, the permeances of the individual components $L_{i,k}$, the fugacity coefficients at the retentate side membrane surface and on the permeate side $\varphi_{i,k,RM}$ and $\varphi_{i,k,P}$, the mole fractions on the retentate and permeate sides as well as at the retentate side membrane surface $y_{i,k,R}$, $y_{i,k,P}$, and $y_{i,k,RM}$, the average fugacity $(p_k \cdot y_{i,k} \cdot \varphi_{i,k})_{av}$, the retentate pressure $p_{k,R}$, the average temperature $T_{k,av}$, the retentate and permeate side temperatures $T_{k,R}$ and $T_{k,P}$, the enthalpies of the retentate and permeate sides as well as that of the transmembrane flux $\tilde{H}_{k,R}$, $\tilde{H}_{k,P}$, and $\tilde{H}_{k,M}$, $\dot{n}_{k,R}$ and $\dot{n}_{k,P}$, the concentration on the retentate side $c_{k,R}$, h and the density on the retentate side $\rho_{k,R}$. This

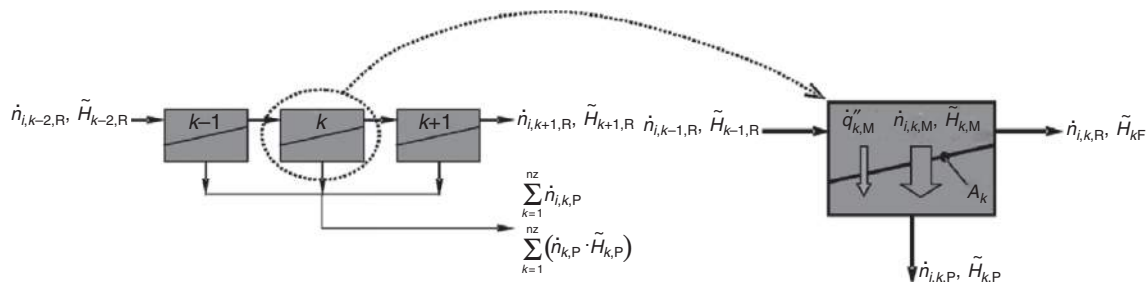


Figure 8 Representation of a Göteborgs Kungl. Segel Sällskap (GKSS) GS-type module and permeation cell. Reproduced with permission from Ohlrogge, K., Ebert, K. *MEMBRANEN, Grundlagen Verfahren und industrielle Anwendungen*; WileyVCH Verlag GmbH & Co. KGaA, 2006; pp 299, 306, 379, 425 [48].

amounts to a total number of unknowns of $10nc + 11$. Hence, the system of equations representing one permeation cell can be solved using an appropriate numerical method.

Several approaches for implementing the above equations for one cell and their interconnection to represent a module are possible. One option is to use a programming language as C, C++, Fortran, or Java and develop a stand-alone model. It is also possible to use a spreadsheet program with an included macro language as, for example, Microsoft Excel/Visual Basic for Applications. The disadvantages of this approach are the necessity to provide subroutines for the required numerical methods and physical properties and that the model cannot be used to represent interactions with the other unit operations making up the entire or part of the process. An advantage of this approach is the relatively low cost for software licensing. Numerical routines well suited for the modeling of membrane modules can be found in Press *et al.* [29]. Gmehling and Kolbe [28] published a collection of subroutines for the determination of thermodynamic properties as fugacities and enthalpies. Relationships for the calculation of transport properties can be found in Reid *et al.* [30].

However, the leading commercial process simulation packages all have interfaces that allow including user-written models into flowsheets. In addition, the property packages can be interfaced. In the case of Aspen Plus[®] [31], it is possible to use Fortran subroutines, Excel spreadsheets, or the Cape Open standard [32]. The latter is a development resulting from a European Union project where standardized interfaces for models and property packages were defined.

A further possibility to model membrane modules equation-oriented process simulators. The most

popular ones are probably Aspen Custom Modeler[®] [31] and gProms[®] [33]. These simulators provide an integrated development environment in which an object-oriented scripting language is implemented. The elements of these languages are types, which reflect the typical modeling tasks in process engineering, that is, different physical quantities as temperatures or pressures have their own variable types, port types handle the feed and product streams of a unit, etc. The resulting models allow for different depths controlled by parameters that switch desired blocks of equations active or inactive. Hence, the natural way of modeling, that is, starting with a simple model and making it increasingly more complex by considering, for example, nonideal thermodynamic behavior or additional transport resistances, is supported. Numerical methods and physical property calculations are automatically implemented. Furthermore, the equation-oriented simulators support the implementation of dynamic models.

An example for the approach to model an envelope-type membrane module presented above is the separation of *n*-butane and carbon dioxide from nitrogen. This process was investigated in the scope of a diploma thesis [18], whereas the model was presented at the Euromembrane Conference 2004 [27]. **Figure 9** shows a simplified flow sheet of a pilot plant into which an envelope-type membrane module was installed. The module was equipped with approximately 3 m^2 of POMS membrane and a number of sample ports along the membrane surface. Hence, the composition profiles developing inside the membrane module could be determined experimentally by means of a gas chromatograph. The feed gas was mixed by using pure gases and introduced into the feed vessel. A typical composition was 88 vol.% N_2 , 6 vol.% *n*- C_4H_{10} , and 6 vol.% CO_2 . A liquid ring compressor provided the feed

Table 1 System of equations for permeation cell with free permeate withdrawal

Equation		Number
Material balance, cell	$\dot{n}_{i,k-1,R} - \dot{n}_{i,k,R} - \dot{n}_{i,k,P} = 0$	nc
Material balance, retentate side	$\dot{n}_{i,k-1,R} - \dot{n}_{i,k,R} - \dot{n}_{i,k,M} = 0$	nc
Permeation	$\dot{n}_{i,k,M} - A_k \cdot L_k \cdot \frac{p_{std}}{R \cdot T_{std}} \cdot (\varphi_{i,k,RM} \cdot y_{i,k,RM} \cdot p_{k,R} - \varphi_{i,k,P} \cdot y_{i,k,P} \cdot p_P) = 0$	nc
Free-volume model	$L_i - L_{i,\infty}^0 \cdot \exp \left[-\frac{E_{i,act}}{R \cdot T_{k,av}} + \sum_{j=1}^{nc} \left(\frac{\sigma_j}{\sigma_j} \right)^2 \cdot m_{j,0} \cdot (p_k \cdot y_{j,k} \cdot \varphi_{j,k})_{av} \cdot \exp(m_{j,T} \cdot T_{k,av}) \right] = 0$	nc
Pressure drop, retentate side	$p_{k,R} - p_{k-1,R} + \zeta_{k,R} \cdot \frac{A_k}{d_{h,R} \cdot b_R} \cdot \frac{\rho_{k,R}}{2} \cdot v_{k,R}^2 = 0$	1
Mass transfer, boundary layer	$\dot{n}_{i,k,M} - A_k \cdot c_{k,R} \cdot \sum_{j=1}^{nc-1} \beta_{ij,k,R} \cdot (y_{j,k,R} - y_{j,k,RM}) - y_{i,k,RM} \cdot \sum_{j=1}^{nc} \dot{n}_{j,k,M} = 0$	$nc-1$
Mole fraction summation, retentate side membrane surface	$\sum_{j=1}^{nc} y_{i,k,RM} - 1 = 0$	1
Energy balance, cell	$\dot{n}_{k-1,R} \cdot \tilde{H}_{k-1,R} - \dot{n}_{k,R} \cdot \tilde{H}_{k,R} - \dot{n}_{k,P} \cdot \tilde{H}_{k,P} = 0$	1
Energy balance, retentate side	$\dot{n}_{k-1,R} \cdot \tilde{H}_{k-1,R} - \dot{n}_{k,R} \cdot \tilde{H}_{k,R} - \dot{n}_{k,M} \cdot \tilde{H}_{k,M} - A_k \cdot k_{k,R} \cdot \underbrace{(T_{k,R} - T_{k,R})}_{=\dot{q}} \cdot k_{k,M} = 0$	1
Average cell temperature	$T_{k,av} = 0,5 \cdot (T_{k,R} + T_{k,P})$	1
Average cell fugacity	$(p_k \cdot y_{i,k} \cdot \varphi_{i,k})_{av} = 0,5 \cdot (\varphi_{i,k,RM} \cdot y_{i,k,RM} \cdot p_{k,R} + \varphi_{i,k,P} \cdot y_{i,k,P} \cdot p_P)$	nc
Total flow rate, retentate side	$\dot{n}_{k,R} = \sum_{j=1}^{nc} \dot{n}_{j,k,R}$	1
Total flow rate, permeate side	$\dot{n}_{k,P} = \sum_{j=1}^{nc} \dot{n}_{j,k,P}$	1
Molefractions, retentate	$y_{i,k,R} = \frac{\dot{n}_{i,k,R}}{\dot{n}_{k,R}}$	nc
Molefractions, permeate	$y_{i,k,P} = \frac{\dot{n}_{i,k,P}}{\dot{n}_{k,P}}$	nc
Fugacity coefficient, retentate side, membrane surface	$\varphi_{i,k,RM} = F_{EOS}(T_{k,R}, p_{k,R}, y_{j=1, \dots, nc, k, RM})$	nc
Fugacity coefficient, permeate side	$\varphi_{i,k,P} = F_{EOS}(T_{k,P}, p_{k,P}, y_{j=1, \dots, nc, k, RM})$	nc
Enthalpy, retentate side	$\tilde{H}_{k,P} = F_{EOS}(T_{k,R}, p_{k,R}, y_{j=1, \dots, nc, k, R})$	1
Enthalpy, permeate side	$\tilde{H}_{k,P} = F_{EOS}(T_{k,P}, p_{k,P}, y_{j=1, \dots, nc, k, P})$	1
Enthalpy, transmembrane flux	$\tilde{H}_{k,M} = F_{EOS}(T_{k,R}, p_{k,R}, y_{j=1, \dots, nc, k, P})$	1
Density, retentate side	$\rho_{k,R} = F_{EOS}(T_{k,R}, p_{k,R}, y_{j=1, \dots, nc, k, R})$	1
Concentration, retentate side	$c_{k,R} = F_{EOS}(T_{k,R}, p_{k,R}, y_{j=1, \dots, nc, k, R})$	1
Number of equations		$10 nc + 11$

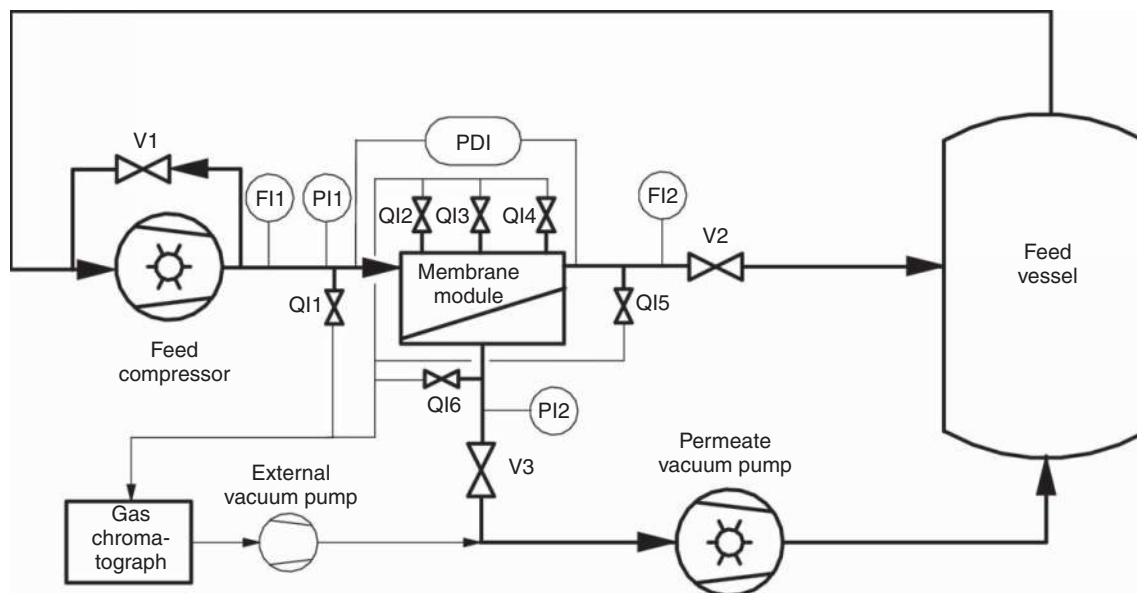


Figure 9 Gas permeation pilot plant.

pressure of up to 4 bar at flow rates between 29 and $45 \text{ m}^3_{(\text{STP})} \text{ h}^{-1}$. Furthermore, the product stream of the compressor was water saturated, since water was used as the service liquid. The N_2 -rich retentate (i.e., high pressure) product stream of the membrane module was throttled and recycled to the feed vessel. Next to the feed compressor, a liquid ring vacuum pump also contributed to the required driving force by applying a permeate pressure of approximately 400 mbar. The $n\text{-C}_4\text{H}_{10}$ and CO_2 -enriched permeate was recompressed by this pump and also recycled to the feed vessel. Hence, a closed circuit system was investigated.

Figure 10 shows the measured and simulated composition profiles for $n\text{-C}_4\text{H}_{10}$ and CO_2 on the feed/retentate side of the investigated module. The model for the membrane module was implemented in Aspen Custom Modeler[®]. A discretization of the membrane area into 60 permeation cells was chosen. For each of the cells, the system of equations as detailed in **Table 1** was solved. The cells were interconnected as shown in **Figure 8**. For this application, the consideration of real gas behavior (use of fugacities and Joule–Thomson effect) probably was not necessary due to the low process pressures. Of great importance, however, was the calculation of the permeances of the individual components and the consideration of the mass transfer resistance of the feed-side boundary layer.

The former was evaluated by means of the free-volume model (Equation (3)). An important fact to be mentioned is that the parameters used in the model were evaluated from single gas permeation measurements as shown in **Figure 6**, that is, no experimental mixed gas data were used as input for the simulation. This is a great advantage for the practical application of the model to predict operating performances of membrane units for the removal of VOCs, since the amount of experimental work required is considerably reduced. The concentration polarization was calculated assuming the linearized equation for multicomponent mass transfer (Equation (8), as outlined above). Furthermore, the pressure drop on the feed/retentate side of the module was calculated. The predictions of the model shown in **Figure 10** correspond well with the experimental data. The stage cut of this particular experiment was measured to be 29.4%, while the simulation gave a result of 30.2%. Hence, it can be assumed that the model is well suited for the design gas permeation units equipped with silicone-based membranes for the removal of hydrocarbons from permanent gas streams. The model has been extensively employed for these tasks, which included more complex layouts similar to the ones presented here. Some examples are the inclusion of other unit operations as heat exchangers, condensers, and distillation columns or the use of recycle

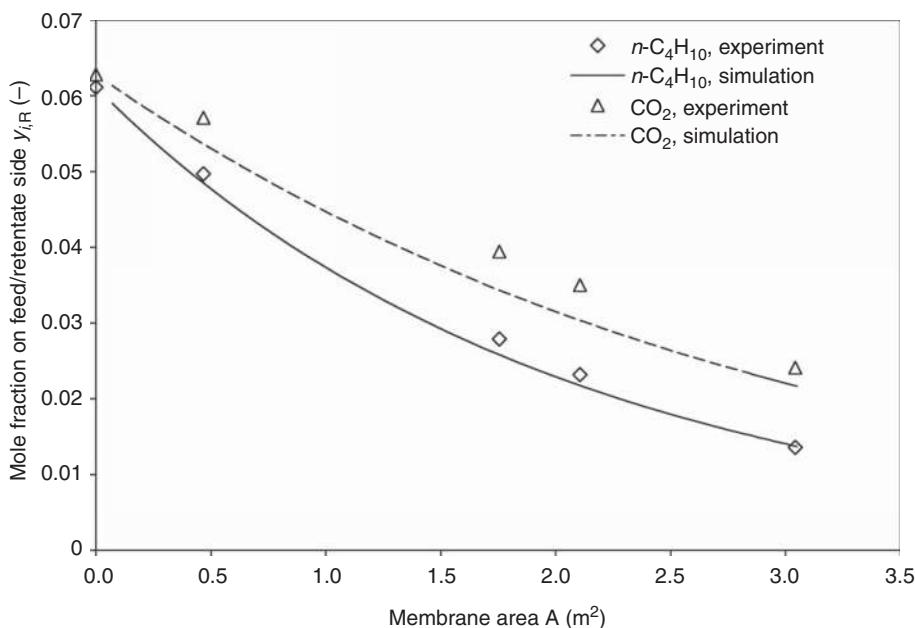


Figure 10 Measured and simulated $n\text{-C}_4\text{H}_{10}$ and CO_2 concentration profiles.

streams. An example is simultaneous recovery of hexane from and drying of a N_2 purge gas stream in a polyethylene (PE) production process presented in [34].

A detailed optimization of processes is possible and also the most effective selection of membrane type, membrane thickness, and flow distribution can be found.

As an example for membrane module optimization, the effect of membrane thickness and feed gas velocity has been calculated for a hexane separation process in accordance with the flow sheet depicted in Figure 20. The separation has been calculated for POMS membranes with different nitrogen permeances, which can be taken as a measure for the separation layer thickness.

The nitrogen permeances have been set to:

- membrane A: $0.1 \text{ m}^3_{(\text{STP})} \text{ m}^{-2} \text{ h}^{-1} \text{ bar}^{-1}$
- membrane B: $0.2 \text{ m}^3_{(\text{STP})} \text{ m}^{-2} \text{ h}^{-1} \text{ bar}^{-1}$
- membrane C: $0.4 \text{ m}^3_{(\text{STP})} \text{ m}^{-2} \text{ h}^{-1} \text{ bar}^{-1}$

The membrane areas used in a GKSS envelope-type module were adjusted in accordance to the different thicknesses of the membranes. A feed gas flow of $100 \text{ m}^3_{(\text{STP})} \text{ h}^{-1}$ was assumed.

Figure 11 shows that increasing the feed gas velocity reduces the effect of concentration polarization. It is obvious that the effect of concentration

polarization increases with decreasing membrane thickness. The overall selectivities shown are calculated mean values for a complete module taking all interaction effects into account.

From Figure 12 it can be seen that it is not the highest gas velocity that produces the best separation effect. This is due to the pressure drop in the membrane module, which increases significantly with higher gas velocities and leads to a reduction in driving force. In this example, it was not possible to achieve the same retentate vapor concentration using the more permeable membrane because the membrane area has been set exactly to halve the value when the thickness was reduced in the same manner. A small additional amount of membrane area would lead to the same retentate concentration but with slightly increased permeate volume flow.

The optimal choice of the membrane arrangement can be found when all aspects, such as membrane costs, investment for compressors, vacuum pumps, and operating costs, are taken into account.

2.09.7 General Layout Criteria

Organic VRUs are used for off-gas treatment as end-of-pipe systems or as integrated system to separate compounds interfering with a process or the quality

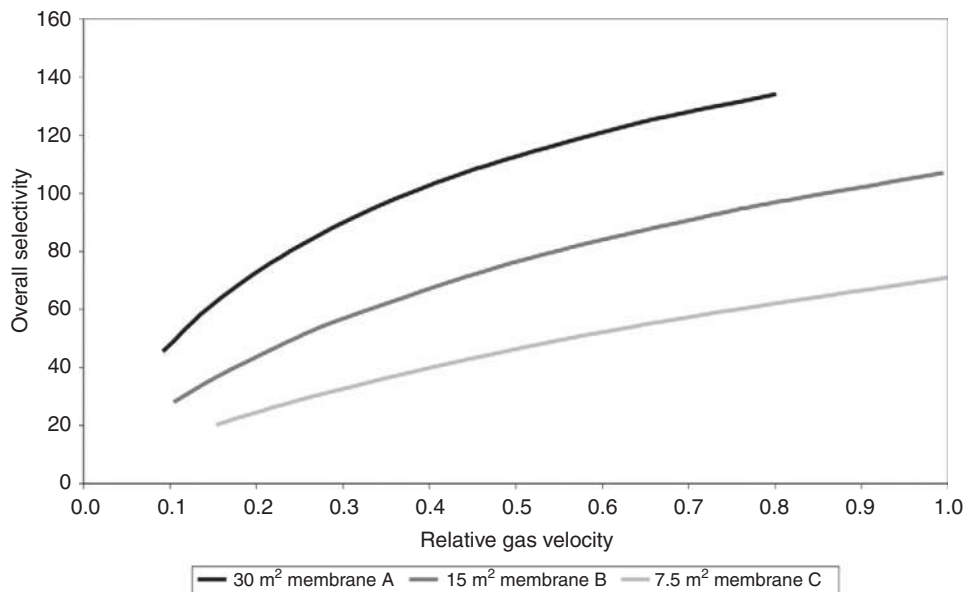


Figure 11 Hexane/nitrogen overall selectivity over relative feed gas velocity.

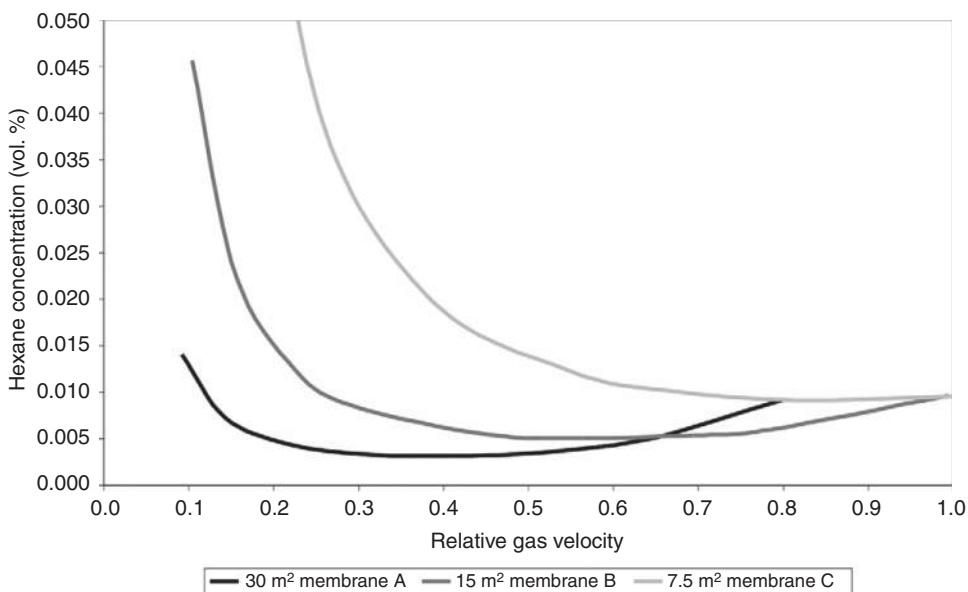


Figure 12 Hexane retentate concentration over relative feed gas velocity.

of the gas streams. The membrane systems are used for an efficient recovery of a valuable product, purification of off-gas streams, or feed gas concentration control. Commonly, end-of-pipe organic vapor separation units have to meet stipulated clean air standards. Effluents are collected and fed to a booster pump or compressor. In the case of pressure increase, the recovery of organic compounds occurs by condensation in

the recovery stage after the compressor. The condenser exhaust gas containing a residual organic vapor concentration is fed to the membrane stage. The membrane separation process can be performed at elevated pressure or by applying vacuum at the permeate side or a combination of both. The adjustment of the pressure ratio depends on feed pressure, membrane selectivity, and required separation efficiency.

The pressure ratio Φ is defined as follows:

$$\Phi = \frac{P_F}{P_P} \quad (10)$$

The applied pressure ratio has to be chosen depending on the membrane selectivity. Highly selective membranes require the highest possible pressure ratio. On the other hand, it does not make sense to apply a high-pressure ratio to low selectivity membranes [35]. The units are designed as single unit system or the membrane stage and can easily be combined with other separation or recovery techniques such as condensation, adsorption, absorption, or with posttreatment systems to destroy any residual organic vapor content by combustion or catalytic conversion. A simplified flow scheme of a membrane-based separation process is shown in Figure 13.

The size of an organic vapor recovery membrane stage mainly depends on applied feed pressure, pressure ratio, and required retentate concentration. The organic-vapor-enriched permeate is fed back to the intake of feed pump. Organic vapors are recovered by condensation or absorption downstream of feed compressor or vacuum pump.

Some process-integrated separation systems require only a membrane stage to control the organic vapor content of the feed gas. Permeate is discharged to further treatment.

2.09.8 Technical Applications

2.09.8.1 Gasoline Vapor Recovery

The stipulation of new clean air standards for large refineries and tank farms by the Technical Instructions on Air Quality Control – TI Air in Germany [36] necessitated the development of membrane-based gasoline vapor recovery systems. The new standards required the development of new technologies or the improvement of existing techniques to reduce the concentration of organic compounds in the gasoline handling off-gas to $<150 \text{ mg m}^{-3}$. Other legal requirements for gasoline storage and distribution are the two “ordinances on the reduction of hydrocarbon emissions arising during the handling of otto-engine fuels (20. and 21. BImSchV)” [37, 38]. The strong provisions stipulated by German law are in contrast to the European Directive 94/63/EC. This directive provides an emission limit of 35 g m^{-3} hydrocarbons in

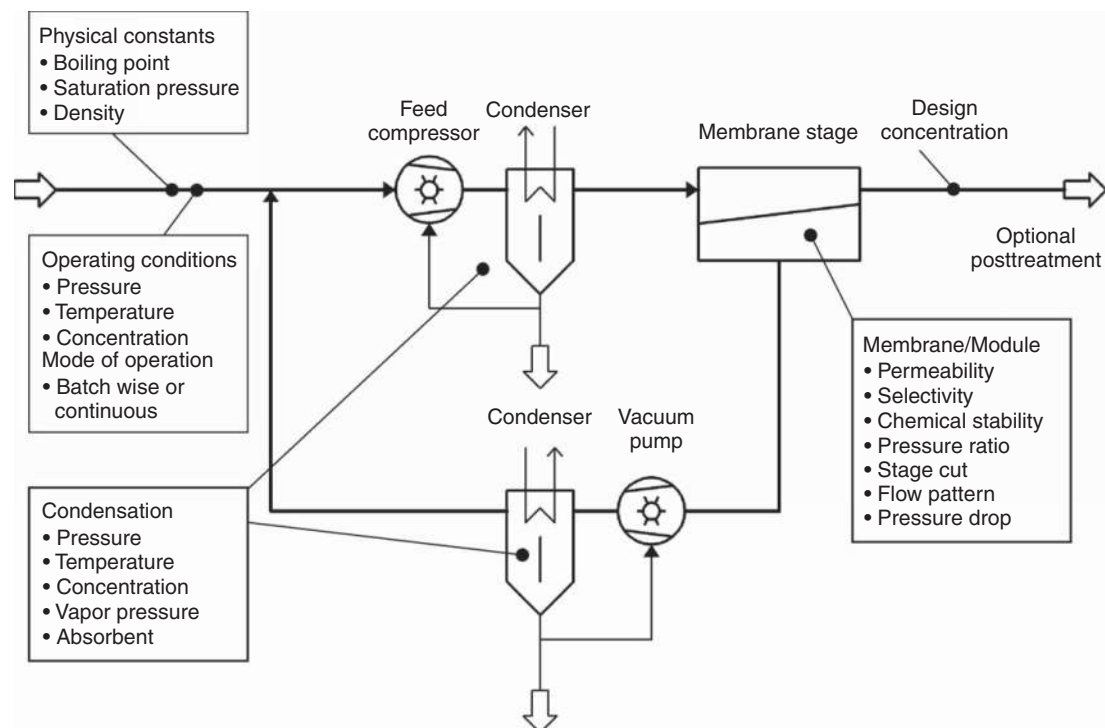


Figure 13 Flow scheme of a membrane-based organic vapor separation process.

air, which was far from the state-of-the-art emission reduction technology and is approximately 230 times higher in comparison with the stipulated TI-Air values.

The commonly used technologies to recover gasoline vapor, at that time, were adsorption on activated carbon or condensation by cryogenic systems.

The advantages of membrane separation for gasoline vapor recovery are:

- membranes are considerably more selective for gasoline vapor compounds than for air;
- variation of feed concentration can be accepted;
- passage of organic vapor concentration from greater than upper explosion limit to less than lower explosion limit occurs in a static apparatus;
- ease of start-up and shutdown operations;
- low maintenance;
- simple design;
- easily combined with recovery techniques or posttreatment systems;
- energy efficient; and
- small footprint.

Loading terminals of tank farms are characterized by intermittent operations, and several peak times during the day can be expected. In order to design the most economical unit, it makes sense to install a gasholder to balance the off-gas volume during peak loading times. The VRU can be designed according to an average gas volume flow. This often leads to lower investment costs, lower energy

consumption, and steady-state operation of the unit. The simplified flow scheme in **Figure 14** shows the design options of a gasoline VRU.

The design most applied in Germany is the combination of membrane technology and pressure swing adsorption (PSA).

The tank farm off-gas is sucked by means of a liquid ring compressor and compressed to a pressure of approximately 3 bar. Lean gasoline is used as service liquid to operate the compressor and the scrubber to recover gasoline vapors. The feed gas, containing a residual concentration, leaves the scrubber top and is fed to the membrane stage. Commonly, the membrane separation process is supported by applying vacuum to the permeate side. The enriched permeate is mixed with the off-gas to the suction line of the compressor. The concentration at the compressor intake is typically enhanced to a level higher than the upper explosion limit of gasoline vapor/air mixtures. In the case of a hybrid system consisting of membrane separation and PSA, the hydrocarbon outlet concentration of the membrane stage is reduced to approximately $2\text{--}10\text{ g m}^{-3}$. The PSA system typically consists of two adsorption beds arranged in parallel. One bed is in the adsorption phase, while the other one is being regenerated. The feed pressure of the membrane stage is used for an enhanced adsorption; the process vacuum is used to support desorption of the carbon bed. Clean vent gas of the PSA system is used as purge gas in the desorption phase (**Figure 15**).

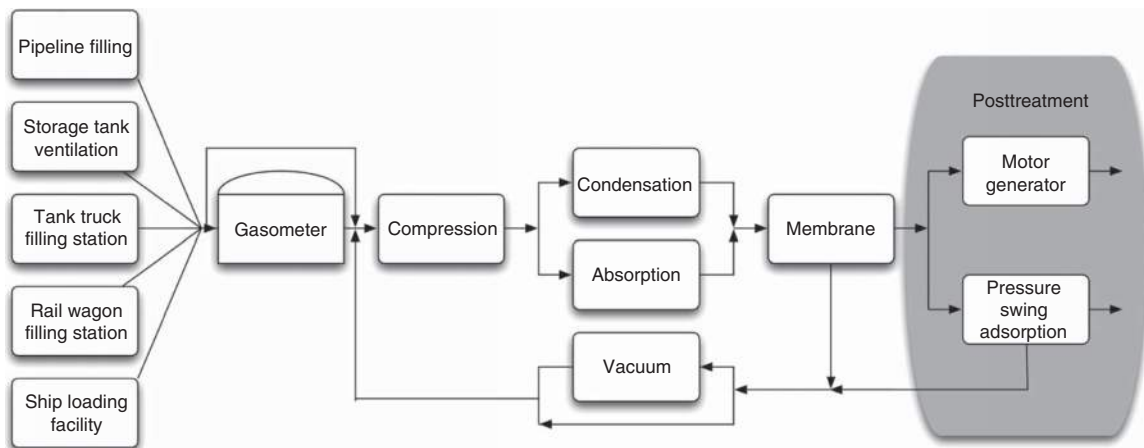


Figure 14 Design options of gasoline vapor recovery units. Reproduced with permission from Ohlrogge, K., Stürken, K. *Membranes: Separation of Organic Vapors from Gasstreams*. In *Ullmann's Encyclopedia of Industrial Chemistry*; Wiley-VCH Verlag GmbH & Co. KGaA, 2005 [46].

stack of a storage tank are likely, a vapor recovery system with a minimum efficiency of 97% has to be employed in order to prevent vent stack emissions.

The driving force to develop a gasoline vapor recovery system at petrol stations was provided by new and more stringent air quality control ordinances and money savings by the recovery of a valuable product. The vapor recovery process has to not only meet a high degree of efficiency but also ensure that all types of equipment meet the suitable safety standards. Equipment and process have to be approved by certified organizations.

The initial situation was the following. Without any environmental precautionary measures, approximately 1 g gasoline vapors per liter of refueled gasoline was emitted in an uncontrolled manner. The pumped liquid volume from storage tank to the car tank was replaced by lean air balancing by the storage tank vent stack. Additional emissions occur by saturation of headspace atmosphere. Change of atmospheric pressure or filling of the storage tank from tank trucks causes breathing of headspace vapors via the vent stack. The vapors vented at the car filler neck are collected by vapor-balancing devices of the dispenser nozzles. Two principles are available: active systems, that is, vacuum-assisted vapor return and passive systems having a close connection between car filler neck and gasoline nozzle. Because of the greater comfort in handling, vacuum-assisted vapor return is the commonly used and widely accepted technology.

A second option to recover refueling emissions is on-board refueling vapor recovery (ORVR). Large carbon canisters (LCCs) are installed into new vehicles that would allow gasoline vapor from vehicle fuel tanks to be contained within the vehicle instead of being vented to the atmosphere. Vapor is displaced into an activated carbon-filled canister during car tank refueling. The adsorbed vapors are desorbed by airflow, drawn into the engine, and burned. This principle is used for new cars in the United States. In this case, the volume balancing in storage tanks takes place by lean air return and creates emissions by saturation of headspace volume. A treatment of vent stack emissions is absolutely essential.

European cars are commonly equipped with small carbon canisters to avoid the so-called running losses and to catch emissions created during parking and heating up by solar radiation. Refueling of cars with small carbon canisters required vapor return during refueling.

If only active vapor return is installed, some emissions may occur. The efficiency of return depends on

the design of the car filler neck and the type of vapor return nozzle. Investigations of TÜV Rheinland have shown that the vapor return efficiency is limited to approximately 75%, depending on the car type [39]. New observations show an improved filler neck design, which leads to an average vapor return efficiency of 85% [40]. The vapor return rate can be improved up to 95–99% by increasing the air-over-liquid ratio (A/L) from 1:1 to 1:1.2 or higher [41]. In order to avoid an emission transfer from interface filler neck to storage tank vent, a treatment of vent stack gases is required [38] (Figure 16).

An essential requirement for the operation of an environment-friendly petrol station is a leak-proof installation of tanks, piping, and dispensers (Figure 17). An installation of pressure/vacuum valves (P/V valves) (12/13) on top of the storage tank vent pipes and an electronic level gauge (17) is also required.

The vent gas treatment unit is installed in parallel to the storage tank vent stack. Only a single unit is necessary to treat the vent gas of a petrol station. A pressure sensor (9) with an integrated pressure switch monitors the differential pressure of atmospheric pressure over tank pressure. Vapors generated by vehicle refueling are returned to the storage tank by means of a vapor return pump of a dispenser and the vapor spout of the vapor return nozzle. A pressure buildup may occur by return of extra volume, evaporation of gasoline to saturate the headspace above the liquid level, or by change of atmospheric pressure. At a given set point, the vacuum pump of the recovery unit (8) is activated. The applied vacuum opens the pneumatic retentate valve as well as the vent line (6) to atmosphere. The gas from headspace flows over the membrane surface of module (7). Gasoline vapors permeate through the membranes and feed back to the storage tank. Clean air is released to atmosphere. Some installations are equipped with a retentate pump (10).

The use of the retentate pump provides some advantages:

- adjustment of a constant flow velocity; and
- adjustment of start-up and shutdown set points close to atmospheric pressure.

The constant flow volume allows an optimized design of module compartment staging to achieve the highest possible separation efficiency. Start and stop set points close to atmospheric will avoid the impact of possible diffusive emissions caused by small leakages in the petrol-station infrastructure.

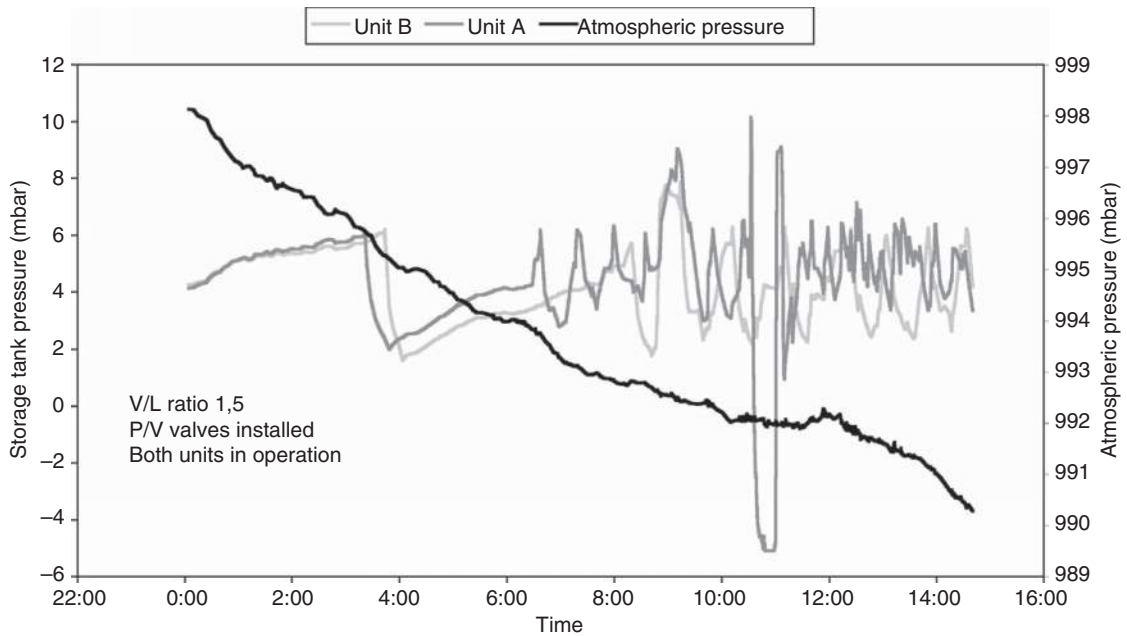


Figure 18 Tank pressure curve from station closing time to frequent operation.

Figure 18 shows the developing of tank pressure over 16 h from station closing time at 11 p.m. to afternoon next day. The start-up set point was adjusted at 6 mbar and the shutdown set point at 2 mbar. It can be seen that a pressure buildup takes place during nighttime. This is because of the saturation of tank headspace above liquid level, which is associated with an increase of tank pressure. The start of the recovery unit is activated and the tank pressure is decreased by release of gas volume

to atmosphere. When the petrol station opens at 6 a.m., the pressure buildup is caused by vapor return and there is a decrease of atmospheric pressure from 998 to 990 mbar. At 11 a.m., a refilling of storage tank 'A' takes place. This procedure creates overpressure and negative pressure. The graph shows the frequent operation during peak sales time (**Figure 18**).

The technical implementation of vent gas treatment system started in the mid-1990s in Germany and Luxembourg and, by the end of the decade, the

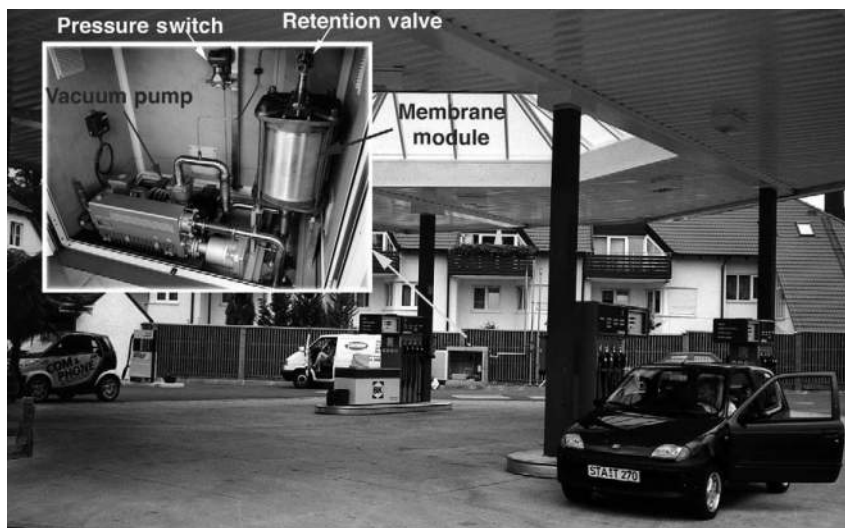


Figure 19 Gasoline vapor separation system.

first unit was installed in the United States. Besides the treatment of petrol station, off-gas was the system used by car manufacturers to reduce emissions generated by the first fueling of new cars in the final assembly line. The real breakthrough of the technology came in early 2002 in the United States. The system, marketed in the United States under the trade name Permeator[®], was granted ORVR approval by Texas Commission on Environmental Quality (TCEQ) and the Maryland Department of Environment certified the compliance with the Code of Maryland Regulation. In March 2007, the system achieved the certification by the California Air Resources Board (CARB). In Europe, the system was certified by TÜV Rheinland, by TÜV Süddeutschland, and, in Switzerland, by Bundesamt für Umwelt, Wald und Landschaft (BUWAL).

The latest demand for implementation of this technology was caused by clean air requirements in highly populated areas in China. To improve the air quality in Beijing, several gas stations have been equipped with storage tank vent processing.

It was proved by third-party testing that storage-tank evaporative losses are between 0.1% and 0.5% of gasoline stations' throughput [42]. The variations in range are due to various site-specific factors as installation of stage I equipment, Reid vapor pressure (RVP) of gasoline, fuel tank temperature, altitude, use of vent stack P/V valves, and population of

ORVR-equipped vehicles. Recovery rates of 97% to >99% have been confirmed.

Meanwhile, approximately 300 systems are installed worldwide. The acceptance is growing because of the increasing oil price and clean air requirements, especially in highly populated cities.

2.09.8.3 PE Powder Treatment

Membrane separation can be used to separate hexane from the purge gases of the PE powder treatment and to purify the purge gas for further reuse. PE powders are purged in a purge bin with heated nitrogen [43].

The membrane process is used for

- recovery of hexane for the reuse as feedstock for the polymerization process;
- purification of nitrogen for reuse as recycle gas or to minimize the off-gas treatment facility; and
- separation of water and traces of HCl from the recovered hydrocarbons.

Figure 20 shows the flow scheme of a PE powder treatment.

The hydrocarbon-enriched purge gases are fed to an in-line cooler. By means of spray cooling, the gas temperature is decreased from 100 to 40 °C. The cooling water is provided by a bypass of the service liquid loop of the liquid ring compressor. Hexane has negligible solubility in water. The purge gas is

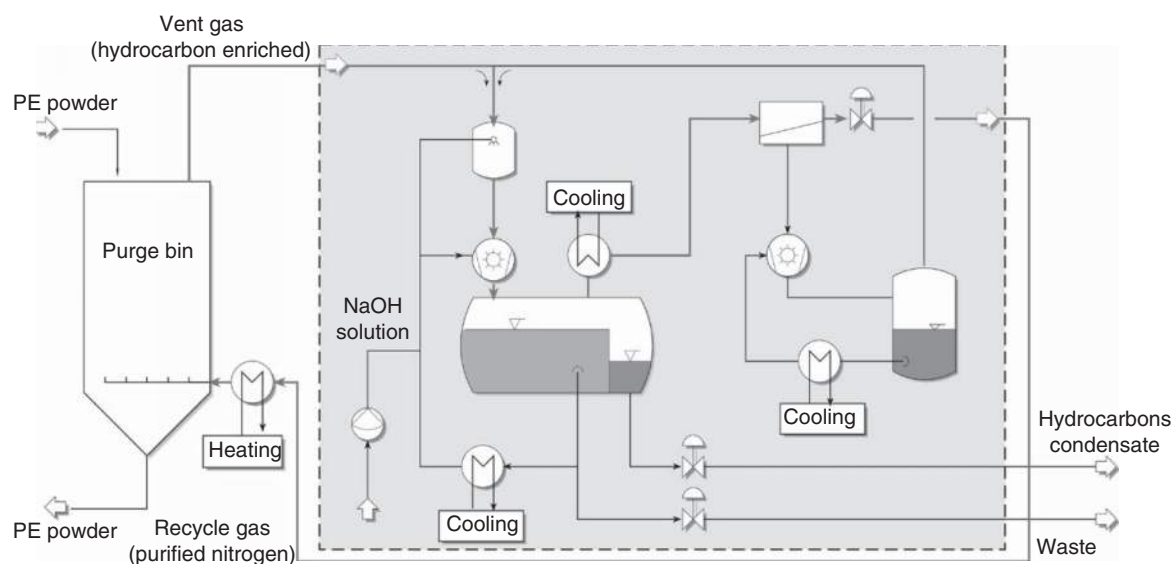


Figure 20 Flow scheme of polyethylene (PE) powder treatment [43]. Reproduced with permission from Ohlrogge, K., Stürken, K. Membranes: Separation of Organic Vapors from Gasstreams. In *Ullmann's Encyclopedia of Industrial Chemistry*; Wiley-VCH Verlag GmbH & Co. KGaA, 2005 [46].

compressed by means of the liquid ring compressor to 7 bar. The vapor is cooled down to 30 °C and partial condensation takes place. The condensate forms an aqueous and an organic (hydrocarbon) phase. The liquid ring service water tank also acts as a phase separator. The water phase is further used as service liquid for the compressor, and hydrocarbons are fed to a collection tank for reuse. The gas/vapor mixture exiting the cooler is fed to hydrocarbon-selective membrane stage. A liquid-ring vacuum pump creates a vacuum of 200 mbar to provide an additional driving force for the permeation of the residual hydrocarbons. The hydrocarbon vapors are recycled to the intake of the liquid ring compressor and purified nitrogen is fed back to degassing bin.

2.09.8.4 Polyolefin Production

Another promising application is the separation of olefins from off-gases of the polyolefin production and the associated purification of purge gas. The olefin recovery is based on following process steps, as shown in **Figures 21 and 22**:

- compression,
- refrigeration/condensation, and
- membrane separation.

In the case of polypropylene production, the off-gas from the purge bin is compressed by means of an oil-lubricated screw compressor. A typical feed pressure is 16 bar. After compression, the gas is released to a cryogenic condensation unit, operating temperature at -20 °C. The noncondensed vapors are then fed to the membrane stage and separated into a hydrocarbon-depleted nitrogen stream (retentate) and an organic-vapor-enriched permeate stream, which is recycled to the intake of the compressor. If high nitrogen purities are required, the membrane stage can be separated into two stages. The first stage operates at atmospheric pressure at the permeate side. In order to achieve high nitrogen purities, the separation of the second membrane stage can be supported by vacuum. The highly purified nitrogen can be returned to the purge bin.

In the case of polyethylene production, the off-gas from the purge bin is compressed to higher pressures. The membrane integration is extremely simple if the already-existing recycle compressor has adequate spare capacities to recompress the additional amount of permeate gas from the membrane stage.

Downstream of the compressor, the first separation of the ethylene takes place in the cryogenic condensation unit. The off-gas ethylene content is reduced to approximately 70 mol.% and the stream is partly fed

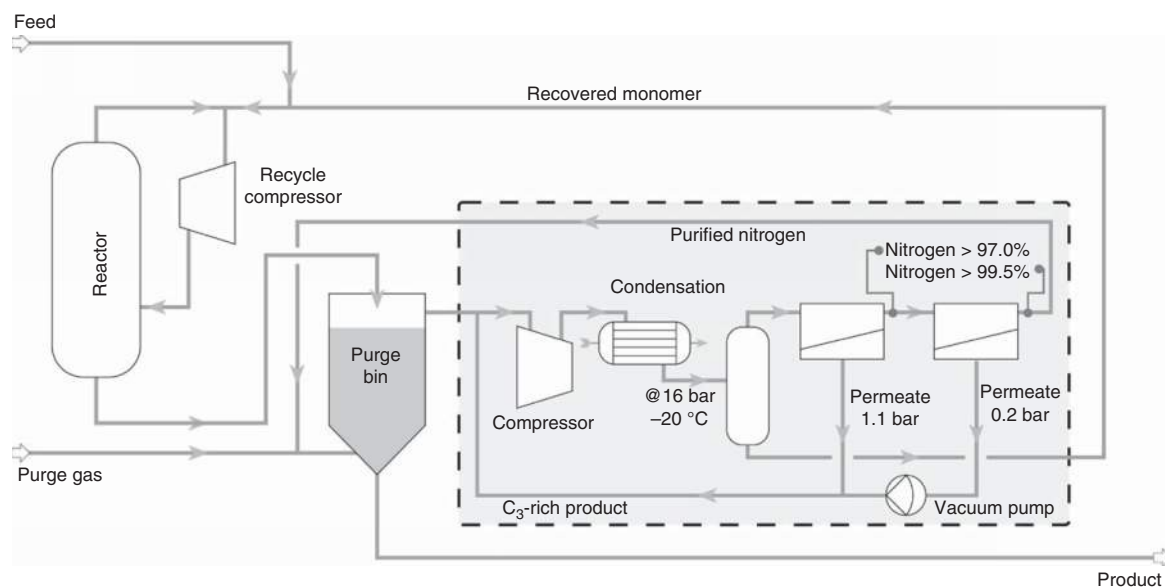


Figure 21 Membrane-based propylene recovery unit. Reproduced with permission from Ohlrogge, K., Stürken, K. Membranes: Separation of Organic Vapors from Gasstreams. In *Ullmann's Encyclopedia of Industrial Chemistry*; Wiley-VCH Verlag GmbH & Co. KGaA, 2005 [46].

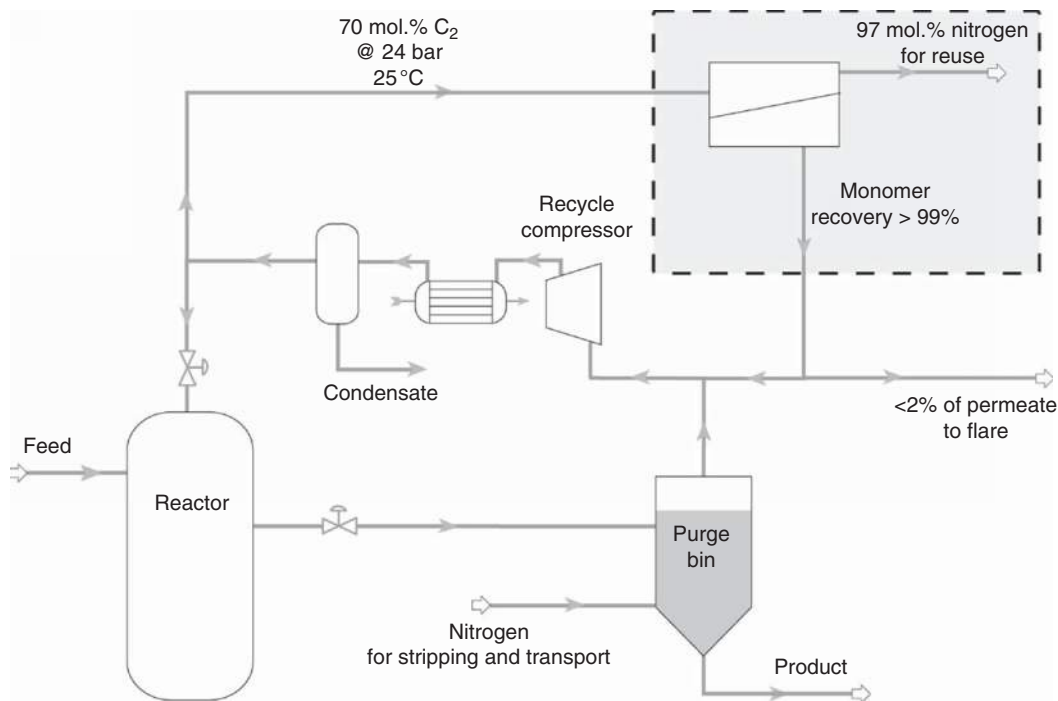


Figure 22 Ethylene recovery unit.

to the membrane stage. The feed gas temperature and pressure are adjusted to reasonable values before the gas enters the membrane, which is not shown in the simplified flow scheme depicted in [Figure 22](#). The temperature of the feed gas to the membrane usually could not be kept to values comparable to the condensation temperature because the additional cooling of the gas in the membrane module caused by the Joule–Thomson effect would lead to extreme low retentate temperatures, which could create problems to the pressure resistance of the stainless steel piping.

The temperature is adjusted to values as low as possible – because the membrane selectivity increases with decreasing temperature – but high enough to avoid pressure resistance problems of the piping. The nitrogen content of the retentate is enriched by the membrane to ≈ 97 mol.% and enables the reuse of the nitrogen in a closed loop. The ethylene recovery rate of the membrane stage is in the range of more than 99%. However, the total permeate is not recycled to the process and a small portion of the ethylene enriched gas is purged to the flare to avoid accumulation of trace gases such as ethane, which is enriched in the permeate stream as well ([Figure 23](#)).



Figure 23 High-pressure module arrangement for ethylene recovery. Picture by courtesy of Sterling SIHI GmbH.

2.09.8.5 Ethylene Oxide and Vinyl Acetate Production

The production of ethylene oxide and vinyl acetate is based on the reaction of ethylene and oxygen in a catalytic reactor. Trace gases, which are found in small amounts, could interfere with the process if these gases accumulate to higher concentrations in the recycle loop as depicted in [Figure 24](#).

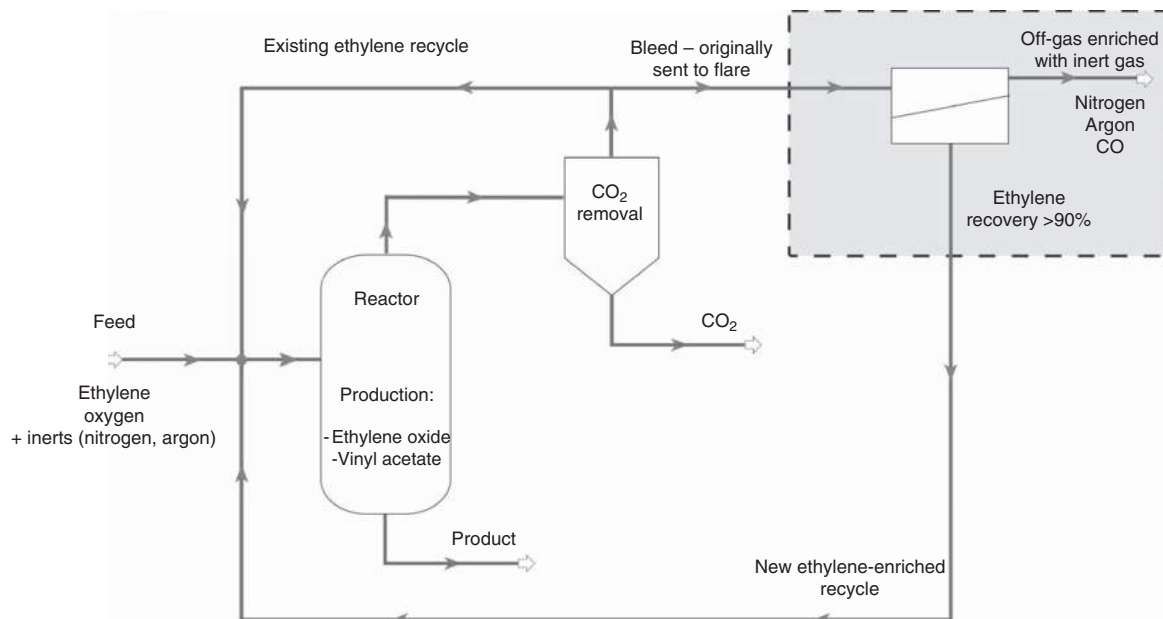


Figure 24 Membrane separation to treat recycle streams of ethylene oxide and vinyl acetate production.

Ethylene, oxygen, including the trace gases, are fed to the reactor [44].

The product is discharged and the nonreacted gases have to be treated and recycled. In the first stage, CO₂ is separated by scrubbing and discharged to atmosphere or to CO₂ utilization plant. In a second step, inert gases have to be removed. This can be done by means of PSA or membrane separation. Because of the limited lifetime of activated carbon in an existing production plant, the operator decided to use membrane technology to treat the process gas stream. The membrane separates the nonreacted ethylene from the recycle stream. The inert gas at the retentate side of the membrane will be fed to further off-gas treatment.

2.09.9 Conclusions and Outlook

Organic vapor recovery by means of membranes can be considered as state-of-the-art technology. Membrane technology is established in various end-of-pipe applications as well as in process-integrated systems. Membrane technology is also used as part of hybrid systems in order to achieve highly efficient separations to meet stringent clean air requirements. Typical applications are solvent recovery in the chemical and pharmaceutical industry and gasoline vapor recovery in the gasoline distribution chain.

Associated with the development of membranes and modules, engineering tools to design separation units have been evaluated.

Accurate models describing the flow patterns in industrial-scale membrane modules as well as the transport phenomena and thermodynamics important to transmembrane mass transfer have been developed. Combined with process simulation tools, these models allow process engineers and plant operators to design optimized integrated processes consisting of membrane units and other separation equipment. The integration of membrane design tools into existing flow-sheet programs was an important step for the acceptance and extension of membrane-based organic vapor separation processes.

Particularly, the increase of oil prices has a considerable impact on the development of new utilizations of organic vapor selective membranes.

Spin-off applications based on the experience gained from established solvent recovery and gasoline recovery systems are treatment of natural gas streams for hydrocarbon dewpointing and methane number control of fuel gas for gas engines.

Modified organic vapor separation membranes are used for oxygen enrichment from air. A typical use is the oxygen enrichment up to 30 vol.%.

The treatment of off-gases from coalmines is in the focus of research activities because of environmental as well as economical reasons. The coalmine off-gases

have typically fluctuating methane concentrations and are often flared to the atmosphere. If a certain minimum methane concentration can be provided, the methane can be used as feedstock for power-generation units. A silicone-based membrane can be used for the upgrading of coalmine off-gas to fuel gas. Membrane variations and module optimizations are tested to review the performance. Experience gained from experiences with organic vapor recovery provide the background to evaluate the applicability of membranes for this application [45].

Experience gained from the development of organic vapor selective membranes has also a high impact on the improvement of new membranes in pervaporation and organophilic nanofiltration applications.

Acknowledgments

The authors would like to thank Carsten Scholles and Thorsten Wolff for the preparation of flow schemes and figures.

References

- [1] Mitchell, J. K. *J. Med. Sci. (Lond.)* **1831**, 13, 36.
- [2] Mitchell, J. K. *J. Roy. Inst.* **1831**, 2(101), 307.
- [3] Graham, T. *Philos. Mag.* **1866**, 32, 401.
- [4] Stern, A. *J. Membr. Sci.* **1994**, 94, 1–65.
- [5] Pixton, M. R., Paul, D. R. Relationship between Structure and Transport Properties for Polymers with Aromatic Backbones. In *Polymeric Gas Separation Membranes*; Paul, D. R., Yampolski, Yu. P., Eds.; CRC Press: Boca Raton, FL, 1994; pp 83–153.
- [6] Freeman, B. *Macromolecules* **1999**, 32, 375.
- [7] Fritsch, D., Peinemann, K.-V., Behling, R.-D., Just, R. (GKSS), Membran auf Basis von Graftpolymeren. DE Pat. 04,213,217 A1, 22 April 1992.
- [8] Alpers, A., Keil, B., Lüdtkke, O., Ohlrogge, K. *Ind. Eng. Chem. Res.* **1999**, 38(10), 3754–3760.
- [9] Cocker, D. T., Allen, T., Freemann, B., Fleming, G. K. *AIChE J.* **1999**, 45, 1451–1468.
- [10] Kaldis, S. P., Kapantaidakis, G. C., Sakellariopoulos, G. P. *J. Membr. Sci.* **2000**, 173, 61–71.
- [11] Qui, R., Henson, M. A. *Ind. Eng. Chem. Res.* **1997**, 36, 2320–2331.
- [12] Pan, C. Y. *AIChE J.* **1983**, 29, 545–552.
- [13] Savolainen, P. Modelling of Non-Isothermal Vapor Membrane Separation with Thermodynamic Models and Generalized Mass Transfer Equations. PhD Thesis, Lappeenranta University of Technology, 2002.
- [14] Tessendorf, S., Gani, R., Michelsen, M. L. *Comput. Chem. Eng.* **1996**, 20, 653–658.
- [15] Rautenbach, R., Knauf, R., Struck, A., Vier, J. *Chem. Eng. Technol.* **1996**, 19, 391–397.
- [16] Marriott, J., Sørensen, E. *Chem. Eng. Sci.* **2003**, 58, 4975–4990.
- [17] Davies, R. A. *Chem. Eng. Technol.* **2002**, 25, 717–722.
- [18] Wolff, T. Vergleich zweier Membranmodultypen für die Gaspermeation. Diploma Thesis, Technical University Hamburg – Harburg, 2003.
- [19] Fang, S. M., Stern, S. A., Fritsch, H. L. *Chem. Eng. Sci.* **1975**, 15, 773–778.
- [20] Alpers, A. Hochdruckpermeation mit selektiven Polymermembranen für die Separation gasförmiger Gemische. PhD Thesis, University of Hannover, 1997.
- [21] Soave, G. *Chem. Eng. Sci.* **1972**, 27, 1197–1203.
- [22] Peng, D.-Y., Robinson, D. B. *Ind. Eng. Chem. Fundam.* **1976**, 15, 59–64.
- [23] Bird, R. B., Stewart, W. E., Lightfoot, E. N. *Transport Phenomena*; Wiley: New York, 1960.
- [24] Froment, G. F., Bischoff, K. B. *Chemical Reactor Analysis and Design*; Wiley: New York, 1990.
- [25] Taylor, A., Krishna, R. *Multicomponent Mass Transfer*; Wiley: New York, 1993.
- [26] Alopaeus, V., Nordén, H. V. *Comput. Chem. Eng.* **1999**, 23, 1177–1182.
- [27] Brinkmann, T., Hapke, J., Ohlrogge, K., Wind, J., Wolff, T. *Proceedings Euromembrane*, Hamburg, 26 September–1 October; Book of Abstracts, **2004**, p 172.
- [28] Gmehling, J., Kolbe, B. *Thermodynamik*. Thieme Verlag: Stuttgart, 1988.
- [29] Press, W. H., Teukolosky, S. A., Vetterling, W. T., Flannery, B. P. *Numerical Recipes in C*. Cambridge University Press: Cambridge, 1992.
- [30] Reid, R. C., Prausnitz, J. M., Sherwood, T. K. *The Properties of Gas and Liquids*; McGraw-Hill: New York, 1977.
- [31] AspenTech: Optimizing Process Manufacturing, <http://www.aspentech.com> (accessed November 2009).
- [32] CO-LaN, <http://www.colan.org> (accessed November 2009).
- [33] Process Systems Enterprise, <http://www.psenterprise.com> (accessed November 2009).
- [34] Brinkmann, T. Modellierung und Simulation der Membranverfahren Gaspermeation, Dampfermeation und Pervaporation. In *Membranes*; Ohlrogge, K., Ebert, K., Eds. Wiley-VCH: Weinheim, 2006; pp 273–333.
- [35] Ohlrogge, K., Wind, J., Peinemann, K.-V. Membranverfahren zur Gaspermeation. In *Membranes*; Ohlrogge, K., Ebert, K., Eds.; Wiley-VCH: Weinheim, 2006; pp 375–409.
- [36] Technische Anleitung zur Reinhaltung der Luft (TA-Luft) vom 27. Februar 1986, Gemeinsames Ministerialblatt, pp 92–202, novelliert am 1. oktober 2002.
- [37] Verordnung zur Begrenzung der Kohlenwasserstoffemissionen beim Umfüllen und Lagern von Ottokraftstoffen, 20. BImSchV, novelliert am 24. Juni 2002.
- [38] Verordnung zur Begrenzung der Kohlenwasserstoffemissionen bei der Betankung von Kraftfahrzeugen, 21. BImSchV, novelliert am 6. Mai 2002.
- [39] Hassel, D. *Praxis – Forum Umweltmanagement* **1994**, 23/94, 183–203.
- [40] Luft und Luftreinhaltung, VOC – Betankungsverluste bei Tankstellen, <http://www.umweltbundesamt.de/luft/schadstoffe/voc.htm> (accessed November 2009).
- [41] Ohlrogge, K. *Praxis – Forum Umweltmanagement* **1994**, 23/94, 207–217.
- [42] Arid Technologies, Inc. Independent Third-Party Field Test Confirms Predicted Gasoline Evaporative Losses, <http://www.aridtech.com> (accessed November 2009).
- [43] Ohlrogge, K., Stürken, K. Membranes: Separation of Organic Vapors from Gas Streams. *Ullmann's Encyclopedia of Industrial Chemistry*; Wiley-VCH: Weinheim, 2006.
- [44] Stegger, J. Organic Vapour Separation by Polymeric Membranes. In *Proceeding of Euromembrane*, Hamburg: Book of Abstracts, 2004; p 169.

- [45] Brinkmann, T., Scholles, C., Wind, J., Wolff, T., Dengel, A., Clemens, C. *Desalination* **2008**, 224, 7–11.
- [46] Ohlrogge K., Stürken K., Membranes: Separation of Organic Vapors from Gasstreams. In *Ullmann's Encyclopedia of Industrial Chemistry*; Wiley-VCH Verlag GmbH & Co. KGaA 2005.
- [47] Nunes S. P., Peinemann K.-V., *Membrane Technology in the Chemical Industry*; Wiley-VCH Verlag GmbH & Co. KGaA, 2006; p112.
- [48] Ohlrogge K., Ebert K., *MEMBRANEN, Grundlagen Verfahren und industrielle Anwendungen*; WileyVCH Verlag GmbH & Co. KGaA, 2006; pp 299, 306, 379, 425.

Biographical Sketches



Klaus Ohlrogge received the Dipl.-Ing. degree in ship operation engineering. He started his industrial career in 1970 when he was employed at Continental Gummi-Werke AG, Hannover, as engineer for planning plants for energy applications. In 1975, he moved to GKSS Forschungszentrum Geesthacht GmbH as scientific officer. After seven years of activity in the framework of the research program 'Water desalinization, marine resources' he moved to membrane research for gas and vapor separation applications. From 1982 to his retirement in December 2005, he was head of the Process Engineering Department as part of the Institute of Chemistry (now Institute of Polymer Research). He was also a cofounder of GMT-Membrantechnik GmbH in Rheinfelden (1995). He has made numerous presentations at national and international congresses, has authored many publications, and coinvented several membrane-related patents.



Jan Wind studied bioengineering with a focus on environmental engineering at the University of Applied Science Hamburg-Bergedorf, including a six-month internship oriented to engineering studies at the company Pagendarm – Coating Engineering/Hamburg. He received the Dipl.-Ing. degree in 1983 when he completed his external diploma thesis on the subject 'Application of membrane separation for the reduction of gaseous toxic emissions' at the GKSS Research Centre in Geesthacht, Germany. Since November 1983 he has been employed at the Process Engineering Department of the Institute of Chemistry – now Institute of Polymer Research – at the GKSS. His work focuses on gas, vapor, and organic solvent separation, including process design, development of simulation tools, module design, and also upscaling of membrane preparation. He has coinvented several process and membrane patents. He is also a cofounder of GMT-Membrantechnik GmbH Rheinfelden.



Torsten Brinkmann studied mechanical engineering with specialization in process engineering at the Technical University of Aachen, Germany, graduating with the degree of Dipl.-Ing. in 1993. Subsequently, he was employed as a research officer at the University of Bath, Great Britain. At this time, he conducted research on the subject 'Use of catalytic membrane reactors for *in situ* reaction and separation' for which he received his PhD. Between 1996 and 2000, Torsten Brinkmann worked for AspenTech UK Ltd. He was primarily involved in the modeling and simulation of adsorption processes. Since 2000 he has been employed as a scientific officer at the GKSS Research Centre in Geesthacht, Germany. His main research interests include the development, design, and simulation of pervaporation, gas and vapor permeation processes, as well as the modeling of membrane modules and transport phenomena. In December 2005, he became the head of the Process Engineering Department within the Institute of Polymer Research of GKSS.

2.10 Fundamentals and Perspectives for Pervaporation

K Nagai, Meiji University, Kawasaki, Japan

© 2010 Elsevier B.V. All rights reserved.

2.10.1	Introduction	243
2.10.2	Target Solutions for Separation	245
2.10.3	Separation Mechanisms and Experiments	245
2.10.3.1	Transport Mechanism	245
2.10.3.2	Permeability and Permselectivity	247
2.10.3.3	Solubility and Solubility Selectivity	250
2.10.3.4	Diffusivity and Diffusivity Selectivity	252
2.10.3.5	Combination of Selectivities	258
2.10.3.6	Temperature Dependence	259
2.10.3.7	Experimental Methods	260
2.10.4	Membrane Materials and Pervaporation Properties	262
2.10.4.1	Combination of Solubility Selectivity and Diffusivity Selectivity	262
2.10.4.2	Affinity Control	265
2.10.4.3	Pore Structure Control	267
2.10.4.4	Stability Improvement	268
2.10.5	Concluding Remarks	268
References		269

2.10.1 Introduction

As compared to conventional methodologies, membrane separation technology has various advantages, one of which is its capability to carry out isothermal operation at low temperatures. Moreover, this particular technology imposes no requirements for additives, and enjoys the advantages of low energy consumption and ease of integration into other separation or reaction processes. Historically, membrane science and technology comprise a wide variety of industrial applications in gas separation and water purification, such as the removal of small solids and ions from water. The pervaporation process is one of those identified membrane processes that can separate liquid mixtures.

Since the early stage of membrane engineering, water purification membranes have contributed to the production of drinking water and the process of rinsing water for the electronic industry (e.g., semiconductor manufacture). This technique also finds applications for in-house water purification, and even in large-scale systems for city operations. In addition, the current applications of ultrafiltration, microfiltration, nanofiltration, and electrodialysis include medical, chemical, food, beverage, and fermentation industries.

In 1982, the first commercial-scale membrane system for liquid separation was established to separate ethanol–water mixtures through pervaporation [1]. Since then, more than 50 plants have been installed for ethanol dehydration. However, such pervaporation processes remain largely underdeveloped in the fields of water purification and liquid separation, both of which have been proven suitable in the production of bioethanol.

A separation membrane is the interphase between two adjacent phases acting as a selective barrier, which regulates the transport of substances between the two compartments. It is employed for specific functions, including the separation of gases and liquids, ions, or biological matters. In pervaporation, a liquid mixture is supplied to a membrane on one side and the permeate components are evaporated from the other side (Figure 1). Therefore, the driving force of this process is a gradient of partial pressure or chemical potential located across a membrane. To enhance the flux or the total amount of the product, the permeate side is always maintained at a pressure below the saturated pressure of a given component, either under a vacuum or by sweeping the vapor using a carrier gas. The vapor at the permeate side is then condensed and recovered as liquid. Interestingly, the pervaporation process has been

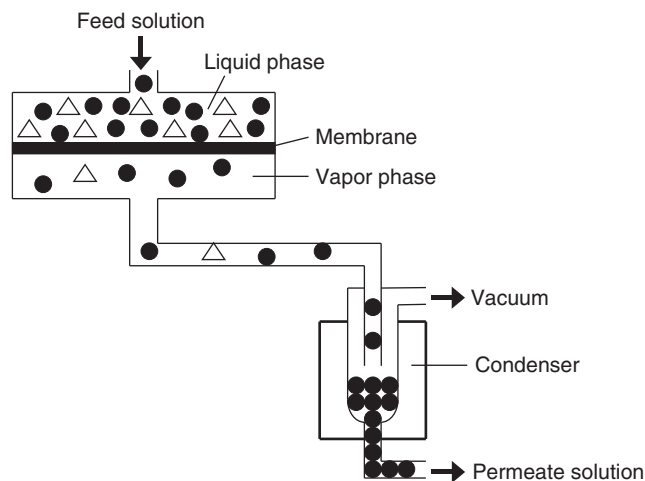


Figure 1 Vacuum-driven pervaporation process.

noted as the only membrane process, in which a mixture's phase transition manifests itself during transport through a membrane (i.e., a change from liquid phase to vapor phase).

In 1917, Kober [2] observed the permeation of a liquid kept in a closed collodion bag suspended in midair. This phenomenon was ascribed the technical word pervaporation, coined from the two concepts, permeation and evaporation. In 1935, Farber [3] developed a pervaporation technique to concentrate solutions of proteins and enzymes by evaporating water through a cellophane bag. By 1956, the separation of liquid mixtures (e.g., ethanol–water mixture) through pervaporation using a cellophane membrane was attempted by Heisler *et al.* [4]. Currently, the pervaporation process being widely used is a result of the process proposed by Binning in the late 1950s [5–8].

Mechanisms for water purification using a membrane-based process, such as ultrafiltration and microfiltration, involve size-sieving filtration which removes small solids from water. In contrast, pervaporation is based on a solution–diffusion, adsorption–diffusion, or size-sieving filtration mechanism. Pervaporation is used to achieve the removal of volatile organic compounds (VOCs), such as ethanol, from water; the dehydration of VOCs (i.e., removal of water from VOCs); or the separation of mixtures of VOC liquids. Among all liquid separation technologies (e.g., distillation), a pervaporation process is noted to be most effective under the following conditions: (1) when liquid mixtures are separated at azeotropic point, (2) when they have similar boiling

temperatures, or (3) if they contain thermally unstable component(s). Based on such separation mechanism, at the permeate side, it is impossible to recover components which have not evaporated (e.g., metals, ions, peptides, or polymers). They may remain in the feed.

The properties of a membrane strongly depend on the chemical structure and microstructure of the membrane material, both of which are substantially affected by the molecular weight of the polymer, the presence of impurities, the membrane formation process, membrane thickness, and membrane pretreatment. Therefore, the synthesis of novel polymer and inorganic materials with well-defined structures as designed membrane materials will not only contribute to the development of new membrane materials, but will lead to a significant advancement in the study of membranes as well.

Permeation through a membrane has been identified as a rate-determining step. As such, a minor component of the mixture must be removed via selective permeation through the membrane in order to minimize the amount of permeate liquid. For example, preferential water permeation (water selectivity) is a characteristic feature of most polymers. However, there have been some reports about VOC-selective polymers to date. Substituted polyacetylenes exhibit a remarkably interesting example of a class of polymer by displaying both their VOC- and water-selectivity characteristics [9]. Therefore, a design to achieve a highly efficient and economically viable membrane material requires the elucidation of the relationship of their transport properties and

molecular structures. This is primarily because membrane functions are governed by the primary and secondary structures of both polymers and inorganic materials.

This chapter reviews the fundamentals and perspectives of pervaporation, and subsequently provides a comprehensive overview of the separation mechanisms, experimental methods, and structure–property relationships of membrane materials in various important applications of the pervaporation processes.

2.10.2 Target Solutions for Separation

In his book, Baker [1] summarized the industrial application fields of pervaporation and focused on three applications: dehydration of solvents, water purification (i.e., separation of dissolved organics from water), and separation of organic liquid mixtures.

This chapter mainly addresses various existing and prospective target solutions for separation by pervaporation as earlier reported in academic research fields. To date, such technique has demonstrated multidimensional potentials in the energy, petroleum, environmental, pharmaceutical, as well as in food and beverage industries. A pervaporation process is expected to purify a target liquid on the permeate side or concentrate it on the feed side.

It is important to emphasize the fact that across separation technologies, the pervaporation process takes prior advantage in the separation of liquid mixtures at the azeotropic point. This is also true when it involves mixtures with similar boiling temperatures or those containing thermally unstable component(s). According to this separation mechanism, the permeate component(s) must involve a vaporization behavior at a given operating temperature and pressure. Components considered as VOCs include hydrocarbons (e.g., hexane, octane, and cyclohexane), BTX (benzene, toluene, and xylene isomers), halogen-containing compounds (e.g., trichloroethylene and chloroform), alcohols (e.g., methanol, ethanol, propanol, and butanol), phenol, oxygen-containing compounds (e.g., acetic acid, methylethylketone, butanone, 1,4-dioxane, and methyl-*tert*-butyl ether (MTBE)), nitrogen-containing compounds (e.g., acetonitrile and acrylonitrile), aromas (e.g., menthol, lactones, higher alcohols, higher ketones, and higher esters), and endocrine disruptors (e.g., dioctylphthalate, 2-*sec*-

butylphenylmethylcarbamate, 2,2-dimethyl-1,3-benzodioxol-4-yl methylcarbamate, and 1,2-dibromo-3-chloropropane).

The above-mentioned VOCs can also be recovered as concentrated products in the feed side. Unlike in the permeate side, it is not necessary for concentrated compound(s) in the feed solution to be evaporated when they are separated through a membrane. Examples of these compounds include ions, large molecules (e.g., saccharin, glucose, fructose, glycosan, ascorbic acid (vitamin C), amino sugars, polyethylene glycol, maltose, lactose, sucrose, trehalose, and raffinose), polymers (e.g., poly(vinyl alcohol (PVC)), polypeptide, starch, glycogen, cellulose, alginic acid, and chitin), as well as enzymes (e.g., amylase and laccase).

The optimum component balance in a solution can also be adjusted through pervaporation, such as in the production of fruit juices and liquors, and in the manufacture of petroleum products. Under these circumstances, pervaporation processes are not required to have high separation abilities.

2.10.3 Separation Mechanisms and Experiments

2.10.3.1 Transport Mechanism

Separation membranes can be divided into two major classes (porous and nonporous membranes) and the respective transport of small molecules through these two types of membranes occurs under different mechanisms (Figure 2).

In a porous membrane, diffusion occurs under mechanisms that are largely dependent on the morphology of the membrane (i.e., pore size) and the size of the diffusing molecule. These mechanisms include Knudsen diffusion, surface diffusion, capillary condensation, and molecular sieving, among others. In Knudsen diffusion, the penetrant collides more frequently with the pore wall than with other penetrant molecules. In surface diffusion, the penetrant is adsorbed onto the surface and then diffused along the pore surface through activated jumps. Meanwhile, in capillary condensation, an interaction between the penetrant and the pore walls causes the condensation, which in turn influences diffusion through the pore. Finally, in molecular-sieving pores, the size of the pore prevents larger molecules from passing.

On the other hand, a nonporous membrane acts accordingly with the solution–diffusion mechanism. Pores do not control the passage of the penetrant as

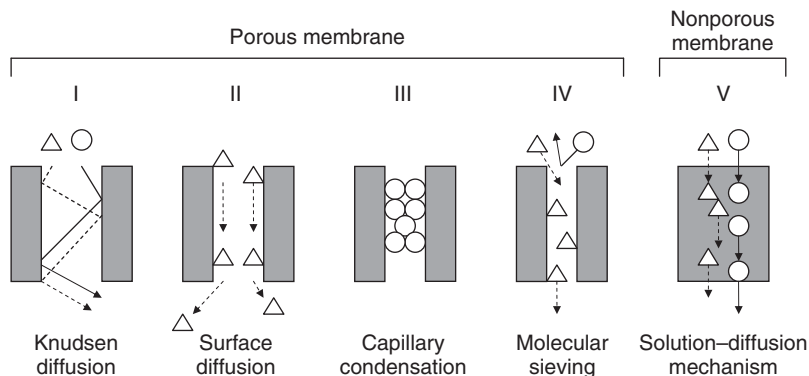


Figure 2 Mechanisms of transport for small molecules through a membrane.

similarly depicted in gas separation and vapor separation. A penetrant is dissolved into the surface of a membrane, its molecule diffuses inside a membrane from one side to the other side, and then it is removed from the surface of the other side of the membrane.

Polymer membranes and inorganic membranes are designed by nonporous and porous structures, respectively. In polymer membranes, the penetrant molecules are dissolved and diffused in transient molecular spaces across assemblies of polymer segments, which appear to be continuously arranged within a nonporous membrane. In inorganic membranes, the penetrant diffuses in fixed pores, which are continuously prepared across a porous membrane. These molecules adsorb onto the surface of the pores, because organic compounds have interactions with inorganic materials. This behavior results in Knudsen diffusion, surface diffusion, and capillary condensation. In this regard, the transports that occur within polymer membranes and inorganic membranes are based on solution–diffusion and adsorption–diffusion mechanisms, respectively. Separation of the mixture occurs when the solution/adsorption phenomena and/or diffusion speed of each component differ from each other.

Among the mechanisms presented in **Figure 2**, the molecular sieving has been observed to produce the highest separation property, and only smaller molecules inside the pores of the membrane. Similar to the others, this transport process for these smaller molecules manifests an adsorption–diffusion mechanism.

The flux (\mathcal{F}_i) of component i found across a membrane at a steady state is expressed below using Fick's law:

$$\mathcal{F}_i = -D_i \frac{dC_i}{dx} \quad (1)$$

where D_i is the diffusion coefficient of component i , and dC_i/dx is the concentration gradient of component i across a membrane with thickness l . If the concentrations of the surfaces of the membrane at the feed and permeate sides are C_{i1} and C_{i2} ($C_{i1} > C_{i2}$), respectively, this equation can be rewritten as

$$\mathcal{F}_i = D_i \frac{C_{i1} - C_{i2}}{l} \quad (2)$$

In addition, for polymer membranes, the concentrations, C_{i1} and C_{i2} , are also described using the solubility coefficient S_i as a function of each partial pressure, p_{i1} and p_{i2} :

$$C_{i1} = S_i p_{i1} \quad (3)$$

$$C_{i2} = S_i p_{i2} \quad (4)$$

Hence, Equation (2) is given as

$$\mathcal{F}_i = D_i S_i \frac{p_{i1} - p_{i2}}{l} = P_i \frac{p_{i1} - p_{i2}}{l} \quad (5)$$

The permeability (P_i) of component i that goes through a membrane can be expressed in terms of solubility and diffusivity factors, which are concepts offered in the following solution–diffusion mechanism:

$$P_i = S_i D_i \quad (6)$$

The feed solution always makes contact with the surface of a membrane. In contrast, the membrane remains dry at the opposite side, because permeate components always evaporate. Unlike gas separation and vapor separation membranes, during the permeation, the cross section of the pervaporation membrane has a gradient structure with the membrane containing liquid in the feed side and vapor in the permeate side.

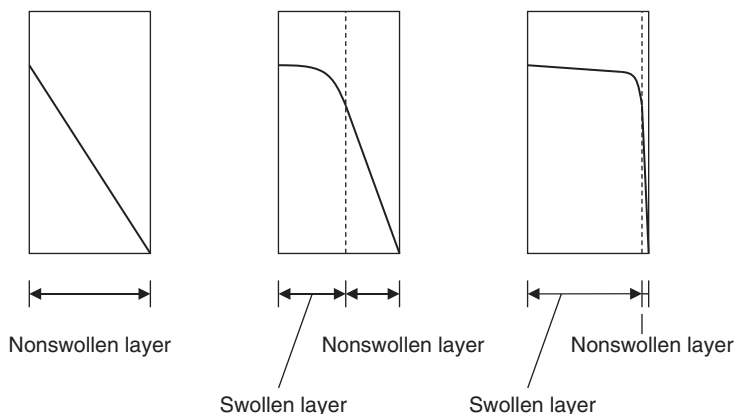


Figure 3 Concentration gradient of a penetrant across a membrane.

The concentration gradient in the pervaporation membrane is classified into three types as described in **Figure 3**. In type I, the concentration gradient is linear across a membrane, which follows Fick's law in Equation (1). The membrane is not swollen by the feed solution, as in the case of several inorganic membranes.

When membrane materials are composed of polymers and some other inorganic materials, they sometimes become swollen by the liquid on the feed side. In contrast, the membrane remains dry continuously maintaining its shape in the permeate side (i.e., moderate swelling for type II and high swelling for type III). During permeation, the polymer membrane is thought to have two layers (i.e., swollen layer and nonswollen layer). Liquid components in the feed solution are selectively dissolved and diffused in the swollen layer. Due to the fact that the polymer segments are expanded in the region swollen by the liquid, all components achieve a high diffusion speed, which is largely similar to the others on the basis of weak size-sieving behavior. In the swollen layer, it is the solubility coefficient, and not the diffusion coefficient, which is considered as the dominant factor of the transport.

These aforementioned components are then selectively dissolved in the interface between the swollen and the nonswollen layers. Under these circumstances, it is important to note that since this interface is not clearly separated as in a laminate membrane, the thickness of the nonswollen layer cannot be determined. Subsequently, the penetrant diffuses through the nonswollen layer and is left in the surface as vapor. Unlike the diffusion process occurring in the swollen layer, the polymer segments herein are densely packed leading to the large

resistance of diffusion by the small molecules. Transport behavior through the nonswollen layer is almost similar to that described in the vapor and gas separation membrane. Hence, the dominant factor of the transport in the nonswollen layer is the diffusion coefficient, and not the solubility coefficient. The nonswollen layer has also been referred to as the dried layer, dense layer, or the active separation layer. In addition, the nonswollen layer is generally thinner than the swollen layer.

2.10.3.2 Permeability and Permselectivity

The flux (\mathcal{J}_i) of component i across a membrane is determined as

$$\mathcal{J}_i = \frac{Q_i}{At} \quad (7)$$

where Q_i is the amount of the permeated product of component i , A is the permeation area of a membrane, and t is the measurement time. There is a time lag in the permeation occurring at the initial stage of measurement. Immediately after the permeation measurement begins, the amount of the permeated product gradually increases (i.e., nonsteady state), before settling down to a constant steady state. In general, the Q_i value is recorded at a steady state. The flux units are represented in practical units of $\text{g m}^{-2} \text{h}^{-1}$, $\text{kg m}^{-2} \text{h}^{-1}$, $\text{cm}^3 \text{cm}^{-2} \text{h}^{-1}$, and $\text{m}^3 \text{m}^{-2} \text{h}^{-1}$, as well as the SI unit $\text{mol m}^{-2} \text{s}^{-1}$. This is because the recovered liquid product is normally measured by weight or volume.

The combination of the pressures at the feed and permeate sides provides variations in flux and permselectivity. For example, in the permeation of pure hexane liquid through the polyethylene

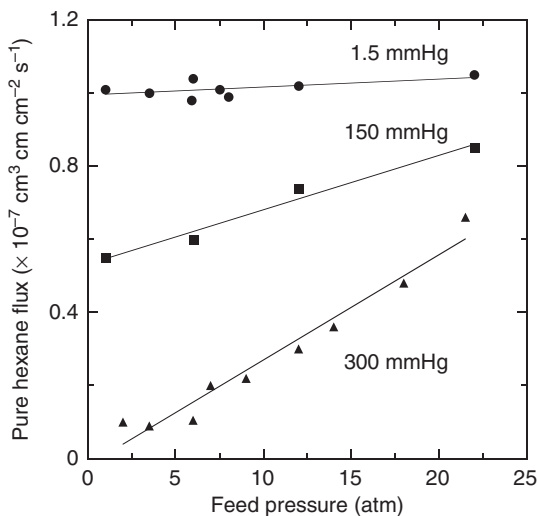


Figure 4 Pure hexane flux of the low-density polyethylene membrane at 30°C, as a function of feed pressure. The permeate pressures: 1.5 mmHg (●), 150 mmHg (■), and 300 mmHg (▲). Reproduced from Greenlaw, F. W., Prince, W. D., Shelden, R. A., Thompson, E. V. *J. Membr. Sci.* **1977**, 2, 141–151.

membrane at 30°C, as the feed pressure increased, the flux of hexane increased linearly when the permeate pressure was set at 300 mmHg, which is higher than that of the saturation pressure of hexane (Figure 4) [10]. In contrast, the flux was almost independent of the feed pressure when the permeate pressure was much lower than that of the saturation pressure of hexane. As the permeate pressure decreased, there occurred an increase in the gradient of partial pressure or chemical potential across a dried nonswollen layer. As a result, when the permeate components became easily vaporized, the flux or the total amount of the product increased.

As the permeate pressure approached zero, the flux began to show the larger values. For hexane/heptane binary mixtures, the permeate pressure is noted to strongly affect permselectivity (Figure 5) [11]. Each component then created a different gradient of partial pressure across the nonswollen layer, because each component incorporated different vapor pressures. Afterwards, there appeared a linear relationship between permselectivity and saturation vapor pressure of the endocrine disruptors in the pervaporation of endocrine disruptor aqueous solutions (concentration: 10 ppm) through the polydimethylsiloxane (PDMS, 1) membrane at 90°C (Figure 6) [12].

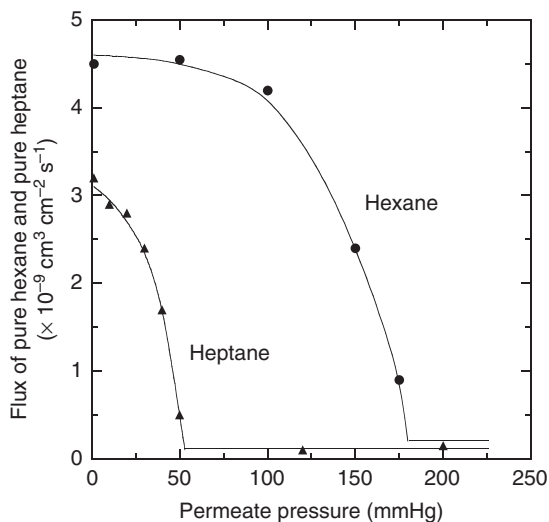
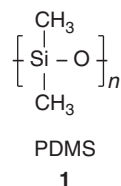


Figure 5 Flux of pure hexane (●) and pure heptane (▲) of the low-density polyethylene membrane at 30°C and at upstream pressure of 1 atm, as a function of permeate pressure. Reproduced from Greenlaw, F. W., Shelden, R. A., Thompson, E. V. *J. Membr. Sci.* **1977**, 2, 333–348.



In this regard, unlike in the other liquid separation membrane processes, such as reverse osmosis and ultrafiltration, the addition of the pressure in the feed is generally unnecessary during pervaporation in polymer membranes. The permeate side is maintained at a pressure below the saturation pressure of a given component either under a vacuum or by sweeping the vapor using a carrier gas.

The permeation process through a membrane involves a rate-determining step. As the membrane thickness becomes thinner, the flux increases. Ideally, the flux of a homogeneous membrane is in proportion to the reciprocal of the membrane thickness. Figure 7 presents a pure water flux at 25°C, which passed through a poly(vinyl pyridine) membrane to study the function of reciprocal membrane thickness [13]. The distinct linear relationship then appeared.

Using Equation (7), the normalized flux can be written as

$$\mathcal{F}_i = \frac{Q_i l}{A t} \quad (8)$$

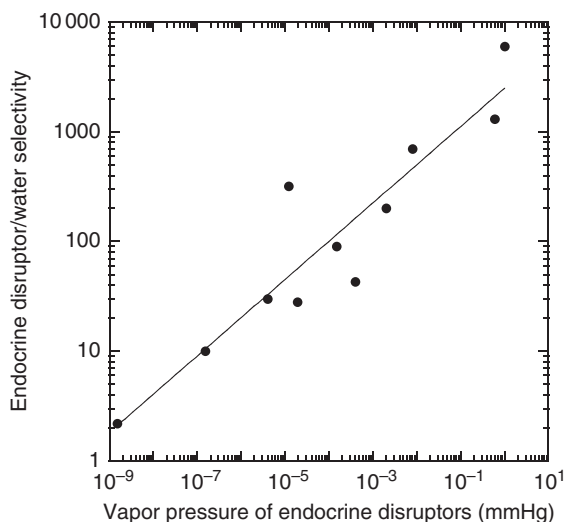


Figure 6 Endocrine disruptor/water selectivity of the polydimethylsiloxane membrane, as a function of their saturation vapor pressure. Temperatures at feed and permeate sides were 90 and 150 °C, respectively. Reproduced from Yoon, B. O., Asano, T., Nakaegawa, K., Ishige, M., Hara, M., Higuchi, A. Separation of Endocrine Disruptors from Aqueous Solutions by Pervaporation: Relationship between the Separation Factor and Solute Physical Parameters. In *Advanced Materials for Membrane Separations*; Pinnau, I., Freeman, B. D., Eds.; American Chemical Society: Washington, DC, 2004; pp 394–410.

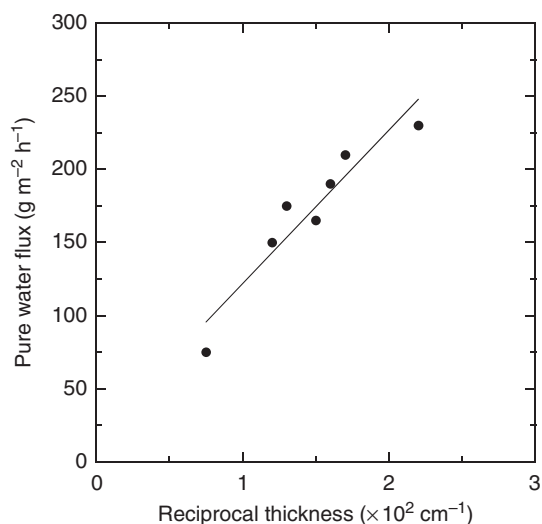


Figure 7 Relationship between pure water flux and reciprocal thickness of the poly(4-vinylpyridine) membrane at 25 °C. Reproduced from Yamada, S., Hamaya, T. *Kobun Ronbun. (Jpn. J. Polym. Sci. Tech.)* **1982**, 39, 407–414.

where l is the membrane thickness. The unit of the flux is represented as $\text{g m}^{-2} \text{h}^{-1}$, $\text{kg m}^{-2} \text{h}^{-1}$, $\text{cm}^3 \text{cm}^{-2} \text{h}^{-1}$, $\text{m}^3 \text{cm}^{-2} \text{h}^{-1}$, or $\text{mol m}^{-2} \text{s}^{-1}$.

The permselectivity or separation factor (α_p) of component i over component j in a binary mixture is obtained from

$$\alpha_p = \frac{\left(\frac{Y_i}{Y_j}\right)}{\left(\frac{X_i}{X_j}\right)} = \frac{Y_i(1-X_i)}{X_i(1-Y_i)} \quad (9)$$

where X_i and X_j are the weights or weight fractions ($X_i + X_j = 1$) of component i and component j in a feed solution, respectively. The variables Y_i and Y_j are the weights or weight fractions ($Y_i + Y_j = 1$) of component i and component j in a permeate solution, respectively. Molar fractions can also be used together with weight fraction. The composition of the feed and permeate solutions can then be determined using an analyzer, such as gas chromatograph. The flux is dependent on membrane thickness, whereas normalized flux and permselectivity are ideally independent of the thickness of such homogeneous membranes.

As membrane thickness reaches a measurement of as low as 100 nm, the study notes high possibility of defects (e.g., pinhole) for both polymer and inorganic membranes, which enhance flux and reduce selectivity. However, in several cases, such as in heterogeneous structures and even thicker thicknesses without any defects, flux had been induced, and as a result permselectivity also cannot be simply correlated to the reciprocal thickness. For example, for aqueous solution pervaporation in chlorinated hydrocarbons, such as 1,1,2-trichloroethane, copolymer membranes composed of trimethylsilylmethylmethacrylate and

n-butyl acrylate did not simply conform to the rule [14]. The chlorinated hydrocarbon/water selectivity of these membranes with a thickness greater than 70 μm was constant, whereas this selectivity gradually decreased as the membrane became thinner than 70 μm. Therefore, when the flux of various membranes is compared, the membranes with similar thickness must be used.

Finally, the permselectivity (α_P) of component *i* over other components in a multicomponent mixture is given as

$$\alpha_P = \frac{\left(\frac{Y_i}{Y_{\text{total}} - Y_i}\right)}{\left(\frac{X_i}{X_{\text{total}} - X_i}\right)} = \frac{Y_i(1 - X_i)}{X_i(1 - Y_i)} \quad (10)$$

where X_{total} and Y_{total} are the total weights or total weight fractions ($X_{\text{total}} = Y_{\text{total}} = 1$) of component *i* in the feed and permeated solutions, respectively.

2.10.3.3 Solubility and Solubility Selectivity

Solubility behavior includes adsorption, absorption, and sorption. In the definitions recommended by the International Union of Pure and Applied Chemistry (IUPAC), adsorption is the enrichment of one or more components in an interfacial layer [15]. In contrast, absorption refers to molecules penetrating the surface layer and entering the structure of the bulk solid. It is important to stress that sometimes it is difficult, impossible, or irrelevant to distinguish between adsorption and absorption. As such, it is more convenient to use the wider term sorption, which encompasses both phenomena.

In pervaporation, the first step of the transport across a membrane is the dissolution of liquid components from the surface of the membrane, while the final step involves the evaporation of vapor components from the other side of the membrane surface. At an equilibrium state, these phenomena are expressed as the partition coefficients of component *i* of the feed side ($K_{i\text{-feed}}$) and the permeate side ($K_{i\text{-permeate}}$) of the membrane:

$$K_{i\text{-feed}} = \frac{C_{i\text{-feed-membrane}}}{C_{i\text{-feed-solution}}} \quad (11)$$

$$K_{i\text{-permeate}} = \frac{C_{i\text{-permeate-membrane}}}{C_{i\text{-permeate-vapor}}} \quad (12)$$

where $C_{i\text{-feed-membrane}}$ and $C_{i\text{-permeate-membrane}}$ are the concentrations of component *i* of the interfaces of the feed and permeate sides of the membrane, respectively. The variables $C_{i\text{-feed-solution}}$ and $C_{i\text{-permeate-vapor}}$

are the concentrations of component *i* of the solution at the feed side and the vapor at the permeate side, respectively.

It is difficult to determine the partition coefficients through mere experiments, because there is a concentration gradient across a membrane. Hence, for polymer membranes, the apparent solubility coefficient in a bulk membrane is used as a measure to describe these phenomena. For inorganic membranes, an adsorption isotherm for a bulk membrane is determined. Various analyses of adsorptions on solid are described thoroughly by the IUPAC and in physical chemistry textbooks [15, 16].

The apparent solubility coefficient of a polymer membrane is correlated to the degree of swelling of a membrane with liquid. The degree of swelling of a liquid mixture in a membrane at the equilibrium state (i.e., steady state) is obtained from

$$\text{Degree of swelling (wt. \%)} = \frac{W_W - W_D}{W_D} \times 100 \quad (13)$$

where W_W is the weight of the membrane which sorbed a liquid mixture at equilibrium, and W_D is the weight of the dry membrane. The degree of swelling shows an apparent solubility phenomenon around the surface of the feed side in types II and III (Figure 3).

The solubility selectivity (α_S) of component *i* over component *j* in a binary mixture is estimated from

$$\alpha_S = \frac{\left(\frac{Z_i}{Z_j}\right)}{\left(\frac{X_i}{X_j}\right)} \quad (14)$$

where X_i and X_j are the weights of component *i* and component *j* in a mixture, respectively. The variables Z_i and Z_j are the weights of component *i* and component *j* sorbed in a membrane, respectively.

Three types of the relationships between permeate (Z_i/Z_j) and feed compositions (X_i/X_j) are illustrated in Figure 8. When either component *i* is preferably dissolved in a membrane or component *j* is selectively rejected from the membrane, the relationship is described as type A (i.e., $\alpha_S > 1$). A type-B line appears when there is no difference in the solubility of both components *i* and *j* (i.e., $\alpha_S = 1$), while type-C curve is observed as an opposite case of type A (i.e., $\alpha_S < 1$). Among the three types, type B is rarely observed.

The solubility is explained by the free energy of mixing Gibbs (ΔG_m) with the enthalpy of mixing (ΔH_m) and the entropy of mixing (ΔS_m) [16]:

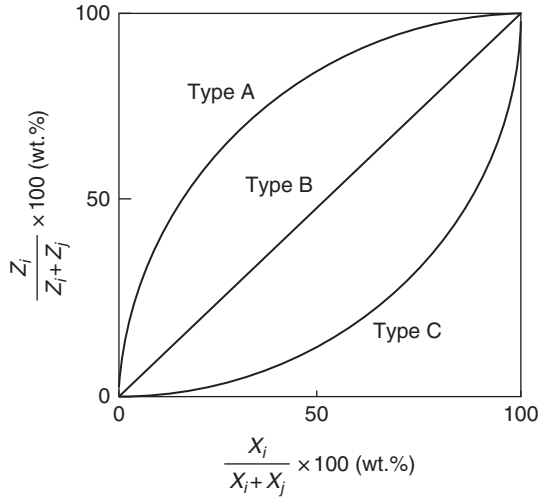


Figure 8 Relationship between permeate and feed compositions by pervaporation.

$$\Delta G_m = \Delta H_m - T\Delta S_m \quad (15)$$

where T is the absolute temperature. When the ΔG_m value is negative, components become soluble with each other. However, since the ΔS_m value is normally positive, the solubility implies dependency on the ΔH_m value.

In the case of the mixture of a liquid and the membrane material, molecules of the liquid and the membrane material are noted to interact independently, before they come in contact. When the molecules of the liquid are dissolved in the membrane, new interaction(s) between the liquid molecule and membrane material must be created. The enthalpy of mixing is then described as [17]

$$\Delta H_m = H_{\text{liquid}} + H_{\text{membrane}} - 2H_{\text{liquid-membrane}} \quad (16)$$

where H_{liquid} is the enthalpy of the liquid, H_{membrane} is the enthalpy of the membrane material, and $H_{\text{liquid-membrane}}$ is the enthalpy between the liquid and the membrane material.

The enthalpy of mixing is defined with the following solubility parameter [17]:

$$\Delta H_m = V(\delta_{\text{liquid}} - \delta_{\text{membrane}})^2 \phi_{\text{liquid}} \phi_{\text{membrane}} \quad (17)$$

where V is the total molar volume of the liquid and the membrane material, and the variables δ_{liquid} and δ_{membrane} are the solubility parameters of the liquid and membrane material, respectively. Meanwhile, ϕ_{liquid} and ϕ_{membrane} are the volume fractions of the liquid and membrane material, respectively. The solubility parameter (δ) can be determined from the cohesive energy (G_{coh}) as [18]

$$\delta = \left(\frac{G_{\text{coh}}}{V} \right)^{1/2} \quad (18)$$

According to Equation (17), the ΔH_m value is always positive, implying endothermic mixing. To produce the negative ΔG_m value, the ΔH_m value must be smaller than the $T\Delta S_m$ value, which requires a smaller difference in the solubility parameters of the liquid and the membrane material. When the solubility parameter of the liquid is equal to that of the membrane material (i.e., $\delta_{\text{liquid}} = \delta_{\text{membrane}}$), the enthalpy of mixing achieves a zero value and the free energy of mixing becomes negative. In this case, the liquid and the membrane material are soluble with each other.

Based on this concept, when a component in a mixture has a solubility parameter similar to that of the membrane material, large solubility of the given component to the membrane is thereby expected. Conversely, when the solubility parameter of a component in a mixture is quite different from that of the membrane material, less solubility (i.e., rejection) of that component to the membrane is expected.

However, when there are specifically strong interactions between molecules of the liquid and the membrane material, or if there are voids or defects in the membrane that are much larger than a molecule of the liquid, the ΔH_m value sometimes becomes negative. Under this circumstance, Equation (17) cannot be governed. In Equation (16), $2H_{\text{liquid-membrane}}$ is larger than H_{liquid} plus H_{membrane} , thereby resulting in an exothermic mixing.

To understand the selective solubility characteristics of a liquid in a membrane, Hansen's three-dimensional solubility parameters are widely demonstrated [17–19]:

$$\delta^2 = \delta_d^2 + \delta_p^2 + \delta_h^2 = \delta_d^2 + \delta_A^2 \quad (19)$$

$$V = \sum_z zV \quad (20)$$

$$\delta_d = \frac{\sum_z zF_d}{V} \quad (21)$$

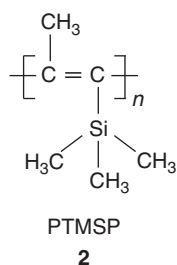
$$\delta_p = \frac{\left(\sum_z zF_p^2 \right)^{1/2}}{V} \quad (22)$$

$$\delta_h = \left(\frac{-\sum_z zU_h}{V} \right)^{1/2} \quad (23)$$

where δ is the total value, δ_d is the dispersion component, δ_p is the polar component, δ_h is the hydrogen-bonding component, and δ_A is the association cohesion parameter (i.e., $\delta_p + \delta_h$). The variable zF_d is the group contribution to the dispersion, zF_p is the group contribution to the polar parameter, zU_h is the group contribution to the hydrogen-bonding parameter, and V is the group molar volume.

Another measure of the solubility parameter is the one which relatively describes the strength of hydrogen bonding in a molecule (i.e., δ (poorly), δ (moderately), or δ (strongly)) [18, 19].

For example, poly(1-trimethylsilyl-1-propyne) (PTMSP, **2**) has less polar structure with a δ value of $15.8 \text{ MPa}^{1/2}$ [20], which was estimated using the group contribution method of Fedors [21]. The solubility of PTMSP in pure organic liquids was dependent on δ_A than δ_d (Figure 9) [22]. There were both solvents and nonsolvents in the δ_d value of $14\text{--}19 \text{ MPa}^{1/2}$, while most of the solvents involved a δ_A value smaller than about $10 \text{ MPa}^{1/2}$. The PTMSP was observed to be preferably soluble to several less polar liquids with smaller δ_A . In addition, PTMSP was soluble to the liquids with a δ (poorly) value of $13.5\text{--}19.4 \text{ MPa}^{1/2}$. The uptake of various pure nonsolvents in the PTMSP membrane at 25°C increased when the δ values of a liquid and PTMSP were similar to each other (Figure 10) [22]. This trend was consistent with the rule provided by Equation (17). The PTMSP was not soluble in the polar liquids even if their δ was near the PTMSP value (e.g., δ (moderately)).



However, as in a contour map, all liquid molecules have a gradient of electronic charge, and it is difficult to find an exact borderline of solubility factors, such as in hydrogen bonding (Figure 11). This indicates the limitation of using the solubility parameter to accurately estimate the solubility phenomena.

2.10.3.4 Diffusivity and Diffusivity Selectivity

In principle, Fick's law (type I, Figure 3) describes the diffusion coefficient for both polymer and

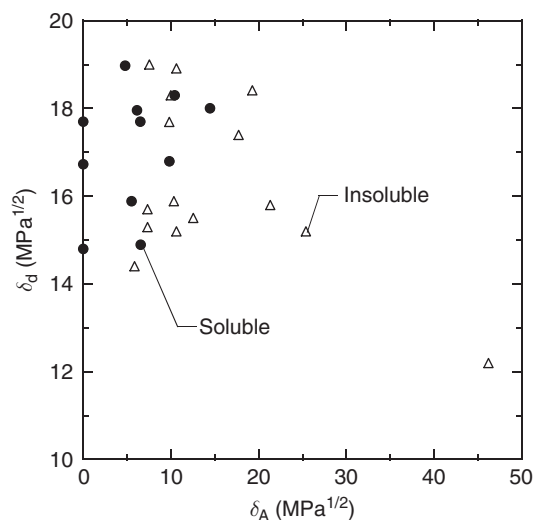


Figure 9 Relationship between δ_d and δ_A values of solvents and nonsolvents of poly(1-trimethylsilyl-1-propyne) at 25°C . Reproduced from Nagai, K., Ohno, M., Nakagawa, T. *Membrane* **1999**, 24, 215–220.

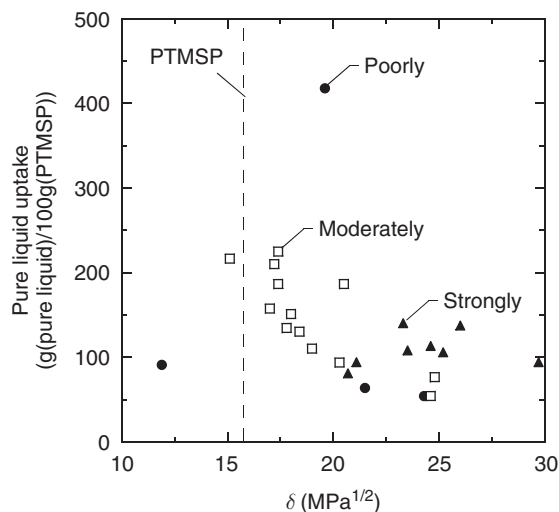


Figure 10 Pure liquid uptake of nonsolvents of poly(1-trimethylsilyl-1-propyne) at 25°C , as a function of solubility parameter (δ) of their nonsolvents with hydrogen bonding factors: δ (poorly), δ (moderately), and δ (strongly). Reproduced from Nagai, K., Ohno, M., Nakagawa, T. *Membrane* **1999**, 24, 215–220.

inorganic membranes. However, it is strongly affected by the concentration of the components in a polymer membrane. The concentration-dependent diffusion coefficient is defined as [23]

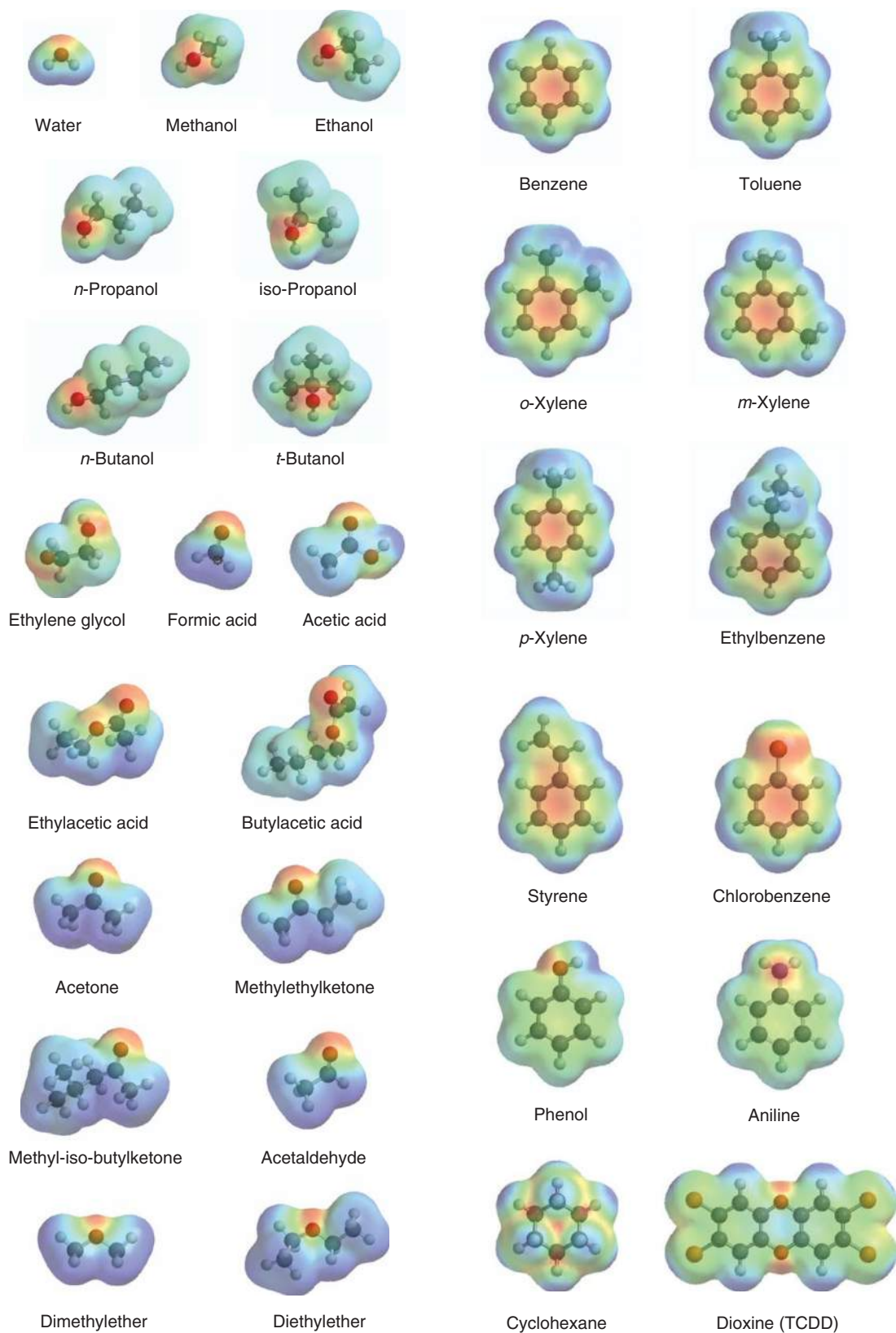


Figure 11 Electronic charge of various small molecules and membrane materials.

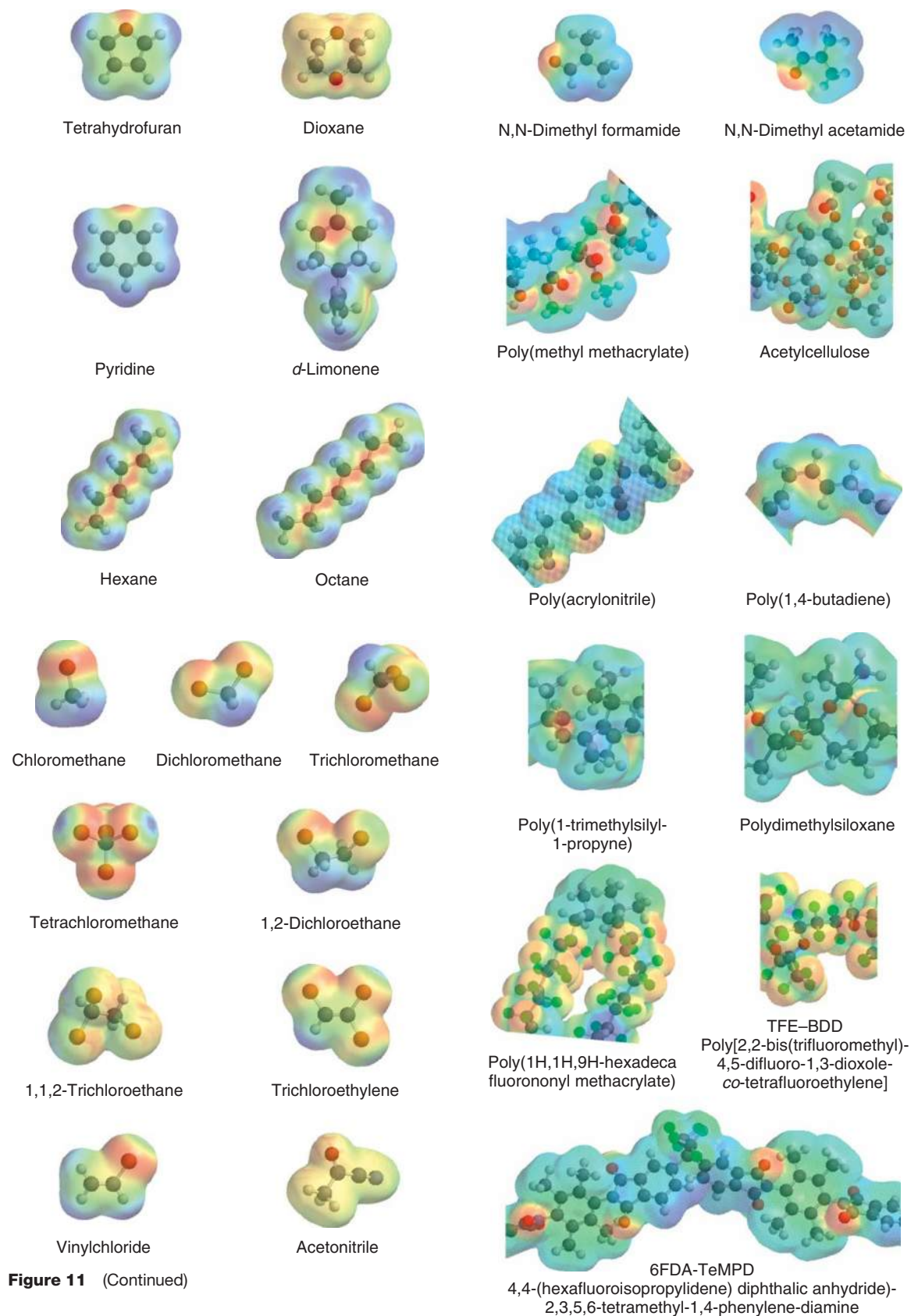


Figure 11 (Continued)

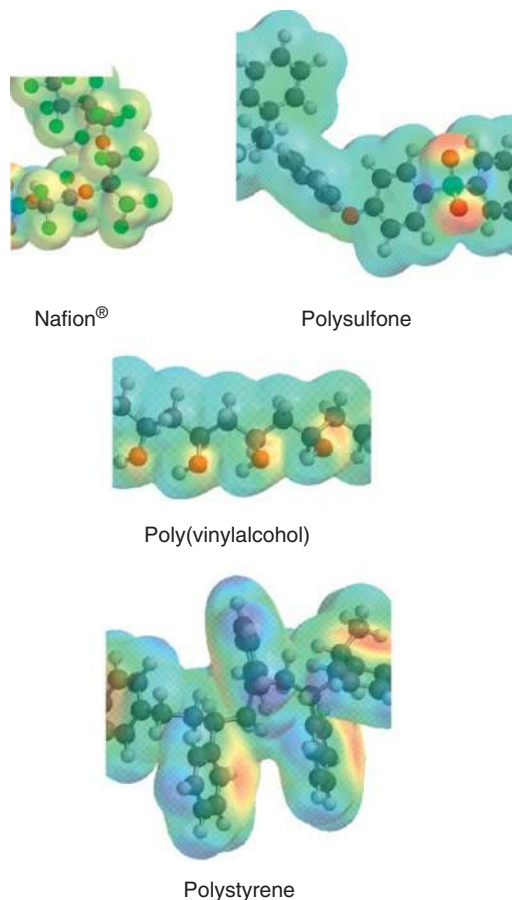


Figure 11 (Continued)

$$D = D_0 \exp(\beta C) \quad (24)$$

where D is the diffusion coefficient at the concentration C , D_0 is the diffusion coefficient at infinite dilution when the concentration C is zero, and β is the plasticization factor, indicating interactions between a membrane material and a component. The larger β value indicates stronger affinity between a membrane material and a component. For example, when (1) the D_0 value is an order of $10^{-9} \text{ cm}^2 \text{ s}^{-1}$, (2) the β value varies from 20 to 90, and (3) a swelling ratio of a membrane to a component is 10 wt.% (i.e., $C=0.1$), the diffusion coefficient becomes more than 1000 times larger than that of the dried membrane (i.e., $C=0$) [24].

The transport of small molecules in the dried non-swollen layer of the polymer membrane in types II and III in **Figure 3** is almost similar for vapor and gas separation membranes, when the permeate side is held under a vacuum. Hence, penetrant-induced plasticization affects both the dried and the liquid-swollen

layer. **Figure 12** presents the pressure dependence on the average diffusion coefficient of carbon dioxide in dried 4,4-(hexafluoroisopropylidene) diphthalic anhydride (6FDA)-2,3,5,6-tetramethyl-1,4-phenylenediamine (TeMPD) polyimide (6FDA-TeMPD, **3**) membranes prepared with dichloromethane to as much as 40 atm (i.e., relative pressure at about 0.5) at a given time with a temperature of 35°C [25]. The average diffusion coefficient increased along with increasing pressure in the feed. **Figure 13** presents the diffusion coefficient of carbon dioxide at a given time in the same 6FDA-TeMPD membrane as a function of CO_2 concentration at 35°C [25]. As can be seen, the diffusion coefficient increased along with the increasing concentration of carbon dioxide. However, in this study, there was no obvious correlation in the carbon dioxide concentration values at the critical plasticization pressure as determined from gas permeability. The critical average diffusion coefficient of carbon dioxide was $(73 \pm 5) \times 10^{-8} \text{ cm}^2 \text{ s}^{-1}$ at 35°C

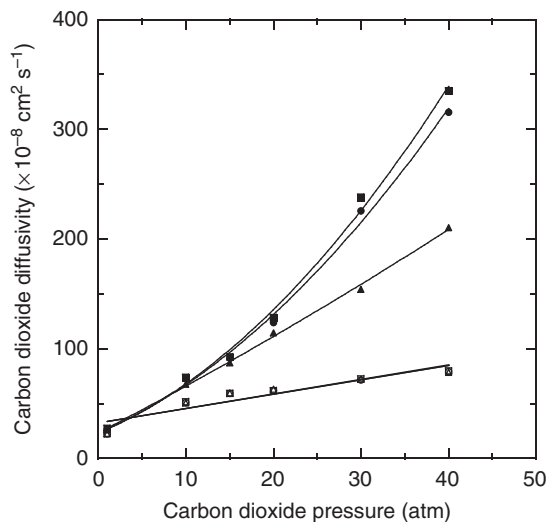


Figure 12 The pressure dependence of carbon dioxide diffusion coefficient in 6FDA-TeMPD prepared from the dichloromethane solution at a given time at 35 °C: (a) after 5 min (\blacktriangle , \triangle), (b) after 360 min (\bullet , \circ), and (c) after 720 min (\blacksquare , \square) for (as-cast, heat-treated). Reproduced from Kanehashi, S., Nakagawa, T., Nagai, K., Duthie, X., Kentish, S., Stevens, G. *J. Membr. Sci.* **2007**, 298, 147–155.

for the dried 6FDA-TeMPD membranes at the critical plasticization pressure, despite membrane preparation protocols (i.e., casting solvent and thermal treatment).

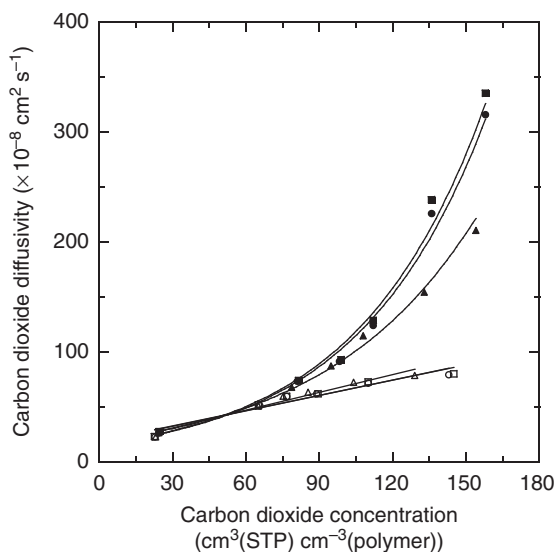
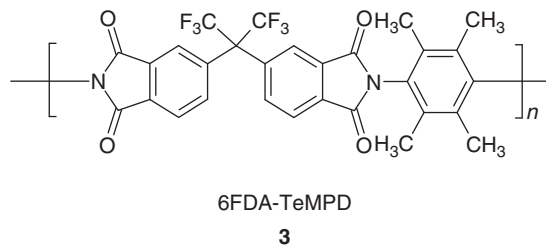


Figure 13 Carbon dioxide diffusion coefficient in 6FDA-TeMPD prepared from the dichloromethane solution at a given time at 35 °C, as a function of carbon dioxide concentration: (a) after 5 min (\blacktriangle , \triangle), (b) after 360 min (\bullet , \circ), and (c) after 720 min (\blacksquare , \square) for (as-cast, heat-treated). Reproduced from Kanehashi, S., Nakagawa, T., Nagai, K., Duthie, X., Kentish, S., Stevens, G. *J. Membr. Sci.* **2007**, 298, 147–155.



During transport in the dried layer of the polymer membrane at the initial stage of measurement (i.e., nonsteady state), there is an observed intermittent relaxation of polymer segments as well as the manifestation of a Fickian diffusion behavior. In general, this has been referred to as non-Fickian diffusion. A kinetic sorption analysis provides the following equation as a function of measurement time t [26]:

$$C = C_F + C_R[1 - \exp(-\tau t)] \quad (25)$$

where C_F and C_R are the concentrations of Fickian diffusion and relaxation contribution at equilibrium, respectively, and τ is the kinetic constant for relaxation.

When the diffusion of small molecules occurs much faster than the relaxation of polymer segments, a distinct interface layer appears between the swollen and the nonswollen layers. With this relaxation becoming the rate-determining step, the interface layer moves at the constant speed across the cross section of the membrane. This behavior is called case II diffusion [27].

$$C = k t^n \quad (26)$$

where k and n are the adjustable parameters. Case II diffusion occurs at $n = 1$ [28]. Fickian diffusion and case II diffusion are simultaneously observed at $0.5 < n < 1.0$.

The diffusion of the small molecules in gas or vapor phase across a polymer membrane is correlated to its fractional free volume (FFV), and this relation holds when there is no or little interaction between the penetrant molecules and the polymer chain. The free-volume theory provides the following equation [29]:

$$D = A_D \exp\left(-\frac{B_D}{\text{FFV}}\right) \quad (27)$$

where A_D and B_D are adjustable parameters, and both of them represent inherent diffusion parameters correlated with the penetrant size and shape.

However, these parameters have not yet been clearly discussed. One reason is that, although there are varying measures of the size and shape of a small molecule, the optimum measure of the penetrant size

and shape has not been defined for this theory. Their measures include kinetic diameter, critical volume, van der Waals volume, and diameter determined from Lennard-Jones force constant [30–32]. As presented in Figure 11, the shape of molecules is not a monatomic structure. Both the area of the cross section (i.e., minimum diffusion gap) and the length of a molecule (i.e., diffusion path) affect diffusion in a membrane [33]. In addition, several vibrations have been monitored in molecules (e.g., stretching, scissoring, and twisting vibrations) as detected by infrared or Raman spectroscopy [16]. These vibrations manifest in different shapes at the moment even if molecules exist in a membrane.

Figure 14 presents the diffusion coefficient of carbon dioxide, of common glassy polymers in a dry state as a function of FFV at a feed pressure of 10 atm (i.e., relative pressure of about 0.1) [34]. The diffusion coefficient tended to decrease with increasing reciprocal FFV as expected from Equation (27). However, these data were scattered with carbon dioxide diffusivity varying from 10^{-6} to 10^{-8} $\text{cm}^2 \text{s}^{-1}$ at the $1/\text{FFV}$ value of 5.5 (i.e., FFV is 0.18), as shown in Figure 14. In contrast, better linear correlation coefficients were reported only for structurally related polymers, such as polycarbonates, polysulfones, or polyarylates. This behavior illustrates the limitations of the use of Equation (27) in estimating the diffusion coefficient of small molecules, and suggests that accurate

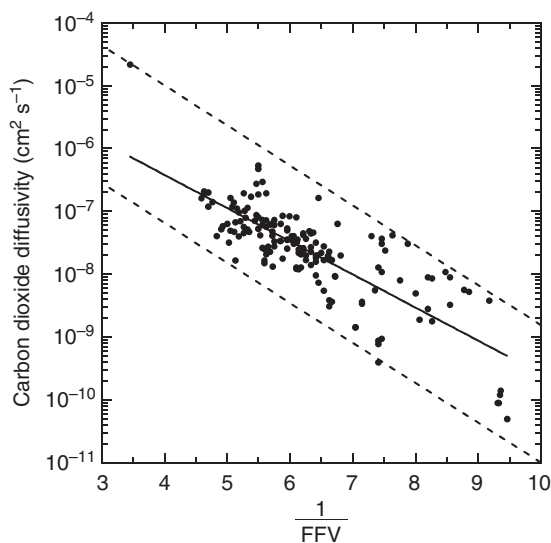
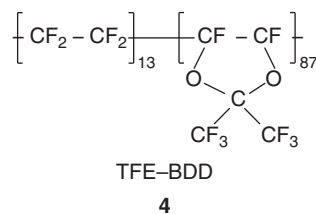


Figure 14 Carbon dioxide diffusion coefficient of various polymers at 35 °C at a feed pressure of 10 atm (i.e., relative pressure: about 0.1), as a function of reciprocal fractional free volume ($1/\text{FFV}$). Reproduced from Kanehashi, S., Nagai, K. *J. Membr. Sci.* **2005**, 253, 117–138.

correlations can only be obtained for structurally related polymers.

These less-accurate correlations are due to the distribution of free-volume space, which can be estimated using positron annihilation lifetime spectroscopy (PALS) [35]. The PALS data are analyzed using parameter τ_n (ns) as space size and parameter I_n (%) as the amount of space τ_n . Space size increases with an increasing n value, and for most of the polymers, the values lie between τ_1 and τ_3 levels. Until now, the τ_4 level space has only been reported for some substituted polyacetylenes (e.g., PTMSP) and fluorinated polymers (e.g., poly(2,2-bis(trifluoromethyl)-4,5-difluoro-1,3-dioxole-*co*-tetrafluoroethylene) (TFE-BDD, **4**) [35–37]. Gas diffusivity is correlated with the reciprocal values of $\tau_3^3 \times I_n$ ($\text{ns}^3\%$), which is the total volume of τ_3 level space in a polymer membrane. Gas diffusion in PTMSP and TFE-BDD is described in terms of $\tau_4^3 \times I_n$ and/or $\tau_3^3 \times I_n + \tau_4^3 \times I_n$ ($\text{ns}^3\%$). Meanwhile, the connectivity of τ_1 – τ_4 level space across a polymer membrane has also been identified as an important factor in determining gas diffusion.



As mentioned previously, the classical free-volume theory does not take into account the effects of interaction between the penetrant molecules and the polymer chains. However, the dielectric constant of polymer membranes is correlated to FFV, which is strongly influenced by the polarity of polymers. Based on Clausius–Mossotti equation, the diffusion coefficient of small molecules is defined as functions of the dielectric constant, ϵ , and is given as [38]

$$D = \gamma_D \exp\left(\frac{-\beta_D}{1-\alpha}\right) \quad (28)$$

where

$$\alpha = 1.3 \frac{V_W \epsilon - 1}{P_{LL} \epsilon + 2}$$

with γ_D and β_D being adjustable constants, V_W the specific van der Waals volume, and P_{LL} the molar polarization.

The diffusion coefficients of small molecules in a family of 6FDA-based polyimides provided a

linear relationship as a function of the reciprocal of $1-\alpha$. Moreover, the $1-\alpha$ values of the 6FDA-based polyimides were 1.6–2.2 times larger than their FFV values. As expected from Equation (27), the FFV was mainly dependent only on the free-volume space in a membrane. On the other hand, the $1-\alpha$ (i.e., FFV determined from Equation (28)) was dependent on free-volume space and electric factors, such as molar polarization, which affected the interactions between the gas molecules and the polymer segments. A comparison across the family of polymers proves that this factor provides for a more actual adjustment for transport of small molecules in a free volume of a polymer membrane.

When a membrane is swollen by the feed solution, as illustrated in types II and III of Figure 3, the apparent average diffusion coefficient of each component in a total membrane (i.e., the liquid-swollen layer plus the dried nonswollen layer) can be estimated according to Aptel's study. The flux of component i (\mathcal{F}_i) and component j (\mathcal{F}_j) through a membrane (thickness, l) is defined as [39]

$$\mathcal{F}_i = \frac{\bar{D}_i k S_i}{l} \quad (29)$$

$$\mathcal{F}_j = \frac{\bar{D}_j k S_j}{l} \quad (30)$$

where \bar{D}_i and \bar{D}_j are the apparent average diffusion coefficients of component i and component j , respectively. The variables S_i and S_j are the degree of swelling of component i and component j , respectively. Similarly, k is obtained as

$$k = \frac{1}{\frac{S_i}{\rho_i} + \frac{S_j}{\rho_j} + \frac{100}{\rho_m}} \quad (31)$$

where ρ_i , ρ_j , and ρ_m are density values of component i , component j , and the membrane, respectively. Finally, the diffusivity selectivity (α_D) of component i over component j in a binary mixture can be estimated as

$$\alpha_D = \frac{\bar{D}_i}{\bar{D}_j} \quad (32)$$

2.10.3.5 Combination of Selectivities

The permselectivity or separation factor (α_P) of component i over component j in a binary mixture is defined as the ratio of the permeabilities or fluxes

of component i over component j (P_i/P_j), and thus, can be expressed as

$$\alpha_P = \alpha_S \alpha_D = \frac{P_i}{P_j} = \left(\frac{S_i}{S_j} \right) \times \left(\frac{D_i}{D_j} \right) \quad (33)$$

The first term represents solubility selectivity, while the second one is concerned with diffusivity selectivity.

When the diffusivities of both components are similar, the diffusivity selectivity is ~ 1 and the permselectivity is approximately equal to the solubility selectivity:

$$\alpha_P \approx \alpha_S = \frac{P_i}{P_j} \approx \frac{S_i}{S_j} \quad (34)$$

In contrast, when the solubilities of both components are similar, the solubility selectivity is ~ 1 . The permselectivity is then approximately equal to the diffusivity selectivity:

$$\alpha_P \approx \alpha_D = \frac{P_i}{P_j} \approx \frac{D_i}{D_j} \quad (35)$$

Membranes are required to have either the component i selectivity (i.e., $(P_i/P_j) > 1$) or the component j selectivity (i.e., $(P_i/P_j) < 1$). When component i is a larger molecule than component j , on the basis of the size-sieving diffusion, the diffusivity selectivity is always $(D_i/D_j) < 1$. On the other hand, the solubility coefficient is correlated to the solubility parameters of a membrane material and a liquid. As previously mentioned, the affinity of a liquid with a membrane is determined by the extent of congruence between their solubility parameters. Thus, when the solubility parameter of component i is closer to that of a membrane material as compared to component j , the membrane shows component i -selectivity (i.e., $(S_i/S_j) > 1$) from the mixture and vice versa. In cases where the diffusivity selectivity is the dominant contributing factor, $(S_i/S_j) < (D_i/D_j)$, the membrane shows a component j -selective behavior (i.e., $(P_i/P_j) < 1$). In contrast, when the solubility selectivity is the dominant factor for separation, $(S_i/S_j) > (D_i/D_j)$, this membrane has a component i -selectivity (i.e., $(P_i/P_j) > 1$). As illustrated in this example, controlling the solubility and/or diffusivity selectivity is a requisite for achieving an increase in both types of permselectivity.

Solubility and diffusivity have concentration-dependent behaviors. When the composition in the feed solution is changed, the solubility and diffusivity of each component change. As a result, each component's permeability is modified as well. This indicates that the composition in the feed solution affects the permselectivity, solubility selectivity, and diffusivity selectivity of a membrane.

Figure 15 presents the total flux of benzene–aniline mixtures through the γ -ray irradiated polyethylene membrane at 25 °C as a function of benzene concentration in the feed solution [40]. This polymer was effectively swollen by benzene as compared to aniline. As the benzene (i.e., the component with better affinity with the membrane) concentration in the feed solution increased, the total flux of the mixtures dramatically increased. Regardless of feed concentration, benzene had always permeated through this membrane faster than aniline (Figure 16) [40]. The permselectivity of benzene over aniline also decreased with increasing benzene concentration in the feed solution (Figure 17) [40]. The benzene molecules swelled the membrane, enabling it to easily accompany the aniline molecules in expanded polymer segments.

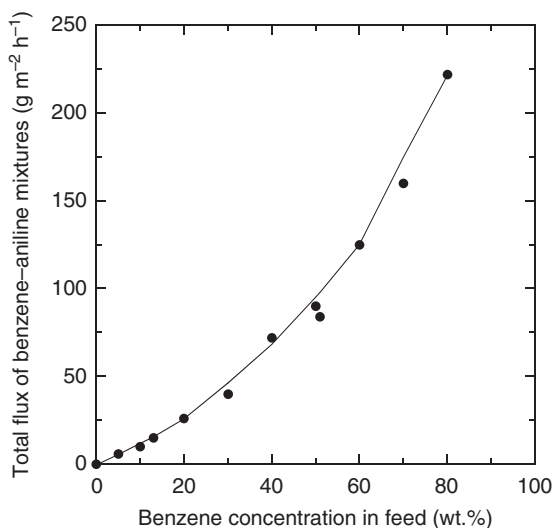


Figure 15 Total flux of benzene–aniline mixtures through the γ -ray irradiated low-density polyethylene membrane at 25 °C, as a function of benzene concentration in the feed solution. Reproduced from Yamada, S., Hamaya, T. *Kobun. Ronbun. (Jpn. J. Polym. Sci. Tech.)* 1976, 33, 217–223.

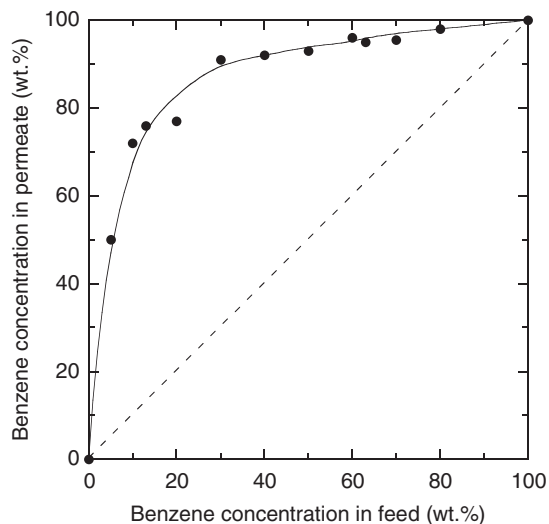


Figure 16 Benzene concentrations in permeate and feed solutions by pervaporation of benzene–aniline mixtures through the γ -ray irradiated low-density polyethylene membrane at 25 °C. Reproduced from Yamada, S., Hamaya, T. *Kobun. Ronbun. (Jpn. J. Polym. Sci. Tech.)* 1976, 33, 217–223.

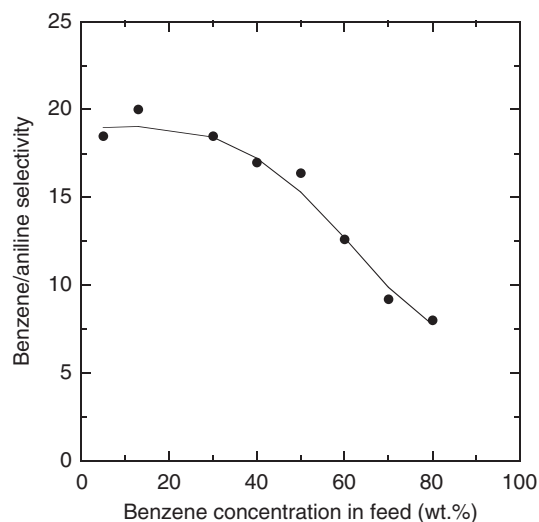


Figure 17 Benzene/aniline selectivity of the γ -ray irradiated low-density polyethylene membrane at 25 °C, as a function of benzene concentration in the feed solution. Reproduced from Yamada, S., Hamaya, T. *Kobun. Ronbun. (Jpn. J. Polym. Sci. Tech.)* 1976, 33, 217–223.

2.10.3.6 Temperature Dependence

Without any transition (e.g., glass transition of a polymer, or boiling point of a liquid) in the membrane materials and penetrant, and when the permeate pressure is maintained much lower than the saturation pressure of a given liquid, the temperature

dependence on mass transport generally follows Arrhenius rule. That is, there is a linear relationship between a transport parameter logarithm and the reciprocal of the absolute temperature (T). The permeability coefficient (P) is expressed as

$$P = P_0 \exp\left(-\frac{E_P}{RT}\right) \quad (36)$$

where P_0 is the pre-exponential factor of permeation, E_P is the activation energy for permeation, and R is the gas constant.

The solubility coefficient (S) and diffusion coefficient (D) are also given the following expressions with van't Hoff–Arrhenius rules:

$$S = S_0 \exp\left(-\frac{\Delta H_S}{RT}\right) \quad (37)$$

$$D = D_0 \exp\left(-\frac{E_D}{RT}\right) \quad (38)$$

where S_0 and D_0 are the pre-exponential factors of solubility and diffusivity, ΔH_S is the heat of sorption, and E_D is the activation energy for diffusion. The heat of sorption is described together with the enthalpy of mixing (ΔH_m) in Equation (15) and the heat of condensation (ΔH_c)

$$\Delta H_S = \Delta H_m + \Delta H_c \quad (39)$$

The ΔH_c value is always negative; however, as previously mentioned, the ΔH_m value is dependent on the situation.

Based on the solution–diffusion mechanism, as described in Equation (6), Equation (36) can be rewritten with Equations (37) and (38):

$$P = P_0 \exp\left(-\frac{E_P}{RT}\right) = S_0 D_0 \exp\left(-\frac{\Delta H_S + E_D}{RT}\right) \quad (40)$$

Hence, P_0 and E_P can be provided by

$$P_0 = S_0 D_0 \quad (41)$$

$$E_P = \Delta H_S + E_D \quad (42)$$

In general, as temperature increases, solubility decreases while diffusivity increases. Therefore, the heat of sorption is negative and the activation energy for diffusion is always positive. When solubility is dominant for permeation as compared to diffusion, the activation energy for permeation must be negative and vice versa.

The permselectivity or separation factor (α_P) of component i over component j in a binary mixture is defined from

$$\alpha_P = \frac{P_i}{P_j} = \frac{P_{i0}}{P_{j0}} \exp\left(-\frac{E_{Pi} - E_{Pj}}{RT}\right) \quad (43)$$

Likewise, the solubility selectivity and diffusivity selectivity are shown as

$$\alpha_S = \frac{S_i}{S_j} = \frac{S_{i0}}{S_{j0}} \exp\left(-\frac{\Delta H_{Si} - \Delta H_{Sj}}{RT}\right) \quad (44)$$

$$\alpha_D = \frac{D_i}{D_j} = \frac{D_{i0}}{D_{j0}} \exp\left(-\frac{E_{Di} - E_{Dj}}{RT}\right) \quad (45)$$

2.10.3.7 Experimental Methods

In journal articles reporting on pervaporation, the flat membrane is most commonly used for polymer materials as compared to the hollow-fiber and tubular-type membrane. In contrast, tubular-type membranes are more popular for inorganic materials. The pervaporation experiment is performed in research laboratories by either a dead-end batch style or a continuous-flow style. In order to provide a driving force for permeation, the permeate side of the pervaporation membrane is maintained either under a vacuum (i.e., vacuum-driven pervaporation, **Figures 18 and 19**) or by sweeping a noncondensable carrier gas, such as nitrogen and helium (i.e., carrier gas-driven pervaporation). Most experimental data reported in journal articles have been recorded at a given constant temperature. However, when a temperature gradient appears across a membrane, the driving force for permeation is enhanced. This method is called thermopervaporation where the feed liquid is heated before permeation.

The permeated vapor is normally condensed as liquid, which is achieved by using a condenser such as liquid nitrogen, and then the weight or volume of the permeated product is determined. The flux is then calculated using Equation (7) along with the data of the membrane area and measurement time data. The compositions of the feed and permeate solutions are determined using an analyzer, such as gas chromatograph, and the permselectivity is calculated using Equations (9) and (10).

In general, the flux and permselectivity are dependent on the concentration in the feed solution. Scientists have then reported on the relationships between permeate composition and feed composition, between permselectivity and feed composition, and between flux and feed composition (see **Figures 15–17**) [40].

As mentioned previously, the phase transition from a liquid phase to a vapor phase appears during

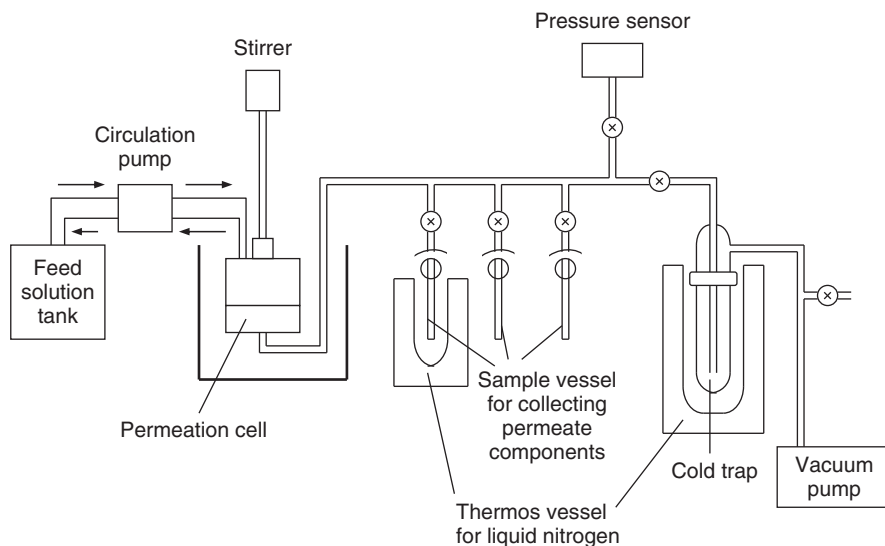


Figure 18 Schematic diagram of a batch-type permeation cell for pervaporation.

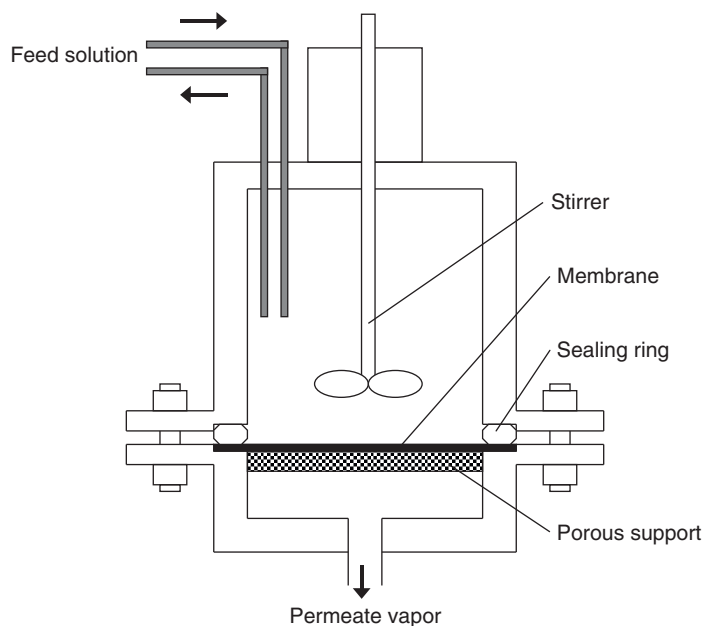


Figure 19 Schematic diagram of a batch-type permeation cell for pervaporation.

transport through a membrane, with a partial pressure difference of about 1 atm. Therefore, as compared to other membrane separation processes, internal stress in a membrane material is large. The pressure loss sometimes induces a significant decrease in the temperature and pressure. The heat of evaporation is always required, because the permeate components are evaporated from the membrane surface.

The composition of a liquid mixture sorbed in a membrane at equilibrium can be analyzed. The sample membrane is soaked in a solution until it achieves an equilibrium sorption state. The liquid mixture sorbed in the membrane is evaporated from the sample and collected with a cold trap cooled by liquid nitrogen, as illustrated in [Figure 20](#) [41]. The composition can be determined using an analyzer, such as gas chromatograph. For example, when the collected

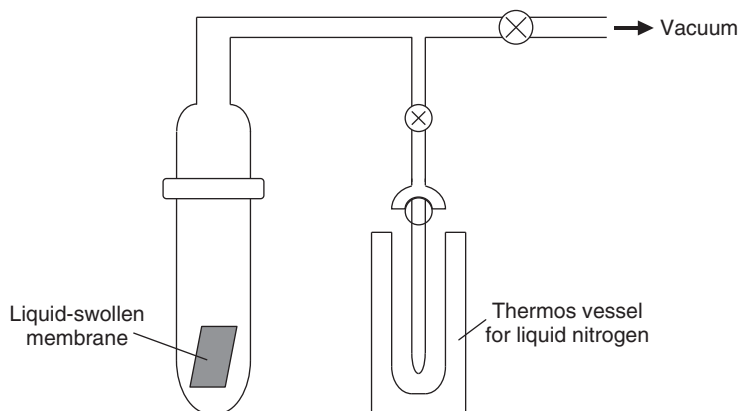


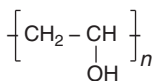
Figure 20 Schematic diagram of a batch-type apparatus for estimation of solubility selectivity.

product is separated in two phases, this can be homogeneously dissolved in an optimum solvent for both components. Finally, the solubility selectivity is calculated using Equation (14).

2.10.4 Membrane Materials and Pervaporation Properties

2.10.4.1 Combination of Solubility Selectivity and Diffusivity Selectivity

The first commercial-scale membrane system of liquid separation was established for the separation of an ethanol–water mixture by pervaporation in 1982 [1]. The composite membrane with a crosslinked PVC 5 dense layer onto a porous polyacrylonitrile support was used [42]. This had water-selective behavior for an ethanol or iso-propanol aqueous solution.



PVC

5

In the case of polymer membranes, a family of polymers has a general tendency to exhibit either water selectivity or VOC selectivity. The transport is thought to conform to the solution–diffusion mechanism. **Table 1** summarizes the strategies for VOC–water separation membranes. As the size of VOC molecules is larger than water, ($D_{\text{VOC}}/D_{\text{H}_2\text{O}}$) is smaller than 1 for the polymers where separation is affected by the size-sieving diffusion. The affinity of

a VOC–water mixture with a polymer membrane is determined by the extent of congruence between the solubility parameters of the two. Hence, hydrophilic polymer membranes normally show ($S_{\text{VOC}}/S_{\text{H}_2\text{O}}$) to be smaller than 1 (i.e., water-selective membrane 1 in **Table 1**), while hydrophobic polymer membranes tend to show that ($S_{\text{VOC}}/S_{\text{H}_2\text{O}}$) is larger than 1 (i.e., water-selective membrane 2 and VOC-selective membrane 1 in **Table 1**). In cases where diffusivity selectivity is the dominant contributing factor, ($S_{\text{VOC}}/S_{\text{H}_2\text{O}} < D_{\text{VOC}}/D_{\text{H}_2\text{O}}$), the membrane shows water-selective behavior even though ($S_{\text{VOC}}/S_{\text{H}_2\text{O}} > 1$) (i.e., water-selective membrane 2 in **Table 1**).

In the process of pervaporation, permeation through a membrane is the rate-determining step; therefore, a minor component of the mixture must be removed by selective permeation through the membrane to minimize the amount of permeate liquid. Preferential water permeation (water

Table 1 Strategies for VOC–water separation membranes

<i>Water-selective membrane 1</i>	<i>Water-selective membrane 2</i>	<i>VOC-selective membrane 1</i>
$\frac{S_{\text{VOC}}}{S_{\text{H}_2\text{O}}} < 1$	$\frac{S_{\text{VOC}}}{S_{\text{H}_2\text{O}}} > 1$	$\frac{S_{\text{VOC}}}{S_{\text{H}_2\text{O}}} \gg \gg 1$
$\frac{D_{\text{VOC}}}{D_{\text{H}_2\text{O}}} < 1$	$\frac{D_{\text{VOC}}}{D_{\text{H}_2\text{O}}} \ll \ll 1$	$\frac{D_{\text{VOC}}}{D_{\text{H}_2\text{O}}} < 1$
$\frac{P_{\text{VOC}}}{P_{\text{H}_2\text{O}}} \ll < 1$	$\frac{P_{\text{VOC}}}{P_{\text{H}_2\text{O}}} \ll < 1$	$\frac{P_{\text{VOC}}}{P_{\text{H}_2\text{O}}} \gg > 1$

Table 2 Ethanol/water selectivity and normalized flux of substituted polyacetylenes in ethanol–water pervaporation (ethanol feed concentration: 10 wt.%) at 30 °C

R^1	$-(-CR^1=CR^2-)_n-R^2$	Permeate pressure (mmHg)	Thickness (μm)	Ethanol/water selectivity	Normalized flux ($10^{-3} \text{ g m}^{-2} \text{ h}^{-1}$)	Reference
(a) Ethanol-selective						
CH ₃	Si(CH ₃) ₃	1.0	ca. 20	12	4.5	[44]
Phenyl	C ₆ H ₄ - <i>p</i> -Si(CH ₃) ₃	2.0	53	6.9	4.2	[44]
Phenyl	Phenyl	2.0	46	6.0	5.9	[44]
β -Naphthyl	C ₆ H ₄ - <i>p</i> -Si(CH ₃) ₃	2.0	32	5.3	6.9	[44]
Phenyl	β -Naphthyl	2.0	45	3.4	14	[44]
Cl	<i>n</i> -C ₆ H ₁₃	1.0	ca. 20	1.1	0.41	[43]
(b) Water-selective						
CH ₃	<i>n</i> -C ₅ H ₁₁	1.0	ca. 20	0.72	0.57	[43]
H	<i>tert</i> -Butyl	1.0	ca. 20	0.58	0.65	[43]
H	CH(<i>n</i> -C ₅ H ₁₁)Si(CH ₃) ₃	1.0	ca. 20	0.52	0.40	[43]
CH ₃	Phenyl	1.0	ca. 20	0.28	0.24	[43]
Cl	Phenyl	1.0	ca. 20	0.21	0.23	[43]

selectivity) is the characteristic feature of most polymers, and there have been some reports about VOC-selective polymers to date. Substituted polyacetylenes show a good example of a class of polymers, which exhibits both VOC- and water-selectivity behaviors [9].

Table 2 summarizes the total flux and ethanol/water selectivity of various VOC- and water-selective substituted polyacetylene membranes [43, 44]. The highly permeable substituted polyacetylene membranes were ethanol selective (i.e., ethanol/water selectivity > 1), whereas the less-permeable substituted polyacetylenes were water selective (i.e., ethanol/water selectivity < 1). The PTMSP membrane with a membrane thickness of about 20 μm had a total flux of $4.5 \times 10^{-3} \text{ g m}^{-2} \text{ h}^{-1}$ with an ethanol/water selectivity of 4.5, whereas the poly(1-phenyl-2-chloroacetylene) membrane had a total flux of $0.23 \times 10^{-3} \text{ g m}^{-2} \text{ h}^{-1}$ with an ethanol/water selectivity of 0.21.

The PTMSP membrane showed the ($S_{\text{EtOH}}/S_{\text{H}_2\text{O}}$) value to be larger than 1 and the ($D_{\text{EtOH}}/D_{\text{H}_2\text{O}}$) value to be smaller than 1. However, as the solubility selectivity was the factor (i.e., ($S_{\text{EtOH}}/S_{\text{H}_2\text{O}}$) > ($D_{\text{EtOH}}/D_{\text{H}_2\text{O}}$)) which dominated the overall permeability selectivity in this case, ($P_{\text{EtOH}}/P_{\text{H}_2\text{O}}$) was larger than 1 for the PTMSP membrane (i.e., VOC-selective membrane 1 in **Table 1**). Some substituted polyacetylene membranes exhibited water selectivity despite their hydrophobic nature, as shown in **Table 2**. They preferentially sorbed ethanol, hence, the solubility selectivity would be larger than 1 of ($S_{\text{EtOH}}/S_{\text{H}_2\text{O}}$), but as the overall permeation selectivity

($P_{\text{EtOH}}/P_{\text{H}_2\text{O}}$) was smaller than 1, the diffusivity effect was probably of greater significance in this case ($S_{\text{EtOH}}/S_{\text{H}_2\text{O}} < D_{\text{EtOH}}/D_{\text{H}_2\text{O}}$) (i.e., water-selective membrane 2 in **Table 1**).

The flux and alcohol/water selectivity of an alcohol–water mixture by pervaporation of alcohol-selective PTMSP membrane decreased (e.g., methanol > ethanol > *n*-propanol) with increasing size of alcohol (e.g., methanol < ethanol < *n*-propanol) [45]. The pervaporation properties of the PTMSP membrane depended on the solubility based on the alcohols' polarity. Less polar PTMSP preferentially sorbed less polar alcohols. The selectivity of isopropanol/water was higher than that of *n*-propanol/water due, presumably, to the higher affinity of isopropanol to PTMSP than *n*-propanol.

Among BTX and xylene isomers, the physical properties are very similar (**Table 3**) [18, 31, 46]. However, in the case of the PTMSP membrane, as summarized in the same table, the normalized flux and BTX/water selectivity were different from each other [47, 48]. The ranking of normalized flux at 25 °C was toluene > benzene > *o*-xylene > *p*-xylene > *m*-xylene. The ranking of BTX/water selectivity was *o*-xylene > *m*-xylene > toluene > *p*-xylene > benzene. As mentioned previously, the total selectivity of the PTMSP membrane was correlated to solubility selectivity. Xylene isomers have the same solubility parameter. The selectivity ranking for xylene isomers was correlated to that of dipole moment. BTX with a larger dipole moment value had larger BTX/water selectivity. The ranking of

Table 3 Physical properties of water and BTX, and pervaporation data of BTX/water binary mixtures through the poly(1-trimethylsilyl-1-propyne) membrane (thickness, 120 μm) at 25 °C at the permeate pressure below 0.1 mmHg

<i>Penetrant</i>	<i>Molar volume [31] ($\text{cm}^3\text{mol}^{-1}$)</i>	<i>Dipole moment [31] (debye)</i>	<i>Solubility parameter [18] ($\text{MPa}^{1/2}$)</i>	<i>Equilibrium vapor pressure at 20 °C [46] (mmHg)</i>	<i>Solubility to water at 25 °C [46] (mg l^{-1})</i>	<i>Feed concentration of BTX [47, 48] (ppm)</i>	<i>BTX normalized flux [47, 48] ($\text{kg } \mu\text{m m}^{-2} \text{h}^{-1}$)</i>	<i>BTX/water selectivity [47, 48]</i>
Water	18.07	1.8	47.9	17.5	-	-	-	-
Benzene	89.4	0.0	18.8	100 ^a	1780	200	1.1	1300
Toluene	106.9	0.4	18.2	22	470	200	1.5	1900
<i>o</i> -Xylene	121.3	0.5	18.0	5.0	171	100	0.93	4600
<i>m</i> -Xylene	123.5	0.3	18.0	6.0	146	100	0.54	2000
<i>p</i> -Xylene	123.9	0.1	18.0	6.5	156	100	0.62	1600

^a 26 °C.

the normalized flux was not consistent with any order of the physical properties shown in **Table 3**, which indicates the influence of diffusion behavior in terms of the solution–diffusion mechanism.

2.10.4.2 Affinity Control

The affinity interaction between a membrane material and a given liquid component in the mixture has been enhanced to increase the solubility selectivity. The introduction of a hydrophobic structure in a membrane material (i.e., increase in hydrophobicity) provides an increase in VOC selectivity for VOC–water mixtures.

One of the modifications of the ethanol/water separation in the PTMSP membrane was the graft of hydrophobic PDMS onto the α -methyl carbon of PTMSP [49]. In the separation of a 7 wt.% ethanol–water solution at 30 °C, the PTMSP membrane had a flux of $1.2 \times 10^{-3} \text{ g m}^{-2} \text{ h}^{-1}$ and an ethanol/water selectivity of 11. When PDMS was grafted onto PTMSP at the 12 mol.% PDMS content in the graft copolymer, the flux increased to $2.5 \times 10^{-3} \text{ g m}^{-2} \text{ h}^{-1}$ and the ethanol/water selectivity was also enhanced up to 28.

The PTMSP membrane displayed faster permeation rates for other VOCs, such as acetone, acetonitrile, and acetic acid, in comparison with water, as presented

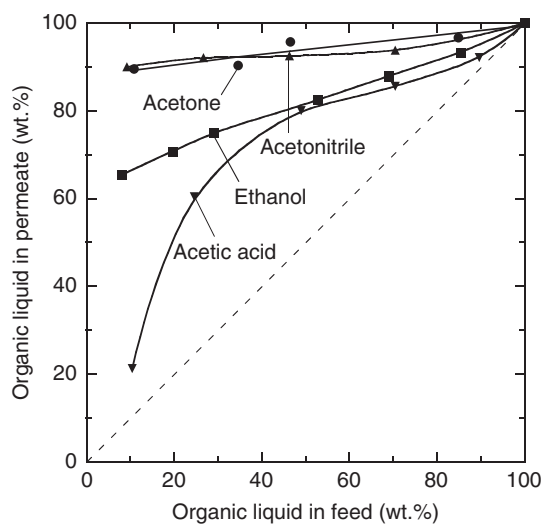


Figure 21 Permeate composition curves for the poly(1-trimethylsilyl-1-propyne) membrane used for organic liquid–water pervaporation at 30 °C. Organic liquids: acetone (●), acetonitrile (▲), ethanol (■), and acetic acid (▼). Reproduced from Masuda, T., Takatsuka, M., Tang, B. Z., Higashimura, T. *J. Membr. Sci.* **1990**, *49*, 69–83.

in **Figure 21** [50]. This substituted polyacetylene increased the acetonitrile content of acetonitrile/water mixture from 7 wt.% to 88 wt.% at 30 °C with a total flux of $7 \times 10^{-2} \text{ g m}^{-2} \text{ h}^{-1}$. The acetonitrile/water selectivity was then 101. As the VOC concentration in the feed solution increased, the total flux of the solution also increased, whereas the VOC/water selectivity decreased except for acetic acid. The selectivity of acetic acid increased up to the 25 wt.% acetic acid concentration in feed mixtures, and then decreased further with increasing concentration.

When the trimethylsilyl group was introduced on a 10 mol.% of the α -methyl carbon of PTMSP, both the flux and acetonitrile/water selectivity were two-fold enhanced at 50 °C [51]. This trimethylsilyl-group-induced PTMSP membrane also showed higher fluxes and higher VOC/water selectivities than the pure PTMSP membrane for various solvents, such as acetone and dioxane.

Hydrophobic fluoroalkyl methacrylate monomers were sorbed in pure PTMSP membranes and then irradiated with γ -rays for polymerization of the monomers inside their membranes [52]. As the fluoroalkyl methacrylate content in the membrane increased, total flux decreased, and chloroform/water selectivity increased and then gradually decreased (**Figures 22 and 23**). The chloroform/water selectivity for 0.8 wt.% chloroform aqueous solution at 25 °C was 860 for pure PTMSP membranes and was above 7000 for 18 wt.% 1H, 1H, 9H-hexadecafluorononyl methacrylate containing PTMSP membranes irradiated with γ -rays.

Blend membranes of PTMSP with 62 wt.% poly(1H, 1H, 9H-hexadecafluorononyl methacrylate) had an ethyl butanoate/water selectivity of about 600 at 0.02 wt.% ethyl butanoate feed mixtures at 25 °C [53]. The diffusivity of ethyl butanoate was much lower than that of water, whereas its solubility was much higher than that of water. As the solubility factor was dominant for the transport, ethyl butanoate permeated faster through this modified polymer than water.

The introduction of a phenyl group in a membrane structure is expected to enhance an affinity interaction between benzene and the membrane. However, in the separation of benzene/water mixtures (benzene concentration: 600 ppm in feed) by pervaporation at 25 °C, the selectivity of benzene over water was 400 for the poly(1-phenyl-1-propyne) (PPP, **6**) membrane, whereas it was 1600 for the PTMSP membrane [54]. As the PPP content increased in PTMSP/PPP blend membranes, the water flux gradually decreased, while the benzene

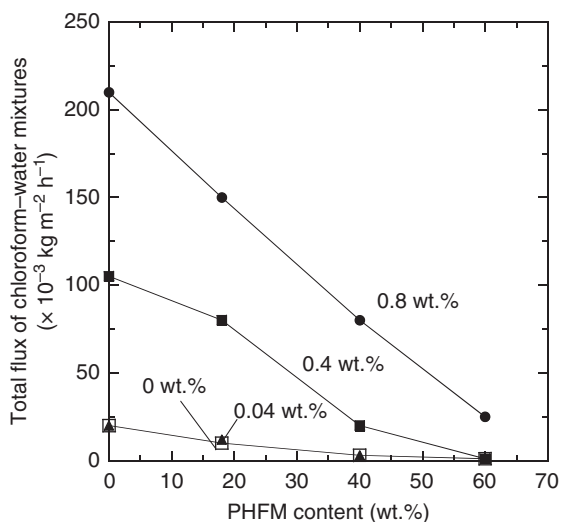


Figure 22 Total flux of chloroform–water mixtures through the γ -ray irradiated poly(1-trimethylsilyl-1-propyne) membrane containing 1H, 1H, 9H-hexadecafluorononyl methacrylate (PHFM) at 25 °C, as a function of PHFM content in the membrane. Concentration of chloroform in chloroform–water mixtures: 0 wt.% (□), 0.04 wt.% (▲), 0.4 wt.% (■), and 0.8 wt.% (●). Reproduced from Nakagawa, T., Arai, T., Ookawara, Y., Nagai, K. *Sen'i Gakkai*. **1997**, 53, 423–430.

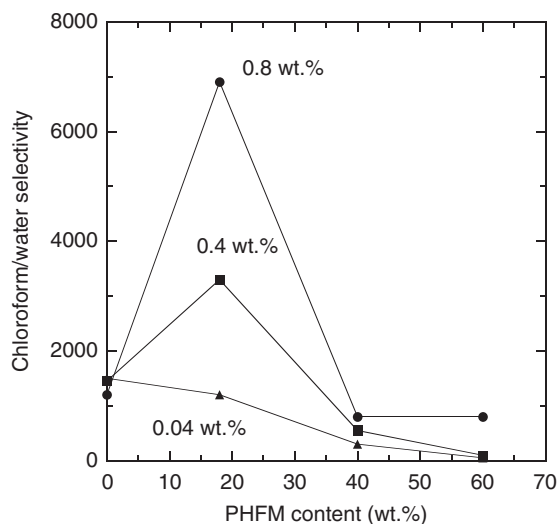
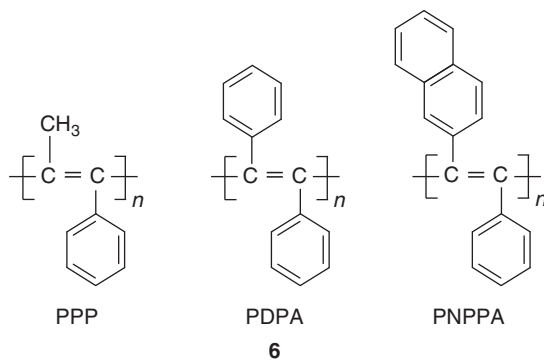


Figure 23 Chloroform/water selectivity for chloroform–water mixtures through the γ -ray irradiated poly(1-trimethylsilyl-1-propyne) membrane containing 1H, 1H, 9H-hexadecafluorononyl methacrylate (PHFM) at 25 °C, as a function of PHFM content in the membrane. Concentration of chloroform in chloroform–water mixtures: 0.04 wt.% (▲), 0.4 wt.% (■), and 0.8 wt.% (●). Reproduced from Nakagawa, T., Arai, T., Ookawara, Y., Nagai, K. *Sen'i Gakkai*. **1997**, 53, 423–430.

flux stayed almost constant up to 25 wt.% of PPP content in the blends. As a result, interestingly, the PTMSP/PPP blend membranes had benzene/water selectivities higher than those of each substituted polyacetylene membrane. For example, PTMSP/PPP (75/25) blend membranes had a benzene/water selectivity of 2900.



In the separation of benzene–cyclohexane mixtures by pervaporation, the phenyl group containing substituted polyacetylene membranes showed benzene permselectivity [44]. When the feed solution contained about 50 wt.% benzene, the benzene/cyclohexane selectivity of the poly(diphenylacetylene) (PDPA, **6**) membrane was 1.6 at 30 °C. It was about 10 times lower than that of cellulose acetate. However, the PDPA membrane with a thickness of 46 μm had a total flux of 191 $\text{g m}^{-2} \text{h}^{-1}$, which was 560 times faster than that of cellulose acetate. When the benzene content was 10 wt.% in the feed solution, the selectivity was slightly higher compared to the value at 50 wt.% benzene concentration, but the flux was about a half of the value at 50 wt.% benzene concentration. The replacement of the phenyl group in PDPA by the β -naphthyl group (PNPPA, **6**) enhanced the selectivity relative to the value of PDPA. The flux was, however, reduced by this replacement. Thus, the substituted polyacetylenes seemed to have little potential for the separation of organic liquid mixtures.

When β -cyclodextrin was added in a cross-linked PVC membrane, this membrane preferentially permeated *n*-propanol as compared to iso-propanol from their mixtures [55]. From the *n*-propanol–iso-propanol mixture with 10 wt.% *n*-propanol, the PVC membrane containing 40 wt.% β -cyclodextrin concentrated this solution to about 45 wt.% *n*-propanol solution at 40 °C.

Poly(tetrafluoroethylene) (PTFE) is one of the higher hydrophobic polymers with a VOC-selective behavior. The mixture of water (boiling temperature

of 100 °C) and *tert*-butanol (boiling temperature of 82.8 °C) (11.8:88.2 wt.%) has the azeotropic temperature of 95.5 °C [46]. The pervaporation of this mixture through PTFE membranes grafted with *N*-vinylpyrrolidone (i.e., introduction of hydrophilic structure) at 25 °C provided water-selective behavior with water/*tert*-butanol selectivity of 41 [56].

Ions have larger affinity for water than for VOCs. When the counter-cation (e.g., H⁺, Li⁺, Na⁺, K⁺, and Cs⁺) of sulfonated polyethylene membranes was replaced, these membranes showed water-selective behavior and the water/alcohol selectivity was enhanced. For example, when the counter-cation was changed from H⁺ to Cs⁺ at 26 °C, the water/ethanol selectivity increased from 2.6 to 725 and the water/*iso*-propanol selectivity increased from 5.5 to about 29 000 [57]. In this membrane and in another ion-exchange membrane Nafion 811, the order of the selectivity and flux did not simply follow the rule of the periodic law [57, 58].

2.10.4.3 Pore Structure Control

According to the separation mechanism in Figure 2, the highest selectivity appears with molecular-sieving membranes. Inorganic materials have an advantage in preparing these types of membranes as compared to polymer materials. In 1955, Kammermeyer and Hagerbaumer attempted the separation of homogeneous liquid mixtures (e.g., ethylacetate–tetrachlorocarbon, ethanol–water, and benzene–methanol) by using porous Vycor glass membrane (this article did not clearly mention whether the penetrant's phase at the interface of the membrane at the permeate side was vapor or liquid) [59].

Silicalite membranes, which were prepared from colloidal silica, tetrapropylammonium bromide, sodium hydroxide, and pure water (1:0.1 :0.05:80) (Figure 24), showed ethanol-selective behavior from ethanol–water mixtures [60]. The ethanol flux was independent of water concentration in the feed solution, whereas the water flux decreased in the presence of ethanol during transport. The ethanol was selectively adsorbed in the silicalite pores, which restricted the transport of water in the pores.

Both NaX and NaY zeolite membranes (SiO₂/Al₂O₃ = 3.6–5.3(X) and 25(Y), Na₂O/SiO₂ = 1.2–1.4(X) and 0.88(Y), and H₂O/Na₂O = 30–50) preferably adsorbed methanol relative to MTBE and then showed methanol permselectivity from methanol–MTBE mixtures [61]. The NaX zeolite membrane had the flux of 0.46 kg m⁻² h⁻¹ and methanol/MTBE selectivity of 10 000 from the methanol–MTBE mixture (10:90 wt.%) at 50 °C, whereas the NaY zeolite membrane showed larger flux, but lower selectivity; flux: 1.70 kg m⁻² h⁻¹; methanol/MTBE selectivity: 5300.

In addition, in pervaporation of the ethanol–water mixture (90:10 wt.%) at 75 °C, the NaA zeolite membrane (Al₂O₃:SiO₂:Na₂O:H₂O = 1:2:2:120 mol) had the flux of 2.2 kg m⁻² h⁻¹ and water/ethanol selectivity of larger than 10 000 [62]. Another NaA zeolite membrane (no information on material composition) showed water/*tert*-butanol selectivity of 21 863 from the water–*tert*-butanol mixture (5.2:94.8 wt.%) at 60 °C [63].

These examples could be explained using an adsorption–diffusion mechanism with a difference in the fluxes of two components; that is, both components were able to penetrate inside the pores. However, template-free secondary growth MFI-type zeolite

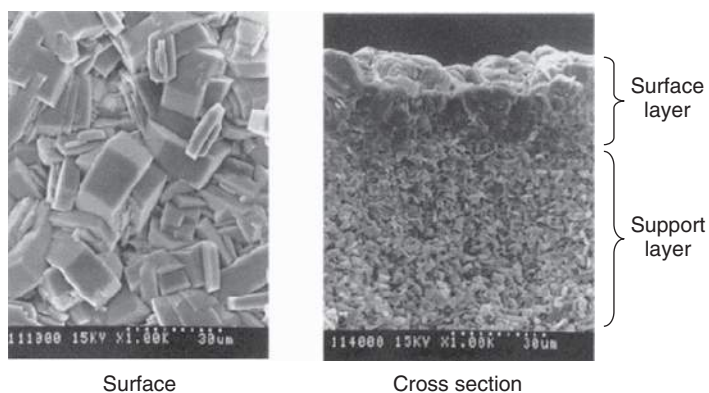


Figure 24 Scanning electron microscope (SEM) photographs of the surface (left) and cross section (right) of a silicalite membrane. Reproduced from Nomura, M., Yamaguchi, T., Nakao, S. *J. Membr. Sci.* **1998**, *144*, 161–171.

(diameter ≈ 0.6 nm) membranes provided a more accurate macroscopic defect-free structure with the high *p*-xylene/*o*-xylene selectivity of 69 from each pure component flux and that of 40 from the 50:50 mol.% binary mixture at 50 °C [64]. This membrane preparation technique provided more significant molecular-sieving pores between the sizes of *p*-xylene (diameter ≈ 0.58 nm) and *o*-xylene (diameter ≈ 0.68 nm) molecules.

2.10.4.4 Stability Improvement

In the pervaporation of mixtures of water and various VOCs, rubbery polymer membranes (e.g., PDMS) are always VOC-selective regardless of the polymer structures [65]. As rubbery polymer membranes had weak mechanical strength as compared with glassy polymer membranes, it could be modified by the introduction of glassy polymer segments in the membrane. Hence, the permeate flux and separation properties were strongly influenced by the composition and the phase-separated structures.

For example, phase-separated graft polymer membranes, composed of PDMS and poly(methylmethacrylate) (PMMA) segments, had a transition point of their flux and benzene/water selectivity for a 0.05 wt.% benzene concentration in the mixture, at PDMS content of about 40 mol.% in the membrane [66]. At this content, the continuous phase in the membrane changed from PMMA to PDMS and, consequently, the flux and benzene/water selectivity underwent dramatic increases. Among the graft polymer membranes, one with 68 mol.% PDMS content displayed the highest benzene/water selectivity of 3730.

When *tert*-butylcalix[4]arene (CA) was added in phase-separated graft or block polymer membranes, composed of PDMS and PMMA segments, because of an increase in the solubility selectivity with specific affinity of CA for benzene, their benzene/water selectivity was enhanced [67]. For example, in the pervaporation of 0.05 wt.% benzene aqueous solution at 40 °C, the benzene/water selectivity of the PMMA-*b*-PDMS (29:71 mol.%) membrane and that containing 40 wt.% CA were about 1700 and about 2300, respectively.

Copolymer membranes composed of trimethylsilylmethylmethacrylate (i.e., this homopolymer was glassy) and *n*-butyl acrylate (i.e., this homopolymer was rubbery) showed 1,1,2-trichloroethane, trichloroethylene, and tetrachloroethylene permselective behaviors from an aqueous solution of 0.2 and 0.4 wt.% chlorinated hydrocarbons [14]. In particular, its rubbery copolymer

membrane with about 70 mol.% of *n*-butyl acrylate exhibited this chlorinated hydrocarbon/water selectivity of 600–1000 at 25 °C.

Cross-linking is also expected to enhance the mechanical strength of a membrane. Copolymer membranes composed of methyl methacrylate and methacrylic acid cross-linked with Fe³⁺ or Co²⁺ ions showed benzene-selective behavior from benzene/cyclohexane mixtures at 40 °C [68]. PMMA membranes cross-linked with ethylene glycol dimethacrylate also showed benzene-selective behavior from benzene/cyclohexane mixtures at 40 °C [69]. Benzene has a larger solubility parameter than cyclohexane, because of its larger hydrogen component (δ_h) value [18, 19]. Hence, benzene is more hydrophilic as compared to cyclohexane, which provided the benzene-selective behavior for the PMMA membrane. In addition, both cross-linking approaches produced the significant depression of swelling of the membranes by the solution.

Furthermore, the pervaporation characteristics were significantly affected by the operation temperature. In the separation of an aqueous phenol solution through polyurethane membranes and of a 10 ppm 1,2-dibromo-3-chloropropane solution through cross-linked PDMS membranes, the VOC/water selectivity attained the maximum value at 60–70 °C [70, 71]. Water vapor pressure underwent a drastic increase above 60–70 °C leading to an increase in water diffusion, and decreased (D_{VOC}/D_{H_2O}), thus resulting in an overall decline in (P_{VOC}/P_{H_2O}).

2.10.5 Concluding Remarks

This chapter has reviewed the fundamentals and perspectives of pervaporation and has provided a comprehensive overview of the separation mechanisms, experimental methods, and structure–property relationships of membrane materials in various important applications of pervaporation processes. Compared to other membrane technologies, the theories on transport and separation in pervaporation have not been established yet. Most of them can explain each phenomenon qualitatively, but several inconsistencies appear, as research continually develops. This fact has not led to the optimum direction of designing membrane materials with well-defined structures for pervaporation applications.

The main reason is that, as mentioned previously, the pervaporation process is the only

membrane process by which the phase transition of the mixture appears during transport through a membrane. The factors on transport and separation include the swelling of a membrane with a feed solution, the interface phenomena between a liquid-swollen layer and a dried nonswollen layer, the interactions among components in the feed solution, and the interactions between the components in the feed solution and a membrane material. These facts complicate the analysis of the pervaporation mechanism.

As the flux and selectivity are strongly affected by feed composition, temperature, and permeate pressure, among others, the operating condition must be strictly controlled. This suggests the limitation of industrial applications with current technologies. Conversely, there remains a wide variety of research possibilities for pervaporation. If these issues on pervaporation are solved, then a huge advantage and benefit for liquid separation will be provided for an enjoyable and productive future.

References

- [1] Baker, R. W. *Membrane Technology and Applications*; McGraw-Hill: New York, 2000.
- [2] Kober, P. A. *J. Am. Chem. Soc.* **1917**, *39*, 944–948.
- [3] Farber, L. *Science* **1935**, *82*, 158.
- [4] Heisler, E. G., Hunter, A. S., Siciliano, J., Treadway, R. H. *Science* **1956**, *124*, 77–79.
- [5] Binning, R. C., James, F. E. *Petrol. Refiner* **1958**, *37*, 214–215.
- [6] Binning, R. C., Lee, R. J., Jennings, J. F., Martin, E. C. *Ind. Eng. Chem.* **1961**, *53*, 45–50.
- [7] Binning, R. C., Lee, R. J. Separation of Azeotropic Mixtures. US 2,953,502, 20 September 1960.
- [8] Binning, R. C., Stuckey, J. M. Method of Separating Hydrocarbons Using Ethyl Cellulose Selective Membrane. US 2,958,657, 1 November 1960.
- [9] Nagai, K., Masuda, T., Nakagawa, T., Freeman, B. D., Pinnau, I. *Prog. Polym. Sci.* **2001**, *26*, 721–798.
- [10] Greenlaw, F. W., Prince, W. D., Shelden, R. A., Thompson, E. V. *J. Membr. Sci.* **1977**, *2*, 141–151.
- [11] Greenlaw, F. W., Shelden, R. A., Thompson, E. V. *J. Membr. Sci.* **1977**, *2*, 333–348.
- [12] Yoon, B. O., Asano, T., Nakaegawa, K., Ishige, M., Hara, M., Higuchi, A. Separation of Endocrine Disruptors from Aqueous Solutions by Pervaporation: Relationship between the Separation Factor and Solute Physical Parameters. In *Advanced Materials for Membrane Separations*; Pinnau, I., Freeman, B. D., Eds.; American Chemical Society: Washington, DC, 2004; pp 394–410.
- [13] Yamada, S., Hamaya, T. *Kobun. Ronbun. (Jpn. J. Polym. Sci. Tech.)* **1982**, *39*, 407–414.
- [14] Nakagawa, T., Kanemasa, A. *Seni Gakkai.* **1995**, *51*, 123–130.
- [15] Sing, K. S. W., Everett, D. H., Haul, R. A. W., et al. *Pure Appl. Chem.* **1985**, *57*, 603–619.
- [16] Barrow, G. M. *Physical Chemistry*, 5th edn.; McGraw-Hill: New York, 1988.
- [17] van Krevelen, D. W. *Properties of Polymers, Their Correlation with Chemical Structure; Their Numerical Estimation and Prediction from Additive Group Contributions*, 3rd edn.; Elsevier: Amsterdam, 1990.
- [18] Barton, A. F. M. *CRC Handbook of Solubility Parameters and Other Cohesion Parameters*, 2nd edn.; CRC: Boca Raton, FL, 1991.
- [19] Grulke, E. A. Solubility Parameter Values. In *Polymer Handbook*, 4th edn.; Brandrup, J., Immergut, E. H., Grulke, E. A., Eds. Wiley: New York, 1999; pp VII675–VII714.
- [20] Nagai, K., Higuchi, A., Nakagawa, T. *J. Polym. Sci. Part B: Polym. Phys.* **1995**, *33*, 289–298.
- [21] Fedors, R. F. *Polym. Eng. Sci.* **1974**, *14*, 147–154.
- [22] Nagai, K., Ohno, M., Nakagawa, T. *Membrane* **1999**, *24*, 215–220.
- [23] Barrer, R. M., Barrie, J. A., Slater, J. *J. Polym. Sci.* **1958**, *27*, 177–197.
- [24] Nakagawa, T. Gas Separation and Pervaporation. In *Membrane Science and Technology*; Osada, Y., Nakagawa, T., Eds. Marcel Dekker: New York, 1992; pp 239–287.
- [25] Kanehashi, S., Nakagawa, T., Nagai, K., Duthie, X., Kentish, S., Stevens, G. *J. Membr. Sci.* **2007**, *298*, 147–155.
- [26] Berens, A. R., Hopfenberg, H. B. *Polymer* **1978**, *19*, 489–496.
- [27] Alfrey, T., Gurnee, E. F., Lloyd, W. G. *J. Polym. Sci. Part C: Polym. Symp.* **1966**, *12*, 249–261.
- [28] Jacques, C. H. M., Hopfenberg, H. B., Stannett, V. *Polym. Eng. Sci.* **1973**, *13*, 81–87.
- [29] Fujita, H. Organic Vapors above the Glass Transition Temperature. In *Diffusion in Polymers*; Crank, J., Park, G. S., Eds. Academic Press: London, 1968; pp 75–105.
- [30] Breck, D. W. *Zeolite Molecular Sieves*; Wiley: New York, 1974.
- [31] Poling, B. E., Prausnitz, J. M., O'Connell, J. P. *The Properties of Gases and Liquids*, 5th edn.; McGraw-Hill: New York, 2000.
- [32] Berens, A. R., Hopfenberg, H. B. *J. Membr. Sci.* **1982**, *10*, 283–303.
- [33] Meares, P. *J. Am. Chem. Soc.* **1954**, *76*, 3415–3422.
- [34] Kanehashi, S., Nagai, K. *J. Membr. Sci.* **2005**, *253*, 117–138.
- [35] Freeman, B. D., Hill, A. J. Free Volume and Transport Properties of Barrier and Membrane Polymers. In *Structure and Properties of Glassy Polymers*; Tant, M. R., Hill, A. J., Eds.; ACS Symposium Series 710; American Chemical Society: Washington, DC, 1998; pp 306–325.
- [36] Nagai, K., Freeman, B. D., Hill, A. J. *J. Polym. Sci. Part B: Polym. Phys.* **2000**, *38*, 1222–1239.
- [37] Yampolskii, Y. P., Korikov, A. P., Shantarovich, V. P., et al. *Macromolecules* **2001**, *34*, 1788.
- [38] Miyata, S., Sato, S., Nagai, K., Nakagawa, T., Kudo, K. *J. Appl. Polym. Sci.* **2008**, *107*, 3933–3944.
- [39] Aptel, P., Cuny, J., Jozefonvicz, J., Morel, G., Neel, J. *J. Appl. Polym. Sci.* **1974**, *18*, 365–378.
- [40] Yamada, S., Hamaya, T. *Kobun. Ronbun. (Jpn. J. Polym. Sci. Tech.)* **1976**, *33*, 217–223.
- [41] Akiba, C., Watanabe, K., Nagai, K., Hirata, Y., Nguyen, Q. T. *J. Appl. Polym. Sci.* **2006**, *100*, 1113–1123.
- [42] Brueschke, H. Eur. Pat. EP0096339 (Priority DE3220570), 31 May 1983.
- [43] Masuda, T., Tang, B. Z., Higashimura, T. *Polym. J.* **1986**, *18*, 565–657.
- [44] Sakaguchi, T., Yumoto, K., Kwak, G., Yoshikawa, M., Masuda, T. *Polym. Bull.* **2002**, *48*, 271–276.
- [45] Ishihara, K., Nagase, Y., Matsui, K. *Macromol. Chem. Rapid Commun.* **1986**, *7*, 43–46.

- [46] Lide, D. R. *CRC Handbook of Chemistry and Physics*, 82nd edn.; CRC Press: Boca Raton, FL, 2001.
- [47] Komaki, I., Hasegawa, K., Endo, T., Nagai, K. *Polym. Prepr. Jpn.* **2005**, *54*, 1867.
- [48] Endo, T., Hasegawa, K., Komaki, I., Nagai, K. *Polym. Prepr. Jpn.* **2005**, *54*, 1858.
- [49] Nagase, Y., Ishihara, K., Matsui, K. *J. Polym. Sci. Part B: Polym. Phys.* **1990**, *28*, 377–386.
- [50] Masuda, T., Takatsuka, M., Tang, B. Z., Higashimura, T. *J. Membr. Sci.* **1990**, *49*, 69–83.
- [51] Nagase, Y., Takamura, Y., Matsui, K. *J. Appl. Polym. Sci.* **1991**, *42*, 185–190.
- [52] Nakagawa, T., Arai, T., Ookawara, Y., Nagai, K. *Sen'i Gakkai.* **1997**, *53*, 423–430.
- [53] Mishima, S., Nakagawa, T. *J. Appl. Polym. Sci.* **2002**, *83*, 1054–1060.
- [54] Takahashi, S., Yoshida, Y., Kamada, T., Nakagawa, T. *Kobun Ronbun. (Jpn. J. Polym. Sci. Tech.)* **2001**, *58*, 213–220.
- [55] Miyata, T., Iwamoto, T., Uragami, T. *J. Appl. Polym. Sci.* **1994**, *51*, 2007–2014.
- [56] Aptel, P., Challard, N., Cuny, J., Neel, J. *J. Membr. Sci.* **1976**, *1*, 271–287.
- [57] Cabasso, I., Korngold, E., Liu, Z. Z. *J. Polym. Sci.: Polym. Lett. Ed.* **1985**, *23*, 577–581.
- [58] Cabasso, I., Liu, Z. Z. *J. Membr. Sci.* **1985**, *24*, 101–119.
- [59] Kammermeyer, K., Hagerbaumer, D. H. *AIChE J.* **1955**, *1*, 215–219.
- [60] Nomura, M., Yamaguchi, T., Nakao, S. *J. Membr. Sci.* **1998**, *144*, 161–171.
- [61] Kita, H., Fuchida, K., Horita, T., Asamura, H., Okamoto, K. *Sep. Purif. Technol.* **2001**, *25*, 261–268.
- [62] Okamoto, K., Kita, H., Horii, K., Tanaka, K., Kondo, M. *Ind. Eng. Chem. Res.* **2001**, *40*, 163–175.
- [63] Gallego-Lizon, T., Edwards, E., Lobiundo, G., dos Santos, L. F. *J. Membr. Sci.* **2002**, *197*, 309–319.
- [64] Yuan, W., Lin, Y. S., Yang, W. *J. Am. Chem. Soc.* **2004**, *126*, 4776–4777.
- [65] Nijhuis, H. H., Mulder, M. H. V., Smolders, C. A. *J. Appl. Polym. Sci.* **1993**, *47*, 2227–2243.
- [66] Uragami, T., Yamada, H., Miyata, T. *J. Membr. Sci.* **2001**, *187*, 255–269.
- [67] Uragami, T., Meotoiwa, T., Miyata, T. *Macromolecules* **2003**, *36*, 2041–2048.
- [68] Inui, K., Noguchi, T., Miyata, T., Uragami, T. *J. Appl. Polym. Sci.* **1999**, *71*, 233–241.
- [69] Inui, K., Okumura, H., Miyata, T., Uragami, T. *J. Membr. Sci.* **1997**, *132*, 193–202.
- [70] Higuchi, A., Yoon, B.-O., Asano, T., *et al.* *J. Membr. Sci.* **2002**, *198*, 311–320.
- [71] Hoshi, M., Kogure, M., Saitoh, T., Nakagawa, T. *J. Appl. Polym. Sci.* **1997**, *65*, 469–479.

Biographical Sketch



Kazukiyo Nagai is currently a professor and head of the Department of Applied Chemistry and chair of the Center for Polymer Science at the Meiji University, Japan. Nagai received his BE degree in 1988, his ME degree in 1990, and his DE degree in 1996 from the Department of Industrial Chemistry at Meiji University. He has more than 15 years of research experience in polymer and membrane science and technologies – particularly gas separation and pervaporation. He worked for the Shin-Etsu Chemical Co. Ltd., Japan (1990–93 and 1996–97), the North Carolina State University, USA (1997–2000), and the Commonwealth Scientific and Industrial Research Organization (CSIRO) Petroleum and CSIRO Molecular Science, Australia (2000–02). Nagai joined the faculty of Meiji University in 2002. He was a project leader in the Cooperative Research Center for Greenhouse Gas Technologies, Australia (2003–06), an honorary fellow at the University of Melbourne, Australia (2003–06), and a research advisor for the Japan Railway Technical Research Institute, Japan (2005–07). He was named Young Scientist 2003 by the Membrane Society of Japan. He has contributed to the membrane community as an editorial committee member of the journal *Membrane* since 2005 and *Journal of Packaging Science and Technology, Japan* since 2008.

2.11 Selective Membranes for Purification and Separation of Organic Liquid Mixtures

T Uragami, Kansai University, Osaka, Japan

© 2010 Elsevier B.V. All rights reserved.

2.11.1	Introduction	274
2.11.2	Structural Design of Separation Membrane	274
2.11.2.1	Chemical Design of Separation Membranes	274
2.11.2.2	Physical Construction of Separation Membranes	275
2.11.3	Preparation Methods for Separation Membranes	275
2.11.3.1	Methods for Membrane Preparation	275
2.11.3.2	Membrane Structures	275
2.11.4	Principles of Membrane Separation Techniques for Organic Liquid Mixtures	276
2.11.4.1	Pervaporation	276
2.11.4.2	Evapomeation	276
2.11.4.3	Temperature-Difference-Controlled Evapomeation	277
2.11.4.4	High-Temperature and Pressure Evapomeation	277
2.11.5	Fundamentals of Membrane Permeation and Separation	277
2.11.5.1	Permeation Equation	277
2.11.5.2	Solution-Diffusion Model	278
2.11.5.3	Surface Diffusion	279
2.11.6	Selective Permeation and Separation of Organic Liquid Mixtures	279
2.11.6.1	Water/Alcohol-Selective Membranes	279
2.11.6.2	Alcohol/Water-Selective Membranes	290
2.11.6.3	Water/Organic-Liquid-Selective Membranes	296
2.11.6.4	Selective Membranes for Organic Liquid/Water Mixtures	301
2.11.6.5	Selective Membranes for Organic Liquid/Organic Liquid Mixtures	309
2.11.6.5.1	Bz/Chx-selective membranes	309
2.11.6.5.2	Organic/organic-selective membranes	313
2.11.6.6	Selective Membranes for Isomers	317
2.11.6.7	Selective Membranes for Facilitation of Chemical Reactions	319
2.11.7	Conclusions	319
References		319

Glossary

Evapomeation (EV) A novel membrane separation technique that makes use of the advantages of pervaporation but reduces the negative effects of swelling on membrane performance. In this EV technique, the feed solution is fed to the membrane without directly contacting the membrane. This is accomplished by vaporizing the liquid feed so that only vapor is supplied to the membrane. Therefore, swelling or shrinking of the polymer membranes due to contact with the feed solutions is minimized. There are some advantages in EV technique.

High-temperature and pressure evapomeation (HTPEV) During the evapomeation procedure, vapor under high temperature and high pressure can be applied to the feed vapor side, hence the term high-temperature and pressure evapomeation (HTPEV). The membranes used for HTPEV can also be connected to a distillation system.

Temperature-difference-controlled evapomeation (TDEV) In evapomeation, the temperatures of the feed solution and the membrane surroundings are controlled, and,

consequently, a differential between these temperatures can be established. Such an EV method, in which this temperature difference is controlled, is called temperature-difference-controlled evaporation (TDEV). In TDEV, the most permeable solute has a lower freezing point in a

binary liquid mixture and is selectively permeated. In addition, when the membrane has a stronger affinity to the preferentially permeating mixture component, it can result in an increase in selectivity.

Nomenclature

T_g glass transition temperature

2.11.1 Introduction

Purification and separation of organic liquid mixtures are strongly required in various fields, such as the concentration and recovery of organic solvents in the chemical process industry, removal of volatile organic compounds (VOCs) from water, concentration of alcohol in bio-fermentation, and analytical field. Purification and separation of organic liquid mixtures have been carried out by distillation, solvent extraction, and chromatography. However, these methods are expensive for energy cost and low in treatment efficiency.

Membrane separation techniques with high energy savings and high efficiency are promising techniques for the separation of materials. Because of their characters, membrane separation technologies have been examined as a way to conserve resources, energy, and the environment. If a membrane-based separation process is technically and economically feasible, the key points of purification and separation of organic liquid mixtures are both the design of chemical structure and construction of physical structure of the membrane for high membrane performance.

In this chapter, the methods for membrane preparation, the structural design of highly selective membranes, the principles of membrane separation techniques that can be applied to the purification and separation of organic liquid mixtures, and several applications of these membranes for separation of water/alcohol, alcohol/water, water/organic liquid, organic liquid/water, VOC/water, organic liquid/organic liquid mixtures, and isomers, as well as facilitation of chemical reaction are discussed.

2.11.2 Structural Design of Separation Membrane

The chemical design and physical construction of separation materials are very important considerations in balancing chemical and physical functions of separation membranes. The foundations of membrane structural design are the selection, improvement, and synthesis of membrane materials and the membrane preparation methods [1].

2.11.2.1 Chemical Design of Separation Membranes

Novel candidates for separation membranes are selected based on:

1. the development of systematic structure/property relationships in membrane materials to provide separation membranes with enhanced performance;
2. the ease of membrane preparation; and
3. their stability under application conditions, such as pH, temperature, and pressure.

Furthermore, synthesis of new membrane materials and modification of existing membrane materials are often employed to develop membranes with higher performance. For membrane materials, modification and synthesis of membrane materials are accomplished by blending, cross-linking, formation of internal hydrogen bonding, and graft, block, and multiblock copolymerization. In addition, separation membranes may also be significantly altered by surface modification techniques. There are two general types of surface modification techniques: chemical or

physical modification. In the case of chemical treatment, the separation membranes are contacted with a chemical agent, solvent, coupling agent, vapor, surface-active agent, surface grafting, or other additives. Physical treatment techniques for separation membranes include ultraviolet irradiation, plasma irradiation, and sputtering.

2.11.2.2 Physical Construction of Separation Membranes

For the development of high-performance separation membranes, it is important to choose an optimum membrane material based on its physical and chemical properties. This is reflected in improved permeability, selectivity, and durability of the resultant membrane. The physical structure of separation membranes is strongly dependent on the separation membrane preparation method and the conditions of separation membrane formation. In the membrane permeation, the chemical and physical properties of the separation membrane do not work separately for the membrane performance, and, consequently, both chemically and physically structural factors are significantly related to membrane performance together in almost every case.

2.11.3 Preparation Methods for Separation Membranes

2.11.3.1 Methods for Membrane Preparation

Various membrane preparation methods are summarized in **Table 1**. In the solution-casting method (method 1), there are two types: wet [2–8] and dry [9] methods. In the former method, separation membranes are made by pouring casting solutions onto an applicator for a thin-layer chromatograph, drawing the blade across a glass plate, allowing the solvent to evaporate at a certain temperature for a prescribed period, and immersing the glass plate together with

the membrane into a gelation medium (usually water). After resting in the gelation medium for a desired period, the membranes are removed from the glass plate and annealed as required. The resulting membranes from this wet method are asymmetric structures consisting of dense, thin-skin layers and rough, porous support layers. On the other hand, in the dry method, since a gelation medium is not used and the casting solvent is completely evaporated, the resulting membranes have a dense symmetric structure and are reversible in the wet–dry membrane cycle. In the composite method (method 2), thin active layers, consisting of separation materials with high affinity for a permeant that can be selectively permeated through the membrane, are coated onto a porous support for separation. Asymmetric membranes prepared by solution-casting method have physical-asymmetric structures in which the dense, thin-skin layer and the porous support layer consist of the same material. In the composite method, membranes with physical and chemical asymmetric structures, which consist of different materials, can be prepared. In the casting-reaction method (method 3), membrane materials are cross-linked and chemically modified during the membrane preparation. Modified materials cannot be dissolved in feed mixtures, and membranes can be formed simultaneously. For example, separation membranes are modified by reaction reagents added to the casting solution during membrane formation. In the polyion complex (PIC) method (method 4), membranes are prepared by the formation of PICs with mixing between aqueous solutions of cationic polyelectrolytes and anionic polyelectrolytes. The resulting PIC membranes are not dissolved in water and organic solvents. In the freeze-dry method (method 5), membrane materials are dissolved in a solvent with a relatively high freezing point; this casting solution is casted onto a Teflon dish and frozen, and then the membranes are prepared by drying under reduced pressure [10]. In the surface treatment method (method 6), the property of the membrane surface prepared by methods (1)–(5) is improved by surface modifiers and surface cross-linkers.

Table 1 Membrane preparation methods

(1) Solution-casting method (dry and wet)
(2) Composite method (polymer cast)
(3) Casting-reaction method (cross-link, chemical modification)
(4) Polymer complex method
(5) Freeze-dry method
(6) Surface treatment method (surface modification)

2.11.3.2 Membrane Structures

When we consider the permeation of permeants through the membrane, the interrelationships among the sizes of pores through which permeants transfer, the physical characteristics of the permeants, and the electrochemical interaction between the

membrane materials constituting pores and permeants (physicochemical factors) are very important. If the pore size of the membrane is much larger than the size of a permeant, the interaction between the membrane and the permeant is negligible [11]. Membranes with such large pores are called porous membranes. Conversely, membranes with extremely small pores such as molecular gaps between polymer chains based on thermal vibrations of polymers are called nonporous membranes. Membranes in which physical or chemical structures are the same are termed symmetric membranes, and those in which physical or chemical structures are different from the perspective of the thickness of the membrane are called asymmetric membranes. Porous, nonporous, symmetric, and asymmetric structures of membranes are strongly dependent on membrane preparation methods. Furthermore, the development of fine structures in membranes can be significantly controlled by membrane preparation conditions.

2.11.4 Principles of Membrane Separation Techniques for Organic Liquid Mixtures

2.11.4.1 Pervaporation

Figure 1 shows the principles of pervaporation (PV). In this separation process, when a liquid mixture is fed to the upstream side of a membrane and the downstream side is evacuated, a component in the feed mixture can preferentially permeate through the membrane. In a PV process, differences in the solubility, the diffusivity, and the relative volatility of

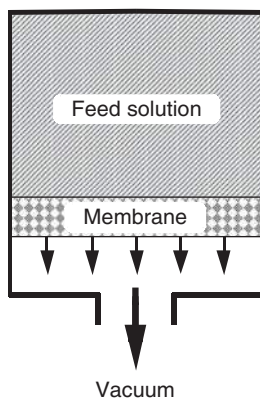


Figure 1 Principle of pervaporation (PV).

permeants in the membrane can influence the permeability and selectivity [12–15]. In general, PV exhibits the following characteristics [16]:

1. Selective transport across a nonporous membrane is achieved by a three-step process consisting of solution, diffusion, and evaporation.
2. As the driving force for permeation is the vapor pressure for each component rather than total system pressure, this method is effective for separation of organic liquid mixtures with high osmotic pressure.
3. PV can be applied to the separation and concentration of mixtures that are difficult to separate by distillation. For example, it is useful for the separation of azeotropic mixtures, close-boiling-point mixtures, and structural isomers.
4. PV can be used for the removal of certain components in equilibrium reactions.
5. Polymer membrane compaction, a frequent problem in high-pressure gas separations, is not encountered in pervaporation because the feed pressure is typically low.

2.11.4.2 Evapomeation

PV is an efficient method for the separation of organic liquid mixtures, and many studies have been performed using this process. As the membranes used in PV are directly in contact with the liquid feed solutions, however, specifically designed chemical and physical membrane properties are often impaired by swelling or shrinking of the membrane due to sorption of the feed components. Swelling or shrinking of the polymer membranes is disadvantageous for the membrane performance with respect to the separation of mixtures. A novel membrane separation technique known as evapomeation (EV) [1, 11, 15–22] makes use of the advantages of PV but reduces the negative effects of swelling on membrane performance. **Figure 2** shows the principles of EV. In this technique, the feed solution is fed to the membrane without directly contacting the membrane. This is accomplished by vaporizing the liquid feed so that only vapor is supplied to the membrane. Therefore, swelling or shrinking of the polymer membranes due to contact with the feed solutions is minimized. The advantages of EV compared to PV are as follows [1, 23]:

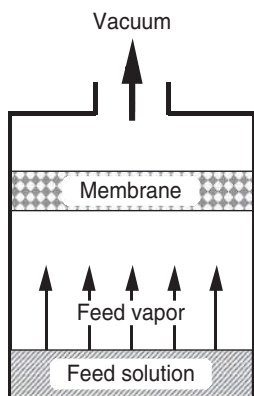


Figure 2 Principle of evapomeation (EV). From Uragami, T., Saito, M. *Makromol. Chem. Rapid Commun.* **1988**, 9, 361–365.

1. In the EV process, membranes are not in direct contact with liquid feed mixtures as only vapors are supplied to the membranes. Accordingly, any swelling or shrinking of the membrane due to the feed mixtures is minimized, and, consequently, an improvement in membrane performance may be expected.
2. As the organic liquid mixtures are vaporized, interactions between component molecules are significantly weakened, and, as a result, the separation performance is remarkably improved.
3. In EV, contaminants in a liquid feed mixture, such as macromolecular solutes, can lead to fouling of the membrane; this problem is avoided in EV.
4. During EV, the temperature of the feed solution and the membrane surroundings can both be controlled; hence, an improvement in the permeation and separation characteristics of the membrane can be achieved.

2.11.4.3 Temperature-Difference-Controlled Evapomeation

As mentioned previously, a new EV method for membrane separation that improves the shortcomings of PV, while keeping the advantages of this technique, was developed [1, 11, 15–22]. In EV, the temperatures of the feed solution (I) and the membrane surroundings (II) are controlled, and, consequently, a differential between these temperatures can be established, as shown in **Figure 3**. Such an EV method, in which this temperature difference is controlled, is called temperature-difference-

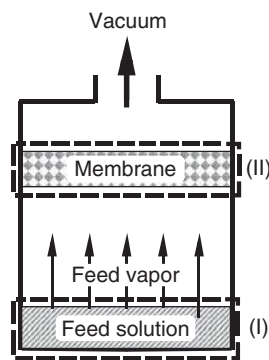


Figure 3 Principle of temperature-difference-controlled evapomeation (TDEV). From Uragami, T., Morikawa, T. *J. Appl. Polym. Sci.* **1992**, 44, 2009–2018.

controlled evapomeation (TDEV) [1, 11, 15, 16, 24–31]. In TDEV, the most permeable solute has a lower freezing point in a binary liquid mixture and is selectively permeated, as shown in **Table 2**. In addition, when the membrane has a stronger affinity to the preferentially permeating mixture component, it can result in an increase in selectivity.

2.11.4.4 High-Temperature and Pressure Evapomeation

During the EV procedure, vapor under high temperature and high pressure can be applied to the feed vapor side. We designated the term high-temperature and pressure evapomeation (HTPEV) for EV under high temperature and high pressure, as shown in **Figure 5**. The membranes used for HTPEV can also be connected to a distillation system [31].

2.11.5 Fundamentals of Membrane Permeation and Separation

2.11.5.1 Permeation Equation

The permeation rate, Q_i , of component i is expressed by Fick's first law as

$$Q_i = -D(C_i)dc_i/dx \quad (1)$$

where $D(C_i)$ is the diffusion coefficient, C_i is the concentration of component i in the membrane, and x is the distance from the membrane/feed-solution interface.

Fick's second law of diffusion is

$$dC_i/dt = D(C_i)d/dx(dc_i/dx) = D(C_i)(d^2C_i/dx^2) \quad (2)$$

Table 2 Effect of the freezing point on the selectivity of the permeant in the organic liquid mixtures through polymer membranes in TDEV

Membrane	Chitosan	PVC	PDMS
Freezing point of permeant	(CH ₃) ₂ SO/H ₂ O 18.5 > 0 °C	CH ₃ COOH/H ₂ O 16.7 > 0 °C	C ₂ H ₅ OH/H ₂ O -114.4 < 0 °C
Selectivity	H ₂ O	H ₂ O	C ₂ H ₅ OH

From Uragami T. Polym. J. **2008**, 40, 485–494.

where $D(C_i)$ is given by the following equation:

$$D(C_i) = D_0 \exp(\gamma C_i) \quad (3)$$

Here, D_0 is the infinite dilution diffusion coefficient and γ is a measure of membrane plasticization that is dependent on temperature.

At steady-state permeation, the boundary conditions are dC_i/dt , $C_i = C_1$ at $x = 0$, $C_i = C_2$ at $x = l$. By substituting Equation (3) into Equation (2) and then integrating, we obtain

$$Q_i = (D_0/\gamma l)(\exp \gamma C_1 - \exp \gamma C_2) \quad (4)$$

The concentration distribution is expressed as

$$C_i = (1/\gamma) \ln \{ \exp \gamma C_1 - x/l(\exp \gamma C_1 - \exp \gamma C_2) \} \quad (5)$$

If the concentration at the boundary of the feed solution and the membrane is equilibrated thermodynamically, the following equations hold:

$$C_1 = C^*(p^0) \quad (6)$$

$$C_2 = C^*(p_2) \quad (7)$$

where C^* is a pressure-dependent function, p^0 is saturated vapor pressure, and p_2 is the vapor pressure on the downstream side of the membrane.

Using these expressions, Equations (4) and (5) may be rewritten with p^0 and p_2 . At the same time, the permeability, P_i , is derived as

$$P_i = Q_i l / \Delta p = (D_0/\gamma \Delta p)(\exp \gamma C_1 - \exp \gamma C_2) \quad (8)$$

where $\Delta p = p^0 - p_2$. When Equations (6) and (7) obey Henry's law, $C^*(p) = Sp$, and Equations (4), (5), and (8) are easily expressed as a function of p^0 and p_2 :

$$Q_i = (D_0/\gamma l)(\exp \gamma Sp^0 - \exp \gamma Sp_2) \quad (9)$$

$$C_i = (1/\gamma) \ln \{ \exp \gamma Sp^0 - x/l(\exp \gamma Sp^0 - \exp \gamma Sp_2) \} \quad (10)$$

$$P_i = (D_0/\gamma \Delta p)(\exp \gamma Sp^0 - \exp \gamma Sp_2) \quad (11)$$

2.11.5.2 Solution–Diffusion Model

When a similar treatment is applied to gas or vapor permeation, the following equations are obtained:

$$Q_i l = \int_{C_1}^{C_2} D(C_i) dC_i \quad (12)$$

$$Q_i = P_i(p_1 - p_2)/l \quad (13)$$

where p_1 and p_2 are the vapor pressures on the high and low concentration sides of the membrane, respectively.

Combining Equations (12) and (13) yields

$$P_i = \left\{ \int_{C_1}^{C_2} D(C_i) dC_i \right\} (p_1 - p_2) \quad (14)$$

Rearrangement gives

$$Q_i l = R = P_i(p_1 - p_2) = \int_{C_1}^{C_2} D(C_i) dC_i \quad (15)$$

where R is the normalized permeation rate. When the concentration-averaged diffusion coefficient, \bar{D}_i , is defined as in Equation (16), P_i and R are expressed as in Equations (17) and (18), respectively:

$$\bar{D}_i = \int_{C_1}^{C_2} D(C_i) dC_i / (C_1 - C_2) \quad (16)$$

$$P_i = \bar{D}_i \{ (C_1 - C_2) / (p_1 - p_2) \} \quad (17)$$

$$R = \bar{D}_i (C_1 - C_2) \quad (18)$$

If the diffusion coefficient is not dependent on permeant concentration, then \bar{D}_i equals D . In PV, the downstream pressure is much lower than the upstream pressure ($p_1 \gg p_2$). Hence, Equations (16)–(18) can be represented as

$$\bar{D}_i = \int_{C_1}^{C_2} D(C_i) dC_i / C_1 \quad (19)$$

$$P_i = \bar{D}_i (C_1 / p_1) \quad (20)$$

$$R = \bar{D}_i C_1 \quad (21)$$

where $C_1/p_1 = S_1$, which is the pseudo-solubility coefficient. Under these conditions P_i may be expressed as

$$P_i = \bar{D}_i S_1 \quad (22)$$

In PV, the separation factor, $\alpha_{B/A}$, a relative measure for the degree of separation, can be represented by

the component mole fractions in the feed and permeate as follows:

$$\alpha_{B/A} = (Y_B/Y_A)/(X_B/X_A) \quad (23)$$

where X_A and X_B are the weight fraction or mole fraction of A and B components in the upstream side, respectively. Y_A and Y_B are the weight fraction or mole fraction of A and B components in the downstream side, respectively.

2.11.5.3 Surface Diffusion

The diffusion behavior of component i in normal bulk solid state is expressed by Fick's first law as

$$\mathcal{F}_i = -D \text{ grad} C_i \quad (24)$$

where \mathcal{F}_i is the permeation rate of component i (component $\text{m}^2 \text{s}^{-1}$), C_i is the concentration of diffused component i (component m^{-3}), and D is the diffusion coefficient ($\text{m}^2 \text{s}^{-1}$).

The behavior of the component on the surface surroundings of the solid is different from that inside of solid. However, the diffusion of the component on the surface of the solid can be defined by Fick's law.

As shown in **Figure 4**, we image a solid in which the concentration of a component is changed only x direction. In this case, the diffusion amount to x direction is expressed as

$$\mathcal{F} = -(dC/dx) \int_0^L D(y) dy \quad (25)$$

The diffusion coefficient is generally defined as a function of the depth direction (y) of solid.

In **Figure 4**, if the component in the solid is homogeneous from interface at $y=0$ to interface at $y=L$, the diffusion amount to x direction is

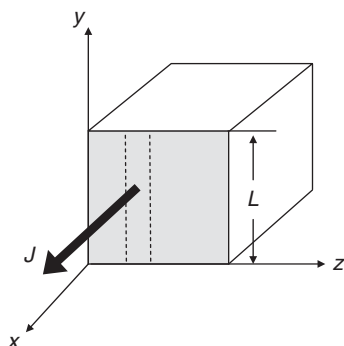


Figure 4 Principle of surface diffusion.

$$\mathcal{F}^B = -D_B(dC/dx)L \quad (26)$$

where D_B is the diffusion coefficient in a homogeneous solid. The permeation rate (\mathcal{F}^S) by the diffusion via a surface is defined as

$$\mathcal{F}^S = 1/2(\mathcal{F} - \mathcal{F}^B) \quad (27)$$

From Equations (25), (26), and (27), \mathcal{F}^S by the diffusion via a surface is

$$\mathcal{F}^S = -1/2(dC/dx) \int_0^L \{D(y)D_B\} dy \quad (28)$$

When the diffusion coefficient of surface is D_s ($\text{m}^2 \text{s}^{-1}$) and the thickness of surface layer is δ , the integral term in Equation (28) is $2D_s\delta$. Namely, the following equation is given:

$$\mathcal{F}^S = -1/2(dC/dx)2D_s\delta = -D_s(dC/dx)\delta \quad (29)$$

2.11.6 Selective Permeation and Separation of Organic Liquid Mixtures

2.11.6.1 Water/Alcohol-Selective Membranes

Water/alcohol-selective membranes are effective for the following scenario. For example, when an aqueous solution of dilute ethanol (~ 10 wt.%) produced by the bio-fermentation is concentrated by distillation, since an aqueous solution of 96.5 wt.% ethanol is an azeotropic mixture, ethanol cannot be concentrated by distillation any more, and, consequently, ethanol is concentrated by azeotropic distillation with the addition of benzene (Bz). If membranes that can preferentially permeate only water at 3.5 wt.% in an azeotropic mixture of aqueous ethanol solution can be developed, significant energy savings would be achieved. The permeation and separation mechanisms in PV, EV, TDEV, and HTPEV [32] through dense membranes consist of the dissolution of the permeants into the membrane, the diffusion of the permeants in the membrane, and the evaporation of the permeants from the membrane. Therefore, the separation of permeants in these membrane separation techniques depends on the differences in the solubility and diffusivity of the permeants in the feed mixture. When the structure of water/alcohol- and water/organic-liquid-selective membranes is dominically designed, hydrophilic materials can be recommended as membrane materials. Therefore, an increase in the solubility of water molecules into the membrane during the solution process can be expected. In order to raise the affinity of membranes for water molecules,

membranes with dissociation groups introduced into their structure are used for dehydration from organic solvents. Various membranes, which permeate water selectively from water/ethanol mixtures, were prepared by the plasma graft polymerization of styrene (*g*-PS) onto porous poly(vinylidene fluoride) (PVF₂) films, by the sulfonation of the grafted membranes, and by the ionization of the sulfonated (*g*-PSS⁻Na⁺) membranes, respectively. The H₂O/EtOH selectivity increased with the ethanol concentration in the feed, and the grafted amount should be controlled for the optimum separation of water. The *g*-PSS⁻Na⁺ membrane with a grafted amount of PS of 0.14 mg cm⁻² was found to have a high permeation rate of 6.6 kg (m² h)⁻¹, and a separation factor of 21 for PV of aqueous 60 wt.% ethanol solution at 50 °C [33].

The PV separation of a concentrated ethanol/water mixture with 90 wt.% of ethanol content through a sodium alginate (NaAlg) membrane was performed to investigate the permeation behavior of the membrane during PV [34]. From the swelling measurements of the membrane in an aqueous solution of 90 wt.% ethanol, the solubility selectivity was about 1000 and the water content in the swollen membrane was 21 wt.% at 40 °C. Its excellent sorption properties could result in the outstanding PV performance for the aqueous solution; higher than a separation factor of 10 000 and 120–290 g m⁻² h⁻¹ permeation rate of 120–290 g (m² h)⁻¹.

The PIC membranes were prepared by ion complex formation between κ -carrageenan and poly {1,3-bis[4-alkylpyridinium]propane bromide}s, with different numbers of methylene units between the two ionic sites within a repeating unit, respectively. The dehydration of a 90 wt.% aqueous ethanol solution was carried out at different temperatures. The selectivity and permeability were very good over a wide temperature range; in the case of the PIC membrane consisting of κ -carrageenan and poly {1,3-bis[4-ethylpyridinium]propane bromide}, the H₂O/EtOH selectivity was 45 000 and the permeability was 150 g (m² h)⁻¹ at 30 °C. With increasing operating temperature, the permeability greatly increased but the selectivity decreased slightly [35]. PIC membranes were prepared by the simultaneous interfacial reaction of aqueous solutions of two oppositely charged polyelectrolytes, that is, from cellulose sulfate and various polycations as well as a cationic surfactant. PV investigations proved that such membranes prepared with polycations might be successfully used for the dehydration of various organic solvents. Measurements of the swelling and PV properties of model membranes

confirm that the anionic polysaccharide, Na-cellulose sulfate, is the only component responsible for good separation capability in the dehydration of organics with PIC membranes [36]. PIC membranes consisting of chitosan (Chito) and poly(acrylic acid) (PAA) were prepared by blending two polymer solutions in different ratios. The thermal properties of PIC membranes constructed from chitosan and PAA by various blend ratios showed a shift in the transition temperature of the PICs. PV performances were investigated with various organic mixtures: water/ethanol, water/1-propanol, and methanol/methyl *t*-butyl ether mixtures. An increase in the PAA content of PIC membranes affected the swelling behavior and PV performance of a water/ethanol mixture. The permeation rate decreased, and the water concentration in the permeate was close to 100% upon increasing the feed alcohol concentration [37]. Asymmetric PIC membranes composed of chitosan membrane and PAA were constructed from an aqueous solution. The absorption quantity of PAA decreased, whereas the water selectivity of the PIC membrane increased with an increase in the molecular weight of PAA. In PV experiments, the water selectivity of the membrane was so high that no ethanol was detected by gas chromatography [38]. The dehydration of an ethanol/water azeotrope during EV using PIC cross-linked chitosan composite (q-Chito-PEO acid PIC/polyethersulfone (PES) composite) membranes, constructed from quaternized chitosan (q-Chito) and polyethylene oxydiglycolic acid (PEO acid) on a porous PES support, was investigated [39, 40]. Both the q-Chito/PES composite and the q-Chito-PEO acid PIC/PES composite membranes showed high H₂O/EtOH selectivity for an ethanol/water azeotrope. Both the permeation rate and the H₂O/EtOH selectivity of the q-Chito/PES composite membrane were enhanced by increasing the degree of quaternization of the chitosan molecule, because the affinity of the q-Chito/PES composite membranes for water was increased by introducing a quaternized ammonium group into the chitosan molecule. Q-Chito-PEO acid PIC/PES composite membranes prepared from an equimolar ratio of carboxylate groups in the PEO acid versus quaternized ammonium groups in the q-Chito showed the best separation factor for H₂O/EtOH selectivity without lowering the permeation rate, as shown in **Figure 5**. With an increasing molecular weight of PEO acid, the separation factor for H₂O/EtOH selectivity increased, but the permeation rate almost did not change. The permeation rate, separation factor for H₂O/EtOH selectivity, and EV

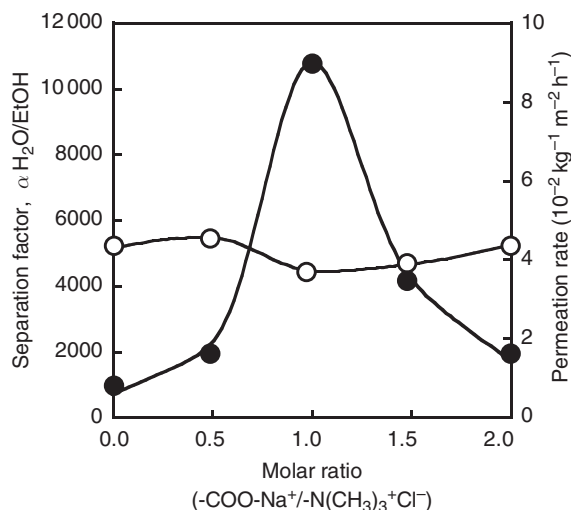


Figure 5 Permeation and separation characteristics for an azeotropic mixture of ethanol/water through q-Chito/PEO acid 4000 polyion complex/PES composite membranes during EV as a function of the molar ratio between the carboxylate groups in PEO acid 4000 and the ammonium groups in q-Chito at 40 °C. From Uragami, T., Yamamoto, S., Miyata, T. *Biomacromolecules* **2003**, *4*, 137–144.

index of the q-Chito-PEO acid 4000 PIC/PES composite membrane with an equimolar ratio of q-Chito were $3.5 \times 10^{-1} \text{ kg (m}^2 \text{ h)}^{-1}$, 6300, and 2205, respectively. The separation factor for aqueous solutions of 1- and 2-propanol was also maximized at an equimolar ratio of carboxylate groups and ammonium groups, and was greater than for an ethanol/water azeotrope.

The dehydration of aqueous alcohol solutions through asymmetric nylon 4 (N4) membranes was investigated using the PV processes. A separation factor of 4.72 and a permeation rate of $0.78 \text{ g (m}^2 \text{ h)}^{-1}$ for the asymmetric membrane were obtained. When compared to conventional homogeneous N4 membranes, the asymmetric membrane can effectively supersede the PV performance of the N4 membrane for the separation of water/alcohol mixtures [41]. A 4-vinylpyridine-grafted-polycarbonate (PC-*g*-4VP) membrane was prepared for PV of water selectivity. Water was permeated through the PC-*g*-4VP membrane preferentially over all feed compositions. The permeation rate and separation factor increased with increasing 4-vinylpyridine content in the membrane. The total permeation rate of a PC-*g*-4VP membrane with grafting of 26.7% was $153 \text{ g (m}^2 \text{ h)}^{-1}$, and the separation factor was above 6300 for an aqueous solution of 90 wt.% ethanol [42]. A hydrophilic PV

membrane was prepared via the homografting polymerization of *N,N'*-(dimethylamino)ethyl methacrylate (DMAEM) onto a nylon N4 backbone, thus generating the DMAEM-*g*-N4 membrane [43]. The water selectivity was improved by the ammonium quaternization of the pendant *N,N'*-dimethylamino group on the DMAEM-*g*-N4 membrane using dimethyl sulfate, resulting in a DMAEMQ-*g*-N4 membrane. The separation factor and permeation rate for both chemically modified N4 membranes were higher than those of the unmodified N4 membrane. Optimum PV was obtained by a DMAEMQ-*g*-N4 membrane with a degree of grafting of 12.7% for a 90 wt.% ethanol feed concentration, giving a separation factor of 36 and a permeation rate of $564 \text{ g (m}^2 \text{ h)}^{-1}$. Temperature-sensitive membranes were synthesized by grafting poly(*N*-isopropylacrylamide) (PNIPAAm) onto a PVA backbone using hydrogen peroxide–ferrous ion as an initiator. Due to the grafting of PNIPAAm, the hydrophilic/hydrophobic balance and the polarity of the pendant groups within the membranes were modified. Significant temperature sensitivity of the grafted membranes was observed close to the lower critical solution temperature (LCST) of linear PNIPAAm membranes during the PV of an ethanol/water mixture. Both the PV and sorption selectivities for water showed a maximum value in the vicinity of 30–32 °C for ethanol contents of 75% and 80%. The temperature sensitivity of the grafted membranes also depended on the ethanol concentration. The maximum PV and solubility selectivities disappeared when the ethanol content was lower than 75%, because the greater degree of swelling reduced the size screening effect of the membrane [44].

Interpenetrating polymer network (IPN) PV membranes were prepared by the free-radical polymerization of acrylamide (AAm) or acrylic acid (AA) in the presence (or absence) of the cross-linking agents allyldextran or *N,N'*-methylenebisacrylamide within cellophane films swollen in the reaction mixture. IPN membranes were selective over a wide range of ethanol concentrations in the feed. The separation factor and the permeation rate improved significantly with increasing PAAm–PAA in the IPN membranes, especially for the cellulose-PAA (K⁺ form) membranes; for an 86% EtOH feed at 50 °C. The separation characteristics of these membranes were in good correlation with their swelling behavior [45].

Three different types of blend membranes, based on Chito and PAA, were prepared, and their performance for the PV separation of a water/ethanol

mixture was investigated. All membranes were highly H₂O/EtOH selective. The temperature dependence of the membrane for H₂O/EtOH selectivity for feed solutions of higher water content (>30 wt.%) was unusual in that both the permeability and the separation factor increased with increasing temperature. A comparison of the PV performance between composite and homogeneous membranes was made, and typical PV results at 30 °C for a 95 wt.% ethanol aqueous solution were as follows. For the homogeneous membrane, the permeation rate was 33 g (m²h)⁻¹ and the separation factor was 2216; for the composite membrane, the permeation rate was 132 g (m²h)⁻¹ and the separation factor was 1008 [46]. Blend membranes were prepared by coagulating a mixture of *O*-carboxymethylated chitosan (CM-Chito) and alginate in an aqueous solution with 5 wt.% CaCl₂, and then by treating it with a 1 wt.% HCl aqueous solution. Polymer interpenetration including a Ca²⁺ cross-linked bridge occurred in the blend membrane, and resulted in a high separation factor for the PV separation of alcohol/water and low permeation rate. The thermostability of the blend membranes was significantly superior to that of alginic acid and cellulose/alginate blend membranes, owing to a strong electrostatic interaction caused by the amino groups of CM-Chito with the carboxylic acid groups of alginic acid [47].

To obtain water-permeable membranes, the introduction of dissociation groups and hydrophilic groups into polymer membrane materials, chemical modification, graft copolymerization, and polymer blends have all been attempted. However, adequate membrane performance cannot be obtained by only improving hydrophilicity of the membrane materials. Most importantly, membrane performance is significantly affected by the swelling of the polymer membrane due to the feed mixture. Cross-linking is one of the methods that can maintain the hydrophilicity of the membrane while attenuating the swelling of the membrane.

In Figure 6, the permeation rate and ethanol concentration in the permeate through Chito and glutaraldehyde (GA) cross-linked chitosan (GAC) membranes during EV, and the degree of swelling of the membrane are shown as a function of the feed composition [48]. The GAC membrane had a 0.5% GA content (3.2% GA in the casting solution). Both the Chito and GAC membranes had a low ethanol concentration in the permeate, and showed high H₂O/EtOH selectivity. Furthermore, there are significant differences between the compositions of the

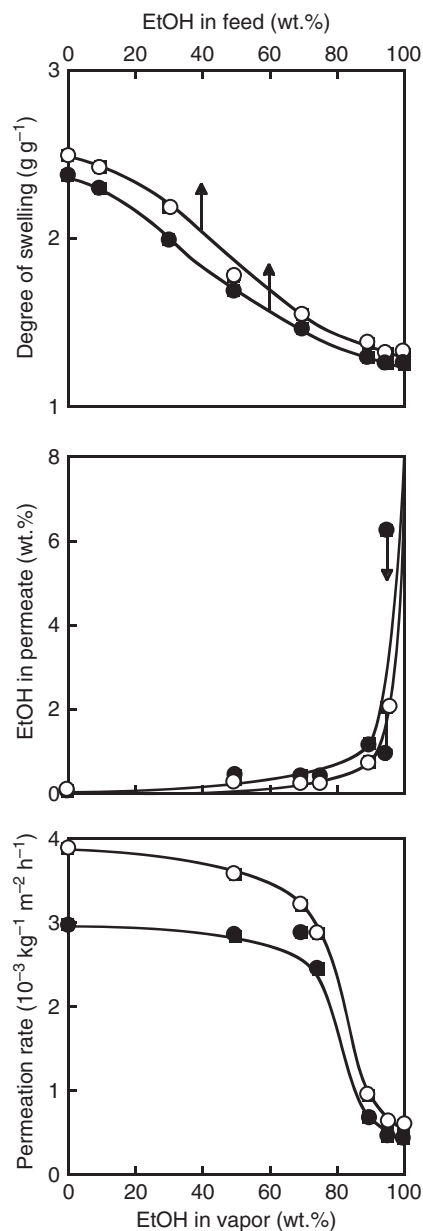


Figure 6 Effects of the ethanol concentration in the feed vapor on the permeation and concentration characteristics and the degree of swelling of the Chito (○) and GAC (●) membranes by EV. From Urugami, T., Matsuda, T., Okuno, H., Miyata, T. *J. Membr. Sci.* **1994**, *88*, 243–251.

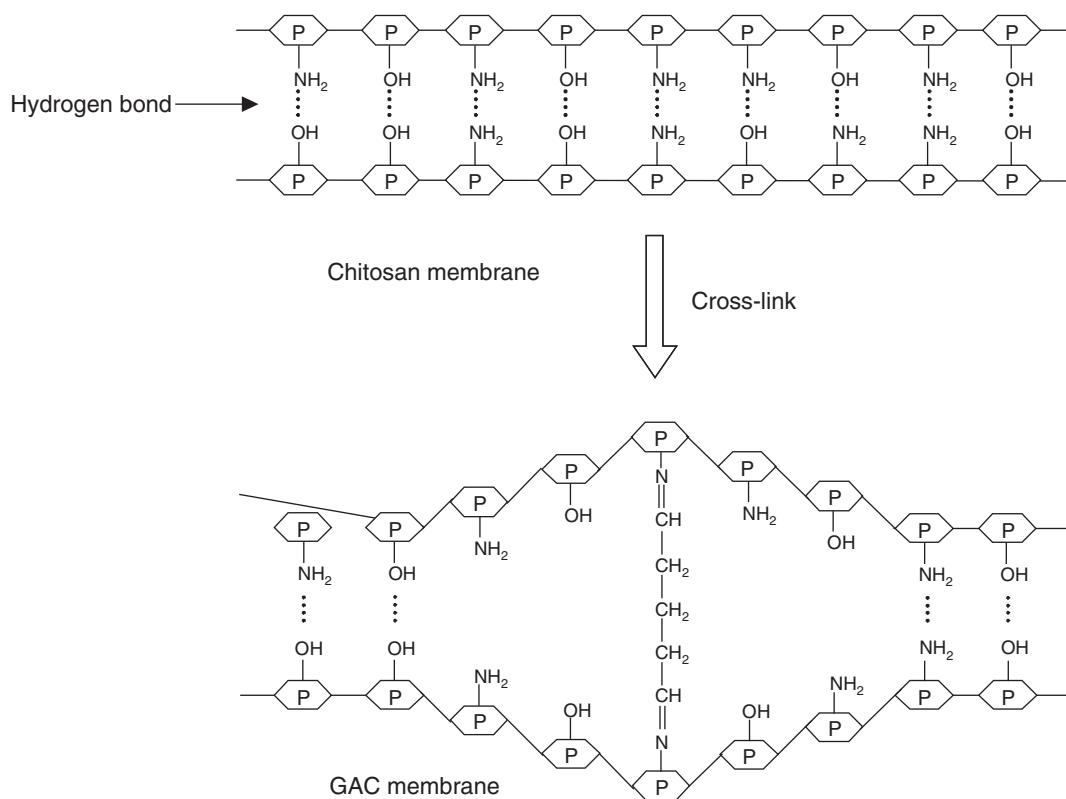
permeate from the Chito and GAC membranes; it was higher than that of the Chito membrane in spite of the fact that the permeation rate of the GAC membrane was greater than that of the Chito membrane. In addition, the degree of swelling of the GAC membrane was higher than that of the chitosan membrane and this tendency increased with decreasing

ethanol concentration in the feed mixture. When polymer membranes are cross-linked, in general, the permselectivity is improved but the permeation rate is decreased because the degree of swelling of the membrane is lowered. In this case, the permeation rate, the H₂O/EtOH selectivity, and degree of swelling of the GAC membrane, however, were higher than those of the Chito membrane. In order to clarify the results in Figure 6, the density and crystallinity of the Chito and GAC membranes were determined by the flotation method and wide-angle X-ray diffraction, respectively.

The density and the correlation crystallinity index decreased with increasing GA content in the casting solution. These results imply that the increase in the cross-linking of the Chito membrane decreased the density and crystallinity of the membrane. Based on the above results, the model structure shown in Scheme 1 is proposed for the Chito and GAC membranes. The chitosan membrane has many intermolecular hydrogen bonds between hydroxyl groups and amino groups. A few of these hydrogen bonds in the GAC membrane are

broken by cross-linking with GA and free hydrophilic groups, such as hydroxyl and amino groups, are formed. These hydrophilic groups have a strong affinity for water molecules, that is, the solubility of water molecules into the GAC membrane is increased. Conversely, since the size of the water molecules sorbed into the GAC membrane is smaller than that of the ethanol molecule, the water molecule can be diffused more easily into the GAC membrane than the ethanol molecule. Consequently, the GAC membranes are moderately swollen by water molecules, and simultaneously increase the H₂O/EtOH selectivity. The increase in the H₂O/EtOH selectivity of the GAC membrane is due to both the increase in the solubility of water molecules into the GAC membrane and the increase in the diffusivity of water molecules into the GAC membrane. From the above discussion, both the increase in the permeation rate and the improved H₂O/EtOH selectivity with increasing GA content cross-linked in the Chito membrane can be understood.

The permeation and separation characteristics during EV of an ethanol/water azeotrope (96.5



Scheme 1 Model structures of the chitosan and GAC membranes. $\langle P \rangle$, pyranose ring. From Uragami, T., Matsuda, T., Okuno, H., Miyata, T. *J. Membr. Sci.* **1994**, *88*, 243–251.

wt.% ethanol) through q-Chito membranes and cross-linked q-Chito membranes, which were cross-linked with diethylene glycol diglycidyl ether (DEGDGE), were studied [49]. Both the q-Chito and the cross-linked q-Chito membranes showed high H₂O/EtOH selectivity for an ethanol/water azeotrope. The permeation rates for both membranes decreased and the H₂O/EtOH selectivity increased, with an increasing degree of quaternization of the chitosan and increasing cross-linker concentration. The mechanism responsible for the separation of an ethanol/water azeotrope through the q-Chito and cross-linked q-Chito membranes was analyzed by the solution-diffusion model. Increasing permeation temperature increased the permeation rate and decreased the H₂O/EtOH selectivity for both membranes. However, the permeation rates of a cross-linked q-Chito membrane at 60–80 °C were almost the same as those of the q-Chito membrane, and the separation factors for H₂O/EtOH selectively in the former were 4100–4200 and greater by two orders of magnitude as compared to those in the latter.

Two types of q-Chito membranes were prepared for the dehydration of ethanol/water mixtures. One was prepared by coating a casting solution of q-Chito containing GA with a HCl catalyst onto a porous PES support (membrane A). The other, membrane B, was further cross-linked in an aqueous GA solution with a H₂SO₄ catalyst (membrane B). These membranes were then used for the dehydration of ethanol/water mixtures in HTPEV. The permeation rate increased with increasing feed vapor pressure, but decreased with an increase in the feed vapor temperature under constant feed vapor pressure. This decrease in the permeation rate could be attributed to a lowering of the vapor density, which is the ratio of the feed vapor pressure over the total pressure (P_1/P_T). The permeation rate derived from the relationship given by an empirical equation, which was driven statistically by the experimental data with a change in the feed vapor temperature under constant feed vapor pressure, agreed closely with that predicted from the equation as a function of the ratio of P_1/P_T . The separation characteristics for H₂O/EtOH selectivity in the water/ethanol vapor increased with a decrease in the difference between P_T and P_1 [50].

To inhibit the swelling of PVA membranes in aqueous solutions, which leads to lowered water permselectivity during separation, organic-inorganic hybrid membranes composed of PVA and tetraethoxysilane (TEOS) were prepared. When an aqueous

ethanol solution was permeated through the PVA/TEOS hybrid membranes during PV, the H₂O/EtOH selectivity increased; however, the permeation rate decreased, with increasing TEOS content. This decreased permeation rate caused a decreased degree of swelling of the membrane. This decrease in the degree of swelling and increase in the membrane density were due to the formation of hydrogen bonds between the silanol groups resulting from the hydrolysis of TEOS and the hydroxyl group of PVA. When the PVA and PVA/TEOS hybrid membranes were annealed, the H₂O/EtOH selectivity of these membranes increased with increasing annealing temperature and time. The fact that annealing at higher temperatures promoted the dehydration-condensation reaction between PVA and TEOS in the PVA/TEOS membranes was related to the enhanced H₂O/EtOH selectivity of the PVA/TEOS membranes [51]. Hydrophilic organic-inorganic hybrid membranes were prepared from hydrophilic q-Chito and TEOS by a sol-gel process, in order to minimize the swelling of the q-Chito membranes. When an azeotrope of ethanol/water was permeated through their q-Chito/TEOS hybrid membranes during PV, the q-Chito/TEOS hybrid membranes showed high H₂O/EtOH selectivity. However, the H₂O/EtOH selectivity of the membranes decreased slightly with increasing TEOS content over 45 mol.%. Furthermore, the H₂O/EtOH selectivity of these membranes is discussed from the viewpoint of their chemical and physical membrane structure [52].

Swelling of poly(vinyl alcohol-co-acrylic acid) (P(VA-co-AA)) membranes in aqueous alcohol solutions operated under PV conditions leads to low H₂O/EtOH selectivity. To reduce swelling, organic-inorganic hybrid membranes composed of P(VA-co-AA) and TEOS were prepared. However, when an aqueous ethanol solution was permeated through the P(VA-co-AA)/TEOS hybrid membranes by PV, the permeation rate increased and the H₂O/EtOH selectivity decreased with increasing TEOS content. The increase in the permeation rate and the decrease in the H₂O/EtOH selectivity were caused by an increase in the degree of swelling of the membrane and a decrease in the membrane density with increasing TEOS content. These effects resulted from insufficient formation of hydrogen bonds between the silanol groups by hydrolysis of TEOS and the hydroxyl and carboxyl groups of P(VA-co-AA). When the P(VA-co-AA)/TEOS hybrid membranes were annealed, the water/ethanol separation factor for H₂O/EtOH selectivity increased with

increasing annealing time and TEOS content. Longer annealing time promoted the dehydration–condensation reaction between P(VA-*co*-AA) and TEOS in P(VA-*co*-AA)/TEOS hybrid membranes, leading to enhanced H₂O/EtOH selectivity of the hybrid membranes [53].

To control the swelling of PVA membranes, mixtures of PVA and an inorganic oligosilane were prepared using sol–gel reactions to yield new PVA/oligosilane hybrid membranes. In the separation of an ethanol/water azeotropic mixture during PV, the effect of the oligosilane content on the H₂O/EtOH selectivity of PVA/oligosilane hybrid membranes was investigated. The H₂O/EtOH selectivity of PVA/oligosilane hybrid membranes was higher than that of PVA membranes, but the H₂O/EtOH selectivity of hybrid membranes decreased with increasing oligosilane content. In order to increase the H₂O/EtOH selectivity, PVA/oligosilane hybrid membranes were annealed. The H₂O/EtOH selectivity of annealed PVA/oligosilane hybrid membranes was greater than that of unannealed hybrid membranes, and significantly governed by the oligosilane content, which could be attributed to both solubility and diffusion selectivities. The relationship between the structure of unannealed and annealed PVA/oligosilane hybrid membranes along with permeation and separation characteristics of an ethanol/water azeotropic mixture during PV are discussed in detail [54].

PV and EV separations of water/alcohol mixtures, through a modified N4 membrane-coated with plasma-deposited, hydrolyzed vinyl acetate (VAc) – (PVA-*p*-N4), were investigated. The separation factor and the permeation rate of this PVA-*p*-N4 membrane are both higher than those of the unmodified N4 membrane for PV of aqueous ethanol solutions. The PVA-*p*-N4 membrane showed a separation factor of 13.5, and a permeation rate of 420 g (m² h)⁻¹ can be obtained. Compared with PV, EV effectively increased the separation factor for the water/alcohol mixtures, but the permeation rate decreased the permeation rate [55].

To improve the hydrophilicity of an N4 membrane for PV and EV processes, and to overcome the hydrolysis of PVA, a PVA-*g*-N4 membrane by γ -ray irradiation grafting of VAc onto N4 membrane was prepared, and then followed by hydrolysis treatment. A separation factor of 13.8 and a permeation rate of 0.352 kg (m² h)⁻¹ can be obtained for a PVA-*g*-N4 membrane with a degree of grafting of 21.2% for a 90 wt.% ethanol feed concentration. Compared to the PV process, the EV process had a significantly

increased separation factor with a decreased permeation rate for the same PVA-*g*-N4 membrane [56].

Twelve types of polyimide membranes were prepared using three dianhydrides (including 2,2-bis[4-(3,4-dicarboxyphenoxy)phenyl]propane dianhydride (BPADA), 3,3',4,4'-benzophenonetetracarboxylic dianhydride (BTDA), and 3,3',4,4'-biphenyltetracarboxylic dianhydride (ODPA)) and four diamines (including benzidine (BZD), bis(4-aminophenyl)phenyl phosphate (BAPP), 4,4'-diaminodiphenylmethane (MDA), and 4,4'-diaminodiphenyl ether (ODA)) via a two-step method. The permeation rate of ethanol/water mixtures through the polyimide membranes with the same dianhydrides increases following the order of BZD < ODA < MDA < BAPP. The permeation rate increases with increase in temperature [57].

Zeolite-embedded hybrid membranes are manufactured by using a casting machine with polyester nonwoven fabric as the supporting layer, polyacrylonitrile (PAN) as the porous backing layer, and PVA as the active separating layer. Experimental results show the H₂O/EtOH selectivity has been greatly improved after adding zeolite 4A and that reasonably high separation factor can be achieved for feed ethanol concentration of above 80 wt.%, probably due to the superior molecular-sieving effect of added zeolite 4A on the water/ethanol system. By incorporation of zeolite, apparent Arrhenius activation energy significantly decreased for water but obviously increased for ethanol. Water molecules require much less energy, whereas ethanol molecules need much more energy to transport through the membrane because of the hydrophilic characteristics of zeolite 4A [58].

The separation of aqueous alcohol mixtures was carried out by the use of a series of novel aromatic polyamide membranes. The aromatic polyamides were prepared by the direct polycondensation of 2,2'-dimethyl-4,4'-bis(aminophenoxy)biphenyl (DBAPB) with various aromatic diacids, such as terephthalic acid (TPAc), 5-*tert*-butylisophthalic acid (TBPAc), and 4,4'-hexafluoroisopropylidenedibenzoic acid (FDAc). The solubility of ethanol in the aromatic polyamide membranes is higher than that of water; however, the diffusivity of water through the membrane is higher than that of ethanol. The effect of diffusion selectivity on the membrane separation performances plays an important role in the EV process. Compared with PV, EV effectively increased the H₂O/EtOH selectivity. Moreover, the effect of aromatic diacids on the polymer chain packing density on the PV and EV performance were investigated. The permeation rate could be increased

by introduction of a bulky group into the polymer backbone [59].

A series of soluble polyimides derived from 3,3',4,4'-benzhydrol tetracarboxylic dianhydride (BHTDA) with various diamines, such as 1,4-bis(4-aminophenoxy)-2-*tert*-butylbenzene (BATB), 1,4-bis(4-aminophenoxy) 2,5-di-*tert*-butylbenzene (BADTB), and 2,2'-dimethyl-4,4'-bis(4-aminophenoxy)biphenyl (DBAPB), were investigated for PV separation of ethanol/water mixtures. Diamine structure effect on the PV of 90 wt.% aqueous ethanol solution through the BHTDA-based polyimide membranes was studied. The H₂O/EtOH selectivity was ranked in the order of BHTDA-DBAPB > BHTDA-BATB > BHTDA-BADTB. The increase in molecular volume for the substituted group in the polymer backbone increased the permeation rate. As the feed ethanol concentration increased, the permeation rate increased, while the water concentration in the permeate decreased for all polyimide membranes. The optimum PV performance was obtained by the BHTDA-DBAPB membrane with an aqueous ethanol solution of 90 wt.%, giving a separation factor of 141, permeation rate of 255 g (m² h)⁻¹, and 36 000 of PSI [60].

Novel organic-inorganic hybrid membranes were prepared through sol-gel reaction of PVA with γ -aminopropyltriethoxysilane (APTEOS) for PV separation of ethanol/water mixtures. The amorphous region of the hybrid membranes increased with increasing APTEOS content, and both the free volume and the hydrophilicity of the hybrid membranes increased when APTEOS content was less than 5 wt.%. The swelling degree of the hybrid membranes has been restrained in an aqueous solution owing to the formation of hydrogen and covalent bonds in the membrane matrix. Permeation rate increased remarkably with an increasing APTEOS content, and H₂O/EtOH selectivity increased at the same time; the tradeoff between the permeation rate and H₂O/EtOH selectivity of the hybrid membranes was broken. The sorption selectivity increased with increasing temperature, but decreased with increasing water content. The hybrid membrane containing 5 wt.% APTEOS has the highest separation factor of 536.7 and permeation rate of 0.035 5 kg (m² h)⁻¹ in PV separation of 5 wt.% water in the feed [61].

Sericin/PVA blend membranes were prepared by blending sericin and PVA, followed by chemical cross-linking with dimethylolurea. The blend membranes were preferentially permeable to water. In the temperature range of 50–70 °C, a permeate water concentration of 93.1–94.1 wt.% was achieved at 8.5 wt.% water in the feed. As a comparison, membranes

were also fabricated from pure sericin and PVA alone, and tested for PV separation under the same conditions. The water selectivity of membrane was primarily derived from sorption selectivity, and there was a strong coupling effect for the permeation and sorption of the permeant in the membranes [62].

Energy-efficient dehydration of low-water-content ethanol is a challenge for the sustainable production of fuel-grade ethanol. Blends of cross-linked mixture of poly(allylamine hydrochloride) and hydrolyzed PVA of 99% and 88% were prepared as pervaporative dehydration membrane. These polymeric membranes had higher H₂O/EtOH selectivity for low feed water concentrations (<5 wt.%) than 99% hydrolyzed PVA [63].

Novel semi-IPN membranes of sodium alginate (NaAlg) and thermoresponsive PNIPAAm were prepared by free radical polymerization using potassium persulfate as an initiator [64]. Membranes were cross-linked with GA and used in PV separation of water/ethanol mixtures at varying feed compositions and temperatures. PV separation characteristics of the membranes showed a dependence on the thermosensitive nature of NIPAAm. Increasing the NIPAAm content of the semi-IPN resulted in an increased selectivity with a decreased permeation rate. The membrane containing 30 wt.% NIPAAm showed the highest H₂O/EtOH selectivity of 18 881 with a permeation rate of 0.137 kg (m² h)⁻¹ at 40 °C, that is, the above LCST of NIPAAm, but below its LCST, that is, at 25 °C, it exhibited considerably a lower H₂O/EtOH selectivity of 92 with a permeation rate of 0.185 kg (m² h)⁻¹ for 15 wt.% water in the feed. The H₂O/EtOH selectivity decreased with decreasing temperature at 15 wt.% water below the LCST region, that is, at 30 °C. The pore size of membrane became larger, the permeation rate increased up to 0.225 kg (m² h)⁻¹, but the H₂O/EtOH selectivity decreased.

Sulfonated poly(phenylene oxide) (SPPO) membranes were prepared for dehydrating water/ethanol mixtures. The effects of hydration of sulfonated membranes on PV performance were discussed by comparing the characteristics of pure PPO and SPPO membranes. The differences in microstructural and hydrophilic properties of membranes were characterized by means of atomic force microscopy and swelling test. The degree of sulfonation of PPO significantly affected the hydrophilicity of sulfonated membranes and played an important role for the dehydration performance of PV membranes. The sulfonated membranes showed excellent water permeation rate

of about $300 \text{ g (m}^2 \text{ h)}^{-1}$ with good selectivity up to 700. SPPO membranes exhibited better PV performance than pure PPO membranes [65].

The asymmetric aluminum ion-exchange polysulfone (PS) membranes were prepared for the dehydration of ethanol/water mixture. The separation performance of those membranes was increased with increasing the degree of aluminum ion exchange in PS membranes. Both the permeation rate and separation factor of these membranes increased with increasing the degree of ion exchange. The increase in separation performance of aluminum ion-exchange membranes was mainly attributed to ion cross-linking in polymer network and the degree of hydration of exchanged ion in membranes. Conversely, the operating temperature in the PV process showed a significant influence on the dehydration of water molecules in the permeate. An increase in temperature, in turn, increased the permeation rate of permeate, but slightly decreased $\text{H}_2\text{O}/\text{EtOH}$ selectivity [66].

Through the complexation of two anionic polysaccharide blends composed of NaAlg and carrageenan with divalent calcium ions, PIC membranes were prepared. The effects of annealing on the structure of the PIC membranes and on their performance at removing water from a methanol mixture were investigated. The annealed membranes exhibited a change in their crystallinity. The change was due to a rearrangement of polymer chains, which was induced by a deformation of the chelate structure and intramolecular or intermolecular interactions between the polysaccharides. Because of the effects of annealing on the resulting membranes, water components nearly penetrated the membranes to the permeate side in the vapor permeation process. Moreover, the membrane performances were gradually enhanced as the operating temperature increased [67].

Cross-linked, dense PVA membranes with different degrees of hydrolysis were prepared and used in the sorption and PV of 2-propanol (IPA)/water mixtures. The partial permeation rate for water permeation was increased with increasing water content in the liquid mixture, but the partial permeation of 2-propanol due to the coupling effect of sorption and permeation reached a maximum value. The degree of PVA hydrolysis and the feed temperature influenced the permeation rate and $\text{H}_2\text{O}/\text{IPA}$ selectivity due to the degree of PVA hydrolysis, and the selectivity of PVA for water was inversely proportional to the degree of PVA hydrolysis [68].

A thin, dense Chito membrane coated onto a hydrolyzed PAN support membrane [69] had a good permeation rate of $0.26 \text{ kg (m}^2 \text{ h)}^{-1}$, and a high separation factor for $\text{H}_2\text{O}/\text{IPA}$ selectivity of more than 8000 for an aqueous solution of 90 wt.% ethanol at 60°C ; the same membrane reached 0.8 and 1 kg $(\text{m}^2 \text{ h)}^{-1}$ for the permeation rates of an aqueous solution of 80 wt.% of 1-propanol and 2-propanol, respectively, with a separation factor of about 10^5 .

The surface of a cellulose triacetate membrane was modified with gaseous plasma in the presence of ammonia gas. The contact angle measurement indicated that the hydrophilicity of the surface increased. These membranes showed excellent $\text{H}_2\text{O}/\text{IPA}$ selectivity for water in the separation of an aqueous solution of 2-propanol. The permeation rate of water increased with an increase in the treatment time for all concentrations of IPA in the feed. Surface-modified cellulose acetate (CA) membranes treated with magnetron-enhanced plasma also showed high $\text{H}_2\text{O}/\text{IPA}$ selectivity for the separation of a 2-propanol/water mixture during PV [70].

Blend membranes of Na-Alg and PAAm-grafted guar gum (PAAm-*g*-GG) in ratios of 3:1 and 1:1 were prepared for the PV separation of a water/2-propanol mixture. Membranes prepared from pure Na-Alg (M-1) and 1:1 blends of Na-Alg and PAAm-*g*-GG (M-3) showed the highest separation selectivity for 10 mass% water in the feed mixture, whereas a membrane prepared with a 3:1 blend ratio of Na-Alg and PAAm-*g*-GG showed the highest permeation selectivity for 20 mass% water in the feed. The $\text{H}_2\text{O}/\text{IPA}$ selectivity decreased with increasing amounts of grafted copolymer in the blend mixture. The permeation rate increased with increasing amounts of water in the mixture; however, the permeation rate did not change markedly with the PAAm-*g*-GG content in the blend membrane at the lower mass% water [71].

Cross-linked organic-inorganic hybrid Chito membranes were obtained from blending Chito and γ -(glycidyoxypropyl) trimethoxy-silane (GPTMS) in acetic acid aqueous solution. The hydrophilicity of the modified membranes was not significantly decreased, so as to result in good $\text{H}_2\text{O}/\text{IPA}$ selectivity and high permeation rate in pervaporative dehydration on a 70 wt.% 2-propanol/water mixture. The chitosan membrane containing 5 wt.% GPTMS had a permeation rate of $1730 \text{ g (m}^2 \text{ h)}^{-1}$ and separation factor of 694 for $\text{H}_2\text{O}/\text{IPA}$ selectivity [72].

The effectiveness of chemical cross-linking modification of P84 copolyimide membranes, using

diamine compounds for PV dehydration, has been investigated and the scheme to enhance separation performance of asymmetric polyimide membranes was developed. Two diamine cross-linking agents, *p*-xylenediamine (XDA) and ethylenediamine (EDA), were used in this study for both dense and asymmetric P84 membranes. Experimental results suggest that the cross-linking reaction induced by EDA is much faster than that by XDA because the former has a smaller and linear structure than that of the latter. However, membranes cross-linked by *p*-XDA are thermally more stable than those by EDA. Membranes modified by *p*-XDA or EDA have increased hydrophilicity. An increase in the degree of cross-linking reaction initially results in an increase in separation factor with the compensation of lower permeation rate for PV dehydration of 2-propanol. However, a further increase in the degree of cross-linking reaction may swell up the polymeric chains because of the hydrophilic nature of these diamine compounds, thus resulting in low separation performance. Posttreatment after cross-linking reaction can significantly enhance as well as tailor membrane performance because of the formation of charge transfer complexes and the enhanced degree of cross-linking reaction. A low-temperature heat treatment developed PV membranes with high permeation rate and medium separation factor for H₂O/IPA selectivity, whereas a high-temperature heat treatment produced membranes with high separation factor with medium permeation [73].

Four cross-linked PVA/trimesoyl chloride (TMC) membranes with different degrees of cross-linking were prepared by applying TMC/hexane to the surfaces of dried PVA membranes. Fourier transform infrared spectroscopy–attenuated total reflectance (FTIR–ATR) spectroscopy revealed that PVA–TMC membranes had asymmetric molecular structures. PV properties were studied through water permeation at different temperatures and dehydration of 2-propanol/water mixtures at different temperatures and with different feed water fractions. Results showed that PVA–3TMC had the best overall PV properties among the four PVA–TMC membranes [74].

Chitosan/poly(tetrafluoroethylene) (Chito/PTFE) composite membranes were prepared from casting a GPTMS-containing chitosan solution on poly(styrene sulfuric acid) grafted expanded poly(tetrafluoroethylene) film surface. The adhesion between the chitosan skin layer and the PTFE substrate was fairly good to warrant the high performance of Chito/PTFE

composite membranes used in PV dehydration processes on 2-propanol. The Chito/PTFE membrane exhibited a permeation rate of 1730 g (m² h)⁻¹ and a separation factor of 775 for H₂O/IPA selectivity of 775 at 70 °C for an aqueous solution of 70 wt.% IPA [75].

β -TDI/MDI (P84)/PES dual-layer hollow fibers for PV dehydration of 2-propanol were developed. The effects of spinning conditions, for example, air-gap distances, outer- and inner-layer dope flow rates on membrane formation, morphology, and PV performance, have been investigated. Compared to the wet-spun dual-layer hollow fibers, macrovoids in the outer layer are significantly suppressed in the dry-jet wet-spun fibers. The intrusion of nonsolvent from the outer layer may propagate the formation of finger-like macrovoids into the inner layer. Because of different phase-inversion rates in the dual layers, the effects of elongational stresses in the air-gap region on the separation performance of dual-layer hollow fibers are much more complicated than that of single-layer hollow fibers. Both, thermal treatment at elevated temperatures and chemical cross-linking modification by XDA, were investigated. Heat treatment at 200 °C increases the separation factor with reduced permeation rate. However, unlike single-layer P84 hollow fibers, further increased heat treatment temperatures do not enhance separation property of P84/PES dual-layer hollow fibers because of the enhanced sublayer resistance via the densification of PES layer. The performance enhancement by XDA cross-linking seems to be very promising for the P84/PES dual-layer hollow fiber because XDA induces cross-linking reactions only in the P84 outer layer. The best H₂O/IPA selectivity is reached at cross-linking time of 2 h. This study demonstrates that a significant material cost saving can be achieved without sacrificing separation performance by choosing the dual-layer hollow-fiber approach with the aid of XDA cross-linking modification [76].

Using a solution technique, novel polymeric membranes were prepared by incorporating water-soluble blocked diisocyanate into Chito. The membrane containing 40 mass% of blocked diisocyanate showed the highest separation for H₂O/IPA selectivity of 5918 with a permeation rate of 2.20×10^{-2} kg (m² h)⁻¹ at 30 °C for 5 mass% of water. The total permeation rate and permeation rate of water were found to be overlapping, particularly for higher cross-linked membranes, suggesting that the membranes developed with higher amount of blocked diisocyanate could be used effectively to break the

azeotropic point of water/2-propanol mixture, so as to remove a small amount of water from 2-propanol [77].

Chito and hydroxypropyl cellulose (Chito/HPC) blend membranes prepared by solution-casting method, followed by cross-linking with urea–formaldehyde–sulfuric acid mixture, were tested for the PV dehydration of 2-propanol. Blend membrane containing 20 wt.% HPC (Chito/HPC-20) gave a high selectivity of 11 241 for 10 wt.% water containing feed mixture. Comparatively, a low selectivity of 488 was observed for plain cross-linked Chito membrane for the same feed mixture; this value further decreased with increasing water composition of the feed mixture. The permeation rate of the plain Chito membrane increased from 0.074 to 0.246 kg (m² h)⁻¹ over the feed water compositions of 10–30 wt.%. For Chito/HPC-20 membrane, permeation rates increased from 0.132 to 0.316 kg (m² h)⁻¹. The observed permeation rate was higher for Chito/HPC blend membranes, but lower for the plain cross-linked Chito membrane; nevertheless, the H₂O/IPA selectivity was higher for Chito/HPC-10 and Chito/HPC-20 blend membranes. For Chito/HPC-40 membrane, the permeation rate was increased from 0.226 to 0.391 kg (m² h)⁻¹, but H₂O/IPA selectivity decreased from 453 to 80 over the composition range of 10–30 wt.% water in the feed. With increasing temperature, flux increased considerably, but the H₂O/IPA selectivity decreased [78].

Mixed-matrix membranes of PVA loaded with phosphomolybdic heteropolyacid (HPA) and cross-linked with GA were prepared by the solution-casting technique. At high content (i.e., 7 wt.% with respect to weight of PVA) of HPA, the mixed-matrix membranes could extract water efficiently on the permeate side with a selectivity of 90 000 and a permeation rate of 0.032 kg (m² h)⁻¹ for 10 wt.% of water containing feed mixture. Permeation rate of the mixed-matrix membranes decreased with increasing concentrations of HPA; however, a significant improvement in PV performance was observed for HPA-loaded membranes than the pristine PVA [79].

CM-Chito/PS hollow-fiber composite membranes were prepared through GA as the cross-linking agent and PS hollow-fiber ultrafiltration membrane as the support. The permeation and separation characteristics for dehydration of 2-propanol were investigated by the PV method. The cross-linked CM-Chito/PS hollow-fiber composite membranes had high H₂O/IPA selectivity and promising permeability. The permeation rate and

separation factor for H₂O/IPA selectivity were 38.6 kg (m² h)⁻¹ and 3238.5, respectively, using 87.5 wt.% of 2-propanol concentration [80].

Matrimid(R) polyimide asymmetric hollow fibers have been fabricated and applied for PV dehydration of IPA. The effectiveness of thermal annealing at high temperatures and/or chemical cross-linking using 1,3-propane diamine (PDA) on the separation property of these fibers has been investigated. An increase in the degree of cross-linking results in an increase in separation factor for H₂O/IPA selectivity and a decrease in the permeation rate. Thermal annealing alone has failed to improve hollow-fiber performance due to the cracks caused by inhomogeneous shrinkage in heating process. Nevertheless, appropriate application of thermal annealing as a pretreatment for cross-linking can produce fibers with the optimal performance. The pristine hollow fibers had a permeation rate and a separation factor for H₂O/IPA selectivity of 6.2 kg (m² h)⁻¹ and 7.9, respectively; with this thermal treatment followed by cross-linking, the permeation rate and separation factor changed to 1.8 kg (m² h)⁻¹ and 132, respectively. The formation of charge-transfer complexes within the polymer matrix during heat treatment not only assists polymeric chain packing and rigidification but also facilitates more efficient PDA cross-linking. Apparently, PDA molecules could also seal the nonselective cracks (defects). These results indicate that the combined thermal and chemical modification possibly is an effective method independent of the initial status of the hollow fiber (e.g., defective or defective free) in revitalizing and enhancing the membrane performance. X-ray diffraction (XRD) characterization confirmed a tighter polymer networking in hollow fibers with the cross-linking modification. Comparison between the dehydration of different alcohols revealed that a better separation performance could be obtained for alcohols having a larger molecular cross section [81].

PV membrane for the separation of diacetone alcohol/water mixtures, using commercially available membranes for organic enrichment and dehydration, was evaluated. Empirical correlations for the effect of the process parameters of feed concentration, feed temperature, permeate-side pressure, and scale-up were developed. The solvent/water mixture was successfully separated with a PVA-based Sulzer PERVAP 2210 dehydration membrane. Various dehydration membranes were evaluated and a comparison of the permeation and separation factor was made. The membrane

performance in separating acetone/water mixtures was also studied. Based on the results, an overall model to predict the membrane area needed for a scale-up was developed [82].

Dense PIC membranes of anionic NaAlg and cationic polyethyleneimine (PEI) were prepared and cross-linked with GA for dehydration of alcohol/water mixtures by PV. PV dehydration characteristics of the membranes were determined as a function of PEI content, cross-linking time, as well as feed water composition. Transport parameters, such as sorption, diffusion, and permeability of water and alcohols through the membranes, were determined. Among the four different membrane compositions, the PIC containing 40% PEI was found to yield optimum separation data in terms of membrane stability, selectivity, and permeability. Conversely, 10% PEI-containing membrane gave the highest selectivity with the lowest permeation rate at ambient temperature, but the membranes were not sufficiently stable [83].

PIC membranes were prepared by the complexation of protonated chitosan with NaAlg doped on a porous, PS-supporting membrane. The PV characteristics of the membranes were investigated with various alcohol/water mixtures. The PIC membranes had an excellent PV performance in most aqueous alcohol solutions and the selectivity and permeability of the membranes depended on the molecular size, polarity, and hydrophilicity of the permeant alcohols. However, the aqueous methanol solutions showed a permeation behavior different from that of the other alcohol solutions. Methanol permeated the prepared PIC membranes more easily than water even though water molecules have stronger polarity and are smaller than methanol molecules [84].

Mordenite (Mo)-filled Chito/PAA PIC membranes were prepared by incorporating mordenite into Chito and PAA blending solution for PV separation of ethylene glycol (EG) aqueous solution. The effects of mordenite content on sorption, diffusion, and PV performance of the membranes were evaluated. The permeation rate decreased while the separation factor first increased and then decreased with increasing the mordenite content. The M04-PIC60/40 containing 4 wt.% mordenite showed the highest separation factor for H₂O/EG selectivity of 258 with a permeation rate of 165 g (m² h)⁻¹ for 80 wt.% EG in feed at 70 °C. High H₂O/EG selectivity was due to the diffusivity of water molecule through PIC membranes [85].

Cross-linked Chito for the separation of EG/water mixture membranes were prepared by using phosphoric acid in alcohol baths. The cross-linked membranes were subjected to sorption studies to evaluate the extent of interaction and degree of swelling in pure as well as in binary mixtures of the two liquids. The membrane had a good potential for breaking the boiling mixture of EG/water since a moderately good selectivity of 234 was obtained at a reasonable permeation rate of 0.37 kg (m² h)⁻¹. The separation factor for H₂O/EG selectivity was improved with decreasing feed water concentration, whereas permeation rate decreased correspondingly. Increasing the membrane thickness decreased the permeation rate but had a less profound effect on the separation factor. Higher permeate pressure caused a reduction in permeation rate and an increase in selectivity [86].

Dehydration of aqueous EG solution by PV was studied by surface cross-linked PVA membrane using GA. When the feed mixture was an aqueous solution of 80 wt.% EG, the permeation rate and separation factor for H₂O/EG selectivity at 70 °C were 211 g (m² h)⁻¹ and 933, respectively. The remarkable dependence of water and EG concentration in permeate side as well as their activity coefficients within the membrane on feed concentration indicate that a strong coupling effect existed between water and EG, which effectively inhibits the permeation of EG, thus considerably enhancing the H₂O/EG selectivity. With feed temperature increasing, the permeation rate increases; however, separation factor for H₂O/EG selectivity decreased significantly due to the difference of activation energies between water and EG. With feed flow rate increasing, both the permeation rate and separation factor for H₂O/EG selectivity increased correspondingly [87].

2.11.6.2 Alcohol/Water-Selective Membranes

Cross-linked PVA composite membranes have been used in commercial PV plants for dehydration of ethanol beyond the azeotrope. However, aqueous ethanol solutions that can be produced by bio-fermentation are dilute (~10 wt.%). Therefore, if ethanol/water (EtOH/H₂O)-selective membranes with high efficiency can be prepared, the distillation process in the first stage to obtain an azeotrope can be replaced which is very advantageous for reduction of energy cost. There are fewer reports on EtOH/H₂O-

selective membranes compared with those of EtOH/H₂O-selective membranes. One reason why the development of efficient high-performance EtOH/H₂O selective membranes is difficult can be attributed to the fact that ethanol has a larger molecular size than water and must be preferentially permeated through the membrane. In fact, permeation and separation in a PV process through dense membranes is based on the solution–diffusion mechanism [12, 88]. Therefore, when it is required that ethanol molecules with larger molecular size preferentially permeate from an aqueous ethanol solution, it cannot be expected to be separated by the diffusion process. Consequently, only a difference of solubility selectivity in the solution process in which both ethanol and water components are dissolved can contribute to the separation. Figure 7 shows the ethanol concentration in the permeate through a poly(dimethyl siloxane) (PDMS) membrane during PV and that sorbed into a PDMS membrane. These results support the hypothesis that the difference in the solubility of the permeants contributes to the EtOH/H₂O selectivity. PDMS membranes show high EtOH/H₂O selectivity, but their mechanical strength is weak, and it is difficult to prepare thin membranes from PDMS. In order to obtain both EtOH/H₂O selectivity and mechanical strength, graft copolymers composed of PDMS macromonomer and vinyl monomers were synthesized.

Graft copolymer membranes, which were either ethanol or water selective, were prepared by copolymerization of an oligo-dimethylsiloxane (DMS) monomer with methyl methacrylate (MMA) [89, 90]. Two glass transition temperatures (T_g) were observed at about 120 and -127°C in the graft

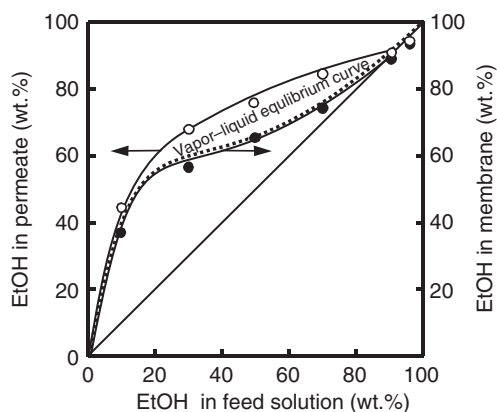


Figure 7 Permeation and separation characteristics of aqueous ethanol solutions through a PDMS membrane during PV.

copolymer membranes. Transmission electron micrograph (TEM) demonstrated that the poly(methylmethacrylate) (PMMA)-*g*-PDMS membranes showed microphase-separated structures. When an aqueous solution of 10 wt.% ethanol was permeated through the PMMA-*g*-PDMS membranes by PV, the ethanol concentration in the permeate and the permeation rate increased drastically with the DMS content in the copolymer. In particular, at a DMS content of less than 40 mol.%, water permeates preferentially from an aqueous solution of 10 wt.% ethanol, whereas membranes with more than about 40 mol.% of DMS are EtOH/H₂O selective, as shown in Figure 8. The change in the EtOH/H₂O selectivity of the PMMA-*g*-PDMS membranes can be explained by a microphase-separated polymer structure using Maxwell's model and a combined model consisting of both parallel and series expressions. Furthermore, image processing of TEMs allowed the determination of the percolation transition of the PDMS phase at a DMS content of about 40 mol.%. These results suggest that the continuity of the PDMS phases in the microphase-separated PMMA-*g*-PDMS membranes directly affects their EtOH/H₂O selectivity for aqueous ethanol solutions [89, 90].

The EtOH/H₂O selectivity of block copolymer membranes, consisting of ethanol-selective PDMS and water-selective PMMA, was compared to the EtOH/H₂O selectivity of graft copolymer membranes for the separation of an aqueous ethanol solution. With increasing DMS content, the block copolymer membranes changed from H₂O/EtOH

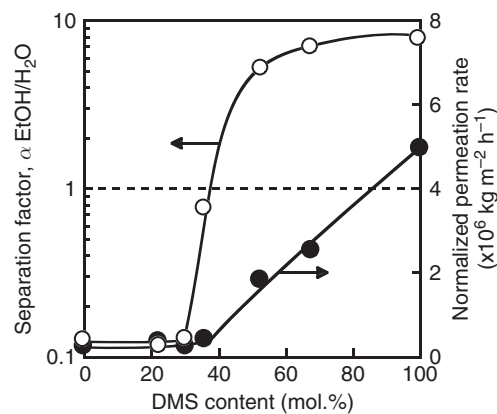


Figure 8 Effects of the DMS content on the normalized permeation rate (○) and separation factor (●) through the PMMA-*g*-PDMS membrane during PV. Feed: aqueous solution of 10 wt.% ethanol. Dashed line is the feed composition. From Miyata, T., Takagi, T., Uragami, T. *Macromolecules* **1996**, 29, 7787–7794.

selective to EtOH/H₂O selective at a DMS content of 55 mol.%. The graft copolymer membranes showed a dramatic change in their EtOH/H₂O selectivity at a DMS content of 40 mol.%. TEMs demonstrated that both membranes had a distinct microphase-separated structure consisting of PDMS and PMMA phases, and that the morphology was quite different between the block and graft copolymer membranes. The morphological changes in these membranes were investigated by image processing of micrographs and analysis using a combined model consisting of both parallel and series models. These investigations revealed that the percolation transition of the PDMS phase in the block and graft copolymer membranes takes place at a DMS content of about 55 and 40 mol.%, respectively. This suggests that the continuity of the PDMS phase in these microphase-separated membranes strongly influences their ethanol selectivity [91].

The effects of annealing on selectivity during PV were also investigated for these block and graft copolymer membranes. The EtOH/H₂O selectivity of the block copolymer membranes was strongly influenced by annealing, but that of the graft copolymer membranes was essentially not affected. The original block copolymer membranes changed from being water selective to ethanol selective at a DMS content of 55 mol.%; however, the annealed block copolymer membranes changed at a DMS content of 37 mol.%. TEMs demonstrated that the annealing of block copolymer membranes with a DMS content between 37 and 55 mol.% resulted in dramatic changes in their morphology. However, annealing of the graft copolymer membranes had very little effect on their microphase-separated morphology, which was quite different from the morphology of the block copolymer membranes. In addition, an analysis using a combined model consisting of parallel and series models revealed that a continuous PDMS phase in the direction of the membrane thickness was readily formed by annealing of the block copolymer membranes. As a result, the continuity of the PDMS phase in the microphase-separated structure governed the ethanol selectivity of these membranes for an aqueous ethanol feed solution [92].

It is well known that poly[1-(trimethylsilyl)-1-propyne] (PTMSP) membranes show high EtOH/H₂O selectivity [97, 98]. In order to enhance the EtOH/H₂O selectivity of PTMSP membranes, surface-modified PTMSP membranes were prepared by adding a small amount of a polymer additive, a graft copolymer (poly(fluoroacrylate) (PFA)-*g*-PDMS)

consisting of PFA and PDMS, in the casting solution of PTMSP. Modified PTMSP membranes were cast on glass plates and the contact angles of water on the membrane surfaces exposed to the air side and the glass side, respectively, were measured. The contact angle for water on surface-modified PTMSP membranes was significantly different on the air side versus that on the glass side; the contact angles on the air side were more hydrophobic. Furthermore, the contact angle for water increased in hydrophobicity with additional amounts of PFA-*g*-PDMS. The high hydrophobicity of the membrane surface on the air side and the increase in hydrophobicity with additional amounts of polymer additive were also confirmed by X-ray photoelectron spectroscopy (XPS). The permeation rate for an aqueous solution of 10 wt.% ethanol in PV experiments using surface-modified PTMSP membranes decreased slightly. However, the EtOH/H₂O selectivity increased considerably with increasing amounts of PFA-*g*-PDMS [99, 100].

The permeation and separation characteristics for aqueous alcohol solutions, such as methanol/water, ethanol/water, and 1-propanol/water, were studied using a dense PDMS membrane in PV and EV mode. The PDMS membrane preferentially permeated methanol, ethanol, and 1-propanol from aqueous solutions in both methods. The concentration of alcohol in the permeate by EV was higher than that obtained by PV. However, the permeation rate in EV was lower. In EV, with a temperature difference between the feed solution and the membrane surroundings (TDEV), when the temperature of the membrane surroundings was kept constant and the temperature of the feed solution was raised, both the permeation rate and the EtOH/H₂O selectivity increased with increasing temperature of the feed solution. Conversely, as the temperature of the feed solution was kept constant and the temperature of the membrane surroundings was changed, the permeation rate decreased. However, the EtOH/H₂O selectivity for ethanol increased remarkably with dropping the temperature of the membrane surroundings, as shown in **Figure 9**. Under TDEV permeation conditions of a feed solution at 40 °C and a membrane surrounding temperature of -30 °C, an aqueous solution of 10 wt.% ethanol in the feed was concentrated to about 90 wt.% in the permeate [93–95]. The selectivity for aliphatic alcohols in PDMS membranes follows the order of methanol < ethanol < 1-propanol [93, 94].

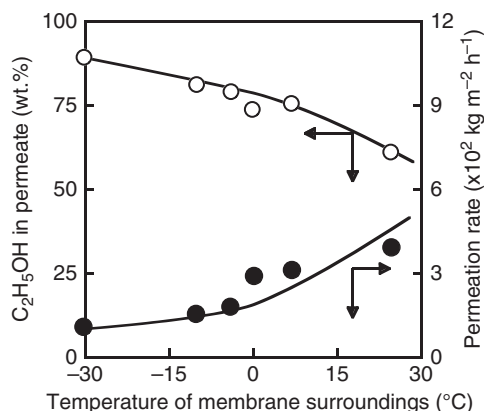


Figure 9 Effects of the temperature of membrane surroundings on the permeation rate (○) and ethanol concentration in the permeate (●) for an aqueous solution of 10 wt.% ethanol through a PDMS membrane. Temperature of feed solution: 40°C. From Uragami, T., Morikawa, T. *J. Appl. Polym. Sci.* **1992**, *44*, 2009–2018.

An integrated fermentation and membrane-based recovery PV process has certain economical advantages in continuous conversion of biomass into alcohols. New PV data obtained for PTMSP samples synthesized in various conditions were reported. Three different catalytic systems, TaCl₅/*n*-BuLi, TaCl₅/Al(*i*-Bu)(3), and NbCl₅, were used for synthesis of the polymers. The catalytic system has a significant influence over the properties of membranes made from PTMSP. Although a combination of a high permeation rate and a high separation factor for EtOH/H₂O selectivity (not <15) was provided by all PTMSP samples, the PTMSP samples synthesized with TaCl₅/*n*-BuLi showed significant deterioration of membrane properties when acetic acid was present in the feed. In contrast, the PTMSP samples synthesized with TaCl₅/Al(*i*-Bu)(3) or NbCl₅ showed stable performance in the presence of acetic acid. When using a multicomponent mixture of organics and water, the co-permeation of different organic components results in lower separation factor for both ethanol and butanol. These data are consistent with nanoporous morphology of PTMSP. It was demonstrated that pervaporative removal of ethanol improved the overall performance of the fermentation process [104].

PV can be utilized for the recovery of ethanol from fermentation broths. A hybrid fermentation–PV–distillation continuous process was considered for the production of 30 000 l d⁻¹ of 95% ethanol. Available data of composite hollow-fiber PDMS

membrane of PV module were used to develop the model equations. Direct production cost of ethanol was estimated and used for the optimization of ethanol concentration in fermenter and retentate. Minimum direct production cost of \$0.2 l⁻¹ of ethanol was found at 55 kg m⁻³ of ethanol mass concentration in fermenter and 50 kg m⁻³ in retentate. A sensitivity analysis of the PV performance parameters, such as permeation rate, separation factor, and membrane cost, was also carried out [105].

A novel inorganic/organic composite membrane was prepared through introducing carbon black (CB) into PDMS membrane. CB was treated with various measures, including extraction, methylation, and high-temperature calcinations, in order to tailor the nature of the surface. The effects of surface treatment, CB loading, particle size, and temperature on the PV performance in the extraction of ethanol from ethanol/water mixtures were explored. In certain ranges of composition, the permeation rate was remarkably increased without reducing the EtOH/H₂O selectivity [106].

Fermentation broths contain ethanol, water, and a variety of other compounds, often including carboxylic acids. The effects of acetic acid on long-term PV of aqueous ethanol mixtures through high-silica ZSM-5 zeolite-filled PDMS membranes were investigated. Addition of acetic acid to the ethanol/water mixture reduced the ethanol removal effectiveness of these membranes and decreased permeation rates of ethanol and water. These results are due to acetic acid competing with ethanol and water for adsorption sites in the membrane. Longer-term exposure to acetic acid resulted in an irreversible, steady decline in the separation factor for EtOH/H₂O selectivity because of declining permeation rate of ethanol. Increasing feed pH to above the dissociation constant (pK_a) of acetic acid diminished the long-term decline in the permeation rate of ethanol and essentially eliminated the effect of competitive adsorption. Measurements of adsorption competition between ethanol, water, and either acetic acid or succinic acid on the zeolite particles suggested that other carboxylic acids have qualitatively similar short-term effects on membrane performance as those observed for acetic acid [107].

The separation of ethanol/water could be cost competitive using PV in the production of renewable biomass ethanol; however, the performance of the modified or unmodified polymeric membranes is still not satisfactory. For the purpose of improving the PV performance of polymeric membranes,

especially for permeation rate, PDMS was deposited uniformly on the surface of tubular asymmetric ZrO_2/Al_2O_3 porous ceramic supports. The thickness of the PDMS layer formed atop the ZrO_2 layer was on the order of 5–10 μm . In the PV experiment of ethanol/water mixtures, as the ethanol concentration increased, the total permeation rate increased but the EtOH/ H_2O selectivity decreased. At the same time, with increasing operating temperature, the total permeation rate of the composite membranes increased, whereas the EtOH/ H_2O selectivity decreased. It was observed that the PDMS/ceramic composite membrane showed a great total permeation rate of $19.5 \text{ kg (m}^2 \text{ h)}^{-1}$ and separation factor for EtOH/ H_2O selectivity of 5.7 at a feed temperature of 70°C , under a pressure of 460 Pa, and in an ethanol concentration of 4.3 wt.%. The total permeation rate of the PDMS/ceramic composite membranes was superior to other reported PDMS membranes [108].

Studies were carried out to improve the effectiveness and cost effectiveness of a semicontinuous ethanol fermentation of lactose mash combined with a PV module [109]. During a 20-day fermentation/PV with an immobilized biocatalyst, the fermentation of the lactose mash (12%) averaged 4.56% m/v ethanol. In the circulation PV module, ethanol from about 2000-g portions of the fermented mash was removed to below 0.7% m/v in 10–12 h. The effectiveness of ethanol separation ranged between 88% and 95% and was determined by the ethanol concentration in the fermented mash. The productivity of 15.6% m/v ethanol obtained in such a system was about 530 g day^{-1} . The PDMS–PAN–PVA membrane applied to the PV system proved to be highly selective toward ethanol, separation factor for EtOH/ H_2O selectivity was >8 , and permeation rate was $2600\text{--}3500 \text{ g (m}^2 \text{ h)}^{-1}$.

In the above-mentioned experiment, dense EtOH/ H_2O -selective membranes for the concentration of aqueous ethanol solutions were applied to PV, EV, and TDEV. In these cases, the permeation and separation of ethanol and water are dependent on the solution–diffusion mechanism. Therefore, in PV, the permeation rate is high but the EtOH/ H_2O selectivity is low; in EV, the permeation rate is low but the EtOH/ H_2O selectivity is high; and, in TDEV, the permeation rate is low but the EtOH/ H_2O selectivity is higher. However, both high permeation rate and high EtOH/ H_2O selectivity are required in the membrane performance. It is presumed that the membrane performance for the concentration of water/ethanol mixtures using dense membranes is

limited. Hence, porous membranes were applied to TDEV to concentrate aqueous ethanol solutions.

Figure 10 shows the effect of the temperature of the membrane surroundings on the permeation rate and the ethanol concentration in the permeate for an aqueous solution of 10 wt.% ethanol through a dense PDMS membrane (1) and a porous PDMS membrane (2) in TDEV. In Figure 10, the temperature of the feed solution was kept constant at 40°C and the temperature of the membrane surroundings was changed; the pressure on the downstream side was kept at 665 Pa. In Figure 10(b), with dropping temperature of the membrane surroundings, the permeation rate decreased and the ethanol concentration in the permeate increased. This decrease in the permeation rate can be explained by the permeation conditions in Table 3, where ΔT is the temperature difference between the temperature of the feed solution, T_L , and that of the feed vapor, T_V ,

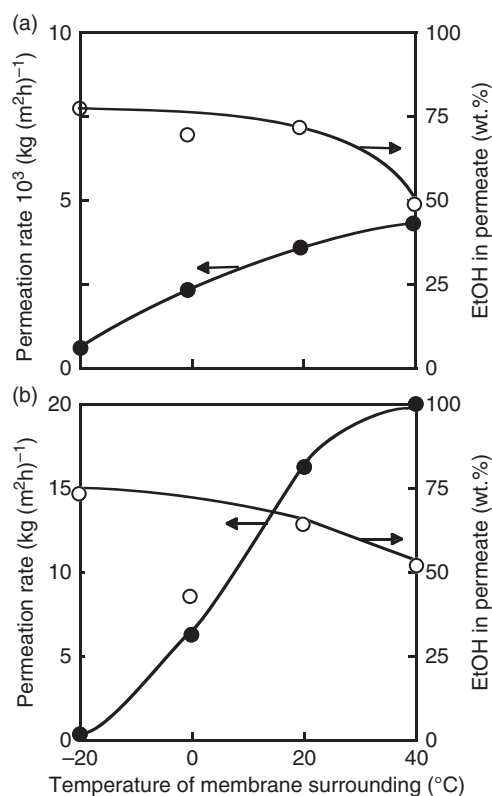


Figure 10 Comparison of the permeation and separation characteristics for an aqueous solution of 10 wt.% ethanol of a dense PDMS membrane (a) and a porous PDMS membrane (b) in TDEV, in which the temperature of the feed solution was kept constant at 40°C and the temperature of the membrane surroundings was changed. From Urugami, T. *Desalination*, **2006**, 193, 335–343.

Table 3 Performance of EtOH/H₂O-selective membranes

Membrane	Feed (wt. %)	Method	Applied temperature (°C)	$\alpha_{\text{EtOH}/\text{H}_2\text{O}}$	NPR ^a (kg $\mu\text{m} (\text{m}^2 \text{h})^{-1}$)	Ref.
PDMS	7	PV	25	11.8	2.1	[96]
PTMSP	7	PV	25	11.2	1.1	[97]
PTMSP	10	PV	30	12.0	4.5	[98]
PFA- <i>g</i> -PDMS/PTMSP ^b	10	PV	40	20.0	24.1	[99, 100]
PPP- <i>g</i> -PDMS	7.28	PV	30	22.5	5.5	[101]
PSt- <i>g</i> -PhdFDA (87.6/12.4)	8	PV	30	45.9	0.6	[102]
TFE/ <i>i</i> -OcVE/C18VE						
Terpolymer (50/25/25)	15	PV	50	7.13	5.0	[103]
Modified silicone	10	PV	40	3.65	11.0	[95]
Modified silicone	10	TDEV	-30/40	19.3	16.6	[95]
PDMS	10	PV	40	7.44	6.4	[93, 94]
PDMS	10	TDEV	-30/40	85.7	0.9	[93, 94]
PMMA- <i>g</i> -PDMS (34/66)	10	PV	40	7.1	4.8	[90]
PMMA- <i>b</i> -PDMS (27/73)	10	PV	40	8.0	5.1	[91]
PMMA- <i>b</i> -PDMS (38/62) ^c	10	PV	40	6.8	3.5	[92]
PTMST	10	TDEV	0/40	77.5	38	[111]
Porous PDMS	10	TDEV	-20/40	23.1	1250	[23, 110]

^a Normalized permeation rate.

^b PFA-*g*-PDMS is 0.2 wt. %.

^c Annealing is 120 °C, 2 h.

From Uragami, T. Polymer Membranes for Separation of Organic Liquid Mixtures. In *Material Science of Membranes for Gas and Vapor Separation*; Yampolskii, Y., Pinnau, I., Freeman, B.D., Eds., Wiley: New York, 2006; pp 355–372.

and ΔP is the pressure difference between the pressure on the feed side, P_f , and that on the permeate side, P_p . In **Figures 11(a)–11(c)**, the relationships between ΔT and ΔP , and between ΔP and ΔT , and the characteristics of permeation and separation are shown, respectively. It is suggested that an increase in ΔT results in a decrease both in ΔP and in the permeation rate. Consequently, the decrease in the permeation rate with dropping temperature of the membrane surroundings in **Figure 10(b)** significantly depends upon a decrease in ΔP .

Conversely, the increase in the ethanol concentration in the permeate shown in **Figure 10(b)**, that is, the increase in the EtOH/H₂O selectivity through a porous PDMS membrane with dropping temperature of the membrane surroundings, can be attributed to a tentative mechanism shown in **Figure 12** [227].

When water and ethanol molecules, vaporized from the feed solution, come close to the membrane surroundings kept at lower temperature in TDEV, the water vapor aggregates much easier than the ethanol vapor, because the freezing point of water molecules (0 °C) is much higher than that of ethanol molecules (-114.4 °C), and the aggregated water molecules tend to be liquefied as the temperature of the membrane surroundings becomes lower. Conversely, because the PDMS membrane has a

relatively high affinity to the ethanol molecules, they are sorbed inside the pores in a porous PDMS membrane, and this sorbed layer of the ethanol molecules is formed in an initial stage of the permeation. The vaporized ethanol molecule may be able to permeate across the membrane by surface diffusion on the sorbed layer of the ethanol molecules inside the pores.

Both the aggregation of the water molecules and the surface diffusion of the ethanol molecules in the pores are responsible for the increase in the ethanol/water selectivity through a porous PDMS membrane in TDEV. The increase of the EtOH/H₂O selectivity in TDEV can be attributed to both the degree of aggregation of the water molecules on the membrane surroundings and the thickness of the sorbed layer of the ethanol molecules inside the pores, which are significantly governed by the temperature of the membrane surroundings. When the temperature of the membrane surroundings becomes lower, the degree of aggregation of the water molecules and the thickness of the sorbed layer of the ethanol molecules are increased. Therefore, an increase in the EtOH/H₂O selectivity for aqueous ethanol solutions was observed with dropping temperature of the membrane surroundings.

As shown in **Figures 10(a) and 10(b)**, the tendency of the decrease in the permeation rate and increase in the EtOH/H₂O selectivity, with lowering temperature of the membrane surroundings through these two PDMS membranes, was very similar. Despite the fact that the EtOH/H₂O selectivity in these PDMS membranes was almost equal, the permeation rates through these PDMS membranes were remarkably different, that is, the permeation rates in a porous PDMS membrane were higher by three orders of magnitude than those of a dense PDMS membrane [227].

A remarkable difference in the permeation rate between dense and porous PDMS membranes can be attributed to the fact that the permeation through a dense PDMS membrane is due to the solution–diffusion model [12, 88] and that through a porous PDMS membrane is based on pore flow, as shown in **Figure 12**.

Based on the above results, it is suggested that an application of porous hydrophobic polymer membranes to TDEV for the concentration of aqueous ethanol solutions is very advantageous [23, 110].

In **Table 4**, the performance of the ethanol/water-selective polymer membranes is compared. As can be seen in **Table 4**, the addition of PFA-*g*-PDMS to the PTMSP membrane in PV was very effective; the application of TDEV method to the membrane separation technique was also very interesting for the enhancement of the EtOH/H₂O selectivity for the ethanol/water mixtures; and, in particular, the application of porous PDMS membrane to TDEV was a very excellent performance for the ethanol/water mixtures.

A specially designed and manufactured PV cell was used to separate the butanol from butanol/water mixtures of different butanol concentrations. The PV experiment was carried out in butanol/water mixture of 250 cm³ under the pressure of permeation side of 0 bar. Results revealed that butanol concentration changes nonlinearly during the first 3 h, and then proceeds linearly. The percentage of butanol removal increased with increasing feed concentration. A resistance in series model was used to simulate the PV step. The butanol concentration in the feed during the PV step was predicted by using the developed model. There is a fair agreement between butanol concentration in feeding tank of PV cell both experimentally and predicted from the developed model [112].

PV experiments were conducted to recover 1-butanol (BuOH) from model pharmaceutical aqueous

waste using a surface-modified PVF₂ membrane. The surface modification of the membrane was made using silicone grease as an ultrathin layer on the surface to improve the PV performance of the membrane. The effect of operating variables, such as feed composition, feed temperature and feed flow rate on permeation rates, separation factor, and pervaporative separation index, was studied in order to optimize the operating variables. The experimental results showed that surface-modified PVF₂ membrane was BuOH/H₂O selective, especially for low feed compositions. The separation factor for BuOH/H₂O selectivity of 6.4 and total permeation rate of 4.126 kg (m²h)⁻¹ were obtained at a feed composition of 7.5 wt.%, feed temperature of 50 °C, feed flow rate of 600 ml min⁻¹, and permeate pressure of 50 mmHg. The total permeation rate of the surface-modified membrane increased with increasing feed composition, feed temperature, and feed flow rate of the mixture, whereas the separation factor for BuOH/H₂O selectivity was a reversed order except for flow rate. The influence of operating variables, such as feed composition and temperature, on partial permeation rate and permeate composition was modeled based on Fick's first law to understand the process behavior, which will be very useful for design purpose. These models will be used to predict the required membrane surface area for recovery of 1-butanol for the range of experimental feed compositions [113].

2.11.6.3 Water/Organic-Liquid-Selective Membranes

Water/organic-selective membranes are effective for the dehydration of water/organic mixtures. The dehydrated organic solvents can be useful as industrial reaction solvents, washing solvents, and analytical solvents.

In **Figure 13**, the permeation and separation characteristics for an aqueous dimethyl sulfoxide (DMSO) solution through a dense Chito membrane by TDEV are shown. In **Figure 13**, the feed was an aqueous solution of 50 wt.% DMSO; the temperature of the feed solution was kept constant at 40 °C; and the temperature of the membrane surroundings was lowered to less than the temperature of the feed solution [114]. Both the total permeation rate and the separation factor increased with dropping temperature of the membrane surroundings. This increase in the total permeation rate may be due to the increase in the solubility of the vapor in the membrane with increasing temperature of the

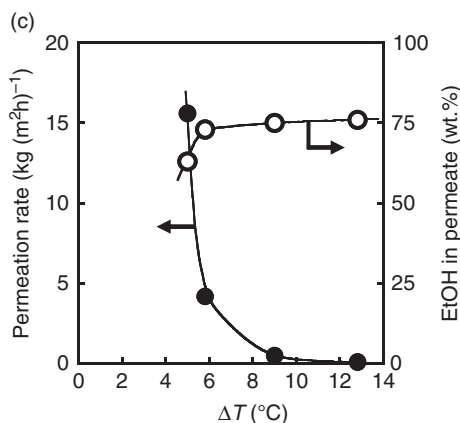
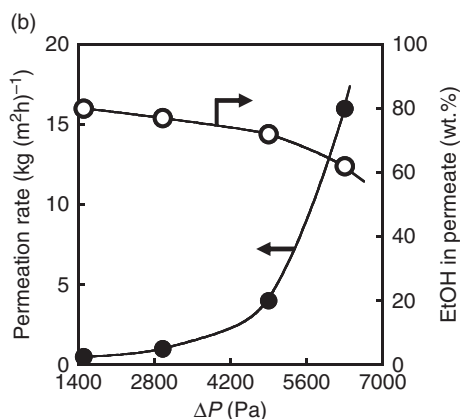
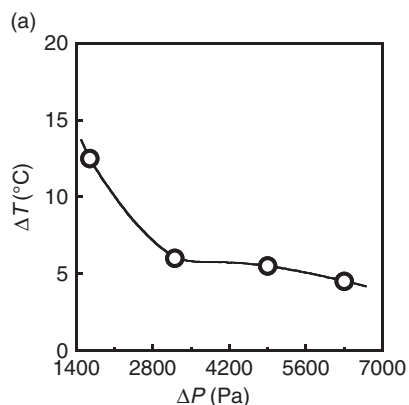


Figure 11 Relationships between the temperature difference, ΔT , and the pressure difference, ΔP (a), between ΔP and the permeation and separation characteristic (b), and between ΔT and the permeation and separation characteristics (c) in TDEV. From Uragami, T. *Polym. J.* **2008**, *40*, 485–494.

membrane surroundings, according to Henry's law. The increase of the separation factor, that is, the improvement of the H₂O/DMSO selectivity, can be explained by the illustration shown in **Figure 14**. When the DMSO and water molecules, which had vaporized from the feed mixture, come close to the

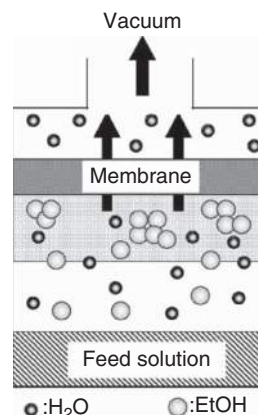


Figure 12 Tentative mechanism of the separation for aqueous ethanol solutions through porous PDMS membrane in TDEV. From Uragami, T. *Polym. J.* **2008**, *40*, 485–494.

membrane surroundings, the DMSO vapor aggregates much easier than the water vapor (because the freezing points of DMSO and water are 18.4 and 0 °C, respectively), and tends to liquefy as the temperature of the surrounding membrane becomes lower. This aggregation of the DMSO molecules is responsible for the increase in the H₂O/DMSO selectivity for water through the Chito membrane. The increase in the separation factor with the TDEV method, in which the temperature of the membrane surroundings is lower than the temperature of the feed solution, can be attributed to the degree of aggregation of the DMSO molecule, which is significantly governed by the temperature of the membrane surroundings. The high H₂O/DMSO selectivity of Chito membrane for an aqueous solution DMSO in TDEV is significantly enhanced by both the high affinity for water of the Chito membrane and the decrease in the solubility selectivity for DMSO molecules into the Chito membrane, based on their aggregation on the membrane surroundings [23, 114]. The mechanism of permeation and separation of a DMSO/water mixture through a dense Chito membrane during TDEV, in **Figure 14**, is effective for understanding that of an ethanol/water mixture through a dense PDMS membrane during TDEV [23].

Novel hybrid composite membranes have been prepared by incorporating 5 and 10 wt.% of sodium montmorillonite (NaMMT) clay particles into NaAlg and cross-linked with GA. PV separation performance of the hybrid composite membranes was investigated for the dehydration of 2-propanol, 1,4-dioxane (DIOX), and tetrahydrofuran (THF) from

Table 4 Permeation and separation characteristic for an aqueous solution of 10 wt.% ethanol through a porous PDMS membrane during TDEV and the permeation conditions in TDEV on changing the temperature of the membrane surroundings as the temperature of the feed solution was kept constant

	Temperature of membrane surroundings (°C)			
	-20	0	20	40
EtOH in permeate (wt.%)	71.8	71.1	62.1	49.8
Permeation rate (kg (m ² h) ⁻¹)	0.14	7.8	16.1	20.1
T_L	33.0	33.8	35.2	40.0
T_V	17.2	22.0	30.2	38.0
ΔT	15.8	11.8	5.0	2.0
ΔP	4934	5692	6357	6903
P_F	5599	6357	7022	7568

T_L , temperature of the feed solution; T_V , temperature of the feed vapor; P_p , pressure on the downstream side; P_F , pressure on the feed side. $\Delta T = T_L - T_V$, $\Delta P = P_F - P_p$.

From Uragami, T. *Polym. J.* **2008**, *40*, 485–494.

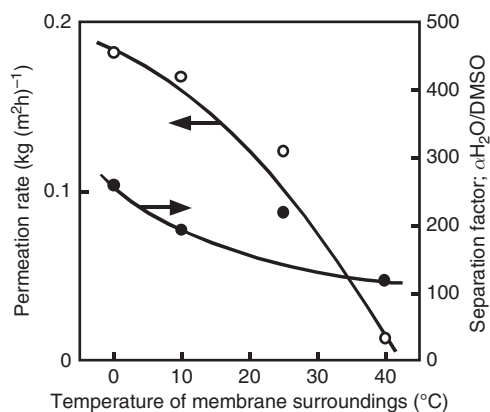


Figure 13 Effects of the temperature of the membrane surroundings on the characteristics of permeation and separation for an aqueous solution of 50 wt.% dimethyl sulfoxide (DMSO) through a Chito membrane in TDEV. Feed temperature: 40 °C. From Uragami, T., Shinomiya, H. *J. Membr. Sci.* **1992**, *74*, 183–191.

their aqueous solutions. NaMMT particles could be intercalated in the aqueous polymer solution. The driving force for NaMMT adsorption is entropic, which involves at least partial replacement of water of hydration associated with exchangeable cations in the clay galleries. The results of PV experiments demonstrated that the addition of NaMMT clay particles increased the selectivity to water over that of pristine NaAlg membrane. Permeation rates of the hybrid composite membranes were lower than those observed for plain NaAlg membrane [115].

Microporous aluminophosphate (AlPO₄-5) has been employed to prepare novel NaAlg-based

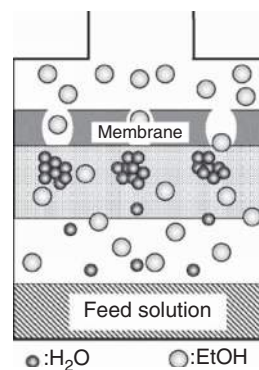


Figure 14 Tentative separation mechanism for aqueous dimethyl sulfoxide solution through a Chito membrane in TDEV. From Uragami, T., Shinomiya, H. *J. Membr. Sci.* **1992**, *74*, 183–191.

composite membranes by solution-casting technique and cross-linking with GA. These membranes were tested for the PV dehydration of 2-propanol (12.6 wt.% water), 1,4-dioxane (18.1 wt.% water), THF (6.7 wt.% water), and ethanol (4 wt.% water) from their aqueous mixtures. However, PV dehydration studies at feed composition from 5 to 20 wt.% were done for pristine NaAlg and 20 wt.% AlPO₄-5-loaded composite membranes. The activation parameter values involved in the permeation process were evaluated. The permeation rate and selectivity near the azeotropic compositions of the feed mixtures were enhanced with increasing AlPO₄-5 content into NaAlg-based matrix. The selectivity to water was higher for water/IPA azeotrope, but the permeation rate was more in case of water/1,4-dioxane and

water/tertahydrofuran azeotropes. The selectivity to water was smaller for water/THF and water/ethanol azeotropes as compared to water/2-propanol and water/1,4-dioxane azeotropes. Molecular-sieving effect due to uniform distribution of microporous molecular sieve particles, and hydrophilic characteristics of the aluminophosphate molecular sieve, in addition to its interaction with the hydrophilic NaAlg matrix, were responsible for such an appreciable increase in membrane performance over that of pristine cross-linked NaAlg membrane [116].

PVA-based nanocomposite membranes were prepared by co-precipitation of different amounts of Fe(II) and Fe(III) taken in an alkaline medium and their PV performances were investigated to dehydrate from aqueous solutions of 10–20 wt.% 2-propanol and 1,4-dioxane, and 5–15 wt.% THF. Thin-layer membranes were cast on polyester fabric cloths as support layers to improve their PV separation performances for all the three mixtures over that of the pristine cross-linked PVA membrane. In particular, the composite membrane prepared by taking 4.5 wt.% of iron oxide showed an improved selectivity with a slight sacrifice in the permeation rate compared to membranes containing lower contents of iron oxide as well as the pristine cross-linked PVA membrane. The permeation rate decreased with increasing content of iron in the PVA matrix, while the selectivity increased systematically [117].

The PV separation of 1,4-dioxane/water mixtures was carried out using cross-linked blend membranes of Chito and nylon 66 (N66). Optimum Chito/N66 ratio was determined as 90/10 (w/w) for the containing water of 4.3 wt.% at 40 °C [118]. Increasing barrier from 30 to 120 μm improved separation factors for H₂O/DIOX selectivity from 767 to 1123, but permeation rates were lowered from 0.118 to 0.028 kg (m² h)⁻¹. An azeotrope of 1,4-dioxane/water mixture (1,4-dioxane of 82 wt.%) was easily broken with a separation factor for H₂O/DIOX selectivity of 865 and permeation rate of water was 0.089 kg (m² h)⁻¹.

Acrylonitrile (AN) was copolymerized with 2-hydroxyethyl methacrylate (HEMA) at three different copolymer compositions [119] by emulsion polymerization to produce PAN/HEMA copolymer membranes. These membranes were PAN/HEMA-1, PAN/HEMA-2, and PAN/HEMA-3. The PV dehydration of THF over a concentration range of 0–14 wt.% water in the feed through these three copolymer membranes was studied. Among the copolymer membranes, PAN/HEMA-1 membrane exhibited a reasonable permeation rate of water (34.9 g (m² h)⁻¹)

with a very high H₂O/THF selectivity of 264, whereas PAN/HEMA-3 membrane showed a higher permeation rate of water of 52 g (m² h)⁻¹; however, the H₂O/THF selectivity for highly concentrated THF (water of 0.56 wt.% in the feed) at 30 °C was 176.5.

Cross-linked blend Chito/PVA membranes were prepared by casting mixtures of Chito and PVA and a urea formaldehyde/sulfuric acid mixture. Chito was used as the base component in the blend system, whereas PVA concentration was varied from 20 to 60 wt.%. Membranes were tested for PV dehydration of 2-propanol and THF. In close proximity to their azeotropic compositions, the membrane performance was assessed by calculating permeation rate and selectivity. Swelling experiments performed in water/organic mixtures were used to explain the PV results. The cross-linked blend membrane containing 20 wt.% PVA was tested for water of 5 and 10 wt.% in the THF/water mixture and 2-propanol/water mixture. Their separation factors for water selectivity were 4203 and 17 991, respectively. The permeation rate increased with increasing concentration of water in the feed. The selectivity was the highest for the cross-linked blend membrane with PVA of 20 wt.% [120].

Dense polymer membranes were made by mixing aqueous solutions of hydrophilic polymers PVA and PEI for investigating the separation of an azeotrope of THF/water (94 wt.% THF) by PV. The membranes were found to have good potential for breaking an azeotrope of THF. An increase in PVA content in the blend caused a decrease in the permeation rate and an increase in selectivity. The blend membrane of PVA/PEI of 5/1 showed the highest separation factor for H₂O/THF selectivity of 181.5 and the permeation rate of 1.28 kg (m² h)⁻¹ for an azeotropic mixture, respectively [121].

Mixed-matrix polymer membranes containing nanosized (21 nm) TiO₂ particles dispersed in NaAlg were prepared by solution casting and cross-linking with GA. These membranes were tested for PV dehydration of THF and 2-propanol from their aqueous solutions. Plain cross-linked NaAlg membrane could remove up to a water content of 97 wt.% for the feed with high water content. The mixed-matrix membranes of NaAlg had infinite selectivities for the dehydration with reasonable permeation rates. Permeation rates of NaAlg–TiO₂ mixed-matrix membranes were slightly lower than those of the plain NaAlg membrane [122].

Zeolite K-LTL-loaded NaAlg-mixed-matrix membranes were prepared by solution casting and

cross-linked with GA. The PV dehydration of 2-propanol, 1,4-dioxane, and THF was tested at 30–70 °C as a function of membrane thickness and feed compositions. These membranes showed enhancement in both the permeation rate and water selectivity at azeotropic mixtures. These results were due to the addition of K-LTL particles in NaAlg matrix. The permeation rate and selectivity to water were higher for water/1,4-dioxane azeotrope than those of water/2-propanol and water/THF azeotropic mixtures. Molecular-sieving effect, based on uniform distribution of K-LTL zeolite particles, in NaAlg matrix, its hydrophilicity, and hydrophilic NaAlg gave high membrane performance than pristine cross-linked NaAlg membrane [123].

Permeation and separation characteristics of *N,N'*-dimethyl formamide (DMF)/water mixtures were investigated by PV, EV, and TDEV using alginate membranes cross-linked with calcium chloride. The permeation rate was found to be inversely proportional to the membrane thickness, whereas the separation factor increased with increasing membrane thickness. The permeation rates in EV and TDEV were lower than those in PV, and the highest separation factors were obtained with TDEV. Alginate membranes gave permeation rates of 0.97–1.2 kg (m²h)⁻¹ and separation factors for H₂O/DMF selectivity of 17–63, depending on the operation conditions and the membrane separation method. The sorption selectivity was a dominant factor for the separation of DMF/water mixtures [124].

Membranes constructed from pure poly(4-methyl-1-pentene) (TPX) and 4-vinyl pyridine (4-VP)-modified TPX membranes (TPX/P4-VP) were also prepared for PV. The introduction of a hydrophilic 4-VP monomer into the TPX matrix was done by free radical polymerization to form the TPX/P4-VP membrane. The separation factor for H₂O/CH₃COOH selectivity and permeation rate of the TPX/P4-VP membranes were higher than those of the unmodified TPX membranes for the PV of an aqueous acetic acid solution. A good relationship was obtained between the water concentration in the feed and the permeation rate of water by applying the Michaelis–Menten equation [125].

The PV separation of acetic acid/water mixtures was carried out over the full range of compositions at 30–55 °C using PVA membranes modified with PAA. The best condition for the preparation of the membranes was found as PVA/PAA ratio of 75/25 (v/v). PVA/PAA membranes gave separation factors of 34–3548 and permeation rates of 0.03–0.60 kg (m²h)⁻¹,

depending on the operation temperature and feed mixture composition [126].

Itaconic acid (IA) was grafted onto PVA with cerium (IV) ammonium nitrate as an initiator. IA-*g*-PVA membranes were prepared with a casting method, and permeation and separation characteristics of acetic acid/water mixtures were investigated by PV, EV, and TDEV. The permeation rates in EV were lower than those in PV, whereas the separation factors for H₂O/CH₃COOH selectivity in EV were higher. In TDEV, permeation rates decreased and separation factors for H₂O/CH₃COOH selectivity increased with dropping temperature of the membrane surroundings. The highest separation factor for H₂O/CH₃COOH selectivity of 686 was obtained for acetic acid of 90 wt.% in the feed in TDEV [127].

The characteristics of permeation and separation of acetic acid/water mixtures through 85/15 (v/v) PVA/malic acid (MA) membranes were investigated by EV and TDEV. The permeation rates increased; however, separation factors for H₂O/CH₃COOH selectivity decreased with an increase in permeation temperature in EV. When the temperature of feed solution was kept constant and the temperature of the membrane surrounding was dropped, the permeation rate and separation factor for H₂O/CH₃COOH selectivity were significantly influenced by the temperature of membrane surroundings. The increase in the acetic acid concentration in the feed vapor mixture decreased the permeation rate and increased the separation factor for H₂O/CH₃COOH selectivity, except 40 wt.% acetic acid content. The best separation factors were 800 in the EV and 860 in the TDEV for 90 wt.% acetic acid. The separation index of TDEV was higher than that of EV for an azeotropic mixture of acetic acid/water. TDEV in the separation of acetic acid/water mixtures through the PVA/MA membranes was more effective than EV [128].

The separation of acetic acid/water mixtures was carried out using PV and TDEV. For the separation process, 4-VP was grafted on PVA. Membranes were prepared from the graft copolymer by casting method and cross-linked by heat treatment. Permeation rates were found to be high in PV, whereas separation factors for H₂O/CH₃COOH selectivity were high in TDEV. Membranes gave permeation rates of 0.1–3.0 kg (m²h)⁻¹ and separation factors of 2.0–61.0, depending on the composition of the feed mixture and the membrane separation method [129].

The separation of acetic acid/water mixtures by using EV and TDEV was carried out over the full range of compositions at 30–55 °C using PVA/PAA of

75/25 (v/v) alloy membranes. PVA/PAA membranes in EV gave separation factors of 110–5711 and permeation rates of 2.3×10^{-4} – 1.53×10^{-1} kg (m² h)⁻¹, depending on the operation temperature and feed mixture composition. TDEV was also applied to PVA/PAA membranes to separate acetic acid/water mixtures; high permeation rates (1.7×10^{-3} – 3.0×10^{-1} kg (m² h)⁻¹) and separation factors for H₂O/CH₃COOH selectivity (1335–8924) were obtained. Azeotrope of acetic acid and water was also separated by TDEV with a separation factor of 297 and permeation rate of 1.50×10^{-1} kg (m² h)⁻¹ [130].

AN and HEMA were grafted onto PVA using cerium (IV) ammonium nitrate as initiator at 30 °C. The PVA-*g*-AN/HEMA membranes were prepared by a casting method, and used in the separation of acetic acid/water mixtures by PV. PVA-*g*-AN/HEMA membranes gave separation factors for H₂O/CH₃COOH selectivity of 2.26–14.60 and permeation rates of 0.18–2.07 kg (m² h)⁻¹. Grafted membranes gave lower permeation rates and greater separation factors for H₂O/CH₃COOH selectivity than PVA membranes [131].

Novel composite membranes were prepared from two hybrid materials of class I and class II. Membranes exhibited a remarkable increase in the degree of swelling with increasing zeolite loading in class-II hybrid material. The PV performance of these membranes for the separation of water/acetic acid mixtures was investigated in terms of feed composition and zeolite loading. Both the permeation rate and H₂O/CH₃COOH selectivity increased simultaneously with increasing zeolite content in the membrane matrix. These results were explained based on the enhancement of hydrophilicity, selective adsorption, and the establishment of molecular-sieving action. Among the membranes developed, the membrane containing 15 mass% of zeolite exhibited the highest separation factor for H₂O/CH₃COOH selectivity of 2423 with a permeation rate of 8.35×10^{-2} kg (m² h)⁻¹ for 10 mass% of water in the feed at 30 °C [132].

A new type of NaAlg composite membrane, by incorporating cobalt (III) (3-acetylpyridine-*o*-aminobenzoylhydrazone) (Co-APABZ) complex as filler particles in different ratios, was developed. Membranes were prepared by solution casting, followed by solvent evaporation, and cross-linked with GA. NaAlg composite membranes in the presence of Co-APABZ particles preferentially absorbed water molecules to facilitate diffusion of water through the membranes, thus enhancing the H₂O/

CH₃COOH selectivity in the acetic acid/water mixture. However, the membrane performance was significantly affected by the content of Co-APABZ in the NaAlg matrix and the degree of swelling of the membrane. The membrane with Co-APABZ of 5 wt.% in NaAlg matrix resulted in the separation factor for H₂O/CH₃COOH selectivity of 174 and the permeation rate of 0.123 kg (m² h)⁻¹ for an aqueous solution of 90 wt.% acetic acid [133].

Novel hydrophilic polymer membranes based on cross-linked mixtures of poly(allylamine hydrochloride)-PVA are developed. The high selectivity and permeation rate characteristics of these membranes for the dehydration of organic solvents are evaluated using PV technology and are found to be very promising when compared to existing membranes [134].

2.11.6.4 Selective Membranes for Organic Liquid/Water Mixtures

Organic-liquid/water-selective membranes are effective for the removal of organics in water and recovery of organic solvents from water. These membranes can contribute to the environmental problem and effective use of organic solvents.

The removal and enrichment of chlorinated hydrocarbons, such as 1,1,2-trichloroethane (TCE), trichloroethylene (TCET), and tetrachloroethylene (TECET), from dilute aqueous solutions by PV was investigated [135]. Novel polymers with high selectivity for these solvents were synthesized by radical polymerization, that is, glassy copolymers composed of (trimethylsilyl)methyl methacrylate (TMSMMA), and rubbery *n*-butyl acrylate (*n*-BA). The effect of the molar ratio of TMSMMA/*n*-BA on the permeation rate of TCE and the separation factor for TCE/H₂O selectivity was examined. The glass transition temperatures of the copolymers decreased with an increase in *n*-BA content, which resulted in high segmental mobility and, thus, high diffusivity. The copolymer membrane containing about 70 mol.% of *n*-BA showed the highest separation factor, in the range of 600–1000, for TCE. The high selectivity of these copolymer membranes for chlorinated hydrocarbons was mainly attributed to high partition coefficients for chlorinated hydrocarbons [135].

Silicalite-filled poly(siloxane imide) (PSiI) membranes were prepared for the separation of VOCs from water by PV. PSiI copolymer was synthesized by polycondensation of 3,3',4,4'-benzophenonetetracarboxylic dianhydride (BTDA) with a siloxane-containing diamine, for example, PDMS,

bis(3-aminopropyl) terminated (PSX), added with 3,3-diaminodiphenyl sulfone (DDS). 2,4,6-triamine pyrimidine (TAP) was added into the casting solution in order to enhance the compatibility between the polymeric matrix and the filler, that is, silicalite. The surface morphology for the membrane, with the addition of TAP, differed from that without TAP. The latter seems to be consisting of particles in the membrane surface. The solubility selectivity of the PSiI membranes for chloroform (CHCl_3)/water solutions was investigated, and there was a highest value for it around 50 wt.% of PSX content. The PV performance of the membranes was studied with the separation of chloroform/water mixture. The silicalite-filled membrane with 120- μm thickness exhibited a high total permeation rate of 280 $\text{g}(\text{m}^2\text{h})^{-1}$ with separation factor for $\text{CHCl}_3/\text{H}_2\text{O}$ selectivity of 52.2 for chloroform of 1.2 wt.% of the chloroform/water mixture [136].

Hydroxy-terminated polybutadiene (HTPB)–polyurethaneurea (PUU)–PMMA IPN membrane has been developed for the selective removal of chlorinated VOCs, such as 1,1,2,2-tetrachloroethane (TCEN), CHCl_3 , carbon tetrachloride (CCl_4), and TCET in water, in very low concentration by PV. IPNs of different PMMA content and also different cross-linking densities were used. Since the selective permeation and diffusion of the VOCs through the membrane are dependent on their interaction with the membrane material, their sorption and diffusion behaviors through the membrane were also investigated by swelling the membrane in pure VOCs. The sorption and diffusion behaviors were explained with the help of their solubility parameter data and calculated interaction parameter data of the membrane polymers with the VOCs. Based on the swelling kinetics data, diffusion coefficients of the VOCs through the membrane were calculated. Diffusion coefficients increased with the increase in cross-linking density and PMMA content in the membrane. In PV experiment, concentrations of chlorinated organic compounds in feed were varied from 100 to 1000 ppm. All the three IPN membranes showed excellent separation performances of the chlorinated VOCs from water. One IPN containing PMMA of 26% produced TCET of 88.7% in the permeate and resulted in the permeation rate of 0.2 $\text{kg}(\text{m}^2\text{h})^{-1}$ and a separation factor of 7842 for 0.1% aqueous feed at 30 °C. All three IPN membranes of different compositions showed the separation performances, namely, permeation rate and separation factor in the order of $\text{TCEN} < \text{CCl}_4 < \text{CHCl}_3 < \text{TCET}$ [137].

Surfactants are widely used for the remediation of groundwater contaminated with chlorinated solvents. The reuse of surfactants is quite important for the economic feasibility of the remediation process. PV with a PDMS membrane was conducted to simultaneously separate TCE and TCEN from waste solution of the nonionic surfactant Tween 80. Membrane thickness between 200 and 300 μm did not affect the PV performance. The permeation rate of organic did not increase above the flow rate of 100 ml min^{-1} . The increase in the feed concentration and feed temperature enhanced the permeation rate of organic. Organic selectivity reduced significantly with increasing feed temperature. This was due to an increase in the thermal motion of polymer chains. The reduction in the permeation rate was small, below surfactant of 1.0 wt.% (Tween 80) in feed solution. The permeation rate and selectivity for TCE were higher than those of tetrachloroethylene (PCE) because an extracellular portion of TCE was higher than that of TCEN. In simultaneous PV of TCE and TCEN, the permeation rate and organic selectivity decreased due to the competitive sorption of TCE and TCEN. However, the reduction percentage in permeation rate and selectivity was less than 10% in TCE/TCEN of 1/1. With operation for 100 h, over 95% of TCE and 90% of TCEN were simultaneously removed from 0.5 wt.% of Tween 80 solution with TCE and TCEN of 1000 ppm [138].

The permeation and separation characteristics of a series of chlorinated hydrocarbons, which have different carbon and chlorine numbers, were investigated through a PDMS membrane in the PV of pure hydrocarbon organics and dilute organic aqueous mixtures, respectively. The permeation behavior of the chlorinated hydrocarbon aqueous solutions was interpreted in terms of the effects of the interaction between the organic permeant and the membrane material, and the interaction between the water and organic molecules absorbed in the membrane, resulting in a corresponding plasticization action on the membrane material. The permeation of an organic permeant through the rubbery membrane was dominated by the solubility process rather than by the diffusion process [139].

The application of an integrated PV process to improve the PV performance of acetic acid/water mixtures was investigated. This integrated PV process was based on a plain PDMS membrane with a hydrophobic ionic liquid composed of a heterocyclic cation and $[\text{PF}_6]^-$ anions. The hydrophobic ionic liquid was introduced as the third phase between the

aqueous phase and the plain PDMS membrane for improving mass transfer of acetic acid from its aqueous matrix to the PDMS membrane. The primary results indicated that the ionic liquid as an extractant prior to PV was favorable for improving the $\text{CH}_3\text{COOH}/\text{H}_2\text{O}$ selectivity and the permeation rate of acetic acid compared with those in a plain PDMS membrane. This performance could be attributed to the incorporation of acetic acid molecules and rejection of water molecules by the ionic liquid prior to PV. Extraction of a real effluent containing acetic acid from an antibiotic pharmaceutical plant was carried out using the above integrated PV, and the results imply that this integrated PV process could be scaled up for recovering acetic acids over its water-rich effluents [140].

HTPB-based PUU membranes were synthesized and used for pervaporative recovery of *N*-methyl-2-pyrrolidone (NMP) from dilute aqueous solution. The sorption of NMP in cross-linked PUU membranes was found to vary with the NMP concentration in the feed and soft segment content of the membrane. A linear sorption isotherm was observed. The effects of membrane soft segment content, NMP concentration, operating temperature, and membrane thickness on the PV performance of the synthesized PUU membranes were studied. With decrease in soft segment content of the membrane, the permeation rate decreased slightly but the separation factor for $\text{NMP}/\text{H}_2\text{O}$ selectivity increased to some extent. With increase in concentration of NMP in the feed solution, the permeation rate was improved significantly. Both the permeation rate and the separation factor for $\text{NMP}/\text{H}_2\text{O}$ selectivity increased with increase in operating temperature [141].

HTPB-based porous PUU membranes were prepared. The porosity was developed by incorporation of lithium chloride into polymer matrix with subsequent leaching of the same in hot water. The PV performance of synthesized membranes was studied with aqueous 4-nitrophenol solution as feed. PUU membrane was found to permeate 4-nitrophenol selectively with high separation factors for the organic component. Pore size and number of pores on the surface of the membrane were calculated from scanning electron microscope (SEM) image of the membranes, and effects of pore size and porosity on PV permeation were also investigated [142].

IPN membrane of HTPB-based PUU and PMMA was developed and used in the PV separation of water/DMF mixtures of different compositions. At a higher temperature, the permeation of diffusing

molecules through the membrane became easier, resulting in an increase of permeation rate of DMF. With the increase in PMMA content in the membrane, the permeation rate of DMF and separation factor for $\text{DMF}/\text{H}_2\text{O}$ selectivity increased. This increase was due to the presence of more polar groups of PMMA. The highest permeation rate of DMF was $0.231 \text{ kg (m}^2\text{h)}^{-1}$ for the PUU-PMMA-3 membrane at 60°C for DMF of 80% in the feed [143].

The separation of propyl propionate/water mixtures by PV using poly(ether-*b*-amide) (PEBA) membranes, which is relevant to aroma compound recovery from dilute aqueous solutions, was studied. Under the experimental conditions tested, the permeate concentration was much higher than the solubility limit, and, upon phase separation, substantially pure propyl propionate could be achieved. The diffusivity of propyl propionate through the membrane from its dilute aqueous solutions was affected by the solution concentration exponentially. The permselectivity of the membrane for propyl propionate/water separation was mainly derived from its solubility selectivity due to the organophilicity of the membrane. The diffusivity of pure propyl propionate in the membrane was about 29 times higher than the diffusivity of pure water [144].

The PV characteristics of the EVA copolymer membranes with different VA content for recovery of ethyl acetate (EA) from aqueous EA solutions were investigated. The separation factor for $\text{EA}/\text{H}_2\text{O}$ selectivity decreased with increasing VA content from 26 wt.% (EVA26) to 100 wt.% (poly vinyl acetate, PVAc) in EVA copolymer membranes. A maximum permeation rate ($\mathcal{J}_{\text{EA, max}}$) of EA of a EVA membrane with a VA content of 38 wt.% for 2.5 wt.% aqueous EA solution at 30°C was $550 \text{ g (m}^2\text{h)}^{-1}$ and the separation factor for $\text{EA}/\text{H}_2\text{O}$ selectivity was 118. These PV characteristics of EVA membranes were explained in terms of the crystallinity of EVA copolymer and the affinities between EA or water and VA segment in EVA copolymer membrane. Experimental results also showed that both the separation factor for $\text{EA}/\text{H}_2\text{O}$ selectivity and \mathcal{J}_{EA} increased with increasing feed temperature and feed concentration [145].

Separation of multicomponent liquid systems containing nonvolatile compounds (e.g., salts, sugars, or proteins) became an important and interesting case of the application of PV process. The influence of NaCl on the performance of PV removal of methyl acetate (MeAc) from water using hydrophobic membrane was evaluated [146]. The selective and

transport properties were determined for a hydrophobic PDMS membrane in contact with pure water, binary water/MeAc, and ternary water/MeAc/NaCl systems. The presence of electrolyte in the feed solution caused the decrease of the permeation rate of water and the increase of permeation rate of MeAc simultaneously; thus, the increase in the membrane selectivity and the overall performance of the separation process were enhanced. Such behavior of the membrane system can be explained by the salting-out effect and described using the Setschenov empirical equation. In contact with binary mixture (1 wt.% MeAc), the separation factor for MeAc/H₂O selectivity was 160 and the permeation rate of MeAc $\bar{J}_{(\text{MeAc})}$ was 202 g (m² h)⁻¹, whereas in contact with ternary mixture (1 wt.% MeAc, 4 mol. NaCl/kg⁻¹) and \bar{J}_{MeAc} was 430 g (m² h)⁻¹.

PEBA membranes were prepared by casting a solution on a nonsolvent surface. The effects of the solvent ratio (*n*-butanol/2-propanol), temperature, and polymer concentration on the quality of the membranes were studied. The results show that the film quality was enhanced with increasing 2-propanol ratio in the solvent. This behavior was related to the reduction of the solution surface tension and the interfacial tension between the solution and nonsolvent. Uniform films were made at a temperature range of 70–80 °C and a polymer concentration of 4–7 wt.%. The qualities of the films improved with increasing 2-propanol ratio in the solvent. With these membranes, the PV of ethyl butyrate (ETB)/water and 2-propanol/water mixtures was studied. For ETB/water mixtures, with increasing ETB content, both the permeation rate and separation factor for ETB/H₂O selectivity increased. However, for 2-propanol/water mixtures, with increasing 2-propanol content, the permeation rate increased, but the separation factor for IPA/H₂O selectivity was decreased. Increasing temperature in a limited range resulted in a decreasing separation factor and an increasing permeation rate [147].

The removal of VOCs, such as Bz and chloroform, from aqueous Bz and chloroform solutions using PMMA-*g*-PDMS, poly(ethylmethacrylate)-PDMS (PEMA-*g*-PDMS), and poly(*n*-butylmethacrylate)-PDMS (PBMA-*g*-PDMS) graft copolymer membranes was investigated by PV. When aqueous solutions of dilute VOCs were permeated through the PMMA-*g*-PDMS and PEMA-*g*-PDMS membranes, these membranes were Bz/H₂O and CHCl₃/H₂O selective. The permeation and separation characteristics of the PMMA-*g*-PDMS and

PEMA-*g*-PDMS membranes changed drastically at a DMS content of about 40 and 70 mol.%, respectively, as shown in Figure 15. The permeation rate and VOC/water selectivity of the PBMA-*g*-PDMS membranes, however, increased gradually with increasing DMS content, unlike those of PMMA-*g*-PDMS and PEMA-*g*-PDMS membranes. Furthermore, TEM observations revealed that the PMMA-*g*-PDMS and PEMA-*g*-PDMS membranes had microphase-separated structures, consisting of a PDMS phase and a poly(alkyl methacrylate) phase. Conversely, the PBMA-*g*-PDMS membrane was homogeneous. It was found that the permeability and selectivity of these graft copolymer membranes for treatment of aqueous VOC solutions by PV were significantly related to a PDMS continuous layer in the phase-separated structure [148, 149].

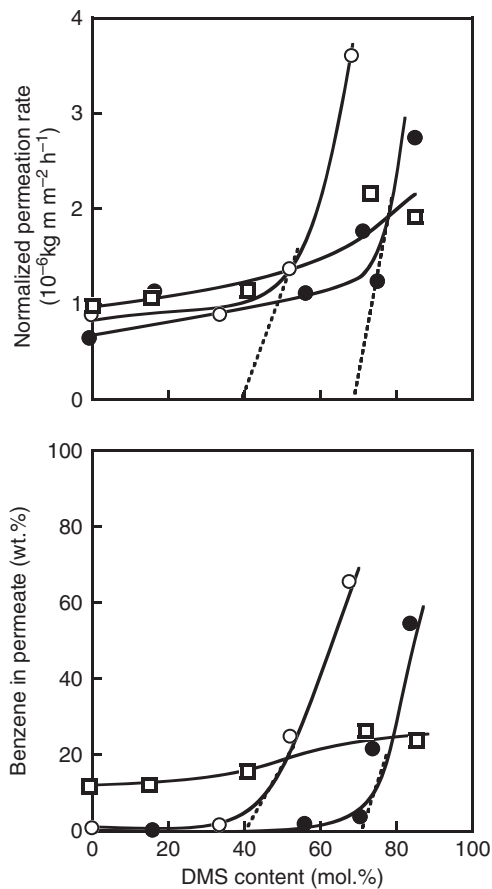


Figure 15 Effects of the DMS content on the benzene concentration in the permeate and normalized permeation rate for an aqueous solution of 0.05 wt.% benzene through PMMA-*g*-PDMS (○), PEMA-*g*-PDMS (●), PBMA-*g*-PDMS (□) membranes during PV. From Uragami, T., Yamada, H., Miyata, T. *J. Membr. Sci.*, **2001**, *187*, 255–269.

Hydrophobically surface-modified membranes were prepared by adding a fluorine-containing graft copolymer to a microphase-separated membrane consisting of PDMS and PMMA. Contact angle measurements and XPS revealed that the addition of a fluorine-containing copolymer produced a hydrophobic surface at the air side of the membrane due to surface localization of the fluorinated copolymer. It was apparent from TEM that adding a fluorine-containing copolymer of less than 1.2 wt.% did not affect the morphology of the microphase-separated membrane. However, adding a fluorine-containing copolymer over 1.2 wt.% resulted in a morphological change, from a continuous PDMS phase to a discontinuous PDMS phase. The addition of a small amount of fluorine-containing copolymer to the microphase-separated membranes enhanced both their permeability and Bz/cyclohexane (Chx) selectivity for a dilute aqueous solution of Bz during PV because of their hydrophobic surfaces and microphase-separated structures. Specifically, the microphase-separated membrane with 1.2 wt.% of fluorine-containing copolymer concentrated an aqueous solution from 0.05 to 70 wt.% Bz, and, therefore, removed the Bz from water very effectively [150].

Effects of the addition of fluorine-containing graft- or block-copolymer additives composed of PFA and PDMS or PDMS macro-azo-initiator to a microphase-separated membrane consisting of PDMS and PMMA on the Bz/H₂O selectivity by PV, and the surface characteristics and structures of the surface-modified PMMA/PDMS membranes were investigated. Addition of the fluorine-containing copolymer additives, PFA-*g*-PDMS and PFA-*b*-PDMS to a PMMA-*g*-PDMS membrane, yielded hydrophobic surfaces at the air side of surface-modified membranes due to the localization of their additives on the air-side surface of these membranes. The addition of a small amount of the PFA-*g*-PDMS and PFA-*b*-PDMS enhanced both the Bz/H₂O selectivity and the permeability for an aqueous dilute Bz solution during PV because of the formation of their hydrophobic surfaces and the existence of the microphase-separated structures with a continuous PDMS phase in the inner layer of these membranes. When a larger amount of the PFA-*g*-PDMS and PFA-*b*-PDMS were added to a PMMA/PDMS, the latter additive could keep the microphase-separated structures with a continuous PDMS phase, but the former did not [151].

PMMA-*g*-PDMS and PMMA-*b*-PDMS membranes containing *tert*-butylcalix [4] arene (CA) (CA/PMMA-*g*-PDMS and CA/PMMA-*b*-PDMS) were applied to the removal of Bz from a dilute aqueous solution of Bz by PV [152]. When an aqueous solution of 0.05 wt.% Bz was permeated through CA/PMMA-*g*-PDMS and CA/PMMA-*b*-PDMS membranes, these membranes showed high Bz/water selectivity. Both the permeability and Bz/H₂O selectivity of the CA/PMMA-*g*-PDMS and CA/PMMA-*b*-PDMS membranes were enhanced by increasing the CA content, due to the affinity of CA for Bz. The permeability and Bz/H₂O selectivity of CA/PMMA-*b*-PDMS membranes were much greater than those of CA/PMMA-*g*-PDMS membranes. TEM observations revealed that both the CA/PMMA-*g*-PDMS and CA/PMMA-*b*-PDMS membranes had microphase-separated structures consisting of a PMMA phase and a PDMS phase-containing CA. The microphase-separated structure of the latter membranes was much clearer than that of the former and was lamellar. The distribution of CA in the microphase-separated structure of the CA/PMMA-*g*-PDMS and CA/PMMA-*b*-PDMS membranes was analyzed by differential scanning calorimetry (DSC) and CA was distributed in a PDMS continuous layer in micro-phase-separated structure [152, 153].

In previous works, it has been reported that the PMMA-*b*-PDMS membranes show high VOC/water selectivity. Thus, for the purpose of improvement of the VOC/water selectivity, graft- and block-copolymer membranes composed of polystyrene (PSt), which is more hydrophobic than PMMA and has higher affinity for VOCs, and PDMS were prepared. Conversely, recently, ionic liquids are becoming the focus in a great number of fields, such as inorganic, organic, biological, and electrochemical applications, because they have outstanding properties, such as very low vapor pressure, nonvolatility, heat stability, high polarity, good solvent for various organic and inorganic compounds, and high conductivity. Such ionic liquids are playing an increasingly important role in separation science [228]. Then, PSt-*b*-PDMS membranes containing an ionic liquid, 1-allyl-3-butylimidazolium bis(trifluoromethane sulfonyl)imide ([ABIM]TFSI) ([ABIM]TFSI/PSt-*b*-PDMS), were tested for the removal of VOCs from an aqueous solution of dilute VOC by PV [229]. These [ABIM]TFSI/PSt-*b*-PDMS membranes showed high VOC/water selectivity, and both the permeability and

VOC/H₂O selectivity were enhanced by increasing the [ABIM]TFSI content, due to the affinity of [ABIM]TFSI for VOCs.

It was found that a continuous PDMS layer in PMMA-*g*-PDMS and PMMA-*b*-PDMS membranes play an important role for the removal of VOCs from water. For the purpose of constructing the membrane matrix from PDMS component mainly, polydimethylsiloxane dimethylmethacrylate macromonomer (PDMSDMA) was selected as a membrane material. The effects of cross-linkers of the cross-linked PDMS membranes derived from PDMSDMA and divinyl compounds, on the PV characteristics of the removal of Bz from an aqueous solution of dilute Bz. When an aqueous solution of 0.05 wt.% Bz was permeated through the cross-linked PDMSDMA membranes, they showed high Bz/H₂O selectivity. Both the permeability and Bz/H₂O selectivity of the membranes were enhanced with increasing divinyl compound content as the cross-linker, and were significantly influenced by the type of divinyl compound. PDMSDMA membranes cross-linked with divinyl siloxane (DVS) showed very high membrane performance during PV. The best normalized permeation rate, separation factor for Bz/H₂O selectivity, and PV separation index (PSI) [157, 158], which is the product of the

permeation rate and the separation factor, and can be used as a measure of the membrane performance during PV, of a PDMSDMA–DVS membrane were $1.96 \times 10^{-5} \text{ m kg (m}^2 \text{ h)}^{-1}$, 98, and 192, respectively [154]. When divinyl perfluoro-*n*-hexane (DVF), which is much more hydrophobic, was employed as a cross-linker of PDMSDMA, the best normalized permeation rate, separation factor for Bz/H₂O selectivity, and PSI of a PDMSDMA–DVF membrane were $1.72 \times 10^{-5} \text{ m kg (m}^2 \text{ h)}^{-1}$, 4316, and 7423, respectively [155].

The effect of the addition of CA to the cross-linked PDMS membranes derived from PDMSDMA, and various divinyl compounds, on the PV characteristics of the removal of Bz from an aqueous solution of dilute Bz. Both the Bz/H₂O selectivity and permeability of the membranes were enhanced with increasing both divinyl compound content as the cross-linker and additional amount of CA, and were significantly influenced by the type of divinyl compound. Addition of CA to PDMSDMA membranes cross-linked with DVF gave very high effect for the PV performance [156].

In Table 5, the permeation and separation characteristics of various polymer membranes consisting of the PDMS components are compared under the same PV condition: feed solution, an aqueous

Table 5 Performance for Bz/H₂O of various membranes containing PDMS component

Various PDMS membranes ^a	$\alpha_{\text{sep. Bz/H}_2\text{O}}$	$\alpha_{\text{sorp. Bz/H}_2\text{O}}$	$\alpha_{\text{diff. Bz/H}_2\text{O}}$	NPR ^b	PSI ^c	Ref.
PMMA	53	422	0.13	0.29	16	[149]
PMMA- <i>g</i> -PDMS ^d	620	739	0.86	0.13	226	[152]
CA/PMMA- <i>g</i> -PDMS ^e	1772	1267	1.40	0.71	1240	[152]
PFA- <i>g</i> -PDMS/PMMA- <i>g</i> -PDMS ^f	4492			0.64	2879	[150]
PDMSDMA–DVB ^g	3171	1436	2.21	1.46	4629	[154]
PDMSDMA–DVS ^h	2886	1270	2.46	1.96	5656	[154]
PDMSDMA–DVF ⁱ	4316	1804	2.49	1.72	7423	[155]
CA/PDMSDMA–DVB ^j	4021	1689	2.18	1.75	7037	[156]
CA/PDMSDMA–DVS ^k	3866	1620	2.39	1.97	7616	[156]
CA/PDMSDMA–DVF ^l	5027	1998	2.52	1.86	9350	[156]

^a PV experimental conditions: feed solution, an aqueous solution of 0.05 wt.% benzene; permeation temperature, 40 °C; pressure of permeation side, 1×10^{-2} Torr (1.33 Pa).

^b normalized permeation rate ($10^{-5} \text{ m kg (m}^2 \text{ h)}^{-1}$).

^c PV separation index (NPR $\times \alpha_{\text{sep. Bz/H}_2\text{O}}$).

^d PDMS content: 74 mol.%.

^e PDMS content: 74 mol.%; CA content: 40 mol.%.

^f PDMS content: 74 mol.%; PFA-*g*-PDMS content: 1.2 wt.%.

^g DVB content: 80 mol.%.

^h DVS content: 90 mol.%.

ⁱ DVF content: 90 mol.%.

^j DVB content: 80 mol.%; CA content: 0.5 wt.%.

^k DVS content: 90 mol.%; CA content: 0.5 wt.%.

^l DVF content; CA content.

From Ohshima, T. Miyata, T. Uragami, T. *Macromol. Chem. Phys.* **2005**, 206, 2521–2529.

solution of 0.05 wt.% Bz; permeation temperature, 40 °C; and pressure of permeation side, 1.33 Pa. As can be seen in **Table 5**, both the normalized permeation rate and the Bz/H₂O selectivity of each of the CA/PDMSDMA-divinyl benzene (DVB), CA/PDMSDMA-DVS, and CA/PDMSDMA-DVF membranes were improved as compared to each of the PDMSDMA-DVB, PDMSDMA-DVS, and PDMSDMA-DVF membranes. Although the separation factors of the CA/PDMSDMA-DVB, CA/PDMSDMA-DVS membranes were lower than those of the PFA-*g*-PDMS/PMMA-*g*-PDMS membranes, the PSI of the former membranes was much greater than that of the latter one. In previous studies [154, 155], the introduction of cross-linking structure into the membrane matrix using a suitable cross-linker with a high affinity for permeant was a very effective method to give both a high permeation rate and a high Bz/H₂O selectivity. In **Table 5**, it is shown that the addition of CA into the cross-linked PDMSDMA membranes cross-linked with a suitable cross-linker is significantly effective to obtain a higher permeation and separation characteristics. A CA/PDMSDMA-DVF membrane with DVF of 90 mol.% and CA of 0.4 wt.% showed the best membrane performance, that is, the normalized permeation rate, separation factor for Bz/H₂O selectivity, and PSI were $1.86 \times 10^{-5} \text{ m kg (m}^2 \text{ h)}^{-1}$, 5027, and 9350, respectively.

The air-stripping removal of VOCs, such as toluene and phenol, from water by microporous poly(propylene) (PP) hollow fibers was studied. The VOC stream passed through the lumen side of the module, while air (stripping gas) flowed across the shell side. Experiments were performed at different liquid flow rates (8–16 cm³ min⁻¹), gas flow rates (60–180 cm³ min⁻¹), feed VOC concentrations (100–1000 ppm), and temperatures (24–35 °C). The removal was more effective when feed VOC level and liquid or gas flow rate increased. The applicability of a mass transfer model that considers diffusion in the liquid layer, membrane, and gas layer under steady state was checked. Unlike phenol with a very small dimensionless Henry's law constant (equilibrium gas concentration divided by liquid concentration) and a relatively low amount of sorption on PP fibers, the measured overall mass transfer coefficients for toluene reasonably agreed with those predicted from the model. The large deviation observed for phenol indicated unsteady state nature, likely due to its small concentration difference between air and liquid phase/fiber matrix. The air-

stripping removal and separation of binary VOCs, including *O*-xylene and chloroform, from water were also examined [159].

Membranes with CB as a filler to PV of toluene from the diluted aqueous solution were applied. PDMS composite membranes, PDMS and PEBA membranes, filled with CB, were used. The membranes were prepared in a laboratory scale especially for this purpose. Both PEBA and PDMS membranes showed excellent properties to separate toluene from the water; however, toluene solubility in the PDMS membrane was better. The removal of this compound from the feed was better when PDMS membrane was used. In some cases, total permeation rate as well as toluene permeation rate decreased for the membranes with the filler comparing to those without the filler [160].

The permeation and separation characteristics of VOCs, such as chloroform, Bz, and toluene, from water by PV through cross-linked PDMS membranes prepared from PDMSDMA and divinyl compounds, such as ethylene glycol dimethylmethacrylate (EGDM), DVB, DVS, and DVF, were studied [161]. These membranes showed high VOC/H₂O selectivity and permeability. Both, VOC/water selectivity and permeability, were affected significantly by the divinyl compound. Furthermore, cross-linked PDMSDMA membranes showed the highest CHCl₃/H₂O selectivity. The VOC/H₂O selectivity was mainly governed by the solubility selectivity rather than the diffusion selectivity. However, the difference in the VOC/H₂O selectivity between different types of VOCs depended on differences in the diffusivity of permeants. With increasing downstream pressure, the VOC/H₂O selectivity of all cross-linked PDMSDMA membranes increased, but the permeability decreased. A PDMSDMA-DVF membrane exhibited a normalized permeation rate of $1.9 \times 10^{-5} \text{ kg m (m}^2 \text{ h)}^{-1}$; this and a separation factor for CHCl₃/H₂O of 4850 yielded a separation index of 9110.

Atom transfer radical polymerization of HEMA from initiators immobilized on porous supports yields PV membranes with high permeation rate that can be readily modified to control their properties. Derivatization of poly(2-hydroxyethyl methacrylate) (PHEMA) coatings with octyl (C8-PHEMA), hexadecyl (C16-PHEMA), or penta-decafluorooctyl (fluorinated PHEMA) side chains provides films that are sufficiently hydrophobic to allow selective PV of VOCs from water. For all of these derivatized PHEMA membranes, VOC/water

selectivities generally increased with decreasing solubility of the VOC in water, and TCET/water selectivities are about 500. Sorption data suggested that fluorinated PHEMA has the highest free volume and that C16-PHEMA had the lowest, and, consistent with this inference, permeation rate decreased in the order of fluorinated PHEMA > C8-PHEMA > C16-PHEMA. The permeation rate was generally an order of magnitude greater than those through high-performance PDMS membranes [162].

Five types of PDMS/PVF₂ composite membranes were prepared using asymmetric PVF₂ hollow-fiber membranes as the substrate where a very thin layer of silicone-based coating material was deposited via a developed dip-coating method. In the optimal coating procedure, homogenous and stable oligo-PDMS coating layers, as thin as 1–2 μm, were successfully deposited on the surface of the PVF₂ membranes. The developed PDMS/PVF₂ composite membranes were applied for separation of a wide variety of VOC (Bz, chloroform, acetone, EA, and toluene). The results showed that the PDMS/PVF₂ hollow-fiber composite membranes that had been developed exhibited very high removal efficiency (>96%) for all the VOCs examined under favorable operating conditions [163].

VOCs can be separated from aqueous micellar surfactant solutions with high efficiency by PV processes using organophilic polymer membranes. This seems to be a surprising result because the transmembrane permeation rate of a VOC strongly depends on its volatility, which is rather low in the presence of a surfactant at concentrations far above the critical micellar concentration. Based on the results of equilibrium measurements in micellar systems and PV experiments, a theoretical analysis of the mass transfer was given. The mass transfer for VOCs in the liquid boundary layer of a PV membrane in the presence of a micellar phase cannot be described by molecular diffusion processes alone. Obviously, the mass transfer was enhanced considerably by diffusing micelles which transport the solubilized VOC molecules in direction to the surface of the membrane [164].

A novel composite membrane, using supramolecule CA-filled PDMS as the top active layer and nonwoven fabric as the support layer, was developed for the pervaporative removal of Bz from water. Compared to unfilled PDMS homogenous membrane, the composite membrane exhibited both higher separation factor for Bz/H₂O selectivity and higher permeation rate by 1.8- and 3.2-fold,

respectively. The permeation rate of Bz was proportional to both the Bz concentration in feed and the downstream pressure [165].

The study was aimed at removing organic solvents from aqueous solutions using PV. The tests were carried out on a composite PDMS membrane manufactured by GKSS/Forschungszentrum Geesthacht, Germany, and a PDMS membrane filled with CB prepared in a laboratory. There were two runs: the first one tested an aqueous toluene solution as feed, while the other used a mixture of solvents—toluene, acetone, and EA. The PDMS membrane without CB removed all the components of the mixture, displaying a very high efficiency of the process. However, the selectivity and enrichment factors turned out to be relatively low. The PDMS/CB membrane produced slightly lower removal degrees as well as the permeation rate of acetone and EA compared to the PDMS membrane, yet their concentration at the permeate side of the membrane was considerably higher. The presence of other solvents did not greatly affect toluene permeation – its final removal seemed to be independent of the composition of the feed used [166].

The syntheses of siloxane-grafted poly(amide-imide) and polyamide were carried out by a macromonomer method, in order to develop a highly permeable and durable membrane material for PV. A novel compound, 3,5-bis(4-aminophenoxy)benzyloxypropyl-terminated polydimethylsiloxane (BAPB-PDMS), was synthesized as a macromonomer. BAPB-PDMSs with different PDMS segment lengths were prepared by hydrosilylation of 3,5-bis(4-nitrophenoxy) benzyl allyl ether with hydrosilyl-terminated PDMS using Pt catalyst, followed by hydrogenation reduction of the terminal dinitro groups. The polycondensations of BAPB-PDMSs with trimellitic anhydride chloride and terephthaloyl chloride yielded the desired siloxane-grafted poly(amide-imide) (PAI-*g*-PDMS) and polyamide (PA-*g*-PDMS) copolymers, respectively. The copolymer membranes were prepared by solvent-casting method, and the gas permeability and PV property of these membranes were evaluated. As the solubility of the copolymers depended on the main chain structure, PA-*g*-PDMS membrane was insoluble in any solvents after it was dried *in vacuo*. The gas permeability coefficients of these copolymer membranes were increased with increasing of PDMS segment length, and these values of PAI-*g*-PDMS were higher than those of PA-*g*-PDMS containing the same PDMS segment length. From the results of

PV of the dilute aqueous solutions of organic solvents, it was found that PA-*g*-PDMS membrane exhibited the excellent organic/water selectivity toward several organic solvents, such as alcohols, acetone, THF, chloroform, dichloromethane, and Bz with a high and stable permeation. Furthermore, it was confirmed that the removal of THF from its dilute aqueous solution was efficiently achieved by the PV using PA-*g*-PDMS membrane [167].

2.11.6.5 Selective Membranes for Organic Liquid/Organic Liquid Mixtures

Organic/organic-selective membranes are effectively used for the purification and separation of industrial products and reuse of organic solvents based on separable recovery of organic mixtures.

2.11.6.5.1 Bz/Chx-selective membranes

The separation of Bz and Chx by distillation is a very energy-intensive process, because the boiling points of the components are very similar. PV may be an alternative, more energy-efficient process for the separation of Bz/Chx mixtures. Therefore, many workers have studied the PV properties of polymeric membranes for Bz/Chx separation.

For example, Inui *et al.* [168] selected PMMA and PEMA membranes which have a strong affinity for Bz. The PV permeation and separation characteristics for Bz/Chx mixtures in these poly(alkyl methacrylate) membranes cross-linked with EGDM were studied [168]. The cross-linked poly(alkyl methacrylate) membranes exhibited Bz/Chx (Bz/Chx) selectivity for Bz/Chx mixtures, and the permeation rate increased with increasing Bz concentration in the feed solution. The Bz/Chx selectivity of these membranes was strongly governed by the diffusion selectivity, and depended on the difference in molecular size between the Bz molecule and the Chx molecule. With increasing cross-linker content in the membrane, swelling of the membranes was reduced, enhancing the Bz/Chx selectivity. This result was attributed to an increase in the solubility selectivity caused by reduced swelling of the membrane. Cross-linked tertiary copolymer (PMMA-PEMA-EGDM) membranes also showed excellent Bz/Chx selectivity. These results suggested that both the increase in the affinity of the membrane for Bz and the reduction in the swelling of the membrane are very important variables in the separation of Bz/Chx mixtures [168].

Poly(dimethyl acrylamide-random-methyl methacrylate) (DMAA-*r*-MMA) and poly(dimethyl acrylamide)-graft-poly(methyl methacrylate) (DMAA-*g*-MMA) membranes were also examined for Bz/Chx separation by PV. The Bz selectivity of the DMAA-*r*-MMA membrane changed from diffusion-selectivity-controlled to solubility-selectivity-controlled with increasing DMAA content. In contrast, DMAA-*g*-MMA membranes with higher DMAA content had higher apparent diffusion selectivity than the apparent solubility selectivity. Furthermore, the apparent Bz/Chx solubility selectivity for the DMAA-*r*-MMA membrane and the DMAA-*g*-MMA membrane with a higher DMAA content was remarkably different. These results were attributed to the difference in structure between the copolymers [169].

A side-chain liquid-crystalline polymer (LCP) was synthesized by the addition of mesogenic monomer to poly(methylsiloxane) with a Pt catalyst. When Bz/Chx mixtures were permeated through the LCP membranes by PV at various temperatures, the permeation rate increased with increasing Bz concentration in the feed solution and permeation temperature. Although the LCP membranes exhibited Bz/Chx selectivity, the mechanism responsible for the permeation and separation of the Bz/Chx mixtures was different in the glassy, liquid-crystalline state versus the isotropic state of the LCP membranes. These results suggested that the Bz/Chx selectivity was moderately influenced by the change in LCP membrane structure (i.e., a state transformation). The balance between the orientation of the mesogenic groups and the flexibility of the siloxane chain is very important with respect to permeability and Bz/Chx selectivity [170, 171]. When Bz/Chx, toluene/Chx, and *o*-xylene/Chx mixtures were subjected to PV through an LCP membrane in the liquid-crystalline state, the permeation rate increased with increasing temperature and the LCP membrane exhibited selectivity for the aromatic hydrocarbons. The permeation rate and selectivity of the LCP membrane for each mixture decreased with increasing molecular size of the aromatic hydrocarbon in the binary feed mixture [172]. When Bz/Chx mixtures were permeated through nematic and smectic side-chain LCP (*n*- and *s*-LCP) membranes under various conditions during PV, the *n*- and *s*-LCP membranes exhibited Bz/Chx selectivity. The selectivity of the *n*-LCP membrane changed from solubility-selectivity-controlled to diffusion-selectivity-controlled upon the state transformation of the membrane, induced

by an increase in the permeation temperature. In contrast, the selectivity of the *s*-LCP membrane was governed by diffusion selectivity regardless of the state of this membrane. At low permeation temperatures, the *n*-LCP membrane in the liquid-crystalline state exhibited lower permeability but higher selectivity than the *s*-LCP membrane. However, at high permeation temperatures, the relationship between the permeability and Bz/Chx selectivity of the *n*-LCP and *s*-LCP membranes in the liquid-crystalline state was reversed. These results are a result of differences in the chemical and physical structure of the *n*-LCP and *s*-LCP membranes [173].

Chito and its derivatives have been used as membrane materials for a wide variety of PV applications, including dehydration of ethanol/water mixtures. Uragami *et al.* synthesized benzoylchitosan (BzChitos) with different degrees of benzylation as a durable membrane material for the separation of Bz/Chx mixtures. The characteristics of BzChito membranes, such as contact angle, crystallinity, and the degree of swelling, were significantly influenced by the degree of benzylation. As shown in **Figure 16**, the BzChito membranes showed high Bz/Chx selectivity for a mixture containing 50 wt.% Bz during PV. The difference in Bz/Chx selectivity of the BzChito membranes with different

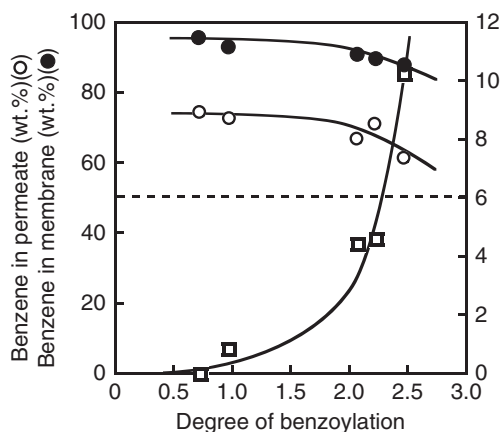


Figure 16 Effects of the degree of benzylation on the benzene concentration in the permeate (○) and the permeation rate (□) through the benzoylchitosan membranes for a benzene/cyclohexane mixture of 50 wt.% benzene by PV. The composition of benzene/cyclohexane sorbed into the membranes (●) for a benzene/cyclohexane mixture. Dotted line is the feed mixture composition (benzene/cyclohexane = 50/50, w/w). From Inui, K., Tsukamoto, K., Miyata, T., Uragami, T. *J. Membr. Sci.* **1998**, 138, 67–75.

degrees of benzylation corresponded to differences in the physical structure of the membranes. When a Bz/Chx mixture of 50 wt.% Bz was permeated through the BzChito membranes, the permeation rate increased and Bz/Chx selectivity decreased slightly with an increasing degree of benzylation [174, 175].

Modified cellulose-based membranes for Bz/Chx separation was developed [176, 177]. Various types of benzoylcellulose (BzCell) were synthesized and the effect of the degree of benzylation on the PV properties of the membranes was investigated [176]. A BzCell membrane with a benzylation degree of 2 showed high Bz/Chx selectivity for Bz/Chx mixtures during PV. The permeation rate of the BzCell membrane increased, but the Bz/Chx selectivity decreased with increasing Bz concentration in the feed mixture. This increase in the permeation rate was due to an increase in the swelling of the membrane, whereas the Bz/Chx selectivity decrease was attributed to a decrease in the solubility selectivity. With increasing benzylation of the BzCells, the permeation rate increased significantly, but the Bz selectivity decreased slightly. These results cannot be explained by the degree of swelling, the density, or the contact angle of the BzCell membranes [176].

Tosylcellulose (TosCell) with different degrees of tosylation were synthesized as membrane materials for the separation of Bz/Chx mixtures. TosCell membranes also showed high Bz/Chx selectivity when tested in PV mode [177]. An increase in the Bz concentration of the feed mixtures increased the permeation rate but decreased the Bz/Chx selectivity of the TosCell membranes. This increase in the permeation rate was attributed to an increase in the degree of swelling of the TosCell membranes due to sorption of the feed mixture. The decrease in Bz/Chx selectivity was mainly caused by a decrease in solubility selectivity. With low Bz concentrations in the mixtures, the permeation rate of a TosCell membrane with a higher degree of tosylation was greater than that with a lower degree of tosylation; however, the reverse was observed for high Bz concentrations. The Bz/Chx selectivity of the former TosCell membrane was higher than that of the latter membrane. Differences in the permeation rate and Bz/Chx selectivity with changes in the Bz concentration of the feed mixture and the degree of tosylation of the TosCell membrane were significantly influenced by the degree of swelling of the TosCell membrane, which is related to the Bz concentration sorbed into the membrane. The mechanism responsible for the

separation of Bz/Chx mixtures through the TosCell membranes was analyzed and discussed using the solution–diffusion model.

Methyl methacrylate-methacrylic acid copolymer (P(MMA-*co*-MAA)) membranes ionically cross-linked with Fe^{3+} and Co^{2+} ions P(MMA-*co*-MAA- Fe^{3+} and - Co^{2+}) were prepared, and their permeation and separation characteristics for a Bz/Chx mixture containing 50 wt.% Bz by PV were studied. Although the introduction of the metal ions into the MMA-*co*-MAA membrane enhanced both Bz/Chx selectivity and permeability for a Bz/Chx mixture, the PV characteristics of the MMA-*co*-MAA- Fe^{3+} and - Co^{2+} membranes were significantly different. The difference in performance between these membranes was strongly governed by differences in their membrane structures, as indicated by their glass transition temperature, contact angle to methylene iodide, degree of swelling, and mixture composition sorbed into the membrane [178].

Ren *et al.* [179] investigated the PV properties of a series of cross-linked 4,4'-hexafluoro-isopropylidene dianhydride (6FDA)-based copolyimide membranes for the separation of Bz/Chx mixtures. The glassy, highly rigid copolyimides were obtained by polycondensation of 6FDA with various diamines. To obtain high permeability as well as high selectivity, a combination of the diamines 2,3,5,6-tetramethyl-1,4-phenylene diamine (4MPD), 4,4'-hexafluoro-isopropylidene dianiline (6FpDA), and 3,5-diaminobenzoic acid (DABA) as monomers with a cross-linkable group were used. Cross-linking is necessary to prevent undesirable swelling effects, which generally occur with noncross-linked polyimides, especially if high Bz concentrations are reached during PV. The degree of cross-linking was kept constant at 20%, whereas the ratio of the diamine monomers 6FpDA and 4MPD was varied. The PV experiments were performed at 60 °C, using Bz/Chx mixtures with Bz concentrations covering the entire concentration range. All of the cross-linked polymers had excellent chemical and thermal stability in the PV experiments. In all cases, conditioning of the membrane samples with pure Bz was a suitable pretreatment to enhance the permeation rate without decreasing the Bz/Chx selectivity significantly. For the most promising membrane material, 6FDA-4MPD/DABA of 4:1 cross-linked with EG, the PV experiments were performed with a Bz/Chx feed mixture of 50/50 (w/w) over a temperature range between 60 and 110 °C to determine the effect of temperature on the separation characteristics [179].

The sorption and PV properties of poly(vinyl chloride) (PVC) membranes in Bz/Chx mixtures were studied by Yildirim *et al.* [180]. The effects of the Bz/Chx mixture composition and the temperature on the sorption and PV characteristics were determined at 30, 40, and 50 °C, respectively, for membranes containing 8 wt.% PVC polymer. The total sorption increased with increasing concentrations of Bz. Increasing the concentration of Bz resulted in an increase in the permeation rate and a decrease in the Bz/Chx selectivity. Permeation rates increased, and Bz/Chx selectivities decreased with increasing temperature. The Bz/Chx selectivity was not affected significantly by varying the concentration of polymer in the casting solution; however, as expected for a nonporous membrane, the permeation rate decreased with increasing concentration of the polymer in the casting solution. This was due to an increase in membrane thickness [180].

Polyvinylacetalized PVA (PVAc) membranes added *O,O*-bis(diethoxyphosphoryl)-*tert*-butyl calixarene (BEPCA) as a molecular recognition compound were applied to the separation of Bz/Chx mixture. These membranes were highly Bz/Chx selective. When evaluated against pure Bz and Chx, PVA/BEPCA showed an ideal selectivity tending toward infinity but a poor permeation rate ($5.9 \text{ kg } \mu\text{m} (\text{m}^2 \text{ h})^{-1}$) for Bz. The permeation rate of Bz was significantly higher in PVAc and increased from $20 \text{ kg } \mu\text{m} (\text{m}^2 \text{ h})^{-1}$ for 20% (v/v) Bz/Chx mixture to $65.8 \text{ kg } \mu\text{m} (\text{m}^2 \text{ h})^{-1}$ for pure Bz. The swelling index also increased with the increasing concentration of Bz in the feed. PV in PVAc was thus solubility controlled. The high interaction of PVAc with Bz was interpreted in terms of solubility parameters and free volume in the polymer [181].

The PV characteristics of Bz/Chx mixtures through a fixed carrier membrane consisting of CA as a base polymer and dinitrophenyl (DNP) group as a selective fixed carrier was investigated. The result of the PV of Bz/Chx mixture using the unmodified CA membrane and the CA/DNP membrane showed that the DNP group was effective to increase the Bz/Chx selectivity [182].

PVAc was synthesized by the acid-catalyzed acetalization of PVA. Three different morphologically modified variants of the polymer were prepared by the addition of supramolecules; α -cyclodextrin (α -CD) and β -cyclodextrins (β -CDs), and *tert*-butylcalix [4] arene (CA) were added to the PVAc of 20% (w/v) in THF. The PV behavior of modified membranes was evaluated for the separation of a wide

composition of Bz/Chx mixtures. Addition of α -CD or CA to PVAc reduced the overall permeation rate, while dispersion of β -CD favored an enhanced permeation rate, especially in low Bz concentration and an azeotropic mixture [183].

The effect of carbon molecular sieve (CMS) incorporated into PVA on PV of Bz/Chx mixtures was studied [184]. The characterization results showed that filling of CMS decreased the hydrogen-bond interaction among PVA polymer chains and made chains more flexible and relaxed, which resulted in decreasing of PVA membrane crystallinity, thus creating higher free volume in the membranes. CMS filling effectively increased the degree of swelling of membranes in almost the whole feed composition range. Due to the more relaxed polymer chain packing and stronger sorption ability, the permeation rate of CMS-filled PVA membranes increased effectively, but excessive filling would decrease the permeation rate. With increase of Bz weight fraction, operating temperature, and feed flow rate, the permeation rate of Bz increased, while the separation factor for Bz/Chx selectivity decreased. Compared with unfilled PVA membrane (permeation rate of Bz $21.87 \text{ g (m}^2 \text{ h)}^{-1}$, separation factor 16.7), permeation rate of Bz of PVA–CMS–06 membrane (mass ratio of CMS to PVA was 6%) increased remarkably to $59.25 \text{ g (m}^2 \text{ h)}^{-1}$ and separation factor for Bz/Chx selectivity increased to 23.21.

A novel type of hybrid membrane was prepared by filling carbon graphite (CG) into PVA and Chito blending mixture, with the expectation of improving the separation performance of the membranes by the synergistic effect of blending and filling. The results showed homogenous distribution of graphite particles, considerable alteration of hydrogen-bonding interaction, remarkable decrease of crystallinity degree, dramatic enhancement of mechanical properties, and significant increase of free volume in CG–PVA/Chito hybrid membranes. Sorption studies indicated that the degree of swelling of CG–PVA/Chito hybrid membranes increased with increasing graphite content and the separation factor for Bz/Chx selectivity was dominated by solubility selectivity rather than diffusivity selectivity. The PV properties of CG–PVA/Chito hybrid membranes for separation of Bz/Chx mixtures were investigated through varying graphite content and mass ratio of PVA to Chito in hybrid membranes. Higher permeation rate and separation factor of CG–PVA/Chito hybrid membranes were desirably obtained, compared to PVA and PVA/Chito membranes. In particular, a

CG06–PVA60/Chito40 membrane exhibited the highest separation factor of 59.8 with a permeation rate of $124.2 \text{ g (m}^2 \text{ h)}^{-1}$ at 50°C , 1 kPa [185].

β -CD-filled cross-linked PVA membranes were cross-linked with GA (β -CD/PVA/GA). The β -CD/PVA/GA membranes showed strong Bz/Chx selectivity. The permeation rates of β -CD/PVA/GA membranes increased when the β -CD content was 0–8 wt.%, but the permeation rate decreased slightly more than β -CD content of 8 wt.%. The separation factor for Bz/Chx selectivity increased when β -CD content was in the range 0–10 wt.% and decreased slightly in the range of β -CD content of 10–20 wt.%. Compared with the β -CD-free PVA/GA membrane, the separation factor for Bz/Chx selectivity of the β -CD/PVA/GA membrane considerably increased from 16.7 to 27.0, and the permeation rate of Bz increased from 23.1 to $30.9 \text{ g (m}^2 \text{ h)}^{-1}$ for Bz/Chx (50/50 w/w) mixtures at 50°C . The analysis based on the solution–diffusion model and β -CD inclusion phenomena (complex stabilities) revealed that β -CD in PVA membranes played an important role as a carrier to partition Bz selectively from Bz/Chx mixtures [186].

Novel hybrid membranes were prepared from PVA and carbon nanotube (CNT) of β -CD [187]. Both pure PVA and PVA/CNT hybrid membranes were uniform and these hybrid membranes exhibited significant improvement in Young's modulus and thermal stability as compared to pure PVA and β -CD/PVA membranes. These membranes were applied to PV separation of Bz/Chx mixtures, and showed excellent PV properties. The permeation rate of Bz was $61.0 \text{ g (m}^2 \text{ h)}^{-1}$ and separation factor for Bz/Chx selectivity was 41.2.

An aliphatic type of hyperbranched polyester (HBPE), which was synthesized from 2,2-dihydroxymethyl propanyl acid (DMPA) and 1,1,1-trihydroxymethyl propane (TMP), was end-capped with acrylic group, and the photo-polymerizable hyperbranched polyester (AHBPE) was obtained [188]. These AHBPEs were employed as the macromolecular cross-linking agents to enhance the PV performance of ethyl cellulose (EC) membrane for the separation of Bz/Chx mixtures. The effects of the content of AHBPE and benzophenone (BP) as well as the radiating time on the separation factor and the total permeation rate were investigated in detail. The results show that the performance of EC membranes incorporating AHBPEs of higher generations exhibited much higher permeation rate, in comparison to the membranes cross-linked with EG dimethacrylate.

A membrane from AHBPE of 40 wt.% and BP of 10 wt.% showed the total permeation rate of $42.5 \text{ kg } \mu\text{m} (\text{m}^2 \text{ h})^{-1}$ and the separation factor for Bz/Chx selectivity of 6.82.

2.11.6.5.2 Organic/organic-selective membranes

The preferential sorption and PV selectivities of a PVC membrane for various binary liquid mixtures were evaluated [189]. Methanol/1-propanol, Bz/*n*-hexane, and ethanol/water mixtures were selected as model mixtures in this study. For the methanol/*n*-propanol mixture, methanol preferentially sorbed in the PVC membrane, resulting in selective methanol permeation. For the Bz/*n*-hexane mixture, Bz exhibited higher sorption uptake and permeated preferentially. In the ethanol/water mixture, ethanol preferentially sorbed in the PVC membrane, but water was the preferentially permeating component. This result suggested that the overall selectivity in the membrane was determined by a high water/ethanol diffusion selectivity. The sorption data were analyzed according to Mulder's model [226] derived from Flory–Huggins thermodynamics. The PV selectivity in these systems was analyzed using a solubility and diffusion selectivity model [189].

Composite membranes of PSt and a hydrophilic polymer were prepared via the concentrated emulsion polymerization method [190]. In the concentrated emulsion precursor, styrene containing styrene–butadiene–styrene (SBS) block copolymers constituted the dispersed phase, and a solution of a hydrophilic monomer in water was the continuous phase. The polymerized systems were transformed into membranes by hot pressing at 150°C . The mechanical properties of the membranes were affected by the amount of SBS in the dispersed phase and by the nature of the hydrophilic monomer of the continuous phase. SBS improved the mechanical properties of the membrane significantly. The membranes were then subjected to sorption and PV of Bz/ethanol mixtures. They exhibited preferential sorption of Bz over the entire Bz concentration range. The swelling ratio increased with increasing Bz concentration, and the solubility selectivity decreased. These membranes had permeation rates as high as $1040 \text{ g } (\text{m}^2 \text{ h})^{-1}$, and separation factors as high as 25 for Bz/ethanol mixtures [190].

Zhou *et al.* [191] developed composite membranes based on a selective polypyrrole layer for the separation of ethanol and Chx. Polypyrrole films were

deposited on stainless steel meshes by anodic electro-polymerization of pyrrole dissolved in acetonitrile. Electrochemical and morphological studies on the growth of the polypyrrole films, both oxidized with PF_6^- as the counterion and neutral polypyrrole membranes, were conducted. The performance of these membranes for Chx separation of ethanol/Chx mixture by PV was investigated. The results indicated preferential permeation of ethanol, and clearly demonstrated the feasibility of exploiting conducting polymers in the PV process [191].

The PV characteristics for acetone/chlorinated hydrocarbon mixtures using blend membranes of natural rubber (NR) with epoxidized NR (ENR) were studied [192]. The permeation rate and selectivity of these membranes were determined both as a function of the blend composition and of the feed mixture composition. The membrane performance could be optimized by adjusting the blend composition. NR/ENR 70/30 and NR/ENR 30/70 compositions showed a decrease in permeation rate and chlorinated hydrocarbon/acetone selectivity, whereas the 50/50 composition showed an increased permeation rate and increased hydrocarbon/acetone selectivity. Chlorinated hydrocarbons permeated preferentially through all of the tested membranes. The feed mixture composition also strongly influenced the PV characteristics of the blend membranes. The chlorinated hydrocarbon/acetone selectivity was found to depend on the molecular size of the penetrants [192].

The permeation behavior of methanol and MeAc in the PV experiments is compared with those in VP experiments using a PVA-based composite membrane. The selected membrane was found to be MeOH/MAC selective. Results showed higher permeation rate but a similar separation factor for MeOH/MAC selectivity in PV than in VP. For PV operation, the resulting separation factor for MeOH/MAC selectivity at 60°C showed a monotonous decrease (6.4–4.1) with increasing methanol concentration in the feed mixture (2.3–34 wt.%), whereas the total permeation rate increased from 0.97 to $7.9 \text{ kg } (\text{m}^2 \text{ h})^{-1}$. Based on the solution–diffusion theory, a mathematical model that satisfactorily described the permeation rates of methanol and MeAc in both the PV and VP processes was applied. The permeation rates of both permeants could be explained by the solution–diffusion model with variable diffusion coefficients dependent on methanol concentration in the membrane. Both PV and

VP processes can be described with the same model but using different fitting parameters [193].

NR and PSt-*co*-butadiene rubber (SBR) were cross-linked chemically with sulfur and accelerated by efficient vulcanization. These were then compounded for physical cross-linking with high-abrasion CB filler with three different doses, that is, 5, 10, and 20 phr to obtain three filled membranes from each of these two rubbers (NR-5, NR-10, and NR-20 and SBR-5, SBR-10, and SBR-20). These six filled rubber membranes were used for PV separation of toluene (Tol)/methanol mixtures up to 11 wt.% of toluene in feed. With increase in filler doses from membrane-5 to membrane-20, the selectivities and mechanical properties of the membranes increased. All of these membranes showed reasonably good range of permeation rate ($20.8 \text{ g (m}^2 \text{ h)}^{-1}$ for SBR-5 to $10.7 \text{ g (m}^2 \text{ h)}^{-1}$ for NR-20) and separation factor for Tol/MeOH selectivity (286.4 for NR-5 to 183.7 for SBR-5) for 0.55 wt.% of toluene in feed. Among these membranes, NR-20 and SBR-20, with highest cross-linking density, showed maximum separation factor for Tol/MeOH along with good permeation rate. For comparable cross-linking density NR membranes showed better separation factor than SBR membranes [194].

Ionic liquids are used as a bulk liquid membrane for separation of toluene from *n*-heptane (Hep). Aromatic hydrocarbon, toluene, is successfully transported through the ionic liquid membrane based on 1-methyl-3-octyl imidazolium chloride. Using silver ion as a carrier in 1-methyl-3-octyl imidazolium chloride membranes, batchwise extraction experiments are carried out. The separation performances, represented by the permeation rate and separation factor for Tol/Hep selectivity, were analyzed systematically by varying the operating parameters: the contact time, concentration of Ag^+ , stirring effect, initial feed phase concentration, and temperature [195].

PV separation of ternary and quaternary mixtures of EA, water, ethanol, and acetic acid, which are present in the hydrolysis of EA encountered in pharmaceutical industries, was investigated. Water concentrations in the feed mixtures are in the range of 90–98 wt.%, while the concentrations of EA, ethanol, and acetic acid are much lower. PDMS was used as membrane to separate organic compounds from aqueous streams. PV experiments showed that PDMS membrane was much more selective to EA than other organic components. Increase in the EA

concentration in feed mixture resulted in higher total permeation rates but lower selectivities of EA [196].

The blend membranes with different PAA content were used to separate dimethyl carbonate (DMC)/methanol azeotrope in PV. The blend membrane containing 70 wt.% PAA had the highest separation factor for DMC/MeOH selectivity of 13 and a permeation rate of $577 \text{ g (m}^2 \text{ h)}^{-1}$ at 60°C for separating an azeotrope [197].

Chito-silica (Chito/Si) hybrid membranes were prepared by cross-linking Chito with 3-aminopropyl-triethoxysilane (APTEOS). During the PV processes, the amorphous region of the membranes increased and the contact angle for methanol on the surface of membrane decreased within a range of operating time, and then they remained almost constant by a reconstruction occurred on the membrane surface. The silica was well distributed in the Chito/Si matrix and the thermal stability of the (Chito/Si) was enhanced. The time for a PV process to reach a steady state decreased with increasing methanol concentration or feed temperature, and it was longer for the Chito/Si than the Chito membrane. The degree of swelling was greatly depressed by cross-linking CS with APTEOS. Sorption data indicated that the selectivity of solubility and diffusion of the Chito/Si membrane were greatly improved over the Chito membrane. The Chito/Si membrane showed the permeation rate of $1265 \text{ g (m}^2 \text{ h)}^{-1}$ and the separation factor of 30.1 in PV separation of 70 wt.% MeOH in feed at 50°C [198].

Copoly(diethyl vinylbenzylphosphonate/hydroxyethyl methacrylate) [copoly(VBP-HEMA)] and copoly(diethyl vinylbenzylphosphonate/vinylbenzyl chloride) [copoly(VBP-VBC)] were prepared and their membranes cross-linked by a reaction of EGDE and ED with, respectively, hydroxyl and methylene chloride groups in their side chains. PV and sorption of Bz/*n*-hexane, Bz/Chx, and toluene/*n*-octane mixtures were investigated. The membranes were in a rubbery state and preferentially permeable to aromatics. They had higher specific permeation rate and a lower PV separation factor compared with the cross-linked membranes of methacrylate copolymers with analogous pendant groups. They displayed better PV performance for toluene/*n*-octane. Sorption isotherms of Bz/*n*-hexane mixtures were represented by the Flory-Rehner model [199].

Different types of membranes based on polyelectrolytes were developed for the separation of aromatic/aliphatic hydrocarbon mixtures by PV. For this purpose, composite membranes with

different polyelectrolytes, soluble either in water (sulfoethylcellulose) or in ethanol (custom-made copolymers of MMA and methacrylic acid [3-sulfo-propyl ester] potassium salt), were prepared by an interfacial reaction with oppositely charged ionic surfactants. The latter copolymer could also be cross-linked with Co^{2+} ions. Both membrane types showed a clear enrichment of aromatic components (toluene or Bz) in the course of the PV process (20 wt.% in the feed and about 55 wt.% in the permeate). The permeation rates were in the range of $1 \text{ kg (m}^2 \text{ h)}^{-1}$ at 80°C . The separation of a Bz/Chx mixture was also successful at 50°C . In all cases, permeation rates in Bz/Chx mixtures were higher than those. In addition, in multicomponent feed mixtures, Bz exhibited the better permeate rates [200].

AgCl/PMMA organic/inorganic hybrid membrane has been fabricated by reverse microemulsion polymerization using MMA as oil phase [201]. The membrane structure is analyzed by SEM, which showed that core-shell organic-inorganic hybrid materials were formed with AgCl as the core and PMMA as the shell. AgCl particulate under $2 \mu\text{m}$ are uniformly dispersed in the PMMA. The swelling-sorption behavior of the Chx and cyclohexene in AgCl/PMMA hybrid membrane were measured, the sorption capacity of cyclohexene in the hybrid membrane was enlarged comparing with pure PMMA membrane, but the change of the sorption behavior of Chx was less. The equilibrium swelling-sorption amount ratio of cyclohexene to Chx in membranes was up to 130.4, which was larger than 54.7 in the pure PMMA membranes.

The possibility of using ionic liquids in bulk (nonsupported) and supported liquid membranes for the selective transport of organic molecules was demonstrated. A systematic selective transport study, in which 1,4-dioxane, 1-propanol, 1-butanol, cyclohexanol, cyclohexanone, morpholine, and methylmorpholine was served as a model seven-component mixture of representative organic compounds, and, in which four ion liquids based on the 1-*n*-alkyl-3-methylimidazolium cation (*n*-butyl, *n*-octyl, and *n*-decyl) are used together with the anions PF₆⁻ or BF₄⁻, immobilized in five different supporting membranes, confirms that the combination of the selected ion liquid with the supporting membranes was crucial to achieve good selectivity for a specific solute. The use of the 1-*n*-butyl-3-methylimidazolium hexafluorophosphate, immobilized in a PVF₂ membrane, allows an extremely highly selective transport of secondary amines over

tertiary amines (up to a 55:1 ratio). The selective transport of a given solute through the ion liquid/membrane system resulted from the high partitioning of the solute to the liquid membrane phase [202].

As part of a research project focusing on the development of a sustainable biocatalytic process for production of chiral secondary alcohols, the pervaporative separation of ethanol from ethanol/EA/1-methoxy-2-propanol/1-methoxy-2-propyl acetate mixtures through a commercial PVA-based membrane was investigated. PV of the nondiluted multicomponent mixture was shown to be strongly influenced by interactions between the permeants and the membrane. Investigation of these interactions contributed to the understanding of the mass transport mechanism of this mixture. Overall, high permeation rates were obtained, but small differences between the fastest permeating species were found. The fastest permeating species was ethanol, EA, or 1-methoxy-2-propanol, depending on the feed composition [203].

Whether a membrane solution can be utilized for hydrocarbon separation by using a supported liquid membrane was investigated. Aromatic hydrocarbons, Bz, toluene, and *p*-xylene were successfully transported through the membrane based on the ionic liquids. Although the permeation rates through the membrane based on the ionic liquids were less than those of water, the selectivity of aromatic hydrocarbons was greatly improved. The maximum selectivity to heptane was obtained using Bz in the aromatic permeation and 1-*n*-butyl-3-methylimidazolium hexafluorophosphate in the liquid membrane phase [204].

PDMS composite membrane was used to separate the binary and multicomponent alkane/thiophene mixtures by PV. The total permeation rates for different alkane/thiophene mixtures decreased with increase of carbon number in the alkanes. In PV results of ternary systems, the increase of content of lighter alkane in feed resulted in a larger total permeation rate, but a smaller selectivity to thiophene. A quaternary system, the mixture of *n*-heptane, *n*-octane, *n*-nonane, and thiophene, was employed to simulate the desulfurization process of gasoline. With the membrane having a PDMS layer of $11 \mu\text{m}$, the total permeation rate was measured to be about $1.65 \text{ kg (m}^2 \text{ h)}^{-1}$, with the corresponding separation factor for thiophene of 3.9 at 30°C [205].

The blend membranes from a polymer blend of PAA and PVA were evaluated for the separation of methanol from methyl *tert*-butyl ether (MTBE) by

PV [206]. Methanol permeated preferentially through all blend membranes tested, and the MeOH/MTBE selectivity increased with increasing PVA content in the blends. However, a decrease in the permeation rate was observed with increasing PVA content. Upon increasing the feed temperature, the permeation rate increased and the MeOH/MTBE selectivity remained constant. In addition, the influence of cross-linking on the MeOH/MTBE selectivity was investigated. The PV permeation rate decreased with increasing cross-linking density; however, this was coupled with an increase in MeOH/MTBE selectivity. This was due to a more rapid decrease in the partial permeation rate of MTBE compared to that of methanol [206].

Thin-film composite membranes were prepared by coating a thin film of polystyrenesulfonate (PSS) onto the surface of a microporous alumina (Al_2O_3) support [207]. The PSS/ Al_2O_3 composite membrane was applied to the separation of MTBE/methanol mixtures in PV mode and exhibited excellent performance. The PSS/ Al_2O_3 composite membranes showed high MeOH/MTBE. The methanol concentration in the permeate was always greater than 99.5 wt.% for all membranes tested and for all feed solution compositions studied. Membranes of the Mg^{2+} -counterion form (PSS-Mg) showed higher separation factors for MeOH/MTBE selectivity than membranes having Na^+ as the counterion (PSS-Na). Extremely high separation factors (25 000–35 000) were observed for the PSS-Mg/ Al_2O_3 composite membrane containing 27.5 mol.% sulfonate [207].

The PV properties of a poly(urethane imide) block-copolymer membrane for separation of ethyl *tert*-butyl ether/ethanol mixtures were investigated by Jonquieres *et al.* [208] over the entire composition range. The PV selectivity for ethanol was higher than the simple solubility selectivity of ethanol over ethyl *tert*-butyl ether. The features of sorption were examined in relation to the corresponding PV properties, and were analyzed in terms of the activity of each penetrant to take into account the nonideality of the system. Sorption isotherms could be expressed in terms of a single linear relationship for ethyl *tert*-butyl ether, but required two linear relationships in the case of ethanol. The discontinuity in the ethanol isotherm corresponded to the composition of a critical feed mixture, and was ascribed to the complete mono-solvation of the polymer's most basic site, that is, urethane groups, by the protic penetrant [208].

The composite membranes, with PVA as separating layer material and PAN or CA as supporting

layer material, were prepared for separating MTBE/methanol mixture by PV. The results showed that PV performance of the composite membrane with PVA membrane as separating layer was superior to that with CA membrane as separating layer, and the PV performance of PVA/CA composite membrane with CA membrane as supporting layer was better. The parameters to prepare the composite membrane remarkably affected PV performance of the composite membrane. The permeate rate of both composite membranes of PVA/PAN and PVA/CA was over $400 \text{ g (m}^2 \text{ h)}^{-1}$, and the concentration of methanol in the permeate reached over 99.9 wt.% for separating MTBE/methanol mixture [209].

Polyelectrolyte-surfactant complex (PELSC) membranes were prepared by the interaction of the anionic groups of sodium cellulose sulfate (Na-CS) or sulfoethyl cellulose (SEC) with different types of cationic surfactants. The membrane properties were investigated using PV experiments with different organic feed mixtures, containing methanol as a polar component. Methanol was mixed with Chx, MTBE, and dimethylcarbonate. The results of the separation experiments employing the methanol-containing mixtures showed that the membranes reveal both very high permselectivity and permeability even at moderate temperatures [210].

Sorption and PV experiments were carried out with cellulose triacetate membranes for the separation of methyl *tert*-butyl ether and methanol mixtures. In the PV experiments, the total and methanol permeation rates increased with the increasing methanol concentration in the feed, while the permeation rates of MTBE first increased and then decreased. The total permeation rates are significantly enhanced with increasing temperature. This temperature dependence was more pronounced at low methanol concentration, but the extent of increase of the total permeate rate was relatively constant when methanol concentrations are greater than 10%. The MeOH/MTBE selectivity decreased with increasing of methanol concentration and became more or less constant at high methanol concentrations [211].

Sorption and PV experiments were carried out with PVA/PAA cross-linked membranes for the separation of an azeotropic MTBE/methanol mixture. With increasing PAA content in the membranes, solubilities and permeation rates decreased and MeOH/MTBE selectivities increased. Total sorption and permeation rates increased with

increasing concentration of methanol. Increasing the concentration of methanol resulted in decreasing MeOH/MTBE selectivities. Because of polarity, methanol permeated selectively through the membranes. Sorption results showed the same tendency with PV results [212].

PV separation process was used for separation of methanol/MTBE mixtures encountered during manufacturing of MTBE. Three different copolymers of acrylamide with increasing amount of HEMA, that is, PAMHEMA-1, -2, and -3, were synthesized and the cross-linked (gelled) copolymer membranes made from these sol copolymers were used for pervaporative separation of methanol from its mixtures with MTBE over the concentration range of 0–10 wt.% methanol in feed. These hydrophilic gel copolymer membranes were found to be highly methanol selective in both sorption and diffusion through the membranes. The permeation rate of methanol was found to decrease with increasing degree of cross-linking from PAMHEMA-1 to -3 copolymer membranes. Among the three membranes, the PAMHEMA-3 membrane showed the highest MeOH/MTBE selectivity and permeation rate and they were 511.7 and 9.9 g (m² h)⁻¹, respectively, for 0.53 wt.% of methanol in feed, while maximum permeation rate with high selectivity was shown by PAMHEMA-1 membrane. Their permeation rate and MeOH/MTBE selectivity were 18.49 g (m² h)⁻¹ and 243, respectively, for 0.53 wt.% of methanol in feed. MTBE was also found to have a negative coupling effect on methanol permeation [213].

The separation of ethanol/ethyl-tertio-butylether mixtures by PV was studied with new membranes prepared from *N*-vinyl-pyrrolidinone (NVP) and *N*-[3-(trimethylamoniopropyl)] methacrylamide-methylsulfate (TMA). The PV results showed that highly ethanol-selective membranes could be obtained from PVP blends and from pyrrolidinone-based cross-linked copolymers. Whatever the exact NVP/TMA composition used, the membranes strongly favored the PV of ethanol. The ethanol selectivity was higher for the lower PVP/TMA ratio. On the one hand, these results were ascribed to the high pyrrolidinone residues content, which is responsible for the enhanced ethanol sorption affinity. The observed permeation selectivity was in agreement with the swelling data also recorded with the different polymers, showing higher affinity for ethanol with PVP-enriched materials compared with TMA ones. This was a direct consequence of the Lewis base feature of pyrrolidinone sites toward

ethanol molecules. On the other hand, the TMA residues improved the overall stability and selectivity of the membranes depended upon cross-linking reactions, which were induced by thermal treatment. A close comparison made between polymer blend and copolymer PV results helped to clarify the TMA role of the membrane transport properties [214].

2.11.6.6 Selective Membranes for Isomers

Propanol and xylene-isomer-selective membranes are very important for the separation of industrial chemical products and energy saving for the separation of those mixtures.

PVA membranes containing β -CD (PVA/CD membrane) were prepared and the permeation and separation characteristics for propanol isomers through the PVA/CD membranes were investigated by PV and EV [215]. EV was more effective for the separation of propanol isomers through the PVA/CD membrane than PV. The PVA/CD membrane preferentially permeated 1-propanol rather than 2-propanol from their mixtures. In particular, a mixture of 10 wt.% 1-propanol concentration was concentrated to about 45 wt.% through the PVA/CD membrane. The permeation mechanism of propanol isomers through the PVA/CD membrane was discussed based on the solution–diffusion model.

The characteristics of permeation and separation for xylene isomers through PVA membranes containing β -CD (PVA/CD membranes) were investigated by PV and EV. EV was more effective for the separation of xylene isomers through the PVA/CD membrane than PV. The increase in CD content gave an increase in *p*-xylene/*o*-xylene selectivity through the PVA/CD membrane by EV. This was attributed to the stronger affinity of CD for *p*-xylene compared with *o*-xylene. Particularly, the PVA/CD membrane at a CD content of 40 wt.% showed a higher separation factor for *p*-xylene/*o*-xylene selectivity than has ever been reported. When the *p*-xylene concentration in the feed was lower, the *p*-xylene/*o*-xylene selectivity was improved. The mechanism of permeation and separation for xylene isomers was discussed from the standpoint of solution–diffusion model [216].

PAA membranes containing α -, β -, or γ -CD were prepared and used for the separation of *o*-/*p*-xylene mixture by PV. The native PAA membrane was almost impermeable for the xylene isomers, and the incorporation of CDs in the PAA membranes resulted in membranes having molecular recognition function,

which selectively facilitated the transport of the xylene isomers. For all types of CDs, the facilitated transport occurred at CD concentrations higher than the threshold concentration. As the CD concentration increased, the permeation rates increased, while the *o*-xylene/*p*-xylene selectivities were almost constant. The selectivity for *o*-xylene/*p*-xylene selectivity of the membranes was strongly influenced by the types of CDs incorporated in the membranes [217].

Polymer membranes containing α -CD were prepared by the casting method using cross-linking reaction with hexamethylenediisocyanate. The film synthesis conducted with and without dibutyltin dilaurate as catalyst resulted in two series of materials in which α -CD host entities were chemically linked to PVA and physically entrapped in PVA, respectively. The obtained membranes were successfully applied to the separation of *o*-/*p*- and *o*-/*m*-xylene isomer mixtures by pertraction from water. *p*- and *m*-xylenes were found to be the faster permeants compared to the *o*-isomer. The separation factor for *p*-xylene/*o*-xylene selectivity varied from 7.75 to 0.35, depending on the membrane α -CD content and the feed concentration. The permeation rate and separation selectivity data were discussed in terms of molecular recognition by α -CD and of coupling transport effect [218].

The PV characteristics of xylene isomer mixtures through a fixed carrier membrane consisting of CA as a base polymer and DNP group as a selective fixed carrier were studied. In the PV of xylene isomer mixtures, the DNP group selectively facilitated the transport of xylene isomers through the membrane. The order of the preferentially permeating component was *p*-xylene > *m*-xylene > *o*-xylene [219].

The selective extraction of the geometrical isomers of xylene using a hydrogel consisting of a PVA grafted with α -CD and β -CD as the complexing moieties was described. The membrane contactors were prepared by the casting method following cross-linking reaction with hexamethylene diisocyanate (HMDI). The transfer of xylenes across the CD-containing membranes was facilitated compared to PVA. The better discrimination was observed for membranes based on α -CD, the more efficient being that containing ~21 wt.% CD. The order of permeation rate *p*-xylene > *m*-xylene > *o*-xylene followed the affinity order inferred from the stability constants α -CD. The permeate composition was independent of the feed composition [220].

Fractionation of *o*- and *p*-xylene isomeric mixtures was performed using PV with PU membranes containing ZSM zeolite. The xylene vapor sorption isotherms exhibited a Henry's law relationship in this PU-zeolite blend. In binary solutions, the individual xylene uptake was also proportional to the solvent composition. Although incorporating zeolite into the PU-zeolite membrane rendered a decrease in xylene solubility as compared with that sorbed in the PU film without zeolite addition, the increase of diffusion coefficient and diffusivity selectivity increases enhanced the separation efficiency using the PU-zeolite blend. Increasing the operating temperatures enhanced the xylene permeation rate of xylene. The permeation rates of xylene and selectivity increased with increasing zeolite content [221].

Palygorskite-polyacrylamide (PGS/PAM) hybrid materials were synthesized via intercalation polymerization initiated by redox initiator consisting of modified PGS (reducer) and ceric salt Ce^{4+} (oxidant), and used as PV membranes. The swelling behavior of hybrid membranes was investigated in single xylene isomer (*p*-xylene, *m*-xylene, and *o*-xylene), binary xylene isomer mixtures (*p*-/*o*-xylene (the mixtures of *p*- and *o*-xylene), *o*-/*m*-xylene (the mixtures of *o*- and *m*-xylene), and *p*-/*m*-xylene (the mixtures of *p*- and *m*-xylene)), and ternary isomer mixture (*p*-/*m*-/*o*-xylene (the mixtures of *p*-, *m*-, and *o*-xylene)). A maximum value of degree of swelling at equilibrium (DSequilibrium) in single xylene isomer at 30 °C exhibited for the hybrid membrane with a PGS of 1.92 wt.%. Negative deviation and both negative and positive deviations of the DSequilibrium based on the addition rule existed in binary or ternary xylene isomer mixtures, respectively, for hybrid membranes with different PGS content at 30 °C. In addition, a maximum value of separation factor of the hybrid membrane revealed for each pair of binary xylene isomer mixtures when the PGS content was 1.92 wt.% in the hybrid membrane. A reversion of the preferential selectivity and a high permeation activation energy of the hybrid membrane occurred at the concentration region with high *p*-xylene content in *p*-/*m*-xylene binary xylene isomer mixtures. The swelling behavior and PV performance of PGS-PAM hybrid membranes were discussed in terms of the entrapping channel in the PGS for the potential introduction of xylene isomers, the interaction between xylene isomers in feed and the solution-diffusion mechanism in the PV process [222].

2.11.6.7 Selective Membranes for Facilitation of Chemical Reactions

Selective membranes for facilitation of chemical reactions are useful for reactors coupled with membrane separation technology such as PV, EV, and TDEV. These systems can help to enhance the conversion of reactants for thermodynamically or kinetically limited reactions via selective removal of one or more product species from reaction mixtures.

PVA membranes cross-linked with sulfosuccinic acid (SSA) were used for the removal of water in the esterification with acetic acid by isoamylic alcohol. In order to study the effects of the cross-linking degree and, simultaneously, the amount of sulfonic groups, different membranes were prepared with SSA/PVA ratios in the range of 5–40 mol.%. To eliminate the dependence between the amount of acid sites and the cross-linking degree, PVA membranes with the $-\text{SO}_3\text{H}$ groups which were introduced by anchoring 5-sulfosalisilic acid (SA) on the PVA chains were also prepared. The consumed conversion of isoamylic alcohol increased when the amount of SSA used in the polymer cross-linking was increased from 5% to 20%. However, when the cross-linking degree increased from 20% to 40%, its conversion increased only slightly, probably due to the increase of molecular mobility restriction in the PVA matrix. In the case of the PVA membranes introduced the $-\text{SO}_3\text{H}$ groups, the membrane activity for esterification increased with increasing content of cross-link [223].

Esterification of lactic acid and succinic acid with ethanol to generate ethyl lactate ($\text{C}_5\text{H}_{10}\text{O}_3$) and diethyl succinate, respectively, was studied in well-mixed reactors with solid catalysts (Amberlyst XN-1010 and Nacion NR50) and two PV membranes (GFIF-1005 and T1-b). Experiments were carried out by a closed-loop system of a batch catalytic reactor and a PV unit employing GFIF-1005. The kinetics of PV is studied to obtain a working correlation for the permeation rate of water in terms of temperature and water concentration on the feed side of the pervaporator. The efficacy of PV-aided esterification was illustrated by attainment of near-total utilization of the stoichiometrically limiting reactant within a reasonable time. Protocols for recovery of ethyl lactate and diethyl succinate from PV retentate were discussed, and simultaneous esterification of lactic and succinic acids, which is an attractive and novel concept, is proposed [224].

Reaction–PV hybrid processes can be an alternative to classical chemical processes to enhance the conversion of equilibrium-limited reactions, such as esterification and trans-esterification. The esterification of acetic acid with isopropanol coupled with PV was investigated. The synthesis and hydrolysis of isopropyl acetate have been studied using the commercial polymeric membrane PERVAP (R) 2201. The effect of temperature and feed composition on the permeation characteristics of the membrane was analyzed and preferential water permeation from the quaternary mixture involved in the esterification of acetic acid with isopropanol was discussed under the experimental conditions [225].

2.11.7 Conclusions

The H_2O /organic-selective membranes designed for the dehydration of organic/water mixtures by PV have already been applied to practical use, and further expansion is expected in future. These membranes have found applications in the chemical and electronics industry and dehydration of alcohols as fuel. Specifically, H_2O /alcohol-selective membranes, such as hydrophilic PVA, are currently used for dehydration of alcohols. Conversely, organic/ H_2O - and organic/organic-selective membranes are still being developed with improvements in selectivity, permeability, and the durability necessary for their practical use. The membrane materials, membrane preparation techniques, and separation process parameters for organic-selective membranes are still being studied. It will be important to develop novel membrane separation techniques other than membrane separation methods based on the solution–diffusion mechanism as well as development of organic-selective membranes. We expect that superior membranes for organic liquid mixtures and membrane separation techniques can be developed in the near future.

References

- [1] Uragami, T. Polymer Membranes for Separation of Organic Liquid Mixtures. In *Materials Science of Membranes for Gas and Vapor Separation*; Yampolskii, Y., Pinau, I., Freeman, B. D., Eds.; Wiley: New York, 2006; pp 355–372.
- [2] Loeb, S., Sourirajan, S. UCLA, Department of Chemical Engineering Report No. 60-60, 1960.
- [3] Merten, U. *Desalination by Reverse Osmosis*; MIT Press: Cambridge, MA, 1966.

- [4] Sourirajan, S. *Reverse Osmosis*; Loges Press: London, 1970.
- [5] Kesting, R. E. *Synthetic Polymeric Membrane*; McGraw-Hill: New York, 1971.
- [6] Kesting, R. E. *Synthetic Polymeric Membranes: A Structural Perspective*, 2nd edn.; Wiley Interscience: New York, 1985.
- [7a] Uragami, T., Fujino, K., Sugihara, M. *Angew. Makromol. Chem.* **1976**, *55*, 29.
- [7b] Uragami, T., Fujino, K., Sugihara, M. *Angew. Makromol. Chem.* **1978**, *68*, 39–53.
- [7c] Uragami, T., Fujino, K., Sugihara, M. *Angew. Makromol. Chem.* **1978**, *70*, 119–134.
- [8a] Uragami, T., Tamura, M., Sugihara, M. *Angew. Makromol. Chem.* **1976**, *55*, 59–72.
- [8b] Uragami, T., Tamura, M., Sugihara, M. *Angew. Makromol. Chem.* **1978**, *66*, 203–220.
- [9] Kesting, R. E. *J. Appl. Polym. Sci.* **1973**, *17*, 1771–1785.
- [10] Uragami, T. Separation of Organic Liquid Mixtures through Chitosan and Chitin Derivative Membranes by Pervaporation and Evaporation Methods. In *Advances in Chitin and Chitosan*; Brine, C. J., Sandford, P. A., Zikakis, J. P., Eds.; Elsevier Applied Science: New York, 1992; pp 594–603.
- [11] Uragami, T. Separation Materials Derived from Chitin and Chitosan. In *Material Science of Chitin and Chitosan*; Uragami, T., Tokura, S., Eds.; Kodansha: Tokyo; Springer: Berlin, 2006; pp 113–163.
- [12] Binding, R. C., Lee, R. J., Jennings, J. F., Mertin E. C. *Ind. Eng. Chem.* **1961**, *53*, 45–50.
- [13] Choo, C. Y. Membrane Permeation. In *Advances in Petroleum Chemistry and Refining*; Kobe, K. A., McKetta, J. J., Eds.; Interscience: New York, 1962; pp 73–117.
- [14] Yamada, S. Pervaporation. In *Estimation of Performance of Artificial Membranes*; Kitami Shobo: Tokyo, 1981; pp 118–123.
- [15] Uragami, T. Structures and Properties of Membranes from Polysaccharide Derivatives. In *Polysaccharides: Structural Diversity and Functional Versatility*; Dumitriu, S., Ed.; Marcel Dekker: New York, 1998; pp 887–924.
- [16] Uragami, T. Structures and Functionalities of Membranes from Polysaccharide Derivatives. In *Polysaccharides: Structural Diversity and Functional Versatility*, 2nd edn.; Dumitriu, S., Ed.; Marcel Dekker: New York, 2005; pp 1087–1122.
- [17] Uragami, T., Saito, M. *Makromol. Chem. Rapid Commun.* **1988**, *9*, 361–365.
- [18] Uragami, T., Saito, M. *Sep. Sci. Technol.* **1989**, *24*, 541–554.
- [19] Uragami, T. Method of Separating a Particular Component from Its Liquid Solution. Jpn. Pat. 1883353, 1994.
- [20] Uragami, T. Method of Separating a Particular Component from Its Liquid solution. US Pat. 4,983,303, 8 January 1991.
- [21] Uragami, T. Method of Separating a Particular Component from Its Liquid Solution. Eur. Pat. 0273267, 1993.
- [22] Uragami, T. Method of separating a Particular Component from Its Liquid Solution. T. Brazilian Pat. P-8.707.041-3, 1993.
- [23] Uragami, T. *Polym. J.* **2008**, *40*, 485–494.
- [24] Uragami, T., Morikawa, T. *Makromol. Chem. Rapid Commun.* **1989**, *10*, 287–291.
- [25] Uragami, T., Tanaka, Y. Method of Separating a Particular Component from Its Liquid Solution. Jpn. Pat. 1,906,854, 1994.
- [26] Uragami, T., Tanaka, Y. Method of Separating Liquid Component from a Solution Containing Two or More Liquid Component. Eur. Pat. 0346739, 1991.
- [27] Uragami, T., Shinomiya, H. *Makromol. Chem.* **1991**, *192*, 2293–2305.
- [28] Uragami, T., Morikawa, T. *J. Appl. Polym. Sci.* **1992**, *44*, 2009–2018.
- [29] Uragami, T., Shinomiya, H. *J. Membr. Sci.* **1992**, *74*, 183–191.
- [30] Uragami, T., Tanaka, Y. Method for Separating a Liquid Component from a Solution Containing Two or More Liquid Components. US Pat. 5,271,846, 21 December 1993.
- [31] Uragami, T., Tanaka, Y., Nishida, S. *Desalination* **2002**, *147*, 449–454.
- [32] Uragami, T. Dehydration of Ethanol by Chitosan Derivative Thin Membranes on Porous Supports. In *Advances in Chitin Science* Vårum, K. M., Domard, A., Smidsrød, O., Eds.; NTNU: Trondheim, 2003; Vol. VI, pp 19–26.
- [33] Ihm, C. D., Ihm, S. K. *J. Membr. Sci.* **1995**, *98*, 89–96.
- [34] Yeom, C. K., Jegal, J. G., Lee, K. H. *J. Appl. Polym. Sci.* **1996**, *62*, 1561–1576.
- [35] Jegal, J., Lee, K. H. *J. Appl. Polym. Sci.* **1996**, *60*, 1177–1183.
- [36] Richau, K., Schwarz, H.-H., Apostel, R., Paul, D. *J. Membr. Sci.* **1996**, *113*, 31–41.
- [37] Nam, S. Y., Lee, Y. M. *J. Membr. Sci.* **1997**, *135*, 161–171.
- [38] Iwatsubo, T., Kusumocahyo, S. P., Shinbo, T. *J. Appl. Polym. Sci.* **2002**, *86*, 265–271.
- [39] Uragami, T., Yamamoto, S., Miyata, T. *Network Polym.* **1999**, *20*, 203–208.
- [40] Uragami, T., Yamamoto, S., Miyata, T. *Biomacromolecules* **2003**, *4*, 137–144.
- [41] Lai, J. Y., Chu, Y. H., Huang, S., Yin, Y. L. *J. Appl. Polym. Sci.* **1994**, *53*, 999–1009.
- [42] Chen, S. H., Lai, J. Y. *J. Appl. Polym. Sci.* **1995**, *55*, 1353–1359.
- [43] Lee, K. R., Lai, J. Y. *J. Appl. Polym. Sci.* **1995**, *57*, 961–968.
- [44] Sun, Y. M., Huang, T. L. *J. Membr. Sci.* **1996**, *110*, 211–218.
- [45] Buyanov, A. L., Revel'skaya, L. G., Kuznetsov, Y. P., Shestakova, A. S. *J. Appl. Polym. Sci.* **1998**, *69*, 761–769.
- [46] Shien, J. J., Huang, R. Y. M. *J. Membr. Sci.* **1997**, *127*, 185–202.
- [47] Zhang, L. N., Guo, J., Zhou, J. P., Yang, G., Du, Y. M. *J. Appl. Polym. Sci.* **2000**, *77*, 610–616.
- [48] Uragami, T., Matsuda, T., Okuno, H., Miyata, T. *J. Membr. Sci.* **1994**, *88*, 243–251.
- [49] Uragami, T., Takuno, M., Miyata, T. *Macromol. Chem. Phys.* **2002**, *203*, 1162–1170.
- [50] Uragami, T., Tanaka, Y., Nishida, S. *Desalination* **2002**, *147*, 449–454.
- [51] Uragami, T., Okazaki, K., Matsugi, H., Miyata, T. *Macromolecules* **2002**, *35*, 9156–9163.
- [52] Uragami, T., Katayama, T., Miyata, T., Tamura, H., Shiwaiba, T., Higuchi, A. *Biomacromolecules* **2004**, *5*, 2116–2121.
- [53] Uragami, T., Matsugi, H., Miyata, T. *Macromolecules* **2005**, *38*, 8440–8446.
- [54] Uragami, T., Yanagisawa, S., Miyata, T. *Macromol. Chem. Phys.* **2007**, *208*, 756–764.
- [55] Lee, K. R., Chen R. Y., Lai, J. Y. *J. Membr. Sci.* **1992**, *75*, 171–180.
- [56] Lai, J. Y., Chen, R. Y., Lee, K. R. *Sep. Sci. Technol.* **1993**, *28*, 1437–1452.
- [57] Xu, Y. X., Chen, C. X., Zhang, P. X., Sun, B. H., Li, J. D. *J. Chem. Eng. Data* **2006**, *51*, 1841–1845.
- [58] Huang, Z., Shi, Y., Wen, R., Guo, Y. H., Su, J. F., Matsuura, T. *Sep. Purif. Technol.* **2006**, *51*, 126–136.
- [59] Fan, S. C., Wang, Y. C., Li, C. L., Lee, K. R., Liaw, D. J., Lai, J. Y. *J. Appl. Polym. Sci.* **2003**, *88*, 2688–2697.

- [60] Li, C. L., Lee, K. R. *Polym. Int.* **2006**, *55*, 505–512.
- [61] Zhang, Q. G., Liu, Q. L., Jiang, Z. Y., Chen, Y. *J. Membr. Sci.* **2007**, *287*, 237–245.
- [62] Gimenes, M. L., Liu, L., Feng, X. S. *J. Membr. Sci.* **2007**, *295*, 71–79.
- [63] Namboodiri, V. V., Vane, L. M. *J. Membr. Sci.* **2007**, *306*, 209–215.
- [64] Teli, S. B., Gokavi, G. S., Aminabhavi, T. M. *Sep. Purif. Technol.* **2007**, *56*, 150–157.
- [65] Shih, C. Y., Chen, S. H., Liou, R. M., Lai, J. Y., Chang, J. S. *J. Appl. Polym. Sci.* **2007**, *105*, 1566–1574.
- [66] Chen, S. H., Liou, R. M., Shih, C. Y., Lai, C. L., Lai, J. Y. *J. Appl. Polym. Sci.* **2007**, *106*, 1412–1420.
- [67] Kim, S. G., Lee, K. S., Lee, K. H. *J. Appl. Polym. Sci.* **2006**, *102*, 5781–5788.
- [68] Lee, C., Hong, W. H. *J. Membr. Sci.* **1997**, *135*, 187–193.
- [69] Wang, X. P., Shen, Z. Q., Zhang, F. Y. *J. Membr. Sci.* **1996**, *119*, 191–198.
- [70] Bhat, N. V., Wavhal, D. S. *Sep. Sci. Technol.* **2000**, *35*, 227–242.
- [71] Toti, U. S., Aminabhavi, T. M. *J. Appl. Polym. Sci.* **2002**, *85*, 2014–2024.
- [72] Liu, Y. L., Su, Y. H., Lee, K. R., Lai, J. Y. *J. Membr. Sci.* **2005**, *251*, 233–238.
- [73] Qiao, X. Y., Chung, T. S. *AIChE J.* **2006**, *52*, 3462–3472.
- [74] Xiao, S. D., Huang, R. Y. M., Feng, X. S. *J. Membr. Sci.* **2006**, *286*, 245–254.
- [75] Liu, Y. L., Yu, C. H., Lee, K. R., Lai, J. Y. *J. Membr. Sci.* **2007**, *287*, 230–236.
- [76] Liu, R. X., Qiao, X. Y., Chung, T. S. *J. Membr. Sci.* **2007**, *294*, 103–114.
- [77] Choudhari, S., Kittur, A., Kulkarni, S., Kariduraganavar, M. *J. Membr. Sci.* **2007**, *302*, 197–206.
- [78] Veerapur, R. S., Gudasi, K. B., Aminabhavi, T. M. *J. Membr. Sci.* **2007**, *304*, 102–111.
- [79] Teli, S. B., Gokavi, G. S., Sairam, M., Aminabhavi, T. M. *Colloids Surf. Phys. Eng.* **2007**, *301*, 55–62.
- [80] Shen, J. N., Wu, L. G., Qiu, J. H., Gao, C. J. *J. Appl. Polym. Sci.* **2007**, *103*, 1959–1965.
- [81] Jiang, L. Y., Chung, T. S., Rajagopalan, R. *Chem. Eng. Sci.* **2008**, *63*, 204–216.
- [82] Slater, C. S., Schurmann, T., MacMillian, J., Zimarowski, A. *Sep. Sci. Technol.* **2006**, *41*, 2733–2753.
- [83] Devi, D. A., Smitha, B., Sridhar, S., Jawalkar, S. S., Aminabhavi, T. M. *J. Chem. Tec. Biotech.* **2007**, *82*, 993–1003.
- [84] Kim, S. G., Lee, K. S., Lee, K. H. *J. Appl. Polym. Sci.* **2007**, *103*, 2634–2641.
- [85] Hu, C. L., Guo, R. L., Li, B., Ma, X. C., Wu, H., Jiang, Z. Y. *J. Membr. Sci.* **2007**, *293*, 142–150.
- [86] Rao, P. S., Sridhar, S., Wey, M. Y., Krishnaiah, A. *Ind. Eng. Chem. Res.* **2007**, *46*, 2155–2163.
- [87] Guo, R. L., Hu, C. L., Li, B., Jiang, Z. Y. *J. Membr. Sci.* **2007**, *289*, 191–198.
- [88] Aptel, P., Cuny, J., Jozefonvicz, J., Morel, G., Neel, J. *J. Appl. Polym. Sci.* **1974**, *18*, 351–364.
- [89] Miyata, T., Takagi, T., Kadota, T., Uragami, T. *Makromol. Chem. Phys.* **1995**, *196*, 1211–1220.
- [90] Miyata, T., Takagi, T., Uragami, T. *Macromolecules* **1996**, *29*, 7787–7794.
- [91] Miyata, T., Obata, S., Uragami, T. *Macromolecules* **1999**, *32*, 3712–3720.
- [92] Miyata, T., Obata, S., Uragami, T. *Macromolecules* **1999**, *32*, 8465–8475.
- [93] Uragami, T., Morikawa, T. *Makromol. Chem. Rapid Commun.* **1989**, *10*, 287–291.
- [94] Uragami, T., Morikawa, T. *J. Appl. Polym. Sci.* **1992**, *44*, 2009–2018.
- [95] Uragami, T., Shinomiya, S. **1992**, *192*, 2293–2305.
- [96] Eustache, H., Histi, G. *J. Membr. Sci.* **1981**, *8*, 105–114.
- [97] Ishihara, K., Nagase, Y., Matsui, K. *Makromol. Chem. Rapid Commun.* **1986**, *7*, 43–46.
- [98] Masuda, T., Tang, B. Z., Higashimura, T. *Polym. J.* **1986**, *18*, 565–567.
- [99] Uragami, T., Doi, T., Miyata, T. *Inter. J. Adhes. Adhes.* **1999**, *19*, 405–409.
- [100] Uragami, T., Doi, T., Miyata, T. Pervaporation Property of Surface Modified Poly[1-(Trimethylsilyl)-1Propyne] Membranes. In *Membrane Formation and Modification*; Pinnau, I., Freeman, B. D., Eds.; ACS Symposium Series 744; American Chemical Society: Washington, DC, 2000; pp 263–279.
- [101] Nagase, Y., Mori, S., Matsui, K. *J. Appl. Polym. Sci.* **1989**, *37*, 1259–1267.
- [102] Ishihara, K., Matsui, K. *J. Appl. Polym. Sci.* **1987**, *34*, 437–440.
- [103] Kashiwagi, T., Okabe, K., Okita, K. *J. Membr. Sci.* **1988**, *36*, 353–362.
- [104] Volkov, V. V., Fadeev, A. G., Khotimsky, V. S., et al. *J. Appl. Polym. Sci.* **2004**, *91*, 2271–2277.
- [105] Wasewar, K. L., Pangarkar, V. G. *Chem. Biochem. Eng. Quart.* **2006**, *20*, 135–145.
- [106] Shi, S. P., Du, Z. J., Ye, H., Zhang, C., Li, H. Q. *Polym. J.* **2006**, *38*, 949–955.
- [107] Bowen, T. C., Meier, R. G., Vane L. M. *J. Membr. Sci.* **2007**, *298*, 117–125.
- [108] Xiangli, F. J., Chen, Y. W., Jin, W. Q., Xu, N. P. *Ind. Eng. Chem. Res.* **2007**, *46*, 2224–2230.
- [109] Lewandowska, M., Kujawski, W. *J. Food Eng.* **2007**, *79*, 430–437.
- [110] Uragami, T. *Desalination* **2006**, *193*, 335–343.
- [111] Uragami, T., Honda, T. *Macromolecules* (submitted).
- [112] Ei-Zanati, E., Abdel-Hakim, E., El-Ardi, O., Fahmy, M. *J. Membr. Sci.* **2006**, *280*, 278–283.
- [113] Srinivasan, K., Palanivelu, K., Gopalakrishnan, A. N. *Chem. Eng. Sci.* **2007**, *62*, 2905–2914.
- [114] Uragami, T., Shinomiya, H. *J. Membr. Sci.* **1992**, *74*, 183–191.
- [115] Bhat, S. D., Aminabhavi, T. M. *Sep. Purif. Technol.* **2006**, *51*, 85–94.
- [116] Bhat, S. D., Mallikarjuna, N. N., Aminabhavi, T. M. *J. Membr. Sci.* **2006**, *282*, 437–483.
- [117] Sairam, M., Naidu, B. V. K., Nataraj, S. K., Sreedhar, B., Aminabhavi, T. M. *J. Membr. Sci.* **2006**, *283*, 65–73.
- [118] Smitha, B., Dhanuja, G., Sridhar, S. *Carbohydr. Polym.* **2006**, *66*, 463–472.
- [119] Ray, S., Ray, S. K. *J. Appl. Polym. Sci.* **2007**, *103*, 728–737.
- [120] Aminabhavi, T. M. *J. Appl. Polym. Sci.* **2007**, *103*, 1918–1926.
- [121] Rao, P. S., Sridhar, S., Wey, M. Y., Krishnaiah, A. *Polym. Bull.* **2007**, *59*, 289–297.
- [122] Reddy, K. M., Sairam, M., Babu, V. R., Subha, M. C. S., Rao, K. C., Aminabhavi, T. M. *Design. Monom. Polym.* **2007**, *10*, 297–309.
- [123] Bhat, M., Santoshkumar, D., Aminabhavi, T. M. *J. Membr. Sci.* **2007**, *306*, 173–185.
- [124] Solak, E. K., Sanli, O. *Sep. Sci. Technol.* **2006**, *41*, 627–646.
- [125] Lai, J. Y., Yin, Y. L., Lee, K. R. *Polym. J.* **1995**, *27*, 813–818.
- [126] Asman, G., Sanli, O. *Sep. Sci. Technol.* **2003**, *38*, 1963–1980.
- [127] Isiklan, N., Sanli, O. *J. Appl. Polym. Sci.* **2004**, *93*, 2322–2333.
- [128] Isiklan, N., Sanli, O. *Sep. Sci. Technol.* **2005**, *40*, 1083–1101.

- [129] Asman, G., Sanli, O. *J. Appl. Polym. Sci.* **2006**, *100*, 1385–1394.
- [130] Asman, G., Sanli, O. *Sep. Sci. Tec.* **2006**, *41*, 1193–1209.
- [131] Al-Ghezawi, N., Sanli, O., Isiklan, N. *Sep. Sci. Technol.* **2006**, *41*, 2913–2931.
- [132] Kulkarni, S. S., Tambe, S. M., Kittur, A. A., Kariduraganavar, M. Y. *J. Membr. Sci.* **2006**, *285*, 420–431.
- [133] Veerapur, R. S., Gudasi, K. B., Sairam, M., et al. *J. Mater. Sci.* **2007**, *42*, 4406–4417.
- [134] Namboodiri, V. V., Ponangi, R., Vane, L. M. *Eur. Polym. J.* **2006**, *42*, 3390–3393.
- [135] Nakagawa, T., Kanemura, A. *Seni Gakkai Shi* **1995**, *51*, 123–130.
- [136] Liu, Q. L., Xiao, H. *J. Membr. Sci.* **2004**, *230*, 121–129.
- [137] Das, S., Banthia, A. K., Adhikari, B. *Chem. Eng. Sci.* **2006**, *61*, 6454–6467.
- [138] Kim, K. S., Kwon, T. S., Yang, J. S., Yang, J. W. *Desalination* **2007**, *205*, 87–96.
- [139] Park, Y. I., Yeom, C. K., Lee, S. H., Kim, B. S., Lee, J. M., Joo, H. J. *J. Ind. Eng. Chem.* **2007**, *13*, 272–278.
- [140] Yu, J., Li, H., Liu, H. Z. *Chem. Eng. Commun.* **2006**, *193*, 1422–1430.
- [141] Ghosh, U. K., Pradhan, N. C., Adhikari, B. *J. Membr. Sci.* **2006**, *285*, 249–257.
- [142] Ghosh, U. K., Pradhan, N. C., Adhikari, B. *Bull. Mater. Sci.* **2006**, *291*, 225–231.
- [143] Das, S., Banthia, A. K., Adhikari, B. *Desalination* **2006**, *197*, 106–116.
- [144] Mujiburohman, M., Feng, X. S. *J. Membr. Sci.* **2007**, *300*, 95–103.
- [145] Bai, Y. X., Qian, J. W., An, Q. F., Zhu, Z. H., Zhang, P. J. *J. Membr. Sci.* **2007**, *305*, 152–159.
- [146] Kujawski, W., Krajewski, S. R. *Sep. Purif. Technol.* **2007**, *57*, 495–501.
- [147] Mohammadi, T., Kikhavandi, T., Moghbeli, M. *J. Appl. Polym. Sci.* **2008**, *107*, 1917–1923.
- [148] Uragami, T., Yamada, H., Miyata, T. *Trans. Mater. Res. Soc. Jpn.* **1999**, *24*, 165–168.
- [149] Uragami, T., Yamada, H., Miyata, T. *J. Membr. Sci.* **2001**, *187*, 255–269.
- [150] Miyata, T., Yamada, H., Uragami, T. *Macromolecules* **2001**, *34*, 8026–8033.
- [151] Uragami, T., Yamada, H., Miyata, T. *Macromolecules* **2006**, *39*, 1890–1897.
- [152] Uragami, T., Meotoiwa, T., Miyata, T. *Macromolecules* **2001**, *34*, 6806–6811.
- [153] Uragami, T., Meotoiwa, T., Miyata, T. *Macromolecules* **2003**, *36*, 2041–2048.
- [154] Uragami, T., Ohshima, T., Miyata, T. *Macromolecules* **2003**, *36*, 9430–9436.
- [155] Ohshima, T., Miyata, T., Uragami, T. *J. Mol. Struct.* **2005**, *739*, 47–55.
- [156] Ohshima, T., Miyata, T., Uragami, T. *Macromol. Chem. Phys.* **2005**, *206*, 2521–2529.
- [157] Huang, R. Y. M., Ed. *Pervaporation Membrane Separation Processes*; Membrane Science and Technology Series 1; Elsevier: Amsterdam, 1991; Chapter 3, pp 115–139.
- [158] Huang, R. Y. M., Yeom, C. K. *Int. Bibliogr. Inf. Doc.* **1990**, *51*, 273–278.
- [159] Juang, R. S., Lin, S. H., Yang, M. C. *J. Membr. Sci.* **2005**, *255*, 79–87.
- [160] Panek, D., Konieuny, K. *Sep. Purif. Technol.* **2007**, *57*, 507–512.
- [161] Ohshima, T., Kogami, Y., Miyata, T., Uragami, T. *J. Membr. Sci.* **2005**, *260*, 156–163.
- [162] Sun, L., Baker, G. L., Bruening, M. L. *Macromolecules* **2005**, *38*, 2307–2314.
- [163] Zhen, H. F., Jang, S. M. J., Teo, W. K., Li, K. J. *J. Appl. Polym. Sci.* **2006**, *99*, 2497–2503.
- [164] Gittel, T., Hartwig, T., Schaber, K. *J. Res. Phys. Chem. Phys.* **2005**, *219*, 1243–1259.
- [165] Wu, H., Liu, L., Pan, F. S., Hu, C. L., Jiang, Z. Y. *Sep. Purif. Technol.* **2006**, *51*, 352–358.
- [166] Panek, D., Konieczny, K. *Desalination* **2006**, *200*, 367–373.
- [167] Nagase, Y., Ando, T., Yun, C. M. *React. Funct. Polym.* **2007**, *67*, 1252–1263.
- [168] Inui, K., Okumura, H., Miyata, T., Uragami, T. *J. Membr. Sci.* **1997**, *132*, 193–202.
- [169] Inui, K., Okumura, H., Miyata, T., Uragami, T. *Polym. Bull.* **1997**, *39*, 733–740.
- [170] Inui, K., Miyata, T., Uragami, T. *J. Polym. Sci. Part B: Polym. Phys.* **1997**, *35*, 699–707.
- [171] Inui, K., Miyata, T., Uragami, T. *J. Polym. Sci. Part B: Polym. Phys.* **1998**, *36*, 281–288.
- [172] Inui, K., Miyata, T., Uragami, T. *Macromol. Chem. Phys.* **1998**, *199*, 589–595.
- [173] Inui, K., Okazaki, K., Miyata, T., Uragami, T. *J. Membr. Sci.* **1998**, *143*, 93–104.
- [174] Uragami, T., Tsukamoto, K., Inui, K., Miyata, T. *Macromol. Chem. Phys.* **1998**, *199*, 49–54.
- [175] Inui, K., Tsukamoto, K., Miyata, T., Uragami, T. *J. Membr. Sci.* **1998**, *138*, 67–75.
- [176] Uragami, T., Tsukamoto, K., Miyata, T., Heinze, T. *Macromol. Chem. Phys.* **1999**, *200*, 1985–1990.
- [177] Uragami, T., Tsukamoto, K., Miyata, T., Heinze, T. *Cellulose* **1999**, *6*, 221–231.
- [178] Inui, K., Noguchi, T., Miyata, T., Uragami, T. *J. Appl. Polym. Sci.* **1999**, *71*, 233–241.
- [179] Ren, J., Standt-Bickel, C., Lichenthaler, R. *Sep. Purif. Technol.* **2001**, *22–23*, 31–43.
- [180] Yildirim, A., Hilmioglu, N., Tullbentci, S. *Chem. Eng. Technol.* **2001**, *24*, 275–279.
- [181] Pandey, L. K., Saxena, C., Dubey, V. *J. Membr. Sci.* **2003**, *227*, 173–182.
- [182] Kusumocahyo, S. P., Ichikawa, T., Shinbo, T., et al. *J. Membr. Sci.* **2005**, *253*, 43–48.
- [183] Dubey, V., Pandey, L. K., Saxena, C. *Sep. Purif. Technol.* **2006**, *50*, 45–50.
- [184] Sun, H. L., Lu, L. Y., Peng, F. B., Wu, H., Jiang, Z. Y. *Sep. Purif. Technol.* **2006**, *52*, 203–208.
- [185] Lu, L. Y., Sun, H. L., Peng, F. B., Jiang, Z. Y. *J. Membr. Sci.* **2006**, *281*, 245–252.
- [186] Peng, F. B., Jiang, Z. Y., Hu, C. L., Wang, Y. Q., Lu, L. Y., Wu, H. *Desalination* **2006**, *193*, 182–192.
- [187] Peng, F. B., Hu, C. L., Jiang, Z. Y. *J. Membr. Sci.* **2007**, *297*, 236–242.
- [188] Luo, Y. J., Xin, W., Li, G. P., Yang, Y., Liu, J. R., Lv, Y., Jiu, Y. B. *J. Membr. Sci.* **2007**, *303*, 183–193.
- [189] Okuno, H., Nishida, T., Uragami, T. *J. Polym. Sci. Part B: Polym. Phys.* **1995**, *33*, 299–307.
- [190] Ruckenstein, E., Sun, F. *J. Membr. Sci.* **1995**, *103*, 271–283.
- [191] Zhou, M., Persin, M., Kujawski, W. J., Sarrazin, J. J. *Membr. Sci.* **1995**, *108*, 89–96.
- [192] Johnson, T., Thomas, S. *J. Appl. Polym. Sci.* **1999**, *71*, 2365–2379.
- [193] Gorri, D., Ibanez, R., Ortiz, I. *J. Membr. Sci.* **2006**, *280*, 582–593.
- [194] Ray, S., Ray, S. K. *J. Membr. Sci.* **2006**, *285*, 108–119.
- [195] Chakraborty, M., Bart, H. J. *Fuel Process. Technol.* **2007**, *88*, 43–49.
- [196] Hasanoglu, A., Salt, Y., Keleser, S., Ozkan, S., Dincer, S. *Chem. Eng. Proc.* **2007**, *46*, 300–306.
- [197] Wang, L. Y., Li, J. D., Lin, Y. Z., Chen, C. X. *J. Membr. Sci.* **2007**, *305*, 238–246.
- [198] Chen, J. H., Liu, Q. L., Fang, J., Zhu, A. M., Zhang, Q. G. *J. Colloid Interface Sci.* **2007**, *316*, 580–588.

- [199] Wang, Y., Hirakawa, S., Tanaka, K., Kita, H., Okamoto, K. *J. Appl. Polym. Sci.* **2003**, *87*, 2177–2185.
- [200] Schwarz, H. H., Malsch, G. *J. Membr. Sci.* **2005**, *247*, 143–152.
- [201] Shen, J. N., Zheng, X. C., Ruan, H. M., Wu, L. G., Qiu, J. H., Gao, C. J. *J. Membr. Sci.* **2007**, *304*, 118–124.
- [202] Branco, L. C., Crespo, J. G., Afonso, C. A. M. *Chem. – Eur. J.* **2002**, *8*, 3865–3871.
- [203] Berendsen, W., Radmer, P., Reuss, M. *J. Membr. Sci.* **2006**, *280*, 684–692.
- [204] Matsumoto, M., Inomoto, Y., Kondo, K. *J. Membr. Sci.* **2005**, *246*, 77–81.
- [205] Qi, R. B., Wang, Y. J., Li, J. D., Zhao, C. W., Zhu, S. L. *J. Membr. Sci.* **2006**, *280*, 545–552.
- [206] Park, H. C., Ramaker, N. E., Mulder, M. H. V., Smolders, C. A. *Sep. Sci. Technol.* **1995**, *30*, 419–433.
- [207] Chen, W. J., Martin, C. R. *J. Membr. Sci.* **1995**, *104*, 101–108.
- [208] Jonquieres, A., Roizard, D., Lochon, P. *J. Chem. Soc. Faraday Trans.* **1995**, *91*, 1247–1251.
- [209] Cai, B. X., Yu, L., Ye, H., Gao, C. J. *J. Membr. Sci.* **2001**, *194*, 151–156.
- [210] Schwarz, H. H., Apostel, R., Paul, D. *J. Membr. Sci.* **2001**, *194*, 91–102.
- [211] Niang, M., Luo, G. S. *Sep. Purif. Technol.* **2001**, *24*, 427–435.
- [212] Hilmioğlu, N. D., Tulbentci, S. *Desalination* **2004**, *160*, 263–270.
- [213] Ray, S., Ray, S. K. *J. Membr. Sci.* **2006**, *278*, 279–289.
- [214] Touchal, S., Roizard, D., Perrin, L. *J. Appl. Polym. Sci.* **2006**, *99*, 3622–3630.
- [215] Miyata, T., Iwamoto, T., Uragami, T. *J. Appl. Polym. Sci.* **1994**, *51*, 2007–2014.
- [216] Miyata, T., Iwamoto, T., Uragami, T. *Macromol. Chem. Phys.* **1996**, *197*, 2909–2921.
- [217] Kusumocahyo, S. P., Kanamori, T., Sumaru, K., Iwatsubo, T., Shinbo, T. *J. Membr. Sci.* **2004**, *231*, 127–132.
- [218] Touil, S., Tingry, S., Palmeri, J., Bouchtalla, S., Deratani, A. *Polymer* **2005**, *46*, 9615–9625.
- [219] Kusumocahyo, S. P., Ichikawa, T., Shinbo, T., et al. *J. Membr. Sci.* **2005**, *253*, 43–48.
- [220] Touil, S., Tingry, S., Bouchtalla, S., Deratani, A. *Desalination* **2006**, *193*, 291–298.
- [221] Lue, S. J., Liaw, T. H. *Desalination* **2006**, *193*, 137–143.
- [222] Zhang, P., Qian, J. W., Yang, Y., Bai, Y. X., An, Q. F., Yan, W. D. *J. Membr. Sci.* **2007**, *288*, 280–289.
- [223] Castanheiro, J. E., Ramos, A. M., Fonseca, I. M., Vitai, J. T. *J. Appl. Catal.: Gen.* **2006**, *311*, 17–23.
- [224] Benedict, D. J., Parulekar, S. J., Tsai, S. P. *J. Membr. Sci.* **2006**, *281*, 435–445.
- [225] Sanz, M. T., Gmehling, J. *Chem. Eng. J.* **2006**, *123*, 1–8.
- [226] Mulder, M. H. V., Franken, T., Smolders, C. A. *J. Membr. Sci.* **1985**, *22*, 155–173.
- [227] Uragami, T. *Polym. J.* **2008**, *40*, 485–494.
- [228] Han, X., Armstrong, D. W. *Acc. Chem. Res.* **2007**, *40*, 1079–1086.
- [229] Uragami, T., Matsuoka, Y., Fukuyama, E., Miyata, T. *Preprints PMSE Division, 237th ACS National Meeting, 2009.*

Biographical Sketch



Tadashi Uragami was born in Hyogo, Japan in 1943. He received his PhD from Kansai University in 1971. He then joined the areas of membrane science and technology and he has 38 years of expertise in the field of membrane for separation of liquid, gas, and vapor, and characterization of polymers for their application. He was promoted to professor of Faculty of Engineering of Kansai University, Osaka, Japan in 1989. He was vice-president at Kansai University from 1997 to 2000 and president for Japanese Society of Chitin and Chitosan in 2000–01. He received Society of Polymer Science, Japan (SPSJ) Mitsubishi Chemical Award in 2007. His research focuses on science and technology of polymer membranes. His research areas are as follows: (1) structure of polymer membranes for ultrafiltration and their permeation and separation characteristics; (2) material transport by polymer membranes with function of carrier transport and their transport mechanism; (3) functional membranes from chitin and chitosan for material separation; (4) preparation of polymer membranes with catalytic function and their separation characteristics; (5) mechanism of permeation and separation of gases by glassy polymer membranes; (6) structural design of polymer membranes for separation of organic liquid mixtures and their permeation and separation characteristics; (7) design of membranes using function of biopolymers and their characteristics for separation; (8) preparation of stimuli-responsive polymer gel membranes and their permeation characteristics; and (9) structural design of polymer membranes containing ionic liquid and concentration of alcohols and removal of volatile organic compounds by their membranes.

His achievements are as follows: (1) he has edited two books, and also published chapters in 61 books, 171 papers, and 60 reviews; (2) he has presented 133 invited lectures in Japan and 43 invited lectures in other countries; and (3) he has 26 Japanese patents and 18 foreign patents to his credit.

2.12 Supported Liquid Membranes for Pervaporation Processes

D Gorri, A Urtiaga, and I Ortiz, Universidad de Cantabria, Santander, Spain

© 2010 Elsevier B.V. All rights reserved.

2.12.1	Pervaporation	326
2.12.1.1	Fundamentals	326
2.12.1.2	Membranes for Pervaporation	327
2.12.2	Liquid Membranes	328
2.12.2.1	Introduction	328
2.12.2.2	Facilitated Transport	328
2.12.2.3	Supported Liquid Membranes	329
2.12.3	Pervaporation with Supported Liquid Membranes	330
2.12.3.1	Introduction	330
2.12.3.2	Supports for Supported Liquid Membranes	330
2.12.3.3	Stability of Supported Liquid Membranes	331
2.12.3.4	Theoretical Analysis	332
2.12.4	Supported Ionic Liquid Membranes	334
2.12.5	Applications	334
2.12.6	Concluding Remarks	345
References		345

Glossary

Asymmetric membrane Membrane constituted of two or more structural planes of nonidentical morphologies.

Composite membrane Membrane with chemically or structurally distinct layers.

Concentration polarization Due to retention of the slow permeating component on the membrane surface, the concentration of the fast permeating component on the membrane surface is lower than that in the bulk phase.

Facilitated transport Process in which chemically distinct carrier species form complexes with a specific component in the feed stream, thereby increasing the flux of this component relative to other components.

Flux Mass of a specified component i passing per unit time through a unit of membrane surface area normal to the thickness direction.

Liquid membrane Liquid phase existing in either supported or unsupported form that serves as a membrane barrier between two phases.

Membrane stability The ability of a membrane to maintain both the permeability and selectivity under

specific system conditions for extended period of time.

Mobile carrier Distinct species moving freely within a membrane for the purpose of increasing the selective sorption and flux of a specific component in a feed stream relative to all other components.

Partition (distribution) coefficient Parameter equal to the equilibrium concentration of a component in a membrane divided by the corresponding equilibrium concentration of the component in the external phase in contact with the membrane surface.

Permeability coefficient Parameter defined as a transport flux, per unit transmembrane driving force per unit membrane thickness.

Permeance Transport flux per unit transmembrane driving force.

Solution-diffusion Molecular-scale process in which permeant is sorbed into the upstream membrane face from the external phase, moves by molecular diffusion in the membrane to the

downstream face, and leaves into the external fluid phase in contact with the membrane.

Sweep Nonpermeating stream directed past the downstream membrane face to reduce downstream permeant concentration.

Nomenclature

A	membrane area (m^2)
C	concentration (g m^{-3})
D	diffusion coefficient ($\text{m}^2 \text{s}^{-1}$)
J	total permeation flux ($\text{g m}^2 \text{h}^{-1}$)
J_i	permeation flux of component i through the membrane ($\text{g m}^2 \text{h}^{-1}$)
k	mass transfer coefficient (m s^{-1})
l	membrane thickness (m)
m	mass of permeate (g)
P	permeability coefficient ($\text{m}^2 \text{s}^{-1}$)
P_C	critical displacement pressure (kPa)
r	pore radius (m)

S	equilibrium partition coefficient (dimensionless)
t	time (s)
α	separation factor (dimensionless)
β	enrichment factor (dimensionless)
γ	interfacial tension (N m^{-1})
θ	contact angle between the membrane pores and the impregnating liquid (degree)

Subscripts

i permeating component

m membrane

Superscripts

f feed solution

p permeate

2.12.1 Pervaporation

2.12.1.1 Fundamentals

Pervaporation (PV) is a separation technology where a liquid mixture (feed) is placed in contact with one side of a membrane and the permeated product (permeate) is removed as a low-pressure vapor from the other side (Figure 1). The permeate vapor can be condensed and collected or released as desired. The chemical potential gradient across the membrane is the driving force for the mass transport. The driving force may be created by applying either a vacuum pump or an inert purge (normally air or steam) on the permeate side to maintain the permeate vapor pressure lower than the partial pressure of the feed liquid [1].

Three main applications of the technology have received considerable attention over the past decades: (1) dehydration of organic solvents, (2) removal of organic compounds from aqueous solutions, and (3) separation of anhydrous organic mixtures. Dehydration of alcohols and of other organic solvents and removal of small amounts of organic compounds from polluted waters have reached the commercial scale, solvent dehydration being the main application [2–4].

PV is a promising technique for the separation of solvents from low-concentration aqueous solutions

[5]. Fermentation processes can generate a variety of by-products, such as acetone, ethanol, butanol, acetic acid, and propionic acid. These compounds can be used as solvent, fuel, or a chemical intermediate. However, their concentrations in a fermentation broth are often quite low, around 1–2%. In this range of solvent concentration in the fermentation broth, distillation is not an economical technology to recover the solvents from the solution. A variety of

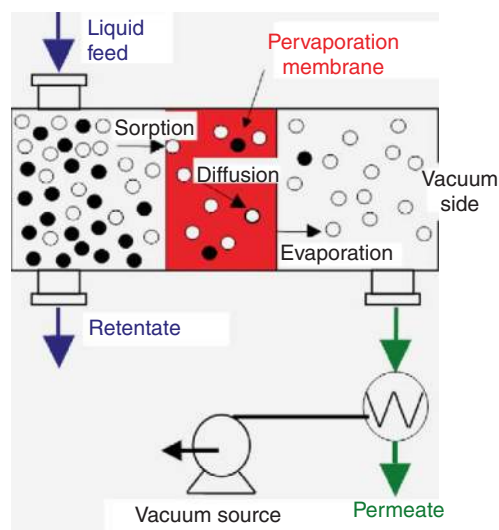


Figure 1 The pervaporation process.

membranes has been used in the PV process for these dilute solutions [6, 7]. These include polymeric membranes made of polydimethylsiloxane (PDMS) (and its composites), polytetrafluoroethylene (PTFE), polyether block amides (PEBA), and inorganic membranes, such as silicalite (zeolite) membranes.

PV separation is governed by the chemical nature of the macromolecules that comprise the membrane, the physical structure of the membrane, the physicochemical properties of the mixtures to be separated, and the permeant–permeant and permeant–membrane interactions. PV transport is usually described to be a three-step process: solution–diffusion–evaporation. The separation is based on the selective solution and diffusion, that is, the physical–chemical interactions between the membrane material and the permeating molecules, not the relative volatility as in distillation.

Vapor permeation (VP) is an alternative technology, where the feed enters as saturated vapor [8, 9]. This avoids the phase change across the membrane surface, and makes VP systems less complex than similar PV systems. In addition to its simplicity, VP is less sensitive to concentration polarization on the feed side of the membrane; the membrane lifetime is expected to be longer than for PV due to the low degree of membrane swelling, and the transport rates across the membrane may be enhanced by raising the feed pressure. Shortcomings in VP, however, are the strong dependence of the separation characteristics on the feed pressure, the sensitivity to friction losses in the feed stream, and the possibility of condensation, and, hence, of the formation of stagnant condensate films, partially covering the membrane on the feed side.

PV is a rate-controlled separation process. In developing PV membranes, three issues must be addressed: (1) membrane productivity, (2) membrane selectivity, and (3) membrane stability. The productivity is defined by the flux of the components across the membrane. The total permeate flux, \mathcal{J} , is obtained from experimental data as

$$\mathcal{J} = \frac{m}{A\Delta t} \quad (1)$$

where m is the mass of collected permeate, A is the membrane surface area, and Δt is the permeation time.

When describing the selectivity of a membrane for the separation of a mixture composed of components i and j , the separation factor is defined as

$$\alpha = \frac{C_i^p/C_j^p}{C_i^f/C_j^f} \quad (2)$$

Parameter α is similar to the membrane selectivity which is widely used in gas permeation, and which is defined as a ratio of the permeabilities of the membrane to two different pure gases under comparable conditions. In PV, the two penetrants are no longer transported independently through the membrane due to strong coupling effects. It should be pointed out that only when the concentration polarization is negligible, the selectivity expressed by Equation (2) would be an intrinsic property of the membrane. Occasionally, membrane selectivity is expressed in terms of the enrichment factor, β , which is simply defined as the ratio of concentrations of the preferentially permeating species in the permeate and in the feed. The use of parameter β makes it easier to formulate the mathematical equations governing the performance (production capacity, operational yield, and energy cost), which characterizes a PV module [10].

2.12.1.2 Membranes for Pervaporation

In conventional PV, the membranes used are preferentially nonporous, in the sense of not possessing pores that are visible with an electron microscope. They can be composed of different materials of polymeric or inorganic nature or from polymeric and inorganic materials themselves. With regard to the structure of the membranes, they can be homogeneous or asymmetrical, and they can also be composite membranes in which case they are constituted of different layers of different materials and/or morphologies.

A comprehensive review of polymeric membranes for PV was recently reported by Shao and Huang [11]. They investigated the potential of PV with regard to separating liquid mixtures in the areas of alcohol and solvent dehydration, organic removal from water, and organic/organic separations. They also reported on the fundamentals of PV transport in detail, discussing modifications made to solution-diffusion theory and discussed the importance of solvent coupling in diffusive transport and how this coupling can be accounted for. A detailed review on membranes for the dehydration of solvents by PV had also been conducted by Chapman *et al.* [3].

In the so-called organophilic PV application, pollution control and solvent recovery can be carried out simultaneously. Organophilic PV mainly involves the

use of polymeric membranes typically based on PDMS. A variety of other polymers have also been used as organophilic PV membranes. As reported in literature [6, 12], these organophilic membranes offer an extremely high selectivity ($\alpha > 1000$) to volatile organic compounds (VOCs), such as benzene, toluene, xylenes, methylene chloride, chloroform, tetrachloromethane, trichloroethane, trichloroethylene (TCE), and chlorobenzene; a high selectivity ($100 < \alpha < 1000$) for VOCs, such as acetates, butanoates, methyl *tert*-butyl ether (MTBE), tetrahydrofuran, and methyl isobutyl ketone (MIBK); a moderate selectivity ($20 < \alpha < 100$) for moderately polar VOCs, such as *n*-butanol, *tert*-butyl alcohol, methyl ethyl ketone, aniline, and pyridine; and a low selectivity ($\alpha < 20$) for highly polar VOCs, such as methanol, ethanol, *n*-propanol, 2-propanol, phenol, and acetone.

On the other hand, ceramic membranes can offer some significant advantages over polymeric ones when used in PV applications, mainly a higher chemical and thermal stability than most polymeric materials for specific applications. Thus, membranes made from ceramic materials can be operated at higher temperatures and in the presence of solvents that would cause polymeric membranes to fail. They offer much better mechanical stability and do not swell and thus achieve a more constant performance with varying feed concentrations [13]. Zeolite membranes do not present this swelling phenomenon and, on the contrary, can be very selective toward water permeation, a property that is particularly useful when very low water concentrations should be reached (<1%). However, due to their ion-exchange nature they are susceptible to be attacked by salts, acids, and alkaline compounds. Ceramic PV membranes, mostly silica-based membranes, are very robust but they are often somehow less selective than polymeric or zeolite membranes. In principle, high-temperature operation is possible with both zeolite and silica PV membranes; however, at present, most industrial applications use polymeric membranes.

In the development of high-flux membranes, much effort has been made to change the membrane structure from a dense thick film to an asymmetric or composite structure, in order to reduce the effective thickness of the membrane. However, the reduction in thickness is typically accompanied by a decrease in selectivity, due to a higher number of defects. To make PV a more economically attractive process for removal, recovery, and concentration of a variety of

VOCs, more efficient membranes are needed. Membranes displaying higher selectivities would reduce the energy required for organic recovery. Membranes with higher organic fluxes would reduce the membrane area requirement.

2.12.2 Liquid Membranes

2.12.2.1 Introduction

A liquid membrane (LM) is a fluid or quasi-fluid phase, which separates two other phases that are immiscible with the LM. LMs were developed because of the relatively small transmembrane flux of polymer membranes. They have gained increasing significance in recent years in combination with the so-called facilitated transport which utilizes selective carriers transporting certain components such as metal ions selectively and at a comparatively high rate across the LM interphase [14, 15].

It is relatively easy to form a thin fluid film. It is difficult, however, to maintain and control this film and its properties during a mass separation process. In order to avoid a breakup of the film, some type of reinforcement is necessary to support such a weak membrane structure. Today, two different techniques are used for the preparation of LMs [16]. In the first case, the selective liquid barrier material is stabilized as a thin film by a surfactant in an emulsion-type mixture. In the second technique for making LMs, a microporous polymer structure is filled with the LM phase. In this configuration, the microporous structure provides the mechanical strength and the liquid-filled pores provide the selective separation barrier.

2.12.2.2 Facilitated Transport

Carrier-facilitated transport membranes incorporate a reactive carrier in the membrane [17]. The solute has to react first with the carrier to form a solute-carrier complex, which then diffuses through the membrane to finally release the solute at the permeate side. The overall process can be considered as a passive transport since the solute molecule is transported from a high to a low chemical potential. Much of the work on carrier-facilitated transport has employed LMs containing a dissolved carrier agent held by capillary action in the pores of a microporous film.

The membrane permeance (permeant flux divided by permeant driving force) for the

transported species is a key parameter in process design and development. Membrane permeance has to be as high as possible, and it is commonly determined by the expression $S * D_m/l$, where S is the distribution coefficient related to the chemical affinity of the membrane to the transported solute, l is the membrane thickness, and D_m the diffusion coefficient of the solute through the membrane; the permeance value can be increased by increasing either the distribution coefficient or the diffusivity and by decreasing the thickness of the membrane. The idea of using a thin organic liquid layer as PV membrane seems to be very attractive from this point of view simply because the value of D_m in liquids is at least three to four orders of magnitude higher than values in solid polymers and in inorganic membranes. Besides, it is possible to dissolve some hydrophobic chemicals in the organic liquid, so that they will be able to interact with the transported hydrophilic species, increasing the affinity of the solute and, thus, the process selectivity. The complex species resulting from the solute–membrane interaction could easily diffuse through the organic liquid. Although the value of D for the formed complex species is slightly lower than that for smaller species penetrating directly, the value of S can be increased by many orders of magnitude, which results in the so-called facilitated transport allowing for much higher rates of the separation process [18].

2.12.2.3 Supported Liquid Membranes

Supported liquid membranes (SLMs), which have been of interest in research for more than 30 years, are formed by liquids immobilized within nanostructured porous supports. In comparison to conventional solid membranes, they display a

number of advantages [19] but often lack the long-term stability needed in industrial applications.

The capacities of performing selective solute transport and treating dilute solutions make the SLM technique an attractive alternative to solvent extraction, that is, it combines the processes of extraction, stripping, and regeneration in a single step [20]. LMs were first applied to gas transport (oxygen, carbon dioxide, carbon monoxide, etc.). Metal ion separation has received considerable interest in order to recover metals, as well as to control pollution. Finally, biotechnological applications and recovery of other products, such as acetic acid and phenols, have been reported. An extensive review including industrial applications has been published [21–23].

In an SLM process, the organic extractive phase is immobilized by capillary forces in the pores of a thin microporous polymeric support separating the feed solution and the stripping solution (Figure 2). The support geometry which offers more advantages is the hollow fiber, where the highest surface-area-to-volume ratios are obtained.

General advantages of facilitated transport membranes are improved selectivity, increased flux, and, especially if compared with membrane contactors, the possibility to use expensive carriers. Despite the advantages, the suitability of an SLM system for the simultaneous extraction and stripping depends on the solute flux rate, the stability of the membrane, and the working lifetime of the system.

The mass-transfer rate through the LM will be affected by variables such as the solubility and diffusivity of the solutes in the immobilized organic phase. The properties of the solid, such as support thickness, porosity, and tortuosity of the pores, also have an influence on the separation rate [24].

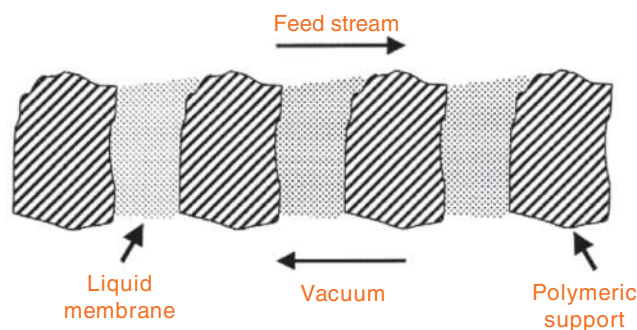


Figure 2 Pervaporation with supported liquid membranes.

The preparation of SLMs is extremely simple, when certain requirements concerning the selective barrier and the microporous support material are fulfilled [14]. The LM material should have a low viscosity and low vapor pressure, that is, high boiling point and, when used in aqueous feed solutions, low water solubility. Otherwise, the useful lifetime of the membrane is rather limited. The microporous structure should have a high porosity, a pore size small enough to support the LM phase sufficiently under hydrostatic pressure and the polymer of the substructure should be hydrophobic in nature for most LMs used in contact with aqueous feed solutions. In practice, LMs are prepared by soaking a hydrophobic microporous membrane in the hydrophobic liquid, which may consist of a selective carrier dissolved in an organic solvent. The disadvantage of supported membranes is their thickness which is determined by the thickness of the microporous support structure, which is in the range of 10–50 μm , and, therefore, about 100 times the thickness of the selective barrier of an asymmetric polymer membrane. Thus, the fluxes of SLMs can be low even when their permeabilities are high.

2.12.3 Pervaporation with Supported Liquid Membranes

2.12.3.1 Introduction

In order to successfully use SLM in PV at least the following conditions are required: the liquid immobilized in the porous support must have a very low volatility to avoid its evaporation under vacuum and, on the other hand, it must be essentially immiscible with the main component (solvent) in the feed mixture; the target solute from feed mixture should have a high affinity with the component of the LM and a partial pressure high enough to allow the existence of separation driving force. According to the Laplace equation (Equation (3)), the breakthrough pressure increases with the interfacial tension between feed solution and SLM phase. Since PV usually operates under vacuum, with the liquid feed mixture at pressure close to the atmospheric pressure, the breakthrough pressure for the LM immobilized in the porous should be higher than 1 bar.

PV through SLMs has been mainly researched to separate volatile fermentation products and other VOCs from aqueous solutions. Oleyl alcohol (OA), iso-tridecanol, beeswax, and silicone oil have been used as LMs [12]. The SLM consisting of OA yielded

a butanol flux and selectivity higher than those of PDMS membranes and stability over periods of 100 h. Since the characteristics of the SLM can be easily changed by selection of solvents, this separation process would be applicable to many volatile materials, such as alcohols, esters, ketones, hydrocarbons, and acids. The limited number of investigations on SLMs for PV can be attributed to the well-known instability of SLMs for practical applications.

2.12.3.2 Supports for Supported Liquid Membranes

SLMs consist of three main components: (1) support membrane, (2) organic solvent, and (3) carrier (in case of facilitated transport) [25]. The most widely used approach to prepare SLMs has been to impregnate the pore structure of a thin, microporous substrate, such as an ultrafiltration membrane, with the liquid containing the complexation agent. As a free liquid film is not very stable, the function of the porous support membrane is to act as a framework. Stability of the immobilized liquid is one of the main constraints of this process, as discussed in the following section. In fact, all types of membrane materials can be used as the support membrane, provided they are stable under the experimental conditions employed and have suitable chemical properties. Indeed, highly stable materials, such as polypropylene, polyethylene, and poly(vinylidene fluoride), are often used as supports. Way *et al.* [24] discuss the chemical and physical properties that must be considered when an SLM support is selected. The surface porosity and overall porosity of such support materials should be high in order to obtain an optimal flux. Table 1 lists some porous membranes frequently used as porous polymeric support. In addition to the above-mentioned materials, other more dense membranes can be used in principle,

Table 1 Some porous membranes frequently used as supports for supported liquid membranes

Material	Characteristics
Polypropylene	Hydrophobic
Polytetrafluoroethylene	Hydrophobic
Polyethylene	Hydrophobic
Polyvinylidene fluoride	Hydrophobic
Polyamide (Nylon)	Hydrophilic
Polycarbonate	Hydrophilic
Polyethersulphone	Hydrophilic
Cellulose acetate	Hydrophilic

such as polysulfone and cellulose acetate. Although the most-used supports are polymeric, there are several studies that have used porous ceramic membranes as support [26–28]. In addition to the porosity, membrane thickness also directly determines the permeation rate because the flux is inversely proportional to the membrane thickness, suggesting that the membrane should be as thin as possible.

An SLM can be made in at least three different geometries [21]. A planar or flat geometry is very useful for laboratory purposes. For industrial purposes, a planar geometry is not very effective since the ratio of surface area to volume is too low. Hollow fiber and spiral wound modules can be used to provide high surface-area-to-volume ratios. Surface-area-to-volume ratios can approach $10\,000\text{ m}^2\text{ m}^{-3}$ for hollow fiber and $1000\text{ m}^2\text{ m}^{-3}$ for spiral wound modules. Nevertheless, to our knowledge there are no references using SLM in spiral wound modules.

2.12.3.3 Stability of Supported Liquid Membranes

LMs supported by hollow fibers are relatively easy to make and operate, and the membrane fluxes can be high. However, membrane stability is a problem. The detailed mechanism for flux instability is not completely established but appears to be related to loss of the organic complexing agent phase from the support membrane [29, 30]. Although membrane fluxes could be restored to their original values by reloading the membrane with fresh complexing agent, this is not practical in a commercial system.

Instability of SLMs is due to the loss of carrier and/or membrane solvent from the membrane phase, which has an influence on both flux and selectivity of the membrane. Depending on the amounts of carrier and solvent lost from the support pores, the solute flux might increase, decrease, or stay almost equal. When all LM phase is lost, the membrane breaks down and a direct transport between the two phases adjacent to the LM takes place with a complete loss of selectivity. The time period after which instability phenomena are observed varies from less than 1 h to several months depending on the system [31].

The major degradation mechanisms are [18, 29–33]:

- progressive wetting of the pores in the membrane support by the aqueous phase;
- pressure difference over the membrane;

- mutual solubility of species from the aqueous phase and LM phase;
- emulsion formation in the LM phase; and
- blockage of membrane pores by precipitation of a carrier complex at the surface.

SLM stability can be affected by the type of polymeric support and its pore radius, organic solvent used in the LM, interfacial tension between the aqueous phase and membrane phase, flow velocity of the aqueous phases, and method of preparation [18]. The minimum transmembrane pressure required to push the impregnating phase out of the largest pores can be calculated using Laplace equation [33]:

$$P_C = \frac{2\gamma \cos\theta}{r} \quad (3)$$

where γ is the interfacial tension between strip or feed solution and SLM phase, θ the contact angle between the membrane pores and the impregnating liquid, and r is the pore radius. Usually, for commercial hollow fiber membrane contactors and hydrocarbon solvents, P_C is much larger than transmembrane pressure, which indicates that pressure difference is not the main cause of SLM degradation [31]. It was proposed that only two mechanisms are the major important factors resulting in the membrane instability: the solubility of the SLM components in the adjacent feed or strip solutions and an emulsification of the SLM phase due to lateral shear forces [18].

Many research groups have been working on improving the stability of SLMs by using various approaches. The alternatives proposed have been summarized by Kocherginsky *et al.* [18]:

1. *Continuous reimpregnation of the support with LM phase* [34]. Such continuous impregnation methods are mainly applied for hollow fiber modules and can be found in different configurations. This regeneration of LMs works well, but feed and/or strip solutions are still polluted with the membrane liquid. Only the effects of LM loss are cured, but the problem of instability itself is not tackled. Other disadvantages are the necessity to fill up the membrane liquid, the complex modules, and the procedures required [31].
2. *Formation of barrier layers on a membrane surface either by physical deposition or by interfacial polymerization* [35]. It works well to prevent emulsification of the membrane liquid in the aqueous solutions and to minimize displacement of LM solutions from the

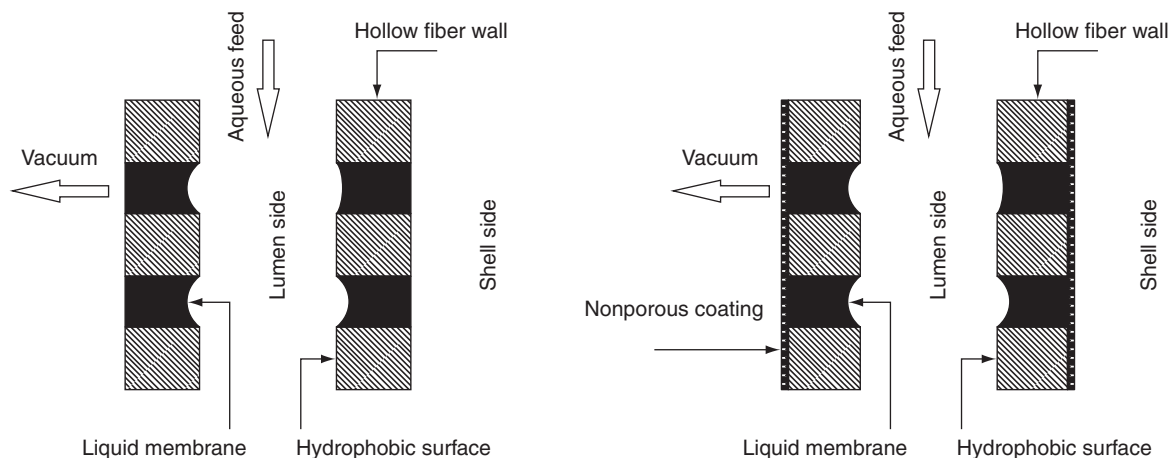


Figure 3 Schematic diagram of the liquid membrane for a pervaporation process: (a) an uncoated membrane is used as the substrate; (b) a coated membrane is used as the substrate. Reproduced from Qin, Y., Sheth, J. P., Sirkar, K. K. *Ind. Eng. Chem. Res.* **2002**, *41*, 3413–3428.

support pores by pressure difference over the membrane (Figure 3). However, the reproducibility of SLMs coated with the polymerized film is poor and the adhesion to the substrate is not strong. Besides, the additional layer can decrease the membrane permeability.

3. *Stabilization of SLM by plasma polymerization surface coating* [12, 36]. This also reduces the size of the membrane surface pores and increases mass transfer resistance, resulting in a decreased permeability of the membrane system.

Details about each of these techniques can be found elsewhere [25].

2.12.3.4 Theoretical Analysis

In membrane processes, it is well recognized that transport is a function of the membrane itself and of the mass transfer resistances that may develop on either side of the membrane. In PV, when the preferentially permeating compound is present in trace amounts in the bulk of the feed, and its flux is relatively high, concentration polarization may develop at the surface of the membrane. As the Reynolds number is increased, eventually into the turbulent regime, liquid film resistance should be reduced/eliminated and the membrane resistance may become rate controlling.

Transport across a dense membrane can be described as a solution/diffusion process [37–39]. In PV, there may be additional resistances to mass transfer in the liquid and in the gas boundary layers

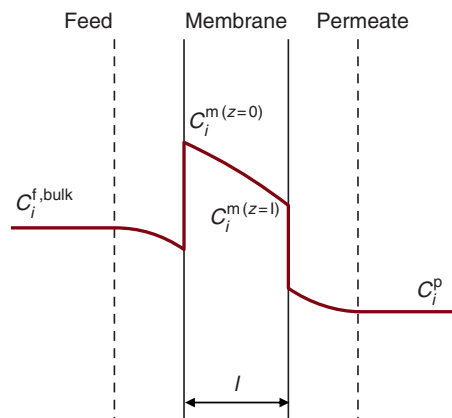


Figure 4 Solute concentration profile across the membrane.

that form at the interfaces with the membrane. With reference to Figure 4, the following expression for the steady-state flux of a component from the liquid side to the vapor side is derived:

$$\mathcal{J}_i = \frac{1}{\frac{1}{k_l} + \frac{1}{S_{ml} * k_m} + \frac{1}{\frac{S_{ml}}{S_{mv}} * k_v}} * \left(C_i^{f,bulk} - \frac{S_{mv}}{S_{ml}} * C_i^p \right) \quad (4)$$

where C is the volumetric concentration, k is the mass transfer coefficient, and S is the dimensionless equilibrium partition coefficient representing the conditions at the interfaces:

$$S_{ml} = \frac{C_i^{m,equil}}{C_i^{f,equil}} \quad (5)$$

$$S_{mv} = \frac{C_i^{m, \text{equil}}}{C_i^{p, \text{equil}}} \quad (6)$$

Maintaining a good vacuum, the vapor side mass transfer limitation is negligible ($1/k_v \approx 0$) and the vapor concentration is small ($C_i^p \approx 0$); hence, Equation (4) can be simplified. Furthermore, if the diffusion coefficient, D_m , is not concentration- and position-dependent, the mass transfer coefficient can be expressed as $k_m = D_m/l$, where l is the membrane thickness.

A dimensionless form of Henry's law constant can be defined as

$$S_{vl} = \frac{S_{ml}}{S_{mv}} = H' \quad (7)$$

The product $P_m = S_{ml} * D_m$ is normally defined as the membrane permeability:

$$P_m = S_{ml} * D_m \quad (8)$$

Substituting Equations (7) and (8) into Equation (8) results in

$$\mathcal{F}_i = \frac{1}{\frac{1}{k_l} + \frac{l}{P_m} + \frac{1}{H'k_v}} * \left(C_i^{f, \text{bulk}} - \frac{C_i^p}{H'} \right) \quad (9)$$

Equation (9) is similar to conventional heat and mass transfer equations, which express fluxes as a ratio of the driving force over the total mass transfer resistance. The partial resistances for the feed side, membrane side, and permeate side are defined, respectively, as

$$R_l = \frac{1}{k_l} \quad (10)$$

$$R_m = \frac{l}{P_m} \quad (11)$$

$$R_v = \frac{1}{k_v H'} \quad (12)$$

The driving force is taken as a difference between the solute concentration in the feed, C_i^f , and the concentration of solute, C_i^p , in the vapor mixture; C_i^p is dependent on the permeate pressure and permeate composition.

Referring to a gradient in composition within the feed phase next to the membrane surface, concentration polarization is a consequence of the slower permeating feed component accumulating near the feed-membrane interface as the faster permeating

component moves on [40]. Since in PV the solute or minority component permeates preferentially, solute depletion near the membrane boundary causes a lower than bulk concentration. A theoretical analysis about the effect of external mass-transfer resistance on the transport through LMs has been reported by Noble *et al.* [41].

Since C_i^p increases with increasing permeate pressure, the solute concentration in the vapor mixture cannot always be considered as negligible compared to the concentration in the feed solution. The solution-diffusion model has been successfully used for the testing and comparison of membranes, when the coupling of fluxes can be neglected (i.e., for very low concentrations of the preferentially permeating components in the feed) [39].

Qin *et al.* [12] reported a detailed mathematical model for the description of VOC removal from water by using SLM-based PV, considering three cases: (1) porous hollow fiber used as substrate, (2) silicone-coated porous hollow fiber used as substrate, and (3) partially wetted substrate. The proposed model allows predicting the exit concentration, permeation flux, and selectivity from the properties of the membrane and VOCs and the operating conditions.

When the immobilized phase (LM) contains a carrier, the flux of the species i is given by the sum of two contributions [42]: the diffusion of the free species through the immobilized phase and the diffusion of the species as a complex. Carrier-facilitated transport involves a combination of chemical reaction and diffusion. A possible approach [43, 44] is to make the simplification that the rate of chemical reaction is fast compared to the rate of diffusion; that is, the membrane diffusion is rate controlling. This approximation is a good one for most facilitated transport processes and can be easily verified by showing that flux is inversely proportional to membrane thickness. If interfacial reaction rates were rate controlling, the flux would be constant and independent of membrane thickness. Assuming chemical equilibrium is reached at the membrane interfaces allows the facilitated transport process to be modeled easily [15, 44].

Noble [45] developed a model for transport in fixed-site carrier membranes (the complexing agents are cast directly into the polymer films). This model yields a dual-mode sorption kind of description in the case of diffusion-limited transport. The diffusion, in this case, is determined by the diffusion coefficient of the solute-carrier complex. This implies that the transport is morphology dependent. Furthermore, it was

shown that the change in mobility caused by changes in morphology might result in a percolation limit.

2.12.4 Supported Ionic Liquid Membranes

Recent studies suggest that ionic liquids (ILs) have great potential as solvents with novel functions as well as replacements for volatile organic solvents [46]. However, using a large amount of ILs as solvents in liquid–liquid extraction systems is expensive due to the extremely high cost of ILs compared with conventional organic solvents.

The concept of supported ionic liquid membranes (SILMs) allows one to combine the recent developments in the field of membrane technology, for example, in nanofiltration, SLMs, and in PV, with the use of ILs for providing novel solutions in downstream processing or process intensification [27]. ILs are currently explored as new reaction media for chemical synthesis or electrochemical applications, and have emerged as a new class of solvents in the last decade. They seem to have a large potential in downstream processing, especially when applied in a form that requires only a small amount of IL, for example, in SLMs. The most outstanding property of ILs is their nonmeasurable vapor pressure that makes their application in LMs attractive for PV. A very useful source of information for properties of ILs is the ILs database (ILThermo), which is a free web research tool that allows users worldwide to access an up-to-date data collection from the publications on experimental investigations of thermodynamic, and transport properties of ILs as well as binary and ternary mixtures containing ILs. Physical properties of some ILs and common solvents for SLMs are shown in **Table 2**.

Many ILs also exhibit unique gas solubility, transport, and separation properties, providing opportunities for developing new gas separation/gas enrichment technologies using a thin layer of IL as the separation barrier, a largely undeveloped field for potential commercial application of ILs [47, 48]. To the best of our knowledge, the first application of SILMs for gas separations was reported by Noble and coworkers [49]. The first report about the molecular interactions between room-temperature ionic liquids (RTILs) and Nafion and PDMS membranes, proving that in contact with these polymers RTILs behaved like electrolytes rather than solvents, was published in 2005 [50]. Scovazzo *et al.* [51] concluded

that by combining the negligible vapor pressure of RTILs with their ability to produce application-specific RTILs, there is potential for producing highly selective membranes with high permeabilities in comparison to classical polymer membranes. So far, SILMs have been mainly studied for applications in selective extraction of organic compounds [52–55] and gas separation [26, 51, 56, 57].

The selectivity of the separation in LMs is not based on the solid support of a given membrane, but on the properties of the liquid. SILMs offer a range of possible advantages [28, 58]:

1. Molecular diffusion is higher in ILs than in polymers.
2. The selectivity of the separation can be influenced by variation of the liquids; especially ILs offer the advantage of a wide variety of properties.
3. ILs as LMs allow three phase systems easily due to their special mixing behavior.
4. Contrary to the extraction, only small amounts of liquids are necessary to form the LM, thus allowing the use of more expensive materials as well.
5. Due to their good thermal stability, reactive processes may take place at high temperatures (up to around 250 °C), which leads to faster kinetics in the case of endothermic reactions.
6. The usage of nano-, ultra-, and microfiltration ceramic modules could help to diminish concentration polarization due to a rough liquid-membrane surface.
7. Since ILs do not show measurable vapor pressures, they might overcome stability problems of common SLMs caused by evaporation of the membrane phase. In addition, mechanical stability of the SLM is increased due to the improved wetting properties of ILs.

2.12.5 Applications

Main applications reported in literature have been addressed to separate volatile fermentation products and other VOCs from their dilute aqueous solutions. Compared to the large number of PV studies using solid membranes, investigations on LMs for PV are rare. This can be attributed to the well-known instability of SLMs for practical applications. A summary of the experimental studies by using SLM-PV reported in the literature is presented in **Table 3**.

Earlier works have shown that PV could play an important role in the continuous removal of

Table 2 Physical properties of solvents for preparing liquid membranes (at 20 °C)

<i>Solvent</i>	<i>CAS number</i>	<i>Melting point (K)</i>	<i>Boiling point (K)</i>	<i>Density (kg m⁻³)</i>	<i>Viscosity (mPa s)</i>	<i>Surface tension (mN m⁻¹)</i>
Oleyl alcohol	143-28-2		480 (at 1.7 kPa)	850	26	31.6
Hexadecane	544-76-3	291.3	560	773	3.4	28
Trioctylamine	1116-76-3	238.5	639.2	811	15	21
Triethylene glycol	112-27-6	265.8	561.5	1119	38.7	45
1- <i>n</i> -butyl-3-methylimidazolium hexafluorophosphate	174501-64-5	283.1		1372	340	48.8 (298.1 K)
1-butyl-3-methylimidazolium tetrafluoroborate	174501-65-6	188.1		1205	136	48.8 (298.1 K)
1-butyl-3-methylimidazolium bis[(trifluoromethyl)sulfonyl]imide	174899-83-3	271.1		1442	63	46.6 (298.1 K)
1-ethyl-3-methylimidazolium bis[(trifluoromethyl)sulfonyl]imide	174899-82-2	256.1		1524	39	32.8 (298.1 K)
1-ethyl-3-methylimidazolium trifluoromethanesulfonate	145022-44-2	264.1		1388	50	41.6 (298.1 K)

Table 3 Experimental studies on pervaporation with SLM

<i>Feed mixture</i>	<i>Support</i>	<i>Liquid membrane</i>	<i>Operative conditions</i>	<i>Reference</i>
Acetone/water (0–16%) butanol/water (0–6%)	Microporous polypropylene flat sheet, thickness 25 μm , porosity 45%, maximum size of slender pore $0.04 \times 0.4 \mu\text{m}$	Oleyl alcohol	Permeate pressure 100 Pa, 30 °C	[63]
Ethanol from fermentation broths	Flat microporous polytetrafluoroethylene, thickness 65 μm , pore size 0.2 μm	Isotridecanol	Sweeping gas operation with air at atmospheric pressure	[64]
Butanol, isopropanol, and other acids in aqueous solution	Microporous polypropylene flat sheet, thickness 25 μm , porosity 45%, maximum size of slender pore $0.04 \times 0.4 \mu\text{m}$	Oleyl alcohol	Permeate pressure 133 Pa	[65]
Diacetyl from fermentation broths	Microporous polypropylene hollow fiber, thickness 22 μm , porosity 45%	Oleyl alcohol	Permeate pressure 1330 Pa, 30 °C	[66]
TCE/water (50–950 ppm)	(1) Microporous polypropylene hollow fiber; (2) plasma-polymerized silicone-coated microporous polypropylene hollow fiber membranes	Hexadecane	Permeate pressure 80–9330 Pa, 25 °C	[12]
Acetic acid/water, butyric acid/water	(1) Microporous polypropylene hollow fiber; (2) plasma-polymerized silicone-coated microporous polypropylene hollow fiber membranes	(1) Trioctylamine and (2) tridodecylamine	Permeate pressure 80–667 Pa, 25–65 °C	[67]
Acetone, ethanol, and butanol from dilute aqueous solutions	(1) Microporous polypropylene hollow fiber; (2) microporous polypropylene hollow fiber coated with nanoporous fluorosilicone on the outside of fibers	Trioctylamine	Permeate pressure 400–667 Pa, 25–54 °C	[68]
Nitrogen, 86 vol.% hydrocarbon vapors (benzene and cyclohexane), 11.5 vol.% and water vapor, 2.5 vol.%	Double-layered liquid membrane. (1) Top layer: conventional SLM. A hydrophilic-treated PTFE microporous membrane of 1 μm in pore size, 35 μm in thickness and 83% in porosity was soaked in triethylene glycol. (2) The liquid membrane was placed on a highly hydrophobic microporous membrane (PVDF)	Triethylene glycol	Permeate pressure 200 Pa, room temperature (295–300 K)	[70]

C5–C8 hydrocarbons, in which 72–87% was aromatic. Gas carrier: nitrogen	Double-layered liquid membrane. (1) Top layer: conventional SLM. A hydrophilic-treated PTFE microporous membrane of 1 μm in pore size, 35 μm in thickness, and 83% in porosity was soaked in triethylene glycol. (2) The liquid membrane was placed on a highly hydrophobic microporous membrane (PVDF)	Triethylene glycol	Permeate pressure 100 Pa, room temperature (293–296 K)	[71]
Toluene-N ₂ , methanol-N ₂ , acetone-N ₂	Plasma-polymerized silicone-coated microporous polypropylene hollow fiber membranes	Silicone oil	Permeate pressure 133–4400 Pa, 25 °C	[72]
1,3-propanediol/ water (1–3%)	Ceramic nanofiltration module, pore size 0.9 nm	Hydrophobic IL (tetrapropylammonium tetracyanoborate)	Permeate pressure 80 Pa, 22 °C	[27]
Acetone/butanol/ water	Ceramic ultrafiltration module made from TiO ₂ with pore size 60 nm	(1) PDMS + 1-ethenyl-3-ethyl-imidazolium hexafluorophosphate (2) PDMS + tetrapropylammonium tetracyano-borate	Permeate pressure 20 Pa, 23 °C	[58]
Acetone/butanol/ water	Ceramic ultrafiltration module made from TiO ₂ with pore size 60 nm	PDMS + tetrapropylammonium tetracyano-borate	37 °C	[73]

biosolvents with inhibitory effects on the production rate, such as ethanol, butanol, and acetone, from fermentation broths [7, 59, 60]. By integrating a PV unit into a bioreactor, which selectively removes volatile inhibitory substances, significantly better bioconversion rates and lower downstream processing costs may be achieved. Since the characteristics of the SLM can be easily changed by selection of solvents, PV process with SLM would be applicable to many volatile materials, such as alcohols, esters, ketones, hydrocarbons, and acids. A brief comparison between different PV membranes with its performances for PV separation of 1-butanol from 1-butanol/water mixtures is shown in **Table 4**.

Matsumura and Kataoka [63] reported a PV method which uses an SLM prepared with OA for removal of butanol and acetone from diluted aqueous solutions. The reported separation factor for butanol was 180, and the permeation flux was 10 times higher than that of the silicone tubing. This higher permeation flux can be attributed to the difference in the diffusivity of butanol in liquids and solids. The OA LM was also applicable to dilute aqueous acetone solutions and showed a good separation factor of 160 when a double-trapping method was employed. The authors reported that PV process could be carried out continuously for a period of up to 100 h without any change in separation performance.

PV across high-flux solvent-selective membranes can in principle render a solvent fermentation process continuous, enhance its efficiency, and minimize the waste biomass. Christen *et al.* [64] used an SLM system for the extraction of ethanol during semicontinuous fermentation of *Saccharomyces bayanus*. The membrane consisted of a porous Teflon sheet as support, soaked with isotridecanol. These authors reported that the assembly permitted combining biocompatibility, permeation efficiency, and stability. The removal of ethanol from the cultures led to decreased inhibition and, thus, to a gain in conversion of 345 g l^{-1} glucose versus 293 g l^{-1} glucose without extraction. Besides these improvements in fermentation performances, the process resulted in ethanol purification, since the separation was selective toward microbial cells and carbon substrate, and probably selective to mineral ions present in the fermentation broth. **Figure 5** compares the ethanol concentration in the broth and the permeate during the course of fermentation; for operation in PV mode, a concentration of ethanol 4 times was obtained in the collected permeate. As shown in **Figure 5**, the ethanol concentration in the broth did not rise above

107 g l^{-1} . This limited the inhibition phenomena and extended the culture activity in time.

Another case of a bioreactor coupled with PV using SLMs has been investigated by Matsumura *et al.* [65]. Continuous butanol/isopropanol fermentation with immobilized *Clostridium isopropylicum* was performed in a downflow column reactor using molasses as the substrate. In order to prevent product inhibition and, at the same time, obtain high concentration of the products, the column reactor was coupled with a PV module. The LM was prepared with OA nontoxic to the microorganism. In comparison with the continuous fermentation without product removal, the specific butanol production rate was 2 times higher. The butanol concentration in the permeate was 230 kg m^{-3} , which was about 50 times higher than that in the culture broth. A stable fermentation continued up to 270 h, and the average butanol concentration was maintained at a rather low value of 4.5 kg m^{-3} owing to the PV. The butanol concentration in the reactor without product removal was estimated to be 7.9 kg m^{-3} from the experimental result at the same dilution rate of 0.129 h^{-1} . In this manner, the butanol inhibition was alleviated by coupling the fermentation with PV, and this resulted in increased specific rates of substrate consumption and solvent production. In a later study [66], this research group reported the application of the same methodology to diacetyl fermentation by immobilized lactic acid bacteria. OA immobilized in the porous of polypropylene hollow fiber was used as LM. Diacetyl productivity in fermentation coupled with PV was about $10 \text{ g m}^{-3} \text{ h}^{-1}$, while productivity during batch fermentation was about $6 \text{ g m}^{-3} \text{ h}^{-1}$. Diacetyl yield from consumed glucose was about 0.04 g g^{-1} , which was 4 times as large as that of batch fermentation. The PV functioned favorably on actual fermentation broth and no membrane fouling was observed. The flux of the permeate and the diacetyl separation factor for the PV were about $9 \text{ g m}^{-2} \text{ h}^{-1}$ and 36, respectively, and these values were maintained at almost constant levels during fermentation. Diacetyl concentration in the permeate was about 2 kg m^{-3} , which is considered sufficiently high for commercial use.

Qin *et al.* [12] reported the separation of TCE from their aqueous solutions by using an LM consisting of nonvolatile hydrophobic hydrocarbons immobilized in the micropores of hydrophobic porous propylene hollow fibers with or without a plasma-polymerized ultrathin silicone membrane on the outside diameter of the fibers. In that study, the feed TCE concentration was varied between 50 and

Table 4 Separation of *n*-butanol from dilute aqueous solutions by pervaporation through SLM and polymeric membranes

<i>Membrane</i>	<i>Feed concentration</i> (wt. %)	<i>Permeate concentration</i> (wt. %)	<i>Separation</i> <i>factor</i>	<i>Total flux</i> (g m ⁻² h ⁻¹)	<i>Operative</i> <i>conditions</i>	<i>References</i>
Oleyl alcohol supported by microporous polypropylene flat sheet, 25- μ m thickness	0.5	46	171	50	30 °C, permeate pressure 133 Pa	[63]
	1.0	64	176	81		
	1.5	75	197	109		
	3.0	85	183	284		
Trioctylamine supported by microporous polypropylene hollow fiber, 50- μ m thickness	1.5	62.3	108.4	6.4	25 °C, permeate pressure 467 Pa	[68]
	2.0	72	126.4	8.2		
	2.5	78.3	141.2	10		
PDMS, 180- μ m thickness	0.5	25	66	50	30 °C, permeate pressure 100 Pa	[63]
	1.0	42.5	72	87		
	2.6	67.5	78	135		
	6.1	84	82	170		
Silicone rubber, 50- μ m thickness	1.0	37	58.1	70	50 °C	[61]
Polyurethane, 50- μ m thickness	1.0	11	13	88	50 °C	[61]
Polyether block amide, 50- μ m thickness	1.0	20	25	278	50 °C	[61]
Silicalite-silicone composite membrane (Pervap-1070), active layer thickness 29 μ m	1.0	30.8	44	50	30 °C, permeate pressure 400 Pa	[62]

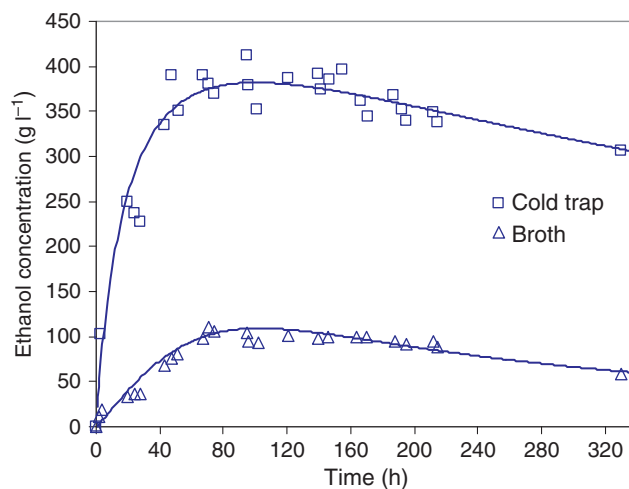


Figure 5 Evolution of ethanol concentration in broth and condensed permeate vs. time. Adapted from Christen, P., Minier, M., Renon, H. *Biotechnol. Bioeng.* **1990**, 36, 116–123.

950 ppm and the operative conditions were 25 °C, essentially atmospheric pressure at the feed side (lumen side), and the permeate pressure range was 80–9330 Pa. In most of the experiments, pure hexadecane (C₁₆H₃₄) and pure dodecane (C₁₂H₂₆) were employed as LMs, spanning the whole thickness of the microporous substrate with or without a silicone coating. Based on experimental results with dodecane immobilized, it can be concluded that when the LM material does not fully fill the micropores on the wall, there will be an increase in the water flux and decreases in the TCE flux, the fractional TCE removal, and the selectivity because the micropores are at least partially wetted by the feed in the presence of the LM. On the other hand, the volatility of dodecane could not provide stable operation for an extended period. The hexadecane SLM was found to be permselective for TCE: the experimental selectivity was 30 000, and the intrinsic selectivity (in absence of concentration polarization) could be as high as 2×10^5 , much higher than the values reportedly obtained by any solid membrane. The performance of a hexadecane LM for TCE removal is illustrated in [Figure 6](#) for pure hexadecane immobilized in the micropores of hollow fibers without any silicone coating. Because of the large partition coefficient of TCE between hexadecane and water, the LM resistance to TCE was found to be much less than the lumen-side boundary resistance. The hexadecane SLM performance indicated long-term stability: about 30% decreases in both PV flux and selectivity were observed in a run lasting 4 months.

Qin *et al.* [67] studied the removal and enrichment of acetic acid from its dilute aqueous solutions by PV through an SLM with reactive extractants. The SLM consisted of a fatty amine, as well as its mixtures with a higher fatty alcohol (OA). When tested as an LM in PV, most extractants used for conventional extraction of acetic acid from aqueous solutions were acetic acid selective. The influence of the LM composition, LM thickness, feed concentration, and temperature on the permeability, selectivity, and stability of the SLM was studied. Limited studies of butyric acid were also done. Among various extractants tested, trioctylamine (TOA) and tri-laurylamine (TLA) demonstrated defect-free performances for more than 500 h. During this period, the acetic acid concentration in the permeate, the selectivity, and the acetic acid permeation flux decreased gradually. This is because the properties of the substrate membrane, porous hydrophobic polypropylene hollow fiber, changed gradually with operation; it is also due to the loss of extractants from the LM through evaporation to the permeate side and the solubilization to the feed during the operation. Several complexes can exist in the organic phase, and the complex can be stabilized by the modifier. It was found that the resistance for the diffusion of species in the LM is much larger than the resistance for the diffusion of acetic acid in the bulk feed. The acetic acid selectivity can be as high as 33 for a feed of 1 M at 60 °C, an order of magnitude higher than that obtained by any solid polymeric membrane reported in the literature; however, the acetic acid permeation flux was much lower than those obtained for polymer membranes

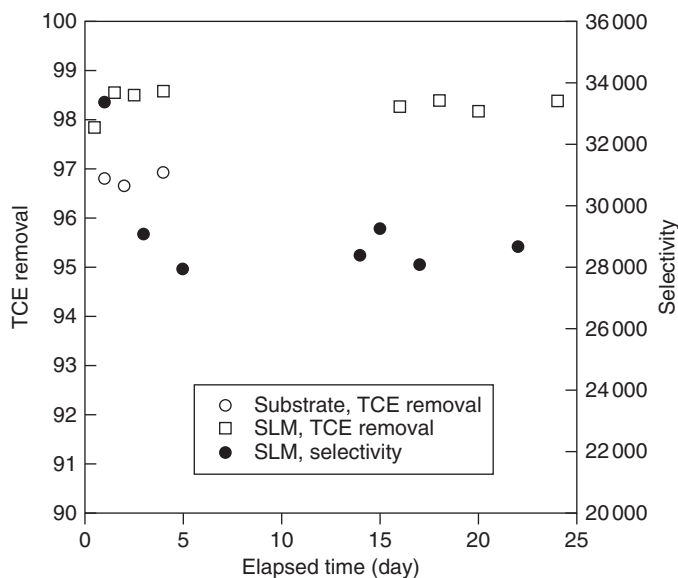


Figure 6 Trichloroethylene (TCE) removal and selectivity of the hexadecane supported liquid membrane (SLM) as a function of time (hollow fibers without silicone coating, $P_{\text{perm}} = 133$ Pa, $C_{\text{feed-in}} = 850\text{--}950$ ppm, $V = 2.5$ ml min^{-1}). Reproduced from Qin, Y., Sheth, J. P., Sirkar, K. K. *Ind. Eng. Chem. Res.* **2002**, *41*, 3413–3428.

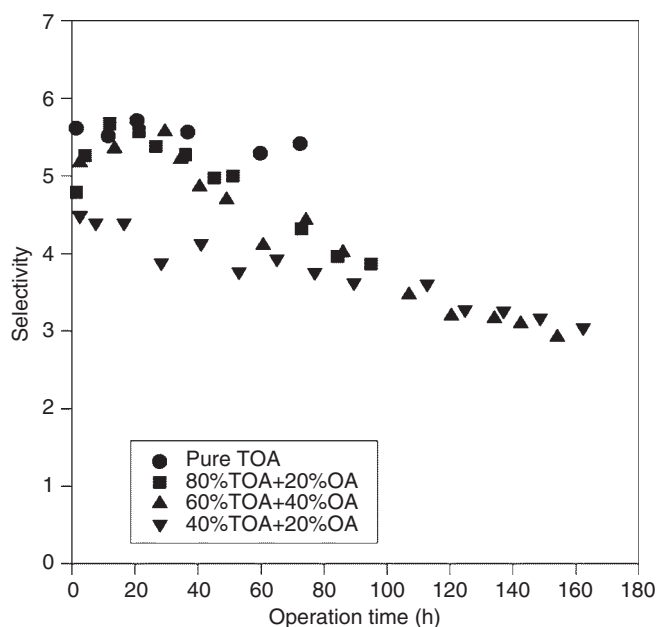


Figure 7 Dependence on the liquid membrane composition of the acetic acid selectivity (microporous polypropylene hollow fibers as support, $T = 35^\circ\text{C}$, $P_{\text{perm}} = 667$ Pa, $C_{\text{feed-in}} = 1$ M, $V = 1$ ml min^{-1}). Reproduced from Qin, Y., Sheth, J. P., Sirkar, K. K. *Ind. Eng. Chem. Res.* **2003**, *42*, 582–595.

having low acetic acid selectivities. In addition, it was found that a higher vacuum (lower permeate pressure) always led to a higher acid concentration in the permeate, a higher acetic acid selectivity, and a higher acetic acid flux. In this work, OA was evaluated as a modifier; **Figure 7** shows the effect of

different compositions of the TOA/OA LM on the selectivity; it can be seen that pure TOA provided the highest acetic acid selectivity and stability.

Recently, Thongsukmak and Sirkar [68] reported a new LM-based PV technique that has been developed to ensure stability and prevent contamination of

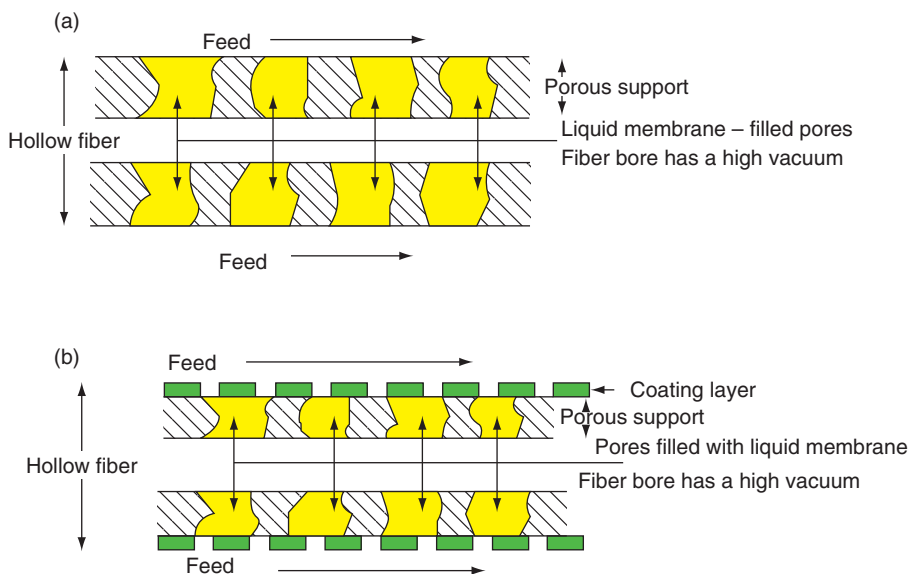


Figure 8 Liquid membrane immobilized in porous hydrophobic hollow fiber membranes: (a) fiber without any coating and pores completely filled by liquid membrane; (b) fiber with a nanoporous coating on the outside surface. From Thongsukmak, A., Sirkar, K. K. *J. Membr. Sci.* **2007**, *302*, 45–58.

the fermentation broth. TOA as an LM was immobilized in the pores of a hydrophobic hollow fiber substrate having a nanoporous coating on the broth side and studied for PV-based removal of solvents (acetone, ethanol, and butanol) from their dilute aqueous solutions. A scheme of used membranes is shown in **Figure 8**. The LM of TOA in the coated hollow fibers demonstrated high selectivity and reasonable mass fluxes of solvents in PV. Experiments were carried out with the feed mixture at various temperatures up to 54°C. The selectivity and mass flux of solvents were increased at elevated temperatures as shown in **Figure 9**. The selectivities of butanol, acetone, and ethanol achieved were 275, 220, and 80, respectively, with 11.0, 5.0, and 1.2 g m⁻² h⁻¹ for the mass fluxes of butanol, acetone, and ethanol, respectively, at a temperature of 54°C for a feed solution containing 1.5 wt.% butanol, 0.8 wt.% acetone, and 0.5 wt.% ethanol. However, acetic acid in the feed solution reduced the selectivities of the solvents without reducing the solvent fluxes due to coextraction of water which increases the rate of water permeation to the vacuum side.

Another membrane process, VP, is also promising for hydrocarbon separation. This process has the advantage of selecting the membrane material, because the membrane does not contact the organic liquids which may cause deterioration of the membrane material. On the other hand, a drawback of the

VP process is its low flux compared to the PV process. Recently, there is a rapid development in the field of separation of hydrocarbons focused on the isolation of aromatics from aliphatic hydrocarbons. Particularly, the separation of benzene is one of the most important and most difficult processes in the petrochemical industry [69]. VP of a benzene and cyclohexane mixture was studied by Yamanouchi *et al.* [70] using an LM of triethylene glycol (TEG), which is supported on the surface of a microporous hydrophobic membrane. Permeation experiments were conducted using a flat-type membrane cell under the conditions of atmospheric pressure on the feed side and a vacuum on the permeate side. Mixed vapors of benzene/cyclohexane and water were fed into the membrane cell by a carrier gas. The benzene vapor preferentially permeated through the TEG LM; the separation factor for benzene over cyclohexane was around 8. This selectivity corresponded to the vapor–liquid equilibrium of hydrocarbons dissolved in TEG. Adding a salt to the TEG LM caused an increasing aromatic selectivity as well as a decreasing VP rate. In another study [71], this research group reported the permeation of gasoline vapor using the same LMs. The feed vapor consisted of C5–C8 hydrocarbons, in which 72–87% was aromatic. The vapor that permeated through the TEG LM was 98–99% aromatic. The selectivities for C6 and C7 aromatic hydrocarbons over paraffin

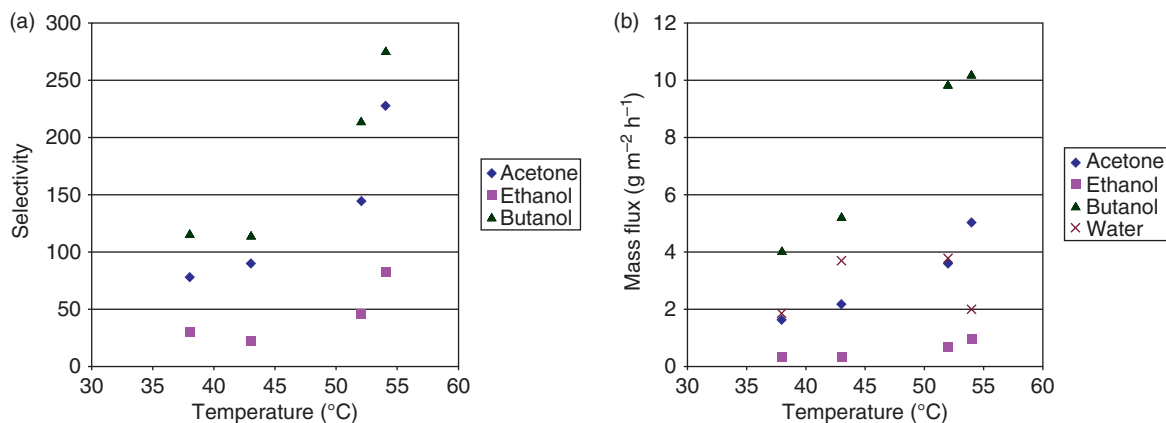


Figure 9 Performance of trioctylamine (TOA) as the liquid membrane with coated hollow fibers as the support with a feed mixture at different temperatures: (a) selectivity and (b) mass flux (pure TOA as liquid membrane, feed composition: acetone 0.8 wt.%, ethanol 0.5 wt.%, butanol 1.5 wt.%). From Thongsukmak, A., Sirkar, K. K. *J. Membr. Sci.* **2007**, 302, 45–58.

hydrocarbons were 47 and 15, respectively. Obuskovic *et al.* [72], in a study about the selective removal of VOCs from nitrogen, used a thin SLM of silicone oil incorporated in the micropores of a hydrophobic hollow fiber with a silicone rubber coating. The observed benefits of having the thin immobilized LM incorporated in the microporous structure were 2–5 times more VOC-enriched permeate since the nitrogen flux was drastically reduced, and the separation factor was 5–20 times increased depending on the type of the VOC and the feed gas flow rate. These authors report that the SLM was stable over an extended period (6 months to 2 years) demonstrating the potential utility of such an SLM-based hollow fiber device for VOC-N₂/air separation.

Recent works in this field have been addressed to the use of ILs as material for LMs to constitute the so-called SILMs. Izák *et al.* [27] reported the use of PV with SILMs for removal of 1,3-propanediol from aqueous solutions. A hydrophobic IL (tetrapropylammonium tetracyanoborate [(C₃H₇)₄N][B(CN)₄]) and a nanofiltration ceramic module with pore size 0.9 nm as support were used. First, they evaluated the transport of the solute (1,3-propanediol) from aqueous mixture through an empty ceramic nanofiltration module under low pressure (80 Pa) at room temperature; then PV experiments with an impregnated module were performed. When the IL is in the pores of module due to its hydrophobicity, the preferentially permeating component is 1,3-propanediol, with an average separation factor of 5.6, in comparison with a separation factor of 0.4 obtained with the nanofiltration module without IL. Further coating with

PDMS of the ceramic module with IL inside the pores caused an important increase of separation factor (Figure 10); however, it also decreased the 1,3-propanediol flux through the permselective barrier.

As for other options to increase the stability of LMs, Izák *et al.* [58] immobilized a mixture of IL-polymer in the porous of a ultrafiltration membrane. The ultrafiltration membranes were impregnated by two ILs (1-ethenyl-3-ethyl-imidazolium hexafluorophosphate (IL1) and tetrapropylammonium tetracyano-borate (IL2)) and PDMS. These SILMs were used for separation of ternary mixtures butan-1-ol–acetone–water by vacuum PV. In comparison with a PDMS membrane, the enrichment factor of butan-1-ol increased from 2.2 (PDMS) to 3.1 (PDMS–IL1) and to 10.9 (PDMS–IL2). In the case of acetone, the enrichment factor increased from 2.3 (PDMS) to 3.2 (PDMS–IL1) and to 7.9 (PDMS–IL2). Although the separation process with IL–PDMS membranes is a little bit slower, its higher selectivity shows a good potential for the improvement of downstream separation processes. The PV of the system was checked after 5 months and no changes in transport properties or stability of the SILM were observed. In a later study [73], this research group reported the experimental results obtained with acetone–butanol–ethanol (ABE) fermentation coupled to PV, as shown in Figure 11. The SILM was impregnated with 15 wt.% of an IL (tetrapropylammonium tetracyano-borate) and 85 wt.% of PDMS. As a support matrix for the nonporous membrane, we used the ceramic ultrafiltration membrane made from TiO₂ with a pore size of 60 nm. Using this membrane, butan-1-ol concentration in the permeate increased

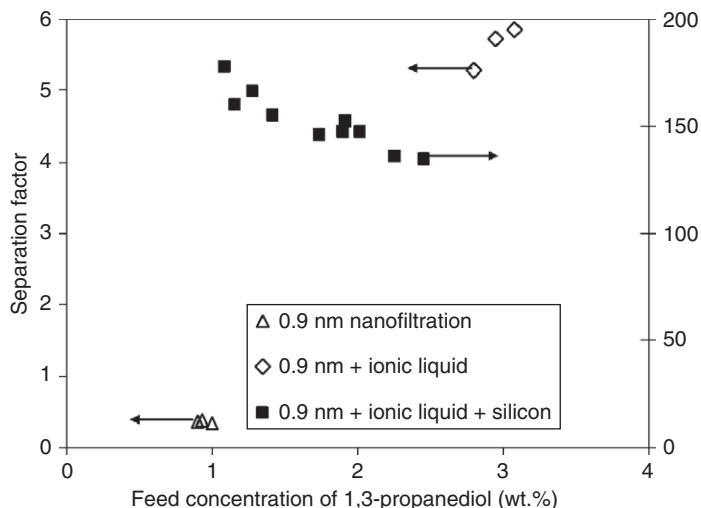


Figure 10 Separation of 1,3-propanediol from aqueous solutions by pervaporation with supported ionic liquid membrane (SILM). Dependence of selectivity on feed concentration of 1,3-propanediol at 22 °C. From Izák, P., Köckerling, M., Kragl, U. *Desalination* **2006**, 199, 96–98.

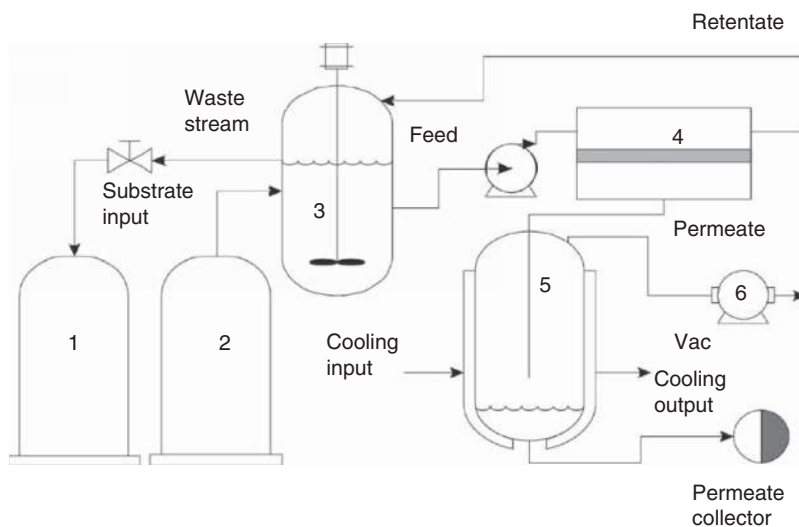


Figure 11 Schema of continuous culture fermentation connected with pervaporation. 1, waste tank; 2, tank with substrate; 3, culture vessel; 4, pervaporation cell; 5, cold trap; 6, vacuum pump. From Izák, P., Schwarz, K., Ruth, W., Bahl, H., Kragl, U. *Appl. Microbiol. Biotechnol.* **2008**, 78, 597–602.

more than 5 times in comparison with the concentration in the culture vessel. In addition, the other products of ABE fermentation (ethanol and acetone) were enriched several times in the permeate.

In another procedure by Yu *et al.* [74], combining ILs and PV, a hydrophobic IL (BMImPF_6) was introduced as the third phase between the aqueous phase and the plain PDMS membrane for improving mass transfer of acetic acid from its aqueous matrix to the PDMS membrane. Their primary results indicated

that the IL as an extractant prior to PV was favorable for improving the permeate selectivity and the permeate flux of acetic acid compared with using only a plain PDMS membrane.

Recently, several applications of SILMs to gas separation have been reported in literature [75]. ILs can selectively dissolve gases; this makes them potential solvents for gas separations. Four different ILs were immobilized in porous hydrophilic polyether-sulfone supports and examined for the flux and

selectivity of CO₂/N₂ and CO₂/CH₄. The selectivities for CO₂/N₂ (61) and CO₂/CH₄ (20) were achieved with the 1-ethyl-3-methylimidazolium dicyanamide supported membrane [51]. Another research group used an alumina membrane filled with [BMIm][NTf₂] to achieve a selectivity of 127 for CO₂/N₂ [26]. With nanofiltration membranes as support, four ILs were immobilized. The permeability of the gas molecules H₂, O₂, N₂, and CO was examined. A selectivity of 4.3 for H₂/CO₂ was achieved [76].

There are several promising applications of SILM/PV, such as aroma recovery, separation of olefin/paraffin mixtures, and product recovery from fermentation broths for enhanced bioconversions. The separation of organic–organic mixtures is presently the least developed application of PV because of the problems normally associated with membrane stability under relatively harsh conditions; however, it represents the largest opportunity for energy and cost savings. In the development of LMs for olefin/paraffin separation, the concept of carrier-mediated facilitated transport is often combined with the so-called silver complexation [77, 78]. A silver salt reversibly binds to an olefin molecule building a complex. This complex diffuses to the permeate side of the membrane where the olefin is unbound from the complex. Hence, the facilitated transport constitutes a combination of physical diffusion enhanced by reversible chemical reaction and diffusion of the complex. Recently, the selective absorption of propylene from their mixtures with propane by chemical complexation with silver ions in IL solutions has been performed [79].

2.12.6 Concluding Remarks

The membrane permeability value can be increased by increasing either the distribution coefficient or the diffusivity for the transported solute. The idea of using thin organic liquid layers as PV membranes seems to be very attractive from this point of view simply because the value of diffusivity in liquids is at least three to four orders of magnitude higher than values in solid polymers and in inorganic membranes. Besides, it is possible to dissolve some selective carriers in the immobilized liquid, so that they will be able to interact with the transported species, increasing the affinity of the solute and, thus, the process selectivity.

There are two primary constraints associated with the use of SLMs. Solvent loss can occur by evaporation, dissolution, or large pressure differences forcing the solvent out of the pore support structure. In addition, carrier loss can occur. This loss can be due to irreversible side reactions or solvent condensation on one side of the membrane. Pressure differences can force the liquid to flow through the pore structure and leach out the carrier. In comparison to solid membranes for PV, LMs are used at moderate temperatures, because the stability problems increase at high temperatures. The stability of LMs can be increased drastically by placing a thin polymer layer on top of the LM; however, often it implies a reduction of the permeation flux.

Since ILs do not show measurable vapor pressures, they might overcome stability problems of common SLMs caused by evaporation of the membrane phase. In addition, mechanical stability of the SLM is increased due to the improved wetting properties of ILs.

Main applications reported in literature have been addressed to separate volatile fermentation products and other VOCs from their dilute aqueous solutions. The use of PV coupled to a fermenter acts not only as a means of separation, but also as a production enhancer by reducing product inhibition. Further applications (i.e., organic–organic separations) should be explored taking into account the use of suitable ILs as immobilized liquid in SLMs. ILs can dissolve a very broad spectrum of organic compounds, and their miscibility with these substances can be fine-tuned by changing the nature of the cation and/or anion. However, so far the separations of organic–organic mixtures by using hydrophilic ILs have been limited by interfacial instability phenomena at the feed/membrane interface. Future efforts should be directed toward developing systems with improved stability.

Acknowledgments

The authors gratefully acknowledge the financial support from projects CTQ2008-00690/PPQ and CTM2006-00317.

References

- [1] Feng, X., Huang, R. Y. M. *Ind. Eng. Chem. Res.* **1997**, *36*, 1048–1066.
- [2] Jonquière, A., Clément, R., Lochon, P. *J. Membr. Sci.* **2002**, *206*, 87–117.

- [3] Chapman, P. D., Oliveira, T., Livingston, A. G., Li, K. J. *Membr. Sci.* **2008**, *318*, 5–37.
- [4] Urriaga, A. M., Gorri, D., Gómez, P., Casado, C., Ibáñez, R., Ortiz, I. *Dry. Technol.* **2007**, *25*, 1819–1828.
- [5] Urriaga, A. M., Gorri, D., Ortiz, I. *AIChE J.* **2002**, *48*, 572–581.
- [6] Lipnizki, F., Hausmanns, S., Ten, P.-K., Field, R. W., Laufenberg, G. *Chem. Eng. J.* **1999**, *73*, 113–129.
- [7] Vane, L. M. *J. Chem. Technol. Biotechnol.* **2005**, *80*, 603–629.
- [8] Schäfer, T., Crespo, J. G. *Vapour Permeation and Pervaporation. In Green Separation Processes; Afonso, C. A. M., Crespo, J. G., Eds.; Wiley-VCH: Weinheim, 2005; pp 271–289.*
- [9] Gorri, D., Ibáñez, R., Ortiz, I. *J. Membr. Sci.* **2006**, *280*, 582–593.
- [10] Néel, J. *Pervaporation; Lavoisier: Paris, 1997.*
- [11] Shao, P., Huang, R. Y. M. *J. Membr. Sci.* **2007**, *287*, 162–179.
- [12] Qin, Y., Sheth, J. P., Sirkar, K. K. *Ind. Eng. Chem. Res.* **2002**, *41*, 3413–3428.
- [13] Li, K. *Ceramic Membranes for Separation and Reaction; Wiley: Chichester, 2007; Chapter 1, pp 1–20.*
- [14] Strathmann, H. *Synthetic Membranes and Their Preparation. In Handbook of Industrial Membrane Technology; Porter, M. C., Ed.; Noyes Publications: Park Ridge, NJ, 1990; pp 1–60.*
- [15] Cussler, E. L. *Diffusion – Mass Transfer in Fluid Systems, 2nd edn.; Cambridge University Press: Cambridge, 1997.*
- [16] Urriaga, A. M., Ortiz, M. I., Alonso, A. I., Irabien, J. A. *Trends Chem. Eng.* **1993**, *1*, 103–121.
- [17] Noble, R. D., Way, J. D. *Facilitated Transport. In Membrane Handbook; Ho, W. S. W., Sirkar, K. K., Eds.; Chapman and Hall: New York, 1992; pp 833–866.*
- [18] Kocherginsky, N. M., Yang, Q., Seelam, L. *Sep. Purif. Technol.* **2007**, *53*, 171–177.
- [19] Boyadzhiev, L., Lazarova, Z. *Liquid Membranes (Liquid Pertraction). In Membrane Separations Technology: Principles and Applications; Noble, R. D., Stern, S. A., Eds.; Elsevier: Amsterdam, 1995; Chapter 7, pp 284–285.*
- [20] Urriaga, A. M., Ortiz, M. I., Salazar, E., Irabien, J. A. *Ind. Eng. Chem. Res.* **1992**, *31*, 877–886.
- [21] Noble, R. D., Way, J. D., Eds. *Liquid Membranes: Theory and Applications; ACS Symposium Series 347; American Chemical Society: Washington, DC, 1987.*
- [22] Noble, R. D., Way, J. D. *Description of Facilitated Transport and Environmental Applications. In Membrane Processes in Separation and Purification; Crespo, J. G., Bøddeker, K. W., Eds.; Kluwer: Dordrecht, 1994; pp 317–342.*
- [23] Noble, R. D., Koval, C. A. *Review of Facilitated Transport Membranes. In Materials Science of Membrane for Gas and Vapor Separation; Yampolskii, Y., Pinnau, I., Freeman, B. D., Eds.; Wiley: Chichester, 2006; Chapter 17, pp 411–435.*
- [24] Way, J. D., Noble, R. D., Bateman, B. R. *Selection of Supports for Immobilized Membranes. In Materials Science of Synthetic Membranes; Lloyd, D. R., Ed.; ACS Symposium Series; American Chemical Society: Washington, DC, 1985; Vol. 269, pp 119–128.*
- [25] Mulder, M. *Basic Principles of Membrane Technology, 2nd edn.; Kluwer: Dordrecht, 1996.*
- [26] Baltus, R. E., Counce, R. M., Culbertson, B. H., et al. *Sep. Sci. Technol.* **2005**, *40*, 525–541.
- [27] Izák, P., Köckerling, M., Kragl, U. *Desalination* **2006**, *199*, 96–98.
- [28] Krull, F. F., Medved, M., Melin, T. *Chem. Eng. Sci.* **2007**, *62*, 5579–5585.
- [29] Nørgaard, A. M., Bargeman, D., Smolders, C. A. J. *Membr. Sci.* **1992**, *67*, 133–148.
- [30] Zha, F. F., Fane, A. G., Fell, C. J. D. *J. Membr. Sci.* **1995**, *107*, 59–74.
- [31] Kemperman, A. J. B., Bargeman, D., Van Den Boomgaard, Th., Strathmann, H. *Sep. Sci. Technol.* **1996**, *31*, 2733–2762.
- [32] Danesi, P. R., Reichley-Yinger, L., Rickert, P. G. J. *Membr. Sci.* **1987**, *31*, 117–145.
- [33] Zha, F. F., Fane, A. G., Fell, C. J. D., Schofield, R. W. J. *Membr. Sci.* **1992**, *75*, 69–80.
- [34] Nakano, M., Takahashi, K., Takeuchi, H. *J. Chem. Eng. Jpn.* **1987**, *20*, 326–328.
- [35] Kemperman, A. J. B., Rolevink, H. H. M., Bargeman, D., van den Boomgaard, Th., Strathmann, H. *J. Membr. Sci.* **1998**, *138*, 43–55.
- [36] Yang, X. J., Fane, A. G., Bi, J., Griesser, H. J. *J. Membr. Sci.* **2000**, *168*, 29–37.
- [37] Côté, P., Lipski, C. *Mass Transfer Limitations in Pervaporation for Water and Wastewater Treatment. In Proceedings of Third International Conference on Pervaporation Processes in the Chemical Industry, Nancy, France, 19–22 September 1988; Bakish, R., Ed.; Bakish Materials Corporation: Englewood, NJ, 1988.*
- [38] Liu, M. G., Dickson, J. M., Côté, P. *J. Membr. Sci.* **1996**, *111*, 227–241.
- [39] Lipnizki, F., Trägårdh, G. *Sep. Purif. Methods* **2001**, *30*, 49–125.
- [40] Bøddeker, K. W. *Liquid Separations with Membranes; Springer: Berlin, 2008.*
- [41] Noble, R. D., Way, J. D., Powers, L. A. *Ind. Eng. Chem. Fundam.* **1986**, *25*, 452–455.
- [42] Drioli, E., Criscuoli, A., Curcio, E. *Membrane Contactors: Fundamentals, Applications and Potentialities; Elsevier: Amsterdam, 2006; Chapter 9, pp 308–344.*
- [43] Baker, R., Blume, I. *Coupled Transport Membranes. In Handbook of Industrial Membrane Technology; Porter, M. C., Ed.; Noyes Publications: NJ, 1990; pp 551–558.*
- [44] Baker, R. *Membrane Technology and Applications, 2nd edn.; Wiley: New York, 2004; Chapter 11, pp 425–463.*
- [45] Noble, R. D. *J. Membr. Sci.* **1991**, *56*, 229–234.
- [46] Zhao, H., Xia, S., Ma, P. *J. Chem. Technol. Biotechnol.* **2005**, *80*, 1089–1096.
- [47] Gan, Q., Rooney, D., Zou, Y. *Desalination* **2006**, *199*, 535–537.
- [48] Dupont, J. *Ionic Liquids: Structure, Properties and Major Applications in Extraction/Reaction Technology. In Green Separation Processes; Afonso, C. A. M., Crespo, J. G., Eds.; Wiley-VCH: Weinheim, 2005; pp 229–250.*
- [49] Scovazzo, P., Visser, A., Davis, J., et al. *Supported Ionic Liquid Membranes and Facilitated Ionic Liquid Membranes. In Ionic Liquids: Industrial Applications for Green Chemistry; Rogers, R., Seddon, K., Eds.; American Chemical Society: Washington, DC, 2002; Chapter 6, pp 69–89.*
- [50] Schäfer, T., Paolo, R. E. D., Franco, R., Crespo, J. G. *Chem. Commun.* **2005**, 2594–2596.
- [51] Scovazzo, P., Kieft, J., Finan, D. A., Koval, C., DuBois, D., Noble, R. *J. Membr. Sci.* **2004**, *238*, 57–63.
- [52] Branco, L. C., Crespo, J. G., Afonso, C. A. M. *Chem. Eur. J.* **2002**, *8*, 3865–3871.
- [53] Fortunato, R., González-Muñoz, M. J., Kubasiewicz, M., et al. *J. Membr. Sci.* **2005**, *249*, 153–162.
- [54] Hernández-Fernández, F. J., de los Ríos, A. P., Rubio, M., Tomás-Alonso, F., Gómez, D., Villora, G. *J. Membr. Sci.* **2007**, *293*, 73–80.
- [55] Marták, J., Schlosser, Š., Vičková, S. *J. Membr. Sci.* **2008**, *318*, 298–310.
- [56] Ilconich, J., Myers, C., Pennline, H., Luebke, D. *J. Membr. Sci.* **2007**, *298*, 41–47.

- [57] Myers, C., Pennline, H., Luebke, D., *et al.* *J. Membr. Sci.* **2008**, *322*, 28–31.
- [58] Izák, P., Ruth, W., Fei, Z., Dyson, P. J., Kragl, U. *Chem. Eng. J.* **2008**, *139*, 318–321.
- [59] Strathmann, H., Gudernatsch, W. Pervaporation in Biotechnology. In *Pervaporation Membrane Separation Processes*; Huang, R. Y. M., Ed.; Elsevier: Amsterdam, 1991; pp 363–389.
- [60] Hickey, P. J., Slater, C. S. *Sep. Purif. Methods* **1990**, *19*, 93–115.
- [61] Boddeker, K. W., Bengtson, G., Pingel, H. *J. Membr. Sci.* **1990**, *54*, 1–12.
- [62] Huang, J., Meagher, M. M. *J. Membr. Sci.* **2001**, *192*, 231–242.
- [63] Matsumura, M., Kataoka, H. *Biotechnol. Bioeng.* **1987**, *30*, 887–895.
- [64] Christen, P., Minier, M., Renon, H. *Biotechnol. Bioeng.* **1990**, *36*, 116–123.
- [65] Matsumura, M., Takehara, S., Kataoka, H. *Biotechnol. Bioeng.* **1992**, *39*, 148–156.
- [66] Ishii, N., Matsumura, M., Kataoka, H., Tanaka, H., Araki, K. *Bioprocess Eng.* **1995**, *13*, 119–123.
- [67] Qin, Y., Sheth, J. P., Sirkar, K. K. *Ind. Eng. Chem. Res.* **2003**, *42*, 582–595.
- [68] Thongsukmak, A., Sirkar, K. K. *J. Membr. Sci.* **2007**, *302*, 45–58.
- [69] Garcia Villaluenga, J. P., Tabe-Mohammadi, A. *J. Membr. Sci.* **2000**, *169*, 159–174.
- [70] Yamanouchi, N., Ito, A., Yamagiwa, K. *J. Chem. Eng. Japan* **2003**, *36*, 1070–1075.
- [71] Yamanouchi, N., Ito, A., Yamagiwa, K. *J. Chem. Eng. Japan* **2004**, *37*, 1271–1273.
- [72] Obuskovic, G., Majumdar, S., Sirkar, K. K. *J. Membr. Sci.* **2003**, *217*, 99–116.
- [73] Izák, P., Schwarz, K., Ruth, W., Bahl, H., Kragl, U. *Appl. Microbiol. Biotechnol.* **2008**, *78*, 597–602.
- [74] Yu, J., Li, H., Liu, H. *Chem. Eng. Comm.* **2006**, *193*, 1422–1430.
- [75] Han, X., Armstrong, D. W. *Acc. Chem. Res.* **2007**, *40*, 1079–1086.
- [76] Gan, Q., Rooney, D., Xue, M., Thompson, G., Zou, Y. *J. Membr. Sci.* **2006**, *280*, 948–956.
- [77] Kovvali, A. S., Chen, H., Sirkar, K. K. *Ind. Eng. Chem. Res.* **2002**, *41*, 347–356.
- [78] Duan, S., Ito, A., Ohkawa, A. *J. Membr. Sci.* **2003**, *215*, 53–60.
- [79] Ortiz, A., Ruiz, A., Gorri, D., Ortiz, I. *Sep. Purif. Technol.* **2008**, *63*, 311–318.

Relevant Website

<http://ilthermo.boulder.nist.gov> – IUPAC Ionic Liquids Database.

Biographical Sketches



Daniel Gorri received his diploma in chemical engineering (1995) from the Universidad Tecnológica Nacional, Argentina, and his PhD in chemical engineering (2000) from the University of Cantabria, Spain, where he is currently an associate professor of chemical engineering at the School of Engineering. During 1988–96 he worked for the National Institute of Vitiviniculture, Analytical Laboratory Section (Argentina). He was a visiting researcher at the University of Bologna. His research interests focus on the development of membrane technologies in separation and reaction.



Ane Urtiaga received her bachelor's degree in chemistry (1986) from the University of the Basque Country, Spain, and her MSc in Materials Engineering (1987), Cranfield Institute of Technology, UK. She received her PhD in chemical engineering (1991) from the University of the Basque Country for her thesis "Application of supported liquid membranes to phenol recovery in hollow fiber contactors."

During 1991–92 she worked for the company Unión Española de Explosivos (UEE) SA. Thereafter, she joined the University of Cantabria, where she became a full professor in 2007. Dr. Urtiaga is now the head of the Chemical Engineering Department at the UC.

Dr. Ane Urtiaga is responsible for the research on membrane technology for the development of clean industrial processes, the separation and recovery of heavy metals and organic compounds from industrial wastewaters, recovery of spent solvents, dehydration of raw materials, and the separation of high added-value components. Her current research is also focused on the advanced treatment of reclaimed water for industrial uses.

Dr. Urtiaga has published numerous scientific papers in the fields of chemical engineering and membrane processes. In addition, she has been responsible for research projects with the financial support of the Spanish Ministries of Science and Environment and the European Commission, as well as research contracts with industrial companies. She has supervised five PhD theses.



Inmaculada Ortiz is currently a professor of chemical engineering and former head of the department at Universidad de Cantabria, Spain. She obtained her BS degree and PhD in sciences (chemistry) at the Universidad del País Vasco in 1980 and 1985, respectively. After lecturing in chemical engineering at the Universidad del País Vasco, she joined Cantabria in 1992. She was a scientific officer of the National R&D Programmes on Environment, Chemical Processes and Products and Natural Resources: Environmental Technologies during 1998–2000 and 2000–02, respectively. She was proposed as a coordinator of the chemical technology area of the Spanish ANEP (National Agency of Evaluation and Prospective) for the period 2005–08. Recently (May, 2008), she has been nominated as correspondent member of the Spanish Real Academia de Ciencias Exactas, Físicas y Naturales.

She is currently the leader of the research group Advanced Separation Processes. The research interests of Inmaculada Ortiz are in the areas of (1) design, intensification, and integration of separation processes according to the concept of sustainability and (2) R&D of clean techniques and clean processes for the treatment of wastewaters and hazardous effluents.

She has been responsible of the development of more than 40 R&D projects funded by international (UE) and national public and private organizations. She has authored more than 150 papers and has advised 20 PhD students.

2.13 Progress in the Development of Membranes for Kidney-Replacement Therapy

C Zweigart, M Neubauer, M Storr, T Böhler, and B Krause, Gambro Dialysatoren GmbH, Hechingen, Germany

© 2010 Elsevier B.V. All rights reserved.

2.13.1	Introduction	352
2.13.2	Renal-Replacement Therapy	353
2.13.3	Dialysis Membranes	353
2.13.3.1	Membrane Requirements in RRT	353
2.13.3.2	Membrane Materials	354
2.13.3.2.1	Cellulose membranes	355
2.13.3.2.2	Regenerated cellulose	356
2.13.3.2.3	Synthetically modified cellulose	356
2.13.3.2.4	Synthetic polymeric membranes	356
2.13.3.2.5	Polysulfone/polyethersulfone/polyvinylpyrrolidone (PVP)/ polyamide membranes	357
2.13.3.2.6	PAN membranes	358
2.13.3.2.7	Polymethylmethacrylate membranes	359
2.13.3.2.8	Ethylenvinylalcohol membrane	359
2.13.3.3	Membrane Characteristics: Low- and High-Flux Membranes	359
2.13.4	Biocompatibility of Dialysis Membranes	361
2.13.5	Operation Modes of Dialysis Treatment	363
2.13.5.1	Hemodialysis	364
2.13.5.2	Hemofiltration	364
2.13.5.3	Hemodiafiltration	364
2.13.6	Ultrafiltration Membranes for Dialysate and Infusate Preparations	365
2.13.7	Large-Scale Production of Synthetic Dialysis Hollow Fiber Membranes	366
2.13.7.1	Membrane Formation	366
2.13.7.2	Precipitation of the Membrane and Subsequent Washing	368
2.13.7.3	Recycling of Solvents and Precipitating Agents	368
2.13.7.4	Finishing Treatments	368
2.13.7.5	Winding	368
2.13.7.6	Dialyzer Assembly	369
2.13.7.6.1	Bundle transfer into housing	369
2.13.7.6.2	Potting	369
2.13.7.6.3	Integrity test	369
2.13.7.6.4	Sterilization	370
2.13.8	High Cutoff Dialysis Membranes	370
2.13.8.1	Membrane Description	370
2.13.8.2	HCO Membranes in the Treatment of Kidney Myeloma	372
2.13.8.2.1	Renal disease MM	372
2.13.8.2.2	Therapeutic interventions in myeloma-cast nephropathy	372
2.13.8.2.3	Recovery from renal failure following FLC removal with HCO dialysis	374
2.13.9	High Cutoff Membranes for the Treatment of Sepsis-Induced ARF	375
2.13.9.1	AKI Induced by Sepsis	375
2.13.9.2	Clinical Investigations with HCO in AKI and Sepsis	375
2.13.10	Membranes for Bioartificial Kidneys	376
2.13.10.1	Background and Motivation	376
2.13.10.2	The Concept of Bioartificial Kidneys	377
2.13.10.3	Membranes Used for Bioartificial Kidneys	377

2.13.11	Achievements and Perspectives for using Bioartificial Kidneys	380
2.13.12	Membranes for Stem Cell-Based Approaches to Treat Kidney Diseases	382
2.13.12.1	Background	382
2.13.12.2	Status of Stem Cell Therapies for Kidney Disease	382
2.13.12.3	Technologies and Membranes to Realize Stem Cell Therapies	383
References		385

Glossary

Albumin An abundant protein in the blood.

Biocompatibility The lack of adverse biological effects from the use of materials.

Cast nephropathy Free light chains precipitated with Tom–Horsfall protein, forming casts in the tubules of the kidney leading to renal failure.

Complement reaction A biological reaction cascade of blood components, which results, for example, in blood coagulation and clotting.

Cytokines Proteins secreted by cells, which function as cellular mediators.

Extra cellular matrix (ECM) Proteins secreted by cells, which play a crucial role in, for example, cell adhesion to artificial material.

Free light chains (FLCs) Constitutes of antibodies, which appear due to antibody catabolism in the blood as free light chains.

Hemodialysis (HD) Diffusive transport of substances across semipermeable membranes, driven by an osmotic gradient.

Hemofiltration (HF) Convective transport of substances across semipermeable membranes, driven by a transmembrane pressure gradient.

Hemodiafiltration (HDF) A combination of HD and HF.

High cutoff membrane A membrane with defined increased pore size, which allows the removal of molecules up to a molecular weight of 45 kDa.

Interleukin-6 (IL-6) A pro-inflammatory cytokine.

Interleukin-10 (IL-10) An anti-inflammatory cytokine.

Ischemia Oxygen deprivation.

Lipopolysaccharide (LPS) An integral part of the outer membrane of Gram-negative bacteria, which is a potent stimuli of the innate immune system provoking sepsis.

Microdomain structure Hydrophilic and hydrophobic domains of the inner membrane surface to improve biocompatibility.

Multi-organ failure (MOF) This describes the self-destruction of organs by a hyper-inflammatory, overreacting immune response during sepsis.

Multiple myeloma (MM) Bone marrow cancer characterized by unlimited proliferation of B-cells and dramatically increased concentration of free light chains in the blood.

Sepsis Sepsis is characterized by a whole-body inflammatory state and the presence of an infection.

Stem cell A cell that has, under certain conditions, the ability to reproduce itself for a long time. It also can give rise to specialized cells that make up the tissues and organs of the body.

Tubule A renal system of tubules which contains the fluid filtered through the glomerulus and has specific functions, including concentration of the primary urine.

Tumor necrosis factor- α (TNF- α) A pro-inflammatory cytokine.

2.13.1 Introduction

Today, most patients who require renal-replacement therapy (RRT) are conventionally treated using dialysis membranes. To improve the outcome of chronic dialysis patients, unique developments have been made in the past decades. Cellulose membranes

have been replaced by synthetic polymeric membranes with improved biocompatibility. The development of high-flux membranes and more efficient treatment modes, for example, hemodiafiltration (HDF), have resulted in improved removal rates of uremic toxins.

In 2007, approximately 160 million dialyzers (with an average surface area of 1.7 m²) were

manufactured for the treatment of 1.6 million dialysis patients worldwide. This large membrane-surface area requires highly automated manufacturing plants to produce high-quality and safe products.

Apart from membranes used for conventional hemodialysis (HD), new membranes with increased pore size have been developed for specific treatments. These specialized membranes allow removal of higher-molecular-weight molecules, such as mediators of sepsis/inflammation, or the removal of nephro-toxic light chains of immunoglobulins derived from multiple myelomas (MMs) (bone marrow cancer).

Membranes have also been utilized in cell-based extracorporeal systems to treat patients with kidney disease. In addition, specialized, highly efficient membranes have been developed for stem-cell growth in hollow fiber bioreactors as a technological prerequisite for cellular therapies and other applications.

2.13.2 Renal-Replacement Therapy

RRT replaces kidney function in patients with renal failure; however, the natural secretion of kidney hormones, which influences blood pressure, cannot be duplicated. There are two alternatives: organ transplantation or, more commonly, dialysis. In medicine, dialysis is the process of removing blood from a patient, purifying that blood through an artificial kidney (dialyzer), and then returning it to the patient's bloodstream.

Based on the developments of Willem Kolff and Nils Alwall in the 1940s, the dialyzer membrane systems (i.e., the filter housing as well as the membrane) have undergone multiple development cycles and are now the basis of an effective, reliable, and cost-effective treatment approach. In the early days of dialysis, large and unwieldy plate dialyzers that were made of cellulose membranes were used. Today, almost all dialyzers sold worldwide contain hollow fiber membranes. These changes have increased their versatility in clinical applications and are more cost-effective.

The newest generation of highly efficient dialyzers is equipped with synthetic polymeric hollow fibers.

In a dialyzer, the porous membranes separate the bloodstream from the dialysate stream, which is the core element of the dialyzer. Uremic toxins are removed from the blood while essential blood proteins and formed blood components are retained due to size exclusion of the membrane. Nowadays, a

dialyzer is composed of a bundle of hollow fibers (8000–15 000 fibers), which provide a large exchange surface area (up to 2.5 m²) in a compact and well-designed housing. In 2007, 88% of the ~1.6 million dialysis patients, worldwide, were treated with HD.

Because of the (1) aging population, (2) rising number of diabetes and hypertension patients, (3) optimization of dialysis treatment, and (4) economic opportunities of developing countries to treat kidney failure, the number of dialysis patients treated worldwide is now growing by 6–7% annually.

2.13.3 Dialysis Membranes

2.13.3.1 Membrane Requirements in RRT

To fulfill the requirements for efficient and safe blood transport and the particularities of individual therapies, membranes, in the past few years, have been developed with very specific properties. The morphology of dialyzer membrane structure and the active separation layer are key elements in dialysis membranes [1, 2]. Optimal characteristics of dialysis membranes, as based on theoretical considerations of the transport through the membrane structure, can be defined as follows:

- the active separation layer should be as thin as possible to achieve a high transmembrane flow,
- hydrophilic surface properties for spontaneous wetting are needed to ensure low protein adsorption,
- the surface of the membrane and its overall porosity should be high to achieve high hydraulic permeability,
- the separation layer of the membrane should have a narrow pore-size distribution in order to achieve the greatest selectivity,
- the maximum pore size of the membrane should not exceed a certain limit to prevent loss of necessary proteins, for example, albumin, and
- the mechanical stability of the membrane should be sufficient to withstand the pressures that occur during the treatment and manufacturing processes.

In addition to these basic requirements, there are other functional requirements for dialysis membranes to ensure optimal therapy:

- minimum roughness of the membrane surface that is in contact with the blood to reduce interaction with blood components;
- formation of hydrophilic and hydrophobic domains on membranes that is in contact with

blood to achieve high biocompatibility (low activation of blood components and low protein adsorption);

- prevention of transfer of cytokine-inducing substances (e.g., endotoxins) through the membrane from the dialysate circuit into the bloodstream; and
- design of dialysis membranes in terms of inner diameter, thickness, and geometry (fiber undulation) to achieve the greatest mass transfer through the membrane.

However, the above functional requirements for a dialysis membrane only give an idea of the specific requirements needed in various medical applications.

2.13.3.2 Membrane Materials

The type of membrane material is crucial in determining its separation properties and its biocompatibility. The basic functions and requirements of the membrane are as follows [1]:

1. separation of toxins and excess enriched fluid from the patient;
2. restoration of electrolyte balance in the body;
3. the lowest possible activation of blood components through the membrane surface (hemocompatibility); and
4. sufficient thermal, mechanical, and chemical stability so that the manufacturing steps as well as the types of sterilization and cleaning cycles do not alter the membrane's properties.

First, one can differentiate dialysis membranes according to the raw materials used to manufacture them: (1) unmodified regenerated cellulose, (2) modified regenerated cellulose, and (3) synthetic

polymers. Second, one can differentiate dialysis membranes according to their structure: symmetric or asymmetric.

Symmetric membranes have a uniform homogeneous structure throughout the entire membrane wall and often have similar pore sizes in the inner and outer layers (e.g., Hemophan[®], **Figure 1(a)**). Usually, this type of membrane is made of cellulose and its derivatives. Due to their high mechanical stability, they can be very thin-walled (wall thicknesses of the dry fibers are between 6 and 10 μm). Symmetric membranes can also be synthetic polymeric membranes made of polyacrylonitrile (PAN) (e.g., AN69[®]ST) or polymethylmethacrylate.

Asymmetric membranes, on the other hand, are mainly made of synthetic polymeric materials that have a thin inner selective layer, usually 1–3 μm thick, where the actual separation process takes place. The pore entrances of the inner surface of an asymmetric membrane (Polyamix[™]) can be clearly seen in an scanning electron microscopy (SEM) image (**Figure 2(a)**). Atomic force microscopy (AFM) has been applied to characterize the roughness of the Polyamix[™]/Polyflux membrane (**Figure 2(b)**). Because the smallest pore radii are on the inner surface, penetration of proteins into the Polyflux membrane is prevented.

Dialysis-membrane dialyzers are generally divided into two categories according to the material they are made of: either cellulose-based or synthetic polymeric membranes. The fraction of dialyzers containing synthetic polymeric membranes was $\sim 80\%$ of the total dialyzer market worldwide in 2007. This high percentage is because of their advantages, that is, variability in pore sizes, methods to adjust surface characteristics, and improved biocompatibility compared to cellulosic

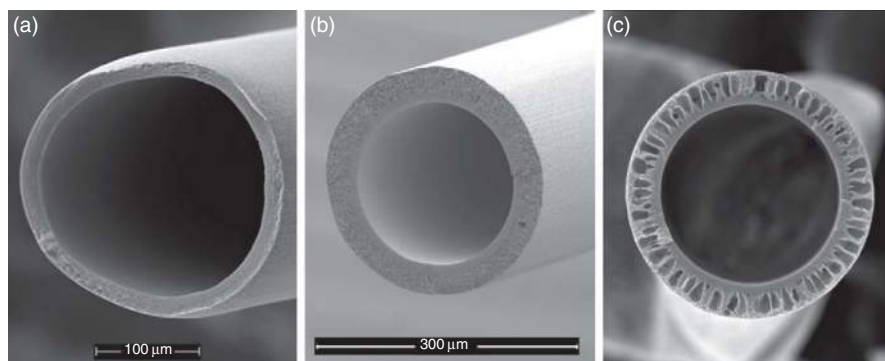


Figure 1 Scanning electron microscopic (SEM) images of the cross section of the (a) cellulosic Hemophan[®] membrane with its symmetric structure, (b) Fresenius Polysulfone[®] membrane with its foam-like asymmetric structure, and (c) a Polyamix[™] membrane with its finger-like asymmetric structure.

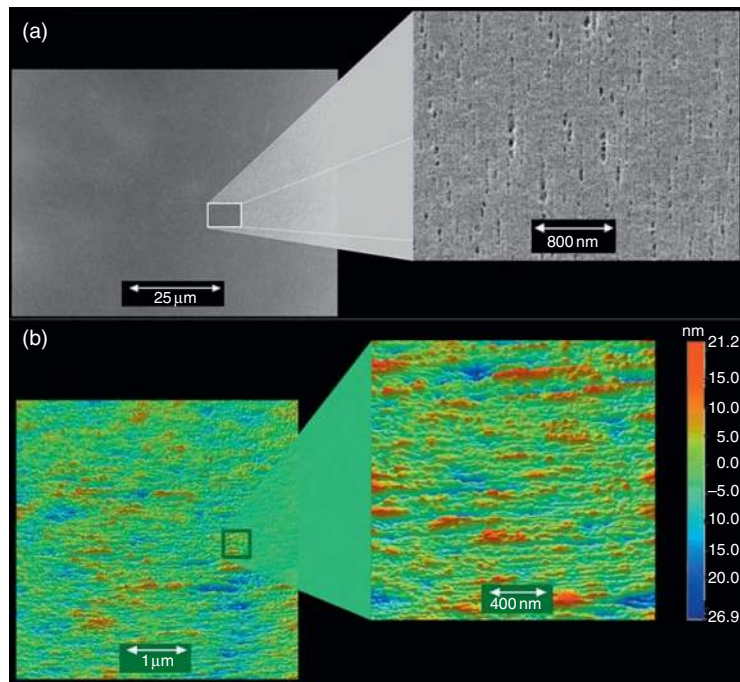


Figure 2 Scanning electron microscopic (SEM) image of an asymmetric membrane (Polyamix™) with the blood contacting the inner surface (a), and the corresponding atomic-force microscopy (AFM) image (b).

materials [1]. In a few years, it is expected that all cellulosic membranes will disappear from the dialysis market.

However, the thin selective layer and the reduced mechanical stability of synthetic polymeric membranes result in increased wall thickness compared to cellulose membranes. Different design approaches have been chosen for the subsequent support structure on top of the selective membrane layer. The support structure frequently shows a sponge-like structure, for example, Fresenius Polysulfone (Figure 1(b)). Nearly all dialysis

membranes made of polysulfone or polyethersulfone show this type of structure.

A higher diffusive resistance in terms of the elimination of small molecules due to the wall's large thickness can be compensated for by a higher porosity of the supporting layer, especially a finger-like structure (e.g., Gambro Polyamix™, Figure 1(c)).

2.13.3.2.1 Cellulose membranes

Table 1 shows the most commonly used cellulosic membranes and lists the materials they are constructed from.

Table 1 Overview of cellulosic materials used for dialysis membranes and their manufacturers

Classification	Membrane	Membrane manufacturer
Regenerated cellulose	Cuprophan®*	Membrana
Modified cellulose	Celluloseacetate	Toyobo, Helbio, Teijin
	Cellulosediacetate	Toyobo, Helbio
	Cellulosetriacetate	Toyobo, Helbio
Coated cellulose	Hemophan®*	Membrana
	Excebrane®*	Terumo
	SMC®*	Membrana
	Biomembrane®*	Asahi Kasei Medical Co., Ltd.

* Not manufactured anymore.

2.13.3.2.2 Regenerated cellulose

Cuprophane[®] is a brand name for cellulose fibers. Cellulose is a natural molecule, enzymatically formed, and semi-crystalline, consisting of a sequence of Cellobiose. To form a semipermeable membrane, the water-insoluble polymer must first be dissolved. Cuprophane[®] was one of the first cellulose membranes used in dialysis and is prepared by the Cuprammonium process [4]. In this process, cellulose is dissolved in an ammoniac solution of cupric oxide and is then precipitated in acid: this process is termed regenerated cellulose.

The Cuprophane[®] membrane is symmetrically structured and is extremely polar and hydrophilic due to its high proportion of hydroxyl groups, resulting in good wettability. However, the water uptake of Cuprophane[®] membranes is limited, that is, 45–50% water related to polymer weight [3].

Its permeability is slightly reduced by this water content. To retain permeability of the membrane during transportation and storage, 5–40% of glycerol is added to the cellulose membranes as a pore stabilizer. However, there is a risk of glycerol reaching the blood stream, for example, by using an inadequately washed filter, which can lead to hypersensitivity reactions and anaphylactic shock.

Cellulose has increased mechanical stability when it interacts with water than when in a dry state. This makes it possible to create very thin-walled membranes (6–10 μm wall thickness) with favorable diffusive transport properties for low-weight molecules.

Cuprophane membranes (used in dialysis) have an average pore radius of 1.72 nm [4]. This allows molecules with a size in range of between 500 and 1000 Da to pass only slowly through the membrane. Molecules above 1000 Da cannot pass through.

The Cuprammonium Rayon membrane is constructed from regenerated cellulose and is produced via the Cuprammonium process [4]. Other membranes made of regenerated cellulose are the RC[®] membrane, Saponified Cellulose Ester (SCE[®]), and FIN-type cellulose membranes.

It is known that Cuprophane membranes can activate the complement system [5] and create other adverse biological reactions, for example, leucopenia, by accumulation of granulocytes in lung capillaries, inhibition of granulocyte metabolism, and release of enzymes from granulocytes and monocytes [6]. This is caused by free

hydroxyl groups found on their linear polysaccharide layer.

2.13.3.2.3 Synthetically modified cellulose

The drawbacks caused by the reduced hemocompatibility of cellulosic membranes can be improved by partial substitution of the hydroxyl groups with: 1. acetylation, 2. introduction of diethylamino groups, or 3. benzyl groups [1].

Cellulose acetate is a cellulose membrane that has been modified by esterification. Depending on the degree of substitution, the membrane shows amounts of cellulose acetate, cellulose diacetate, or cellulose triacetate.

Cellulose ester membranes are unlike Cuprophane membranes in that they have modified side groups in the polymer chain. They also uptake significantly less water than Cuprophane membranes and, thus, have a more hydrophobic membrane surface. Because of this, membrane proteins are adsorbed significantly faster than through Cuprophane membranes [3, 4].

Cellulose acetate membranes have an asymmetric structure and a broad pore-size distribution, resulting in increased permeability of molecules greater than 5000 Da in size compared to Cuprophane membranes.

Hemophane[®] membranes are produced by etherified cellulose with diethylaminoethanol (DEAE). This product's cellulose surface is better tolerated by the patient, that is, no complement activation occurs and the membrane shows improved biocompatibility. Furthermore, Synthetically Modified Cellulose (SMC[®]) membranes are produced by etherification of cellulose with benzene groups.

Another biocompatibility improvement of cellulosic membranes is to surface-coat them with polyethylene glycol (PEG), PAN-RC[®] [7], or vitamin E (Excebrane[®]). The use of vitamin-E-coated membranes seems to significantly decrease the activation and migration of monocytes and granulocytes compared to uncoated cellulose membranes [8].

2.13.3.2.4 Synthetic polymeric membranes

Today, a number of different polymers and polymeric blends are used to manufacture synthetic polymeric dialysis membranes. The membrane materials (except for EVAL[®]) are primarily hydrophobic and, therefore, are combined with hydrophilic additives (e.g., polyvinylpyrrolidone (PVP) or PEG), or

are processed with hydrophilic copolymers such as methallylsulfonate.

Membranes prepared from hydrophobic/hydrophilic polymer blends are the predominant type of synthetic polymeric membrane [1]. The hydrophobic-base material is either polysulfone or polyethersulfone (polyarylethersulfone). A key feature of polyethersulfone- and polysulfone-based membranes, in addition to their good transport properties, is their excellent biocompatibility. These membranes exhibit only slight complement activation [9], the drop in leukocytes is minimal [10], and the release of leukocyte elastase is low [11]. Polyethersulfone- and polysulfone-based membranes contain only small amounts of water and are, in contrast to Cuprophane membranes, free from pore stabilizers.

In the past, dialysis membranes have been defined according to the material used to manufacture them and the characteristics of these special polymers. Today, advances in polymer recipes, advances in technology, and the whole dialyzer-manufacturing concept (including increased high-technology equipment) have resulted in the production of improved safe and high-quality products.

Table 2 gives an overview of the most common synthetic polymer membranes and their manufacturers.

2.13.3.2.5 Polysulfone/polyethersulfone/polyvinylpyrrolidone (PVP)/ polyamide membranes

Depending on the manufacturer, polysulfone can be a homo- or copolymer [2]. The difference between polysulfone and polyarylethersulfone, in short polyethersulfone, lies in their chemical structure: besides the sulfone and alkyl or aryl (e.g., aryether) groups that both polymers contain, polysulfone additionally contains isopropylidene.

Polyarylethersulfone (polyethersulfone) and polysulfone polymers are described as engineering polymers. These thermoplastic polymers show excellent mechanical, chemical, and thermal properties. Polysulfone/polyethersulfone hollow fibers can be sterilized by steam, as well as with radiation, such as beta or gamma.

PVP is obtained by the vinylation of pyrrolidone plus a subsequent polymerization. PVP is widely used as an excipient in the pharmaceutical industry. It is added to the polymer solution of dialysis membranes when made of polysulfone or polyethersulfone to increase the hydrophilicity and porosity of the membrane. This is achieved by a partial washout procedure during the precipitation process. This process creates a gradient of PVP in the membrane wall with the highest concentration being on the inside of the membrane.

Table 2 Synthetic polymer membranes and their manufacturers

<i>Synthetic polymers</i>	<i>Membrane</i>	<i>Manufacturer</i>
Polyethersulfone/polyvinylpyrrolidone/polyamide	Polyamix™	Gambro
Polyethersulfone/polyvinylpyrrolidone	Revaclear	Gambro
	DIAPES®,	Membrana
	PUREMA®	
	POLYNEPHRON™	Nipro
	ARYLANE®	Gambro/Hospital
	Polyphen®	Minnotech
Polysulfone/polyvinylpyrrolidone	Polysulfone®,	Fresenius Medical Care
	Helixone®	
	Toraysulfone®	Toray Industries
	Diacap®alpha	B. Braun
	Minnotech PS	Minnotech
	REXBRANE,	Asahi Kasei Kuraray Medical Co.
	APS™,	Ltd.
	VitabranE™,	
	Biomembrane™ PEG	
Polyacrylonitrile	AN69®ST,	Gambro/Hospital
	Evodial	
Polymethylmethacrylate	PMMA®	Toray Industries
Ethylvinylalcohol copolymer	EVAL®	Asahi Kuraray Membrane Manufacturing Co., Ltd.
Polyester/polyvinylpyrrolidone	PEPA®	Nikkiso

In 1937, polyamide was used in the production of nylon. Around the same time, Perlon[®] was developed and polyamides became used in the textile industry. The scope and range of applications that polyamides can be utilized in are virtually unlimited, and they are also used in the production of dialysis membranes. Today, an aromatic–aliphatic copolyamide is used as additive to the Polyamix[™] membrane (Gambro) to improve its performance.

1. *The polysulfone/PVP membrane.* All polysulfone-based dialysis membranes show a foam-like support structure. The formation of this support structure can be designed to achieve specific separation characteristics. The increased hydraulic resistance of a foam-like support structure is partially compensated for by a reduction in wall thickness [1].

2. *The polyethersulfone/PVP/polyamide membrane.* The Polyamix[™] membrane has a unique asymmetric, three-layer structure where the outer layer, referred to as the supporting layer, is characterized by a very open finger-like morphology. The actual inner separation layer of the membrane is formed by an extremely thin inner skin supported by an intermediate layer. This middle layer forms a foam-like structure, which is very permeable. Thus, low resistance for convection and diffusion are ensured. The outer layer provides high mechanical stability.

High elimination capacity and clearance, as well as efficient retention of endotoxins, are among the most outstanding characteristics of Polyamix[™] membranes. This is due to the membrane's unique polymer blend, with polyamide as an essential component, and to its configuration and improved biocompatibility [12]. The contact between blood and membrane therefore affects neither the immune system nor the coagulation cascade [13, 14].

Its reduction in specific interactions with proteins and cells is a result of its hydrophobic and hydrophilic polymers, which, when combined, form a micro-domain structure (its hydrophilic domains reduce the intensity of interactions; see Figure 3) [15]. In addition, blood contact with a Polyamix[™] membrane causes no symptoms of functional vascular interference [16].

3. *The polyethersulfone/PVP membrane.* Most membranes made of polyethersulfone and PVP are characterized by their asymmetric structure, a dense selective inner skin, which is in contact with blood, and a supportive porous outer layer. By appropriately adjusting the membrane-manufacturing

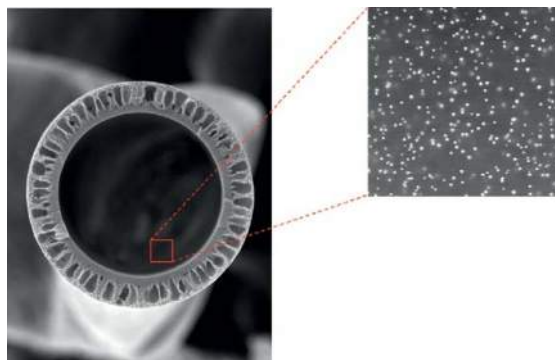


Figure 3 Micro-domain structure on the inner surface of the asymmetric three-layer Polyamix[™] membrane of Gambro.

parameters, as well as the use of different molecular weights of PVPs, the underlying membrane's physicochemical properties, morphological structure, solute-rejection behavior, and filtration performance can be refined. Newer developments follow a current trend for higher removal of middle-molecular-weight products, such as β 2-microglobulin, while retaining albumin. Such membranes (e.g., Revaclear, Gambro; PUREMA[®], Membrana) show excellent diffusive transport properties, high selectivity, biocompatibility.

2.13.3.2.6 PAN membranes

PAN was the first synthetic material developed for dialysis membranes.

The material of the old AN69[®] membrane developed by Hospal, is a copolymer of acrylonitrile and sodium methallylsulfonate. The combination of acrylonitrile and sodium methallylsulfonate is crucial, with the addition of sodium methallylsulfonate heavily influencing membrane structure. Pure PAN membranes usually have large pores. The additional methallylsulfonate leads to a finer, homogeneous high-flux membrane, with good diffusive and convective transport properties. AN69[®] membranes have a high adsorption capacity for proteins, including β 2-microglobulin [17], cytokines [18], as well as for endotoxins [19].

However, in those patients receiving ACE inhibitors and who have been treated with PAN dialysis membranes (AN69[®]), contact activation, particularly activation of kallikrein and secession of bradykinin, seems to occur. This is due to the negatively charged membrane surface. However, this drawback can be overcome by coating the membrane surface with polycationic polyethylenimine, which has the

additional benefit of binding heparin, thus allowing lower heparin dosage during dialysis. Today, this membrane is available as AN69®ST.

In contrast to Cuprophan membranes, which are not permeable to β 2-microglobulin, a weekly loss of ~400–600 mg of β 2-microglobulin can be expected with an AN69® membrane [20].

2.13.3.2.7 Polymethylmethacrylate membranes

This membrane consists of modified polymethylmethacrylate (PMMA). As a high-flux membrane, the PMMA® membrane was used in 1977 for HD, as well as for new therapies, such as hemofiltration (HF) and HDF. This was because of this membrane's higher permeability to liquid and so-called middle molecules compared to cellulose membranes, and the membrane also possessed good albumin-retention properties [21, 22]. In the manufacturing process, this membrane is treated, after rinsing with glycerol, to stabilize the pores. Any elimination of β 2-microglobulin by PMMA® membranes is mainly due to adsorption.

2.13.3.2.8 Ethylenvinylalcohol membrane

In comparison to cellulosic membranes, the EVAL® membrane has a symmetric membrane structure with improved biocompatibility, even though the material it is manufactured from, ethylenvinylalcohol copolymer is naturally highly hydrophilic. This membrane structure is also stabilized with pore fillers, for example, glycerol.

2.13.3.3 Membrane Characteristics: Low- and High-Flux Membranes

Dialysis membranes are split into 'high' and 'low'-flux membranes. The difference between them is primarily the ultrafiltration coefficient, that is, the hydraulic permeability of the membrane. Hydraulic permeability is a measure of the volume that can pass through the membrane within a defined surface area, time, and pressure. Low-flux membranes have a water permeability of $<300 \text{ l m}^{-2} \text{ h}^{-1} \text{ MPa}^{-1}$. High-flux membranes typically have a value of greater than $1200 \text{ l m}^{-2} \text{ h}^{-1} \text{ MPa}^{-1}$ [1]. This increased hydraulic permeability is achieved by increasing the pore size of the membrane, which results in an increased nominal cutoff.

Mass transfer through the membrane is essentially controlled by the nanostructure of the membrane. The relationship between the structural properties

of the membrane and the diffusive and convective mass transfer through the dialysis membrane is approximated by [23]:

$$\text{Diffusive transfer: } \lim_{\Delta P \rightarrow 0} \mathcal{J}_i = \frac{\varepsilon D_i^M S}{\tau \Delta z} (C_{Bi} - C_{Di}) \quad (1)$$

$$\text{Convective transfer: } \lim_{\frac{dc}{dz} \rightarrow 0} \mathcal{J}_i = \frac{\varepsilon r^2 S C_{Bi}}{8\eta\tau} \frac{\Delta P}{\Delta z} \quad (2)$$

These equations describe the specific flux, \mathcal{J}_i , of component i ; ε the porosity; τ the tortuosity of the membrane; η the dynamic viscosity; r the pore diameter of the selective pores; Δz the thickness of the membrane; S the sieving coefficient; C_{Bi} and C_{Di} the concentration of component i in the blood and dialysate, respectively; D_i^M the diffusion coefficient of component i through the membrane; and ΔP the hydrostatic pressure gradient between the two phases separated by the membrane. Based on theoretical considerations (Equations (1) and (2)), dialysis membranes can be designed for a particular therapy and for the prevailing transport mechanisms.

Differences in permeability are also reflected in the diffusive properties of the membrane. By definition, dialysis is a process of separating elements in a solution by diffusion across a semipermeable membrane (diffusive solute transport) down a concentration gradient. The diffusion properties of a dialysis membrane are dependent on the overall wall thickness, the thickness of the separating layer, the porosity and tortuosity of the membrane, and can be expressed by diffusion coefficients. The diffusion coefficient is a constant of proportionality that represents the amount of a particular substance diffusing across a unit area through a unit concentration gradient in a unit time. The effective diffusion coefficient, D^M , is calculated by $D^M = P^M \times \Delta z$, where P^M is the permeability of the membrane and Δz the wall thickness of the membrane. Diffusivity decreases with increasing molecule size (see Figure 4). The diffusion coefficient for solutes with increasing molecular weight differs for low- and high-flux membranes.

In addition, low- and high-flux dialyzers differ in their exclusion criteria (Cut-off), which correlate with their pore size and pore-size distribution (pore diameters ranging from 3 to 6 nm) within the membrane. Measurement conditions, as well as the media used, have a significant impact on the sieving profile. The sieving coefficient (S) for experiments with hollow

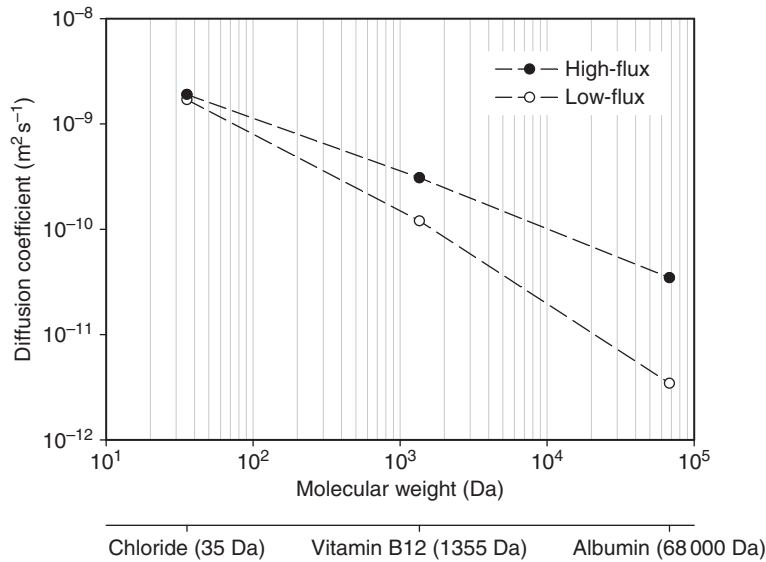


Figure 4 Diffusion coefficients for the substances chloride, vitamin B12, and albumin passing through Polyamix™ high- and low-flux membranes.

fiber membranes can be calculated according to Equation (3), which describes the concentration in the filtrate (C_F), the plasma/blood concentration at the entrance (C_{Bi}), and the concentration at its exit (C_{Bo}):

$$\text{Sieving coefficient : } S = \frac{2C_F}{C_{Bi} + C_{Bo}} \quad (3)$$

Figure 5 shows the sieving profiles for a high-flux membrane for different proteins measured in

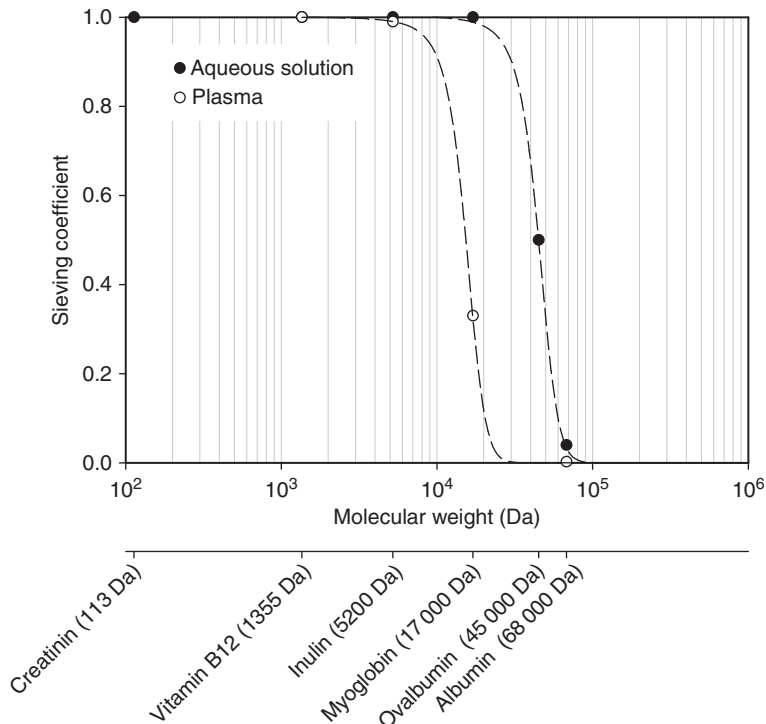


Figure 5 Sieving coefficients for a synthetic high-flux membrane (Polyflux, Gambro) for different proteins. The measurements were performed in aqueous solution (●) and in plasma (○) at a fixed intrinsic flow rate $J_v = 0.704 \text{ cm s}^{-1}$ and a wall shear rate of $\gamma = 461 \text{ s}^{-1}$. The concentration of these particular substances was 0.1 g l^{-1} .

aqueous solution and in bovine plasma, depending on the molecular weight (in Da) of different substances.

Proteins within plasma can create a layer on the membrane surface that is in contact with blood, acting as an additional barrier to protein permeability, thus resulting in a sieve profile shift toward lower molecular weights compared to measurements taken in an aqueous solution.

In **Figure 6**, the sieving coefficient profiles for both low- and high-flux Gambro membranes are shown for different proteins in aqueous solution, and are plotted against their molecular weights (in Da).

Low-flux membranes are capable of eliminating substances of up to 5000 Da and rejecting nearly 100% of β 2-microglobulin, whereas high-flux membranes are highly permeable to β 2-microglobulin. The mass transfer of low-flux membranes is mainly diffusive and is not suitable for use in therapies that require high convective transport, for example, HF and HDF. The pore structure of high-flux membranes allows the passage of so-called middle molecules up to 20 000 Da. In addition, significant

protein loss, that is, albumin (68 000 Da), is prevented. Besides the immunoglobulins, albumin is the most important plasma protein that needs to be retained in the chronic dialysis patient. High-flux membranes are suitable for HD, HF, and HDF.

2.13.4 Biocompatibility of Dialysis Membranes

Mass transfer through membranes is essentially determined by the membrane's structure, though interactions between the membrane surface and blood can lead to changes. In particular, the adsorption of proteins on the membrane surface, and in the pores and the pore entrances, has to be considered. Apart from adsorption, activation of the complement system, coagulation, hemolysis, and adhesion of blood platelets can occur as a result of interactions between the membrane surface and blood. The above-mentioned phenomena are summarized here. The sum of the polymer and surface characteristics

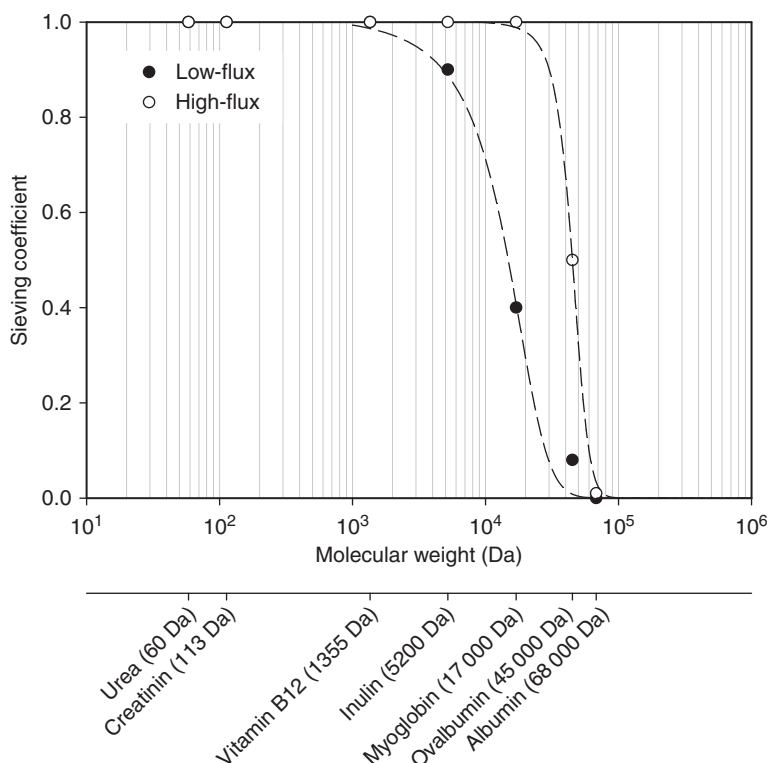


Figure 6 Sieving coefficients for synthetic low-flux (●) and high-flux (○) membranes (Polyflux, Gambro) for different proteins. The measurements were performed in aqueous solution at a fixed intrinsic flow rate $J_v = 0.704 \text{ cm s}^{-1}$ and a wall shear rate of $\gamma = 461 \text{ s}^{-1}$. The concentration of these particular substances was 0.1 g l^{-1} .

that form the hemocompatible surface are complex and are, as yet, not fully understood.

By definition, a biocompatible material has the property of not producing a toxic, injurious, or immunological response in living tissue.

In HD, biocompatibility is related to multiple interactions that occur between the artificial membrane surface and the humoral and cellular components of the patient's blood. This includes both general and inflammatory immune responses.

Humoral changes are induced by the activation of systems or the adsorption and/or denaturation of humoral factors. Disturbances of cellular systems include changes in cell population, cellular function, and cellular release of substances. In the human body, the typical response to coming into contact with synthetic material is the deposition of proteins with specific products of complement activation (immunologically potent substances, such as C3a, C4a, and C5a) from the body fluids onto the surface of the material.

Complement is a principal mediator of the acute inflammatory response, and contributes to the non-specific recognition and elimination of foreign substances from the body. Apart from activation, blood-material interactions promote the adsorption of plasma proteins and other macromolecules onto the surface of the material, which can change its conformation and reactivity due to adsorption. Some substances may desorb from the material surface and recirculate in the blood stream, and possibly exhibit different properties than when they were in their preadsorbent state.

The contact phase activation (kallikrein-kinin system) is triggered after contact of blood with a negatively charged surface. After a complex cascade of enzymatic reactions, vasodilatation and coagulation of blood occurs.

Platelets and coagulation factors respond to different characteristics of the dialysis membrane and stimulate the coagulation process. This results, finally, in platelet activation and aggregation. Furthermore, in these pre-thrombotic reactions, leukocytes are also involved, leading eventually to pre-inflammatory effects.

In addition, leukocytes can be activated, leading to degranulation and mediator release. Stimulated monocytes produce inflammatory mediators such as interleukin (IL) and tumor-necrosis factor (TNF) [24].

Although allergic reactions are generally rare, a main trigger is ethylene oxide, which is used in some forms of sterilization. If any residues remain in the

dialyzer, this can contact albumin during dialysis, which can then become an effective allergen and a main trigger for an allergic reaction during dialysis.

In HD, the whole dialysis system needs to be considered with respect to biocompatibility. Therefore, not only are the chemical composition and surface structure of all the artificial components important (e.g., dialysis membrane, tubing system), but also physical effects such as the geometry of the dialyzer, blood flow and pump effects, as well as potential bacterial contamination by the dialysate or inadequate anticoagulation. Materials do interact with blood differently, but such effects can also depend on the patient's disease type and disease state. For a chronic dialysis patient, a mild interaction can lead cumulatively to a significant clinical effect because dialysis treatment is performed for many years 3–4 times a week.

With regard to the membrane, the properties of the surface that makes contact with blood can significantly influence its biocompatibility. Therefore, surface roughness, chemical composition and structure, with respect to functional groups or charge, as well as hydrophilicity, all play crucial roles.

Based on the surface properties of proteins, an 'ideal' membrane surface should have hydrophilic, hydrophobic, and negatively and positively charged areas [25, 26]. The concept of hydrophilic and hydrophobic micro-domains has been experimentally confirmed and is found, today, in both synthetic polymer and synthetically modified cellulose membranes [27–29].

With the knowledge of the manifold potential interactions between artificial materials and the patient, the need for pre-clinical testing of these materials for their biocompatibility is undisputed. Three important effects of the blood-artificial membrane contact layer are often analyzed *in vitro* when developing membranes.

1. Complement activation, by measuring the concentration and generation rate of terminal complement complexes (TCCs). Some specific proteins, such as C3 or C5, become adsorbed at the surface and commence a cascade of complicated reactions, which finally lead to clot formation. In order to study this phenomenon, the concentration of factors, such as TCC or C3a, is usually measured.

2. Activation of the coagulation cascade (thrombin formation and thrombocyte activation). Thrombin-antithrombin III (TAT) levels are measured and platelets are counted.

3. Contact phase activation: testing for kallikrein-like activity. The cascade starts with adsorption of high-molecular-weight kininogen (HMWK) and prekallikrein (PK), and results in conversion of prekallikrein to kallikrein (KK). After a complex cascade of enzymatic reactions, vasodilatation and coagulation of blood can occur.

2.13.5 Operation Modes of Dialysis Treatment

In general, dialysis treatments are performed 3 times a week for time periods of 3–5 h. The extracorporeal circulation begins at the ‘artery’, that is, the vascular access. With the help of a blood pump, usually a roller pump, the blood is pumped at a flow rate of 200–500 ml min⁻¹ through the dialyzer. The cleaned blood returns to the patient at the venous access. In addition, there is an anticoagulation medium added, for example, heparin, to prevent coagulation of blood. For patient safety, other devices and air traps are integrated into the extracorporeal blood circuit. These components allow elimination of any small quantities of air from the tubular system and avoid treatment interruption in unexpected situations (e.g., leakage, air in the system, and so on).

The effectiveness of the separation of particular components by the different processes is expressed in the medical community by the term ‘clearance’, and

describes the removal rate in ml min⁻¹ [3]. This term refers to the purified blood volume and is both a function of the membrane’s properties as well as the process design. The clearance (C_L) for the different treatment modes is calculated as follows:

$$\text{Hemodialysis : } C_L = \frac{(C_{Bi} - C_{Bo})Q_{Bi}}{C_{Bi}}$$

$$\text{Hemofiltration : } C_L = \frac{C_F}{C_{Bi}} Q_F$$

$$\text{Hemodiafiltration : } C_L = \frac{(C_{Bi} - C_{Bo})Q_{Bi} + Q_F C_{Bo}}{C_{Bi}}$$

where Q is the flow, C the concentration, and subscripts B, D, F, I, and o denote blood, dialysate, filtrate, inlet, and outlet, respectively. Diffusive clearance is dependent on the molecular size of the substance.

Clearance of the uremic toxin, urea, is of particular interest, acting as a sensitive indicator of dialysis efficiency. With a molecular weight of 60 Da, it is classed as a small-molecular-weight substance. Urea exhibits high membrane permeability and is completely eliminated by dialysis. For higher-molecular-weight substances, such as vitamin B12 (1355 Da) or inulin (5200 Da), clearances are reduced. Blood flow is of importance in the clearance of different substances; its influence at defined dialysate flow rates can be seen in **Figure 7**. At low blood-flow rates, clearance increases linearly with the blood flow.

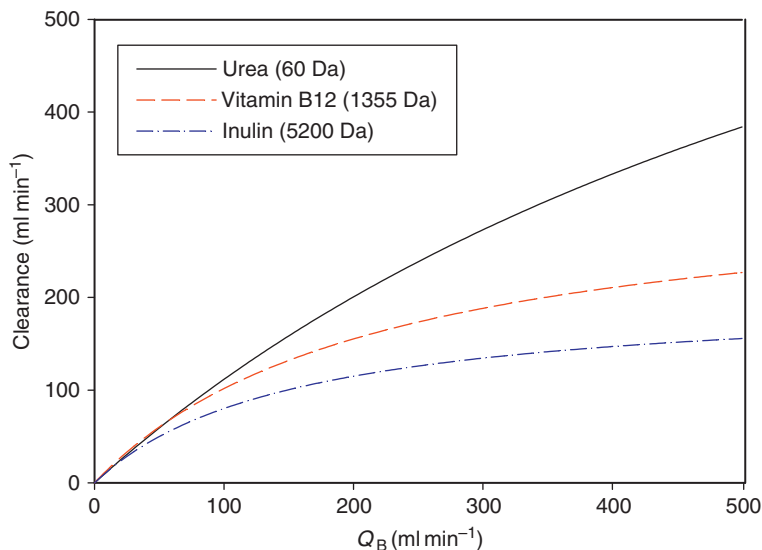


Figure 7 Clearances for small- and middle-molecular-weight proteins depending on blood flow (Q_B) in a dialyzer (Revaclear, Gambro, $A = 1.8 \text{ m}^2$) with a PolyamixTM high-flux membrane. $Q_D = \text{const.} = 500 \text{ ml min}^{-1}$. For low Q_B , the clearance was identical with Q_B .

A clearance plateau is reached at certain blood-flow rates, which is lowered with increasing molecular weight of the substance removed.

At low blood-flow rates, the dialysate flow fully controls the clearance. In particular, for small-molecular-weight substances, clearance increases with increasing dialysate flow.

The control of transmembrane pressure, flow rates, and mass balance during dialysis treatment in the different therapy modes can be comprehensively managed by the currently available modern dialysis machines.

2.13.5.1 Hemodialysis

In HD, the uremic toxins of the blood are eliminated mainly under diffusive isobar conditions; the removal rates of the different substances depend mostly on their molecular size (with increasing size of molecule leading to a reduced removal rate). The dialysate runs counter-current to the blood, to provide a high concentration gradient along the whole dialyzer. Sodium and potassium concentrations of the dialysate are similar to those of normal plasma, to prevent their loss. Sodium bicarbonate is also added to the dialysate to correct for blood acidity. By adjusting negative pressure relative to the blood compartment, excess fluid from the patient is removed (ultrafiltration). Mass transfer due to ultrafiltration in HD mode is negligible. In HD treatment, low- and high-flux dialyzers are utilized. **Figure 8** shows a schematic drawing of HD.

2.13.5.2 Hemofiltration

In contrast to HD (diffusion), convective transport is used to eliminate uremic substances from the hemofiltrate by applying a hydrostatic pressure difference. In

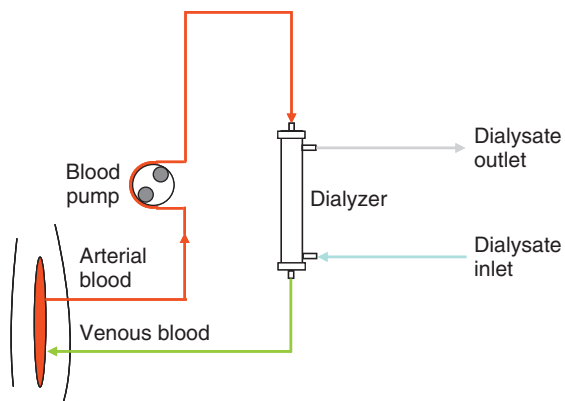


Figure 8 Schematic drawing of a hemodialysis setup.

this method, middle-molecular-weight substances are removed more efficiently, and removal rates are independent of molecular weight up to a molecular weight of 20 000 Da. For this process, a high-flux membrane is required, which allows high filtration rates (20–30 l per treatment), and a dialysate flow is not applied. However, the high fluid loss is compensated for by the addition of a sterile fluid (substitute) to the bloodstream. However, this fluid substitution generates high costs; thus, HF is not a routine treatment for chronic kidney failure, but is mainly applied in intensive care. If the substitution fluid is introduced into the bloodstream after passing through the dialyzer/filter, one speaks of post-dilution. In contrast, if the substitution fluid is introduced into the bloodstream prior to passing through the dialyzer/filter, this is defined as pre-dilution. The principle of the HF mode (during post-dilution) is shown in **Figure 9**.

2.13.5.3 Hemodiafiltration

HDF is a combination of HD and HF (see **Figure 10**). The elimination of uremic toxins takes place by diffusive and convective transport, resulting in high removal rates for both low- and middle-molecular-weight substances. Similar to the HF mode, only high-flux dialyzers can be used because of the high filtration rates required. In the classic HDF mode, the substitution solution is supplied in bags. However, utilizing infusion fluid from bags leads to greater technical requirements

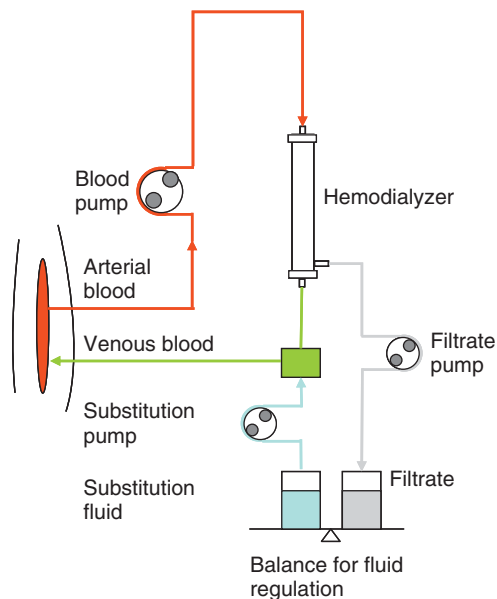


Figure 9 Schematic drawing of a hemofiltration with a post-dilution setup.

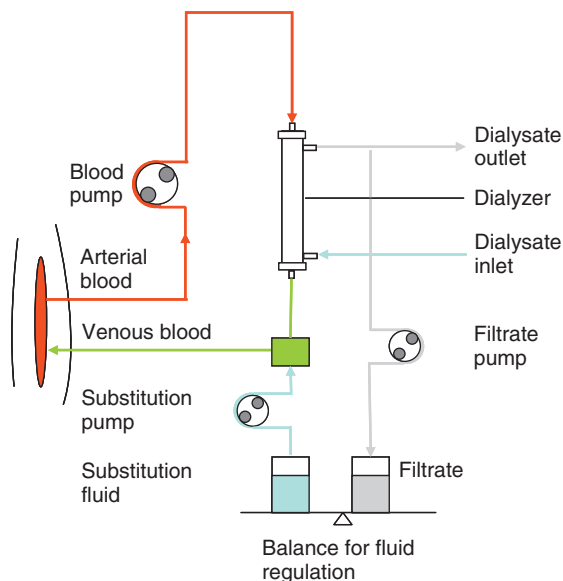


Figure 10 Schematic drawing of a hemodiafiltration with a post-dilution setup.

and costs, and results in limited exchange volumes (8–12 l per treatment). However, because of the development of online systems, the costs of supplying substitution solutions have been drastically lowered, and can now provide an economic treatment.

Online HDF provides high removal rates over a wide molecular-weight spectrum, and is achievable with present-day RRTs. The ultrafiltered excess volume, approximately 20–70 l per treatment, is automatically replaced continuously by a substitution solution. The solution is generated by stepwise ultrafiltration of dialysate direct into the machine: this fulfills the quality demands of commercially available infusion solutions with regard to sterility and quantities of pyrogen. Online HDF is preferably performed in the post-dilution mode [30].

Online HDF is considered to be the most effective and safest dialysis treatment due to its superior blood purification of all uremic toxins, and it reduces the incidence of cardiovascular events.

Hemodialysis can also be considered as a form of HF due to its increased ultrafiltration rate because of its backfiltration and, thereby, also its increased convective mass transfer.

The choice of the dialysis technique depends on multiple factors, including the primary need (e.g., solute or water removal, or both), underlying indications (e.g., acute or chronic failure, and poisoning), vascular access, hemodynamic stability, availability, local expertise, and patient preference.

Dialysis and filtration can be performed intermittently or continuously. Continuous therapy is used exclusively for acute renal failure; benefits over intermittent therapy are improved tolerability as a result of slower removal of solute and water.

All three different modes are normally performed at blood flows of between 200 and 500 ml min⁻¹. Dialysate flows in HD and HDF modes are 500–800 ml min⁻¹. Filtration rates during HDF/HF are heavily dependent on the treatment mode (pre- or post-dilution flows) and blood flow, and range from ~25% during post-dilution (HDF) to 100% during predilution (HF) [30–32].

Volume flows are adjusted specifically to the patient, the treatment's requirements, and to the dialysis system (dialysis machine and filter assembly). The distribution of blood and dialysate flow in dialysis modules has a significant influence on the efficiency of mass transfer. For this reason, the blood inlets are constructed accordingly. To ensure uniform distribution of dialysate flow in the bundle cross-section (to avoid channel formation), there are at least three methods: (1) installation of threads by a spacer between the hollow fiber bundles [20, 21], (2) a special bundle configuration by arranging individual membranes to a specific angle during the manufacturing process and (3) undulation (creation of a wavy fiber profile) with the membranes forming an open bundle that ensures unimpeded dialysate flow across the bundle cross section. In addition, combinations of these methods are possible. These configurations lead to more efficient exchange of materials and a significant increase in removal rates of uremic toxins.

2.13.6 Ultrafiltration Membranes for Dialysate and Infusate Preparations

All impurities and other components of the dialysate can theoretically be transferred into the blood of patients due to a missing or insufficient transmembrane pressure gradient in the direction of the dialysate compartment. These substances may also reach the blood due to partial backfiltration, which is of greater risk when utilizing high-flux membranes.

If endotoxins (bacterial-degradation products) in the dialysate pass through the membrane, pyrogenic reactions in patients (e.g., feeling generally unwell, fever or development of sepsis) can occur. The transport of bacterial fragments is dependent on the membrane material, the pore radius, and membrane-surface

properties (hydrophilic/hydrophobic). However, some high-flux dialysis membranes have a more hydrophobic exterior and are made of special materials that allow removal of bacterial contamination by adsorption.

Guidelines for the different dialysates and infusates regarding endotoxin concentrations have been established. The European Directive allows an upper limit of bacteria of 100 CFU ml^{-1} (colony forming unit), and for endotoxins of 0.25 EU ml^{-1} (endotoxin unit) [33–35]. The fluid quality description, ‘ultrapure’, means practically free from bacteria and endotoxins. In quantitative terms, it is defined as $<0.1 \text{ CFU ml}^{-1}$ and $<0.03 \text{ EU ml}^{-1}$. By applying one additional step to controlled ultrafiltration, ultrapure dialysis fluid can be further purified to such a high microbiological quality that it can be used for infusion [36].

Various authorities require regular endotoxin checks of the dialysate. Optimally, a general bacterial- and endotoxin-free dialysate is created by filtration (ultrafiltration membranes) at the dialysis machine. In modern dialysis machines, up to three filters with ultrafiltration membranes (hollow fiber systems) of different sizes are implemented in the fluid circuit of the dialysis machine, or in the tubing system used for re-infusion (in HDF and HF). The use of multistep ultrafiltration allows the online production of a high-quality infusion liquid, which is a prerequisite for convective HDF or HF treatments.

During dialysis treatment, the clinical staff need to maintain high hygienic standards to ensure the health of the patient. It is recommended that, during dialysis, a continuous water supply and a continuous flow of dialysate in the device are maintained [37]. Further, the entire water and dialysate system should be regularly cleaned and disinfected, in order to prevent the formation of a biofilm [30].

The bicarbonate used in the buffer solution is also an ideal medium for microorganisms. Therefore, it is recommended that bicarbonate be used in powdered form and stored dry until needed. In modern dialysis machines, cartridges with dry sodium bicarbonate are introduced into the machine, allowing online production of liquid dialysis fluid [30].

2.13.7 Large-Scale Production of Synthetic Dialysis Hollow Fiber Membranes

Hollow fiber- and flat-sheet-based dialyzers have been developed and used in parallel for decades. Today, nearly 97% of all treatments are performed

with hollow fiber dialyzers. The technical advantages of hollow fiber systems are their reduced manufacturing costs and the compact design of the dialyzer. In addition, they are simpler to use and can be used in different treatment modes.

The manufacture of dialysis membranes is comparable with the production of other hollow fiber membranes: the world annual production in 2007 for ~150 million dialyzers was ~1.8 m² surface area of membrane. The majority (~80%) of these dialyzers are equipped with synthetic polymeric membranes: no other application in membrane technology has reached this advanced level of development. Production of dialyzers is a continuous process, whereby membrane production is integrated into the manufacture of the dialyzer. For optimized application, the inner diameter of the hollow fiber membranes range from 180 to 220 μm. Synthetic polymeric membranes have a wall thickness of between 30 and 50 μm. In contrast, cellulosic membranes have a wall thickness of between 5 and 8 μm.

The design of the membrane and the dialyzer are crucial. Optimal mass transfer between blood and dialysate has to be guaranteed, and this is also influenced by the dimensions of the membrane surface. The effective membrane-surface area of the dialyzer chosen to treat a patient has to be adjusted to the size of the patient: pediatric filters (for small patients) have a surface area of between 0.01 and 0.6 m², and standard filters for adults range from 1.0 to 2.4 m².

The blood-filling volume, flow resistance, and the dimensions and weight of the dialyzer should be as small as possible. The performance characteristics of a dialyzer must be precisely documented in a data sheet and must be reproducibly detectable for each dialyzer. Due to the high frequency of treatments needed by dialysis patients (~150 times per year), the cost of a dialyzer is important. However, generally, the dialyzer costs less than 10% of the total treatment.

To ensure sterile products, the entire manufacturing process is carried out in sterile rooms. In modern manufacturing facilities, the production of a dialyzer is a sequence of several individual and complex processing steps. The most relevant processing steps are presented in [Figure 11](#).

2.13.7.1 Membrane Formation

The continuous process of production of hollow fiber membranes can be divided into six individual steps:

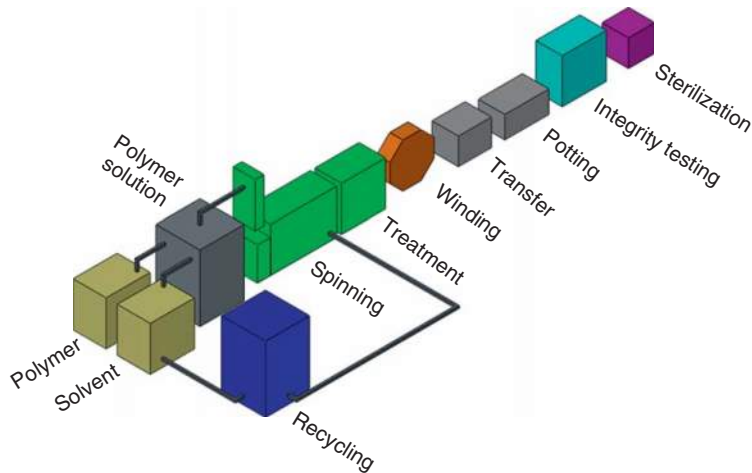


Figure 11 The most relevant process steps in dialyzer manufacturing.

1. manufacture of the polymer solution and the bore liquid;
2. formation of hollow fibers;
3. precipitation of the membrane in a coagulation bath and subsequent washing;
4. finishing treatments, for example, undulation, fiber drying, and surface treatments;
5. winding of the membrane bundles; and
6. recycling of solvent and precipitating liquid.

The entire membrane-manufacturing process (spinning process), from membrane formation to winding bundles, is shown schematically in [Figure 12](#). These steps are described in detail below.

The production of dialysis membranes uses different polymers and processes to allow the manufacture of a range of dialysis membranes with defined properties. Today, mainly diffusion-induced phase separation (DIPS) processes are used, which

allow the use of a combination of polymers, and fine-tune pore-size and diffusive transport characteristics. The polymers are dissolved in a suitable solvent, and precipitation takes place in a nonsolvent bath, preferably water. The concentration of the polymer in the polymer solution is approximately 20 wt.%, depending on the particular recipe.

The polymer solution is pumped through an annular die (spinneret) to form a hollow fiber. The inner void of the hollow fiber is formed by a bore liquid (mixture of solvent and nonsolvent), which is introduced into the inner part of the spinneret. In a third step, the hollow fiber is guided through a nonsolvent bath. The nonsolvent bath and bore liquid are required to convert the homogeneous liquid-polymer solution into a two-phase system by diffusive solvent-nonsolvent exchange (immersion precipitation). The demixing process stops at the vitrification point of the polymer-rich phase. A rigid membrane

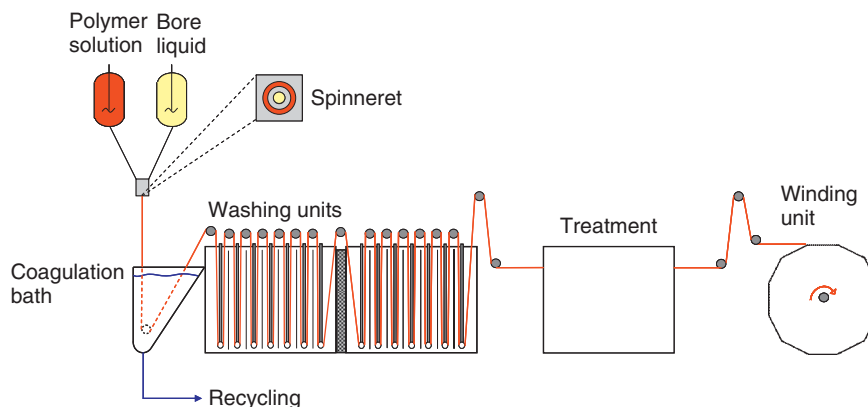


Figure 12 Schematic drawing of a synthetic hollow fiber membrane-manufacturing plant.

structure is formed during the polymer-rich phase, and the membrane pores are formed during the liquid–polymer-poor phase.

The main influences on membrane properties during the manufacturing process are: composition, viscosity and temperature of the polymer solution, the use of additives, the ability to crystallize or aggregate, nozzle design, composition of the coagulation bath, and the conditions between nozzle and coagulation-bath entrance.

The quality of a membrane strongly depends on the quality of the polymers used and the preparation procedure of the polymer solution (spinning solution). Reproducibility of the membrane properties can only be guaranteed if polymer quality (molecular-weight distribution, moisture, etc.) and solution quality (free of gel particles, viscosity, free of dissolved gas) are constant throughout the year from batch to batch. The size of the batch of the polymer solutions is dependent on the number of spinning machines connected to one polymer-solution manufacturing plant and the number of nozzles per spinning machine. The solution batches can vary from a few hundred to several thousand kilograms.

Typically, the membrane-manufacturing process is continuous, and spinning machines will only need maintenance work for only a few days a year. Modern spinning machines may have more than 1000 spinning nozzles, and spinning speeds of up to 100 m min^{-1} may be realized.

2.13.7.2 Precipitation of the Membrane and Subsequent Washing

After passing through the nozzle, the membrane is guided into a coagulation bath where the external structure of the membrane is formed. The composition and temperature of the coagulation bath play an important role in determining the membrane's structural properties. In the coagulation bath, the largest part of the solvent from the polymer solution is removed. For complete removal of the solvent, subsequent rinsing units are installed. The membranes formed are guided through these baths until fully stabilized. Several techniques have been developed whereby the membranes are guided through either connected or separated washing baths or water/non-solvent spraying chambers.

2.13.7.3 Recycling of Solvents and Precipitating Agents

In particular, environmental aspects are considered in the membrane-manufacturing process. Some examples of this are the use of water to precipitate the media, and the recovery of this water and solvent in a recycling plant. These processes reduce the consumption of water and solvents to a minimum.

The total length of a spinning line can be up to 100 m in length, and the length of a membrane from the spinneret to the winding wheel can be more than 1 000 m to ensure adequate extraction of the solvent. Thus, guidance of the membrane requires precise control with driving units and pulleys.

2.13.7.4 Finishing Treatments

After rinsing, the hollow fiber is dried online (directly within the manufacturing process, leading to reduced processing time). Subsequently, different processes, such as coating, undulation, and surface modifications, can be applied.

Undulation changes the geometry of the fibers. This special technique forms waves with different amplitudes and wavelengths of the fibers (see [Figure 13\(b\)](#)). By applying this technique, in combination with advanced bundle formation, an ideal bundle is formed, which has been proven to be efficient in increasing mass transfer through the membrane into the dialyzer.

2.13.7.5 Winding

The spinning machines lead on to the winding unit. All single hollow fiber membranes, originating from one or more spinning machines, are guided together into one winding unit. To increase mass transport,

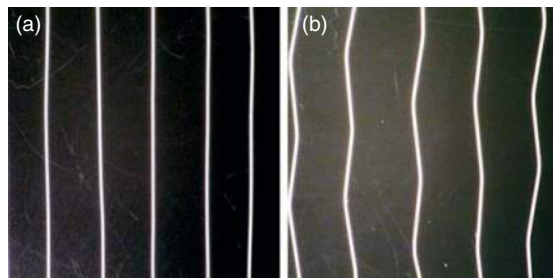


Figure 13 Photographs of (a) straight fibers and (b) undulated fibers.

the winding equipment often places the membranes in parallel or in defined patterns, for example, cross winding, to add inert support fibers. The bundle configuration is of crucial importance for the distribution of the dialysate in the dialyzer.

All modern dialysis (ultrafiltration) membranes are prepared free of pore stabilizers. This is one example of the highly sophisticated manufacturing process and the level of membrane development. Manufacturing of pore-stabilizer-free membranes improves handling of the product in clinical applications and allows reduction in the number of process steps.

2.13.7.6 Dialyzer Assembly

2.13.7.6.1 Bundle transfer into housing

After winding the membrane bundles, the bundle is transferred into the dialyzer housing. High package densities for highly efficient dialyzers require a well-designed technique for precise bundle transfer without damaging a single fiber within the bundle. The material of the housing needs to provide mechanical stability, transparency, and stability against the different types of sterilization (steam, γ -radiation, and ethylene oxide). The design of the housing itself, and the endcaps for the blood inlet and outlet, are important as they largely determine the distribution of the blood and dialysate, as well as any pressure drops in the system.

2.13.7.6.2 Potting

In the dialyzer assembly, the membrane bundles are merged with the housing parts. To separate the blood compartment from the dialysate compartment, polyurethane (two components: polyol and multi-functional isocyanates) is used as the membrane

potting material. Polyurethane has been proven not to release any toxic substances or substances that could lead to blood clotting.

To attach the ends of the membrane bundle effectively with the potting material, and to get a defect-free sealing of each individual membrane between the blood and dialysate compartments, special centrifuge systems are utilized. To avoid chemical reactions between residual water of the fibers and the potting material, the membranes are carefully dried prior to potting, and the fiber ends are sealed so that no potting material can penetrate. The potting conditions, the curing time, and the viscosity and strength of the potting material have to be adjusted to the specific characteristics of the hollow fiber membrane.

To open up the hollow fiber membrane, the ends of the potted bundle are cut. A smooth and flat surface is crucial to prevent hemolysis or blood clotting. Today, specialized knives are usually used for cutting. **Figure 14(a)** shows an acceptable cutting quality, whereas **Figure 14(b)** shows a cutting surface that is too rough.

2.13.7.6.3 Integrity test

After applying the endcaps to the dialyzer housing, the integrity of the dialyzer is checked. This test verifies the integrity of all the housing components, the connections, and the membrane itself. Normally, a dialyzer contains between 8000 and 14000 fibers and the specially designed membrane-integrity tests allow detection of a single fiber leak or deviation in membrane performance from that specified. Finally, a visual control guarantees that each product is safe and within the specifications given. Products that are not within specification are scrapped.

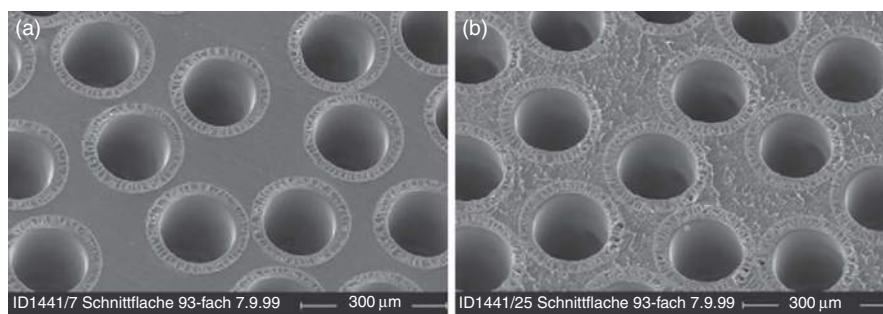


Figure 14 Scanning electron microscopic (SEM) images of the cutting surface of two different dialyzers: (a) a smooth surface of the blood-contacting surface of a standard product; (b) a rough cut surface not meeting quality requirements. White bar = 300 μm .

2.13.7.6.4 Sterilization

A prerequisite before use by the patient is verification of the dialyzer's sterility [38]. Three different sterilization methods are in common usage: γ -radiation, steam, and ethylene oxide (ETO). The choice of sterilization method can influence membrane performance, for example, pore-size distribution, depending on the condition of the membrane (in aqueous solution, moist or dry) during sterilization.

ETO reacts with the proteins and nucleic acids of microorganisms to destroy them. The influence of ETO is dependent on the membrane material and its structural properties. The disadvantage of ETO is its solubility in polyurethane. Due to the high toxicity and reactivity of polyurethane, the dialyzer must be degassed after the sterilization process to allow safe limits in the final product prior to its application. The use of ETO as a sterilizing agent for products used in chronic applications is steadily declining.

The worldwide acceptance for γ -sterilized medical devices has increased and is, today, with steam sterilization, a standard technique. The radiation dose for γ -sterilization is between 5 and 40 kGy, and bacteria are killed physically.

In steam sterilization, microorganisms are destroyed by heat denaturation of their cell walls and proteins, and no use of toxic or radioactive substances is required. Steam sterilization is performed for at least 20 min at a temperature of at least 121 °C and at a pressure of at least 0.1 MPa.

The choice of sterilization method depends on the stability of the materials of the membrane, the housing, and the potting material. Steam sterilization is, however, in terms of environmental impact and patient application, the method of choice.

2.13.8 High Cutoff Dialysis Membranes

2.13.8.1 Membrane Description

Low- and high-flux membranes are commonly used for the treatment of chronic and acute kidney failure. However, even high-flux membranes have a limited ability to clear molecules that exceed a molecular weight of 20 000 Da and those that are effectively cleared by the native kidney, such as low-molecular-weight proteins (LMWPs), which have a molecular weight spectrum of \sim 1000—50 000 Da. More effective transmembrane elimination of these molecules from the circulation is particularly desirable in conditions where LMWPs that are involved in pathophysiological

mechanisms are rapidly produced and accumulate in the circulation. Examples include free light-chain proteins and inflammatory cytokines. Monoclonal light chains of immunoglobulin are excessively produced by malignant plasma cells in patients with MM, and can cause renal lesions such as cast nephropathy. In this condition, serum concentrations can be elevated by more than 100-fold compared to normal serum concentrations. Pro-inflammatory cytokines are overexpressed in acute inflammatory diseases and contribute to the pathogenesis of septic acute kidney injury (AKI). In order to maximize LMWP removal and to enlarge the molecular-weight spectrum of solutes removed during dialysis treatments, high cut-off (HCO) membranes with increased pore sizes have been developed and investigated in clinical studies.

In HCO membranes, pore sizes are shifted toward larger pore diameter compared with conventional high-flux membranes. Accordingly, significantly higher permeability for substances in the molecular-weight range of 15–50 kDa can be achieved with this membrane compared to permeability rates achieved with conventional high-flux membranes. **Figure 15** shows the pore-size distribution for an HCO membrane, with the maximum number of pores in the range of 10 nm radius.

A narrow distribution ensures a sharp upper cutoff and limits the permeability for essential larger proteins, such as albumin, clotting factors, and immunoglobulins. Comparisons of the pore-size distributions of a conventional high-flux membrane and an HCO membrane have been made. High-flux membranes show typical pore sizes of between 3 and 6 nm, whereas HCO membranes have pore sizes of $>$ 200 nm, and allow the unrestricted passage of all plasma proteins.

The increase in pore sizes of HCO membranes translates to an increase in both convective and diffusive permeabilities of LMWPs. The sieving coefficient (i.e., the ratio between solute concentration in the ultrafiltrate and its average plasma concentration) characterizes the convective membrane's permeability for a given solute. The sieving coefficient is inversely related to the solute's molecular weight. HCO solutes, with molecular weights that range from 20 to 50 kDa, which do not pass through the high-flux membrane, can filtrate through the HCO membrane to a significant extent (see **Figure 16**).

A much higher diffusive permeability of larger molecules is also observed. Whereas the diffusion rates for smaller solutes are quite similar for HCO and high-flux membranes, diffusive transport is less

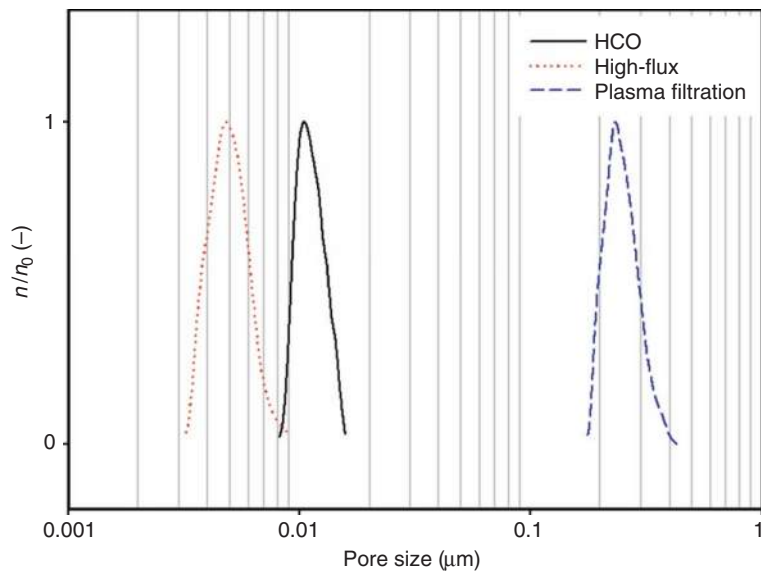


Figure 15 Pore-size distribution of high-flux (Polyflux S), high cut-off (HCO), and plasmafiltration membranes.

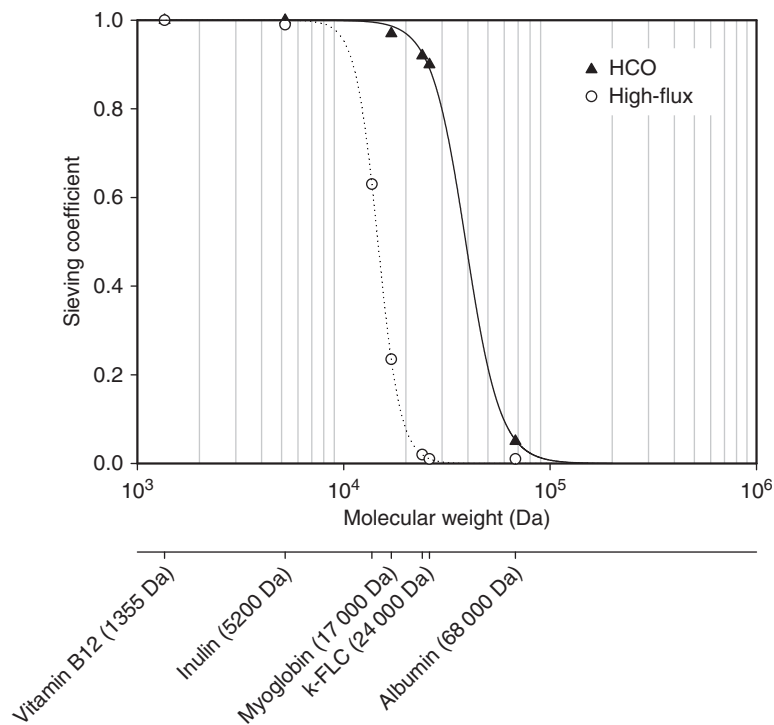


Figure 16 Sieving coefficients for high-flux (Polyflux S) and HCO membranes, as determined with blood.

hindered for larger molecules. For the HCO membrane, there is less steric interaction between the solute and the larger pores of its membrane compared with those of high-flux membranes (see [Figure 17](#)).

Over the last decade, various membranes, such as the cellulose triacetate-based FH 70/150 (Sureflux,

Nipro [39]), the polysulfone-based APS-1050 (Asahi [40]), the PMMA-based BK-F/BG 2.1 (Torry [41]), and the Helixone polysulfone-based FX-E (Fresenius Medical Care [42]), have been manufactured with the purpose to gain increased membrane permeability. These different membranes have

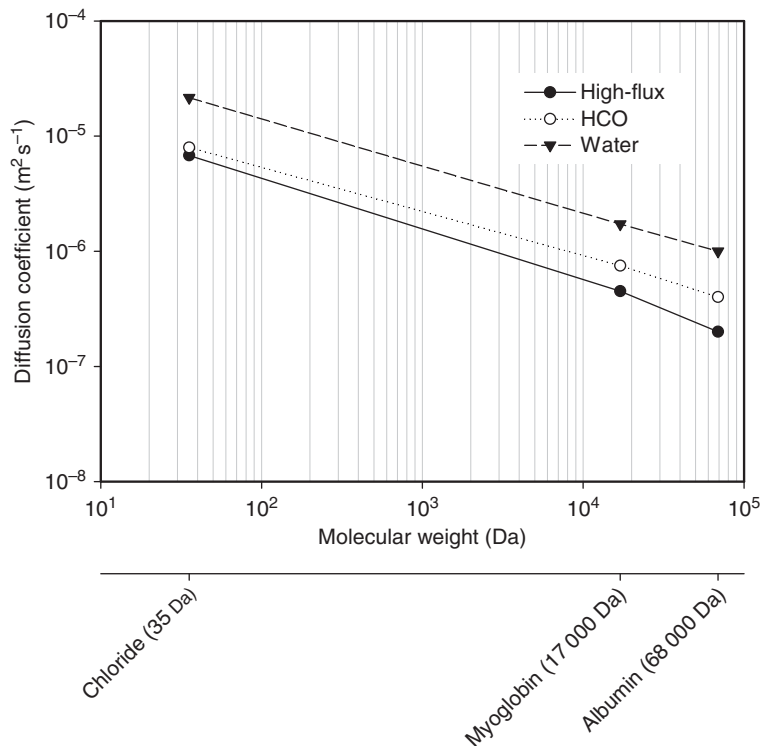


Figure 17 Diffusion coefficient in water and effective membrane diffusion coefficients for high-flux (Polyflux S) and HCO membranes as a function of solute size.

recently been compared for their free light chains (FLC)-removal capacity [43]. Hutchison and colleagues found that the HCO membrane exerted the highest elimination rate of FLC. Interestingly, the FLC-elimination capacity of PMMA-based BK-F/BG 2.1 was more caused by absorption than dialysis, which indicates an obstacle in removing sufficient amounts of FLC from MM patients. These test results are summarized in **Table 3**.

2.13.8.2 HCO Membranes in the Treatment of Kidney Myeloma

2.13.8.2.1 Renal disease MM

MM is a plasma-cell dyscrasia that accounts for almost 10% of all hematologic malignancies. The annual incidence of MM is 4–5 per 100 000 people [44]. Renal involvement remains a major complication in MM, particularly in advanced stages of the disease. Renal impairment is found in up to 30% of patients at initial presentation, and in up to 50% of patients at some stage of the disease. In about 10–20% of patients, severe renal dysfunction that requires dialysis develops, with most of these patients becoming dependent on chronic hemodialysis. Renal failure limits

therapeutic options for these patients and aggravates prognosis. It is amply documented that patient survival decreases in proportion to the severity of renal failure [45, 46]. ‘Myeloma kidney’ or cast nephropathy is the most common cause of renal disease in MM, and is caused by FLCs excessively produced in the bone marrow by a clone of the neoplastic plasma cells. Large amounts of FLCs are released into the circulation. In the kidney, these proteins readily pass through the glomerular apparatus, which can overwhelm the absorptive capacity of the proximal tubules and initiate a stress response. In the distal tubules, the light chains can co-aggregate with Tamm–Horsfall protein, which is produced in the thick ascending limb of the loop of Henle. This finally results in apoptosis of tubular cells, tubulointerstitial fibrosis, tubular cast formation, and tubular obstruction. Less frequent renal lesions, caused by free light chains, are AL amyloidosis and light-chain-deposition disease.

2.13.8.2.2 Therapeutic interventions in myeloma-cast nephropathy

Shortening the time in which the patients’ kidneys are exposed to toxic levels of light chains lowers the risk for long-term renal damage. Therefore, prompt

Table 3 FLC elimination by different membranes in patients with multiple myeloma

Class	Make	Model	Membrane material	Surface area (m ²)	Molecular cutoff in Blood (kDa)	Mean FLC concentration in UF (%)	
						κ	λ
High flux	B. Braun	Hi-PeS 18	PES	1.8	10	17	12
	Asahi	APS-1050	PS	2.1	10	30	18
	Nikkiso	FLX 8GWS	PEPA	1.8	10	12	11
	Idemsa	200 mHP	PES	2.0	10	21	16
Super flux	Toray	BK-F 2.1	PMMA	2.1	20	0.1	0.2
	Toray	BG 2.1	PMMA	2.1	20	0.1	0.1
High cutoff	Gambro	HCO 1100	PAES	1.1	45	62.5	90

FLC, free light chains; PAES, polyarylethersulfone; PEPA, polyester polymer alloy; PES, polyethersulfone; PMMA, polymethylmethacrylate; PS, polysulfone; UF, ultrafiltrate.

intervention that aims at rapid reduction of pre-renal FLC load is essential to facilitate the recovery of renal function and to avoid irreversible renal impairment: chronic hemodialysis then becomes mandatory for the rest of the patient's life. Rapid administration of cytoreductive chemotherapy induces reduction of the tumor burden and of production of FLC in these patients. To acutely reduce FLC plasma levels, additional FLC removal from the circulation by extracorporeal blood-treatment therapies have been investigated in clinical studies. Hutchison *et al.* [43] showed that, daily extended hemodialysis represents an effective treatment for removal of large quantities of FLC, provided the pore size of the membrane is large enough to facilitate significant transmembrane transport of FLC, which exist as monomers (23 kDa) and dimers (45 kDa). The results of serum FLC removal in patients with MM using different membranes are shown in **Table 4**.

Significantly higher FLC dialysate concentrations, and greater serum reductions and FLC clearance rates were achieved using the HCO membrane compared to less open porous dialysis membranes. Treatments with the HCO membrane have provided post-dialysis reduction rates of greater than 50%. **Figure 18** shows the serum and dialysate FLC concentrations during an 8-h hemodialysis session using the HCO membrane.

A total of more than 20 g of λ-FLCs were removed in this single dialysis session. **Figure 19** shows the daily pre- and post-dialysis serum kappa FLC concentrations, and the amounts of FLC removed in the dialysate fluid (per 10-day period) for a patient who had 42 g l⁻¹ of serum FLC at clinical presentation.

In this patient, measurement of dialysate FLC concentrations during a 6-week period indicated removal of 1.7 kg. This study has demonstrated that extended dialysis using an HCO membrane could

Table 4 Concentration of FLCs in serum and dialysate fluid of a patient with acute renal failure caused by multiple myeloma, and who was undergoing dialysis using a high cut-off dialyzer

Membrane dialyzer	Pre-dialysis serum conc. (mg ⁻¹ l)	Mean % reduction in serum conc.	Mean (range) dialysate conc. (mg ⁻¹ l)	Mean dialysate (mg ⁻¹ h)	Mean clearance (ml min ⁻¹)
Toray BK-F2.1	11 580	3.2	6.9 (0.8–20.3)	200	0.29
B. Braun Hi-Pes18	1 795	5.6*	5.3* (2.7–9.5)	160*	1.5*
Toray BK-F2.1	2 950	24.2*	2* (0.5–3.5)	60*	0.5*
Gambro HCO 1100	9 155	58.5	265.6 (88–648)	7,800	22

*Significant less than the Gambro HCO 1100 result for this patient (P < 0.02).

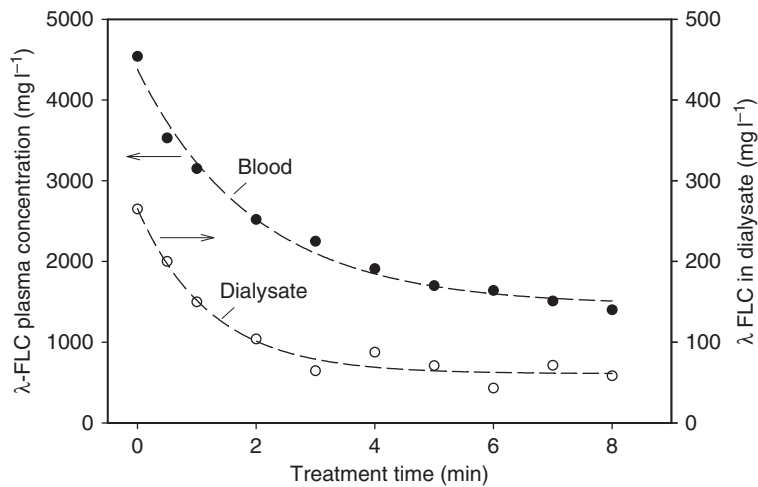


Figure 18 Serum and dialysate lambda FLC concentrations during an 8-hemodialysis session using the HCO membrane.

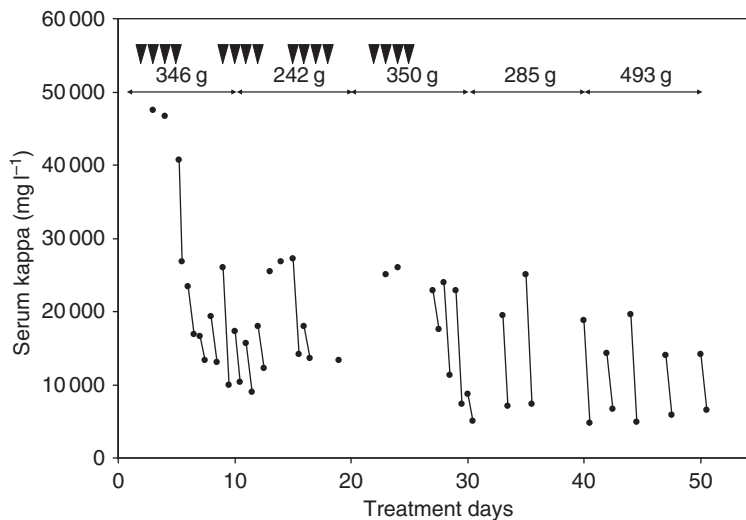


Figure 19 Pre- and post-dialysis serum kappa FLC concentrations in a patient treated with the HCO membrane over a period of 50 days. Pre- and dialysis samples are connected by a line. Numbers indicate the amount of FLCs (in grams) removed in the dialysate per 10-day period. The arrowheads (▼) correspond to a daily application of chemotherapy.

continuously remove large quantities of FLC. This elimination leads to early sustained reductions in serum FLC concentrations provided that FLC production rate by the tumor can be switched off by an effective chemotherapy.

2.13.8.2.3 Recovery from renal failure following FLC removal with HCO dialysis

Historically, the combination of dialysis dependence and FLC-induced renal pathology secondary to MM has been associated with very poor renal outcomes, with most patients becoming dependent on chronic dialysis. In a pilot trial with 17 patients with FLC-

induced AKI, it was shown that rapid reduction of FLC serum concentrations, using an effective chemotherapy and FLC removal with HCO dialysis, facilitated recovery of renal function [47]. All patients who achieved a sustained reduction of greater than 60% of FLCs recovered renal function and became independent of hemodialysis. The renal-recovery rate for these treated patients is shown in **Figure 20**, alongside the historical recovery rates at the same hospital.

Clearly, patients who received FLC removal with HCO dialysis had better renal-recovery rates. These results suggest that renal recovery is possible in most

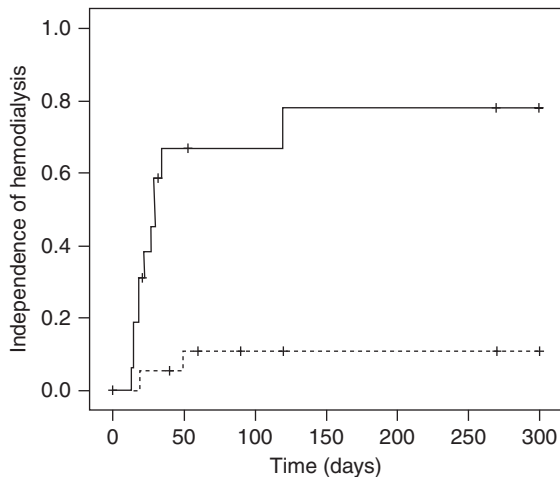


Figure 20 Kaplan–Meier plot of renal recovery in 17 patients with multiple myeloma (MM) and acute renal failure (ARF) treated by chemotherapy and dialysis with HCO membranes (—). The control group (□) comprises 17 patients treated with a similar chemotherapy, but using conventional hemodialysis.

patients with MM who present with acute renal failure from cast nephropathy, if a rapid reduction of FLCs to normal concentration has been achieved using HCO membranes in combination with an effective chemotherapy.

2.13.9 High Cutoff Membranes for the Treatment of Sepsis-Induced ARF

2.13.9.1 AKI Induced by Sepsis

Severe sepsis, a whole-body systemic inflammatory response syndrome (SIRS), is one of the most frequent causes of death. Mortality rate of SIRS varies from 30% to 100%, depending on the number of organs involved.

The body may develop SIRS as an inflammatory response to microbes or to traumatic events such as burned skin. Severe sepsis can lead to low blood pressure and insufficient blood flow (septic shock), and cause AKI or multiple-organ failure (MOF). Endotoxins (lipopolysaccharides (LPS)), derived from Gram-negative bacteria, are principal mediators, which stimulate the synthesis of cytokines (TNF- α , IL-1, and IL-6) and other pro-inflammatory mediators (thromboxane A₂, prostacyclin, platelet-activating factor, and nitric oxide) by monocytes. Sepsis is usually treated in the intensive care unit with intravenous-fluid replacement and antibiotics. If fluid replacement

is insufficient to maintain blood pressure, specific vaso-pressor drugs are used. Artificial ventilation and dialysis may be needed to support the function of the lungs and kidneys, respectively.

Under normal physiological conditions, the kidneys' filtration units (glomeruli) are capable of removal of cytokines. In cases of acute renal failure (ARF), cytokines and other pro-inflammatory mediators are not eliminated.

Much clinical and molecular biological research suggests that cytokines and other septic-shock mediators are pivotal contributors to the pathogenesis of septic shock and multiple organ failure, including ARF.

The vast majority of cytokines are water soluble and of middle molecular weight (5–50 kDa). These properties make them potentially removable by HF or HD. However, standard HF or HD membranes, even when used in a high-volume HF mode, can remove few cytokines, either by transmembrane transport or by adsorption. Hence, conventional RRTs have failed to significantly eliminate cytokines and sustainably reduce plasma levels. This is attributable to the limited pore size and the limited adsorption capacity of standard membranes. An approach to overcome these limitations is the use of a membrane with moderately increased pore sizes, facilitating a high permeability for cytokines and, at the same time, a high retention of larger proteins.

2.13.9.2 Clinical Investigations with HCO in AKI and Sepsis

The HCO membrane has been investigated in a series of *ex vivo* studies. In summary, these studies show that treatment with HCO is safe and efficient regarding elimination of substances with molecular weights up to \sim 50 kDa. These *ex vivo* studies were performed to determine and optimize performance characteristics of cytokine removal and albumin retention.

In one of the first *ex vivo* studies, HCO hemodialysis of LPS-stimulated blood from six healthy volunteers was tested in a closed extracorporeal circuit. It was the first study to demonstrate that cytokine dialysis is achievable through a membrane with a high cutoff point, and is associated with negligible albumin loss [48].

Another *ex vivo* study was performed to evaluate the difference between diffusion versus convection on the performance characteristics of HCO membranes. HCO-HF, hemodialysis, and albumin

dialysis of LPS-stimulated blood from 15 healthy volunteers was tested in a closed extracorporeal circuit for 4 h. High cutoff hemofilters achieved high clearances for inflammatory IL-6 and TNF- α . Using diffusion instead of convection significantly reduced the loss of albumin [49].

A prospective, randomized, controlled trial, with two study arms, was performed to evaluate the safety of HCO treatment by continuous venovenous hemofiltration (CVVH) and post-dilution for a period of 5 days in 32 patients with MOF induced by septic shock. In the treatment arm, patients were treated for 12 h per day with a HCO-membrane and for 12 h per day with a conventional high-flux membrane. In the control group, patients were treated for 24 h per day with a conventional high-flux membrane. Treatment by HCO-HF significantly eliminated cytokines leading to a sustainable decline in the total amount of circulating IL-6. The median 12-h albumin loss was 4.8 g. Plasma levels of coagulation factors and albumin remained unchanged throughout the treatment period. The authors concluded that HCO-HF had no unexpected adverse events and, overall, was well tolerated [50].

Furthermore, it was investigated whether surrogate biomarkers of immune status were influenced by HCO-HF. It could be demonstrated that collected HCO filtrates of patients could activate the release of TNF- α (and phagocytosis rates) of peripheral blood monocyte cultures derived from healthy volunteers [51]. This indicates that HCO-HF successfully eliminated mediators that could have contributed to immune-pathophysiological cellular activities.

In addition, it was shown that incubation of peripheral blood leucocytes with HCO filtrates restored the proliferation of T-lymphocytes, indicating that the HCO-HF treatment may have improved the immune status of patients with severe sepsis [52].

In another prospective randomized clinical trial, HCO-membrane effects were investigated using different dialysis modalities. Twenty-four patients with septic shock complicated by ARF were tailored into four study arms to compare diffusive (CVVH: UF = 11 h⁻¹, and UF = 2.51 h⁻¹) versus convective hemodiafiltration (continued venous to venous hemodialysis (CVVHD)) HCO treatment for 3 days. It was shown that both HCO-CVVH and CVVHD were effectively cleared of cytokines (IL-6, IL-1 β , IL-1ra). However, HCO-CVVHD was associated with less plasma protein loss than CVVH. It was further

demonstrated that antithrombin III (MW = 58 kDa) was not affected by these HCO treatments [53].

In order to evaluate the positive clinical effect, a prospective, randomized, clinical trial with two study arms was conducted to compare HCO versus conventional high-flux-CVVH for 48 h. Thirty patients with sepsis-induced ARF were included in this study. In this patient population, norepinephrine treatment was needed to stabilize the circulation of these patients with severe sepsis. It was found that HCO-HF was superior in eliminating IL-6 and IL-1ra, and that HCO-HF exerted a beneficial effect on the need for norepinephrine. Furthermore, a trend towards a decline in a sepsis severity score was observed in the HCO group [54].

In a double-blind, crossover, randomized, controlled, phase 1 trial, 10 patients with septicemia induced by ARF were treated for 4 h with HCO intermittent hemodialysis (IHD) versus high-flux IHD, at a blood flow, Q_B , of 200 ml min⁻¹, and a dialysate flow, Q_D , of 300 ml min⁻¹. In those patients who also had acute renal failure, HCO-IHD exerted increased diffusive cytokine clearance and a greater relative decrease in plasma cytokine concentrations than standard high-flux IHD. Control of uremia was achieved equally in both treatment modes. Clinically, a trend for improved mean arterial pressure and a decrease in norepinephrine (from 8–2 μ g min⁻¹) was shown for the HCO group [55].

The use of different protein-leaking dialyzers has been tested by academic working groups to treat septic AKI. A systematic review by Haase *et al.* [56] concluded that HCO membranes provided a feasible and safe method to remove pro- and anti-inflammatory mediators from patients with sepsis when this was complicated by AKI.

2.13.10 Membranes for Bioartificial Kidneys

2.13.10.1 Background and Motivation

Membranes used for extracorporeal treatments of chronic and acute renal failure in the dialysis setting have been described above. Here, membranes suitable for integration of cells into an extracorporeal system such as bioartificial kidneys are discussed.

Even though conventional dialysis treatments are mandatory and pivotal for the survival of kidney failure patients, the mortality rates for AKI patients on hemodialysis or continuous RRT range from 50%

to 70%, without substantial improvement over the past few decades [57–59]. If a hospitalized patient develops AKI, which occurs in 5–7% of hospitalized patients, the risk of death is five- to eightfold higher compared to hospitalized patients without AKI [60, 61]. The cost of ARF is estimated to be ~\$8 billion per year, equivalent to ~\$130 000 per life-year saved in the US [62]. Damage to kidney-tissue function is a key element in the pathophysiological sequence of AKI. At a molecular level, tissue injury to endothelial and epithelial cells of the tubule system is critical in the pathophysiology of AKI [63, 64]. Vasoconstriction and damage of the vasculature accompanied by endothelial injury are important contributors to inflammation [63]. Tubule epithelial cells undergo cell death by necrosis and apoptosis, and have the capacity to express a large variety of cytokines, which contribute to the inflammatory response [65, 66].

It is of particular interest that renal tubules have a high regenerative capacity. Particularly after short ischemia periods, that is, short periods of kidney damage, damage to renal function is reversible, and the kidney can almost completely regenerate [59, 65]. However, exceeding a certain severity threshold (e.g., prolonged periods of ischemia), renal failure leads to diminished solute and water excretion, and finally to total organ failure [67].

Currently applied and conventional RRTs are limited to partially substituting the function of the glomerulus. The glomerulus represents a highly selective filter for removal of small solutes and fluid volume. This function can be replaced by membranes in dialyzers or filters. However, membranes used in RRTs do not replace the biological function of the whole kidney tubule system, that is, the metabolic, endocrine, and immune functions. Tubule epithelial cells play an important role in a variety of metabolic activities, such as glutathione reclamation, activation of vitamin D, or re-absorption of molecules such as proteins, glucose, or acids from the tubule. The endocrine functions of the kidney include, among many others, biosynthesis of proteins (e.g., parathyroid hormone, erythropoietin, renin, and peroxidase), production of prostaglandins, and secretion of growth factors and cytokines [68]. Furthermore, the tubule cells may exert immune functions, which include endotoxin depletion or production of bactericidal defensins. These are antigen-presenting cells that possess co-stimulatory molecules and synthesize inflammatory cytokines upon stimulation [69, 70]. Consequently, a replacement system needs to be able to mimic not only the glomerulus as a filter for the kidney,

but also the tubule as metabolic, endocrine, and immunoregulatory unit of the kidney.

2.13.10.2 The Concept of Bioartificial Kidneys

The concept of bioartificial kidneys was proposed, in the late 1980s, to cover semipermeable hollow fiber membranes with renal epithelial cells as a design for a bioartificial kidney [71]. The idea was to design an extracorporeal support that used renal epithelial cells as an equivalent biohybrid construct. It was hoped that this would provide an extended and more efficient blood purification process and, at the same time, act as a substitute for the endocrine, metabolic, and immune functions of the renal tubule system. In addition, it was hoped that this construct could improve the metabolic milieu and enable substitution of tubule tissue function, or even regeneration of tubular tissue. All proposed bioartificial kidney concepts rely on a combination of ultrafiltration, using conventional hemofilters, and a secondary epithelial cell-based bioreactor to replace tubular reabsorption and secretion of cell-derived factors. One of many potential designs of an epithelial cell-based extracorporeal treatment system to utilize bioartificial kidneys in clinical settings is shown in [Figure 21](#).

The patient's blood is passed through a primary dialysis and filtration unit, as is used today in RRTs. The filtrate of the primary unit is then passed through the inner side of a secondary hollow fiber cartridge, which contains hollow fibers lined with a confluent and a tight monolayer of functional epithelial cells on the intra-capillary side. The blood leaving the primary unit undergoes additional filtering through the extra-capillary side of the secondary cartridge.

After exposure to the cell-processed and modified filtrate via the membrane, the blood is then returned to the patient. There are many possible alternatives to this design, such as incorporation of different epithelial cell types from different parts of the tubule system (proximal, distal, and collecting duct), positioning of the cells in the hollow fiber cartridges (extra-capillary side or intra-capillary side), configuration of the hollow fiber device, etc.

2.13.10.3 Membranes Used for Bioartificial Kidneys

Following the concept of seeding renal tubule cells onto membranes as part of an extracorporeal system, porous membranes are the first choice and are used in

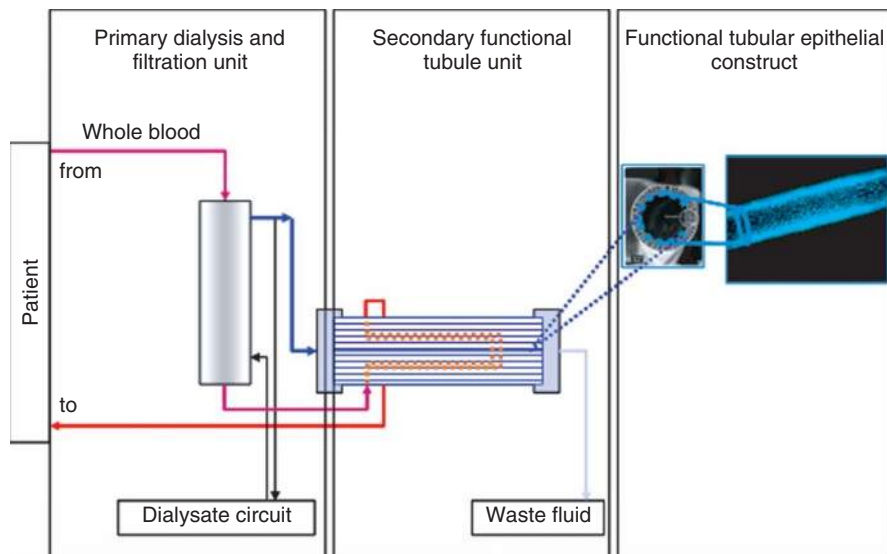


Figure 21 Possible design of a bioartificial kidney system connected to a patient. The patient is connected to an extracorporeal system. The patient's blood is passed through a primary dialysis and filtration unit, as used today in renal-replacement therapies (RRTs). The filtrate of the primary unit is subsequently flowed through the inner side of a secondary hollow fiber cartridge that contains cells on the intra-capillary side. The patient's blood leaving the primary unit is pumped through the extra-capillary side of the secondary cartridge and is returned to the patient (adopted from Humes [70]). The right panel illustrates cells seeded into a hollow fiber, and shows the blue-stained nuclei of epithelial cells.

most applications. Most cultured adherent cells are grown on solid substrates, primarily tissue-culture plates or flasks. However, epithelial cells, such as renal tubule epithelial cells, form tight monolayers, as they are usually supplied with nutrients from the baso-lateral surface, that is, the side where the epithelial cell surface is in closest proximity to blood vessels *in vivo* [72]. If epithelial cells grow to form a tight monolayer on a solid substrate, a sufficient supply of nutrients cannot be assured and, as a consequence, those cells lose their polarity accompanied by dedifferentiation processes [73]. Loss of polarity and dedifferentiation processes of epithelial cells can be avoided by growing the cells on a porous substrate with a nutrient-supplying medium that supplies both the apical and baso-lateral surfaces [74].

Porosity is an important property of substrates for cultivating epithelial cells. Another crucial feature is to mimic the *in vivo*-like conditions in a three-dimensional (3D) context, for instance, gels or hollow fibers [72]. In addition, the 3-D context gives epithelial cells an increased resistance to apoptosis [75]. Other conditions, such as medium composition, concentration of calcium, and mechanical stiffness of the substrate, influence the growth and functional properties of epithelial cells.

In developing a bioartificial kidney, hollow fiber membranes have been shown to be far superior in various respects compared to flat membrane configurations. Hollow fibers exhibit a high surface-to-volume ratio, resulting in a reduced need for incubation space, reduced material consumption, which is a prerequisite for automation of the culture process when integrated into a closed system (see also Reference 67).

The requirements for membrane materials and cell culture systems suitable for epithelial cell growth, and the maintenance of cells in a differentiated functional state to use in bioartificial kidneys are, among others, the following:

1. long-term stability of the polymeric substrate to allow long-term cell culture;
2. maintenance of tubule cell function in long-term cultures;
3. possibility to integrate the membrane device in a hollow fiber perfusion system to facilitate adherence and confluent growth of epithelial tubule cells; and
4. development of small-lumen hollow fibers with a biocompatible outer surface.

Different membrane materials, including synthetic materials or materials coated with proteins, have

been used in various approaches to form an epithelial-based tubule-type bioartificial kidney. Membrane materials used in dialyzer devices are designed to exhibit high biocompatibility, which is achieved by high resistance of the membrane surface to protein adsorption and cell interaction. Surfaces of such types can mostly be modified with extra-cellular matrix proteins, such as fibronectin or derivatives, collagen, laminin or derivatives, or Matrigel to allow cell adhesion and cell growth. In the earliest approaches toward producing a bioartificial kidney, by the Aebischer and Galetti group, epithelial cell lines were grown on the outer surface of a polyvinylchloride-acrylic copolymer and polysulfone membrane coated with extra-cellular matrix proteins, such as a mixture of collagen type I and III or Matrigel [76, 77]. In later publications, this group also describes cellulose-nitrate flat membranes coated with collagen I and III, Matrigel, or mussel-adhesive protein [78–80].

Fey-Lamprecht *et al.* [81–83] investigated the suitability of flat and hollow fiber membranes made from polysulfone or polysulfone-PVP blends with PAN for their adhesion, growth, and maintenance properties regarding confluent monolayers of canine Madin-Darby kidney epithelial cells (MDCK). Both membrane types were able to support and maintain epithelial cells, although polysulfone was reported to show decreased cell adhesion. Exceptionally, a surface modification of the polysulfone-PVP membrane with extra-cellular matrix proteins was not applied (in contrast to most other studies that have applied polysulfone-based membranes). In addition to these materials, Fey-Lamprecht *et al.* used poly(acrylonitrile-*N*-vinylpyrrolidone) (P(AN-PVP)), which was found to be suitable for epithelial cell culture. Fey-Lamprecht *et al.* designed fiber-in-fiber bioreactors, that is, inner fibers with an inner diameter of ~400–500 μm , that could be placed in the intra-capillary space of outer fibers (diameters of 750 or 820 μm). Cells were grown in the space between the inner layer of the outer fiber and the outer layer of the inner fiber. The authors suggest that this configuration might lead to improved cell growth due to an improved supply of oxygen and the presence of mitogenic factors secreted by the cells. However, undesired overgrowth of MDCK cells, which formed multilayers, were observed, though this was less pronounced using P(AN-PVP) membranes.

Saito *et al.* intended to develop a bioartificial kidney consisting of continuous HF with 101 day^{-1} of filtrate and an epithelial cell-based cartridge in conjunction.

An investigation into the functional and transport properties of epithelial cells, MDCK and wild-type and Aquaporin-1 transfected Lewis-lung cancer porcine kidney cells (LLC-PK₁), was carried out using polycarbonate flat membranes. The membranes were coated with Pronectin-F, an engineered tripeptide RGD-containing protein [84], fibronectin [85, 86], or laminin [85]. Artificial membranes as hollow fiber substrates for epithelial cells including polysulfone membranes, optionally coated with collagen I and IV or Pronectin-F, as well as membranes made from polyimide or (EVAL)copolymer were used to grow mainly MDCK, HK-2, or LLC-PK₁ [87–89].

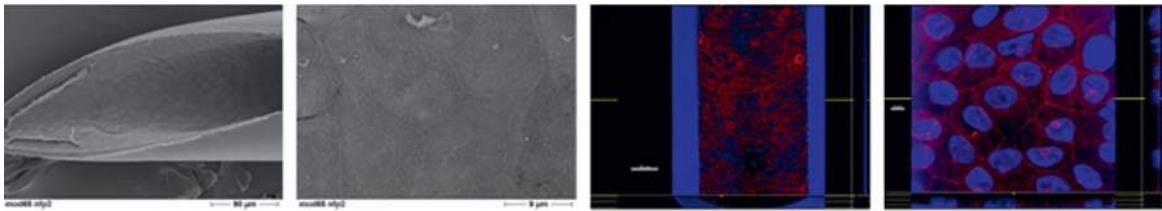
Confluent monolayers of epithelial cells have been obtained using polyimide and EVAL membranes. However, polysulfone was not suitable for epithelial cell culture, except for polysulfone membranes that are coated with extra-cellular matrix proteins. In addition, cellulose acetate membranes without and with a coating of matrix proteins are proven candidates for bioartificial kidneys [90]. Saito *et al.* [90] concluded that there are several membrane candidates although it has not been confirmed, which one is the most appropriate for application as a membrane for bioartificial kidneys.

Humes *et al.* developed the so-called renal assist device (RAD), which represents the most advanced bioartificial kidney system, and has been evaluated in a multicenter, randomized, controlled, open-label phase II clinical trial. The concepts and underlying technology of the RAD have been presented in multiple reviews [91–99]. Humes *et al.* have used commercial high-flux dialyzers and modified the inner hollow fiber surface using Pronectin-L, a synthetic protein containing intercellular-attachment domains of laminin [100, 101], laminin [102, 103], or collagen type IV [104] to facilitate epithelial cell culture. In a similar way, Huijuan *et al.* [105] utilized polysulfone high-flux dialyzers with a laminin coating as a bioartificial kidneys.

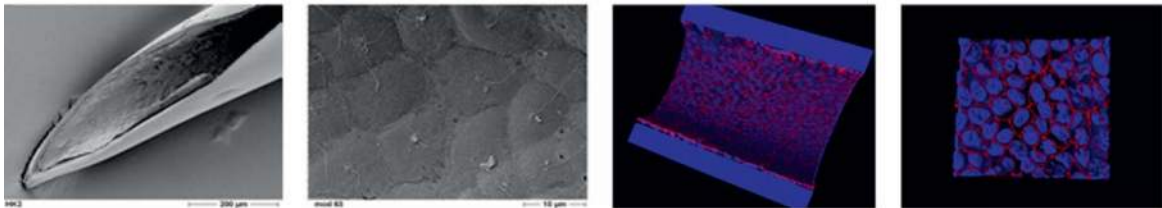
Tsuruoka *et al.* [106, 107] established bioartificial kidneys intended for intoxicification therapy. The hybrid devices consisted of polyethylene hollow fibers modified with type I collagen.

We have developed an epithelial cell culture system using synthetic membranes without the need for coating with an extracellular matrix protein. MDCK cells, human HK-2 cells, and primary human epithelial cells could be attached, expanded, and maintained over several weeks on hollow fiber membranes. As shown in **Figure 22**, we could achieve a homogenous cell distribution that resulted in a confluent monolayer

Human primary renal tubule cell



Human proximal renal epithelial cell line HK2



Canine renal epithelial cell line MDCK

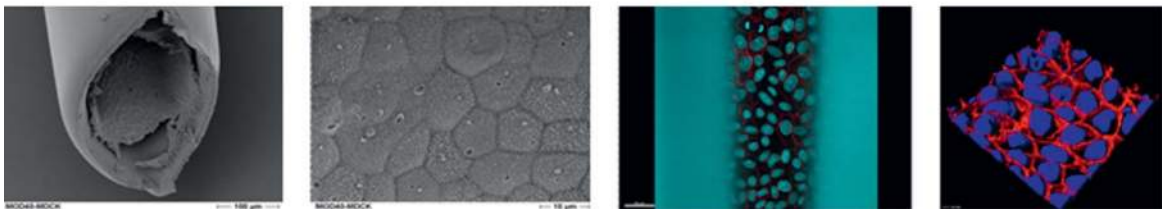


Figure 22 Epithelial cell-covered synthetic hollow fibers. Hollow fibers were intra-capillarially seeded with primary human renal tubule epithelial cells (upper row), human cell line HK-2 (middle row), or MDCK cells (lower row). Scanning-electron micrographs show cells in hollow fibers forming confluent monolayers with microvilli and cilia. Confocal scanning-laser micrographs show cells with stained nuclei (blue) and stained tight or adherent junction molecules (red). Red stains represent ZO-1 for human cells, and E-cadherin for canine cells.

of all epithelial cell types after cell expansion. The hollow fibers are completely covered with epithelial cells and exhibit tight cell–cell junctions, microvilli, and cilia. Scanning electron micrographs show cells in hollow fibers forming confluent monolayers with microvilli and cilia. Confocal scanning-laser micrographs show cells with blue-stained nuclei and red-stained tight or adherent junction molecules. Human cells are stained for the tight junction-associated ZO-1, whereas canine cells are stained for adherent-junction molecule E-cadherin. The expression of functional epithelial marker Aquaporin-1 has also been demonstrated (data not shown).

2.13.11 Achievements and Perspectives for using Bioartificial Kidneys

Early works by Aebischer and Galetti, and Fey-Lamprecht *et al.* (described above) focused on

the first concepts of bioartificial kidneys and have shown proof that renal tubule epithelial cells can be grown and maintained on porous membranes. Those groups have identified some membrane materials, such as polyvinyl chloride acrylic copolymer, poly-sulfone and blends thereof, as well as PAN and derivatives without and with modification with adhesion proteins. It has been shown that cells can form tight, confluent monolayers that allow active transport of physiological substances. Saito *et al.* have contributed to this area of study with additional evidence that functional tubule epithelial-cell monolayers can be tightly grown on various substrates, showed metabolic and functional parameters, and they have also introduced genetically modified epithelial cells that have a high capacity for water transport. Huijuan *et al.* [105] have previously reported the application of a bioartificial kidney in a porcine model of multi-organ failure that included acute renal failure, and showed the beneficial effects of their cell-based system with regard to blood

pressure, partial improvement of cytokine profile, and survival time of the animals.

The most systematic, preclinically and clinically advanced bioartificial kidney system and therapy has been developed by Humes *et al.*, starting in the late 1990s. Isolation and stable cultivation of proximal tubule cells were established in studies [100, 103]. It was demonstrated that epithelial cells attach to hollow fibers and can be maintained in long-term culture on the intracapillary membrane surface. These cells also exhibited typical *in vitro* transport of, for example, glucose, bicarbonate, and glutathione, and displayed metabolic characteristics. In addition, as a prerequisite, a perfusion system was established that performed epithelial-cell culture in hollow fibers in order to study flow rates, media composition, etc. In a next step, the model was upscaled using hollow fiber cartridges (up to 0.4 m^2), and the bioreactors were maintained in steady-state-perfusion for more than 6 months before use. They displayed only minor cell loss during a typical treatment period of 24–72 h [108].

In further steps, Humes *et al.* have reported canine and porcine animal studies carried out using AKI [101, 104] or sepsis [94, 102] models. In AKI models, RADs with more than 1 billion kidney cells were applied to 24-h post-bilateral nephrectomies. Bicarbonate, phosphate, and potassium levels were closer to normal values in the RAD group compared to a sham control group. Interestingly, 40–50% of the ultrafiltrate was reabsorbed in the RAD cartridges. Ammonia excretion, vitamin D metabolism, as well as glutathione processing were improved in the RAD versus sham control-treated animals. In the sepsis models, survival time of animals treated with RAD was significantly prolonged and cytokine levels were partially modulated by RAD treatment. RAD-treated animals showed significantly decreased plasma levels of the pro-inflammatory cytokines, IL-6 and interferon- γ . A phase I clinical study with 10 AKI or MOF patients was performed using RADs containing ~ 1 billion tubule cells [69]. RAD proved to be viable and safe in this *ex vivo* clinical setting. Six of 10 treated patients survived past 30 days. Glutathione degradation and vitamin D conversion were also shown in this study. Significant declines in granulocyte colony-stimulating factor, IL-6, IL-10, and IL-6/IL-10 ratio, were

determined for a subset of patients with excessive pro-inflammatory levels. In a follow-up phase II multicenter, randomized, controlled, open-label trial, 40 patients were treated with RAD and 18 patients participated in the control group [67]. The primary endpoint was 28-day mortality, which was reduced from 61% to 33% when using the RAD, although the decrease in mortality was not statistically significant. After 180 days, the secondary endpoint measure of mortality was significantly reduced by 50%. The authors state that the RAD therapy was well tolerated, and that the most common adverse events were hypotension, thrombocytopenia, and hypoglycemia, with hypoglycemia associated with insulin residuals from the cell culture process. A follow-up phase IIb bridging study with 53 patients was discontinued after an interim analysis predicted that the study would not meet its efficacy goals.

In summary, these bioartificial kidney approaches have provided initial evidence that incorporation of functional tubule epithelial cells may result in beneficial therapy of AKI or MOF as compared to conventional RRTs. However, some limitations, open questions, and unknown factors have come to light when reviewing the entire body of published data on this subject.

1. Significant complexity in the production of cell-based cartridges for extracorporeal treatments has become evident and been confirmed [67]. There is a clear need for a commercial scaled-up manufacturing process, which is further discussed in the next paragraph of this article.

2. When using primary human cells, the availability of tubule cells may be a limiting factor when scaling up a bioartificial kidney system to make it accessible to AKI and MOF patients [87, 108]. Finding alternative cell sources, such as stem cells or stem cells differentiated into tubule epithelial cell-like cells, may be a future challenge for research in this field.

3. Logistic arrangements to ship bioartificial kidneys containing living cells worldwide may require more research to ensure a high quality of products at the site of application.

4. There is a lack of systematic testing of membrane materials to identify membrane substrates that exhibit the optimum conditions for adhesion, expansion, and maintenance of tubule epithelial or epithelial-like cells in a functional state. Most studies have been performed using conventional dialysis cartridges.

Hollow fibers were modified with extracellular matrix proteins in order to allow for cell adhesion and growth. When scaling up the technology, the availability of matrix proteins at the required quality for human use has to be ensured. The development of synthetic membranes, which make matrix proteins redundant, has to be a major goal in the field of membrane development for cell culture purposes (see also next paragraph of this article).

5. Bioincompatibility, especially the risk of blood clotting, of the hemofilter, and the cell-containing cartridge has been reported as a major risk and the most common cause of early treatment terminations [67, 87]. Specifically, whole blood perfusion of the extra-capillary side of the cell-seeded cartridge may be problematic because, if conventional dialyzers are used, the outer membrane surface is not designed for blood contact.

6. There is a lack of systematic permeability testing of the primary filter to identify the optimum primary filtrate being processed and modified in the corresponding secondary cell-seeded cartridge and also to identify the permeability of the secondary filter to identify the optimum exchange conditions of the cell-processed filtrate and blood.

As a long-term perspective, contributors to the field see further developments directed toward wearable or implantable bioartificial kidneys for both chronic and acute kidney failure patients. Such developments require a systematic approach that includes all the systems' components, such as miniaturized filters, materials suitable for implantation, tailored membranes and membrane surfaces, regeneration of dialysate or filtrate, miniaturized pumps, nanoelectronics, etc. [87, 109]. An interdisciplinary approach involving engineering, biological, and medical competence will also be a crucial prerequisite for successful future developments.

2.13.12 Membranes for Stem Cell-Based Approaches to Treat Kidney Diseases

2.13.12.1 Background

Regenerative therapies using stem cells represent a promising and innovative alternative to conventional symptomatic therapies for the causal treatment of chronic and acute diseases.

Besides using kidney-derived cells in extracorporeal systems to replace cellular kidney function, there

are several approaches to the use of stem cells [110]. Stem cells are special kinds of immature cells that have a capacity to renew themselves and to give rise to specialized cell types [111]. In general, two types of stem cells are the focus of regenerative medicine: embryonic (ES) and adult (AS) stem cells [112]. ESs represent the most immature stem cells, which can be propagated most extensively and which can differentiate into virtually any body cell type. However, there are ethical concerns associated with ES, and clinical development is in a very early stage, with only one company being cleared to begin a clinical trial using ESs [113]. In contrast, AS cells are undergoing advanced phases of clinical trials, with a high probability of their usage in clinical treatments in the near future.

AS cells reside in virtually any tissue of the body. Bone marrow-derived AS cells have drawn the attention of researchers and clinicians. In bone marrow, at least two types of stem cells are present: hematopoietic stem cells (HSCs) and mesenchymal stromal cells (MSCs). HSCs are known as precursor cells of blood cells whereby MSCs can differentiate into many mesenchymal cell types, such as adipocytes, osteoblasts, chondrocytes, myocytes, and stromal cells, both *in vitro* and *in vivo*.

2.13.12.2 Status of Stem Cell Therapies for Kidney Disease

Since 2001, an increasing number of publications have reporting the administration of bone marrow-derived MSCs to treat both chronic and acute kidney diseases in preclinical settings (reviewed in References 114–129). MSCs have been administered parenterally using animal and, most frequently, rodent models of various kidney diseases. Regarding chronic renal failure, rat and murine models have shown proven beneficial effects in the treatment of chronic diseases after partial nephrectomy [130–132], in a model of anti-Thy1.1 glomerulonephritis [133], and in models of Alport disease [134, 135]. The effects of MSCs have also been studied in chronic models in conjunction with acute models [131, 132]. Most evidence has been generated in the successful application of stem cells, mostly bone marrow-derived MSCs, for the treatment of AKI. In nephrotoxic [136–139] and ischemia/reperfusion [140–146] models of AKI, MSCs are suggested to mostly exert their renoprotective action through differentiation-independent mechanisms [146]. In many more preclinical studies, additional early evidence has reported the efficacy of

stem cells to treat kidney diseases, including the usage of kidney-derived stem or progenitor cells [147–151a,b], although the role of kidney-derived stem cells in renal repair has been controversially discussed [152]. The clinically most advanced study (phase 1) is currently being run by the Salt Lake City-based company Allocure, with the aim of demonstrating that application of allogeneic MSCs at defined doses is safe in patients who are at high risk of developing significant AKI after undergoing on-pump cardiac surgery [153].

2.13.12.3 Technologies and Membranes to Realize Stem Cell Therapies

In summary, stem cells and especially bone marrow-derived MSCs represent a promising alternative to conventional treatment modalities for acute and chronic renal diseases. However, a huge technological challenge to enable routine large-scale clinical application of stem cells is the cell expansion process. Stem cells are very rare cells in the body. For instance, MSCs make approximately 0.01–0.001% of mononucleated cells in human bone marrow [154]. This means that several thousand MSCs can be obtained from a few deciliters of bone marrow. As a therapeutic dose, 1–10 million MSCs per kilogram body weight of the patient are administered and, depending on the disease, multiple doses may be required over the course of treatment [155]. Today's standard technology for MSC expansion can be ascribed to the usage of conventional polystyrene-based cell culture flasks or cell stacks, which are multiple flask-type culture devices that can be stacked to up to 40 layers [156, 157]. The technological realization of cellular therapies and tissue engineering applications requires the entire process chain, from harvesting stem cells, expansion of cells, to harvesting of cells, to develop into a system that allows for automation and provides for up-scaling to an industrial scale. It is commonly acknowledged that there is a strong need for bioreactor technologies in the field of cellular therapies and tissue engineering in order to facilitate the transition from discovery-level science to large-scale clinical markets [158]. Because transition to large-scale manufacturing technologies needs to ensure precision, reliability, regulatory compliance, and prerequisites for standardization of manufacturing processes of cellular products, while still providing an economically reasonable structure, the success of this transition is considered to be strongly connected to the success

of the industry in such breakthrough medical technologies [159].

Several different kinds of bioreactor systems for various applications are available as commercial products. Applications include recombinant protein production, manufacturing of vaccines, liver-assist devices, or cell expansion processes [160–163]. Some of these bioreactors contain hollow fiber membranes as cell growth substrates. Most bioreactors are designed to cultivate anchorage-independent cells, such as cell lines used for protein production. The above-mentioned MSCs, which currently represent the most promising cellular candidate for stem cell-based treatments for renal disease, are cells that grow in an anchorage-dependent way.

In contrast to flask-based devices for cell expansion, which represent planar and solid substrates, hollow fiber-based bioreactors provide several advantages. Hollow fiber bioreactors have the capacity to be integrated into a closed system. A closed system is mandatory for safety reasons in terms of avoiding microbial contamination. Furthermore, a closed bioreactor system is a basic prerequisite to expand cells independently of clean room facilities. Once the bioreactor is part of a closed system, the cell expansion process can be automated. Automation has benefits regarding time consumption to avoid, for example, manually performed media exchange or cell harvest procedures in flask culture, reduced labor, reduced handling steps, and, therefore, decreased number of mistakes and increased reliability and reproducibility. Furthermore, electronic documentation of all process steps can be facilitated. The benefits of the high surface-to-volume ratio of hollow fibers compared to flat and planar cell substrates enable reduced space requirements and potentially reduce consumption of cell culture media.

An example of a hollow fiber-based bioreactor system for expansion of anchorage-dependent cells, such as MSCs, is currently under development at CaridianBCT (Figure 23) [164]. The system contains two principal flow pathways: the intra-capillary (IC) loop (red lines) and the extra-capillary (EC) loop (blue lines). This setup provides freedom for the user to use variable media at each side and to exchange media on the IC and the EC sides at different rates. The cells that need to expand are attached to the inner surface of the hollow fibers. The major innovations of this cell expansion system (CES), as compared to conventional flask or stack cultures, include reduced space requirement, reduced labor

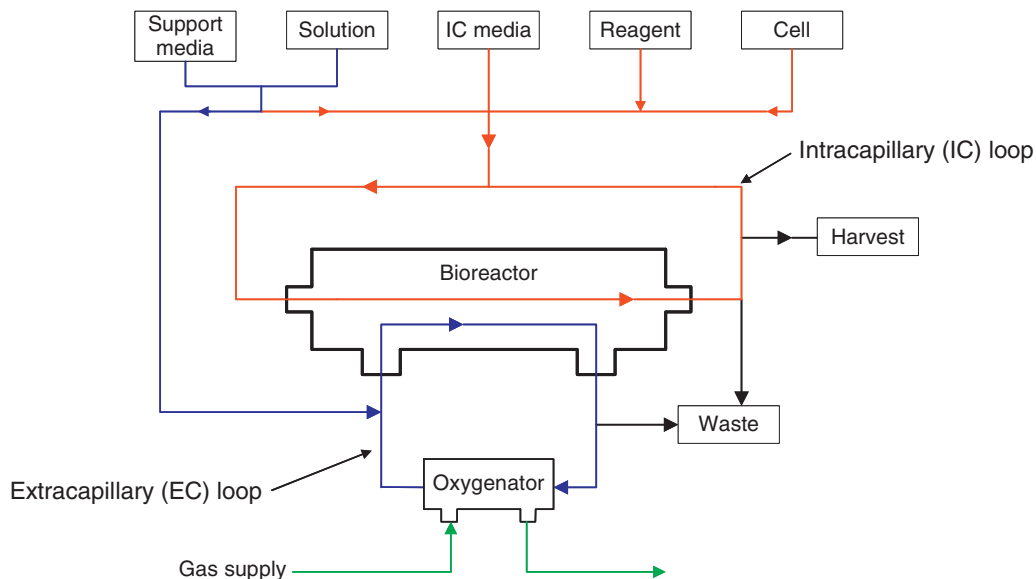


Figure 23 Systematic, simplified flow diagram of the CES. The system contains two principle flow pathways: the intra-capillary (IC) loop (red lines) and the extracapillary (EC) loop (blue lines). Cells to expand are attached to the inner surface of the hollow fibers. Gas supply is managed by a hollow fiber oxygenator.

due to automation, and decreased contamination risk due to it being a closed system. The system is a computer-controlled automated culture system. Cells are grown inside a hollow fiber bioreactor that is part of a closed sterile single-use disposable set. Cells, media, and other support fluids are contained in sterile docked bags with an attached waste bag for the collection of spent fluids. Typical culture process steps, such as cell seeding, media exchange, and cell harvesting, are all managed by the system using pumps and automated valves. The CES disposable set also contains a small oxygenator for gas management.

Membranes used in bioreactors for the cultivation of anchorage-dependent cells, such as MSCs in the CES, consist of synthetic material or synthetic materials coated with matrix proteins, as described above. The advantage of eliminating the need for matrix proteins as attachment-mediating foci, that is, the usage of pure synthetic membrane materials, simplifies the system. Using pure synthetic membranes results in less operating steps prior to loading the cell or tissue material, and the application of chemically defined materials lacks the batch-to-batch variations that frequently occur with biologic materials. As a large-scale application, the availability of matrix proteins at the required quality for human use may represent

an issue. We have developed synthetic membranes suitable for adhesion and expansion of cryopreserved MSCs or MSCs from unprocessed bone marrow. Several hundred million MSCs could be expanded within 4 weeks starting with 10–50 ml of bone marrow (data not shown). Characterization of cells harvested from synthetic membrane bioreactors in the CES show that cells fulfill the criteria defined for MSCs [165]. Harvested MSCs were plastic adherent when maintained in standard culture conditions, expressed CD105, CD73, and CD90, and lacked expression of hematopoietic markers, such as CD45, CD34, or HLA-DR (data not shown). In addition, MSCs have differentiated into osteoblasts, adipocytes, and chondroblasts *in vitro* (data not shown). **Figure 24** shows MSCs expanded in a bioreactor in the CES. The scanning electron microscope image shows MSCs growing as a monolayer on the inner surface of the membrane, and exhibiting the spindle-shaped morphology typical for MSCs.

The CES represents a valuable tool for future applications in the field of cell therapy and aims to provide a technological tool to make cell therapies become a reality for a large number of patients. The therapy market is an emerging market: it is undergoing transition from clinical trial phase, to implementation into clinical routine.

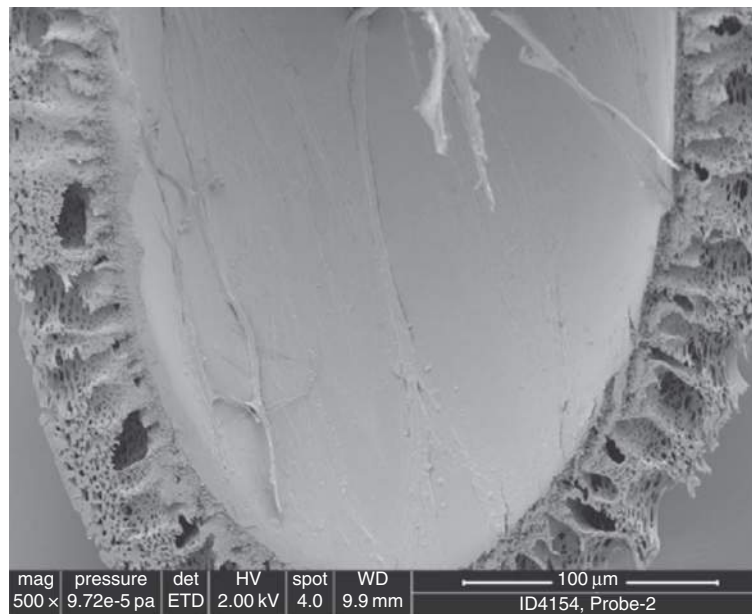


Figure 24 Human bone marrow-derived MSCs expanded in a hollow fiber bioreactor, as shown by scanning-electron microscopy (SEMs).

References

- [1] Ohlogge, K., Ebert, K. *Membranen Grundlagen, Verfahren und industrielle Anwendungen*; Wiley-VCH: Weinheim, 2006; Chapter 6.
- [2] Henderson, L. W., Ford, C., Colton, C. K. *Trans. Am. Soc. Artif. Intern. Organs* **1977**, 23, 234.
- [3] Ward, R. A., Feldhoff, P. W., Klein, E. Membrane Materials for Therapeutic Applications in Medicine. In *Material Science of Synthetic Membranes*; Lloyd, D. R., Ed.; American Chemical Society: Washington, DC, 1985; Chapter 5, pp 99–118.
- [4] Klein, E., Holland, F. F., Eberle, K. J. *J. Membr. Sci.* **1979**, 5, 19.
- [5] Hakim, R. M., Fearon, D. T., Lazarus, J. M. *Kidney Int.* **1984**, 26, 194–200.
- [6] Franz, H. E. *Dialyse 2001*; Pabst Science Publishers: Lengerich, 2002.
- [7] Franz, H. E. *Blutreinigungsverfahren*; Thieme Verlag: Stuttgart, 1997; Chapter 2.
- [8] Zaluska, W. T., Ksjazek, A., Roliski, J. *ASAIO J.* **2001**, 47, 619–622.
- [9] Stannat, S., Bahlmann, J., Kiessling, D., Koch, K. M., Deicher, H., Peter, H. H. *Contrib. Nephrol.* **1985**, 46, 102–108.
- [10] Streicher, E., Schneider, H. *Contrib. Nephrol.* **1985**, 46, 1–13.
- [11] Schaefer, R. M., Heidland, A., Hörl, W. H. *Contrib. Nephrol.* **1985**, 46, 109–117.
- [12] Ronco, C., Gepaldi, C., Brendolan, A., et al. *Nephrol. Dial. Transplant.* **2003**, 18 (supplement 7), 10–20.
- [13] Hoenich, N. A., et al. *ASAIO J.* **2000**, 46(1), 70–75.
- [14] Tielemans, C., et al. *Blood Purif.* **2002**, 20(2), 214–215.
- [15] Deppisch, R., Goehl, H., Smeby, L. *Nephrol. Dial. Transplant.* **1998**, 13, 1354–1359.
- [16] Mourad, A., et al. *Nephrol. Dial. Transplant.* **2004**, 19, 2797–2802.
- [17] Jørstad, S., Smeby, L. C., Balstad, T., Widerøe, T.-E., *Blood Purif.* **1988**, 6, 96–105.
- [18] Lonnemann, G., Koch, K. M., Shaldon, S., Dinarello, C. A. *J. Lab. Clin. Med.* **1988**, 112, 76–86.
- [19] Laude-Sharp, M., Caroff, M., Simard, L., Pusineri, C. M., Kazatchkine, M. D., Haeffner-Cavaillon, N. *Kidney Int.* **1990**, 38, 1089–1094.
- [20] Floege, J., Bartsch, A., Schulz, M., Shaldon, S., Koch, K. M., Smeby, L. C. *J. Lab. Clin. Med.* **1991**, 118, 153–165.
- [21] Kunitomo, T. *Am. J. Surg.* **1984**, 148, 594–598.
- [22] Ota, K., Okazawa, T., Kumagaya, E., et al. *Proc. Eur. Dial. Transplant. Assoc.* **1975**, 12, 559–564.
- [23] Strathmann, H. *Trennung von molekularen Mischungen mit Hilfe synthetischer Membranen*; Dr. Dietrich Steinkopf Verlag: Darmstadt, 1979.
- [24] Horl, W. H. *J. Am. Soc. Nephrol.* **2002**, 13(supplement 1), 62–71.
- [25] Singer, S. J., Nicolson, G. L. *Science* **1972**, 175, 720–731.
- [26] Andrade, J. D. *Surface and Interfacial Aspects of Biomedical Polymers*; Plenum: New York, 1985; Vol. 2.
- [27] Hoenich, N. A., Stamp, S., Robert, S. *Artif. Organs* **1999**, 23, 650.
- [28] Deppisch, R., Buck, R., Dietrich, R., Storr, M., Goehl, H., Smeby, L. *Int. J. Artif. Organs* **1997**, 20, 553.
- [29] Bowry, S. K., Rintelen, T. *ASAIO J.* **1998**, 44, M579–M583.
- [30] Ledebro, I. *Adv. Ren. Replace. Ther.* **1999**, 6, 195–208.
- [31] Ledebro, I. *Int. J. Artif. Organs* **1995**, 18, 735–742.
- [32] Ledebro, I. *Blood Purif.* **1999**, 17, 178–181.
- [33] Braun, N., Bosch, T. *Expert. Opin. Investig. Drugs* **2000**, 9, 2017–2038.
- [34] Lauterbach, G. *Handbuch der Kardiotechnik*; Urban and Fischer: München, 2002.
- [35] Tschaud, R. J. *Extrakorporale Zirkulation in der Theorie und Praxis*; Pabst Science Publishers: Lengerich, 1999.

- [36] Ledebro, I. *Blood Purif.* **2004**, *22*(supplement 2), 20–25 (doi:10.1159/000081869).
- [37] Nowack, R., Birck, R., Weinreich, T. *Dialyse und Nephrologie für Pflegeberufe*, 2. Auflage; Springer: Berlin, 2002.
- [38] Ronco, C., La Greca, G. In *Hemodialysis Technology*; Berlyne, G. M., Ronco, C., Eds.; Contributions to Nephrology; Karger: Basel, 2002; Vol. 137.
- [39] Delanaye, P., Lambermont, B., Dogné, J. M., et al. *Int. J. Artif. Organs.* **2006**, *29*(10), 944–948.
- [40] Tomo, T., Matsuyama, M., Nakata, T., et al. *Blood Purif.* **2008**, *26*(4), 347–353.
- [41] Galli, F., Benedetti, S., Floridi, A., et al. *Kidney Int.* **2005**, *67*(2), 750–759.
- [42] Kerr, P. G., Sutherland, W. H., de Jong, S., Vaithalingham, I., Williams, S. M., Walker, R. J. *J. Kidney Dis.* **2007**, *49*(4), 533–539.
- [43] Hutchison, C. A., Cockwell, P., Reid, S., et al. *J. Am. Soc. Nephrol.* **2007**, *18*(3), 886–895.
- [44] Korbet, S. M., Schwartz, M. M. *J. Am. Soc. Nephrol.* **2006**, *17*, 2533–2545.
- [45] Bladé, J., Fernández-Llama, P., Bosch, F., et al. *Arch. Intern. Med.* **1998**, *158*, 1889–1893.
- [46] Winearls, C. G. *Kidney Int.* **1995**, *48*(4), 1347–1361.
- [47] Hutchison, C. A., Basnayake, K., Cook, M., Bradwell, A. B., Cockwell, P. *Nephrol. Dial. Transplant. Plus* **2008**, *1*(supplement 2), ii9–ii10.
- [48] Uchino, S., Bellomo, R., Morimatsu, H., et al. *ASAIO J.* **2002**, *48*, 650–653.
- [49] Morgera, S., Klonower, D., Rocktäschel, J., et al. *Nephrol. Dial. Transplant.* **2003**, *18*, 1361–1369.
- [50] Morgera, S., Haase, M., Rocktäschel, J., et al. *Nephrol. Dial. Transplant.* **2003**, *18*, 2570–2576.
- [51] Morgera, S., Haase, M., Rocktäschel, J. et al. *Nephron Clin. Pract.* **2003**, *94*, c75–c80.
- [52] Morgera, S., Rocktäschel, J., Haase, M., et al. *Intensive Care Med.* **2003**, *29*, 1989–1995.
- [53] Morgera, S., Slowinski, T., Melzer, C., et al. *Am. J. Kidney Dis.* **2004**, *43*, 444–453.
- [54] Morgera, S., Haase, M., Kuss, T., et al. *Crit. Care Med.* **2006**, *34*, 2099–2104.
- [55] Haase, M., Bellomo, R., Baldwin, I., et al. *Am. J. Kidney Dis.* **2007**, *50*, 296–304.
- [56] Haase, M., Bellomo, R., Morgera, S., Baldwin, I., Boyce, N. *Int. J. Artif. Organs* **2007**, *30*, 1031–1041.
- [57] Mehta, R. L., Pascual, M. T., Soroko, S., et al. *Kidney Int.* **2004**, *66*, 1613–1621.
- [58] Ympa, Y. P., Sakr, Y., Reinhart, K., Vincent, J. L. *Am. J. Med.* **2005**, *118*, 827–832.
- [59] Schrier, R. W., Wang, W., Poole, B., Mitra, A. *J. Clin. Invest.* **2004**, *114*, 5–14. Erratum in: *J. Clin. Invest.* **2004**, *114*, 598.
- [60] Chertow, G. M., Levy, E. M., Hammermeister, K. E., Grover, F., Daley, J. *Am. J. Med.* **1998**, *104*, 343–348.
- [61] Bates, D. W., Su, L., Yu, D. T., et al. *Clin. Infect. Dis.* **2001**, *32*, 686–693.
- [62] Ramesh, G., Reeves, W. B. *Kidney Int. Suppl.* **2004**, *91*, 56–61.
- [63] Bonventre, J. V., Weinberg, J. M. *J. Am. Soc. Nephrol.* **2003**, *8*, 2199–2210.
- [64] Lameire, N. H., Vanholder, R. *Best Pract. Res. Clin. Anaesthesiol.* **2004**, *18*, 21–36.
- [65] Bonventre, J. V. *J. Am. Soc. Nephrol.* **2003**, *14*(supplement 1), S55–S61.
- [66] Lieberthal, W., Nigam, S. K. *Am. J. Physiol.* **1998**, *275*, F623–F631.
- [67] Tumlin, J., Wali, R., Williams, W., et al. *J. Am. Soc. Nephrol.* **2008**, *19*, 1034–1040.
- [68] Flanigan, M. J., Lim, V. S. Endocrine Function in Uremia. In *Replacement of Renal Function by Dialysis*; Hoerl, W. H., Koch, K. M., Lindsay, R. M., Ronco, C., Winchester, J. F., Eds.; Kluwer: Dordrecht, 2004; pp 999–1011.
- [69] Humes, H. D., Weitzel, W. F., Bartlett, R. H. et al. *Kidney Int.* **2004**, *66*, 1578–1588.
- [70] Nitschke, M., Wiehl, S., Baer, P. C., Kreft, B. *Exp. Nephrol.* **2002**, *10*, 332–337.
- [71] Aebischer, P., Ip, T. K., Panol, G., Galletti, P. M. *Life Support Syst.* **1987**, *5*, 159–168.
- [72] Rodriguez-Boulan, E., Powell, S. K. *Annu. Rev. Cell Biol.* **1992**, *8*, 395–427.
- [73] Zegers, M. M., O'Brien, L. E., Yu, W., Datta, A., Mostov, K. E. *Trends Cell Biol.* **2003**, *13*, 169–176.
- [74] Simons, K., Fuller, S. D. *Annu. Rev. Cell Biol.* **1985**, *1*, 243–288.
- [75] Weaver, V. M., Lelièvre, S., Lakins, J. N., et al. *Cancer Cell* **2002**, *2*, 205–216.
- [76] Aebischer, P., Ip, T. K., Miracoli, L., Galletti, P. M. *ASAIO Trans.* **1987**, *33*, 96–102.
- [77] Aebischer, P., Ip, T. K., Panol, G., Galletti, P. M. *Life Support Syst.* **1987**, *5*, 159–168.
- [78] Ip, T. K., Aebischer, P., Galletti, P. M. *ASAIO Trans.* **1988**, *34*(3), 351–355.
- [79] Ip, T. K., Aebischer, P. *Artif. Organs* **1989**, *13*(1), 58–65.
- [80] Uludag, H., Ip, T. K., Aebischer, P. *Int. J. Artif. Organs* **1990**, *13*(2), 93–97.
- [81] Fey-Lamprecht, F., Gross, U., Groth, T. H., et al. *J. Mater. Sci. Mater. Med.* **1998**, *9*, 711–715.
- [82] Fey-Lamprecht, F., Groth, T., Albrecht, W., Paul, D., Gross, U. *Biomaterials* **2000**, *21*(2), 183–192.
- [83] Fey-Lamprecht, F., Albrecht, W., Groth, T., Weigel, T., Gross, U. *J. Biomed. Mater. Res. A* **2003**, *65*(2), 144–157.
- [84] Terashima, M., Fujita, Y., Sugano, K., et al. *Artif. Organs* **2001**, *25*(3), 209–212.
- [85] Fujita, Y., Kakuta, T., Asano, M., et al. *Tissue Eng.* **2002**, *8*(1), 13–24.
- [86] Fujita, Y., Terashima, M., Kakuta, T., et al. *Tissue Eng.* **2004**, *10*(5–6), 711–722.
- [87] Saito, A., Aung, T., Sekiguchi, K., et al. *J. Artif. Organs* **2006**, *9*, 130–135.
- [88] Ozgen, N., Terashima, M., Aung, T., et al. *Nephrol. Dial. Transplant.* **2004**, *19*(9), 2198–2207.
- [89] Saito, A. *Artif. Organs* **2004**, *28*(1), 58–63.
- [90] Saito, A., Aung, T., Sekiguchi, K., Sato, Y. *Ther. Apher. Dial.* **2006**, *10*(4), 342–347.
- [91] Ding, F., Humes, H. D. *Nephron Exp. Nephrol.* **2008**, *109*(4), e118–e122.
- [92] Woods, J. D., Humes, H. D. *Semin. Nephrol.* **1997**, *17*(4), 381–386.
- [93] Humes, H. D. *Semin. Nephrol.* **2000**, *20*(1), 71–82.
- [94] Maguire, P. J., Stevens, C., Humes, H. D., Shander, A., Halpern, N. A., Pastores, S. M. *Crit. Care Clin.* **2000**, *16*(4), 681–694.
- [95] Humes, H. D., Fissell, W. H., Weitzel, W. F. *Kidney Int. Suppl.* **2002**, *80*, 121–125.
- [96] Humes, H. D., Weitzel, W. F., Fissell, W. H. *Blood Purif.* **2004**, *22*(1), 60–72.
- [97] Tiranathanagul, K., Eiam-Ong, S., Humes, H. D. *Crit. Care Clin.* **2005**, *21*(2), 379–394.
- [98] Tiranathanagul, K., Brodie, J., Humes, H. D. *Nephrology (Carlton)* **2006**, *11*(4), 285–291.
- [99] Fissell, W. H., Fleischman, A. J., Humes, H. D., Roy, S. *Transplant. Res.* **2007**, *150*(6), 327–336.
- [100] Humes, H. D., MacKay, S. M., Funke, A. J., Buffington, D. A. *Kidney Int.* **1999**, *55*(6), 2502–2514.
- [101] Humes, H. D., Buffington, D. A., MacKay, S. M., Funke, A. J., Weitzel, W. F. *Nat. Biotechnol.* **1999**, *17*(5), 451–455.
- [102] Fissell, W. H., Dyke, D. B., Weitzel, W. F., et al. *Blood Purif.* **2002**, *20*(1), 55–60.

- [103] MacKay, S. M., Funke, A. J., Buffingto, D. A., Humes, H. D. *ASAIO J.* **1998**, 44(3), 179–183.
- [104] Humes, H. D., Fissell, W. H., Weitzel, W. F., et al. *Am. J. Kidney Dis.* **2002**, 39(5), 1078–1087.
- [105] Huijuan, M., Xiaoyun, W., Xumin, Y., Hengjin, W., Xia, S. *ASAIO J.* **2007**, 53(3), 329–334.
- [106] Tsuruoka, S., Sugimoto, K. I., Ueda, K., Suzuki, M., Imai, M., Fujimura, A. *Kidney Int.* **1999**, 56(1), 154–163.
- [107] Tsuruoka, S., Nishiki, K., Sugimoto, K. I., Suzuki, M., Imai, M., Fujimura, A. *Kidney Int.* **2002**, 62(4), 1332–1337.
- [108] Fissell, W. H. *Expert Rev. Med. Devices* **2006**, 3, 155–165.
- [109] Prokop, A. *Ann. N. Y. Acad. Sci.* **2001**, 944, 472–490.
- [110] Bussolati, B., Camussi, G. *Contrib. Nephrol.* **2007**, 156, 250–258.
- [111] Winslow, T. *Stem Cells: Scientific Progress and Future Research Directions*; NIH Publication, Bethesda, MD, 2001, <http://stemcells.nih.gov/info/> (accessed February 2010).
- [112] Winslow, T. *Regenerative Medicine*; NIH Publication: Bethesda, MD, 2006, <http://stemcells.nih.gov/info/> (accessed February 2010).
- [113] Geron, Visionary Therapeutics, <http://www.geron.com> (accessed February 2010).
- [114] Yokoo, T., Kawamura, T., Kobayashi, E. *Kidney Int.* **2008**, 74(7), 847–849.
- [115] Sagrinati, C., Ronconi, E., Lazzeri, E., Lasagni, L., Romagnani, P. *Trends Mol. Med.* **2008**, 14(7), 277–285.
- [116] Liu, K. D., Brakeman, P. R. *Crit. Care Med.* **2008**, 36(supplement 4), S187–S192.
- [117] Gupta, S., Rosenberg, M. E. *Am. J. Nephrol.* **2008**, 28(4), 607–613.
- [118] Humphreys, B. D., Bonventre, J. V. *Annu. Rev. Med.* **2008**, 59, 311–325.
- [119] Imai, E., Iwatani, H. *J. Am. Soc. Nephrol.* **2007**, 18(9), 2423–2424.
- [120] Haller, H. *Internist* **2007**, 48(8), 813–818.
- [121] Sharples, E. J. *Curr. Opin. Crit. Care* **2007**, 13(6), 652–655.
- [122] Hishikawa, K., Fujita, T. *Hypertens. Res.* **2006**, 29(10), 745–749.
- [123] Morigi, M., Benigni, A., Remuzzi, G., Imberti, B. *Cell Transplant.* **2006**, 15(supplement 1), S111–S117.
- [124] Lin, F. *Pediatr. Res.* **2006**, 59(4 Pt 2), 74R–78R.
- [125] Patschan, D., Plotkin, M., Goligorsky, M. S. *Curr. Opin. Pharmacol.* **2006**, 6(2), 176–183.
- [126] Cantley, L. G. *Nat. Clin. Pract. Nephrol.* **2005**, 1(1), 22–32.
- [127] Ricardo, S. D., Deane, J. A. *Nephrology* **2005**, 10(3), 276–282.
- [128] Bates, C. M., Lin, F. *Curr. Opin. Pediatr.* **2005**, 17(2), 215–220.
- [129] Perin, L., Giuliani, S., Sedrakyan, S., Da Sacco, S., De Filippo, R. E. *Pediatr. Res.* **2008**, 63(5), 467–471.
- [130] Choi, S., Park, M., Kim, J., Hwang, S., Park, S., Lee, Y. *Stem Cells Dev.* **2008**, 22 July [Epub ahead of print].
- [131] Kirpatovskii, V. I., Kazachenko, A. V., Plotnikov, E. Y., et al. *Bull. Exp. Biol. Med.* **2007**, 143(1), 160–165.
- [132] Kirpatovskii, V. I., Kazachenko, A. V., Plotnikov, E. Y., et al. *Bull. Exp. Biol. Med.* **2006**, 141(4), 500–506.
- [133] Kunter, U., Rong, S., Djuric, Z., et al. *J. Am. Soc. Nephrol.* **2006**, 8, 2202–2212.
- [134] Ninichuk, V., Gross, O., Segerer, S., et al. *Kidney Int.* **2006**, 70, 121–129.
- [135] Prodromidi, E. I., Poulosom, R., Jeffery, R., et al. *Stem Cells* **2006**, 24, 2448–2455.
- [136] Herrera, M. B., Bussolati, B., Bruno, S., Fonsato, V., Romanozi, G. M., Camussi, G. *Int. J. Mol. Med.* **2004**, 14, 1035–1041.
- [137] Bi, B., Guo, J., Marlier, A., Lin, S. R., Cantley, L. G. *Am. J. Physiol. Renal Physiol.* **2008**, 295(4), F1017–F1022.
- [138] Magnasco, A., Corselli, M., Bertelli, R., et al. *Cell Transplant.* **2008**, 17(10–11), 1157–1167.
- [139] Herrera, M. B., Bussolati, B., Bruno, S., et al. *Kidney Int.* **2007**, 72(4), 430–441.
- [140] Mias, C., Trouche, E., Seguelas, M. H., et al. *Stem Cells* **2008**, 26(7), 1749–1757.
- [141] Togel, F., Cohen, A., Zhang, P., Yang, Y., Hu, Z., Westenfelder, C. *Stem Cells Dev.* **2008**, 19 June [Epub ahead of print].
- [142] Behr, L., Hekmati, M., Fromont, G., et al. *Nephron Physiol.* **2007**, 107(3), 65–76.
- [143] Semedo, P., Wang, P. M., Andreucci, T. H., et al. *Transplant. Proc.* **2007**, 39(2), 421–423.
- [144] Lange, C., Tögel, F., Itrich, H., et al. *Kidney Int.* **2005**, 68(4), 1613–1617.
- [145] Rabb, H. *Am. J. Physiol. Renal Physiol.* **2005**, 289(1), F29–F30.
- [146] Tögel, F., Hu, Z., Weiss, K., Isaac, J., Lange, C., Westenfelder, C. *Am. J. Physiol. Renal Physiol.* **2005**, 289(1), F31–F42.
- [147] Mazzinghi, B., Ronconi, E., Lazzeri, E., et al. *J. Exp. Med.* **2008**, 205(2), 479–490.
- [148] Kinomura, M., Kitamura, S., Tanabe, K., et al. *Cell Transplant.* **2008**, 17(1–2), 143–158.
- [149] Lazzeri, E., Crescioli, C., Ronconi, E., et al. *J. Am. Soc. Nephrol.* **2007**, 18(12), 3128–3138.
- [150] Sagrinati, C., Netti, G. S., Mazzinghi, B., et al. *J. Am. Soc. Nephrol.* **2006**, 17(9), 2443–2456.
- [151a] Humphreys, B. D., Duffield, J. D., Bonventre, J. V. *Minerva Urol. Nefrol.* **2006**, 58(1), 13–21.
- [151b] Humphreys, B. D., Duffield, J. D., Bonventre, J. V. *Minerva Urol. Nefrol.* **2006**, 58(4), 329–337.
- [152] Humphreys, B. D., Valerius, M. T., Kobayashi, A., et al. *Cell Stem Cell* **2008**, 2, 284–291.
- [153] AlloCure, <http://www.allocure.com> (accessed February 2010).
- [154] Pittenger, M. F., Mackay, A. M., Beck, S. C., et al. *Science* **1999**, 284(5411), 143–147.
- [155] Le Blanc, K., Frassoni, F., Ball, L., et al. *Lancet* **2008**, 371(9624), 1579–1586.
- [156] Brooke, G., Rossetti, T., Pelekanos, R., et al. *Br. J. Haematol.* **2009**, 144(4), 571–579.
- [157] Müller, I., Kordowich, S., Holzwarth, C., et al. *Cytotherapy* **2006**, 8(5), 437–444.
- [158] Martin, I., Wendt, D., Heberer, M. *Trends Biotechnol.* **2004**, 22(2), 80–86.
- [159] Lysaght, M. J., Hazlehurst, A. L. *Tissue Eng.* **2004**, 10(1–2), 309–320.
- [160] Wang, D., Liu, W., Han, B., Xu, R. *Curr. Pharm. Biotechnol.* **2005**, 6(5), 397–403.
- [161] Martin, Y., Vermette, P. *Biomaterials* **2005**, 26, 7481–7503.
- [162] Tzanakakis, E. S., Hess, D. J., Sielaff, T. D., Hu, W. S. *Annu. Rev. Biomed. Eng.* **2000**, 2, 607–632.
- [163] Marten, D., Suck, K., Diederichs, S. et al. *Chemie-Ingenieur-Technik* **2008**, 80, 1803–1808.
- [164] Antwiler, D. and team, Deppisch, R., Neubauer, M. and team, Zander, A. and team, Westenfelder, C. and team *Annual Meeting of the International Society for Cellular Therapies (ISCT)*, Miami, FL, USA, 17–20 May 2008.
- [165] Dominici, M., Le Blanc, K., Mueller, I., et al. *Cytotherapy* **2006**, 8, 315–317.

Biographical Sketches



Carina Zweigart was born on 3rd July 1981 in Rottweil, Germany. She studied process engineering at the University of Applied Science in Furtwangen, which she completed in 2005. Her diploma thesis was a study of influencing parameters on the hydraulic permeability of dialysis membranes in their membrane production process. Since September 2005 she has been working in a membrane research group of Gambro Dialysatoren GmbH in Hechingen, where she is involved in developments of new membranes for blood purification, separation processes, or other applications of porous polymeric membranes. Her working fields also include studying and developing production process steps and new membrane technologies. Mrs. Zweigart is co-owner of several patents concerning membranes with special performances and production thereof.



Markus Neubauer was born on 30th April 1974 in Kolbermoor, Germany. He studied pharmacy at the University of Regensburg, Germany. From 2000 to 2004, he worked on stem-cell-based tissue engineering at the Department of Pharmaceutical Technology of Professor Goepferich and Dr. Blunk at the University of Regensburg where he received his PhD. in 2004. He took over the position of a research manager within R&D at Gambro Dialysatoren GmbH in Hechingen, Germany, in 2005. He is author of numerous papers and publications in the field of tissue engineering and stem cells and owns patents in the field of membranes for cellular applications.



Markus Storr was born on 20th July 1964 in Altomünster, Germany. He studied chemistry at the Technical University Munich. From 1991 to 1994, he worked as a research associate on the development of heterogeneous biocatalysts at the Department of Technical Chemistry at Technical University Munich, where he received his PhD in 1994. In the same year, he took over the position of a senior scientist and research manager at Gambro Dialysatoren GmbH in Hechingen, Germany. In his current position, he is responsible within the Gambro research organization for the development of new therapies based on extracorporeal blood purification treatments with membrane and adsorption devices.



Torsten Böhrer was born on 7th April 1967 in Konstanz, Germany. He studied biology at the universities of Konstanz (Germany), Jerusalem, and Tel Aviv (Israel). Thereafter, he graduated at the Nephrology Department of Charité-Hospital, Humboldt University, Berlin (Germany). As a postdoctoral fellow, Torsten Böhrer worked at the Stanford Medical School (USA) and at the Institut National de la Santé et de la Recherche Médicale (INSERM), Toulouse (France) on different projects in the field of nephrology, dialysis, and transplantation, and received research awards from the American Society of Transplantation (AST) and European Society of Organ Transplantation (ESOT). He is author of more than 50 peer-reviewed articles and numerous book chapters and teaching articles. Since 2008, Torsten Böhrer has been working as a medical research manager at the R&D department of Gambro, conducting clinical proof-of-concept trials. He is a member of the European Renal Association-European Dialysis and Transplant Association (ERA-EDTA).



Bernd Krause was born on 31st August 1966 in Otterndorf, Germany. He completed a three-year apprenticeship as a chemical laboratory technician at the Vereinigte Aluminium Werke (VAW) in Stade, Germany. He stayed with the VAW at different locations for 10 years, for example, at the R&D center in Bonn and at the plant in Schwandorf. Subsequently, he studied chemical engineering at the University of Applied Science Münster, Germany. Performing six-month's practical training with German Remedies Ltd. in Mumbai, India, he also completed his studies with a master thesis at the R&D Department of British Oxygen Company in Murray Hill, USA. In 1997, he moved to the Membrane Technology Group at the University of Twente, Netherlands, and worked for four years on a solvent-free process for membrane formation along with the group of Professor Heiner Strathmann and Professor Matthias Wessling, where he also received his PhD. In 2001, he took over the position as a membrane research manager within the R&D department at Gambro Dialysatoren GmbH in Hechingen, Germany. At the beginning of 2009, he became R&D director, Membrane and Devices, at Gambro Dialysatoren GmbH in Hechingen. He is the author of numerous papers and publications and has more than 15 patents to his credit in the field of membranes.

2.14 Electromembrane Processes: Basic Aspects and Applications

H Strathmann, University of Stuttgart, Stuttgart, Germany

© 2010 Elsevier B.V. All rights reserved.

2.14.1	Introduction	393
2.14.2	Ion-Exchange Membranes, Their Function, and Preparation	393
2.14.2.1	Ion-Exchange Membranes, Their Properties, and Preparation	393
2.14.2.2	Properties of Ion-Exchange Membranes	393
2.14.2.3	Preparation of Ion-Exchange Membranes	394
2.14.2.3.1	Preparation of heterogeneous ion-exchange membranes	394
2.14.2.3.2	Preparation of homogeneous ion-exchange membranes	395
2.14.2.3.3	Special-property membranes	396
2.14.3	Transport of Ions in Membranes and Solutions	397
2.14.3.1	Electric Current in Electrolyte Solutions and Ohm's Law	397
2.14.3.1.1	Ion conductivity, drift speed, and mobility	398
2.14.3.2	Mass Transport in Ion-Exchange Membranes and Electrolyte Solutions	399
2.14.3.2.1	Fluxes and driving force in ion transport	399
2.14.3.2.2	Electrical current and ion flux	400
2.14.3.2.3	The transport number and the membrane permselectivity	400
2.14.3.2.4	The Donnan equilibrium and Donnan exclusion	401
2.14.3.2.5	Membrane counterion permselectivity	402
2.14.4	Ion-Exchange Membrane Deionization Processes	402
2.14.4.1	Electrodialysis	403
2.14.4.1.1	The principle of electrodialysis	403
2.14.4.1.2	Principle of electrodialysis with bipolar membranes	403
2.14.4.1.3	Electrodialysis equipment and process design	405
2.14.4.1.4	Electrodialysis process costs	409
2.14.4.1.5	Electrodialysis with bipolar membrane system design and process costs	412
2.14.4.1.6	Practical applications of electrodialysis	413
2.14.4.1.7	Applications of bipolar membrane electrodialysis	417
2.14.4.2	Continuous Electrodeionization	419
2.14.4.2.1	System components and process design aspects	419
2.14.4.2.2	Operational problems and the practical applications of electrodeionization	421
2.14.4.3	Diffusion Dialysis	421
2.14.4.3.1	The process principle	421
2.14.4.3.2	System design, costs, and application	422
2.14.4.4	Donnan Dialysis	423
2.14.4.5	Capacitive Deionization	424
2.14.5	Ion-Exchange Membranes in Electrochemical Synthesis	425
2.14.5.1	The Chlorine/Alkaline Production	425
2.14.6	Ion-Exchange Membranes in Energy Conversion and Storage	426
2.14.6.1	Ion-Exchange Membranes in Low-Temperature Fuel Cells	426
2.14.6.2	Energy Production by Reverse Electrodialysis	427
References		427

Nomenclature

a	constant –; activity (mol m^{-3}); ion radius (m)
A	area (m^2)
b	constant (–)
C	concentration (mol m^{-3})
\bar{C}	average concentration (mol m^{-3})
D	diffusion coefficient ($\text{m}^2 \text{s}^{-1}$)
e	elementary charge (As)
E	energy (A V s)
f	friction coefficient (kg s^{-1})
F	Faraday constant (A s eq^{-1})
F_a	acceleration force (kg m s^{-2})
F_f	friction force (kg m s^{-2})
G	Gibbs free energy (J)
i	current density (A m^{-2})
i_{lim}	limiting current density (A m^{-2})
\bar{i}	average current density (A m^{-2})
I	current (A)
J	flux ($\text{mol m}^{-2} \text{s}^{-1}$)
k	coefficient (various)
l	length (m)
L	coefficient ($\text{mol}^2 \text{N}^{-1} \text{m}^{-2} \text{s}^{-1}$)
N	number (–)
p	pressure (Pa)
Q	volume flow rate ($\text{m}^3 \text{s}^{-1}$)
r	area resistance (Ωm^2)
R	electrical resistance (Ω)
\bar{R}	average electrical resistance (Ω)
R	gas constant ($\text{J mol}^{-1} \text{K}^{-1}$)
s	drift speed (ms^{-1})
S	conductivity (Ω^{-1})
T	temperature (K)
t	time (s); transport number (–)
u	ion mobility ($\text{m}^2 \text{s}^{-1} \text{V}^{-1}$)
U	electrical potential (V)
V	volume (m^3)
\bar{V}	partial molar volume ($\text{m}^3 \text{mol}^{-1}$)
x	directional coordinate (m)
z	charge number (eq mol^{-1})
γ	activity coefficient (–)
Δ	cell thickness (m); recovery rate (–); difference (–)
∇	gradient (–)
κ	specific conductivity ($\Omega^{-1} \text{m}^{-1}$)
λ_{eq}	equivalent conductivity ($\text{m}^2 \Omega^{-1} \text{eq}^{-1}$)
$\lambda_{+/-}$	ion conductivity ($\text{m}^2 \Omega^{-1} \text{ion}^{-1}$)
μ	chemical potential (J mol^{-1})
$\bar{\mu}$	electrochemical potential (A V s mol^{-1})
ν	stoichiometric coefficient (–)
π	osmotic pressure (Pa)

Ψ	membrane permselectivity (–)
η	viscosity ($\text{kg m}^{-1} \text{s}^{-1}$)
φ	electrical potential (V)
ρ	specific resistance (Ωm)
Λ_{mol}	molar conductivity ($\text{m}^2 \Omega^{-1} \text{mol}^{-1}$)
ξ	current utilization (–)

Subscripts

a	anion
c	cation
cell	cell or cell pair
co	coion
cou	counterion
des	desalination
Don	Donnan
e	electric charge
eff	efficiency
eq	equivalent
fix	fixed ion
i	component
lim	limited value
mol	mole
p	pumping
pro	product
ref	reference
s	salt
spec	specific
st	stack
tot	total
unit	cell element
w	water

Superscripts

am	anion-exchange membrane
b	bulk solution
bm	bipolar membrane
c	concentrate
cm	cation-exchange membrane
e	electrode rinse
d	diluate
diff	diffusion
f	feed
fc	feed concentrate
fd	feed diluate
in	inlet
m	membrane
max	maximum value
mig	migration
out	outlet
pro	product
s	solution

2.14.1 Introduction

During the middle of the last century, electrodialysis was first applied on an industrial scale for the desalination of brackish water. Since then a number of new applications of electrodialysis and related processes based on ion-exchange membranes have been developed and are utilized today on a large technical scale, such as the chlorine–alkaline synthesis, the production of ultrapure water by the continuous electrodeionization, and the production of acids and bases by electrodialysis with bipolar membranes. With the development of processes, such as diffusion dialysis and Donnan dialysis or capacitive deionization on a laboratory scale, a number of new applications in the chemical and pharmaceutical industry and in the treatment and recycling of industrial effluents have more recently been identified and have extended the range of application of electromembrane processes beyond their traditional use in brackish-water desalination. The term electromembrane process is used to describe an entire family of processes that can be quite different in their basic concept and their application. However, they are all based on the coupling of a mass transport with an electrical current through an ion-permeable membrane. Electromembrane processes are used today mainly in three areas: (1) the deionization of salt solutions, (2) the electrochemical synthesis of inorganic and organic compounds, and (3) the conversion of chemical energy into electrical energy [1–3].

2.14.2 Ion-Exchange Membranes, Their Function, and Preparation

The key components in electromembrane processes are the ion-exchange membranes. They can be characterized in terms of their properties into cation-exchange and anion-exchange membranes or in terms of their structure in heterogeneous and homogeneous membranes. Ion-exchange membranes should have high permselectivity, low electrical resistance, and good mechanical and chemical stability.

2.14.2.1 Ion-Exchange Membranes, Their Properties, and Preparation

There are three different types of ion-exchange membranes: (1) cation-exchange membranes, which contain negatively charged groups fixed to the

polymer matrix; (2) anion-exchange membranes, which contain positively charged groups fixed to the polymer matrix; and (3) bipolar membranes, which are composed of an anion- and a cation-exchange layer laminated together.

In a cation-exchange membrane, the fixed negative charges are in electrical equilibrium with mobile cations in the interstices of the structure. The mobile cations are referred to as counterions and the mobile anions, which carry the same electrical charge as the membrane, are referred to as coions. Due to the exclusion of the coions, a cation-exchange membrane is more or less impermeable to anions. An anion-exchange membrane is preferentially permeable to anions and more or less impermeable to cations. To which extent the coions are excluded from an ion-exchange membrane depends on the membrane as well as on the solution properties. Bipolar membranes enhance the dissociation of water molecules into H^+ and OH^- ions and are used in combination with monopolar membranes to convert salts into the corresponding acids and bases [4, 5].

2.14.2.2 Properties of Ion-Exchange Membranes

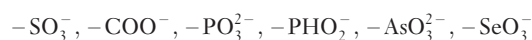
The most desired properties of ion-exchange membranes are:

- high permselectivity;
- low electrical resistance; and
- good mechanical, chemical, and thermal stability.

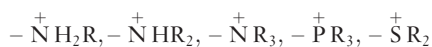
Many of today's commercially available membranes meet most of these requirements. Especially, cation-exchange membranes based on fluorocarbon polymers have quite satisfactory properties [6, 7].

The properties of ion-exchange membranes are determined by two parameters, that is, the basic material they are made from and the type and concentration of the fixed ionic moiety. The basic material determines to a large extent the mechanical, chemical, and thermal stability of a membrane [8–10]. The type and the concentration of the fixed ionic charges determine its permselectivity and electrical resistance, but they also have a significant effect on the mechanical properties of the membrane. The degree of swelling, especially, is affected by the type of the fixed charges and their concentration.

The following moieties are used as fixed charges in cation-exchange membranes:



In anion-exchange membranes, fixed charges may be



The sulfonic acid group is completely dissociated over nearly the entire pH range, while the carboxylic acid group is hardly dissociated in the pH range <3. The quaternary ammonium group again is completely dissociated over the entire pH range, while the secondary ammonium group is only weakly dissociated. Accordingly, ion-exchange membranes are referred to as being weakly or strongly acidic or basic in character.

2.14.2.3 Preparation of Ion-Exchange Membranes

The preparation of ion-exchange membranes is described in numerous publications and patents [11–14]. Ion-exchange membranes can be divided according to their structure and the way they are prepared into homogeneous and heterogeneous membranes. In homogeneous ion-exchange membranes, the fixed charged groups are evenly distributed over the entire membrane polymer matrix. Heterogeneous ion-exchange membranes have distinct macroscopic domains of ion-exchange resins in the matrix of a polymer.

The structure of a homogeneous membrane is illustrated in **Figure 1** which shows schematically a cation-exchange membrane with negative charges fixed to the polymer matrix that are neutralized by mobile cations and a few anions in the interstices of the polymer backbone. The ion-exchange capacities of homogeneous ion-exchange membranes are in the

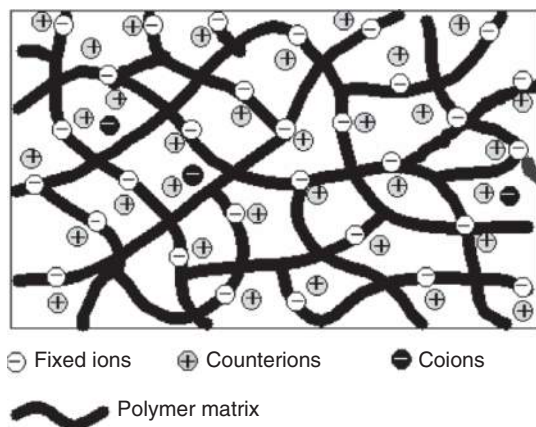


Figure 1 Schematic drawing illustrating the structure of a homogeneous cation-exchange membrane.

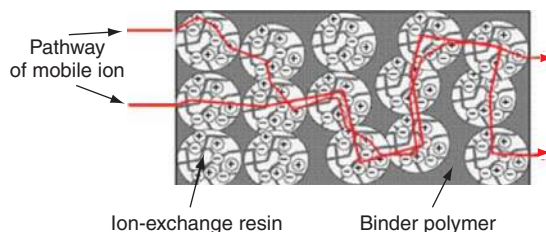


Figure 2 Schematic drawing illustrating the structure of a heterogeneous cation-exchange membrane and the pathway of an ion in the membrane.

range of 2–3 equivalent per kilogram dry membrane. Their water sorption in an electrolyte solution is between 10 and 30 wt.% depending on the ion-exchange capacity, the membrane polymer matrix, and the electrolyte concentration.

The structure of a heterogeneous membrane is illustrated in **Figure 2** which shows a cation-exchange membrane composed of fine cation-exchange particles embedded in an inert binder polymer, such as polyethylene or polyvinylchloride. Heterogeneous ion-exchange membranes are characterized by the discontinuous phase of the ion-exchange material. The efficient transport of ions through a heterogeneous membrane requires either a contact between the ion-exchange particles or an ion-conducting solution between the particles. Therefore, heterogeneous membranes have generally a higher electric resistance and a lower permselectivity as homogeneous membranes. The ion-exchange capacities of heterogeneous membranes are in the range of 1–2 equivalent per kilogram dry membrane and thus significantly lower than that of homogeneous membranes which is between 2 and 3 equivalent per kilogram dry resin. The water sorption is generally higher than that of homogeneous membranes.

2.14.2.3.1 Preparation of heterogeneous ion-exchange membranes

Heterogeneous ion-exchange membranes can be easily prepared by mixing an ion-exchange powder with a dry binder polymer, followed by extrusion of sheets under the appropriate conditions of pressure and temperature, or by dispersion of ion-exchange particles in a solution of a film-forming binder polymer, followed by casting a film and then evaporating the solvent.

Heterogeneous ion-exchange membranes with useful properties contain 64–68 wt.% of the ion-exchange particles. Membranes that contain significantly less

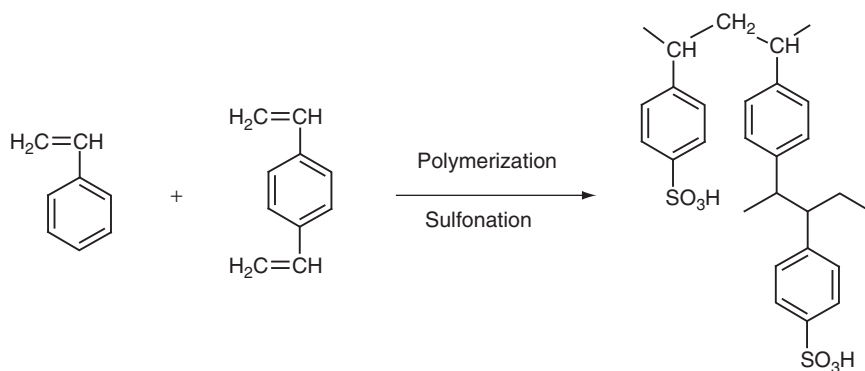
than 64 wt.% ion-exchange particles have high electric resistance and membranes with significantly more resin particles than 68 wt.% have poor mechanical strength. Furthermore, heterogeneous membranes often develop water-filled channels in the polymer matrix during the swelling process, which affects both the mechanical properties as well as the permselectivity.

2.14.2.3.2 Preparation of homogeneous ion-exchange membranes

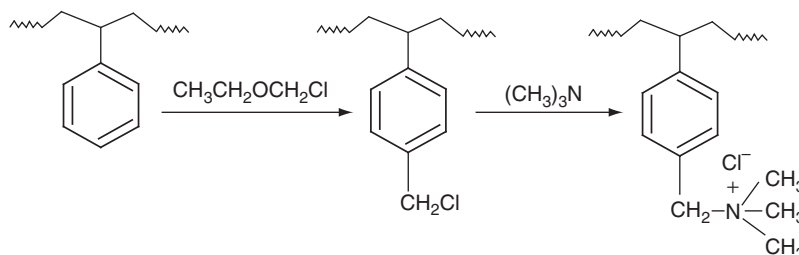
Homogeneous ion-exchange membranes can be prepared by polymerization of monomers that contain a moiety that either is or can be made anionic or cationic, or by polymerization of a monomer that contains an anionic or a cationic moiety, or by introducing anionic or cationic moieties into a dissolved polymer by a chemical reaction, or by grafting functional groups into a preformed polymer film.

A widely applied method for preparing a cation-exchange membrane is based on the polymerization of styrene and divinylbenzene and its subsequent sulfonation according to [Scheme 1](#).

In a first step, styrene is partially polymerized and crosslinked with divinylbenzene; and, then in a second step, sulfonated with concentrated sulfuric acid.



Scheme 1



Scheme 2

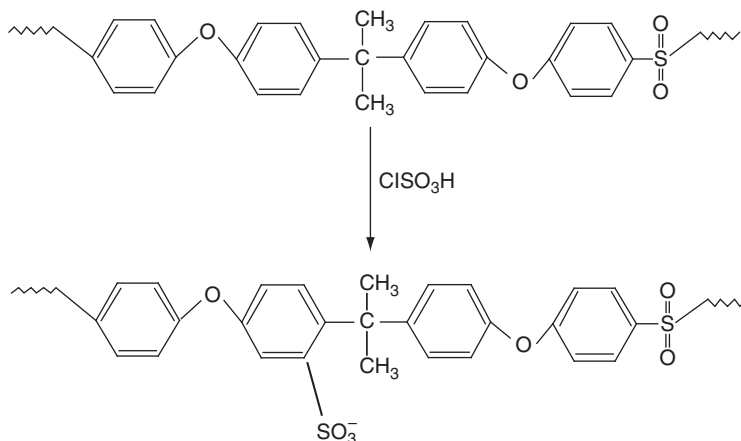
A homogeneous anion-exchange membrane, which is used on a large commercial scale, is obtained by introducing a quaternary amine group into polystyrene by a chloromethylation procedure followed by an amination with a tertiary amine according to [Scheme 2](#).

The membranes are cast on a support screen to increase their mechanical strength and form stability.

The membrane structures and their preparation described above are just two examples. There are many variations of the basic preparation procedure resulting in slightly different products. Instead of styrene, often, substituted styrene, such as methylstyrene or phenylacetate, is used. Instead of divinylbenzene, monomers, such as divinylacetylene or butadiene, are used.

More recently, cation-exchange membranes with good mechanical and chemical stability and well-controlled ion-exchange capacity are prepared by sulfonation of dissolved polysulfone [13]. The sulfonation is carried out with chlorosulfonic acid according to [Scheme 3](#).

To obtain membranes with different ion-exchange capacity, the sulfonated polysulfone can be mixed with unsulfonated polymer in a solvent, such as *N*-methylpyrrolidone. By changing the ratio of the



Scheme 3

sulfonated to unsulfonated polymer, the fixed charge density can easily be adjusted to a desired value.

Anion-exchange membranes based on polysulfone can be prepared by halomethylation of the backbone polymer and subsequent reaction with a tertiary amine according to [Scheme 4](#).

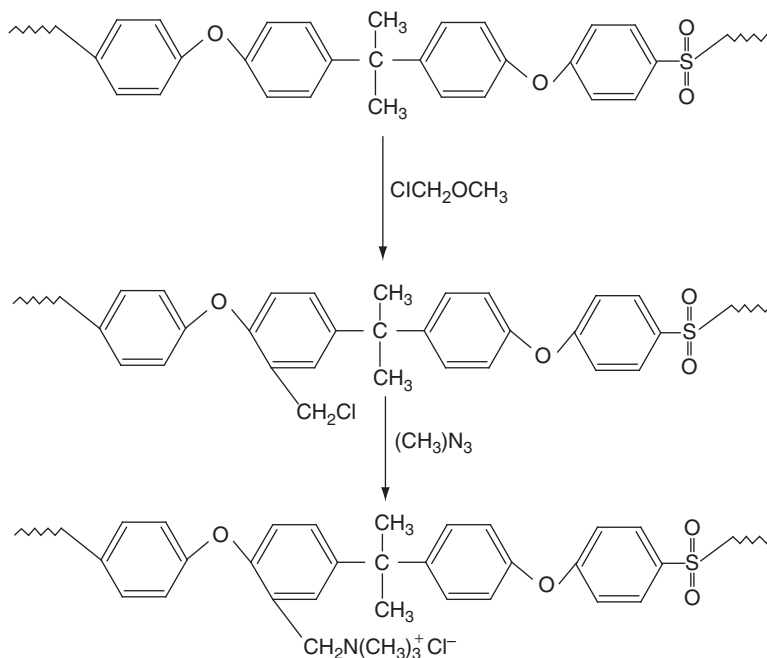
Ion-exchange membranes based on polysulfone have excellent chemical and thermal stability.

For the preparation of cation-exchange membranes also polyetheretherketone is used as the basic polymer [14]. It can very easily be sulfonated with concentrated sulfuric acid according to [Scheme 5](#).

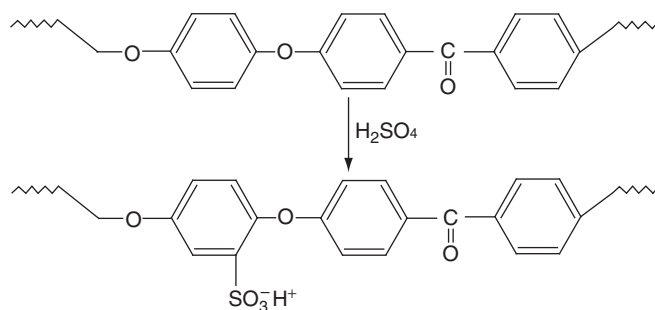
The sulfonation occurs on one polyetherether block only and is thus very easy to control. To obtain membranes with different ion-exchange capacity, the sulfonated polyetheretherketone can be mixed with polyethersulfone in a solvent, such as *N*-methylpyrrolidone. By changing the ratio of the sulfonated polyetheretherketone to polyethersulfone, the fixed charge density can easily be adjusted to a desired value.

2.14.2.3.3 Special-property membranes

In addition to the monopolar membrane described above, a large number of special-property membranes

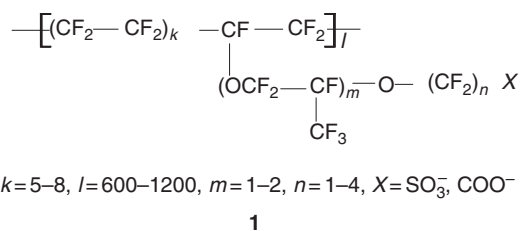


Scheme 4



Scheme 5

are used in various applications. One of the commercially most important special-property cation-exchange membranes is based on a fluorocarbon polymer. This membrane has extreme chemical and thermal stability and is a key component in the chlorine/alkaline electrolysis as well as in most of today's fuel cells. It can be prepared by copolymerization of tetrafluoroethylene with perfluorovinylether having a carboxylic or sulfonic acid group at the end of a side chain as indicated in 1.



The synthesis of perfluorocarbon membranes is rather complex and requires a multistep process. There are several variations of a general basic structure commercially available today [15]. In addition to the various perfluorinated cation-exchange membranes, an anion-exchange membrane also has been developed which so far has not reached the same commercial relevance as the cation-exchange membrane.

Other special-property membranes are the so-called low-fouling anion-exchange membranes used in certain wastewater treatment applications or composite membranes with a thin layer of weakly dissociated carboxylic acid groups on the surface, and the bipolar membranes which resemble a laminate of an anion- and a cation-exchange layer used in the production of protons and hydroxide ions to convert a salt in the corresponding acids and bases by electrodialysis. The preparation techniques are described in detail in numerous publications [16–18].

2.14.3 Transport of Ions in Membranes and Solutions

The transport rate of a component in a membrane and an electrolyte solution is determined by its concentration, its mobility in a given environment, and by the driving force or forces acting on the component. The mobility of a component is determined by its interaction with other components in its surrounding. The driving forces for the transport ions are gradients in the electrochemical potential. For applying an electrical potential in an electrolyte solution, two electron conductors, generally two electrodes, must be in contact with an electrolyte. At the electrode/electrolyte interface, the electron conductance is converted into an ionic conductance by an electrochemical reaction. In electrolyte solutions, the electrostatic forces must always be balanced, that is, the number of positive and negative electrical charges must always be equal in a macroscopic electrolyte volume.

2.14.3.1 Electric Current in Electrolyte Solutions and Ohm's Law

When an electrical potential difference is established between two electrodes in contact with an electrolyte solution, the anions will migrate toward the anode where they are oxidized by releasing electrons to the electrode in an electrochemical reaction. Similarly, cations will migrate toward the cathode where they are reduced by receiving electrons from the electrode. Thus, the transport of ions in an electrolyte solution between electrodes results in a transport of electrical charges, that is, an electrical current. In an electrolyte solution without concentration gradients, the relation between the electrical current and electrical potential driving force can be described by the same equation as the transport of

electrons in a metallic conductor, that is, by Ohm's law which is given by

$$U = RI \quad (1)$$

Here, U is the electrical potential between two points in an electron-conducting material, such as a metal or an ion-conductive system such as an electrolyte solution, I is the electrical current, and R the electrical resistance.

The resistance R is a function of the specific resistance of the material which is referred to as resistivity, the distance between the two points in the conducting material, and the cross-sectional area of the material through which the electric current passes. It is given by

$$R = \rho \frac{l}{A} \quad (2)$$

Here, R is the resistance, ρ is the resistivity which is often also referred to as specific resistance, l is the length, and A the cross-sectional area of the conducting material.

The reversal of the resistance or of the resistivity, respectively, is the conductance and the conductivity; thus

$$S = \frac{1}{R} \quad \text{and} \quad \kappa = \frac{1}{\rho} \quad (3)$$

where S is the conductance and κ the conductivity.

2.14.3.1.1 Ion conductivity, drift speed, and mobility

The conductivity of electrons in metal conductors, however, is generally three to five orders of magnitude higher than that of ions in electrolyte solutions. Furthermore, the conductivity of metals is decreasing with increasing temperature, while the conductivity of electrolyte solutions is increasing with temperature. The most important difference between electron and ion conductivity, however, is the fact that ion conductivity is always coupled with a transport of mass. The conductivity of an electrolyte solution is given by

$$\kappa = \Lambda_{\text{mol}} C_s \quad (4)$$

where Λ_{mol} is the molar conductivity and C_s is the molar concentration of an electrolyte in solution.

The molar conductivity is the sum of the contributions of its individual ions. This is referred to as the law of independent migration of ions. Thus

$$\Lambda_{\text{mol}} = (\nu_+ \lambda_+ + \nu_- \lambda_-) \quad (5)$$

Here, λ is the ion conductivity and ν is a stoichiometric coefficient referring to the number of ions in a mole electrolyte; the subscripts $+$ and $-$ refer to cation and anion, respectively.

The ion conductivity is a function of the ion mobility, which is given by

$$\lambda = |z| u F \quad (6)$$

Here, u is the ion mobility, z is the charge number of an ion, and F is the Faraday constant. The ion mobility is related to the so-called drift speed of an ion in solution.

Combination of Equations (4)–(6) leads to

$$\begin{aligned} \kappa &= C_s \Lambda_{\text{mol}} = C_s \sum_i \nu_i \lambda_i = C_s \sum_i |z_i| \nu_i \lambda_{\text{eq}} \\ &= F C_s \sum_i |z_i| \nu_i u_i = F C_{\text{eq}} \sum_i u_i \end{aligned} \quad (7)$$

Here, λ and λ_{eq} are the ion and the equivalent conductivity, respectively; C_s and C_{eq} are the molar and the equivalent concentration, respectively, of the electrolyte in the solution; $|z_i|$ is the charge number of ions in absolute value; ν_i is the stoichiometric coefficient referring to the number of ions in an electrolyte; and u is the ion mobility. Furthermore,

$$C_{\text{eq}} = \sum_i |z_i| \nu_i C_s \quad (8)$$

and

$$\Lambda_{\text{mol}} = \sum_i |z_i| \nu_i \lambda_{\text{eq}} \quad (9)$$

Thus, the stoichiometric coefficient gives the number of ions in a mole electrolyte and the charge number gives the number of charges related to an ion.

For example, for NaCl, the stoichiometric coefficients for cations and anions, that is, ν_c and ν_a are identical and equal to 1, and also the charge numbers of anions and cations are the same, that is, z_c and z_a are 1. However, for MgCl₂, ν_c is 1 and ν_a is 2, and z_c is 2 and z_a is 1.

The drift speed of an ion is reached when the acceleration force acting on an ion is balanced by friction forces and the ion moves with constant velocity. The acceleration force is given by an electrical potential difference and the friction force is caused by viscous drag.

The acceleration force is given by

$$F_a = F_f = \frac{|z| e d \varphi}{dx} = f_s \quad (10)$$

The drift speed is given by

$$s = \frac{|z|e}{f} \frac{d\varphi}{dx} = \frac{|z|e}{6\pi\eta a} \frac{d\varphi}{dx} = u \frac{d\varphi}{dx} \quad (11)$$

Here, F_a and F_f are the acceleration and the friction force, respectively, f is the friction factor, s the drift speed, e the electrical charge, z is the charge number of an ion, φ is the electrical potential, x a directional coordinate, u is the ion mobility, a is the ion radius, and η the dynamic viscosity of the solution.

The friction factor is given by Stokes–Einstein relation:

$$f = 6\pi\eta a \quad (12)$$

and the ion mobility is related to the friction coefficient by

$$u = \frac{|z|e}{f} = \frac{|z|e}{6\pi\eta a} \quad (13)$$

2.14.3.2 Mass Transport in Ion-Exchange Membranes and Electrolyte Solutions

To describe the mass transport in an electrolyte solution or in an ion-exchange membrane, three independent fluxes must be considered, that is, the fluxes of the cations, the flux of anions, and the flux of the solvent [19]. The transport of ions can be accomplished by diffusion and migration on a molecular level or by convection, that is, viscous flow, on a macroscopic level. The transport of ions is the result of an electrochemical potential gradient, and the transport of the solvent through the membrane is a result of chemical potential differences of the solvent, that is, by osmosis or coupled with an electric current, that is, electroosmosis.

2.14.3.2.1 Fluxes and driving force in ion transport

The driving force for the flux of a component i in electromembrane processes on a molecular level without convective flux is a gradient in its electrochemical potential which is given at constant temperature by

$$\nabla\tilde{\mu}_i = \nabla\mu_i + \nabla\varphi = \bar{V}_i\nabla p + RT\nabla \ln a_i + z_iF\nabla\varphi \quad (14)$$

Considering the one-dimensional case in the direction of the x coordinate, Equation (14) can be expressed by

$$\frac{d\tilde{\mu}_i}{dx} = \frac{d\mu_i}{dx} + \frac{d\varphi}{dx} = \bar{V}_i \frac{dp}{dx} + RT \frac{d \ln a_i}{dx} + z_i F \frac{d\varphi}{dx} \quad (15)$$

Here, $\tilde{\mu}_i$, μ_i , a_i , and \bar{V}_i are the electrochemical potential, the chemical potential, the activity, and the partial molar volume, respectively, of a

component i ; p and φ are the hydrostatic pressure and the electrical potential, x is the directional coordinate, F is the Faraday constant, R the gas constant, and T the temperature.

The mass transport of a component i at constant temperature can be described as a function of the driving force by a phenomenological equation [20], that is,

$$\mathcal{J}_i = L_i \frac{d\tilde{\mu}_i}{dx} = L_i \left(\bar{V}_i \frac{dp}{dx} + RT \frac{d \ln a_i}{dx} + z_i F \frac{d\varphi}{dx} \right) \quad (16)$$

Here, \mathcal{J}_i and L_i are the flux and a phenomenological coefficient relating the driving force to the corresponding flux, and the subscript i refers to a components in the system.

The activity of a component a_i is given by the concentration C_i multiplied by the activity coefficient γ_i that is,

$$a_i = C_i \gamma_i \quad (17)$$

Here, a_i is the activity and γ_i is the activity coefficient of a component i .

Furthermore,

$$\begin{aligned} \frac{d \ln a_i}{dx} &= \frac{d \ln C_i + d \ln \gamma_i}{dx} = \frac{d \ln C_i}{dx} \left(1 + \frac{d \ln \gamma_i}{d \ln C_i} \right) \\ &= \frac{1}{C_i} \left(1 + \frac{d \ln \gamma_i}{d \ln C_i} \right) \frac{d C_i}{dx} \end{aligned} \quad (18)$$

The flux of a component can also be expressed by

$$\mathcal{J}_i = C_i (s_i - s_{\text{ref}}) \quad (19)$$

Here, s_i the velocity with which a component moves in a system and s_{ref} is the reference velocity of the system, that is, the frame of reference for the moving component.

In electromembrane processes, generally the solvent or the membrane is used as frame of reference and thus s_{ref} is 0.

The velocity s_i is identical to the drift speed as expressed in Equation (11), which relates the drift speed with friction coefficient, the ion mobility, the phenomenological, and the diffusion coefficient.

Introducing the drift speed, the ion mobility, and the diffusion coefficient into Equation (16) leads to

$$\mathcal{J}_i = C_i s_i = C_i \frac{d\tilde{\mu}_i}{f_i dx} = u_i C_i \frac{d\tilde{\mu}_i}{dx} = L_i \frac{d\tilde{\mu}_i}{dx} = D_i C_i \frac{d\tilde{\mu}_i}{dx} \quad (20)$$

Here, f_i , L_i , u_i , and D_i are the friction coefficient, the phenomenological coefficient, the ion mobility, and the diffusion coefficient, respectively; C_i is the concentration; and $\tilde{\mu}_i$ is the electrochemical potential of the component i .

Assuming the solution is infinitely diluted and can be considered ideal, and the activity coefficient is 1, then the term $d \ln y_i / d \ln C_i$ becomes 0.

If

$$\frac{d \ln y_i}{d \ln C_i} = 0$$

then

$$\frac{d \ln a_i}{dx} = \frac{d \ln C_i}{dx} = \frac{1}{C_i} \frac{dC_i}{dx} \quad (21)$$

For an ideal solution and constant pressure and temperature, the flux of a component i can be expressed by

$$\mathcal{J}_i = -D_i \left(\frac{dC_i}{dx} + \frac{z_i F C_i}{RT} \frac{d\varphi}{dx} \right) \quad (22)$$

Here, D_i is the diffusion coefficient, φ_i is the electrical potential, C_i the concentration, and z_i the charge number of a component i .

Equation (22) is identical to the Nernst–Planck flux equation [21].

The term $D_i(dC_i/dx)$ represents the diffusion in Equation (22) and the term

$$D_i \frac{z_i C_i F}{RT} \frac{d\varphi}{dx}$$

the migration of a component. Thus, the Nernst–Planck equation is an approximation of the more general phenomenological equation assuming the activity coefficient to be unity and neglecting all kinetic coupling between different fluxes.

For an ideal solution, the relation between the Fickian diffusion coefficient, the phenomenological coefficient, the ion mobility, and the friction coefficient is given by

$$D_i = \frac{L_i RT}{C_i} = u_i \frac{RT}{|z_i| F} = C_i \frac{RT}{f_i} \quad (23)$$

2.14.3.2.2 Electrical current and ion flux

The flux of electrical charges, that is, the electrical current in an electrolyte is proportional to the flux of ions and given by

$$I = \frac{U}{R} = iA = F \sum_i z_i \mathcal{J}_i A \quad (24)$$

Here, I is the current, U is the applied voltage, R is the resistance, i is the current density, A is the cross-sectional area of the conducting media, F is the Faraday constant, \mathcal{J} is the flux, and subscript i refers to ions.

Introducing Equation (22) into (24) and rearranging leads to

$$i = F \sum_i z_i \mathcal{J}_i = F^2 \sum_i z_i^2 \frac{C_i D_i}{RT} \left(\frac{RT}{z_i C_i F} \frac{dC_i}{dx} + \frac{d\varphi}{dx} \right) \quad (25)$$

Here, i is the current density, C is the concentration, F is the Faraday constant, φ is the electrical potential, z is the valence, D is the ion diffusivity, R is the gas constant, T is the absolute temperature, and the subscript i refers to anions and cations.

The term $\frac{RT}{z_i C_i F} \frac{dC_i}{dx}$ has the dimension of an electrical potential gradient and represents the concentration potential which is established between two electrolyte solutions of different concentrations.

2.14.3.2.3 The transport number and the membrane permselectivity

In an electrolyte solution, the current is carried by both ions. However, cations and anions usually carry different portions of the overall current. In ion-exchange membranes, the current is carried preferentially by the counterions.

The fraction of the current that is carried by a certain ion is expressed by the ion transport number which is given by

$$t_i = \frac{z_i \mathcal{J}_i}{\sum_i z_i \mathcal{J}_i} \quad (26)$$

Here, t_i is the transport number of the component i , \mathcal{J}_i is its flux, and z_i its valence.

The transport number t_i indicates the fraction of the total current that is carried by the ion i , the sum of the transport number of all ions in a solution is 1.

The membrane permselectivity is an important parameter for determining the performance of a membrane in a certain ion-exchange membrane process. It describes the degree to which a membrane passes an ion of one charge and retains an ion of the opposite charge. The permselectivity of cation- and anion-exchange membranes can be defined by the following relations [4]:

$$\Psi^{cm} = \frac{t_c^{cm} - t_c}{t_a} \quad \text{and} \quad \Psi^{am} = \frac{t_a^{am} - t_a}{t_c} \quad (27)$$

Here, Ψ is the permselectivity of a membrane, t is the transport number, the superscripts cm and am refer to cation- and anion-exchange membranes, and the subscripts c and a refer to cation and anion, respectively.

An ideal permselective cation-exchange membrane would transmit positively charged ions only, that is, for a transport number of a counterion in a cation-exchange membrane is $t_c^{cm} = 1$ and the permselectivity of the membrane is $\Psi = 1$. The permselectivity approaches zero when the transport number within the membrane is identical to that in the electrolyte solution, that is, for $t_c^{cm} = t_c$ is $\Psi^{cm} = 0$. For, the anion-exchange membrane holds the corresponding relation.

The transport number of a certain ion in the membrane is proportional to its concentration in the membrane which again is a function of its concentration in the solutions in equilibrium with the membrane phase, due to the Donnan exclusion. Thus, the selectivity of ion-exchange membranes results from the exclusion of coions from the membrane phase.

2.14.3.2.4 The Donnan equilibrium and Donnan exclusion

The concentration of a coion in an ion-exchange membrane can be calculated from the Donnan equilibrium, which is established between phases, such as an ion-exchange membrane and a solution that are in electrochemical equilibrium. It can be calculated from Equation (15) under the condition that $\frac{d\tilde{\mu}_i}{dx} = 0$.

$$\frac{d\tilde{\mu}_i}{dx} = 0 = \bar{V}_i \frac{dp}{dx} + RT \frac{d \ln a_i}{dx} + z_i F \frac{d\varphi}{dx} \quad (28)$$

Integrating and rearranging leads to

$$\varphi_{\text{Don}} = \varphi^m - \varphi^s = \frac{1}{z_i F} \left(RT \ln \frac{a_i^s}{a_i^m} + \bar{V}_i (p^s - p^m) \right) \quad (29)$$

Here, φ is the electrical potential, p is the pressure, a is the activity, z is the charge number, \bar{V} is the partial molar volume, the subscript i refers to ions, the subscript Don refers to the Donnan potential, and the superscripts s and m refer to the solution and the membrane, respectively.

Introducing the osmotic pressure difference $\Delta\pi$ for the pressure difference $p^s - p^m$ between the membrane and the solution into Equation (29) leads to

$$\varphi_{\text{Don}} = \varphi^m - \varphi^s = \frac{1}{z_i F} \left(RT \ln \frac{a_i^s}{a_i^m} + \bar{V}_i \Delta\pi \right) \quad (30)$$

The numerical values of the Donnan potentials calculated from the cations and anions are identical; thus

$$\begin{aligned} \varphi_{\text{Don}} &= \frac{1}{z_a F} \left(RT \ln \frac{a_c^s}{a_c^m} + \bar{V}_c \Delta\pi \right) \\ &= \frac{1}{z_a F} \left(RT \ln \frac{a_a^s}{a_a^m} + \bar{V}_a \Delta\pi \right) \end{aligned} \quad (31)$$

and

$$\frac{1}{z_a F} \left(RT \ln \frac{a_a^s}{a_a^m} + \bar{V}_a \Delta\pi \right) = \frac{1}{z_c F} \left(RT \ln \frac{a_c^s}{a_c^m} + \bar{V}_c \Delta\pi \right) \quad (32)$$

Furthermore

$$z_a \nu_a = -z_c \nu_c \quad \text{and} \quad \bar{V}_s = \nu_a \bar{V}_a + \nu_c \bar{V}_c \quad (33)$$

Here, ν and z are the stoichiometric coefficient and the charge number, respectively, \bar{V} is the partial molar volume, and the subscripts a , c , and s refer to anion, cation, and salt.

Introducing Equation (33) into Equation (32) and rearranging leads to

$$\left(\frac{a_a^s}{a_a^m} \right)^{\frac{1}{z_a}} \left(\frac{a_c^s}{a_c^m} \right)^{\frac{1}{z_c}} = e^{-\frac{\Delta\pi \bar{V}_s}{RT \nu_c z_c}} \quad (34)$$

Equation (34) describes the Donnan equilibrium between the solution and the membrane. Depending on the fixed ions of the membrane, the anion or cation can be the coion, that is, in a cation-exchange membrane the anion is the coion and in the anion-exchange membrane the cation is the coion.

Introducing the ion concentration and the activity coefficient for the ion activities in Equation (34) and rearranging leads to

$$\left(\frac{C_{\text{co}}^s}{C_{\text{co}}^m} \right)^{\frac{1}{z_{\text{co}}}} \left(\frac{C_{\text{cou}}^m}{C_{\text{cou}}^s} \right)^{\frac{1}{z_{\text{cou}}}} = \left(\frac{\gamma_{\text{co}}^m}{\gamma_{\text{co}}^s} \right)^{\frac{1}{z_{\text{co}}}} \left(\frac{\gamma_{\text{cou}}^s}{\gamma_{\text{cou}}^m} \right)^{\frac{1}{z_{\text{cou}}}} e^{-\frac{\Delta\pi \bar{V}_s}{RT \nu_c z_c}} \quad (35)$$

Here, C and γ are the concentration and the activity coefficient, the subscripts co and cou refer to coion, and counterion, respectively, the superscripts s and m refer to solution and membrane, respectively, the subscripts c and s refer to cation and salt. All other symbols are the same as in the previous equations.

The calculation of the coion concentration in the membrane for a multicomponent electrolyte under practical conditions is rather complicated. However, for a monovalent electrolyte the coion concentration in an ion-exchange membrane can be estimated when certain assumptions are made:

- exponential function $e^{-\frac{\Delta\pi \bar{V}_s}{RT \nu_c z_c}} \cong 1$;
- the ratio of the activity coefficient in the solution and the membrane is 1; that is,

$$\left(\frac{\gamma_{\text{co}}^m}{\gamma_{\text{co}}^s}\right)^{\frac{1}{z_{\text{co}}}} \left(\frac{\gamma_{\text{cou}}^s}{\gamma_{\text{cou}}^m}\right)^{\frac{1}{z_{\text{cou}}}} \cong 1; \text{ and}$$

- the counterion concentration is close to the fixed ion concentration, that is,

$$C_{\text{cou}}^m = C_{\text{fix}} + C_{\text{co}} \cong C_{\text{fix}}$$

In many practical applications of electro dialysis, these assumptions are valid to a first approximation and the coion concentration in the membrane for a monovalent salt is given by

$$C_{\text{co}}^m = \frac{C_s^2}{C_{\text{fix}}} \quad (36)$$

Here, C is the concentration, the subscripts co, s, and fix refer to coion, salt, and fixed ion of the membrane, the superscripts s and m refer to solution and membrane, respectively.

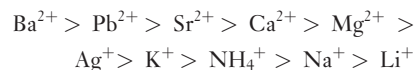
Equation (36) indicates that the coion concentration in the membrane and, thus, the permselectivity of the membrane is decreasing with increasing salt concentration in the solution.

2.14.3.2.5 Membrane counterion permselectivity

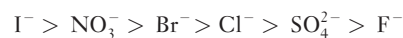
The transport number of counterions in an ion-exchange membrane is always quite high compared to that of the coions. However, the permselectivity of a membrane for counterions can also be quite different. The transport rates of ions through a membrane are determined by their concentration and their mobility in the membrane. The concentration of the counterions in the membrane is always close to the concentration of the fixed charges of the membrane. The mobility of the ions in the membrane depends mainly on the radius of the hydrated ions and the membrane structure. The mobility of different ions in an aqueous solution does not differ very much with the exception of H^+ and OH^- ions. Their mobility is about a factor 5–8 higher than that of other ions. This exceptionally high mobility of the H^+ ion can be explained by the transport mechanism of protons and hydroxide ions. Because of the molecular interaction of water dipoles with electrical charges, protons form hydronium ions. Common salt ions move with their hydrate shell through the solution. The proton, however, is transported by a mechanism that does not involve an actual motion through the solution. According to the chain mechanism, protons migrate through a solution by the rearrangement of bonds in a cluster

of water molecules. The proton conductivity is governed by the rate at which the water molecules can rotate into orientations in which they can accept or donate protons and by the rate at which the protons tunnel from one end of a hydrogen bond to another. This explains not only the extraordinary high mobility of protons but it is also one of the reasons for the high permeability of anion-exchange membranes for protons, while these membranes generally have a very low permeability for salt cations. The same mechanism also holds true for the transport of hydroxide ions, thus the permeability of hydroxide ions in an aqueous solution and also in a cation-exchange membrane is much higher than that of other salt anions. As protons and hydroxide ions are transported only to a small extent as individual ions surrounded by a hydration shell, their water transport number in the membrane is always quite low and they contribute very little to the electroosmotic transport of water.

The concentration of the different counterions in the membrane is determined mainly by electrostatic effects referred to as electroselectivity [10]. Generally, multivalent counterions are stronger absorbed than monovalent ions in an ion-exchange membrane. A typical counterion-exchange permeability sequence of a cation-exchange membrane containing SO_3^- -groups as fixed charges is [4]



A similar counterion-exchange sequence is obtained for anions in an anion-exchange membrane containing quaternary ammonium groups as fixed charges:



2.14.4 Ion-Exchange Membrane Deionization Processes

The processes that utilize ion-exchange membranes as key components can conveniently be divided into three types [22]:

- electrodeionization such as electro dialysis or continuous electrodeionization;
- electrosynthesis such as chlorine-alkaline or the hydrogen production; and
- electrochemical energy conversion such as fuel cells or batteries.

In the first type, an electrical potential gradient is used to remove charged components, such as dissociated salts, from a solution. In the second type, the transport of ions is combined with an electrochemical reaction producing certain chemicals. The third type involves the conversion of chemical energy into electrical energy.

2.14.4.1 Electrodialysis

Among the ion-exchange membrane deionization processes, electrodialysis is today by far the most important one. Other processes such as diffusion and Donnan dialysis or continuous electrodeionization and capacitive deionization have had so far only minor commercial impact.

Electrodialysis is a well-developed process with reliable equipment and significant application know-how commercially available.

2.14.4.1.1 The principle of electrodialysis

The principle of electrodialysis is illustrated in **Figure 3**, which shows a schematic diagram of an electrodialysis cell arrangement.

An electrodialysis cell arrangement consists of a series of anion- and cation-exchange membranes arranged in an alternating pattern to form individual cells stacked between an anode and a cathode [23]. If an ionic solution, such as an aqueous salt solution, is pumped through these cells and an electrical potential is established between the anode and cathode, the positively charged cations migrate toward the

cathode and the negatively charged anions toward the anode. The cations pass through the negatively charged cation-exchange membrane, but are retained by the positively charged anion-exchange membrane. Similarly, the negatively charged anions pass through the anion-exchange membrane, and are retained by the cation-exchange membrane. The overall result is an increase in the ion concentration in alternate compartments, while the other compartments simultaneously become depleted. The depleted solution is referred to as the diluate and the concentrated solution as the brine. The space between two contiguous membranes is occupied by the diluate or the brine and the two contiguous anion- and cation-exchange membranes make up a cell pair which is a repeating unit in a so-called electrodialysis stack, which may have a few hundreds cell pairs between two electrodes.

2.14.4.1.2 Principle of electrodialysis with bipolar membranes

The conventional electrodialysis can be combined with bipolar membranes and utilized to produce acids and bases from the corresponding salts [24, 25]. In this process, monopolar cation- and anion-exchange membranes are installed together with bipolar membranes in alternating series in an electrodialysis stack as illustrated in **Figure 4**. A typical repeating unit of an electrodialysis stack with bipolar membranes is composed of three cells, two monopolar membranes, and a bipolar membrane. The cell between the monopolar membranes

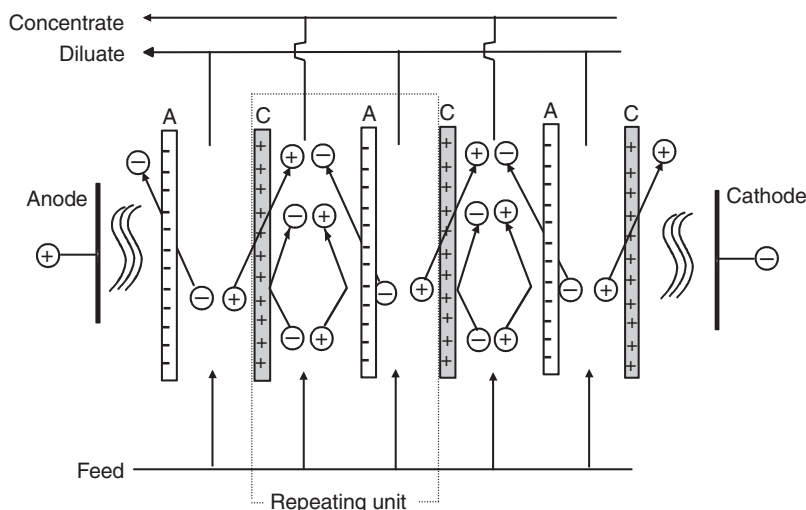


Figure 3 Schematic diagram illustrating the principle of desalination by electrodialysis in a stack with cation- and anion-exchange membranes in alternating series between two electrodes.

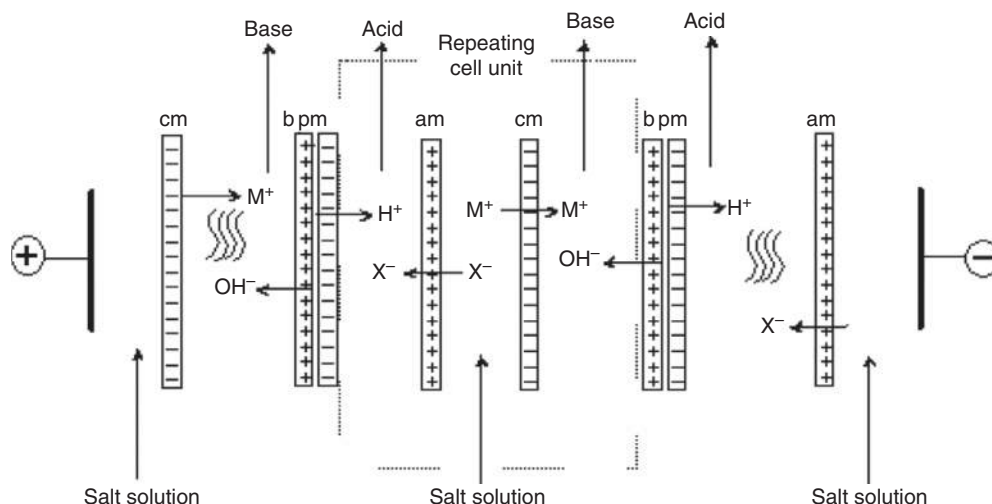


Figure 4 Schematic drawing illustrating the principle of an electrodiolytic production of acids and bases from the corresponding salts with bipolar membranes.

contains a salt solution and the two cells between the monopolar and the bipolar membranes contain a base and an acid solution. When an electrical potential gradient is applied across a repeating unit, protons and hydroxide ions form, with the cations and anions removed from the salt solution, an acid and a base, respectively.

The utilization of electrodiolysis with bipolar membranes to produce acids and bases from the corresponding salts is economically very attractive and has a multitude of interesting potential applications as discussed later.

The function of the bipolar membrane. The function and structure of a bipolar membrane are illustrated in **Figure 5**, which shows an anion- and a cation-exchange membrane with a 4–5-nm-thick interphase arranged in between two electrodes. When an electrical potential difference is established between the electrodes, all charged components will be removed from the interphase, and only water is left between the two ion-exchange membranes. Further transport of electrical charges can be accomplished only by protons and hydroxyl ions of the dissociated water. However, H^+ and OH^- ions removed from the interphase are regenerated due to the water dissociation equilibrium which is given by



The transport of H^+ and OH^- ions from the transition region into the outer phases is determined by the water diffusion rate into the interphase and by the

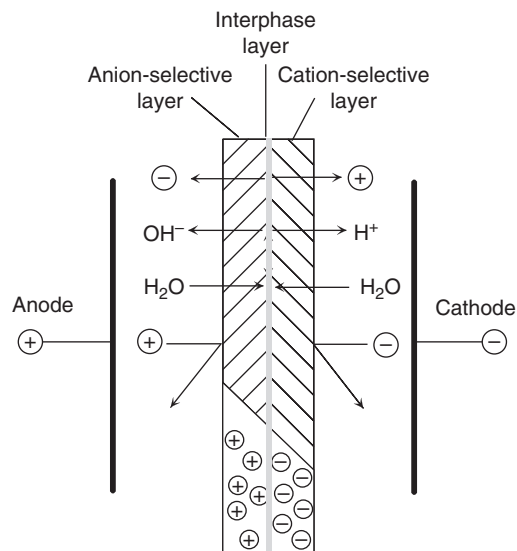


Figure 5 Schematic diagram illustrating the structure and the function of a bipolar membrane which is composed of a cation- and an anion-exchange layer with a 4–5-nm-thick interphase transition layer arranged between two electrodes.

regeneration rate of H^+ and OH^- ions which is drastically increased in a bipolar membrane compared to the rate obtained in water due to a catalytic reaction [26–28]. Therefore, very high production rates of acids and bases can be achieved in electrodiolysis with bipolar membranes.

The energy required for the water dissociation can be calculated from the Nernst equation for a

concentration chain between solutions of different pH values. It is given by

$$\Delta G = F\Delta\varphi = 2.3RT\Delta\text{pH} \quad (37)$$

Here, ΔG is the Gibbs free energy, F is the Faraday constant, R is the gas constant, T is the absolute temperature, and ΔpH and $\Delta\varphi$ are the pH value and the voltage difference between the two solutions separated by the bipolar membrane, respectively. For 1 mol l^{-1} acid and base solutions in the two phases separated by the bipolar membrane, ΔG is $0.022 \text{ kWh mol}^{-1}$ and $\Delta\varphi$ is 0.828 V at 25°C .

2.14.4.1.3 Electrodialysis equipment and process design

The performance of electrodialysis in a practical application is determined by several equipment components, such as membranes and the arrangement in a system, pumps, and rectifier, and also by several process parameters, such as the flow velocities of the different flow streams across the surface of the membrane, the applied current density, and the product recovery from a feed solution.

The electrodialysis stack. A key element in electrodialysis is the so-called stack, which is a device to hold an array of cation- and anion-exchange membranes between two electrodes. A typical electrodialysis stack used in water desalination contains 200–600 membranes stacked between the electrodes [4]. The electrode containing cells at both ends of a stack are often rinsed with a separate solution, which does not contain Cl^- ions to avoid chlorine formation.

The membranes in an electrodialysis cell are separated by spacer gaskets as indicated in **Figure 6**, which

shows schematically the design of a so-called sheet-flow electrodialysis stack. The spacer gasket consists of a screen, which supports the membranes and controls the flow distribution in the cell. The gasket that seals the cell to the outside also contains the manifolds to distribute the process fluids in the different compartments. To minimize the resistance of the solution in the cell, the distance between two membranes is kept as less as possible and is in the range of 0.5–2 mm in industrial electrodialysis stacks. A proper electrodialysis stack design ensures uniform flow distribution and mixing of the solutions to minimize concentration polarization at the membrane surfaces at minimized pressure loss of the solution flow in the stack.

Concentration polarization and limiting current density.

The limiting current density is the maximum current which may pass through a given cell pair area without detrimental effects. If the limiting current density is exceeded, the electric resistance in the diluate will increase and water dissociation may occur at the membrane surface, which effects the current utilization and can lead to pH changes in the solutions.

The limiting current density is determined by concentration polarization at the membrane surface in the diluate containing compartment, which is also a function of the diluate concentration. Concentration polarization in electrodialysis is the result of differences in the transport number of ions in the solution and in the membrane. The effect of concentration polarization is illustrated in **Figure 7**, which shows the salt-concentration profiles and the fluxes of cations and anions in the concentrate and diluate solution at the surface of a cation-exchange membrane.

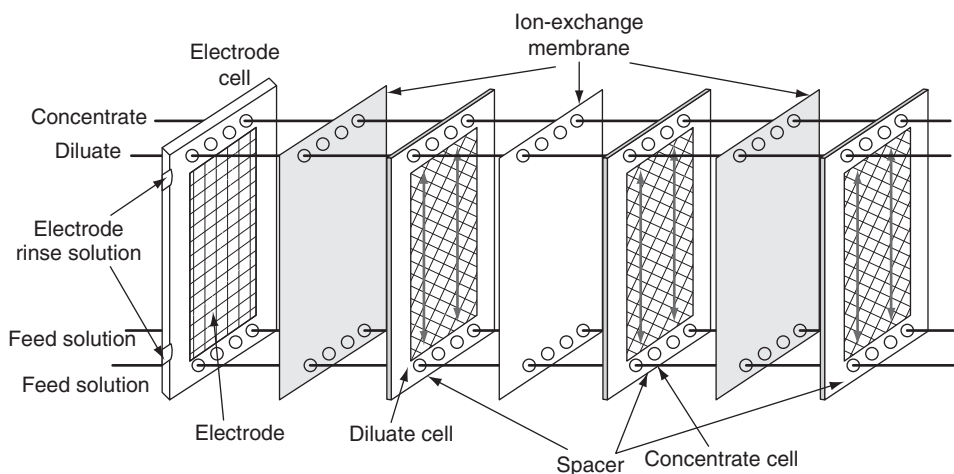


Figure 6 Exploded view of a sheet-flow type electrodialysis stack arrangement indicating the individual cells and the spacer gaskets containing the manifold for the distribution of the different flow streams.

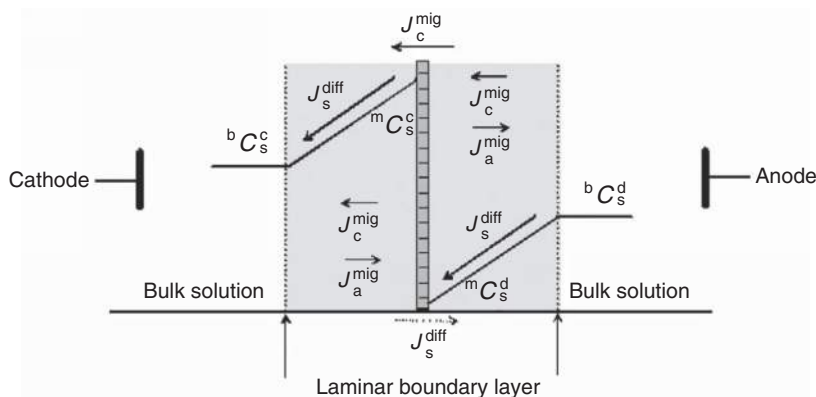


Figure 7 Schematic drawing illustrating the concentration profiles of a salt in the laminar boundary layer on both sides of a cation-exchange membrane and the flux of ions in the solutions and the membrane.

J and C in **Figure 7** denote the fluxes and the concentrations of ions; the superscripts mig and diff refer to migration and diffusion, respectively; the superscripts d and c refer to diluate and concentrate solution; the superscripts b and m refer to bulk phase and membrane surface, respectively; and the subscripts a and c refer to anion and cation, respectively.

The transport number of a counterion in an ion-exchange membrane is generally close to 1 and that of the coion close to 0, while in the solution, the transport numbers of anion and cations are not very different and are close to 0.5. At the surface of a cation-exchange membrane, the cation concentration in the solution is reduced due to the high transport number of the cations in the membrane. Since anions migrate in the opposite direction, the electrolyte concentration in the diluate solution at the surface of the membrane is reduced and a concentration gradient is established between the membrane surface and the well-mixed bulk solution. This concentration gradient results in a diffusive electrolyte transport toward the membrane surface. A steady-state situation is obtained when the migration of ions from the membrane surface is balanced by the diffusive transport of salt toward the membrane surface. On the other side of the cation-exchange membrane, which is facing the concentrate solution, the electrolyte concentration at the membrane surface is increased for the same reason.

The concentration polarization in electrodialysis can be calculated by a mass balance taking into account all fluxes in the boundary layer and the hydrodynamic conditions in the flow channel between the membranes. In practical applications, the so-called Nernst film model, which neglects the

entrance and exit effects of the flow streams in the stack, is used to estimate concentration polarization effects. Due to the spacer effect, the flow distribution in an electrodialysis stack and, thus, the thickness of the laminar boundary is difficult to determine. Nevertheless, the Nernst model provides a reasonable description of the concentration polarization, which results in an expression for the current density as a function of the bulk solution concentration, the transport number of the ions, the diffusion coefficient of the electrolyte, and the thickness of the laminar boundary layer.

$$i = \frac{z_i F D_i}{(t_i^m - t_i^s)} \frac{\Delta C_i^d}{\Delta x} \quad (38)$$

Here, t is the transport number of the counterion, ΔC is the concentration difference between the solutions at the membrane surface and in the bulk, D is the diffusion coefficient, F is the Faraday constant, z is the charge number, and Δx is the boundary layer thickness; the subscript i refers to cations or anions; the superscripts d, m, and s refer to diluate, membrane, and solution, respectively.

When the flow conditions are kept constant, the boundary layer will be constant and the current density will reach a maximum independent of the applied electrical potential. This maximum current density, which is referred to as the limiting current density, is reached when the counterion concentration at the membrane surface becomes 0; thus

$$i = i_{\text{lim}} \text{ for } {}^m C_s^d \rightarrow 0: i_{\text{lim}} = \frac{z_i F D_s}{(t_i^m - t_i^b)} \left(\frac{{}^b C_s^d}{\Delta x} \right) \quad (39)$$

Here, i_{lim} is the limiting current density and ${}^b C_s^d$ is the salt concentration of the diluate in the bulk

solution. All other symbols have the same meaning as in Equation (38).

In practical applications, the limiting current density is often experimentally determined and described as a function to the diluate flow velocity and the concentration by the following relation:

$$i_{\text{lim}} = a u^b F C_s^d \quad (40)$$

Here, C_s^d is the concentration of the solution in the diluate cell, u is the linear flow velocity of the solution through the cells parallel to the membrane surface, F is the Faraday constant, and a and b are the characteristic constants for a given stack design and must be determined experimentally.

Water transport in electro dialysis. Water transport in electro dialysis from the diluate to the concentrate can affect the process efficiency significantly. If a convective flux, as a result of pressure differences between flow streams, can be excluded, there are still two sources for the transport of water from the diluate to the concentrate solution. The first one is the result of an osmotic pressure difference between the two solutions and the second is due to electroosmosis, which is caused by the coupling of water to the ions that transported through the membrane due to the driving force of an electrical potential.

Each of the two fluxes may be dominant, depending on the ion-exchange membrane, the salt concentrations in the solutions separated by the membrane, and the current density. In electro dialysis with relatively large differences in the salt concentration of the diluate and concentrate, the electroosmotic flux is dominant and generally much higher than the osmotic flux. The water flux due to electroosmosis is proportional to the flux of ions and given by

$$\mathcal{F}_w = {}^m t_w \sum_i \mathcal{F}_i \quad (41)$$

Here, ${}^m t_w$ is the water transport number, \mathcal{F}_w is the water flux, and \mathcal{F}_i is the flux of ions. The water transport number thus is

$${}^m t_w = \frac{\mathcal{F}_w}{\sum_i \mathcal{F}_i} \quad (42)$$

The water transport number refers to the number of water molecules transferred by one ion through a given membrane. It depends on the membrane and on the electrolyte, that is, on the size of the ions, their valence, and their concentration in the solution. In aqueous salt solutions and commercial ion-exchange membranes, the water transport number is in the

order of 4–8, that is, one mole of ions transports ~ 4 –8 moles of water through a typical commercial ion-exchange membrane.

Current utilization. In practical applications, electro dialysis is affected by incomplete current utilization, which is the result of poor membrane permselectivity, parallel current through the stack manifold, and water transport by convection by osmosis and electroosmosis. In a well-designed stack with no pressure difference between diluate and concentrate, the convective water transport is negligibly low and also the current through the manifold can be neglected. Under these conditions, the overall current utilization is given by

$$\xi = N_{\text{cell}} (\psi^{\text{cm}} t_a^s + \psi^{\text{am}} t_c^s) (1 - [t_w^{\text{cm}} + t_w^{\text{am}}] \bar{V}_w (C_s^c - C_s^d)) \quad (43)$$

Here, ξ is the current utilization, ψ is the membrane permselectivity, t is the transport number, N_{cell} is the number of cell pairs in the stack, \bar{V}_w is the partial molar volume of water, C is the concentration; the subscripts a, c, s, and w refer to anion, cation, solution, and water, respectively, and the superscripts cm, am, c, and d refer to cation-exchange membrane, anion-exchange membrane, concentrate, and diluate.

Electro dialysis equipment and plant design. In an electro dialysis stack, the membranes are separated by spacers that also hold the manifolds for the distribution of the individual flow channels for the diluate and concentrate. There are two major concepts as far as the construction of the spacers is concerned. One is the so-called sheet-flow spacer concept which is illustrated in **Figure 8(a)** and the other is the so-called tortuous path concept which is illustrated in **Figure 8(b)**.

The sheet-flow spacer is generally installed vertically in a stack as shown in **Figure 6**. The flow velocity in the cells is between 2 and 3 cm s⁻¹ and the pressure drop in the stack is generally less than 0.2 bar. The tortuous path spacer is generally installed horizontally in a stack, the flow velocity in the cells is between 6 and 10 cm s⁻¹, and the pressure drop in the stack is 1–2 bars. However, the process path length is significantly longer than in a sheet-flow spacer stack.

In the practical application of electro dialysis, there are two main process operation modes. The first one is referred to as the unidirectional electro dialysis and the second one as electro dialysis reversal [29]. In a unidirectionally operated electro dialysis system, the electric field is permanently applied in

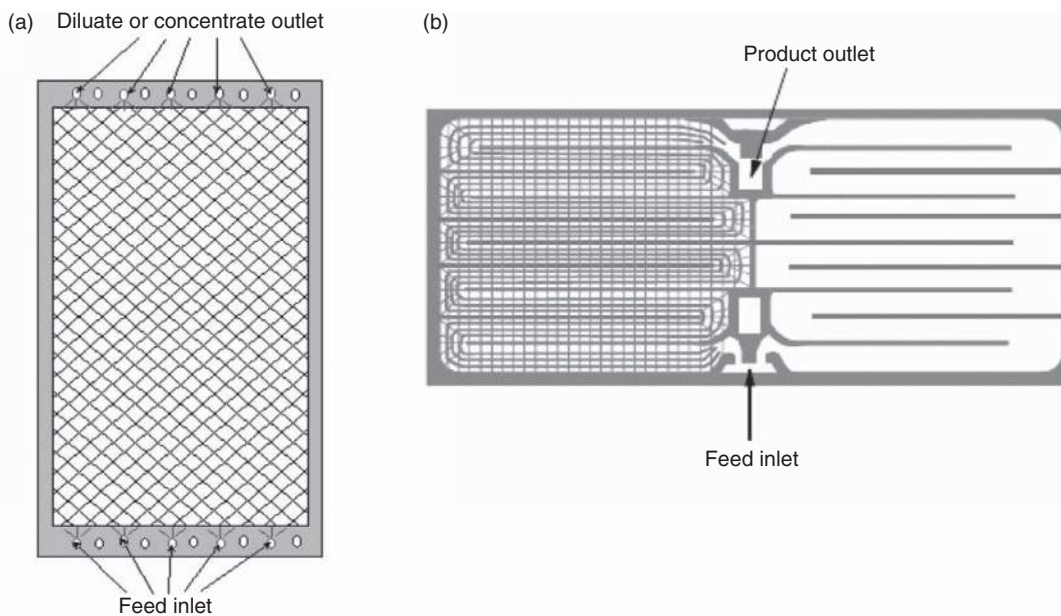


Figure 8 Schematic drawing illustrating (a) the sheet-flow and (b) a tortuous path spacer concept.

one direction and the diluate and concentrate cells are also permanently fixed over the period of operation. Unidirectionally operated electro dialysis plants are rather sensitive to membrane fouling and scaling and require periodical rinsing of the stack with acid or detergent solutions. In the desalination of brackish or surface waters, generally, electro dialysis reversal is applied. In the electro dialysis reversal operating mode, the polarity of the electric field applied to the electro dialysis stack is reversed in certain time intervals. Simultaneously, the flow streams are

reversed, that is, the diluate cell becomes the concentrate cell and vice versa with the result that the matter that has been precipitated at the membrane surface will be redissolved and removed with the flow stream passing through the cell. The principle of the electro dialysis reversal is illustrated in **Figure 9**, which shows schematically an electro dialysis cell formed by a cation- and an anion-exchange membrane between two electrodes and a feed solution containing negatively charged large fouling components. If an electric field is applied, these

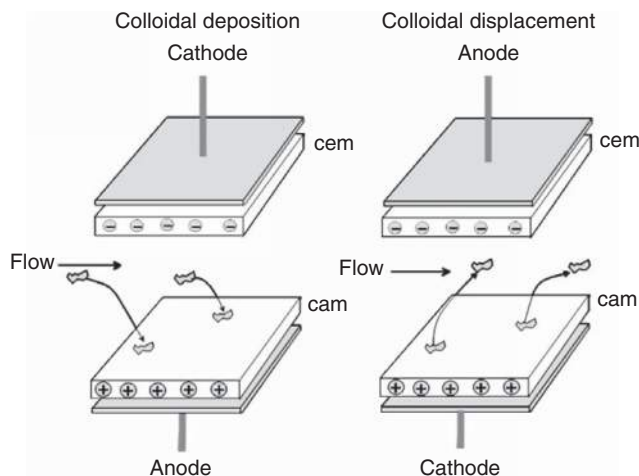


Figure 9 Schematic drawing illustrating the removal of deposited negatively charged colloidal components from the surface of an anion-exchange membrane by reversing the electric field in the electro dialysis reversal operating mode.

components will migrate to the anion-exchange membrane and will be deposited on its surface to form a so-called fouling layer, which affects the efficiency of the electrodiagnosis process. If the polarity is reversed, the negatively charged components will now migrate away from the anion-exchange membrane back into the feed stream and the membrane properties are restored. This procedure, which is referred to as clean in place, is very effective not only for the removal of colloidal fouling materials but also for removing precipitated salts and is used today in almost all electrodiagnosis water desalination systems.

However, reversing the polarity of a stack has to be accompanied with a reversal of the flow streams. This requires a more sophisticated flow control. The flow scheme of an electrodiagnosis plant operated with reversed polarity is shown in **Figure 10**. In the reverse polarity operating mode, the hydraulic flow streams are reversed simultaneously with the polarity, that is, the diluate cell will become the brine cell and vice versa. In this operating mode, the polarity of the current is changed at specific time intervals ranging from a few minutes to several hours. During the reversal of the polarity and the flow streams, there is a brief period when the concentration of the desalted product exceeds the product quality specification. The product water outlet has a concentration sensor, which controls an additional three-way valve. This valve diverts the concentrated product to waste and, then, when the concentration returns to the specified quality, directs the flow to the product outlet. Thus,

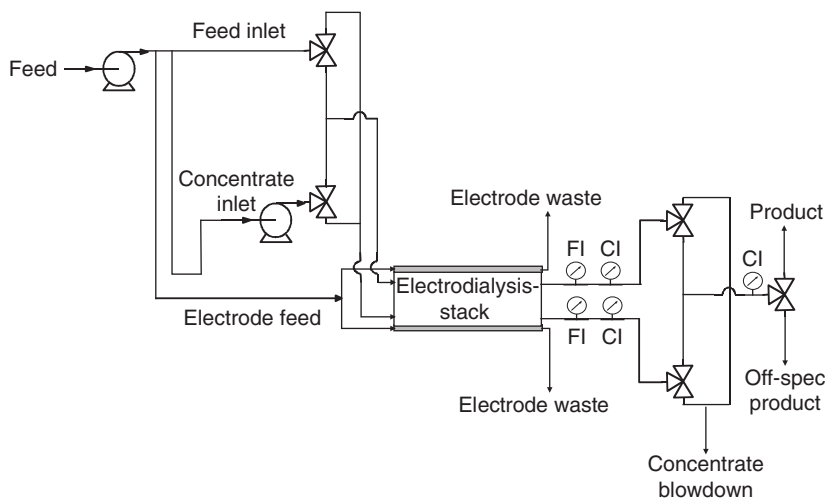


Figure 10 Flow scheme of electrodiagnosis reversal in a continuous operating mode with the feed solution also used as electrode rinse.

in electrodiagnosis reversal, there is always a certain amount of the product lost to the waste stream which in praxis is less than 2%.

The degree of desalination that can be achieved in passing the feed solution through a stack is a function of the solution concentration, the applied current density, and the residence time of the solution in the stack. If the degree of desalination or concentration that can be achieved in a single path of the feed through the stack is insufficient, several stacks are operated in series or part of the diluate or concentrate is fed back to the feed solution as shown in **Figure 11**.

In the feed and bleed operating mode, both the brine and the product concentration can be determined independently and very high recovery rates can be achieved.

2.14.4.1.4 Electrodiagnosis process costs

The total costs in electrodiagnosis are the sum of fixed charges associated with the plant investment costs and the plant operating costs. Both the capital-related costs as well as the plant operating costs per unit product are a function of the feed solution concentration and the required product and brine concentrations. They are also strongly affected by the plant capacity and the overall process design [30, 31].

Investment-related costs. The investment costs are determined mainly by the required membrane area for a certain plant capacity. Costs of other items, such as maintenance, pumps, and process control equipment, can be considered as being proportional to the required membrane area. The required membrane area

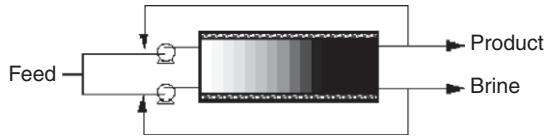


Figure 11 Flow scheme of an electrodiagnosis stack operated in a feed and bleed mode, that is, with partial recycling of the diluate and concentrate solutions.

for a given capacity plant can be calculated from the total current required to remove a certain number of ions from the feed solution and the current density. Thus, the total current required for the desalination process is proportional to the concentration difference between the feed and diluate solution and the total volume flow of the diluate through the stack. It is inversely proportional to the number of cell pairs in the stack and the current utilization. The total current passing through a cell pair and the stack is given by

$$I = A_{\text{cell}} i = \frac{Q_{\text{cell}}^{\text{d}} F (C_{\text{eq}}^{\text{f}} - C_{\text{eq}}^{\text{d}})}{\xi} \quad (44)$$

Thus

$$\begin{aligned} N_{\text{cell}} Q_{\text{cell}}^{\text{d}} &= Q_{\text{st}}^{\text{d}} \quad \text{and} \quad N_{\text{cell}} A_{\text{cell}} = A_{\text{st}} \quad \text{and} \quad A_{\text{st}} \\ &= \frac{Q_{\text{st}}^{\text{d}} F (C_{\text{eq}}^{\text{f}} - C_{\text{eq}}^{\text{d}})}{i \xi} \end{aligned} \quad (45)$$

Here, I and i are the electric current and the current density, A is the cell pair area, N_{cell} refers to the number of cell pairs in the stack, Q is the volume flow, C is the concentration expressed in equivalent per volume, F is the Faraday constant, and ξ is the current utilization. The subscripts eq, st, and cell refer to equivalent, the stack, and cell pair, and the superscripts d and f refer to diluate and feed solution.

The equivalent concentration determines the charges in an electrolyte solution in mole as has been discussed earlier. For a monovalent salt, such as NaCl, the equivalent concentration is equal to the molar concentration. For a multivalent electrolyte, the equivalent concentration is $z_a \nu_a C_s = z_c \nu_c C_s$. Since on a macroscopic scale electroneutrality must prevail, the number of positive and negative charges must be identical $z_a \nu_a = z_c \nu_c$. Thus, the number of charges removed from a feed solution is identical for cations and anions.

The voltage drop across the stack is constant, while the current density is changing over the cell length from the feed inlet to the product outlet because the resistance is changing from the feed

inlet to the product outlet. The average current density is given by

$$\bar{i} = \frac{U_{\text{cell}}}{\bar{R} A_{\text{cell}}} \quad (46)$$

Here, U_{cell} is the voltage drop across a cell pair, A_{cell} is the area, and \bar{R} and \bar{i} are the average resistance and current density of a cell pair, respectively.

The average resistance of a cell pair is

$$\bar{R} = \frac{1}{A_{\text{cell}}} \left[\frac{\Delta}{\lambda_{\text{eq}}} \left(\frac{1}{\bar{C}_{\text{eq}}^{\text{d}}} + \frac{1}{\bar{C}_{\text{eq}}^{\text{c}}} \right) + r^{\text{am}} + r^{\text{cm}} \right] \quad (47)$$

Here, Δ is the cell thickness, \bar{C} is the average concentration, λ_{eq} is the equivalent conductivity of the salt solution, r is the area resistance, the superscripts d, c, am, and cm refer to the diluate, the concentrate, and the anion- and the cation-exchange membranes.

The average resistance of a cell pair is a function of the average concentrations of the solutions, which are changing from the inlet to the outlet of the cells. The integral average concentrations are given by

$$\bar{C}_{\text{eq}} = \frac{\ln \left(\frac{C_{\text{eq}}^{\text{out}}}{C_{\text{eq}}^{\text{in}}} \right)}{C_{\text{eq}}^{\text{out}} - C_{\text{eq}}^{\text{in}}} \quad (48)$$

Here, \bar{C}_{eq} is the average equivalent concentration of the diluate and the concentrate in a cell pair and the superscripts in and out refer to the cell inlet and outlet, respectively.

Introducing Equation (48) into Equation (47) gives the average resistance in a cell pair:

$$\bar{R} = \frac{1}{A_{\text{cell}}} \left[\frac{\Delta \ln \left(\frac{C_{\text{eq}}^{\text{fd}} C_{\text{eq}}^{\text{c}}}{C_{\text{eq}}^{\text{fc}} C_{\text{eq}}^{\text{d}}} \right)}{\lambda_{\text{eq}} (C_{\text{eq}}^{\text{fd}} - C_{\text{eq}}^{\text{d}})} + r^{\text{am}} + r^{\text{cm}} \right] \quad (49)$$

Here, \bar{R} is the average resistance, A_{cell} is the area of a cell pair, C^{fd} and C^{d} are the salt concentrations of the diluate at the inlet and outlet of the cell, respectively, C^{fc} and C^{c} are the salt concentrations of the concentrate cell at the inlet and outlet, respectively, Δ is the cell thickness, λ_{eq} is the equivalent conductivity, and r^{am} and r^{cm} are the area resistances of the anion- and cation-exchange membranes, respectively.

The current density in a stack should not exceed the limiting current density. Thus, the applied cell voltage should not exceed a certain maximum value since the concentration of the diluate is lowest at the cell pair outlet. Thus, the highest resistance and the lowest current density are obtained at the outlet of

the stack. This current density determines the maximum cell voltage, which is given by

$$U_{\text{cell}}^{\text{max}} = i_{\text{lim}} \left[\frac{\Delta}{\lambda_{\text{eq}}} \left(\frac{1}{C_{\text{eq}}^{\text{d}}} + \frac{1}{C_{\text{eq}}^{\text{c}}} \right) + r^{\text{am}} + r^{\text{cm}} \right] \quad (50)$$

Here, Δ is the cell thickness, λ_{eq} is the equivalent conductivity of the salt solution, r is the area resistance, the superscripts d, c, am, cm, and max refer to the diluate, the concentrate, and the anion- and the cation-exchange membranes, and maximum values, respectively.

The membrane area required for a certain plant capacity as function of the feed and product concentration is obtained by combination of Equations (44)–(50) and rearranging:

$$A_{\text{st}} = \frac{\left[\ln \frac{C_{\text{eq}}^{\text{fd}} C_{\text{eq}}^{\text{c}}}{C_{\text{eq}}^{\text{cd}} C_{\text{eq}}^{\text{d}}} + \frac{\lambda_{\text{eq}} (r^{\text{am}} + r^{\text{cm}}) (C_{\text{eq}}^{\text{fd}} - C_{\text{eq}}^{\text{cd}})}{\Delta} \right] Q_{\text{st}}^{\text{d}} F C_{\text{eq}}^{\text{d}}}{\left[\frac{C_{\text{eq}}^{\text{cd}}}{C_{\text{eq}}^{\text{c}}} + 1 + \frac{\lambda_{\text{eq}} C_{\text{eq}}^{\text{d}}}{\Delta} (r^{\text{am}} + r^{\text{cm}}) \right] i_{\text{lim}} \xi} \quad (51)$$

Here, A_{st} is the total membrane area in a stack and N_{cell} is the number of cell pairs in a stack. All other symbols are as explained in Equations (44)–(50).

The total investment-related costs depend on the price of the membranes and the additional plant components and their useful life under operating conditions, which in practical applications is 5–8 years.

Operating costs. The operating costs are energy and plant costs. The maintenance costs are proportional to the size of the plant and calculated as a percentage of the investment-related costs.

The energy required in an electro dialysis process is an additive of two terms: (1) the electrical energy to transfer the ionic components from one solution through membranes into another solution and (2) the energy required to pump the solutions through the electro dialysis unit. The energy consumption due to electrode reactions can generally be neglected since more than 200 cell pairs are placed between the two electrodes in a modern electro dialysis stack. The energy required for operating the process control devices can generally also be neglected.

The energy required in electro dialysis for the transfer of the ions from a feed solution to the concentrate solution is given by the current passing through the electro dialysis stack multiplied with the total voltage drop encountered between the electrodes:

$$E_{\text{des}} = I_{\text{st}} U_{\text{st}} t = I_{\text{st}} N_{\text{cell}} U_{\text{cell}} t = I^2 N_{\text{cell}} \bar{R} t \quad (52)$$

Here, E_{des} is the energy consumed in a stack for the transfer of ions from a feed to a concentrate solution, I_{st} is the current passing through the stack, U_{st} and

U_{cell} are the voltage applied across the stack, that is, between the electrodes, and across a cell pair; t is the time of operation.

The total current through the stack is given by Equation (44) and the average resistance is given by Equation (49). Combination of the two equations and dividing by the diluate so produced gives the desalination energy per volume product:

$$\begin{aligned} E_{\text{des,spc}} &= \frac{N_{\text{cell}} \bar{R}_{\text{cell}} I^2 t}{V_{\text{pro}}} \\ &= \frac{N_{\text{cell}} t}{AV_{\text{pro}}} \left[\frac{\Delta \ln \frac{C_{\text{eq}}^{\text{fd}} C_{\text{eq}}^{\text{c}}}{C_{\text{eq}}^{\text{cd}} C_{\text{eq}}^{\text{d}}}}{\lambda_{\text{eq}} (C_{\text{eq}}^{\text{fd}} - C_{\text{eq}}^{\text{cd}})} + r^{\text{am}} + r^{\text{cm}} \right] \\ &\quad \times \left[\frac{Q_{\text{cell}}^{\text{d}} F (C_{\text{eq}}^{\text{fd}} - C_{\text{eq}}^{\text{cd}})}{\xi} \right]^2 \end{aligned} \quad (53)$$

Here, E_{des} and $E_{\text{des,spc}}$ are the desalination energy and the specific desalination; I is the total current, t is the time of operation; C^{fd} and C^{fc} are the equivalent concentrations of the diluate and the concentrate at the cell inlet, respectively; C^{d} and C^{c} are the concentrations of the diluate and the concentrate at the cell outlet, respectively; λ_{eq} is the equivalent conductivity of the salt solution; r^{am} and r^{cm} are the area resistances of the anion- and cation-exchange membrane, respectively; Δ is the cell thickness; ξ is the current utilization; $Q_{\text{cell}}^{\text{d}}$ is the diluate flow rate in a cell; \bar{R} is the average resistance of a cell pair; A is the cell pair area; N_{cell} is the number of cell pairs in a stack; and V_{pro} is the volume product water.

Equation (53) shows that the energy dissipation due to the resistance of the solutions and membranes is increasing with the current density. The electrical energy for a given resistance is proportional to the square of the current, whereas the salt transfer is directly proportional to the current. Hence, the energy necessary for the production of a given amount of product increases with the current density. However, the required membrane area for a given capacity is decreasing with the current density as illustrated in **Figure 12**, which shows the total costs of desalination, the membrane costs, and current-density-related costs as a function of the current density. The figure shows that at a certain current density the total desalination costs reach a minimum. However, in a practical application the operating current density must be lower than the limiting current density.

The operation of an electro dialysis unit requires one or more pumps to circulate the diluate, the concentrate, and the electrode rinse solution through the

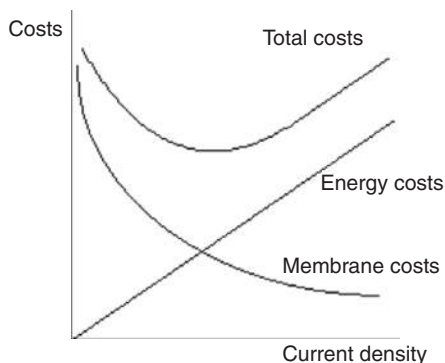


Figure 12 Schematic diagram illustrating the various cost items in electrodialysis as function of the applied current density.

stack. The energy required for pumping these solutions is determined by the volumes of the solutions to be pumped and the pressure drop. It can be expressed by

$$E_{p,\text{spec}} = \frac{E_p}{Q^{d,r}} = k_{\text{eff}} \frac{(Q^d \Delta p^d + Q^c \Delta p^c + Q^e \Delta p^e)}{Q^d} \quad (54)$$

Here, $E_{p,\text{spec}}$ is the total energy for pumping the diluate, the concentrate, and the electrode rinse solution through the stack per unit diluate water; k_{eff} is an efficiency term for the pumps; and Q^d , Q^c , and Q^e are the volume flow rates of the diluate, the concentrate, and the electrode rinse solution through the stack, respectively.

The pressure losses in the various cells are determined by the solution flow velocities and the cell design. The energy requirements for circulating the solution through the system may become a significant or even dominant portion of the total energy consumption for solutions with rather low salt concentration.

2.14.4.1.5 Electrodialysis with bipolar membrane system design and process costs

The design of an electrodialysis process with bipolar membranes is closely related to that of a conventional

electrodialysis desalination process as shown in the schematic flow diagram of **Figure 13**. The main difference is in the stack construction which requires three independent flow streams, that is, the salt solution, the base, and the acid flow stream. Furthermore, additional energy is required for the water dissociation, and the mono- and bipolar membranes (as well as other hardware components) must have excellent chemical stability in strong acids and bases, respectively.

The determination of the costs for the production of acids and bases from the corresponding salts follows the same general procedure as applied for the costs analysis in electrodialysis desalination. The contributions to the overall costs are the sum of the investment-related cost and the operating costs.

Investment costs in electrodialysis with bipolar membranes. The investment costs are directly related to the required membrane area for a certain plant capacity and can be expressed as a certain percentage of the total required membrane area for a given capacity plant, which can be calculated from the current density by

$$A_{\text{unit}} = \frac{Q_{\text{pro}} F C_{\text{pro}}}{i \xi} \quad (55)$$

Here, A_{unit} is the required cell unit area which contains a bipolar membrane, and a cation- and an anion-exchange membrane, i is the current density, Q_{pro} is the product volume flow, F is the Faraday constant, ξ is the current utilization, and C_{pro} is the concentration of the product.

Operating costs in electrodialysis with bipolar membranes. The operating costs in electrodialysis with bipolar membranes are strongly determined by the energy requirements which are composed of the energy required for the water dissociation in the bipolar membrane and the energy necessary to transfer the salt ions from the feed solution, and protons and hydroxide ions from the transition region of the bipolar membrane into the acid and base solutions. The energy

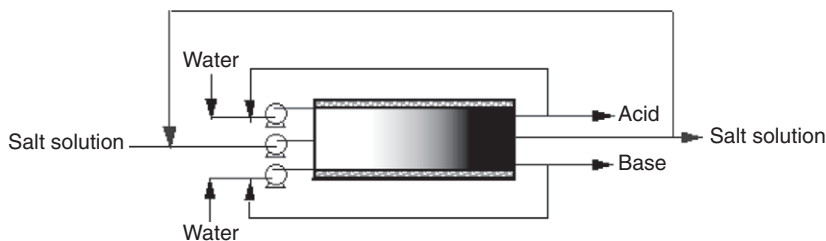


Figure 13 Schematic diagram indicating the production of acids and bases from the corresponding salt in a stack with feed and bleed operation.

consumption due to the pumping of the solutions through the stack can generally be neglected.

The total energy for the production of an acid and a base from the corresponding salt is, as in electro-dialysis desalination, which has been discussed earlier, given by the total current passing through the stack and the voltage drop across the stack. The total energy required in electro-dialytic water dissociation in a practical process is given by the current passing through the stack multiplied with the total voltage drop encountered between the electrodes.

$$E_{\text{pro}} = IUt \quad (56)$$

Here, E_{pro} is the energy consumed in a stack for the production of an acid and a base, I is the current passing through a stack or a series of stacks, U is the voltage applied across the stack, that is, between the electrodes, and t is the time of operation.

The current passing through the stack can be derived by rearranging Equation (31):

$$I = Ai = \frac{Q_{\text{pro}} F C_{\text{pro}}^{\text{in}} - C_{\text{pro}}^{\text{out}}}{\xi} \quad (57)$$

Here, A is a cell unit area, i is the current density, I is the current, Q_{pro} is the flow rate of the product, C_{pro} is the concentration of the product, F is the Faraday constant, ξ is the current utilization, and the superscripts in and out refer to the in and outlet of the stack.

The voltage drop across the stack is the result of the electrical resistance of the membranes, that is, that of the cation- and anion-exchange membranes and the bipolar membranes and the resistances of the acid, the base, and the salt containing flow streams in the stack. In addition to the voltage drop required to overcome the various electrical resistances of the stack, additional voltage drop is required to provide the energy for the water dissociation, which is given by Equation (37). Assuming that the three cells of a cell unit in the stack have the same geometry and flow conditions, the total energy consumption in an electro-dialysis stack is given by

$$E_{\text{pro}} = N_{\text{cell}} A_{\text{cell}} \left(\sum_i \frac{\Delta}{\lambda_i \bar{C}_i} + r^{\text{am}} + r^{\text{cm}} + r^{\text{bm}} + \frac{2.3RT}{Fi} \Delta\text{pH} \right) \left(\frac{Q_{\text{pro}} F (C_{\text{pro}}^{\text{out}} - C_{\text{pro}}^{\text{in}})}{N_{\text{cell}} A_{\text{cell}} \xi} \right)^2 t \quad (58)$$

Here, E_{pro} is the energy for the production of a certain amount of acid and base; I is the current passing through the stack; N_{cell} is the number of cell

units in a stack; A_{cell} is the cell unit area; C and \bar{C} are the concentration and average concentration in a cell, respectively; Δ is the thickness of the individual cells; λ_{eq} is the equivalent conductivity; r is the area resistance; ξ is the current utilization; R is the gas constant; T is the absolute temperature; F is the Faraday constant; ΔpH is the difference in the pH value between the acid and base; the subscript pro refers to product; the subscript i refers to salt, acid, and base; the superscripts am, cm, and bm refer to the cation-exchange, the anion-exchange, and the bipolar membrane, respectively; the superscripts out and in refer to cell outlet and inlet, respectively; Q_{pro} is the total flow of the acid or base through the stack; and t is the time.

The average concentrations of the acid, the base, and the salt in the bulk solutions are the integral average of the solutions given by Equation (48).

The total costs of the electro-dialytic water dissociation with bipolar membranes are determined, as in electro-dialysis, by cost related to fixed charges associated with the amortization of the plant investment costs, the energy costs for the transfer of ions, and pumping the different solutions through the stack, and by operating costs, which include maintenance and all pre- and posttreatment procedure costs.

2.14.4.1.6 Practical applications of electro-dialysis

Currently, brackish water desalination is the largest industrial-scale applications of conventional electro-dialysis. However, other applications in the food and chemical industry and in the treatment of wastewater are becoming increasingly more important. In Japan, electro-dialysis is also used widely for the preconcentration of seawater to the production of table salt. Several of the more important applications of conventional electro-dialysis and the stack and process design used in this application as well as the major limitations are listed in **Table 1**.

Brackish water desalination by electro-dialysis. The production of potable water from brackish water electro-dialysis is competing directly with reverse osmosis. Since, in electro-dialysis, both the energy consumption and the required membrane area are strongly increasing with increasing feed water concentration, reverse osmosis is considered to have an economic advantage for the desalination of brackish water with total dissolved salts in excess of 10 000 mg l⁻¹. Electro-dialysis is mainly used with feed water having a salinity of 1000–5000 mg l⁻¹ total

Table 1 Industrial applications of conventional electro dialysis

<i>Industrial applications</i>	<i>Stack and process design</i>	<i>Status of application</i>	<i>Limitations</i>	<i>Key problems</i>
Brackish water desalination	Sheet flow, tortuous path stack, reverse polarity	Commercial	Concentration of feed and costs	Scaling, costs
Boiler feed water production	Sheet flow, tortuous path stack, reverse polarity	Commercial	Product water quality and costs	Costs
Waste and process water treatment	Sheet-flow stack, unidirectional	Commercial	Membrane properties	Membrane fouling
Ultrapure water production	Sheet flow, tortuous path stack, reverse polarity	Commercial	Product water quality and costs	Membrane biofouling
Deminerlization of food products	Sheet flow, or tortuous path stack, unidirectional	Commercial or pilot phase	Membrane selectivity and costs	Membrane fouling, product loss
Table salt production	Sheet-flow stack, unidirectional	Commercial	Costs	Membrane fouling
Concentration of reverse osmosis brine	Sheet-flow stack, unidirectional	Pilot phase	Costs	Waste disposal

dissolved solids in small- to medium-size plants with capacities less than a few $100 \text{ m}^3 \text{ d}^{-1}$ to more than $20\,000 \text{ m}^3 \text{ d}^{-1}$. The plants are generally operated in the polarity reversal mode. The advantages of electro dialysis compared to reverse osmosis are:

- high water recovery rates;
- operation at elevated temperatures up to 50°C possible;
- less membrane fouling or scaling due to process reversal; and
- less raw water pretreatment requirements.

For the production of potable water, a severe disadvantage of electro dialysis compared to reverse osmosis is that neutral toxic components, such as viruses or bacteria, are not removed. Brackish water desalination plants used for the production of potable water can be rather different in size ranging from 50 to $300 \text{ m}^3 \text{ d}^{-1}$ plant capacity used to supply potable water in hotels and villages located in isolated areas or larger installations with capacities between $10\,000$ and $20\,000 \text{ m}^3 \text{ d}^{-1}$ used for municipal water supply. A typical large-scale electro dialysis water desalination plant is shown in **Figure 14**. The plant is built by Ionics Incorporated,

**Figure 14** Industrial-size electro dialysis reversal drinking water plant. Courtesy of Ionics Incorporated.

Watertown, MA, USA using the Aquamite XX EDR system.

Treatment of industrial process water and wastewater by electrodialysis. Depending on the application, industrial process water must meet certain quality standards in terms of total dissolved solids and colloidal material. Traditionally, precipitation, filtration, and ion exchange are used in the production of industrial water. Today, these processes are replaced or complimented increasingly by microfiltration, reverse osmosis, and electrodialysis. Major applications of electrodialysis in industrial water processing include predemineralization of boiler feed water, desalination of contaminated industrial water for reuse, and the recovery of valuable wastewater components. In many of these applications, electrodialysis is in competition with conventional ion-exchange techniques. However, for certain raw water compositions electrodialysis has a clear cost advantage over the competing processes. A typical application of electrodialysis is the recycling of cooling tower blow-down water. Electrodialysis seems to be particularly suited for this purpose because high recovery rates up to 95% and thus, high brine concentrations up to 100 g l^{-1} can be achieved which result in a significant reduction in wastewater discharge compared to conventional ion-exchange techniques. Another example of a successful application of electrodialysis is the recycling of produced water from crude oil production. In many oil wells, steam is being injected into the ground to heat and liquify the crude oil so that it can be pumped. In the process, the steam is condensed and pumped out of the ground mixed with the oil but it also contains large quantities of salts extracted from the ground. The water is first separated from the oil by an oil/water separator. To be reused as boiler feed for the generation of steam, the produced water must be softened. Since the salt concentration in the produced water is relatively

high, that is, in the order of $5000\text{--}10\,000\text{ mg l}^{-1}$ large quantities of salt are used for the regeneration of the ion-exchange resin. Substantial savings in regeneration costs can be achieved by using electrodialysis as a presoftening desalination step. The process is illustrated in the simplified flow scheme of **Figure 15** which shows a typical produced water recycling plant with an oil skimmer, an electrodialysis predesalination unit, and a water softener. In this application, electrodialysis is superior to other desalination processes, such as reverse osmosis, because of the thermal and chemical stability of the ion-exchange membranes which can operate reliably at temperatures in excess of $50\text{ }^{\circ}\text{C}$ with a minimum of feed water pretreatment.

Very closely related to the recycling of industrial water is the recovery of toxic or valuable components from an industrial effluent to avoid pollution of the environment and to save costs. A major source of pollution are effluents of the metal processing industry containing heavy metal ions such as nickel, zinc, cadmium, chromium, silver, mercury, and copper ions which are highly toxic even at relatively low concentrations. In combination with other processes, such as ion-exchange, ultra-, and microfiltration, the application of electrodialysis provides a solution to severe pollution problems and can save substantial production costs by recovering and recycling valuable components and water.

A typical example is the recovery of nickel, cadmium, and copper from rinse solutions of galvanic processes. Metal parts that have been plated in a galvanic bath are rinsed in a series of rinse tanks to remove metal ions carried out of the plating bath. The first tank is referred to as still rinse. In this tank, most of the components carried out of the plating bath are rinsed off leading to a rapid increase in the concentration of metal ions.

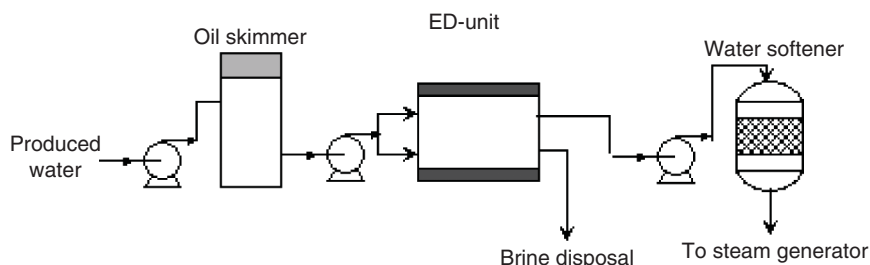


Figure 15 Simplified flow diagram illustrating a produced water recovering plant with an integrated electrodialysis unit.

The ion concentration in the still rinse tank, however, determines the amount of material carried into the next rinse tanks and must be removed by ion-exchange from the last tank. The amount of ions that must be removed by the ion-exchange process and thus, ion-exchange regeneration costs depend on the concentration in the still rinse tank. When a certain concentration in this tank is reached, it must be discharged to limit the amount of dragged out metal ions. The concentration of the still rinse tank, however, can be kept on a low level by treating the solution of the still rinse tank by electro dialysis. The concentrate of the electro dialysis processes is recycled after further treatment to the galvanic bath and the diluate is fed back into the still rinse keeping the metal ion concentration at a predetermined low level and the ion drag-over into the last water rinse tank is kept correspondingly low. Due to the recovery of the metal ions and the reduction of sludge and wastewater treatment substantial cost reduction is achieved [32, 33].

The prevailing method of metal surface treatment is pickling with acids. The acids used are H_2SO_4 , HCl , HNO_3 , HF , etc. The pickling solution, however, deteriorates with time and becomes ineffective. Since the spent pickling solution contains various heavy metals and substantial amounts of acids it must be neutralized and the obtained sludge must be deposited safely. For economic reasons, it is interesting to recover the acids from the spent pickling solution and reduce the sludge disposal. One of the methods used today to recover and recycle acids is retardation in combination with electro dialysis.

There are many more interesting applications of electro dialysis in wastewater treatment. Some of these applications require only relatively small electro dialysis units, as for example, the treatment of small amounts of effluents from galvanic industry containing highly toxic compounds. In other

applications, rather large quantities of water must be treated. This is the case in the paper and pulp industry. Here, electro dialysis has been successfully used to remove $NaCl$ selectively from the chemical recovery cycle of Kraft pulp production [34]. The removal of nitrate from polluted water is an option that has been tested on a pilot plant scale.

Food processing by electro dialysis. Not only in the food and beverage industry but also in biotechnology and the pharmaceutical industry electro dialysis has found a large number of potential applications. Some of these applications can be considered as the state-of-the-art processes such as the deionization of whey. Other applications such as the removal of salts from protein and sugar solutions or salts and organic acids (such as lactic acid and certain amino acids from fermentation) have been tested in the laboratory and on a pilot plant scale. Typical applications of electro dialysis in the food industry are summarized in **Table 2**. Most of the applications listed in the table require small units and special application know how. Therefore, the introduction of electro dialysis in the food industry on a large industrial scale has been rather slow in spite of the clear advantages of the process compared to conventional ion-exchange technology. The only application which presently has reached some significance is the deionization of cheese whey and skimmed milk [35].

Other applications of electro dialysis in the food industry such as the demineralization of soy sauce, sugar molasses, and amino acids or the deacidification of fruit juice have not yet reached the same industrial relevance. In most cases, only pilot plant studies have been carried out and only a few applications have been commercialized.

Several applications of electro dialysis in biotechnology and the pharmaceutical industry such as recovery of lactic acid from fermentation broth have been studied on a laboratory scale [36].

Table 2 Examples for potential applications of electro dialysis in the food and beverage industry

<i>Industry</i>	<i>Application of electro dialysis</i>
Dairy industry	Demineralization of cheese whey, demineralization of nonfat milk
Sugar industry	Demineralization of molasses in sugar production, demineralization of waste molasses, demineralization of polysaccharide
Fermentation industry	Demineralization of soy sauce, desalination of amino acids, recovering of organic acids
Wine industry	Removal of tartrate
Beverage industry	Deacidification of fruit juice

But, very few commercial units have been installed so far.

Preconcentration of salts by electrodialysis. The concentration of dilute salt solutions by electrodialysis is of interest for the production of salts such as KBr or KI from certain raw water sources prior to evaporation. Of special interest is the preconcentration of NaCl from seawater for the production of table salt in countries that do not have native salt deposits such as Japan. Conventional evaporation is rather costly and with evaporation all seawater constituents are equally concentrated. For the production of table salt and as raw material for the chlorine-alkaline production, it is desirable to have NaCl as pure as possible. Using electrodialysis as a preconcentration step not only substantial energy savings can be achieved but with the development of low resistance monovalent ion selective membranes a more effective concentration of NaCl was achieved. Further improvements of the seawater pretreatment process have eliminated the extensive cleaning procedures. Operation for several years and cleaning without disassembling the stack are now possible. Large plants with a capacity of 20 000 to more than 200 000 tons of table salt per year are in operation in Japan [37, 38].

2.14.4.1.7 Applications of bipolar membrane electrodialysis

Since bipolar membranes became available as commercial products in 1977, a very large number of potential applications of electrodialysis with

bipolar membranes has been identified and has been studied extensively on a laboratory or pilot plant scale. However, in spite of the obvious technical and economical advantages of the technology large-scale industrial plants are still quite rare. The main reasons for the reluctant use of bipolar membrane electrodialysis are shortcomings of the available bipolar and monopolar membranes which result in poor current utilization and high product contamination. However, there are a number of smaller-scale applications in the chemical process industry, in biotechnology, in food processing, and in wastewater treatment where bipolar membranes are successfully used [39, 40]. Some of the potential applications of electrodialysis are summarized in Table 3.

Production of acids and bases by bipolar membrane electrodialysis. The largest potential application of bipolar membrane electrodialysis is the production of acids and bases from the corresponding salts. Presently, caustic soda is produced as a coproduct with chlorine by electrolysis. Bipolar membrane electrodialysis would be an interesting alternative process for economic reasons [41]. However, presently the process has still severe problems due to shortcomings of both the commercially available mono- and bipolar membranes. The useful life of the membranes in concentrated acids and bases is insufficient leading to high membrane replacement costs. The incomplete permselectivity of the bipolar membrane in concentrated solutions results in salt leakage into the acid and base and thus to a contamination of the products. The poor permselectivity of the monopolar membranes for

Table 3 Potential applications of electrodialysis with bipolar membranes, their state of development, and possible advantages and experienced problems

<i>Application</i>	<i>State of process development</i>	<i>Potential advantages</i>	<i>Problems related to application</i>
Production of mineral acids and bases	Pilot plant operation	Lower energy consumption	Contamination of products
Recovery of organic acids from fermentation processes	Commercial and pilot plant operation	Simple integrated process, lower costs	Unsatisfactory membrane stability and fouling
pH control in chemical and processes	Laboratory tests	Fewer by-products, less salt production	Application experience, process costs
Removal of SO ₂ from flue gas	Extensive pilot plant test	Decreased salt production	Long-term membrane stability
Recycling of HF and HNO ₃ from steel pickling solutions	Commercial plants	Cost savings due to recovered acids and less salt disposal	Relatively complex process, high investment costs
Ion-exchange resin regeneration	Pilot plant tests	Decreased salt disposal	High investment costs
High-purity water production	Laboratory tests	Better removal of weak acids and bases	No long-term experience

protons and hydroxide ions results in low current utilization. Therefore, the production of high-quality concentrated acids and bases is presently not yet feasible.

However, the situation is different when acids or bases can be recovered from salts of chemical reactions or neutralization processes. In these cases, the requirements for the concentration and the purity of the recovered acids or bases are not as stringent as in the production of high-quality commercial products.

Applications of bipolar membranes in wastewater treatment. Recovering acids and bases from their salts generated in neutralization reactions to control pollution and minimize waste disposal is one of the most promising applications of bipolar membrane electro dialysis. One of the first commercial applications of bipolar membrane electro dialysis was the recovering of hydrofluoric and nitric acid from wastewater-containing potassium fluoride and nitrite generated by neutralization of a steel pickling bath [42].

The process is illustrated in the simplified flow diagram of **Figure 16**.

The spent pickling acid is neutralized with potassium hydroxide. The solution is then filtered and the precipitated heavy metal hydroxides are removed. The neutral potassium fluoride and nitrite-containing solution is fed to the bipolar membrane electro dialysis unit in which the salts are converted to the corresponding acids and potassium hydroxide. The potassium hydroxide is recycled to the neutralization tank and the acids to the pickling bath. The depleted salt solution from the bipolar membrane electro dialysis unit is concentrated in a conventional electro dialysis system and recycled directly to the bipolar membrane unit.

The treatment of alkaline or acid scrubbers that are used to remove components which are harmful to the environment, such as NO_x , SO_2 , or certain amines from waste air streams, is another interesting application for bipolar membrane electro dialysis [43].

Other applications of bipolar membrane electro dialysis are the recovering and recycling of an acid from the salt of a spent liquor bath of the rayon spinning process and pulping and bleaching processes. The regeneration of ion-exchanger effluents is another potential application of bipolar membrane electro dialysis.

Applications of bipolar membrane electro dialysis in biotechnology. A very promising application of electro dialysis with bipolar membranes is the recovery of organic acids from fermentation processes. During the fermentation of an organic acid, such as lactic acid, the pH in the fermentation broth shifts to lower values due to the production of the acid. To avoid product inhibition, the pH value of the fermentation broth is maintained at a certain level by addition of sodium or ammonium hydroxide which reacts with the acid and forms a soluble salt. In the conventional batch type fermentation process, illustrated in **Figure 17(a)**, the spent medium is separated from the biomass by filtration and the free acid is recovered by lowering the pH value. The pH-value adjustment in the fermenter as well as in the spent medium is costly and creates a substantial amount of salts mixed with the product, which complicates the final purification of the acid and creates an additional waste disposal problem. By integrating bipolar membrane electro dialysis, the production of additional salts in the fermentation broth can be eliminated and the fermentation and thus the production of acid can be carried out more efficiently in a continuous process as illustrated in the

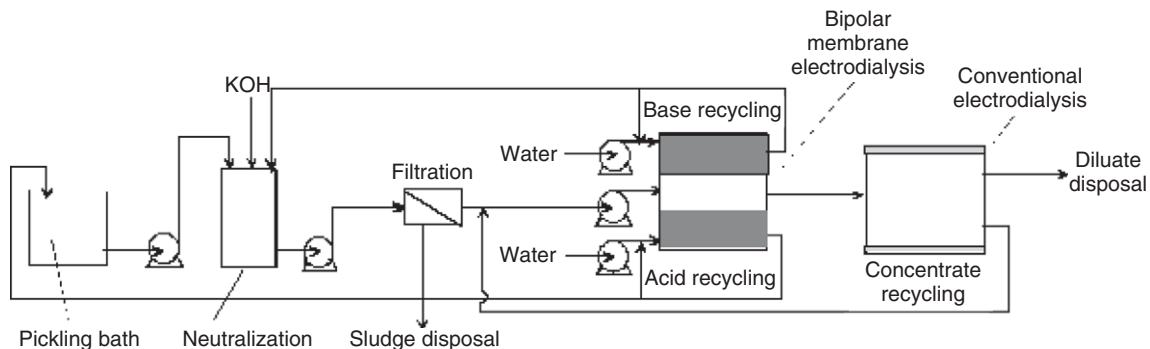


Figure 16 Simplified flow diagram illustrating the acid recycling from steel pickling neutralization bath with bipolar membrane electro dialysis.

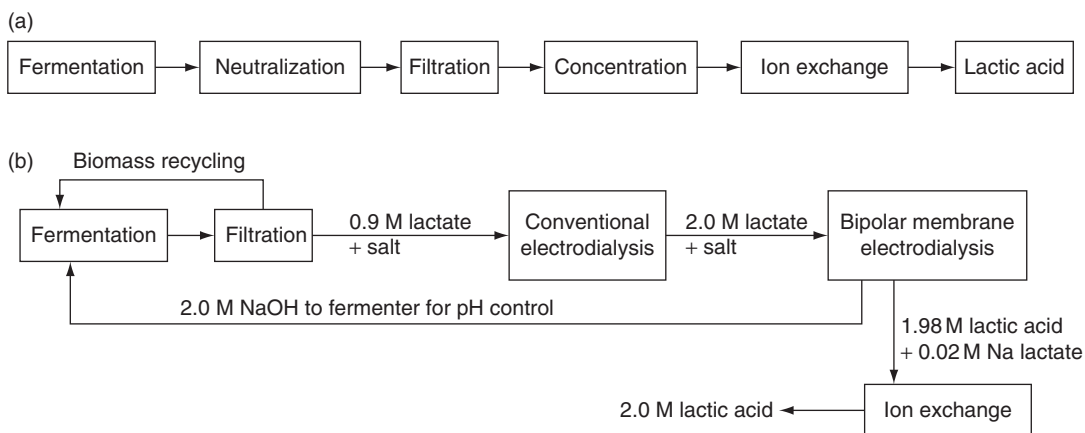


Figure 17 Simplified flow diagram illustrating (a) the conventional lactic acid production process and (b) the production process with integrated electro dialysis.

simplified flow diagram of **Figure 17(b)**. In the first process step, the fermenter constituents are passed through a filtration unit where the biomass is separated from the product containing solution. In the second step, the lactate and salts are concentrated by conventional electro dialysis and in the third step the lactate is converted into lactic acid by bipolar membrane electro dialysis. The simultaneously produced base is recycled to the fermenter to control the pH value.

Other applications of bipolar membrane electro dialysis in biotechnology are the recovery of gluconic acid from sodium gluconate and the production of ascorbic acid from sodium ascorbate. For organic acids with an anion of high molecular weight, the migration of the ion through conventional anion-exchange membranes is very slow and the membrane exhibits a high electrical resistance. In this case, the use of a bipolar membrane unit with two-cell repeating units seems to be better suited than the three-cell unit in spite of an additional purification step that might be required.

Many applications of bipolar membrane electro dialysis for other separation problems in biotechnology have been tested on a laboratory scale [44]. Some of these applications are quite promising; others are presently not economic or do not provide the same quality products as competitive conventional processes.

2.14.4.2 Continuous Electrodeionization

Continuous electrodeionization is a combination of ion exchange and electro dialysis. The process is similar to conventional electro dialysis. There are

some variations of the basic design of the process as far as the distribution of the ion-exchange resin is concerned. In some cases, the diluate cell is filled with a mixed-bed ion-exchange resin; in other cases, the cation- and anion-exchange resins are placed in series in the cell [45]. More recently also bipolar membranes are used in the process [46]. Continuous electrodeionization is widely used today for the preparation of high-quality deionized water to be used as ultrapure water in the electronic industry or in analytical laboratories.

2.14.4.2.1 System components and process design aspects

The process design and the different hardware components needed in electrodeionization are very similar to those used in conventional electro dialysis. The different concepts used for the distribution of the cations and anions in the cell are illustrated in **Figures 18(a)** and **18(b)**. **Figure 18(a)** shows an electrodeionization stack with the diluate cell filled with a mixed-bed ion-exchange resin which removes the ions of a feed solution. Due to an applied electrical field, the ions migrate through the ion-exchange resin toward the adjacent concentrate cells and highly deionized water is obtained as a product. Compared to the deionization by a conventional mixed-bed ion-exchange resin the continuous electrodeionization has the advantage that no chemical regeneration of the ion-exchange resins is needed which is time consuming, costly, and generates a salt-containing wastewater.

However, in continuous electrodeionization using a stack with mixed-bed ion-exchange resins

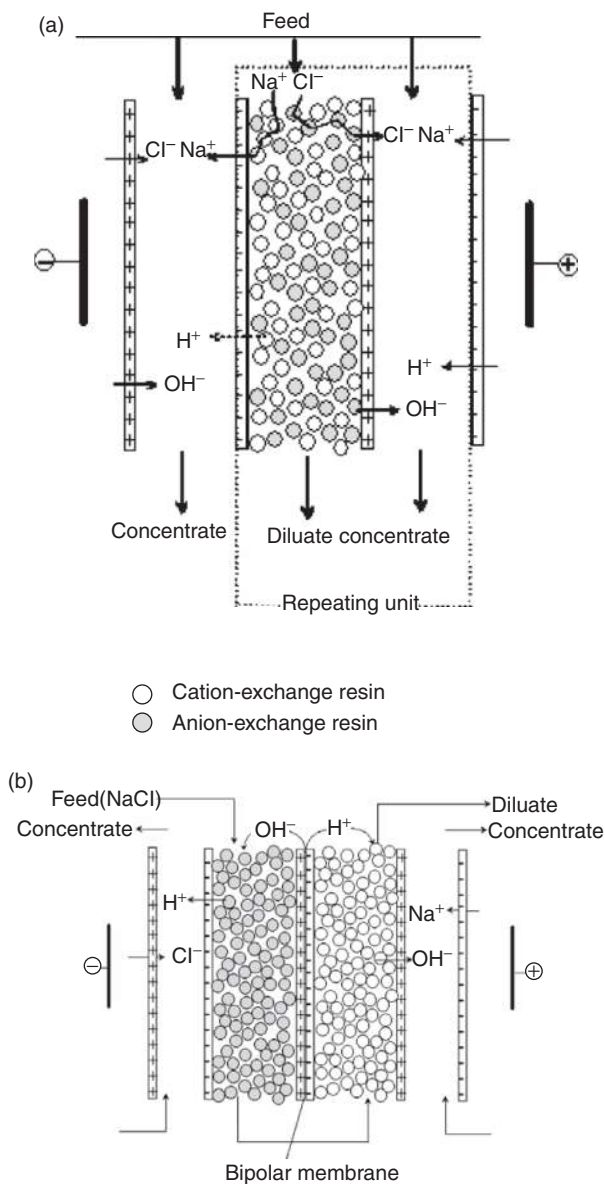


Figure 18 Schematic drawing illustrating different stack concepts used in continuous electrodeionization: (a) a conventional stack with the diluate cells filled with a mixed-bed ion-exchange resin, and (b) a stack with cation-exchange and anion-exchange resins in different diluate cells and the regeneration of the ion-exchange resins by H⁺ and OH⁻ ions generated in a bipolar membrane.

weak acids and bases such as boric or silicic acid are only poorly removed [30]. Much better removal of weakly dissociated electrolytes can be achieved in a system in which the cation- and anion-exchange resins are placed in a stack in separate beds with a bipolar membrane placed in between as illustrated in **Figure 18(b)** which shows a diluate cell filled with a cation-exchange resin facing toward the cathode separated by a bipolar membrane from a

diluate cell facing the anode. A cation-exchange membrane, a cation-exchange resin, a bipolar membrane, an anion-exchange resin, an anion-exchange membrane, and a concentrate cell build a repeating unit between two electrodes.

The main difference between the electrodeionization system with the mixed-bed ion-exchange resins and the system with separate beds is that in mixed-bed electrodeionization systems anions and cations

are simultaneously removed from the feed while the solution leaving the diluate cell is neutral. In the electrodeionization system with separate ion-exchange beds and bipolar membranes, the cations will first be exchanged by the protons generated in the bipolar membrane with the result that the solution leaving the cation-exchange bed is acidic. This solution is then passed through the cell with the anion-exchange resin where the anions are exchanged by the OH^- ions generated in the bipolar membrane and the solution is neutralized. Both the mixed and the separate bed ion-exchange continuous electrodeionization systems are widely used today on a large industrial scale.

2.14.4.2.2 Operational problems and the practical applications of electrodeionization

In addition to the problems of removing weak acids or bases in the electrodeionization system with the mixed-bed ion-exchange resins, there are problems of uneven flow distribution in the resin beds which lead to poor utilization of the ion-exchange resins. The fouling of the ion-exchange resins by organic components such as humic acids, and bacterial growth on the surface of the resin is a problem which requires a very thorough pretreatment of the feed solution to guarantee a long-term stability of the system.

The main application of continuous electrodeionization is in the production of ultrapure water. Not only the electronic industry but also analytical laboratories and power stations need water which is free of particles and has a conductivity of less than $0.06 \mu\text{S cm}^{-1}$. Conventionally, well or surface water is purified in a series of processes that include water softening, microfiltration, reverse osmosis, UV sterilization, and mixed-bed ion exchange. While reverse osmosis, microfiltration, and UV sterilization can all be operated in a continuous mode, the mixed-bed ion

exchanger must be regenerated in certain time intervals. This regeneration requires long rinse down times to remove traces of regeneration chemicals and is also affected by biological fouling due to microorganisms brought into the resin during the regeneration process. By replacing the mixed-bed ionexchanger in the ultrapure water production line, the process can be substantially simplified producing consistently high-quality water in a completely continuous process. The process is illustrated in **Figure 19** which shows a simplified flow scheme of an ultrapure water production line with a continuous electrodeionization unit instead of a mixed-bed ionexchanger.

The advantages of the ultrapure water production with an integrated electrodeionization unit compared to the use of a mixed-bed ion exchanger are a more simple process, no regeneration chemicals, less raw water consumption, and a substantial reduction in costs.

2.14.4.3 Diffusion Dialysis

In diffusion dialysis, the separation of ionic components is not the result of an externally applied electrical potential but a concentration gradient. Diffusion dialysis is utilizing anion- or cation-exchange membranes only to separate acids and bases from mixtures with salts. The process has so far gained only limited practical relevance [47].

2.14.4.3.1 The process principle

The principle of the process is illustrated in **Figure 23** which shows a schematic diagram of a typical diffusion dialysis cell arrangement consisting of a series of anion-exchange membranes arranged in parallel to form individual cells. If a feed solution containing a salt in a mixture with an acid is separated by an anion-exchange membrane from a compartment containing pure water, the so-called

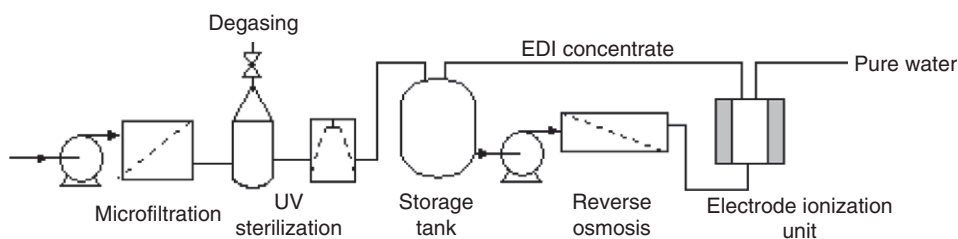


Figure 19 Schematic diagram illustrating an ultrapure water production process using a continuous electrodeionization step in stead of a mixed bed ion-exchange resin.

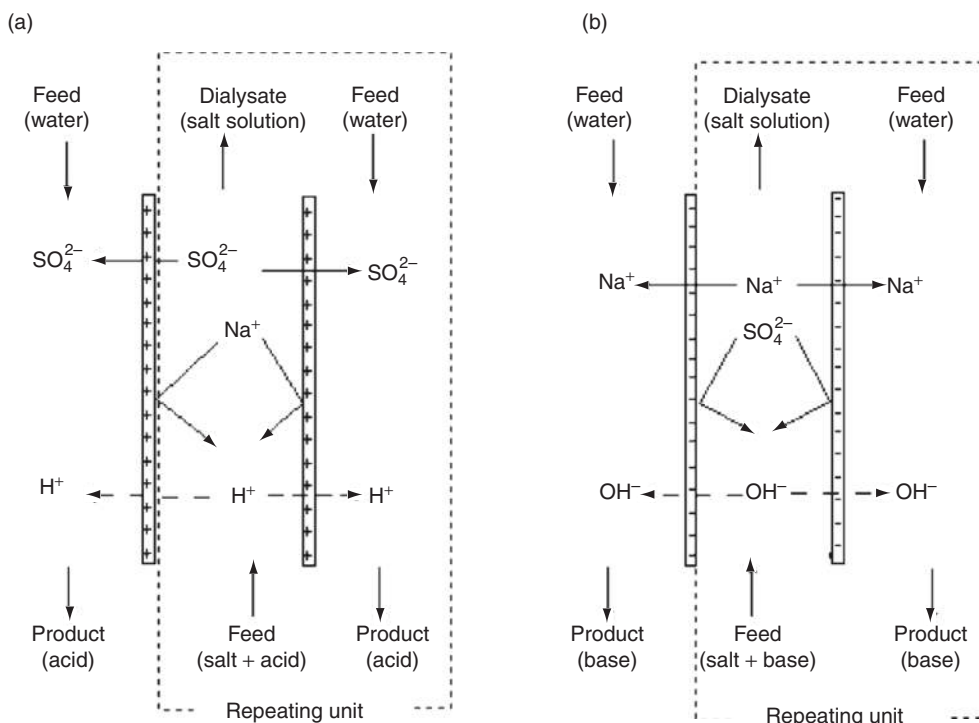


Figure 20 Schematic drawing illustrating the principle of diffusion dialysis used to recover (a) an acid from a mixture with salt in a stack of anion-exchange membranes only and (b) a base in a stack with cation-exchange membranes.

stripping solution anions will diffuse from the feed solution through the ion-exchange membrane into the stripping solution due to a concentration difference, but the salt cations will be retained by the membrane. The protons, however, can pass the anion-exchange membrane in spite of their positive charge. Thus, the acid will be removed from the salt solution. Correspondingly, a base can be removed from mixtures with salts if cation-exchange membranes are used (Figure 20).

2.14.4.3.2 System design, costs, and application

Diffusion dialysis is used mainly to recover acids from pickling solutions in the metal surface treating industry. However, its commercial relevance is still rather limited. Since the diffusion through the relatively thick ion-exchange membranes is a rather slow process, large membrane areas are required to remove a significant amount of ions from a feed solution resulting in high investment costs for a given capacity plant.

A typical diffusion dialysis plant used to recover acids such as HF, HNO₃, or HCl from a pickling bath is shown in the simplified flow diagram of Figure 21.

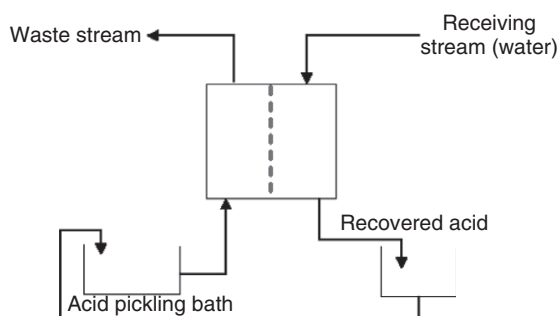


Figure 21 Simplified flow diagram of the diffusion dialysis process used to recover acid from a pickling bath.

Depending on the specific application the diffusion dialysis plant consists of a pretreatment unit and the actual diffusion dialysis stack with pumps, filters, flow control devices, and concentration-monitoring instrumentation. The key component in the process is the dialysis stack. Its construction is very similar to that of a conventional electrodesalination unit with 200–400 membranes in a stack. However, the flow of the receiving solution and the feed solutions is countercurrent and the linear flow velocities in the stack are usually quite low, that is, generally less than a few centimeters per second. Due to chemical

potential gradients, and the fact that anion-exchange membranes are permeable to protons, acid is transported from the feed solution into the receiving solution. When pure water is used as a stripping solution and the system is operated in countercurrent flow of the feed and stripping solutions in a stack where all cells have the same geometry and flow velocities, a simple relation can be used to describe the mass transport [48]. The amount of the component i removed from the feed solution and transferred across the membrane is equal to the amount of the component i received in the stripping solution. Due to a mass balance

$$C_i^d = C_i^f - C_i^{\text{pro}} \quad (59)$$

The membrane flux is

$$\mathcal{J}_i = k^* A^m (C_i^f - C_i^{\text{pro}}) = Q^{\text{pro}} C_i^{\text{pro}} \quad (60)$$

and the recovery rate is

$$\Delta = \frac{C_i^{\text{pro}}}{C_i^f} = \frac{k^*}{k^* + \frac{Q^{\text{pro}}}{A^m}} \quad (61)$$

Here, C_i^f and C_i^d are the concentrations of the component i in the feed at the cell entrance and the cell exit, C_i^{pro} is the concentration of the component i in the product solution, that is, the concentration in the stripping solution at the cell exit, \mathcal{J}_i is the flux of the component i across the membrane, k^* is a mass transfer coefficient describing the mass transport through the membrane, A^m is the membrane area, Δ is the recovery rate of the acid, and Q^{pro} is the volume flow rate of the stripping solution, that is, the product.

Equations (59)–(61) give a simple relation between the concentration of a component i in the feed and stripping solution, the recovery rate, and the total amount of the component i transferred through the membrane. Modeling the diffusion dialysis process and designing a plant for a typical practical industrial effluent is complicated due to the complex composition of the feed solution, which generally contains a multitude of different ions in a relatively high concentration, which results in a high osmotic water flux. Thus, Equations (59)–(61) can only be considered as a first approximation for designing the diffusion dialysis process.

A key component in diffusion dialysis for recovering acids from a feed solution is the anion-exchange membrane. The membrane should provide high ion fluxes and should also provide satisfactory chemical stability in strong acid solutions. Of major concern in

operating a diffusion dialysis plant is also the flow distribution in the stack.

The total costs in diffusion dialysis are determined mainly by charges related to the capital investment while operating and energy costs are generally quite low compared to other membrane processes.

There are also some intrinsic limitations of the diffusion dialysis process. An acid in a mixture with its salt cannot be completely recovered because a certain concentration difference between the feed solution and the receiving solution is needed as driving force for acid transport through the membrane. In addition, some salt will diffuse into the acid because of the limited permselectivity of the anion-exchange membranes at high ion concentrations. This means the recovered acid will always be contaminated with salt.

2.14.4.4 Donnan Dialysis

Donnan dialysis is an ion-exchange process between two solutions separated by a membrane. Only cation- or anion-exchange membranes are installed in a stack. The driving force for the transport of ions is their concentration difference in the two solutions. A typical application of Donnan dialysis is the removal of divalent ions such as Ca^{2+} ions from a feed stream by exchange for monovalent ions such as Na^+ ion as illustrated in **Figure 22** which shows a feed solution containing CaCl_2 in a relatively low concentration and a stripping solution containing NaCl in a relatively high concentration placed into alternating cells of a stack of cation-exchange membranes. Because of the concentration difference in the feed and the stripping solution, Na^+ ions diffuse from the stripping solution through the cation-exchange membrane into the feed solution. Since the Cl^- ions cannot permeate the negatively charged cation-exchange membrane, an electrical potential is generated between the two solutions which acts as driving force for the transport of Ca^{2+} ions from the feed to the stripping solution. Because of the required electroneutrality the identical charges are exchanged between the two solutions, that is, for two Na^+ ions diffusing from the stripping into the feed solution one Ca^{2+} ion is removed from the feed solution if the membrane is completely impermeable for Cl^- ions. In addition to water softening, there are several other interesting potential applications in wastewater treatment, but presently there is no significant commercial use of Donnan dialysis.

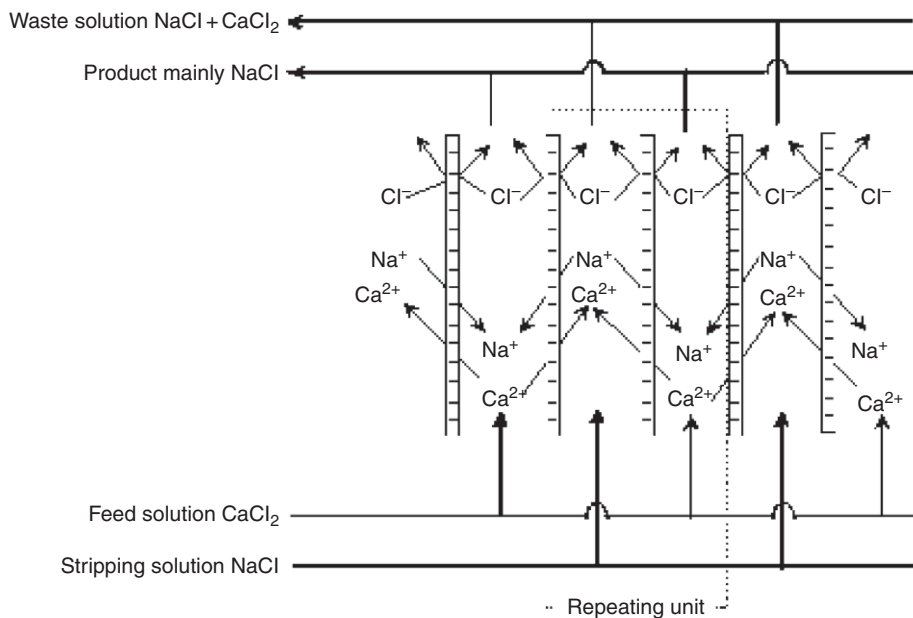


Figure 22 Schematic drawing illustrating the principle of the Donnan dialysis water softening process by the exchange of Na^+ and Ca^{2+} ions in a stack with cation-exchange membranes only.

2.14.4.5 Capacitive Deionization

Capacitive deionization is an electrosorption process that can be used to remove ions from an aqueous solution by charge separation [49, 50]. The process is illustrated in **Figure 23** which shows schematically a capacitive deionization cell unit consisting of two electrodes made out of activated carbon separated by a spacer that acts as a flow channel for an ion-containing solution.

In capacitive deionization, the anolyte and catholyte are contained within the porous electrodes and electrons are not transmuted by oxidation and reduction reactions but by electrostatic adsorption.

The system resembles a flow-through capacitor. If an electrical potential is applied between the electrodes, ions are removed from the solution and adsorbed at the surface of the charged electrodes. When the carbon electrodes are saturated with the charges the ions are released from the electrodes by reversing the potential, that is, the cathode becomes the anode and vice versa; the anode becomes the cathode. Thus, capacitive deionization is a two-step process. In a first step as shown in **Figure 23(a)**, ions are removed from a feed solution by electrosorption and migration in the feed solution under an electrical potential driving force resulting in

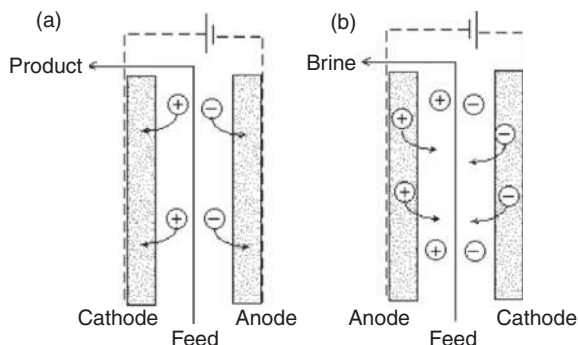


Figure 23 Schematic diagrams illustrating the capacitive deionization process: (a) sorption of ions from a feed solution at the porous carbon electrodes producing deionized product water and (b) desorption of ions from the porous carbon electrodes into the feed solution due to a change of polarity producing concentrated brine.

deionized product water. In a second step as shown in **Figure 23(b)**, the adsorbed ions are released from the carbon electrodes and transported back into the feed solution by reversing the electrical potential producing a concentrated brine.

A key component in this process is the carbon electrode. The number of ions adsorbed at the electrodes is directly proportional to the available surface area. Therefore, the specific surface area, that is, the surface area per unit weight of the electrodes should be as high as possible. Activated carbon, carbon nanotubes, and carbon aerogels are the most promising materials for the preparation of electrodes. Their specific surface area is up to $1100 \text{ m}^2 \text{ g}^{-1}$. Another parameter is the applied potential which not exceeds a certain maximum value to avoid water dissociation caused by electrode reactions. In practical applications of capacitive deionization, cells are operated at a voltage drop of between 0.8 and 1.5 V. The efficiency of capacitive deionization is impaired by incomplete sorption and desorption of ions and by sorption of counterions from the concentrate during the regeneration step. However, this effect can be reduced significantly by placing an ion-exchange membrane between the feed solution and the electrodes [51] as illustrated in **Figure 24** which shows schematically the ion transport in membrane capacitive deionization.

During the deionization step anions are prevented to diffuse into the product water by cation-exchange membrane on the cathode and an anion-exchange membrane on the anode as shown in **Figure 24(a)**. During the regeneration step under reverse polarity condition, the cation-exchange

membrane prevents the transport of anions toward the anode and the anion-exchange membrane prevents the transport of cations toward the cathode as shown in **Figure 24(b)** and thus, avoids an ion adsorption at the electrodes during the regeneration step. The consequence of introducing an ion-exchange membrane between the feed solution and the electrode is that more ions are adsorbed during the deionization step and more ions are desorbed and released during the regeneration step in a capacitive deionization process with ion-exchange membranes than in a capacitive deionization process without ion-exchange membranes between feed solution and electrodes.

2.14.5 Ion-Exchange Membranes in Electrochemical Synthesis

Ion-exchange membranes are also used in electrochemical synthesis of certain organic and inorganic compounds, such as chlorine and caustic soda, or, oxygen and hydrogen.

2.14.5.1 The Chlorine/Alkaline Production

Today, the electrolytic production of chlorine and caustic soda is one of the most important processes using ion-exchange membranes in electrochemical synthesis [7]. The process is illustrated in the schematic drawing of **Figure 25**. The cell unit used in this process is composed of two electrodes separated by a cation-exchange membrane forming two compartments. The compartment with the anode contains

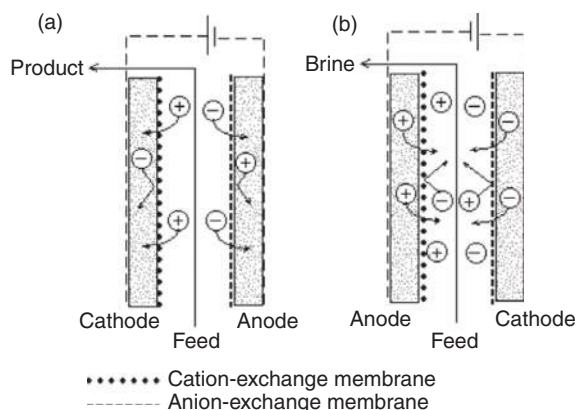


Figure 24 Schematic diagrams illustrating the capacitive deionization process with ion-exchange membranes between the feed solution and the porous carbon electrodes: (a) shows sorption, that is, the deionization step and (b) shows the desorption of ions due to a change of polarity producing concentrated brine, that is, the regeneration step.

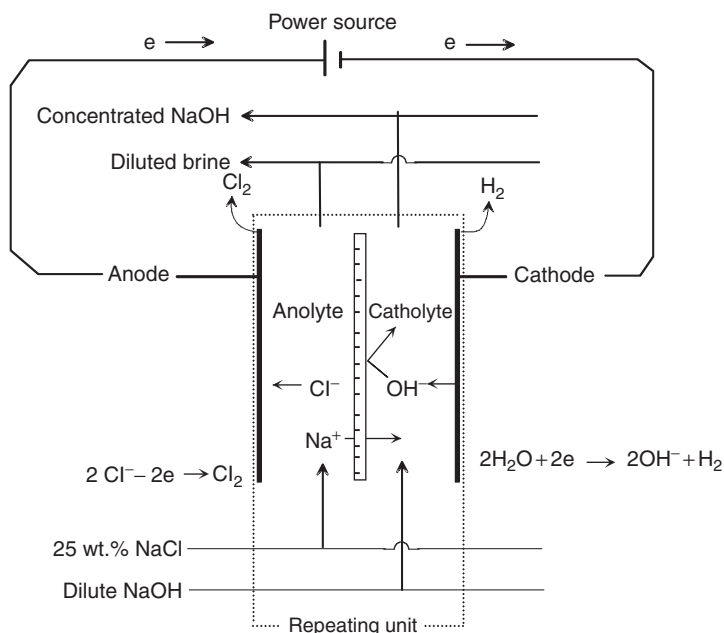


Figure 25 Schematic drawing illustrating the principle of the electrolytic production process of chlorine and sodium hydroxide.

the anolyte, that is, a 25 wt.% NaCl solution, and the other compartment with the cathode contains the catholyte, that is, dilute sodium hydroxide. When an electrical potential between the electrodes is applied, the chloride ions in the anode compartment migrate toward the anode where they are oxidized and released as chlorine gas. The sodium ion from the salt solution migrates through the cation-exchange membrane toward the cathode where it is reduced to sodium metal, which immediately reacts with the water to sodium hydroxide and hydrogen, which is then released as gas. A multitude of the cell units are integrated in a stack using bipolar electrodes. High-performance perfluorinated membranes with excellent chemical stability are used in the process. There are many more very interesting processes with ion-exchange membranes as key elements used today in organic synthesis and catalytic membrane reactors.

2.14.6 Ion-Exchange Membranes in Energy Conversion and Storage

Ion-exchange membranes play an increasingly important role in energy storage and conversion systems such as battery separators and fuel cells. They are also considered in generating electrical energy from mixing salt solutions and surface water.

2.14.6.1 Ion-Exchange Membranes in Low-Temperature Fuel Cells

The most prominent application of ion-exchange membranes in energy conversion systems is in low-temperature fuel cells [52]. The principle of a fuel cell based on the electrochemical oxidation of hydrogen by oxygen is illustrated in **Figure 26** which

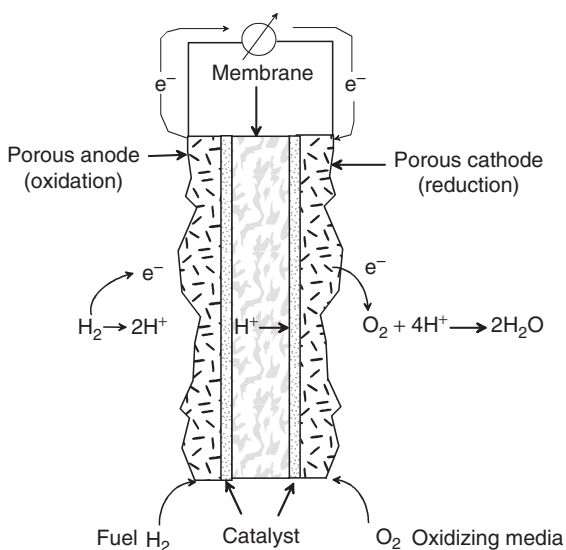


Figure 26 Schematic drawing illustrating the principle of the fuel cell based on the electrochemical oxidation of hydrogen by oxygen.

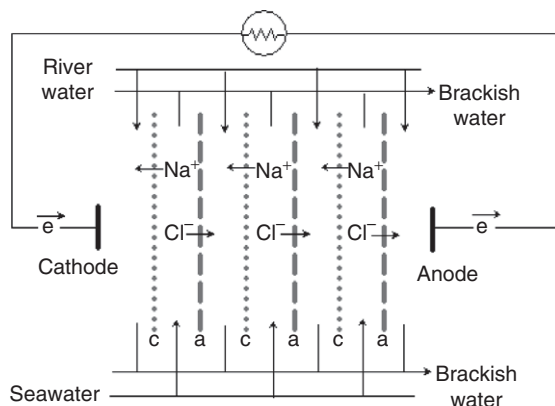


Figure 27 Schematic drawing illustrating the concept of reverse electrodialysis to regeneration of electrical energy by mixing river and seawater.

shows a single unit cell consisting of two porous electrodes and two catalyst layers separated by a cation-exchange membrane.

Hydrogen gas is passed through the porous anode. It reacts in the catalyst layer forming protons and releasing electrons at the anode to an electric circuit. The protons diffuse through the ion-exchange membrane and react in the catalyst layer at the surface of the porous cathode with oxygen gas to form water and take up electrons from the electric circuit. The overall reaction in a fuel cell is the oxidation of hydrogen by oxygen to water. Instead of hydrogen hydrocarbons also, such as methanol or ethanol, are used as fuel and often air is used as oxidation medium instead of oxygen.

2.14.6.2 Energy Production by Reverse Electrodialysis

The production of energy by mixing seawater with river water through ion-exchange membranes is a process referred to reverse electrodialysis. The process, which is illustrated in [Figure 27](#), provides a clean and sustainable energy source and is certainly very interesting.

The design of a stack to be used in reverse electrodialysis is very similar to the stack used in electrodialysis. The main difference is that the cells arranged in parallel between the electrodes are rinsed in alternating series by sea and by river water as indicated in [Figure 27](#). The ions in the seawater indicated as Na^+ and Cl^- ions permeate from the seawater into the river water through the corresponding ion-exchange membrane due to their electrochemical potential gradient. This leads to an

electrical current between the cathode and anode. The maximum amount of energy that can be recovered is the Gibbs free energy of mixing fresh water and seawater which is $\sim 10.7 \text{ kWh}$ when 1 m^3 of fresh water is mixed with seawater that has a total salt content of $\sim 35 \text{ kg m}^{-3}$. The driving force for the ion transport through the cation- and anion-exchange membranes which separates the seawater from the fresh water is the electrochemical potential difference between the sea and the river water. The flux that can be achieved with today's ion-exchange membranes is in the range of a few $\text{kg m}^{-2} \text{ h}^{-1}$. Concentration polarization effects at the membrane surface will further reduce the effective flux and energy needed to pump the sea and the fresh water through the membrane device will reduce the efficiency of the process further. Therefore, it seems that membrane costs must be drastically decreased and membrane ion transport rates must be increased to make reverse electrodialysis a competitive energy-production process!!

References

- [1] Spiegler, K. S. *Electrochemical Operations*. In *Ion-Exchange Technology*; Nachod, F. C., Schubert, J., Eds.; Academic Press: New York, 1956.
- [2] Wilson, J. R. *Deminceralization by Electrodialysis*; Butterworth: London, 1960.
- [3] Schaffer, L. H., Mintz, M. S. *Electrodialysis*. In *Principles of Desalination*; Spiegler, K. S., Ed.; Academic Press: New York, 1966; pp 3–20.
- [4] Strathmann, H. *Ion-Exchange Membrane Separation Processes*; Elsevier: Amsterdam, 2004.
- [5] Liu, K. J., Chlanda, F. P., Nagasubramanian, K. J. *J. Membr. Sci.* **1977**, *2*, 109.
- [6] Eisenberg, A., Yeager, H. L. *Perfluorinated Ionomer Membranes*; ACS Symposium Series 180; American Chemical Society Washington, DC, 1982.

- [7] Jackson, C. *Modern Chlor-Alkali Technology*; Society of Chemical Industry, Ellis Horwood: Chichester, 1983; Vol. 2.
- [8] Flett, D. S. *Ion-Exchange Membranes*; E. Horwood: Chichester, 1983.
- [9] Bergsma, F., Kruissink, Ch. A. *Fortschr. Hochpolym.-Forsch.* **1961**, 21, 307.
- [10] Helfferich, F. *Ion-Exchange*; McGraw-Hill: London, 1962.
- [11] Sata, T. *Pure Appl. Chemistry* **1986**, 58, 1613.
- [12] Grot, W. *Chem. Ing. Tech.* **1975**, 47, 617.
- [13] Zschocke, P., Quellmalz, D. J. *Membr. Sci.* **1985**, 22, 325.
- [14] Kerres, J., Tang, C. M., Graf, C. *Ind. Eng. Chem. Rev.* **2004**, 43, 4571.
- [15] Grot, W. G. Films of Fluorinated Polymer Containing Sulfonyl Groups with One Surface in the Sulfonamide or Sulfonamide Salt Form and a Process for Preparing Such. US Pat. 3,784,399, 1974.
- [16] Simons, R. J. *Membr. Sci.* **1993**, 78, 13.
- [17] Wilhelm, F. W. Bipolar Membrane Preparation. In *Bipolar Membrane Technology*; Kemperman, A. J. B., Ed.; Twente University Press: Enschede, The Netherlands, 2000.
- [18] Pourcelly, G. *Desalination* **2002**, 147, 359.
- [19] Spiegler, K. S. *Trans. Faraday Soc.* **1958**, 54, 1408.
- [20] Kedem, O., Katchalsky, A. J. *Gen. Physiol.* **1961**, 45, 143.
- [21] Planck, M. *Ann. Physik u. Chem., N.F.* **1890**, 39, 161.
- [22] Strathmann, H. Electrodialysis and Related Processes. In *Membrane Separation Technology*; Nobel, R. D., Stern, S. A., Eds.; Elsevier: Amsterdam, 1995; pp 213–281.
- [23] Huffmann, E. L., Lacey, R. E. Engineering and Economic Considerations in Electromembrane Processing. In *Industrial Processing with Membranes*; Lacey, R. E., Loeb, S., Eds.; Wiley: New York, 1972; pp 39–55.
- [24] Mani, K. N. J. *Membr. Sci.* **1991**, 58, 117.
- [25] Kemperman, A. J. B. *Handbook on Bipolar Membrane Technology*; Twente University Press: Enschede, The Netherlands, 2000.
- [26] Strathmann, H., Krol, J. J., Rapp, H. J., Eigenberger, G. J. *Membr. Sci.* **1997**, 125, 123.
- [27] Mafé, S., Ramirez, P., Alcaraz, A., Aguilera, V. Ion Transport and Water Splitting in Bipolar Membranes. In *Bipolar Membrane Technology*; Kemperman, A. J. B., Ed.; Twente University Press: Enschede, The Netherlands, 2000.
- [28] Rapp, H. J. Die Elektrodialyse mit bipolaren Membranen - Theorie und Anwendung. PhD Thesis, University of Stuttgart, Germany 1965.
- [29] Katz, W. E. *Desalination* **1979**, 28, 31.
- [30] Lee, H. J., Safert, F., Strathmann, H., Moon, S. H. *Desalination* **2002**, 142, 267.
- [31] Mintz, M. S. *Ind. Eng. Chem.* **1963**, 55, 18.
- [32] Ito, S., Nakamura, I., Kawahara, T. *Desalination* **1980**, 32, 383.
- [33] Korngold, E., Kock, K., Strathmann, H. *Desalination* **1978**, 24, 129.
- [34] Rapp, H. J., Pfromm, P. H. *Ind. Eng. Chem. Res.* **1998**, 37, 4761.
- [35] Ahlgreen, R. M. Electromembrane Processing of Cheese Whey. In *Industrial Processing with Membranes*; Lacey, R. E., Loeb, S., Eds.; Wiley Interscience: New York, 1972 pp 57–69.
- [36] Kim, H. Y., Moon, S. H. *J. Chem. Technol. Biotechnol.* **2001**, 76, 169.
- [37] Yamane, R., Ichikawa, M., Mizutani, Y., Onoue, Y. *Ind. Eng. Chem. Process Des. Dev.* **1969**, 8, 159.
- [38] Nishiwaki, T. Concentration of Electrolytes Prior to Evaporation with an Electromembrane Process. In *Industrial Processing with Membranes*; Lacey, R. E., Loeb, S., Eds.; Wiley: New York, 1972.
- [39] Pourcelly, G., Gavach, G. Electrodialysis Water Splitting- Application of Electrodialysis with Bipolar Membranes. In *Handbook Bipolar Membrane Technology*; Kemperman, A. J. B., Ed.; Twente University Press: Enschede, The Netherlands, 2000.
- [40] Simons, R. J. *Membr. Sci.* **1993**, 78, 13.
- [41] Liu, K. J., Chlanda, F. P., Nagasubramanian, K. J. J. *Membr. Sci.* **1977**, 2, 109.
- [42] McArdle, J. C., Piccari, J. A., Thornburg, G. G. *Iron Steel Eng.* **1991**, 68, 39.
- [43] Mani, K. N., Chlanda, F. P. Electrodialytic Water Splitter and Process for Removal of SO₂ from Gases Containing Same for the Recovery of SO₂ and NaOH. US Pat. 4,629,545, 1986.
- [44] Huang, C., Xu, T., Zhang, Y., Xue, Y., Chen, G. J. *Membr. Sci.* **2007**, 288, 1.
- [45] Ganzi, G. C. Electrodeionization for High Purity Water Production. In *New Membrane Materials and Processes for Separation*; Sirkar, K. K., Lloyd, D. R., Eds.; AIChE Symposium Series; American Institute of Chemical Engineers; Washington, DC, 1988; Vol. 84, p 73.
- [46] Grabowskij, A., Zhang, G., Strathmann, H., Eigenberger, G. J. *Membr. Sci.* **2006**, 281, 297.
- [47] Kobuchi, Y., Motomura, H., Noma, Y., Hanada, F. J. *Membr. Sci.* **1987**, 27, 173.
- [48] Kobuchi, Y., Matsunaga, Y., Noma, Y., Hanada, F. Application of Ion-Exchange Membranes to the Recovery of Acids by Diffusion Dialysis and Electrodialysis. In *Synthetic Polymeric Membranes*; Sedlacek, B., Kahovec, J., Eds.; W. de Gruyter: Berlin, Germany, 1987 pp 412–428.
- [49] Welgemoed, T. J., Schutte, C. F. *Desalination* **2005**, 183, 327.
- [50] Farmer, J. Method and Apparatus for Capacitive Deionization, Electrochemical Purification and Regeneration of Electrodes. US Pat. 5,425,858, 1995.
- [51] Lee, J.-B., Park, K.-K., Eum, H.-M., Lee, C.-W. *Desalination* **2006**, 196, 125.
- [52] Williams, K. R. *An Introduction to Fuel Cells*; Elsevier: London, 1966.

Biographical Sketch



Heinrich Strathmann was born in Detmold, Germany in 1934. He received his *Diplôme d'Ingénieur* (Dipl.-Ing.) in chemistry from the University of Darmstadt, Germany in 1961. In 1965, he was awarded a doctorate degree in chemistry by the University of Darmstadt, Germany. In 1982, he was awarded the habilitation degree, by the University of Tübingen, Germany. Since 1988, he has been a professor at the University of Stuttgart, Germany.

From 1962 to 1966, he worked as a research assistant at the University of Aachen, Germany. Between 1966 and 1971, he was associated with Amicon Corp., Lexington, MA, USA. From 1971 to 1982, he was associated with Forschungsinstitut Berghof GmbH, Germany. Between 1982 and 1992, he worked with the Fraunhofer Institute for Bioengineering, Stuttgart, Germany. From 1988 to 1992, he was a professor at the University of Stuttgart, Germany. Between 1992 and 1999, he was a professor at the University of Twente, the Netherlands. From 1999 to 2000, he was a professor at the University of Colorado, Boulder, USA. He has been professor emeritus at the University of Stuttgart, Germany since 2000.

He was with the editorial board of the *Journal of Membrane Science* in 1976. He was an editor of *Separation and Purification Technology* (1997–2002). He worked in the fields of desalination (1978), filtration and separation (1987–2002), and gas separation and purification (1982–96).

Apart from being a member of the scientific advisory board of various companies, he holds membership in various scientific organizations such as DECHEMA, Frankfurt, Germany and European Membrane Society. He is also a member of the board of scientific organizations such as the European Membrane Society (1984–98) (vice-president), UNESCO Center for Membrane Technology, Sydney, Australia (1993–98), and the UN-University, Environmental Science, Gwangju, Korea (2003–06).

He has authored three textbooks on *Membrane Science and Technology*, coauthored eight reference books, and has more than 200 scientific publications and 36 patents to his credit.

His responsibilities include teaching chemical engineering and supervising PhD students.

He is a recipient of various awards including the 1994 Honorary Professor at the Dalian Institute Chemical Physics, 1998 Willy Hager Price and gold medal, 2005 Honorary Professor at the South China Central University, and 2007 R. Barrer Price of the European Membrane Society.

2.15 Basic Aspects in Proton-Conducting Membranes for Fuel Cells

G Alberti and M Casciola, Università di Perugia, Perugia, Italy

© 2010 Elsevier B.V. All rights reserved.

2.15.1	Introduction	433
2.15.2	General Properties of Polymer Electrolyte Membranes	433
2.15.2.1	Ion Exchange	434
2.15.2.2	Sorption of Nonelectrolyte Substances from Solutions or Vapors	435
2.15.2.3	Sorption of Electrolyte Solutes (Donnan Exclusion)	435
2.15.2.4	Swelling	435
2.15.2.5	Kinetics of Swelling and Shrinking	436
2.15.2.6	Water-Vapor Sorption Isotherms in Cross-Linked Polymer Electrolytes	436
2.15.2.7	Schroeder Paradox	438
2.15.3	General Consideration on Membranes for PEMFCs	438
2.15.3.1	Desirable Operating Temperature of the Stacks	439
2.15.3.2	Membrane Resistance to Radical Attack	439
2.15.3.3	Permeability to Gases	439
2.15.3.4	Lifetime	439
2.15.3.5	Thickness of the Membranes	439
2.15.4	Perfluorinated Membranes Containing Superacid $-\text{SO}_3\text{H}$ Groups	440
2.15.4.1	Nafion Membranes	440
2.15.4.1.1	Preparation	440
2.15.4.1.2	Nafion morphology	441
2.15.4.1.3	Water uptake in liquid water at different temperatures	442
2.15.4.1.4	Water-vapor sorption isotherms of Nafion	442
2.15.4.1.5	Curves T/n_c	445
2.15.4.1.6	Water uptake and tensile modulus	447
2.15.4.1.7	Proton conductivity	449
2.15.4.1.8	Instability maps for proton conductivity	449
2.15.4.2	Composite Nafion Membranes	450
2.15.4.2.1	Oxide-filled membranes	450
2.15.4.2.2	Heteropolyacid-filled membranes	452
2.15.4.2.3	Zirconium-phosphate-filled membranes	452
2.15.4.3	Some Information on Dow and on Recent Hyflon Ion [®] Ionomers	453
2.15.5	Nonperfluorinated Membranes	454
2.15.5.1	Poly(ether ketone)s	454
2.15.5.2	Poly(sulfone)s	455
2.15.5.3	Poly(imide)s	456
2.15.5.4	Sulfonated Block Copolymers	457
2.15.5.5	Polybenzimidazole	458
2.15.5.6	Poly(phosphazene)s	459
2.15.6	Some Final Remarks	460
References		461

Glossary

Casting procedure A method for the preparation of polymer electrolyte membranes in which a solution (or dispersion) of the ionomer is cast on a suitable flat solid surface (e.g., a glass plate). After the elimination of the solvent (usually by heating), the formed membrane is detached from the support. In industrial preparations, percolating films of ionomer dispersions are rapidly air-dried during their percolation.

Copolymerization A chemical reaction in which macromolecules are formed from different kinds of monomers.

Counter-osmotic pressure The external pressure required to prevent the flow of water entering into the osmotic cells. With reference to ionomer membranes, counter-osmotic pressure is produced by the counter-elastic force of the membrane matrix that balances the inner osmotic pressure.

Cross-linking The formation of covalent bonds between adjacent chains of macromolecules (polymers). The introduction of cross-linking in ionomer membranes can significantly reduce their swelling due to water uptake.

Four-probe impedance measurements A direct (DC) or alternating (AC) electrical current (I) is driven through a membrane strip by two electrodes located at the ends of the strip. The potential drop along the strip (V) is measured by a couple of electrodes, separated by a distance d . For DC measurements, the membrane conductivity is: $\sigma = (d)/(VA)$, where A is the area of the membrane cross section. The same relation also holds for AC measurements if the phase angle is close to zero.

Impedance measurements Impedance is a quantity, usually indicated by Z , that relates the alternating current (I) passing through a circuit to the alternating potential (V) applied to it. It consists of two components: resistance (R) and reactance (X). If V is expressed as the sum of a component (V') in phase with I and a component (V'') leading or lagging I by $\pi/2$, then $R = V_0'/I_0$ and $X = V_0''/I_0$, where V_0' , V_0'' , and I_0 are the

amplitudes of V' , V'' , and I , respectively. Impedance measurements within a suitable frequency range (e.g., from mHz to MHz) are usually employed to separate the ohmic resistance of an electrolyte from the impedance of the electrode–electrolyte interface (see Nyquist plot).

Keggin structure A cage-like structure, which is built up by four equivalent sets of octahedra made of oxygen atoms (oxide ions, together with hydroxyl ions and water molecules) coordinating a central metal ion. Each set is formed by three condensed octahedra sharing edges and is connected to the other three sets through octahedron corners. Within each set, there is one oxide ion shared by three octahedra. These oxide ions are also tetrahedrally coordinated to a p-block element located at the center of the cage.

Nyquist plot A representation of the data obtained from impedance measurements drawn by plotting Z'' as a function of Z' . The analysis of the Nyquist plot usually allows for the separation of the ohmic resistance of an electrolyte from the impedance of the electrode–electrolyte interface.

Osmotic water inside an ionomer membrane The fraction of water (usually expressed as the number of water moles per equivalent weight of fixed ionogenic groups) that enters an ionomer for equilibrating differences between the water activity inside and outside the ionomer.

Polycondensation A chemical reaction in which compounds of high molecular mass are formed from monomers with the elimination of small molecules, such as water.

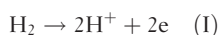
Swelling An expansion of the volume of the dry membrane due to the uptake of water or other polar solvents.

Water-sorption isotherms of polymeric electrolytic membranes Plots in which, at constant temperature, the water uptake of the membrane is reported as a function of the external relative humidity.

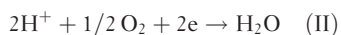
2.15.1 Introduction

Both the continuous increase in petrol costs and the necessity for reduction of pollution, especially in large towns, have reinforced interest in electrical cars based on fuel cells (FCs). Among the recently developed types of FCs, preference is given to polymeric electrolyte membrane fuel cells (PEMFCs) because these cells exhibit the best characteristics of weight, volume, and current density for automotive applications [1].

We recall that hydrogen PEMFC is a primary electrochemical device [2] where a fuel (e.g., hydrogen) is fed to a catalytic electrode (usually Pt) that is able to catalyze, at the working temperature, the anodic semi-reaction:



while an oxidant (usually air or oxygen) is fed to a catalytic electrode (usually Pt) specific for the cathode semi-reaction:



Hydrogen and oxygen (air) are separated by a proton-conducting polymeric membrane. The protons produced at the anode cross the membrane and react at the cathode with the formation of water. The chemical energy derived from the fuel oxidation is therefore continuously converted into electrochemical energy.

At temperatures lower than 130 °C, only hydrogen and a few other fuels (e.g., alkanols) are able to produce protons at an acceptable rate. Therefore, our attention will be limited to membranes for PEMFC types using hydrogen or methanol as fuel.

Before discussing current knowledge of these membranes, it is assumed that there are still many unsolved problems which delay the commercialization of PEMFCs being used in cars.

In short, the main problems in PEMFCs using hydrogen as fuel are related to: (1) the high costs of both proton-conducting polymeric membranes and catalysts; (2) the low proton conductivity of the presently available membranes at low relative humidity (RH); and (3) their instability and short lifetime at temperatures higher than about 80 °C (see later for details).

Other problems that arise in PEMFCs using methanol as fuel are either too high methanol cross-over through the present polymeric membranes or

the high costs and low efficiency of catalysts at the anodic electrode.

In this situation, it is now becoming clear that intensive efforts must be made to develop completely new types of polymeric membranes with the required characteristics for automotive application.

However, since it is not probable that new PE membranes better than the existing ones based on perfluorosulfonic acid (PFSA) will be found in the near future, efforts to improve the characteristics of existing membranes by appropriate modifications must also be made. In order to do this in the best manner, we need to know the basic aspects of unmodified proton-conducting membranes.

Therefore, in the first part of this chapter, we begin by examining the general properties of PE membranes such as ion exchange, sorption of electrolyte and nonelectrolyte solutes, swelling, and shrinking. Then, after a short discussion of the reasons for which, especially for automotive applications, we need membranes of high conductivity, high stability, and a long lifetime, we examine the properties of some unmodified PFSA membranes.

Especially for Nafion, the morphology, the evolution of its conformation during hydration/dehydration processes, the equilibrium water uptake, and its relation to the tensile modulus and proton conductivity are discussed in some detail. The very recent advancement in understanding the reasons for their thermal instability at medium temperatures will then be illustrated.

Nonperfluorinated ionomers with polyaromatic or inorgano-organic backbones, which are considered as possible alternatives to Nafion membranes, are also described and compared with Nafion. Due to the large variety of these materials, only representative examples are reported here with focus on the main synthetic procedures and physicochemical properties.

Finally, some remarks on the expected developments of membranes for PEMFCs in the near future, including recent progress on thermal-annealing procedures for increasing their durability in the temperature range 80–130 °C, are reported.

2.15.2 General Properties of Polymer Electrolyte Membranes

Other than in solutions or in ionic liquids, ionic conduction can also take place in the solid state. The solids that exhibit ionic conduction are called

solid-state ionic conductors (SSICs). Fundamental aspects of the conduction mechanism for inorganic SSICs are not discussed here. The interested reader is referred to [3]. Based on the charge of ionic species responsible for conduction, they are divided into cationic and anionic conductors; then, based on specific species involved in the conduction, they are further subdivided into sodium ion conductors, proton conductors, fluorine ion conductors, and so on. The class of inorganic solid-state proton conductors (SSPCs) has been particularly investigated for its potential applications [4].

If the solid conductor is a polymer, we refer more specifically to polymer electrolytes (or ionomers). Many ionic groups such as $-\text{SO}_3^-$, $-\text{PO}_3\text{H}^-$, $-\text{COO}^-$, $-\text{NH}_3^+$, and $=\text{N}^+=$, whose electric charge is balanced by mobile counterions of opposite sign, can be easily attached to a variety of polymers and the chemistry of the obtained materials has been developed since 1935, when the first polymer-ion exchangers were obtained by Adams and Holmes [5]. The interest in these materials has grown considerably after World War II for their application as cation and anion exchangers and a large variety of polymeric ion exchangers were developed. Many books on this subject are available. Among them, we recommend, in particular, the book *Ion Exchange* by Helfferich [6].

The most important cation exchangers are sulfonation products of cross-linked polystyrene. The most important anion exchangers are cross-linked polystyrene into which strong- or weak-base groups have been introduced by chloromethylation and subsequent amination. Reaction with tertiary alkyl amines gives strong-base quaternary ammonium groups. Most part of the polymer-ion exchangers exhibits some amount of ionic conduction. The importance of this conduction is due to the fact that thin sheets or membranes can be easily obtained by casting procedure or by extrusion of polymer electrolytes at high temperatures. These thin membranes are usually flexible and very compact and can be used as separators in many electrochemical processes and electrochemical devices.

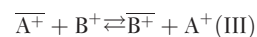
PEMs in sodium form are used as separators in the electrolytic preparation of Cl_2 and NaOH and in the processes of electrodialysis, in which desalting of brackish water can be obtained by an alternating arrangement of cationic and anionic PEMs. Finally, there is an increasing interest in the use of PEM in H^+ form as separators in FCs, and also in the

electrolytic processes for the local production of hydrogen.

An almost unlimited variety of resins with different fixed ionic groups and different compositions and degrees of cross-linking of the matrix can be prepared. However, in spite of the large number of possible polymer electrolytes, only a few are able to exhibit the required electrochemical properties for their use as membranes in electrochemical processes of interest.

2.15.2.1 Ion Exchange

As a rule, polymer electrolytes are insoluble in aqueous solutions. When a polymer electrolyte containing A^+ as counterion is placed in an electrolyte solution containing the cation B^+ , an exchange between the two counter ions takes place:



The original counter ion A^+ in the ionomer is partially replaced by B^+ . Ion-exchange equilibria are of great practical and theoretical importance and have therefore been extensively investigated. Without getting into the details of these studies, it has been observed that the polymer electrolyte usually retains or takes up certain counter ions in preference to others (ion-exchange selectivity). Independently of specific interactions with the fixed ionic groups, counter ions of higher valence are greatly preferred. This selectivity is known as electroselectivity. The presence of counter ions of high valence or having specific interactions with the fixed ionic groups must therefore be carefully avoided in PEMs which are used in electrochemical processes because, as a rule, the higher the selectivity of a certain counter ion, the lower its mobility in the membrane. This is why proton-conducting membranes employed in FCs are boiled in 0.5 mol l^{-1} sulfuric acid before being used.

The ion-exchange capacity is usually expressed in milliequivalents per gram (meq. g^{-1}) of dry ionomer in H^+ form. Polymer electrolytes in H^+ form and $-\text{OH}^-$ form can also be considered as insoluble polyacids and polybases, respectively. Therefore, their weighed amounts can be titrated with standard bases and acids. In such a titration, the insoluble polyelectrolyte gel reaches equilibrium with the solution to which the titrant is added. If the equilibrium is slowly reached, a new titrant must be added only when the previous one has been completely

consumed. The neutralization of the acid or basic fixed groups can be easily observed by recording the pH of the supernatant solution by an automatic titrator. The titration curve obtained can be evaluated to give the number of ionogenic groups. Information on the acid strength of fixed ionogenic groups can also be obtained by the titration curves.

2.15.2.2 Sorption of Nonelectrolyte Substances from Solutions or Vapors

Nonelectrolytes are sorbed by ionomers in a manner similar to that by nonionic sorbents. Sorption is favored by specific interactions between the substance under consideration and the polymer electrolyte. These interactions can occur either with the polymeric matrix (London interactions) or with the counter ions. The latter interaction is particularly important in the case of strong acidic ionomers that can take up many protonable molecules such as water and basic organic solvents. The sorption of water is essential for proton transport in PEM for FCs and this subject is dealt later in the Sections 2.15.2.4 and 2.15.2.6. The sorption of methanol is also very important for PEMFCs using methanol as fuel (Me PEMFCs). Finally, some basic solvents such as dimethylformamide (DMF), *N*-methylpyrrolidone (NMP), and alkanols are used in the preparation of membranes for FCs by the so-called casting procedure. Large amounts of these solvents can remain inside the membranes even after drying. Strong acidic membranes such as Nafion in H⁺ form must be stored in closed systems because many organic vapors present in the air even in small concentrations can be taken up. The basic solvents present in the membranes must be eliminated before their use in FCs. This elimination can be done either by oxidation with a boiling solution of 3% H₂O₂ or by washing with acid solutions.

2.15.2.3 Sorption of Electrolyte Solutes (Donnan Exclusion)

Sorption of electrolytes is affected by electrostatic forces. The origin of these electrostatic forces when an electrolyte polymer with fixed negative charge is placed in a dilute solution of a strong electrolyte is first discussed briefly. As in this case the concentration of positively charged counter ions inside the polymer electrolyte is higher than in the external solution, there is a natural tendency for these counter ions to diffuse out into the solution in order to level

out the concentration differences. On the contrary, the concentration of the negative species is higher in the solution, and a diffusion of these species from the solution into the electrolyte polymer must be expected. However, because the moving species are charged, the diffusion process disturbs electroneutrality. Even a limited migration of both cations into the solution and anions into the electrolyte polymer produces an excess of positive charge in the solution and of negative charge in the polymeric phase. The electric potential difference at the interface is known as Donnan potential. This potential attracts the cations back into the negatively charged polymeric phase and repels anions back into the positively charged solution. An equilibrium is established at which the natural tendency of both positive and negative ions to migrate is balanced by the attractive and repulsive forces of the electric field. The result is that the concentration of the counter ions in the polymeric phase remains higher than in solution, while the opposite takes place for the anions (co-ions). Owing to the requirement of electroneutrality, low coion uptake is equivalent to low electrolyte sorption in the polymeric phase. In other words, the electrolyte is, at least partially, excluded inside a cationic polymer electrolyte (Donnan exclusion). The situation within a polymer electrolyte carrying fixed positive charges can be described in a similar manner and Donnan exclusion of the electrolytes also occurs in this case. Obviously, the Donnan potential will take an opposite sign to that previously described. Donnan exclusion increases with increasing concentration of the fixed charges and decreases with the concentration of the electrolyte in solution. Donnan exclusion also decreases if counter ions and coions have high and low valence, respectively.

2.15.2.4 Swelling

As seen before, dried polymer electrolytes are able to sorb a large variety of solvents. The solvent uptake provokes an expansion of the polymeric matrix. Particularly important is the uptake of water and we refer essentially to this solvent; however, large amounts of other solvents such as alkanols and some basic solvents such as NMP and DMF are also taken up. The driving forces for solvent uptake are the solvation tendency of the counter ions and fixed ionic groups, as well as the tendency of the highly concentrated polyelectrolyte solution to dilute itself. The elastic matrix is stretched to make room for the incoming solvent. Swelling equilibrium is achieved

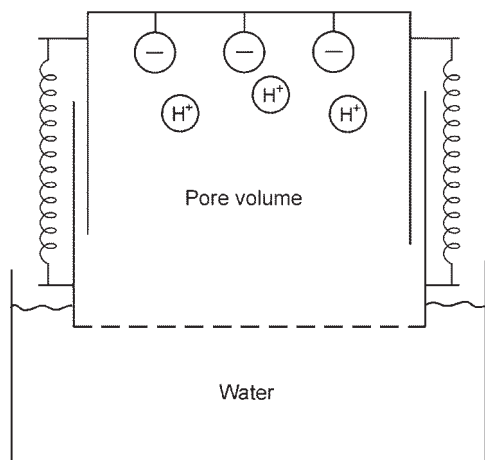


Figure 1 The mechanical model of Gregor in which the matrix of a polymer electrolyte is represented as an elastic spring that is stretched when water enters into the liquid pores.

when the swelling pressure balances the driving forces for solvent uptake. As early as 1948, Gregor [7] developed a very simple model for solvent uptake that is schematically illustrated in **Figure 1**. According to this model, the matrix of the polymer electrolyte is an elastic network that acts as an elastic spring. When the polymer swells, the network is stretched and exerts a pressure on the internal water-filled pores just as the skin of an inflated toy balloon exerts a pressure on the air inside. In the Gregor model, solvation shells are considered as being part of both fixed charged groups and counter ions. This choice is not well defined from a thermodynamic point of view, but it brings out a clear picture of the physical action of the swelling pressure.

2.15.2.5 Kinetics of Swelling and Shrinking

Swelling and shrinking may be described in terms of diffusion of solvent molecules. No electric coupling is involved because the solvent molecules are not charged. The fact that swelling progresses from the external surface of the membrane toward its center should be taken into account. As the external part of the matrix progressively expands, the solvent molecules become more and more mobile in the already swollen part. Thus, swelling equilibrium is rapidly attained in the external part of the membranes, while the solvent diffusion remains low in the still shrunken inner part of the membrane. The result is that there is the formation of a sharp phase boundary that moves

from the external part toward the center of the membrane. When the swollen membrane is dehydrated, the external layers are the first to lose their solvent. The shrinking of the external part increases the resistance to solvent diffusion, whereas in the inner part, the higher solvent mobility keeps the solvent concentration rather uniform. The result is that the formation of a moving phase boundary does not occur. Furthermore, shrinking is much slower than swelling, particularly in the last stages of dehydration, because the solvent must travel long distances in the shrunken polymer matrix.

Swelling and shrinking are important properties for PE membranes, which are discussed in detail later.

2.15.2.6 Water-Vapor Sorption Isotherms in Cross-Linked Polymer Electrolytes

Especially for FC membranes, it is important to know the water uptake when the polymer electrolyte is equilibrated at constant temperature and various values of RH. The water taken up by a polymer electrolyte is conveniently reported as the number of water molecules per ionogenic group and usually denoted by λ .

A typical water-vapor sorption isotherm at room temperature for the H^+ forms of sulfonated styrene at various degrees of cross-linking [8] is shown in **Figure 2**.

Note that, for $RH < 0.3$, the water uptake is low and almost independent of the degree of cross-linking. As shown later (see Equation (3)), the reason is that the osmotic water taken up for the different water activities outside and inside the ionomer (λ_{os}) is very less at low RH values. Thus, at low RH values, the most important factor for the water uptake is the hydration tendency of the ionogenic groups (which is independent of the degree of cross-linking). In other words, the first water that enters into the anhydrous pores at low RH is very likely strongly bound as a hydration shell (λ_{hyd}).

The λ_{os} appreciably increases with RH. Generally, very high values can be obtained at $RH > 0.7$, even for low degrees of cross-linking of the ionomer. Taking into account that the cross-linking is expected to increase the counter-elastic force of the polymer matrix, the strong dependence of water uptake on the degree of cross-linking can be simply explained by the Gregor model discussed earlier.

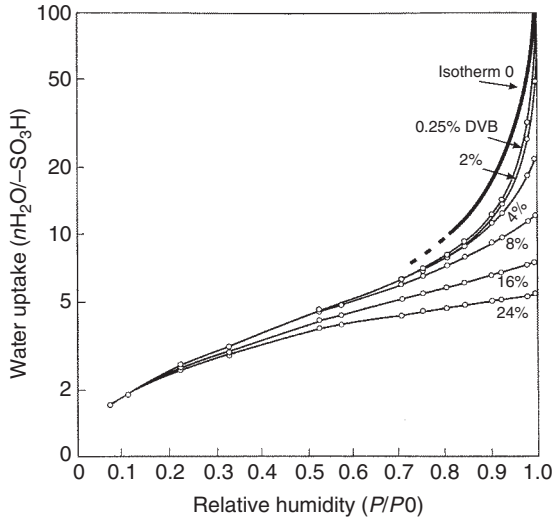


Figure 2 Typical water-vapor sorption isotherms for the H^+ form of sulfonate styrene ion exchange resin at various degrees of cross-linking. The isotherm 0 for an ideal ionomer with counter-elastic force 0 (calculated using Equation (7)) has been inserted and taken as the isotherm of 0 cross-linking. DVB, divinylbenzene. Redrawn from data of Boyd, G. E., Soldano, B. A. Z. *Elektrochem.* **1953**, 57, 162–166.

To account for the possibility of anisotropic swelling, the counter-elastic forces in the three space directions can be introduced into the original model [9]. Furthermore, by eliminating fixed ionized groups, a simple three-dimensional model for the study of water-vapor sorption isotherms of solutions under different applied pressures can also be obtained (Figure 3(a)).

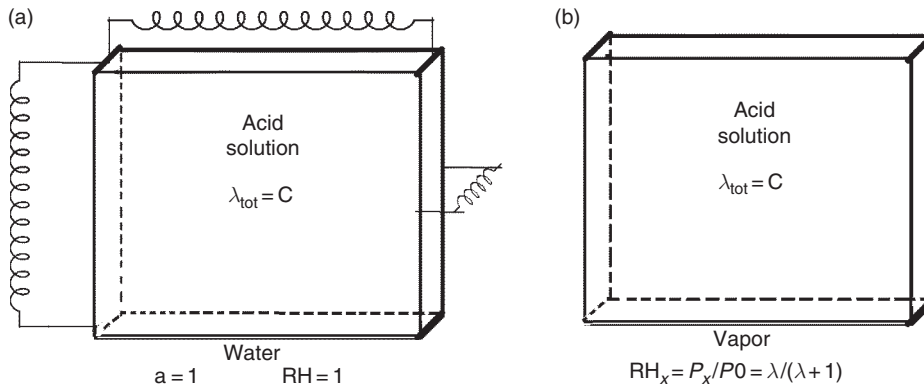


Figure 3 A simplified model of (a) a three-dimensional cell filled with acid solutions. The surface of the cell is considered to be a semipermeable membrane. The cell is immersed in liquid water. An equilibrium between the external and inner water is reached when the osmotic pressure is balanced by the counter-elastic force of the springs (in absence of anisotropic swelling, the counter-elastic force is the same in the three directions). (b) The cell (a), without any applied counter-elastic force.

Let us suppose that inside this three-dimensional model, without any applied pressure (Figure 3(b)) there is a solution of an undissociated solute which does not appreciably interact with water.

We can write

$$X_s = 1 - X_w \quad (1)$$

where X_s and X_w are the molar fraction of the solute and of the water, respectively.

Taking into account Raoult's law, we can also write

$$X_w = \frac{P}{P^0} = RH \quad (2)$$

Finally, by remembering that

$$X_w = \frac{n_w}{n_w + n_s}$$

where n_w and n_s are the number of water and solute molecules, respectively; by dividing numerator and denominator by n_s , we obtain

$$X_w = \frac{\lambda_{os}}{\lambda_{os} + 1} = RH \quad (3)$$

where λ_{os} is the osmotic water due to the difference in activity between the water in the external vapor phase and the water inside the osmotic box. If the solute strongly interacts with water with formation of hydration shells, additional water is taken up for hydration (λ_{hyd}).

Since in the Gregor model the solvation shell is considered as being part of the protons and anions, the total water becomes

$$\lambda_{\text{tot}} = \lambda_{\text{os}} + \lambda_{\text{hyd}} \quad (4)$$

Thus, Equation (3) can be written as

$$\text{RH} = \frac{\lambda_{\text{tot}} - \lambda_{\text{hyd}}}{(\lambda_{\text{tot}} - \lambda_{\text{hyd}}) + 1} \quad (5)$$

Let us now apply similar considerations to a polymer electrolyte containing $-\text{SO}_3\text{H}$ groups. In this treatment, $-\text{SO}_3\text{H}$ groups are considered as completely dissociated when $\lambda_{\text{tot}} \geq 3$ [10]. However, unlike soluble acids, only dissociated protons contribute to the osmotic pressure, while the dissociated $-\text{SO}_3^-$ groups contribute only to the total hydration. By defining total hydration (λ_{hyd}) as the sum of the hydration numbers of protons (λ_{hyd}^+) and $-\text{SO}_3^-$ groups (λ_{hyd}^-), we have

$$\lambda_{\text{hyd}} = \lambda_{\text{hyd}}^+ + \lambda_{\text{hyd}}^- \quad (6)$$

Thus, the osmotic behavior of a polymer electrolyte can be described using Equation (5), by inserting the hydrations of protons and fixed charges, similar to Equation (6) derived for an acid solution.

There are various methods for the estimation of λ_{hyd} that cannot be discussed here. In short, as an average of much data (based on various vapor sorption isotherms of solutions of sulfuric and phosphoric acids at various temperatures), a useful estimation for the proton hydration at 20 °C could be the following: ~ 1 for $\text{RH} < 0.1$; ~ 3 for $\text{RH} = 0.25$; and ~ 3.5 for $\text{RH} = 0.4$. For $\text{RH} > 0.4$, the estimation is more difficult because λ_{hyd} begins to be influenced by the counter-elastic force of the ionomer while additional water can also be taken from the fixed $-\text{SO}_3^-$ groups. By assuming that the protons are completely dissociated when $\lambda_{\text{tot}} > 3$, it can be estimated that the hydration number of the proton at $\text{RH} = 0.8$ is about 6 for an ionomer that exhibits a λ_{tot} in the range 12–16 when equilibrated in liquid water at 20 °C. Taking into account the hydration of the fixed dissociated groups, the total λ_{hyd} can be assumed to be about 7. Equation (5) can therefore be written as

$$\text{RH} = (\lambda_{\text{tot}} - 7) / (\lambda_{\text{tot}} - 6) \quad (7)$$

According to Equation (7), λ_{tot} greatly increases with increasing RH and becomes ∞ for $\text{RH} = 1$.

The fact that finite water-uptake values are experimentally found at $\text{RH} = 1$ is due to the counter-elastic force of the polymeric matrix that prevents its dissolution.

A plot of Equation (7) can be considered as an isotherm for an ideally soluble polymer electrolyte with degree of cross-linking equal to zero and in which no interactions between adjacent polymeric chains occur. Note that this ideal isotherm 0, reported in Figure 2 as an isotherm of reference, is very near to the experimental curve with degree of cross-linking 0.25 divinylbenzene (DVB).

Now, we can apply an increasing degree of cross-linking to the ionomer. It can be shown [9] that due to the increased counter-elastic force, the isotherm 0 is shifted more and more toward the right, as experimentally observed. The derivation of these shifts as a function of the counter-elastic force of the polymeric matrix is discussed in Section 2.15.4.1.4.

2.15.2.7 Schroeder Paradox

About 100 years ago, Schroeder [11] reported that the water taken up by a sample of gelatin immersed in liquid water is greater than that taken up by the same sample when equilibrated in vapor at 100% RH. This phenomenon was called the Schroeder paradox because, the chemical potential of liquid water being equal to that of its saturated vapor at the same temperature, no differences in water uptake were expected. In the last century, the Schroeder paradox was then reported for many other amorphous materials, including ionomers, and many different explanations have been reported. Due to the large number of papers on this subject, this thermodynamic paradox was believed to be true and therefore taken into account in many papers concerning the water uptake of ionomer membranes. In our systematic investigations on the water uptake of Nafion 117 membranes (see later), the Schroeder paradox was never clearly found. This led us to conclude that many of the previous water determinations were strongly influenced by differences in permanent deformations in ionomers that were not well controlled [9]. These conclusions were then confirmed in a recent paper of Onishi *et al.* [12] in which it has been definitively confirmed that the Schroeder paradox does not exist, at least for ionomer membranes.

2.15.3 General Consideration on Membranes for PEMFCs

Before describing the state of the art of important proton-conducting membranes for PEMFCs, some general considerations about the desirable operating

temperature of the stacks, membrane resistance to radical attack, gas permeability, lifetime, and thickness of the membranes are reported. For additional information, the reader is referred to Li *et al.* [13]

Next, two main types of polymeric membranes are taken into consideration: (1) perfluorinated membranes containing superacid protogenic $-\text{SO}_3\text{H}$ groups and (2) nonperfluorinated membranes containing acid protogenic $-\text{SO}_3\text{H}$ groups.

There is a brief information on membranes containing basic groups (e.g., PBI) soaked with phosphoric acid, to give suitable proton conductivity at low RH and high temperature.

2.15.3.1 Desirable Operating Temperature of the Stacks

In contrast to an internal combustion engine (ICE), which rejects almost half the heat through the exhaust, an FC has to reject most of the heat through the radiator. On the other hand, for reasons of weight and dimensions, the size of a PEMFC radiator must be smaller or comparable with that of existing ICEs of similar power. The cooling efficiency obviously depends on the difference between the stack temperature and the external temperature. From a practical point of view, in order to use a radiator having a front area comparable with that of an ICE of similar power, we need membranes that are able to operate up to 90°C when the external temperature is lower than about 25°C and in the range $90\text{--}110^\circ\text{C}$ when the external temperature is in the range $25\text{--}40^\circ\text{C}$. Further reductions in the radiator front area obviously require higher stack temperatures. However, temperatures higher than $130\text{--}140^\circ\text{C}$ are not desired by car producers because they prefer to use the same radiators of the existing ICE without any change of cooling liquid and thermal resistance of the connecting tubes. Other problems also arise on very cold days. In this case, especially when the membrane hydration is greater than 3–4 molecules of water for each $-\text{SO}_3\text{H}$ group, freezing of water can provoke irreversible damages to the membrane. Furthermore, in subzero conditions, the proton conductivity of the membrane becomes very low and problems can arise in starting the FC. Finally, the water generated at the cathode can freeze near the electrode interface leading to limited or totally blocked oxygen permeation.

2.15.3.2 Membrane Resistance to Radical Attack

Superoxide radicals can be formed in a working PEMFC by oxygen crossover through the membrane onto the anode side with formation of HO_2^\bullet at the platinum catalyst. Furthermore, hydrogen peroxide is formed at the cathode side in sufficient amounts for its detection. In the presence of catalytic platinum, H_2O_2 decays, especially at high temperature, into HO^\bullet radicals. These species are all very reactive, and are therefore responsible for the degradation of membranes [14]. Thus, to ensure long-term durability of the membranes, we need ionomers of high chemical stability. The first comparative assessment of membrane stability can be carried out using the Fenton reaction ($\text{H}_2\text{O}_2/\text{Fe(II)}$) and characterizing membrane physical integrity, conductivity, mechanical properties, etc. as a function of time.

2.15.3.3 Permeability to Gases

The permeability of both oxygen and hydrogen through the membrane is of the order of 10^{-11} to $10^{-10} \text{ mol s}^{-1} \text{ atm}^{-1}$, corresponding to an equivalent loss of $1\text{--}10 \text{ mA cm}^{-2}$, approximately 1% of the performance.

2.15.3.4 Lifetime

The Teflon-like molecular backbone provides excellent long-term stability to PFSA membranes. A lifetime of over 60 000 h under the working condition of FCs at temperatures lower than 90°C has been achieved, for example, with commercial Nafion membranes.

At temperatures $>90^\circ\text{C}$, the durability is till date too short for practical applications.

2.15.3.5 Thickness of the Membranes

Weight and volume of the PEMFC are particularly important for automotive applications; thus, very thin membranes which also exhibit high proton conductivity are required in order to reach current density of about $7\text{--}10 \text{ kA m}^{-2}$. The thickness of the membranes is, however, limited by the mechanical properties of the polymer used and by its permeability to hydrogen and oxygen. The membrane must prevent the diffusion of these reacting gases as much as possible. High permeability would defeat the main

purpose of the FC because the oxidation of hydrogen occurring for diffusion of oxygen to the anode or for diffusion of hydrogen to the cathode will not contribute to the generation of electricity. It would simply result in wasting heat, thus reducing the efficiency of the PEMFC. The thickness of many membranes is therefore between 50 and 200 μm . High energy density sufficient for automotive application can be obtained with this thickness only if proton conductivity is of the order of 0.1 S cm^{-1} .

2.15.4 Perfluorinated Membranes Containing Superacid $-\text{SO}_3\text{H}$ Groups

The PFSA membranes are characterized by high mechanical stability, excellent chemical inertness, very interesting thermal stability, and high proton conductivity. For these unique characteristics, they have been the material of choice for automotive PEMFCs for many years. We may recall that the use of PFSA membranes in PEMFCs started about 45 years ago with the US space program Gemini in which the first successful realization of low-temperature PEMFCs was possible. In spite of their high cost and some important limitations, that are discussed later, they are used even now because better proton-conducting membranes with fixed protogenic groups are not commercially available for automotive PEMFCs.

Many commercial forms of PFSA membranes exist today. Some of these are listed in **Table 1**. Our attention here is essentially limited to Nafion[®], being till date the most investigated membrane. Some comparisons between Nafion[®] and the recent Hyflon Ion[®] membranes are also made.

2.15.4.1 Nafion Membranes

Nafion 1 membranes differ from conventional ion-exchange membranes in that they are not formed by cross-linked polyelectrolytes but by thermoplastic perfluorinated polymers with pendant side chains terminated by $-\text{SO}_3\text{H}$ groups.

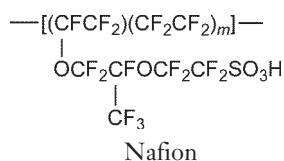


Table 1 Perfluorinate sulfonic acid membranes

Some Nafion[®] 1100 membranes, produced by Du Pont de Nemours:

Nafion 117 (180 μm)
Nafion 115 (130 μm)
Nafion RE212 (50 μm)^a
Nafion 112 (50 μm)

Some Hyflon Ion membranes, produced by Solvay Solexis:

Aquivion E87-10S (100 μm)
Hyflon Ion 890 (50 μm)
Hyflon Ion 790 (30 μm)

PFSA membranes, produced by Fumatech[®]:

Fumapem F950
Fumapem FZP-930^b

Aciplex membranes produced by Asahi Chemical Company

Flemion membranes produced by Asahi Glass Company

Dow membranes produced by DowChemical (not commercially available)

^a Prepared by casting procedure.

^b Composite PFSA-zirconium phosphate membrane.

In commercial materials, m varies from about 5 to 11. This generates an equivalent weight (EW) ranging from about 1000 to 1500 g of dry Nafion per mole of sulfonic acid groups, corresponding to an ion-exchange capacity ranging from 1.0 to 0.67 meq. g^{-1} .

Nafion membranes are designated by three numbers, the first two referring to the EW and the last one to the thickness. For example, the numbers 112, 115, and 117 refer to Nafion membranes having 1100 EW and a nominal thickness of 2×10^{-3} , 5×10^{-3} , and 7×10^{-3} inches, respectively. The molecular weight is in the range 10^5 – 10^6 Da.

Due to the presence of the electronegative fluorine atoms, the acidity of the $-\text{CF}_2-\text{SO}_3\text{H}$ groups is very high (the value of the Hammett acid function is equal to -12). Thus, this particular polymer electrolyte combines in one macromolecule the high hydrophobicity of the backbone with the high hydrophilicity of the sulfonic superacid groups.

2.15.4.1.1 Preparation

A sulfonylfluoride precursor of Nafion membranes is first obtained by copolymerization of sulfonylfluoridevinylether with tetrafluoroethylene. This $-\text{SO}_3\text{F}$ precursor is thermoplastic and therefore it can be extruded into membranes of required thickness. These precursor membranes possess Teflon-like crystallinity and this morphology persists even when the precursor is converted into, for example, Na^+ form. In the $-\text{SO}_3\text{H}$ form, the clustered

morphology, that is essential for proton percolation, is achieved only in hydrated dissociated forms. Extrusion of the sulfonylfluoride precursor can cause microstructural orientation in the machine direction resulting in some anisotropy in the swelling and proton-conductance properties of Nafion membranes.

2.15.4.1.2 Nafion morphology

It is widely accepted that hydrogen bonding between the $-\text{SO}_3\text{H}$ groups in Nafion is favored and, with even minimal amount of water, there is the formation of a continuous network of water among these groups. In other words, the sulfonic acid groups aggregate to form interconnected hydrophilic domains (or ionic clusters) and a nanoseparation of hydrophobic–hydrophilic domains takes place.

Whereas the connected hydrophilic domain is responsible for the transport of protons and water, the hydrophobic domain gives morphological stability to the matrix, avoiding excessive swelling unlike that produced due to cross-linking in ion-exchange resins.

Ion clustering in Nafion was first suggested by Gierke [15]. In this historical model, the ionic clusters were approximately spherical in shape with an inverted micellar structure. The cluster diameter, the number of exchange sites per cluster, and the number of water molecules per exchange site increase linearly with water content. To explain the percolation of protons, the spherical ionic clusters were proposed to be interconnected in the fluorocarbon backbone network by narrow channels of around 1 nm diameter. The growth of cluster size with increasing hydration was supposed to occur due to a combination of expansion in cluster size and a redistribution of the sulfonate sites to yield fewer clusters in a highly hydrated Nafion. Although this model gained fairly wide acceptance, it became clear that the spherical shape of the clusters is an oversimplification. Many other morphological models were therefore proposed. These models are shown and discussed in a recent review of Mauritz and Moore [16] and the interested reader is referred to this review. Here, only the recent representation of the hydrated morphology of Nafion derived from experiments and modeling is illustrated in **Figure 4**.

Presently, it is accepted that there is a continuous morphological reorganization of Nafion with hydration. According to Gebel, for a water-volume fraction greater than 0.5, the spherical interconnected ionic clusters are transformed in a connected network of

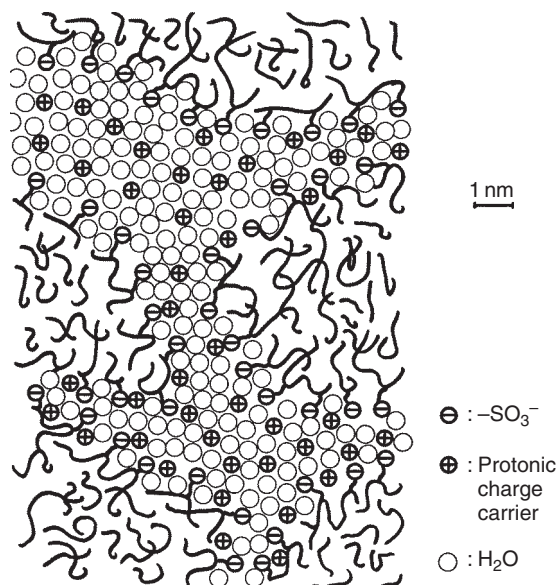


Figure 4 Schematic representation of the nanophase separation in hydrophobic/hydrophilic domains for Nafion. Reproduced with permission from Kreuer, K. D. *J. Solid State Ionics* **2001**, 185, 29–39.[20]

polymer rods and finally, for water-volume fraction greater than 0.75, a colloidal dispersion of rod-like particles is formed. We discuss this part in greater detail in Section 2.15.4.1.6.

For its unique properties, Nafion has been largely investigated (in the literature about 33 000 papers, patents, and so forth dealing with Nafion can be found, and the number is growing). However, although a significant number of critical relationships between structure and properties of Nafion have been elucidated, much remains to be discovered.

In our opinion, the difficulty in obtaining reliable comparisons between results obtained from various laboratories is due to the fact that Nafion is essentially composed of an amorphous matrix in which some microcrystalline phases are embedded. All amorphous materials can have metastable phases that can appear kinetically stable although thermodynamically unstable, as previously discussed. Many of the properties of Nafion determined in conditions of apparent equilibrium strongly depend on the previous pretreatment procedures of the membranes (Nafion history or memory). The thermal treatments in dry or nearly dry conditions are particularly important. Yeo and Yeager have observed that water uptake is reduced by thermal treatments and the original uptake is gained again only after long equilibration in warm water (see later). More

importantly, recent research performed in our laboratory showed that the memory effects of thermal treatment are particularly important at temperatures lower than 50 °C. Large hysteresis loops in the water uptake are therefore found at room temperature. These loops decrease with increasing temperature and completely disappear at about 140 °C. Since the same value of the water uptake was reached from two opposite directions, it can be concluded that memory effects due to previous treatments are completely cancelled at this temperature. As the pretreatments performed in the various laboratories can be considerably different, many different results, in some cases in apparent contrast, can also be found in recent literature. To avoid these unpleasant disagreements, all the measurements of Nafion, or similar ionomers, must be accompanied with complete information on the previous membrane pretreatments. In the case of comparison, very similar pretreatments of the membranes must be performed. A typical standard procedure useful for the elimination of metal cations and organic impurities is as follows: Nafion membranes, as received, are boiled for a half an hour in 3% H₂O₂, then half an hour in 0.5 M H₂SO₄, and later in distilled water for 1 h. The membrane is then dried at about 70–80 °C for 3 h and finally thermally treated in air at 120 °C for 15 h. This procedure is useful in comparing data collected in different laboratories because it assures that the characterization has been made on membranes that have received the same pretreatment and therefore have the same history.

2.15.4.1.3 Water uptake in liquid water at different temperatures

The water uptake of Nafion 117 when equilibrated in liquid water at different temperatures has been investigated by Hinatsu *et al.* [17] and Zawodzinsky *et al.* [18]. As the time necessary to reach equilibrium values was not reported, more recently, Alberti *et al.* [9] investigated the water uptake, for each temperature, as a function of the equilibration time. Furthermore, because water-uptake was influenced by the thermal annealing of the examined sample (see later), all measurements were made using a well-defined thermal treatment (120 °C in air for 15 h).

It was found that the time necessary for these membranes (thickness 180 μm) to attain equilibrium was very long (150–225 h). Furthermore, the percentage of equilibrium after 1 h is sufficiently high at low

temperatures but appreciably decreases with the increase in temperature of liquid water [9].

Both the long equilibration times and the decrease in kinetic rate with temperature can be explained if the total water uptake is the result of two distinct processes, the first, very fast and the second, very slow. Reasonably, the fast process can be attributed to the water diffusion within the thin membrane while the slow process can be associated with a modification of the Nafion conformation with temperature (see later).

The equilibrium λ values obtained at the various temperatures of water are plotted in **Figure 5**. In agreement with other authors [17, 18], the hydration process was not reversible when the temperature was again decreased. As indicated by the arrows, hydration reached at a given temperature tends to be maintained at lower temperatures (memory of the higher hydration attained). As is discussed later in detail, this behavior has to be related to the viscoelastic properties of perfluorinated ionomers.

2.15.4.1.4 Water-vapor sorption isotherms of Nafion

Water-uptake sorption isotherms for cross-linked ionomers with different degrees of cross-linking have already been discussed (see Section 2.15.2.6). We discuss now water-uptake sorption isotherms for ionomers that are not cross-linked. Nafion was chosen as a typical example of a noncross-linked ionomer since many investigations on its water-vapor sorption isotherms have been carried out.

Let us now examine before the effect of an applied external pressure on the isotherm 0 previously discussed using the model shown in **Figure 3**. For simplicity, we assume that the Nafion membrane examined is isotropic and therefore springs with equal elastic force are applied to the three-dimensional model (**Figure 3(a)**). The applied springs counteract the inner osmotic pressure and the water content inside the osmotic cell decreases. Note that the pressure exerted by the springs can be calculated by the following ideal experiment [9]. Suppose that the model is first equilibrated in water (100% RH). A given λ value, depending on the strength of the springs, is obtained at equilibrium (see **Figure 3(a)**). The springs are then removed and the tendency of the water to enter in the osmotic cell is now balanced by decreasing the external water activity. This can be obtained by equilibrating the cell at a certain external RH value whereby the same λ_{os} value is obtained (**Figure 3(b)**).

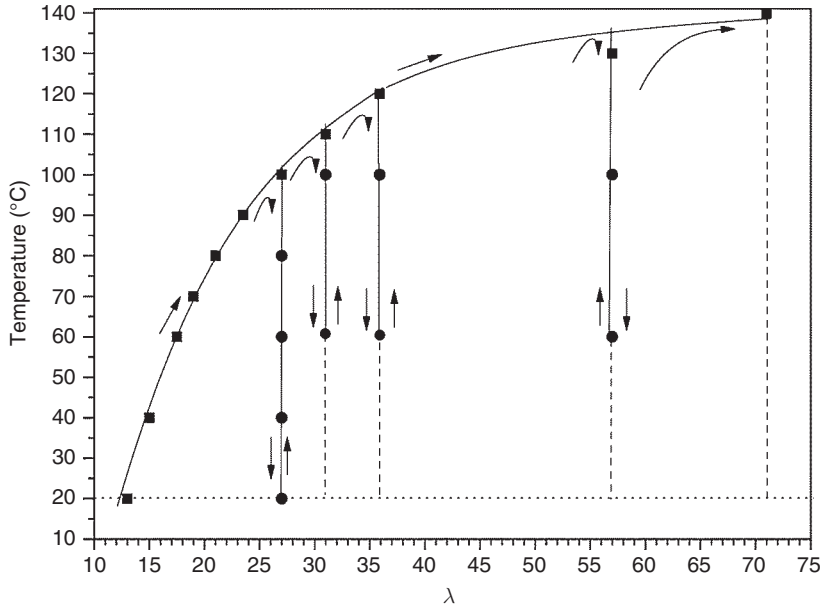


Figure 5 Water uptake of Nafion 117 (120–15) sample when equilibrated in liquid water at increasing temperatures between 20 and 140 °C. [9] At the indicated temperatures, the water was cooled to a lower temperature and then again warmed to the original temperature. The arrows show the path followed during the hydrothermal treatments. Reproduced with permission from Alberti, G., Narducci, R., Sganappa, M. *J. Power Sources* **2008**, 178, 575–583.

Since λ_{os} is not changed, the shift $(1-RH)$ corresponds to the pressure exerted on the osmotic cell by the applied springs. The value $(1-RH)$ can therefore be taken as an index of this pressure. We called this index of counter-elastic force (n_c) the shift in RH% unit in order to maintain the same value of λ_{os}

$$n_c = 100(1 - RH) \quad (8)$$

As an example, in **Figure 6**, these shifts are shown for a solution of phosphoric acid (**Figure 6(a)**) and for an ideal solution of Nafion (**Figure 6(b)**). We remember that isotherm 0 for an ideal solution of Nafion is obtained by plotting Equation (7).

The inner counter-elastic force of Nafion can therefore be estimated using Equation (8) by replacing RH with Equation (5). This equation, after simple rearrangements, becomes

$$n_c = 100/(\lambda_{tot} - \lambda_{hyd}) + 1 \quad (9)$$

Finally, if we assume $\lambda_{hyd} = 7$ for Nafion equilibrated in liquid water at 20 °C, we can write the simple relation

$$n_c = 100/(\lambda_{tot} - 6) \quad (10)$$

Note that the experimental determination of n_c for Nafion is very simple. It is sufficient to determine λ_{tot} in liquid water at 20 °C and apply Equation (10).

The expected water-vapor sorption isotherm at 20 °C of a given sample M will be the one obtained by shifting toward right, the isotherm 0 by the number of RH% units equal to the n_c value found for the examined sample.

Referring to Alberti *et al.* [9] for particulars, we note here that Equation (3) can be replaced by the equivalent equation

$$\lambda_{os} = RH\%/(100 - RH\%) \quad (11)$$

Thus, the shifted isotherms of **Figure 6** can also be calculated by the equation

$$\lambda_{os} = (RH\% - n_c)/(100 - (RH\% - n_c)) \quad (12)$$

From the above considerations of the water-vapor sorption isotherm of noncross-linked ionomers, it is evident that reproducible isotherms for Nafion can be expected only if samples of the same conformation (hence characterized by same n_c values) are examined. Therefore, as discussed in Alberti *et al.* [9], the large differences in the water-vapor sorption isotherms of Nafion reported by various authors [17–21] are not due to experimental errors but due to the fact that these isotherms have been determined with samples not having a defined history, very likely due to different thermal treatments, and hence exhibit different n_c values.

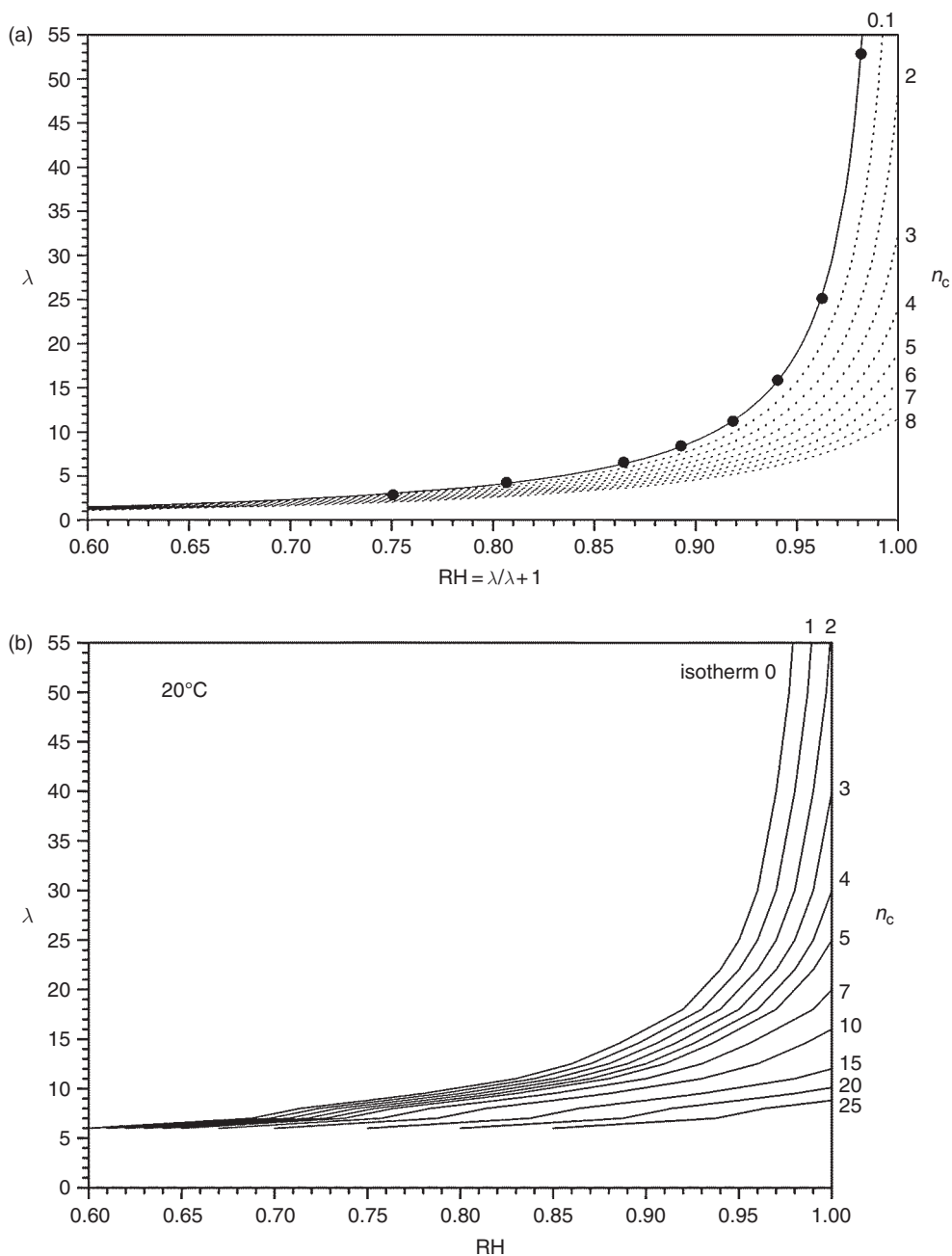


Figure 6 (a) Calculated water-vapor isotherms for a solution of phosphoric acid at 100 °C under different applied pressures. The original isotherm 0 is shifted toward right and cuts the abscissa axis at $RH = 1$. For each λ value corresponding to the cut, the difference $(1 - RH) \times 100$ is called n_c index. The meaning of this index is explained in the text. [9] (b) Calculated isotherm 0 at 20 °C for an ideal Nafion solution (i.e., without any applied counter-elastic force of the matrix and related shifted isotherms obtained when increasing counter-elastic forces, expressed as n_c indices, are applied as in real Nafion. Each n_c unit at 20 °C corresponds to an applied pressure of 1.35 MPa. [9] (a, b) Reproduced with permission from Alberti, G., Narducci, R., Sganappa, M. *J. Power Sources* **2008**, 178, 575–583.

It is of interest to compare the Nafion isotherms with those of cross-linked ionomers previously discussed (Figure 2). Note that the shape is very similar

and that the index of the counter-elastic force of the matrix plays the same function as the degree of cross-linking. However, the index of the counter-elastic

force of the matrix produces a marked dependence of many important properties of the noncross-linked ionomer on their previous history. Thus, n_c index can also be taken as an index of the actual conformation of the ionomer, which reassumes all the effects of the previous history of the ionomer membrane. For example, the low n_c values of Nafion samples after the standard treatment with H_2O_2 and sulfuric acid can be increased by thermal annealing. Thus, thermal treatments reinforce the morphological stability of the Nafion matrix in the same way as the degree of cross-linking reinforces styrene cation exchangers.

2.15.4.1.5 Curves T/n_c

We have seen that the Nafion conformation depends on RH, temperature, and time of equilibration. The introduction of the n_c index greatly facilitates the study of this dependence because this index, besides being proportional to the counter-elastic force of the ionomer matrix, can also be taken as an index of the actual ionomer conformation. For this reason, a systematic investigation on the variation of the initial n_c values of well-defined samples of Nafion membranes after equilibration for different times at different temperatures and different RH values was recently carried out [21].

In this study, the inner osmotic pressure is considered as a force for surface unit applied in the three

space directions to a viscoelastic polymeric matrix. In other words, the elastic spring balancing the inner osmotic pressure is replaced by a polymeric viscoelastic spring in which a permanent deformation can remain when the inner osmotic pressure is removed or reduced by decreasing the external RH and/or the system is quickly cooled.

A first set of Nafion 117 membranes, after a standard treatment with H_2O_2 and sulfuric acid was annealed in air at 120°C for 15 h. These samples had an initial n_c value of 13.6 and are denoted as Nafion 117 (120–15).

These samples were then equilibrated for 360 h at constant RH of 94% and at different temperatures. Then, the samples were equilibrated in liquid water at 20°C for 24 h, the water uptakes were determined, and n_c values were calculated using Equation (10). A plot of n_c obtained at different temperatures is shown in Figure 7.

At the same time, another set of membranes, after the above standard treatment, was hydrothermally treated in water at 130°C in order to obtain an initial n_c value of 1.5. In addition, these samples were equilibrated for 360 h at constant RH of 94% and at different temperatures and the results are reported in Figure 7 [21]. Note that the samples with an initial n_c value of 13.6 decrease their index of counter-elasticity when the temperature is increased, while

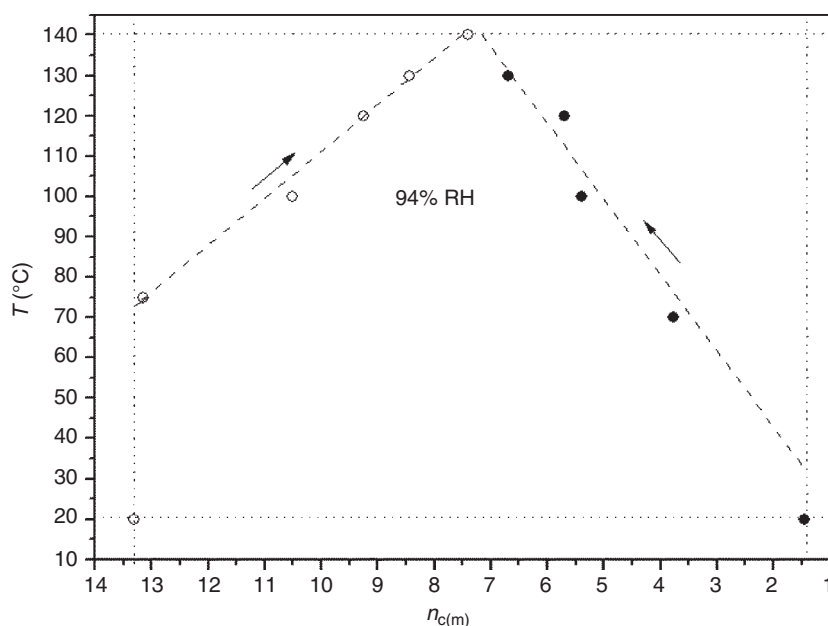


Figure 7 Change of n_c values at 94% RH when the temperature is increased from 20 to 140°C for two Nafion 117 membranes having initial n_c values of 13.6 and 2.1, respectively.

the opposite occurs for the samples with an initial n_c value of 2. Two series of n_c values are therefore obtained, corresponding to undersaturated and oversaturated hydrated samples, respectively. The arrows show the direction of these changes. Very large hysteresis loops between the two series of samples, indicating the presence of metastable conformations, can be noted. This hysteresis considerably decreases with increasing temperature and practically disappears at about 140 °C.

The memory due to permanent deformations and the evolution of this memory with the change in experimental conditions can therefore be quantitatively followed by the experimental determination of the variation of the counter-elastic index of the matrix with RH and temperature.

From a detailed examination of many other equilibrium data on the n_c evolution of undersaturated Nafion 1100 samples (see Figure 8), it was discovered that same n_c values can be obtained with different couples of RH–temperature. The couples RH– T giving the same n_c value are called iso-(RH; T) couples.

Note that the experimental T/n_c curves at constant RH values fit well parallel curves (shown in Figure 8 as dashed curves) to that obtained in liquid

water (i.e., RH = 100%). Although T/n_c curves of Nafion 117 are not linear in the large range of examined temperatures, two ranges of temperatures (20–50 °C and 50–140 °C) can be found where n_c is roughly linear with the temperature. The linearity in the range of 50–140 °C is of high interest for medium-temperature PEMFCs and therefore is examined here in more detail. Taking as reference the curve with RH = 100%, the linear dependence is of the type

$$n_{c(T)} = n_{c(50)} - (T - 50)/11.4 \quad (13)$$

Being 9.2 the experimental value of $n_{c(50)}$, we can write

$$n_{c(T)} = 9.2 - 0.087(T - 50) \quad (14)$$

in which $T \geq 50$ °C. Note that the initial $n_{c(T)}$ value at 50 °C decreases by one unit for each increment of temperature of 11.4 °C.

Let us now consider the change in the counter-elastic index with RH at constant temperature ($n_{c(RH)}$). This change can be easily found by recalling Equation (8). Taking RH = 100% as reference, we can write: $n_{c(RH)} = 100 - \text{RH}\%$. Thus, at constant temperature, $n_{c(RH)}$ increases by one unit for each decrement of one RH% unit. Therefore, taking

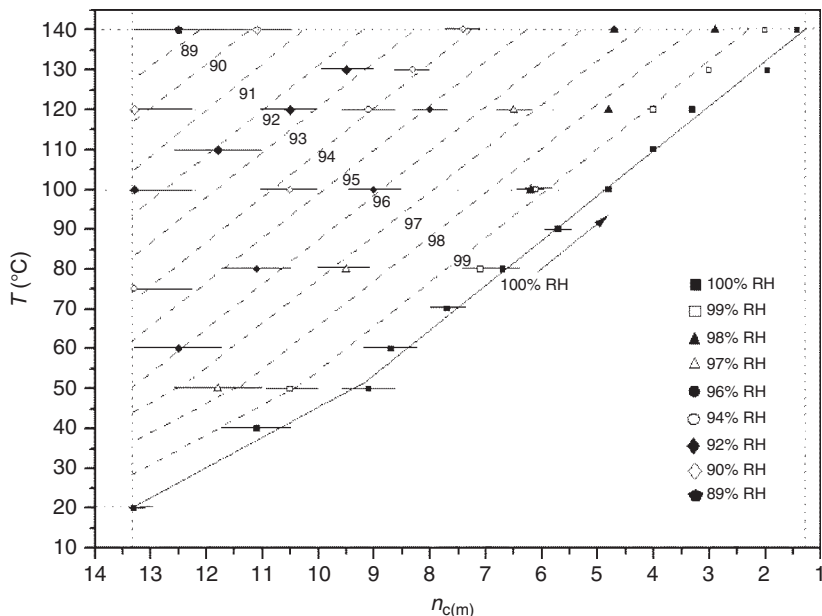


Figure 8 T – n_c plot for samples of Nafion 117 (120–15) equilibrated at the indicated RH values. The dashed lines were drawn by shifting the solid line referring to 100% RH by steps of 1 RH% unit, corresponding to 1 n_c unit (see Equation (8)). Note the good agreement between these dashed lines and experimental points.

$n_c = 9.2$ as reference point for $T = 50^\circ\text{C}$ and $\text{RH}\% = 100$, we can write

$$\begin{aligned} n_{c(\text{RH}-T)} &= n_{c(\text{RH})} + n_{c(T)} \\ &= 9.2 + (100 - \text{RH}\%) - 0.087(T - 50) \end{aligned} \quad (15)$$

Preliminary experiments seems to indicate that a general equation of the type

$$n_{c(\text{RH}-T)} = n_{c(50)} + (100 - \text{RH}\%) - k(T - 50) \quad (16)$$

is valid not only for Nafion 117 but also for many other PFSA membranes and, very probably, for all the ionomer membranes. This equation can be very useful to estimate the water uptake of an ionomer after equilibration at a couple of given $\text{RH}-T$ values. By recalling Equation (10), we can write

$$\lambda_{(\text{RH}-T)} = (100/n_{c(\text{RH}-T)}) + 6 \quad (17)$$

By replacing $n_{c(\text{RH}-T)}$ with Equation 15, we obtain

$$\lambda_{(\text{RH}-T)} = 100/((100 - \text{RH}\%) + 9.2 - 0.087(T - 50)) + 6 \quad (18)$$

Finally, by recalling Equation (12), we can also write the equivalent equation

$$\lambda_{(\text{RH}-T)} = (\text{RH}\% - n_{c(T)}) / (100 - (\text{RH}\% - n_{c(T)})) + 7 \quad (19)$$

As an example, suppose that we wish to estimate the value of water uptake of a sample Nafion 117 (120–15) after an equilibration at 80°C and $97\% \text{RH}$. By applying Equation (18), we obtain $\lambda_{(97\%; 80^\circ)} = 16.3$. Note that if the value of $n_{c(T)}$ obtained by Equation (14) (i.e., $n_{c(80^\circ)} = 6.59$) is placed in Equation (19), the same value for the water uptake is obtained. This estimated value is in good agreement with the experimental value of 16.2. Indeed, a very good agreement between estimated and experimental values has been obtained for many other samples of Nafion 117 membranes [21].

Furthermore, a similar comparison is presently being developed for Hyflon Ion membranes and a good agreement was found in this case too [22]. Thus, we believe that the calculated indices of conformation really allow reliable predictions for the equilibrium vapor water uptake of ionomers at different temperatures and RH values. This discovery is expected to be very important in the prediction of the fundamental properties of ionomer membranes in medium-temperature FCs.

2.15.4.1.6 Water uptake and tensile modulus

It is reasonable to suppose that tensile modulus and counter-elasticity of the matrix are related to each other. Therefore, the water uptake of many thermally treated samples was first determined by equilibrating the samples in liquid water at 20°C ; their n_c was then calculated using Equation (10) and their tensile modulus was experimentally determined. By plotting the tensile modulus as a function of water uptake in the λ_{tot} range 10–100 (see Figure 9), it was found that the experimental points fit a curve of the equation

$$E = 500/(\lambda_{\text{tot}} - 6) \quad (20)$$

where E is the tensile modulus (in MPa).

Note that this equation, apart from the multiplicative factor, is identical to that previously found for n_c (Equation (10)). The ratio between the two equations is $E/n_c = 5$. Both the tensile modulus and the counter-elastic index can be considered as indices of ionomer conformation. The determination of the counter-elastic index is, however, very simple and does not require an expensive apparatus.

Note that in both Equations (3) and (4), the protons are considered to be hydrated. It must be recalled that ion solvation is thermodynamically not well defined, and therefore the distinction between free solvent and solvation shells is, to a certain extent, arbitrary. Nevertheless, the hydration of the ions is largely accepted and greatly helps in understanding and explaining quite a number of phenomena, at least in a semi-quantitative way.

The classic representation of the Nafion conformations proposed by Gebel [23] for the various water contents is reported in Figure 10. To make clear the correspondence between the counter-elastic index and tensile modulus with Nafion conformation at various stages of hydration, the water-volume fraction has been converted into λ_{tot} and the corresponding n_c and E values are also reported.

Note that the n_c index can replace, in a more quantitative way, the qualitative nomenclature introduced by Yeo and Yeager [24] who, on the basis of thermal treatments performed, classified the membranes in E-, N-, and S-form (expanded-, normal-, and shrunken-form); a further shrunken-form (indicated as FS-form) was then introduced by Sone *et al.* [25].

Other important properties such as the conductivity and the electro-osmotic drag depend on the

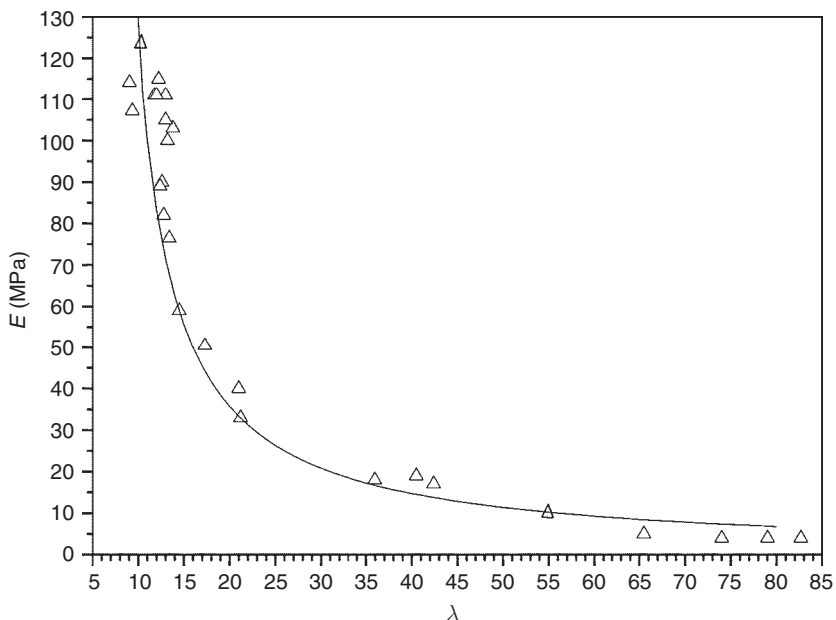


Figure 9 A plot of experimental tensile modulus (MPa) as a function of the water uptake (λ_{tot}) when the Nafion samples are equilibrated in liquid water at 20 °C. The experimental points fit the curves of Equation (15). Reproduced with permission from Alberti, G., Narducci, R., Sganappa, M. *J. Power Sources* **2008**, 178, 575–583.

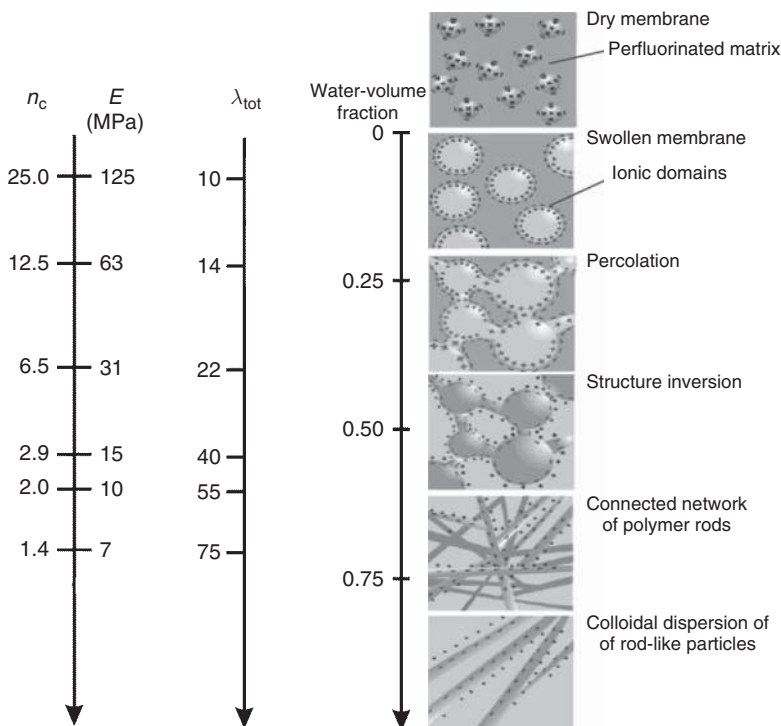


Figure 10 Changes in the morphological conformation of Nafion with increasing water content proposed by Gebel. The corresponding λ_{tot} , tensile modulus, and n_c values have been inserted to make evident the relationship between these properties and morphological conformation. The asterisked values are calculated using Equation (19). Reproduced with permission From Alberti, G., Narducci, R., Sganappa, M. *J. Power Sources* **2008**, 178, 575–583.

water content, while lower crossover of methanol is expected for high values of counter-elasticity index of the membranes.

Taking into account the previous discussions, it can be easily understood why previous thermal pretreatments greatly influence many important properties of Nafion membranes. In conclusion, if low RH is used to avoid cell pressurization, the conductivity of Nafion membranes becomes too low. On the other hand, if pressurization and high RH are used, an irreversible decay of Nafion conductivity takes place (see Section 2.15.4.1.8).

2.15.4.1.7 Proton conductivity

Hydration is a crucial aspect as far as proton conductivity of Nafion is concerned. In the presence of water, even for λ values as low as 3, the sulfonic groups are fully dissociated and proton conductivity arises from both proton diffusion (through water as vehicle) and intermolecular proton transfer (Grotthuss transport). The prevalence of one or the other mechanism depends on the hydration of the membrane [26]. It was observed that at high water content, the mobility of the protonic charge carriers (D_σ), as obtained from conductivity data through the Nernst–Einstein equation, is somewhat higher than the water self-diffusion coefficient ($D_{\text{H}_2\text{O}}$). This is due to the fact that intermolecular proton transfer is involved in the mobility of protonic charge carriers as in the case of dilute aqueous solutions of acids. However, with decreasing hydration, D_σ approaches $D_{\text{H}_2\text{O}}$ thus indicating the prevalence of the vehicle-type mechanism. At room temperature, the conductivity of Nafion 1100 shows a nearly linear dependence on λ and reaches 0.1 S cm^{-1} for $\lambda \approx 22$ [27, 28].

2.15.4.1.8 Instability maps for proton conductivity

Above about 80°C and at constant RH, the through-plane conductivity of Nafion 117 membranes (i.e., the conductivity measured with the electric field perpendicular to the membrane surface) remains nearly constant within a more or less wide temperature range [29]. However, when temperature and RH exceed certain critical values, the conductivity undergoes an irreversible decay: in particular, the higher the RH, the lower the temperature threshold at which the decay occurs. The analysis of the evolution of both frequency response and through-plane conductivity during the decay suggested that it arises from changes in the bulk-transport properties of the

Nafion membrane [30]. This was confirmed by determining, under stability conditions, the conductivity of membranes pretreated under decay conditions. Since the decay does not occur when the membrane is free to swell, it is inferred that it is associated with the anisotropic deformation taking place, under certain conditions of temperature and RH, when the membrane is constrained between the electrodes and forced to swell only in the direction parallel to the them. In this case, the effects of the anisotropic swelling can be considered to be similar to those provoked by an applied stretching parallel to the membrane surface. It must be pointed out that the conductivity decay was found to be associated with a significant decrease in the membrane density even in the anhydrous state thus indicating that the anisotropic membrane deformation gives rise to changes in the ionomer conformation. Research on the characterization of the membrane after decay is still in progress [31].

Conductivity measurements can therefore give information on the membrane dimensional stability under temperature and RH conditions that are of interest for FC operation but hardly accessible with the standard equipment for testing mechanical properties. More specifically, the results of systematic conductivity determinations at controlled temperature, RH, and applied pressure on the electrodes can be used to build up an instability map, that is, a plot providing the (T –RH) couples for which the conductivity is unstable. To define the instability domain, the conductivity is recorded as a function of time for a maximum of 150 h at controlled temperature and RH, using a new membrane sample each time in order to avoid the influence of previous thermal treatments. The border of the instability domain is the line separating the (T –RH) couples for which the conductivity is stable for at least 150 h from those for which the conductivity decays within 150 h.

Figure 11 shows the instability map of an as-received Nafion 117 membrane. The plot is step shaped because conductivity measurements were carried out at temperature and RH intervals of 5 – 10°C and 5 RH units, respectively. In the temperature range 70 – 130°C , the stability-to-instability transition is weakly affected by temperature changes, being confined between 95% and 100% RH. However, in the range 130 – 150°C , the transition is suddenly shifted to RH values as low as 70%. This behavior could be related to a different physical origin of the membrane swelling in the two ranges

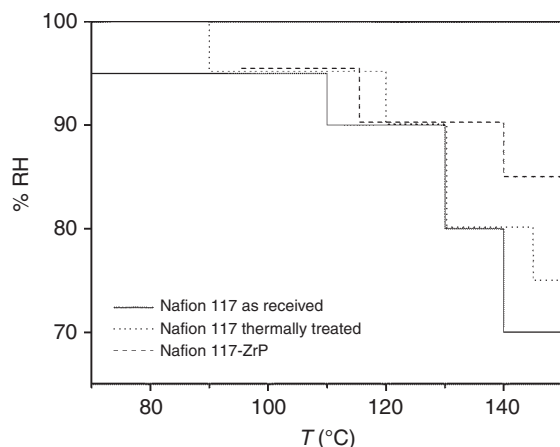


Figure 11 Instability maps for a Nafion 117 membrane as received, after thermal treatment for 2 h at 120 °C, and for a composite membrane containing *in situ* grown 10 wt.% ZrP. Reproduced with permission from Alberti, G., Casciola, M. In *Membrane Technology. Volume 2: Membranes for energy conversion*; Peinemann, K.V., Nunes, S. P., Eds. Wiley-VCH: Weinheim, 2008; Chapter 4.

of temperature. While at low temperature the instability is probably due to the sharp increase in hydration at RH close to 100% and to the consequent plasticizing effect of water, at high temperature, and in particular above the glass transition temperature, the weakening of the hydrophobic interactions between the ionomer chains is expected to lower the RH value at which the swelling occurs.

Thermal treatment of Nafion 117 (2 h at 120 °C) reduces the swelling and therefore an enhancement of stability is found between 70 °C and 100 °C. A significant increase in stability in the range 135–150 °C is achieved by growing nanosized zirconium phosphate within the hydrophilic clusters of Nafion 117 [32–34] (see Section 2.15.4.2.3). In agreement with the fact that the conductivity decay depends on the occurrence of an anisotropic deformation of the membrane, the enhanced stability of the conductivity is associated with higher values of the elastic modulus.

2.15.4.2 Composite Nafion Membranes

A possible approach to the solution of the problems hindering the development of suitable polymeric proton-conducting membranes for FCs working at low RH and temperature above 80 °C (see Introduction) is the improvement of the membrane properties through the incorporation, preferably on a nanometric scale, of an inorganic solid (filler) into the

polymer that serves as the matrix component. In a composite system, the filler–polymer interaction can range from strong (covalent, ionic) bonds to weak physical interaction. In the last decade, several studies reported consistent improvements of the performance of PEMFCs at temperatures above 80 °C when inorganic nanoparticles, such as metal oxides, zirconium phosphate/phosphonates, or heteropolyacids, were inserted into the polymeric membrane [34–37]. According to the literature, there are several membrane properties that may benefit from the presence of homogeneously dispersed inorganic fillers. These improvements include reduced permeation of reaction gases and radical species that could contribute to oxidative degradation, reduced swelling, enhanced water management and mechanical properties, as well as improved conductivity if the filler possesses higher proton conductivity compared to the neat polymer. The main types and properties of Nafion-based composite membranes are reviewed in the following sections.

2.15.4.2.1 Oxide-filled membranes

The first nanocomposite Nafion–SiO₂ membranes were obtained by growing the silica particles inside a preformed membrane [38–45]. According to this approach, tetraethoxysilane is incorporated into previously swollen Nafion membranes and then hydrolysed via a sol–gel reaction catalyzed by the superacid sulfonic groups of Nafion. The *in situ* grown silica is represented by the formula SiO_{2(1-x/4)(OH)_x} with *x* significantly higher than zero. Characterization of these nanocomposites by Fourier transform-infrared (FT-IR) spectroscopy [38], dielectric relaxation [39], thermal analysis [40], and small-angle X-ray scattering (SAXS) [41] suggested that the nanophase-separated morphology of Nafion acts as a template for the growth of the silica particles because the SAXS peak characteristic of quasi-ordered clusters in unfilled Nafion persists in the composites filled with silica. *In situ* hydrolysis of metal alkoxides was also used to prepare a number of nanocomposite Nafion membranes containing zirconium oxide [45, 46], titanium dioxide [46], mixed silicon–titanium oxide, and mixed silicon–aluminum oxide [47].

Nafion–MO₂ membranes (with M = Si, Ti, Zr) displayed a larger water uptake than Nafion in the range 90–120 °C at a given RH value [46] according to the sequence ZrO₂ > TiO₂ > SiO₂. However, in the same temperature range, only the Nafion–ZrO₂ membrane showed slightly higher conductivity than

Nafion. The FC performance of perfluorosulfonic membranes filled with *in situ* grown silica was tested in the temperature range 80 to 140 °C. At 130 °C, under a pressure of 3 atm, the composite membranes delivered a current density at least six times higher than that of the unmodified membranes due to their better water management and higher rigidity [48].

Nafion-SiO₂ composite membranes were also obtained by hydrolysis/polycondensation of alkoxy silanes in water-propanol Nafion solutions [49, 50]. Since the growth of the inorganic polymer is not limited to already existent ionic clusters, this approach offers the possibility of obtaining diverse morphologies depending on the amounts of the incorporated inorganic component. Transparent but brittle films, containing up to 54 wt.% silica, were obtained using tetraethylorthosilicate (TEOS) as a precursor to the inorganic polymer. The film flexibility was increased by replacing 1,1,3,3-tetramethyl-1,3-diethoxydisiloxane (TMDES) for TEOS. However, for substitution higher than 10%, phase separation was observed by electron microscopy. The conductivity of these films was determined by impedance measurements in the range 25–100 °C in an argon atmosphere. The highest conductivity ($\sigma \approx 2.10^{-3} \text{ S cm}^{-1}$ at 100 °C) was found for the film prepared using a Nafion/TEOS/TMDES mixture of composition 50/40/10 wt.%, respectively. Unfortunately, a direct comparison with the conductivity of Nafion under the same experimental conditions is missing.

On the basis of the same synthetic approach, a significant enhancement of the conductivity of Nafion 117 and recast Nafion was achieved with Nafion-bifunctional silica composite membranes, where sol-gel-derived silica particles bear both -SiOH and -SO₃H functional groups [51]. These membranes were prepared by casting Nafion-ethanol solutions mixed with sulfonated phenethylsilica sol. Due to the presence of sulfonated silica, their ion-exchange capacity increases linearly with silica loading from $0.9 \times 10^{-3} \text{ mol-SO}_3\text{H g}^{-1}$ for bare recast Nafion up to about $2 \times 10^{-3} \text{ mol-SO}_3\text{H g}^{-1}$ for 7.5 wt.% silica. Concomitantly, the water content per gram of dry membrane grows from 0.26 to 0.4 g at room temperature, and from 0.36 to 0.7 g at 80 °C. However, the degree of hydration, expressed as number of water molecules per sulfonic group, is fairly constant and nearly coincident with that of Nafion 117. At 80 °C and 100% RH, the conductivity of composite membranes loaded with 2.5–5 wt.% silica ($\sigma = 0.11$ and 0.23 S cm^{-1} , respectively) is 2.7–5.8

times higher than that of Nafion 117 under the same conditions.

Nanocomposite Nafion membranes can also be prepared by bulk mixing of a polymer solution with oxide nanocrystallites and subsequent casting. This approach was first described by Watanabe [52, 53]. Membranes containing 3 wt.% SiO₂ were also loaded with highly dispersed platinum by ion exchange of the Pt(II) tetra-amino complex and subsequent Pt reduction with hydrazine. When used as proton electrolytes in FCs, these membranes effectively suppressed H₂ and O₂ crossover and allowed efficient operation at 80 °C even without gas humidification. This is possible because the Pt particles catalyze the combination of crossover hydrogen and oxygen to generate water, which in turn is retained by the membrane.

Thermal treatment of Nafion-3 wt.% SiO₂ nanocomposite membranes by hot pressing up to 160 °C was shown to increase the polymer crystalline fraction [54, 55]. Direct methanol FCs based on this type of membrane and fed with 2M methanol were characterized by low methanol crossover and were able to work up to 145 °C with open circuit voltages of 0.82–0.95 V and power density peaks of 150–240 mW cm⁻² in air and oxygen, respectively.

The FC performance of Nafion filled with TiO₂ [56] and ZrO₂ [57] preformed nanoparticles turned out to be better than that of neat recast Nafion, over the temperature range 80–130 °C at 3 abs. bar H₂/air, with power densities of 500–600 mW cm⁻² at 110 °C and 250–390 mW cm⁻² at 130 °C.

A series of Nafion composite membranes containing binary oxides (M_xO_y, with M = Si, Ti, Zr, Hf, Ta, and W) were recently prepared by casting of mixtures of the polymer solution with the oxide nanopowder [58–60]. FT-IR and FT-Raman studies indicated that the hydrophobic polytetrafluoroethylene (PTFE) domains of these membranes consist of a blend of fluorocarbon chains with helical conformation 15₇ and 10₃ and that the presence of the filler affects the relative amounts of the two conformations. Particularly along group IV of the periodic table, the 10₃ conformation increases in the order Ti < Zr < Hf, while along group VI, it decreases in the order Hf > Ta > W. Four different species of water domains were detected including (1) bulk water, (2) water-solvating oxonium ions directly interacting with the sulfonic group, [H₃O⁺···SO₃⁻](H₂O)_m (3) acid water, [H₃O⁺···(H₂O)_n], and (4) water molecules interacting with metal oxoclusters, [M_xO_y···(H₂O)_m]. It was found that the amount of each type of water

domain depends on the acidity of the M_xO_y oxoclusters and that the mechanical, thermal, and dynamic characteristics of the host polymer depend on the dynamic cross-links, $R-SO_3H \cdots M_xO_y \cdots HSO_3-R$.

Composite Nafion membranes containing ZrO_2 nanoparticles covered with a layer of SiO_2 were also investigated [60]. These membranes are represented by the general formula Nafion/ $[(ZrO_2) \cdot (SiO_2)_{0.67}]_x$, where x is the $ZrO_2/-SO_3H$ molar ratio, and their conductivity is higher than that of neat Nafion for x in the range 0.313–1.253. The best conductivity value, 0.043 S cm^{-1} , was found for $x = 0.313$ at 135°C and 100% RH.

2.15.4.2.2 Heteropolyacid-filled membranes

Heteropolyacids, besides being electrocatalytically active [61, 62], possess strong acidity and high proton conductivity in hydrated form [63]. Most of them exhibit the Keggin structure and their molecules (about 1 nm in diameter) can be regarded as nanoparticles. Due to these characteristics, heteropolyacids appear to be suitable membrane fillers to increase the number of protonic carriers and to improve the hydrophilic character of the membranes.

Composite Nafion membranes containing heteropolyacids were obtained either by simple impregnation of preformed membranes with a heteropolyacid solution [64] or by mixing a Nafion solution with an appropriate amount of a heteropolyacid followed by casting [65,66]. Nafion-recast membranes loaded with silicotungstic acid (STA), phosphotungstic acid (PTA), and phosphomolybdic acid (PMA) were systematically investigated by ionic conductivity, water uptake, tensile strength, and thermal behavior determinations. In comparison with Nafion 117, all these membranes exhibited larger water uptake, higher proton conductivity especially at low RH and temperature above 100°C , enhanced FC performance with increasing temperature, but decreased tensile strength.

Although Nafion membranes filled with heteropolyacids maintain sufficient proton conductivities for FC operation at atmospheric pressure and temperature above 100°C , the membrane and the membrane electrode assembly (MEA) processing is severely curtailed because of the solubility of the filler in aqueous media. To overcome this problem, the protons of PTA were partially or fully exchanged by Cs^+ ions and the thus-modified PTA was used for the preparation of recast Nafion membranes [67]. After protonation treatment in 1 M sulfuric acid at

85°C , these membranes turned out to be more stable toward PTA leaching compared to those containing the unmodified heteropolyacid.

If the ion-exchange process is applied to an entire MEA, both the Nafion membrane and the Nafion in the electrodes are converted to a melt-processible form, which permits thermal treatment at temperatures as high as 200°C and greatly simplifies the MEA manufacturing [68]. The thermal treatment does not alter FC performance at elevated temperatures and low RH and does not hamper the integrity of the membrane.

A different approach to the problem of reducing the heteropolyacid leaching consists in the immobilization of the heteropolyacid onto a metal dioxide support, which in most cases is made of silica. Three main synthetic procedures were used to prepare the Nafion/metal oxide/heteropolyacid composite membranes: (1) impregnation of the heteropolyacid onto oxide particles, dispersion of the impregnated oxide within a Nafion solution, and membrane formation by casting of the Nafion/oxide/heteropolyacid mixture [69–72]; (2) formation of oxide particles by sol-gel within a preformed Nafion membrane and subsequent impregnation of the heteropolyacid onto the oxide [73]; and (3) hydrolysis of oxide precursors within a Nafion solution in the presence of the heteropolyacid and subsequent membrane formation by casting [74]. The last procedure was also used to obtain membranes where silica/heteropolyacid particles were functionalized with sulfonic groups to make the filler more hydrophilic [75].

2.15.4.2.3 Zirconium-phosphate-filled membranes

Nafion/zirconium phosphate (ZrP) composite membranes can be prepared using two main synthetic procedures. According to the earlier procedure, the filler is grown within the preformed ionomeric matrix by ion exchange of the ionomer protons with zirconium cationic species and subsequent membrane treatment with an aqueous solution of phosphoric acid [33, 76–86]. The more recent synthetic approach is based on the coprecipitation of the filler and the ionomer from a solution containing the ionomer and a ZrP precursor [32, 87].

The composite membranes prepared by the two procedures have similar physicochemical properties although the ZrP particles show different morphologies as proved by the different features of the X-ray powder patterns [32, 33, 80, 82, 88]. However, in both

cases, strong decrease of the crystallinity degree of the matrix with increase in the filler concentration is observed.

The presence of ZrP results in an increase of the tensile modulus and a decrease in the peak of the $\tan \delta$ versus temperature curve with increasing ZrP loading [32, 33, 82, 85]. In the presence of water, the differences in mechanical behavior between Nafion and its composites with ZrP are progressively less evident as the water content increases and nearly vanish at $\lambda \approx 12$.

In all cases, the composite membranes take up more water than Nafion at the same water activity, but both water and methanol diffusion are reduced relative to diffusion in the pure ionomer [80, 82]. In spite of the larger water content, the composite membranes do not show improved conductivity in comparison with Nafion over the entire range of water activities at temperatures from 80 to 140 °C [32, 33, 79, 80, 83, 85] with the only exception of a composite containing 10 wt.% ZrP which is slightly more conductive than Nafion for RH < 50% [86]. The fact that at 100% RH the activation energies for the conductivity of the composite membrane and unmodified Nafion are close indicates that the presence of ZrP does not significantly change the proton-conduction mechanism in well-hydrated membranes.

Taking into account that the conductivity of amorphous ZrP approaches 0.01 S cm^{-1} at 80 °C in water [89], it can be inferred that the lower proton conductivity of the composites arises to some extent from the fact the filler is less conductive than Nafion. Surprisingly, the Nafion/ZrP composites exhibit better FC performance than bare Nafion under high temperature and low RH conditions as reported independently by several groups [77–81]. Even when the performance is slightly decreased, as is the case of some composites in a direct methanol fuel cell (DMFC) environment [84], higher efficiencies can be reached due to the reduced methanol permeability of the composite membrane. The factors underlying the better FC performance above 100 °C at RH values lower than 100% are not yet completely understood. However, it was shown that after FC operation in hydrogen and oxygen at 130 °C, the Nafion 117 composite membranes underwent much less dimensional changes than bare Nafion 117 [84].

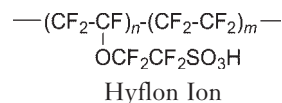
It was recently reported that treatment of Nafion/ZrP composite membranes with sulfophenylphosphonic acid leads to partial replacement of the

monohydrogen phosphate group of ZrP through a topotactic anion-exchange reaction. The membrane thus obtained showed improved conductivity and stiffness with respect to both Nafion 117 and the parent composite membrane [33].

2.15.4.3 Some Information on Dow and on Recent Hyflon Ion[®] Ionomers

A perfluorinated ionomer with a structure similar to that of Nafion, except for a shorter pendant side chain carrying the $-\text{SO}_3\text{H}$ ionogenic group, was prepared by Dow Chemicals in the beginning of the 1980s. This perfluorinated ionomer, called Dow ionomer, was investigated for its use in FCs with encouraging results by Ballard Power Systems. In spite of these results, the industrial development of the Dow ionomer was unfortunately abandoned, probably due to the high costs of the production.

Recently, a more simple route for the synthesis of the base monomer was found by Arcella *et al.* [90]. On the basis of these results, Solvay Solexis has restarted the development of membranes based on short side-chain perfluorinated ionomers. These membranes, known earlier by the trade name Hyflon Ion and recently renamed Aquivion[®] 2, are now under investigation with very interesting results.



A comparison of a polarization curve at 75 °C obtained with a Hyflon Ion membrane (EW = 850; thickness 50 μm) with that obtained with Nafion N112 shows that Hyflon Ion exhibits a slightly better performance, especially in FCs at high current density [91]. However, we note that it is too early for definitive conclusions because information on the previous pretreatments of the membranes was not reported. Furthermore, different equivalent weights for Hyflon Ion and Nafion were used. Memory effects of the employed membranes could therefore be responsible for the small variation of the performance curves.

Short-side-chain Dow membranes (therefore similar to Hyflon Ion) of different equivalent weights have been recently characterized with respect to water sorption, transport (proton conductivity, electro-osmotic drag, and water diffusion), microstructure, and viscoelastic properties as a function of temperature and degree of hydration [92].

The data are compared to those of Nafion 117. From this comparison, it is concluded that “no distinct differences in water and proton transport and in the hydrophobic/hydrophilic separation as a function of water-volume fraction were observed for Dow ionomers compared to Nafion of the same equivalent weight. The significant higher elastic modulus of Dow may be the sole reason for its superior performance as electrolyte in a fuel cell.”

Further research on these very interesting membranes is therefore necessary, especially concerning their conductivity at low RH and their durability in the temperature range 80–130 °C.

2.15.5 Nonperfluorinated Membranes

A different approach to overcome the limits of PFSA membranes is based on the design of nonfluorinated ionomer matrices with polyaromatic or inorgano-inorganic backbones. An excellent review covering the field of nonfluorinated ionomers till the year 2003 can be found in Reference 93.

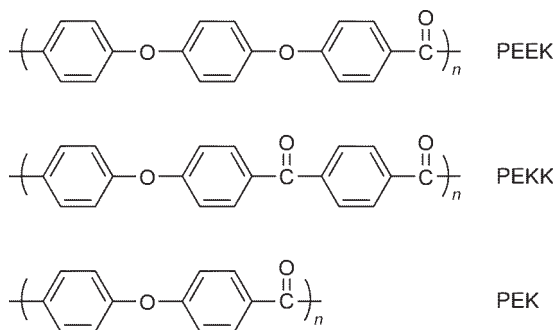
Polyaromatic ionomers are considered as an alternative to perfluorosulfonic ionomers mainly because of the good oxidation resistance of the aromatic carbon atoms. In most cases, the structure of these polymers is built up by $(-Ar-X-)$ units where Ar is an aryl group (e.g., phenyl) and X is an oxygen or sulfur atom (which gives the polymer chain a certain degree of flexibility and hence processability) or a group such as $-CO-$ in polyketones, $-SO_2-$ in polysulfones, $-COO-$ in polyesters, or $-NHCO-$ in polyamides. The polymer repeat unit may consist in a single $(-Ar-X-)$ unit or in a combination of different units.

Aromatic polymers are easily sulfonated by direct sulfonation using concentrated sulfuric acid, fuming sulfuric acid, or sulfur trioxide. This approach is simple but has some drawbacks such as the occurrence of side reactions, the possibility of degradation of the polymer backbone, and the fact that the thus-formed material is not necessarily the most stable toward desulfonation. Alternatively, the sulfonated polymer can be prepared by grafting of sulfonated functional groups onto a polymer main chain or by direct copolymerization of sulfonated monomers. The last approach allows building up repeat units that are sulfonated on deactivated sites. This is of interest because sulfonic groups attached to electron-deficient sites are expected to possess enhanced

stability and higher acidity [94]. Due to the very large variety of sulfonated aromatic polymers, only representative examples, including poly(ether ketone)s, poly(sulfone)s, poly(imide)s, block copolymers, and PBI, are reported in the following sections. Among polymers with inorgano-inorganic backbones, polyphosphazenes are briefly reviewed.

2.15.5.1 Poly(ether ketone)s

Poly(ether ketone)s **3** are a class of polyarylenes linked through varying sequences of ether (E) and ketone (K) units. Depending on the prevalence of one of the two units, these polyarylenes can be rich in ethers (e.g., poly(ether ether ketone) (PEEK)), ketones (e.g., poly(ether ketone ketone) (PEKK)), or balanced (e.g., poly(ether ketone) (PEK)). These polymers possess a number of beneficial attributes for use in FCs including good thermal stability, mechanical strength, and adequate conductivity, which is brought on by sulfonation of the polymer backbone. Oxidative and hydrolytic stability are expected to increase with increase in the proportion of ketone segments.



Examples of poly(ether ketone)s: poly(ether ether ketone), PEEK; poly(ether ketone ketone), PEKK; and poly(ether ketone), PEK

Sulfonated PEEK (sPEEK) and sulfonated poly(ether ether ketone ketone) (sPEEKK), with the sulfonic group attached to the aromatic backbone, were synthesized by either direct sulfonation or copolymerization of sulfonated monomers [93, 95–99]. sPEEK obtained by direct sulfonation is substituted at one of the four equivalent sites of the hydroquinone unit situated between the ether groups. The solubility of sPEEK in *N*-methylpyrrolidinone, ethanol, and water increases with the degree of sulfonation. Dissolution in *N*-methylpyrrolidinone, needed for membrane casting, is only possible for an exchange

capacity >0.9 meq. g^{-1} . The problem of the insolubility of the PEEK matrix can be overcome by introducing a phthalide unit in the PEEK repeat unit [97, 100].

The proton conductivity of sPEEK was determined under various conditions of temperature and RH for samples with different ion-exchange capacities [29, 97, 100, 101]. The dependence of conductivity on RH, at constant temperature, is affected to a great extent by the degree of sulfonation in such a way that the lower the degree of sulfonation, the more sensitive the conductivity to changes in RH. In addition, RH changes have greater influence on the sPEEK conductivity than on the Nafion conductivity: for RH decreasing from 100% to 66%, the conductivity of Nafion and that of sPEEK, with ion-exchange capacity of 1.6 meq. g^{-1} , decrease by a factor of 4 and 10, respectively. This is probably due to the stronger acidity of the sulfonic function in Nafion and to the fact that the higher flexibility and hydrophobic character of the perfluorinated backbone of Nafion in comparison with the polyaromatic backbone of sPEEK results in a larger nanophase separation in Nafion and, consequently, in more continuous conduction pathways even at low hydration levels [102]. In agreement with this model, it was found that, at $150^\circ C$ and 75% RH, the conductivity of sPEEK approaches that of Nafion 117 only for ion-exchange capacity as high as 2.48 meq. G^{-1} [29].

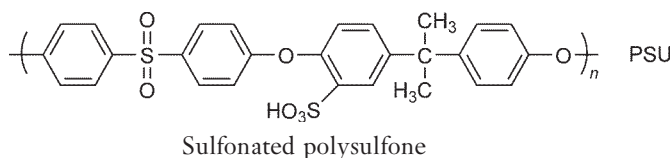
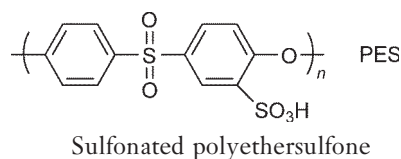
The different morphology of sulfonated poly(ether ketone)s in comparison with Nafion also seems to be responsible for the low methanol permeability of this class of polymers. Either sPEEK [98] and sPEEK [99] synthesized by copolymerization or sPEEK obtained by direct sulfonation [96, 97] shows conductivity to methanol permeability ratios that in

the most favorable cases are nearly 10 times higher than that of Nafion.

sPEEK was also investigated as an ionomer in the catalyst layer for DMFC [103]. The optimum ion-exchange capacity and content (wt.%) of the SPEEK ionomer in the catalyst layer were found to be, respectively, 1.33 meq. g^{-1} and 20 wt.%. The MEAs fabricated with sPEEK membrane and sPEEK ionomer in the electrodes exhibited superior performance in DMFC compared to those fabricated with Nafion ionomer.

2.15.5.2 Poly(sulfone)s

The repeat unit in poly(arylene ether sulfone)s, PES **4**, consists of phenyl rings separated by alternate ether and sulfone linkages, whereas the repeat unit in polysulfones, PSU **5**, contains four phenyl rings connected through two ether oxygens, one sulfone, and one 2-propylidene group. Direct sulfonation reactions lead to PES and PSU sulfonated at the *ortho* position to the ether bond which for PSU is located in the bisphenol A part of the repeating unit. However, it is also possible to sulfonate PSU at the *ortho* position to the sulfone group through a procedure based on PSU lithiation, reaction with SO_2 , and oxidation of the sulfinate thus obtained [104]. Polymers with ion-exchange capacity in the range 2.5 – 3 meq. g^{-1} have conductivity close to that of Nafion, but they swell significantly at $80^\circ C$ [105].



Sulfonated PES, with the sulfonic function at the more stable *ortho*-sulfone position, was obtained by copolymerization of 4,4'-dichlorodiphenylsulfone, 4,4'-biphenol, and 3,3'-disulfonate-4,4'-dichlorodiphenylsulfone [106, 107]. These random copolymers

showed a hydrophilic/hydrophobic nanophase separation where the hydrophilic domains increase in size with the percentage of the disulfonated monomer (%DS, in mol.) and form a semicontinuous morphology once %DS exceeds 50 mol.%.

Concomitantly, an increase in water uptake is observed and a dramatic swelling occurs for %DS > 50 mol.%. The proton conductivity of these membranes is in the range 0.08–0.17 S cm⁻¹ for ion-exchange capacities of 1.72 and 2.42 meq. g⁻¹, respectively.

High-molecular-weight sulfonated poly(arylene ether benzonitrile) random copolymers, containing as much as 55 mol.% disulfonate units, were also synthesized from disulfonated and unsulfonated monomers [108]. In comparison to Nafion, the benzonitrile-containing copolymers with up to 35 mol.% disulfonated units adsorbed less moisture. Nevertheless, the conductivity of the 35 mol.% disulfonated copolymer reached values of 0.1 S cm⁻¹ at 110 °C under full hydration, therefore being comparable with the conductivity of Nafion 117.

Disulfonated PES copolymers containing carboxylic acid groups were synthesized for use in DMFC applications [109]. Membrane conductivity and methanol permeability increased with the degree of sulfonation and the conductivity to permeability ratio reached a maximum for 20 mol.% disulfonated units, being about 5 times higher than the value correspondingly found for Nafion 117.

Sulfonated poly(arylene) ionomers containing merely electron-accepting sulfone units (–SO₂–) connecting the phenyl rings have recently been synthesized and characterized, particularly with respect to properties relevant for their application as membrane materials in PEMFCs [110]. This new class of polymers with extremely electron-deficient aromatic rings shows very high thermal, thermooxidative, and hydrolytic stabilities, low solubilities, and reduced swelling in water at high temperature compared to other sulfonated poly(arylene)s. The latter property allows for the preparation of membranes with very high ion-exchange capacity and high proton conductivity especially at high temperature and low humidification, which makes them

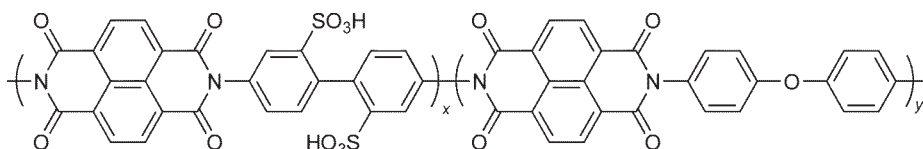
interesting materials for applications such as PEMFCs.

PSUs with very high local concentration of immobilized phosphonic acid were prepared by grafting poly(vinylphosphonic acid) side chains onto the PSU backbone through anionic polymerization of diethyl vinylphosphonate initiated from lithiated PSU [111]. Fully polymeric membranes were cast from solutions and showed high thermal stability with decomposition temperatures exceeding 300 °C in air. These membranes are among the best proton-conducting polymers under nominally dry conditions, their conductivity being around 5 × 10⁻³ cm⁻¹ at 120 °C.

2.15.5.3 Poly(imide)s

Polyimides are a class of high-performance materials endowed with thermal and oxidative stability. Random and sequenced sulfonated copolyimides were first synthesized by reacting naphthalene-1,4,5,8-tetracarboxylic dianhydride (NTCD) or 4,4'-oxydiphthalic anhydride (OPDA) with 4,4'-diaminobiphenyl-2,2'-disulfonic acid (BDSA) and nonsulfonated diamine monomers, such as 4,4'-oxydianiline (ODA), according to a two-step synthetic route, which allows for controlling the degree of sulfonation [112–116]. The first step consists in the preparation of short sequences of BDSA condensed with NTCD or OPDA. Adjusting the diamine/dianhydride molar ratio allows the creation of different block lengths of the sulfonated sequence. In the second step, the degree of sulfonation can be precisely controlled by regulating the unsulfonated diamine/BDSA molar ratio.

As far as use in FC is concerned, naphthalenic polyimides **6** are favored in comparison with phthalic polyimides because of lower ring strain and better hydrolytic stability [117, 118].



Naphthalenic sulfonated polyimide

However, naphthalenic polyimides have, in general, poor solubility, which limits membrane formation. Solubility can be enhanced by making a suitable choice of the unsulfonated diamine used in the second step of the synthesis [114, 119].

For BDSA–NTCD–ODA polyimides, the length of the ionic block for a constant equivalent weight has greater influence on water uptake than a variation of the equivalent weight for polymers with the same block length [115]. Surprisingly, while the number of water molecules per sulfonic group increases when the ionic block length (x) goes from 1 to 9, the highest proton conductivity ($\sim 0.02 \text{ S cm}^{-1}$ for fully hydrated membranes at room temperature) is observed for $x=3$. According to Rozière *et al.* [93], this behavior seems to indicate the occurrence of microstructural changes accompanying the increase in the ionic block length. It should be pointed out that both the number of water molecules per ionic group and conductivity are systematically lower for random microstructures than for sequenced copolymers [120].

In general, sulfonated polyimides may have proton conductivity as high as that of Nafion membranes with significantly lower methanol permeability [117, 118, 121]. Nevertheless, the short-term DMFC performance of several polyimide copolymer membranes is similar to the performance of Nafion 117.

Successful H_2 /air FC operation for 5000 h at 80°C and 60–90% RH was recently reported for sulfonated polyimides containing aliphatic segments [122, 123]. This is one of the longest successful FC operations for a nonfluorinated ionomer membrane. It was suggested that introducing aliphatic segments both in the main and side chains could significantly reduce the chances of nucleophilic attack by water onto the imide linkage resulting in enhanced hydrolytic stability of polyimide ionomers [124].

2.15.5.4 Sulfonated Block Copolymers

Block copolymers are made of chemically different oligomers (blocks) which are bonded to each other by covalent bonds [125, 126]. Blocks of different nature (in terms of length, structure, and chemical composition) tend to produce a nanophase separation, which is responsible for the fact that, in general, these copolymers combine the properties of different polymers.

Block copolymers, where oligomers with a high density of acid groups (e.g., sulfonic groups) are covalently linked to neutral oligomers, are expected

to show improved properties as compared to the properties of random copolymers of the same chemical composition. The nanoseparated morphology should favor the formation of proton-conducting channels, hinder the swelling of the conducting phase, and therefore reduce methanol permeability. Due to these properties, block copolymers appear to be suitable materials for the design of proton-conducting polymer electrolytes for FC applications.

As in the case of random copolymers, the preparation of sulfonated block copolymers can be performed either by postsulfonation of nonsulfonated block copolymers at specific sites (e.g., phenyl rings of styrene block copolymers) or from monomers bearing sulfonic acid groups. A large number of styrene block copolymers were prepared by postsulfonation. Here, only the phenyl rings of the poly(styrene) blocks are sulfonated so as to favor a phase separation between the different types of blocks [127–133]. The poly(styrene)–poly(isobutylene)–poly(styrene) system may be taken as a representative example [129] showing highly ordered hexagonally packed poly(styrene) cylinders dispersed in a poly(isobutylene) matrix. As demonstrated by TEM and SAXS, the distances between the cylinders remain unchanged with increase in poly(styrene) weight fraction while the cylinder diameters are changed.

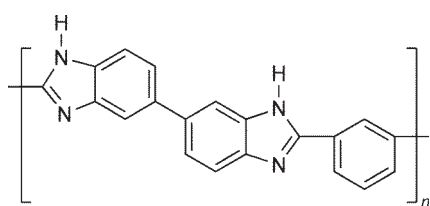
A large variety of sulfonated poly(imide)s, sulfonated poly(aramide)s, and sulfonated poly(arylene ether)s were synthesized from sulfonated monomers. An interesting comparison between the properties of sulfonated poly(aramide) block copolymers, obtained from terephthaloyl chloride, 4,4'-oxydianiline, and 2,5-diamino benzene sulfonic acid, and those of the corresponding random copoly(aramide)s was reported [134, 135]. It was shown by wide-angle X-ray diffraction that a phase separation between sulfonated and nonsulfonated domains occurs when the block length exceeds 20 repeating units. This phase separation results in reduced methanol permeability and water uptake as compared to Nafion and random copoly(aramide)s. In particular, water uptake decreases with increase in block length, thus proving that nonsulfonated domains restrict the swelling of the sulfonated blocks. Unfortunately, the performance of these poly(aramide) membranes in DMFC is much lower than that of Nafion because the lower methanol diffusion coefficient is also associated with a reduced proton-diffusion coefficient.

A comparison between the properties of block and random copolymers, in terms of proton conductivity, methanol permeability, and self-diffusion coefficient

of water, was also recently reported for biphenol-based sulfonated poly(arylene ether sulfone)s [136]. As far as proton conductivity is concerned, it is interesting to observe that the decrease in conductivity caused by the decrease in hydration is much more severe for the random than for the block copolymers. Moreover, under partial hydrated conditions, the block copolymers with the longest blocks are more conductive than those with the shortest blocks in spite of their very low ion-exchange capacity and hydration level. This is an indirect evidence for an increase in both nanophase separation and connectivity between hydrophobic domains with an increase in block length. Another remarkable difference is found for methanol permeability, which increases with the water-diffusion coefficient for random copolymers and is independent of it for block copolymers. Therefore, it can be inferred that in ionomeric block copolymers, the hard hydrophobic segments lower methanol permeability, while the soft hydrophilic segments provide pathways for water and proton transport.

2.15.5.5 Polybenzimidazole

PBI **7** is a basic polymer endowed with high thermal stability (melting point above 600 °C) and good mechanical properties (glass transition temperature of 425–436 °C). PBI by itself is a poor proton conductor for use in FCs with conductivity of the order of 10^{-4} S cm⁻¹ at 40 °C–100% RH [137].



Polybenzimidazole

Attempts were made to improve PBI conductivity by replacing the imidazole hydrogen with aryl or alkyl substituents. This method provides an opportunity to tune the properties of the polymer by a suitable choice of the substituent. Benzylsulfonate PBI [137, 138] is remarkably stable in solutions of 3% H₂O₂/F(II) and starts to decompose at around 360 °C, thus showing better thermal stability than polyarylene polymers where the sulfonic group is directly bonded to the polymer chain. By increasing the degree of sulfonation up to about 75%, the water

uptake increases up to 33 wt.%, corresponding to a λ value ≈ 7 almost independent of the degree of sulfonation. Concomitantly, the conductivity increases up to a maximum of 0.02 S cm⁻¹ in water at 25 °C [95]. The same synthetic route used to graft benzylsulfonate groups onto the PBI backbone allowed the preparation of phosphorylated PBI, but the resulting polymer turned out to be insoluble in organic solvents and could not be recast as a membrane [139].

The presence of a basic site on the imidazole ring (pK ≈ 5.5) enables PBI to form blends with polymers possessing acidic groups, such as sulfonated poly(etheretherketone) and poly(sulfone) [140], sulfonated poly(phosphazene) [141], sulfonated poly(arylenethioether)s [142], poly(arylenethioether-sulfone) [143], and Nafion [144, 145]. PBI complexes with strong acids, such as sulfuric and phosphoric acid [93], exhibit strongly enhanced proton conductivity in comparison with pristine PBI. However, this is not the case of complexes of PBI with heteropolyacids, unless the heteropolyacid is supported by high surface area inorganic fillers such as hydrated silica, which is supposed to provide the main pathway for proton conduction [146–148]. Relatively high conductivity ($\approx 4 \times 10^{-3}$ S cm⁻¹ at 200 °C and 100% RH) was instead obtained for PBI incorporating 50 wt.% zirconium tricarboxybutylphosphonate [149].

Due to its outstanding properties in terms of high proton conductivity in a dry environment at temperature up to 200 °C, low methanol permeability, and low electro-osmotic drag, the system PBI/H₃PO₄ was extensively investigated since 1994 [150–156]. PBI/H₃PO₄ complexes can be obtained by treating the preformed PBI membrane with phosphoric acid, by casting from a solution of PBI and phosphoric acid in trifluoroacetic acid [93], or by casting from solutions of high-molecular-weight PBI in polyphosphoric acid (PPA) [157]. In comparison with pristine PBI, the acid-doped polymer has much higher oxygen and hydrogen permeability, higher by a factor of ≈ 1000 and ≈ 100 , respectively.

The investigation of the influence of molecular weight on the physicochemical properties of PBI [158, 159] showed that at high acid-doping levels the membrane mechanical strength decreases especially for polymers of low molecular weight. However, changes in molecular weight do not significantly affect proton conductivity. For the PBI/H₃PO₄ complex containing 1 mol H₃PO₄ per repeat unit ($x=1$), the proton conductivity is lower than 0.01 S cm⁻¹ even at 200 °C. However, at the

same temperature, the conductivity rises from 0.025 S cm^{-1} for $x=2$ to about 0.08 S cm^{-1} for $x=5.7$ and is high enough for FC applications [160]. The effect of inorganic fillers on the conductivity of acid-doped PBI was also investigated. Membranes containing 15–20 wt.% of zirconium phosphate had higher conductivity than the corresponding PBI/ H_3PO_4 membranes, while membranes incorporating 20–30% PWA or SiWA had higher or comparable conductivity to PBI/ H_3PO_4 up to 140°C .

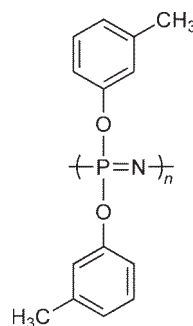
One of the problems affecting PBI/ H_3PO_4 membranes is the leaching of phosphoric acid at high acid-doping levels, although it was shown that for PBI/PPA membranes operating at 160°C , the phosphoric acid loss was sufficiently low to allow long-term operation ($>10\,000 \text{ h}$) [161]. To improve the acid-retention capability, it was recently suggested to increase the basic character of the polymer by modulating the number of nitrogen atoms and their interspacing along the polymer backbone [162], or to incorporate silica particles functionalized by an imidazole-based structure endowed with good chemical affinity toward PBI [163]. In both cases, a significant improvement in the acid-retention properties and in the permanent proton conductivity after leaching was observed.

A different approach to avoid electrolyte leaching consists in replacing H_3PO_4 with polyvinylphosphonic acid (PVPA) which is immobilized in the PBI matrix by interpenetration, cross-linking, and covalent bonding [164]. PBI acts as the host material, while the continuous PVPA network serves as proton electrolyte. This membrane was designed for application in DMFC and showed lower methanol crossover, water permeability, and electro-osmotic drag in comparison with Nafion 117.

Finally, a novel sulfonated polybenzimidazole (SOPBI) was recently synthesized [165] by postsulfonation of the phenylene rings of poly[2,2'-(*p*-oxydiphenylene)-5,5'-bibenzimidazole]. SOPBI showed good solubility in dimethyl sulfoxide (DMSO), high thermal stability, good film-forming ability, and excellent mechanical properties. Cross-linked SOPBI membranes were also prepared by thermal treatment of phosphoric-acid-doped SOPBI membranes and showed much improved water stability and radical oxidative stability in comparison with the corresponding noncross-linked ones, while the proton conductivity did not change largely ($\approx 0.15 \text{ S cm}^{-1}$ at 120°C in water).

2.15.5.6 Poly(phosphazene)s

Among inorgano-organic polymers, poly(phosphazene)s have been considered as suitable materials for the development of proton-conducting membranes due to their good thermal and chemical stability. Poly(phosphazene)s have a general formula $(\text{P}(\text{R}^1\text{R}^2)=\text{N})_n$ and their backbone consists of alternating phosphorus and nitrogen atoms where each phosphorus atom bears two side groups (R^1, R^2). The main advantage of poly(phosphazene)s over hydrocarbon polymers is that the properties of the final polymer can be finely tuned through substitution reactions starting from the parent poly(dichlorophosphazene), PDCP, because the chlorine atoms can be replaced by a wide range of different organic groups. Aryloxy substituted poly(phosphazene)s **8** are considered the most suitable poly(phosphazene)s for PEM application because they combine barrier properties with high thermal, mechanical, and chemical stability. In addition, the possibility to cross-link the polymer by γ radiation allows one to improve mechanical and barrier properties.



Poly[bis(3-methylphenoxy)phosphazene]

Several poly(dialkylphosphazene)s, with R^1 and $\text{R}^2 = \text{methyl, ethyl, propyl, butyl, and hexyl}$, were considered for the fabrication of solid proton-conducting electrolytes due to their capacity to be protonated at the chain N atom [166]. Protonated poly(dipropylphosphazene) ($\text{PDPrP} \cdot n\text{H}^+$) turned out to be the most suitable material for this purpose. The proton conductivity and structural stability of $\text{PDPrP} \cdot n\text{H}^+$, with molar ratio $\text{H}_3\text{PO}_4/\text{N} = 1$, in composite materials with poly(phenylsulfide) (Ryton[®]) were studied by thermal analysis, nuclear magnetic resonance (NMR) spectroscopy, and impedance measurements as a function of temperature up to 79°C at RH in the range 0–33%. The highest conductivity turned out to be of the order of $10^{-3} \text{ S cm}^{-1}$ at 52°C at 33% RH.

In order to make the poly(phosphazene)s highly proton conductive, acidic groups including $-\text{SO}_3\text{H}$, $-\text{PO}_3\text{H}_2$, and sulfonimide were incorporated into the polymer matrix. Two main approaches can be used to prepare sulfonated poly(phosphazene)s. In the first, an already sulfonated aryl oxide, alkoxide, or arylamine substitutes the chlorine atoms in PDCP. According to this approach, PCDP reacts in a single step with the nucleophile–hydroxybenzenesulfonic acid using the noncovalent protection of the sulfonic acid functionality with a hydrophobic ammonium ion which can be easily removed after the completion of the reaction [167].

Alternatively, sulfonation can be carried out on unsubstituted aryloxy side groups of a preformed poly(phosphazene). Chlorosulfonic acid, concentrated and fuming sulfuric acids [168], SO_3 [169, 170], and propanesulfone [171] were used as sulfonating agents. Sulfonation with chlorosulfonic and fuming sulfuric acid causes some chain cleavage depending on temperature and reaction time, while sulfonation of side groups with SO_3 occurs after the initial formation of a complex between SO_3 and the backbone nitrogen atoms.

The conductivity at 25 °C of noncross-linked sulfonated poly(bis(3-methylphenoxy) phosphazene) with an ion-exchange capacity in the range 0.8–1.6 meq. g^{-1} increases with water uptake from 10^{-8} to 10^{-7} S cm^{-1} up to about 0.1 S cm^{-1} for membrane swelling in the range 0–50 vol.% [172]. It was also shown [173] that cross-linked sulfonated poly(bis(3-methylphenoxy)phosphazene) with an ion-exchange capacity of 1.4 meq. g^{-1} combines high conductivity (0.08 S cm^{-1} at 65 °C) with a low methanol-diffusion coefficient ($8.5 \cdot 10^{-8}$ $\text{cm}^2 \text{s}^{-1}$ at 45 °C).

Sulfonated poly(bis(phenoxy) phosphazene) (s-BPP) was used to build up an interpenetrating network with cross-linked hexa(vinyloxyethoxy)cyclotriphosphazene (CVEEP) [174]. Membranes with good mechanical and thermal stabilities were obtained exhibiting high ion-exchange capacities in the range of 1.62–1.79 mmol g^{-1} and proton conductivity of 0.013 S cm^{-1} at 25 °C in liquid water. The same sample held at 75 °C and $\approx 12\%$ RH exhibited a conductivity as high as 5.7×10^{-3} S cm^{-1} .

Phenylphosphonic acid functionalized poly(phosphazene)s cosubstituted with 4-methylphenoxy or 3-methylphenoxy side groups were synthesized for use in PEMFCs. These materials have an ion-exchange capacity in the range 1.17–1.43 meq. g^{-1} and ionic conductivity between 0.04 and 0.06 S cm^{-1} in fully hydrated state at room

temperature [175]. At 80 °C, the methanol crossover of 3-methylphenoxy-substituted poly(phosphazene) in contact with a 3 M aqueous solution is about 12 times lower than that of Nafion. In general, when the conductivity to permeability ratio is taken into account, it is found that sulfonated poly(phosphazene) is superior to Nafion 117 at temperatures below 85 °C while the phosphonated poly(phosphazene) is superior to Nafion 117 over a wide temperature range of 22–125 °C [176].

Cross-linked poly(phosphazene) incorporating 17% aryl sulfonimide side groups and 83% *p*-methylphenoxy side groups had a conductivity of about 0.07 S cm^{-1} in fully hydrated state at room temperature [177] and a maximum power density of 0.47 W cm^{-2} at 1.29 A cm^{-2} and 80 °C [178] was achieved with an MEA based on this kind of poly(phosphazene).

2.15.6 Some Final Remarks

We have seen that in spite of the large number of polymeric proton-conducting membranes available today, the obtained characteristics for their applications in commercial FCs are, unfortunately, rather far from those required by automotive firms, especially with regard to price, durability, and proton conductivity at medium temperatures and low RH.

When hydrogen is used as a fuel, car producers would like to operate in the temperature range 70–130 °C with FCs not pressurized and using only the water produced at the cathode for hydration of the membrane (i.e., at low RH). The recently modified PFSA membranes are able to work, at least for short times, in the desired range of temperature, but the conductivity in the RH range 20–40% is too low even for very thin membranes. Conversely, PBI– H_3PO_4 membranes are able to work well even at low RH values in the range 150–200 °C, but their conductivity is unfortunately too low in the temperature range 70–130 °C and other problems, such as phosphoric acid leaching, are not completely solved. Therefore, efforts must be made either for increasing the conductivity of PFSA membranes at RH lower than about 30–40% or for increasing the conductivity and decreasing phosphoric acid leaching of PBI– H_3PO_4 membranes in the temperature range 70–130 °C.

Note that, if hydrogen containing traces of CO is used as fuel, the temperature range 150–220 °C could be accepted since the poisoning effect of CO is

strongly reduced at high temperature. Concerning membrane durability, efforts must be made in finding more stable ionomer matrices. At the same time, efforts must also be made for reducing the oxygen permeability as much as possible from the cathodic to the anodic side of the membrane as this may lead to the formation of very aggressive oxidized radicals when the oxygen reaches the anode. According to Alberti [21], an excessive hydration of the membrane is usually made in the starting procedures, and this could be responsible for the fast membrane degradations observed in swelling–de-swelling cycles, especially at high temperatures. As discussed before, while hydration equilibrium with the external vapor water activity is quickly attained, the change in the matrix conformation provoked by hydration at high RH values can remain for long times even at high temperatures when vapor activity is drastically reduced. Thus, if the membrane during the starting procedures is equilibrated at a level of hydration greater than that attained under the stationary working conditions, it is reasonable that an appreciable increase of oxygen permeability can take place in these permanently deformed membranes when the water content is decreased.

On the basis of what is discussed above, it is therefore advisable to prepare annealed perfluoro-sulfonic acid membranes exhibiting n_c indexes appropriate to the final working conditions while procedures of excessive hydration in the starting procedures must be avoided. Some experiments on membrane durability at medium temperatures, performed in collaboration with the Electricité de France (EDF), are in progress. Although it is too early for definitive conclusions, the first results seem to confirm our expectations and are really very encouraging [179].

When a liquid aqueous solution of methanol is used as fuel, present research efforts must be mainly addressed to reduce the methanol permeability of the membranes. Here, as discussed before, the presence of nanoparticles in the ionomer matrix could be very important. An association with appropriate thermal annealing could also be of interest.

Finally, PBI–H₃PO₄ membranes working in the temperature range 200–220 °C and/or with reduced permeability to methanol should be the preferred ones when methanol–water vapor mixtures are used as fuel.

In conclusion, the availability of new, less expensive, and efficient membranes is an important

key for the future development of PEMFCs for automotive application and appreciable progress in this field can be expected in the forthcoming years. However, the problem of the commercial production of medium-temperature PEMFCs cannot be solved even with substantial progress in proton-conducting membranes if more efficient and less expensive catalytic electrodes with long durability are not found.

References

- [1] Doyle, M., Rajendran, G. Perfluorinated Membranes. In *Handbook of Fuel Cells*; Vielstich, W., Lamm, A., Gasteiger, H. A., Eds.; Wiley: New York, 2003; Vol. 3, pp 351–395.
- [2] Bockris, J. O. M., Reddy, A. K. N., Eds. *Modern Electrochemistry*; Plenum: New York, 1977; Vol. 2.
- [3] Hagenmuller, P., Van Gool, W., Eds. *Solid Electrolytes: General Principles, Characterization, Materials, Applications*; Academic Press: New York, 1978.
- [4] Colomban, Ph., Ed. *Proton Conductors: Solids, Membranes and Gels – Materials and Devices*; Cambridge University Press: Cambridge, 1992.
- [5] Adams, B. A., Holmes, E. L. *J. Soc. Chem. Ind.* **1935**, 54, 1T–6T.
- [6] Helfferich, F. *Ion Exchange*; McGraw-Hill: New York, 1962.
- [7] Gregor, H. P. *J. Am. Chem. Soc.* **1948**, 70, 1293–1298.
- [8] Boyd, G. E., Soldano, B. A. *Z. Elektrochem.* **1953**, 57, 162–166.
- [9] Alberti, G., Narducci, R., Sganappa, M. *J. Power Sources* **2008**, 178, 575–583.
- [10] Paddison, S. J. *Annu. Rev. Mater. Res.* **2003**, 33, 289–319.
- [11] Schroeder, P. Z. *Phys. Chem.* **1903**, 45, 57–69.
- [12] Onishi, L. M., Prausnitz, J. M., Newman, J. J. *Phys. Chem. B* **2007**, 111, 10166–10173.
- [13] Li, Q., He, R., Jensen, J. O., Bjerrum, N. J. *Chem. Mater.* **2003**, 15, 4896–4915.
- [14] Liu, W., Zuckerbrod, D. J. *Electrochem. Soc.* **2005**, 152, A1165–A1170.
- [15] Gierke, T. D., Munn, G. E., Wilson, F. C. *J. Polym. Sci. Part B: Polym. Phys.* **1981**, 19, 1687–1704.
- [16] Mauritz, K. A., Moore, R. B. *Chem. Rev.* **2004**, 104, 4535–4585.
- [17] Hinatsu, J. T., Mizuhata, H., Takenaka, J. *J. Electrochem. Soc.* **1994**, 141, 1493–1498.
- [18] Zawodzinski, T. A., Derouin, C., Radzinski, S., et al. *J. Electrochem. Soc.* **1993**, 140, 1041–1047.
- [19] Reucroft, P. J., Rivin, D., Schneider, N. S. *Polymer* **2002**, 43, 5157–5161.
- [20] Kreuer, K. D. *J. Solid State Ion.* **2001**, 185, 29–39.
- [21] Alberti, G., Narducci, R. *Fuel Cells* **2009**, 9, 410–420.
- [22] Alberti, G., Narducci, R. (in preparation).
- [23] Gebel, G. *Polymer* **2000**, 41, 5829–5838.
- [24] Yeo, R. S., Yeager, L. Structural and Transport Properties of Perfluorinated Ion-Exchange Membranes. In *Modern Aspects of Electrochemistry No 16*; Conway, B. Z., White, R. E., Bockris, J. O. M., Eds.; Plenum: New York, 1985; pp 437–504.
- [25] Sone, Y., Ekdunge, P., Simonsson, D. *J. Electrochem. Soc.* **1996**, 143, 1254–1259.
- [26] Kreuer, K. D. *J. Membr. Sci.* **2001**, 185, 29–39.

- [27] Zawodzinski, T. A., Derouin, C., Radzinski, S., et al. *J. Electrochem. Soc.* **1993**, *140*, 1041–1047.
- [28] Kreuer, K. D. *Solid State Ion.* **1997**, *97*, 1–15.
- [29] Alberti, G., Casciola, M., Massinelli, L., Bauer, B. J. *Membr. Sci.* **2001**, *185*, 73–81.
- [30] Casciola, M., Alberti, G., Sganappa, M., Narducci, R. J. *Power Sources* **2006**, *162*, 141–145.
- [31] Alberti, G., Casciola, M., Sganappa, M., Narducci, R. (in progress).
- [32] Alberti, G., Casciola, M., Capitani, D., et al. *Electrochim. Acta* **2007**, *52*, 8125–8132.
- [33] Casciola, M., Capitani, D., Comite, A., et al. *Fuel Cells* **2008**, *8*, 217–224.
- [34] Alberti, G., Casciola, M. Membrane for Medium Temperature PEFC Based on Nafion filled with Layered Matel Phosphates and Phosphonates. In *Membrane Technology. Volume 2: Membranes for Energy Conversion*; Peinemann, K. V., Nunes, S. P., Eds.; Wiley-VCH: Weinheim, 2008; Chapter 4, pp 97–122.
- [35] Jones, D. J., Rozière, J. Inorganic/Organic Composite Membranes. In *Handbook of Fuel Cells – Fundamental, Technology and Applications*; Vielstick, W., Gasteiger, H. A., Lamm, A., Eds.; Wiley: New York, 2003; Vol. 3, pp 447–455.
- [36] Alberti, G., Casciola, M. *Annu. Rev. Mater. Res.* **2003**, *33*, 129–154.
- [37] Premchand, Y. D., Di Vona, M. L., Knauth, P. Proton-Conducting Nanocomposites and Hybrid Polymers. In *Nanocomposites*; Knauth, P., Schoonman, J., Eds. Springer: Cambridge, 2008; pp 71–117.
- [38] Mauritz, K. A., Warren, R. M. *Macromolecules* **1989**, *22*, 1730–1734.
- [39] Mauritz, K. A., Stefanithis, I. D. *Macromolecules* **1990**, *23*, 1380–1388.
- [40] Stefanithis, I. D., Mauritz, K. A. *Macromolecules* **1990**, *23*, 2397–2402.
- [41] Mauritz, K. A., Stefanithis, I. D., Davis, S. V., et al. *J. Appl. Polym. Sci.* **1995**, *55*, 181–190.
- [42] Gummaraju, R. V., Moore, R. B., Mauritz, K. A. *J. Polym. Sci. B: Polym. Phys.* **1996**, *34*, 2383–2392.
- [43] Mauritz, K. A. *Mater. Sci. Eng. C* **1998**, *6*, 121–133.
- [44] Baradie, B., Dodelet, J. P., Guay, D. *J. Electroanal. Chem.* **2000**, *489*, 101–105.
- [45] Apichatchutapan, W., Moore, R. B., Mauritz, K. A. *J. Appl. Polym. Sci.* **1996**, *62*, 417–426.
- [46] Jalani, N. H., Dunn, K., Datta, R. *Electrochim. Acta* **2005**, *51*, 553–560.
- [47] Shao, P. L., Mauritz, K. A., Moore, R. B. *Chem. Mater.* **1995**, *7*, 192–200.
- [48] Adjemian, K. T., Srinivasan, S., Benziger, J., Bocarsly, A. B. *J. Power Sources* **2002**, *109*, 356–364.
- [49] Zoppi, R. A., Yoshida, I. V. P., Nunes, S. P. *Polymer* **1997**, *39*, 1309–1315.
- [50] Zoppi, R. A., Nunes, S. P. *J. Electroanal. Chem.* **1998**, *445*, 39–45.
- [51] Wang, H., Holmberg, B. A., Huang, L. et al., *J. Mater. Chem.* **2002**, *12*, 834–837.
- [52] Watanabe, M., Uchida, H., Seki, Y., Emori, M., Stonehart, P. *J. Electrochem. Soc.* **1996**, *143*, 3847–3852.
- [53] Watanabe, M., Uchida, H., Emori, M. *J. Electrochem. Soc.* **1998**, *145*, 1137–1141.
- [54] Antonucci, P. L., Aricò, A. S., Creti, P., Ramunni, E., Antonucci, E. *Solid State Ion.* **1999**, *125*, 431–437.
- [55] Arico, A. S., Antonucci, V. Polymeric Membrane Electrochemical Cell Operating at Temperatures above 100 °C. Eur. Pat. Ep 0926754, 30 June 1999.
- [56] Sacca, A., Carbone, A., Passalacqua, E., et al. *J. Power Sources* **2005**, *152*, 16–21.
- [57] Sacca, A., Gatto, I., Carbone, A., Pedicini, R., Passalacqua, E. *J. Power Sources* **2006**, *163*, 47–51.
- [58] Di Noto, V., Gliubbizzi, R., Negro, E., Pace, G. *J. Phys. Chem. B* **2006**, *110*, 24972–24986.
- [59] Di Noto, V., Gliubbizzi, R., Negro, E., Vittadello, M., Pace, G. *Electrochim. Acta* **2007**, *53*, 1618–1627.
- [60] Di Noto, V., Piga, M., Piga, L., Polizzi, S., Negro, E. *J. Power Sources* **2008**, *178*, 561–574.
- [61] Savadogo, O. *J. Electrochem. Soc.* **1992**, *139*, 1082–1087.
- [62] Savadogo, O. *Electrochim. Acta* **1992**, *37*, 1457–1459.
- [63] Nakamura, O., Ogino, I., Kodama, T. *Solid State Ion.* **1981**, *3/4*, 347–351.
- [64] Malhotra, S., Datta, R. *J. Electrochem. Soc.* **1997**, *144*, L23–L26.
- [65] Tazi, B., Savadogo, O. *Electrochim. Acta* **2000**, *45*, 4329–4339.
- [66] Tazi, B., Savadogo, O. *J. New Mater. Electrochem. Syst.* **2001**, *4*, 187–196.
- [67] Ramani, V., Kunz, H. R., Fenton, J. M. *Electrochim. Acta* **2005**, *50*, 1181–1187.
- [68] Ramani, V., Kunz, H. R., Fenton, J. M. *J. Power Sources* **2005**, *152*, 182–188.
- [69] Staiti, P., Aricò, A. S., Baglio, V., Lufrano, F., Passalacqua, E., Antonucci, V. *Solid State Ion.* **2001**, *145*, 101–107.
- [70] Carbone, A., Casciola, M., Cavalaglio, S., et al. *J. New Mater. Electrochem. Syst.* **2004**, *7*, 1–5.
- [71] Shao, Z. G., Joghee, P., Hsing, I. M. *J. Membr. Sci.* **2004**, *229*, 43–51.
- [72] Sacca, A., Carbone, A., Pedicini, R., et al. *Fuel Cells* **2008**, *8*, 225–235.
- [73] Xu, W., Lu, T., Liu, C., Xing, W. *Electrochim. Acta* **2005**, *50*, 3280–3285.
- [74] Ramani, V., Kunz, H. R., Fenton, J. M. *J. Membr. Sci.* **2006**, *279*, 506–512.
- [75] Kim, H. J., Shul, Y. G., Han, H. *J. Power Sources* **2006**, *158*, 137–142.
- [76] Grot, W., Rajendran, G. Membranes Containing Inorganic Fillers and Membrane and Electrode Assemblies and Electrochemical Cells Employing Same. Pat. WO9629752, 29 September 1996.
- [77] Yang, C., Srinivasan, S., Aricò, A. S., Creti, P., Baglio, V., Antonucci, V. *Electrochem. Solid-State Lett.* **2001**, *4*, A31–A34.
- [78] Yang, C., Costamagna, P., Srinivasan, S., Benziger, J., Bocarsly, A. B. *J. Power Sources* **2001**, *103*, 1–9.
- [79] Costamagna, P., Yang, C., Bocarsly, A. B., Srinivasan, S. *Electrochim. Acta* **2002**, *47*, 1023–1033.
- [80] Yang, C., Srinivasan, S., Bocarsly, A. B., Tulyani, S., Benziger, J. B. *J. Membr. Sci.* **2004**, *237*, 145–161.
- [81] Lee, H.-K., Kim, J.-I., Park, J.-H., Lee, T.-H. *Electrochim. Acta* **2004**, *50*, 761–768.
- [82] Bauer, F., Willert-Porada, M. *J. Membr. Sci.* **2004**, *233*, 141–149.
- [83] Bauer, F., Willert-Porada, M. *J. Power Sources* **2005**, *145*, 101–107.
- [84] Bauer, F., Willert-Porada, M. *Fuel Cells* **2006**, *6*, 261–269.
- [85] Bauer, F., Willert-Porada, M. *Solid State Ion.* **2006**, *177*, 2391–2396.
- [86] Bauer, F., Müller, A., Wojtkowiak, A., Willert-Porada, M. *Adv. Sci. Technol.* **2006**, *45*, 787–792.
- [87] Alberti, G., Casciola, M., Donnadio, A., Narducci, R., Pica, M., Sganappa, M. *Desalination* **2006**, *199*, 280–282.
- [88] Truffier-Boutry, D., De Geyer, A., Guetaz, L., Diat, O., Gebel, G. *Macromolecules* **2007**, *40*, 8259–8264.
- [89] Alberti, G., Casciola, M., Costantino, U., Levi, G., Ricciardi, G. *J. Inorg. Nucl. Chem.* **1978**, *40*, 533–537.

- [90] Arcella, V., Ghielmi, A., Tommasi, G. *Ann. N.Y. Acad. Sci.* **2003**, *984*, 226–244.
- [91] Ghielmi, A., Vaccarone, P., Troglia, C., Arcella, V. *J. Power Sources* **2005**, *145*, 108–115.
- [92] Kreuer, K. D., Schuster, M., Obliers, B., et al. *J. Power Sources* **2008**, *178*, 499–509.
- [93] Rozière, J., Jones, D. J. *Annu. Rev. Mater. Res.* **2003**, *33*, 503–555.
- [94] Kim, Y. S., Wang, F., Hickner, M., et al. *J. Polym. Sci. Part B: Polym. Phys.* **2003**, *41*, 2816–2828.
- [95] Jones, D. J., Rozière, J. *J. Membr. Sci.* **2001**, *185*, 41–58.
- [96] Li, L., Zhang, J., Wang, J. *J. Membr. Sci.* **2003**, *226*, 159–167.
- [97] Drioli, E., Regina, A., Casciola, M., Oliveti, A., Trotta, F., Massari, T. *J. Membr. Sci.* **2004**, *228*, 139–148.
- [98] Li, X., Zhao, C., Lu, H., Wang, Z., Na, H. *Polymer* **2005**, *46*, 5820–5827.
- [99] Gil, M., Ji, X., Li, X., Na, H., Hampsey, J. E., Lu, Y. *J. Membr. Sci.* **2004**, *234*, 75–81.
- [100] Regina, A., Fontananova, E., Drioli, E., Casciola, M., Sganappa, M., Trotta, F. *J. Power Sources* **2006**, *160*, 139–147.
- [101] Bauer, B., Jones, D. J., Rozière, J., et al. *J. New Mater. Electrochem. Syst.* **2000**, *3*, 93–98.
- [102] Kreuer, K.-D. *J. Membr. Sci.* **2001**, *185*, 29–39.
- [103] Lee, J. K., Li, W., Manthiram, A. *J. Power Sources* **2008**, *180*, 56–62.
- [104] Kerres, J., Cui, W., Reichle, S. *J. Polym. A* **1996**, *34*, 2531–12438.
- [105] Nolte, R., Ledjef, K., Bauer, M., Mülhaupt, R. *J. Membr. Sci.* **1993**, *83*, 211–220.
- [106] Wang, F., Hickner, M., Kim, Y., Zawodzinski, T. A., McGrath, J. E. *J. Membr. Sci.* **2002**, *197*, 231–242.
- [107] Wang, F., Hickner, M., Ji, Q., et al. *Macromol. Symp.* **2001**, *175*, 387–396.
- [108] Summer, M., Harrison, W. L., Weyers, R. M., et al. *J. Membr. Sci.* **2004**, *239*, 199–211.
- [109] Kim, D. S., Shin, K. H., Park, H. B., Chung, Y. S., Nam, S. Y., Lee, Y. M. *J. Membr. Sci.* **2004**, *278*, 428–436.
- [110] Schuster, M., Kreuer, K.-D., Andersen, H. T., Maier, J. *Macromolecules* **2007**, *40*, 598–607.
- [111] Parvole, J., Jannasch, P. *Macromolecules* **2008**, *41*, 3893–3903.
- [112] Cornet, N., Diat, O., Gebel, G., Jousse, F., Marsacq, D., Mercier, R., Pineri, M. *J. New Mater. Electrochem. Syst.* **2000**, *3*, 33–42.
- [113] Genies, C., Mercier, R., Sillion, B., et al. *Polymer* **2001**, *42*, 5097–5105.
- [114] Genies, C., Mercier, R., Sillion, B., Cornet, N., Gebel, G., Pineri, M. *Polymer* **2001**, *42*, 359–373.
- [115] Cornet, N., Beaudoin, G., Gebel, G. *Sep. Purif. Technol.* **2001**, *22–23*, 681–687.
- [116] Besse, S., Capron, P., Diat, O., et al. *J. New Mater. Electrochem. Syst.* **2002**, *5*, 109–112.
- [117] Einsla, B. R., Hong, Y. T., Kim, Y. S., Wang, F., Gunduz, N., McGarth, J. E. *J. Polym. Sci. Part A: Polym. Chem.* **2004**, *42*, 862–874.
- [118] Einsla, B. R., Kim, Y. S., Hickner, M. A., et al. *J. Membr. Sci.* **2005**, *255*, 141–148.
- [119] Vallejo, E., Pourcelly, G., Gavach, C., Mercier, R., Pineri, M. *J. Membr. Sci.* **1999**, *160*, 127–137.
- [120] Hickner, M. A., Ghassemi, H., Kim, H. S., Einsla, B. R., McGrath, J. E. *Chem. Rev.* **2004**, *104*, 4587–4611.
- [121] Miyatake, K., Zhou, H., Matsuo, T., Uchida, H., Watanabe, M. *Macromolecules* **2004**, *37*, 4961–4966.
- [122] Asano, N., Aoki, M., Suzuki, S., Miyatake, K., Uchida, H., Watanabe, M. *J. Am. Chem. Soc.* **2006**, *128*, 1762–1769.
- [123] Aoki, M., Asano, N., Miyatake, K., Uchida, H., Watanabe, M. *J. Electrochem. Soc.* **2006**, *153*, A1154–A1158.
- [124] Miyatake, K., Zhou, H., Watanabe, M. *Macromolecules* **2004**, *37*, 4956–4960.
- [125] Meier-Haack, J., Taeger, A., Vogel, C., Schlensted, K., Lenk, W., Lehmann, D. *Sep. Purif. Technol.* **2005**, *41*, 207–220.
- [126] DeLuca, N. W., Elabd, Y. A. *J. Polym. Sci. Part B: Polym. Phys.* **2006**, *44*, 2001–2225.
- [127] Serpico, J. M., Ehrenberg, S. G., Fontanella, J. J., et al. *Macromolecules* **2002**, *35*, 5916–5921.
- [128] Weiss, R. A., Sen, A., Willis, C. L., Pottick, L. A. *Polymer* **1991**, *32*, 1867–1874.
- [129] Storey, R. F., Baugh, D. W. *Polymer* **2000**, *41*, 3205–3211.
- [130] Kim, J., Kim, B., Jung, B. *J. Membr. Sci.* **2002**, *207*, 129–137.
- [131] Lu, X. Y., Steckle, W. P., Weiss, R. A. *Macromolecules* **1993**, *26*, 5876–5884.
- [132] Edmondson, C. A., Fontanella, J. J., Chung, S. H., Greenbaum, S. G., Wnek, G. E. *Electrochim. Acta* **2001**, *46*, 1623–1628.
- [133] Elabd, Y. A., Napadensky, E., Sloan, J. M., Crawford, D. M., Walker, C. W. *J. Membr. Sci.* **2003**, *217*, 227–242.
- [134] Taeger, A., Vogel, C., Lehmann, D., et al. *React. Funct. Polym.* **2003**, *57*, 77–92.
- [135] Taeger, A., Vogel, C., Lehmann, D., Lenk, W., Schlensted, K., Meier-Haack, J. *Macromol. Symp.* **2004**, *210*, 175–184.
- [136] Roy, A., Hickner, M. A., Yu, X., Li, Y., Glass, T. E., McGrath, J. E. *J. Polym. Sci. Part B: Polym. Phys.* **2006**, *44*, 2226–2239.
- [137] Glipta, X., Hadda, M. E., Jones, D. J., Rozière, J. *Solid State Ion.* **1997**, *97*, 323–331.
- [138] Pu, H., Liu, Q. *Polym. Intl.* **2004**, *53*, 1512–1516.
- [139] Rikukawa, M., Sanui, K. *Prog. Polym. Sci.* **2000**, *25*, 1463–1502.
- [140] Walker, M., Baumgartner, K.-M., Kaiser, M., Kerres, J., Ulrich, A., Rauchle, E. *J. Appl. Polym. Sci.* **1999**, *74*, 67–73.
- [141] Wycisk, R., Lee, J. K., Pintauro, P. N. *J. Electrochem. Soc.* **2005**, *152*, A892–A898.
- [142] Lee, J. K., Kerres, J. *J. Membr. Sci.* **2007**, *294*, 75–83.
- [143] Bai, Z., Price, G. E., Yoonessi, M., Juhl, S. B., Durstock, M. F., Dang, T. D. *J. Membr. Sci.* **2007**, *305*, 69–76.
- [144] Ainla, A., Brandell, D. *Solid State Ion.* **2007**, *178*, 581–585.
- [145] Wycisk, R., Chisholm, J., Lee, J., Lin, J., Pintauro, P. N. *J. Power Sources* **2006**, *163*, 9–17.
- [146] Staiti, P., Freni, S., Hocevar, S. *J. Power Sources* **1999**, *79*, 250–255.
- [147] Staiti, P., Minutoli, M. *J. Power Sources* **2001**, *94*, 9–13.
- [148] Staiti, P. *J. New Mater. Electrochem. Syst.* **2001**, *4*, 181–186.
- [149] Jang, M. Y., Yamazaki, Y. *J. Power Sources* **2005**, *139*, 2–8.
- [150] Wainright, J. S., Wang, J.-T., Savinell, R. F., Litt, M., Moaddel, H., Rogers, C. *Proc. Electrochem. Soc.* **1994**, *94*, 255–264.
- [151] Wainright, J. S., Wang, J.-T., Weng, D., Savinell, R. F., Litt, M. *J. Electrochem. Soc.* **1995**, *142*, L121–L123.
- [152] Glipta, X., Bonnet, B., Mula, B., Jones, D. J., Rozière, J. *J. Mater. Chem.* **1999**, *9*, 3045–3049.
- [153] Kawahara, M., Morita, J., Rikukawa, M., Sanui, K., Ogata, N. *Electrochim. Acta* **2000**, *45*, 1395–1398.
- [154] Pu, H., Meyer, W. H., Wegner, G. *J. Polym. Sci. B* **2002**, *40*, 663–669.

- [155] Qingfeng, L., Hjuler, H. A., Bjerrum, N. J. *Polym. Sci.* **2001**, *31*, 773–779.
- [156] Li, Q., He, R., Jensen, J. O., Bjerrum, N. J. *Fuel Cells* **2004**, *4*, 147–159.
- [157] Xiao, L., Zhang, H., Scanlon, E., et al. *Chem. Mater.* **2005**, *17*, 5328–5333.
- [158] Lobato, J., Canizares, P., Rodrigo, M. A., Linares, J. J., Aguilar, J. A. *J. Membr. Sci.* **2007**, *306*, 47–55.
- [159] He, R., Li, Q., Jensen, J. O., Bjerrum, N. J. *J. Membr. Sci.* **2006**, *277*, 38–45.
- [160] He, R., Li, Q., Xiao, G., Bjerrum, N. J. *J. Membr. Sci.* **2003**, *226*, 169–184.
- [161] Yu, S., Xiao, L., Benicewicz, B. C. *Fuel Cells* **2008**, *8*, 165–174.
- [162] Carollo, A., Quartarone, E., Tomasi, C., et al. *J. Power Sources* **2006**, *160*, 175–180.
- [163] Mustarelli, P., Quartarone, E., Grandi, S., Carollo, A., Magistris, A. *Adv. Mater.* **2008**, *20*, 1339–1343.
- [164] Gubler, L., Kramer, D., Belack, J., Ünsal, Ö., Schmidt, T. J., Scherer, G. G. *J. Electrochem. Soc.* **2007**, *154*, B981–B987.
- [165] Xu, H., Chen, K., Guo, X., Fang, J., Yin, J. *Polymer* **2007**, *48*, 5556–5564.
- [166] Dotelli, G., Gallazzi, M. C., Mari, C. M., Greppi, F., Montoneri, E., Manuelli, A. *J. Mater. Sci.* **2004**, *39*, 6937–6943.
- [167] Andrianov, A. K., Marin, A., Chen, J., Sargent, J., Corbett, N. *Macromolecules* **2004**, *37*, 4075–4080.
- [168] Allcock, H. R., Fitzpatrick, R. J., Salvati, L. *Chem. Mater.* **1991**, *3*, 1120–1132.
- [169] Montoneri, E., Ricca, G., Gleria, M., Gallazzi, M. C. *Inorg. Chem.* **1991**, *30*, 150–152.
- [170] Wycisk, R., Pintauro, P. N. *J. Membr. Sci.* **1996**, *119*, 155–160.
- [171] Allcock, H. R., Klingenberg, E. H., Welker, M. F. *Macromolecules* **1993**, *26*, 5512–5519.
- [172] Tang, H., Pintauro, P. N. *J. Appl. Polym. Sci.* **2001**, *79*, 49–59.
- [173] Guo, Q., Pintauro, P. N., Tang, H., O’Conner, S. J. *Membr. Sci.* **1999**, *154*, 175–181.
- [174] Burjanadze, M., Paulsdorf, J., Kaskhedikar, N., Karatas, Y., Wiemhofer, H.-D. *Solid State Ion.* **2006**, *177*, 2425–2430.
- [175] Allcock, H. R., Hofmann, M. A., Ambler, C. M., et al. *J. Membr. Sci.* **2002**, *201*, 47–54.
- [176] Zhou, X., Weston, J., Chalkova, E., et al. *Electrochim. Acta* **2003**, *48*, 2173–2180.
- [177] Hofmann, M. A., Ambler, C. M., Maher, A. E., et al. *Macromolecules* **2002**, *35*, 6490–6493.
- [178] Chalkova, E., Zhou, X., Ambler, C., et al. *Electrochem. Solid-State Lett.* **2002**, *5*, A221–A222.
- [179] Marrony, M., Barrera, R., Quenett, S., Ginocchio, S., Alberti, G. Progress in MEA Components for Medium and High Temperature Polymer Electrolyte Fuel Cells. In *Proceedings of the First CARISMA International Conference*, La Grande Motte, France, 21–24 September 2008; p 129.

Biographical Sketches



Giulio Alberti began his scientific career at Rome University where he became full professor in inorganic chemistry in 1971. A year later he moved to Perugia University, where he is still active in scientific research. His long research activity ranges from the synthesis and characterization of solid-state proton conductors to their applications in the field of proton-conducting composite membranes. For his research on two-dimensional solids he received a gold medal in 1998 from the Italian Chemical Society. In the last 10 years, his research interest has gradually shifted to the study of polymeric electrolytic membranes and their use in hydrogen fuel cells (FCs) for cars. In particular, most of his research in this field has been focused on the preparation of membranes able to operate in medium-temperature FCs. Particular attention was devoted to annealing procedures for perfluorosulfonic acid membranes, to their water uptake at medium temperatures, and to the preparation and characterization of new composite membranes. He is the author of 175 scientific papers, 30 reviews, 14 chapters in books, 24 patents, and is coeditor of the book *Two and Three Dimensional Inorganic Networks*, Vol. 7 of the series *Comprehensive Supramolecular Chemistry*, Pergamon 1996.



Mario Casciola is a full professor in general and inorganic chemistry at the Faculty of Natural Sciences of Perugia University (Italy). His scientific interests are mainly focused on the chemistry of layered materials belonging to the class metal (IV) phosphates and phosphonates. In recent years he has contributed to the development of the chemistry of layered zirconium phosphonates bearing acidic groups in the interlayer region and to the investigation of their ion exchange and intercalation behavior, mainly their proton-transport properties. This research activity led to the development of original synthetic procedures that allow the disperse zirconium phosphate and zirconium phosphonates, on a nanometric scale, within various neutral and charged polymeric matrices, and to prepare hybrid proton-conducting membranes. His research activity has been documented by more than 100 articles and review papers in international journals and by five patents.